Diagnostic Radiology
Genitourinary Imaging

PIONEERS OF AIIMS-MAMC-PGI IMAGING SERIES

Manorama Berry

Sudha Suri

Veena Chowdhury

PAST EDITORS

Sima Mukhopadhyay

Sushma Vashisht

Diagnostic Radiology
Genitourinary Imaging

3rd Edition

Editors

Niranjan Khandelwal MD DNB FICR
Professor and Head
Department of Radiodiagnosis
Postgraduate Institute of Medical Education and Research, Chandigarh, India

Veena Chowdhury MD
Director Professor and Head
Department of Radiodiagnosis
Maulana Azad Medical College, New Delhi, India

Arun Kumar Gupta MD MAMS
Professor and Head
Department of Radiodiagnosis
All India Institute of Medical Sciences, New Delhi, India

Associate Editor

Anupam Lal MD
Associate Professor
Department of Radiodiagnosis
Postgraduate Institute of Medical Education and Research, Chandigarh, India

JAYPEE BROTHERS MEDICAL PUBLISHERS (P) LTD

St Louis (USA) • Panama City (Panama) • New Delhi • Ahmedabad • Bengaluru
Chennai • Hyderabad • Kochi • Kolkata • Lucknow • Mumbai • Nagpur

Published by

Jitendar P Vij
Jaypee Brothers Medical Publishers (P) Ltd

Corporate Office
4838/24, Ansari Road, Daryaganj, **New Delhi** 110 002, India, Phone: +91-11-43574357, Fax: +91-11-43574314

Registered Office
B-3, EMCA House, 23/23B Ansari Road, Daryaganj, **New Delhi** 110 002, India
Phones: +91-11-23272143, +91-11-23272703, +91-11-23282021, +91-11-23245672
Rel: +91-11-32558559, Fax: +91-11-23276490, +91-11-23245683
e-mail: jaypee@jaypeebrothers.com, Website: www.jaypeebrothers.com

Branches

- 2/B, Akruti Society, Jodhpur Gam Road Satellite
  Ahmedabad 380 015 Phones: +91-79-26926233, Rel: +91-79-32988717
  Fax: +91-79-26927094 e-mail: ahmedabad@jaypeebrothers.com
- 202 Batavia Chambers, 8 Kumara Krupa Road, Kumara Park East
  Bengaluru 560 001 Phones: +91-80-22285971, +91-80-22382956, +91-80-22372664
  Rel: +91-80-32714073 Fax: +91-80-22281761 e-mail: bangalore@jaypeebrothers.com
- 282 IIIrd Floor, Khaleel Shirazi Estate, Fountain Plaza, Pantheon Road
  Chennai 600 008 Phones: +91-44-28193265, +91-44-28194897, Rel: +91-44-32972089
  Fax: +91-44-28193231 e-mail: chennai@jaypeebrothers.com
- 4-2-1067/1-3, 1st Floor, Balaji Building, Ramkote Cross Road
  Hyderabad 500 095 Phones: +91-40-66610020, +91-40-24758498 Rel:+91-40-32940929
  Fax:+91-40-24758499, e-mail: hyderabad@jaypeebrothers.com
- No. 41/3098, B & B1, Kuruvi Building, St. Vincent Road
  Kochi 682 018, Kerala Phones: +91-484-4036109, +91-484-2395739, +91-484-2395740
  e-mail: kochi@jaypeebrothers.com
- 1-A Indian Mirror Street, Wellington Square
  Kolkata 700 013 Phones: +91-33-22651926, +91-33-22276404, +91-33-22276415
  Rel: +91-33-32901926 Fax: +91-33-22656075, e-mail: kolkata@jaypeebrothers.com
- Lekhraj Market III, B-2, Sector-4, Faizabad Road, Indira Nagar
  Lucknow 226 016 Phones: +91-522-3040553, +91-522-3040554
  e-mail: lucknow@jaypeebrothers.com
- 106 Amit Industrial Estate, 61 Dr SS Rao Road, Near MGM Hospital, Parel
  Mumbai 400012 Phones: +91-22-24124863, +91-22-24104532, Rel: +91-22-32926896
  Fax: +91-22-24160828, e-mail: mumbai@jaypeebrothers.com
- "KAMALPUSHPA" 38, Reshimbag, Opp. Mohota Science College, Umred Road
  Nagpur 440 009 (MS) Phone: Rel: +91-712-3245220, Fax: +91-712-2704275
  e-mail: nagpur@jaypeebrothers.com

North America Office
1745, Pheasant Run Drive, Maryland Heights (Missouri), MO 63043, USA Ph: 001-636-6279734
e-mail: jaypee@jaypeebrothers.com, anjulav@jaypeebrothers.com

Central America Office
Jaypee-Highlights Medical Publishers Inc. City of Knowledge, Bld. 237, Clayton, Panama City, Panama Ph: 507-317-0160

Diagnostic Radiology: Genitourinary Imaging

First Edition: 1996

Second Edition: 2003

Third Edition: **2009**

ISBN 978-81-8448-682-7

Typeset at JPBMP typesetting unit

Printed at

CONTRIBUTORS

Ajay Gulati MD
Assistant Professor
Department of Radiodiagnosis
Postgraduate Institute of Medical Education and Research
Chandigarh

Ajay Kumar MD
Assistant Professor
Department of Radiodiagnosis
Postgraduate Institute of Medical Education and Research
Chandigarh

Alpana Manchanda MD
Associate Professor
Department of Radiodiagnosis
Maulana Azad Medical College
New Delhi

Anjali Prakash DMRD DNB MNAMS
Assistant Professor
Department of Radiodiagnosis
Maulana Azad Medical College
New Delhi

Anju Garg MD
Professor
Department of Radiodiagnosis
Maulana Azad Medical College
New Delhi

Anupam Lal MD
Associate Professor
Department of Radiodiagnosis
Postgraduate Institute of Medical Education and Research
Chandigarh

Arun Kumar Gupta MD MAMS
Professor and Head
Department of Radiodiagnosis
All India Institute of Medical Sciences, New Delhi

Ashu Seith Bhalla MD
Associate Professor
Department of Radiodiagnosis
All India Institute of Medical Sciences, New Delhi

Atin Kumar MD
Assistant Professor
Department of Radiodiagnosis
(Trauma Centre)
All India Institute of Medical Sciences, New Delhi

Deep Narayan Srivastava MD MAMS
Professor
Department of Radiodiagnosis
All India Institute of Medical Sciences, New Delhi

Hina Arif Mumtaz MD, DNB
Senior Research Associate
Department of Radiodiagnosis
Postgraduate Institute of Medical Education and Research
Chandigarh

Kusum Joshi MD, PhD
Professor and Head
Department of Histopathology
Postgraduate Institute of Medical Education and Research
Chandigarh

Mahesh Prakash MD
Assistant Professor
Department of Radiodiagnosis
Postgraduate Institute of Medical Education and Research
Chandigarh

Manavjit Sandhu MD
Professor
Department of Radiodiagnosis
Postgraduate Institute of Medical Education and Research
Chandigarh

Mandeep Kang MD
Associate Professor
Department of Radiodiagnosis
Postgraduate Institute of Medical Education and Research
Chandigarh

Manphool Singhal MD, DNB
Senior Research Associate
Department of Radiodiagnosis
Postgraduate Institute of Medical Education and Research
Chandigarh

Naveen Kalra MD
Associate Professor
Department of Radiodiagnosis
Postgraduate Institute of Medical Education and Research
Chandigarh

Niranjan Khandelwal MD, DNB
Professor and Head
Department of Radiodiagnosis
Postgraduate Institute of Medical Education and Research
Chandigarh

Paramjeet Singh MD
Additional Professor
Department of Radiodignosis
Postgraduate Institute of Medical Education and Research
Chandigarh

Radhika Srinivasan MD, PhD
Additional Professor
Department of Cytology and Gynaec-pathology
Postgraduate Institute of Medical Education and Research
Chandigarh

Raju Sharma MD
Additional Professor
Department of Radiodiagnosis
All India Institute of Medical Sciences, New Delhi

Rakesh Kumar MD
Associate Professor
Department of Nuclear Medicine
All India Institute of Medical Sciences, New Delhi

Rama Mohan Reddy MD
Department of Radiodiagnosis
All India Institute of Medical Sciences, New Delhi

Rashmi Dixit MD
Professor
Department of Radiodiagnosis
Maulana Azad Medical College
New Delhi

Sameer Vyas MD
Senior Research Associate
Department of Radiodiagnosis
Postgraduate Institute of Medical Education and Research
Chandigarh

Sanjay Thulkar MD
Associate Professor
Department of Radiodiagnosis (BRA IRCH)
All India Institute of Medical Sciences, New Delhi

Sapna Singh MD DNB MNAMS
Assistant Professor
Department of Radiodiagnosis
Maulana Azad Medical College
New Delhi

Shamim Ahmed Shamim MD
Department of Radiodiagnosis
All India Institute of Medical Sciences, New Delhi

Shivanand Gamanagatti MD
Assistant Professor
Department of Radiodiagnosis (Trauma Centre)
All India Institute of Medical Sciences, New Delhi

Smriti Hari MD.
Assistant Professor
Department of Radiodiagnosis
All India Institute of Medical Sciences, New Delhi

Sumedha Pawa MD
Professor
Department of Radiodiagnosis
Maulana Azad Medical College
New Delhi

Veena Chowdhury MD
Director Professor and Head
Department of Radiodiagnosis
Maulana Azad Medical College
New Delhi

FOREWORD

The last few decades have seen tremendous advancement in the field of medical imaging leading to a significant change in the perception of many diseases. The advent of sonography and computed tomography (CT) was a breakthrough in the history of medical imaging and had changed the outlook of many diseases. With the ever-increasing advancement in the field of technology and the advent of MRI, PET and specialized fluoroscopy units, the management of many urological diseases has also altered significantly. There is a close inter-relationship between the advancement of knowledge and complexity of research technology required. The field of uroradiology has benefited significantly from these technological advances in recent past taking the management of many urological diseases to a new platform.

The new generation of imaging procedures namely MRA, MRS and PET are superior to currently available technologies. These have been used to investigate a wide spectrum of urogenital disorders. The development of DSA and identification of percutaneous/ endovascular routes for access to the kidneys, ureter and bladder has lead to the firm establishment of interventional radiology as an important subspeciality of radiology.

The present volume on genitourinary imaging is the Third edition in the series of diagnostic radiology courses organized by the Departments of Radiodiagnosis and Imaging PGIMER Chandigarh, AIIMS and MAMC, New Delhi. A number of dedicated workers from these institutes have contributed to this volume. They have not only covered major recent advances in the field of genitourinary radiology but have also dealt with more conventional forms of imaging.

These volumes would be a valuable addition to the libraries of all Medical Practitioners not only in this country or the subcontinent but all over the world. Dr N Khandelwal, Dr Veena Chowdhury and Dr Arun Kumar Gupta deserve to be congratulated for their continuing vision and efforts in promoting these invaluable courses on diagnostic radiology.

Vinay Sakhuja
MD, DM(Neph), MNAMS(Neph), FISN, FAMS
Dean, PGIMER Chandigarh, India

Preface to the Third Edition

The first edition of Diagnostic Radiology on "Genitourinary Imaging" was published in 1996 and the second edition in 2003. Encouraged by the response to the previous editions and to keep up the pace of advances in imaging, we decided to update the third edition. We are very hopeful that this edition will be more comprehensive for residents, practicing radiologists, nephrologists and urologists.

We wish to take this opportunity to thank our faculty from AIIMS, MAMC and PGIMER for their active contribution and support without which this endeavor would not have been possible.

We would also like to thank Shri Jitendar P Vij (Chairman and Managing Director) along with Mr Tarun Duneja (Director-Publishing) of M/s Jaypee Brothers Medical Publishers (P) Ltd, New Delhi and other staff for their professional help and cooperation in publishing this book in a very short time.

Niranjan Khandelwal
Veena Chowdhury
Arun Kumar Gupta
Anupam Lal

Preface to the First Edition

Urogenital radiology is practised today quite differently in many ways than a decade ago. This is mainly due to the technological advances in ultrasound, computed tomography and magnetic resonance imaging. With the ever-increasing number of diagnostic techniques, the radiologists and the referring clinicians are faced with the dilemma of determining the most appropriate test or tests for a given clinical problem.

Keeping this in view, the present book aims to present the most current information on the role of various techniques, viz conventional radiology, ultrasound, computed tomography and magnetic resonance imaging in the urogenital practice, their merits and limitations and to determine the approach to complex problems in this decade. The comprehensive discussion on the indications of various imaging techniques in urogenital practice are presented throughout this text. Recommendations are offered regarding the role of each technique in various clinical situations based on the collective experience of the faculty of radiology at the All India Institute of Medical Sciences, Maulana Azad Medical College, Postgraduate Institute of Medical Education and Research and other renowned Indian radiologists.

We hope this book will help the postgraduate students, practising radiologists and internists develop an indepth understanding and appreciation of the contemporary radiologic evaluation of the urogenital tract.

We wish to take this opportunity to thank the authors for their cooperation and prompt submission of their contributions to this volume.

Manorama Berry
Sushma Vashisht
Veena Chowdhury

CONTENTS

MISCELLANEOUS URINARY TRACT LESIONS

RETROPERITONEUM

INTERVENTIONS

DISEASES OF FEMALE PELVIS

SCROTUM AND MALE SEXUAL DYSFUNCTION

Chapter 1

Current Status of Conventional Techniques in Urogenital Imaging

Naveen Kalra, Manavjit Sandhu

The history of uroradiology dates back to July 11, 1896 when MacIntyre, Glasgow first reported the X-ray demonstration of a renal calculus in a patient.[1] Subsequently, urologists developed cystography, retrograde pyelography and retrograde urethrography within a span of next 15 years. In 1929, Moses Swick[2] introduced a successful intravenous urographic contrast agent called uroselectan (5-iodo-2-pyridone N acetic acid) which ushered in IVU (intravenous urography) that became an integral part of the urological work-up of patients. Plain X-ray of kidney, ureter and bladder (KUB) and intravenous urography (IVU) continued to be used as the primary imaging techniques for the diagnostic evaluation of urinary tract for several years (Figs 1.1A to C). However, recently with the development of ultrasound (US), computed tomography (CT) and magnetic resonance imaging (MRI), there are now several techniques in the diagnostic armamentarium of the uroradiologist. While a multimodality approach is often required to come to a final conclusion, the strengths and weaknesses of each technique must be known so that both conventional and newer techniques can be used to the maximum

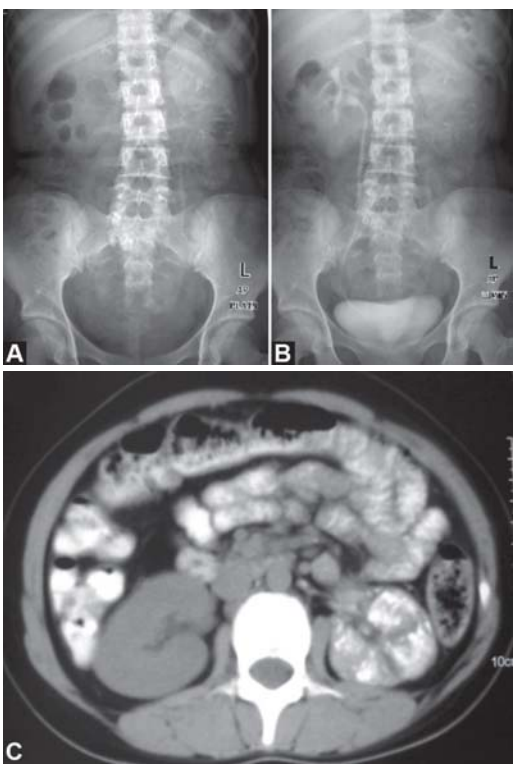

Figs 1.1 A to C: (A) Plain radiograph of the abdomen shows extensive calcification in the left kidney and along the course of left ureter as a result of tuberculosis infection. **(B)** IVU shows no contrast excretion into the calyceal system on the left side. The right kidney and ureter are normal. **(C)** Non-enhanced axial CT section shows extensive parenchymal calcification in the left kidney

benefit of patients. Availability, cost-effectiveness and radiation dose are some of the other important factors determining the choice of the imaging modality while investigating various clinical problems. This chapter will discuss the current status of conventional radiological procedures vis-à-vis the newer techniques in common clinical situations.

Patients suspected to have urolithiasis may present with acute flank pain, hematuria or recurrent urinary tract infections. A plain film of the abdomen (X-ray KUB) is usually the first radiological investigation performed in these patients. However, the diagnostic accuracy of plain film for the detection of urinary tract calculus depends on the chemical composition of the stone, its size, location, overlying bowel gas shadows and technical quality of the film. Levine et al[3] in their study of 178 patients found that plain radiographs had a sensitivity of only 45 percent for detecting ureteral calculi which marginally increased to 59 percent when the plain films were retrospectively reviewed with CT as the standard of reference. However, plain films are still good as baseline study and for follow-up of stone disease post-treatment.

Recently, ultrasound on account of its simplicity, freedom from radiation and ready availability has been proposed as an alternative technique when used in combination with KUB for diagnostic evaluation of patients presenting with acute flank pain. In a prospective study conducted by Lewis-Jones et al,[4] X-ray KUB and ultrasound provided similar information as that obtained by IVU in 81.4 percent of patients. Considering the cost effectiveness, the authors concluded that KUB and US could replace IVU in patients of renal colic. In a series of 180 patients, Dalla Palma et al showed a 95 percent negative predictive value of the KUB/US combination indicating that IVU was unlikely to be helpful, if the KUB/US tests were negative.[5] While US is highly sensitive for detection of dilated collecting system, it has several limitations. Calculi smaller than 5 mm can be easily missed and ureteral stones that are seen in association with undilated collecting system cannot be detected.

In the last decade unenhanced CT has rapidly gained popularity for investigating a patient of renal colic and there are several studies which have reported high sensitivity and specificity (95-97%) for detection of renal and ureteral calculi.[6,7] CT detects virtually all stones regardless of their composition. In a study of 20 patients by Smith et al,[8] 5 patients had shown calculi on both IVU and CT, 6 had a stone that was detected only on CT and one patient had a stone that was not detected either on CT or IVU. With the availability of fast spiral CT scanner, the technique is specially useful in the emergency setting. There are many centers where plain films and IVU have been replaced by helical CT in patients presenting with flank pain and hematuria. In addition the extent of perinephric edema seen on CT has been used to predict the degree of ureteral obstruction and chances of spontaneous passage of ureteral stone with an accuracy of 94 percent.[9] Thus in centers where there is free access to spiral CT, unenhanced CT has actually replaced plain films and IVU for diagnosis of stones in the urinary tract. KUB and ultrasound may be used as the initial screening modality which is followed by spiral CT if the KUB and US are negative (Figs 1.2A and B). However, IVU is still the best investigation if CT is not available. The KUB/US combination has also been compared to spiral CT. In a prospective study of 66 patients, the KUB/US combination had a sensitivity of 79 percent for detecting ureteric stones.

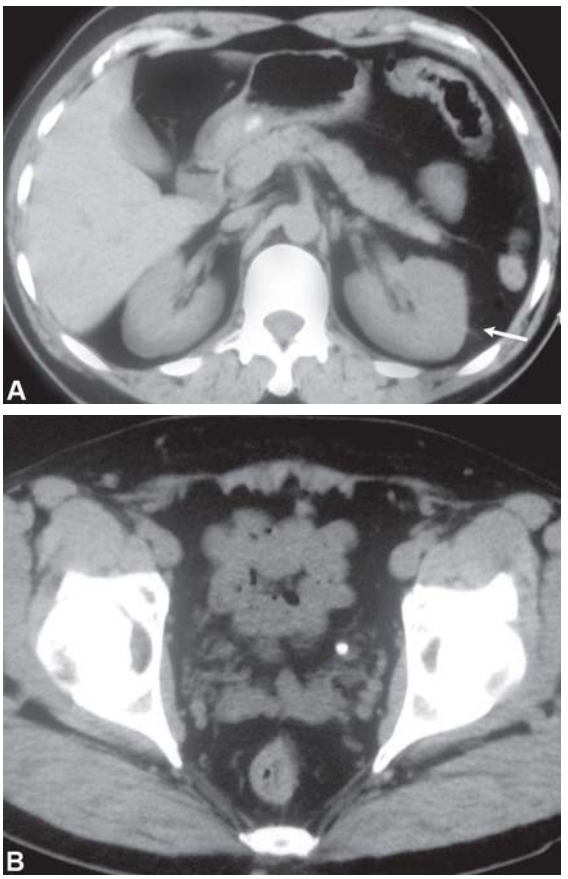

Figs 1.2 A and B: Non-enhanced axial helical CT sections of a patient with renal colic and normal X-ray KUB and US. **(A)** The left kidney is enlarged with mild perinephric stranding (arrow). **(B)** A small calculus is seen in the left lower ureter

However, all the missed cases had spontaneous passage of stone and it was concluded that CT would not add useful information after a negative KUB/US study.[10]

Radiation dose is one of the major factors which influences the choice of appropriate imaging modality. The radiation dose of unenhaced CT is greater than that of IVU even though patients with obstruction may require more number of radiographs than those without obstruction. The low dose CT protocol for stone detection proposed by Liu et al [7] still results in approximately double the effective dose equivalent in comparison with IVU (2.8 mSv for CT, 1.33 mSv for conventional IVU).

Painless hematuria is another major urological problem which needs evaluation of both renal parenchyma and urothelium to rule out urinary tract malignancy. Traditionally IVU has been used as the baseline investigation in these patients. IVU is a time tested technique which is most acceptable to the urologist as it gives a global view of the renal parenchyma and the collecting system. However, with advent of helical CT and CT/MR urography the exact place of IVU in this clinical setting is again under question and there is no universal agreement about the first imaging modality to be used in patients with hematuria. The American Urological Association Best Practice Policy Guidelines include either IVU or CT urography as the initial imaging test for asymptomatic microscopic hematuria.[11] In addition, the American College of Radiology has rated IVU and CT urography equal as to their appropriateness for evaluation of patients with hematuria.[12] In patients with hematuria due to renal parenchymal disease, US is the best imaging modality for evaluating renal volume and morphology.

It is generally agreed that imaging with US/CT/MRI is superior to IVU for detection and characterization of renal masses. In addition a urogram or retrograde pyelogram may be required to visualize the urothelium of the renal collecting system and the ureters in patients when there is suspicion of urothelial neoplasm. CT urography is an evolving technique wherein three-dimensional (3D) coronal reconstruction of contrast enhanced CT images is

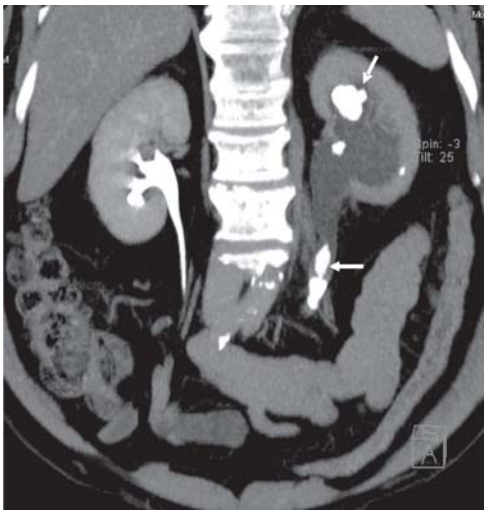

Fig. 1.3: CT urography in the pyelogram phase showing good opacification of the calyceal system and ureter on the right side. There is presence of left hydroureteronephrosis with renal and ureteric calculi (arrows)

achieved using the maximum intensity projections (Fig. 1.3). McNicholas et al [13] found no significant differences in the ability of CT urography and IV urography in opacifying the calcyces, pelvis and ureter and opined that CT urography has the potential for evaluating the urothelium. Chow et al [14] concluded that CT urography in conjunction with the axial images is a single examination which alone may be required for the work-up of patients with hematuria as it is capable of imaging both the parenchyma and the collecting system. On the other hand, Hattery and King[15] have reported their experience of CT urography and found 10 percent of urinary tract abnormality were either better or only detected by IVU compared to 5 mm axial sections and CT urography. The authors listed several examples such as pyeloureteritis cystica, papillary necrosis and transitional cell carcinoma where CT urography may not provide the high quality images needed for diagnosis. The authors supported the notion that CT with digital reformatted images does not provide sufficient detail for evaluation of subtle urothelial neoplasms. Cowan et al[16] compared CT urography with retrograde pyelography for the detection of urothelial carcinoma in 106 patients. The only false negative CT urogram was a small urothelial tumor that was not detected in an unopacified segment. From the aforesaid, it is clear that as refinement of CT urography continues, IVU will be replaced by CT urography subject to availability and affordability.

IVU is the only modality to detect early changes in renal calyces in tuberculosis, papillary necrosis, etc. US, CT and MRI may be totally normal in these early cases. Hence, in a suspected case of urinary tract TB, IVU is the first imaging modality for diagnosis and subsequent follow-up.[17] However, it is always advisable to intergrate IVU with cross-sectional imaging in patients with suspected tuberculosis.

Children presenting with repeated attacks of UTI have been traditionally investigated with IVU and cystourethrography. The aim of imaging is to diagnose any underlying congenital renal anomaly that may predispose to recurrent urinary tract infections and detect the presence of renal scarring and vesicoureteric reflux. Recent studies have shown that diagnostic yield of IVU in this clinical setting is unacceptably low (8.3%)[18] and the abnormalities detected rarely change the management. Risks of IVU in terms of radiation and possibility of adverse reaction to contrast media outweigh its benefits and there is thus a strong case for withdrawal of routine IVU as a screening test in patients with recurrent UTI. Renal scintigraphy using ^{99m}TcDMSA is superior to IVU for detection of renal scarring. Despite many proponents of radionuclide cystography (RNC), conventional contrast voiding cystourethrography (VCUG) continues to be the gold standard

for detecting and grading of the vesicoureteric reflux (VUR) on account of false-negative studies and poor grading accuracy of radionuclide cystography.[19] RNC has a much lower radiation dose than VCUG, but the low spatial resolution cannot identify the anatomic abnormalities of the urethra, bladder and ureters. RNC is recommended for follow-up of VUR and for screening the asymptomatic siblings of patients with VUR. Initial evaluation of VUR in girls may be done with RNC but in boys RNC is inadequate as anatomic imaging of urethra and bladder can only be done with VCUG.

In children and pregnant patients being investigated for obstructive uropathy, MR urography also has the potential to replace IVU due to the absence of radiation exposure (Figs 1.4A and B). Using T2-weighted (static-fluid urography) and contrast enhanced dynamic T1-weighted sequences (excretory urography), images of sufficient diagnostic quality can be obtained in infants with oral sedation.[20] Blandino et al in 2001[21] in their study of 115 patients found that the specificity of MR urography in detecting hydronephrosis was 98 percent and the accuracy in revealing the level of obstruction was 100 percent. The sensitivity of detecting stones, strictures and congenital ureteropelvic junction obstructions was 68.9 percent, 98.5 percent and 100 percent respectively. The sensitivity of detecting ureteral calculi is technique dependent, with higher sensitivity being reported for excretory urography than for static-fluid urography.[22]

In patients of renal trauma, IVU and renal arteriography were the main diagnostic tools in the past. With introduction of US and CT, IVU is no longer used in these patients and CT is considered the technique of choice for detection and characterization of renal injuries and for assessment of vascular status.

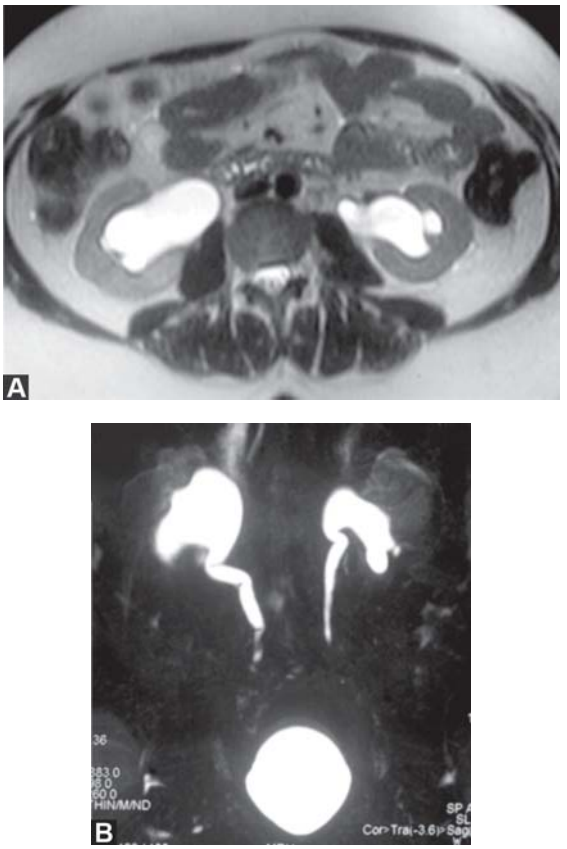

Figs 1.4A and B: MR urography in a patient with retroperitoneal fibrosis. **(A)** Axial T2-weighted image shows hydronephrosis on both sides. **(B)** Static-fluid MRU image shows hydroureteronephrosis on both sides with medially deviated ureters

Angiography is reserved for patients who require interventional treatment such as embolisation of traumatic pseudoaneurysm or AV fistula. Contrast cystography, micturating cystourethrography and retrograde urethrography continue to be the techniques of choice for diagnosing bladder and urethral injuries and urethral strictures (Figs 1.5A and B).

Pretransplant work-up of renal donor used to include IVU and conventional angiography. Precise information of number of ureters, site of joining in case of duplication of ureter and vascular anatomy is mandatory

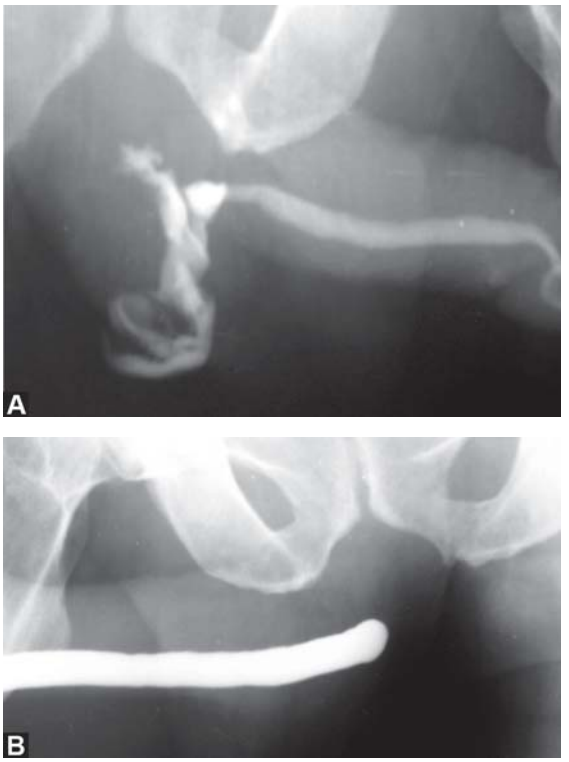

Figs 1.5A and B: (A) Retrograde urethrography (RGU) in a patient following pelvic trauma shows contrast extravasation from the bulbar urethra. **(B)** Follow-up RGU in the same patient shows stricture at the level of bulbar urethra

before donor selection. The reported sensitivity and specificity of MDCT angiography for the detection of accessory renal arteries, prehilar branching and venous anomalies are 88 percent and 98 percent, 100 percent and 97 percent and 100 percent and 97 percent respectively. In one of the studies, CT findings agreed with surgical findings for accessory renal arteries, prehilar branching and venous anomalies in 94 percent, 93 percent and 98 percent of patients respectively.[23]

At times before pelvic surgery for bladder, uterus, ovaries, etc. the surgeon needs exact relationships of the lower ureters in the surgical field or involvement of ureters by the pelvic pathology to reduce the chances of ureteral injury. However, IVU should not be used routinely before hysterectomy but should be performed in patients with large pelvic masses or known pelvic cancer.[24]

CONCLUSION

To conclude it appears that conventional uroradiology continues to play an important but limited role in urogenital imaging. Nonenhanced helical CT has nearly replaced conventional uroradiology for evaluation of urinary tract calculi. However, in countries such as ours, a blanket substitution may not be feasible due to cost factor and availability. CT and MR urography at present cannot fully substitute contrast urography although CT urography is the current heir apparent to IVU. Technical improvements in CT urography like reduction in radiation exposure and MR urography like faster imaging time and consistent image quality are required to further enhance the utility of CT and MR urography in the future.

REFERENCES

1. MacIntyre J. Photograpy of renal calculus: Description an adjustable modification in the focus tube. Lancet 1896;2:118.
2. Swick M. Visualization of the kidney and urinary tract on roentgenograms by means of intravenous administration of a new contrast: Uroselectan. Klin Wochenschr 1929;8:2087.
3. Levine JA, Neitlich J, Verga M, et al. Ureteral calculi in patients with flank pain: correlation of plain radiography with unenhanced helical CT. Radiology 1997;204:27-31.
4. Lewis-Jones HG, Lamb GH, Hughes PL. Can ultrasound replace the intravenous urogram in preliminary investigation of renal tract disease? A prospective study. Br J Radiol 1989;62:977-80.
5. Palma DL, Stacul F, Bazzocchi M, et al. Ultrasound and plain film versus intravenous urography in ureteric colic. Clin Radiol 1993; 47:333-36.

6. Boulay I, Holtz P, Foley WD, et al. Ureteral calculi: Diagnostic efficacy of helical CT and implications for treatment of patients. AJR 1999;172:1485-90.
7. Liu W, Esler SJ, Kenny BJ, et al. Low dose non-enhanced helical CT of renal colic: Assessment of ureteric stone detection and measurement of effective dose equivalent. Radiology 2000; 215:51-54.
8. Smith RC, Rosenfield AT, Choe KA, et al. Acute flank pain: Comparison of non-contrast enhanced CT and intravenous urography. Radiology 1995;194:789-94.
9. Boridy IC, Kawashima A, Goldman SM, et al. Acute ureterolithiasis: Nonenhanced helical CT findings of perinephric edema for prediction of degree of ureteral obstruction. Radiology 1999;213:663-67.
10. Ripolles T, Agramunt M, Errando J, et al. Suspected ureteric colic: Plain film and sonography vs unenhanced helical CT. A prospective study in 66 patients. Eur Radiol 2004;14:129-36.
11. Grossfeld GD, Litwin MS, Wolf JS Jr, et al. Evaluation of asymptomatic microscopic hematuria in adults : The American Urological Association best practice policy. II. Patient evaluation, cytology, voided markers, imaging, cystoscopy, nephrology evaluation, and follow-up. Urology 2001;57:604-610.
12. Choyke PL, Bluth EI, Bush WH Jr, et al. Radiological investigation of patients with hematuria. American College of Radiology, ACR Appropriateness Criteria, 2005.
13. McNicholas MMJ, Raptopoulos VD, Schwartz RK, et al. Excretory phase CT urography for opacification of the urinary collecting system. AJR 1998;170:1261-67.
14. Chow LC, Sommer FG. Multidetector CT urography with abdominal compression and three dimensional reconstruction. AJR 2001;177: 849-55.
15. Hattery RR, King BF. Invited Commentary. Radiographics 2001;21:822-23.
16. Cowan NC, Turney BW, Taylor NJ, et al. Multidetector computed tomography urography for diagnosing upper urinary tract urothelial tumor. BJU Int 2007;99;1363-70.
17. Palma DL. What is left of IV urography? Eur Radiol 2001;11:931-39.
18. Little MA, Johnson DBS, O'Callaghan JP, et al. The diagnostic yield of intravenous urography. Nephrol Dial Transplant 2000;15:200-04.
19. Kass EJ,Kernen KM, Carey JM. Paediatric urinary tract infection and the necessity of complete urological imaging. BJU Int 2000;86:94-96.
20. Riccabona M, Simbrunner J, Ring E, et al. Feasibility of MR urography in neonates and infants with anomalies of the upper urinary tract. Eur Radiol 2002;12:1442-50.
21. Blandino A, Gaeta M, Minutoli F, et al. MR pyelography in 115 patients with a dilated renal collecting system. Acta Radiol 2001;42:532-36.
22. Silverman SG, Leyendecker JR, Amis SE Jr. What is the current role of CT urography and MR urography in the evaluation of the urinary tract? Radiology 2009;250:309-23.
23. Namasivayam S, Small WC, Kalra MK, et al. Multidetector-row CT angiography for preoperative evaluation of potential laparoscopic renal donors: How accurate are we? Clin Imag 2006;30:120-26.
24. Mushlin AI, Thornbury JR. Intravenous pyelography: The case against its routine use. Annals of Int Med 1989;111:58-70.

Chapter

2

Ultrasound of Urogenital Tract: Techniques and Normal Appearances

Anju Garg

Ultrasonography is an indispensable modality for morphological evaluation of the urogenital tract**.** It is accurate, safe, does not require exposure to ionizing radiation or normal renal function for image production. With modern instrumentation, bedside sonography and guided procedures can be performed on even the most seriously ill patients.

KIDNEYS AND URETERS

Technique

A 3 to 5 MHz sector/linear transducer is used to scan the urinary tract. Although no specific preparation is required for scanning the kidneys, fasting optimises the visualization. Evaluation of the renal vessels is augmented by adequate patient hydration, and a full bladder is essential for visualising the lower ureters, vesicoureteric junction, and the bladder. The kidneys are scanned in the supine or lateral decubitus position. Varying the degree of respiration can help in complete evaluation of the kidneys. The left kidney is more difficult to visualize because gas in small bowel and splenic flexure interfere with the anterior or anterolateral approach. A posterolateral approach often gives a good visualization of left kidney. Scanning in prone position is rarely required in adults, except for renal guidance procedures, but in young children it remains a useful approach.

Some of the common indications for evaluating the upper urinary tract are:

- Evaluation of collecting system obstruction
- Evaluation of suspected or known nephrolithiasis
- Evaluation of cystic renal disease
- Detection of a renal or perirenal mass lesion
- Characterization of a renal mass lesion
- Guidance for diagnostic or therapeutic interventional procedures

Normal Sonographic Appearance

The kidneys lie retroperitoneally on either side of the spine enclosed in fascial layers. The adult kidney is reniform in shape with a smooth outline. It is surrounded by a fibrous capsule which demarcates it from the surrounding perirenal fat. The cortex forms the outer part of renal parenchyma surrounding the medulla which is made up of renal pyramids arranged around the renal sinus (Fig. 2.1).

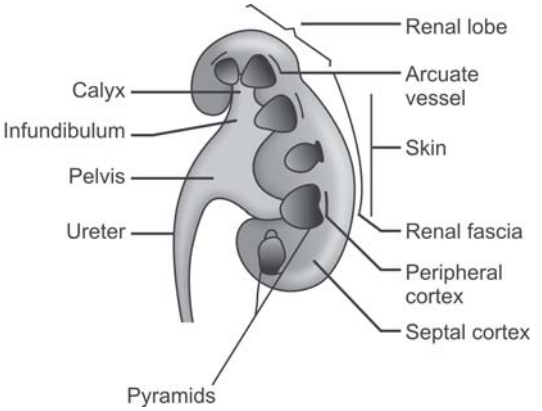

Fig. 2.1: Diagram depicting the normal sectional anatomy of kidney

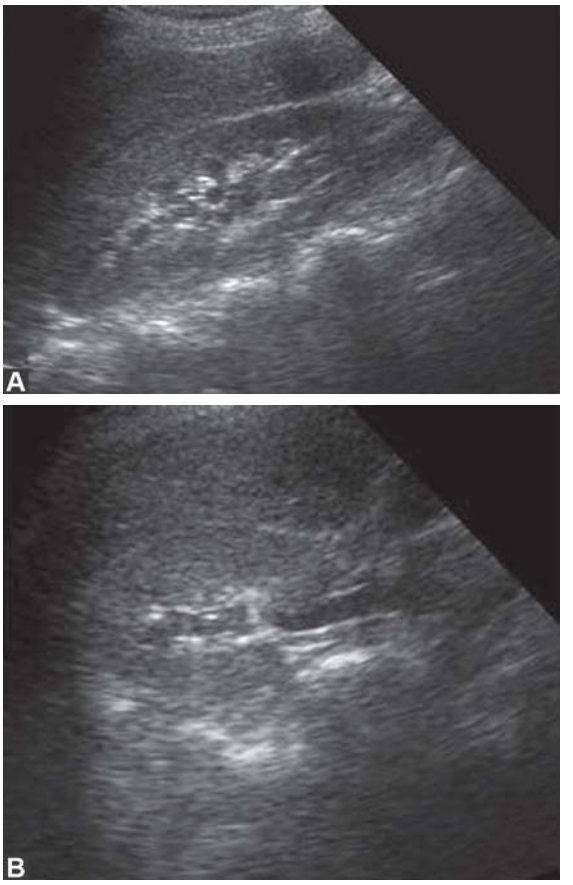

Figs 2.2 A and B: Normal kidney: **(A)** Sagittal view showing cortex and hypoechoic pyramids with bright central sinus echoes. **(B)** Transverse view at level of renal hilum

On sonography, the cortex has a fine homogeneous texture with a reflectivity less than that of the adjacent liver and spleen (Figs 2.2A and B), but the degree of differentiation is to some extent dependent on the equipment. However, if the renal cortex is brighter than the liver, it strongly suggests the presence of disease. Medullary pyramids are seen as echopoor oval areas evenly distributed around the inner margin of the cortex. Arcuate vessels mark the true corticomedullary junction and can be seen as punctuate echogenic foci (Fig. 2.3A) in approximately 25% of patients.[1] The **cortical thickness** is the distance between the capsule and the outer margin of the medullary pyramid while **parenchymal thickness** is the distance between the capsule and the margin of the sinus (Fig. 2.3B). It is often easier and more consistent to measure the parenchymal thickness.

The renal sinus contains the calyces, infundibulum, a portion of the renal pelvis, fibrous tissue, fat, vessels and lymphatics. On US, the renal sinus appears as a central hyperechoic area, largely because of its fat content. When collapsed, the collecting system merges with the echoes of the renal sinus. However, in well-hydrated patients it may be slightly distended with echo free urine.

The **neonatal kidney** is sonographically more echogenic than that of the older infant and adults (Fig. 2.4). Echogenicity is equal to or greater than the adjacent liver. It assumes the adult appearance by 2-3 months of age.[2] Other differences are tabulated in Table 2.1.

Table 2.1: Differences between neonatal and adult kidney

	Neonatal	*Adult*
Contour	Lobed	Smooth
Cortex reflectivity	++	+
Medullary reflectivity	—	—
Sinus	Echo poor	Echogenic
Collecting system	Apparent	Inapparent

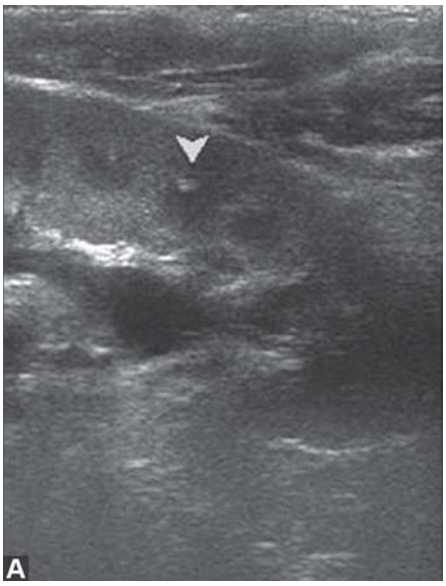

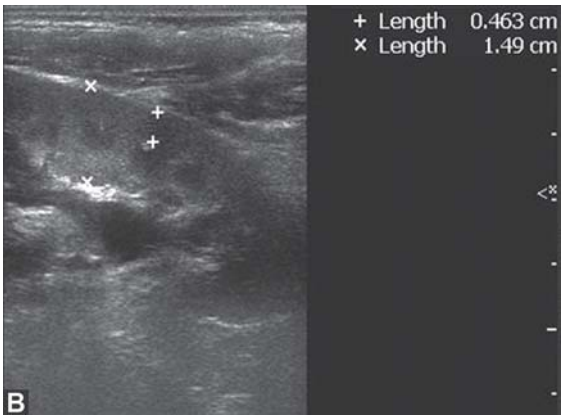

Figs 2.3A and B: Corticomedullary differentiation. **(A)** Echogenic arcuate vessel (arrowhead) seen at cortico-medullary junction, **(B)** Cortical thickness(++) and parenchymal thickness (××)

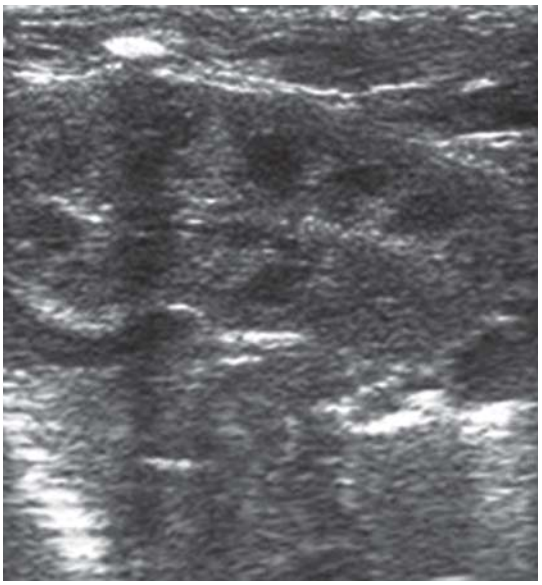

Fig. 2.4: Normal neonatal kidney. The cortex of the kidney is relatively thin and moderately reflective. The medullary pyramids appear disproportionately large and are very poorly reflective. Only minimal renal sinus structures are seen

The determination of renal size with US is more accurate than with intravenous urography because the kidney is imaged without magnification and contrast induced osmotic diuresis. As a result renal size is approximately 15% smaller**.** Renal size is related to sex, age and built of the patient. The length of the normal adult kidney is usually 10-12 cm but can range from 7-14 cm in patients with normal renal function (Table 2.2). Length can also vary in the same individual depending on the state of hydration.

On sonography the longest cranio-caudal length is imaged by rotating the probe around its vertical axis.[3] Care must be taken to measure the longest length as it is easy to get a false low measurement due to the ellipsoid shape of the kidney. For more accurate measurement of renal size, a renal

volume assessment can be made, either by measuring the area of kidney in serial slices and subsequently calculating the volume or by using the modified 3D ellipsoid formula. The precise value is probably not as important as consistency so that changes in volume over a period of time can be measured. Emamian et al[4] measured the renal size in 665 healthy adult volunteers and showed that the parenchymal volume of the right kidney is smaller than the left. Possible explanation for this could be: (1) The spleen is smaller than the liver and so there is more space for left kidney growth and (2) The left renal artery is shorter than the right and, therefore, increased blood flow on the left results in an increase in renal volume.

Table 2.2: Normal kidney length in adults

	Adult female (cm)	*Adult male (cm)*
Left kidney	11 (9.9-12.1)	11.5 (10.4-12.6)
Right kidney	10.7 (9.5-12)	11.2 (10.1-12.4)

Normal Variations

The kidneys may vary in **position** due to ptosis or an ectopic location. The most common site for the ectopic kidney is the pelvis, where it may be difficult to detect, as it can be obscured by bowel gas. **Renal duplication** is common and spans a range from complete to minimal. However, sonography may only show an elongated kidney perhaps with separation of the renal sinus into two parts (Fig. 2.5). A double pelvis may be visualised when the collecting system is distended. Residual **fetal lobulations** may be seen. A **dromedary hump** can be seen sometimes which is a bulge along the lateral border of the left kidney due to moulding by the adjacent spleen (Fig. 2.6).

A **hypertrophied column of Bertin** is a normal variant and represents unresorbed

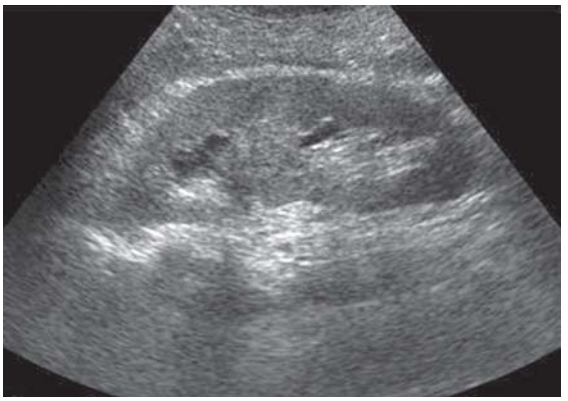

Fig. 2.5: Duplex collecting system. Sagittal sonogram shows central parenchyma separating the upper and lower moities. There is mild dilatation of upper moity

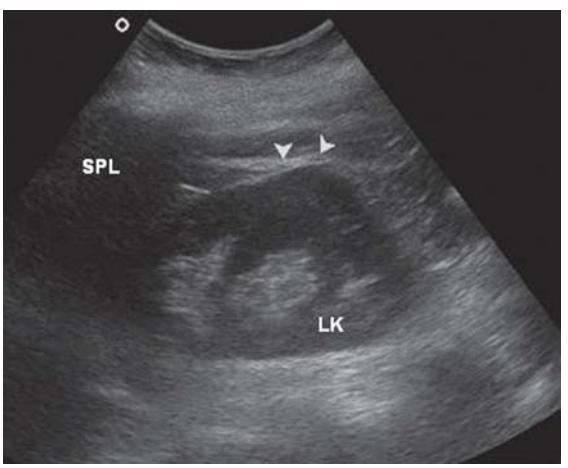

Fig. 2.6: Dromedary hump seen as a focal bulge along the lateral aspect of the left kidney (arrowheads)

polar parenchyma from one or both of the 2 subkidneys that fuse to form the normal kidney.[5] Sonographic criteria to diagnose a hypertrophied column of Bertini include isoechogenicity and continuity with rest of the renal cortex, lack of mass effect, indentation of renal sinus laterally, generally less than 3 cm in size with a normal vascular pattern on Doppler. Occasionally it may be difficult to differentiate a small avascular tumour from a hypertrophied column of

Bertini when further investigations maybe required.

A wedge-shaped echogenic defect or an echogenic line, the **intervesicular fissure or parenchymal junctional defect**, may sometimes be seen running obliquely from the sinus to the capsule in upper anterior or lower posterior part of the kidney (Fig. 2.7). It was thought to represent connective tissue at the junction of the development of anterior and posterior components of the kidney. However, subsequent reassessment suggests that this line represents an extension into the parenchyma of hilar/sinus fat in patients with a deep renal sinus, rather than a true plane of fusion between embryological components.[6] It may mimic a scar or rarely a small echogenic tumor.

The **renal sinus thickness** is normally equal to the parenchymal thickness. However, it may vary depending on the fat content of the sinus. An increase in fat content of the renal sinus can occur in obese individuals, in renal sinus lipomatosis, and in cases of parenchymal atrophy. It is decreased in neonates and in cachectic patients.

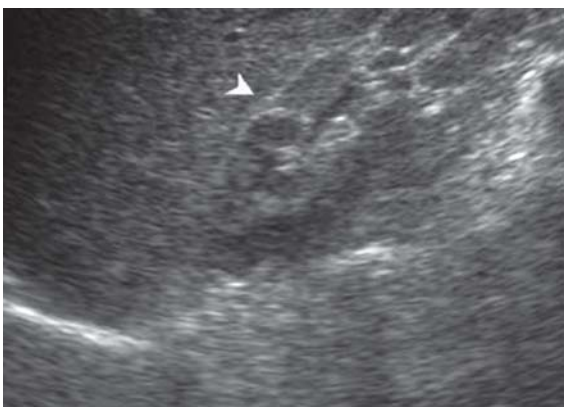

Fig. 2.7: Anterior junction line. Sagittal sonogram demonstrating the echogenic line (arrowhead) that extends from the renal sinus to the perinephric fat

A mild distension of the collecting system can occur due to physiological filling. This can be seen in a fluid loaded subject,a patient on diuretics, diabetics, recovery phase of acute tubular necrosis, single kidney, neonatal kidney and patients with an overdistended bladder.

Doppler Evaluation

The renal arteries arise from the aorta, slightly below the origin of the superior mesenteric artery. The right renal artery (RRA) arises from the anterolateral aspect of the aorta and then passes posterior to the IVC as it courses towards the right renal hilum. The left renal artery (LRA) arises from the lateral or posterolateral aspect of the aorta and follows a posterolateral course to the left renal hilum. Accessory renal arteries may arise from the aorta in as many as 20 percent individuals, either superior or inferior to the main renal artery. The renal arteries typically divide into anterior and posterior divisions that lie anterior and posterior to the renal pelvis, respectively. These divisions give rise to the segmental arteries which branch further within the renal sinus, forming interlobar arteries that penetrate the renal parenchyma. These terminate in arcuate arteries that curve around the corticomedullary junction giving rise to cortical branches.

Each renal vein is formed from tributaries that coalesce in the renal hilum. The left renal vein passes anterior to the aorta and posterior to SMA, to enter the left side of IVC. The right renal vein, which is shorter, extends directly to the IVC from the right renal hilum.

Technique

With the patient supine, the RRA can be identified arising approximately 1 cm below

the origin of the SMA. Occasionally, LRA can be identified at its origin from the postero-lateral or lateral surface of aorta. Both renal veins and their junction with the IVC can usually be demonstrated in this plane. In slim patients it is occasionally possible to follow the renal artery and vein into the hilum of the kidney. The right and left posterior oblique positions can also be used to identify the vessels in the midline. Throughout the course of examination of renal vessels, colour Doppler is frequently switched on to confirm the nature and direction of flow. The optimum pulse repetition frequency is selected to detect moderate flow velocities, although it may need to be modified to detect high velocities if a stenosis with aliasing of colour signals is present. With the system set to detect low or moderate flow velocities, flow can be identified in almost all patients in the vessels at the renal hilum. Angling of the probe medially from the right or left flank will allow assessment of the intrarenal vessels. Though the hilar and interlobar vessels are demonstrated in all patients, the arcuate and striate arteries may be seen only in slimmer patients. Power doppler can show smaller vessels with slow flow, though with loss of directional information (Fig. 2.8). The use of ultrasound contrast material can further enhance visualization of parenchymal vessels.

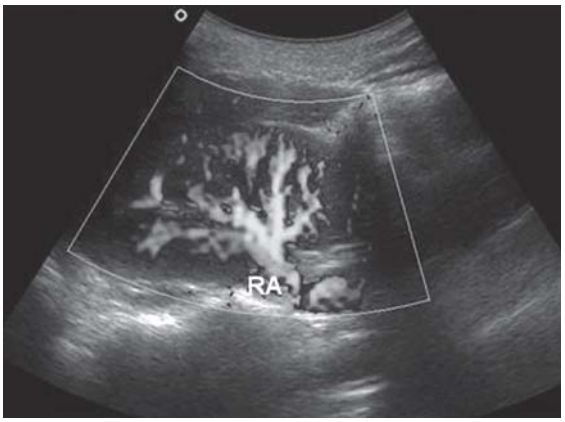

Fig. 2.8 : Power Doppler image of the renal vasculature. RA = Renal Artery

Normal Doppler Pattern

The typical spectral pattern of the renal artery is shown in (Fig. 2.9A). There is a rapid systolic upstroke, which is occasionally followed by a secondary slower rise to peak systole. Subsequently there is a gradual diastolic decay but with persistent forward flow in diastole.[7] Spectral indices are measu-red in the renal artery at proximal,

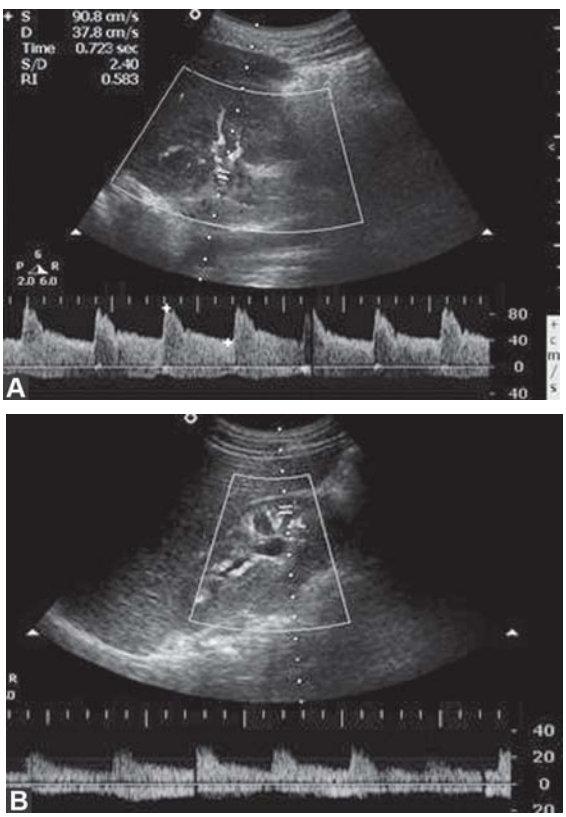

Figs 2.9 A and B: (A) Normal renal spectral pattern. The normal renal artery spectral waveform shows a steep systolic peak, and a smooth downslope to diastole **(B)** Spectral waveform in an intrarenal vessel showing lower velocities

middle and at the hilum. Normal range of values is shown in Table 2.3. Further, indices should also be measured in the intrarenal vessels at the superior, middle and inferior pole of the kidney. The RI and PI values measured in healthy subjects show a significant dependence on age and the area sampled. The values in the main artery are higher than in the more distal smaller arteries and they are lowest in the interlobular arteries (Fig. 2.9B).

The renal vein spectra are often different for right and left veins. The RRV is short and often mirrors the pulsatility of the IVC, while the left, particularly if it is sampled to the left of the SMA, may show only slight variability of flow velocities.

Table 2.3: Normal renal indices[7]

Index	*Range*
Pulsatility index (PI)	0.7-1.4
Resistance index (RI)	0.56-0.7
Peak systolic velocity (PSV)	60-140 cm/sec (< 180)
Renal artery/aorta ratio (RAR)	< 3.5
Acceleration time	0.04-0.05 secs
Acceleration index	2.5-3.8 m/sec^2

Indications

- Renovascular hypertension
- Characterisation of mass lesions.
- Differentiation between obstructive and nonobstructive hydronephrosis
- Evaluation of transplant kidney
- Renal vein thrombosis
- Miscellaneous, e.g. trauma, AVM, etc.

Ureters

The ureter is a long (30-34 cm) mucosal lined tube varying in diameter from 2-8 mm.[8] The normal ureters are usually difficult to visualise as they are thin, collapsed structures. However, dilated ureters can be imaged in their proximal and distal parts. The proximal ureters are best visualised in a coronal oblique view, using the kidney as a window. An attempt can be made to follow the ureter upto the bladder using the same approach. The distal ureters can be seen suprapubically through the full bladder.

URINARY BLADDER AND URETHRA

Technique

Examination of the bladder necessitates a well filled bladder for its detailed evaluation and for the study of entire pelvic cavity. The urinary bladder is scanned transabdominally using 3 to 5 MHz transducers or transperineally using 7 to 10 MHz transducers. Endocavitary high frequency probes (transrectal/transurethral) can give excellent detail of the bladder wall. The full bladder and postmicturition residual volume can be calculated using the formula for a prolate ellipsoid (0.523 × length × width × height).

Common **indications** for sonography of the lower urinary tract are:

- Determination of the existence and rate of urine flow through the vesicoureteric junction in patients with dilated ureters
- Determination of pre- and post-void bladder volume
- Detection of bladder calculi or mass
- Detection and quantification of bladder wall thickening
- Guidance for diagnostic or therapeutic interventional procedures

Normal Sonographic Appearance

The normal distended bladder is an anechoic structure occupying the midline of the true pelvis. It is triangular in the sagittal plane and oval in the transaxial plane. It has thin

walls (less than 3 mm in the distended state and 5-6 mm when nondistended), which are regular and smooth. The ureteric orifices appear as small focal thickenings of the bladder base. Transabdominal evaluation of the ureteral jets is helpful to assess for any proximal obstruction. On gray scale, a stream of low level echoes can be seen entering the bladder from the ureteric orifice. Density differences between the jet and bladder urine allow its sonographic visualization.[9] Doppler evaluation improves the detection of ureteric jets (Fig. 2.10). Depending on the state of hydration, the jet frequency may vary from less than 1 per minute to continuous flow; however, both sides should be symmetrical in a healthy individual. Detection of these jets excludes complete ureteric obstruction and establishes renal function.

Transrectal and transurethral scanning can evaluate the layers of the bladder wall, and evaluate the extent of a mass lesion through tissue planes in and around the urinary bladder. Guidance for biopsy can also be better provided with endocavitary probes.

Urethra

The posterior male urethra can be best evaluated by the endorectal route. Penile urethra can be visualised through the penile shaft using a 7 to 10 MHz linear probe after filling the penile urethra with gel or fluid. The normal penile urethra is seen as an anechoic tubular structure when distended.

The female urethra can be visualized on transabdominal scanning in 35 percent of the patients, and in 100 percent of the patients with a catheter in place. It can also be well identified in all patients by translabial or endovaginal scanning with the probe placed at the introitus or just partially inserted into the vagina. It is seen throughout its length as a short anechoic channel (Fig. 2.11).

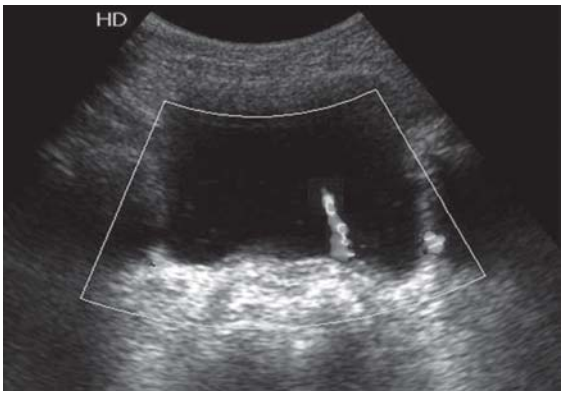

Fig. 2.10: Color doppler evaluation showing a left ureteric jet on a transverse sonogram of the urinary bladder

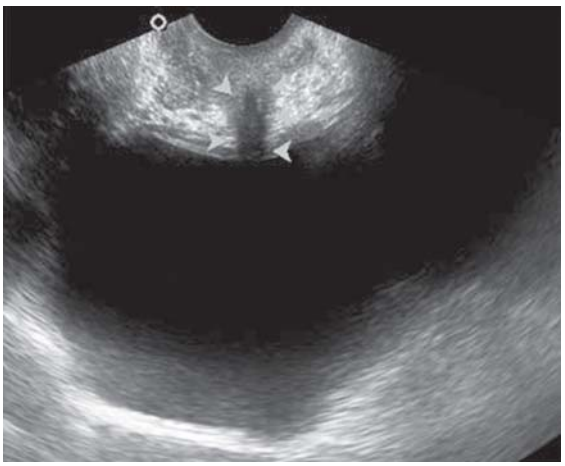

Fig. 2.11: Translabial ultrasound of the female urethra showing the hypoechoic tubular urethra (arrowheads) extending from the bladder

PROSTATE AND SEMINAL VESICLES

Technique

The prostate and seminal vesicles can be examined sonographically via the transabdominal (TAS) and the transurethral (TRUS) routes. Transabdominally, a 3-5 MHz sector probe is used with the full bladder acting as an acoustic window. The prostate is visualized posterior to the bladder in both axial and sagittal planes. A 5 to 7.5 MHz

specially designed probe with a multiplanar facility is used for TRUS. The most commonly used commercially available probes fire from the end and can be used for both transrectal and transvaginal imaging. The bladder should be empty and a cleansing enema may be given. The patient is examined in the left lateral decubitus position with the knees flexed. The probe is lubricated and covered by a rubber balloon or condom. It is then inserted gently into the rectum. Sagittal and axial scans are obtained by rotating the probe through 90°.

In the sagittal plane, the gland is systematically surveyed from right to midline to left; while in the axial plane, cranial to caudal viewing is done from a plane just superior to the prostate (showing the seminal vesicles) to the apex of the prostate caudally.

Prostatic volume can be calculated on TAS and TRUS by using the prolate ellipsoid formula (0.523 × length × width × height). The volume measured can be converted to weight because the specific gravity of prostatic tissue is 1, thus 1 ml of prostate tissue is equal to 1 gm.

The presence of anal or rectal strictures or advanced rectal carcinoma may disallow the transrectal method. In these cases transperineal evaluation approach can be used. However, it is compromised by beam scattering artifacts. A transurethral route has also been used to visualize the prostate. It needs specially designed probes and is an invasive technique.

Common **Indications** for sonograhic evaluation of the prostate are:

- To quantify prostate volume
- Assessment of a palpable nodule
- Evaluation of infertile patients
- Guided prostatic biopsy

Normal Sonographic Appearance

The normal prostate gland is shaped like a pyramid and lies posteroinferior to the bladder (Fig. 2.12). The base of the prostate lies adjacent to the bladder and apex adjacent to the membranous urethra. It measures approximately 4 cm in length (cephalocaudal), 4 cm in transverse diameter, and 3 cm in height (anteroposterior); the normal volume (weight) ranges from 20-25 ml (gm). The border of the prostate appears sharply defined, except at the posterolateral margins where the neurovascular enters the prostate gland.

The prostate glandular structure can be divided into three zones, peripheral, transition, and central (Fig. 2.13). More than 80 percent of prostate cancers arise in the peripheral zone (PZ), which contains 70 percent of the prostate glandular elements. The central zone surrounds the ejaculatory

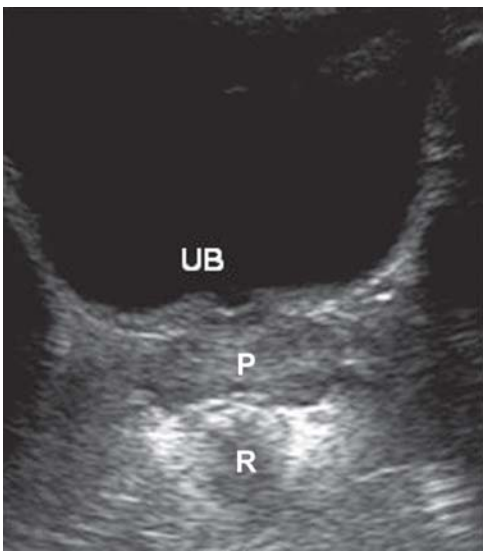

Fig. 2.12: Normal prostate. Transabdominal axial scan shows the prostate (P) between the bladder (UB) and the rectum (R)

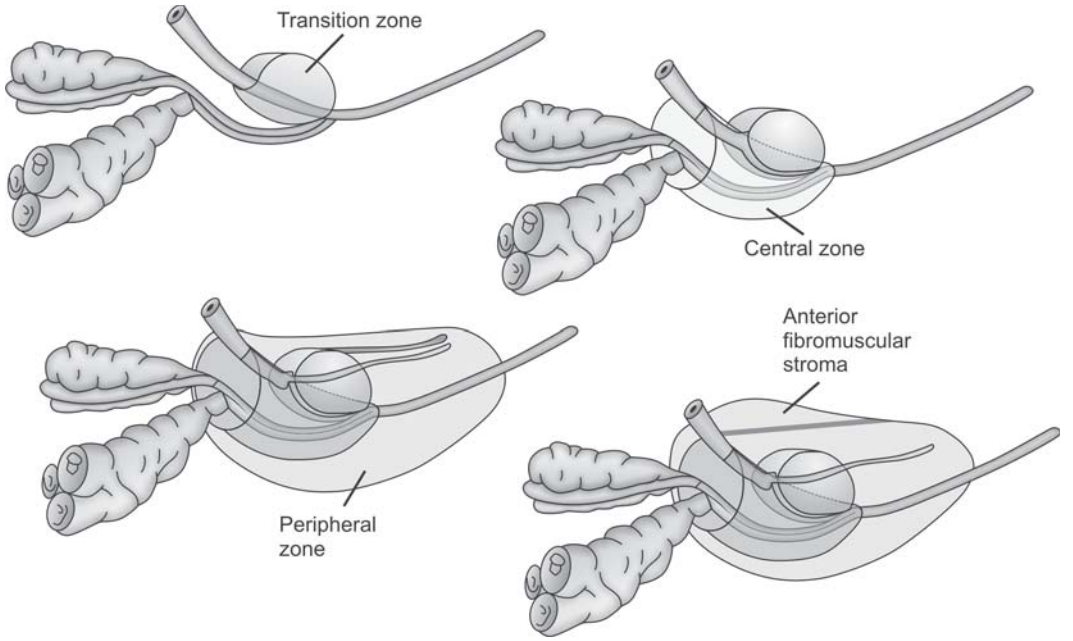

Fig. 2.13: Zonal anatomy of prostate

ducts and is the site of the primary lesion in fewer than 10% of cases. The transition zone (TZ), the site of development of benign prostatic hyperplasia (BPH), contains 10 percent of the glandular elements (although up to 80 percent in cases of BPH) and is the site of origin for less than 20 percent of prostate cancers.

On TRUS, axial scans show the gland as a homogeneous bean shaped structure with well defined margins. It is often difficult to distinguish the PZ from the inner gland in a young male. In older men, with benign prostatic hyperplasia (BPH), the surgical capsule becomes more evident as a thin hypoechoic line between the PZ and inner gland (Figs 2.14A and B). The PZ is more uniform in texture and slightly more echogenic. This echogenicity is taken as the standard and echogenicity in other areas of the gland is compared to that of the PZ.[10] The posterior urethra and its surrounding smooth muscle and glandular area appear relatively hypoechoic and can be quite prominent measuring upto 2 cm in diameter. The urethra and ejaculatory ducts may be identified. At the level of verumontanum, the ejaculatory ducts and urethra merge. Near the apex of the gland most of the tissue is the peripheral zone.

In the sagittal plane, the most parasagittal images of the gland show only PZ tissue with uniform echotexture in young men. With BPH, the transition zone may extend laterally, compressing the PZ posteriorly. At the base of the gland, the seminal vesicles immediately adjoin the central and peripheral zones. In the midsagittal section the collapsed urethra is seen as an echogenic line surrounded by the hypoechoic smooth muscle forming the internal urethral sphincter. The ejaculatory ducts can be seen coursing

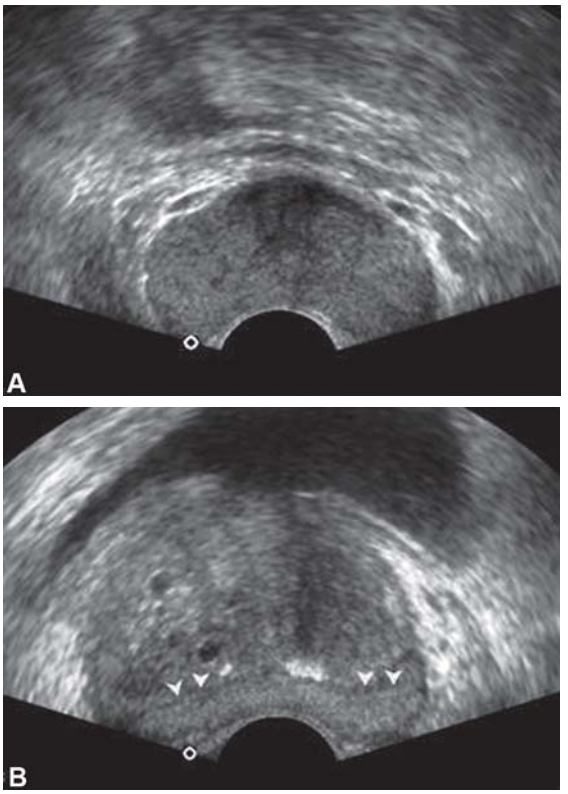

Figs 2.14A and B: Transrectal axial sonograms of prostate at midgland level. **(A)** In a young male Note the normal hypoechoic muscular internal sphincter (arrow). **(B)** In an older male with BPH. The more echogenic PZ is seen posteriorly compressed by the anterior enlarged TZ. The surgical capsule(arrowheads) is well seen as a thin hypoechoic line between PZ and TZ

through the CZ from the seminal vesicles and joining the urethra at the verumontanum.

With color **Doppler**, particularly using the power mode, the prostate is seen as a very vascular structure. The capsular and urethral arteries are easily seen, and branches to the inner gland and peripheral zone are usually very prominent.

The **seminal vesicles** are seen as paired, relatively hypoechoic, symmetric structures cephalad to the base of the prostate (Fig. 2.15). They are imaged in the long axis on the axial

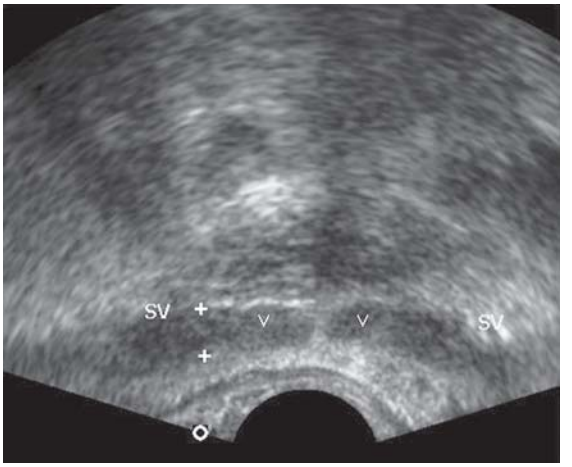

Fig. 2.15: TRUS: Axial image above base of prostate showing the seminal vesicles (SV) and vas (V)

images and in cross-section on sagittal images. They are up to 1 cm in width, but occasionally they may be very large in normal men.[11] Cysts representing the remnants of the Wolffian and Müllerian ducts are not uncommon in this region.

Normal Variants

Benign ductal ectasia is seen in older men due to atrophy and dilatation of peripheral prostatic ducts. They are seen either singly or grouped, radially oriented, 1-2 mm in diameter, tubular structures in the peripheral zone, starting at the capsule and radiating towards the urethra.[10] Their significance lies in that they can be mistaken for a cancerous lesion.

Prostatic calcification and corpora amylacea are frequently seen in the older age group of patients as bright echogenic foci or areas in the prostate. Corpora amylacea are proteinaceous debris in dilated prostatic ducts and are most commonly seen in the periurethral glands along the surgical capsule (Fig. 2.16), but can occur anywhere in the

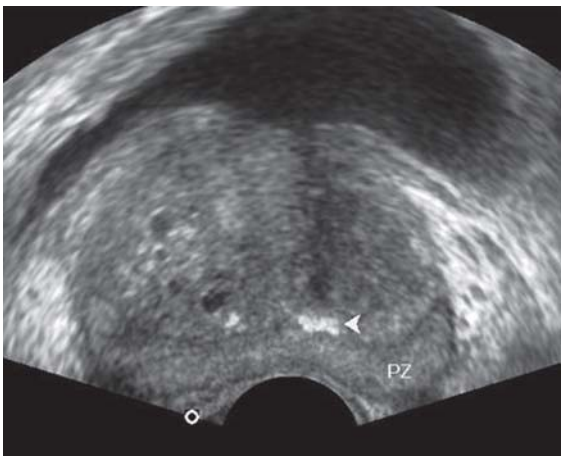

Fig. 2.16: Corpora amylacea seen as echogenic foci (arrowhead) just anterior to the surgical capsule

prostatic gland. They can be very dense, thus causing marked attenuation of the sound beam. However, they are usually not palpable.

SCROTUM

Technique

A high frequency (7.5-15 MHz) linear array transducer is used to scan the scrotum. The examination is done with the patient in supine position, thighs are adducted, and a towel or sheet is placed underneath the scrotum and held taut. This supports the scrotum and eases the examination. Alternatively, the scrotal sac maybe supported by the examiner's hand. Palpation prior to, and during scanning is useful specially if a small mass is suspected. The scrotum is scanned by direct contact after application of a suitable gel. Both testes are visualized in the transverse and sagittal planes. If possible, a transverse scan showing both testes for comparison should be obtained using a dual image or extended field of view technique. Scanning from the opposite side helps in identification of small lesions.

Normal Appearances

The testis is an ovoid organ measuring 3-5 cm in length, 2-4 cm in width and 3 cm in anteroposterior diameter. Each testis weighs 12.5-19 gm. Testicular size and weight decrease with age.[12,13] It is surrounded by a dense fibrous capsule, the tunica albuginea. It comprises of 200-300 lobules separated by thin septae (Fig. 2.17). Seminiferous tubules from each lobule converge into large collecting tubules and form the rete testis adjacent to the mediastinum (which is a longitudinal condensation of fibrous tissue on one side of the testis). Efferent ductules from the rete testis exit the testis over its upper half to form the epididymis. The epididymis lies closely applied to the testis in the long axis with two expansions – the head at the upper pole and the tail at the lower pole. The vas, a tubular structure, is a continuation of the epididymal tail and runs upwards from the lower pole parallel to the epididymis to form the spermatic cord.

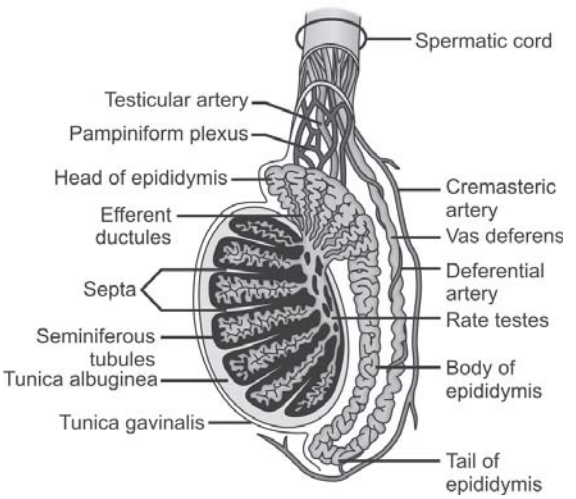

Fig. 2.17: Normal intrascrotal anatomy. *(From Sudakoff GS, Quiroz F, Kaarcaaltincaba M, Foley WD. Scrotal ultrsonography with emphasis on the extratesticular space: Anatomy, embryology and pathology . Ultrasound Quarterly 18:255-273, 2002)*

The cord, testis and epididymis are enveloped by a thin membrane, the tunica vaginalis, which is reflected back onto the scrotal wall posteriorly.

Sonographically, the **testis** is seen as an organ of homogeneous granular echotexture with medium level echoes surrounded by an echogenic capsule (Fig. 2.18A). The mediastinum is seen as a thin echogenic band on the same side as the epididymis with fine hypoechoic strands of septa radiating from it into the testicular parenchyma. The appearance of the medistinum testis varies according to the amount of fibrous and fatty tissue present. It is best visualsed between the ages of 15 – 60 years.[13] The **epididymis** is of varying reflectivity with the head being isoechoic or slightly hyperechoic to the adjacent testis, measuring approximately 10-12 mm in diameter and lying lateral to the superior pole of the testis, while the main body is hypoechoic measuring less than 4 mm in diameter and lies along the posterolateral aspect of testis.[14] The tail, appendix epididymis and appendix testis are most often identified sonographically as separate structures when a hydrocele is present. The **appendix testis**, a remnant of the paramesonephric duct is a small ovoid structure located most commonly on the superior pole of the testis (Fig. 2.18B) or in the groove between the testis and the head of the epididymis and is seen in almost 80% of testes.[15]

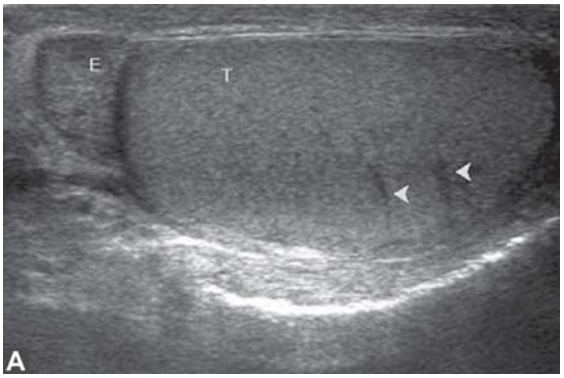

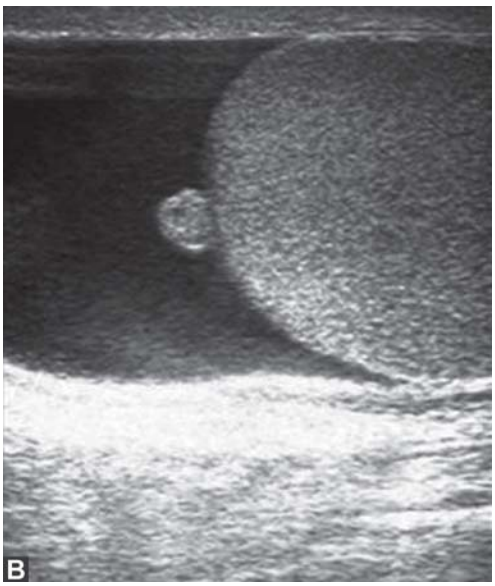

Figs 2.18 A and B: (A) Normal homogeneous echotexture of the testis (T) with septula tesis (arrowheads) seen as linear hypoechoic structures within the testis. E = head of epididymis. **(B)** Appendix testis well seen in a patient with hydrocele

The **vas** is more difficult to identify, but may be seen as a fine hypo-echoic tubular structure with a hyperechoic lumen running along the epididymis. The **spermatic cord** consists of the vas deferens; the cremasteric, deferential and testicular arteries; a pampiniform plexus of veins; the lymphatics and the nerves of the testis. Sonographically, the normal spermatic cord is difficult to distinguish from the adjacent soft tissues of the inguinal canal, but its position can be identified by the pulsations of the testicular artery within it.

The **scrotal sac** is composed of several layers that are derived from the skin, abdominal wall muscles and the peritoneum (tunica vaginalis). The **tunica vaginalis** is derived from the peritoneum and is a closed

pouch folded around the testis. The inner or visceral layer of the tunica vaginalis covers the testis, epididymis, and the lower portion of the spermatic cord, while the outer or parietal layer lines the walls of the scrotal pouch and is attached to fascial coverings of the testis. A small amount of fluid is normally present between these two layers, specially in the polar regions and between the epididymis and testis. Sonographically, the layers of the normal scrotal wall cannot be identified separately and are seen as a 5-7 mm thick hyperechoic stripe.

Indications

- Evaluation of acute scrotal pain
- Evaluation of scrotal enlargement
- Evaluation of infertility
- Localization of undescended testis
- Evaluation of scrotal trauma
- Detection of occult tumor in patients with known metastases.

Doppler Evaluation

The main arterial supply to the testis is from the testicular artery which arises from the mid abdominal aorta and passes into the scrotum via the inguinal canal along with cremasteric artery and deferential artery. The testicular artery forms a network of capsular branches over the testis which pass through the tunica albuginea and form another network in the testicular substance. The pampiniform plexus of draining veins is formed around the upper half of the testis. This drains into the testicular vein. The right testicular vein drains into the IVC, while the left drains into the left renal vein.

On colour Doppler, the normal testis shows little flow in the testicular tissue, but larger centripetal and centrifugal vessels are seen in the lobular septa and around the capsule. A prominent transmediastinal artery may sometimes be seen traversing the testis. The velocity waveforms of the normal capsular and intratesticular arteries show high levels of antegrade diastolic flow throughout the cardiac cycle, reflecting the low vascular resistance of the testis (Fig. 2.19). In a study of normal subjects, peak systolic flow velocities in intratesticular arteries, including capsular arteries, ranged from 4 to 23.4 cm/sec (mean 10.8), end-diastolic velocities ranged from 1.6 to 9.2 cm/sec (mean 3.8) and RI from 0.46 to 0.78 (mean 0.64).[16] Supratesticular arterial waveforms vary in appearance. Two main types of waveform exist: A low resistance waveform (testicular artery and its branches) and a high resistance waveform with a sharp, narrow systolic peak and little or no diastolic flow which is believed to reflect the high vascular resistance of the extratesticular tissues (branches of cremasteric and deferential arteries). The pampiniform venous plexus is seen as a network of venous channels (less than 2 mm in width) around the upper half of the testis, generally on the same side as the epididymis and vas.

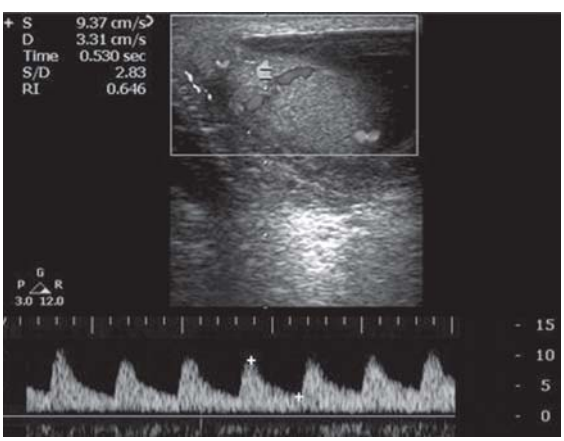

Fig. 2.19: Spectral waveform of the testicular artery showing typical low impedance flow

Indications

- Testicular inflammation—acute and chronic
- Testicular torsion
- Varicocele
- Testicular tumors

PENIS

Technique and Normal Appearance

Sonographic examination of the penis is performed with the patient in the supine position, with the penis lying on the anterior abdominal or supported with towels between the thighs, using a high frequency (7.5-15 MHz) linear array transducer. Examination is performed in transverse and longitudinal planes, starting at the level of the glans and moving towards the base of the penis. A transperineal approach maybe used to assess the base of the penis.

The penis contains three longitudinal columns of erectile tissue: the paired dorsal corpora cavernosa and the ventral corpus spongiosum. The urethra passes through the corpus spongiosum. The deep cavernosal arteries run centrally through the length of each corpus cavernosum with dorsal arteries lying superficially. The dorsal vein of the penis lies between the two dorsal arteries.

The corpora cavernosa are seen as two circular structures adjacent to each other, of medium echogenicity with the deep arteries lying medially within them on the transverse section (Fig. 2.20). The normal cavernosal artery diameter ranges from 0.3-1 mm (mean 0.3-0.5 mm),[17] with a peak systolic velocity of 10-15 cm/sec in the flaccid state.[18] The corpus spongiosum is often compressed and is difficult to visualize optimally from the ventral aspect. It is more hypoechoic with the urethra seen as an anechoic central area within it. The tunica albuginea is seen as a hyperechoic capsule surrounding the periphery of the corporal structures.

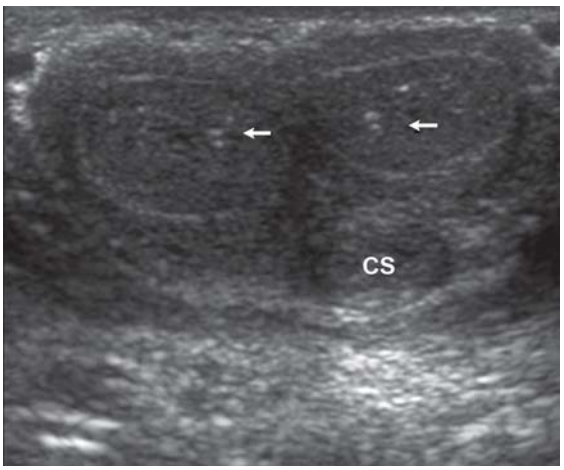

Fig. 2.20: Normal penile sonogram. Transverse section through the mid shaft shows the paired dorsal corpora cavernosa and the ventral corpus spongiosum (CS). The deep arteries are seen as echogenic foci in the corpora cavernosa (arrows)

Indications

- Penile masses
- Trauma
- Urethral strictures
- Peyronie's disease
- Impotence

UTERUS AND ADNEXA

Technique

Sonographic evaluation of the uterus and the adnexa can be done by the transbdominal (TAS) and transvaginal (TVS) routes. They are complementary techniques and both are used extensively in evaluation of the female pelvis. The **transabdominal** scan is performed with 3.5 to 5 MHz sector transducer, with a full bladder as an essential prerequisite. The urinary bladder is considered adequately full when it covers the entire fundus of the uterus. Overdistension is to be

avoided as it may distort the anatomy and may push the pelvic organs beyond the focal zone of the transducer.

Imaging of the uterus is performed in both sagittal and axial planes. The adnexa are imaged by scanning obliquely from the contralateral side, although in many cases good visualisation may be achieved by scanning directly over the adnexa.

The limitations of this technique are as follows.

1. Patients unable to fill the bladder
2. Patients with retroverted uterus in whom fundus may be beyond the focal zone of the transducer
3. Limited resolution.

Transvaginal scanning affords improved resolution of the pelvic organs. Specially designed probes of 5 to 8 MHz frequency are used for this procedure. The bladder should be empty. However, a minimal distension may be required if the uterus is severely anteflexed.

The patient is positioned supine with the knees flexed and hips slightly elevated. The probe is prepared as for TRUS and inserted gently into the vagina till the uterus is identified. The uterus is imaged in its longitudinal axis, first sweeping from left to right. Short axis images are then obtained. The relative position of the uterus can be inferred by the orientation of the probe that best images the uterus, e.g. if the uterus is best imaged with a posterior inclination, the uterus is retroflexed and vice versa. For imaging the cervix, the transducer should be withdrawn to the mid vaginal level.

The ovaries are imaged by tilting the transducer to either side of the midline in the transverse section. The internal iliac vessels can be identified as anechoic tubular structures along the pelvic side walls. The ovaries usually lie anterior and medial to these vessels.

Limitations of this technique are:

1. Limited field of view
2. Vaginal atrophy may disallow examination.

Normal Appearances

The uterus lies between the bladder anteriorly and rectosigmoid posteriorly (Fig. 2.21). Its size and shape vary throughout life related to age, hormonal status and parity. The infantile or prepubertal uterus has an inverse pear shaped appearance with a disproportionately larger cervix occupying upto one-half to two thirds the size of the uterus (Fig. 2.22). In the immediate neonatal period the uterus is slightly larger and shows an echogenic endometrium, because of residual maternal hormonal stimulation. A small amount of endometrial fluid may also be seen in 25% of neonatal uteri.[19] There is little growth of the prepubertal uterus from infancy till about 8 years of age when the uterus gradually increases in size till puberty when it attains a pear shaped appearance with the body of the uterus becoming approximately double the cervix. The normal postpubertal or adult uterus varies considerably in size. The maximal dimensions of the nulliparous uterus are approximately 8 cm in length by 5 cm in width and 4 cm in AP diameter. Parity increases the normal dimensions by more than 1 cm in each dimension[20] (Table 2.4). After menopause the uterus atrophies with the most rapid decrease in size occurring in the first ten years following the cessation of menstruation.

Table 2.4: Uterine size

	Length (cm)	*Width (cm)*	*AP diameter (cm)*
Neonates	2.3 - 4.6		0.8-2.1
2-11 years	2-4	-	0.5-1
Adult	8 -9	5 - 6	4 -5
Postmenopausal	3.5-6.5		1.2-1.8

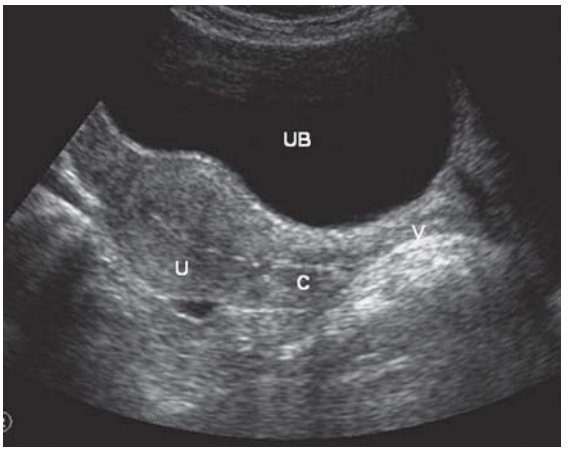

Fig. 2.21: Normal uterus (U), cervix(C), and vagina (V) on a transabdominal sagittal scan. Central linear echo representing apposed surfaces of vaginal mucosa (V)

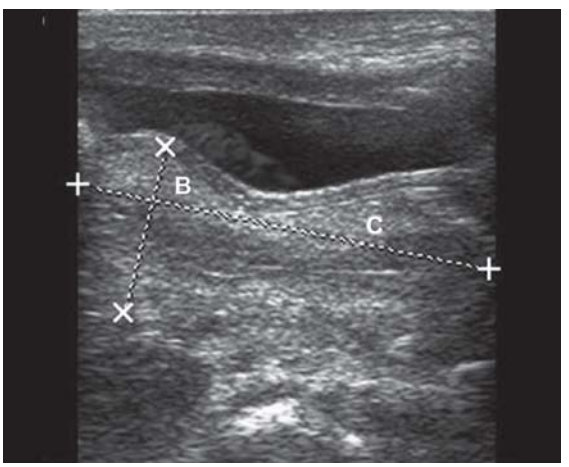

Fig. 2.22: Normal neonatal uterus — sagittal scan. Inverse pear shape with cervix (C) having greater width than body (B) of uterus

The uterus usually assumes a position that is both anteverted and anteflexed (Fig. 2.23). The degree of bladder filling alters the lie of the uterus; on transvaginal scanning with an empty bladder the uterus is angled forwards from the lie of the vagina, whereas a full bladder straightens the uterus. In case of retroverted or retroflexed uterus, the fundus lies posteriorly. It is often not possible to distinguish between retroversion and retroflexion on sonography so the general term retroposition is used. On transabdominal scanning the deeper portions of the fundus may be difficult to delineate and may even appear abnormal because of shadowing from the intervening body and cervix. Transvaginal scanning gives an excellent visualization of the retropositioned uterus as the probe can be directed posteriorly.[21]

The uterus consists of an an external serosa (perimetrium), a middle muscle layer (myometrium) and the internal mucosa (endometrium). The perimetrium is not visible on ultrasound examination, although subserosal veins may be seen as a normal variant. On sonography the the myometrium has three layers. The inner myometrium (or the subendometrial halo) appears as a thin hypoechoic area surrounding the echogenic endometrium. The intermediate layer is the thickest and has a uniformly homogeneous low to moderate echogenicity. The thin outer layer is less echogenic and separated from the intermediate layer by the arcuate vessels, which can be visualized on ultrasound as small anechoic foci in the periphery of the uterus. Calification may be seen in the arteries in postmenopausal women. Sometimes small highly echogenic foci may be seen in the inner layer of myometrium. These small, single or multiple, nonshadowing foci are thought to represent dystrophic calcification related to previous instrumentation like dilatation and curettage or endocervical biopsy.[22]

The normal endometrial cavity is seen as a central echogenic line as a result of specular reflection from the interface between apposing surfaces of the endometrium. It should be straight or smoothly curved. The sonographic appearance of the

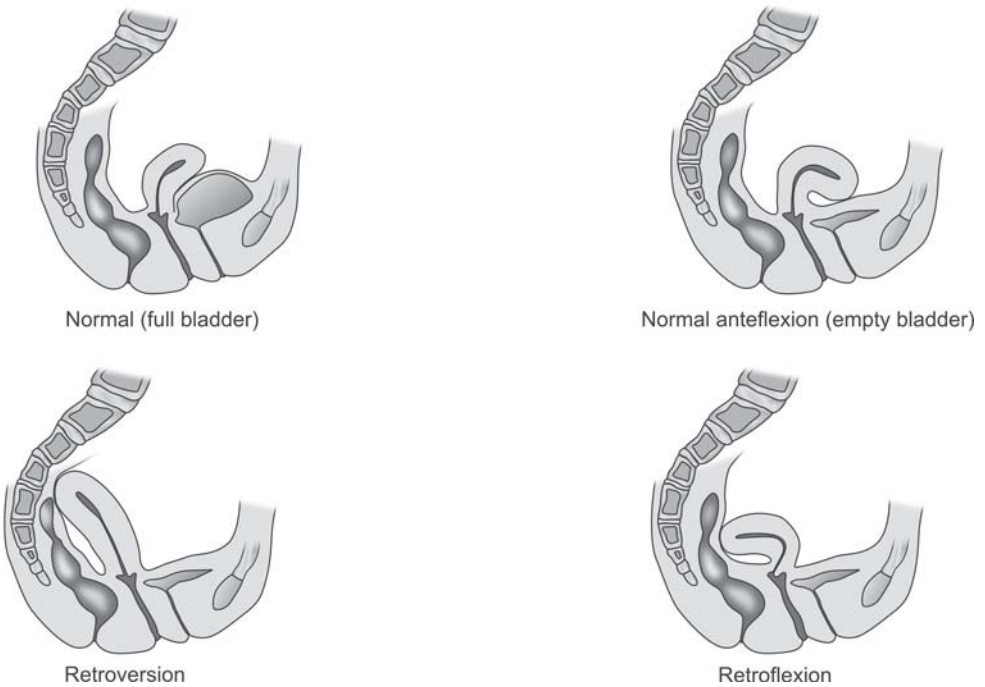

Fig. 2.23: Alterations in uterine position. The normal position of uterus in most women is anteverted with a mild degree of anteflextion. In retroversion, the long axis of the uterus and cervix points more posteriorly than the long axis of the vagina. In retrofexion, the body of the uterus is angled posteriorly relative to the cervix

endometrium varies during the menstrual cycle and has been correlated with histology.[23] The appearance during the various phases of the menstrual cycle has been given in Table 2.5 (Figs 2.24A to C). The endometrium is best measured on the midline sagittal scan of the uterus. The measurement is taken from the proximal to the distal interfaces between the subendometrial halo that surrounds the endometrium and the more echogenic endometrium. This is the double layer thickness.

In postmenopausal women, the normal sonographic endometrial appearance varies according to presence or absence of hormonal replacement therapy (HRT). Additionally, the type of HRT (i.e. continuous, combined or sequential) is important.[24] In asymptomatic postmenopausal women not receiving HRT, several reports suggest endometrial thickness should not exceed 4 mm, whereas others use 8 mm as the upper normal value. For women receiving HRT, the sonographic appearance of the endometrium depends on whether the patient takes continuous estrogen or a combination of estrogen and progesterone (either continuously or sequentially). Sequential HRT results in monthly withdrawal bleeding and cyclic endometrial thickening. At mid cycle, maximal endometrial thickness frequently exceeds 8 mm, and in some cases may approach 15 mm. In these women, it is important to do a

Table 2.5: Appearance of endometrium in a normal menstrual cycle

Date of cycle	*Phase*	*Thickness(mm)*	*Appearance*
1-4	Menstrual phase	1-4	Small amounts of fluid may be seen endovaginally. Thin interrupted central echo.
5-14	Proliferative phase	4-8	Central hyperechoic line with surrounding thin hypoechoic band
	Periovulatory	6-10	Trilayered appearance ; the hypoechoic band becomes more prominent with thin echogenic lines on either side
15-28	Secretory phase	8-16	Thick Echogenic with through transmission.

follow-up scan. In women taking either continuous estrogen or continuous estrogen and progesterone the maximal endometrial thickness is 8 mm, and cyclic endometrial changes should not occur. Postmenopausal women may often have a trace of fluid (approximately 1 mm in thickness) in the endometrial cavity due to cervical stenosis.[24]

Sonohysterography can be done to visualize the intracavitary anatomy and any pathology within the cavity. The endometrial cavity is distended with fluid introduced via a self-retaining catheter, prior to transvaginal sonography. The fluid within the cavity gives an excellent visualization of any pathology within the cavity and also differentiates bet-ween intracavitary versus extracavitary pathology (Figs 2.25A and B).

CERVIX AND VAGINA

The **cervix** is better visualized by transvaginal sonography as a tubular structure of homogeneous echogenicity (Fig. 2.26). The mucus within the endocervical canal usually appears as an echogenic interface which may become hypoechoic during the periovulatory period as the fluid content increases. Retention (nabothian) cysts of the cervix are commonly seen during routine sonography. They may vary in size from a few mm to four cm. They may be single or multiple and usually diagnosed incidentally, although they may be associated with chronic cervicitis.

The **vagina** runs anteriorly and caudally from the cervix between the bladder and rectum. It is best seen on the mid sagittal transabdominal scans as a collapsed hypoechoic tubular structure with a central hyperechoic line representing the apposed surfaces of the vaginal mucosa (Fig. 2.21). In patients who have had a hysterectomy , the vaginal cuff should not be mistaken for a mass. The normal upper limit of the AP diameter of the vaginal cuff is 2.1 cm.[25]

ADNEXA

The adnexae consist of the ovaries, the fallopian tubes, ligaments and vessels. The **ovaries** most commonly lie lateral to the uterus (usually within a few centimeters) at about the level of the cornua. Variations are common and insignificant. A relatively constant relationship of the ovaries is their location anterior to internal iliac vessels, which serves as a useful landmark for the ovaries particularly during TVS.

The ovaries are typically seen as oblong structures with a relatively homogeneous echotexture. Well-defined small anechoic

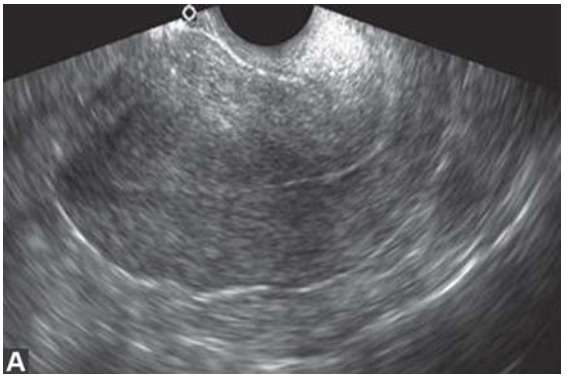

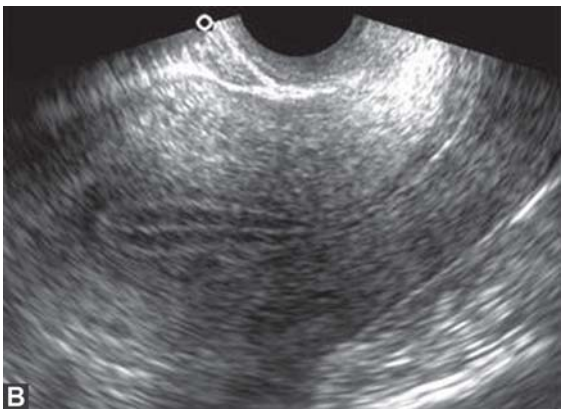

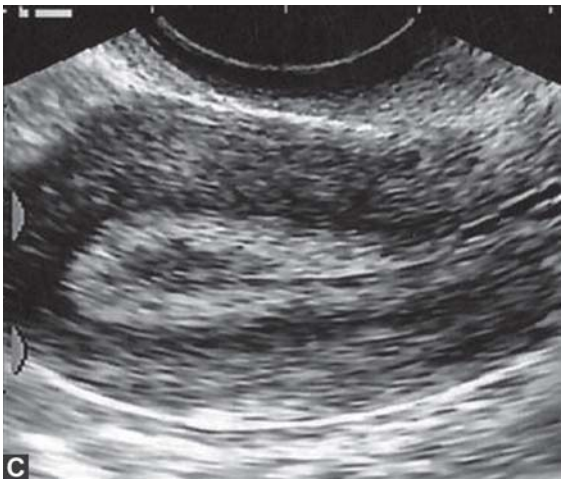

Figs 2.24A to C: Endometrium – spectrum of appearances. **(A)** Normal thin early proliferative endometrium. **(B)** Normal late proliferative endometrium with triple layer appearance. **(C)** Normal thick hyperechoic secretory phase endometrium

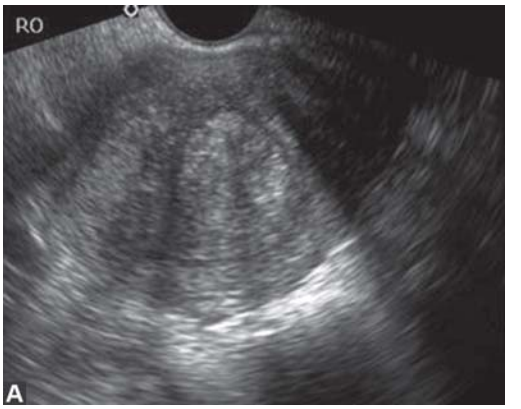

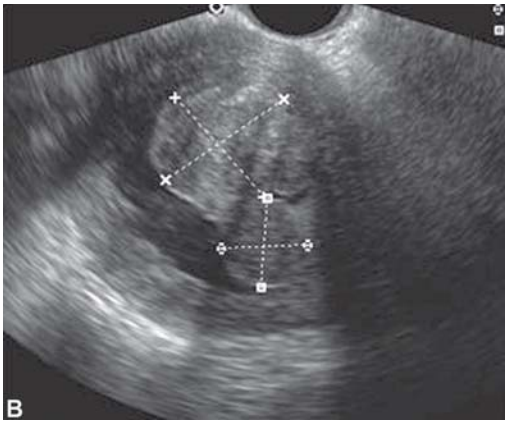

Figs 2.25A and B: Sonohysterography. **(A)** transvaginal scan shows hyperechoic masses within the uterus;it is not possible to determine their realtion with the endometrium. **(B)** On intillation of intracavitary saline, 2 well defined masses (within calipers) are seen projecting into the endometrial cavity – submucous fibroids

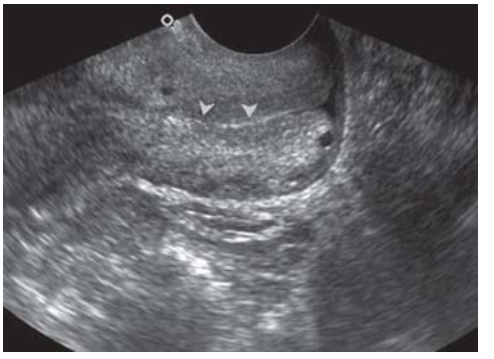

Fig. 2.26: The normal cervix as seen on sagittal transvaginal scan, with a central echogenic line (arrowheads) representing the cervical canal. Two small Nabothian cysts are seen

follicles may be seen peripherally in the cortex. By day 8 or 9 of the menstrual cycle, one follicle becomes dominant and reaches up to 2 to 2.5 cm in size, and the others become atretic (Figs 2.27A and B). Non-dominant follicles are usually less than 14 mm in diameter. Following ovulation, a corpus luteum develops which can commonly be seen as a hypoechoic or isoechoic structure preipherally within the ovary (Fig. 2.27C), but may show a very varied sonographic appearance. Sometimes, it may form a cyst and become very large (Fig. 2.28). Its irregular walls and low level internal echoes with low impedance Doppler signals may be a cause for concern. However, unless a pregnancy occurs, the corpus luteum involutes towards the end of the cycle, so that a repeat scan 2-6 weeks later will usually resolve the dilemma.

Because of the variability in shape, **ovarian volume** is considered the best method for evaluating the ovarian size (0.523 × length × width × AP diameter). For this measurement any cyst larger than 1 cm in diameter is excluded. In the first 2 years of life the ovarian volume ranges between 1-3 cc (largest in the first 3 months). It remains relatively stable upto 5 years of age and then gradually increases upto menarche when the mean volume is 4.2 + 2.3 cc with an upper limit of 8 cc.[26] The normal ovarian volume ranges from 6 to 15 cc in an average adult female.[27] The two ovaries should be approximately equal in volume, neither should be more than twice the volume of the other.

Small echogenic, nonshadowing foci may sometimes be seen in a normal ovary, which are thought to be due to specular reflection from tiny unresolved cysts below the spatial resolution of the ultrasound machine.[28]

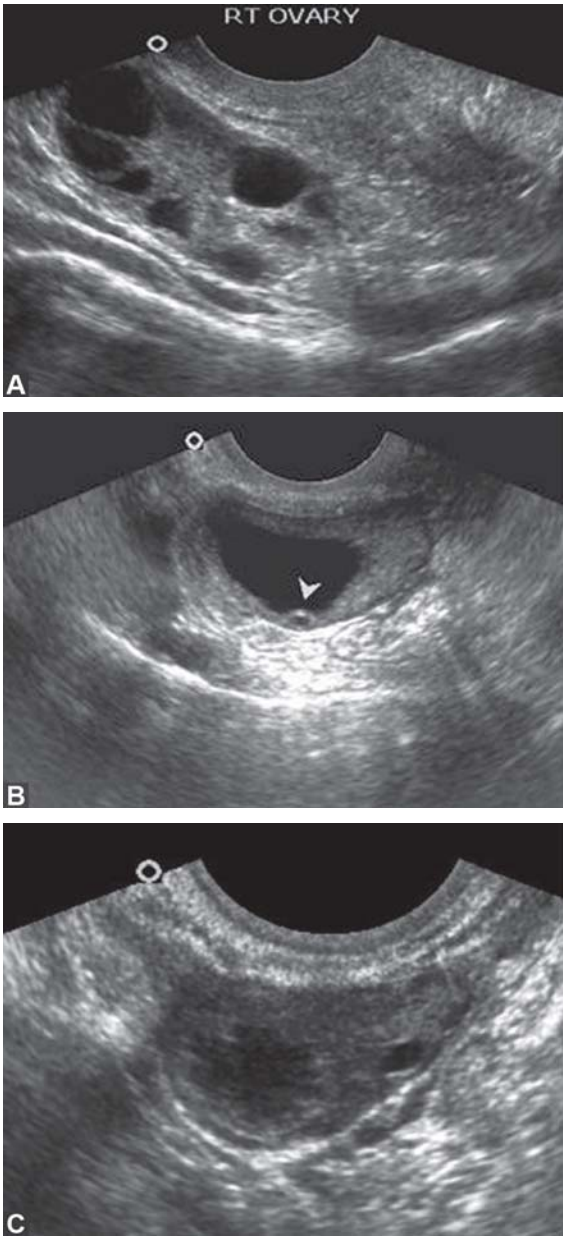

Figs 2.27A to C: Normal ovary—transvaginal scans. **(A)** Ovary in proliferative phase showing multiple small follicles. **(B)** Dominant follicle with cumulus oophrus (arrowhead) seen just prior to ovulation. **(C)** Corpus luteum seen as a small hypoechoic mass with crenated margins within the ovary

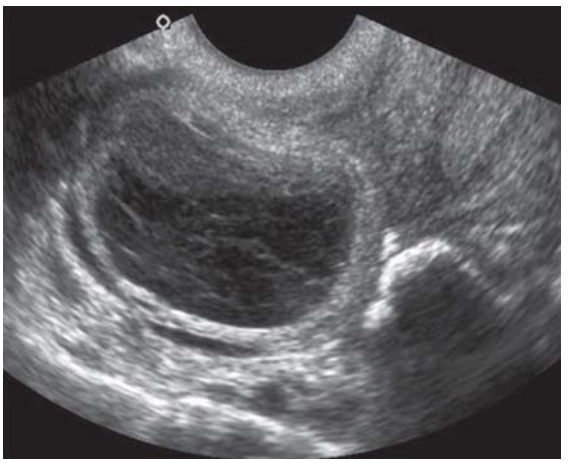

Fig. 2.28: Hemorrhagic corpus luteum cyst. Characteristic reticular pattern of internal echoes seen within the cyst

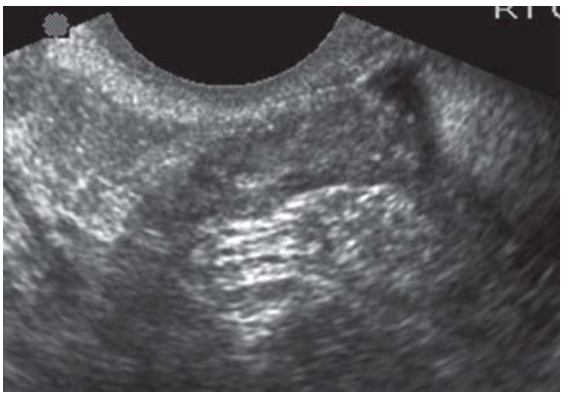

Fig. 2.29: Postmenopausal ovary: Small in size with no follicles, often difficult to identify

The **postmenopausal ovaries** may be difficult to recognise sonographically as they are relatively small and do not contain follicles (Fig. 2.29). Wolf et al[29] in a study of 290 postmenopausal ovaries known to be present, using both transabdominal and transvaginal sonography, visualized only 40 percent of ovaries transvaginally and 58 percent transabdominally. Using both techniques resulted in 68 percent visualization. Mean postmenopausal ovarian volume ranges between 1.2-5.8 cc, with the volume decreasing in size with increasing age. An ovarian volume of more than 8 cc is definitely abnormal. Small anechoic cysts (less than 3 cm) may be seen in upto 15 percent of post menopausal ovaries and are not related to age, length of time since menopause or hormone use. These cysts can disappear or change in size overtime.[29]

The non-distended fallopian tubes are difficult to see on ultrasound. Delineation of the tubes is possible if intraperitoneal fluid is present in the cul-de-sac or if they are distended by saline/contrast agent. Sonosalpingography can be done to establish the patency of the fallopian tubes by instilling fluid or contrast agent into the uterus and then visualizing sonographically its passage through the tubes, or presence of fluid in the pouch of Douglas. The use of color Doppler in conjunction with ultrasound contrast improves the sensitivity of the technique in the detection of tubal spill.

The posterior cul-de-sac (pouch of Douglas) is the most posterior and inferior reflection of the peritoneal cavity located between the rectum and vagina. Small quantities of fluid in the cul-de-sac is a normal finding in asymptomatic women, and can be seen in all phases of the menstrual cycle.

Indications for Evaluation of Uterus and Adnexa

- Menstrual disorders
- Post menopausal bleeding
- Pelvic inflammatory disease
- Pelvic mass
- Infertility
- Guided procedures

Doppler Evaluation

The blood supply to the uterus is via the uterine artery, a branch of the internal iliac artery. The uterine artery enters the uterus at the cervicocorporal junction and ascends along the lateral aspect of the uterine body to the cornua. At the cornua an adnexal branch originates that supplies the ipsilateral ovary and anastomoses with the ipsilateral ovarian artery. The uterine arteries anastomose through the anterior and posterior arcuate arteries which are located in the outer one-third of the myometrium. The endometrium is supplied by branches of the uterine arteries. Radial arteries arise from the arcuate vessels and extend through the myometrium upto the endometrium where they from (i) the basal arteries which supply the basalis layer of endometrium and (ii) the spiral arteries which supply the functional layer of endometrium. The spiral arteries are responsive to hormonal changes similar to the endometrium.

The ovarian arteries arise from the abdominal aorta and enter the pelvis through the infundibulopelvic ligament. They reach the ovaries through the hilus via the mesovarium. After supplying the ovary, terminal branches anastomose with branches of the uterine artery.

The uterine and ovarian vessels can be identified on color Doppler. The course of the uterine artery is ideally suited for transvaginal assessment with ideal geometry for Doppler signal recording. It is also possible to record Doppler signals transabdominally with an empty bladder when the uterus is anteverted. The ovarian arteries are more difficult to assess as they run a transverse course through the pelvis. The branches of the uterine artery extending towards the ovary can be identified in the broad ligament and the superior aspect of the ovary respectively. Because of their tortuosity, only short segments of the arteries are usually identified in any scan plane. The lowest possible filter, with a high color gain should be used to detect slow flow.

During the reproductive years of a normal female both color and duplex Doppler patterns change concomitant with grey scale changes.[30]

The general pattern of uterine blood flow throughout the menstrual cycle is that perfusion increases in response to rising plasma oestrogen and progesterone and decreases with periovulatory fall in estrogen. The typical spectral waveform shows a high resistance pattern characterized by high flow velocity with an early diastolic notch (Fig. 2.30). The normal values are given in Table 2.6. Endometrial vascularity can also be evaluated by Doppler sonography. The extent of vascular penetration into the

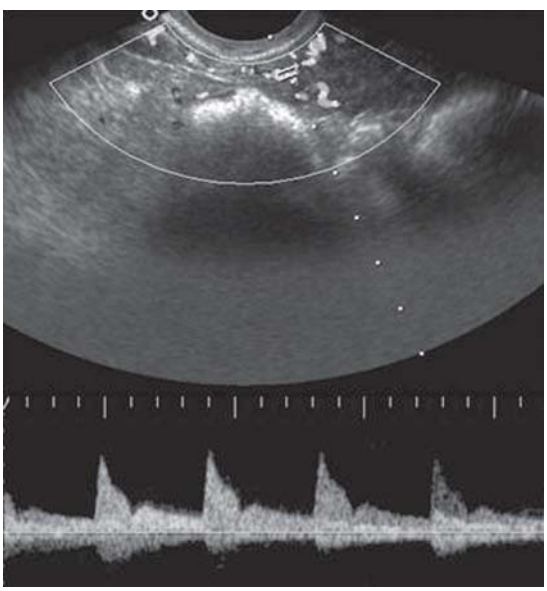

Fig. 2.30: Normal spectral waveform of the uterine artery characterised by a high flow velocity, a post-systolic notch and low diastolic flow

endometrium correlates well with successful conception and it is possible to see variations in the depth of vascular penetration before, during and after the mid-cycle.

The ovarian arterial supply also exhibits different flow characteristics during different phases of a normal menstrual cycle. In general, the index value is high during the early follicular phase, progressively decreases till the early luteal phase and then rises again in the late luteal phase[31] (Table 2.6). Differences in flow characteristics may also be seen between the dominant and non-dominant ovaries. In the ovary containing the dominant follicle, continuous diastolic flow may be seen by the early luteal phase. In contrast, both diastolic flow and cyclical changes may be absent in the non dominant ovary.

Doppler ultrasound can demonstrate the neovascularity within the wall of the corpus luteum. Demonstrable colour flow surrounding the developing dominant follicle becomes more apparent as the midcycle approaches and continues around the corpus luteum until the late luteal phase. In the event of pregnancy both the low resistance flow and the color flow to the corpus luteum may remain until the eleventh week of amenorrhea.[30]

Table 2.6: Variation in Doppler indices in the uterine and ovarian arteries

	*RI OVA**	*PI OVA**	*PI UTA*
Early proliferative	0.65-0.7	1.8-2.2	1.67± 0.22
Late proliferative/ Ovulation	0.55-0.6	1.0-1.3	1.89 ± 0.4
Luteal	0.6-0.65	1.3-1.8	1.23 ± 0.67
Postmenopausal	0.6-1.0	1.3-4.0	1.8 – 3.8

RI = resistance index, PI = pulsatility index; OVA = ovarian artery, UTA = uterine artery

Indications

- Characterization of uterine/ovarian masses.
- Infertility and assisted reproduction.

Three-dimensional Sonography

Three-dimensional imaging has several obvious benefits that relate to an improved spatial orientation and the demonstration of multiplanar views, of which the coronal plane is particularly useful[32] (Fig. 2.31). It offers a more objective and reproducible measurement of volume and vascularity of the region of interest, and an improved assessment of normal and pathological pelvic organs through further postprocessing modalities, including tomographic ultrasound imaging and various rendering modalities. It also has the benefit of offering reduced scanning time, the option of teleconsultation and storage of images for re-evaluation.

There are different types of 3D acquisition, manual, sensor-based and automatic.

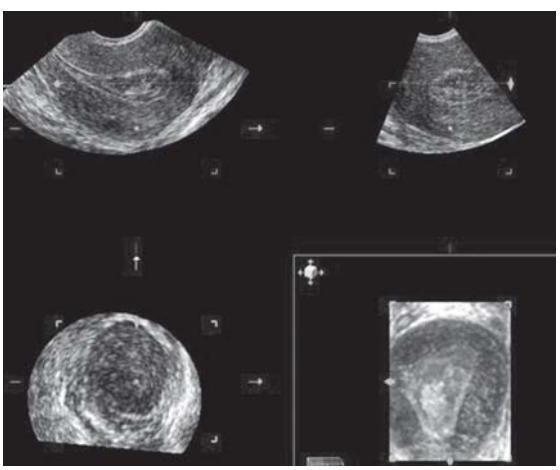

Fig. 2.31: 3-D ultrasound permits collection and review of data obtained from a volume of tissue in multiple imaging planes and allows visualization of the third or coronal plane of the uterus

For manual acquisitions the user moves the probe during the data acquisition. The smoothness and speed at which the probe is moved should be constant. Since the time for post-processing depends on the acquired number of frames, it is recommended to start with a high frame rate. Low frame rates result in fewer acquired frames for the 3D dataset, which results in more intensive post-processing (interpolation). Manual acquisitions are much more user dependant and are unable to be used for measurement. When performing sensor-based acquisitions a transmitter is used to generate a pulsed electro-magnetic field, which is detected by a sensor attached to the transducer. As the sweep is done the position information is detected and used to calculate a 3D data set. Automatic acquisitions are more uniform and consistent due to the ultrasound system driving the movement of the acoustic array. The anatomy is acquired as a dataset and each anatomical scan plane can be rotated on the X, Y or Z-axis to obtain the optimal image, allowing for more accurate 2D and volume measurements.

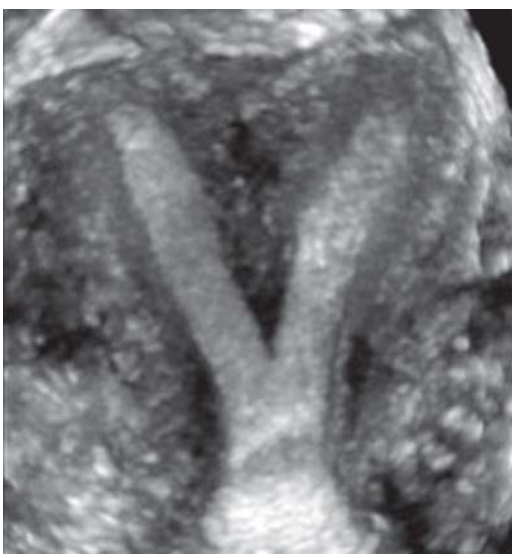

Fig. 2.32: 3-D reconstructed coronal view showing a subseptate uterus

Indications

- Diagnosing congenital uterine malformations (Fig. 2.32).
- Accurate volume measurement, e.g. endometrial, ovarian cysts and follicles, tumour masses, prostate.
- Exact localisation of pathology—intrauterine fibroid, IUCD, etc.
- Characterisation of adnexal masses.
- Extent of tumor infiltration into adjacent tissues/organs.
- 3-D power Doppler can aid in characterisation of vessel morphology.

Extended Field of View (EFOV) Imaging[33]

Overcomes the drawback of limited field of view of sonography, enabling the visualization of large fields of view in a single image. This technology is now available in most of the modern equipments. The technique is relatively simple and requires only a steady sweep of the transducer over the concerned area to acquire the data. The EFOV image is then reconstructed automatically by the computer. Although EFOV plays its most important role in the evaluation of relatively superficial structures, e.g. in evaluation of scrotal masses and establishing their relation with the testes (Fig. 2.33), it can also help in localization and orientation of lesions in the abdomen and pelvis. Doppler EFOV allows a panoramic visualization of vascularity in mass lesions, helping in their characterization. Transvaginal EFOV is also possible to illustrate the relation of smaller pelvic masses with the uterus and ovaries in a single image. EFOV images are comparable to CT/MRI images as it provides a panoramic view.

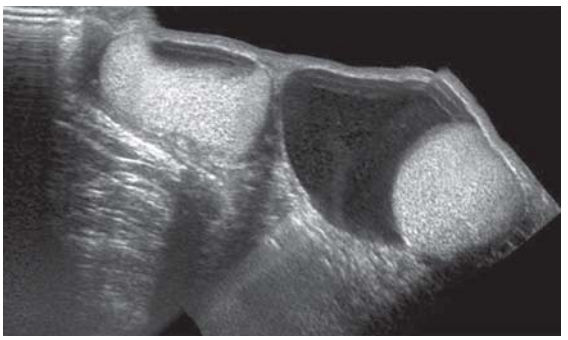

Fig. 2.33: EFOV image of the scrotum showing left hydrocele with normal left testis, alongwith the normal right testis

Image enhancement tools like **spatial compound imaging** and **tissue harmonic imaging** can add to the diagnostic confidence. Spatial compound imaging is a technology by which the unwanted speckle and clutter or "noise" can be reduced , thus giving better contrast resolution and clearer borders. Tissue harmonic imaging takes advantage of nonlinear propagation of ultrasound in tissue. It diminishes low frequency , high amplitude noise and improves imaging of technically difficult patients.

Elastography[34]

Elastography is a recently introduced ultrasound imaging technique that evaluates the elasticity of tissue. Neoplastic tissue has a greater cell density leading to increase in hardness if the tissue, thus causing a change in its elasticity. Elastography shows promising results in the evaluation of prostate cancer.[35]

Contrast-enhanced Ultrasonography (CEUS)

Contrast agents can help delineate vascular structures and enhance Doppler signals from small volumes of blood making it possible to image organ and lesion perfusion in real time.[36] Gas filled microbubbles are used as ultrasound contrast agents. They are in the size range of 1-4 microns in diameter and can be administered intravenously. There are two forms of CEUS, untargeted CEUS, which is used in echocardiography and targeted CEUS, which is a disease/organ specific technique and can be used in cases of inflammatory or malignant lesions of the liver, prostate, kidney, uterus , ovaries, and other organs. However, targeted CEUS has not yet been approved for clinical use. If these microbubble based techniques are successful , future application will likeky expand to include detection and staging of malignancies, as well as monitoring response to therapy.[37]

CONCLUSION

Ultrasound remains the first line investigation when evaluating the urogenital tract. Other than its inherent advantages of lack of ionizing radiation and low cost, it gives an excellent visualization of the organs of the urogenital tract. With the addition of Doppler, the vascular pattern and morphology can also be very well-evaluated. The introduction of contrast agents has made it possible to interrogate even the slow flow areas. Multiplanar and surface rendered images are possible with 3-D technology. However, it is essential to recognize that operator skill, regardless of the equipment used, ultimately determines the final benefit of ultrasound in patient care.

REFERENCES

1. Zagoria RJ. An Introduction to Radiologic methods. In Genitourinary Radiology. The Requisites; (2nd Edn). Mosby 2004;1 -50.
2. Swischuk LE. Genitourinary Tract and Adrenal Glands. In Imaging of the Newborn, Infant & Young Child. (5th Edn) Lippincott Williams & Wilkins: 2004;590-724.

3. Allan Paul. The normal kidney. In Meire HB, Cosgrove D, Dewbury KC, Tarrant P (Eds). Abdominal and General Ultrasound Edinburgh. Churchill Livingstone 2001;515-27.
4. Emamian SA, Nielsen MB, Pedersen JF, et al. Kidney dimensions at sonography: Correlation with age, sex and habitus in 665 adult volunteers. AJR 1993;160:83-86.
5. Yeh HC, Halton KP, Shapiro RS, et al. Junctional parenchyma. Revised definition of Hypertrophied Column of Bertin, Radiology 1992; 185:725-32.
6. Dalla Palma L, Bazzichi M, Cressa C, et al. Radiological anatomy of the kidney revisited. Br J Radiol 1990;63: 680-90.
7. Dubbins PA. The kidney in Allan PL, Dubbins PA, Pozniak M, Mc Dicken WN (Eds). Clinical Doppler Ultrasound. Churchill Livingstone 2000;169-90.
8. Thurston W, Wilson SR. The Urinary Tract in Rumack CM, Wilson SR, Charboneau JW (Eds). Diagnostic ultrasound 3rd edition Elseiver Mosby 2005;321-93.
9. Price CI, Adler RS, Rubin JM. Ultrasound depiction of differences in density: Explanation of ureteric jet phenomenon and implications for new ultrasound applications. Invest Radiol 1989;24:876-83.
10. Bree RL Toi A. The Prostate in Rumack CM, Wilson SR, Charboneau JW (Eds). Diagnostic ultrasound (3rd Edn). Elseiver Mosby 2001; 395-424.
11. Rickards D, Hare C. The lower urinary tract. In Meire HB, Cosgrove D, Dewbury KC, Farrant P (Eds). Abdominal and General Ultrasound. Edinburgh, Churchill Livingstone 585-611, 2001.
12. Krone KD, Caroll BA. Scrotal Ulatrasound. RCNA 1985;23:121–139.
13. Rifkin MD, Foy PM, Goldberg BS. Scrotal Ultrasound: Acoustic characteristics of the normal testis and epididymis defined with higher resolution superficial scanners. Med Ultrasound 1984;8: 91–97.
14. Gorman B, Caroll BA. The Scrotum in Rumack CM, Wilson SR, Charboneau JW (Eds): Diagnostic ultrasound. (3rd edn). Elseiver Mosby 2001;849-888.
15. Johnson KA, Dewbury KC. Ultrasound imaging of the appendix testes and appendix epididymis. Clinical Radiology 1996;51:335-37.
16. Middleton WD, Thorne DA, Melson GL. Colour Doppler ultrasound of the normal testis. AJR 1989;152: 293-97.
17. Benson CB, Doubilet PM, Vickers MA. onography of the male genital tract. AJR 1989;153: 705-13.
18. Schwartz AN, Wang KY, Mark LA, et al. Evaluation of normal erectile function with color flow Doppler sonography. AJR 1989;153: 1155- 60.
19. Siegel MJ. Pediatric gynaecologic sonography. Radiology 1991;170:593-600.
20. Salem S, Wilson SR. Gynaecologic Ultrasound in Rumack CM, Wilson SR, Charboneau JW (Eds). Diagnostic ultrasound (3rd Edn). Elseiver Mosby 2001;527-87.
21. Coleman BG, Arger PH, Grumbach K, et al. Transvaginal and transabdominal sonography: Prospective comparison. Radiology 1988; 168:639-43.
22. Burks DD, Stainken BF, Burkhard TK, et al. Uterine inner myometrial echogenic foci: Relationship to prior dilatation and curettage and endocervical biopsy. J Ultrasound Med 1991;10:487-92.
23. Forrest TS, Elyaderani MK, Muilenburg MI. Cyclic endometrial changes: US assessment with histologic correlation. Radiology 1988;167:233.
24. Laing FC, Douglas MD, et al. Gynecologic ultrasound. RCNA 2001;39(3):523-40.
25. Schoenfield A, Levavi H, Hirsch M, et al. Transvaginal sonography in postmenopausal women. J Clin Ultrasound 1990;18:350-58.
26. Orsini LF, Salardi S, Pilu G, et al. Pelvic organs in premenarchal girls: Real-time ultrasonography. Radiology 1984;153:113 -16.
27. Van Nagell JR Jr. Higgins RV, Donaldson ES, et al. Transvaginal sonography as a screening method for ovarian cancer. Cancer 1990;65: 573-77.
28. Muradali D. Colgin T, Hayeems E, et al. Echogenic ovarian foci without shadowing: Are they caused by psammomatous calcifications? Radiology 2002;224:429–35.
29. Wolf SI, Gosink BB, Feldesman MR, et al. Prevalence of simple adnexal cysts in postmenopausal women. Radiology 1991;180:65-71.
30. Applebaum M in The menstrual cycle, menopause, ovulation induction and *in vitro* fertilization. Copel JA, Reed KL (Eds). Doppler ultrasound in Obstetrics and Gynaecology 1994;71-86.

31. Dubbins PA. The female pelvis. In Allan PL, Dubbins PA, Pozniak MA, et al (Eds). Clinical Doppler Ultrasound. Churchill Living-stone 2000;237-58.
32. Pretorirus DH, Borok NN, Coffler MS, et al. Three Dimensional Sonography in Obstetrics and Gynaecology, RCNA 2001;39(3): 499-521.
33. Henrich W Fuchs I Schmider A Transvaginal and Transabdominal Extended Field of View (EFOV) and Power Doppler EFOV Sonography in Gynecology: Advantages and Applications. Journal of Ultrasound in Medicine 2002;21: 1137–44.
34. Ophir J, et al. Elastography: A quantitative method for imaging the elasticity of biological tissues. Ultrason Imaging 1991;13(2):111-34.
35. Pallwein L, Fauscher F, Mitterberger M. Value of contrast enhanced ultrasound & elastography in imaging of prostate cancer. Curr Opin Urol, 2007;17(1):39-47.
36. Burns PN. Microbubble Contrast for Ultrasound Imaging: Where, How and Why in Rumack CM, Wilson SR, Charboneau JW (Eds). Diagnostic ultrasound (3rd Edn) Elseiver Mosby 2001; 55-76.
37. Halpern EJ. Contrast-Enhanced Ultrasound Imaging for Prostate Cancer. Rev Urol 2006; 8(Suppl):S29- S37.

Chapter

3

Computed Tomography of Urogenital Tract: Techniques and Normal Appearances

Sapna Singh, Veena Chowdhury

INTRODUCTION

With the advent of the modern, cross-sectional imaging modalities of computed tomography (CT) and magnetic resonance imaging (MRI) and refinement in their techniques, the kidney is a much better understood organ as CT has enlarged the capacity to visualize the genitourinary tract noninvasively. The anatomical characteristics of the kidney and perirenal region can be accurately and consistently visualized. Further perfusion of the kidney can also be studied. Therefore, CT is a vital component of a uroradiologic diagnosis and plays a valuable role in evaluating patients with renal masses, renal cystic disease, renal infections, renal trauma and flank pain of unknown etiology. It is unsurpassed in evaluating lesions containing fat or calcium.

Helical CT has overcome the limitations of conventional CT (CCT) and is now the standard CT technology. It allows rapid volumetric assessment of the kidneys and is highly accurate in the evaluation of renal masses and blood vessels. 3D postprocessing capabilities allow the assessment of the renal vascular pedicle noninvasively by CT angiography. Gapless volume scanning and improved resolution in the Z-axis during the excretory phase enables improved visualization of the renal collecting system and ureters, resulting in a better demonstration of intraluminal and extraluminal pathology.[1] Thus, helical CT enables an improved characterization of renal lesions, reducing the diagnosis of indeterminate masses and thus, facilitating a better theraupetic management.

NORMAL RENAL STRUCTURE AND CT ANATOMY OF KIDNEYS

The retroperitoneum is divided into three compartments namely the anterior pararenal, posterior pararenal and the perinephric spaces. The perinephric space contains the kidneys, renal vessels, the adrenals, the IVC and lower aorta, perinephric fat and the renal collecting system. Each kidney is about 11cm in length, 6 cm in breadth and 3 cm in antero-posterior dimension. The left kidney is little longer, narrower and is higher in position.The kidney itself, has an internal medulla, external cortex and an outer capsule. The capsule is surrounded by perinephric fat, which is enveloped by the renal fascia. The renal fascia is in two layers, the anterior and posterior, which are named Gerota's fascia and the fascia of Zuckerkandl respectively.

The renal fascia fuses superiorly with the diaphragmatic fascia and laterally with the lateroconal fascia, inferiorly the layers of renal fascia fuse weakly with the iliac fascia and blend loosely with the periureteric connective tissue. The inferior apex of the compartment remains open towards the iliac fossa. The weakest point of the perinephric compartment through which urine or perinephric effusions escape most easily is at the inferomedial angle adjacent to the ureter. The posterior renal fascia fuses medially with the psoas and the quadratus lumborum fascia.[2,3]

On axial scanning, the kidney appears smooth and oval with an anteromedial break in the region of hilum where the vascular pedicle enters. The renal hilum is at the level of L1-2 vertebra on the right side and is 1-2 cm higher on the left side. The renal vascular pedicle lies anterior to the pelvis and it may not be always possible to differentiate renal artery and vein on conventional scannings. The renal veins are usually larger than the renal artery and the longer left renal vein crosses anterior to the aorta and enters the inferior vena cava at the uncinate process of the pancreas (Fig. 3.1). The aorta and superior mesenteric artery may pinch the left renal vein which causes the left renal vein to appear larger than the right.

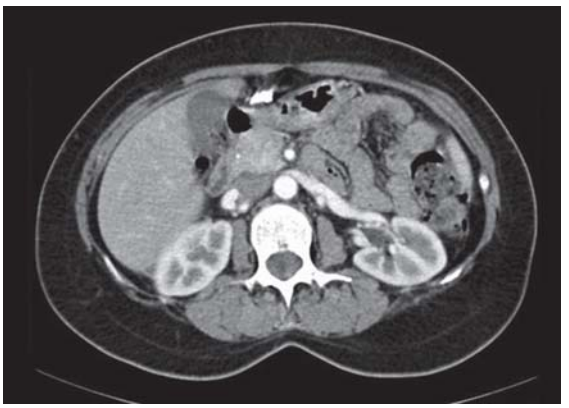

Fig. 3.1: Contrast-enhanced axial scan CT showing the longer left renal vein crossing anterior to the aorta and entering the inferior vena cava at the level of the uncinate process of the pancreas.

NORMAL CT ANATOMY OF THE PELVIS

The pelvis contains the bony structures and within it the soft tissue structures including the ureters, urinary bladder, vascular structures, male and female genital organs. The ureters are best seen after intravenous administration of iodinated contrast material. At the level of the sacral promontory, the ureters are located anteromedial to the psoas major and anterior to the common iliac artery or lateral to the external iliac artery. The ureters then course medially and posteriorly to the external iliac arteries until they reach the midportion of the internal obturator muscle. At this level they course anteromedially to reach the trigone of the urinary bladder (Figs 3.2A to D). The configuration of the urinary bladder depends on the degree of filling and imaging is greatly improved when the bladder is fully distended. In the distended state, bladder wall is 1 to 3 mm thick. Partial volume artifacts may obscure a small area of the fundus and base of the bladder. Peritoneal reflections extend from the fundus of the bladder to the rectum in males, while in females; the peritoneum is first reflected onto the uterus and then to the rectum. These peritoneal reflections form small cul-de-sacs, which are the earliest site of small collections in pelvic inflammatory disease.

The prostate appears on CT scans as a homogeneous well-marginated soft tissue structure, 2-4 cm in length located just beneath the symphysis pubis immediately anterior to the rectum (Fig. 3.3). Anteriorly prostate is anchored to the pubis with

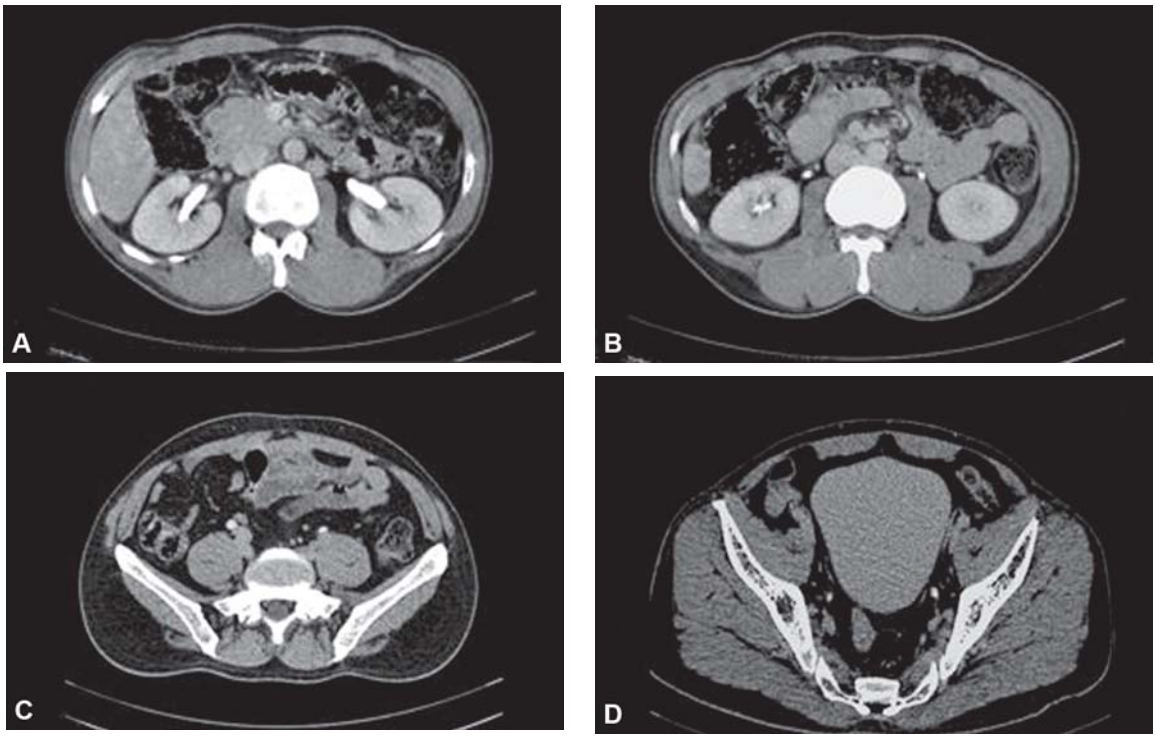

Figs 3.2A to D: Transverse CT images obtained with a multidetector row CT scanner showing the normal anatomy progressing from superior to inferior **(A)** the renal pelvis **(B)** upper ureters **(C)** mid ureters and **(D)** distal ureters

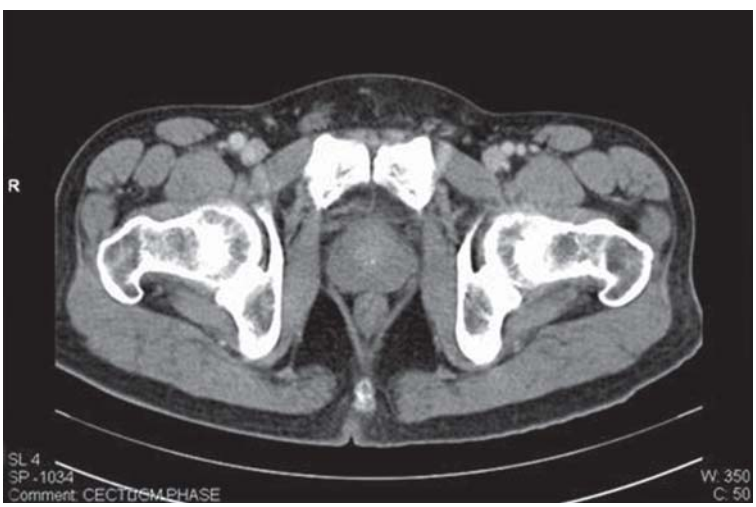

Fig. 3.3: Axial CT scan showing the normal prostate as a homogeneous well-marginated soft tissue 2-4 cm in length located beneath the symphysis pubis anterior to the rectum

ligaments and posteriorly Denonvilliers fascia separates it from the rectum.The size of the gland increases with advancing age. The seminal vesicles lie posterior to the urinary bladder and superior to the prostate. They are separated by a wedge shaped layer of fat from the posterior wall of the bladder forming the seminovesical angle (Fig. 3.4).

Female pelvic viscera is constituted by the uterus,fallopian tubes, ovaries, cervix and vagina. The vagina, urethra and rectum are bounded laterally by ligaments of the levator ani muscle. Prior to scanning, the lumen of vagina should be demarcated by inserting a tampon.[2] The uterine cervix appears as a transverse oval soft tissue structure with a diameter not exceeding 3 cm and is sharply demarcated from surrounding fat. The cross sectional diameter of a normal uterus in a reproductive age group female should be < 5 cm (Fig. 3.5). The uterine cavity is visible as a T-shaped structure after administration of IV contrast media. The broad ligaments are two fibrous sheets extending laterally from the uterus to the pelvic side wall and covered on their anterior and posterior surfaces by peritoneum.[3] They are not routinely seen on CT unless outlined by ascites. Between the leaves of the broad ligaments, are the parametrium, uterine artery, fallopian tube and round ligament. The round ligaments demarcate the superolateral border of the uterus and ascend anterolaterally over the external iliac vessels, pass through the inguinal canal and insert in the labia major. The triangular cardinal ligaments are located at the base of the broad ligament and fan out from their attachments at the cervix to insert on fascia covering the pelvic diaphragm. The uterosacral ligaments arise in continuity with the cardinal ligaments and pass posterolaterally around the rectum to insert on the sacrum.[3] The ovarian fossa is located between the external iliac vessels laterally and the pelvic ureter posteriorly. The ovaries, which are normally 3 × 1.5 cm in size are variable in position (Fig. 3.6).

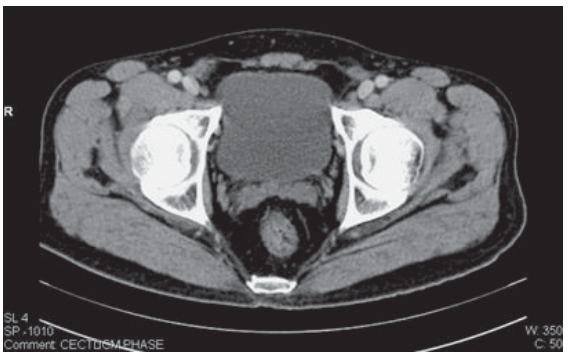

Fig. 3.4: Axial CT scan showing the seminal vesicles which lie posterior to the urinary bladder and separated by wedge shaped layer of fat from the posterior wall of the bladder forming the seminovesical angle

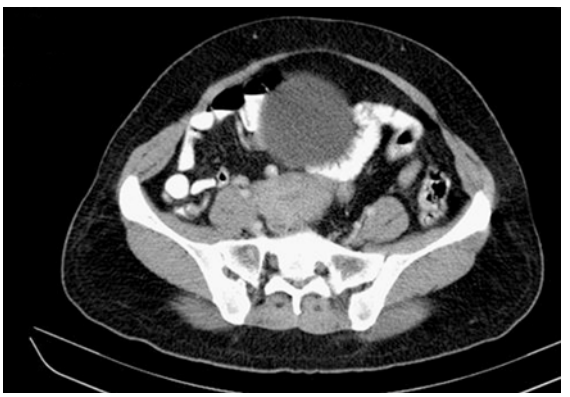

Fig. 3.5: Axial CT scan showing the normal uterus posterior to the bladder

MULTIDETECTOR CT (MDCT)

Multidetector CT (MDCT) is the most recent advance in CT technology. Also known as multislice, multichannel or multisection CT, it uses a multiple row detector array instead of the single row detector array used in single slice helical CT.[4] These new CT scanners with reduced gantry rotation times

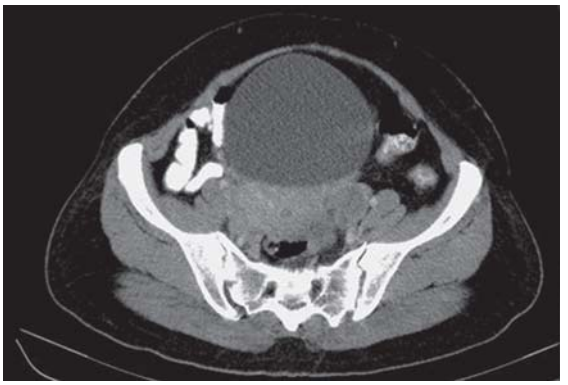

Fig. 3.6: CT scan showing the normal uterus and a cyst in the left ovary

(0.5 sec or less for one 360° rotation) allow 2 to 25 times faster scan times than helical CT with the same or better image quality.[5] The faster scan times result in decreased breath hold times with reduced motion artifact and more diagnostic images. Increased volume coverage is combined with thinner slice thickness to obtain better quality volume data sets for three dimensional (3D) images. MDCT allows images to be obtained in multiple phases of renal parenchymal enhancement and excretion in the collecting system after administration of a single bolus of intravenous (IV) contrast material. Detection and characterization of small renal masses, display of the arterial and venous supply similar to conventional angiography and demonstration of the collecting system using different 3D display technique are possible with MDCT.[6]

Advantages of Renal Multidetector Row CT

The main advantages of MDCT are faster scanning time, increased volume coverage and improved spatial and temporal resolution.[7]

Increased Diagnostic Images

As MDCT uses multiple rows of detector, it allows for registration of more than one channel per gantry rotation whereas single detector helical CT allows registration of only one channel of image information of the scanned body part per gantry rotation.[8]

Increased Temporal Resolution

Current MDCT scanners have very fast gantry rotation time that is equal to or less than 0.4 seconds. Decreased gantry rotation time provides reduced scanning times and increased coverage along the Z-axis. Therefore, image acquisitions in multiple phases of renal parenchymal enhancement and contrast excretion in the collecting system after administration of a single bolus of IV contrast media are possible.[9]

Isotropic Data Acquisition and Increased Spatial Resolution

Isotropic data acquisition is defined as obtaining images with equal voxel size in three axes. MDCT scanners permit acquisition of thin sections with isotropic voxel size. Their effective section thickness is between 0.75 and 1.6 mm. MDCT scanners permit reconstruction of images at various thicknesses different from that chosen before the scan.[9] Isotropic imaging minimizes the importance of patient positioning and obviates obtaining axial, coronal and sagittal planes directly. Increased temporal resolution and acquisition of thin slices with isotropic voxel allows excellent quality MPR images to be obtained and 3D rendering of virtually any plane.[10] Optimal imaging of the renal hilar anatomy requires small slice widths and isotropic or near – isotropic data sets which can be achieved on MDCT scanners.[11]

EXAMINATION TECHNIQUE AND IMAGING PROTOCOLS OF MULTIDETECTOR ROW CT OF THE KIDNEY

Imaging protocols and parameters vary depending on the type of MDCT scanner (number of detectors and name of manufacturer). Every imaging department should optimize its imaging protocols and parameters. The CT examination phases of the kidney are precontrast (noncontrast), corticomedullary, nephrographic, and excretory (delayed or urographic) phases.

Noncontrast CT

Noncontrast scans are obtained to locate the kidneys, evaluate urolithiasis, detect acute hematoma, and obtain baseline density measurements of renal masses.[12] Noncontrast CT is accepted as primary imaging to detect urinary calculi.

Contrast-enhanced CT Oral Contrast Medium

In the evaluation of urolithiasis, dense oral contrast medium in the bowel can make detection of ureteral stones more difficult. In addition, for 3D CT angiography, positive oral contrast medium should not be given in order to improve postprocessing image quality and to avoid major overlay in postprocessed images.[13] Some investigators suggest drinking 500 to 750 ml of water over a 15 to 20 minutes period before the start of a renal CT examination and do not advocate the use of oral contrast medium for renal MDCT.[14]

Administration of Intravenous Contrast Medium

For the contrast-enhanced phases, the optimal timing depends on the volume of the contrast medium, the rate of its administration, and patient's cardiac output. The difference between the start of contrast medium injection and the start of scanning is referred to as delay time. 100 to 120 ml of nonionic contrast medium is sufficient at an infusion rate of 2 to 3 ml per second for routine renal imaging. Contrast is injected through an 18-gauge catheter placed in the antecubital vein.

PHASES OF RENAL ENHANCEMENT / MULTIPHASIC HELICAL CT

Normal CT Nephrogram

The first perfusion phase, the cortical nephrogram or the **corticomedullary phase (CMP)** becomes visible 25-80 seconds after contrast administration. When contrast material enters the cortical capillaries and peritubular capillary spaces and filling of the lumina of the proximal cortical tubules starts, the renal cortex is distinctly differentiated from the unenhanced medulla[15,16] (Fig. 3.7).

The second phase, the tubular nephrogram or **nephrographic phase** begins **90-120** seconds after contrast injection and

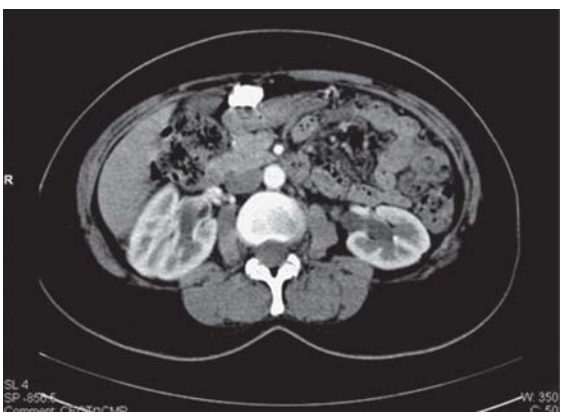

Fig. 3.7: Contrast-enhanced scan of the kidney in the corticomedullary (CM) phase showing dense cortical enhancement, the renal cortex is distinctly differentiated from the unenhanced medulla

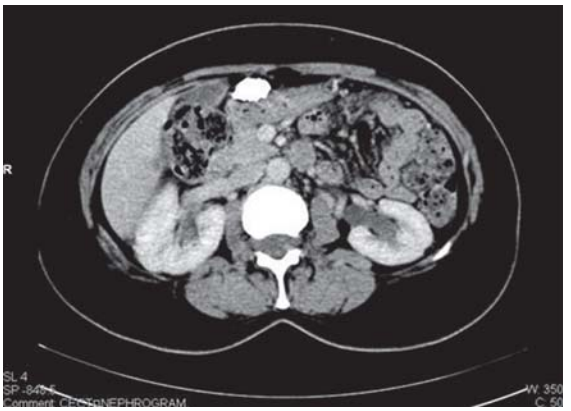

Fig. 3.8: CECT of the kidney in the nephrogram phase showing dense homogeneous parenchymal enhancement and disappearance of the corticomedullary differentiation during this phase

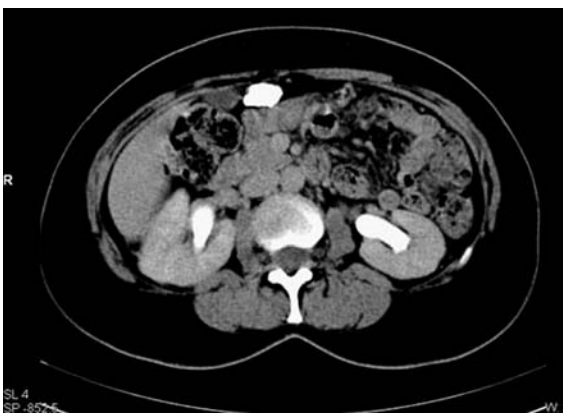

Fig. 3.9: Excretory phase or the delayed phase (5 minutes) axial CT image demonstrating calyceal opacification

includes the passage of contrast material through the renal tubule system.[15,16] During this phase the corticomedullary differentiation disappears and the renal parenchyma enhances homogeneously (Fig. 3.8).

The third phase, the **excretory phase** (EP) begins 3-5 minutes after contrast administration and begins when contrast material is excreted into the collecting system (Fig. 3.9).

Corticomedullary Phase (CMP)

The advantages of CMP include differentiation of normal variants of renal parenchyma from renal masses and better depiction of tumor hypervascularity improving the characterization of solid renal mass lesions (Figs 3.10A to C). However, assessing the CMP alone may result in clinically significant errors[17] since small hypovascular tumors of the renal medulla may be missed since they are not sufficiently enhanced and hypervascular cortical renal cell carcinomas may enhance to the same degree as the normal cortex and may be missed. Thus imaging of the kidney during CMP should be completed by scanning the kidney during nephrographic phase (NP).

Nephrographic Phase (NP)

This is considered the optimal phase for the detection and characterization of renal masses, in particular of small renal masses < 3 cm providing both homogeneous enhancement of cortex and medulla and lesion enhancement.[18] Lesion enhancement > 20 HU which is considered sufficient proof for a malignant mass may be delayed and not visualized until the nephrographic phase (NP) (Figs 3.11A and B). Homogeneous enhancement of NP also provides the visualization of renal infarction, traumatic parenchymal lesions and acute pyelonephritis.

Pathological CT Nephrogram

Helical CT enables an improved depiction of renal pathology caused by abnormal vascular perfusion and/or reduced tubule transit rates.

Impaired renal perfusions with focal reduction of the nephrogram include renal infarction, blunt renal trauma and acute

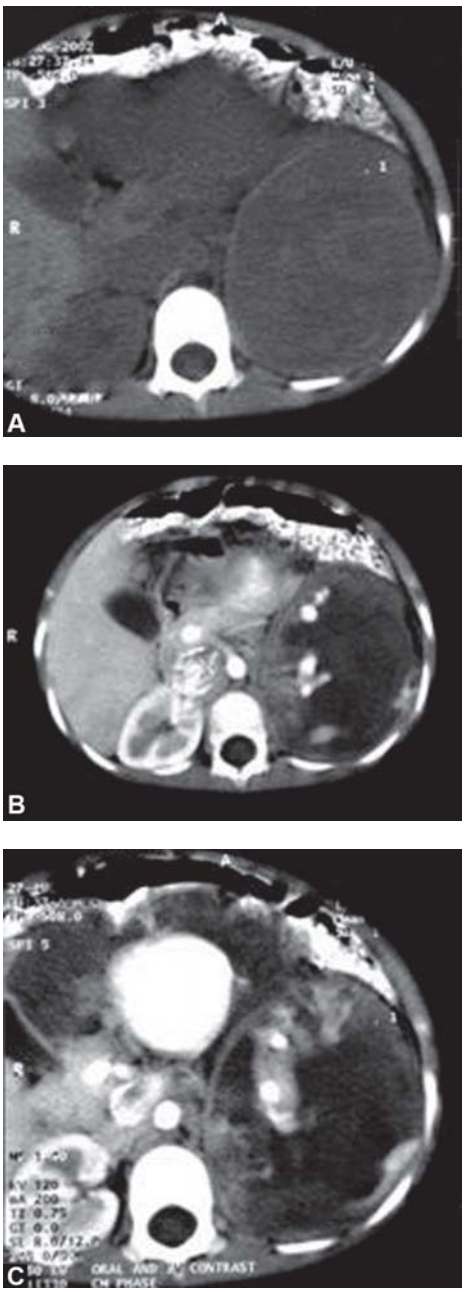

Figs 3.10A to C: (A) Noncontrast axial CT showing a large hypodense mass with no differential density replacing the left kidney. **(B and C)** The corticomedullary phase shows multiple tortuous feeder vessels depicting tumor hypervascularity. Thrombus is also seen in IVC – Wilm's tumor

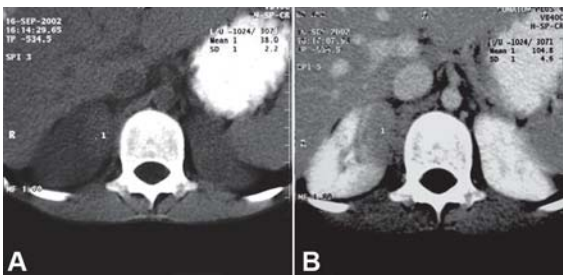

Figs 3.11A and B: Noncontrast CT scan: **(A)** Showing an indeterminate mass in the right kidney. Nephrogram phase of renal enhancement **(B)** Demonstrating significant enhancement > 20 HU suggestive of malignant mass

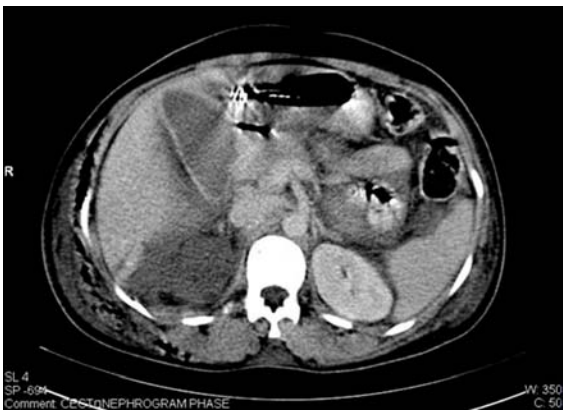

Fig. 3.12: Contrast-enhanced axial scan of the kidney showing lack of nephrogram on the right side suggesting devascularization of the renal parenchyma in a case of trauma. The normal nephrogram with homogeneous enhancement of the renal parenchyma is seen on the left side

pyelonephritis. In blunt renal trauma, lack of the nephrogram is a feature of devascularization of renal parenchyma which may be segmental/total depending on the localization of the vessel injury (Fig. 3.12). In acute pyelonephritis, hypoperfusion is combined with reduced tubule transit rates due to inflammatory obstruction. Delayed perfusion of the renal tubule system is visualized as a striated nephrogram of the infiltrated parenchyma. An initially reduced density and slowed temporal progression of the three phases of the nephrogram is caused by

significant stenoses of the main renal artery, acute obstruction of the renal vein and acute ureteral obstruction. A bilaterally reduced density and persistence of the nephrogram is observed in shock due to diminished glomerular filtration rate and tubular stasis caused by severe systemic hypotension.

Excretory Phase (EP)

The excretory phase (the delayed or urographic phase), used to evaluate renal collecting system and ureters, begins 3 minutes after the start of contrast medium injection. In this phase, while the intensity of the nephrogram declines, excretion of the contrast medium permits opacification of the calyces, renal pelvis, and ureters. The opacification of the renal collecting system allows the depiction of intraluminal pathology.

Thus, Multiphasic HCT is the preferred technique in the evaluation of the kidney in clinically suspected/known renal disease.[19] It includes an unenhanced scan as well as scanning after rapid bolus injection (3-4 ml/sec) of contrast (100-120 ml/300 mgl/ml) during both CMP and NP and/or EP respectively. Scan parameters include 120 KV, 220-280 mA, a collimation of 3-5 mm, a reconstruction interval of 2-4 mm and a pitch of 1.5 during a scan acquisition time of one breath hold.

IMAGE PROCESSING AND POSTPROCESSING TECHNIQUES

Four main 3-D visualization techniques currently are used on clinical 3-D workstations: MPR, maximum intensity projections (MIP), shaded surface displays (SSD), and a volume-rendering technique (VRT).

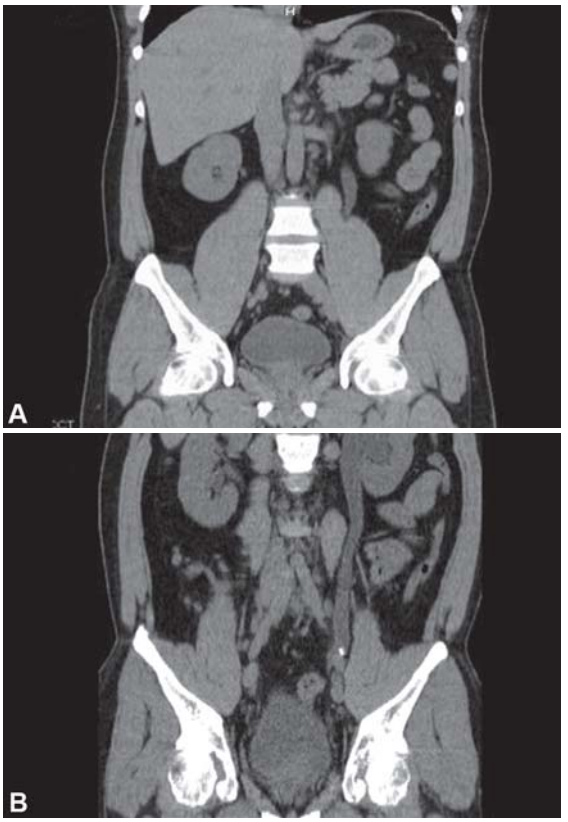

Figs 3.13A and B: (A) Coronal MPR image demonstrating only a small segment of the left ureter in its mid portion **(B)** Curved multiplanar reformation displaying a left ureteric calculus, the consequent hydronephrosis and the entire dilated ureter proximal to it in a single image regardless of opacificaion

Multiplanar Reformation (MPR)

MRP is the postprocessing technique used most commonly and represents simple reordering of the image voxel. A known limitation of MPR is the visualized structures must be in the same plane. Because most structures of interest are not within a single plane, a MRP cannot be created that demonstrates an entire structure (Figs 3.13A and B). As structures course in and out of the MPR, pseudostenoses are created. To solve this problem, curved planar reformation (CPR)

are used. CPR have a single voxel thick tomogram, but it is capable of demonstrating an uninterrupted longitudinal cross-section as the display plane curves along the structure of interest.[20] CPR images can be obtained manually by drawing a line over a structure of interest or it can be produced automatically or semiautomatically by dedicated software. CPR provide the most useful luminal assessment (such as of blood vessels, airways, bowel and ureters) and are useful in improving the visualization of vessels of small diameter or tortuous anatomy such as the ureters[21] (Fig. 3.14). CPR have an important limitation in that they are highly dependent on the accuracy of the curve.

Maximum Intensity Projection (MIP)

MIP displays the maximum voxel intensity along a line of viewer projection in a given volume. High density structures, such as contrast filled vessels and the collecting system, are demonstrated nicely in images, such as angiograms or urograms (Fig. 3.15). The main disadvantage of MIP is that it obscures the area of interest by high density material, such as bone, calcium, and oral contrast medium. With the MIP technique, a 3-D effect can be obtained with rotational viewing of multiple projections, but it lacks depth orientation.[14]

Shaded Surface Displays (SSD)

SSD enables accurate 3-D representations of anatomy, relying on the gray scale to encode surface reflections from an imaginary source of illumination. SSD images are limited by their dependence on user-selected threshold setting.

Volume Rendered Technique (VRT)

With this technique, all attenuation values within a voxel are used to obtain the final image (that each voxel contributes brightness, color, and opacity to the final image). Anatomic structures with different levels of opacity (e.g. renal parenchyma, renal veins and arteries, and the collecting system) can

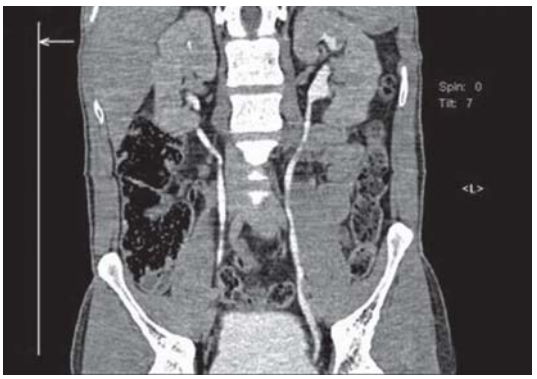

Fig. 3.14: Curved multiplanar reformation (CPR) image after contrast opacification of the pelvicalyceal system showing an uninterrupted course of the left ureter in its entirety as this technique displays all voxel values on the curve randomly drawn by the operator

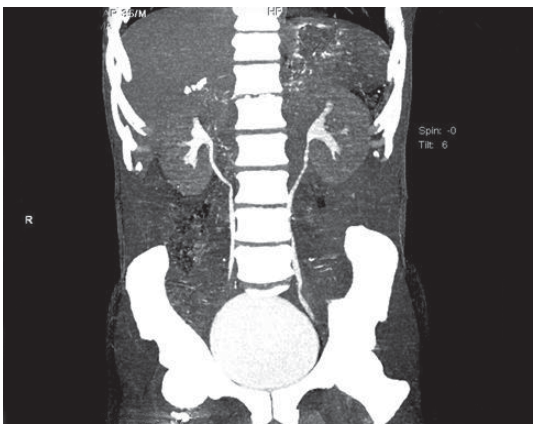

Fig. 3.15: Maximum intensity projection (MIP) in the excretory phase demonstrating the normally opacified calyces, the ureters and the bladder. This technique displays the maximum voxel value along a line of viewer's projection through a given volume

be demonstrated simultaneously (Fig. 3.16). VRT is an excellent 3-D technique for presentation that provides a roadmap for surgery and summary picture for the referring physician.[22] The most important limitation of VRT is its need for more powerful computers and costly workstation. Using editing techniques, structures overlaying the area of interest can be removed for better visualization and desired orientation (Figs 3.17 and 3.18).

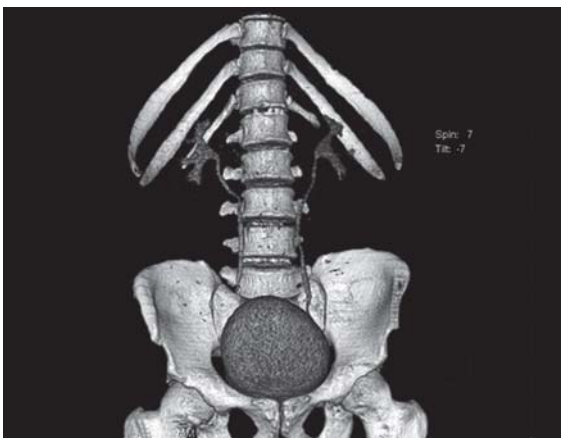

Fig. 3.16: Volume rendering technique (VRT) displaying the entire urinary tract. This technique takes the entire volume of data and displays anatomic structures with different levels of opacity/attenuation *(For color version see Plate 1)*

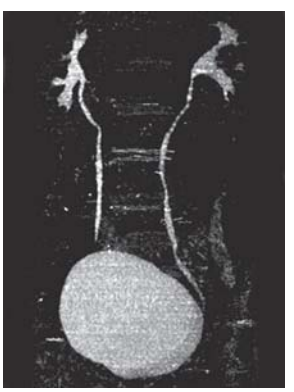

Fig. 3.17: Normal CT urogram image using maximum intensity projection (MIP) with bone editing displaying the entire urinary tract

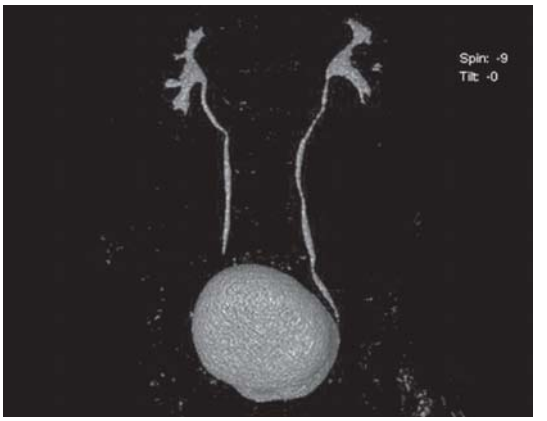

Fig. 3.18: Normal CT urogram image using volume rendering with bone editing displaying the entire urinary tract *(For color version see Plate 1)*

MULTIDETECTOR CT UROGRAPHY (MDCTU)

Multidetector CT urography may be defined as the examination of the urinary tract by MDCT in the excretory phase following intravenous administration.

Indication of CT Urography

- Calculi
- Renal tumors
- Urothelial tumors
- PUJ obstruction
- Congenital anomalies.

Calculi

It has been established unequivocally that currently MDCT is the most sensitive and specific test for the diagnosis of urinary tract calculi.[23] MDCTU can not only detect calculi but also accurately determine the level of obstruction (Figs 3.19A and B). MDCTU has an advantage over IVU that is, the ability to exclude extraurinary pathologies that may mimic calculi.[24] MDCT can also detect calculi in unusual positions such as in calyceal divertculae and is more accurate than IVU

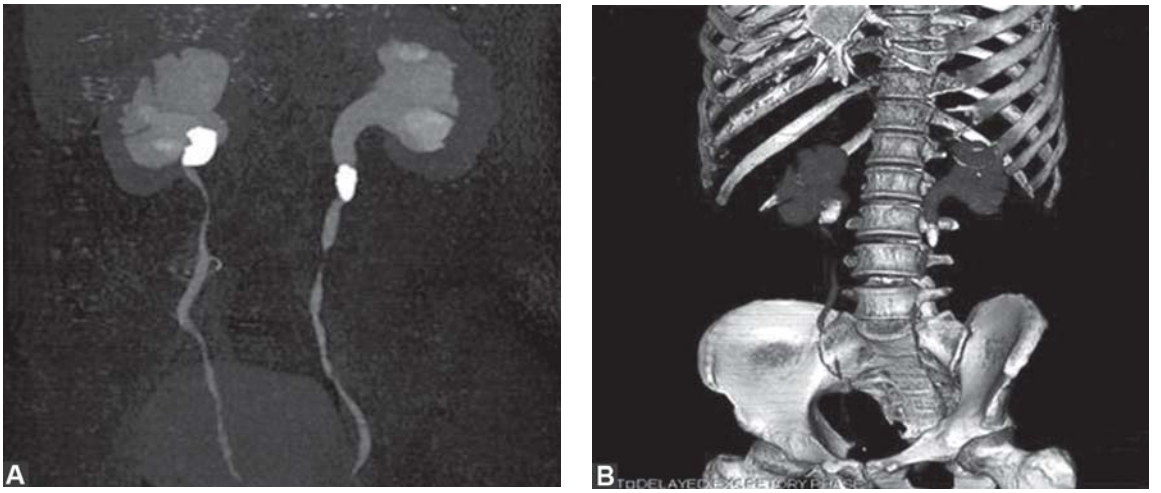

Figs 3.19A and B: CT urogram using MIP technique **(A)** depicting a calculus at the pelviureteric junction on the right side and a calculus in the proximal left ureter. There are backpressure changes on both sides. VRT image **(B)** displaying the same *(For color version of Fig. 3.19B see Plate 1)*

for detecting presence, size and location of urinary tract calculi. MDCTU also has the IVU advantage of demonstrating physiologic information, gained from the degree of delayed excretion, which was considered an index of severity of obstruction. Hydronephrosis, hydroureter, ipsilateral renal enlargement perinephric and periureteral fat stranding, perinephric fluid, ureter rim sign and ureterovesical edema are secondary signs of obstructing calculi (Figs 3.20A to C). The presence of "soft time rim sign", namely, a circumferental rim of soft tissue attenuation surrounding a calcification is a reliable indicator that the calcification in question represents a calculus within the ureter. Calculi associated with a "soft tissue rim sign" have a mean size of 4 mm.[26,27] Conversely a "comet tail sign" namely a linear or curvilinear soft tissue structure extending from an abdominal/pelvic calcification, has been stated to represent a phlebolith.

Renal Tumors

MDCTU is an appropriate imaging test for the detection and characterization of renal masses. The initial unenhanced CT is obtained to serve as the baseline for measurements of enhancements on the nephrographic phase images.[25] Most renal cell cancers are solid, with attenuation greater than 20 HU on unenhanced CT.[28] Lesion enhancement greater than 20 HU is considered highly suspicious of a malignant lesion. The location of the tumor may also be helpful in the diagnosis and characterization of solid renal masses. Renal cell carcinoma is frequently located at the periphery or near the corticomedullary junction of the kidney as it originates in the renal cortex, while transitional cell carcinoma extends into the kidney from the renal pelvicalyceal system and occurs more centrally in the kidney.[29] These features are well-demonstrated by MDCT. Renal tumors with nephron sparing surgery require a precise depiction of the

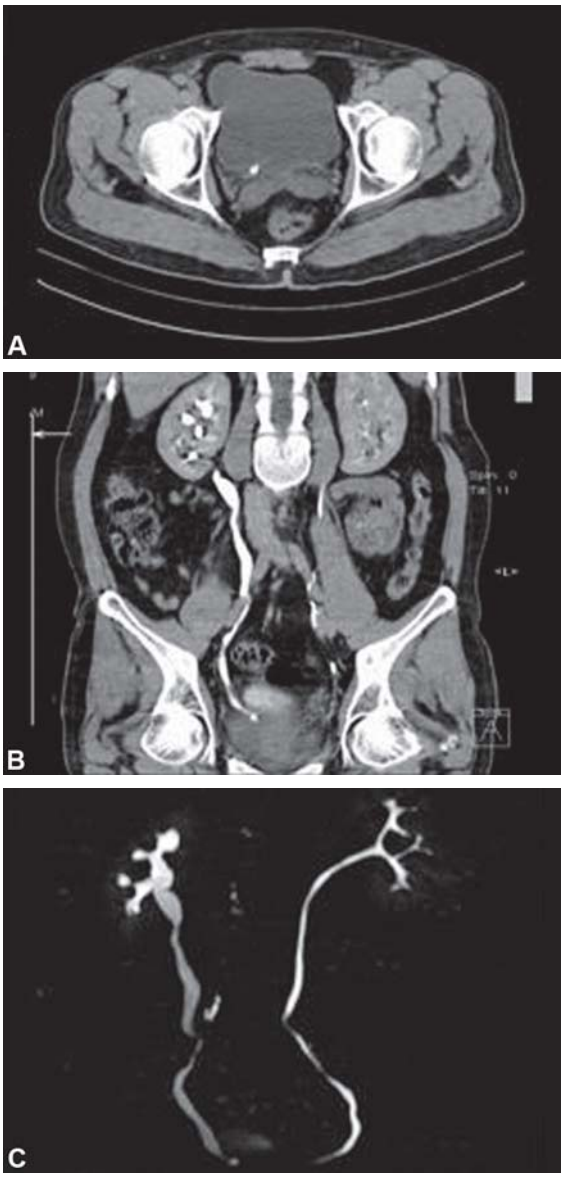

Figs 3.20A to C: Noncontrast axial CT **(A)** showing a radiodensity at the right ureterovesical junction (UV junction) s/o calculus. Curved MPR image after contrast opacification **(B)** depicting the calculus at the right UV junction with proximal hydronephrosis and hydroureter. CT urography using MIP **(C)** image showing the dilated hydroureter and hydronephrosis proximal to the calculus. The normal nondilated pelvicalyceal system and ureter is seen on the left side

tumor and its relation to the collecting system (Figs 3.21A to C). MDCT urogram demonstrates not only the pelvicalyceal system as in conventional urography but also renal, perirenal and vascular tissues.

Urothelial Tumors

Transitional cell carcinoma is the most common malignant neoplasm of the urotheluim. Many urologists believe that intravenous urography is still the gold standard for evaluating the urothelium, however, it has been reported in the literature to have detection rates for urothelial neoplasms of only 43 to 64 percent.[30] In the early stages, these neoplasms are seen as subtle filling defects or mural thickening. A filling defect in the renal pelvis or ureter can be caused by a neoplasm, calculus, clot, mycetoma or vascular impression. MDCTU has shown increased sensitivity and specificity for detecting urothetial tumor compared with retrograde ureterography, an imaging test assumed to be superior to IVU in evaluating the collecting system and ureters.[31] A recent study suggests that MDCTU is an accurate means for detection and staging of upper urinary tract TCC with accuracy for peritumoral invasion with positive and negative predictive values of 88.8 and 87.5 percent respectively.[32] One of the main advantages of MDCTU over IVU includes identification of intrinisic and extrinsic causes of ureteric obstruction including mural thickening with short segment malignant strictures retroperitoneal masses or lymphadenopathy retroperitoneal fibrosis, benign ureteric strictures and iatrogenic causes.[33] It can also show ureteic infiltration in malignant pelvic masses. (Figs 3.22A to D).

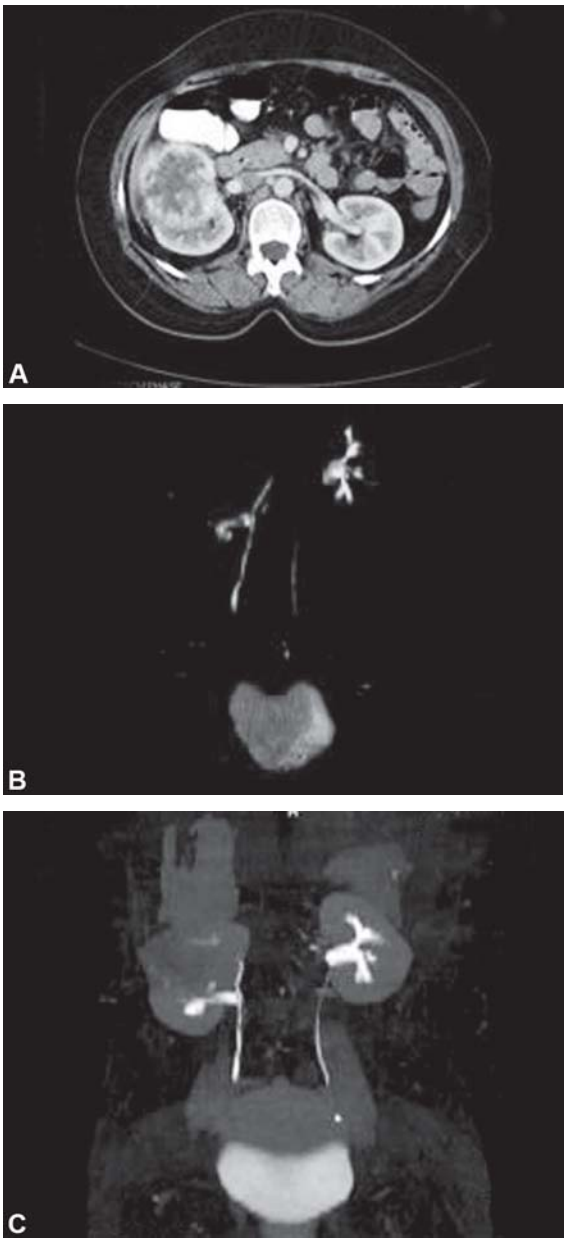

Figs 3.21A to C: Contrast-enhanced axial CT scan: **(A)** showing an enhancing mass in the upper and mid pole of the right kidney. CT urogram using volume rendering **(B)** showing distortion of the calyces by the mass lesion. CT urogram using MIP technique **(C)** showing splaying, distortion and amputation of the calyces on the right side – right renal cell carcinoma *(For color version of Fig. 3.21B see Plate 1)*

Cystoscopy remains the "gold standard" for evaluating the urinary bladder but MDCT urogram is playing an important role in the detection of bladder urothelial neoplasms (Figs 3.23A and B). As with urothelial tumors of the upper urinary tract, bladder neoplasms present as a filling defect, a focal mass or an area of focal bladder wall thickening[34] (Fig. 3.24). In a study a sensitivity of 93 percent and specificity of 99 percent has been quoted for MDCTU in detecting bladder neoplasms, when compared with cystoscopy.[35]

PUJ Obstruction

In patients with PUJ obstruction the success rate of endopyelotomy depends an whether there are crossing vessels at the UPJ. The sucesss rate is only 42% in patients with a crossing vessel and 80% if no crossing vessel is present. A combination of CT angiography with CT urography demonstrates the crossing vessel in relation to the renal pelvis very well.[36]

Congenital Anomalies

In congenital lesion such as retrocaval ureter, not only does CT urography demonstrate the ureteric compression but also the IVC which is the cause for the retrocaval ureter. Ureteral duplication is another congenital anomaly (Figs 3.25A to C). The entire course of both upper and lower moiety must be demonstrated as well as the ectopic opening. Often the upper moiety with lower ectopic opening is hydronephrotic with a hydroureter. MCDTU has ability to demonstrate both functioning and nonfunctioning components.[37] MDCT can also display anomalies such as crossed fused ectopia, horseshoe kidney and renal ectopia (Figs 3.26A to C).

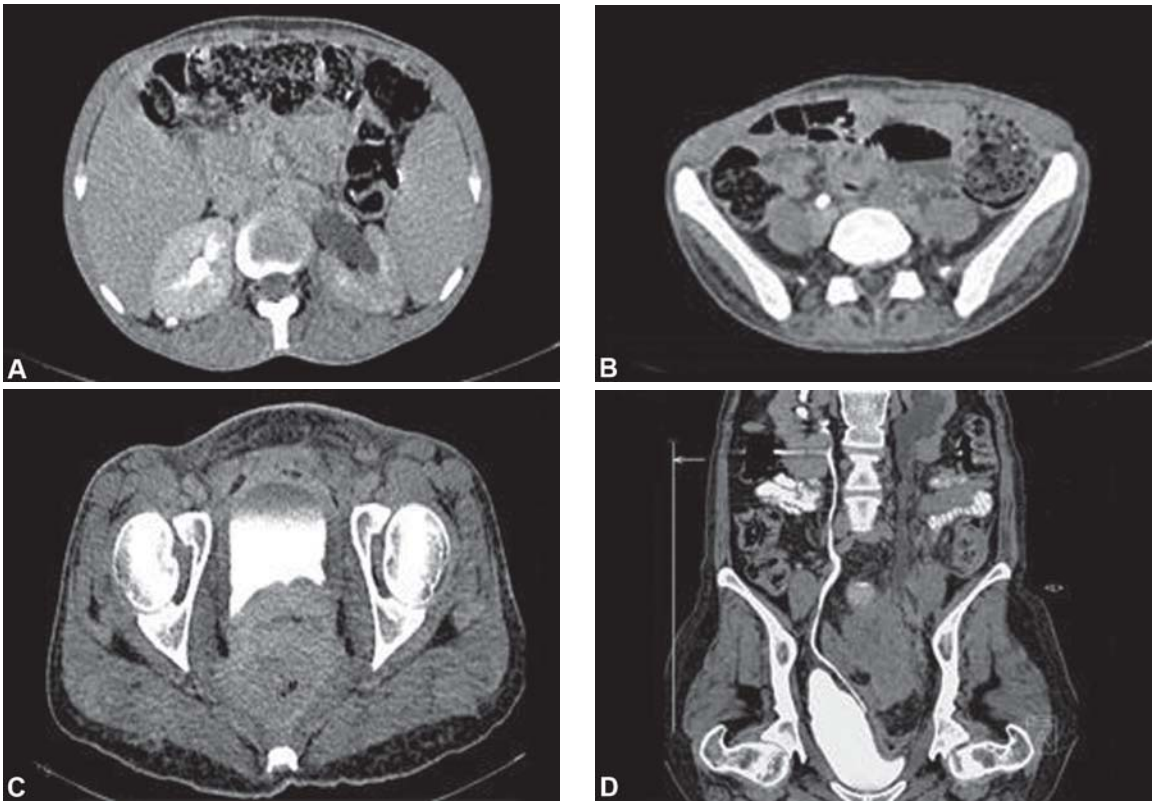

Figs 3.22A to D: Contrast enhanced axial scans of the abdomen showing left hydronephrosis **(A)** dilated left ureter **(B)** Consequent to carcinoma cervix which has infiltrated the left ureter. The mass is also showing loss of planes with the bladder and rectum **(C)** Curved MPR image **(D)** Depicting the infiltration of the left ureter by cervical mass and proximal hydroureteronephrosis with delayed opacification of the pelvicalyceal sysem on the left side. The normal well-opacified pelvicalyceal system and ureter is seen on the right side

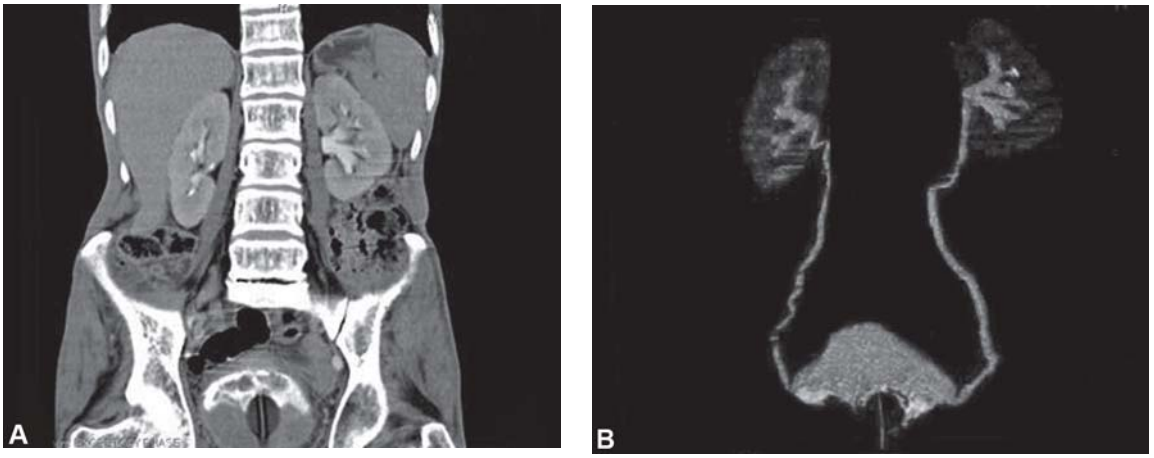

Figs 3.23A and B: Coronal MPR image: **(A)** revealing diffuse circumferential thickening of the bladder base with hydronephrosis seen in both kidneys (left > right). Foley's bulb is seen *in situ*. VRT image **(B)** showing the mass at the bladder base with backpressure changes on both sides, more marked on the left side—Carcinoma bladder *(For color version of Fig. 3.23B see Plate 2)*

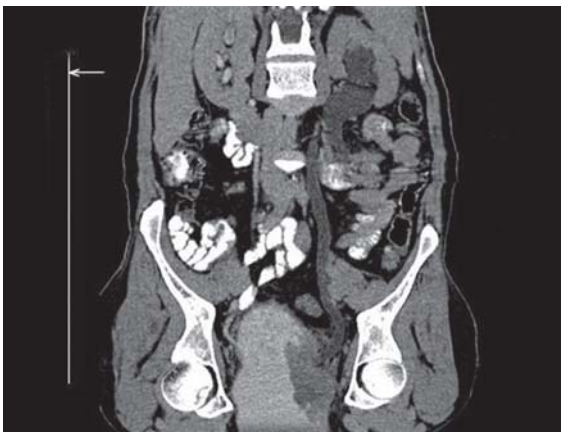

Fig. 3.24: Curved MPR image depicting a mass involving the left lateral wall of the urinary bladder with involvement of the left ureterovesical junction and consequent left hydroureteronephrosis and delayed opacification of the left side as compared to the normal contralateral right side—carcinoma bladder.

MDCTU Protocol

The most commonly used MDCTU protocol comprises a three phase protocol, which consists of an initial unenhanced phase, a second phase following the administration of nonionic contrast material (100-150 ml of 300 mg/ml iodine concentration at a rate of 2-4 ml/second) acquired following 90-100 sec delay also known as the nephrographic phase. This phase is followed by pyelographic phase contrast taken 12-15 minutes following contrast to evaluate the urothelium from the pelvicalyceal system to the bladder.[23] A four phase protocol consists of two excretory phases (5 mintues and 7.5 minutes) to optimize ureteric distension and opacification. However, because of radiation dose a three phase protocol is considered sufficient.

Split Bolus MDCT Urography with Synchronus Nephrographic and Exceretory Phase Enhancement

Chai and colleagues have proposed the use of a split bolus technique in place of a single

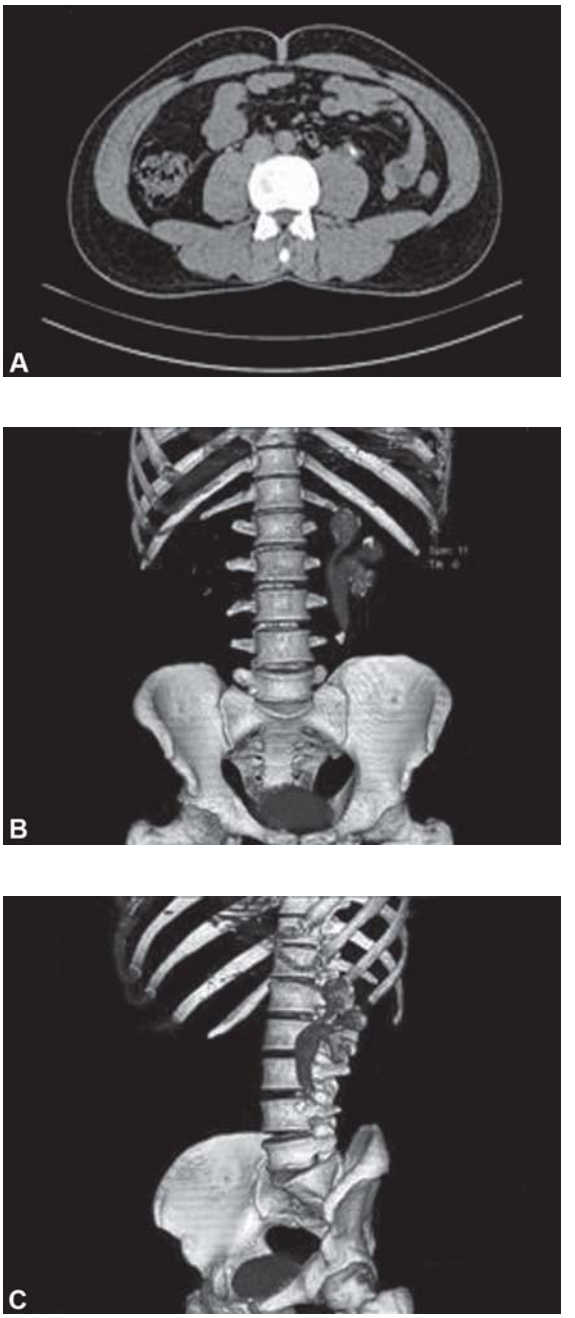

Figs 3.25A to C: Noncontrast CT: **(A)** Depicting a left ureteric calculus. CT urogram using volume rendering **(B and C)** shows the pelvicalyceal system to be bifid and the calculus in the upper left ureter *(For color version of Figs 3.25B and C see Plate 2)*

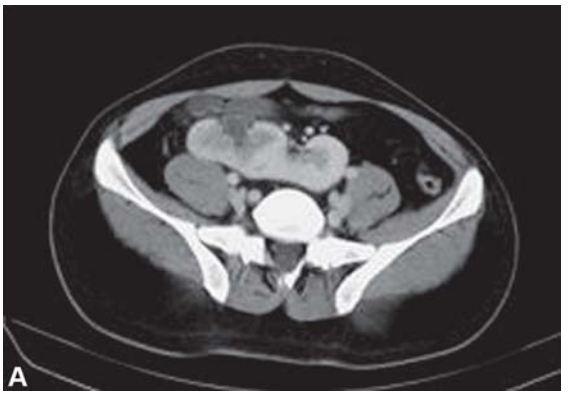

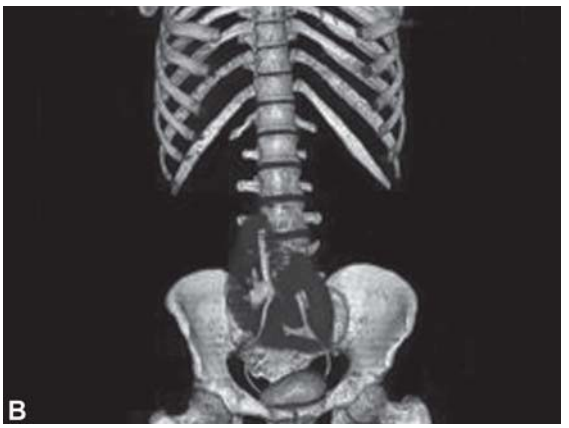

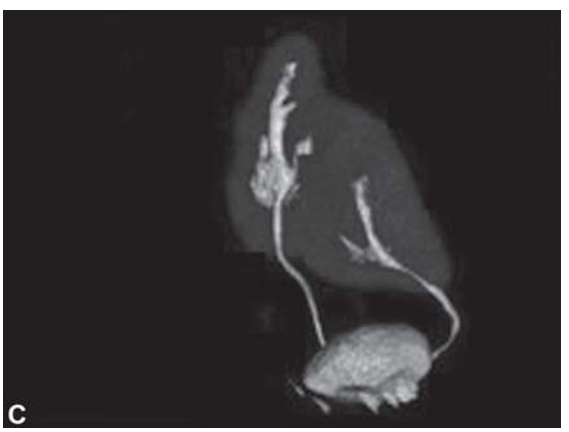

Figs 3.26A to C: Contrast-enhanced axial scans **(A)** Revealing a low lying ectopic kidney with fusion of renal parenchyma of both kidneys. Volume rendered image in the excretory phase **(B)** Depicting the fused low lying ectopic kidney. Volume rendered image with the bone edited out **(C)** Revealing the same – ectopic pancake kidney *(For color version of Fig. 3.26C see Plate 2)*

intravenous injection to facilitate a two phase protocol, namely an unenhanced series of images, and a second phase in which nephrographic and pyelographic phases are simultaneously acquired called the "nephro-pyelographic" phase.[38] With this protocol, after the initial noncontrast administration, 30 CC of nonionic contrast material is infused intravenously and the patient is removed from the CT table. The patient is encouraged to walk for 10 minutes. 10-15 minutes later, the patient is placed in the CT table in the prone-position. A dynamic contrast-enhanced CT is then performed following the administration of and additional 100 cc of nonionic contrast material (300 mg/ml injected at 2 cc/second) following a delay of 100 seconds. Thus in a single "nephro-pyelographic phase" acquisition, the renal paremchyma (nephrographic phase) and the collecting system, ureters and bladder (pyelographic phase) are assessed. The main objective with MDCT urography is to detect all possible causes of hematuria while using the lowest possible radiation dose to the patient. The split bolus technique has the potential to reduce both radiation dose and the number of images generated by MDCT urography.[39]

Techniques to improve urinary tract distension and opacification have been done to achieve adequate opacification and distension of the pelvicalyceal system and ureters.

Compression

Analysis of various data have suggested that the percentage of nonvisualized segments reached upto 25 percent which is not significantly different from CT urography without compression. External compression is not recommended in patients with

abdominal pain or in patients with history of urinary tract obstruction, radical cystectomy, recent surgery and aortic aneurysm. The benefits are outweighed by the added inconvenience and discomfort to the patient. Thus compression is not advocated in most of the centers.

Saline Infusion

It has been seen that saline infusion did not significantly improve ureteric distension or opacification and may simulate ureteric peristalsis in certain cases.[40] Thus saline infusion is usually not included in the MDCTU protocol.

Diuretic Administration

Proponents of low dose diuretic administration have recommended that the diuretic be administered 1 minute before contrast administration. The administration of intravenous diuretic has been reported to increase ureteric distension.

Patient Positioning

It has been reported that MDCTU performed with the patient in the prone position achieved higher opacification of the mid and distal ureters than supine scanning.[41]

Image Interpretation

Interpretation of MDCTU involves review of a large number of images, which includes comparison of unenhanced and enhanced images for presence of calculi and for degree of contrast enhancement which is particularly important for characterization of renal masses. The importance of the state of the art user friendly workstations cannot be overemphasized. MPR and MIP images are most commonly used and are very useful in the evaluation of the ureter and in localizing the exact level of the abnormality. These reformats are also useful in the characterization of urinary tract anomalies.

Thus MDCTU can be used as a "one stop imaging test" for the entire urinary tract.

MULTIDETECTOR CT IN RENAL MASSES

MDCT is accepted as the state of art technology in staging renal cell carcinomas [RCCs] due to its ability to obtain multiple scans through the area of interest. The multiphasic HCT with small and overlapping sections provides increased sensitivity in detection and better characterization of small RCCs and accurate staging of RCCs due to diagnosis of venous tumor extension. For optimal evaluation of a renal mass with MDCT, multiphase imaging is necessary.[28] For all renal imaging, the use of thin (5 mm or less) collimation is essential.[42] Preliminary noncontrast scans are used to detect calcifications and allow quantification of enhancement on the postcontrast scans.

The first phase of contrast enhancement is the **corticomedullary phase** that is essential for accurate staging of RCC. Maximal opacification of the renal arteries and veins allows confident diagnosis of venous extension of tumoral tissue. In evaluation of renal mass special attention is given to visualization of renal vein and IVC junction. Venous extension is shown best during the corticomedullary phase (Figs 3.27A to C). The most specific sign of venous extension is the presence of a hypodense, filling defect within the vein (Figs 3.28A to C). A sudden change in caliber of the renal vein and the presence of a clot within collateral veins are useful ancillary signs. Direct continuity of the thrombus with the primary tumor and heterogeneous enhancement of the thrombus

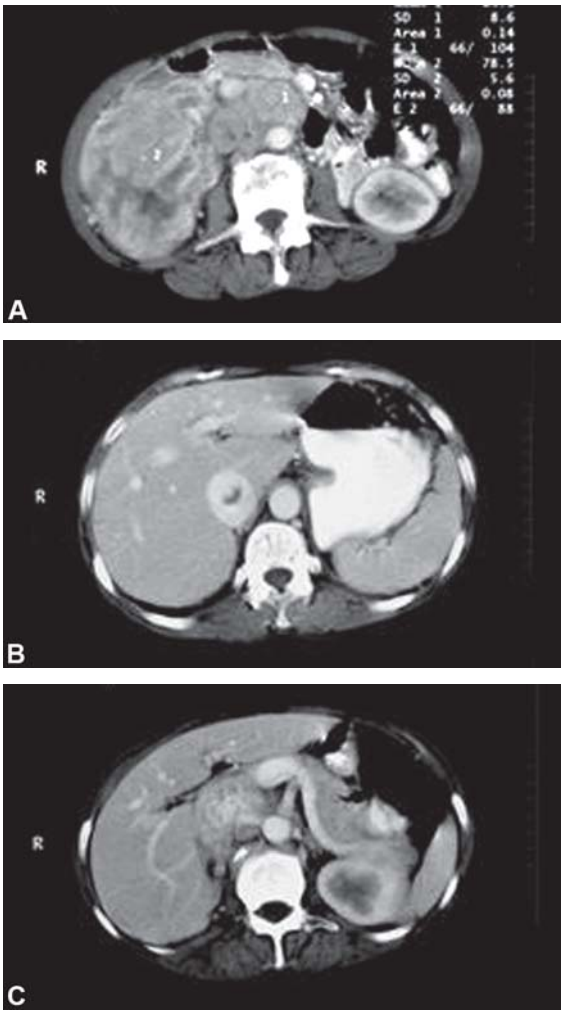

Figs 3.27A to C: Contrast-enhanced axial scan depicting a large and heterogeneous solid mass replacing the right kidney with retroperitoneal lymphadenopathy **(A)** There is a hypodense filling defect in the inferior vena cava **(B)** With patchy contrast enhancement **(C)** s/o Tumoral thrombus with neovascularity – Right RCC with tumoral thrombus

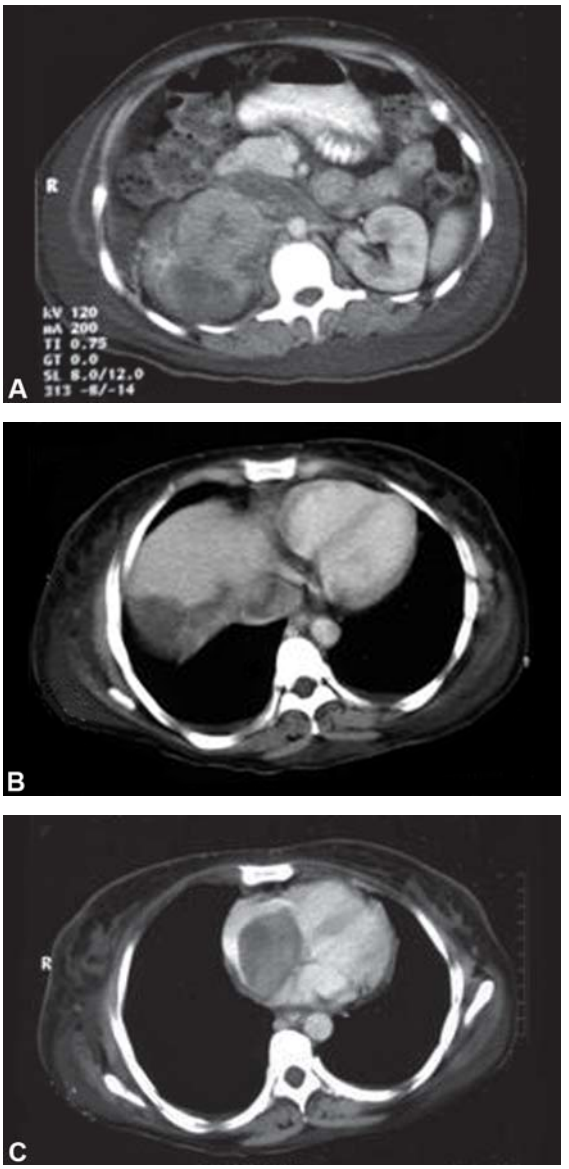

Figs 3.28A to C: Corticomedullay phase of contrast enhancement phase showing a large heterogeneous mass in the right kidney with thrombus in the right renal vein **(A)**. Extension of the thrombus into the IVC **(B)** The right atrium is seen **(C)**

with contrast indicate tumoral thrombus. Accurate demonstration of the arterial anatomy is useful in selected cases to plan nephron sparing surgery.

The **nephrographic phase** is the most useful for detecting renal masses and for characterizing indeterminate lesions. A small lesion can be detected that may blend with the cortex on corticomedullary images. As most RCCS have a rich vascular supply they enhance significantly after contrast administration on

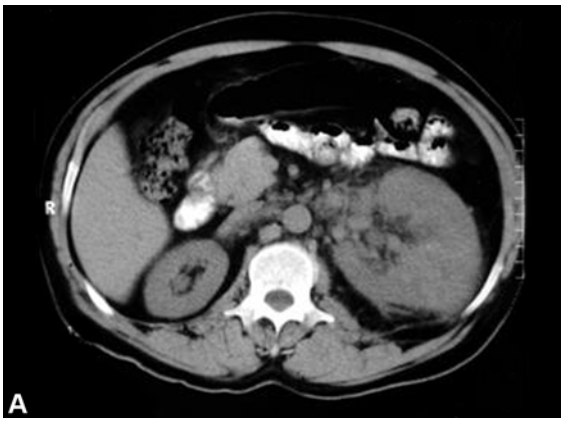

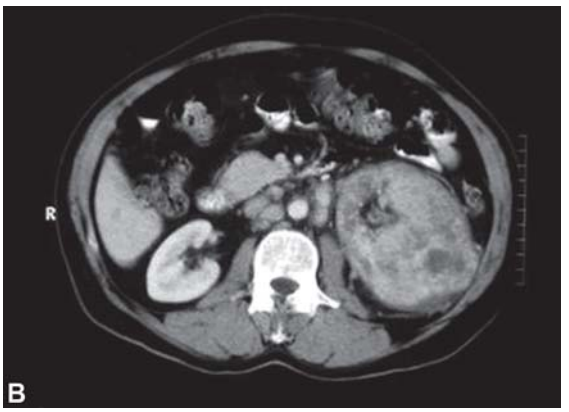

Figs 3.29A and B: Noncontrast axial scan **(A)** showing an indeterminate ill defined mass in the left kidney. Contrast enhanced scan in the nephrogram phase **(B)** shows enhancement of the lesion > 20 HU consistent with a malignant mass

the nephrographic phase. Enhancement value of more than 20 HU is considered suspicious for malignancy.[43] (Figs 3.29A and B). Some less vascular RCC masses enhance 10 to 20 HU and this level of enhancement is seen more frequently with cystic RCC. Sometimes this level of enhancement can be seen in some benign lesions such as complicated cysts.[43]

The excretory phase is useful to delineate the relationship of a centrally located mass with the collecting system better and to define potential involvement of the calyces and the renal pelvis.[28] This phase is useful for detecting transitional cell carcinoma. Measurement of wash out of contrast material from a lesion at 15 minutes may allow differentiation between hyperdense cysts and renal neoplasm.[44] A decrease of 15 HU or more is consistent with a tumor. Alternately, a hyperdense renal cyst shows no change in density between corticomedullary and delayed phase images.[44]

There dimensional CT combined with CT angiography has the potential to provide all the critical information needed to plan the required surgical procedure. The images can be viewed in multiple planes and orientations to define the tumour and its relationship to the renal surface, the collecting system and adjacent organs.[28] A 3-D CT angiogram can display the renal arterial and venous anatomy.

MDCT IN BLUNT RENAL TRAUMA

When examining trauma patients MDCT involving fast volume scanning requires less patient cooperation and creates fewer artifacts. A nonenhanced scan is essential followed by enhanced multiphasic HCT data acquisition. The CMP (Corticomedullary phase) images are best suited to visualize injury of the renal arteries including nonocclusive intimal injury of the main renal artery and renal vein thrombosis. Rapid image acquisition also allows distinguishing extravasations of contrast material due to active hemorrhage visualized during the CMP, from urine extravasations due to rupture of the renal collecting system. Bright enhancement close to the density of nearby arteries within a laceration or around an injured kidney during the CMP phase of CT scanning indicates either contained or active hemorrhage. A contained hemorrhage or

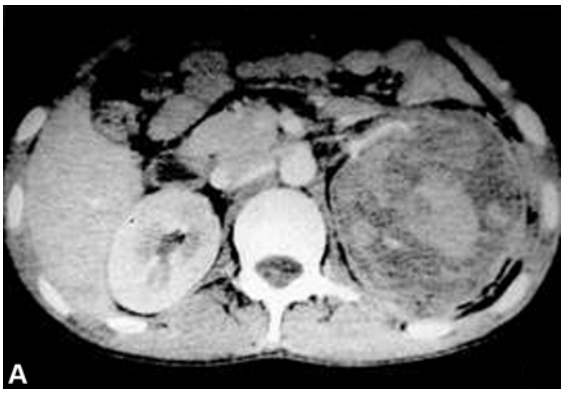

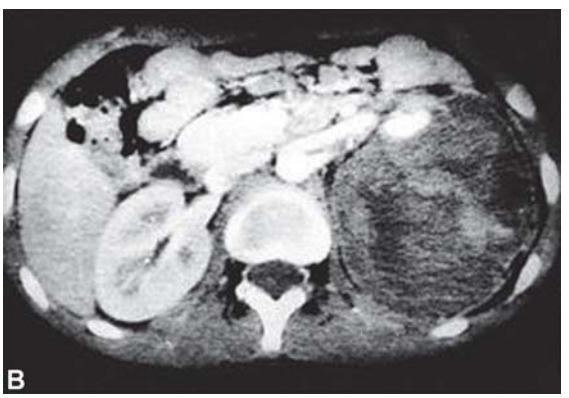

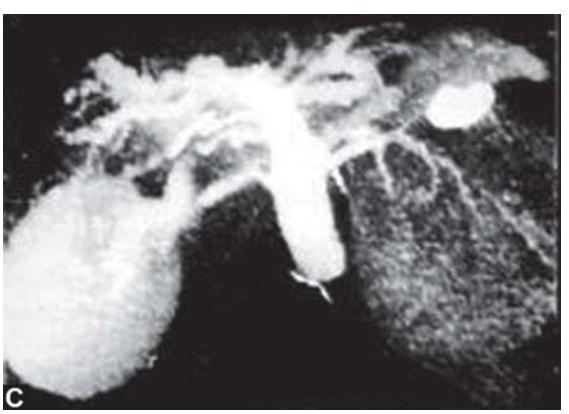

Figs 3.30A to C: Corticomedullary phase **(A and B)** of contrast enhanced CT depicting a large hematoma replacing the left kidney with injury and pseudoaneurysm of the left renal artery. 3-D CT angiogram, MIP technique in oblique axial plane **(C)** Depicting the pseudoaneurysm

pseudoaneurysm is well-circumscribed and contained within the renal parenchyma or laceration (Figs 3.30A to C). Active hemorrhage is ill-defined or flame or waterfall shaped with an associated fresh hematoma which often shows dependent or circumferential layering of older and fresh hemorrhage.[45]

During the nephrographic phase, renal parenchymal injuries and nonperfused parenchymal injuries are best assessed (Fig. 3.31 A and B). The EP images enable to detect contrast extravasation caused by rupture of the renal collecting system. Delayed images

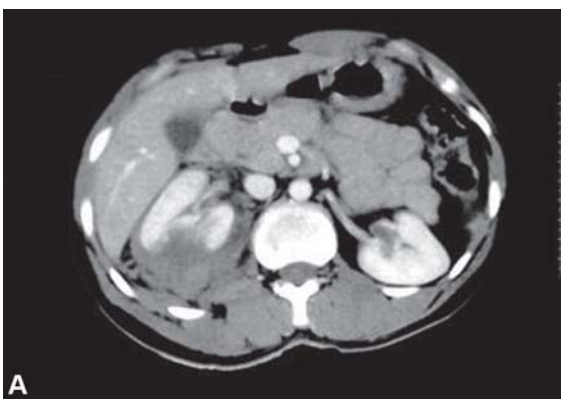

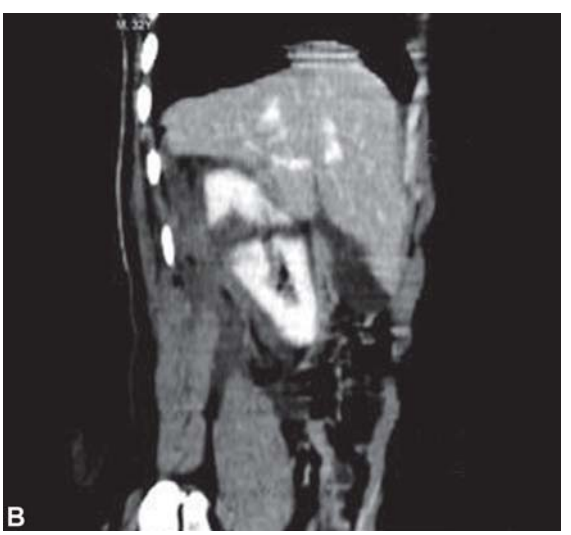

Figs 3.31A to B: Nephrogram phase image **(A)** showing laceration of the right renal parenchyma with perinephric hematoma. Sagittal MPR image **(B)** depicting the fracture of the right kidney

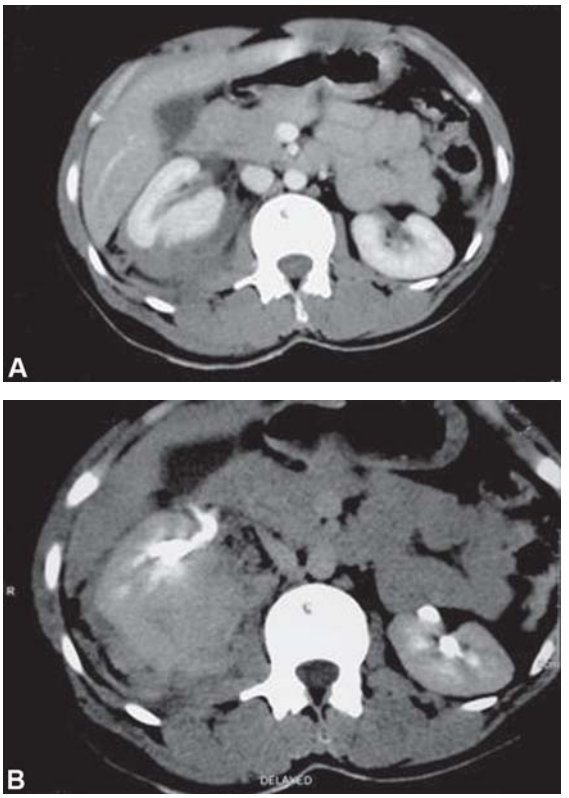

Figs 3.32A and B: CT in the nephrogram phase **(A)** depicting a perinephric hematoma on the right side. Excretory phase image **(B)** depicting the opacified pelvicalyceal system and extravasation of contrast in the perinephric hematoma suggesting rupture of the pelvicalyceal system

(10 to 15 minutes) are obtained to evaluate for urinary contrast extravasations (Figs 3.32A and B). Multiplanar reconstructions [MPR] provide better demonstration of complex injuries of the renal parenchyma and improves the demonstration of the size of the hematomas and urinomas.

If bladder injury is a clinical concern (gross hematuria or pelvic ring fracture) a cystogram or CT cystogram should be performed. CT cystography is capable of distinguishing intraperitoneal, extraperitoneal or combined bladder rupture.[46] For CT cystography once the abdominal CT is complete a retrograde instillation of dilute iodine based contrast (10-12 ml of 300 strength contrast in 500 ml normal saline) is done and the pelvis is scanned again when the bladder is fully distended taking care to include the entire urinary bladder.

MDCT IN EVALUATION OF FLANK PAIN AND URINARY CALCULI

Unenhanced CT has been demonstrated to be the most accurate and efficient diagnostic imaging means to evaluate urinary lithiasis. Fielding et al have reported a 98% sensitivity and 100% specificity.[47] Niall et al have reported a sensitivity of 100% and specificity of 92% in detection of urolithiasis.[48] Using MDCT, thin collimation (3 to 5 mm) noncontrast scans are obtained through the abdomen from the superior aspect of the kidneys (or from the dome of the liver) through the inferior aspect of bladder base or pubic symphysis within seconds. Regardless of their calcium content, almost all urinary tract calculi are radiopaque on noncontrast scans. Reconstructed images such as MPR and CPR are useful in demonstrating the exact location of stones and their relationship to the ureter. Noncontrast CT is also helpful in detecting nonobstructing calculi in patients who have hematuria. Stone size is the single most reliable indicator of stone passage and can be measured accurately on CT[49] (Fig. 3.33).

The most specific diagnostic finding of urolithiasis is the identification of a stone within the ureter. The second important finding is the "rim sign," seen as 1 to 2 mm of soft tissue thickening around the stone secondary to ureteral wall edema at the site of stone impaction.[50] (Fig. 3.34). Other secondary CT findings of urolithiasis are dilatation of the ureter or collecting system, asymmetric

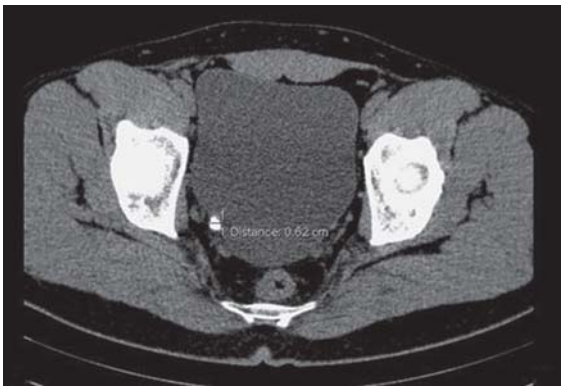

Fig. 3.33: Noncontrast CT shows a radiodense focus at the right uretero vesical junction suggestive of a calculus. The calculus is measuring 6 mm in size

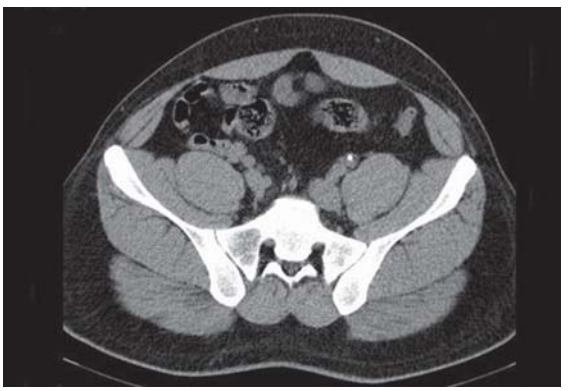

Fig. 3.34: Noncontrast CT scan showing a calculus in the midureter with a soft tissue rim around it consistent with the "rim sign" seen in a calculus

enlargement or decreased density of the kidney, and perinephric stranding. Renal edema from obstruction results in loss of the hyperdense pyramid (white pyramid sign) and the attenuation of the parenchyma on the obstructed side is 5 to 14 HU less than on the normal side, an objective finding of obstruction.[51] (Fig. 3.35)

Some degree of uretral edema and thickening can be seen if a stone already has passed into the bladder. To decide whether or not a distal ureteral stone is in the ureterovesical junction or in the bladder, prone position imaging can be useful.

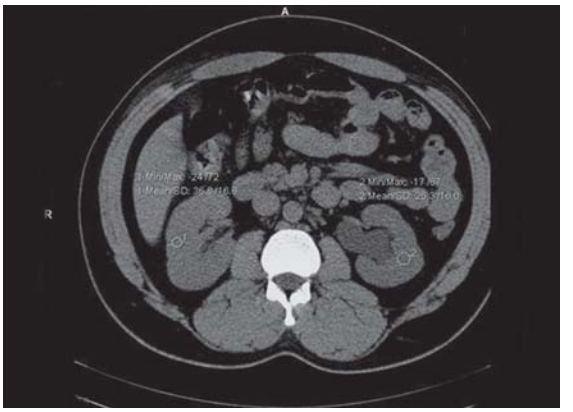

Fig. 3.35: Noncontrast CT showing a hydronephrotic left kidney with attenuation of the renal parenchyma on the left side 10 HU less than that of the contralateral right side, an objective finding of obstruction on the left side

Pelvic phleboliths, arterial vascular calcification, calcified vas deferens, and a calcified appendicolith can be considered a differential diagnosis of ureteric calculi. Phleboliths often show a central lucency, whereas true calculi are as dense or more dense at the center than at the periphery. Another useful sign for diagnosing phlebolith is the comet-tail sign, which is a linear or curvilinear soft tissue structure represented by the noncalcified vessel, extending from an abdominal or pelvic calcification; its positive predictive value for phlebolith is 100%.

Another advantage of CT is its ability to detect nongenitourinary and nonstone disease which may be the cause of pain such as appendicitis, diverticulitis biliary colic, etc.[52]

MDCT IN RENAL INFECTIONS

MDCT is more useful than IVU or ultrasonography for the assessment of renal infection.[53] The main purpose of renal imaging is to obtain information regarding the nature and extent of the disease process

and to identify any significant complications such as gas forming infection, abscess and urinary obstruction.[54]

The diagnosis of acute pyelonephritis is based on clinical and laboratory finding in most cases, and routine imaging, therefore, is unnecessary. When a definite diagnosis of acute renal infection is not established or patients present with recurrent episodes of infection, renal imaging is indicated because of an increased possibility of stones, obstruction, abscess, or a congenital anomaly. After noncontrast CT, a contrast-enhanced study is essential, including angionephrographic or corticomedullary and nephrographic phases, for a complete evaluation of patients who have renal inflammatory disease to demonstrate alterations in the renal parenchymal perfusion and excretion of contrast material that may occur as a result of the inflammatory process.[54] The most common CT finding of acute pyelonephritis is ill-defined, wedge-shaped lesions of decreased attenuation radiating from the papilla to the cortical surface, with or without swelling. This finding may be subtle in the corticomedullary phase. This perfusion abnormality is detected best in the nephrographic phase. Another characteristic finding of acute pyelonephritis is a striated nephrogram on contrast-enhanced CT, consisting of linear bands of alternating hypoattenuation and hyperattenuation oriented parallel to the axes of the tubules and collecting ducts.[55] (Figs 3.36A to C). Diminished concentration of contrast material in the tubules, caused by tubular obstruction by inflammatory cells and debris, ischemia, and interstitial edema, results in this characteristic CT finding. Other useful secondary CT findings of acute pyelonephritis are global or focal enlargement of the kidney, thickening of the pelvicalyceal wall, obliteration of the renal sinus and

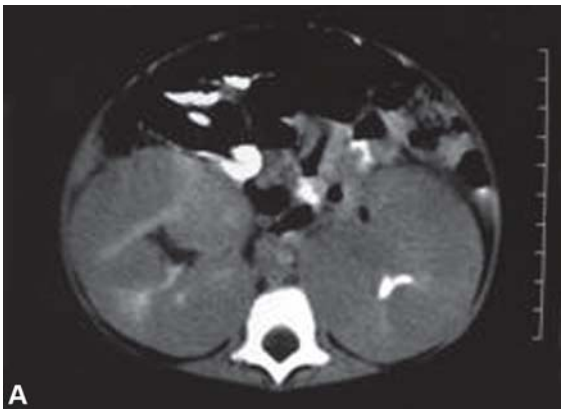

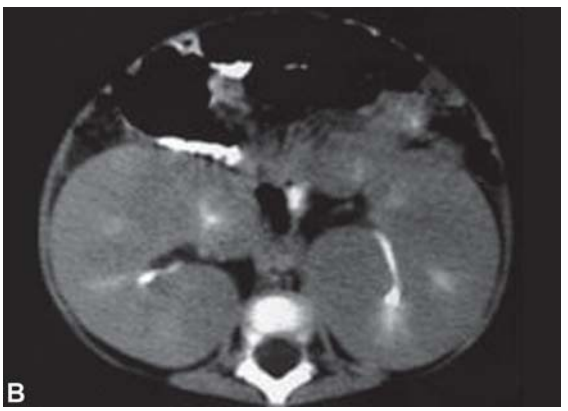

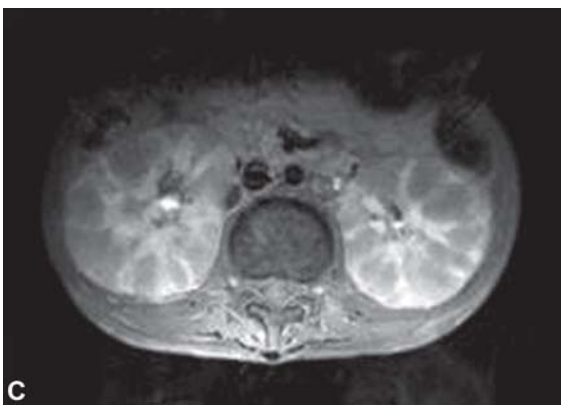

Figs 3.36A to C: Nephrogram phase images **(A and B)** revealing a striated nephrogram consisting of linear bands of alternating hypoattenuation and hyperattenuation oriented parallel to the collecting ducts. Both the kidneys are enlarged. Haste axial MR image **(C)** depicting hypointense areas radiating from the papilla to the cortical surface—acute pyelonephritis

perinephric fat planes, focal calyceal obliteration, and thickening of the fascia of Gerota.[56] Scarring resulting from pyelonephritis may be demonstrated by MDCT as focal thining of the cortex or extensive contour abnormalities. VRT images may be useful for demonstrating focal defects resulting from abscess foci related to pyelonephritis.

HELICAL CT FOR LOWER URINARY TRACT AND PELVIS

Oral contrast opacification of small and large bowel is essential to perform a diagnostic pelvic CT. Patients drink 450 ml of water soluble contrast medium 10 to 12 hours before the examination to opacify the large bowel and 450 ml, 45 mins preceding the study to opacify pelvic small bowel. In patients with suspected ovarian cancer, pelvic inflammatory disease, endometriosis, diverticulitis or rectal cancer 200 ml water soluble contrast enema may be ideal to delineate disease extent. Intravenous contrast medium is used to opacify the bladder and ureter, enhance solid tumor components of bladder and ovarian cancer, endometrial sarcoma and gestational trophoblastic disease, differentiate iliac vessels from lymph nodes, enhance myometrium and visualize the endometrial cavity. With current high resolution fast CT scanners an optimum contrast enhancement technique uses mechanical injector to give 150 ml of 60 percent contrast at the rate of 2 ml/second.

A standard pelvic CT scan consists of contiguous 8 to 10 mm sections from the level of the symphysis pubis cephalad to the iliac crest. This protocol optimizes parenchymal enhancement as well as vascular opacification for lymph nodes metastasis detection. In cancer staging or abdominopelvic mass evaluation, sections are then taken at 1 to 1.5 cm intervals from the iliac crest to the diaphragm to screen for hydronephrosis and metastatic disease. At the end of the abdominal study additional 2 to 5 mm sections may be taken through pelvic tumor or small masses to define local extension better and eliminate the problem of volume averaging of mass and normal adjacent structures. Delayed thin sections through the pelvis delineate the interface between a mass and the contrast filled bladder and pelvic ureters. (Figs 3.37A and B).

Measurement of the volume of an organ can be readily calculated by tracing the organ of interest with an electronic computer cursor

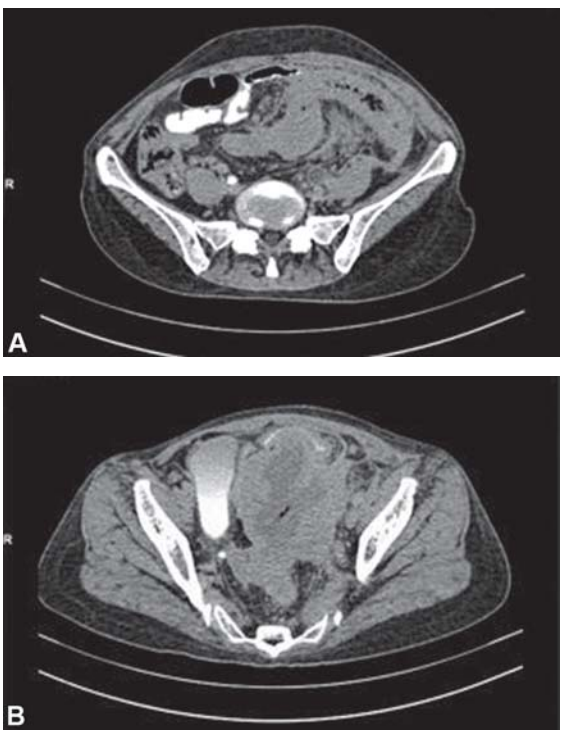

Figs 3.37A and B: Contrast-enhanced axial scans in a case of carcinoma cervix showing the mass in the cervix with normal opacified right ureter. The left ureter is infiltrated by the mass and shows absence of contrast opacification

and summating the surface area measurements obtained on the individual scans. This area is then multiplied by the slice thickness to determine the segmental volume. The total volume of the organ to be measured is computed by the addition of all segmental volumes. CT of the pelvis, in either males or females, usually is obtained in conjunction with CT, of the abdomen. Incidental gynecologic finding are visualized more frequently now, because the adnexa, for example, are better seen with MDCT than on single-slice CT. This improvement results largely from the decrease in partial-volume averaging. Suspected local or systemic disease in the pelvis that prompts CT evaluation can affect the adnexa or uterus, and these abnormalities now can be seen better with MDCT. CT also plays a leading role in the aspiration or drainage of fluid collections such as pus or blood.

MDCT has been used successfully for staging and treatment planning of cervical and ovarian malignancy. CT has an advantage over clinical examination for staging, particularly for detecting ascites, metastases to the liver and pelvic and para-aortic lymph node involvement.[57] In the past, inability to resolve abnormalities smaller than 1 cm has been cited as a disadvantage of CT, but resolution is much improved with new MDCT technology, and partial-volume averaging is significantly decreased. Ultrasound had been claimed to be superior to CT for staging ovarian cancer, because scanning occurs in both transverse and longitudinal planes; however, two-dimensional and three-dimensional reconstructions are now available with new MDCT technology. Coronal, sagittal, and obliqaue multiplanar reconstruction (MPRs) are performed using the source data obtained in the axial plane and can be used to evaluate the complex female pelvic anatomy. In addition to its capability of multiplanar imaging, CT is superior to ultrasound in detecting tumor adherence to bowel, retroperitoneal lymphadenopathy, and peritoneal implants. Further more, oncologists may be more familiar with cross-sectional anatomy as seen with CT as opposed to ultrasound.

Evaluation of female pelvic vasculature has included MDCT of fibroids after uterine artery embolization and of pelvic arteriovenous malformations after embolization.

CT ANGIOGRAPHY (CTA) OF RENAL ARTERIES

The diagnostic accuracy achieved by CTA of the renal arteries is highly dependent on the selection and acquisition of imaging parameters and optimization of contrast injection. The quality of CTA of renal arteries is maximized by minimizing collimation, reconstruction interval and table feed. Because of the small diameter of the vessels of interest and their parallel or near parallel course to the imaging plane thin nominal section thickness of 1.25 mm and overlapping reconstruction are necessary. An individually timed bolus injection of 150 ml of contrast material (300 mgI/ml) with flow rate of 4 ml/sec provides scanning during the plateau phase of contrast enhancement and improves the quality of CTA. Indications for CTA of renal arteries include the preoperative assessment of number and course of renal arteries in renal donors, assessment of renal vessels crossing the ureteropelvic junction prior to repair of obstruction, the evaluation of renal artery involvement in abdominal aortic aneurysms, the detection of renal artery aneurysms and the evaluation of occlusive renal artery disease. MDCT of the kidney allows delineation of size, number and course of the renal arteries and vein, evaluation of the renal

parenchyma and collecting system and diagnosis of unsuspected conditions that precuide organ donation. CT angiography can depict 100% of the main renal arteries and veins.[58]

The region of interest for scan volume is determined by the initial topogram/axial scans. Conventionally, the region between the superior mesenteric artery and lower border of L3 is chosen so as to include sites of origin of accessory renal arteries. Delay time is determined through prior time density curves of dynamic scanning and patient is instructed for breath holding. Maximum intensity projection [MIP]/shaded surface display [SSD] modes are used. SSD clearly depicts the complex vascular anatomy since it is the best technique for assessing regions of overlapping vessels and vessel origins in relationship to aneurysms of the abdominal aorta. However, SSD cannot display attenuation values of structures which are not within the threshold range and is therefore unable to show intravascular contrast and pathologies such as thrombus and calcification. Further, SSD over or underestimates stenosis depending on the defined threshold. In contrast to SSD, MIP images are not threshold dependent, preserve attenuation information and make structures that do not lie in a single plane visible in their entirety very similar to conventional angiograms (Fig. 3.38). MIP is currently the technique of choice for CTA and is a reliable method for displaying accessory renal arteries. Superimposition of vessels may interfere but this may be overcome by generating multiple images in different projections which can be rotated about an axis to visualize three dimensional vascular relationships.[59]

Volume rendering technique [VRT] avoids extensive loss of information that is inherent in SSD and MIP by retaining all CT data and summing the contributions from all voxels along a line from any viewing angle along the data set. Depth, surface and relative X-ray attenuation are all conveyed with VRT (Fig. 3.39). Adjacent structures to vessels can

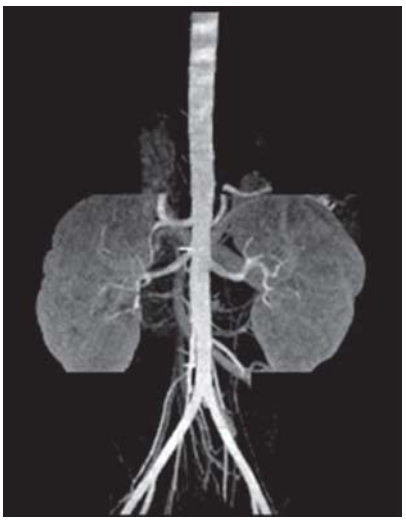

Fig. 3.38: CT angiography using MIP technique depicting the normal renal arteries on both sides

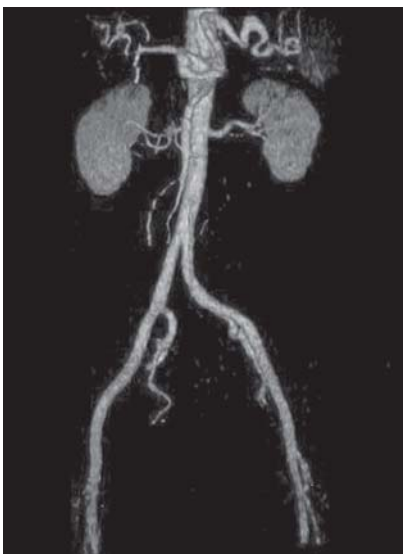

Fig. 3.39: CT angiography using VRT technique depicting the normal renal arteries on both sides *(For color version see Plate 2)*

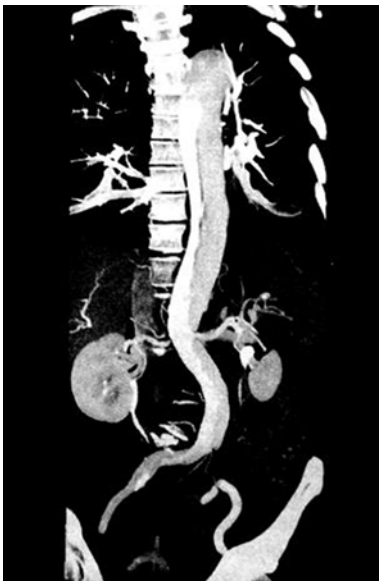

Fig. 3.40: CT angiography using volume rendering technique depicting fusiform aneurysm of the aorta with dissection. The true lumen opacified with contrast and the non-opacified false lumen are clearly seen. The renal arteries are however normal

be displayed and the 3-D data set can be interactively modified in any orientation to optimize depiction of the renal vascular anatomy[60] (Fig. 3.40).

VIRTUAL CYSTOSCOPY/ENDOSCOPY

Over the last few years the technique of virtual cytoscopy/endoscopy has been significantly refined and clinically tested. A volumetric dataset is acquired, the images are computer rendered to generate 3-D images. Special software then allows navigation through the bladder. Virtual cystoscopy may prove to be useful for detecting bladder lesions greater than 5 mm. Virtual endoscopic techniques may provide ureteral "fly-throughs" allowing the observer to have a ureteroscopic view point of the urinary tract.[60]

CT examination includes unenhanced scanning covering the entire urinary tract, contrast-enhanced scanning covering the abdomen and pelvis at a scan delay of 100-120 seconds and dedicated scanning for bladder evaluation. IV contrast material is administered in a power injector at a dose of 2 ml/kg of body weight at a rate of 3 ml/sec to a maximum of 150 ml. After the first two scans are obtained the patient gets down from the CT machine and is asked to report to the CT room when he or she feels a desire to void (90-140 minutes after IV injection of contrast material) and delayed CT is performed for bladder evaluation. Immediately, before the CT examination, all patients are asked to take supine and prone positions four times to obtain adequate mixing of the contrast material and urine in the bladder. Adequate mixing is obtained when high attenuation fills the entire bladder lumen homogeneously and there is no fluid–fluid level caused by unopacified urine. The CT data is then transferred to a workstation for reconstructing virtual cystoscopy and multiplanar reconstruction images. The interactive navigation and interpretation of 3-D virtual reality imaging is performed.

Virtual cystoscopy has advantages over multiplanar reconstruction and source CT images.[61] First, virtual cystoscopy is dedicated for evaluating the mucosal surface of the bladder and therefore, can detect superficial lesions missed by multiplanar reconstruction or source CT images. Second, virtual cystoscopy can allow the operator to navigate the muscosal surface of the bladder in various projections.[62] A major advantage of virtual cystoscopy is its noninvasive nature. It is not associated with the risk of local infection, bladder perforation stricture or scarring.[63,64] It can be taken as a tool for initial screening of patients with hematuria

and more accurate patient selection for invasive cystoscopy.

In conclusion for every practicing radiologist an adequate knowledge of 3-D anatomy of the urogenital system, a clear understanding of its physiology and that of contrast media is required. Improvements in scanner technology, coupled with affordable and powerful computer graphics systems have resulted in superb image generation and visualization tools for the radiologist and the clinician. Although the advanced visualization techniques do not actually create new anatomic data above and beyond the source cross-sections, using these tools to display the data in new ways that more closely simulate natural 3-D scenes may create additional new visual information about the patient. The current challenge is to prove that the additional effort and expense are justified by improving patient care through more accurate diagnosis, improved patient outcome and improved communication with the referring physician.

REFERENCES

1. Schreyer HH, Uggowitzer MM, Ruppert-Kohlmayr A. Helical CT of the urinary organs. Eur Radiol 2002;12:575-91.
2. Moss AA, Gamsu G, Genant HK. Computed Tomography of the Body with Magnetic Resonance Imaging Philadelphia: WB Saunder Co 1992;2(3):20.
3. Haaga JR, Lanzieri CF, Sartoris D, et al: Computed Tomography and Magnetic Resonance Imaging of the Whole Body St Louis: CV Mosby Co., 1994;3(2):35-38.
4. Mc Collough CH, Zink FE. Performance evaluation of a multislice CT system. Med Phy 1999;26:2223-30.
5. Rydberg J, Buck Walter KA, Caldemeyer KS et al. Multisection CT: Scanning techniques and clinical applications. Radiographics 2000;20:1787-806.
6. Kocakoc E, Bhatt S, Dogra VS. Renal Multidetector Row CT. Radiol Clin N Am 2005;43: 1021-47.
7. Napoli A, Fleischmann D, Chan FP, et al. Computed tomography angiography: State of the art imaging using multidetector row technology. J Comput Assist Tomography 2004;28:S32-45.
8. Rydberg J, Liang Y, Teague SD. Fundamentals of multichannel CT. Radiol Clin North Am 2003;41:465-74.
9. Foley WD. Special focus session. Multidetector CT: Abdominal visceral imaging. Radiographics 2002;22:701-19.
10. Kalra MK, Maher MM, D'souza R, et al. Multidetector computed tomography technology: Current status and emerging developments. J Comput Assist Tomogr 28 (suppl 1): 2004;S2-6.
11. Lawler LP, Jarret TW, Corl FM, et al: Adult ureteropelvic junction obstruction: Insights with three dimensional multidetector row CT. Radiographics 2005;25:121-34.
12. Tunaci A, Yekeler E. Multidetector row CT of the kidneys. Eur J Radiol 2004;52:56-66.
13. Wintersperger BJ, Nikolaou K, Becker CR. Multidetector row CT angiography of the aorta and visceral arteries. Semin Ultrasound CT MR 2004;25:25-40.
14. Sheth S, Fishman EK. Multidetector row CT of the kidneys and urinary tract: Techniques and applications in the diagnosis of benign diseases. Radiographics 2004;24(2):20.
15. Yuh BI, Cohan RH. Helical CT for detection and characterization of renal masses. Semin Ultrasound CT MRI 1997;18:82-90.
16. Saunders HS, Dyer RB, Shifrin RJ. The CT nephrogram: Implications for evaluation of urinary tract disease. Radiographics 1995;15: 1069-85.
17. Szolar DH, Kammerhuber F, Altziebler S, et al. Multiphasic helical CT of the kidney: increased conspicuity for detection and characterization of small (<3 cm) renal masses. Radiology 1997;202: 211-17.
18. Urban BA. The small renal mass: What is the role of multiphasic helical scanning. Radiology 1997;202:22-23.
19. Garant M, Bonaldi UM, Taourel P, et al. Enhancement patterns of renal masses during multiphasic helical CT acquisitions. Abdom Imaging 1998;23:431-36.

20. Rubin GD. 3-D imaging with MDCT. Eur J Radiol 2003;45 (Suppl 1):S37-41.
21. Cademartiri F, Luccichenti G, Van Der Lugt A, et al. Sixteen row multislice computed tomography: Basic concepts, protocols and enhanced clinical applications. Semin Ultrasound CT MR 2004;25:2-16.
22. Lockhart ME, Smith JK.: Technical considerations in renal CT. Radiol Clin N Am 2003;41:863-75.
23. Nolte Ernsting C, Cowan N. Understanding multislice CT urography techniques: many roads lead to Rome. Eur Radiol 2006;16:2670-86.
24. Sourtzis S, Thibeau JF, Damry N, et al. Radiologic investigation of renal colic: Unenhanced helical CT compared with excretory urography. AJR 1999;172:1491-94.
25. Maher MM, Kalra MK, Rizzo S, et al. Multidetector CT urography in imaging of the urinary tract in patients with hematuria. Korean J Radiol 2004;5:1-10.
26. Bell TV, Fenlon HM, Davison BD, et al. Unenhanced helical CT criteria to differentiate distal ureteric calculi from pelvic phleboliths. Radiology 1998;207:363-67.
27. Guest AR, Cohan RH, Korobkin M, et al. Assessment of the clinical utility of rim and comet tail signs in differentiating ureteral stones from phleboliths. AJR 2001;177:1285-91.
28. S heth S, Scatarige JC, Horton KM, et al. Current concepts in the diagnosis and management of renal cell carcinoma: Role of multidetector CT and three dimensional CT. Radiographics 2001;21:S237-54.
29. Browne RF, Meehan CP, Colville J, et al. Transitional cell carcinoma of the urinary tract: Spectrum of imaging findings. Radiographics 2005;25(6):1609-27.
30. Caoili EM, Cohan RH, Korobkin M, et al. Urinary tract abnormalities: Initial experience with multidetector row CT urography. Radiology 2002;222:353-60.
31. Cowan NC, Turney BW, Taylor NJ, et al. Multidetector computed tomography for diagnosing upper urinary tract urothelial tumour. BJU Int 2007;99:1363-70.
32. Fritz GA, Schoellnast H, Deutschmann HA, et al. Multiphasic multidetector row CT (MDCT) in detection and staging of transitional cell carcinomas of upper urinary tract. Eur Radiol 2006;16:1244-52.
33. Kalra MK, Maher MM, Sahani DV, et al. Current status of multidetector computed tomography urography in imaging of the urinary tract. Curr Probl Diagn Radiol 2002;31:210-21.
34. Dillman JR, Caoili EM, Cohan RH. Multidetector CT urography: A one stop renal and urinary tract imaging modality. Abdom imaging 2007;32:519-29.
35. Turney BW, Willatt JM, Nixon D, et al. Computed tomography urography for diagnosing bladder cancer. BJU Int 2006;98(2):345-48.
36. Kim JK, Cho KS. CT urography and virtual endoscopy: Promising modalitiies for urinary tract evaluation. BJR 2003;76:199-209.
37. Kohli A. Has the time come to write the EPITAPH for the intravenous urogram? Ind J Radiol Imaging 2005;15:161-64.
38. Chai RY, Jhaveri K, Saini S, et al. Comprehensive evaluation of patients with hematuria on multislice computed tomography scanner, protocol design and preliminary observations. Australas Radiol 2001;45:536-38.
39. Chow LC, Kwan SW, Olcott EW, et al. Split bolus MDCT urography with synchronous nephrographic and excretory phase enhancement AJR 2007;189:314-22.
40. Sudakoff GS, Runn PP, Hellman RS, et al. Opacification of the genitourinary collecting system during MDCT urography with enhanced CT digital radiography: Nonsaline versus saline bolus. AJR 2006;186:122-29.
41. McNicholas MMJ, Raptopoulos VD, Schwartz RK, et al. Excretory phase CT urography for opacification of the urinary collecting system AJR 1998;170:1261-67.
42. Zagoria RJ: Imaging of small renal masses: A medical success story. AJR 2000;175:945-55.
43. Sliverman SG, Lee BY, Seltzer SE, et al. Small (< or = 3 cm) renal masses: Correlation of spiral CT features and pathologic findings. AJR 1994; 163:597-605.
44. Macari M, Bosniak MA. Delayed CT to evaluate renal masses incidentally discovered at contrast-enhanced CT: Demonstration of vascularity with deenhancement. Radiology 1999;213:674-80.
45. Willkmann JK, Roos JE, Platz A, et al. Multidetector CT: Detection of active hemorrhage in patients with blunt abdominal trauma. AJR 2002;179:437-44.

46. Morgan DE, Nallamala LK, Kenney PJ, et al. CT cystography: Radiographic and clinical predictors of bladder rupture. AJR 2000;174: 89-85.
47. Fielding JR, Steele G, Fox LS, et al. Spiral computerized tomography in the evaluation of acute flank pain: A replacement for excretory urography. J Urol 1997;157:2071-73.
48. Niall O, Russell J, Mac Gregor R, et al. A comparison of noncontrast computerized tomography with excretory urography in the assessment of acute flank pain. J Urol 1999; 161:534-37.
49. Olcott EW, Sommer FG, Napel S. Accuracy of detection and measurement of renal calculi: *In vitro* comparison of three dimensional spiral CT, radiography and nephrotomography. Radiology 1997;204:19-25.
50. Heneghan JP, Dalrymple NC, Verga M, et al. Soft tissue "rim" sign in the diagnosis of ureteral calculi with use of unenhanced helical CT. Radiology 1997;202:709-11.
51. Georgiades CS, Moore CJ, Smith DF. Differences of renal parenchymal attenuation for acutely obstructed and unobstructed kidneys on unenhanced helical CT: A useful secondary sign? AJR 2001;176:965-68.
52. Smith RC, Verga M, Mc Carthy S, et al. Diagnosis of acute flank pain: Value of unenhanced helical CT. AJR 1996;166:97-101.
53. Akbar SA, Mortele KJ, Baeyens K, et al. Multidetector CT urography: Techniques clinical applications and pitfalls. Semin ultrasound CT MR 2004;25:41-54.
54. Kawashima A, Le Roy AJ. Radiologic evaluation of patients with renal infections. Inf Dis Clin North Am 2003;17:433-56.
55. Kundra V, Silverman PM: Impact of multislice CT on imaging of acute abdominal disease. Radiol Clin North Am 2003,41:1083-93.
56. Kawashima A, Sandler CM, Goldman SM, et al. CT of renal inflammatory disease. Radiographics 1997;17:851-66.
57. Pannu HK, Bristow RE, Montz FJ, et al. Multidetector CT of peritoneal carcinomatosis from ovarian cancer, Radiographics 2003;23(3):687-701.
58. Rankin SC, Jan W, Koffman CG. Noninvasive imaging of living related kidney donors: Evaluation with CT angiography and gadolinuim enhanced MR angiography. AJR 2001;177:349-55.
59. Chow LC, Rubin GD. CT angiography of the arterial system. Radiol Clin North Am 2002;40: 729-49.
60. Kim TS Chung JW, Park JH et al. Renal artery evaluation: Comparison of spiral CT angiography to intra-arterial DSA. J Vasc Inter Radiol 1998;9:553-59.
61. Kim JK, Park SY, Kim HS, et al. Comparison of virtual cystoscopy, multiplanar reformation and source CT images with contrast material filled bladder for detecting lesions. AJR 2005;185:689-96.
62. Bernhardt TM, Schmidl H, Philipp C, et al. Diagnostic potential of virtual cystoscopy of the bladder. MRI vs CT preliminary report. Eur Radiol 2003;13:305-12.
63. Merkle EM, Wunderlich A, Aschoff AJ, et al. Virtual cystoscopy based on helical CT scan datasets: Perspectives and limitations. BJR 1998;71:262-67.
64. Bernhardt TM, Rapp Bernhardt U. Virtual cystoscopy of the bladder based on CT and MRI data. Addom Imaging 2001;26:325-32.

Chapter

4

MRI of Urogenital Tract: Techniques and Normal Appearances

Paramjeet Singh, Sameer Vyas

INTRODUCTION

With recent advances in technology, MR imaging has emerged as single most important modality for evaluation of urogenital tract. The high spatial resolution, intrinsic tissue contrast, short scan time, elimination of motion artifacts and more extensive coverage of abdomen and pelvis provide better detection and characterization of anatomy and pathology of the urogenital tract.[1-5] It has become as an alternative technique to CT scan in view of its multiplanar capability, lack of ionizing radiation and angiographic capabilities.[6-7] In addition MR contrast agents (gadolinium-based) are considered relatively safer as compared to iodinated contrast agents. However, they are also associated with few risk factors which include nephrotoxicity, anaphylactic reaction, reaction at the injection site and nephrogenic systemic sclerosis (NSF).[8] NSF is most important delayed reaction seen as sclerodermalike fibrosing condition, especially in patients who have deranged renal functions. Spectroscopic studies especially in prostate are useful for detection and differentiation of malignant from benign pathologies by non-invasively providing the chemical assay of the assessed tissue. Diffusion weighted imaging (DWI) and dynamic contrast enhancement MR imaging holds good promise in the evaluation of cancers of kidneys, urinary bladder, prostate and female genital tract. High field strength imaging (i.e. 3T) is still in infancy in abdominal applications but is likely to play a greater role in future. Malignant lymph node detection also has improved significantly with new contrast agents, such as iron-based particles.

KIDNEY

Renal MRI has evolved as an alternative or complementary imaging modality to intravenous urography, ultrasonography and computed tomography. It is primarily used as an additional tool of renal imaging in a number of situations. It can be used for evaluation and characterization of renal masses and fluid collections. Internal tissue characters of masses, i.e. presence of fat, necrotic areas or hemorrhage in a cyst or mass can often be better assessed on MRI.[1] Small renal masses can be also diagnosed due to signal alteration produced by them. Because of multiplanar imaging capability, MRI has a definite role for staging of masses. This allows better definition of lesions at the renal poles, i.e. differentiating a renal mass from a suprarenal mass as well as demonstrating the tumor extension in a better way and allowing better

surgical planning. Small tumor detection may be aided by fat suppression combined with gadolinium administration. Evaluation of renal vessels by MR angiography is useful in assessing cephalad extension of renal tumors into renal veins and inferior vena cava and evaluation of renal artery pathology. MRI is an alternative modality in patients with equivocal findings on CT or in whom the use of iodinated contrast material is contraindicated because of an increased risk of adverse reactions or nephrotoxicity, MR contrast media like gadolinium DTPA are dialyzable and are relatively safe in patients with compromised renal function or even overt renal failure. However, NSF is a concern in patients with low glomerular filtration rate (GFR < 30 ml/minute/1.73 m^2) particularly nonionic linear chelates. MR contrast agents are freely excreted by kidneys and reflect GFR and tubular absorption and thus MR pyelography can be used as an alternative technique to intravenous pyelography for demonstrating pelvicalyceal system.

Techniques and Recommended Imaging Sequences

The MR pulse sequences and the precise imaging parameters depend upon the available equipment and the clinical problem in question. Usually both T1 and T2-weighted sequences are performed in the axial plane in combination with sections in coronal and sagittal planes.[3] The spin echo technique usually incorporates flow compensation and respiratory gating to reduce artifacts but gradient echo images (GRE) are preferred due to short examination time allowing breath hold images, thus providing better quality images. T2 fast spin echo (FSE) imaging has more or less replaced the conventional spin echo T2 imaging. Good quality T2-weighted images of high-resolution can be obtained in a short-time using these techniques. In addition, in- and opposed-phase breath hold T1 weighted gradient echo sequences provide an excellent anatomic detail of the retroperitoneum and detection of intracellular lipid.[1] Gradient echo fast low angle shot (FLASH) sequences are used for obtaining sections of the kidneys after contrast administration in corticomedullary, nephrographic and excretory phase, and provide information equivalent to the CT scan. Dynamic MR imaging following administration of a contrast agent also referred as MR renography has emerged as imaging modality of choice in suspected renal diseases as it provide comprehensive evaluation of renal anatomy and physiology.[1,3] It allows the visualization of contrast material within distinct time phase in different intrarenal regions and the signal intensity changes of cortex and medulla can be plotted in a time density curve. Cortical enhancement which primarily reflects renal perfusion is seen earliest, followed by medullary enhancement which reflects mainly glomerular filtration rate, and lastly the enhancement of the collecting system that represents the functional status of the renal tubules.

Normal Appearances

Renal MRI provides separate visualization of the renal cortex and medulla on both T1 and T2-weighted images (Figs 4.1A and B). T1-weighted images show good corticomedullary differentiation with cortex being usually higher in signal intensity compared to the medulla. On T2-weighted images, the renal cortex appears slightly hypointense to medulla.[3] This is due to the fact that cortex

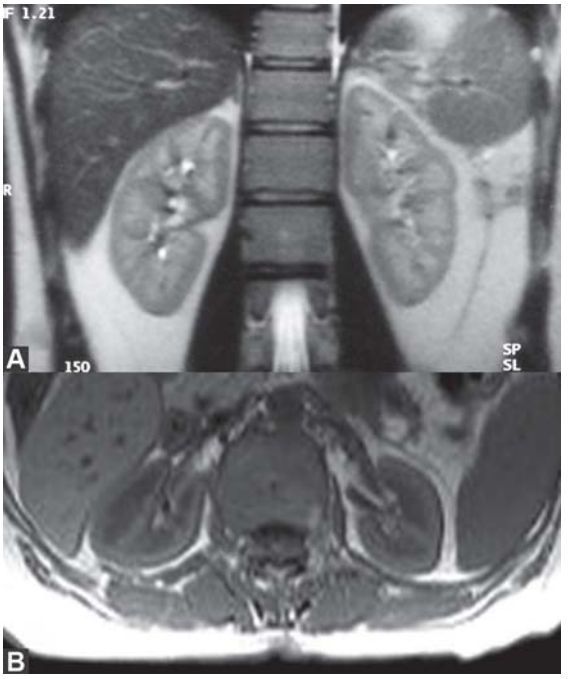

Figs 4.1A and B: Coronal T2 HASTE **(A)** and axial T1 gradient echo FLASH **(B)** images showing good corticomedullary differentiation. The medulla is bright on T2WI compared to cortex. The renal sinus is also bright due to fat and urine. The T1WI show lower signal of the medulla and sinus shows bright fat. The pararenal fat is bright on T1 and intermediate in signal on T2 images

contains less water than the medulla thus has a longer T1 time. The sinus fat at the renal hilum appears bright on both T1 and T2 weighted images. The calyces are generally not well-visualized on MRI but if distended with urine appear dark on T1 and bright on T2 WI. The renal arteries, renal veins, aorta and inferior vena cava are seen as tubular structures that are free from intraluminal signal, although flow related artifacts may cause high signal in these vessels. The renal capsule can be seen as a hypointense line and the pararenal and perirenal fat appears bright. The arterial phase images (20 seconds) provide good corticomedullary differentiation, followed by the venous phase (nephrographic phase; 70 seconds) which are best for detection and characterization of renal masses, and lastly the delayed phase (excretory phase; 180 seconds) delineating the collecting system (Figs 4.2A to D).

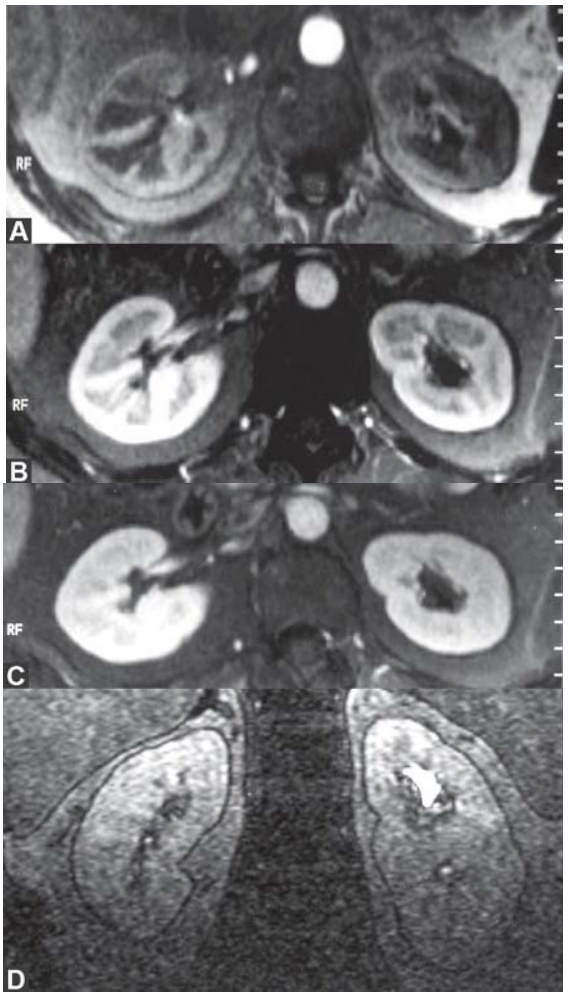

Figs 4.2A to D: Postcontrast dynamic axial **(A,B,C)** and coronal (D) T1 FLASH images. The kidneys show maximal cortical enhancement in arterial phase with good corticomedullary differentiation **(A)**. There is progressive opacification of medulla **(B,C)** with blurred corticomedullary differentiation in venous phase and subsequent appearance of contrast into the pelvicalyceal system **(D)**

MR Urography

MR urography constitutes the evaluation of the collecting system and urinary tract. It is based on the principle that simple fluids, such as urine have very long T2-relaxation time and heavily T2-weighted pulse sequence generate images with high signal intensity from static fluid in the collecting whereas lower signal intensity from parenchymal tissue is suppressed.[4] It is performed using heavily T2-weighted images such as rapid acquisition with relaxation enhancement (RARE) and half fourier acquisition single-shot turbo spin-echo (HASTE) sequences.[5] These sequences are extremely fast and are performed in one breathhold. The fat in the background is suppressed. This is useful in patients where use of ionizing radiation or iodinated contrast material is to be avoided. However, this technique does not provide information about the renal function and may not visualize a non-dilated system. A T1-weighted gadolinium enhanced 3D FLASH sequence is used after a contrast injection of 0.1 mmol/kg and multiple thin sections are obtained. These are processed with maximum-intensity-projection to produce images similar to conventional contrast urography and provide quantitative functional as well as high resolution anatomical information (Figs 4.3, 4.4A and B). Low doses of a diuretic agent can be administered before the examination for better filling of the pelvicalyceal system.

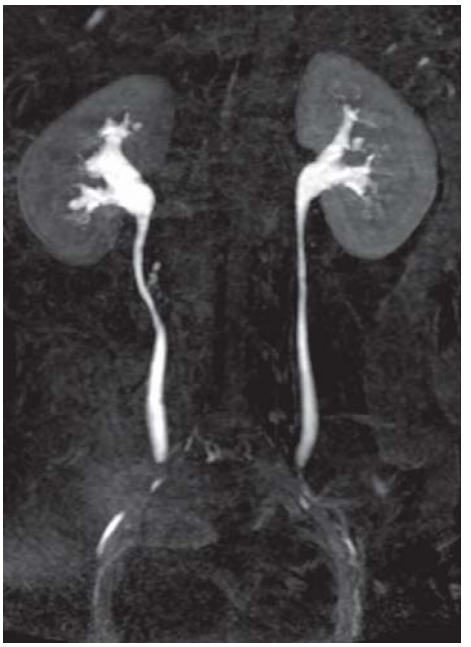

Fig. 4.3: MR urography, T1 FLASH coronal image showing excellent outlining of the pelvicalyceal system and the ureters by excretion of injected gadolinium contrast

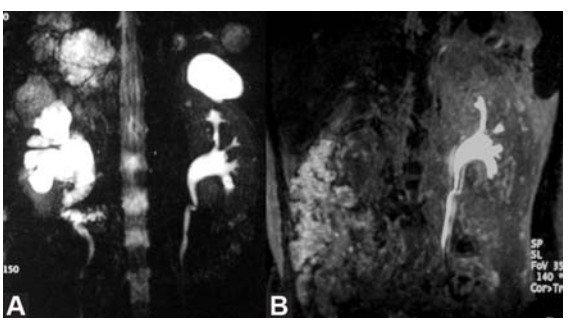

Figs 4.4A and B: Bright fluid (RARE) urogram **(A)** and Gradient contrast excretory urogram **(B)**. Left kidney shows normal appearance of pelvicalyceal system on fluid sensitive sequence **(A)** and shows normal function with actively excreted contrast opacifying pelvicalyceal system on gradient contrast MR urography**(B)**. The right kidney is not functioning due to long standing malignant proximal ureteric obstruction **(B)** while accumulated urine in left PCS Is outlined in A

Renal Angiography and Venography

Contrast-enhanced MR angiography (CEMRA) is accurate and safe technique for evaluation of renal vessels (Figs 4.5A to C). This technique is independent of flow related phenomenon, assesses the true lumen of vessels and has high spatial resolution.[6] Non-contrast MRA techniques such as gradient time of flight (TOF), TRUFISP or phase contrast (PC) techniques render the flowing blood bright (Figs 4.6A to C). However, these techniques

have multiple limitations such as signal loss due to turbulence at the stenosis, over estimation of stenosis due to turbulent jets leading to signal loss, bright signal of fresh thrombus, motion artifacts, non-visualization of small vessels and poor quality due to slow flow.[7] CEMRA is performed during the first pass of contrast, yields arterial detail and later images help in visualization of venous anatomy. An ultra fast 3D T1 gradient echo sequence like FLASH is used to obtain rapid thin slices (1-2 mm) which are reconstructed as maximum intensity projection to yield angiographic images (Figs 4.5 and 4.6).

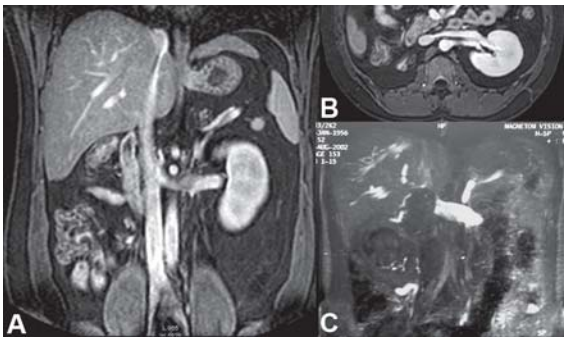

Figs 4.6 A to C: TRUFISP coronal **(A)** and axial **(B)** images showing normal left renal vein lying anterior to the left renal artery **(B).** The vena cava in its entire extent is also shown. **(C)** Left renal vein is obstructed and expanded due to tumor thrombus on a contrast-enhanced venographic image

URINARY BLADDER

Ultrasonography and CT are the primary imaging modalities for evaluation of the urinary bladder. MR plays a limited role in bladder imaging, mostly as a modality for staging of bladder tumors. Its multiplanar capability allows better visualization of tumors located at the bladder base and dome. The exquisite contrast resolution of MRI coupled with multiplanar imaging permits accurate staging of bladder malignancy.[9] MR has also been used for diagnosing fistulas involving the bladder and assessment of the underlying associated abnormalities.

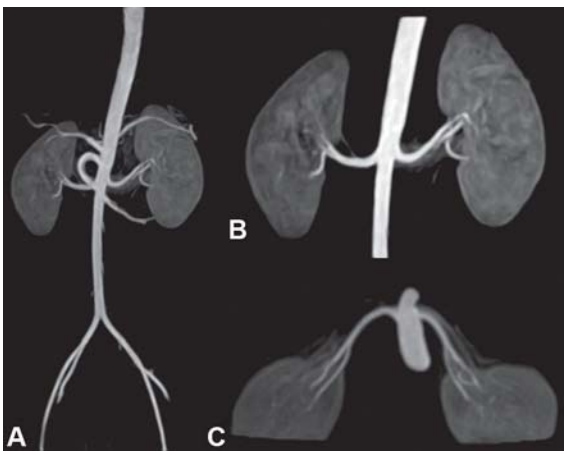

Figs 4.5A to C: 3D Contrast-enhanced angiogram coronal **(A, B)** and axial **(C)** maximum intensity projections showing normal appearance of abdominal aorta and renal arteries. Both the main arterial trunks and segmental branches are outlined

Technique and Recommended Sequences

Phased array coils produce better resolution than the torso coils and have improved the tumour staging capability of MR imaging. They can also show invasion of the bladder wall while body coil can only show gross extra-vesical extension of tumours. Both T1 and T2 W imaging are essential. The T1 SE and T2 FSE are normally used to image bladder in axial, coronal and sagittal planes.[10] It is important to orient the plane perpendicular to the tumor for accurate staging. Lateral walls are best evaluated on axial sections. Sagittal images are essential in evaluating the dome, the base and the anterior and posterior walls of the bladder. Coronal images are complimentary in the evaluation of the dome and base of the bladder and also show the lateral walls in good details. T1WI best demonstrate

exten-sion of the tumor into perivesical fat which normally appears bright. T2WI are most useful for showing invasion of muscular wall and disruption of serosa as these structures show intermediate to low signal intensity on T2-weighted images and invasion by inter-mediate intensity tumor can be better appreciated. Pelvic lymph node metastasis is best assessed on T1WI. An endoluminal coil can be used to assess small tumors at the posterior wall, bladder base or bladder neck. These allow better resolution, signal to noise ratio and field of view.

Normal Appearance

The urinary bladder is clearly demonstrated on MRI regardless of the degree of bladder distension. Since both urine and the muscles have a relatively long T1-relaxation time, both show low signal intensity on T1WI. In contrast to this, the T2-relaxation time of urine and smooth muscles are markedly different, enhancing differentiation between the two on T2WI in which urine appears extremely bright, while bladder wall is hypointense (Figs 4.7A and B). It is important to differentiate the normal low intensity of the bladder wall from the chemical shift artifact caused by different resonant frequency of the hydrogen nuclei of the urine and fat. The chemical shift artifact depends on the direction of the frequency encoding. On axial images, it is seen as a dark band along the lateral wall of one side of the bladder, and a bright stripe along the opposite wall. On sagittal or coronal images the artifact is seen along the base and dome of the bladder. This artifact should not be misinterpreted as bladder pathology. Dynamic contrast enhanced imaging using a fast gradient sequence allows differentiation of tumors from uninvolved bladder wall in most cases if the imaging is completed within 90 seconds as the normal bladder wall enhances later.[9]

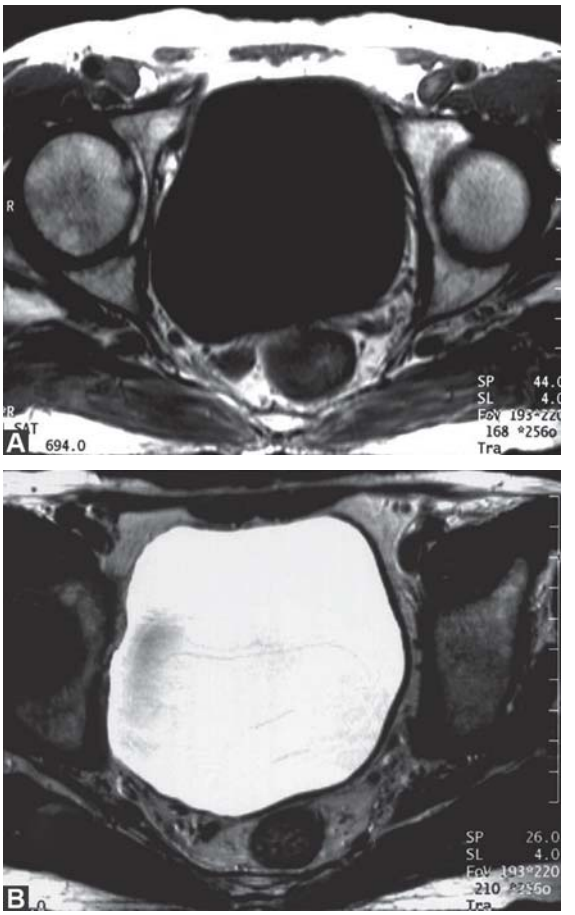

Figs 4.7A and B: T1 and T2-weighted fast spin-echo axial sections **(A,B)** with phased array coil showing normal distended urinary bladder. The urine appears hypointense on T1 with intermediate signal bladder wall (A). The urine appears bright on T2 with low-signal wall (B).The paravesicle fat appears bright on T1 and intermediate signal on T2. The pelvic side walls, rectum and fat planes are well seen

PROSTATE GLAND

Prostate gland is a pyramidal fibromuscular gland which surrounds the urethra from the bladder base to the urogenital diaphragm. It has a thin true capsule, surrounded by

fibrous sheath of pelvic fascia. Between these two layers lies the periprostatic venous plexus. Posterior to the prostate, lie the paired seminal vesicles. The ejaculatory ducts pierce the upper part of the posterior surface of the prostate gland and open into the prostatic urethra at the lateral margin of the prostatic utricle. The prostate gland can be subdivided into two major divisions—the peripheral gland and the central gland. The central gland in turn consists of periurethral glandular tissue, transitional and central zones. MRI has a unique ability to delineate the zonal anatomy of the prostate gland.[12] The zonal anatomy is of clinical importance, as most carcinoma arises in the peripheral zone, whereas benign prostatic hypertrophy affects the transition zone.[11] The relationship of the zones of the gland normally changes with age. In young men the central gland predominantly consists of central zone, whereas in older men with benign prostatic hyperplasia, most of the central gland is transitional zone. The prostate is described conventionally in terms of sextants, based on division of the gland into thirds in the craniocaudal direction (base, midgland and apex), and then into left and right side. Since surgery is potentially curable in a tumor confined to the gland, it is important to diagnose the extracapsular tumor spread, seminal vesicle and other adjacent visceral involvement and pelvic lymphadenopathy. The primary role of MRI is not for tumor detection, but for staging diagnosed cancer. In addition, it helps in cancer localization, in treatment planning and post-treatment follow-up. [13] MR spectroscopic examination is helpful for showing normal and altered tissue metabolism. Functional MR techniques on 3T MRI such as diffusion-weighted images (DWI) and dynamic contrast-enhanced MR imaging (DCEMRI) have evolved as promising new technique in evaluation of prostate cancer. Multimodality MR imaging which includes T2-weighted images, functional imaging and spectroscopic imaging may be able to accurately characterize and stage the carcinoma.

Technique and Recommended Sequences

MRI provides one-stop examination for detailed evaluation of prostate gland, periprostatic and pelvic anatomy. The results of prostate imaging using body coil are not very satisfactory. The combined use of an endorectal coil with a pelvic phased-array coil markedly improves image quality. A balloon mounted endorectal coil placed in the rectum provides the best contrast and spatial resolution for prostate imaging and the pelvic phased array coil provide good pelvic coverage and simultaneously assess pelvic side walls and lymph-adenopathy. Axial spin-echo T1-weighted images are obtained of the entire pelvis, i.e. from aortic bifurcation to the symphysis pubis for detection of the nodal disease.[13] High spatial resolution (thin sections with a small field of view) T2-weighted fast spin echo sections in the axial, coronal and sagittal planes of the prostate and seminal vesicles are useful for tumor detection, localization and staging. Axial T2WI is important in differentiating peripheral and central zones whereas coronal and sagittal images are useful to assess the base and apex of the gland, pelvic muscles, rectum and seminal vesicles. Prostate imaging should not be performed for atleast 4 to 8 weeks (preferably 6 weeks) of a biopsy, as hemorrhage can lead to a false positive and negative interpretation of cancer. Routine use of gadolinium and fat suppression is not recommended. However, contrast may be used in evaluation of prostatic infections and abscesses. However, enhancement of prostate

cancer during the first pass of contrast with fast dynamic imaging has indicated its potential in detecting cancer, especially more aggressive cancers. MR spectroscopy is performed by chemical shift imaging with point resolved spectroscopy (PRESS) voxel excitation and band selective inversion with gradient rephrasing for water and lipid suppression.[13] Diffusion imaging with value from 0 to 800 have been applied to obtain data and create ADC maps which show restriction in high cellularity of tumors. For dynamic contrast-enhanced MR imaging, the data can be evaluated in a semiquantitative (contrast arrival, time to peak, peak enhancement and wash-in-washout gradient) or quantitative approach using pharmacokinetic modeling method.

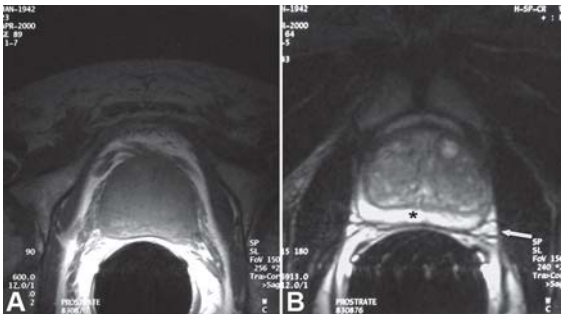

Figs 4.8A and B: T1 **(A)** and T2 **(B)** weighted axial sections of prostate using endorectal coil. The zonal anatomy of prostate is not made out on T1 but the gland contour is well-outlined against bright periprostatic fat. The neurovascular bundle (arrow) is seen at 5 and 7 O'clock positions. T2-weighted image **(B)** shows zonal anatomy, i.e. hyperintense peripheral gland (*) and heterogeneous central zone due to hyperplastic changes. The bright nodule represents glandular hyperplasia and dark areas being stromal hyperplasia. The surgical and anatomical capsules are seen as hypointense structures. The near field signal amplification is seen in proximity of the coil

Normal Appearance of Prostate on MRI

The appearance of prostate on MRI varies depending on the type of coil and technique used. On T1WI the zonal anatomy cannot be appreciated well and the gland is of uniform low signal intensity but post biopsy hemorrhage is better seen in these images. T1WI also show cysts and abscesses well. The zonal anatomy is well-demonstrated on T2WI, where the peripheral zone is seen as a relatively bright area compared to the central gland[12] (Figs 4.8 A and B). It is surrounded by a thin uninterrupted hypointense line comprising true prostatic capsule. The anterior fibromuscular stroma is dark on all pulse sequences (Fig. 4.9). The central and transitional zones are of intermediate signal intensity due to sparse glandular elements. These cannot be differentiated from each other but in older men the transitional zone stands out due to hypertrophy. The verumontanum may be seen on T2WI, where it has high signal intensity. The periprostatic fat is hyperintense on both T1 and T2WI and

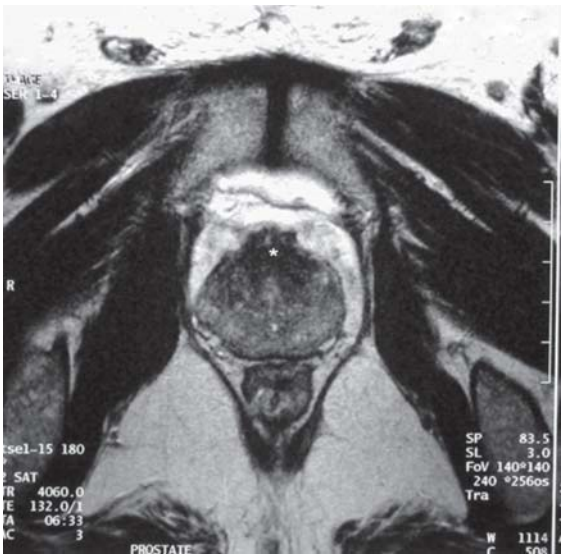

Fig. 4.9: T2-weighted axial section in a young adult. The gland does not show central and peripheral zone distinction or any hyperplastic central gland changes. The fibromuscular stroma anteriorly appears hypointense

allows easy assessment of periprostatic spread of growth. The pelvic bone marrow shows high signal. The neurovascular bundles

are seen at 5 and 7 O'clock position on axial images and are outlined by periprostatic fat, pelvic fascia and muscles. [12] The seminal vesicles are well seen on axial and coronal images (Figs 4.10A and B) and appear bright on T2WI due to the water content. Loss of signal in these structures indicate invasion by malignancy. The prostate volume can be assessed on MR images by using the ellipsoid formula (Half the product of maximum craniocaudal, anteroposterior and transverse dimensions). The vas deferens and seminal vesicles are seen well on axial and coronal images.

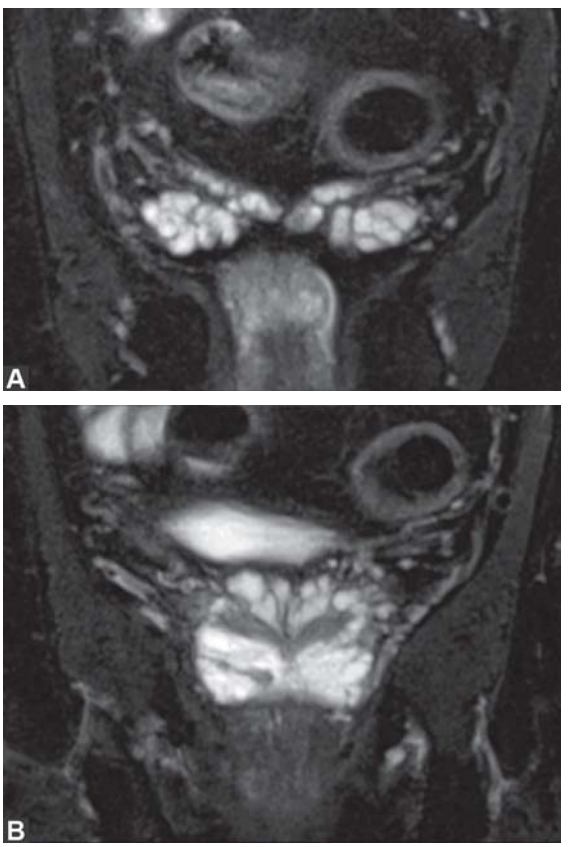

Figs 4.10A and B: Coronal T2 images showing junction of the vas deferens and the seminal vesicle (A) both appearing normally bright due to fluid. More anteriorly the ejaculatory ducts are seen approaching the verumontanum, where they open into the urethra

Prostate spectroscopic examination shows relative concentrations of citrate, creatinine, choline and polyamines within contiguous voxels. Normal prostate tissue contains high levels of citrate (Fig. 4.11).[13] High field strength imaging may improve the quality of the spectra.

UTERUS AND OVARIES

MRI is now recognized as an important modality in evaluation of the female pelvis. Multiplanar capability, higher contrast resolution and lack of significant motion degradation of image in pelvis make MRI an imaging modality of choice for imaging female pelvis. In benign pelvic diseases, ultrasonography remains the most appropriate initial investigation because of its universal availability, lower cost and ease of operation. MRI is reserved as a problem solving technique for the patients in whom ultrasound is suboptimal or equivocal. MRI has become the imaging modality of choice for the diagnosis of congenital uterine anomalies (complex mullerian duct anomalies and ambiguous genitalia) and evaluation of the uterine and cervical malignancy. [14] It is useful in selected cases of leiomyoma prior to the myomectomy, assess response to medical therapy, and in search for submucosal lesions in infertile patients. It is the modality of choice for diagnosis of adenomyosis, and for staging endometrial and cervical malignancy.[15] Leiomyomas are most accurately detected as well as localized (subserosal, submucosal, intramural or cervical) by MRI.

It is the most sensitive imaging technique for the diagnosis of endometriosis and can replace laparoscopy for monitoring response after therapy and when laparoscopy is contraindicated. It is recommended as a

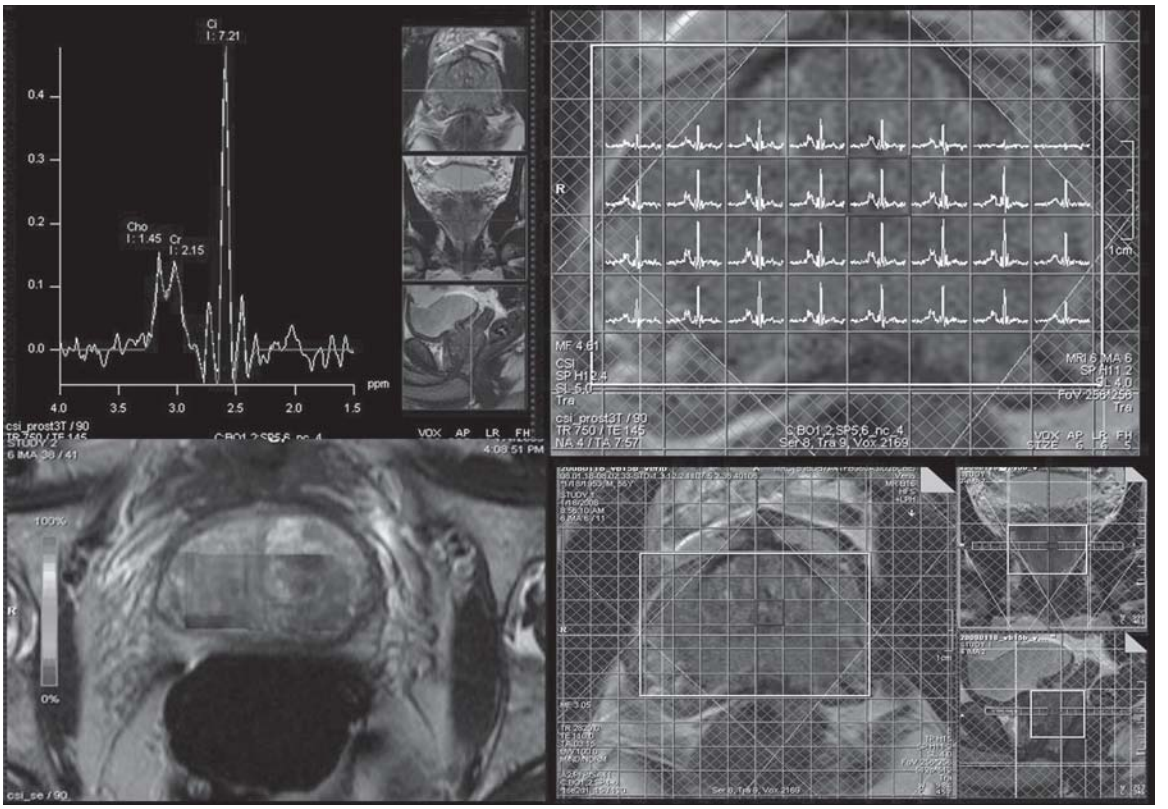

Fig. 4.11: Proton MR spectroscopic imaging (3D CSI- voxel size 8 x 8 x 8, spin echo TE 145, TR 750, total acquisition time 7.57 mins). Spectra from normal prostate tissue shows dominant citrate peak at 2.6 ppm and choline /creatinine complex at 3-3.2 ppm. Metabolite map (lower left) and spectral map (upper right) seen overlaid on the T2 axial image. Volume selection (Lower right) with presaturation slabs is to suppress periprostatic fat *(For color version see plate 3)*

problem solving modality in the evaluation of cystic ovarian lesions, especially dermoids. However, its role in staging ovarian cancer is controversial and needs further evaluation.

Technique and Recommended Sequences

Imaging is performed in supine position with an empty bladder after fasting for atleast 4 hours to limit bowel motion. A variety of receiver coils (body coil allowing better coverage and endoluminal coil for better anatomical depiction) have been used for pelvic imaging but the phased array coils provide the best results. Both T1 and T2-weighted sequences are necessary to evaluate the uterus and vagina. T1-weighted images using spin echo sequence provide excellent organ outline and help in tissue characterization and in evaluation of the nature of fluid collections. Alternatively gradient echo imaging can be done for dynamic studies, useful for staging pelvic malignancies. T2-weighted images are necessary to identify the uterine and vaginal zonal anatomy, and to depict intrauterine pathology.[15] FSE is the recommended T2 sequence. The appearance of uterus on gadolinium enhanced T1-weighted images depends on the phase in which images are acquired. Axial and sagittal planes are both useful for evaluation of the uterus.

It is necessary to use both T1 and T2 weighted spin-echo sequences to identify and evaluate the ovaries. Both transverse and coronal planes are optimal for identification of the ovaries and for confirming that a mass originates in the adnexa rather than the uterus. Chemical shift imaging with fat and water suppression is useful for differentiating lipid and blood products and fat suppressed sequences are useful for the diagnosis of dermoids. A fat suppressed T1WI is helpful in suspected cases of endometriosis.

Normal MR Appearance

On T2-weighted images, three distinct uterine zones can be differentiated in women of reproductive age[14] (Fig. 4.12). The endometrium represents central high signal intensity portion of the uterus. The endometrial thickness depends on phase of menstruation.

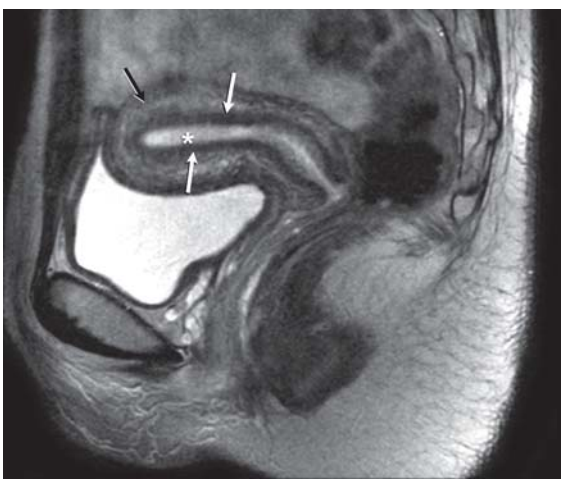

Fig. 4.12: T2-weighted sagittal image of pelvis showing normal anatomy of anteverted and anteflexed uterus. Endometrium (*) appears as a bright signal stripe. Junctional zone (white-arrow) appears hypointense compared to outer myometrium (black-arrow).The uterine isthmus and internal os are seen. The external os of cervix is seen projecting into vaginal fornices

It is thinnest immediately after menstruation and thickest during the midsec-retory phase (3-7mm). The low signal intensity middle layer is the junctional zone and represents the inner myometrium. The thickness of junctional zone is less than 8 mm. The outer medium signal intensity represents the outer myometrium. The zonal anatomy is important to assess the depth of the myometrial invasion of the endometrial carcinoma. On T1 weighted images, uterus is seen as an organ with medium to low signal intensity. Uterus is small with indistinct zonal anatomy in postmenopausal women.

The cervix shows four layers on T2-weighted images.[14] The central high signal intensity represents mucus, which is surrounded by high-signal intensity endocervix. The hypointense fibrous stroma surrounds the endocervix and is continuous with the junctional zone (Figs 4.13A and B). The outer intermediate signal intensity corresponds to smooth muscles and is continuous with the outer myometrium. The vagina has three layers on T2-weighted images. The central high-signal intensity represents mucus-fluid complex, middle low signal intensity represents submucosa and muscularis and outer high signal intensity representing vaginal venous plexus.

On MRI, normal ovaries can be identified in 85 percent of the women of reproductive age. They are identified by following the course of the gonadal vessels or round ligament.[15] On T1-weighted images, the ovaries are seen as low or medium signal intensity structures, and on T2WI, they show low-signal intensity central stroma and high-signal intensity follicles and functional cyst of varied sizes (Figs 4.14A and B). A low intensity rim around ovaries represents fibrous capsule.

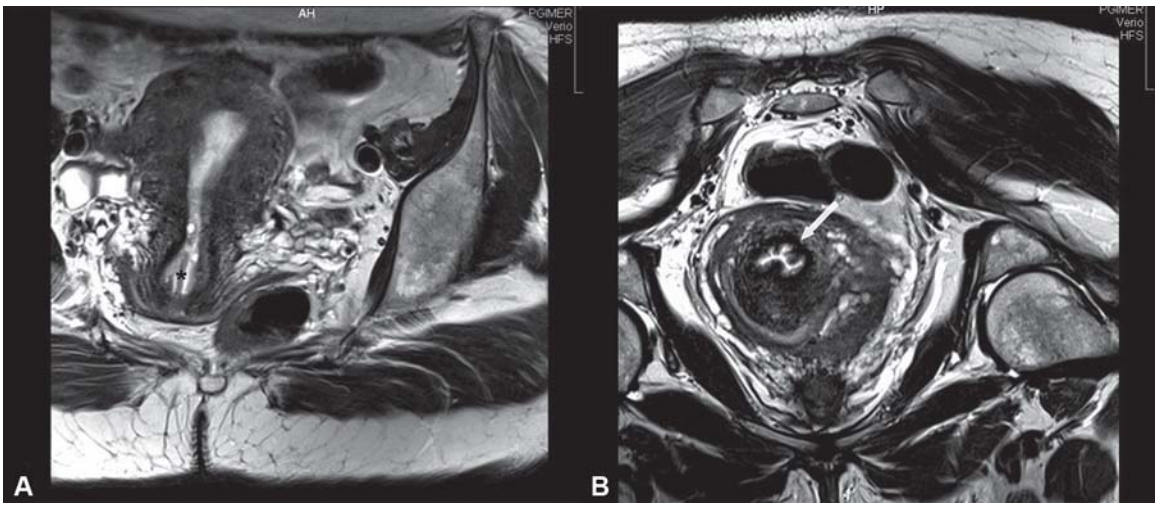

Figs 4.13A and B: Coronal **(A)** and axial views **(B)** showing high signal endocervix and mucosal folds(*), and lower signal fibrous stroma (white-arrow) which continues with the junctional zone. The outer layer is intermediate in signal and continues with outer myometrium

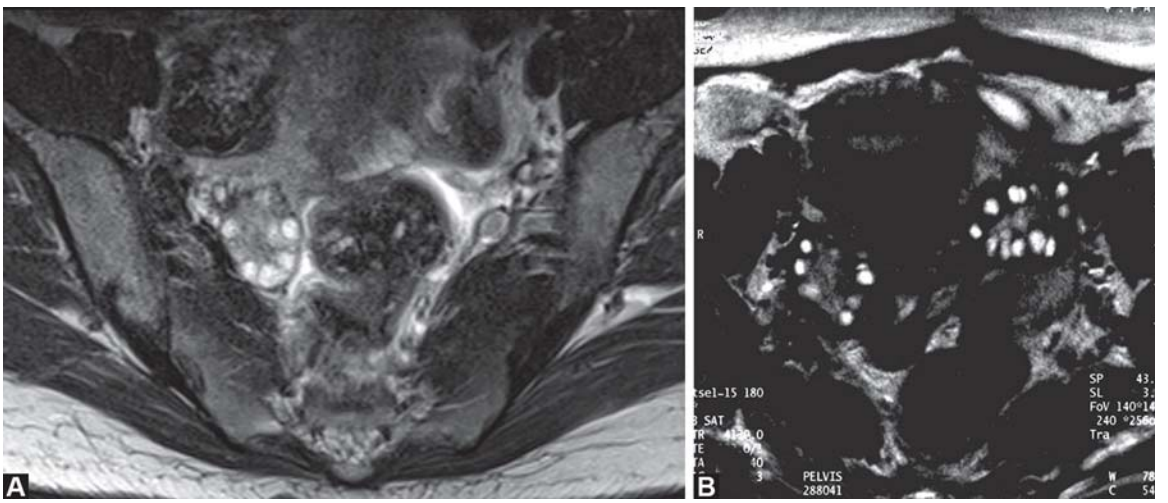

Figs 4.14A and B: T2-axial fast spin echosection with a phased array coil shows excellent details of ovarian anatomy. Note the peripherally distributed hyperintense cysts and relatively low signal ovarian stroma

PELVIC LYMPH NODES

MR imaging plays an important role in staging, accurate treatment and assessing prognosis of genitourinary cancers within the pelvis by allowing detailed evaluation of primary tumor along with pelvic lymph node. [16] The pelvic nodes are seen in relation to major pelvic vessels and are anatomically divided into the common iliac, external iliac, internal iliac and inguinal chains. MRI is useful for detection, localization and characterization of pelvic lymph nodes. The nodes are hypointense on T1WI and hyperintense on T2WI. Currently, MR imaging uses size criteria, presence of

central necrosis and enhancement pattern in differentiating benign from malignant lymph nodes. MR lyphangiography using ultrasmall supraparamagnetic iron oxide (USPIO) is an evolving technique for characterization of nodal function independent of size.[16]

REFERENCES

1. Zhang J, Pedrosa I, Rofsky NM. MR technique for renal Imaging. Radiol Clin North Am 2003;41:877-907.
2. Huang AJ, Lee VS, Rusinek H. MR Imaging of renal function. Radiol Clin North Am 2003; 41:1001-17.
3. Pedrosa I, Rofsky NM: Kidneys. Edelman RR, Hessslink JR, Zlatkin MB, Crues III JV: In Clinical Magnetic Resonance Imaging, Saunders 2006; 2792-862.
4. Kawashima A, Glockener JF, King BF. CT urography and MR urography. Radiol Clin North Am 2003;41:945-61.
5. Grattan-Smith JD, Jones RA. MR Urography: Technique and results for the evaluation of urinary obstruction in the pediatric population. Magn Reson Imaging Clin of North Am 2008; 16:643-60.
6. Michaely HJ, Schoenberg SO, Rieger JR, Reiser MF. MR angiography in patients with Renal Disease. Magn Reson Imaging Clin of North Am 2005;13:131-51.
7. Leiner T, Michaely H. Advances in contrast-enhanced MR angiography of the renal arteries. Magn Reson Imaging Clin of North Am 2008; 16:685-96.
8. Thomsen HS, Marckmann P, Logager VB. Update on Nephrogenic Systemic Fibrosis. Magn Reson Imaging Clin of North Am 2008; 16:551-60.
9. Taveras N, Demas BE, Hricak H. MR imaging of bladder neoplasms. Urol Radiol 1990; 12: 27-33.
10. Mallampati GK and Siegelman ES. MR imaging of the bladder. Magn Reson Imaging Clin of North Am 2004;12:545-56.
11. Akin O, Hricak H. Imaging of Prostate Cancer. Radiol Clin North Am 2007;45:207-22.
12. Somford DM, Futterer JJ, Hambrock T, and Barentsz JO. Diffusion and perfusion MR imaging of the prostate. Magn Reson Imaging Clin of North Am 2008;16:685-96.
13. Rajesh A, Coakley FV. MR imaging and MR Spectroscopic imaging of prostate cancer. Magn Reson Imaging Clin of North Am 2004;12: 557-80.
14. Brown MA, Sirlin CB. Female pelvis. Magn Reson Imaging Clin of North Am 2005;13:381-96.
15. Aubel S, Wozney P, Edwards RP. MRI of female uterine and juxtauterine masses: Clinical application in 25 patients. Magn Reson Imaging 1991; 9:485-91.
16. Kim JY, Harisinghani MG. MR imaging staging of pelvic lymph nodes. Magn Reson Imaging Clin of North Am 2004;12:581-86.

Chapter

5

Current Status of Nuclear Medicine in Urinary Tract Imaging

Rakesh Kumar, Shamim Ahmed Shamim, Rama Mohan Reddy

INTRODUCTION

Renal structure can be investigated in great detail with X-ray method, ultrasound and even with MRI, but functional evaluation of renal and urinary tract need complimentary nuclear medicine technique. With the advent of gamma-camera imaging and high-quality radiopharmaceuticals has greatly facilitated the advances in radionuclide studies of the urinary tract. The techniques of renography, renal scanning, clearance studies, and voiding cystography have reached a point where a wealth of information is available to the nephrologist and urologist conversant with their capabilities and limitations. Besides being highly sensitive, these procedures are noninvasive, simple, rapid, nontoxic and allow acquisition of information often unavailable from other sources. Using these techniques, it has now become possible to assess split renal function in various renal and urinary tract disorders, evaluate kidney size in advanced azotemia, detect the presence of kidneys which are poorly functioning, evaluate renal perfusion, obtain a differential diagnosis of the upper urinary tract dilatation, diagnose urinary tract obstruction, detect intrarenal space-occupying lesions and monitor the renal function in renal failure.

A spectrum of nuclear medicine techniques are now available for the investigation of patients with nephro-urological disorders. These can be broadly classified into four categories: (i) Dynamic renography, (ii) Renal cortical scintigraphy, (iii) Radionuclide cystography and voiding cystography and (iv) Clearance studies, i.e. GFR estimation, ERPF estimation, etc. Various interventional techniques like diuresis and captopril/losarton have further improved the diagnostic capability of obstruction and renovascular hypertension simultaneously using radionuclide studies.

RADIOPHARMACEUTICALS

The various radiopharmaceuticals used in the evaluation of kidneys classified into two groups. The first group includes those that are rapidly eliminated by the kidneys and thus enable evaluation of renal function and urine drainage. ^{99m}Tc-LLEC, ^{99m}Tc-MAG-3, ^{99m}Tc-DTPA, ^{99m}Tc-GHA and ^{123}I-OIH are included in this group and with the exception of GHA, these agents are not used for static imaging because just minutes after intravenous injection, they appear only briefly in the renal parenchyma before they are excreted. The second group includes

radiopharmaceuticals, which are concentrated in the renal parenchyma for a sufficiently long time, thus enabling detailed mapping of the renal parenchyma. Included in this group are ^{99m}Tc-DMSA, and ^{99m}Tc-GHA. Note that ^{99m}Tc-GHA is included in both the groups because approximately 10-15% of the injected dose is retained in the renal parenchyma while 65% of the injected dose is eliminated in the urine within 6 hours after injection.

^{99m}Tc-MAG-3

Currently, ^{99m}Tc-MAG-3 (mercapto-acetyl-triglycine) is most commonly used renal radiopharmaceutical. It is cleared principally through active tubular transport.[1] Plasma clearance is in the order of 300 ml/min, approximately 60% that of ^{123}I-OIH,[2,3] and after 3 hours, approximately 90% of the injected dose can be recovered in the urine. It is more extensively protein bound than ^{123}I-OIH (88% versus 65%) and therefore its volume of distribution is lower than that of ^{123}I-OIH. Since it is eliminated by tubular secretion and has a high initial renal uptake, the kidney to background ratio provided by this tracer is high. Moreover, the rapid excretion provides good temporal resolution. ^{99m}Tc-MAG-3 is a superior agent for renal dynamic scintigraphy but a practical limitation to its extensive use is the relatively high cost.

^{99m}Tc-LLEC

Metabolite of the brain perfusion tracer ECD (ethyl cystine dimer). LLEC has similar good imaging properties and higher renal clearance than MAG-3. Ethylene cystine can exit as four different stereo-isomers D, D-EC, L, L-EC, syn D, L-EC, and anti D, L-EC. Labeling EC with ^{99m}Tc doesn't required boiling. Highest labeling yield is obtained at pH of 10-12 (97%). Like OIH and MAG-3 the secretion of ^{99m}Tc-LLEC occurs in proximal tubule.[4] D, D-EC has highest and faster renal clearance while L, L-EC has lower renal excretion and higher tissue retention.[4,5] Protien binding of D, D-EC is 28% and L,L-EC has 50%. Production of D, D-EC form, however, demands HPLC purification, a drawback for clinical use. The clearance of LLEC is about 75%. The disadvantage of EC is unknown amounts of different stereo-isomers and forms produced by the different labeling kit, which have different excretion.

^{99m}Tc-DTPA

^{99m}Tc-DTPA (di-ethylene-triamine-penta-acetic acid) has been the tracer of choice for dynamic renal scintigraphy for almost three decades. However, it is now being replaced by ^{99m}Tc-MAG-3 and ^{99m}Tc-LLEC in many centers for the reasons stated above. It is excreted primarily by glomerular filtration, at a slightly lower rate than inulin, approximately 90 ml/min.[6, 7] This lower rate of filtration is probably due to protein binding, the amount of which varies with the formulation. A maximum concentration in kidneys is usually achieved by 3 minutes after intravenous injection. This is the best agent for renal dynamic study and estimation of GFR in same sitting.

^{123}I-OIH

^{123}I-OIH (orthoiodohippurate) is useful for dynamic renal scintigraphy because of its high uptake by renal tubules followed by the rapid excretion in the urine.[8] The excretion pattern is similar to para-aminohippuric acid (PAH), which is the standard for the measurement of effective renal plasma flow

(ERPF). Approximately 20% of PAH is eliminated by glomerular filtration and 80% by tubular secretion, with an extraction ratio of approximately 0.9:1.0.[5] The extraction ratio of ^{123}I-OIH is approximately 85% that of PAH.

^{99m}Tc-GHA

^{99m}Tc-GHA (glucoheptonate) is rapidly taken up by the kidneys and by 1 hour, 8 to 10% of the initial tracer activity is present in the kidneys and almost 40% of the administered dose is eliminated in the urine.[9] Static renal scintigraphy is possible at approximately 2 hours or more after injection. Uptake of GHA occurs principally by active renal tubular transport and to a lesser extent by glomerular filtration and the tracer retained within the kidney is associated with cells of the proximal convoluted tubules.[10] Thus it is possible to perform adequate dynamic renal imaging with rapid visualization of renal parenchyma, collecting system, pelvis, ureter and bladder. However, in children with obstructive diseases, some tracer may be retained within the pelvicalyceal system causing interference in the imaging of functional renal parenchyma leading to false interpretation of the study, therefore, late imaging should be considered in such cases. Hepatobiliary system is an alternate route of excretion of GHA, and in patients with severe renal failure, late images at 4 to 6 hours may show tracer activity in the bowels.

^{99m}Tc-DMSA

^{99m}Tc-DMSA (dimercapto-succinic acid) is currently the agent of choice for cortical static renal scintigraphy both in planar and SPECT studies. The renal uptake of this agent is about 50% of the injected dose at 1 hour and about 70% at 24 hours after injection.[11] One hour or more postinjection, the tracer is found principally in the proximal convoluted tubules with very minimal activity elsewhere in the kidney. In most patients, therefore, excellent images of renal cortex can be obtained approximately 4 hours after injection of ^{99m}Tc-DMSA. Here again, patients with obstructive pathology may have tracer retention within the pelvicalyceal system leading to false interpretation. In such a case, delayed imaging upto 24 hours postinjection is recommended to allow tracer in the urine to be eliminated.

IMAGING TECHNIQUES

Renal Dynamic Scintigraphy

This refers to serial continuous imaging following intravenous injection of radiotracer. It encompasses three principal techniques. (a) Dynamic renography, (b) Diuretic renography (c) Captopril renography.

Dynamic Renography

Patient preparation Patient should be well-hydrated before study. Patients should be encouraged to drink fluids prior to the study. Before the examination begins, the patients are asked to empty their bladder. In suspected cases of obstruction, when patients cannot void or in children with VUR, a bladder catheter (Foley's type) should be inserted. The bladder should be allowed to drain through the catheter throughout the entire duration of the study. Intravenous line is established to avoid extravasations of the tracer, which may yield erroneous interpretation.

Radiopharmaceuticals ^{99m}Tc-MAG-3, ^{99m}Tc-DTPA, ^{99m}Tc-LLEC, ^{99m}Tc-GHA or ^{123}I-OIH

can all be used in performing dynamic renal scintigraphy. The dose administered is given Table 5.1.

Imaging Patients are examined in the supine position with the gamma-camera placed underneath the examination table viewing the kidney and bladder area. In this position, the distance from the skin to each of the kidneys is approximately the same and for calculation of the left/right renal uptake ratio, depth correction is not critical. In renal transplants, however, the camera is placed anteriorly over the patient in supine position, viewing the allograft and bladder. In children, appropriate immobilization should be attained during acquisition. Once the patient is appropriately positioned, a rapid intravenous bolus of the tracer is injected and acquisition begun simultaneously. One frame per two seconds is recorded for 60 seconds followed by one frame per 15 seconds for a total of 20-30 minutes.

Interpretation A dynamic renal study is evaluated for the parenchymal phase, the cortical transit time, and the urine drainage phase.

1. *Parenchymal phase:* Evaluation of this phase is very critical. During the first few minutes of the dynamic study, after the initial vascular distribution of the tracer and before its appearance in the renal collecting system, the tracer is concentrated in the renal parenchyma. At this point there is progressive decrease in the blood level of the tracer with increasing concentration in the parenchyma till a peak is reached where maximum concentration has been attained. After this, the tracer appears outside the renal parenchyma with progressive decrease in levels within the parenchyma, marking the beginning of the drainage phase. The parenchymal phase is usually visualized 60-120 seconds after the IV injection and provides the following information:
   a. Relative and absolute size of the functional renal parenchymal units.
   b. Total renal function (Kidney/Background ratio).
   c. Relative or split renal function (right versus left).
   d. Overall renal morphology and redistribution of functioning parenchyma.
   e. Position of the renal units.

   The relative renal size can be estimated by simple visual observation. Renal dimensions in longitudinal and transverse planes can be measured with a calibrated system or by imaging a radioactive ruler placed by the side of the patient. Parenchymal phase shows the position of the renal units. A qualitative estimate of the renal function can be obtained by visually evaluating the ratio of the renal

Table 5.1: Different radiopharmaceutical and their doses

Radiopharmaceutical	*Dose (mCi/kg)*	*Minimum dose (mCi)*	*Maximum dose (mCi)*
^{99m}Tc-MAG-3	0.100	0.5	10.0
^{99m}Tc-DTPA	0.100	0.5	8.0
^{99m}Tc-GHA	0.100	0.5	8.0
^{123}I-OIH	0.010	0.1	0.5
^{99m}Tc-LLEC	0.100	0.5	10.0

and background activity. Normally, very little tracer activity should be present in the background, the blood pool and the liver during the parenchymal phase. If a high level of tracer activity is noted within these regions, then the renal uptake shall be low indicating a poor renal function. Split renal function can be assessed visually and also by calculating the individual renal uptake as a fraction of the total renal uptake from renal regions of interests (ROIs). Placement of ROIs should be strictly over the parenchymal region but under certain special circumstances such as hydronephrosis, this may be difficult. Background ROIs should be placed with caution since this step is usually done manually and different size and position can produce different results, a particular problem when renal function is low and/or severe hydronephrosis is present.

Information about intrarenal distribution of radiotracer can be obtained during the parenchymal phase. Hydronephrosis is usually seen as a "photon deficient" area within the renal pelvis. Depending on the severity of hydronephrosis, the cortical uptake appears as a rim of varying size. It is important to note that absence of a photon deficient area within the renal outline does not rule out hydronephrosis. Reduced or absent tracer activity in a relatively large portion of the kidney such as a malfunctioning upper pole in a duplex kidney, trauma, tumor, or cyst can be detected.

2. *Cortical transit time*: Cortical transit time is defined as the time interval between the intravenous injection of the radiotracer and its first appearance within the renal collecting system. Normally, this is about 3-6 minutes. A normal cortical transit time indicates that renal parenchymal function is not compromised, even in the presence of dilatation of the pelvicalyceal system. Conversely, therefore, the poorer the renal function, the longer is the cortical transit time. As the tracer is eliminated into the renal pelvis, there is gradual decline in the parenchymal activity. Even if the cortical transit time appears to be within the normal range, it is important to determine if it is associated with a decrease of tracer activity from the renal cortex. Cortical retention of tracer activity indicates renal dysfunction. A number of conditions may prolong the cortical time. These include ureteral obstruction, acute and chronic pyelonephritis, nephrotoxicity, trauma, renal artery stenosis, renal vein thrombosis, acute tubular necrosis and allograft rejection.
3. *Drainage phase*: Drainage phase comprises of the passage of the radiotracer from the pelvicalyceal system through the ureter into the bladder. Usually, at the end of 20 minutes of study, much of the tracer would leave the renal parenchyma. At this time, minimal or no tracer should be visible in the renal collecting system. Time activity curves are generated from ROI over an entire kidney and reveal a peak time at 4-7 minutes with subsequent decrease to 30-50% of the peak activity at 15 minutes. Time activity curves should always be interpreted along with careful evaluation of images in the parenchymal phase and drainage phase, keeping in mind the cortical transit time. It is possible to see a normal cortical transit time with complete cortical clearance of tracer at 20 minutes accompanied by a time activity curve that reveals a delayed peak and a

high-residual value. Such a pattern indicates delayed drainage without parenchymal dysfunction and is almost always without any clinical significance. The possibility of a vesico-ureteric reflux of tracer during the drainage phase should also be kept in mind in order to be able to differentiate it from outflow tract obstruction.

Normal Dynamic Renal Study

There is an intense and rapid concentration of tracer in the renal parenchyma at 1-3 minutes postinjection. Subsequently, the tracer passes into the renal calyces and pelvis by 3-6 minutes. Ureters may be visualized in normal patients and in those with slow ureteral transit time. However, a dilated ureter with or without obstruction is always visible. The renal parenchyma is usually completely cleared of radiotracer by 20 minutes but a small residual amount may sometimes be present and is usually of no clinical significance. This residual tracer usually clears spontaneously with change in the patient's position or after the patient voids. The bladder is seen 3-6 minutes after injection and there is a progressive increase in tracer concentration with time. The background activity is usually a reflection of blood clearance of tracer or rather the renal extraction of tracer from the blood pool, which rapidly decreases with time in a patient with normal renal function. The dynamic acquisition can be terminated at 15-20 minutes, when there is no retention of tracer within the pelvicalyceal system or ureters (Fig. 5.1). If at the end of the initial 20 minutes, there is evidence of tracer retention, then the patient should be asked to

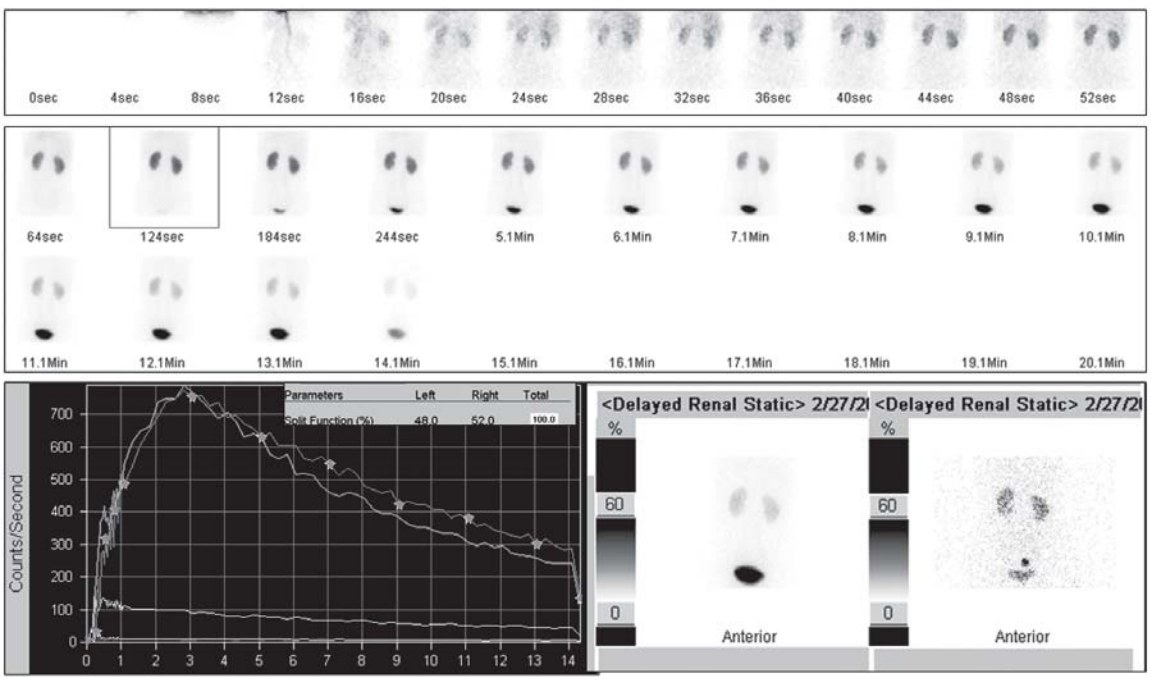

Fig. 5.1: Normal ^{99m}Tc-LLEC scan: Normal dynamic function images with prompt symmetric radiotracer perfusion (upper row), uptake and rapid clearance (middle row). Normal time activity curves with steep uptake slope, distinct peak, and rapid clearance with normal early and delayed static images (lower row) *(For color version see Plate 4)*

get-up and move for a few minutes (a small child should be picked up for a few minutes) to encourage postural drainage. An additional image is recommended to determine the tracer clearance, which, if adequate, should be considered normal, and the outflow tract not obstructed. A diuretic renogram is indicated if an obstruction is present or suspected.

Diuretic Renography

Furosemide causes a rapid diuretic response that drains out tracer from dilated nonobstructed system. In significant outflow tract obstruction, tracer in the renal area may decrease slowly or fail to decrease or even increase in response to a diuretic challenge. The urine flow depends not only on the function and amount of renal parenchyma, but also on the ability of the parenchyma to respond to a diuretic. Drainage is directly proportional to urine flow and inversely proportional to the volume of the renal pelvis and ureters, the poorer the function, the longer is the drainage time. Compliance and volume of the pelvicalyceal system are also important in that a large flaccid renal pelvis usually causes slow drainage of radiotracer. There are several factors that can limit the usefulness of diuretic renography. Severe hydroureteronephrosis may partly or wholly mask the effect of a diuretic on the emptying of the renal pelvis. Other factors include poor response of the renal parenchyma to the diuretic, poor delivery of the diuretic to the kidneys, bladder over distension, complex pelvic surgeries, prune-belly syndrome and ectopic kidney.

Imaging Diuretic renography can be performed using the same radiopharmaceuticals mentioned earlier. It is important to ensure that tracer has filled the renal pelvis and postural drainage has not occurred before the diuretic is administered. The diuretic can be administered 15 minutes postinjection or simultaneously with the radiotracer. Forced hydration has been suggested as a means to differentiate obstruction from nonobstruction in diuretic renography. The diuretic effect is usually seen within 1-2 minutes after administration of furosemide. Patients with intermittent hydronephrosis who complain of intermittent flank pain may have reproduction of pain on administration of diuretic. In some cases with otherwise balanced drainage and urinary flow, a diuretic may cause rapid over distension of the renal pelvis resulting in the disruption of the status of the system. It is important to note that in patients with urinary diversions, even in the absence of obstruction, flow dynamics may be slow, making the diagnosis of obstruction difficult. Overlap of kidney and an ileal or colonic diversion may give rise to confusing images. Imaging in various projections, removal or replacement of external urine collecting devices and attempts at postural drainage may sometimes be helpful.

Interpretation Careful evaluation of the dynamic renal study preceding a diuretic administration is important during interpretation. In the absence of obstruction, rapid and complete washout of radiotracer occurs from the pelvicalyceal system (Fig. 5.2). On the other side of the spectrum is an obstructed system with slow or no drainage of radiotracer following a diuretic challenge (Figs 5.3 and 5.4). Interpretation of intermediate diuretic renographic patterns is difficult. Usually, a comparison is made of images obtained prior to and after a diuretic injection. A cinematic display verifies whether the patient moved during acquisition or not.

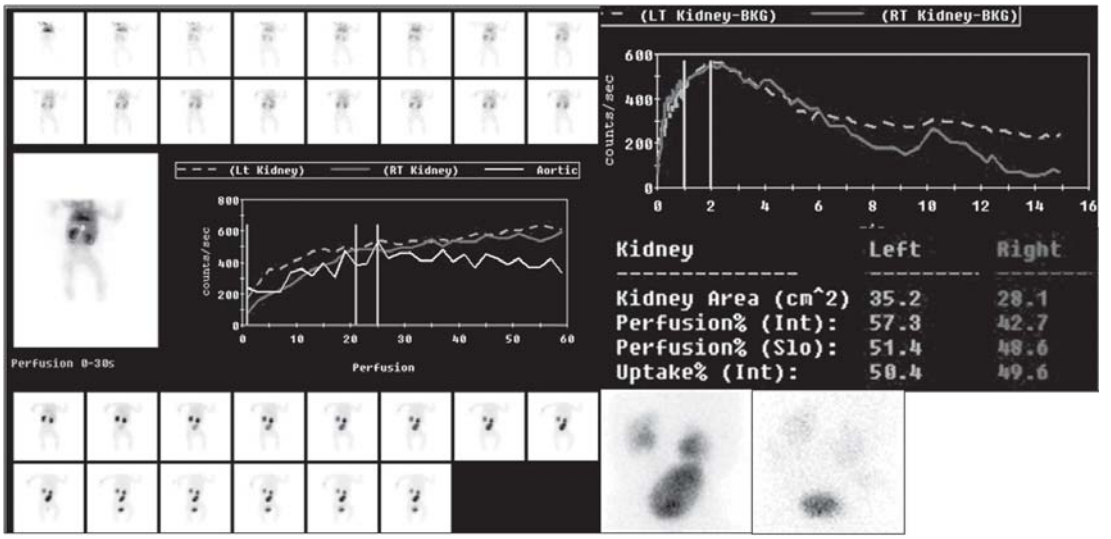

Fig. 5.2: ^{99m}Tc-LLEC scan in non-obstructive hydronephrosis: Dynamic and static renal images showing initial photopenia which is filling-up and non-obstructed clearance, findings are consistent with non-obstructed hydronephrosis *(For color version see Plate 4)*

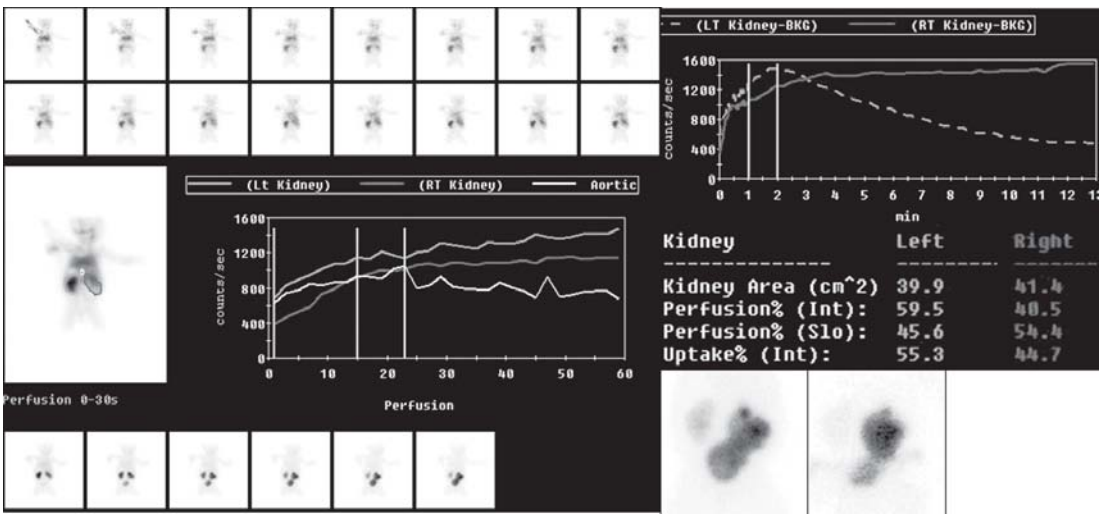

Fig. 5.3: ^{99m}Tc-LLEC scan in obstructed hydronephrosis: Progressive filling of enlarged dilated collecting system is seen on right side, where as the left kidney clears normally. Time activity curves shows washout on the left side and obstructed pattern on right side. Early and delayed static images showing persistent activity in dilated PCS without clearance on right side *(For color version see Plate 5)*

The diuretic washout $T_{1/2}$ is estimated using an exponential interpolation between a point on the initial descent of the time activity curve and another point on the down slope while the curve is decaying monotonically. The diuretic $T_{1/2}$ should be only one of the several factors, which are considered while assessing urinary obstruction. Although there may be many variations in the time of diuretic injection and subsequent time of acquisition following a diuretic response, the overall sensitivity of a diuretic renography

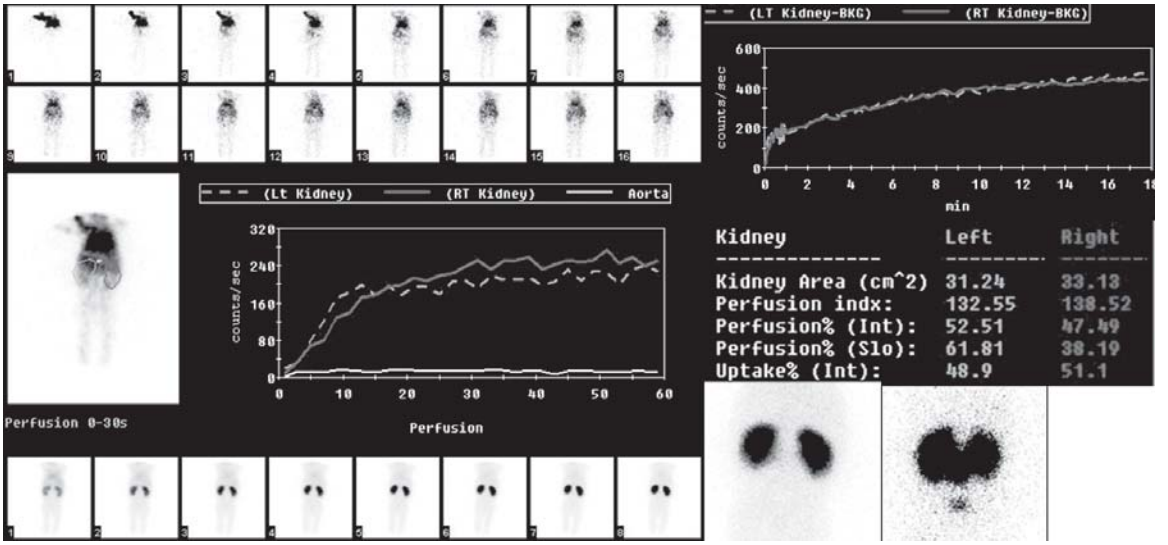

Fig. 5.4: ^{99m}Tc-LLEC scan in bilateral pelvic-uretric junction obstruction: Dynamic images showing progressive filling of enlarged dilated collecting system is seen on both side. Time activity curves shows obstructed pattern on both side. Early and delayed static images showing persistent activity in dilated PCS *(For color version see plate 5)*

for the detection of obstruction in children has been estimated at 93%.[12]

Drainage pattern of renogram

O' Reilly et al (1978) classified patients on the basis of the renogram curve of ^{99m}Tc-DTPA with diuretic.[13]

Response I: Normal initial renography and remained so after diuretics.

Response II: Obstructive initial renography and remained so after diuretics.

Response IIIa: Obstructive initial renography and showed rapid clearance after diuretics.

Response IIIb: Obstructive initial renography and showed mild/partial clearance after diuretics.

Combined: Many centres go for combined approach.

Captopril Renography

Secondary hypertension is more common in children and renal disease is perhaps the most common cause in this group. In a study conducted by Londe S et al in 1978,[14] 563 pediatric patients with secondary hypertension were evaluated. 78% had renal abnormalities and 12% had renal artery disease. Secondary hypertension may be caused less frequently by endocrinal, cardiovascular or nervous system disorders. The renal causes of hypertension are infarction, postpyelonephritic scarring and post-traumatic lesions, which are easily diagnosed by conventional renal scintigraphy. A dynamic study usually shows the affected kidney to be smaller with lesser uptake than the contralateral normal kidney. The more severe the affliction, the lower is the renal uptake of tracer. ^{99m}Tc-DMSA scintigraphy in patients with renovascular hypertension typically reveals renal asymmetry. The affected kidney is smaller and shows lesser tracer uptake than the normal one. In the presence of unilateral renal artery stenosis, there may be reduced renal

perfusion and function on the affected side. However, sometimes the same kidney may remain adequately perfused and owing to the auto regulation mechanism the radionuclide study may remain normal in a significant number of cases. Thus conventional radionuclide studies are not reliable screening tests for the diagnosis of renovascular hypertension and that angiotensin converting enzyme (ACE) inhibitor renal scintigraphy is a markedly improved technique.

ACE inhibitors such as captopril block the formation of angiotensin II, producing dilatation of efferent arterioles and a fall in transcapillary pressure gradient. This causes a significant decrease in GFR of the kidney with renal artery stenosis that can be easily diagnosed by renography.[15-19] Initially ^{99m}Tc-DTPA was used, but subsequent experience has shown that both glomerular and tubular agents can be used.[16] To ensure better absorption of captopril patients should not take solid food atleast four hours before the study. Enalapril another agent has a distinct advantage over captopril as this can be administered intravenously and therefore does not depend on the variations of absorption in the gastrointestinal tract. Caution should be taken about the potentially serious hypotensive episodes following intravenous enalapril. Significant hypotension is also seen after a single dose of captopril and therefore the patient should be well-hydrated and an intravenous access maintained throughout the study. Blood pressure should be monitored every 5-15 minutes. Diuretics may exaggerate the hypotensive effect and should not be used in conjunction with captopril renography.

A baseline study is obtained followed by a repeat examination either one-hour after oral captopril (1 mg/kg, upto 50 mg), or 15 minutes after intravenous enalapril (0.03 mg/kg). Some authors obtain the initial study with an ACE inhibitor and repeat later without the ACE inhibitor only if the first study is abnormal. Since the primary effect of ACE inhibitor is decreased GFR, studies using glomerular agents show decreased extraction of tracer and delayed visualization of the collecting system whereas with tubular agents prolonged retention of the tracer is seen. Moreover, detection of cortical retention of tracer is easier to appreciate than focal decreased extraction, tubular agents are probably more effective than glomerular agents in the detection of segmental renal artery stenosis. The typical findings of a positive captopril study are an increase in differential renal uptake, increase in cortical transit time, prolongation of time to peak and retention of tracer in the renal parenchyma (Fig. 5.5). The most important parameter however is the split renal uptake. In patients with bilateral renal artery stenosis, the narrowing is usually asymmetrical and so is the effect of ACE inhibitor on each kidney. Cases in which captopril does not induce scintigraphic changes are usually associated with failure of revascularisation or nephrectomy.[20-23]

CORTICAL SCINTIGRAPHY/STATIC RENAL SCINTIGRAPHY

^{99m}Tc-DMSA is administered intravenous by a dose of 0.04-0.05 mCi/kg (1.5-1.9 MBq/kg) with a minimum of 0.3 mCi (11.1 MBq) and a maximum of 3 mCi (111 MBq). Imaging is started about 3 to 4 hours after injection. Planar magnified and SPECT images can be acquired.

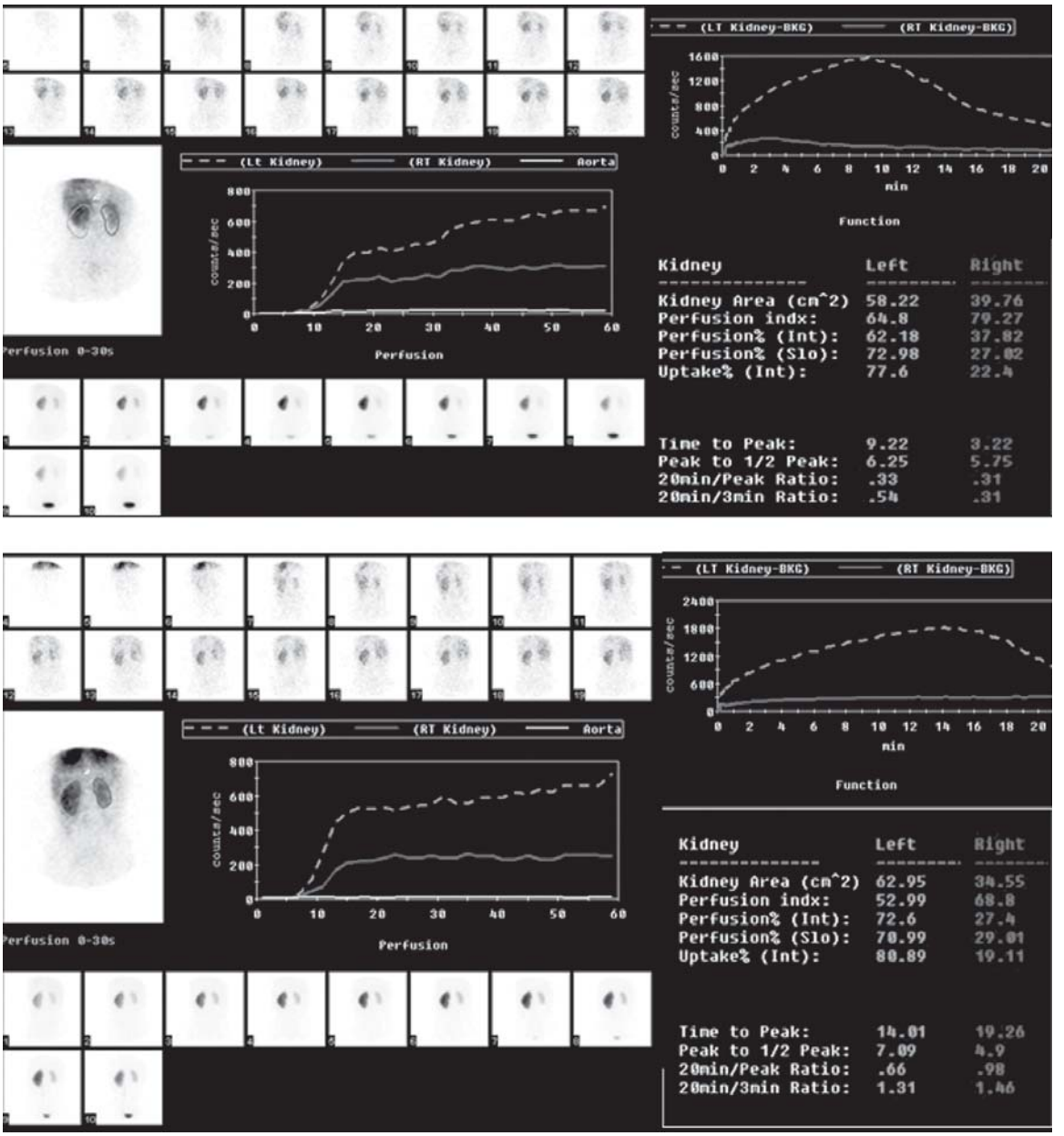

Fig. 5.5: Positive captopril study with ^{99m}Tc-LLEC: Baseline study (upper) showing normal functioning left kidney and impaired functioning right kidney. Captopril study (lower) showing retention of radiotracer on left side and further impairment of function on right side with retention as well *(For color version see Plate 6)*

Imaging Techniques

Planar renal scintigraphy Patient is examined supine with the gamma-camera placed posterior recording 300,000 to 500,000 counts using a high resolution or preferably a ultra high-resolution collimator on a 256 × 256

matrix. Left and right posterior oblique projections are acquired which sometimes prove useful in the identification of cortical defects. Split renal uptake can be calculated by placing ROIs over posterior images. In cases of renal duplication, the upper and lower moieties can be outlined and differential renal function ascertained.

Magnified renal scintigraphy Pinhole magnification or zoomed acquisition is mandatory in neonates and infants and may be useful in identification of cortical defects in older children and adults. Cortical defects following pyelonephritis, infarction, duplication and fetal lobulation can be discerned more frequently with pinhole magnification than with parallel hole high-resolution collimators since the former with an internal diameter of 2 mm provide images of higher spatial resolution than the latter. Posterior and posterior oblique projections are usually acquired.

SPECT Mapping of regional functional parenchyma is best done with ^{99m}Tc-DMSA SPECT. The surface and volume rendered SPECT images permit a superior overall view of the functional anatomy of the kidneys. Using the modern multi-headed SPECT cameras, acquiring 120 images over 360° on a 128 × 128 matrix usually requires 15-20 minutes. Proper sedation is mandatory in acquiring SPECT images.

Radionuclide Cystography

This has been accepted as the technique of choice for evaluation and follow-up of children with urinary tract infection and reflux. The estimated gonadal radiation dose is one-hundredth of the voiding cystourethergraphy. Radionuclide cystography is more sensitive than voiding cystography in detecting vesico-ureteric reflux. Other parameters like residual urine volume, bladder volume at the time of reflux and the rate of clearance of refluxed urine can also be calculated. The only disadvantage of radionuclide cystography is poor anatomical resolution of the bladder and urethra.

Clinical Applications

In urology practice, the most important clinical areas, where radionuclide studies may be of particular importance in patient management, can be considered under the following headings:

1. Urinary tract obstruction
2. Urinary tract infection
3. Renovascular hypertension
4. Congenital anomalies
5. Renal failure
6. Renal transplant evaluation

Urinary tract obstruction Radionuclide studies may be necessary to establish or confirm the diagnosis of obstruction, to ascertain its site or level, to determine its extent or severity or to measure how well the obstructed kidney is functioning.[24] In addition, radionuclide studies may be needed in other situation when any change in the function or condition of the kidney, or of the site and severity of obstruction, is to be determined if desirable clinically to assess patients prognosis and in differential diagnosis of urinary obstruction. In the differential diagnosis of urinary obstruction, diuretic renography is of immense value especially in those patients with a non-obstructed dilated collecting system associated with indeterminate flow curve (Fig. 5.2). Injection of diuretic is essential, if obstruction at the pelvi-ureteric junction is suspected, as this diagnosis can only be confirmed at high urine

flow rate. However, one of the major drawbacks of diuretic renography is a large number of indeterminate results in poorly functioning kidneys. Some progress has been made in this regard by correcting furosemide response for level of renal function. Estimation of renal output efficacy (ROE), which is calculated by a technique independent of variations in uptake rate by the kidneys, provides an accurate diagnosis of renal outflow obstruction in patients with significantly impaired renal function.[25]

Urinary tract infection Renal infection may be clinically obvious, but can be easily overlooked. Clinically, it is frequently difficult or impossible to differentiate infection of the bladder and ureters from the acute renal parenchymal infection. The lack of sensitivity of intravenous urography (IVU) and ultrasonography in the demonstration of early renal infection is well-known. ^{99m}Tc-DMSA is valuable in the identification of renal damage due to early pyelonephritis. Even in the absence of urographic or ultrasonographic abnormalities, regional parenchymal uptake of DMSA may be altered in acute pyelonephritis. ^{99m}Tc-DMSA is also useful to quantify the degree of renal damage, to follow the progress of antibiotic therapy, and to assess recovery and/or residual renal damage.

Imaging with ^{99m}Tc-DMSA facilitates detection of cortical scarring of pyelonephritis (Fig. 5.6). Unlike urography, cortical scarring can detect cortical defects that do not deform the renal outline or the collecting system. In the detection of renal scars ^{99m}Tc-DMSA scan is more sensitive (96%) and specific (98%) as compared with IVU.[26] Besides, in patients with chronic pyelonephritis with uncontrolled hypertension, demonstration of a severe segmental scar on a DMSA scan may guide the surgeon in undertaking partial nephrectomy (Figs 5.7 and 5.8).

One of the most common and routinely employed procedures in children with urinary tract infection is the direct radionuclide cystogram (DRCG) and urine flowmetry (UFMT) in conjunction with cortical scanning (Figs 5.9 to 5.11). In the diagnosis of vesicouretic reflux this procedure is much superior and the radiation exposure to the patient is much less as compared to micturating cystourethrogram (MCU).[27]

Renovascular hypertension Renovascular hypertension is the most common cause of

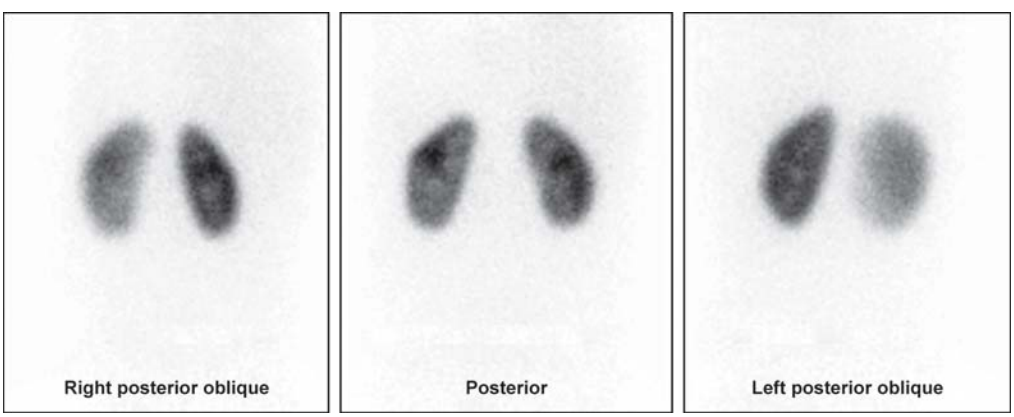

Fig. 5.6: Normal ^{99m}Tc-DMSA scan: Bilateral kidneys are normal in size with smooth cortical outline and normal function

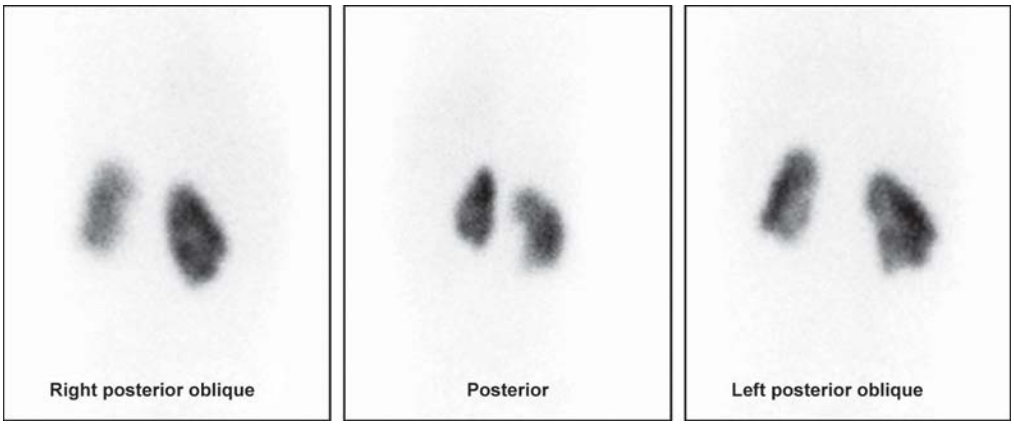

Fig. 5.7: ^{99m}Tc-DMSA study in patient with bilateral vesicouretic reflux. All three views of ^{99m}Tc-DMSA scan show cortical break suggestive of renal scarring (multiple on left side and lower polar on right side)

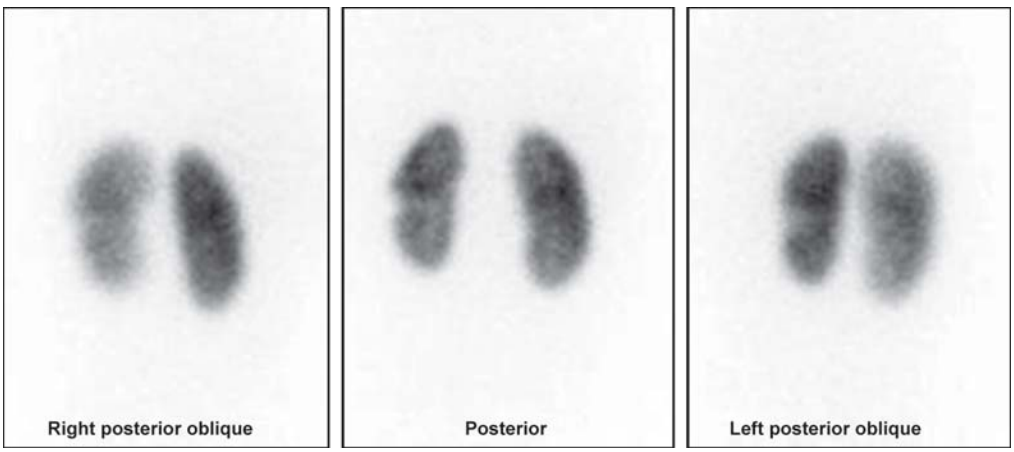

Fig. 5.8: ^{99m}Tc-DMSA study in patient with left vesicouretic reflux. All three views of 99mTc-DMSA scan show cortical break in left kidney suggestive of left renal scarring

secondary and potentially curable hypertension. Regardless of the problems associated with the routine renogram, availability of gamma-camera computer system has made meaningful pre-intervention renal assessment possible in such patients. This test as a follow-up procedure for evaluating the result of percutaneous angioplasty or surgery on the function in the affected kidney of the patients with renovascular disease is an extremely important but often overlooked application.

A major approach to the nuclear medicine diagnosis of the renovascular hypertension has been the introduction of captopril, an angiotensin converting enzyme (ACE)-inhibitor. The concept for the use of ACE-inhibitors in the differential diagnosis of the renovascular hypertension arose from the observation that patients with bilateral renal artery stenosis (RAS), or patient with solitary kidney having RAS had a tendency to develop acute renal failure when treated with these drugs. The theoretical basis for

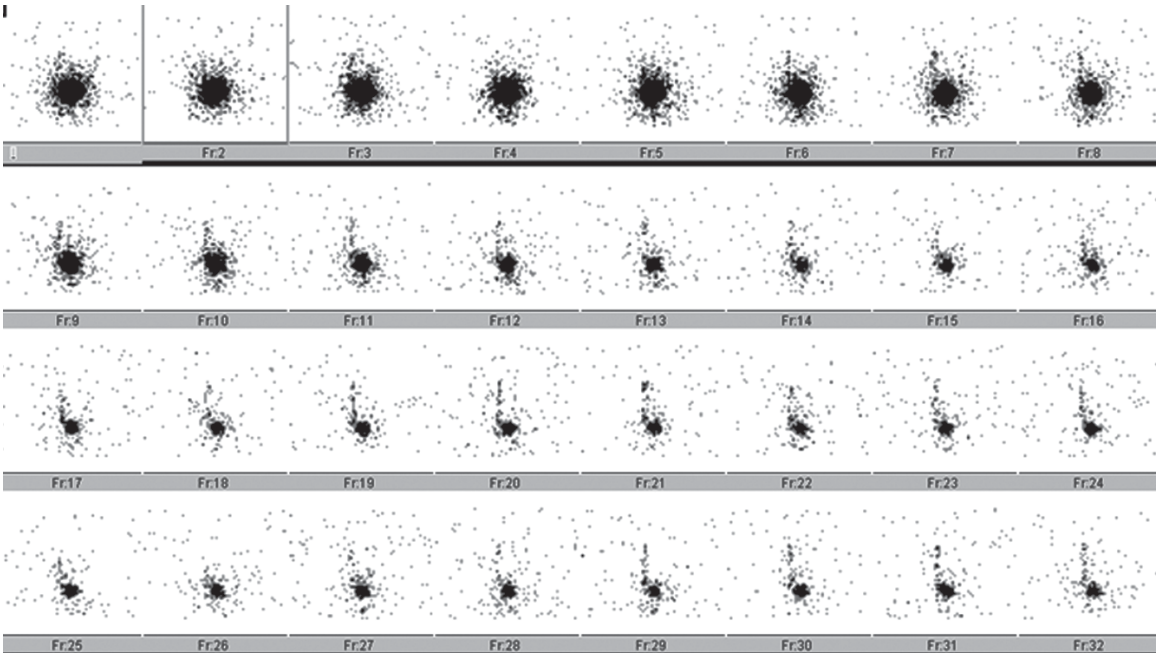

Fig. 5.9: DRCG study: Dynamic images showing vesicoureteral reflux of radiotracer from bladder into left ureter (Grade-II)

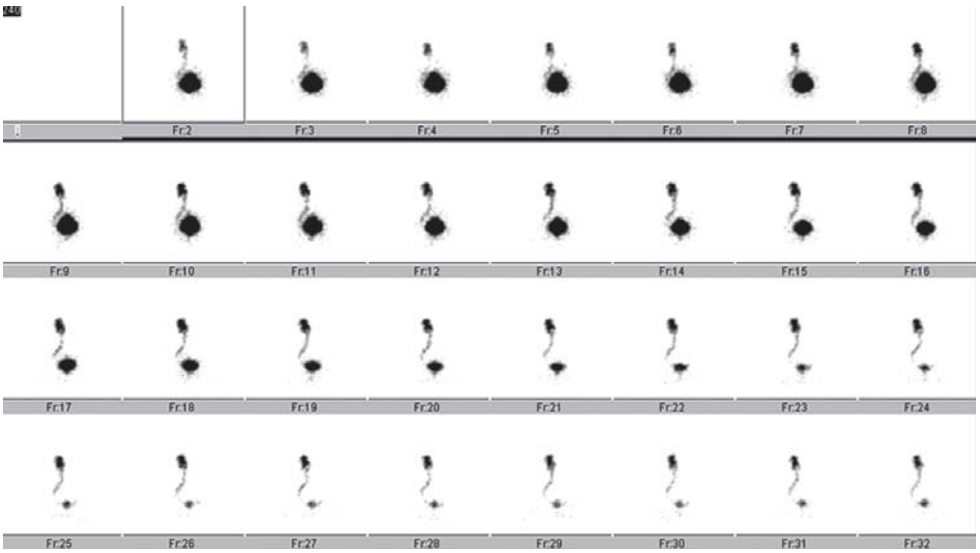

Fig. 5.10: DRCG study in unilateral reflux: Dynamic images showing vesicoureteral reflux of radiotracer from bladder into left ureter (Grade-III)

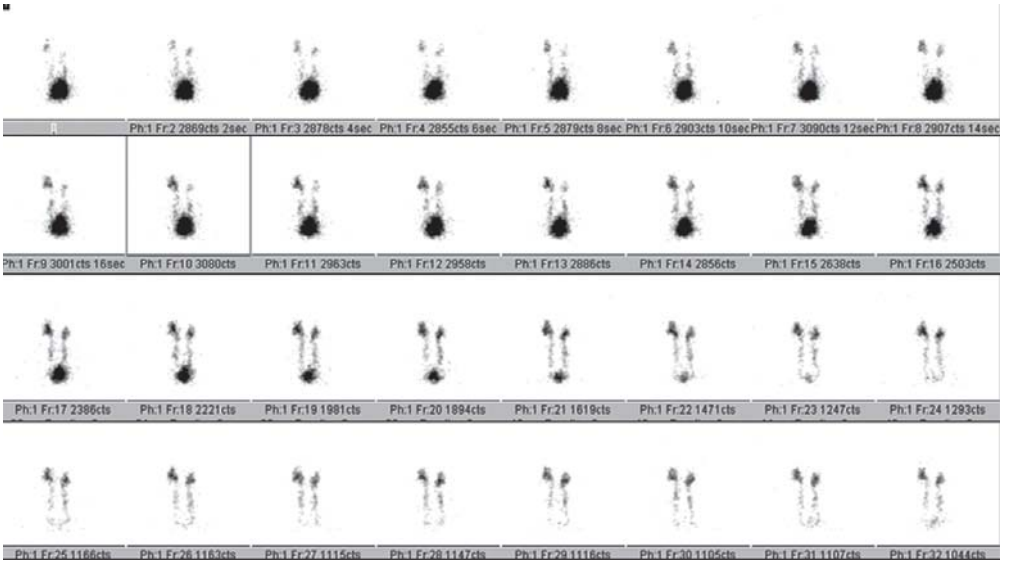

Fig. 5.11: DRCG study in bilateral vesicoureteral reflux: Dynamic images showing vesicoureteral reflux of radiotracer from bladder into both ureters (Grade-III)

complication of ACE-inhibitor therapy and the rationale for the captopril renography test are essentially the same. The renin-angiotension system is thought to be a compensatory mechanism by which the kidney maintains perfusion, when it is subjected to low perfusion pressure, as may result distal to a renal artery stenosis. ACE-inhibitors act to block the step where angiotensin I is converted to angiotensin II, and as a result prevent the subsequent increase in the efferent arteriolar tone. In the absence of this compensatory mechanism, the glomerular filtration rate (GFR) drops significantly in the affected kidney.[16-19] A normal base line study followed by unilateral decreased in split renal function are the hallmark of unilateral renovascular hypertension (Fig. 5.5). Widespread application of the captopril renography and improved surgical techniques as well as perfection of the catheter techniques for percutaneous transluminal angioplasty, has caused tremendous excitement in the field of renovascular disease, and resulted in sudden repopularization of radioisotope renography.

Congenital anomalies Renal radionuclide studies are helpful in the diagnosis and functional evaluation of a spectrum of congenital disorders. Serial evaluation of the parenchymal and drainage function may be essential in patients with polycystic kidneys, and in medullary sponge kidneys. Radionuclide investigations have a definite "functional" edge over the urography in the management of ectopic kidneys, horseshoe-shaped kidney, cross ectopias, or malrotated kidneys.[28,29] Radionuclide studies are useful in the evaluation of regional cortical renal function in patients with duplications of the ureters and renal pelvis. Preoperative and serial postoperative functional as well as morphologic evaluation of the kidney, upper urinary tracts, and the urinary bladder can be effectively done in patients with posterior

urethral valves by the renal dynamic, DMSA cortical imaging and DRCG-IFMT studies. Functional evaluation of the kidney and the urinary bladder by radionuclide studies in patients with neurogenic bladder has also been very well-established.

Renal failure The radionuclide studies in renal failure provide information about renal perfusion, the handling of the renal agent by the kidneys and if urine flow through the collecting system. Significant renal function has been reported on radionuclide studies in a large percentage of the patients with nonfunctioning kidneys seen on intravenous urography. The result is still better when ^{99m}Tc-DMSA is used for renal imaging.

Radionuclide clearance studies provide valuable information and help in monitoring glomerular or tubular function in nephropathies of various origins, the most important being the diabetic nephropathy. Kidney disease in diabetic patients has a devastating effect on survival, most evident in those with juvenile onset disease. It has been advocated that in such patients, the prospective monitoring of diminishing renal function should include precise measurement of GFR by radionuclide techniques combined with determination of fractional clearance of high molecular weight proteins. This is particular important when the effects of treatment on the early proteinuric phase of the diabetic nephropathy are being evaluated.[30, 31] The considerable loss of glomerular filtration capacity at this stage is undetected by inverse creatinine measurement, which remains a valuable tool for monitoring the late stage of nephropathy, when metabolic correction is unlikely to be effective.

Renal transplant evaluation Radionuclide techniques offer rapid, effective and non-invasive means for the correct diagnosis of many of the ischemic, immunological and mechanical complications of the renal transplantation. Renal perfusion and function studies using ^{99m}Tc-DTPA or ^{99m}Tc-MAG-3 offer comprehensive evaluation of the renal blood flow, function and drainage (Fig. 5.12). Many techniques have been described for establishing the cause of acute renal failure in the transplant patients, especially for the diagnosis of acute rejection and acute tubular necrosis (ATN) (Fig. 5.13). Some of the surgical complications like urinary obstruction, urinary extravasations, urinoma, non-urinary pelvic collections, e.g. hematoma or lymphocele and vesicoureteric reflux (VUR) can be diagnosed on radionuclide studies. Despite the relative merits and demerits of the radionuclide studies vis-a-vis other noninvasive diagnostic modalities, nuclear medicine has made an impact in clinical practice in at least three ways:

i. By reducing the number of invasive biopsies in transplant patients
ii. Diagnosing or confirming acute rejection very early for prompt treatment
iii. By being able to reassure the transplant surgeon regarding the viability of the allograft in uncomplicated ATN with prolonged period of oliguria or anuria. With improved techniques and increasing availability of the renal transplantation procedures at many more centers around the country, nuclear medicine is bound to play an important role in evaluation and management of renal transplant.[32, 33]

Management of a clinical nephrourological problem can be best done by a multi-disciplinary approach. The various diagnostic modalities like X-ray, CT, US, magnetic resonance spectroscopy and nuclear medicine often support and complement each other.[34] However, radionuclide techniques have the

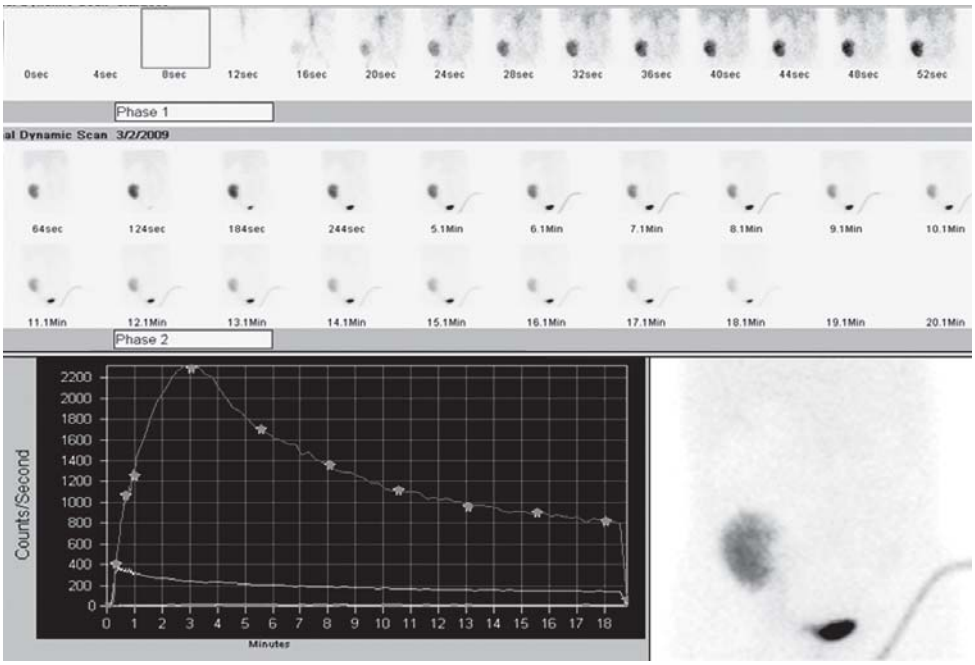

Fig. 5.12: ^{99m}Tc-LLEC scan in normal functioning transplanted kidney. Dynamic images show normal perfusion and uptake with prompt clearance. Time activity curves shows steep uptake slope, distinct peak and rapid clearance *(For color version see Plate 7)*

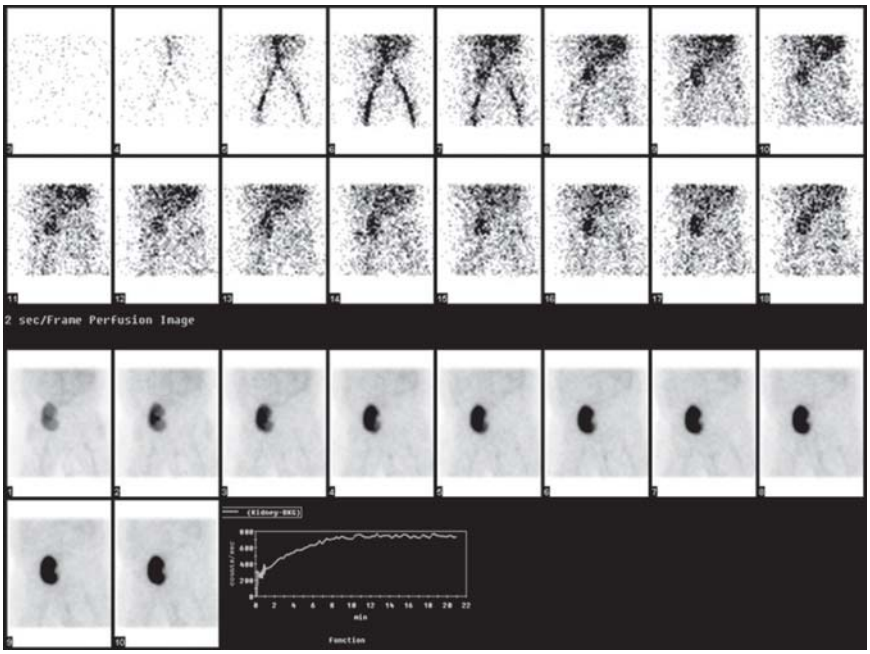

Fig. 5.13: 99mTc-LLEC scan in vasomotor nephropathy (ATN). Baseline images show normal perfusion and uptake but significant retention. Time activity curve not going down consistent with ATN

most important "functional edge" over many other diagnostic methods. With further refinements in technology, instrumentation and radiopharmaceuticals, nuclear medicine destined to improve more in future.

Measurement of Renal Function

Glomerular filtration rates Renal function can be assess by clinical methods using blood urea nitrogen (BUN) and serum creatinine level but these are relatively crude process, as significant decreased in function must occur before changes in BUN and creatinine are seen. Other factors which affect creatinine level are diet, difference in muscle mass and certain medication.

GFR is the clearance rate of substance that is excreated from the body by glomerular filtration and not secreted or reabsorbed by tubules, the model molecule for this is inulin. Those substance has complete first pass extraction through kidney are used to calculate renal plasma flow (RPF). Para-amino hippurate is about 90% extracted and can be used for calculation of RPF. As it is not completely excreated the term effective renal plasma flow (ERPF) is used.

Many radiopharmaceuticals are used to calculate GFR; these include ^{99m}Tc-DTPA and ^{131}I-iothalamate. In India, ^{99m}Tc-DTPA is manly used for GFR calculation. Initially, multiple blood sample technique were used but now two blood sample technique most commonly used. Blood sample are taken at 1 hr and 3 hr after injection. Normal GFR value is approximately 106±27 for adult. In small children adult level GFR reach at about 2 year of age.

Effective renal plasma flow (ERPF) ERPF is another parameter of renal of renal function. As inulin clearance is gold standard for GFR calculation, PAH is used for the calculation of ERPF. Measurement with PAH is accurate but this method need continuous infusion which is inconvenient and lack of precision. The radiolabeled form of hippuric acid, ^{131}I OIH and I-123 OIH, has been used to quantify ERPF. The urinary clearance of ^{131}I OIH is about 85% of the PAH. Currently, ^{99m}Tc-MAG-3 is commonly used for ERPF calculation. Plasma clearance of ^{99m}Tc-MAG-3 is 30-40% lower than that of OIH, but the ratio between their plasma clearance is identical at normal and reduced renal function.[35,36] For accurate calculation of ERPF need multiple blood samples but in clinical practice it is difficult to take multiple blood samples. Several methods have been published to assess the plasma clearance of ^{99m}Tc-MAG-3 using single blood sample.[36, 37] Blood sample at 44 minutes has shown to reproducible within 19 ml/min.

Positron Emission Tomography—Computed Tomography (PET-CT)

PET-CT is a relatively new non-imaging modality which provides functional/metabolic and structural details in the same setting. At present, 2-deoxy-2-[18F]-fluorodeoxyglucose ([18F]-FDG) is most commonly used for PET/PET-CT imaging throughout the world. ([18F]-FDG is a radiolabeled analogue of glucose and as such it is able to detect altered glucose metabolism in various disease conditions. Frequently, there is a significant increase in glucose metabolism in cancer cells compared with that in the surrounding tissues. The role of FDG-PET in the initial staging, monitoring response to the therapy, and management of many types of cancer has been well-documented.[38] There are relatively few FDG-PET reports describing its role in assessing primary urologic tumors at their sites of origin due to the potential problem of tracer excretion through the kidneys. The

usefulness of FDG-PET-CT has been documented in the detection of distant metastasis from these malignancies.[39,40] In recent years, however, special PET-CT techniques have been evolved over the time to make PET-CT imaging possible in patients with primary kidneys and urinary bladder cancers. Moreover, the introduction of other PET radiotracers, such as C11-choline and C11-acetate, the role of this technique in patients with urologic cancer and especially in those with prostate cancer has been enhanced.[41] The main role of PET-CT in urologic malignancies is initial diagnosis and staging, evaluation of treatment response and detection of recurrent/metastatic disease.

Renal Cancer

Despite significant uptake and excretion through the kidneys, FDG has been used in the diagnosis and management of renal cell carcinoma (RCC). Bachor et al[42] studied 29 patients with solid renal masses and found that PET was positive in 20 (77%) of 26 patients of RCC. PET was false-positive in an angiomyolipoma, a pericytoma, and a pheochromocytoma. Ramdave et al[43] evaluated the accuracy of FDG-PET for staging and management of 17 patients with known or suspected RCC. PET and CT had an accuracy of 94%. In addition, PET detected pulmonary metastases in two patients. Miyakita et al[44] compared biologic characteristics of RCC with FDG and concluded that PET-positive tumors had higher tumor grade and increased GLUT-1. Kumar et al,[45] showed good results in 28 solid renal masses of which 10 were primary (nine malignant, one benign) and 18 were metastatic renal tumors. FDG-PET accurately depicted 23 of 27 (85%) malignant renal 27 masses. Of the 10 primary renal tumors (Fig. 5.14), FDG-PET was true positive in eight of nine (89%), true 28 negative in one and false negative in one. In addition to the characterization of primary tumors, FDG-PET was valuable in 31 primary staging and altered treatment in 30% of patients (three of 10). Of the 18 metastatic renal 32 masses,

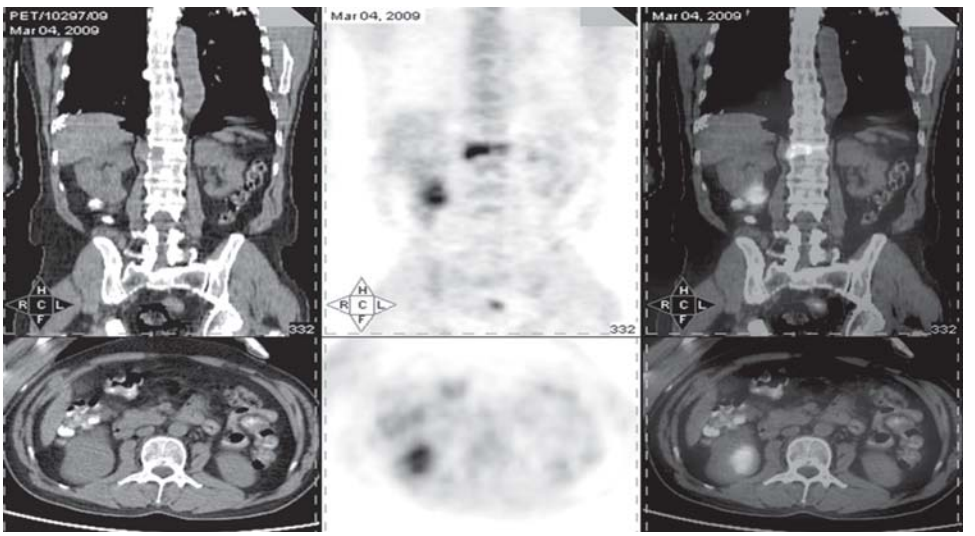

Fig. 5.14: ^{18}F-FDG PET-CT study: Coronal and axial sections of CT, PET and PET-CT showing soft tissue mass at lower pole of right kidney. Note FDG uptake in T12 *(For color version see Plate 7)*

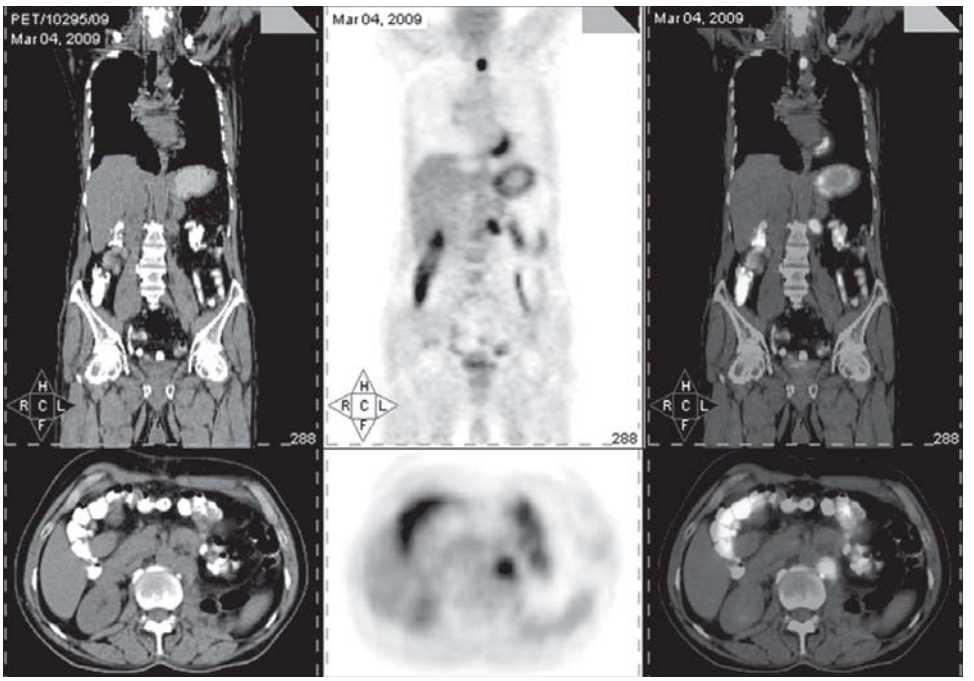

Fig. 5.15: ^{18}F-FDG PET-CT study: Coronal and axial sections of CT, PET and PET-CT showing soft tissue mass in left renal bed suggestive local recurrence *(For color version see Plate 8)*

FDG-PET was positive in 15 (83%) masses. For detection of recurrent and distant disease, PET was found to have an accuracy of 100% in detecting local recurrence and metastases as compared CT which had accuracy of 88% (Fig. 5.15). Majhail et al[46] evaluated FDG-PET in the detection of distant metastases in 24 patients with RCC. FDG-PET results were compared with those abstracted with biopsy in 33 lesions. Overall sensitivity, specificity, and PPV of FDG-PET were 64%, 100% and 100% respectively.

Urinary Bladder Cancer

Previously, FDG-PET was thought to have limited use in diagnosis and management of bladder cancer. However, with modified techniques (after injection of diuretic and delayed imaging) it is possible to image primary as well as recurrent urinary bladder cancer (Fig. 5.16). Kosuda et al[47] studied 12 patients with FDG-PET for the evaluation of recurrent or residual disease. PET identified 100% (17 of 17) of distant metastases (lung, bones, and remote lymph nodes) and 67% (2 of 3) of local lymph nodes. Heicappell et al[48] also had similar detection rate of 67% for local lymph node involvements. Ahlstrom et al[49] attempted to improve the accuracy of PET by using C11-methionine, which has no urinary excretion. The authors reported a sensitivity of 78% (18 of 23) and there was good correlation of tracer uptake and tumor stage.

In conclusion, PET-CT has shown very encouraging results in a limited number of studies, and has also demonstrated a good sensitivity for initial staging in patients with renal and bladder cancer. FDG-PET seems

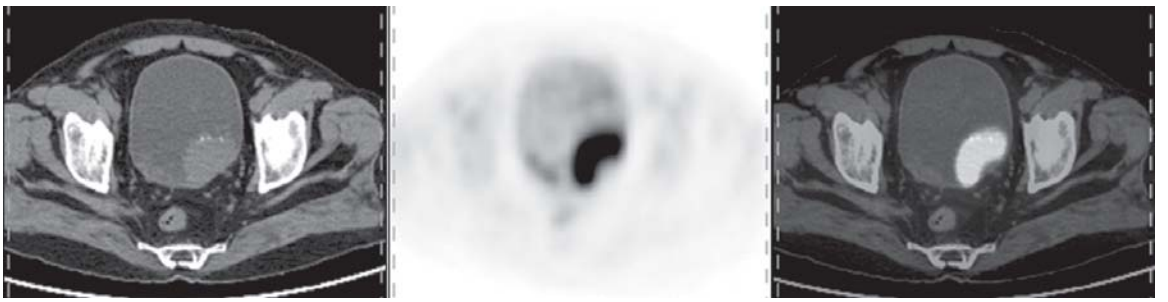

Fig. 5.16: ^{18}F-FDG PET-CT study: Axial sections of CT, PET and PET-CT showing soft tissue mass in urinary bladder suggestive primary bladder cancer *(For color version see Plate 8)*

to be superior to conventional imaging modalities for detecting local disease and recurrence, and distant metastases.

REFERENCES

1. Berkhin EF, Humphreys MH. Regulation of tubular secretion of organic compounds. Kindney Int 2001;59:17-30.
2. Bubek B, Brandau W, Steinbacher M. Tc-99m labeled renal function and imaging agent. II. Clinical evaluation of Tc-99m MAG-3. Nucl Med Biol 1988;15:109-18.
3. Jafri RA, Britton KE, Nimmon CC. Tc-99m MAG-3: A comparison with I-125 and I-131 OIH, inpatients with renal disorders. J Nucl Med 1988;29:147-58.
4. Gutsche HU, Scheffler M, Muller-Surr R et al. Micropuncture study on filtration and reabsorption of technium-99m L, L-Ethylenedicysteine in rats, In: Taylor A, Nally JV, Thomsen H (Eds). Radionuclides in nephrourology. Society of nuclear medicine, Reston, Virbinia. 1997;160-64.
5. Taylor A, Hansen L, Eshima D, et al. Comparison of ^{99m}Tc-LL-EC in rats and humans. J Nucl Med 1997;38:821-26.
6. Atkins HL, Cardinale KG, Eckelman WC, et al. Evaluation of Tc 99m DTPA prepared by three different methods. Radiology 1971;98:674-77.
7. Cohen ML, Smith FGJ, Mindell RS, Vernier RL. A simple reliable method of measuring glomerular filtration rate using single low dose iothalamate I-131. Pediatrics 1969;43:407-15.
8. Chervu LR, Freeman LM, Blaufox MD. Radiopharmaceuticals for renal studies. Semin Nucl med 1974;4:3-22.
9. Arnold RW, Subramanian G, McAfee JG Blair BJ, Thomas FD. Comparison of Tc-99m complexes for renal imaging. J Nucl Med 1975; 16:357-67.
10. Lee HB, Blaufox MD. Mechanism of renal concentration of Tc99m-glucoheptonate. J Nucl Med 1985;26:1308-13.
11. Enlander D, Weber PM, dosRemedios LV. Renal cortical imaging in 35 patients: Superior quality with Tc99m-DMSA. J Nucl Med 1974;15:743-49.
12. Meller St, Eckstein HB. Renal scintigraphy: Quantitative assessment of upper urinary tract dilatation in children. J Paeditr Surg1981;16: 123-26.
13. O'Reilly PH, Testa HJ, Lawson RS, Farrar DJ, Charlton EG. Diuresis renography in equivocal urinary tract obstruction. Br J Urol 1978;50: 76-80.
14. Londe S. Causes of hypertension in the young. Pediatr Clin North Am1978;25:55-66.
15. Blaufox MD, Fine EJ, Heller S, Hurley J, Jagust M, Li Y, Mann SJ, Pickering TG, Zanzonico P, Zhang CG. Prospective study of simultaneous orthoiodohippurate and diet hylenetriamine-penta-acetic acid Captopril renography. The Einstein/Cornell Collaborative Hypertension Group. J Nucl Med 1998;39(3):522-28.
16. Majd M, Potter BN, Guzzeta PC, Ruley EJ. Effect of captopril on efficacy of renal scintigraphy in detection fo renal artery stenosis. J Nucl Med 1983;24:23-27.
17. Sfakianakis GN, Sfakiankis E. Lasix captopril renography in the diagnosis of renovascular hypertension. Contrib Nephrol 1990;79:219-27.
18. Consensus Report on Captopril Renogram in Renovascular Hypertension. JNM 1996; 1876–82.

19. Wenting GJ, Tan-Tjiong HI, Derkx FH. Split renal function after captopril in unilateral renal artery stenosis. BMJ 1984;288:886-90.
20. Dondi M. Captopril renal scintigraphy with Tc99m-MAG-3 for detection renal artery stenosis. Am J Hypertens 1991;4:737S-40S.
21. Arendshorst WJ, Brannstrom K, Ruan X. Actions of angiotensin II on the renal microvasculature. J Am Soc Nephrol Jan;10 1999;Suppl 11:S149-61.
22. Kumar R, Padhy Ajit Kumar, Machineni, Sriram Padey Anil Kumar, Malhotra A. Individual kidney GFR in the interpretation of non-diagnostic curves on captopril renography. Nucl Med Comm 2000;21:637-43.
23. Setaro JF, Chenn CC, Hoffer PB, Black HR. Captopril renography in the diagnosis of renal artery stenosis and the prediction of improvement with revascularisation: The Yale vascular center experience. Am J Hypertens 1991;4:698S-705S.
24. Padhy AK, Gopinath PG, Basu AK: Role of ^{99m}Tc-DTPA renal study in children with upper urinary tract dilation. Indian J Med Res 1985;82:238-47.
25. Chaiwatanrat T, Padhy AK, Bomanji J, Nimmon CC, Sonmezoglu K, Britton KE. Validation of renal output efficiency as an objective quantitative parameter in the evaluation of upper urinary tract obstruction. J Nucl Med 1993; 34:845-48.
26. Sfakianakis GN, Damoulaki-Sfakianaki E. Nuclear medicine in pediatric urology and nephrology. J Nuc1 Med 1988;29:1287-1300.
27. Padhy AK, Gopinath PG, Mitra DK, et al. Direct radionuclide cystogram (DRCG) and urine flowmetry in the evaluation of patients with VUR and/or associated obstructive/neurogenic pathology of lower urinary tract in children. Indian J paeditr 1989;56:423.
28. Sfakianakis GN. Nuclear medicine in congenital urinary tract anomalies. In: LM Freeman (Ed) Nuclear Medicine Annua11991: New York: Raven Press, 1991;129-92.
29. Kumar R, Ritesh Gupta, Malhotra A. Nephroptosis: GHA scan as a diagnostic modality. Clin Nucl Med 2000;25:473-74.
30. Bell EG, Blaufox MD. Clinical application of renal imaging. In EJ (Eds): Diagnostic Nuclear Medicine. Gottschalk A, Potchen Baltimore: Williams and Wilkins Co 1976;476-91.
31. Viberti GC, Bilous RW, Mackintosh D, Keen H. Monitoring Glomerular function in diabetic nephropathy: A prospective study. Am J Med 1983;74:256-64.
32. Padhy AK, Gopinath PG, Mehta SN, et al. Significance of transplant perfusion index in the diagnosis of acute rejection—experience in live-related renal transplant recipients. Indian J Med Res 1989;90:113-23.
33. Hilson AJW, Maisey MN, Brown CE, et al. Dynamic renal transplant imaging with ^{99m}Tc-DTPA (Sn) supplemented by a transplant perfusion index in the management of renal transplants. J Nucl Med 1978;19:994-1000.
34. Padhy AK, Gopinath PG, Mehta SN, et al. Tc-99m renal transplant scintigraphy in the diagnosis of urinoma. Clin Nucl Med 1989; 14:769-71.
35. Bubeck B, Brandau W, et al. Pharmacokinetics of technetium-99m-MAG-3 in humans. J Nucl Med 1990;3:1285-93.
36. Russell CD, Thorstad BL, et al. Quantation of renal function with technetium-99m MAG3. J Nucl Med 1988;29:1931-33.
37. Relling M, Nielsen BV, et al. Renal and extrarenal clearance of ^{99m}Tc-MAG-3: A comparison with I-125 OIH and Cr-51-EDTA inpatients representing all levels of glomerular filtration rate. Eur J Nucl Med 1995;22:1379-84.
38. Kumar R, Zhuang H, Alavi A. PET in the management of urologic malignancies. Radiol Clin North Am 2004;42(6):1141-53.
39. Seltzer MA, Barbaric Z, Belldegrun A, Naitoh J, Dorey F, Phelps ME, et al. Comparison of helical computerized tomography, positron emission tomography and monoclonal antibody scans for evaluation of lymph node metastases in patients with prostate specific antigen relapse after treatment for localized prostate cancer. J Urol 1999;162:1322-28.
40. Hofer C, Laubenbacher C, Block T, Breul J, Hartung R, Schwaiger M. Fluorine-18-fluorodeoxyglucose positron emission tomography is useless for the detection of local recurrence after radical prostatectomy. Eur Urol 1999;36: 31-35.
41. Oyama N, Miller TR, Dehdashti F, Siegel BA, Fischer KC, Michalski JM, et al. 11C-acetate PET imaging of prostate cancer: Detection of recurrent disease at PSA relapse. J Nucl Med 2003;44:549–55.
42. Bachor R, Kotzerke J, Gottfried HW, Brandle E, Reske SN, Hautmann R. Positron emission

tomography in diagnosis of renal cell carcinoma. Urologe A 1996;35:146-50.

43. Ramdave S, Thomas GW, Berlangieri SU, Bolton DM, Davis I, et al. Clinical role of F-18 fluorodeoxyglucose positron emission tomography for detection and management of renal cell carcinoma. J Urol 2001;166:825-30.
44. Miyakita H, Tokunaga M, Onda H, Usui Y, Kinoshita H, et al. Significance of 18F-fluorodeoxyglucose positron emission tomography (FDG-PET) for detection of renal cell carcinoma and immunohistochemical glucose transporter 1 (GLUT-1) expression in the cancer. Int J Urol 2002;9:15–18.
45. Kumar R, Chauhan A, Lakhani P , Xiu Y, Zhuang H, Alavi A. F18-FDG-PET in characterization of solid renal masses. Mol Imaging Biol 2005; 7(6):431-39.
46. Majhail NS, Urbain JL, Albani JM, Kanvinde MH, Rice TW, Novick AC, et al. F-18 fluorodeoxyglucose positron emission tomography in the evaluation of distant metastases from renal cell carcinoma. J Clin Oncol 2003;21:3995-4000.
47. Kosuda S, Kison PV, Greenough R, Grossman HB, Wahl RL. Preliminary assessment of fluorine-18 fluorodeoxyglucose positron emission tomography in patients with bladder cancer. Eur J Nucl Med 1997;24:615-20.
48. Heicappell R, Muller-Mattheis V, Reinhardt M, Vosberg H, Gerharz CD, Muller-Gartner H, et al. Staging of pelvic lymph nodes in neoplasms of the bladder and prostate by positron emission tomography with 2- [(18)F]-2-deoxy-D-glucose. Eur Urol 1999;36:582-87.
49. Ahlstrom H, Malmstrom PU, Letocha H, Andersson J, Langstrom B, Nilsson S. Positron emission tomography in the diagnosis and staging of urinary bladder cancer. Acta Radiol 1996;37:180-85.

Chapter

6

Current Status of Urographic Contrast Media

Sumedha Pawa

INTRODUCTION

Iodinated radiographic contrast media are used widely for imaging of the genitourinary system. These are required for urography and for direct intraluminal studies of the genitourinary tract, such as urethrography, cystography, retrograde pyelography, and loopograms. Their use is essential when CT scan examinations are performed to detect or to characterize renal masses and for CT staging of renal adenocarcinoma.[1] Contrast media are also required for diagnostic and therapeutic angiography.

The compounds used as contrast media in radiological practice should have the basic requirement of effective contrast-enhancement properties and complete inertia towards biological substrates which exert no impact on the physiology of the organs and tissues with which they come into contact. Because they are administered purely for diagnostic reasons, they are expected to have higher risk margins and improved safety profiles compared to therapeutic agents. Furthermore, the excretion should be rapid and complete.[2-4]

DEVELOPMENT OF CONTRAST MEDIA

The long search for a contrast medium featuring the ideal qualities, began in the 1920s, following the advent of the first iodinated compound, **sodium iodide**. Since then, research has developed along two parallel and complementary lines which characterise all pharmaceutical research: increased efficacy and reduced toxicity.

Binding iodine to organic molecules marked the first breakthrough in the development of safer contrast media, making it possible to obtain a three-fold reduction of iodine toxicity compared with sodium iodide, an inorganic salt. However, the development of the first organic agent-**uroselecton**, did not mark increased efficacy in terms of contrast enhancement, as each molecule bound to only one iodine atom. An initial increase in efficacy and reduced toxicity was achieved with uroselecton B, a bisodium salt with two iodine atoms. A further step forwards in terms of efficacy was attained with the development of diodone, with 2 iodine atoms and 2 particles in solution.

Acetrizoic acid, a tri-iodinated compound was introduced in the early 1950s.[5] Strategies to improve efficacy and safety are demonstrated by modifications of the first tri-iodinated contrast medium, acetrizoate. It was suggested that the presence of a hydrogen

atom on the tri-iodinated benzene ring gives a higher degree of protein binding than when the hydrogen atom has been substituted. It was hypothesized that an increase in protein binding factor incited anaphylactoid reactions. In diatrizoate, the unsubstituted hydrogen of acetrizoate has been exchanged for another accetamido unit; this has led to higher biologic tolerance.[6]

In the 1960s, all water soluble contrast media were salts of iodinated fully substituted benzoic acid derivatives. These organic acids have three hydrogen atoms replaced by iodine atoms and three hydrogen atoms replaced by simple side chains. For every three iodine atoms in solutions, two particles exist one anion and one cation in the ratio of 3:2.

Further strategies to decrease general toxicity have been to decrease both osmotoxicity and ionicity by replacing the ionizing carboxyl group (i.e. $COO^- Na^+$ and $COO^- Meg^+$) with hydrophilic structures that could be covalently bound to the benzene ring to get a nondissociating (nonionic) water soluble contrast medium molecule. In 1969, Almen suggested that nonionic molecules could reduce osmolality.[7] The first major breakthrough along these lines was the historic introduction, by Almen of the ratio 3 nonionic monomer, metrizimide released in 1977.[8] This generation of low osmolar contrast media (LOCM) now in widespread clinical use includes iohexol, ioversol, iopamidol and iobitridol.[9] In the 1980s and 1990s, there has been an ongoing development of nonionic isotonic dimers. These agents are consequence of further applications of principles to eliminate ionicity, increase hydrophilicity, lower osmotoxicity, and increase the iodine atoms per molecule.[9]

TYPES OF RADIOGRAPHIC CONTRAST MEDIA

Contrast media are characterized as ionic or nonionic and as monomers or dimers. Ionic media break down into charged particles when entering a solution such as blood.[10] The iodinated benzene ring contains the ionizing carboxyl group with a cation, usually sodium or meglumine. The carboxyl groups ionize in solution, making the agents water soluble. Because these compounds dissociate into ions in water and contain only one iodinated benzene ring, they are referred to as **ionic monomeric agents**. Commonly used contrast material anions are diatrizoate and iothalamate. In solution, the negatively charged contrast anions are conjugated with one of two positively charged cations: sodium or methylglucamine (also called meglumine). In some contrast agents only one of these two cations is used, whereas in others both are used in combination.[1]

Ionic monomers have a relatively high osmolality (> 1400 mOsm/kg at 50 to 76 percent by weight concentrations) because each molecule which contains three iodine atoms dissociates into two particles in solution (ratio 3:2).

Amongst ionic monomers, meglumine iothalamate, sodium iothalamate, and meglumine and sodium diatrizoate preparations are available in India.

Of the many lower-osmolality contrast agents introduced, **nonionic monomers** are the most popular. In nonionic monomers the tri-iodinated benzene ring is made water soluble by the addition of five or six hydrophilic hydroxyl groups to organic side chains placed at 1,3, and 5 positions. Because there is no carboxyl group, nonionic monomers do not ionize in solution. Nonionic contrast agents have the desirable property of being

soluble in water (hydrophilic) and yet do not dissociate in solution. They have relatively low osmolality (500 to 700 m Osm/Kg) at comparable iodine concentrations. Each nonionic monomer molecule contains three iodine atoms per one particle in solution (ratio = 3:1). The nonionic monomers currently in use in India include Iohexol, Iopromide, Ioversol and Iopamidol.

Ionic dimers are formed by joining two ionic monomers together and eliminating one of the carboxyl groups. These agents therefore, contain six iodine atoms for every two particles in solution (ratio of 6:2). The only commercially available ionic dimer is ioxaglate. It has concentration of 59 percent (320 mg iodine/ml) and a relatively low osmolality of 600 m Osm/Kg at comparable iodine concentrations. Due to its viscosity, it is not manufactured at higher concentrations. Ionic oxaglate has been used more widely for peripheral arteriography than for intravenous studies. **Nonionic dimers** such as iotrol and iodixanol consist of two joined nonionic monomers. These substances contain six iodine atoms for every one particle in solution (ratio of 6:1), and therefore for a given iodine concentration they have the lowest osmolality of all the contrast agents (approximately 300 m Osm/Kg). At approximating 60 percent by weight concentration they are iso-osmolar with plasma.[1] However, it results in higher viscosity and greater resistance to cathetar injection.[9]

Thus, currently, there are four classes of contrast media available for clinical use, high osmolar ionic monomers, low osmolar non-ionic monomers, low osmolar ionic dimers and iso-osmolar non-ionic dimers. They are provided at various iodine concentrations and have different physicochemical properties (osmolality, viscosity, hydrophilicity, ions content and pH). All contrast media are distributed in the extracellular phase, they do not penetrate an intact blood-brain barrier and all are excreted via glomenular filtration.[4]

Ionic dimer is not available in India, while the nonionic dimer iodixanol was introduced in India in 2002.

The ratio of iodine atoms to dissolved particles is an important characteristic of contrast media and is a commonly used term. This describes the important relationship between the imaging effect (attenuation of X-rays) and the osmotoxic effect of the media. Since the ratio represents the number of iodine atoms divided by the numbers of particles of the contrast medium in solution, a higher ratio is more desirable, since more iodine means better opacification and fewer particles of contrast medium means a lower osmotoxic effect.[11] Agents with a ratio of 1.5 (3:2) have been termed high-osmolar contrast media (HOCM). This group consists of ionic monomers, e.g. sodium iothalamate, meglumine iothalamate, sodium diatrizoate and meglumine diatrizoate. Agents with a ratio of 3 (3:1) have been termed low osmolar contrast media (LOCM) which include nonionic monomers like iohexol, iopamidol, ioversol etc. and ionic dimer called ioxaglate. Agents with a ratio of 6 (6:1) are termed isotonic contrast media (IOCM) which are nonionic dimers, e.g. iodixanol, iotrolan.[9]

PHARMACOKINETICS OF EXTRA CELLULAR IODINATED CONTRAST AGENTS

X-ray contrast media molecules have very low lipid solubility and extremely low chemical reactivity with body fluids, and they range in molecular weight from 600 to 1650. Molecules of this type distribute throughout the extracellular spaces of the body. There is

no evidence of any substantial penetration of these contrast media molecules through the cell membrane or into the interior of viable cells, with the single exception of the proximal tubular cells of the kidney. Theoretically, the differences in the molecular weight and size between the monomeric and the dimeric contrast agents could lead to slightly slower distribution rates into the extracellular space for the larger dimers. This effect, however, appear to be quite small and is probably not clinically important, though the increased renal intratubular viscosity effects of the isotonic dimers are yet to be fully assessed.[12,13]

When the contrast media molecules reach the systemic circulation, the molecules quickly equilibrate across capillary membranes (except an intact blood-brain barrier).[14] In the first phase of distribution, the increase in intravascular osmolality for the hypertonic agents, including the LOCM, causes a rapid fluid shift across capillary membranes toward the hypertonic (intravascular) compartment. As the contrast medium molecules pass through the capillary bed, there is rapid movement through capillary pores into the interstitial, extracellular space, as well as glomerular filtration into the renal tubules.

The clearance of X-ray contrast media is primarily by means of glomerular filtration and renal clearance. Although older media such as iodopyracet (Diodrast) were excreted by means of both glomerular filtration and tubular secretion, none of the currently employed molecules are reabsorbed or secreted by the renal tubules. Under normal physiologic conditions, nearly 100 percent of the contrast medium is eliminated through the kidney, and the instantaneous rate of removal is equal to the glomerular filtration rate times the plasma iodine concentration. Less than one percent is excreted through extrarenal routes that include liver, bile, small and large intestines, sweat, tears and saliva. Vicarious excretion through extrarenal routes occurs most commonly in association with a renal insult or renal failure.

The clearance of contrast media molecules is usually described by the half-time for the renal clearance portion of plasma decay curves. The half-time (the time required for elimination of 50 percent of the agent from the body) in patients with normal renal function is 1-2 hours for each of the four groups of contrast media.[9] In the total absence of renal function, the extracellular concentration of iodine will approach a value given by the total iodine injected divided by the extracellular volume, which is approximately 200 ml per kilogram of body weight.

In patients with renal failure, the issue has been debated, whether patients with renal failure must undergo emergent dialysis after examination in which contrast medium is used. No definitive studies have addressed this issue. Since contrast agents are not protein bound and possess relatively low molecular weights, they are readily dialyzable. Approximately one-third of either HOCM or LOCM will have already been naturally eliminated through extrarenal routes before dialysis can be set up and begun.[9]

PHYSICO-CHEMICAL PROPERTIES OF CONTRAST MEDIA

The biocompatibility of iodine and its physical properties (k edge at photon energy of 33 Kev) allow the safe intravascular injection of large volumes at high concentration. All the other chemical elements in the molecules serve only to carry, or protect the iodine on the benzene ring. It is the iodine in the radio-

graphic beam and the volume distribution of the contrast material that provide optimal contrast enhancement for imaging.[15]

The ideal contrast medium must exhibit low molecular toxicity. The contrast medium solution should have physico-chemical properties (osmolality, viscosity) as close as possible to those of blood and its formulation should be free of substances interfering with physiological homeostasis.

Water Solubility, Hydrophilicity and Osmolality

Solubility of ionic compounds depends on their formation of salts in solution. The presence of charged groups while increasing the water solubility also increase the intrinsic molecular toxicity. The presence of ions (charged groups) in solution increases the conductivity of body fluids, and changes the overall electrolyte balance.

Hydrophilicity: Nonionic compounds are made water soluble by their high hydrophilicity attributable to the presence of numerous hydroxyl groups on the molecule. This further decreases their protein-binding and tissue-binding propensities and makes them more biologically inert.

Osmolality: The osmolality of any solution is a measure of the number (not size) of dissolved particles, whether ions, molecules, or aggregates, in a liter.

Many of the LOCM used for urography (with the exception of the newest agents, which are iso-osmotic) have osmolalities that range from 483 to 844 mosmol/kg H_2O, whereas those of many of the commonly used HOCM range approximately 1400 to 1515 mosmol/kg H_2O.[16] There is greater potential for tissue damage by contrast agents with greater osmolality. The hyperosmolality of solutions is responsible for the sudden and drastic drawing of water from the cellular and interstitial spaces towards plasma, thereby producing local effects; such as heat and pain. The high osmolality of the contrast medium solution can induce systemic effects such as vasodilation, alteration to the permeability of vessel endothelia, hypervolemia, and osmotic diuresis.[5] For urography and to some extent for CT scanning some degree of osmotic diuresis is necessary to distend the urinary tract optimally. With HOCM the osmotic diuretic effect is strong. The lower osmotic effect of LOCM, however is not a significant disadvantage because of a higher iodine concentration achieved in the urine.

Viscosity

When the contrast-medium is injected into a vessel at a high rate, a substantial slowing in the blood flow in the vessel is observed during administration, which is commensurate with the viscosity of the solution.[17] A lower viscosity is required for agents that have to be rapidly injected intravascularly. With increasing concentrations of any contrast agent, the viscosity increases. The viscosity is largely controlled by the composition of the side chains on the molecules. With conventional ionic compounds, the meglumine side chain helps to achieve water solubility and biologic tolerance but also increases the viscosity.

Contrast medium solutions today feature either reduced viscosity and high hyperosmolality at medium-high concentrations (300 mg/ml) (ionics); or reduced viscosity and limited hyperosmolality (nonionics); or high viscosity and is osmolality (nonionic dimers).

Viscosity also plays a role at the level of the nervous system, as a direct correlation

has been observed between viscosity of solution and magnitude of damage to the blood-brain barrier.[18] If associated with high viscosity, isotonicity of radiopaque solutions also produces unwanted effects at renal level.

Pharmaceutical Characteristics: The Role of Formulation

Elements in the formulation (e.g. chelating agents, buffering agents, counter-ions) have a role in inducing adverse effects.

Diatrizoate compounds cause significant reduction in ionic calcium because of chelating agents (e.g. sodium citrate) which are mixed with the contrast material for the purpose of stabilization of the solution. Calcium supplemented solutions have been developed. Sodium EDTA was replaced with calcium-sodium EDTA.

Nonionic compounds produce little or no decrease in ionic-serum calcium because of absence of chelating additives. Potential undesirable side effects on the cardiovascular system, therefore can be avoided by using nonionic contrast media. These also may be preferred in patients with hypertensive cardiovascular disease who are taking calcium channel blockers.

ADVERSE REACTIONS TO CONTRAST MEDIA

Adverse effects of contrast media are believed to be primarily related to their (1) osmotoxicity, (2) chemotoxicity, (3) ion toxicity, and (4) dose. Other factors, such as viscosity and lipophilicity may also play a role. Osmotoxic effects include pain and discomfort, vasodilatation with hypotension, and rigidification of red blood cells. Chemotoxicity may be directly responsible for the release of vasoactive substances that cause allergic-like symptoms. High dosages that disturb the ionic and osmotic balance in the body will elicit adverse reactions without exhibiting a direct interaction with other molecules.[19]

Chemotoxicity of contrast media is believed to increase as the number of carboxyl groups increase and the number of hydroxyl groups decrease. Ion toxicity occurs when ionic sustances (either the ionic contrast medium anion itself, the cation it is conjugated with, or ionic components in additives) interfere with cellular functions.[20]

Adverse reactions to intravascular contrast media are not frequent and generally classified as either idiosyncratic or chemotoxic. Idiosyncratic (i.e. anaphylactoid) reactions occur unpredictably and independently of the dose or concentration of the agent. Most anaphylaxis-like reactions relate to release of active mediators. Conversely, chemotoxic – type effects relate to dose, the molecular toxicity of each agent and the physiological characteristics of the contrast agents (i.e. osmolality, viscosity, hydrophilicity, calcium-binding properties and sodium content). Chemotoxic effects of contrast media are more likely in patients who are debilitated or medically unstable.[4]

Guidelines on Prevention and Management of Acute Reactions

Acute reactions to contrast media can be divided into minor, intermediate and severe life threatening reactions. The minor reactions include flushing, nausea, arm pain, pruritis, vomiting, headache and mild urticaria. Such reactions are usually mild in severity, of short duration, self-limiting and generally require no specific treatment. Intermediate reactions include more serious degrees of the above symptoms, moderate

degrees of hypotension and bronchospasm. They usually respond readily to appropriate therapy. Severe life threatening reactions include severe manifestation of all of the symptoms included under minor and intermediate reactions, convulsions, unconsciousness, laryngeal edema, severe bronchospasm, pulmonary edema, severe cardiac dysrhythmias and arrest, cardiovascular and pulmonary collapse. The prevalence of adverse reactions with low osmolar contrast media is lower in comparison to high osmolar contrast media by a factor of five to six. Lethal reactions occur rarely.[4]

In the era of ionic contrast media corticosteroid prophylaxis was recommended to patients who had a history of previous generalized moderate or severe contrast medium reaction, asthma or allergy requiring medical treatment. Nowadays with the exclusive use of nonionic contrast media in most radiology departments in the developed world opinion is divided with regard to use of corticosteroid prophylaxis.[4] In a survey performed by the European Society of Urogenital Radiology[21] asthma was considered a significant risk factor but only 48% of the responders gave corticosteroid prophylaxis to these patients. Administration of a very short course of steroids is relatively safe and inexpensive but should be avoided in patients with diabetes mellitus active tuberculosis, peptic ulcer disease and in the presence of systemic infection.[22,23] However, even in patients who receive both corticosteroid premedication and low osmolar contrast media, severe adverse reactions may still occur.[21,24]

The contrast media safety committee recommends that nonionic agents should be used in patients with increased risk (previous generalized contrast medium reaction, either moderate or severe, asthma or allergy requiring medical treatment of an adverse reaction).[24] Resuscitation drugs should be available in the examination room and the patient should be observed for 20-30 minutes after the contrast medium injection. For extravascular applications of contrast media in high risk patients if absorption or leakage into the circulation is possible, the same precautions as for intravascular administration should be implemented.[4] The guidelines on prevention of generalized contrast medium reactions in adults are shown in Table 6.1.[21]

The radiologist must be prepared to treat the acute serious adverse reactions immediately. In patients at high risk of these reactions most radiologists avoid giving intravascular contrast media if at all possible.[21] If the examination is considered essential, nonionic contrast media should be used, the potential risks of the procedure must be explained to the patient and the resuscitation team should be present when the contrast medium is given.[21] The vast majority of patients with severe anaphylactoid—type reactions recover if they are treated quickly and appropriately[4] (Table 6.2).

The ability to assess and treat the contrast reaction effectively is an essential skill that the radiologist should have and maintain. The first line drugs and equipment such as oxygen, adrenaline 1:1000, antihistamine H1 suitable for injection, atropine, β2-agonist metered dose inhaler, IV fluids—normal saline or Ringer's solution, anti-convulsive drugs (diazepam), sphygmomanometer and an one-way mouth "breather" apparatus should be readily available in rooms in which contrast material is injected.[25]

Table 6.1. European Society of Urogenital Radiology (ESUR) guidelines on prevention of generalized contrast medium reactions in adults[21]

A. Risk factors for reactions:
Previous generalized contrast medium reaction, either moderate (e.g. urticaria, bronchospasm, moderate hypotension) or severe (e.g. convulsions, severe bronchospasm, pulmonary oedema, cardiovascular collapse)

Asthma
Allergy requiring medical treatment

B. To reduce the risk of generalized contrast medium reactions:
Use non-ionic agents

C. Pre-medication is recommended in high risk patients (defined in A):
When ionic agents are used
When non-ionic agents are used, opinion is divided about the value of pre-medication

Recommended pre-medication:
Corticosteroids
Prednisolone 30 mg orally or methylprednisolone 32 mg orally 12 h and 2 h before contrast medium
Corticosteroids are not effective if given less than 6 h before contrast medium
Antihistamines H1 and H2 may be used in addition to corticosteroids, but opinion is divided
Remember for all patients:
Have a trolley with resuscitation drugs in the examination room
Observe patients for 20-30 min after contrast medium injection
Extravascular administration:
When absorption or leakage into the circulation possible, take the same precautions as for intravascular administration

Table 6.2: Simple guidelines for first line treatment of acute reactions to contrast media[4]

- Nausea/vomiting
  Transient: Supportive treatment
  Severe, protracted: Appropriate antiemetic drugs should be considered
- Urticaria
  Scattered, transient: supportive treatment including observation
  Scattered, protracted: appropriate H1 – antihistamine intramuscularly or intravenously should be considered. Drowsiness and/or hypotension may occur
  Profound: consider adrenaline 1:1000, 0.1 – 0.3 mL (0.1-0.3 mg) intramuscularly in adults, 0.01 mg/kg intramuscularly up to 0.3 max. in children. Repeat as needed
- Bronchospasm
  1. Oxygen by mask (6 – 10 L/min)
  2. β2- Agonist metered dose inhaler (2 -3 deep inhalations)
  3. Adrenaline

  Normal blood pressure
  Intramuscular: 1- 1000, 0.1-0.3 mL (0.1-0.3 mg) (use smaller dose in a patient with coronary artery disease or elderly patient)
  In pediatric patients: 0.01 mg/kg up to 0.3 mg max.
  Decreased blood pressure
  Intramuscular: 1:1000, 0.5 mL (0.5 mg), (in pediatric patients: 0.01mg/kg intramuscularly)
- Laryngeal edema
  1. Oxygen by mask (6-10 L/min)
  2. Intramuscular adrenaline (1:1000), 0.5 mL (0.5 mg) for adults, repeat as needed

Contd...

Contd...

- Hypotension
  - Isolated hypotension
    1. Elevate patient's legs
    2. Oxygen by mask (6 – 10 L/min)
    3. Intravenous fluid: rapidly, normal saline or lactated Ringer's solution
    4. If unresponsive: adrenaline: 1:1000, 0.5 mL(0.5 mg) intramuscularly, repeat as needed
  - Vagal reaction (hypotension and bradycardia)
    1. Elevate patient's legs
    2. Oxygen by mask (6-10 L/min)
    3. Atropine 0.6-1.0 mg intravenously, repeat if necessary after 3 – 5 min, to 3 mg total (0.04 mg/kg) in adults. In pediatric patients give 0.02 mg/kg intravenously (max. 0.6 mg per dose) repeat if necessary to 2 mg total.
    4. Intravenous fluids: rapidly, normal saline or lactated Ringer's solution
- Generalized anaphylactoid reaction
  1. Call for resuscitation team
  2. Suction airway as needed
  3. Elevate patient's legs if hypotensive
  4. Oxygen by mask (6-10 L/min)
  5. Intramuscular adrenaline (1:1000), 0.5 mL (0.5 mg) in adults. Repeat as needed. In pediatric patients 0.01 mg/kg to 0.3 mg (max. dose)
  6. Intravenous fluids (e.g. normal saline, lactated Ringer's)
  7. H1-blocker, e.g. diphenhydramine 25 – 50 mg intravenously

Guidelines on Late Adverse Reactions

Late adverse reactions to intravascular iodinated contrast media are defined as reactions occurring 1 hour to 1 week after contrast medium injection. The reactions include symptoms such as nausea, vomiting, headache, itching, skin rash, musculoskeletal pain and fever. Their prevalence remains uncertain and their pathophysiology is not fully understood.[26] A significant proportion of these reactions are unrelated to the contrast medium. However, allergy-like skin reactions are well-documented side effects of contrast media with an incidence of approximately 2%. Late reactions appear to be commoner after nonionic dimers. Patients at increased risk of late skin reactions are those with a history of previous contrast medium reaction and those on interleukin-2 treatment. Most skin reactions are self-limiting and resolve within a week. Management is symptomatic and similar to the management of other drug-induced skin reactions.[24]

Guidelines on Renal Adverse Reactions

The term contrast medium induced nephropathy refers to the reduction in renal function induced by contrast media. It implies impairment in renal function (an increase in serum creatinine by more than 25 percent or 44 μmol/L) occurred within 3 days following the intravascular administration of contrast media and the absence of alternative etiology.[27]

The patients at highest risk for developing contrast induced acute renal failure are those with pre-existing renal impairment (>132 μmol/L) particularly when the reduction in renal function is secondary to diabetic nephropathy.[27,28] Diabetes mellitus perse without renal impairment is not a risk factor.[28] Large doses of contrast media and multiple injections

within 72 hours increase the risk of developing contrast medium induced nephropathy. The route of administration is also important and contrast media are less nephrotoxic when administered intravenously than when given intra-arterially in the renal arteries or in the aorta proximal to the origin of the renal blood vessels.[27]

Several measures have been recommended to reduce the incidence of contrast medium induced nephropathy.[29,30] They include volume expansion, hydration with intravenous administration of normal saline solution or half strength saline solution, infusion of sodium bicarbonate instead of normal saline, infusion of mannitol, pharmacological manipulation, use of low osmolar nonionic contrast media instead of high osmolar ionic contrast media, use of isoosmolar contrast media instead of low osmolar contrast media, gadolionum based contrast media instead of iodine based contrast media for radiography and CT, hemodialysis rapidly after contrast administration, and avoiding short intervals (less than 48 hours) between procedures requiring intravascular administration of contrast media.

At present it is unclear whether there is a difference in nephrotoxic potential between low osmolar nonionic monomeric and isoosmolar nonionic dimeric contrast media. However, it is clear that all contrast media can cause nephropathy in patients with risk factors.[4]

Although hemodialysis can safely remove iodinated contrast media from the body, it is not effective in preventing contrast nephrotoxicity.[31] The contrast media safety committee concluded that hemodialysis does not protect poorly functioning kidneys against contrast medium induced nephropathy. In contrast to hemodialysis, hemofiltration was reported to be effective in reducing the incidence of this complication in patients with advanced renal impairment undergoing interventional vascular procedures.[30]

Gadolinium based contrast media was recommended by some authors for radiographic examinations instead of iodinated contrast media in patients at high risk of contrast nephrotoxicity. However, this recommendation is not safe as gadolinium based contrast media are nephrotoxic particularly at doses above the ones used for MRI examinations (>0.3 mmol/kg bw). In addition, gadolinium based contrast medium in approved intravenous doses up to 0.3 µmol/kg bw will not give diagnostic radiographic information in most cases. These agents are not approved for radiographic examinations. The contrast media safety committee does not recommend the use of gadolinium based contrast media for radiographic examinations to avoid nephrotoxicity in patients with renal impairment since they are more nephrotoxic than iodinated contrast media in equivalent attenuating doses. However, these can be used in patients with a history of previous severe generalized adverse reaction to iodinated contrast media and in case of imminent thyroid treatment with radioactive iodine providing the renal function of the patient is not impaired.[32]

Since contrast media can induce reduction in renal function, these agents should be used with extra care in diabetic patients receiving metformin to avoid retention of metformin that may lead to lactic acidosis.[33] However, there is no conclusive evidence indicating that the intravascular use of contrast media precipitates the development of metformin induced lactic acidosis in patients with normal

serum creatinine (<132 μmol/L). Serum creatinine should always be monitored before administration of contrast medium in patients receiving metformin. If the serum creatinine level is not elevated the examination can be carried out but the metformin therapy should be stopped. The administration of metformin can be resumed after 48 hours providing the serum creatinine remains within the normal range. In presence of elevated serum creatinine the administration of metformin should be stopped and the injection of contrast media should be deferred for 48 hours.[33]

Guidelines on Prevention and Management of Extravasation of Contrast Media

The use of automated power fast flow intravenous injection in multislice CT examinations has increased the incidence of this complication and may result in extravasation of a large volume in a short period of time that may lead to severe tissue damage. Careful intravenous technique including the use of appropriate size cannula placed in a suitable vein avoiding the dorsum of the hand is recommended to avoid extravasation particularly when automated power injector is used. Fortunately, most extravasations result in no long-term sequelae. However, severe skin necrosis and ulceration may occur. Compartment syndrome may be seen associated with extravasation of large volumes.[24]

EVALUATING THE PATIENT BEFORE CONTRAST MEDIA INJECTION AND IDENTIFYING GROUPS AT INCREASED RISK FOR ADVERSE CONTRAST REACTIONS

The patient should be questioned about any prior contrast material administration. If the patient had a reaction, the nature of the reaction must be investigated. If the reaction was idiosyncratic and mild, premedication should be instituted and low-osmolality contrast material subsequently should be used. If the reaction was idiosyncratic and moderate or severe (significant respiratory reaction) an alternate study, such as sonography or MR imaging, should be considered. For example, contrast - enhanced MR imaging can be performed to evaluate the kidneys for renal masses, because MR imaging contrast agents are entirely different from iodinated radiographic contrast agents and there is no known cross-reactivity. Nonidiosyncratic adverse reactions of nausea and vomiting are not considered routine indications for corticosteroid premedication or even use of nonionic contrast media.[1]

It is important to know whether the patient has asthma, diabetes mellitus, renal insufficiency or cardiac disease. Currently or recently taken medications should be known, because contrast material injection may have to be delayed in patients receiving metformin and may have to be monitored closely in patients who have had interleukin -2. Also, adverse reaction may be more difficult to recognize appropriately or treat in patients who are taking beta adrenergic blockers.[1]

Patients who previously have had adverse contrast media events have been found to be at highest risk. Adverse reactions to ionic contrast media were approximately four times as common in patients who had previous adverse reactions.[34] Katayama et al[35] found that total adverse reactions and severe adverse reactions to any type of contrast agent occurred five to six times as frequently in patients with prior adverse reactions to contrast media in comparison with patients who had been exposed previously to contrast material and who had no adverse reaction. Conversely, the total and severe adverse reaction rate in patients receiving contrast media for the first time was 1.2 to 1.4 times

that of patients who previously had received contrast material without difficulty.

Many other groups have been identified as being at increased risk of having a contrast reaction. Asthmatics have increased risk from 1.2 to 2.2 times the risk of general population. Patients with allergies to substances other than contrast material are between 1.5 and 3 times more likely to have an adverse reaction.[34,35]

In a postmarketing suveillance study of prevalence of acute reactions to Iopromide [2], it was observed that a higher adverse drug reaction (ADR) rate was reported following IV administration compared with IA use. There was no apparent correlation between the incidence of ADRs and the amount of contrast medium received for either IV or IA administration. Serious ADRs were reported on 0.02% of the patients. Patients in the 18-50 years group experienced a higher rate of ADRs than patients in the 50 to over 80 years group; the highest rate were experienced by patients in the 18-30 years group.[2] It was suggested that the higher rate of ADRs in the younger patient group might be attributable to a higher immunocompetence among younger adults, suggesting that an immune-mediated process is involved. This theory is also supported by lack of any significant association of the ADR rate with the concentration of the contrast medium and the total dose of iodine. Females had a significantly higher rate of ADRs than males. This was true up to 70 years of age, peaking in the 18-50 years age group.[2] The increasing prevalence of asthma and other allergic diseases in recent years may be associated with the presence of environmental estrogens, which would support the hypothesis that contrast media reactions, allergy, and anaphylaxis are increased in the presence of high estrogen levels.[36]

Race may be an associated risk factor: in the UK, people of Indian subcontinent and Mediterranean origin have a significantly higher risk than the native population.[10]

AGGRAVATION OF DISEASES BY CONTRAST MEDIA

Many disease processes can be aggravated by contrast media. These include cardiac disease (aggravation of arrhythmias, precipitation of angina or congestive heart failure); phaeochromocytomas (hypertensive crisis); myasthenia gravis (acute worsening of respiratory symptoms of myasthenia); uncontrolled hyperthyroidism (thyroid storm); sickle cell anemia (sickle cell crisis); and paroxysmal nocturnal hemoglobinuria.

Guidelines on the Use of Iodinated Contrast Media in Patients with Thyroid Disease

Radiographic water soluble contrast media solutions contain small amounts of free iodine which may cause thyrotoxic crisis in patients with Grave's disease or with multinodular goiter and thyroid autonomy, espically if they are elderly and living in areas of iodine deficiency. The free iodide may also interfere with nuclear medicine diagnostic procedures and treatment for up to 2 months. Prophylaxis is generally not necessary but in high risk patients particularly those in areas of dietary iodine–deficiency, prophylactic treatment may be given by an endocrinologist.[37]

Guidelines on the Use of Contrast Media in Patients with Catecholamine-producing Tumors (Pheochromocytomas and Paragangliomas)

Secretion of catecholamines by phaeochromocytomas and paragangliomas may be continuous or intermittent. Typical clinical presentations include hypertension resistant to

conventional treatment and intermittent crises—attacks of hypertension, headache, sweating, pallor or flushing. Crises occur when catecholamines are released from the tumor and may be spontaneous or precipitated by drugs including contrast media. The contrast media safety committee recommends that α and β-adrenergic blockade with orally administered drugs should be given to these patients under the supervision of the referring physician before administration of intravenous contrast administration. A nonionic agent should always be used in these patients.[24]

Guidelines on Interaction between Contrast Media with other Drugs and Clinical Tests

The contrast media safety committee recommends that one is aware of the patient's drug history and keeps proper records of the contrast medium injection (time, dose and name). Patients taking drugs like metformin, cyclosporine, cisplatin, aminoglycosides, nonsteroid anti-inflammatory drugs, β-blocker, interleukin-2 and hydralazine should be given special attention before injection of contrast media. In addition, contrast media should never be mixed with other drugs in tubes or syringes. Biochemical analysis of blood or urine, collected within 24 hours of contrast medium injection should be avoided. Contrast medium injection may interfere with some isotope studies, and should be avoided for at least 24 hours before isotope bone scanning and before labeling red blood cells for isotope studies.[38]

Guidelines on the Use of Iodinated Contrast Media during Pregnancy or Lactation

In general, intravenous contrast material should be avoided, when possible, in pregnant women so as to eliminate any theoretic adverse effects on the fetus. Since nonionic agents are, in general, better tolerated, their use is preferred over conventional ionic agents in pregnant women.

The radiation dose associated with examinations that require intravascular contrast material may be a more significant risk to the fetus than the contrast medium itself. Other tests not requiring the use of ionizing radiation should be considered unless there is no satisfactory alternative.

Mutagenic and teratogenic effects have not been described after administration of iodinated contrast media. Free iodine in radiographic contrast medium given to the mother has the potential to depress fetal/neonatal thyroid function. Neonatal thyroid function should be checked during the first week if iodinated contrast media have been given during pregnancy. The contrast media safety committee considers this check mandatory; however in many countries it is done routinely as part of neonatal screening. Only tiny amounts of iodinated contrast medium given to a lactating mother reach the milk and only a minute proportion entering the baby's gut is absorbed. Therefore, stopping breastfeeding after contrast administration is unnecessary.[39]

SELECTIVE VERSUS UNIVERSAL USE OF NONIONIC CONTRAST MATERIAL

Various organizations, including the American College of Radiology (ACR), the American College of Cardiology(ACC), and the Society of Cardiovascular and Interventional Radiology (SCVIR), have formulated guidelines to assist institutions in establishing a policy of limited use of low osmolality contrast media. In general, the guidelines recommend that low osmolality agents be administered to patients with previous

contrast reactions, asthma, and allergies, and patients with those underlying diseases that may be aggravated by contrast media administration. The ACR also suggests that low osmolality contrast media be administrated to patients who are at increased risk for aspiration; severely debilitated; very anxious about the contrast procedure; noncommunicative (so that the existence of any pertinent history cannot be ascertained); or who specifically request low osmolality agents.[40] Many institutions also selectively administer these agents to patients with elevated serum creatinine levels.[41]

It can be difficult consistently to limit use of low osmolality agents to a selected group of patients. This is because some of the recommended guidelines can be interpreted differently by different individuals. Also, there is tendency for physicians directly involved in injecting the contrast media and monitoring patients after injection to use the better tolerated nonionic agents increasingly to reduce patient discomfort or the likelihood of a reaction. There is also a tendency for low-risk patients to choose nonionic agents when they are allowed specifically to select the type of contrast material that they are to receive.

STRATEGIES FOR CLINICAL USE: COST CONTAINMENT

It is universally acknowledged that if the LOCM was not so expensive, a complete switch to ionic or nonionic LOCM would have occurred years ago. Significant concerns persist regarding not only cost but liability. Professional liability is related to the somewhat hostile medicolegal problems today and often stands in opposition to the physician's obligation to follow the prudent course of choosing the best drug or therapy for the patient. A 'universal switch' strategy has extremely burdensome financial implications; therefore, any strategy for use must be rational yet dynamic. The most challenging task is to develop tactics for identification of patients considered to be at risk for the administration of any contrast media. Estimations of patient risk are derived from a variety of sources. Most physicians can recognize seriously ill and unstable patients. However, not all at - risk patients are always readily identified. In emergency situations or when adequate assessment or pretreatment with steroids is not possible, all patients are best served by LOCM. At the same time, concerted efforts should be made to decrease the waste of contrast material and to make every attempt to limit the dose and volume of contrast for any given study.

The ultimate decision on choice of contrast rests with public policy makers, organized medicine, and the individual physician and patient. A basic understanding of contrast media, risks of administration, choice of agents, and premedication regimens for high-risk patients, is beneficial in helping patients prepare for their examinations.

As long as cost remains the major focus of the debate over the choice, however, physicians need to be informed advocates, familiar with the science, yet sensitive to the economic implications of the decisions they make to best serve the interests of their patients.[15]

Finally, inspite of all considerations about the selection of contrast media and care taken about various risk factors outlined above, before an intravascular contrast study, it is not possible to opine confidentally how the patient will ultimately react to contrast media. Therefore, considering the medicolegal aspects, it is advisable that a performa outlining the availability of various

contrast media, their possible reactions, and the cost should be made available to the patient, also one must discuss directly with the patient/his relatives on these issues before planning a study and an informed consent signed by the patient and his relation is mandatory.

REFERENCES

1. Cohan RH, Ellis JH. Iodinated Contrast Material in Uroradiology—Choice of Agent and Management of Complications. Rad Clin North Am 1997;24(3):471-91.
2. Kopp AF, Mortele KJ, Cho YD, et al. Prevalence of acute reactions to Iopromide: Postmarketing surveillance study of 74,717 patients. Acta Radiol 2008;8:902-11.
3. Katzberg RW. "Acute reactions to urographic contrast medium: Incidence, Clinical Characteristics, and relationship to history of hypersensitivity" – A commentary. Am J Roentgenol 2008;190:1431-32.
4. Thomsen HS. European Society of Urogenital Radiology (ESUR) guidelines on the safe use of iodinated contrast media. Eur J Radiol 2006; 60:307-13.
5. Contrast Media – A multifactorial Approach, edited by Carlo Del Favero-Intramed Communications, 1997.
6. Lasser E, Farr RS, Fujimagari T, et al. The significance of protein binding of contrast media in roentgen diagnosis. Am J Roentgenol 1962;87:338-60.
7. Almen T. Contrast agent design: Some aspects of synthesis of water-soluble contrast agents of low osmolality. J Theo Biol 1969;24:216-26.
8. Almen T, Boijsen E, Lindell SE . Metrizamide in angiography. I. Femoral angiography. Acta Radiol Diagn 1977;18:33-38.
9. Katzberg RW. Urography into the 21st Century: New Contrast Media, Renal Handling, Imaging Characteristics, and Nephrotoxicity. Radiology 1997;204:297-312.
10. Peter Dawson. Adverse reactions to intravascular contrast agents: Routine prophylaxis is not supported by evidence. BMJ 2006;333: 663-64.
11. Almen T. Visipaque: A step forward—A historical review. Acta Radiol 36(Suppl 399):1995;2-18.
12. Dobroto M, Powell CJ, Holtz E. Biochemical and morphological effects of contrast media on the kidney. Acta Radiol 1995;36:196-203.
13. Jakobsen JA. Renal effects of iodixanol in healthy volunteers and patients with severe renal failure. Acta Radiol 1995;36(suppl 399): 191-95.
14. Rapport SI, Levitan H. Neurotoxicity of X-ray contrast media: Relation to lipid solubility and blood brain barrier permeability. Am J Roentgenol 1974;122:186-94.
15. McClennan BL, Stolbery HO. Intravascular contrast media—Ionic versus nonionic: Current status. Rad Clin North Am 1991;29(3):437-54.
16. Segal AJ. Optimizing urography. World J Urol 1998;16(1):3-8.
17. Morris TW, Kern MA, Katzberg RW. The effects of media viscosity on haemodynamics in selective arteriography. Invest Radiol 1982;7: 70-76.
18. Wycherley AG, Sage MR, Evill CA. Contrast media viscosity: a contributing factor in blood-brain barrier damage following intracarotid contrast injection? Australas Radiol 1986;30: 96-98.
19. Weinmann HJ, Platzek J, Schirmer H, et al. Contrast media: future aspects. Eur Radiol 2005;Suppl 15 (Suppl 4):70-73.
20. Almen T. The etiology of contrast medium reactions. Invest Radiol 1994;29(S1):S 37.
21. Morcos SK, Thomsen HS, Webb JAW. Contrast Media Safety Committee of the European Society of Urogenital Radiology. Prevention of generalized reactions to contrast media: a consensus report and guidelines. Eur Radiol 2001;11:1720-28.
22. Thomsen HS, Bush WH. Treatment of the adverse effects of contrast media. Acta Radiol 1998;39:212-18.
23. Dunnick NR, Cohan RH. Cost, corticosteroids, and contrast media. AJR 1994;162:527-29.
24. Thomsen HS (Ed). Contrast media: Safety issues and ESUR guidelines. Heidelberg: Springer Verlag; 2006.
25. Thomsen HS, Morcos SK. Members of Contrast Media Safety Committee of European Society of Urogenital Radiology (ESUR). Management of acute adverse reactions to contrast media. Eur Radiol 2006;14:476-81.

26. Webb JAW, Stacul F, Thomsen HS, Morcos SK, Members of the Contrast Media Safety Committee of the European Society of Urogenital Radiology (ESUR). Late adverse reactions to intravascular iodinated contrast media. Eur Radiol 2003;13:181-84.
27. Morcos SK, Thomsen HS, Webb JAW. Members of contrast media safety committee of the European Society of Urogenital Radiology (ESUR). Contrast media induced nephrotoxicity: a consensus report. Eur Radiol 1999;9:1602-13.
28. Rudnik MR, Goldfarb S, Wexler L, et al. Nephrotoxicity of ionic and nonionic contrast media in 1196 patients: a randomized trial. Kidney Int 1995;47:254-61.
29. Thomsen HS, Morcos SK. Members of Contrast Media safety committee of European Society of Urogenital Radiology (ESUR). In which patients should serum–creatinine be measured before contrast medium administration? Eur Radiol 2005;15:749-54.
30. Morcos SK. Prevention of contrast media nephrotoxicity—The story so far. Clin Radiol 2004;59:381-89.
31. Morcos SK, Thomsen HS, Webb JAW. Members of the Contrast Media Safety Committee of European Society of Urogenital Radiology (ESUR). Dialysis and contrast media. Eur Radiol 2002;12:3026-30.
32. Thomsen HS, Almen T, Morcos SK. Members of Contrast Media Safety Committee of European Society of Urogenital Radiology (ESUR). Gadolinium – containing contrast media for radiographic examinations : a position paper. Eur Radiol 2002;12:2600-05.
33. Thomsen HS, Morcos SK. Members of Contrast Media Safety Committee of European Society of Urogenital Radiology (ESUR). Contrast media and metformin. Guidelines to diminish the risk of lactic acidosis in non-insulin dependent diabetics after administration of contrast media. Eur Radiol 1999;9:738-40.
34. Shehadi WH. Adverse reactions to intravascularly administered contrast media: A comprehensive study based on a prospective survey. Am J Roentgenol 1975;124:145-52.
35. Katayama H, Yamaguchi K, Kozuka T, et al. Adverse reactions to ionic and nonionic contrast media. A report from the Japanese Committee on the safety of contrast media. Radiology 1990;175:621-28.
36. Narita S, Goldblum RM, Watson CS, et al. Environmental estrogens induce mast cell degranulation and enhance Ig E-mediated release of allergic mediators. Environ Health Perspect 2007;115:48-52.
37. Molen AJvd, Thomsen HS, Morcos SK, Members of Contrast Media Safety Committee of European Society of Urogenital Radiology (ESUR). Effect of iodinated contrast media on thyroid function in adults. Radiol 2004;14: 902-06.
38. Morcos SK, Thomsen HS, Exley CM. Members of Contrast Media Safety Safety Committee of European Society of Urogenital Radiology (ESUR). Contrast Media : Interaction with other drugs and clinical tests. Eur Radiol 2005;15: 1463-68.
39. Webb JAW, Thomsen HS, Morcos SK. Members of Contrast Media Safety Safety Committee of European Society of Urogenital Radiology (ESUR). The use of iodinated and gadolinium contrast media during pregnancy and lactaion. Eur Radiol 2005;15:1234-40.
40. Manual on Iodinated Contrast Material. Reston, VA, American College of Radiology, 1991.
41. Cohan RH, Ellis JH, Dunnick NR. Use of low-osmolar agents and premedication to reduce the frequency of adverse reactions to radiographic contrast media: A survey of the society of Uroradiology. Radiology 1995;194:357-64.

Chapter 7

Tubercular Infection of the Urinary Tract

Ashu Seith Bhalla, Arun Kumar Gupta, Raju Sharma

INTRODUCTION

Tuberculosis (TB) of the urinary tract is not uncommon in India. A multicentric study carried out in 1973 under Indian Council of Medical Research showed an incidence of 10 to 34 percent, of all patients presenting with various urological diseases.[1] The **genito-urinary** system is one of the most common sites of involvement by extrapulmonary **tuberculosis**, accounting for 15 to 20 percent of infections outside the lungs.[2] Approximately 4 to 8 percent of patients with pulmonary **tuberculosis** will develop clinically significant **genitourinary** infection.[3] There is an increasing concern world over with the onset of HIV epidemic and the emergence of multi-drug resistant strains in the last two decades. TB occurs in approximately 10 percent of patients with AIDS and involves at least one extra-pulmonary site in nearly 50 percent of the patients, with kidneys being the most commonly involved genitourinary site.[4]

Urinary tract TB is an important clinical problem because of its nonspecific clinical presentation and progression to renal failure if undiagnosed and untreated. It is also a diagnostic problem because of variable imaging features which often resemble many other lesions. The disease is predominant between second and fourth decades of life being distinctly low in children, and less prevalent in fifth and sixth decades. The disease shows a male predominance.

PATHOGENESIS

Renal tuberculosis results from hematogeneous dissemination of the tubercle bacilli from a primary infection elsewhere. Past or concurrent pulmonary lesion is the most common primary lesion, followed by bone and joint tuberculosis. There is a latent period of 5 to 20 years between the original pulmonary infection and the appearance of clinical renal disease. This explains the low incidence of disease in children. The organisms may involve both kidneys in the initial phase, and are lodged in the glomerular and peritubular capillary bed. The subsequent course of the infection is determined by virulence of the organisms and host-resistance factors. Most of the initial lesions heal without sequelae, and only one or a few progress to clinically or radiologically apparent abnormalities. This happens when the bacilli erode out of their initial vascular

location and spill into the tubules. This results in granuloma formation along the nephron. Granuloma, caseous necrosis, and cavitation represent stages of progression of the infection. This may communicate with the pelvicalyceal system, and the infection further spreads to the ureter and urinary bladder. The pelvicalyceal and ureteral involvement appears as mucosal ulcerations, focal or generalised dilatation or cicatrisation. Fibrosis and calcium depositions represent healing. The pattern of progression and healing is variable and produces asymmetric histologic, microscopic and radiological findings unique to each patient. If the hydronephrotic kidney becomes nonfunctioning, extensive dystrophic (putty like) calcification may form a cast of the kidney, referred to as autonephrectomy. Nonfunctioning kidneys in TB may be due to autonephrectomy or as a sequelae of obstruction (Fig. 7.1). Important complications of renal TB include perinephritis, perinephric abscess, fistulae and psoas abscesses.

CLINICAL PICTURE

Frequency of urination, burning, dysuria or urgency are the most common presenting symptoms. Nearly 50 percent of the patients at sometime during the course of the disease have hematuria. Dull or chronic renal pain, even acute colic is not uncommon. Constitutional symptoms like fever, weight loss, fatigue are present in about 50 percent of the patients. Obstructive uropathy, and chronic cystitis are not uncommon with TB.[5,6] Patients may develop fistulae particularly in lower urinary tract involvement. The physical examination is often insignificant. Diagnosis of TB should be considered in patients with recurrent urinary tract infection that is not responding to appropriate therapy for typical pathogens.

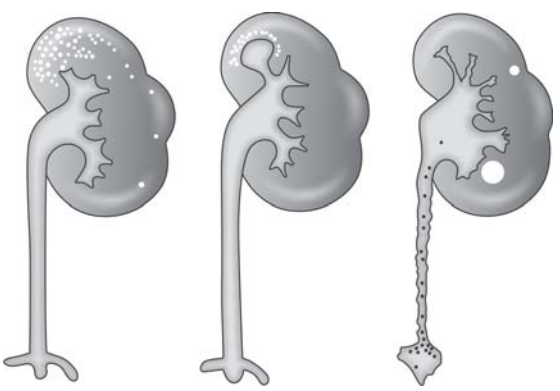

Fig. 7.1: Schematic diagram showing stages of progression of the disease

LABORATORY INVESTIGATIONS

Pyuria which is sterile when cultured on standard media is characteristic. Presence of red blood cells in urine is frequent. The diagnosis is established by demonstration of acid-fast bacilli (AFB) on microscopic examination of urine, urine culture or growth of tubercle bacilli in inoculated guinea-pigs. However, urine culture for acid-fast bacilli is positive in nearly 33 percent, while SAFA (soluble antigen fluorescent antibody) test is strongly positive in only 13 percent, and weak or nonreactive in 87 percent of the patients. Also, routine AFB culture is cumbersome involving a delay of 6-8 weeks with a false negative rate of 10-20 percent, using LJ media. Newer techniques for recovery of mycobacteria from urine specimens include BACTEC 460 and using the automated Mycobacteria Growth Indicator Tube system (MGIT 960), with mean time of positivity of 20 days.[7] As an alternative, polymerase chain reaction (PCR) technique or US-guided fine needle aspiration cytology (FNAC) can be used. PCR is highly sensitive (upto 94 percent), provides a quicker diagnosis but has a relatively poor specificity.[8] FNAC is useful in those with a negative culture to define granulomatous nature of the visible lesions.

CYSTOSCOPY

Visualisation of tubercle, ulcer or retracted ureteric orifice strongly suggest the diagnosis. Generalised cystitis with reduced capacity is almost diagnostic. Biopsy from ulcer, tubercle or inflammatory lesion, particularly in absence of positive urine culture may provide the only diagnostic evidence of the disease.

RADIOLOGICAL EXAMINATION

A key role is often played by the radiologist in the diagnosis of the disease. The balance between local progress and healing of the disease process manifests many abnormal imaging features. Since demonstration of the typical calyceal, ureteral and vesical abnormalities is critical to establish the diagnosis of tuberculosis, conventional radiological studies remain the procedures of choice, while ultrasonography (US) and computerised tomography (CT) have a limited role. Essentially, early findings are best detected on intravenous urogaphy (IVU) while ultrasonography and CT are useful for late or chronic changes. US and CT are especially valuable in the evaluation of areas of mass effect and of the nonvisualised kidney at IVU.[9] MRI had not found a place in the diagnostic protocol for evaluation till recently. However MRI can be useful too in evaluation of the non-functioning kidney and focal lesions. A study by Navarro et al found that Intravenous urography provided the diagnosis in 87.5 percent of cases. The average interval between onset of symptoms and diagnosis was 15 months. They in fact state that the current use of imaging studies other than urography and the finding of other microorganisms in urine culture can delay the diagnosis.[10] The most valuable radiologic feature of **genitourinary tuberculosis** is the multiplicity of abnormal findings. Whenever a imaging pattern of chronic renal inflammatory disease is recognized, particularly in the setting of periureteric or peripelvic fibrosis, **tuberculosis** must be considered.[11]

Plain Films

Plain radiograph of abdomen is an important initial examination before IVU and may provide valuable information such as calcification or evidence of skeletal involvement. Small, enlarged or normal renal size; presence of scarring or focal bulge are all nonspecific findings. Deposition of calcium in an attempt to heal and limit the pathological process often provides a diagnostic clue. Calcification is of two types: (i) Amorphous granular associated with granulomatous masses, and (ii) Dense punctate calcification representing healed tuberculoma. It varies from a few minute areas to a cast of entire kidney (Figs 7.2 and 7.3). The lobar distribution of calcification is quite specific for renal TB. Tubercular calcification of ureter is not as common as renal calcification, and calcification of bladder is relatively rare.[12] Plain films may also reveal an evidence of skeletal tuberculosis in hip, sacroiliac joint or spine with or without a paraspinal abscess and calcification of abdominal lymph nodes. A coexisting focus of extrarenal TB elsewhere ranges from 23 to 53 percent in various series. Chest X-ray is abnormal in about 50 percent of the patients. However, active pul-monary tuberculosis is seen in only 5-10 percent with most patients showing sequelae of past infection.

Intravenous Urography (IVU)

Even though miliary tubercles involve both kidneys, disease progression and hence

Fig. 7.2: Plain radiograph abdomen showing amorphous granular calcification involving the right kidney

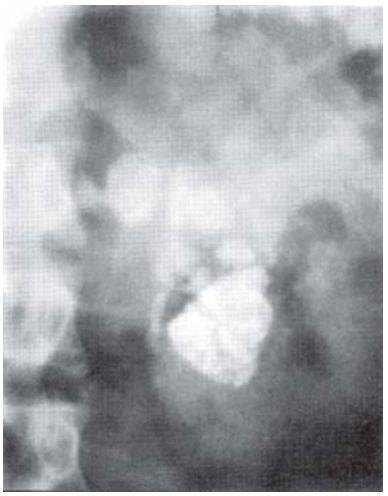

Fig. 7.3: Extensive calcification involving the entire left kidney with no function on intravenous urography–autonephrectomy

radiological abnormalities are confined to a single kidney in over 70 percent of the patients. IVU is a very useful modality to detect early features of urinary tract tuberculosis.[13,14] However, the diagnosis can be made with certainity on urography only if the lesion has ulcerated into the calyx. Hence IVU may be normal in symptomatic renal tuberculosis in the initial stages when the bacilli are lodged in glomerulus and peritubular capillary bed. IVU is essential to assess the extent and severity of involvement, to monitor the response to treatment and to look for complications.

Kidney

The earliest urographic abnormality is the loss of definition of a minor calyx producing an indistinct feathery outline, irregularity of the surface of one or more papillae or calyces with normal renal size and contour (Fig. 7.4).

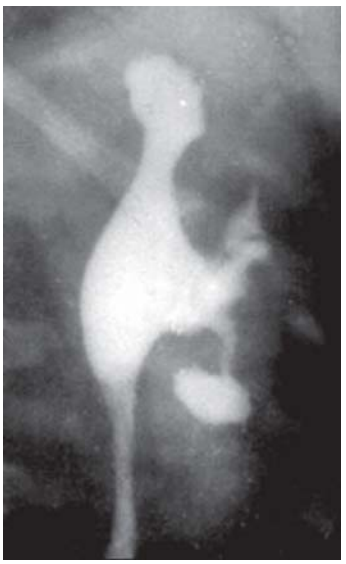

Fig. 7.4: IVU reveals marked dilatation of the inferior calyx with loss of sharpness and fuzziness of its outline. Rest of the calyces are also dilated

Progressive involvement of renal parenchyma occurs in three forms, which occur singly or in combination. First is coalescence of granu-lomas leading to unifocal or multifocal mass lesions. These may enlarge overall renal length or increase thickness of renal substance and cause displacement of adjacent collecting system. Caliectasis occurs with irregularity in contour indicating erosion of the pyramids and cortical necrosis. Depending on the necrosis, a cavity with

irregular walls commu-nicates with a deformed calyx (Figs 7.5 and 7.6). Radiographic appearance of this form simulates papillary necrosis of other origins. The second form seen in advanced renal tuberculosis is parenchymal surface scarring over retracted papillae and dilated calyces. This may be focal or diffuse involving the entire kidney and occurs due to tissue loss leading to fibrosis. Associated calcification or calculi maybe seen. Radiographic identification of calcification associated with renal TB is becoming less common. Calculus disease is rapidly becoming the most frequent form of calcification associated with renal TB.[15] Due to pelvic scarring the calculi formed also tend to take on this deformed shape. Upward pointing renal pelvic calculi may be seen due to 'hiked up' pelvis[15] (Figs 7.7A to C).

Impaired excretion of contrast is seen in either of these two forms. A third form is autonephrectomy, which represents end stage disease. It may be of two types (a) caseo-cavernous type-enlarged sac filled with caseous material, with or without calcification[15] (Fig. 7.8). This can simulate xanthogranulomatous pyelonephritis; (b) calcified shrunken non-functioning kidney.

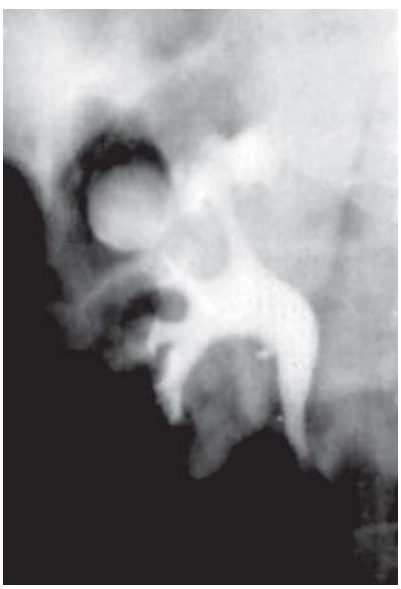

Fig. 7.5: IVU shows a large cavity communicating with a dilated, irregular superior calyx

Following the drainage of a cavity into the collecting system, there is spread of infection to other parts of the urinary tract. Subsequent stimulation of scirrhous reaction causes stenosis and obstruction of parts of the collecting system. The common sites of strictures being the neck of a calyx, pelvi-ureteric junction and lower end of the ureter (Figs 7.9 and 7.10). Depending on the site of narrowing there is dilatation of a single calyx (hydrocalyx) or regional hydrocalycosis or generalized dilatation of the pelvicalyceal system. A completely stenosed infundibulum or calyx may lead to failure of contrast excretion by the involved parenchyma (phantom calyx). A tiny infundibular stump (amputated calyx) may be seen in such cases. The renal pelvis may be dilated or may show filling defects due to caseous debris and granulation tissue. The involvement progresses to fibrosis with scarring. If the inferior margin of the renal pelvis is involved with resultant cephalic retraction, a characteristic deformity called the "hiked up pelvis" results. In addition, deformity of the pelvicalyceal system may be caused by traction from a strictured infundibulum or parenchymal fibrosis kinking the pelvis (Kerr's kink) and involving areas not directly affected by tuberculous ulcerations. Occasionally, obstruction can be of such a high grade and so prolonged that marked hydronephrosis develops[16] (Fig. 7.11).

Ureter

Ureteral involvement is almost always secondary to renal TB with spread of infection by bacilluria. In the early stages

there is dilatation resulting from atony and prolonged bacilluria. With progression of the disease, irregular segments of ureter are seen due to mucosal ulcerations. Further necrosis of ureteral musculature is accompanied by fibrosis resulting in stricutre formation. The ureteric segments which are more superficially involved may heal without stricture formation. This produces a beaded or corkscrew appearance of the ureter.[17] Ureteral strictures have been reported in 10-56 percent of patients with urinary tract TB. The terminal segment of the ureter is most commonly involved (Fig. 7.11). However, any part may be involved with multiple strictures seen in 19 percent cases. In later stages, severe thickening of the wall produces a rigid shortened ureter with narrow lumen termed as "pipe stem ureter." Renal damage secondary to ureteral strictures may be more severe than the effect of the original parenchymal involvement. Dilatation and stenting of the ureter may restore ureteral patency and salvage a kidney.

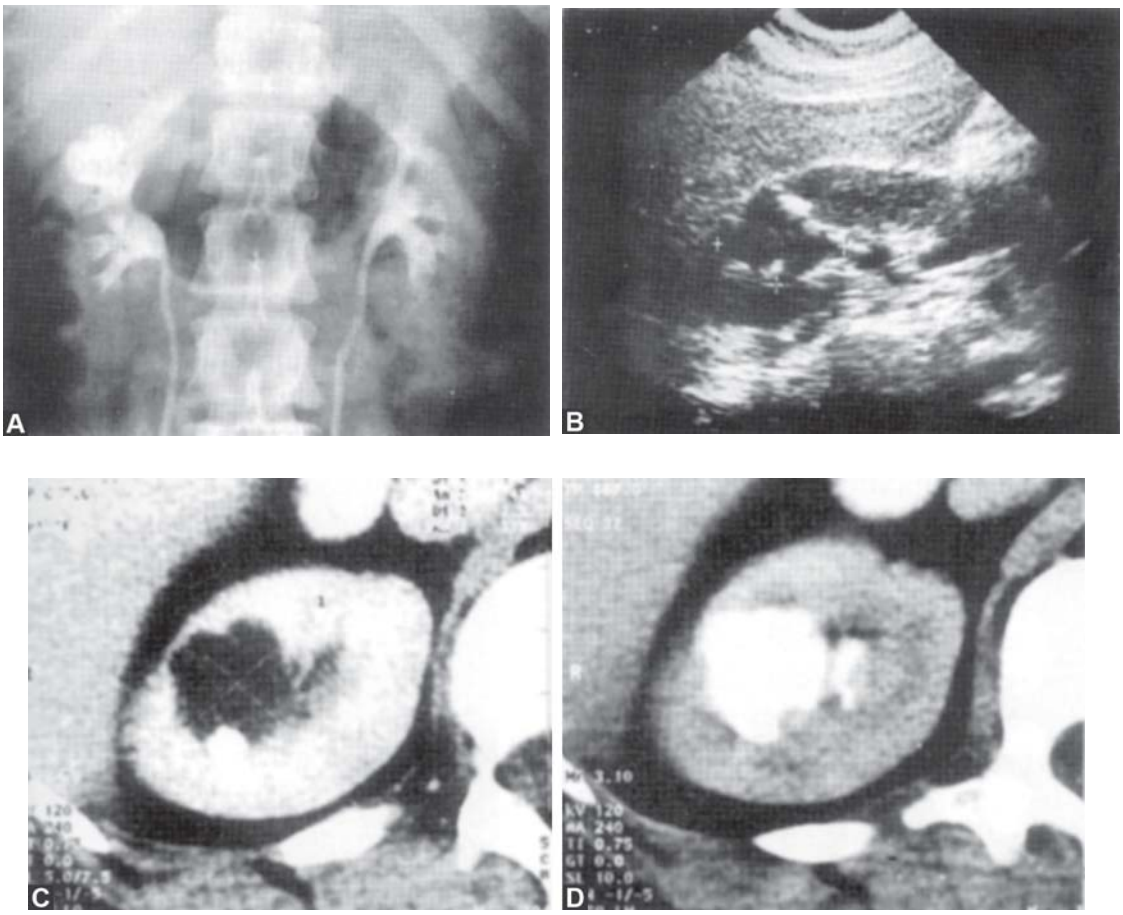

Figs 7.6A to D: (A) IVU reveals a large cavity communicating with the superior calyx of right kidney, **(B)** US shows a hypoechoic focal lesion in the upper polar cortex with an echogenic rim, **(C)** CT confirms the presence of the cavity seen on IVU and US, with pooling of contrast on delayed images, **(D)** due to communication with the pelvicalyceal system

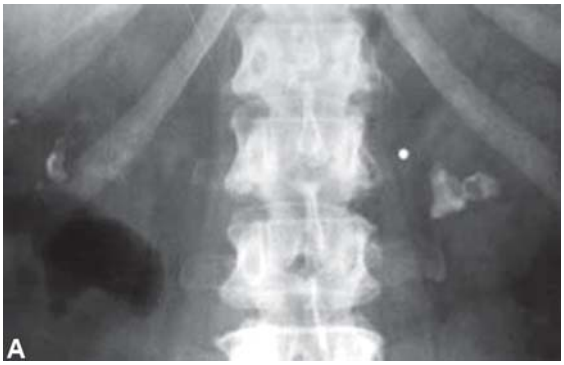

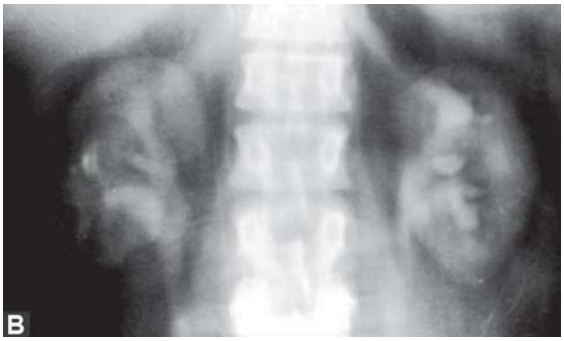

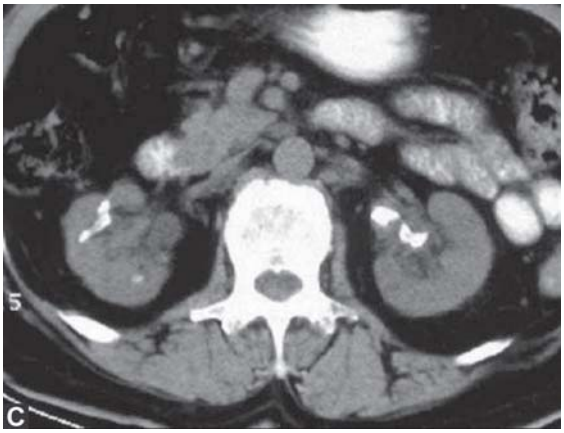

Figs 7.7A to C: Plain radiograph **(A)** reveals deformed calculus in (L) renal pelvis with parenchymal calcification in the right kidney. IVU **(B)** reveals bilateral small kidneys with calyceal dilatation and parenchymal scarring. NCCT scan **(C)** better demonstrates the calcification and scarring

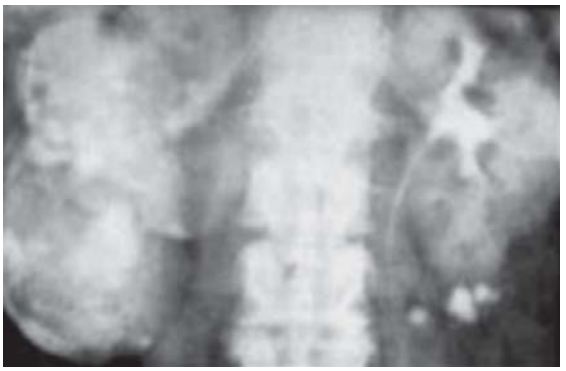

Fig. 7.8: IVU slowing an enlarged, sac like poorly functioning right kidney – Advanced disease of caseo-cavernous type

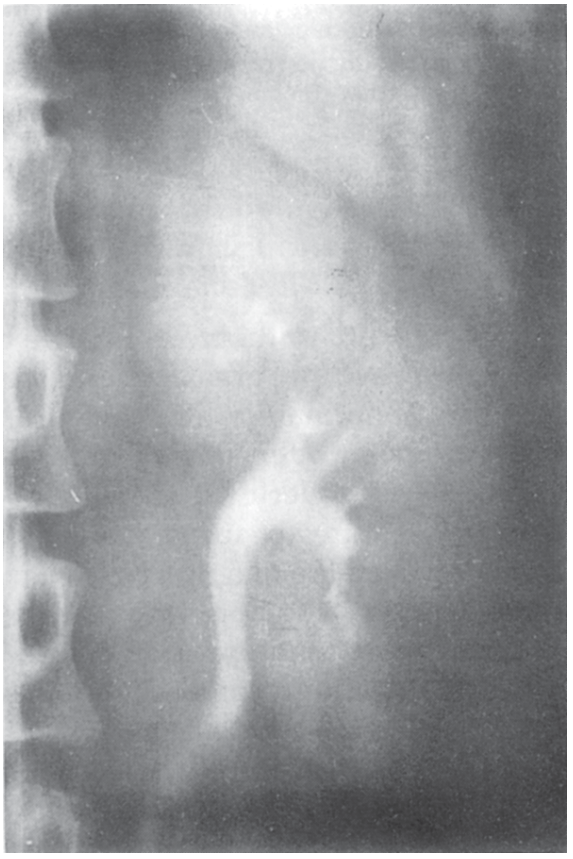

Fig. 7.9: IVU shows irregularity of the superior calyx with intrarenal reflux and infundibular narrowing

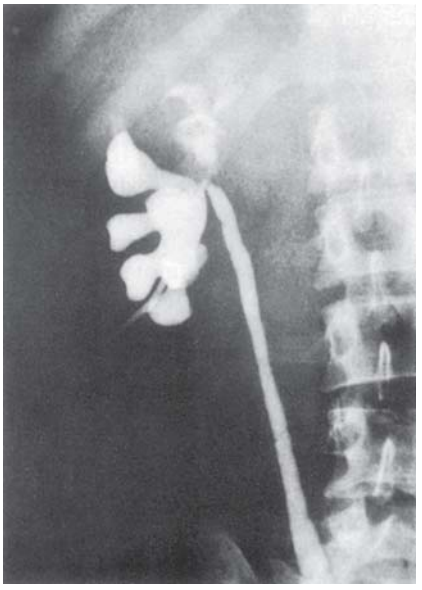

Fig. 7.10: Nephrostogram showing deformed and contracted renal pelvis with proximal dilatation of the pelvicalyceal system. Superior calyx is communicating with an irregular cavity and there is infundibular stenosis. Ureter is also dilated due to lower end stricture

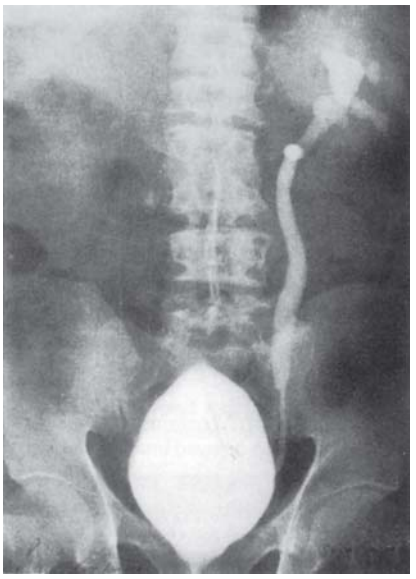

Fig. 7.11: IVU showing long irregular stricture involving lower end of left ureter with hydroureter, hydronephrosis and infundibular stenosis of inferior calyx of left kidney. Also note changes of tuberculosis involving L2-L3 vertebrae

Urinary Bladder

Urinary bladder is involved later in the course of the disease in upto one-third of patients of urinary tract TB. Use of bacillus Calmette-Guérin therapy for bladder cancer can cause symptomatic tubercular infections of the lower genitourinary tract.[5] Tubercular cystitis leads to edema of the bladder mucosa. Large tuberculomas in vesical wall can manifest radiologically as filling defects simulating carcinoma.[18] Advanced disease leads to irregular contracture with thick walls and reduction of bladder capacity – the "thimble bladder" (Figs 7.12A to C and Fig.7.13). Fibrosis in the region of the trigone produces gaping of the ureterovesical junction resulting in free vesicoureteric reflux.

Urethral TB

Tuberculosis of the male urethra is uncommon and usually occurs secondary to renal infection. It may also be associated with prostatic abscess, periurethral abscess or fistula formation. It may result in a nonspecific stricture almost always in the bulbomembranous urethra that is indistinguishable on imaging from strictures due to other causes.

Retrograde Pyelography

Retrograde pyelography is particularly indicated in a patient with nonfunctioning kidney to demonstrate ureteric obstruction and cavitation in the kidney.

Ultrasonography

Ultrasound is not used as the primary imaging modality for diagnosis of urinary tract TB, as it is unable to show early calyceal changes and does not provide information about renal functional status. However,

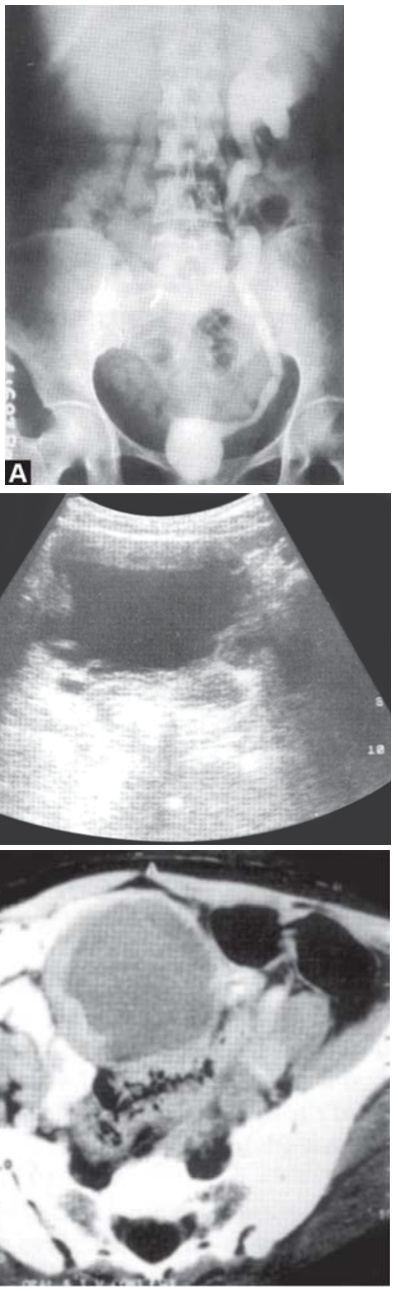

Figs 7.12A to C: Urinary bladder TB: **(A)** IVU reveals a small capacity (thimble) urinary bladder, ureteral stricture with proximal hydroureter and hydronephrosis on left side. Right kidney is non-functioning, **(B)** US shows irregular, asymmetric wall thickening of the urinary bladder with trabeculations. A left adnexal mass is also seen posterior to the bladder **(C)** CT shows a similar appearance of the urinary bladder

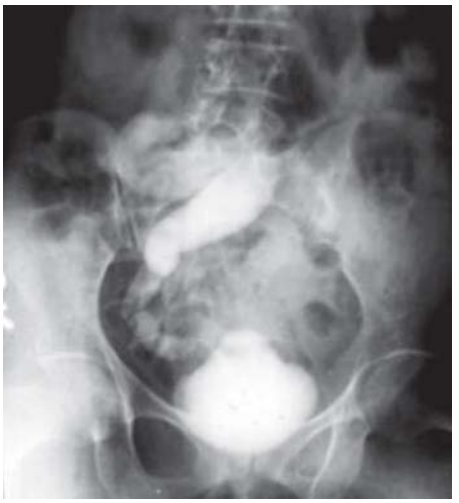

Fig. 7.13: MCU study reveals a small capacity bladder with reflux into a dilated, tortuous right ureter

carefully performed sonogram can show a spectrum of morphological abnormalities.[19,20] The role of sonography is also to provide guidance for the interventional procedures of percutaneous nephrostomy (PCN), antegrade dilatation of ureteral stricture and drainage of the perinephric abscess.

Kidney

A focal renal lesion of varying echogenicity is a frequently encountered sonogra-phic abnormality. In the early stages US demonstrates papillary lesions as areas of hypoechogenicity or hypoechoic foci with echogenic walls or echogenic nonshadowing lesions (Refer Fig. 7.6B).[21] A sloughed calyx is seen as an echogenic flap separated from the normal calyceal wall (Fig. 7.14A). Large liquefying conglomerate cavities or dilated calyces formed as a result of infundibular stricture appear as hypoechoic nodules or masses. The communicating tract from a cavity appears as a sonolucent track entering the dilated calyx (Fig. 7.14B). Heterogeneous echotexture of the parenchyma or normal

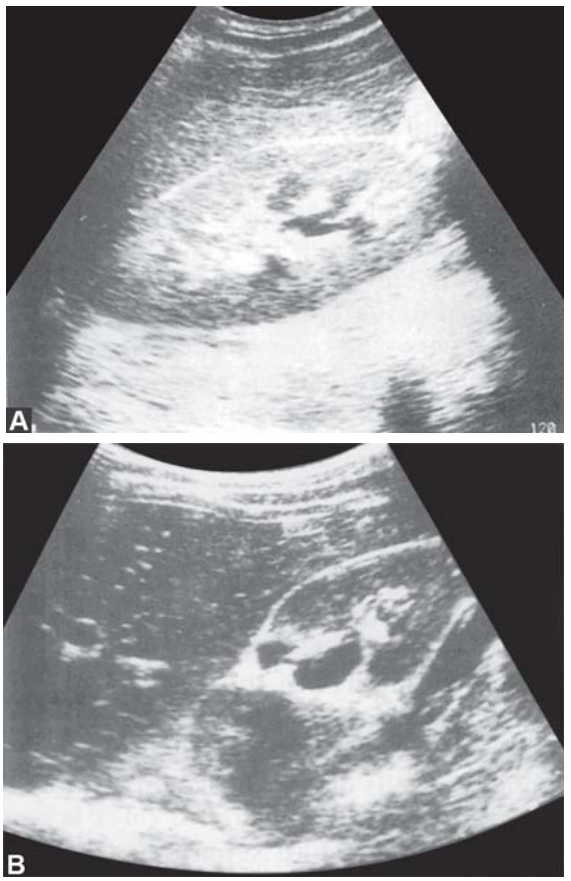

Figs 7.14A and B: US showing echogenic papillary sloughing in the middle calyx of the right kidney. **(B)** US of another patient reveals an anechoic cavity in the renal cortex with a sonolucent track connecting the cavity and the pelvicalyceal system

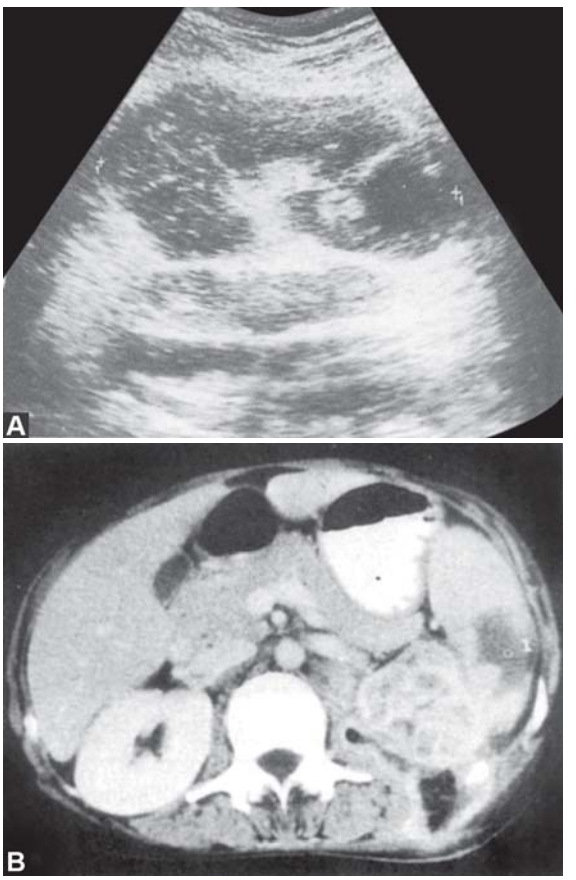

Figs 7.15A and B: (A) US shows an enlarged heterogeneous left kidney with an anechoic cavity in the lower pole. **(B)** Contrast enhanced CT of the same patient reveals poorly functioning heterogeneous left kidney with hypodense areas within. An irregular hypoattenuating splenic abscess and inflammatory changes in the left posterior renal space, left psoas and posterior parietes are also seen

appearing parenchyma may be seen in diffuse involvement (Figs 7.15A and B). Such patients show poor excretory function on IVU and CT. Following pelvicalyceal system involvement, US may characteristically show uneven caliectasis without renal pelvis dilatation. It may also demonstrate hydronephrosis, parenchymal calcification, and perinephric abscess (Figs 7.16A and B).

Xuefang Rui et al [22] reviewed sonographic features of 258 cases of renal tuberculosis. In this series of 258 cases, 152 cases were correctly diagnosed as renal tuberculosis by B-mode ultrasonography, and these were classified under six types. Type I: Nephrectasia type (23 cases); type II: Hydrops type, (21 cases); type III: Empyema type (13 cases); type IV: Inflammatory and atrophy type (15 cases); type V: Calcification type (34 cases); type VI: Mixed type (46 cases). In type I (Nephrectasia), the renal capsule was very irregular. In the renal parenchyma and

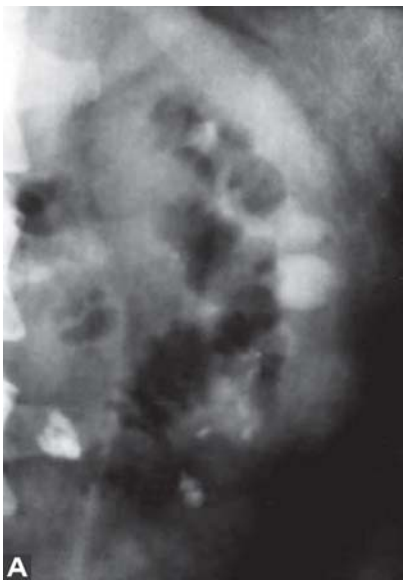

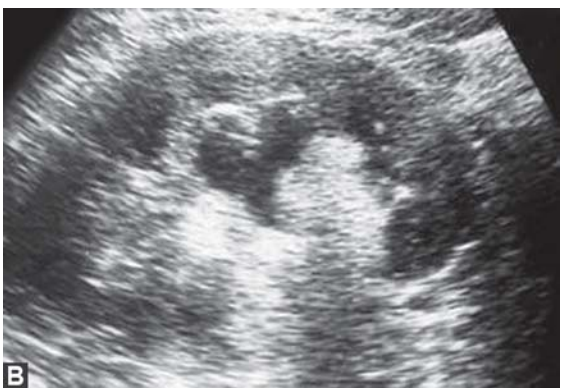

Figs 7.16 A and B: IVU **(A)** and US **(B)** of left kidney of a 28 years male reveals uneven caliectasis with calcification within

renal sinus, there were one or several anechoic zones, of different sizes with irregular margins and some nebulous light spot echoes within. The type II (Hydrops type) also showed an irregular renal capsule. The renal pelvis and calyces were distended, within which there was an anechoic zone, similar to hydronephrosis. However, the inner wall was rough and uneven. In most cases, the ureter was involved and appeared thickened.

Ureter

US does not play a significant role in the acute phase. It is useful in assessment and follow up of back pressure changes and adjoining retroperitoneal disease.

Urinary Bladder

US may detect focal irregularity or thickening of the bladder wall with reduced capacity. Distension of the bladder may be necessary to gauge the bladder capacity accurately. The deformed bladder shape and focal abnormalities are also better appreciated following distension (Fig. 7.12B).

Computed Tomography

Computed tomography is indicated only in patients with strong clinical suspicion but normal or equivocal findings on urography and ultrasonography. Multidetector CT (MDCT) with its multiple reconstructions is useful in demonstrating the extent of involvement, length of ureteric stricture, adjoining retroperitoneal disease and associated spinal or solid organ involvement.

Kidney

CT may show a spectrum of findings including multiple small poorly enhancing nodules, uneven caliectasis and calcification (Figs 7.17A to C). Similar to US the pelvis is typically not distended (Fig. 7.18A to D). Isolated cortical involvement by focal lesions is well-demonstrated on CT. A cavity is well delineated with pooling of contrast in the delayed images (Fig. 7.6C). Compared to US, CT is also able to provide better visualisation of retroperitoneal structures, more detailed information on presence and pattern of calcification and functional status of the kidney (Figs 7.18 to 7.20). In poorly functioning kidneys the nephrogram effect is much better seen on CT than on IVU.

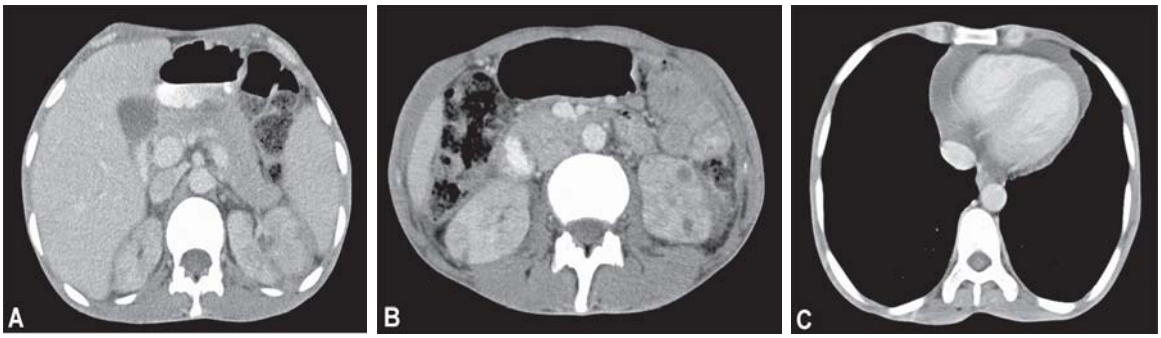

Figs 7.17A to C: CECT of a 36 years old male **(A and B)** showing multiple hypodense lesions in the left kidney with adjoining perinephric collection and fascial thickening. Right kidney reveals a small hypo dense lesion. **(C)** Patient also had pericardial effusion

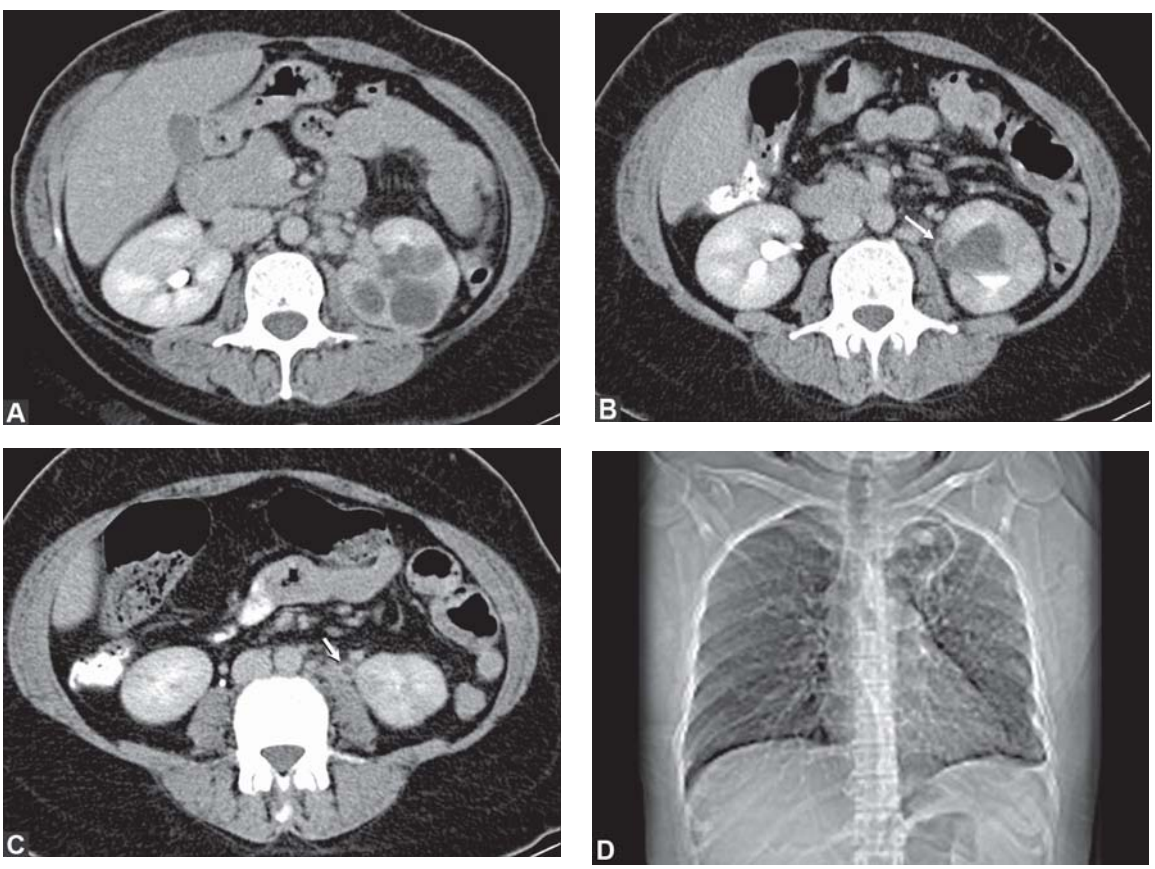

Figs 7.18 A to D: CECT of a young girl reveals a poorly functioning (L) kidney with hydronephrosis. Small retroperitoneal nodes are present **(A)** Renal pelvis is contracted with a thickened wall (arrow) **(B)** The ureteric wall is also thickened (arrowhead) **(C)** Topogram **(D)** reveals a cavity in the left upper lobe of lung

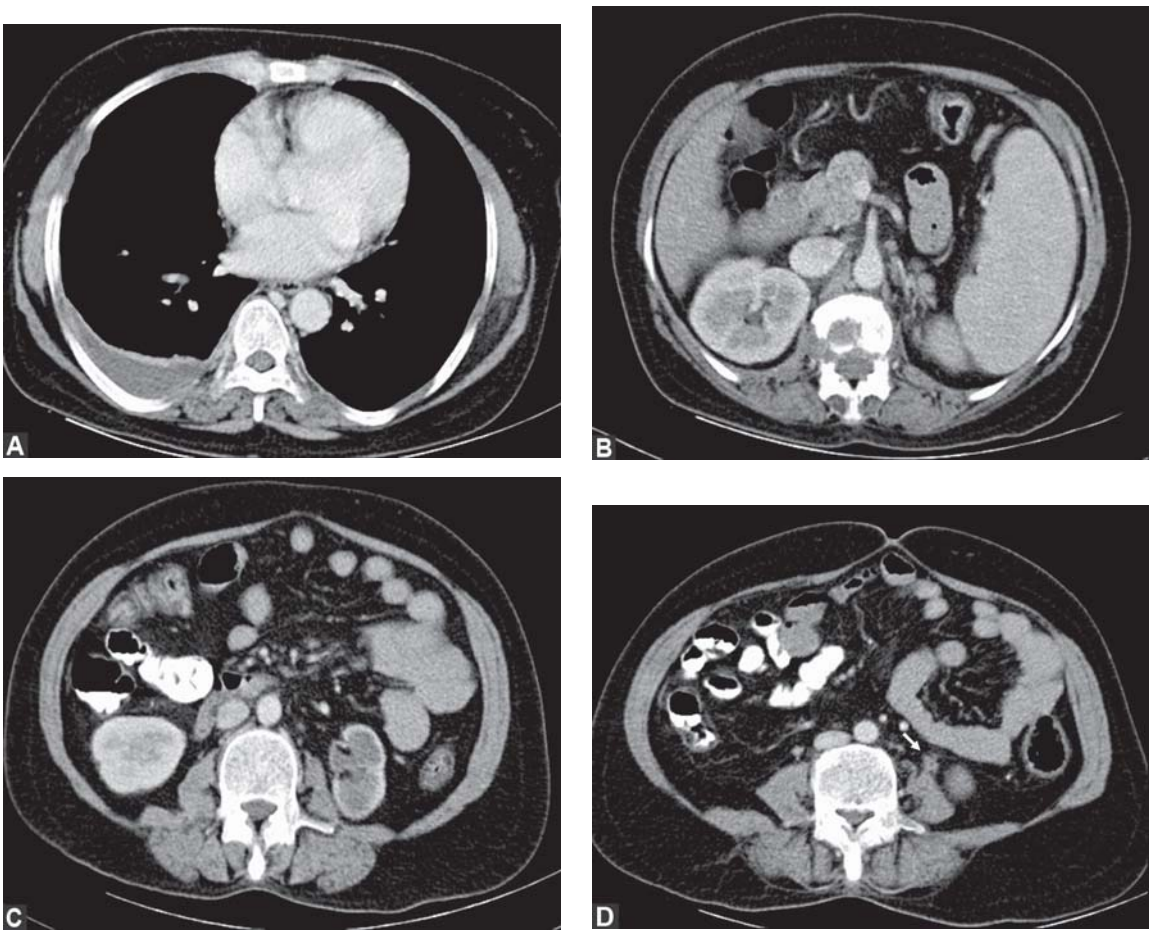

Figs 7.19A to D: CECT of a 43 years old female reveals right pleural effusion **(A)**, destruction of L2 vertebra **(B)**, left kidney is shrunken with hydronephrosis, scarred pelvis and parenchymal thinning **(C)**. Wall thickening of ureter (arrow) is present **(D)**

Ureter

Thickening of the renal pelvis or ureter is highly suggestive of tuberculosis and can be readily identified on CT (Fig. 7.19D).

Urinary Bladder

CT offers no significant advantage in the evaluation of bladder involvement except for detection of faint calcification and demonstration of adjacent genital tract disease (Figs 7.12C and 7.20D).

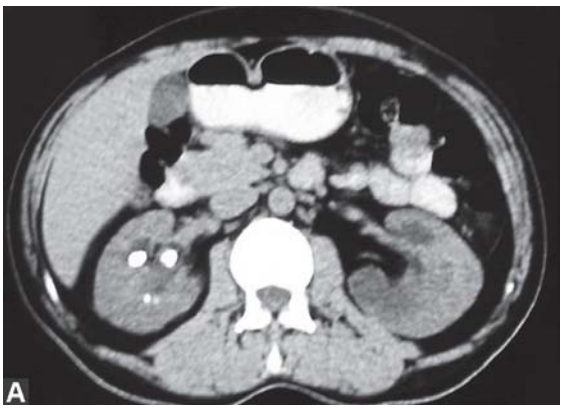

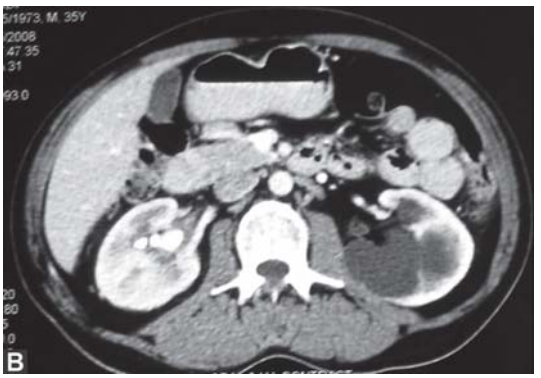

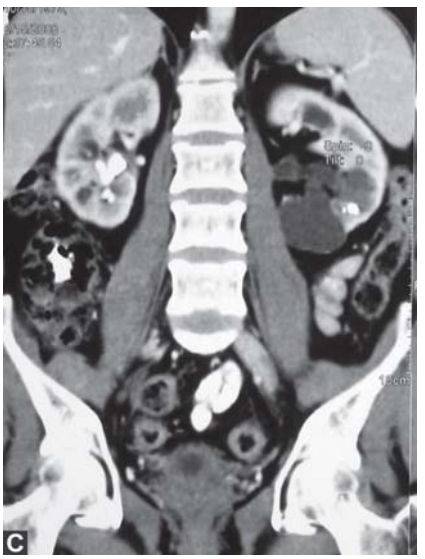

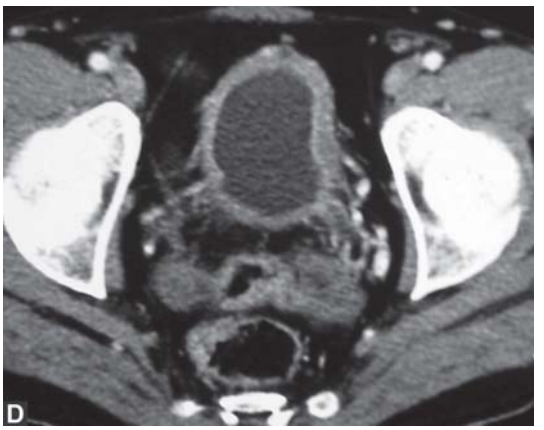

Figs 7.20A to D: MDCT axial **(A and B)** and coronal **(C)** Show a large cavity with irregular caliectasis and calcification involving the lower pole of left kidney. Right kidney has calculi. Scan through pelvis **(D)** reveals urinary bladder thickening with enlarged heterogeneous seminal vesicles

MRI

MRI description of urinary tract TB is limited to sporadic reports. MRI with MR urography can be used to evaluate poorly or nonfunctioning kidney, especially the obstructive form for demonstration of ureteric involvement. MRI also demonstrates the renal parenchymal changes well, while MR urogram details the pelvicalyceal involvement (Figs 7.21 and 7.22). Time-resolved dynamic contrast-enhanced MR urography can be used for the evaluation of ureteral peristalsis.[23]

COMPLICATIONS

The prominent complications include perinephric inflammation/abscess formation including psoas abscesses (Figs 7.22A to E). Fistulae or sinus tracts may develop into adjacent tissues or viscera (Figs 7.23, 7.24A and B).

Differential Diagnosis

The differential diagnosis of urinary TB can be varied depending upon the form of involvement. Early renal TB can simulate papillary necrosis. Focal lesions resemble other infections or even neoplasms. Calcification and extensive inflammation can mimic xanthogranulomatous pyelonephritis. Similarly urinary bladder involvement may be confused with neoplastic involvement.

In conclusion, diagnosis of urinary tract tuberculosis is based on a high index of clinical suspicion supported by a collective evaluation of microbiological, radiological and endoscopic features. While individual radiological features of urinary tract TB can be seen in other diseases such as papillary necrosis due to other causes, infections and neoplasms; the key to diagnosis is pattern recognition. Also, follow-up excretory

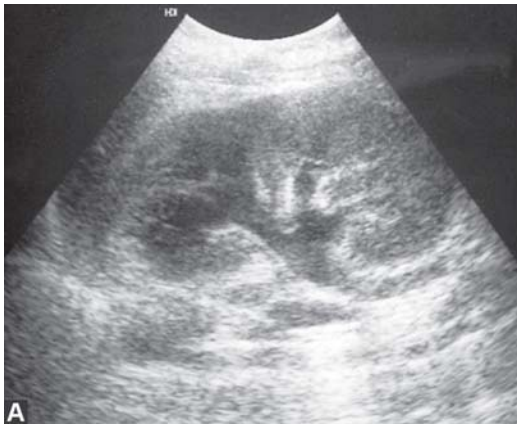

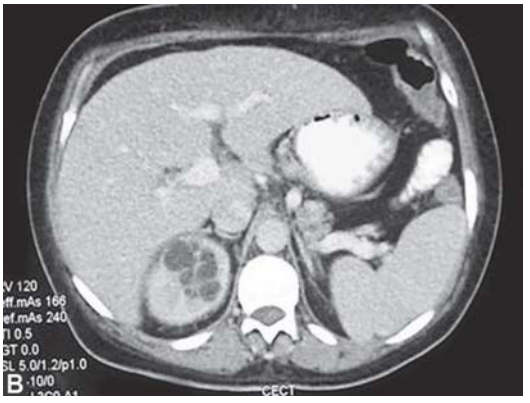

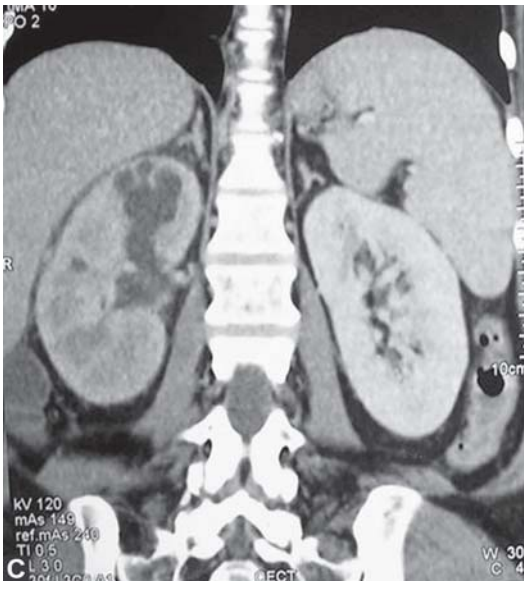

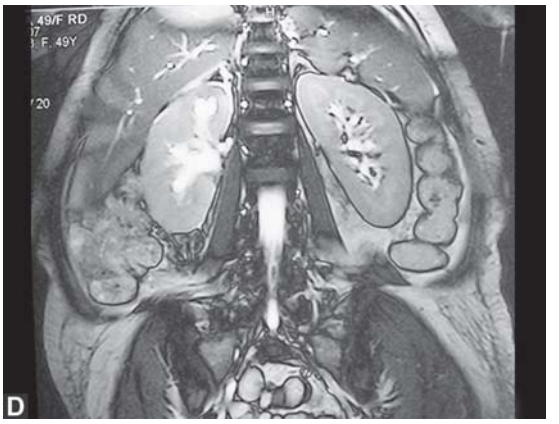

Figs 7.21A to E: Images of a 49 years female. US **(A)** reveals caliectasis of the superior calyx. Axial CECT **(B)** shows multiple cavities involving upper pole of the right kidney. Coronal CECT MPR **(C)** shows the cavities communicating with the superior calyx with parenchymal atrophy of the upper pole, and poor function of the right kidney. Tru-FISP coronal MRI **(D)** reveals increased signal intensity of the right kidney. MR urogram **(E),** in addition illustrates ureteric and bladder irregularity

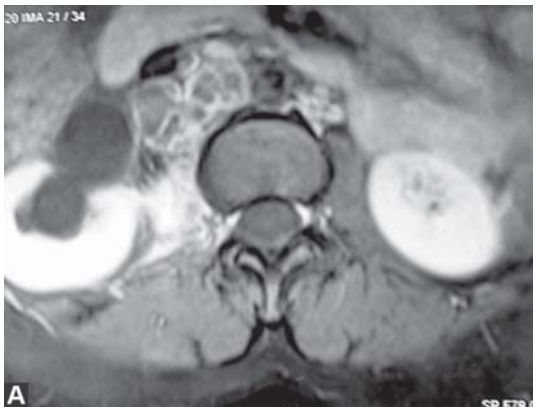

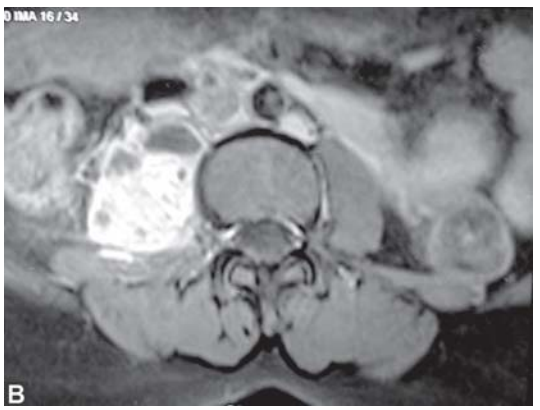

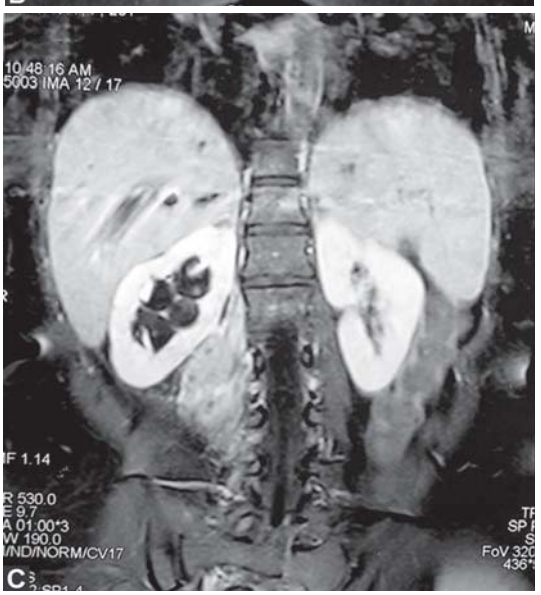

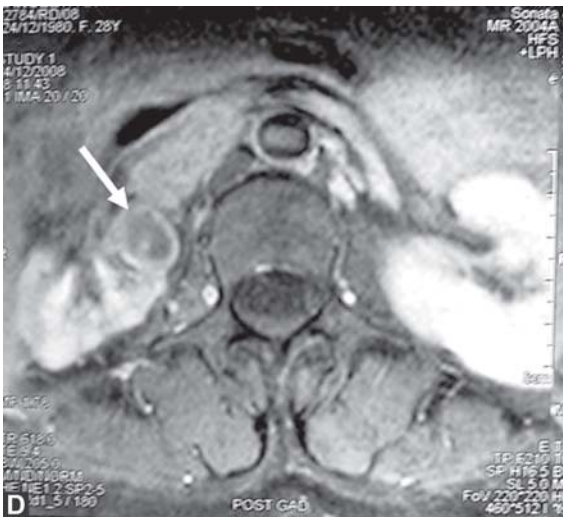

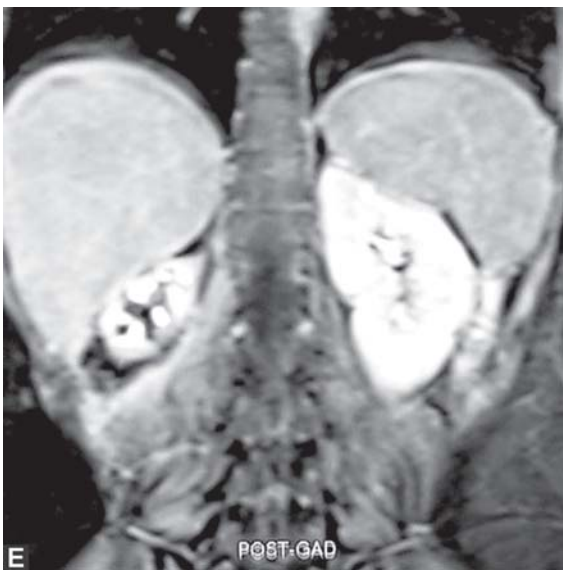

Figs 7.22 A to E: Serial gadolinium enhanced MR images of a 28 years old woman of multi-drug resistant Tuberculosis. Axial **(A and B)** and coronal **(C)** post gad images reveal necrotic retroperitoneal nodes with right psoas abscess encasing the ureter and causing hydronephrosis. MR scan obtained 8 months after second line ATT**(D and E)** shows reduction of the lymphadenopathy and psoas abscess. The right kidney is however shrunken and has a rim enhancing lesion in the renal cortex suggesting an abscess(arrow)

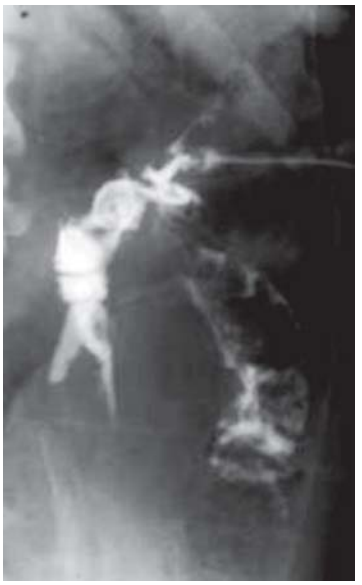

Fig. 7.23: Sinogram performed in a 28 years man with a chronic discharging (L) lumbar sinus reveals opacification of the pelvicalyceal system

urography at regular intervals is useful both for assessment of therapeutic response, and for an early detection of the complications.

GUTB in HIV

The impact of HIV epidemic on the incidence and clinical presentation of genitourinary TB is largely unknown. Navarro et al [10] evaluated clinical and epidemiological characteristics of patients diagnosed with genitourinary TB at their center over the last 10 years, found that of the Forty-five patients analyzed , 33 percent had a coexisting disease (14 were infected by human immunodeficiency virus). In a retrospective study from USA, case records of 16 patients infected with HIV and genitourinary TB were compared with those of 8 patients without HIV infection diagnosed with genitourinary TB. Data abstracted from records included demographics, symptoms, signs, laboratory and radiologic findings, and in-hospital

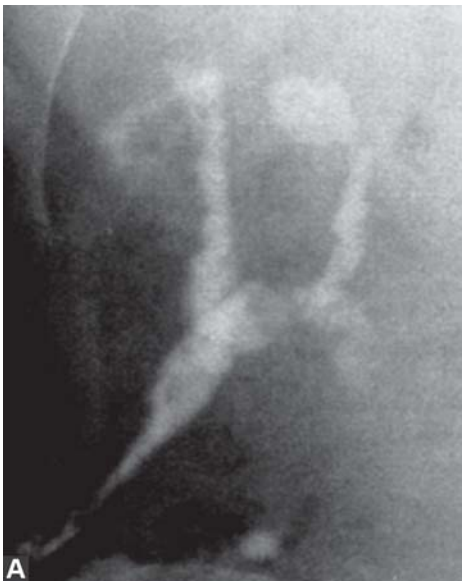

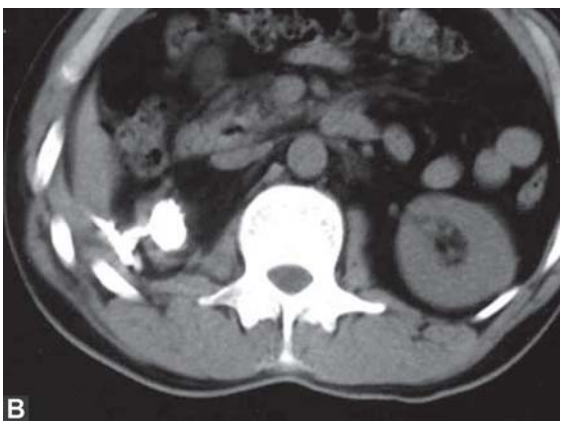

Figs 7.24A and B: Sinogram **(A)** and CT sinogram **(B)** of a different patient shows a shrunken right kidney, with sinus tract extending from the calyces to the skin

mortality. Of 1282 patients with tuberculosis, 24 patients had positive urine cultures for *Mycobacterium tuberculosis.* HIV infection was present in 16 patients (75%). Patients infected with HIV were younger (mean age, 39.1 +/− 6.2 versus 53.9 +/− 17.2, P = 0.047) but did not differ significantly in clinical presentation from patients who did not have HIV infection.[24,25]

REFERENCES

1. Colabawalla BN. Diagnostic evaluation in renal tuberculosis. Indian J Surg 1978;40:109-12.
2. World Health Organization. Stop TB annual report 2001 Geneva, Switzerland: World Health Organization, 2002.
3. Leder RA, Low VH. Tuberculosis of the abdomen. Radiol Clin North Am 1995;33:691-705.
4. Naidich DP, Garay SH, Leitman BS, Mc Gauley DI. Radiographic manifestations of pulmonary disease in the acquired immunodeficiency syndrome. Semin Roentgen 1987;12:14-30.
5. Wise GJ, Shteynshlyuger A. An update on lower urinary tract tuberculosis. Curr Urol Rep 2008;9(4):305-13.
6. Wise GJ, Marella VK. Genitourinary manifestations of tuberculosis. Urol Clin North Am. 2003 Feb;30(1):111-21.
7. Chan DS, Choy MY, Wang S, Sng LH An evaluation of the recovery of mycobacteria from urine specimens using the automated Mycobacteria Growth Indicator Tube system (BACTEC MGIT 960). J Med Microbiol 2008;57(Pt 10):1220-2.
8. Hemal AK, Gupta NP, Rajeev TP, et al. Polymerase chain reaction in clinically suspected genitourinary tuberculosis: Comparison with intravenous urography, bladder biopsy and urine acid fast bacilli culture. Urology 2000; 56(4):570-74.
9. Premkumar A, Lattimer J, Newhouse JH. CT and sonography of advanced urinary tract tuberculosis. AJR 1987;148:65-69.
10. Navarro-Vilasaró M, Font B, Sala M, Prera A, Malet A, Mariscal D, Segura F. Genitourinary mycobacteriosis: Retrospective study of 45 cases in a general hospital. Enferm Infecc Microbiol Clin 2008;26(9):540-45 Article in Spanish, abstract in Pub Med.
11. Goldman SM, Fishman EK, Hartman DS, Kim YC, Siegelman SS. Computed tomography of renal tuberculosis and its pathological correlates. J Comput Assist Tomogr 1985;9:771-76.
12. Hyup S. Urogenital tuberculosis. In Pollack HM, McClennan BL (Eds): Clinical Urography Textbook (2nd Edn) Philadelphia: WB Saunders Co. 2000;2:1193-1228.
13. Dalla Palma L. What is left of IV urography? Eur Radiol 2001;11(6):931-39.
14. Kollins SA, Hartman GW, Carr DT, et al. Roentgenogrpahic findings in urinary tract tuberculosis—a 10-year review. Am J Roentgenol 1974;121:487-96.
15. Merchant SM. Tuberculosis of the genitourinary system. In Diagnostic Radiology and Imaging (2nd Edn). Jaypee Brothers Medical Publishers (P) Ltd. New Delhi 2003;1997;627-56.
16. Narayan AS. Overview of renal tuberculosis. Urology 1982;19:231-37.
17. Wasserman NF. Inflammatory disease of the ureter. Radiol Clin North Am 1996;34(6): 1131-56.
18. Camilien LD, Boyce JG. Diagnostic imaging of gynecological disease – the clinicians view. Urol Radiol 1991;13:3-8.
19. Das KM, Indudhara R, Vaidyanathan S. Sonographic features of genitourinary tuberculosis. AJR 1992;158:327-29.
20. Schaffer R, Becker JA, Goodman J. Sonography of tubercular kidney. Urology 1983;22:209-11.
21. Fan ZM, Zeng QY, Huo JW, et al. Macronodular multi-organs tuberculoma: CT and MR appearances. J Gastroenterol 1998;33(2):285-88.
22. Xuefang Rui, Xin-De Li, SongLiang Cai, Geming Chen and Baisen Cai Ultrasonographic diagnosis and typing of renal tuberculosis International Journal of Urology 2008;15:135–39.
23. Kim S, Jacob JS, Kim DC, Rivera R, Lee VS. Time-resolved dynamic contrast-enhanced MR urography for the evaluation of ureteral peristalsis: initial experience. J Magn Reson Imaging. 2008;28(5):1293-98.
24. Nzerue C, Drayton J, Oster R, Hewam-Lowe K. Genitourinary tuberculosis in patients with HIV infection: Clinical features in an inner-city hospital population. Am J Med Sci. 2000 Nov; 320(5): 299-303Am J Med Sci 2000;320(5):299-303.b
25. Becker JA. Renal tuberculosis. Urol Radiol 1988; 10:25-30.

Chapter

8

Nontubercular Infections of the Urinary Tract

Naveen Kalra, Ajay Kumar

INTRODUCTION

With the availability of US, CT, MRI, nuclear medicine and advances in interventional radiology, diagnosis and management of the renal and perirenal infections have undergone dramatic changes. Plain X-ray and intravenous urography (IVU) have a declining role whereas ultrasonography (US), computed tomography (CT) and magnetic resonance imaging (MRI) play a vital role in detection and delineation of the extent of renal infectious diseases.

The diagnosis of pyelonephritis is based on typical clinical features and laboratory findings.[1-3] Radiological imaging is generally not performed in uncomplicated cases. However, indication of early imaging in suspected cases of urinary tract infection (UTI) includes unusual severe symptoms, high-risk patients (elderly, diabetics or immunocompromised and patient not responding to intravenous antibiotics within 72 hrs).[3] The main objectives of imaging in UTI are (i) To detect the conditions that must be cured immediately, i.e. pyonephrosis, abscesses to preserve renal function and to avoid septic condition, (ii) To search for primary etiological cause of UTI, i.e. obstruction, vesicoureteral reflux (VUR), diabetes, cyst infection.[1,2]

Plain X-ray may provide diagnostic information such as presence of abnormal gas collection in the renal or perirenal area (Fig. 8.1) in patients with emphysematous pyelonephritis and renal abscess or stag-horn calculus in a patient suspected to have

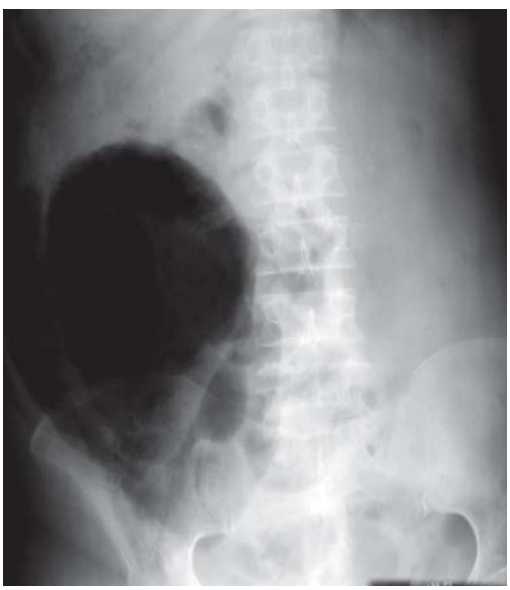

Fig. 8.1: Plain X-ray abdomen showing a large loculus of air overlying the right renal area in a diabetic patient with extensive emphysematous pyelonephritis

pyonephrosis. IVU has a limited role and can exclude congenital anomalies which are important risk factors in patients of recurrent urinary tract infections. Certain conditions like papillary necrosis and early tuberculosis may be diagnosed only on IVU.[4]

Ultrasonography has 98 percent sensitivity in detection of hydronephrosis[5] and is of particular value in patients of renal failure in whom use of contrast media may be hazardous. Extrarenal fluid collections are easily detected, and it is the ideal guiding modality for various interventional procedures such as nephrostomy or cyst aspiration. Limitations of the ultrasound include its inability to detect the subtle changes of microabscesses,[6] small calculi,[7] and papillary necrosis.

CT is the gold standard for diagnosis as well as for delineating the extent of renal infective diseases.

MRI is being increasingly used as an effective modality for both medical and surgical diseases of kidney especially in pregnant women, in patients with renal failure where iodinated contrast cannot be used and in diabetics.[3] The cost and limited availability precludes its routine use, although it provides information similar to CT.

Radionuclide studies with cortical scintigraphy agents such as 99mTc DMSA and glucoheptonate have been shown to be the most sensitive techniques for the diagnosis of acute pyelonephritis and detection of the renal scars in reflux nephropathy.[8]

Renal infections can be divided into acute and chronic infections. Acute infections include: Acute pyelonephritis and its various complications such as focal bacterial nephritis (FBN), renal abscess, emphysematous pyelonephritis, papillary necrosis and pyonephrosis. Chronic renal infections include: chronic pyelonephritis, reflux nephropathy, xanthogranulomatous pyelonephritis, malacoplakia, squamous metaplasia and cholesteatoma.

ACUTE PYELONEPHRITIS

Acute pyelonephritis refers to an inflammatory process affecting the collecting system and the renal interstitium. Inflammation is usually bacterial but may be fungal or viral. *Escherichia coli*, *Proteus* and *Klebsiella* are the common offenders when transmission of infection occurs by the ascending route. Hematogenous infections occur especially in drug addicts and patients with endocarditis. They are usually staphylococcal in origin. Predisposing factors include: prolonged catheter drainage, reflux, obstruction, congenital anomalies, diabetes and pregnancy. Ninety percent of urinary tract infections occur as a single attack with 10 percent being recurrent.[3] Pyelonephritis is more common in sexually active women and there is also a peak increase in men over 60 years due to urinary stasis secondary to prostatic hyperplasia.[3]

Pathology

The affected kidney is enlarged due to edema, and there are multiple foci of inflammation which are characteristically patchy and may lead to microabscesses. With treatment, focal areas of inflammation usually resolve completely, but in the presence of diabetes or other risk factors and inadequate treatment, the infection progresses to result in bacterial nephritis which may be focal or diffuse and may further progress to renal and perirenal abscess.

Radiology

Imaging is usually not required for uncomplicated cases of acute pyelonephritis.

The role of IVU in acute pyelonephritis has rapidly diminished. It is used when CT is not readily available. About 75 percent of all affected uncomplicated patients have normal urograms. Only 25 percent of cases of acute pyelonephritis will have positive IVU findings.[1,3] IVU may show global or focal renal enlargement with decreased, delayed, and persistent nephrogram. Pelvicalyceal system may show minimal dilatation or attenuation of the calyces. In severe cases, the picture may resemble renal vein thrombosis or replacement of the renal tissue with tumor. Ultrasound reveals focal or diffuse enlargement of the kidney with low level echoes and loss of corticomedullary (CM) differentiation. The advent of newer and more user friendly US contrast agents has helped to better demonstrate areas of poor perfusion related to nephritis. Power Doppler is superior to colour Doppler in defining extent of hypoperfusion. USG is considered the modality of choice for pregnant patients.[3] Biphasic/triphasic CECT is superior to both USG and IVU in detecting perinephric fluid collection, obstruction, renal enlargement and inflammatory masses. The CT nephrogram (at 20-45 sec) is felt to be superior in depicting the full extent of the disease and in general defines the abnormalities of acute pyelonephritis the best. Secretory phase (after 2 min) is useful to detect any sloughed papilla or fungus balls. The sensitivity and specificity of CT is about 86.8 percent and 87.5 percent, and of USG is 74.3 percent and 6.7 percent respectively.[3] CECT may reveal wedge-shaped areas of decreased attenuation radiating from papilla due to hypoperfusion in an enlarged kidney (Fig. 8.2). The transverse areas of alternate bands with increased and decreased density represent microstriations due to vaso-constriction and renal edema. Dalla Palma et al[9] have described the role of delayed CT in outlining the true extent of renal infection. Three types of changes were seen on delayed scans: (a) A delayed nephrogram with streaky, wedge-shaped or round high density areas seen at the same site as the reduced density on early scans (b) Focal staining or a hyperdense rim surrounding abscesses (c) Focal areas of increased density distant from the low density areas seen on early scans. These features made it possible to better define the actual extent of infection. Scintigraphic techniques are considered superior to US and IVU for the diagnosis of acute pyelonephritis.[10] Renal cortical scintigraphy with 99mTc DMSA reveals wedge-shaped cortical defects. On MR imaging the affected area has low-signal on T1WI and increased signal on T2WI with loss of CMD. MRI features of pyelonephritis mimic those of CT. MRI may also help in differentiating acute infection from chronic scar. The potential pitfalls of MR imaging are in patients with

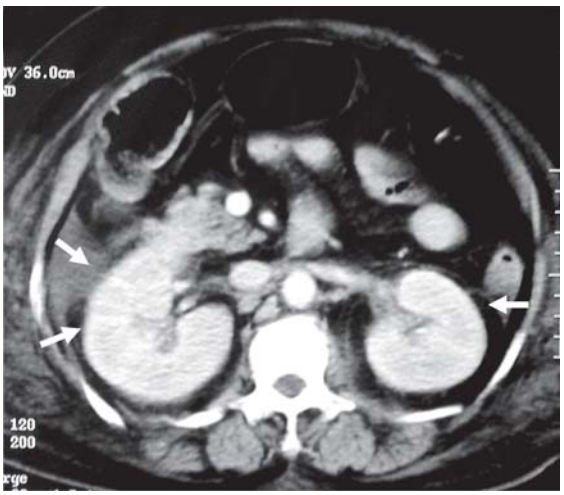

Fig. 8.2: Contrast-enhanced CT scan shows bilateral enlarged kidneys with striated nephrogram (arrows) suggestive of acute pyelonephritis. There is presence of perinephric stranding and thickening of Gerota's fascia and lateral conal fascia

gas forming infections and calculi with the inability of MR to distinguish between the two.[3]

ACUTE FOCAL BACTERIAL NEPHRITIS

IVU reveals presence of a focal renal mass which on follow-up IVU may reveal an area of focal scarring due to healing opposite a normal or clubbed calyx. US reveals hypoechoic poorly defined mass with internal echoes (Fig. 8.3A). The mass will be echogenic if there is haemorrhage.

CT shows focal low density area with patchy enhancement (Fig. 8.3B). Lack of well-defined wall and central low density differentiates it from the renal abscess. Changes of acute pyelonephritis may be seen in the rest of the kidney, which may not have been detected on IVU or ultrasound.

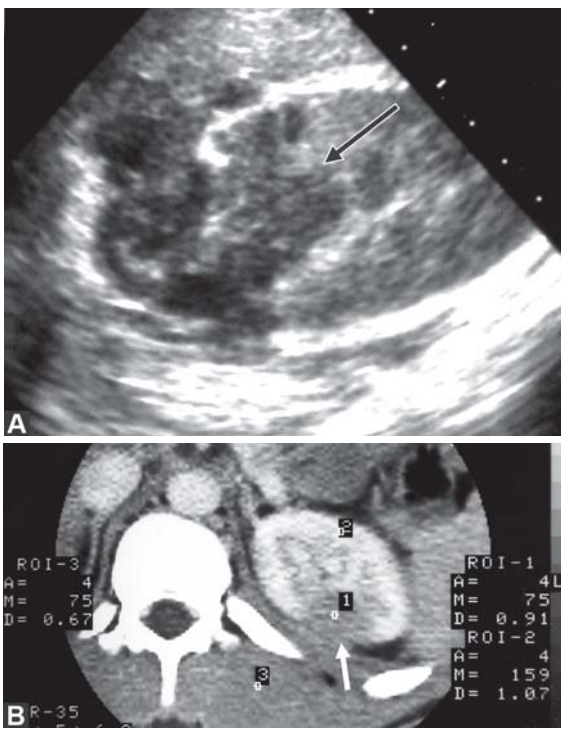

Figs 8.3A and B: (A) Longitudinal ultrasound scan of the kidney showing poorly defined hypoechoic lesion with low level internal echoes in the upper polar region (arrow) which was due to focal bacterial nephritis. **(B)** Contrast enhanced CT scan of another patient showing a focal low density area with patchy enhancement in the posterior aspect of upper pole of left kidney (arrow)

RENAL AND PERIRENAL ABSCESS

Renal and perirenal abscess usually develops as a complication of focal bacterial pyelonephritis, but may result from haematogenous infection or superadded infection in a renal cyst or direct involvement of the perinephric space from pancreas, colon, and retroperitoneum. Plain X-ray abdomen in a case of renal abscess shows renal enlargement, rotation, displacement, presence of mottled gas in the renal areas, and loss of psoas outline. IVU generally shows poorly or nonfunctioning kidney with calyceal attenuation and compression due to mass affect (Figs 8.4A and B). US may reveal a well-defined complex mass with good sound transmission (Figs 8.5A and B). Bright echoes with dirty distal shadowing are seen in the presence of air. However, these findings are nonspecific and may be seen in infected, hemorrhagic cysts or necrotic neoplasms.

CT is the gold standard to assess the renal as well as extrarenal extent of the renal abscess. Changes in the renal contour, parenchymal density, enhancement pattern and perinephric abnormalities such as thickening of the Gerota's fascia, psoas muscle involvement are best seen on CT (Fig. 8.6). Presence of non- enhancing poorly marginated area of decreased attenuation may be seen during the earlier course of renal abscess (Fig. 8.5B). This may be surrounded by an area of decreased enhancement due to presence of infected renal parenchyma. Later in the course of the disease, renal abscess

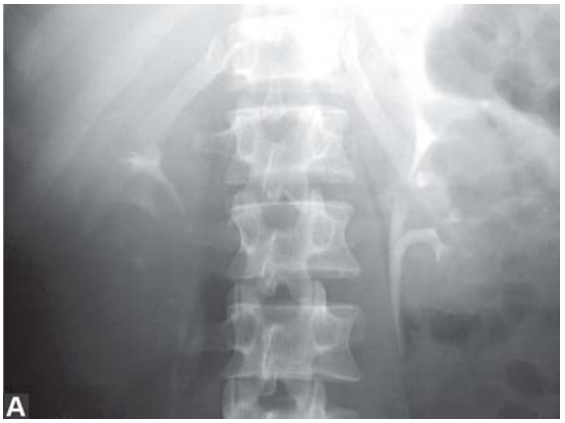

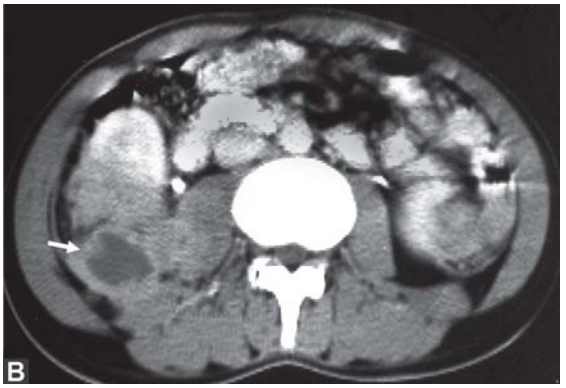

Figs 8.4A and B: (A) IVU showing a mass impression on the collecting system of the upper pole and pelvis due to a right renal abscess. The lower group of calyces are not visualized. The psoas shadow on the ipsilateral side is also obliterated. **(B)** Contrast-enhanced CT scan of the same patient showing an absent nephrogram in the lower pole with a liquefied collection in the perinephric space (arrow) extending medially into the right psoas muscle

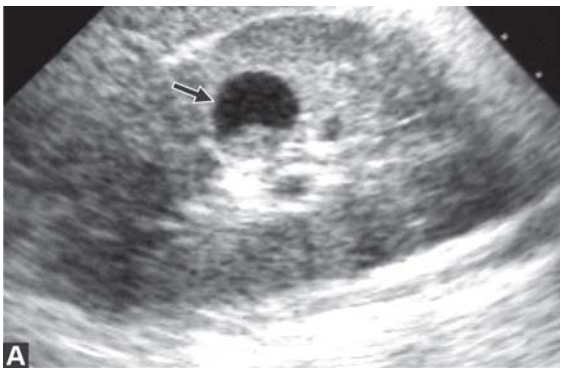

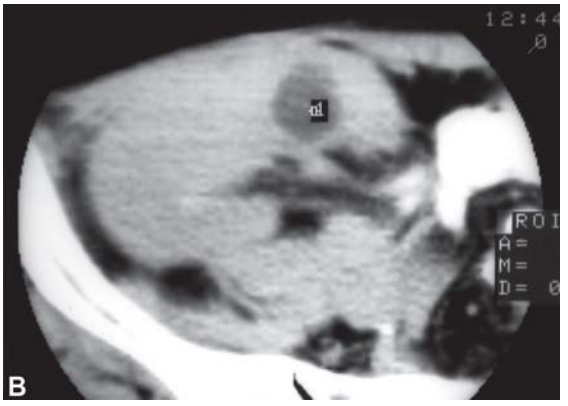

Figs 8.5A and B: (A) Longitudinal ultrasound scan of the transplant kidney shows an anechoic lesion with internal debris in the interpolar region (arrow) suggestive of abscess. **(B)** Contrast-enhanced CT scan of the same patient shows a well-defined hypodense lesion in the anterior parenchyma with minimal peripheral contrast enhancement

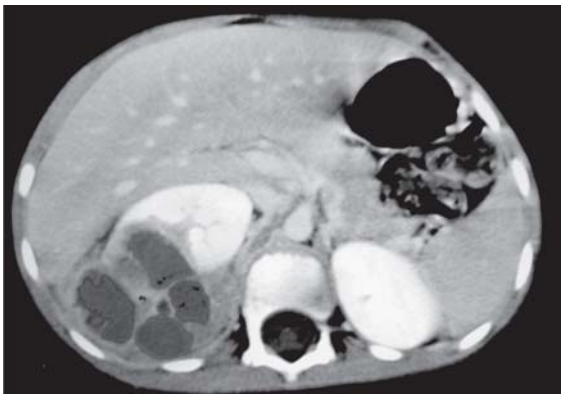

Fig. 8.6: Contrast-enhanced CT scan showing multiple low density lesions with rim enhancement in the right kidney suggestive of renal abscess with extension into the perinephric space

appears as a sharply marginated area of low attenuation due to necrosis surrounded by a peripheral enhancing rim indicating a mature abscess (Fig. 8.6). On MRI a renal abscess is seen as a hypointense lesion on T1WI and a hyperintense lesion on T2WI. On gadolinium administration the lesion shows peripheral enhancement (Figs 8.7A to C). Differential diagnosis includes segmental renal infarct, metastasis, lymphoma, trauma, and renal vein thrombosis. Percutaneous drainage has decreased the mortality with a success rate of 85 to 95 percent.[11]

EMPHYSEMATOUS PYELONEPHRITIS

Emphysematous pyelonephritis (EPN) indicates severe renal infection with gas-forming organisms characterized by presence of gas in the collecting system or renal parenchyma. It is commonly seen in diabetics and patients with ureteral obstruction. Radiologically emphysematous pyelonephritis can be divided into two types: Type I which is less common (33%), has parenchymal destruction and shows streaky/mottled gas in interstitium of renal parenchyma radiating from medulla to cortex, crescent of subcapsular/perinephric gas with no fluid collection. Type II is more common (66%) and shows bubbly/loculated intrarenal gas, renal/perirenal fluid collections and gas within the pelvicalyceal system. Prognosis wise former has worse prognosis having 69 percent mortality with the latter having mortality of only 18 percent.

Plain X-ray can demonstrate air specks in renal area in over 85 percent of cases. However this is frequently misinterpreted as bowel gas. There can be diffuse mottled appearance over the renal shadow with radially oriented air within, corresponding to renal pyramids. The crescent shaped air

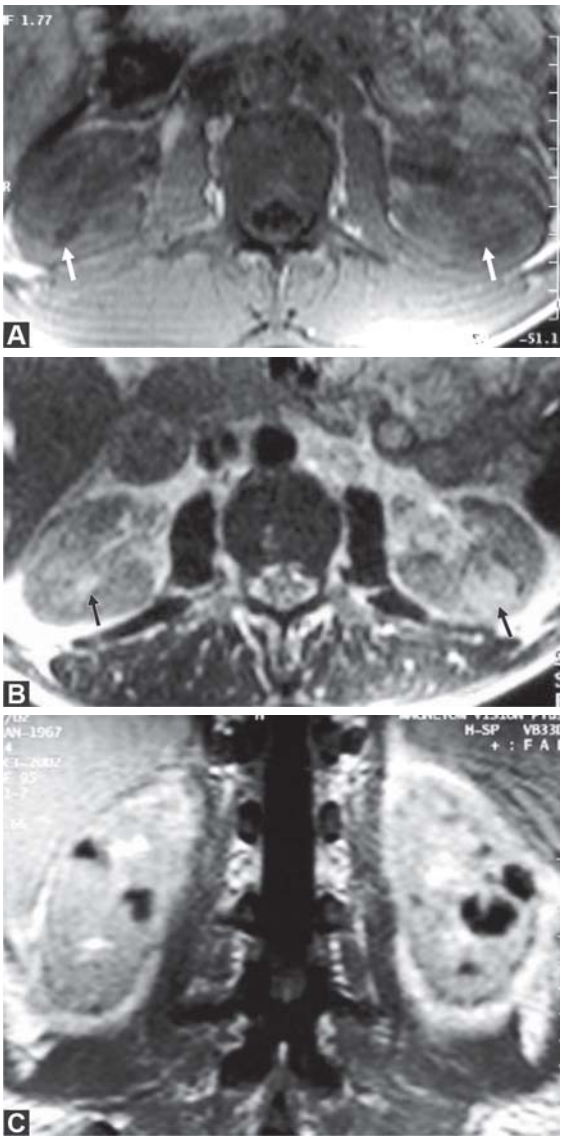

Figs 8.7A to C: (A) Axial T1WI shows hypointense lesions in both kidneys (arrows). **(B)** Axial T2WI shows hyperintense lesions in both kidneys (arrows). **(C)** Gadolinium enhanced coronal T1WI shows multiple hypointense lesions of varying sizes in both kidneys which show peripheral rim enhancement

indicates the extension into perinephric space suggesting the advanced stage. IVU is rarely performed these days, but when performed, reveals a poorly functioning or nonfunctio-

ning kidney. US examination reveals dense echoes with dirty shadowing in intrarenal infection. If the gas enters the perinephric space, there will be nonvisualization of kidney (gassed out kidney). CT is ideal to assess the renal as well as perirenal extent (Fig. 8.8). It detects the presence of air, its precise location within the kidney as well as its extension into the perirenal or pararenal compartments of the retroperitoneal space. The role of MRI is limited as gas appears as an area of signal loss which cannot be differentiated from calculi, renal calcification and flowing blood on T1 and T2WI.

PYONEPHROSIS

Pyonephrosis is the term used to describe infection in an obstructed collecting system with suppurative destruction of the renal parenchyma. Obstruction may be due to renal calculi, stricture or tumor. US is the modality of choice to detect dilated collecting system which contains dependent echoes and shifting debris (Fig. 8.9A). Plain X-ray of the abdomen

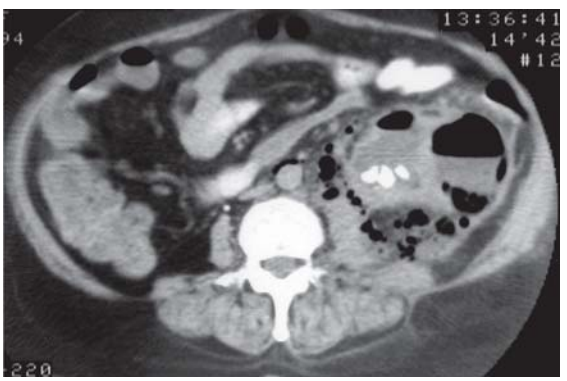

Fig. 8.8: Contrast-enhanced CT scan showing left renal calculi and dilated collecting system with dense urine suggestive of pyonephrosis. In addition extensive collection of air is seen in the renal parenchyma and perinephric space with extension around the aorta due to emphysematous pyelonephritis

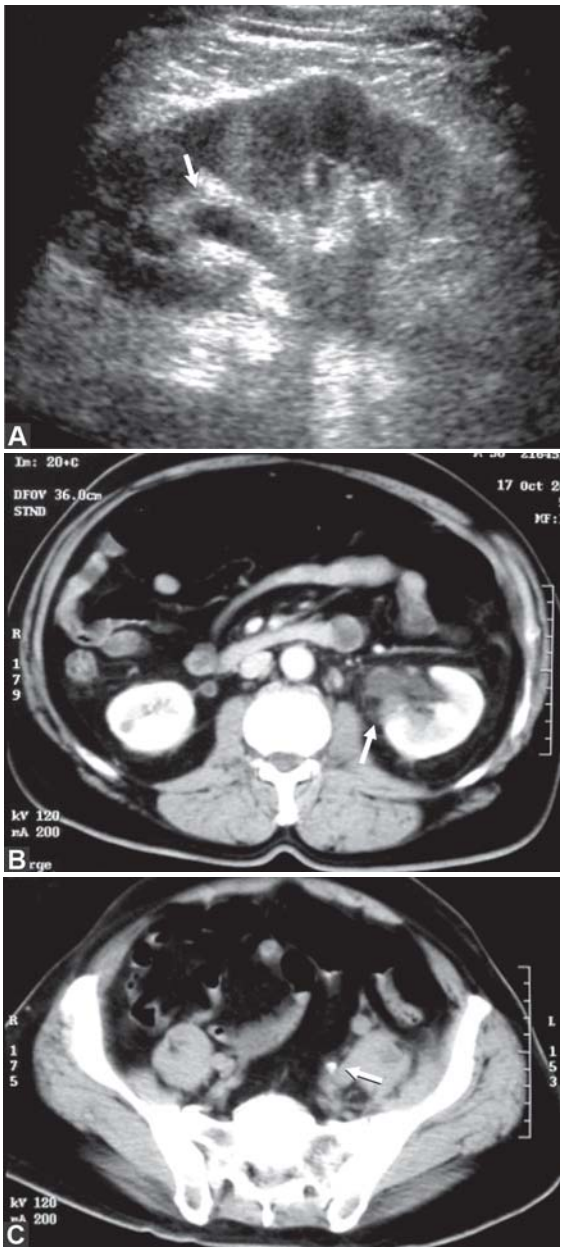

Figs 8.9A to C: (A) Longitudinal ultrasound scan of right kidney showing dilated collecting system filled with echogenic material and thickened echogenic uroepithelium (arrow) suggestive of pyonephrosis. **(B)** Contrast-enhanced CT scan shows hydronephrosis of left kidney with presence of high density urine and perinephric and periureteric stranding (arrow). **(C)** Caudal axial section in the same patient shows a left lower ureteric calculus

may show enlarged kidney with or without stones. IVU shows a nonfunctioning kidney. CT is ideal to show intrarenal changes and the perirenal extension. High-density of urine in the dilated system should suggest infection (Figs 8.9B and C). Thickening of the renal pelvic wall may be detected both on US or CT. Ultrasound guided aspiration may be performed to confirm the diagnosis as well as obtain specimen for culture and sensitivity. Percutaneous nephrostomy may also be performed under US guidance to provide immediate decompression of the collecting system as an adjunct prior to definitive surgery. In case of fungal pyonephrosis, direct infusion of amphotericin B may be accomplished through the PCN catheter. This may be preferable to systemic amphotericin which is more toxic.

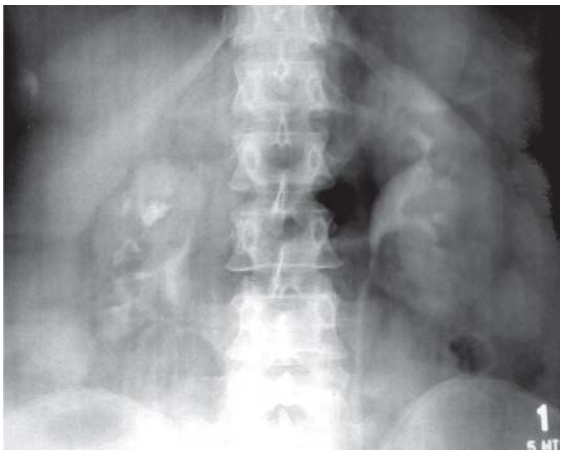

Fig. 8.10: Excretory urogram showing small irregular right kidney with dilated and distorted calyces and thinned out parenchyma especially opposite the polar calyces

CHRONIC PYELONEPHRITIS

Chronic pyelonephritis refers to the chronic inflammation of the kidney characterized by cortical scarring overlying the involved calyx (usually polar). Entire collecting system may be involved resulting in small kidney with clubbed calyces (Fig. 8.10). The opposite kidney may enlarge due to compensatory hypertrophy. Inflammation is generally patchy and the uninvolved areas of parenchyma may hypertrophy to cause mass effect (pseudotumor) which may require scintigraphy for confirmation. Differential diagnosis includes fetal lobulation, ischemia and hypoplastic kidney. In ischemia the adjacent calyx is normal. In fetal lobulation, the scars are in between the calyces. In congenital hypoplastic kidney the number of calyces are less than five.

REFLUX NEPHROPATHY

Reflux nephropathy results from combined effects of the vesicoureteric reflux and bacterial infection. The disease process begins in infancy and childhood, and is more common in females. Due to incompetent papillary duct orifices, there is intrarenal reflux of infected urine which leads to destruction of the tubules and subsequent scarring. Despite the low radiation dose to the patient during radionuclide cystogram, studies have suggested that fluoroscopic voiding cystourethrogram is a better technique to detect and grade the degree of reflux which is an important factor to determine the future treatment planning in these children.[12] In a child with repeated attacks of urinary tract infection, US is still considered the best screening tool to detect obstructive uropathy—an important factor placing the child at risk for recurrent infections and subsequent post-infectious nephropathy. Renal cortical scintigraphy is the best technique to detect renal scarring. Doppler US and power Doppler may be as useful as DMSA scanning for the detection of scarring. Dacher et al[13] showed that power Doppler US could be used to detect acute pyelonephritis in children. They

demonstrated peripheral triangular areas of decreased renal perfusion in these patients. Presence of vesicoureteric reflux needs to be excluded in all these children.

FAT PROLIFERATION IN THE KIDNEY

Sinus fat may increase as a normal phenomenon in an aging kidney, renal sinus lipomatosis (RSL) or it may completely replace the renal parenchyma which is destroyed by chronic inflammation (renal replacement lipomatosis).

RSL is usually seen in patients with extrarenal pelvis. The calyces are stretched and elongated, but there is no hydronephrosis and kidneys are otherwise normal. Differentiation from a parapelvic cyst may require ultrasonography which shows extensive echogenicity in case of RSL whereas parapelvic cyst is sonolucent. On CT, RSL may mimic parapelvic cyst and hydronephrosis (Fig. 8.11).

In renal replacement lipomatosis, plain film frequently reveals calculi. IVU may show absent or poor excretion of contrast with stretched calyces. CT confirms the presence of fat in an atrophic kidney containing calculi. US also shows increased echogenicity indicating fat. Differential diagnosis includes fatcontaining tumors such as angiomyolipoma.

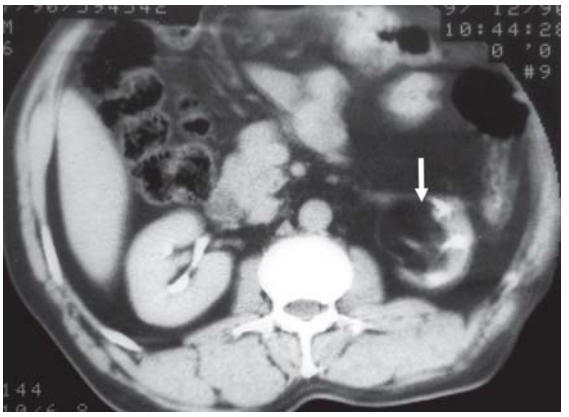

Fig. 8.11: Contrast- enhanced CT scan shows an enlarged renal sinus (arrow) with fat attenuation on the left side suggestive of renal sinus lipomatosis. The fat attenuation differentiates renal sinus lipomatosis from parapelvic cyst

XANTHOGRANULOMATOUS PYELONEPHRITIS

Xanthogranulomatous pyelonephritis (XGPN) is a rare chronic granulomatous inflammation of the kidney usually seen in patients who have stones and obstruction. The disease is characterized by destruction and replacement of the renal parenchyma with lipidladen macrophages which are para-aminosalicylic acid (PAS)-positive (xanthoma cells). The condition is more common in women frequently presenting with mass in the renal area. Two types of the disease, i.e. focal and diffuse have been described. Pathologically depending on the extent, three stages have been described. In Stage I, kidney alone is involved, in Stage II, there is extension into Gerota's fascia and in Stage III, perinephric spaces are also involved.

Imaging features include presence of staghorn calculus and/or also small calcifications scattered throughout the kidney which may be detected on plain X-ray or CT. IVU reveals evidence of a focal mass (tumefactive type), or diffusely enlarged nonfunctioning kidney. Presence of lucent areas on X-ray and nonenhancing cystic areas on CT corresponding to the xanthoma cell collection is characteristic (Fig. 8.12). Renal vein may be thrombosed. Perinephric extent is best seen on CT. US findings include multiple anechoic or hypoechoic areas with central echogenic foci corresponding to the fine calcification. Small cystic collection due to cortical abscesses may be seen. Differential diagnosis from pyonephrosis, tuberculosis,

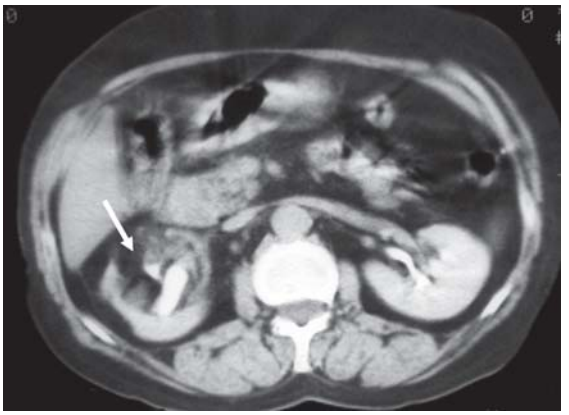

Fig. 8.12: Contrast-enhanced CT scan shows right renal calculi with a well- defined mass lesion with multiple fat attenuation areas (arrow) characteristic of xanthoma cell collection in a case of xantho-granulomatous pyelonephritis

cystic carcinoma, and lymphoma may at times be difficult.

HIV-ASSOCIATED NEPHROPATHY (HIVAN)

HIV can affect any organ of the body and the kidneys have been increasingly shown to be involved by a variety of disease processes in HIV infection. Kidneys may be involved as a collapsing glomerulopathy (HIVAN) or due to secondary infections by bacteria or opportunistic organisms such as *Pneumocystis carinii* and cytomegalovirus. HIVAN is a serious disorder which results in rapidly progressive renal failure. It manifests histologically as focal glomerulosclerosis and as membranous, membranoproliferative, and mesangial proliferative glomerulonephritis.[14] Imaging reveals renal enlargement (>13cm) with increased echogenicity on US. However Atta et al[15] found that only renal echogencity and not kidney size has diagnostic utility for HIVAN. On CECT enlarged kidneys with striated nephrogram are seen.[16,17] On unenhanced CT scans, hyperattenuating medulla may be seen as a result of dilated protein filled tubules. Imaging findings may suggest the diagnosis of HIVAN but it should be confirmed on histology. *Pneumocystis carinii* infection results in punctate areas of calcification within the renal parenchyma similar to those seen with cytomegalovirus or *Mycobacterium avium intracellulare* (MAI).[18]

RENAL PAPILLARY NECROSIS

Most common cause of renal papillary necrosis is analgesic abuse and diabetes. The other causes include urinary tract infection (UTI), renal vein thrombosis, obstruction, dehydration, and sickle cell disease. IVU remains the best technique for demonstrating the changes of papillary necrosis. Presence of extracalyceal contrast, ill-defined calyx, contrast outlining sloughed papillae (ring sign), and filling defect in the calyx or calcification of the papilla may be seen. The sloughed papillae may pass down the collecting system and ureter, and present radiological picture of obstruction.

MALACOPLAKIA

Malacoplakia is a rare granulomatous inflammatory disease seen almost exclusively in women who present with repeated attacks of UTI. Bladder and ureter are most frequently affected. Radiological features include enlarged poorly functioning kidney with presence of filling defect in the bladder and the ureter, similar to the changes seen in pyeloureteritis cystica, or transitional cell carcinoma. Strictures may also form, thus tuberculosis is an important differential diagnosis. Renal involvement results in focal or multiple masses indistinguishable from renal cell carcinoma or XGPN on US, CT or IVU. Diagnosis is usually based on pathology

which reveals van Hanseman cells and Michaelis Gutman bodies in the nodular deposits.

SQUAMOUS METAPLASIA

Squamous metaplasia is the replacement of normal transitional cell epithelium by squamous epithelium as a result of infection. The condition is characterized by the presence of multiple linear radiolucencies in the ureter due to mucosal thickening resulting in so called "tree barking" or "Corduroy appearance" in IVU or RGU.

The term, cholesteatoma is used when there is a filling defect in the collecting system due to sloughed keratinized material. The filling defect on CT has a high attenuation value due to small punctate calcification which differentiates the condition from carcinoma and other causes of filling defects such as sloughed papillae, radiolucent stones, and fungus ball.

Fungal and *parasitic infections* of the kidney are rare, occurring generally in patients with impaired immune status such as diabetics, renal transplants and other chronic infections and on prolonged steroid therapy. Infection by *Candida*, *Aspergillus*, *Cryptococcus*, and mucor has been described. Presence of bilateral poorly functioning/non-functioning enlarged kidneys with multiple low density areas located both in the cortex and medulla on CT should raise the possibility of the diagnosis of mucormycosis.[19] Both *Aspergillus* and mucor are angioinvasive fungi and cause thrombosis of the large as well as small arteries which results in infarction and necrosis of the affected organs. The infection usually occurs by hematogenous route resulting in multiple abscesses which appear as low density areas in the renal parenchyma, and there may be perinephric spread (Fig. 8.13).

PARASITIC INFECTION

Schistosomia usually affects the bladder causing calcification. Renal pelvic striations may be seen. Intrarenal hydatids are rare and

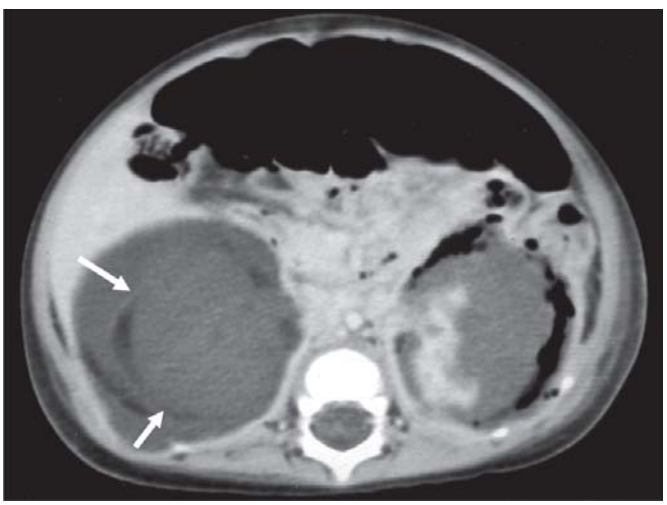

Fig. 8.13: Contrast-enhanced CT scan of a 2-year-old child with proven mucormycosis who presented with renal failure. The right kidney is enlarged and nonfunctioning (arrows) with evidence of perinephric collection. The left kidney shows functioning renal parenchyma on the medial aspect with presence of air in the perinephric space

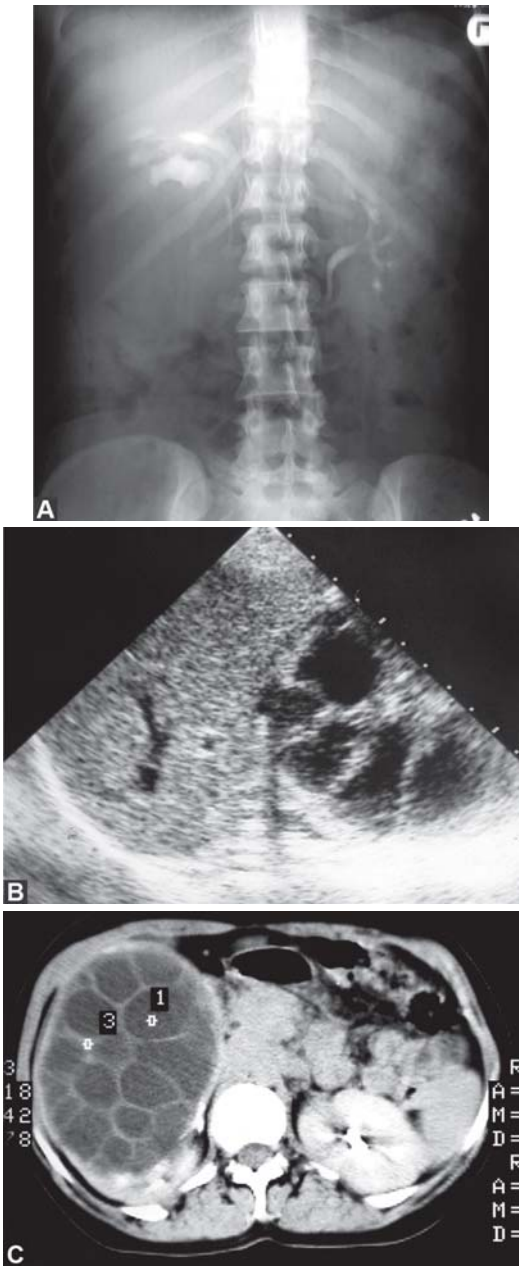

Figs 8.14A to C: **(A)** Excretory urogram showing a mass at the lower pole of right kidney with displacement and dilatation of the collecting system and medial deviation of the ureter. **(B and C)** Ultrasound and contrast-enhanced CT scan of the same patient showing characteristic multiloculated appearance due to daughter cysts of hydatid later confirmed at surgery

appear as focal cystic masses which are usually thick walled and irregular, and may show calcification of crushed eggshell pattern (Figs 8.14A to C).

REFERENCES

1. Kawashima A, Sandler CM, Goldman SM. Imaging in acute renal infection. BJU International 2000;86 Suppl.1,70-79.
2. Bjerklund Johansen TE. The role of Imaging in urinary tract infections. World J Urol 2004; 22:392- 98.
3. Stunell H, Buckley O, Feeney J, et al. Imaging of acute pyelonephritis in the adult. Eur Radiol 2007;17:1820-28.
4. Merenich WM, Popky GL. Radiology of renal infection. Med Clin N Am 1991;75:425-69.
5. Ellenbogen PH, Schieble FW, Talner LB, et al. Sensitivity of gray scale ultrasound in detecting urinary tract obstruction. AJR 1978;130:731-33.
6. Wicks JD, Thornbury JR. Acute renal infections in adults. Radiol Clin N Am 1979;12:245-60.
7. Laing FC, Jeffrey RB (Jr), Wing VW. Ultrasound versus excretory urography in evaluating acute flank pain. Radiol 1985;154:613-16.
8. Conway JJ. The role of scintigraphy in urinary tract infection. Semin Nucl Med 1998;18:308-19.
9. Dalla-Palma L, Pozzi-Mucelli R, Pozzi-Mucelli F. Delayed CT in acute renal infection. Semin Ultrasound CT MR 1997;18:122-28.
10. Talner LB, Davidson AJ, Lebowitz RL, et al. Acute pyelonephritis—can we agree on terminology? Radiol 1994;192:297-305.
11. Van Sonnenberg E, D'Agostino HB, Sanchez RB, et al. Percutaneous abscess drainage. Radiol 1992;184:27-29.
12. Kass EJ,Kernen KM, Carey JM. Paediatric urinary tract infection and the necessity of complete urological imaging. BJU Int 2000;86:94-96.
13. Dacher JN, Pfister C, Monroc M, et al. Power Doppler sonographic pattern of acute pyeloneph-ritis in children: comparison with CT. *AJR* 1996;166:1451-55.
14. Symeonidou C, Standish R, Sahdev A, et al. Imaging and histopathologic features of HIV-related renal disease. Radiographics 2008;28: 1329-54.
15. Atta MG, Longenecker JC, Fine DM, et al. Sonography as a predictor of human immunodeficiency virus- associated nephropathy. J Ultrasound Med 2004;23:603-10.

16. Kuhlman JE, Browne D, Shermak M, et al. Retroperitoneal and pelvic CT of patients with AIDS: Primary and secondary involvement of the genitourinary tract. Radiographics 1991;11: 473-83.
17. Miller FH, Parikh S, Gore RM, et al. Renal manifestations of AIDS. Radiographics 1993;13: 587-96.
18. Bray HJ, Lail VJ, Cooperberg PL. Tiny echogenic foci in the liver and kidney in patients with AIDS: Not always due to disseminated Pneumocystis carinii. AJR 1992;158:81-82.
19. Chugh KS, Sakuja V, Gupta KL, et al. Renal mucormycosis: Computerized tomographic findings and their diagnostic significance. Am J Kidney Dis 22:393-97.

TUMORS OF THE UROGENITAL TRACT

Chapter 9

Pathology of Renal Tumors

Kusum Joshi

INTRODUCTION

Cancer of the kidney amounts to 2 percent of the total human cancers and occur in both adults and children, although the frequency of the cancer types is quite different in the two populations. Although renal tumors can be completely removed surgically, haematgenous spread may occur at an early stage of the disease. The pattern of somatic mutations in kidney tumors has been investigated extensively and has been incorporated, along with histopathology, in the classification of kidney tumors.

Currently, the recent WHO classification (2004) is most acceptable for use and incorporates the cytogenetic features where required.

Since the prevalence of renal tumors is distinctly different in adults and children, the following discussion will be under the subheadings of adult renal tumors and pediatric renal tumors. The following discussion is not a complete review of all types of adult and pediatric renal tumors, but rather a discussion on the common and important ones and those peculiar to the kidney.

ADULT RENAL TUMORS

Renal Cell Tumors

Renal cell carcinoma (RCC) is the most common malignant tumor arising in the kidney and accounts for 2 percent of all new cancers diagnosed, representing 85 percent of all primary renal neoplasms in adults (Fig. 9.1). Renal cell carcinoma is a group of malignancies arising from the epithelium of

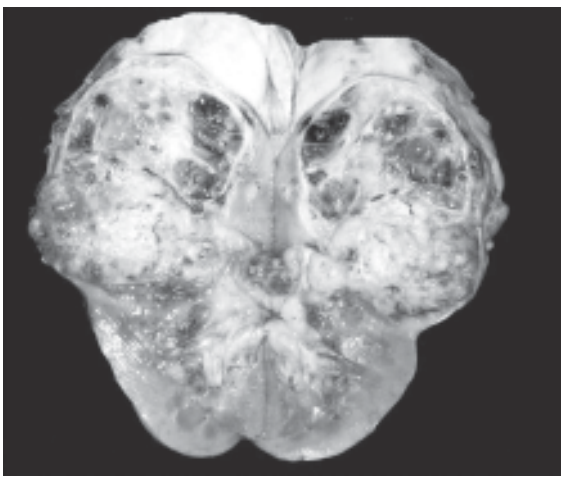

Fig. 9.1: Variegated gross appearance of renal cell carcinoma *(For color version see Plate 9)*

the renal tubules. A male predominance exists with a male to female ratio of 1.6:1.0[1] and the peak incidence is in the sixth and seventh decades although rarely, RCC can occur in children and adolescents. A study from India quotes that renal tumors constitutes 10.64 percent of all the malignant tumors of male urogenital tract or 1.51 percent of all the male cancers. The mean age of the cases for renal cell carcinoma was 50.3 years in this Indian study. An increased incidence of RCC has been associated with end-stage renal disease and with acquired cystic kidney disease.[15] The classic triad of presenting symptoms include hematuria, pain, and flank mass, but nearly 40 percent of patients lack all of these and present with systemic symptoms, including weight loss, abdominal pain, anorexia, and fever. Normocytic anemia unrelated to hematuria occurs in about 33 percent of cases. Hepatosplenomegaly, coagulopathy, elevation of serum alkaline phosphatase, transaminase, and alpha-2- globulin concentrations may occur in the absence of liver metastases and may resolve when the renal tumor is resected. Systemic amyloidosis of the AA type occurs in about 3 percent of patients. Renal cell carcinoma may induce paraneoplastic endocrine syndromes, including hypercalcemia of malignancy (pseudohyperparathyroidism), erythrocytosis, hypertension, and gynecomastia. Hypercalcemia without bone metastases occurs in approximately 10 percent of patients and in nearly 20 percent of patients with disseminated carcinoma. RCCs have been regarded as a single entity in the past; however cytogenetic and molecular studies have proven conclusively that these are group of distinguishable entities, as seen from the Table 9.1.

Clear Cell (or Non-papillary or Conventional) RCC

This is the most common form of RCC, comprising 60 percent of cases. They show a male preponderance of 2:1 and mean age at presentation is 61 years. Clear cell renal cell carcinomas (RCCs) are solitary and randomly distributed cortical tumors that occur with equal frequency in either kidney. Multicentricity and/or bilaterality occur in less than 5 percent of cases. Clear cell RCCs are typically globular tumors which commonly protrude from the renal cortex as a rounded, bosselated mass. The interface of the tumor and the adjacent kidney is usually well-demarcated, with a "pushing margin" and pseudocapsule. Diffuse infiltration of the kidney is uncommon. The average size is 7 cm in diameter. Clear cell renal cell carcinoma is typically golden yellow due to the rich lipid content of its cells; cholesterol, neutral lipids, and phospholipids are abundant. Cysts, necrosis, hemorrhage, and calcification are commonly present. About 50 percent of clear cell RCCs are stage 1 and 2 and less than 5 percent are stage 4. Invasion of perirenal and sinus fat and/or extension into the renal vein occurs in about 45 percent of cases. Clear cell RCC most commonly metastasize hematogenously via the vena cava primarily to the lungs.

Clear cell RCC is architecturally diverse, with solid, alveolar and acinar patterns, being the most common. The alveolar and acinar structures may dilate, producing microcystic and macrocystic patterns. The carcinomas typically contain a regular network of small thin-walled blood vessels. The cytoplasm is commonly filled with lipids and glycogen, giving the appearance of a clear cytoplasm surrounded by a distinct cell membrane. Usually, the nuclei are condensed and

Table 9.1: WHO Histological Classification of Renal Tumors

Renal cell tumors
Clear cell renal cell carcinoma
Multilocular clear cell renal cell carcinoma
Papillary renal cell carcinoma
Chromophobe renal cell *carcinoma*
Carcinoma of the collecting ducts of Bellini
Renal medullary carcinoma
Xp11 translocation carcinomas
Carcinoma associated with neuroblastoma
Mucinous tubular and spindle cell carcinoma
Renal cell carcinoma, unclassified
Papillary adenoma
Oncocytoma

Metanephric tumors
Metanephric adenoma
Metanephric adenofibroma
Metanephric stromal tumor

Nephroblastic tumors
Nephrogenic rests
Nephroblastoma
Cystic partially differentiated nephroblastoma

Mesenchymal tumors
Occurring Mainly in Children
Clear cell sarcoma
Rhabdoid tumor
Congenital mesoblastic nephroma
Ossifying renal tumor of infants
Occurring Mainly in Adults
Leiomyosarcoma (including renal vein)
Angiosarcoma
Rhabdomyosarcoma
Malignant fibrous histiocytoma
Hemangiopericytoma
Osteosarcoma
Angiomyolipoma
Epithelioid angiomyolipoma
Leiomyoma
Hemangioma
Lymphangioma
Juxtaglomerular cell tumor
Renomedullary interstitial cell tumor
Schwannoma
Solitary fibrous tumour

Mixed mesenchymal and epithelial tumors
Cystic nephroma
Mixed epithelial and stromal tumor
Synovial sarcoma

Neuroendocrine tumors
Carcinoid
Neuroendocrine carcinoma
Primitive neuroectodermal tumor
Neuroblastoma
Pheochromocytoma

Hematopoietic and lymphoid tumors
Lymphoma
Leukemia
Plasmacytoma

Germ cell tumors
Teratoma
Choriocarcinoma

Metastatic tumors

hyperchromatic. Sarcomatoid change occurs in 5 percent of tumors and is associated with worse prognosis.[13] Clear cell RCCs frequently react with antibodies to brush border antigens, low molecular weight cytokeratins, CK8, CK18, CK19, AE1, Cam 5.2 and vimentin. The majority of clear cell RCCs react positively for renal cell carcinoma marker, CD10 and epithelial membrane antigen. MUC1 and MUC3 are consistently expressed. Electron microscopical features resembling the proximal tubule can be found, i.e. brush border formation and basal infoldings (Fig. 9.2).

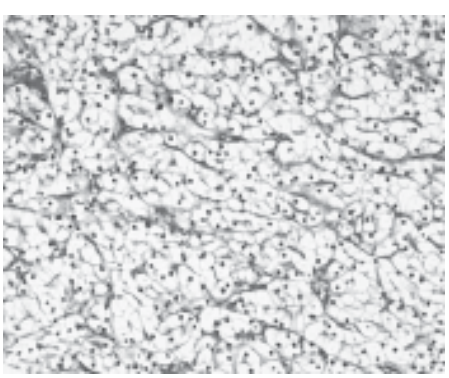

Fig. 9.2: Photomicrograph showing clear cell with grade 1 nuclei in a classical case of renal cell carcinoma *(For color version see Plate 9)*

Multilocular Cystic Renal Cell Carcinoma

This tumor is composed entirely of numerous cysts, the septa of which contain small groups of clear cells indistinguishable from grade 1 clear cell carcinoma. There is male predominance with male: female ratio of 3:1 and age range of 20-76 years with a mean of 51 years. These tumors have excellent prognosis. Multilocular cystic renal cell carcinoma consists of a well-circumscribed mass ranging in size from 25-130 mm and is composed of small and large cysts filled with serous or hemorrhagic fluid separated from the kidney by a fibrous capsule (Fig. 9.3). The cysts are usually lined by a single layer of epithelial cells or occasionally by several layers of cells and even form papillae or may altogether lack an epithelial lining. The lining cells may be flat or plump and their cytoplasm ranges from, clear to pale. The nuclei almost always are small, spherical, and have dense chromatin (Fuhrman grade 1 or 2).

Papillary (or Chromophilic) renal Cell Carcinoma

These tumors are thought to arise from the proximal tubule and comprise 7-14 percent of RCC cases. Papillary renal cell tumors can be divided into adenomas and carcinomas. Papillary adenomas are tumors with papillary or tubular architecture of low nuclear grade and 5 mm in diameter or smaller. Papillary adenomas are the most common neoplasms of the epithelium of the renal tubules. Autopsy studies have found that papillary adenomas increase in frequency in adulthood from 10 percent in patients younger than 40 years to 40 percent in patients older than 70 years. Papillary adenomas are well-circumscribed, yellow to greyish white nodules as small as less than 1 mm in diameter in the renal cortex occurring just below the renal capsule. Usually, papillary adenomas are solitary, but occasionally they are multiple and bilateral. When they are numerous, this has been termed as "renal adenomatosis". Papillary adenomas have tubular, papillary, or tubulopapillary architecture. They are considered as a putative precursor of papillary renal cell carcinoma (PRCC). Bilateral and multifocal tumors are more common in PRCC than in other renal parenchymal malignancies. The tumor papillae contain a delicate fibrovascular core and aggregates of foamy macrophages and cholesterol crystals may be present. Occasionally, the papillary cores are expanded by edema or hyalinized connective tissue. Solid variants of PRCC consist of tubules or short papillae resembling glomeruli. Hemosiderin granules may be present in macrophages, stroma and tumor cell cytoplasm. Two morphological types of PRCC have been described:

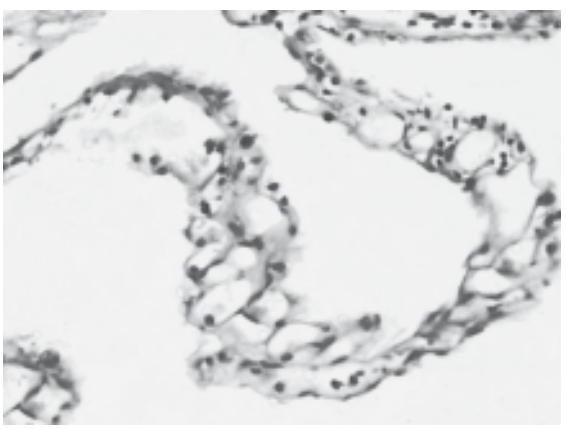

Fig. 9.3: Multilocular cystic renal cell carcinoma, showing clear tumor cells in the septum *(For color version see Plate 9)*

Type 1 tumors have papillae covered by small cells with scanty cytoplasm, arranged in a single layer on the papillary basement membrane (Fig. 9.4).

Type 2 tumor cells are often of higher nuclear grade with eosinophilic cytoplasm and pseudostratified nuclei on papillary

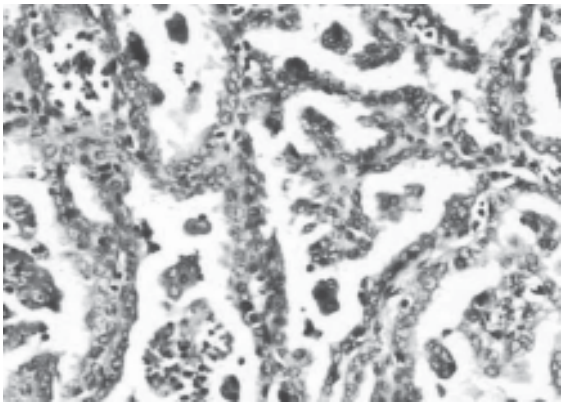

Fig. 9.4: Photomicrograph of papillary (Type 1) renal cell carcinoma *(For color version see Plate 9)*

cores.

Type 1 tumors are more frequently multifocal. Sarcomatoid dedifferentiation is seen in approximately 5 percent of PRCC and has been associated with both type 1 and type 2 tumors.[13] Cytokeratin 7 (CK 7) expression has been reported for PRCC however, this is more frequently observed in type 1 (87%) than type 2 (20%) tumors.[13] For both conventional and papillary RCC, hereditary as well as sporadic cases have been found. Hereditary RCC is characterized by the appearance of multiple and bilateral tumors and an early age of onset. There is no specific grading system for PRCC and the Fuhrman system is accepted as applicable to both clear cell renal cell carcinoma and PRCC.

Chromophobe Renal Cell Carcinoma (CRCC)

The tumor cells resemble and exhibit antigen profile of the intercalated cells type B from the cortical collecting duct. It comprise 6-11 percent of renal epithelial tumors. The mean age of presentation is in the sixth decade, with age range of 27-86 years, and the incidence in men and women is roughly equal. Mortality is less than 10 percent. Chromophobe RCC consists of solid tumor nodules with a slightly lobulated surface. In unfixed specimens the cut surface is homogeneously light brown or tan turning light grey after formalin fixation. The majority of CRCCs are stage T1 and T2 (86%) whereas only 10 percent show extension through the renal capsule into surrounding adipose tissue, and only 4 percent show involvement of the renal vein. In general, the growth pattern is solid, sometimes glandular, with focal calcifications and broad fibrotic septa. In contrast to clear cell renal cell carcinoma, many of the blood vessels are thick-walled and eccentrically hyalinized. The perivascular cells are often enlarged. Chromophobe renal cell carcinoma is characterized by large polygonal cells with transparent slightly reticulated cytoplasm with prominent cell membranes (Fig. 9.5). These cells are commonly mixed with smaller cells with granular eosinophilic cytoplasm. The eosinophilic variant of chromophobe carcinoma is purely composed of intensively eosinophillic cells with prominent cell

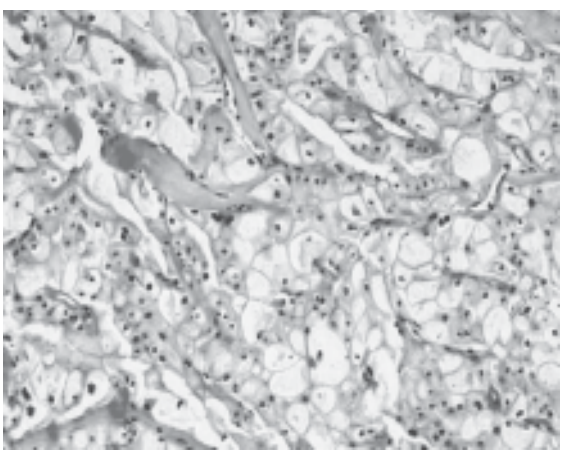

Fig. 9.5: Microscopic appearance of chromophobe carcinoma showing plant like cells with perinuclear clearing of cytoplasm *(For color version see Plate 9)*

membranes. The cells have irregular, often wrinkled, nuclei and some are binucleated. Nucleoli are usually small and perinuclear halos are common.

Another diagnostic hallmark is a diffuse cytoplasmic staining reaction with Hale's colloidal iron stain. Ultrastructurally, the cytoplasm is crowded with glycogen deposits and numerous, sometimes invaginated, vesicles. Chromophobe RCC is positive for carbonic anhydrase C, but does not express band-3 protein.

Collecting Duct (Duct Bellini) RCC (CDC)

This subtype comprises 1 percent of all RCCs. It is a malignant epithelial tumor thought to be derived from the principal cells of the collecting duct of Bellini. Over 100 cases have been described and there is a wide age range from 13-83 years (mean, about 55) with a male to female ratio of 2:1. Upper tract imaging often suggests urothelial carcinoma and patients may occasionally present with positive urine cytology. Collecting duct carcinomas are usually located in the central region of the kidney. When small, origin within a medullary pyramid may be seen. Reported tumors range from 2.5 to 12 cm and they typically have a firm grey-white appearance with irregular borders. Some tumors grow as masses within the renal pelvis and areas of necrosis, satellite nodules and gross renal vein invasion may be present. Collecting duct carcinomas often display infiltration of perirenal and renal sinus fat. About one third of patients have metastases at presentation to the regional lymph nodes, lung, liver, bone and adrenal gland. The prototypic collecting duct carcinoma has a tubular or tubulopapillary growth pattern in which irregular angulated glands infiltrate renal parenchyma and are associated with a desmoplastic stroma. Criteria for diagnosing collecting duct carcinoma have been proposed. Major criteria include — location in a medullary pyramid (small tumors), typical histology with irregular tubular architecture and high nuclear grade, inflammatory desmoplastic stroma with numerous granulocytes, reactive with antibodies to high molecular weight cytokeratin, reactive with Ulex europaeus agglutinin lectin and absence of urothelial carcinoma. Minor criteria include central location (large tumors), papillary architecture with wide, fibrous stalks and desmoplastic stroma, extensive renal, extrarenal, and lymphatic and venous infiltration, intratubular epithelial atypia adjacent to the tumor.

Solid, cord like patterns and sarcomatoid features may be encountered. The sarcomatoid change is a pattern of dedifferentiation similar to that seen in other types of renal carcinoma. The cells of collecting duct carcinoma usually display high grade (Fuhrman 3 and 4) nuclear features. The cells may have a hobnail pattern of growth and the cytoplasm is generally eosinophilic, however, glycogen is usually inconspicuous in collecting duct carcinoma. Both intraluminal and intracytoplasmic mucin may be seen. High molecular weight keratins (34βE12, CK19) are commonly present and co-expression of vimentin may be seen. There is variable immunostaining for CD15 and epithelial membrane antigen. The CD10 and vinculin stains are negative. Lectin histochemistry, usual Ulex europaeus agglutinin-1 and peanut lectin are commonly positive.

Renal Medullary Carcinoma

This is a rapidly growing tumor of the renal medulla associated almost exclusively with

sickle cell trait. With few exceptions these are seen in young people with sickle cell trait between ages 10 and 40 years (mean 22 years) and chiefly in males by 2:1. These are poorly circumscribed tumors ranging in size from 4-12 cm and arising centrally in the kidney. Most of them show extensive hemorrhage and necrosis. A reticular growth pattern and a more compact adenoid cystic morphology are the common features. The cells are eosinophilic with clear nuclei and usually with prominent nucleoli. The sheets of cells can have squamoid or rhabdoid quality. Neutrophils are often admixed with the tumor and the advancing margins are often bounded by lymphocytes. Keratin AE1/AE3 is nearly always positive as is EMA but typically less strongly so. The prognosis is poor and the mean duration of life after surgery has been 15 weeks.

Renal Carcinomas Associated with XP11.2 Translocations/TFE3 Gene Fusions

These carcinomas are defined by several different translocations involving chromosome Xp11.2, all resulting in gene fusions involving the TFE3 gene. These carcinomas predominantly affect children and young adults, though a few older patients have been reported. The ASPL-TFE3 carcinomas characteristically present at advanced stage. Renal carcinomas associated with Xp11.2 translocations are most commonly tan-yellow, and often necrotic and hemorrhagic. The most distinctive histopathologic appearance is that of a carcinoma with papillary architecture comprised of clear cells; however, these tumors frequently have a more nested architecture, and often feature cells with granular eosinophilic cytoplasm. The ASPL-TFE3 renal carcinomas are characterized by cells with voluminous clear to eosinophilic cytoplasm, discrete cell borders, vesicular chromatin and prominent nucleoli. Psammoma bodies are constant and sometimes extensive, often arising within characteristic hyaline nodules. The PRCC-TFE3 renal carcinomas generally feature less abundant cytoplasm, fewer psammoma bodies, fewer hyaline nodules, and a more nested, compact architecture. The most distinctive immunohistochemical feature of these tumors is nuclear immunoreactivity for TFE3 protein. Only about 50 percent express epithelial markers such as cytokeratin and EMA by immunohistochemistry, and the labeling is often focal. The tumors consistently label for the Renal Cell Carcinoma Marker antigen and CD10. Ultrastructurally, Xp11.2-associated carcinomas most closely resemble clear cell renal carcinomas. Very little is known about the clinical behavior of these carcinomas. While the ASPL-TFE3 renal carcinomas usually present at advanced stage, their clinical course thus far appears to be indolent. However, a recent study by Argani et al of 28 Xp11 translocation RCC in patients over the age of 20 years gives a somewhat different picture. Patients ranged from ages 22 to 78 years, with a strong female predominance (F : M = 22 : 6). Five of 6 patients with 1 or more years of follow-up developed hematogenous metastases, with 2 dying within 1 year of diagnosis.

Mucinous Tubular and Spindle Cell Carcinoma

This is a recently described rare entity of low aggressive biological behavior, mostly reported in females of any age. It is a well circumscribed tumor, usually located in the medulla and is composed of elongated inter-

connected tubules, with cords of epithelial cells and interspersed with low grade spindle cell areas. The cells have a bland, monomorphic appearance and stroma can be focally myxoid. It has an ultra-structural resemblance to the Loop of Henle and is nicknamed as a "Loopoma".

Renal Cell Carcinoma—Unclassified

Renal cell carcinoma, unclassified is a diagnostic category to which renal carcinomas should be assigned when they do not fit readily into one of the other categories. Sarcomatoid change has been found to arise in all types of carcinoma in the classification, as well as in urothelial carcinoma of the renal pelvic mucosa. Since there is no evidence that renal tumors arise de novo as sarcomatoid carcinomas, it is not viewed as a type of its own, but rather as a manifestation of high grade carcinoma of the type from which it arose. Occasionally, the sarcomatoid elements overgrow the antecedent carcinoma to the extent that it cannot be recognized; such tumors are appropriately assigned to renal cell carcinoma, unclassified.

Papillary Adenoma

These tumors are 5 mm or smaller in diameter, of lobular or papillary architecture and of low nuclear grade. These are the most common renal neoplasms, often found incidentally in autopsy studies, particularly in older individuals and in patients on hemodialysis or patients of acquired renal cystic disease. They may be multiple. Microscopically, most tumors are Type I, although rare Type II tumors are also seen. Karyotypic aberrations of loss of Y chromosome or trisomy of chromosome 7 and 17 have been identified.

Renal Oncocytoma

This subtype is thought to arise from the distal nephron and comprises 5 percent of RCC and shows a male to female ratio of 2.5:1. Oncocytoma is a benign renal epithelial neoplasm composed of large cells with mitochondria-rich eosinophilic cytoplasm, thought to arise from intercalated cells (Fig. 9.6). Oncocytomas are well-circumscribed, nonencapsulated neoplasms that are classically mahogany-brown and less often tan to pale yellow. A central, stellate scar may be seen in up to 33 percent of cases but is more commonly seen in larger tumors. Hemorrhage is present in up to 20 percent of cases but grossly visible necrosis is extremely rare. Characteristically, these tumours have solid compact nests, acini, tubules, or microcysts. Often there is a hypocellular hyalinized stroma. The predominant cell type is round to polygonal with densely granular eosinophillic cytoplasm, round and regular nuclei with evenly dispersed chromatin, and a centrally placed nucleolus. A smaller population of cells with scanty granular cytoplasm,

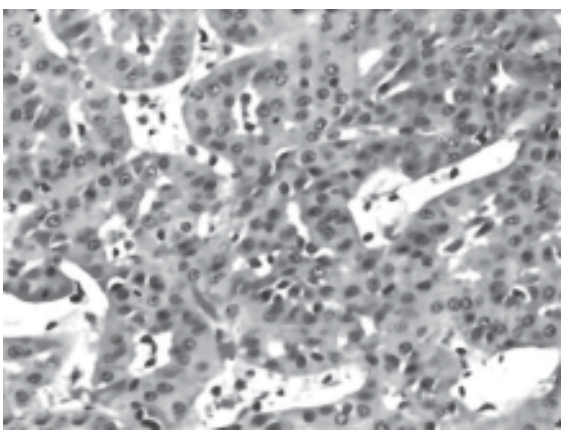

Fig. 9.6: Microscopic appearance of oncocytoma; cells have abundant granular eosinophilic cytoplasm and monomorphic nuclei *(For color version see Plate 9)*

a high nuclear: Cytoplasmic ratio, and dark hyperchromatic nuclei may also be observed.[26] Several cases of Oncocytosis (Oncocytomatosis) have been reported in which the kidneys have contained a large number of oncocytic lesions with a spectrum of morphologic features, including oncocytic tumors, oncocytic change in benign tubules, microcysts lined by oncocytic cells and clusters of oncocytes within the renal interstitium. Ultrastructurally, the cytoplasm is packed with numerous mitochondria. Renal oncocytomas find their origin in the intercalated cells type A of the cortical collecting tubule, which is substantiated by the shared expression of carbonic anhydrase C and band-3 protein.

MOLECULAR/GENETIC FEATURES OF RENAL CELL CARCINOMA

Although classification of renal cell carcinoma is based primarily on histomorphologic criteria, there is molecular genetic evidence that each is an oncogenetically distinct entity. For example, more than 90 percent of clear cell renal carcinomas harbor mutations and/or deletions of the von Hippel-Lindau tumor suppressor gene located on the short arm of chromosome 3. In contrast, the majority of papillary carcinomas have trisomies of chromosomes 7, 16 and 17, and subsets of these tumors have been identified with mutations in the c-met gene. Chromophobe cell carcinomas consistently show abnormalities of chromosomes 1, 2, 6, 10, 13, 17, and 21, whereas some oncocytomas demonstrate a –Y, –1 karyotype and others have translocations involving 11q13.

Clear Cell Renal Cell Carcinoma

The most frequently encountered RCC subtype is characterized by loss of (part of) the short arm of chromosome 3 due to (a) deletion(s) or unbalanced translocation(s). Regions frequently lost are 3p12–14, 3p21–22, and 3p25–26. Loss of at least two of these regions is necessary for kidney cells to develop into common type renal cell carcinoma, and loss of 3p21 is obligatory. Additionally, it was found that allelic losses in adenomas occurred in either 3p25 or 3p12–14, whereas those in carcinomas occurred in 3p21 together with losses in 3p25 or 3p12–14, or both. The most relevant RCC-related gene within 3p25–26 is the Von Hippel Lindau (VHL) gene. The von Hippel–Lindau tumor-suppressor gene was identified in 1993. In Von Hippel–Lindau disease, one VHL allele is inherited with a mutation. Associated focal lesions, such as renal-cell carcinoma, arise from the inactivation or silencing of the remaining normal (wild-type) VHL allele. Defects in the VHL gene also appear to be responsible for about 60 percent of the cases of sporadic clear-cell renal-cell carcinoma, which represents a major portion of all cases of renal-cell carcinoma.

Papillary Renal Adenomas and Carcinomas

Trisomy or tetrasomy 7, trisomy 17 and loss of chromosome Y are the commonest karyotypic changes in PRCC. Most of them are characterized by a unique combination of autosomal trisomies with trisomy 17. Papillary adenomas specifically show a –Y, +7, +17 chromosomal pattern as well as trisomy 3 or gain of the long-arm of chromosome 3, probably reflecting malignant transformation. Trisomy of chromosomes 12, 16, 20 as well as loss of the extra copy of chromosome 17 or loss of 17p are associated with progression from the adenoma into the carcinoma stage, i.e. papillary renal cell

carcinomas. The high incidence of loss of the Y chromosome combined with the strong male preponderance suggests that loss of specific sequences harboured on the Y chromosome probably is important for developing this subtype.

A small subset of papillary RCC is characterized by X;1 autosome translocations. The t(X;1)(p11.2;q21), resulting in a fusion of the transcription factor TFE3 on the X chromosome, with a novel gene, designated PRCC, on chromosome 1, appears to be a specific primary anomaly characterizing a distinct subgroup of papillary RCC with common RCC like features as clear cytoplasm. These tumors occur preferentially in young (male) adults and children.

Renal Oncocytoma

One group is defined by (variant) translocations involving 11q13, and one with specifically defined numerical anomalies, in particular loss of chromosomes 1, and Y/X. The finding of mitochondrial DNA changes and the loss of Y/X in both renal oncocytoma and chromophobe carcinoma might indicate progression from renal oncocytoma to chromophobe renal cell carcinomas through additional chromosome losses, and explaining the occasional malignant behavior of renal oncocytomas.

Chromophobe Renal Carcinomas

Show multiple losses of entire chromosomes, i.e. loss of chromosomes 1, 2, 6, 10, 13, 17, 21, and the Y or X chromosome, leading to a low chromosome number.

Collecting Duct Carcinomas

These tumors do not show consistent chromosomal abnormalities as yet: Probably involvement of the short arm of chromosome 8, loss of the long arm of chromosome 13 as well as loss of part of the long arm of chromosome1q32 are related to poor prognosis. Loss of chromosomal material seems to be a hallmark for all distal nephron tumors.

Sarcomatoid Transformation in RCC

This variant represents the highest form of dedifferentiation and can in principle be derived from all the basic cell types. Cytogenetic data on sarcomatoid RCC is scarce, some tumors show structural abnormalities of chromosomes 1, 5, 16, and 19 and losses of 3p, 4(q), 6q, 8p, 9, 13, 14, 17p, and gain of 5, 12, and 20 as well as TP53 mutations.

NUCLEAR GRADING

Several systems have been proposed over the years for the grading of renal tumors. Of these, one proposed by Fuhrman and colleagues is the most widely used Table 9.2.

Table 9.2: Fuhrman's nuclear Grading system in renal cell carcinoma

Grade	*Nucleus*	*Nuclear size (μ)*	*Nucleoli*
1	Round, uniform	10	Absent/ inconspicuous
2	Slightly irregular	15	evident
3	Very irregular	20	large and prominent
4	Bizarre and multilobated	>20	prominent, chromatin clumped

Pathological Staging

This can be done either by AJCC (2002) method detailed below or by the WHO TNM staging system (2004). The stage designation can be preceded by "pT" to highlight that it is a pathological stage rather than clinical stage.

AJCC Staging

Stage Ia : 4 cm or less, organ confined
Stage Ib : > 4 cm to 7 cm, organ confined

Table 9.3: TNM classification of renal cell carcinoma (WHO)

TNM classification

T – Primary Tumor

TX	Primary tumor cannot be assessed
T0	No evidence of primary tumor
T1	Tumor 7 cm or less in greatest dimension, limited to the kidney
T1a	Tumor 4 cm or less
T1b	Tumor more than 4 cm but not more than 7 cm
T2	Tumor more than 7 cm in greatest dimension, limited to the kidney
T3	Tumor extends into major veins or directly invades adrenal gland or perinephric tissues but not beyond Gerota fascia
T3a	Tumor directly invades adrenal gland or perinephric tissues but not beyond Gerota fascia
T3b	Tumor grossly extends into renal vein(s)b or vena cava or its wall below diaphragm
T3c	Tumor grossly extends into vena cava or its wall above diaphragm
T4	Tumor directly invades beyond Gerota fascia

N – Regional Lymph Nodes

NX	Regional lymph nodes cannot be assessed
N0	No regional lymph node metastasis
N1	Metastasis in a single regional lymph node
N2	Metastasis in more than one regional lymph node

M – Distant Metastasis

MX	Distant metastasis cannot be assessed
M0	No distant metastasis
M1	Distant metastasis

Stage grouping

Stage I	T1	N0	M0
Stage II	T2	N0	M0
Stage III	T3	N0	M0
	T1, T2, T3	N1	M0
Stage IV	T4	N0, N1	M0
	Any T	N2	M0
	Any T	Any N	M1

Stage II : >7 cm, organ confined
Stage IIIa : Spread to perinephric tissue, including renal sinus, but confined within Gerota's fascia
Stage IIIb : Gross tumor in renal vein or its main branches or IVC below diaphragm
Stage IIIc : Gross tumor in IVC above diaphragm
Stage IV : Tumor beyond Gerota's fascia

METANEPHRIC TUMORS

Metanephric adenoma is a highly cellular epithelial tumor composed of small, uniform, embryonic-appearing cells (Fig. 9.7). It occurs in children and adults, most commonly in the fifth and sixth decades. There is a 2:1 female preponderance. Approximately 50 percent of metanephric adenoma are incidental findings with others presenting with polycythemia, abdominal or flank pain, mass, or hematuria. Grossly,size ranges from 30 to 60 mm in diameter. The tumors are typically well-circumscribed but not encapsulated. The cut

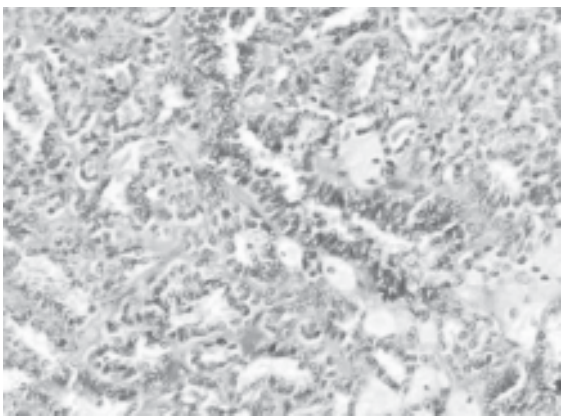

Fig. 9.7: Microscopic appearance of metanephric adenoma showing small embryonic acini *(For color version see Plate 10)*

surfaces vary from grey to tan to yellow and may be soft or firm. Foci of hemorrhage and necrosis are common; calcification is present in approximately 20 percent, and small cysts in 10 percent. Metanephric adenofibromas are typically solitary tan partially cystic masses with indistinct borders. Histology shows that metanephric adenoma is a highly cellular tumor composed of tightly packed small, uniform, round acini with an embryonal appearance. Long branching and angulated tubular structures also are common. The stroma ranges from inconspicuous to a loose edematous stroma. Hyalinized scar and focal osseous metaplasia of the stroma are present in 10-20 percent of tumors. Approximately 50 percent of tumors contain papillary structures, usually consisting of tiny cysts into which protrude blunt papillae reminiscent of immature glomeruli. Psammoma bodies are common and sometimes numerous. Metanephric adenofibroma is a composite tumor in which nodules of epithelium identical to metanephric adenoma are embedded in sheets of moderately cellular fibroblast like spindle cells. Variable amounts of hyalinization and myxoid change are present. Angiodysplasia and glial, cartilaginous, and adipose differentiation occur occasionally. The epithelial component consists of small acini, tubules and papillary structures, as described above in metanephric adenoma. Psammoma bodies are common and may be numerous. Immunohistochemical studies of metanephric adenoma have given variable results. Positive reactions with a variety of antibodies to cytokeratins have been reported, as have positive reactions with antibody to vimentin. Positive intranuclear reactions with antibody to WT-1 are common in metanephric adenoma.

MESENCHYMAL RENAL TUMORS OCCURING IN ADULTS

Although a large number have been described (see classification above), the ones included in the description below are specific for the kidney.

Angiomyolipoma (AML)

These are distinctive tumors composed of variable combinations of abnormal vasculature, smooth muscle and adipose tissue, as the name suggests. AML forms 1 percent of all resected specimens. Most are found within the kidney, but extra-renal sites include liver, lungs, lymph-node and retro-peritoneal tissue. About 80 percent of patients with tuberous sclerosis develop AML; whereas, about one fourth of all AMLs occur in patients of tuberous sclerosis. In non tuberous sclerosis patients, it has a female preponderance (4:1). AML belongs to a family of lesions characterized by proliferation of perivascular epithelioid cells (PEC). The etiology and pathogenesis of the neoplasm are unknown. The different frequency of AML in females and males in the surgical series, the onset of AML after puberty and the frequent progesterone receptor immunoreactivity in AML suggest a hormonal influence. Grossly, AMLs are well-demarcated but not encapsulated (Fig. 9.8). They vary in color from yellow to pinktan, depending on the relative proportions of the various tissue components and may mimic a clear cell RCC or a leiomyoma. Although AMLs may be large, they bulge into rather than infiltrate the perirenal fat. Most AMLs are solitary, but multiple tumors may be present, particularly in association with tuberous sclerosis. Microscopically, most

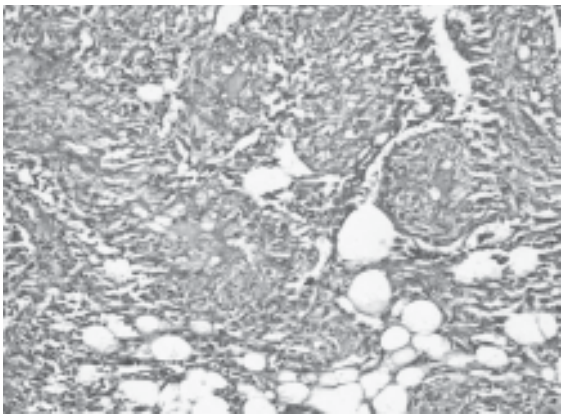

Fig. 9.8: Photomicrograph of angiomyolipoma of kidney, reveals perivascular epithelioid smooth muscle cells along with mature adipocytes *(For color version see Plate 10)*

tumors contain at least focal areas of adipose tissue,either mature or resembling lipoblasts. The smooth muscle cells appear to emanate from blood vessel walls in a radial fashion. The smooth muscle cells are most frequently spindle cells but may appear as rounded epithelioid cells. Rarely, striking degrees of nuclear atypia (occasionally with mitotic activity and multinucleation) may be seen in these cells, raising the possibility of malignancy. Some AMLs that are often located subcapsularly and composed almost entirely of smooth muscle cells (capsulomas) resemble leiomyomas. Cells associated with thin-walled, branching vessels may show a pattern similar to lymphangioleiomyoma. The blood vessels are thick-walled and lack the normal elastic content of arteries, and may mimic a vascular malformation. Prominent cystic change may very rarely be present in AML. Immunoprofile reveals a coexpression of melanocytic markers (HMB45, HMB50, CD63, tyrosinase, Mart1/Melan A and microophthalmia transcription factor) and smooth muscle markers (smooth muscle actin, muscle-specific actin and calponin); CD68, neuron-specific enolase, S-100 protein, estrogen and progesterone receptors, and desmin may also be positive, whereas epithelial markers are always negative. Coexpression of melanocytic and smooth muscle markers in myoid-appearing and lipid-distended cells supports the unitary nature of AML being a neoplasm with ability for phenotypic and immunotypic modulation. Ultrastructural evidence of melanogenesis is reported, and rarely melanin pigment can be abundant.

Epithelioid Angiomyolipoma

This variant of AML is potentially malignant. Tumors are usually large, with infiltrative growth pattern and are composed either exclusively or dominantly of polygonal cells with densely eosinophilic cytoplasm. Variable degrees of nuclear atypia and multinucleated cells are seen. Cells may have a clear cytoplasm. Population of short spindle cells are often present. Hemorrhage and necrosis is more common than in the classic variant. IHC reveals expression of HMB 45, HMB 50, Melan A and variable SMA or muscle specific actin. Allelic loss of chromosomal arm of 16p occurs similar to AML.

Juxtaglomerular Cell Tumor

These are rare tumors, first described by Robertson et al in 1967.The tumor is generally small (2-3 cm), arising in the cortex, solitary and well encapsulated. The histological picture is variable. There are sheets of round to polygonal cells with slightly eosinophilic cytoplasm and distinct cell borders. Glomus like appearance, hemangiopericytomatous areas, ductal and papillary patterns, and areas of spindle cells are seen. PAS stain reveals granular cytoplasm. IHC with anti rennin antibodies is confirmatory and electron microscopy shows distinctive membrane bound rhomboid to polygonal granules.

Renomedullary Interstitial Cell Tumor

Renomedullary interstitial cell tumors are incidental autopsy findings in adult, and are reported to be present in nearly 50 percent of men and women. About half the patients who have one renomedullary interstitial cell tumor have more than one. They are asymptomatic and while renomedullary interstitial cells play a role in regulation of blood pressure, renomedullary interstitial cell tumors have no clear influence on blood pressure. Almost all renomedullary interstitial cell tumors are 1-5 mm in diameter and appear as white or pale grey nodules within a renal medullary pyramid. Microscopically, the renomedullary interstitial cells are small stellate or polygonal cells in a background of loose faintly basophilic stroma reminiscent of renal medullary stroma. At the periphery, renal medullary tubules often are entrapped in the matrix. Interlacing bundles of delicate fibers usually are present. Some renomedullary interstitial cell tumors contain deposits of amyloid.

PEDIATRIC RENAL TUMORS

The major pediatric renal neoplasms with their relative prevalence are:

Nephroblastoma (Wilm's tumor)	85%
Mesoblastic nephroma	3%
Clear cell sarcoma of kidney	3%
Rhabdoid tumor	2%
Miscellaneous	7%
Xp11.2 renal carcinoma	
Papillary renal carcinoma	
Metanephric stromal tumor	
Metanephric adenofibroma	
Renal medullary carcinoma	
PNET	
Renal neuroblastoma	
Angiomyolipoma	
Lymphoma	

Nephroblastoma [Wilm's Tumor (WT)]

The tumor has a peak incidence between 2-5 years and is the most important consideration except during the first 3 months of life.

The WT1 gene, located on chromosome 11p13 is consistently involved in genesis of WAGR (WT associated with aniridia, genital abnormalities and mental retardation) and Denys-Drash syndrome (WT with pseudohermaphrodotism and glomerulopathy). However, WT1 gene is probably normal in 50 percent of sporadic cases of WT. WT2 gene locus maps on chromosome 11p15.

Abnormal substances in the blood or urine of patients of WT include von Willebrand factor, erythropoietin, rennin and neuron specific enolase, which may contribute to coagulopathy, polycythemia and hypertension in these patients. Rarely, they occurs in extrarenal sites. Metastasis is generally restricted to regional lymph nodes, lungs, and liver. Metastatic sites other than these (i.e. bone or brain) are unusual and should suggest alternative diagnoses.

Gross Features

Most tumors are unicentric. However, multicentric masses in a single kidney and bilateral primary lesions can be seen rarely. Wilms tumors are usually solitary rounded masses sharply demarcated from the adjacent renal parenchyma by a peritumoural fibrous pseudocapsule. They are mostly pale grey or tan appearance and of a soft consistency, although they may appear firm and whorled if a large fraction of the lesion is composed of mature stromal elements. Polypoid protrusions of tumor into the pelvicaliceal system may occur resulting in a "botryoid" appearance. Cysts may be prominent. The pathological staging relies on the identification of penetration of the renal capsule,

involvement of renal sinus vessels, positive surgical margins, and positive regional lymph nodes. Bilateral WTs are designated as stage V and their prognosis is determined by the stage of the most advanced tumor and by the presence or absence of anaplasia.

Microscopic Features

Most tumors have a triphasic appearance with variable components of blastemal, stromal and epithelial lineage (Fig. 9.9). Biphasic and monophasic lesions are also often observed. While most of these components represent stages in normal or abnormal nephrogenesis, non renal elements, such as skeletal muscle and cartilage occur (Fig. 9.10). The blastemal cells are small, round or oval with scanty cytoplasm, closely packed, and mitotically active. They have overlapping nuclei containing evenly distributed, slightly coarse chromatin, and small nucleoli. They occur in several distinctive patterns, such as diffuse, nodular, organized, serpentine and basaloid patterns. The diffuse blastemal pattern is characterized by a lack of cellular cohesiveness and an aggressive pattern of invasion into adjacent connective tissues and vessels. An epithelial component of differentiation is present in most nephroblastomas. This pattern may be manifested by primitive rosette-like structures, tubules and papillae. Heterologous epithelial differentiation may occur, the most common elements being mucinous and squamous epithelium. A variety of stromal patterns may occur and may cause diagnostic difficulty when blastemal and epithelial differentiation, are absent. Smooth muscle, skeletal muscle and fibroblastic differentiation may be present. Skeletal muscle is the most common heterologous stromal cell type and large fields of the tumour often contain this pattern. Other types of heterologous stromal differentiation include adipose tissue, cartilage, bone, ganglion cells, and neuroglial tissue. Post-chemotherapy changes include necrosis, xanthomatous histiocytic foci, hemosiderin deposits and fibrosis. There is often maturation of blastoma, epithelial, and stromal components, with striated muscle being the most frequent. Some tumors may show complete necrosis and are considered to be low risk.

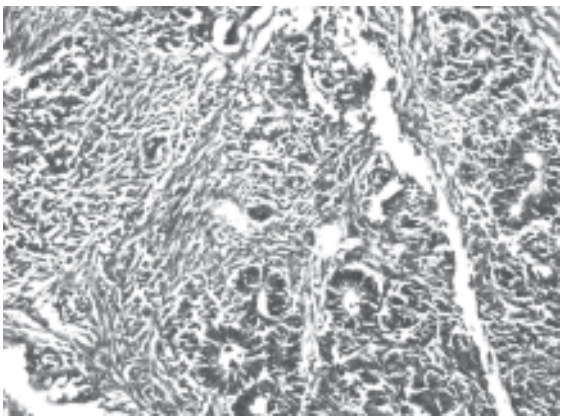

Fig. 9.9: Photomicrograph of nephroblastoma (Wilms tumor), showing a triphasic pattern with blastemal, epithelial and stromal areas *(For color version see Plate 10)*

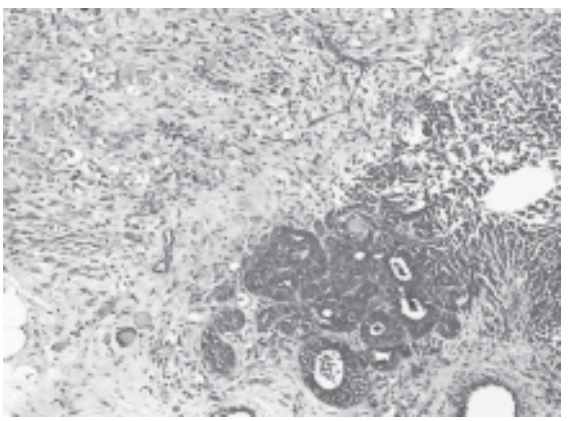

Fig. 9.10: Heterologous skeletal muscle differentiation in Wilms tumor, along with epithelial and blastemal areas *(For color version see Plate 10)*

Anaplasia

Approximately 5 percent of nephroblastomas are associated with an adverse outcome and are recognized pathologically because of their "unfavorable" histology due to the presence of nuclear anaplasia. Histologic diagnosis of anaplasia requires pesence of multipolar polyploid mitotic figures, marked nuclear enlargement and hyperchromasia. Anaplasia is most consistently associated with poor prognosis when it is diffusely distributed and when at advanced stages. For these reasons, pathologic

Distinction have been made between focal anaplasia and diffuse anaplasia. IHC reveals that blastemal cells regularly express vimentin, and may also show focal expression of neuron specific enolase, desmin, and cytokeratin Expression of WT-1 is not present in all nephroblastomas, and may be present in various other tumors. In nephroblastomas, it is confined to the nucleus and correlates with tumor histology: Areas of stromal differentiation and terminal epithelial differentiation show very low levels or no expression of WT-1, whereas areas of blastemal and early epithelial differentiation show high levels of WT-1

Nephrogenic Rests

Nephrogenic rests are abnormally persistent foci of embryonal cells that are capable of developing into nephroblastomas. Nephrogenic rests are encountered in 25 to 40 percent of patients with nephroblastoma, and in 1 percent of infant autopsies. Nephrogenic rests are classified into perilobar (PLNR) and intralobar (ILNR) types. Nephroblastomatosis is defined as the presence of diffuse or multifocal nephrogenic rests. PLNRs are sharply circumscribed and located at the periphery. They may be dormant or may regress. They may also undergo active proliferative overgrowth, resulting in hyperplastic nephrogenic rests, which can be almost impossible to distinguish from nephroblastoma. Rarely, PLNRs may transform into diffuse hyperplastic perilobar nephroblastomatosis. ILNRs are typically located in the central areas of the lobe, are poorly circumscribed and composed of stromal elements as well as epithelial tubules. ILNRs may be dormant, regress, or undergo hyperplasia. Nephroblastmatosis increases the chance of developing into a nephroblastoma.

Cystic Partially Differentiated Nephroblastoma (CPDN)

Rarely, Wilm's tumor may be composed entirely of cysts with delicate septa. Within the septa are small foci of blastoma, immature-appearing stromal cells, and primitive or immature epithelium. Such tumors are called "cystic partially differentiated nephroblastoma" (CPDN). This tumor is a multilocular cystic neoplasm of very young children, composed of epithelial and stromal elements, along with nephoblastomatous tissue. When no nephroblastomatous elements are found, the term "cystic nephroma" has been applied. CPDN is more common in males, and occurs below 2 years of age. Grossly, the tumor is large and multicystic, separated from the remaining kidney by a fibrous pseudocapsule. Microscopically, the cysts are lined with flattened, cuboidal, or hobnail epithelium (Fig. 9.11). The septa contain undifferentiated and differentiated mesenchyme, blastema, and nephroblastomatous epithelial elements. Skeletal muscle, cartilage, fat and myxoid mesenchyme may be present. In the papillonodular variant of CPDN papillae/nodules protrude into the

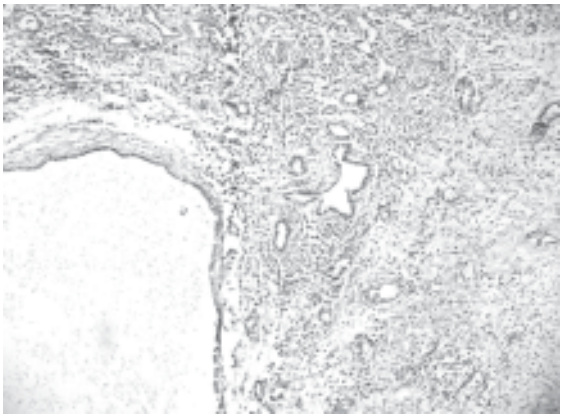

Fig. 9.11: Photomicrograph of cystic partially differentiated nephroblastoma, showing epithelial and blastemal elements within the wall of a cyst *(For color version see Plate 10)*

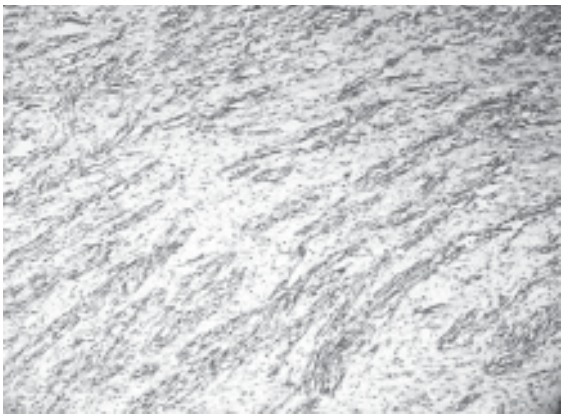

Fig. 9.12: Microscopic appearance of congenital mesoblastic nephroma, shows fibroblastic cells with intervening collagen *(For color version see Plate 10)*

cysts. The epithelial components consist mainly of mature and immature microscopic cysts resembling cross sections of tubules and stubby papillae resembling immature glomeruli. The importance of recognizing CPDN is to know that it is a low grade, potentially malignant tumor when diagnosed and not to miss the diagnosis by inadequate sampling.

Congenital Mesoblastic Nephroma (CMN)

This is the most common congenital renal tumor and occurs in infancy, presenting with an abdominal mass. CMN is a low-grade fibroblastic sarcoma. Gross appearance varies from firm and whorled to soft and cystic. Classic CMN (24% of cases) is morphologically identical to infantile fibromatosis of the renal sinus, composed of interlacing fascicles of fibroblastic cells with collagen deposition, and infiltration into the renal parenchyma (Fig. 9.12). Cellular CMN (66% of cases) has microscopic features akin to infantile fibrosarcoma, These tumors show sheets and poorly formed fascicles with high mitotc activity. Mixed CMN (10% of cases) has features of both classic and cellular CMN within the same tumor. These tumors are immunoreactive for vimentin and actin, and negative for CD34. Cellular CMN but not classic CMN demonstrates a specific chromosome translocation, t(12;15)(p13;q25), which results in a fusion of the ETV6 and NTRK3 genes. Interestingly, the same chromosome translocation and gene fusion present in cellular CMN was first identified in infantile fibrosarcoma, and is not present in infantile fibromatosis Hence, the analogy between cellular CMN and infantile fibrosarcoma, and between classic CMN and infantile fibromatosis, appears appropriate.

Clear Cell Sarcoma of Kidney (CCSK)

Clear cell sarcoma of the kidney (CCSK) is a rare pediatric renal sarcoma with a propensity to metastasize to bone and hence the proposed name "bone metastasizing renal tumor of childhood". It comprises approximately 3 percent of malignant pediatric renal tumors. The mean age at diagnosis is

36 months, with a male to female ratio of 2:1. On gross examination, it is a large tumor, present in the renal medulla, unencapsulated but circumscribed, soft, mucoid, and focally cystic. Microscopically, classic pattern of CCSK consists of nests or cords of cells separated by fibrovascular septa. The cord cells may be epithelioid or spindled, and are loosely separated by extracellular myxoid material that mimics clear cytoplasm. Nuclei are round to oval-shaped, have fine chromatin, and lack prominent nucleoli. The septa may be thin, regularly branching "chicken-wire" capillaries, or thickened sheaths of fibroblastic cells surrounding a central capillary. CCSK can be myxoid or sclerosing. Rarely, the tumor can be anaplastic. Immunoprofile reveals vimentin and BCL2 to be reactive, no reaction with CD34, S100 protein, desmin, MIC2 (CD99), cytokeratin, and epithelial membrane antigen.

Rhabdoid Tumor

Rhabdoid tumor comprises approximately 2 percent of all pediatric renal tumors. It is a highly invasive and malignant neoplasm of young children. The mean age at diagnosis is approximately 1 year, and approximately 80 percent of patients are diagnosed in the first 2 years of life. Grossly, the tumors are typically large, hemorrhagic, necrotic and invasive. Microscopically, it is composed of sheets of cells with vesicular chromatin, prominent red nucleoli, and hyaline intracytoplasmic inclusions. Vascular invasion is usually extensive. A subset of tumors may be composed predominantly of primitive undifferentiated small round cells, but on closer inspection small foci of cells with diagnostic cytologic features can be identified. IHC shows strong vimentin labeling and focal but intense labeling for EMA. Ultrastructurally, the cytoplasmic inclusions reveal whorls of intermediate filaments having a diameter of 8 to 10 nm.

BIBLIOGRAPHY

1. Argani P, Olgac S, Tickoo SK, Goldfischer M, Moch H, Chan DY, et al. Xp11 Translocation Renal Cell Carcinoma in Adults: Expanded Clinical, Pathologic, and Genetic Spectrum. Am J Surg Pathol 2007;31:1149-60.
2. Argani P, Beckwith JB. Renal Neoplasms of Childhood. In Sternberg's Diagnostic Surgical Pathology. Carter D, Greenson JK, Oberman HA, Reuter V, Stoler MH, (Eds). Philadelphia. Lippincott Williams and Wilkins 2004,2001-33.
3. Cohen HT, McGovern FJ. Renal Cell Carcinoma. N Engl J Med 2005;353:2477-90.
4. Eble JN, Sauter G, Epstein JI, Sesterhenn IA, editors. World Health Organization Classification of Tumors. Pathology and Genetics of Tumors of the Urinary System and Male Genital Organs. Lyon: IARC Press; 2004.
5. Iliopoulos O, Eng C. Genetic and clinical aspects of familial renal neoplasms. Semin Oncol 2000; 27:138-49.
6. Kim WY, Kaelin WG. Role of VHL gene mutation in human cancer. J Clin Oncol 2004; 22:4991-5004.
7. Murphy WM, Beckwith JB, Farrow GM. Tumors of the kidney bladder, and related urinary structures. Atlas of tumor pathology, AFIP 1994; 3rd series, fascicle 11.
8. Reuter VE, Tickoo SK. Adult renal tumors. In: In Sternberg's Diagnostic Surgical Pathology 4th edition. Carter D, Greenson JK, Oberman HA, Reuter V, Stoler MH, editors. Philadelphia. Lippincott Williams and Wilkins 2004. 1955-99.
9. Suzigan S, Lopez-Beltran A, Montironi R, Drut R, Romero A, Hayashi T, et al. Multilocular cystic renal cell carcinoma: A report of 45 cases of a kidney tumor of low malignant potential. Am J Clin Pathol 2006;125:1-6.
10. Wang KL, Weinrach DM, Luan C, Han M, Lin F, Teh BT, et al. Renal papillary adenoma: A putative precursor of papillary renal cell carcinoma. Hum Pathol 2007;38:239-46.

Chapter

10 Pathology of Gynecological Malignancies

Radhika Srinivasan

INTRODUCTION

The female genital tract consists of the uterus and cervix, vagina, vulva, bilateral fallopian tubes and ovaries. Among the malignancies affecting the female genital tract, cancer of the uterine cervix is the most frequent malignancy in our country with an age-adjusted incidence of 20-25 per 100,000 women. This is followed by a nearly equal incidence of cancer of the ovary and of the uterus (endometrium). Cancer of the vulva is less common and cancers of the fallopian tube and of the vagina per se are rare.

In general, carcinoma is the most common type of cancer to affect all these organs. Sarcomas are less frequent but do occur in the uterus, cervix, vagina and vulva. Rarely other malignancies such as primary lymphoma and melanomas also are known to involve the genital tract. Germ cell neoplasms and sex cord stromal tumors uniquely affect the ovary and are second to carcinomas in their frequency of occurrence.

Below is an overview of the major neoplasms of the ovary, fallopian tube, uterus, cervix and vulva.

NEOPLASMS OF THE OVARY

General comments: Ovarian carcinoma accounts for the greatest number of deaths from malignancies of the female genital tract. In the West, it is the 5th leading cause of cancer associated mortality. Generally, it occurs in older women (5th/6th decade). In India, the peak is seen almost a decade earlier. Familial ovarian cancer is due to mutations in BRCA1 or BRCA2 gene. Other syndromes such as Lynch type II syndrome are also associated with familial ovarian cancer. Ovarian cancer spreads commonly to the contralateral ovary, peritoneal cavity and the para-aortic and pelvic lymph nodes and the liver. With intra-abdominal spread, ascites develops commonly. Omental and peritoneal deposits also occur. An umbilical metastasis may be the first manifestation of the disease. Lung, pleura and distant metastases also occur. The spread of borderline tumors is mainly in the form of peritoneal implants, which may be invasive or non-invasive; spread to lymph nodes and other organs are also known.

Tumors of the ovary are classified based primarily on the tissue/cell of origin. Thus, we have tumors derived from the:

i. Ovarian surface epithelium, further divided into benign, borderline and malignant.
   a. Serous
   b. Mucinous
   c. Endometrioid

d. Mixed
e. Malignant mixed Müllerian tumor (MMMT)

ii. Germ cells
a. Dysgerminoma
b. Teratoma
c. Endodermal sinus tumor
d. Mixed germ cell tumors

iii. Sex cord
a. Granulosa cell tumor
b. Fibroma-thecoma
c. Sertoli Leydig cell tumor
d. Others

iv. Germ cell-sex cord-stromal tumors

v. Metastatic tumors

Ovarian Surface Epithelial Tumors

These neoplasms constitute the most common ovarian tumors and may be further classified based on the specific cell types as serous, mucinous, endometrioid, mixed and unclassified (Table 10.1).

Table 10.1: Immunohistochemical phenotype of ovarian neoplasms

Tumor type	*Immunophenotype*
Surface epithelial tumors	
• Serous tumors	CA125, CK7+/CK20-
• Mucinous tumors	CK7+, CK20+ in 50%
• Endometrioid tumors	CK7+, CK20-
Germ cell tumors	
• Dysgerminoma	PLAP, CD117, OCT4
• Carcinoid tumor	NSE, Chromogranin and other secretory products
Sex cord stromal tumors	Inhibin alpha, Calretinin, Melan-A, CD99
Endometrial stromal sarcoma	CD10 +, Caldesmon –ve

Serous Tumors

Serous tumors make up about 1/4th of all ovarian tumors and mostly occur in adults. Approximately 30 to 50 percent are bilateral (Figs 10.1A and B).

Gross appearance: Grossly, these tumors have a solid as well as cystic component. The cystic areas are filled with serous fluid and usually have papillary excrescences. Careful inspection of the outer surface is required as sometimes there may be papillary excrescences on outer surface. Benign serous tumors may be uniloculated or multiloculated with thin septae and smooth inner and outer surface. Papillary excrescences may be seen, but usually are focal and small in size. Borderline tumors usually area also cystic but tend to have larger areas (> 10%) covered by papillary excrescences. Malignant tumors are characterized by solid tumors with variable cystic component. The solid areas are usually friable with papillations and show variable degrees of necrosis and hemorrhage.

Microscopy: The cell type of serous tumors resembles the normal tubal epithelium and is cuboidal to low columnar epithelium lining the cysts and papillae. In about 1/3rd cases, psammoma bodies (calcific concretions with concentric lamination) are seen. A morphological spectrum of proliferation exists in these tumors. At one end of the spectrum is the benign serous cystadenoma, in which the cyst and papillae are lined by a single layer of cells without any complexity in the architecture or invasion. At the other end is the papillary serous cystadenocarcinoma characterized by nuclear atypia, invasion and architectural complexity. In between are the tumors designated borderline tumors which

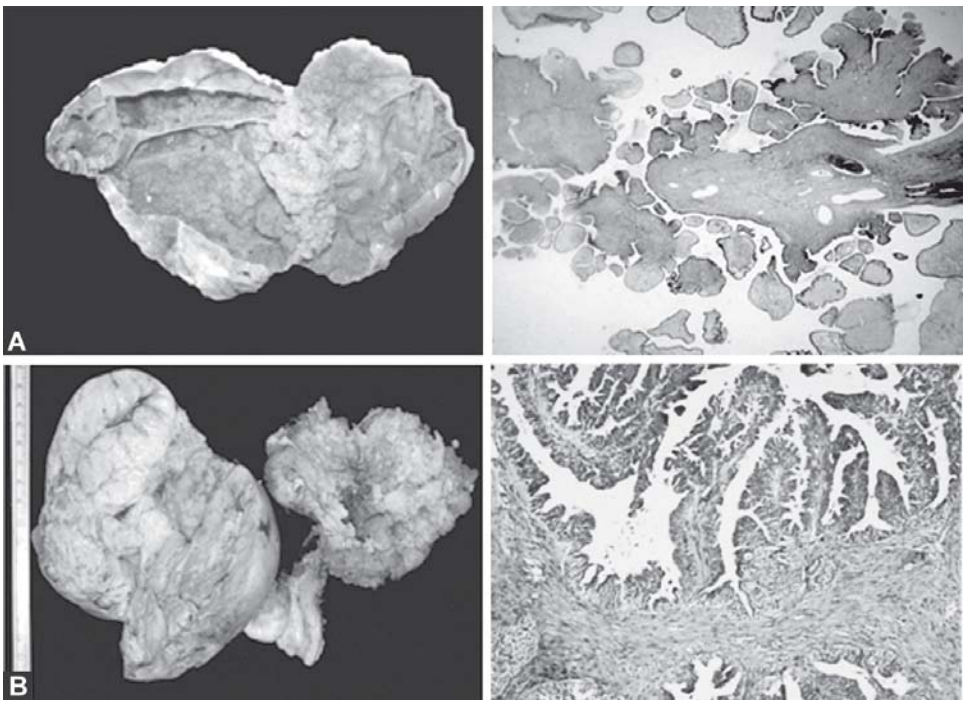

Figs 10.1A and B: (A) Borderline serous tumor: gross and microscopy. Grossly, a large cystic tumor, uniloculated with multiple papillary excrescences are seen. Microscopically, the hierchical papillae are lined by serous epithelial cells showing mild atypia. There is no stromal invasion. **(B)** Papillary serous carcinoma of the ovary: Gross and microscopy. Grossly, a predominantly solid tumor with friable areas and areas of necrosis and hemorrhage *(For color version see Plate 11)*

show proliferation and nuclear atypia but lack the stromal invasion. Tumors which show minimal areas of invasion are placed in the 'microinvasive carcinoma' category. Serous tumors with a significantly fibrous stroma are referred to as cystadenofibroma. These tumors also have benign, borderline and malignant categories as described above.

Mucinous Tumors

Mucinous neoplasms are less common than serous neoplasms and are bilateral in only 10-12 percent cases. As in serous tumors, mucinous cystadenoma, borderline mucinous tumors and mucinous cystadenocarcinomas are recognized (Figs 10.2A and B).

Gross appearance: Mucinous neoplasms usually present as multiloculated cystic tumors. The cysts contain thick viscous mucin. Malignant tumors have larger solid areas and typically areas consisting of smaller cystic spaces filled with mucinous material.

Microscopy: The lining epithelium is tall, columnar and resembles the mucinous lining of the endocervix or the intestine. Benign tumors are lined by a single layer of cells. Papillae and villiform projections into the cystic spaces are also present. The cystic

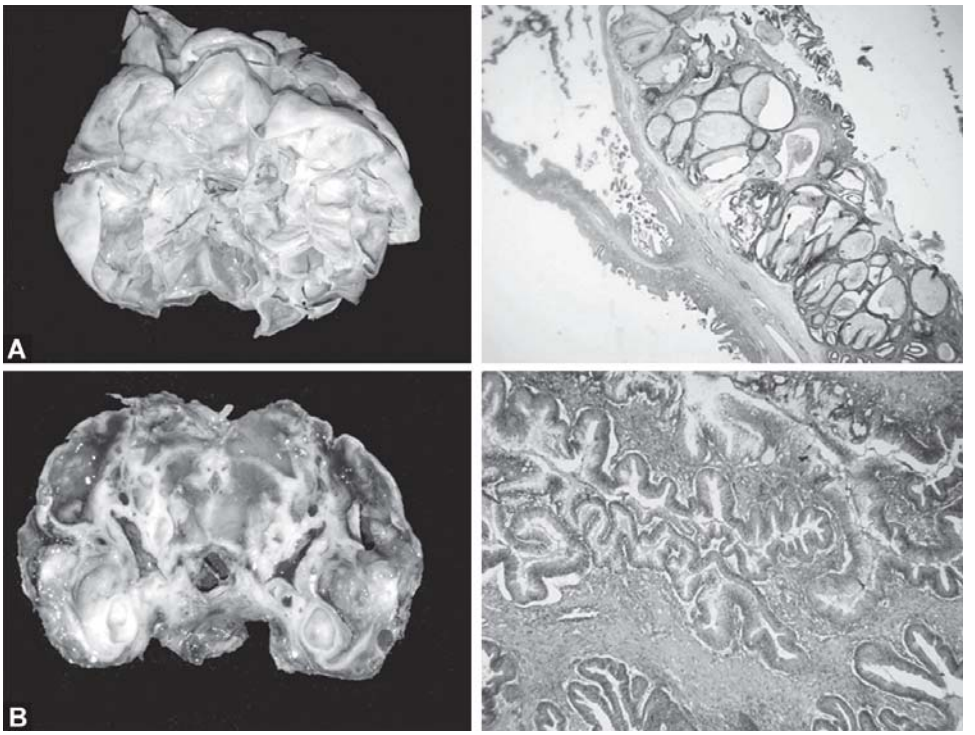

Figs 10.2A and B: (A) Borderline mucinous tumor: Gross and microscopy. Grossly, a multicystic tumor, the cysts filled with gelatinous mucoid material and microscopically complexity of architecture and mild cytological atypia are seen **(B)** Mucinous carcinoma: Gross and microscopy. Grossly, multicystic tumor with thick septae, the cystic spaces filled with mucoid material along with areas of hemorrhage and necrosis. Microscopically, frank stromal invasion is present *(For color version see Plate 11)*

spaces show mucinous material. Foci of inflammatory reaction to the mucin may also be seen. Borderline tumors show greater degree of cellular proliferation and complexity of architecture. Stromal invasion should however be absent for a diagnosis of this type of neoplasms. Tumors with intraepithelial carcinoma and with stromal microinvasion are also recognized. In mucinous cystadenocarcinomas, frank stromal invasion, architectural complexity and nuclear atypia are evident. Mucin may leak into the adjacent ovarian stroma giving rise to an inflammatory reaction comprising of neutrophils, lymphocytes and even giant cells. Mucinous tumors may be associated with a condition called '*pseudomyxoma peritonei*', wherein the peritoneal cavity is filled with thick, gelatinous mucoid material resulting in adhesions between the organs. Careful microscopic evaluation of this material is required to distinguish the relatively benign *peritoneal adenomucinosis* (lacking or with a few strips of benign appearing mucinous epithelium) from the frankly malignant mucinous carcinomatosis.

The subgroup of mucinous tumors with a prominent stromal component is designated as mucinous adenofibroma/mucinous cystadenofibroma and mucinous adenocarcinofibroma, if malignant.

Exceptionally, mucinous adenocarcinomas may contain mural nodules with sarcoma-like nodules comprising of numerous giant cells, true sarcoma or anaplastic carcinoma.

Borderline mucinous tumors are known to have an association with long standing endometriosis.

Endometrioid Tumors

Endometrioid carcinoma comprises 10-25% of all primary ovarian carcinomas. Coexistent endometriosis may be demonstrated in 10-20% cases.

Gross appearance: These neoplasms may be solid or cystic. The contents tend to be hemorrhagic. Visible papillae are absent.

Microscopy: These tumors resemble the usual endometrial adenocarcinoma with glandular spaces lined by tall columnar epithelium with eccentric nuclei. Squamous metaplasia is usually present.

Benign and borderline endometrioid tumors are recognized. These tumors generally have a prominent stromal component (Figs 10.3A to C).

Synchronous endometrioid tumors of the uterus may be present and their frequency varies from 15 to 30 percent.

Clear Cell Adenocarcinoma of the Ovary

Clear cell adenocarcinoma of the ovary shows a spongy, cystic tumor with variable hemorrhage and necrosis. Microscopically, tubular-cystic, papillary and solid patterns of growth may be seen. The cores of the papillae often exhibit prominent hyalinization. The tumors cells are large, pleomorphic and have prominent nucleoli. Some of the nuclei protrude into the lumina resulting in a 'hobnail' configuration. The cytoplasm is clear and may exhibit PAS positive diastase-resistant hyaline globules.

A high association of clear cell carcinomas with pelvic endometriosis is seen and sometimes these tumors are seen to arise directly from endometriotic cysts. These patients are in their 5-6th decades and have a poor prognosis.

Brenner's Tumor

Brenner's tumor constitutes between 1 and 2 percent of all ovarian neoplasms. These tumors are usually unilateral, solid tumors and appear whitish or yellow white.

Microscopy: They consist of solid and cystic epithelial nests of epithelial cells resembling transitional epithelium or urothelium surrounded by an abundant stroma which is fibroblastic. There is a great resemblance to the 'Walthard' cell nests which are common in the mesosalpinx. The cytoplasm is clear and nuclei may show grooves. Cystic areas and mucinous metaplasia may be present. If papillary fronds and nuclear atypia are present, in addition to typical benign areas, then such tumors are referred to as *Proliferating Brenner's tumor***.** Marked nuclear atypia signals malignancy. When both benign and malignant areas are recognized in a Brenner's tumor, it is designated as *malignant Brenner's tumor***.** Tumors without a recognizable benign morphological component are designated as *transitional cell carcinomas*.

Malignant Mixed Müllerian Tumor (MMMT)

This tumor resembles its uterine counterpart. *MMMT homologous variety* is also called carcinosarcoma. The carcinomatous component may appear serous, endometrioid, squamous or clear cell type. The heterologous variety shows diverse sarcomas such as

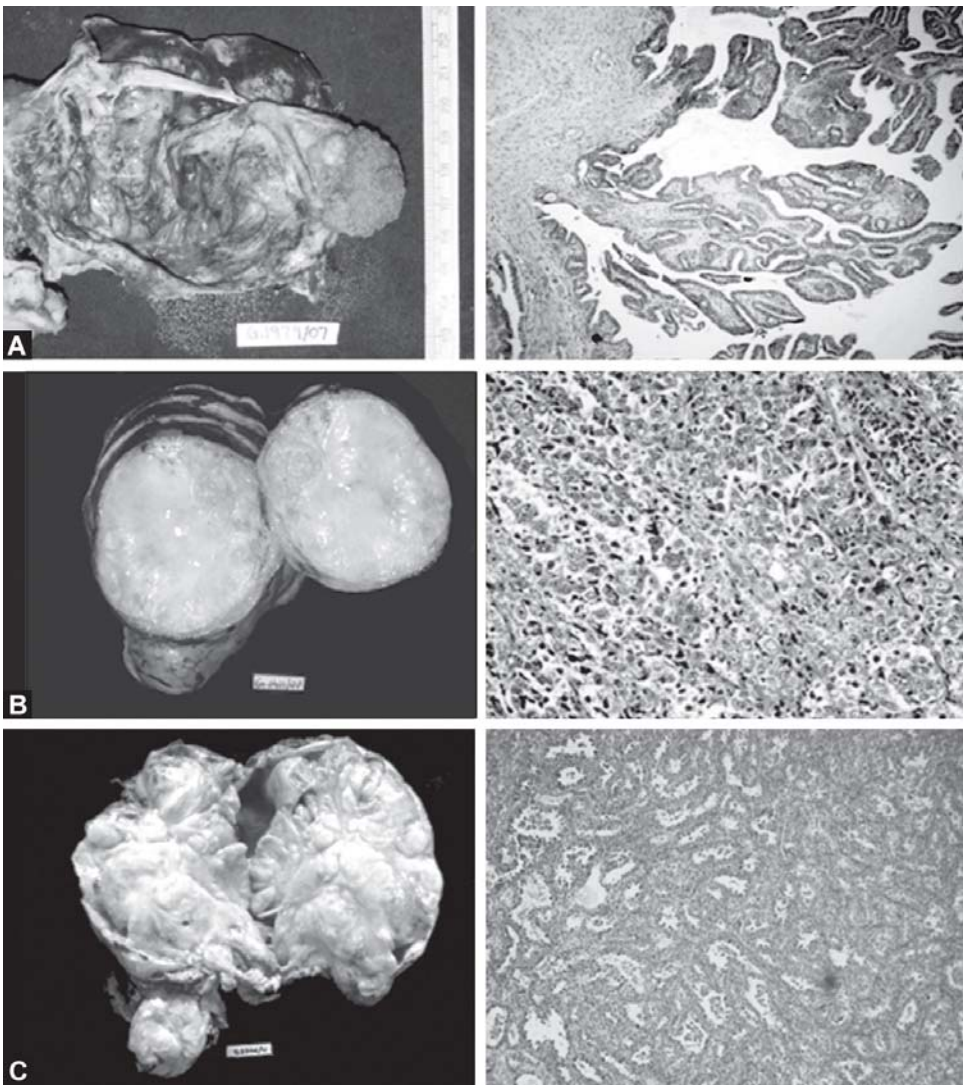

Figs 10.3A to C: (A) Endometrioid carcinoma of the ovary arising in an endometriotic cyst. Note the thick walled cyst with a solid area showing papillary excrescences. Microscopy shows papillae and glands lined by tall columnar endometrioid type of epithelium. **(B)** Endometriod carcinoma of ovary showing a solid tumor with areas of necrosis. Microscopically, a moderately differentiated tumor is noted **(C)** Clear cell carcinoma of ovary, Gross and Microscopy. Glands lined be cells with aclear cytoplasm and pleomorphic nuclei are seen *(For color version see Plate 12)*

chondrosarcoma, osteosarcoma, rhabdomyosarcoma or angiosarcoma. The prognosis of this tumor is extremely poor.

Germ Cell Tumors

Germ cell tumors constitute approximately 20 percent of all ovarian neoplasms and occur predominantly in children and young adults. Approximately 95 percent of these are mature cystic teratomas, whereas the rest are malignant.

Dysgerminoma

Dysgerminoma constitutes approximately 5 percent of all malignant ovarian tumors and

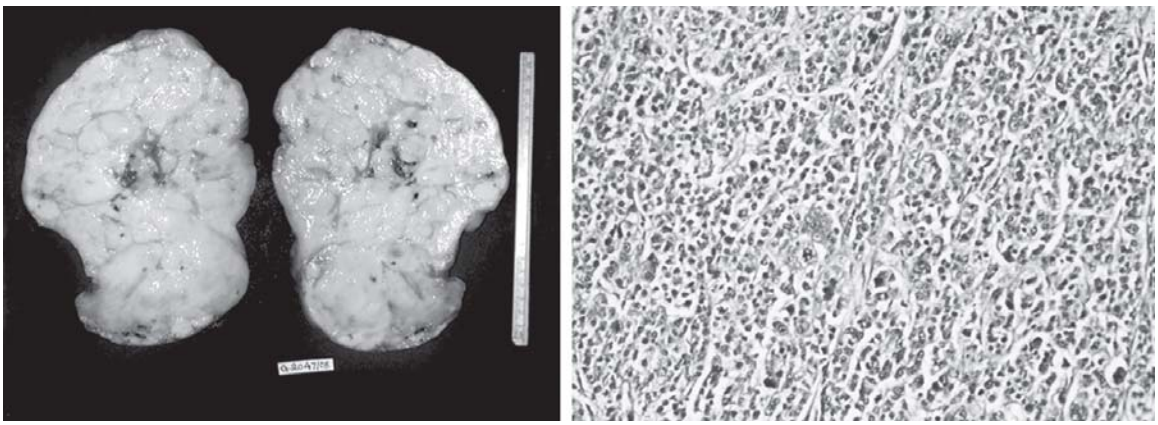

Fig. 10.4: Dysgerminoma: Grossly, a solid, fleshy tumor is seen. Microscopically, nodules of tumor cells separated by fibrous septae showing lymphocytic infiltration *(For color version see Plate 12)*

5 to 6 percent of all malignant tumors in children; approximately 5 percent occur in dysgenetic gonads. It is bilateral in 15 percent cases. Dysgerminomas are also the most common component of mixed germ cell neoplasms. Metastasis occurs to the contralateral ovary, lymph nodes and to the peritoneal cavity (Fig. 10.4).

Gross appearance: Dysgerminoma is usually a large tumor, encapsulated with a smooth outer surface. The cut surface is solid, gray white with foci of hemorrhage and necrosis.

Microscopy: The tumor cells are arranged in well defined nests separated by thin fibrous septae infiltrated with lymphocytes. A granulomatous reaction is not uncommon. The tumor cells are uniform with large nuclei and characteristically have one or more prominent nucleoli and abundant clear to finely granular cytoplasm containing glycogen. Dysgerminoma (in about 3% cases) may show scattered hCG positive syncytiotrophoblastic cells, which may be accompanied by elevated serum hCG levels. Sometimes, there is marked anaplasia when they are designated *anaplastic dysgerminomas.*

Yolk Sac Tumor (Endodermal Sinus Tumor)

Yolk sac tumor (endodermal sinus tumor) is a neoplasm of children and young adults.

Grossly, the tumors are large and on cut surface, have a variegated appearance with areas of necrosis, hemorrhage and cystic change.

Microscopically, the appearance is variable. A variety of patterns are recognized such as microcystic pattern, polyvesicular vitelline pattern and hepatoid pattern. Schiller-Duval bodies are a characteristic feature of this tumor. Intracytoplasmic hyaline globules, which are PAS positive and diastase resistant and are immune-reactive for alphafetoprotein are also noted. The serum AFP is a good tumor marker for this entity.

Embryonal carcinoma is less common in the ovary as compared to the testis. It is usually a component of mixed germ cell neoplasms.

Primary ovarian choriocarcinoma is an exceedingly rare tumor and is morphologically similar to their uterine counterpart.

Immature Teratoma

This is a malignant tumor composed of a mixture of adult and embryonal tissues derived from all the three germ cell layers.

Grossly, immature teratoma is composed of sold and cystic areas.

Microscopically, the main component is primitive neuroepithelium. Primitive mesodermal element is also common. Endodermal derivatives resembling the intestine, liver, etc may be seen in variable amounts. Immature teratomas are graded (described by Norris et al) as:

Grade I: Abundance of mature tissues intermixed with loose mesenchymal tissue with occasional immature focus.

Grade II: Fewer mature tissue; rare foci of neuroepithelium with mitoses but not exceeding three low magnification fields.

Grade III: Few or no mature tissue; numerous neuroepithelial elements occupying four or more low magnification fields.

Thorough microscopic examination is required for proper grading. Further, immature teratomas may also be part of mixed germ cell neoplasms.

Mature Cystic Teratoma

These tumors are the most common ovarian benign neoplasm. Typically, they are cystic containing cheesy sebaceous and keratinous material and grossly evident hair. There is a solid nipple like area referred to as the 'Rokitansky's protuberance, where teeth may be seen. It is important to take sections from this area as a variety of tissues are represented in this area. Variable amounts of fat, cartilage and bone may be identified grossly.

Microscopically, these tumors are characterized by tissues from all the three germ cell layers, which are mature. Thus, skin with pilosebaceous units, adnexae, neuroglial tissue derived from the ectoderm are very common followed by the respiratory epithelium with adjoining cartilage and intestinal tissue representing the endoderm derived tissues. Bone, fat, cartilage representing mesoderm derived tissue may all be present in variable amounts.

Rarely, malignancy can arise in a preexisting mature cystic teratoma in about 2 percent cases. The most common malignancy is squamous cell carcinoma followed by carcinoid tumor and adenocarcinoma.

Carcinoid Tumor and Strumal Carcinoid

Carcinoid tumors of the ovary are uncommon and may represent metastases from elsewhere, part of a teratoma or as a primary neoplasm. Approximately one-third are associated with the carcinoid syndrome. Primary carcinoid carry a good prognosis.

Grossly, they have a smooth outer surface and their cut surface is solid, tan to yellow and homogeneous.

Microscopically, the morphology is similar to carcinoids elsewhere with an insular, trabecular or solid growth patterns. The tumor cells are uniform with fine chromatin. Strumal carcinoid is a tumor that combines features of a carcinoid tumor with struma ovarii.

Sex Cord Stromal Tumors

These constitute approximately 5% of all ovarian neoplasms. The major tumors in this category are (Figs 10.5A to C).

Granulosa Cell Tumor

Adult granulosa cell tumor is usually detected in the child bearing age and 3/4th of them are associated with hyperestrinism. The excessive estrogens may lead to a clinical presentation of precocious puberty in children, metrorrhagia in adults and in postmenopausal women. Some tumors are hormonally inactive, whereas the others may be androgenic.

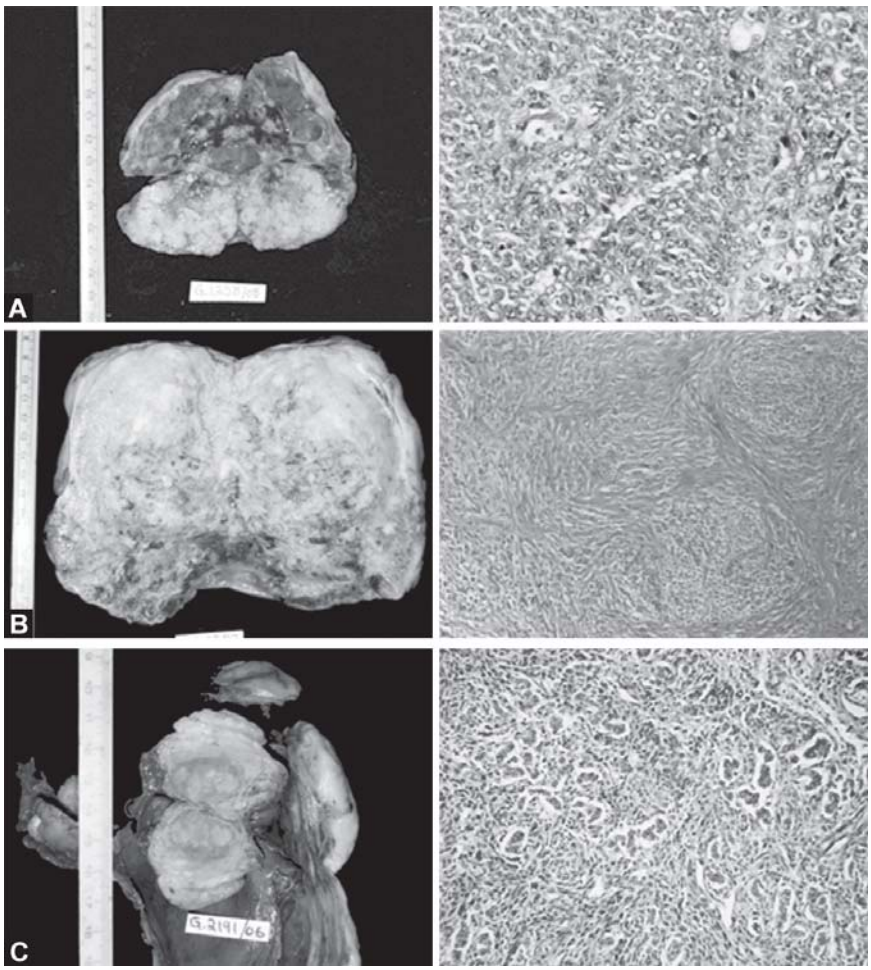

Figs 10.5A to C: Sex cord stromal tumors of the ovary: **(A)** Granulosa cell tumor. Grossly, a solid tumor with areas of hemorrhage and necrosis. Microscopically, diffuse sheets of cell with oval, elongated nuclei which show grooving. **(B)** Fibroma. Grossly, a solid firm tumor and microscopically, spindle cell tumor with collagenization. **(C)** Sertoli-Leydig cell tumor with a characteristic yellow appearance grossly. Microscopically, Sertoli cells forming abortive tubules and Leydig cells with abundant eosinophilic cytoplasm is seen *(For color version see Plate 13)*

Grossly, these tumors are encapsulated with a smooth-lobulated outline and a predominantly sold cut surface. The color may be gray or yellow, if leutinized. Cystic change may be present.

Microscopically, there is a variety of growth patterns such as microfollicular, macrofollicular, trabecular, insular, watered-silk, solid and diffuse (sarcomatoid). Numerous typical 'Call-Exner' bodies may be seen. The nuclei typically show grooves resulting in a 'coffee bean' appearance. Serum inhibin is a useful tumor marker.

Juvenile Granulosa Cell Tumor (JGCT)

JGCT is tumor that presents in 80 percent of cases in the first two decades of life. Most patients present with isosexual precocity.

There is a diffuse or macrofollicular growth pattern with pools of intrafollicular secretion, large tumor cells showing nuclear atypia and a variable but often high mitotic activity. The tumor cells are luteinized.

Thecoma, Fibroma and Other Tumors

These tumors often have an overlapping morphology and are sometime referred to as fibrothecomas.

Thecomas present after menopause, are usually unilateral and varies in size. It has a well-defined capsule and is a solid tumor. The cut surface is solid with a few cysts, and is yellow in color. Microscopically, it is composed of fascicles of spindle cells with moderate amount of cytoplasm. The intervening tissue shows collagen and hyaline plaque formation. Thecoma cells contain abundant intracytoplasmic fat.

Fibromas are common ovarian tumors, usually unilateral and occur after puberty. Grossly, fibromas are solid white tumors. Microscopically, they are composed of closely packed spindle cells with intervening hyalinization and collagenization. Cellularity is variable.

Sertoli-Leydig Cell Tumor

As the name suggests, these tumors are composed of a mixture of cells resembling the male Sertoli-Leydig cells. They are uncommon tumors constituting < 0.1% of ovarian neoplasms. They are seen in young patients and rare after menopause. Nearly 50% show signs of androgen excess. This is manifested as defeminization with amenorrhea and breast atrophy and later by masculinization (voice deepening, clitoral hypertrophy). Some tumors may not have demonstrable endocrine effect, whereas others may secrete estrogen and progesterone.

Grossly, they are solid tumors with a variable cystic component.

Microscopically, they may be well differentiated, intermediate or poorly differentiated (sarcomatoid) or pure Sertoli cell tumors. Heterologous elements such as liver, skeletal muscle, cartilage, etc may be identified. A retiform variant is also identified.

The prognosis of this tumor is usually good and correlates with the stage and the degree of differentiation.

Metastatic Tumors

The ovary is a common site for metastatic tumors. Over half of metastases are bilateral. The most common primary sites are the breast, uterus, stomach, colon, and gallbladder (in India). The eponym Krukenberg tumor is used to designate an ovarian neoplasm, usually bilateral, characterized by multinodular enlargement of the ovaries and microscopically by a diffuse infiltration by signet ring cells containing abundant neutral and acidic mucins in a cellular fibroblastic stroma. Lymphatic tumor emboli are often seen.

CARCINOMA OF THE FALLOPIAN TUBE

Primary fallopian tube carcinoma is rare accounting for 1% of primary genital tract malignancies. Most patients are postmenopausal. Nulliparity is common. Recent studies have shown a strong association of this cancer with carriers of *BRCA1* and *BRCA2* mutation. In developed countries, prophylactic salpingo-oophorectomy is carried out in such women (Fig. 10.6).

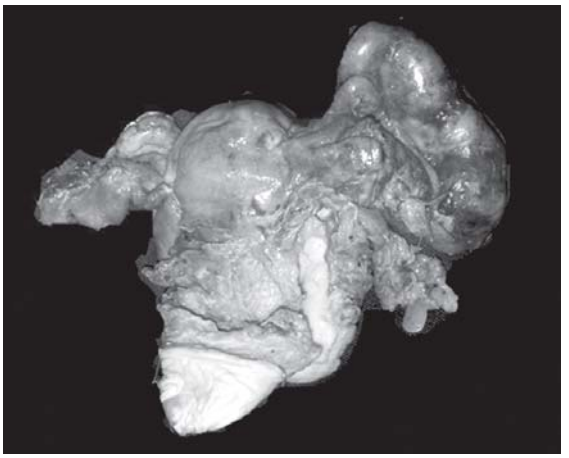

Fig. 10.6: Fallopian tubal carcinoma showing nodular expansion of the left tube by the tumor *(For color version see Plate 13)*

Gross appearance: The tube is enlarged and has fibrous adhesions. The fimbriated end of the tube may be open or closed; a fact of prognostic significance. The cut surface shows a solid or papillary tumor filling and expanding the tubal lumen.

Microscopically, all major types of carcinomas known to occur in the ovary are seen in the tube as well. The most common type is the papillary serous type. Other types include endometrioid, clear cell, sero-mucinous, and transitional carcinomas.

The prognosis depends on the stage of the tumor (77% for stage I tumors vs 20% for stage III).

MALIGNANT TUMORS OF THE UTERUS

These include tumors of the endometrium and of the myometrium. Endometrial cancers include endometrial carcinoma, endometrial stromal sarcoma and malignant mixed Müllerian tumors (MMMT). Leiomyosarcoma arises from the smooth muscle of the myometrium.

Endometrial carcinoma is the most common gynecological malignancy in developed countries. It typically occurs in elderly postmenopausal women. Based on the pathogenesis, two distinct types are noted: *Type I*, which occurs in a background of excess estrogenic stimulation and develops against a background of endometrial hyperplasia; and *Type II*, which occurs de novo. Obesity, hypertension, diabetes and nulliparity are risk factors for type I carcinomas. Other predisposing conditions include polycystic ovarian disease (PCOD), dysfunctional uterine bleeding (DUB), long standing estrogen users, tamoxifen usage and those with functioning granulosa cell tumors.

Type I: Endometrioid Adenocarcinoma

Gross appearance: These tumors may be seen as a polypoidal, predominantly exophytic growth arising from the uterine cavity or as diffusely infiltrating tumors.

Microscopically, they are like the usual adenocarcinomas and are divided into grade I-III tumors based on their degree of differentiation. The most important aspect in the evaluation of a uterine neoplasm especially endometrial adenocarcinoma is the depth of myoinvasion. The second aspect is to evaluate the vertical extent of involvement and to evaluate the involvement of the cervix. These pathological features are important in FIGO staging, which is a surgicopathological staging. Squamous metaplasia is often noted. Other types of metaplasias are also associated with endometrial adenocarcinoma.

Type II: Carcinoma

This category includes *serous carcinoma* and *clear cell carcinoma*. In contrast to type I carcinoma, these tumors are highly

aggressive and occur in older women. Serous carcinoma represents a highly aggressive tumor characterized by a complex papillary growth pattern. The lining cells show moderate to severe pleomorphism and atypia with mitotic figures and sometimes psammoma bodies. Usually deep myoinvasion is present. However, it may remain confined to a polyp or remains intramucosal.

Clear cell carcinoma is composed of large clear cells with distinct cellular margins and abundant cytoplasm containing abundant glycogen. Papillary and glandular differentiation is present. Hobnailing of tumor cells may be seen. Hyaline bodies are also seen.

Endometrial Stromal Tumors

These tumors occur in the 5th decade of life and present clinically with vaginal bleeding (Fig. 10.7).

Gross appearance: They may present as sharply circumscribed nodule with no permeation of the surrounding tissue, when they are designated *Endometrial stromal nodule. Low grade endometrial stromal sarcomas* (ESS) show diffuse permeation of the myometrium and show small nodules on the cut surface. Permeation into the veins and lymphatics may be identified grossly as yellowish, ropy ball-like masses filling dilated channels. ESS can also present as solitary polypoid masses.

Microscopy: These tumors are composed of small ovoid cells resembling the endometrial stromal cells. They are individually enveloped by reticulin fibers. The tumors show numerous finely dispersed small vessels resembling the endometrial spiral arterioles; the tumor cells typically encircle these blood vessels. Low grade ESS usually has a low mitotic activity. Some tumors may show differentiation towards both smooth muscle and endometrial stromal cells. If each component is around 30 percent, then the tumor is designated *a combined smooth muscle-stromal tumor* (Fig. 10.8).

In contrast to low grade ESS, *high grade ESS* show necrosis, high mitotic activity and obvious nuclear atypia and are aggressive neoplasms.

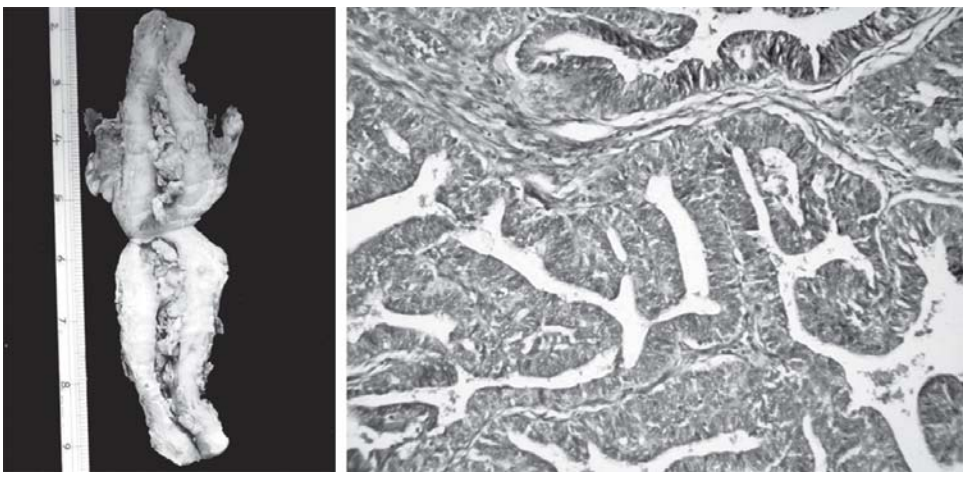

Figs 10.7: Carcinoma endometrium: Grosssly, there is a friable tumor seen filling the uterine cavity with superficial myoinvasion. Microscopy shows a typical endometrioid carcinoma *(For color version see Plate 14)*

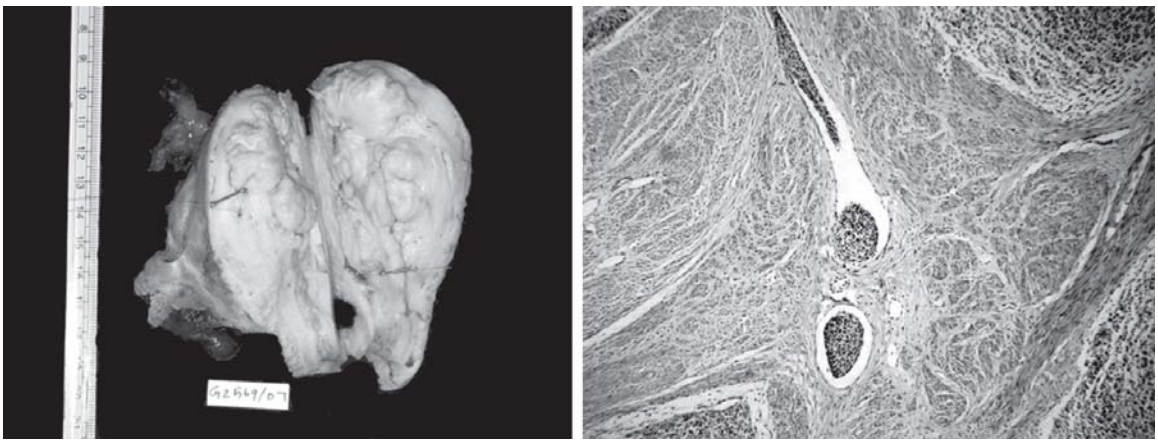

Fig. 10.8: Endometrial stromal sarcoma, low grade: Grossly, there is an infiltrative tumor in the endomyometrium. Microscopically, infiltrating nests of tumor cells are seen in the lymphatics of the myometrium, a characteristic feature of this tumor *(For color version see Plate 14)*

MMMT Carcinosarcoma

MMMT are always seen in postmenopausal women. They present with uterine bleeding and enlargement.

Grossly, they present as soft, polypoidal masses filling the cavity with areas of hemorrhage and necrosis.

Microscopically, the characteristic feature of an MMMT is an admixture of carcinoma and sarcoma-like elements. The carcinoma resembles endometrioid, clear cell or papillary serous types. The sarcomatous component may be homologous or heterologous in nature. Homologous refers to a sarcoma resembling endometrial stromal sarcoma or a spindle cell sarcoma resembling leiomyosarcoma or fibrosarcoma. Heterologous elements may be chondrosarcoma, osteosarcoma or rhabdomyosarcoma in nature. These tumors must be regarded primarily as carcinomas rather than sarcomas based on immunohistochemical and ultrastructural studies.

MMMTs are highly aggressive neoplasms. Extension into the pelvis, lymphatic and vascular permeation and blood-borne metastases are common. Extension of the tumor to the serosa and beyond is a sign of even worse prognosis.

Müllerian Adenosarcoma

This is a distinctive type of tumor and usually presents in the elderly as a bulky polypoidal growth filling the endometrial cavity. *Microscopically*, it shows a combination of epithelial and stromal elements. The epithelial component has a benign appearance whereas the stromal component is malignant and resembles a sarcoma. *Müllerian adenosarcoma with a sarcomatous overgrowth (MASO)* is an aggressive variant of this neoplasm with a poor prognosis (Fig. 10.9).

Leiomyosarcoma

Leiomyosarcoma occurs in older women and grossly is seen as a large fleshy intramural mass with submucous and subserosal extension. Areas of hemorrhage and necrosis are always present.

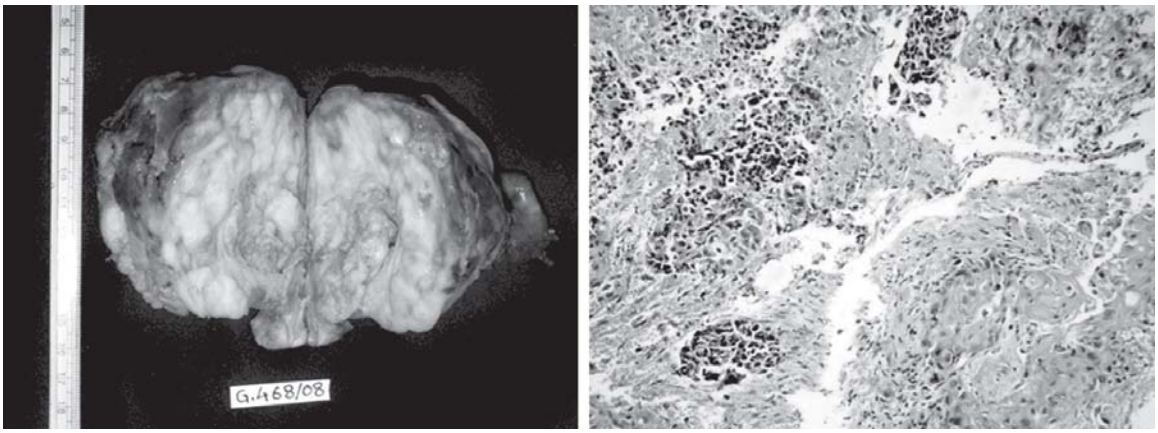

Fig. 10.9: Malignant mixed Mullerain tumor of the uterus: Grossly, a large polypoidal, infiltrative tumor distorting the uterine cavity is seen. Microscopically, there is an admixture on epithelial and mesenchymal elements *(For color version see Plate 14)*

Microscopically, these tumors are highly cellular with large areas of coagulative tumor necrosis. Cellular atypia is obvious and mitoses are numerous (>10/10 high power field). They must be distinguished from cellular and atypical leiomyomas by using histopathological criteria. *Epithelioid and myxoid variants* of leiomyosarcoma are known (Fig. 10.10).

CARCINOMA OF THE UTERINE CERVIX

The cervix is the lower part of the uterus and consists of the endocervix and the ectocervix. The former contains the endocervical canal and the ectocervix continues with the vagina. The ectocervix is covered with stratified squamous epithelium whereas the endocervix is covered by columnar mucin secreting

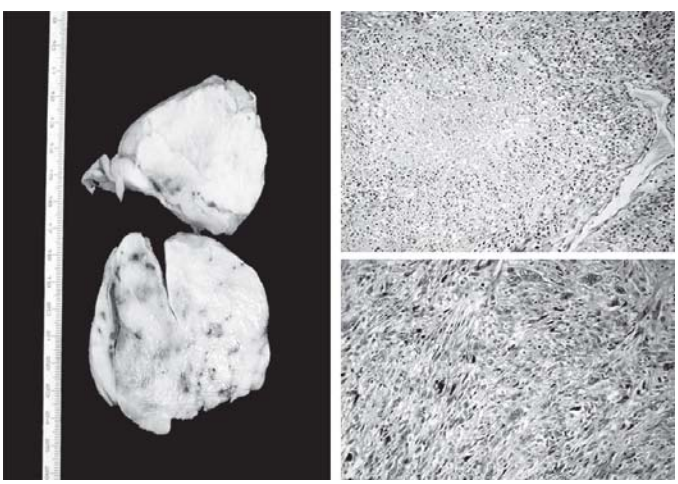

Fig. 10.10: Leiomyosarcoma uterus: Grossly, a fleshy tumor is seen replacing the normal myometrium. Microscopically, coagulative necrosis and diffuse cytological atypia is noted *(For color version see Plate 15)*

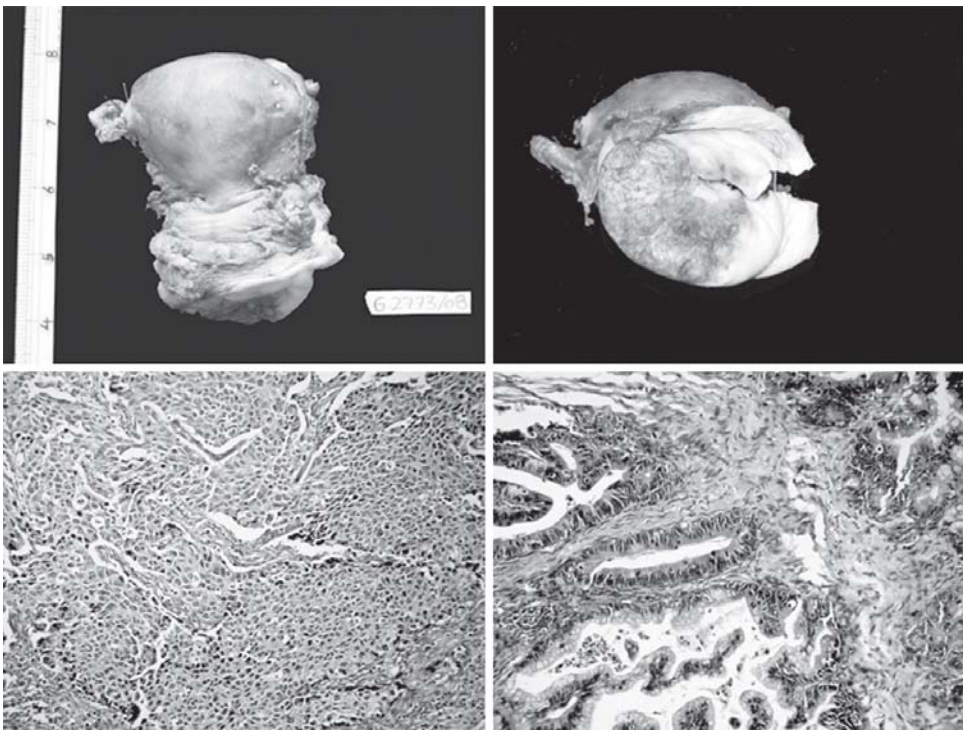

Figs 10.11: Carcinoma cervix: Gross picture of a resected specimen of carcinoma cervix showing an infiltrative growth involving the cervical lips circumferentially. The bottom panel shows a squamous cell carcinoma on the left and an adenocarcinoma on the right, the two principal histological types of invasive carcinoma *(For color version see Plate 15)*

endocervical epithelium. The junction of these two epithelia is called the *squamo-columnar junction (SCJ)*. During puberty and reproductive years of a woman, the squamo-columnar junction moves up and the epithelium between the old and the new SCJ is referred to as the '*transitional zone*' (TZ). It is important to remember that most cervical carcinomas originate in the Transitional Zone. Cervical cancer also has a well defined pre-cancerous state referred to *cervical intra-epithelial neoplasia or CIN* which is graded from CIN I to CIN III. These lesions can be detected in a Papanicolaou smear and forms the basis for screening for cervical cancer (Fig. 10.11).

The association of *human papilloma virus* infection with cervical cancer and precancer is now well established. Out of the several oncogenic HPV types that are associated with cervical cancer, the most important genotypes are HPV 16 and 18 which together account for nearly 75 percent of the cancers. These are also referred to as High-risk HPV types. Screening programmes for cervical cancer now also include testing for these high-risk HPV genotypes.

Invasive Cervical Carcinoma

Gross appearance: These tumors may be polypoid, predominantly exophytic tumors with a cauliflower-like appearance or may be

endophytic, deeply infiltrative resulting in a hard cervix, which is only slightly enlarged. In the evaluation of a surgical specimen, it is important to note the extent of circumferential involvement as well as the upper and lower limits of the tumor. The depth of stromal involvement is also an important aspect. As cervical cancer spreads locally into the parametrium, this also needs careful evaluation.

Microscopically, squamous cell carcinoma is most common followed by adenocarcinoma. Other uncommon types include adenosquamous, verrucous, warty, glassy cell, adenoid-cystic, neuroendocrine and small cell carcinoma. The squamous cell carcinomas may be keratinizing or nonkeratinizing and may be well, moderately or poorly differentiated.

Adenocarcinoma also shows a varied morphology. Endocervical, endometrioid and other subtypes are recognized.

Carcinomas constitute nearly 99% of all malignancies of the cervix. The remaining 1% is made up of a large variety of neoplasms.

Botryoid rhabdomyosarcoma of the cervix is a variant of embryonal rhabdomyosarcoma and presents in children and adolescents as a myxoid polypoid mass covered by attenuated epithelium. This tumor arises in the vagina and less often in the cervix.

Microscopically, the tumor cells are small, ovoid to spindle shaped and form a dense layer beneath the surface lining epithelium called *the 'cambium' layer*. The stroma is loose and myxoid with hypercellular and hypocellular areas. The nuclei are hyperchromatic and mitoses is variable. The tumor cells are positive for myogenic markers like desmin and myogenin.

MALIGNANT TUMORS OF THE VULVA

Squamous Cell Carcinoma

Squamous cell carcinoma accounts for nearly 95% of all malignancies. On the basis of epidemiologic and virologic studies, it is proposed that there are two types of vulval carcinoma; one is HPV negative and occurs in older women and shows a typical keratinizing squamous cell carcinoma microscopically; second is HPV positive and occurs in younger women with associated VIN and has a basaloid or warty histology (Figs 10.12).

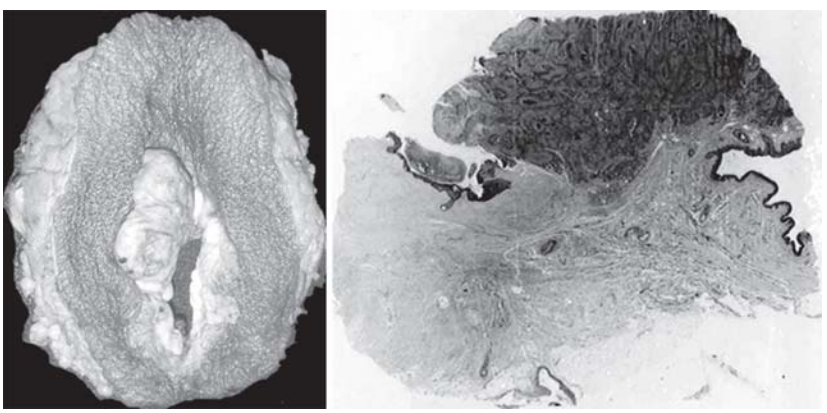

Figs 10.12A : Vulval carcinoma: Grossly, the tumor is seen involving the right labia and extends to the clitoris. Microscopically, it shows a typical squamous cell carcinoma *(For color version see Plate 15)*

Gross Appearance

The tumor frequently arises in the labia majora but may involve the labia minora and clitoris.

Microscopically, squamous cell carcinomas are typically keratinizing. Other subtypes are also known.

Vulval cancer spreads to the regional inguinal lymph nodes. Tumors located in the clitoris can show bilateral node involvement and also involve the deep nodes. Lately, the technique of sentinel lymph node biopsy (similar to breast cancer) has been introduced and practiced as a staging criterion and guide to management for vulvar carcinoma.

Vulvar Paget's Disease

Paget's disease is a malignant tumor of the vulva that clinically presents as a crusting, erythematous, scaling rash on the vulva. A biopsy shows large pale tumor cells forming solid nests or a continuous layer along the basement membrane. These cells are positive for mucin and immunohistochemically for MUC1 and MUC5AC, the latter in striking contrast to the breast. The cells are positive for EMA, CEA keratins and GCDFP-15, a marker of apocrine differentiation. The incidence of an underlying invasive carcinoma varies from 0-30% in vulvar Paget's disease.

BIBLIOGRAPHY

1. Blaustein's Pathology of the Female Genital tract. 5th Edition. Kurman RJ (Ed). Springer-Verlag, New Delhi., 2004.
2. Female Reproductive System in Rosai and Ackerman's Surgical Pathology. Edited by Rosai J. 9th edition, Mosby, Elsevier (Elsevier India), 2004;2:1483-1737.

Chapter

11 Imaging in Renal Tumors

Anjali Prakash

INTRODUCTION

Renal neoplasms that occur in adults constitute a heterogeneous group of tumors with characteristic histology and variable clinicobiological profile. The 2004 WHO classification[1] categorises neoplasms on basis of cell of origin and histopathology. Most renal tumors arise from the parenchyma, refered to as renal cell tumors, with a much smaller number arising from the collecting system and the mesenchyme.

A new classification system proposed in 2006 at Heidelberg subdivides renal cell tumor into benign and malignant parenchymal neoplasm and limits subcategory to the most commonly documented abnormalities (Table 11.1).

BALLS VERSUS BEANS

A useful strategy for the evaluation of renal masses is to divide them on the basis of their growth pattern into ball type or bean type masses. This concept was developed by Hartman and Ros (Oral Communication, October 2006) (Fig. 11.1). Most renal masses like cysts, renal cell carcinomas, angiomyolipoma, metastasis, oncocytoma grow by expansion. These masses are shaped similarly to spheres or balls and they displace and compress, rather that invade normal structure. As these masses enlarge, they expand from normal parenchymal margins, either peripherally to the kidney or into renal sinus. Other renal lesions like transitional cell carcinoma, squamous cell, infiltrating carcinoma, lymphoma, renal medullary carcinoma grow along the latticework of normal renal parenchyma Infiltrating lesions swell the area of involved parenchyma, but do not deform the shape. The kidney retains the 'bean' shape. These are difficult to detect radiologically since little mass effect is associated.

Imaging Modalities

Plain Films

Renal mass may be visible as a soft tissue shadow with displacement of retroperitoneal fat. Calcification can also be detected on plain film. Pattern of calcification may help in differentiating benign from malignant masses. Eighty percent of peripheral calcifications are seen in renal cysts, in 20 percent they are noted in malignant lesions. Renal

Table 11.1: WHO classification of kidney tumors

Familial renal cancer
Renal cell tumors
Malignant
- Clear cell renal cell carcinoma
- Multiocular clear cell renal cell carcinoma
- Papillary renal cell carcinoma
- Chromophobe renal cell carcinoma
- Carcinoma of the collecting ducts of Bellini
- Renal medullary carcinoma
- Xp11 translocation carcinomas
- Carcinoma associated with neuroblastoma
- Mucinous tubular and spindle cell carcinoma
- Renal cell carcinoma unclassified

Benign
- Papillary adenoma
- Oncocytoma

Metanephric tumors
- Metanephric adenoma
- Metanephric adenofibroma
- Metanephric stromal tumors

Mixed mesenchymal and epithelial tumors
- Cystic nephroma
- Mixed epithelial and stromal tumor
- Synovial sarcoma

Nephroblastic tumors
- Nephrogenic rests
- Nephroblastoma
- Cystic partially differentiated nephroblastoma

Neuroendocrine tumors
- Carcinoid
- Neuroendocrine carcinoma
- Primitive neuroectodermal tumor
- Neuroblastoma
- Pheochromocytoma

Other tumors
- Mesenchymal tumors
- Hematopoietic and lymphoid tumors
- Germ cell tumors
- Metastatic tumors

masses that contain central, irregular calcifications are usually malignant (Fig. 11.2).

Skeletal metastasis may also be detected. They appear as lytic expansile foci. Multiple osteomas or bone islands are another abnormality associated with renal mass, particularly in patients with tuberous sclerosis.

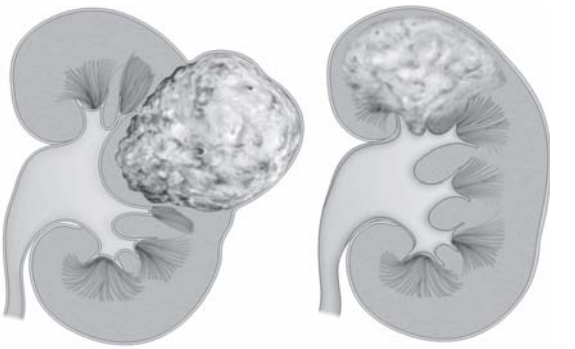

Figs 11.1A and B: Ball versus Bean concept: **(A)** Ball type mass grows exophytically, with a contour deformity. **(B)** Bean type mass uses renal parenchyma as framework for growth with maintained reniform shape. Sinus fat and collecting system elements may be destroyed

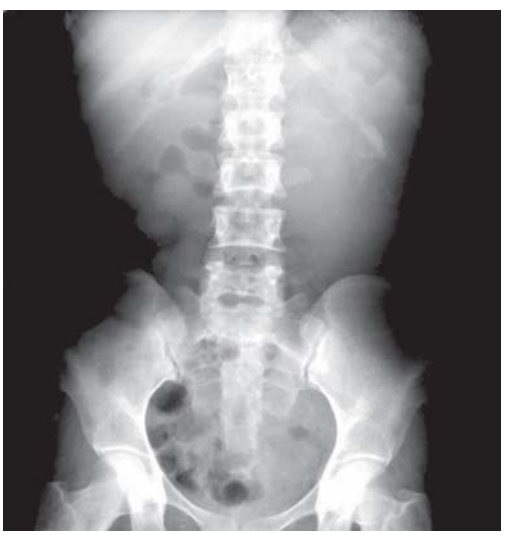

Fig. 11.2: Plain Film showing soft tissue mass with amorphous calcification in left renal fossa

IVU

Excretory urography lacks specificity for accurately characterizing a lesion. Expansile masses cause contour abnormalities, calcyeal splaying, stretching and draping. Infiltrating renal mass produce little parenchymal mass effect and maybe seen as a filling defect in the collecting system.

Ultrasound

Ultrasound is very useful for detection of renal masses and characterizing them as solid or cystic. Ultrasound may also be useful when CT pseudoenhancement is noted, leading to a simple renal cyst being mischaracterized as solid mass. Color Doppler sonography can evaluate renal vein and IVC for presence of thrombus. The vascular flow within a renal mass, identified by color and power Doppler is strongly associated with clear cell carcinoma. The vascular distribution at power Doppler potentially could add information in differentiation of small solid renal masses. Peripheral or mixed peripheral and penetrating patterns are seen in all RCCs and some benign angiomyolipomas and oncocytomas, whereas intratumoral focal and penetrating pattern is characteristic of angiomyolipomas.

CT

CT is accurate in detection, characterization and staging of renal masses. MDCT allows fast, multiphase and high resolution imaging. Comprehensive evaluation of renal masses requires a dedicated CT protocol. For characterization of a renal mass, the examination is to performed before and after administration of IV contrast, the different phases of renal enhancement arterial (15-20 sec delay) corticomedullary (35-80 sec), nephrographic (85-180 sec) and excretory (3 min or more) need to be evaluated.

The nephrographic phase is ideal for detection of masses as there is maximal and homogenous parenchymal enhancement. This allows better delineation of renal masses which do not enhance to the same level as the renal parenchyma. During imaging in corticomedullary phase, small renal masses may be indistinguishable from renal medulla. During excretory phase, masses may be same attenuation as the parenchyma which has deenhanced.

Imaging in corticomedullary phase may help in characterizing pseudotumors such as hypertrophy of column of Bertin. Careful attention is to be given to enhancement that is identified as unequivocal and not due to pseudoenhancement which is elevated HU measurement of cyst due to image reconstruction algorithm. It may be useful to adopt gallbladder or a simple cyst (when present) as internal reference standard for Hounsfield unit measurement. An increase in attenuation of 10 HU or more in a lesion measuring at least 2 cm in diameter indicates enhancement. As enhancement is transient, washout of contrast is also useful. If an area of enhancement decreases subjectively or quantitatively (at least 10 HU), neoplasm is suspected. This is called "de enhancement".

CT urography is beginning to replace IVU as the imaging examination of choice to detect upper urinary tract tumors.

MRI

MRI is useful for characterization of renal masses. This is especially useful in patients in whom iodinated contrast is contraindicated.

The protocol to be used includes a coronal HASTE, axial T2-weighted gradient and spin echo with fat suppression, axial dual echo in phase and opposed phase gradient echo T1 images, and 3D fat suppressed GRE T1 images before and after iv contrast followed by a coronal 3D fast gradient echo sequence with fat suppression after the dynamic series to display renal venous anatomy and IVC, MR imaging is valuable for distinct renal lesions. On MR imaging, hemorrhagic cysts have high signal on T1WI. The combination of high

signal on T1 and lack of enhancement are diagnostic for hemorrhagic cyst. T2-weighted images are useful in distinguishing a simple renal cyst from other lesions. A homogeneous hyperintense lesion on T2 with a thin wall and no enhancement is a renal simple cyst. All 3 phases of renal excretion are obtained after contrast and subtraction images may be obtained to determine, percentage of enhancement. In and opposed phase images help in detecting intratumoral fat.

MR urogram is indicated in patients with suspected collecting system disease.

Angiography

Renal angiography, once a basic element in the diagnosis of renal masses, is of little value now. CT and MR angiography give excellent vascular mapping of the kidney and have replaced catheter angiography for this diagnosis. Angiography may be an alternative to open biopsy in diagnosis of infiltrating renal neoplasm. Hypo and avascular lesion are usually urothelial malignancies.

Retrograde and Antegrade Pyelography

Retrograde and antegrade pyelography may be used for small urothelial tumors, for better mucosal detail.

RENAL CELL CARCINOMA[23]

Renal cell carcinoma, also called hypernephroma, pathologically adenocarcinoma is the most common primary renal malignancy in adults. It accounts for 85 percent of all malignant renal tumors and about 3 percent of all diagnosed neoplasms.

Renal carcinoma occurs more commonly in males, in the 5th to 7th decades. Most are sporadic; some may be associated with syndromes such as von Hippel Lindau (VHL). Risk factors include smoking, exposure to petroleum and asbestos. Usually RCC is unilateral, two percent are bilateral and nine percent are multicenteric in the same kidney. Bilateral and multicenteric tumors arise in patients of VHL syndrome, familial RCC and in patients on long term hemodialysis.

RCC is nowadays most commonly incidentally discovered (30%). These are often smaller and of lower grade and staging. RCC may however present with symptoms like flank pain (37%), hematuria and palpable mass; weight loss, anorexia, fever, GI or neurological symptoms or paraneoplastic syndromes. Superficial tumors can invade and breach the renal capsule and directly involve perirenal fat, adrenal gland and adjacent organs. Metastasis often occurs in regional nodes, invasion of cisterna chylii can lead to hilar and supraclavicular nodes. RCC has a propensity for venous thrombi. Systemic dissemination can take place into liver, bone, adrenal, opposite kidney or brain in decreasing order of frequency.

RCC is composed of different histological subtypes with different disease progression and metastatic potential.

Clear cell RCC is the most common type accounting for 75 percent of RCCs. They typically appear as variegated, expansile, cortical masses with areas of necrosis, hemorrhage, cystic change and calcification (15%). These show hypervascularity. Clear cell RCC, have the greatest metastatic potential and show hematogenous metastasis to lung, liver and bones. There is also a propensity of clear cell RCC for lymphatic and late and unusual sites of metastasis.

Papillary RCC, characterized by papillary or tubopapillary histologic architecture accounts for 10-15 percent of RCC. It presents at 40-50 years of age and is a slow growing tumor. They appear as homogeneous, hypovascular. soft tissue cortical masses with foci of calcification. A low tumor to aorta

enhancement ratio or tumor to normal renal parenchyma enhancement ratio is highly indicative of papillary RCC. Papillary RCCs frequently show necrosis and hemorrhage.

Chromophobe RCC, a recently classified subtype of RCC, represents 5 percent of renal cell cancers and is characterized by large, pale cells with prominent cell membranes. They occur as solitary cortical masses. Bilateral and multicentric chromophobe RCCs are found in association with oncocytomas and Birt-Hogg-Dube syndrome. The tumor is typically large at presentation, homogeneous without necrosis or hemorrhage. The mass is relatively hypovascular. The chromophobe type is associated with the least malignant potential and best prognosis.

Multicystic renal cell carcinoma (MCRCC) is a recently described, rare subtype of RCC. The term is used to describe a cystic RCC with a small volume (25 percent or less) of neoplastic clear cells in the cyst. MCRCC typically manifests as multiseptated cystic masses with thin septations on imaging. Distinction from other cystic masses is difficult.

IVU

An RCC, on IVU appears as an expansile contour bulge. Since the tumor grows by expansion, the tumor usually displaces and distorts the calyces (Fig. 11.3). Increased distance between calyx and cortex is a sensitive sign. Occasionally an RCC grows predominantly outward and no detectable mass effect is exerted on the calyceal system. RCC's that extend either exclusively anteriorly or posteriorly may be difficult to be detected on IVU as the mass contour is superimposed by normal kidney. Other signs on IVU of RCC are secondary to mass effect and the need for increased vascular perfusion. This is in the form of notching of renal pelvis and ureter as a result of enlarged ureteric and renal pelvic vessels which are enlarged to feed a hypervascular RCC. Focal or diffuse hydronephrosis may result due to a large RCC which leads to compression of major calyces, the renal pelvis and upper ureter. Decreased or absent function may be noted. The finding of globally decreased function with a renal mass is suggestive of RCC.

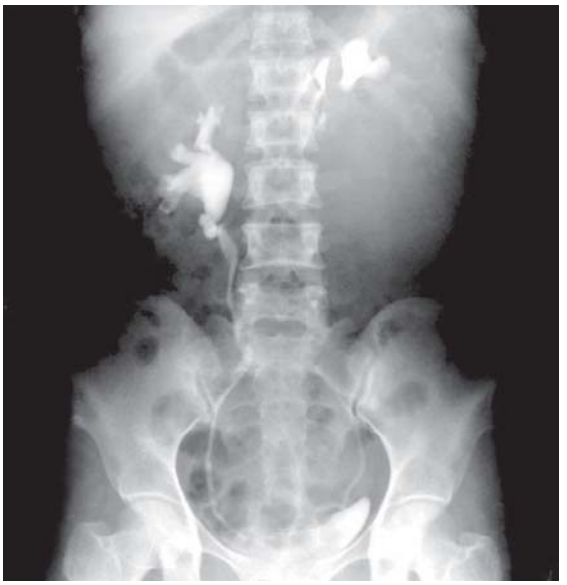

Fig. 11.3: IVU showing compression and displacement of calyces on the left. There is focal hydrocalyx of the upper pole—renal cell carcinoma

Less commonly, an RCC grows by infiltration rather than expansion and in these cases; malignant stricturing of the collecting system occurs, secondary to encasement and invasion of the urothelium.

Small RCCs are undetectable by IVU. One-third of mass lesions less than 3 cm in diameter, cannot be detected with IVU. A normal IVU in patients with clinical evidence of RCC should be supplemented with CT, US or MRI. The detection of mass on IVU is non-

specific and needs further imaging for characterization.

Ultrasound

Renal adenocarcinoma is detected as a well encapsulated solid mass. It may have poorly defined margins. The reflectivity of the mass is similar to that of adjacent parenchyma, although texture is heterogeneous or is of reduced reflectivity. Tumors that are hyperechoic with echogenicity similar to renal sinus fat occur and account for 1/3rd of tumors under 3 cm in diameter, these mimic angiomyolipoma. Features that suggest a malignancy is an echopoor rim and small cysts within the tumor. The echopoor rim is due to a peudocapsule of compressed renal tissue and this is not seen in AML. As tumor grows, inhomogeneity of its appearance increases due to hemorrhage and necrosis (Fig. 11.4). The echopattern of the tumor does not reflect the histological type of tumor. Papillary tumors, which are usually low grade, are of increased reflectivity.

If the tumor is cystic, it presents as a unilocular cystic mass in about 50 percent of such cases. Features such as irregular thickened walls, echoes, and calcification favour malignancy. In 30 percent, the appearance is of a multilocular cystic mass with intervening solid areas, which may calcify. In remaining 20 percent there is a solid mass within the wall of cyst.

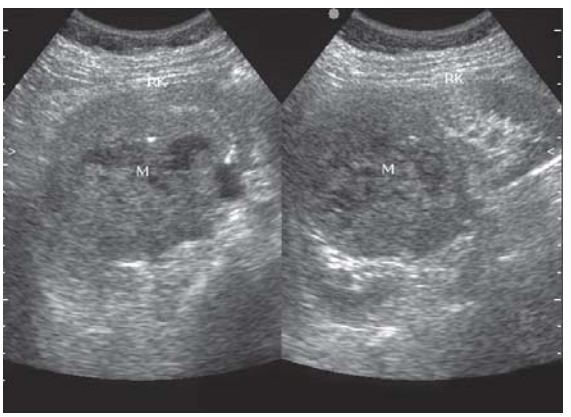

Fig. 11.4: US—Transverse and longitudinal sonogram of the right kidney shows a large well defined heterogeneous mass arising from the upper pole right kidney—renal cell carcinoma

Doppler

An abnormal Doppler signal can be seen in the ipsilateral renal artery as an increase in velocity, spectral broadening and turbulence. These findings may also be seen in some inflammatory lesions making it non-specific (Figs 11.5A and B).

Intraoperative ultrasound is being used in nephron sparing surgery to delineate exact extent of the mass and venous thrombi.

CT

On unenhanced CT, renal cell carcinomas may be hypodense,isodense or hyperdense to the unenhanced renal parenchyma. They are often heterogeneous, with one or more low density central areas, the mass distorts the margin of the kidney in a majority (94%) of cases, irrespective of tumor size. The presence of calcification is also noted in approximately 25 percent and CT is the most sensitive modality for the depiction of parenchymal calcification. The calcification of RCC may be punctate, amorphous, linear or peripheral (Figs 11.6A and B). A zone of relative radiolucency surrounding the tumor or 'halo sign' may be noted. This represents the compressed ischemic renal parenchyma around the tumor–'pseudocapsule'.

Following contrast administration, renal cell carcinomas reveal inhomogeneous enhancement to a lesser degree than normal parenchyma with an indistinct parenchymal interface (Figs 11.7A to D). Clear cell carci-

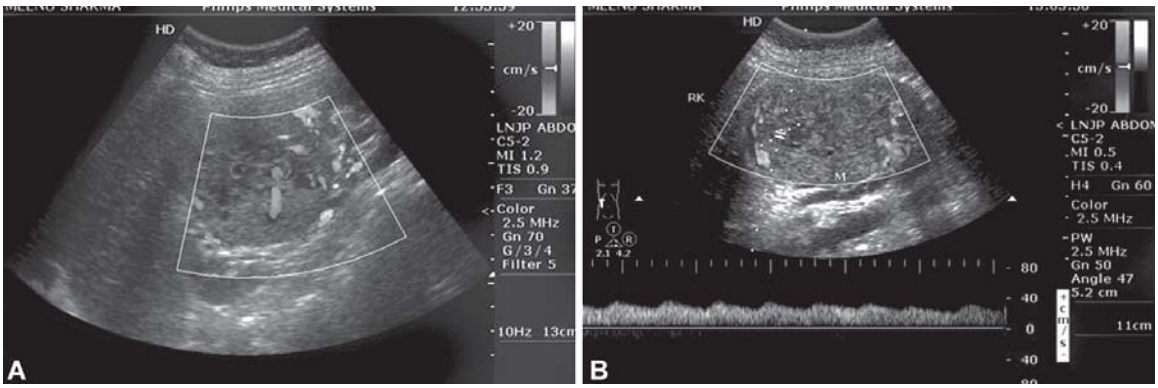

Figs 11.5A and B: Color Doppler: **(A)** and spectral trace **(B)** show vascularity within and surrounding the mass *(For color version see Plate 16)*

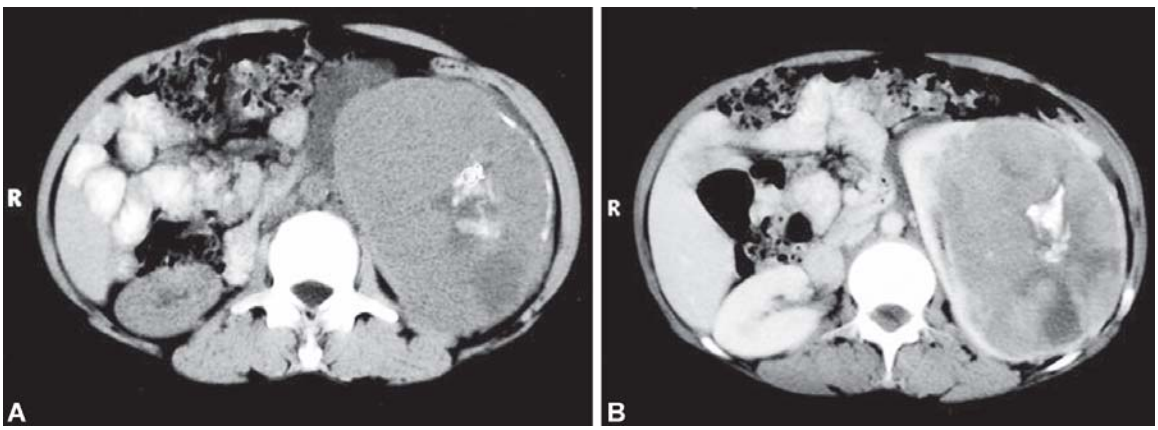

Figs 11. 6A and B: NCCT and CECT showing a large enhancing left renal mass with peripheral and central coarse calcification in the left kidney

nomas enhance to a greater degree than other subtypes of malignant lesions, especially papillary carcinoma.

Most renal carcinomas are solid with an attenuation of atleast 20 HU on precontrast scans. An increase in attenuation of more than 10 HU after contrast suggests a solid mass and enhancement of more than 20 HU indicates malignancy (Figs 11.8A to D). Heterogeneous enhancement correlates with the presence of acellular regions within the tumor, but does not correlate with grade. Cystic and necrotic change is seen in clear cell type, whereas papillary and chromophobe are more homogeneous (Fig. 11.9).

There, often is renal vein invasion and the thrombus may extend into the IVC (30%) CT is specific for renal vein invasion by tumor thrombus with specificity of 98 percent.[4] A hypodense filling defect outlined by contrast in the renal vein on CT using cortico-medullary or nephrographic phase is diagnostic for thrombus (Fig. 11.10). CT for detection of thrombus requires thin (< 5 mm) slices at level of renal vein after pressure injection of contrast. Renal vein enlargement and displacement are not accurate signs for venous invasion, as it may be enlarged due to high flow and displaced due to bulk of tumor.

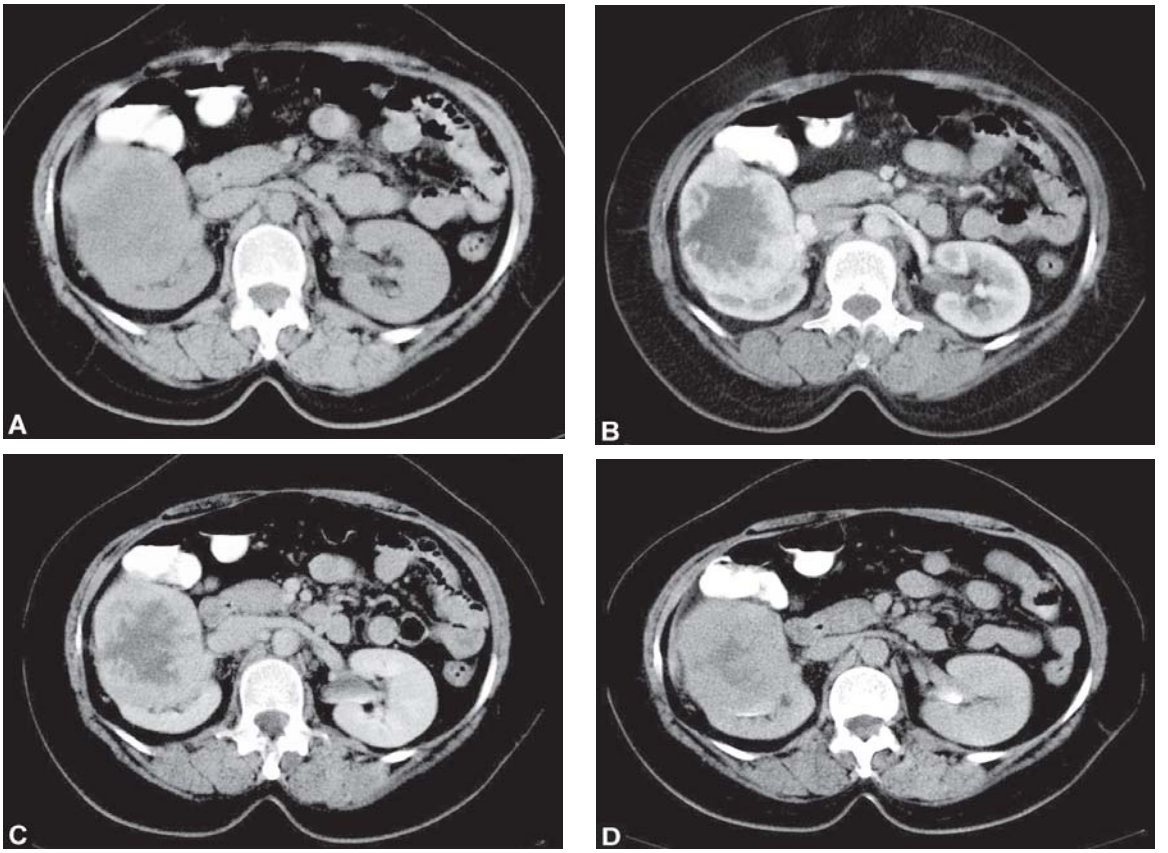

Figs 11.7A to D: CT features of renal cell carcinomas in 4 phases: **(A)** Noncontrast, **(B)** Corticomedullary, **(C)** Nephrographic, **(D)** Excretory phases. The Figures shows a right renal mass with mixed enhancement pattern containing enhancing soft tissue and low attenuation areas representing necrosis or cystic change arising from the anterior renal cortex. The mass is best demarcated on nephrographic phase and shows "de-enhancement" in the later phase

Heterogeneous enhancement of thrombus on nephrographic phase is further diagnostic for tumor thrombus. The flow of unenhanced blood from pelvis may be mistaken for IVC thrombus. In these cases delayed images may be needed for further characterization. Tumor thrombus may extend into IVC, often enlarging the caliber of the IVC. There may be bland thrombus inferior to the tumor thrombus in the IVC, as a result of occlusion of the lumen.

Metastatic adenopathy in the retroperitoneum, associated with RCC has poor prognostic significance. The criterion of 1 cm as a threshold has proved to be unsuccessful in differentiating reactive nodes from metastatic adenopathy. Lymph nodes greater than 2 cm are always malignant. Nodes, less than 1 cm may contain metastasis.

MRI

Diagnosis is made on visualization of a contour disrupting mass, small RCCs are undetectable on MRI. RCC is typically mildly hypointense to the renal cortex on T1 weighted images and mildly high signal on

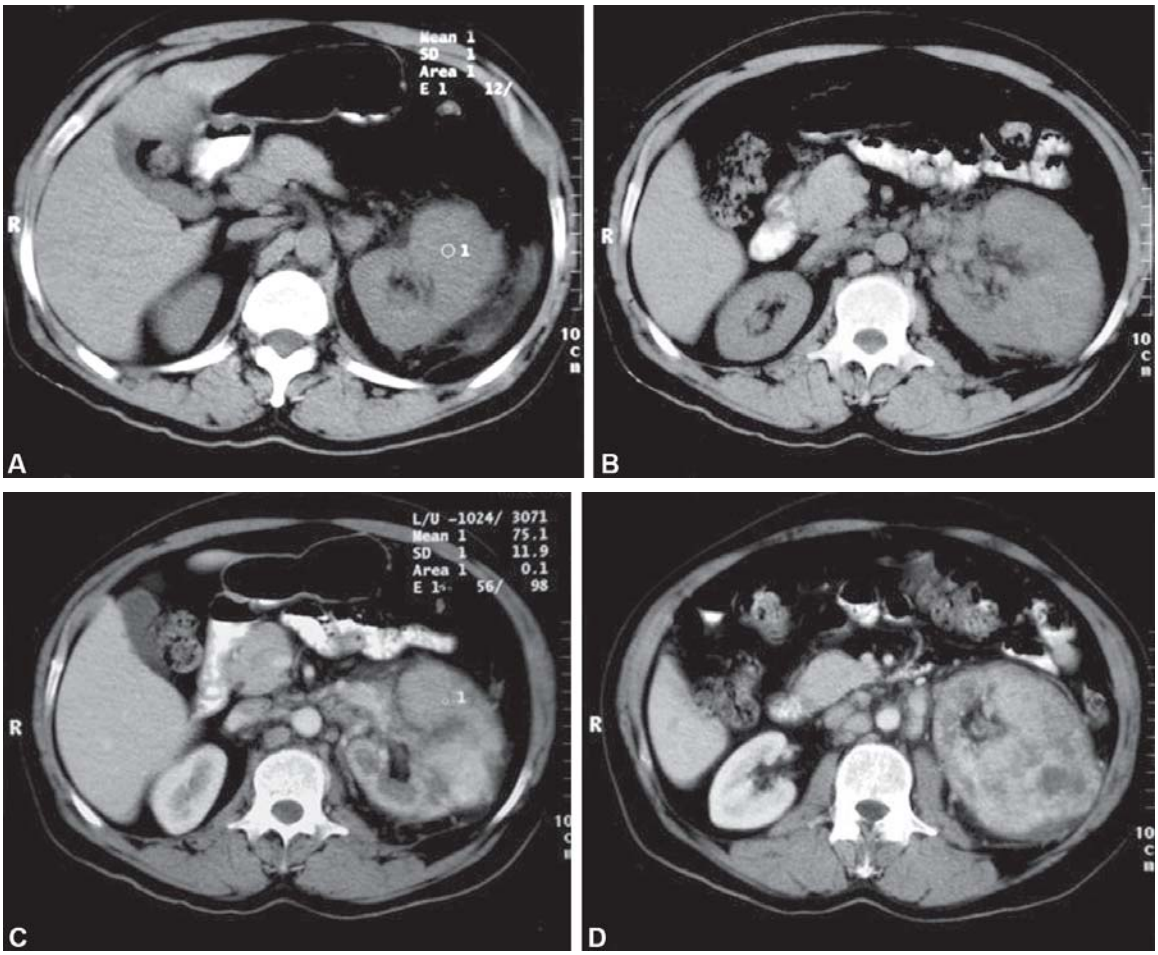

Figs 11.8A to D: CT Pre **(A and B)** and post-contrast **(C and D)** shows solid left renal mass with increase in attenuation of 20 HU-malignant etiology (RCC)

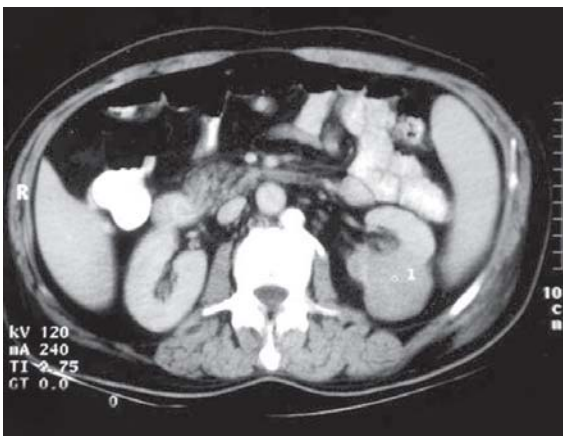

Fig. 11.9: CT abdomen shows a small hypodense well defined cortical mass with no fat density. Possibility of small neoplasm (? papillary RCC) is to be considered

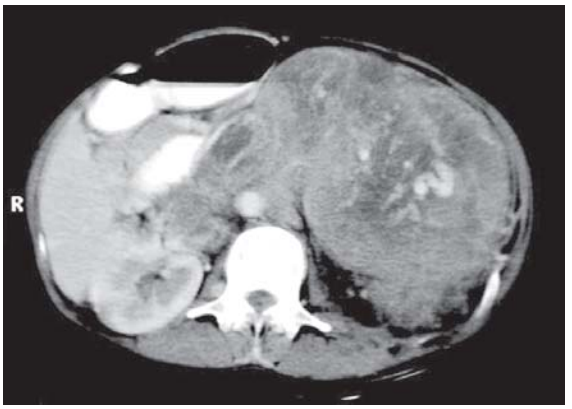

Fig. 11.10: CECT abdomen – shows a large mass in the left kidney with neovascularity, definite extension into perinephric space, left renal vein and IVC – RCC

T2-weighted images. Most RCCs have a hypointense 'pseudocapsule' on TIW (25%) and T2W (60%) at the periphery of tumor on SE images (Figs 11.11A and B). Interruption of this pseudocapsule correlates with advanced stage. Fat saturated images are also recommended as there is a signal drop in AMLs and rare for RCC to contain fat.

Based on T1-weighted images, a 15 to 20 percent enhancement on scans 3-5 minutes after gadolinium is considered diagnostic. When a diagnostic dilemma of enhancement is seen on CT scan, MR imaging is helpful. Subtraction (Gadolinium enhanced fat suppressed T1 weighted images—unenhanced fat suppressed T1 weighted image) is an easy, reliable method. However, it is necessary for subtraction, to have accurate corregisteration of enhanced and enhanced MR images. It is recommended that all MR sequences be obtained during an end expiratory breath hold which is more reproducible. It may also be difficult to detect enhancement on CT in a heavily calcified mass. MR imaging is helpful as calcification not being seen and any enhancement will be detected. MRI is useful in patients for whom iodinated intravascular contrast is contra indicated (Figs 11.12A to D). Multiplanar capability of MRI is helpful in evaluation of vascular thrombosis.GE sequences are used to assess thrombus by depicting flowing blood via a

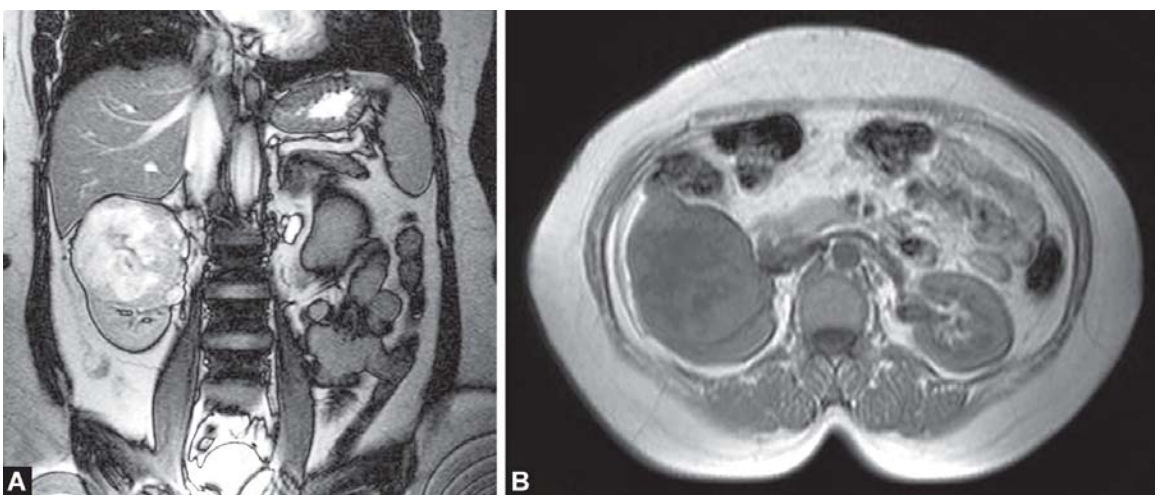

Figs 11.11A and B: Renal cell carcinoma – MRI **(A)** TRUE FISP coronal **(B)** T1W1 axial showing a well-circumscribed mass hypointense on T1 and hyperintense on T2 arising from upper pole of right kidney. IVC appears normal. Necrotic change is noted appearing hyperintense on T2W images

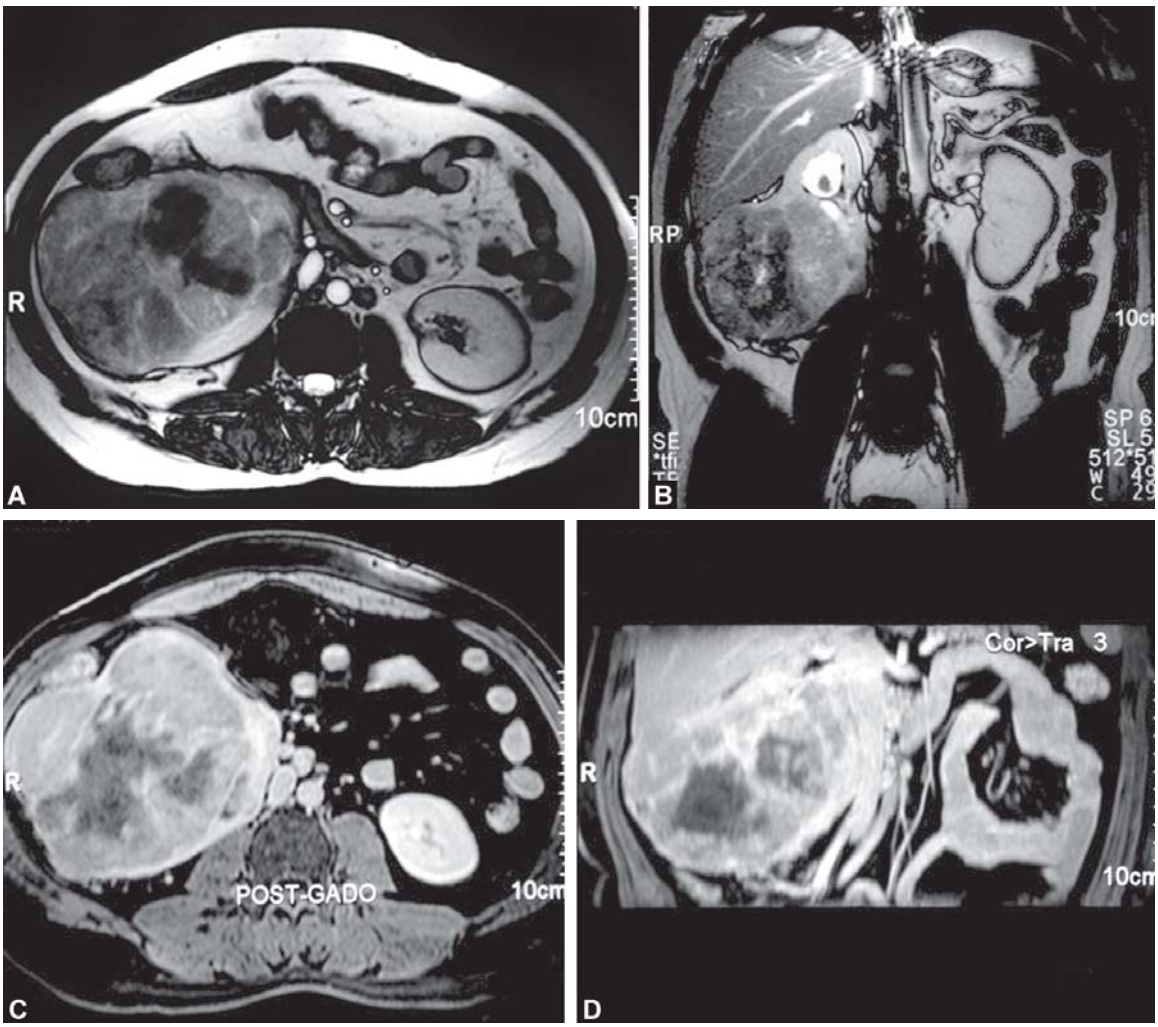

Figs 11.12A to D: MRI—TRU FISP axial **(A)** and coronal **(B)** Mixed intensity right lower renal polar mass with areas of hemorrhage and well defined 'peudocapsule" TI post gadolinium axial **(C)** and MPR **(D)** shows enhancing soft tissue component of the mass

bright signal as opposed to a thrombus which is low signal intensity. GE images maybe helpful in cases with marked caval compression by tumor masses.

Various studies have correlated MRI appearance of renal masses with pathology. An MRI classification system has been proposed to predict the histological subtype and nuclear grade. This is based on certain characteristics like lesion size, peripheral vs central location, T2 signal intensity and degree of enhancement of the lesion, the presence of subvoxel fat on CSI, intratumoral necrosis, retroperitoneal vascular collaterals, vascular thrombosis. Clear cell RCC frequently demonstrates signal intensity similar to renal parenchyma on T1-weighted images and increased signal on T2-weighted images.

Loss of signal intensity within the solid portions of clear cell RCCs on opposed phase images as compared to in phase images is due to cytoplasmic fat and is seen in upto 60 percent of these tumors (Figs 11.13A to H). Central necrosis is common and is typically seen as homogeneous hypointense on T1WI and moderately high signal on T2WI.Clear cell RCCs tend to be hypervascular with heterogeneous enhancement during arterial phase. Retroperitoneal collaterals and renal vein thrombosis are predictive of high grade clear cell RCC. Papillary RCC demonstrate low signal intensity on T2-weighted images due to presence of hemosiderin), small size, peripheral location and low level enhancement. High grade papillary RCC have a more complex appearance with hemorrhage and necrosis. Enhancing papillary projections at periphery of a cystic hemorrhagic mass are seen.[5,6]

Recent studies have shown a promising role of diffusion imaging in evaluation of renal masses. A decrease in ADC values is suggestive of malignant etiology.[7]

Angiography

Angiography, is only very occasionally indicated preoperatively for vascular mapping, especially if nephron sparing surgery is being contemplated for small neoplasm, multiple and bilateral neoplasm or tumors in horseshoe kidney. Most RCCs are hypervascular with presence of tumor vessels which are irregular, tortuous and distributed randomly.

Angioinfarction has a limited role, in large tumors and as palliative procedure to control pain, hematuria in inoperable/unfit for surgery patients.

Nuclear Scintigraphy

FDG-PET has a reported sensitivity for detection of renal malignancy in the range of 40-94 percent.[8] Normal renal excretion of FDG may decrease contrast between tumor and normal renal parenchyma. False-positive results have also been seen in patients with benign inflammatory process of the kidney or benign tumors. FDG-PET may have a role

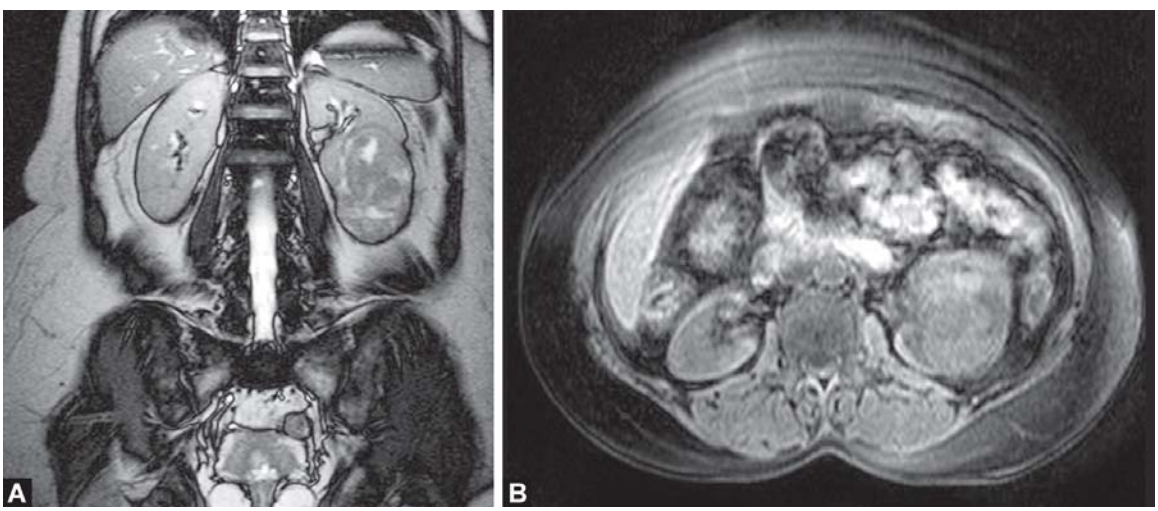

Figs 11.13A and B: MRI T2 TRUE FISP coronal **(A)** TI VIBE axial **(B)** TI in phase (Contd...)

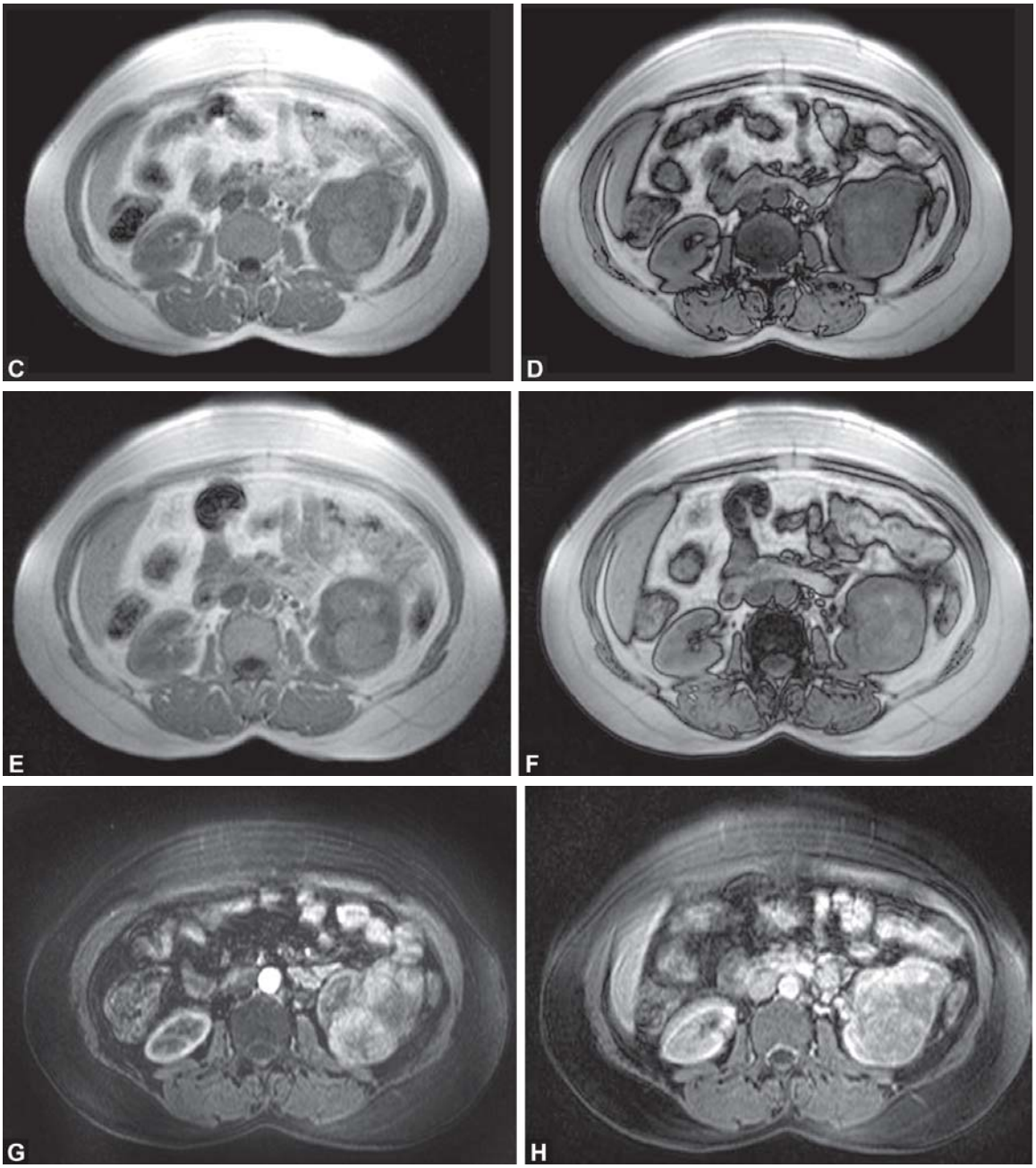

Figs 11.13C to H: T1 in phase **(C and E)**, opposed phase **(D, F)** TI axial post gado **(G, H)**- A solid enhancing mass is seen in left kidney, hypointense on T1,hyperintense on T2,with a drop in signal intensity on opposed phase images compared to in phase images. Note lack of "India Ink "effect on opposed phase—Clear cell RCC

in evaluating distant metastasis and in the differentiation between recurrence and post-treatment changes.

Staging of Renal Cell Carcinoma[2,3,9-11]

Staging is a critical component of evaluation of a patient with renal mass. The staging and histological grading affects the survival and the therapeutic approach. Five-year survival rates vary from 95 percent for T1 to 20 percent for T4. Currently the most commonly used staging system is the TNM system of the American Joint Committee on Cancer (Table 11.2). The patient's overall stage is determined by the American Joint Committee on Cancer stage groupings (Table 11.3).

It is impossible to differentiate between stage I and stage II RCC with CT and MRI. Some signs like stranding of perinephric fat fascial thickening, obliteration/blurring of fat, adrenal involvement, visible collaterals are considered suggestive for extracapsular spread. Perinephric stranding may result from edema, congestion and obliteration of fat may be due to mass effect. The most reliable imaging sign of RCC spread is the presence of discrete perinephric mass >1 cm in diameter (Fig. 11.14). This is usually of not much significance other than prognostication, since radical nephrectomy is the treatment for both, except when there is a solitary kidney or bilateral tumors. The presence of an intact pseudocapsule, composed of compressed normal renal parenchyma and fibrous tissue seen best on T2WI, suggests lack of perinephric invasion.

Stage III includes invasion of renal vein, IVC, adrenal or regional adenopathy. Surgical planning for these patients depends on accurate preoperative staging. If tumor extends only into subdiaphragmatic cava, then a flank approach is sufficient. If it

Table 11.2: TNM staging for renal cancer

T	**Primary tumor**
TX	Primary tumor cannot be assessed
T0	No evidence of primary tumor
T1	Tumor < 7 cm in greatest dimension, limited to the kidney
T1a	Tumor < 4 cm in greatest dimension, limited to the kidney
T1b	Tumor > 4 cm but < 7cm in greatest dimension, limited to the kidney
T2	Tumor > 7 cm in greatest dimension, limited to the kidney
T3	Tumor extends into major veins or invades adrenal gland or perinephric tissues, but not beyond Gerota's fascia
T3a	Tumor directly invades adrenal gland or perirenal and or renal sinus fat, but not beyond Gerota's fascia
T3b	Tumor grossly extends into the renal vein or its segmental (ie, muscle-containing) branches or the vena cava below the diaphragm
T3c	Tumor grossly extends into the vena cava above the diaphragm or invades the wall of the vena cava
T4	Tumor invades beyond Gerota's fascia
N	**Regional lymph nodes**
NX	Regional lymph nodes cannot be assessed
N0	No regional lymph node metastasis
N1	Metastasis in a single regional lymph node
N2	Metastasis in > 1 regional lymph node
M	**Distant metastasis**
MX	Distant metastasis cannot be assessed
M0	No distant metastasis
M1	Distant metastasis

Table 11.3: Stage grouping for renal cancer

Stage I	T1, N0,M0
Stage II	T2, N0, M0
Stage III	T1,N1, M0
	T2, N1, M0
	T3, N0, M0
	T3,N1,M0
Stage IV	T4, N0,M0
	T4,N1,M0
	Any T,N2, M0
	Any T, any N, M1

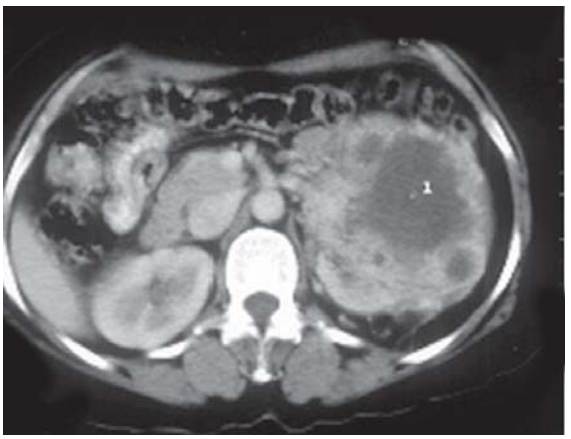

Fig. 11.14: CT—a large left renal mass with definite extension into the perinephric space-stage II

extends beyond this, then thoracoabdominal approach has to be followed. MRI is more sensitive for vascular invasion than CT and the diagnosis is aided by multiplanar ability of MRI. It is more sensitive, for IVC wall invasion and to confirm tumor thrombus (Figs 11.15A to C). On the right side it may be difficult to distinguish between intraluminal tumor thrombus and extrinsic caval compression caused by a large primary tumor or enlarged lymph nodes. Gradient echo images may detect a low-signal defect within the high signal lumen of IVC.

Based on nodal size criteria alone, MRI and CT are similar in sensitivity and specificity for metastatic adenopathy. False-positive rates of 58 percent have been reported, however, when a size criterion of 1 cm is used, owing to reactive or other benign nodal disease. These false-positive are more frequent in patients with tumor involvement of the renal vein and tumor necrosis. Ultrasmall supramagnetic iron oxide particles have shown promise in differentiating metastatic nodes from normal nodes. A normal node will take up this particle and create a drop in T2 signal, whereas no drop in signal is seen in metastatic nodes.

CT has a high negative predictive value for adrenal involvement from RCC. It has been suggested that only when the adrenal gland is not identified, not displaced or enlarged on CT, adrenal is said to be involved.

Stage IV cancer involves distant metastasis or spread to other organs;8 except the adrenal. Metastatic disease involves lung, liver, bone or brain. RCC < 3 cm rarely metastasize. A renal mass may appear to invade the liver or spleen, when it is actually distorting the margin without direct invasion (Figs 11.16A to C). A chest radiograph is essential for the work-up. A chest CT to be done if the radiograph is abnormal or the local disease is advanced. RCC is associated with hypervascular liver metastasis, particularly from clear cell RCC. Portal venous phase imaging detects 90 percent of metastasis. Bone metastases are usually lytic. Bone scan is performed only in patients with bone pain or raised alkaline phosphatase. Bone scan may be negative as the lytic metastasis produce little osteoblastic reaction. MRI may be more sensitive to CT in detection of unsuspected bony metastasis, because of bone marrow imaging capability.

The overall accuracy of MR staging is comparable or superior to CT. It has advantages over CT in the evaluation of tumor vascular extension, differentiation of perihilar vessels from nodes and the assessment of direct tumor extension into other

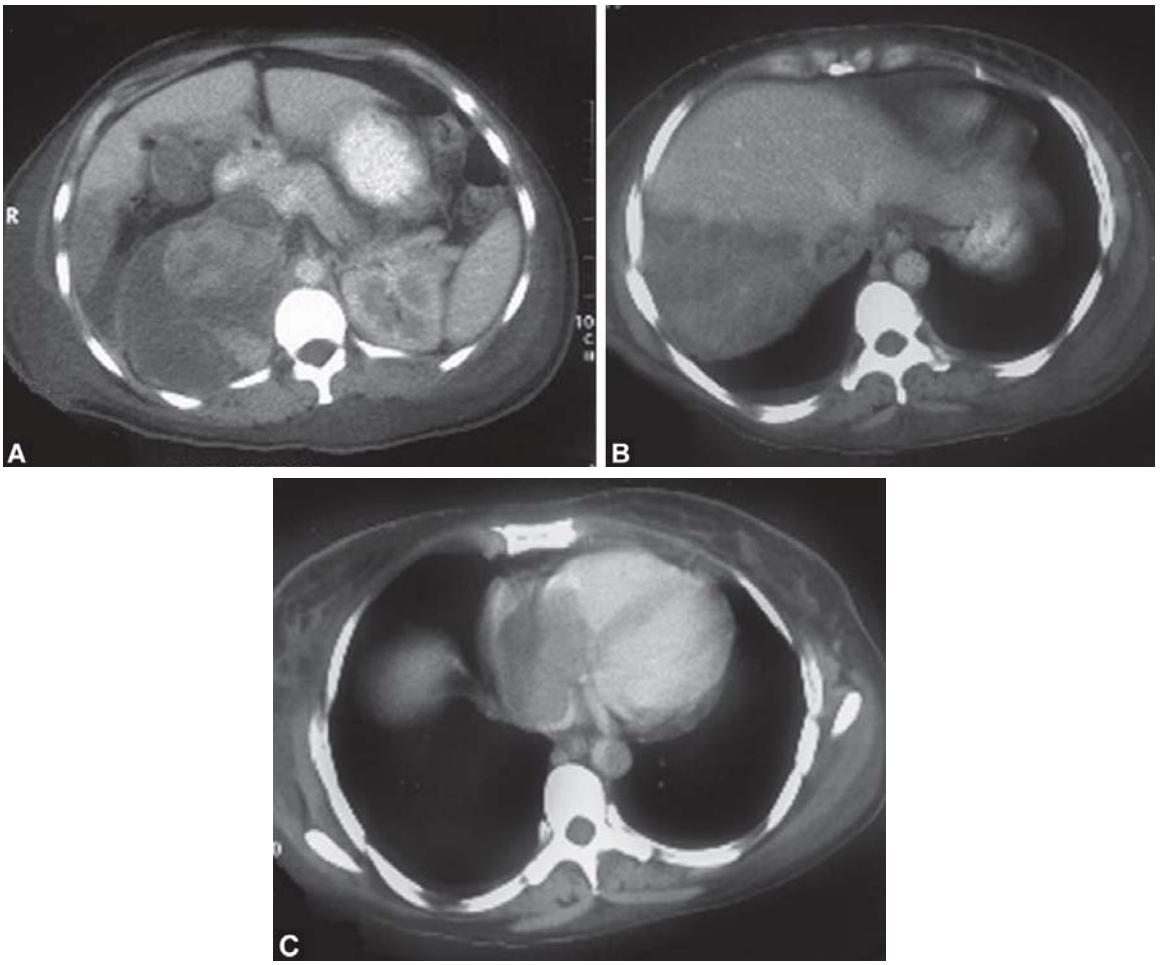

Figs 11.15A to C: Renal cell carcinoma – CT shows a complex solid cystic mass with an intraluminal filling defect seen in the renal vein which is enlarged **(A).** A more cephlad section shows the enhancing thrombus within the IVC and a consequent to this, a perfusion deficit in liver **(B)**. The thrombus is seen to extend into the right atrium **(C)**

organs (Figs 11.17A and B). MRI is an excellent staging modality when the CT findings are equivocal.

Follow-up

Most recurrences occur within 3 years with a median relapse time of 1-2 years. Tumor diameter, T stage, nuclear grade are important determinants for recurrence. For imaging surveillance,CT is the modality of choice for local recurrence as well as distant metastasis. Baseline CT and follow-up CT at 6 months interval is recommended. Normal structures may migrate into the renal fossa after nephrectomy and may simulate recurrent tumor. The liver, ascending colon, 2nd part of duodenum, pancreatic head and small bowel may migrate into the right side. The most likely site of recurrence of tumors is in the nephrectomy site or adjacent

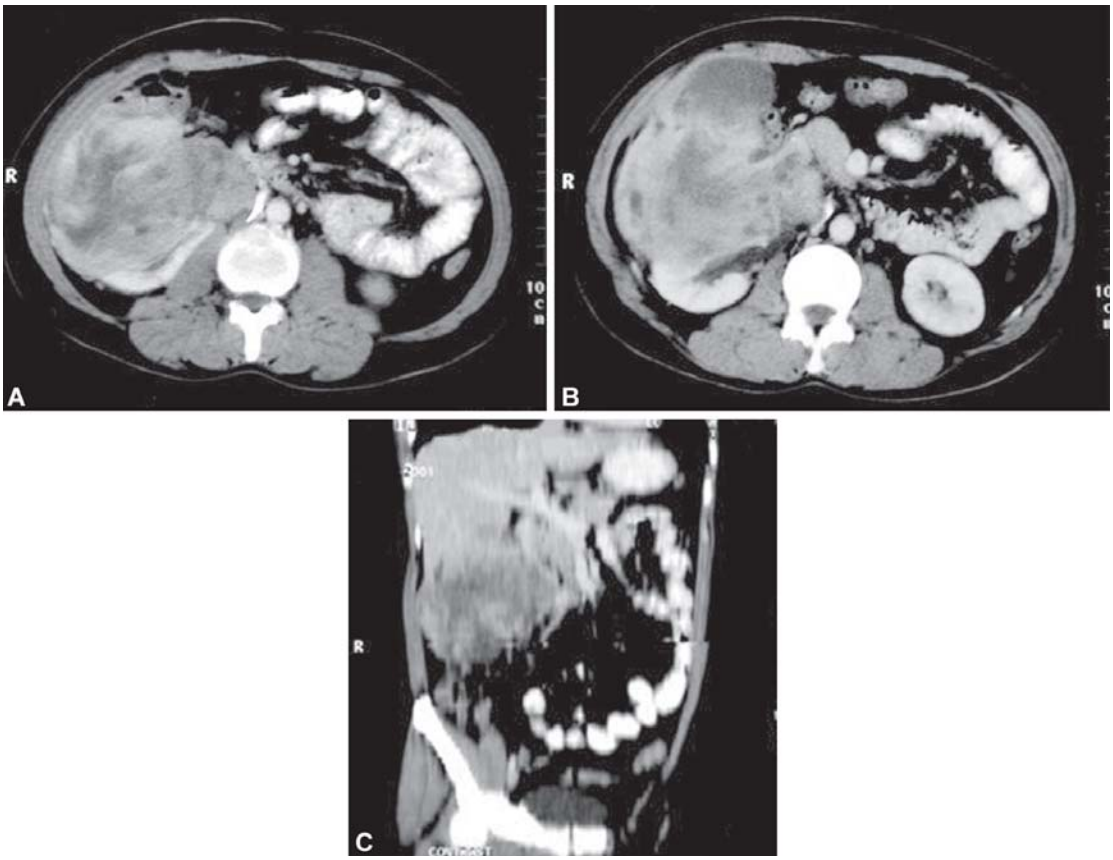

Figs 11.16A to C: CECT abdomen-axial **(A and B)** and MPR **(C)** direct infiltration from right renal mass into liver, gallbladder fossa,duodeneum and colon-stage IV

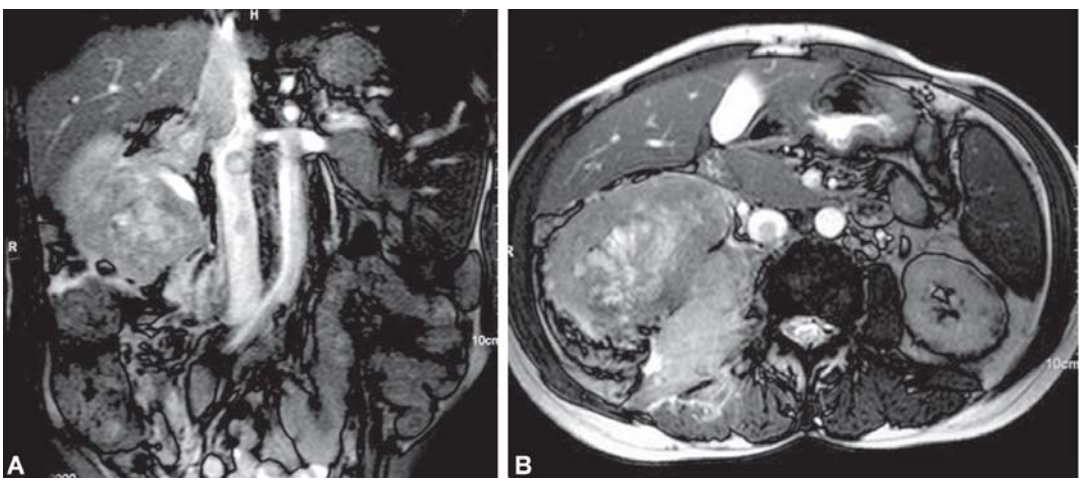

Figs 11.17A and B: T2 TRUE-FISP coronal **(A)** axial **(B)** extension of the renal mass into right renal vein which is enlarged and into the IVC. Direct infiltration into the psoas is also noted

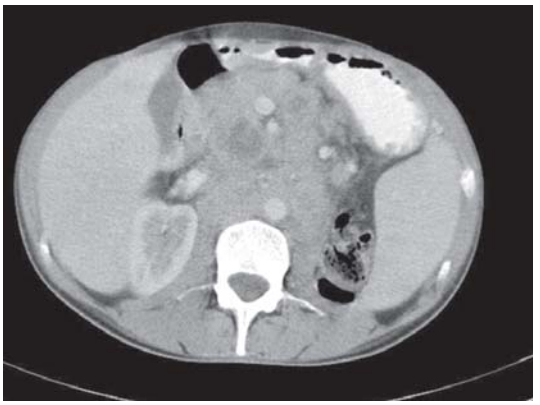

Fig. 11.18: CT abdomen in a postoperative case of RCC, presenting 1 year later with metastatic retroperitoneal lymphadenopathy

structures (Fig. 11.18). Solid organ recurrence also occurs in liver, contralateral kidney or adrenal. FDG-PET may also play a role in follow up with a high positive predictive value.

Stages I and II are treated surgically with a partial or radical nephrectomy. Stage III lesions are usually treated with radical nephrectomy with extirpation of tumor filled veins, tumor thrombectomy, and local lymph node excision. Patients with stage IV are treated palliatively. Renal sparing surgery is now becoming a widely accepted method for removing small cancers. Although partial nephrectomy is offered to patients of bilateral tumors or solitary kidney, it is now being offered to all patients with renal lesions less than 4 cm even in the setting of a normal contralateral kidney. These patients have a decreased risk of chronic renal insufficiency and proteinuria. Image guided percutaneous radiofrequency ablative therapies are also being used. This is to treat patients who are high-risk for surgery and to preserve renal function in multifocal disease. The central tumors are more difficult to ablate than the peripheral exophytic ones.[12]

UROTHELIAL TUMOR

Transitional Cell Carcinoma

Urothelial tumors are less common in the upper urinary tract than renal cell carcinoma. However, TCC is the second most common renal neoplasm in adults. It is most common in urinary bladder, followed in frequency by ureter and pelvis. They may be bilateral in 10 percent and multicentric in 20-44 percent. This known multifocality warrants that the entire collecting system must be evaluated in patients with upper tract TCC because of high prevalence of tumor in the lower tract.

The risk factors for TCC include NSAID abuse, tobacco use or some occupational exposure. The incidence of TCC is more common in males, in the seventh decade. They commonly present with hematuria and flank pain. Hematogenous spread is less common than RCC, but lymphatic spread occurs earlier. High grade tumors are more common in upper tract than the urinary bladder. It has been suggested that stage rather than tumor grade is the main prognostic factor for urothelial tumor of the upper tract.

IVU

This is the primary investigative modality. The findings include a filling defect outlined by excreted contrast. The filling defect may be in pelvis (35%) or calyces (26%). 'Stipple sign' may be seen due to trapping of contrast in the interstices of a papillary growth. There may be obstruction of kidney with non opacification of the collecting system (phantom calyx) due to extensive areas of parenchymal infiltration. Calices may be amputated or obliterated due to malignant infundibular structuring. Calices may be distended with tumor –"oncocalices"

None of the signs on IVU are pathgnomic and can be simulated by a blood clot, radiolucent stone and granuloma.

Retrograde or percutaneous antegrade pyelography may be useful in such situations to delineate the site of obstruction and to obtain brush biopsy.

Ultrasonography

A large TCC is seen as an iso- to hypoechoic solid mass separating the central sinus echoes. A small TCC may not be detected on USG. Focal enlargement of renal cortex suggests infiltration of renal parenchyma. Other non specific findings include hydronephrosis, pyelocaliceal wall thickening. USG can help differentiate a radiolucent calculus from a tumor. It cannot differentiate from a blood clot unless followed up to show change (Fig. 11.19).

CT and MRI[13-15]

CT and MRI urography have increased the diagnostic confidence; however mucosal detail is still best seen on IVP and RGP. For CT or MRI evaluation, images should be obtained to include images in excretory phase (3 to 5 minutes after injection) to show a low attenuation mass involving the collecting system or ureter, as outlined by concentrated dense contrast.

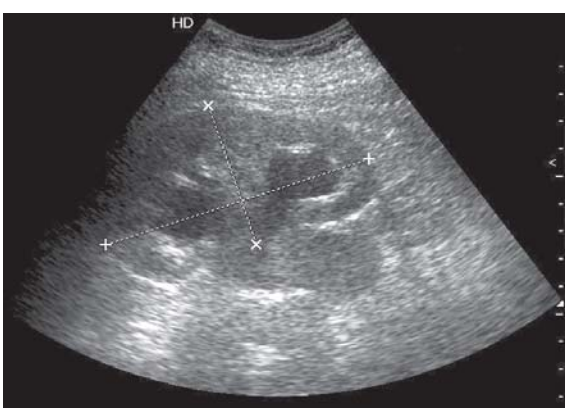

Fig. 11.19: Longitudinal sonogram of the left kidney shows a solid lesion in the renal pelvis and upper ureter with consequent hydronephrosis—Transitional cell carcinoma

There are three appearances on CT of a small TCC, the most common is of a small hypodense lesion in the renal collecting system, the lesion has a soft tissue attenuation (< 40 HU), less than most renal calculi, the attenuation of TCC is slightly lower than a blood clot, but higher than urine. TCC will enhance approx 10-50 HU, with the enhancement being less than renal parenchyma. This mild enhancement helps differentiate it from blood clot and calculi (Figs 11.20A to C). In the kidney, TCC is usually more central than RCC, owing to the origin in the urothelium. TCC does not commonly involve the renal vein, through rare cases of IVC involvement have been reported. The central mass expands the kidney symmetrically and with centrifugal extension preserves the shape. The soft tissue component in the renal sinus obliterates and displaces intervening fat to merge with the renal parenchyma,an appearance described as 'faceless' kidney.[16] This is similar to the appearance on CT of a duplicated system.

TCC may present as a locally aggressive infiltrative renal mass, margins being ill defined. Involvement of renal parenchyma may be seen as a hypoenhancing mass involving parenchyma or heterogeneous abnormal hypoenhancement disrupting the normal parenchyma. A different appearance is thickening of collecting system, Urothelium or ureteral wall. The thickening may be asymmetric or eccentric which may cause focal obstruction.

MR appearance of TCC is of a small focal lesion involving renal pelvis or caliceal system. TCCs are typically isointense relative to renal medulla on T1WI, making the detection of

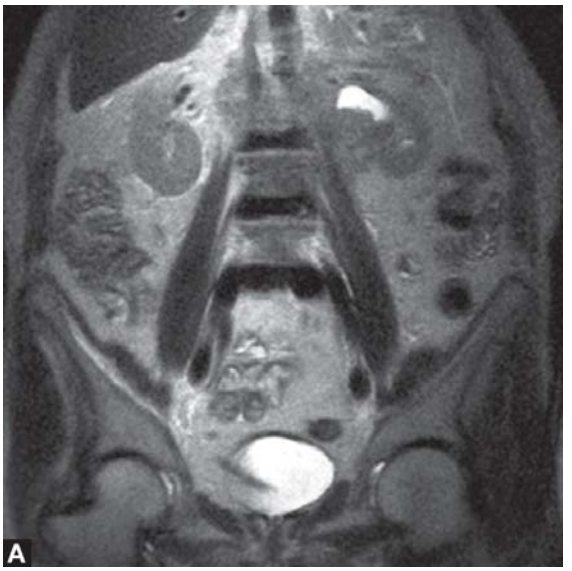

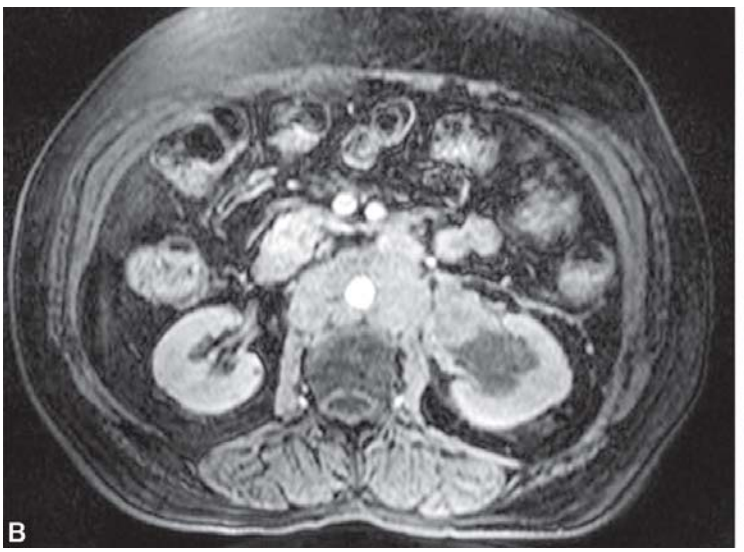

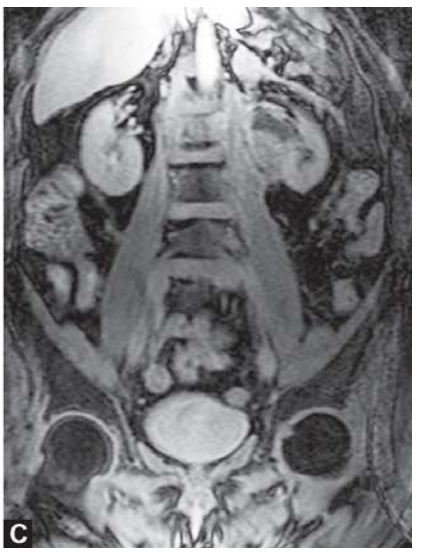

Figs 11.20A to C: MRI T2 TRUE FISP coronal **(A)** T1 VIBE, post-gadolinium axial **(B)** and coronal **(C)** shows an enhancing mass in the renal pelvis with hydronephrosis and retroperitoneal adenopathy—TCC

small tumors virtually impossible. Larger infiltrative tumors may obliterate the fat in the renal sinus. This may be appreciated on T1WI. Bright signal intensity due to urine in the collecting system on T2-weighted images provides excellent soft tissue contrast for detection of TCCs which are seen as hypointense filling defects. Infitrative TCCs may be seen on single shot T2WI as intermediate signal intensity mass infiltrating the renal parenchyma. Enhancement of a focal filling defect in the collecting system is strongly suggestive of TCC.[6] A cup-shaped dilatation of the ureter just distal to a focus of TCC in

the ureter may be seen which is called as "chalice/goblet" sign.[17]

Staging

Staging of TCC in upper urinary tract has different prognostic indications (Table 11.4). Carcinoma *in situ* and tumors limited to submucosa have best prognosis. Tumors beyond subepithelial tissue (stage II) and muscularis (stage III) have worse prognosis. CT cannot accurately distinguish T1 (limited to oroepithelium and lamina propria) from T2 (extending into musularis propria). Indications of stage III disease are parenchymal involvement or peripelvic and periureteral fat involvement.

Focal infiltrative renal lesion may mimic RCC or tuberculosis. TCC tends to be more centrally located and is more likely to expand the kidney centrifugally, while preserving the shape, the coexistence of a stone is a pointer towards SCC. A small area of parenchymal infiltration with papillary necrosis, is a major clue suggesting TB.

Squamous Cell Carcinoma

Squamous cell carcinoma of the renal pelvis is relatively rare tumor. It is highly aggressive, with a poor clinical prognosis. Chronic infection and calculi are implicated in its etiology. It often involves the renal parenchyma and perinephric tissue and may present with metastasis. Intravenous urography may reveal nonvisualization, hydronephrosis, a central mass or a pelvicaliceal filling defect seen in 83 percent of patients. In cross sectional imaging, this cannot be differentiated from transitional cell carcinomas. Pointers towards the diagnosis of SCC include the fact that SCC grow fast, and rapid progression on sequential studies favor SCC. As SCC develops following metaplasia due to chronic inflammation, in up to 50 percent cases renal calculus is noted.

Collecting Duct Carcinoma (Bellini Duct Carcinoma/Renal Medullary Carcinoma)[18,19]

This is a rare tumor arising from the cells lining the epithelium of the distal collecting tubule. The mean age of presentation is mid-fifties with complaints of hematuria. It is an aggressive tumor with poor prognosis. On CT, it is solid or complex-solid and cystic mass in the central portion of the kidney. Slightly hyperdense on CECT, it enhances less than renal parenchyma. On MRI, it is isointense on T1WI and appears hypointense on T2,

Table 11.4: Staging of transitional cell Ca

AJCC	*Disease extent*	*TNM*
0	Noninvasive papillary carcinoma	Ta
1/A	Carcinoma invading the subepithelial tissues	T1
II/B	Invasion of the muscularis	T2
III/C	Extension beyond the muscularis into peripelvic or periureteric fat or extension into the renal parenchyma	T3
IV	Invasion of adjacent organs or extension into perinephric fat (or any nodal or distant metastasis)	T4

which suggests the diagnosis. It has a right kidney predilection (82%). Renal medullary carcinoma is similar and arises from caliceal epithelium, in or near the renal papilla, from which it grows in an infiltrative pattern. It is seen in young African-American children and adults, seen exclusively with patients of sickle cell trait and commonly has metastasis at time of presentation.

Renal Sarcoma[3]

Renal sarcomas arise from the renal parenchyma or the capsule. They are most common in patients more than 40 years of age, and they present with hematuria, abdominal distention, weight loss or pain. Leiomyosarcoma is the most common type of renal sarcoma, comprising half of all renal sarcoma. It is commonly located in the retroperitoneum or the perinehric space. On CT these tumors are heterogeneous with variable enhancement pattern. Liposarcoma of the kidney arises from the renal capsule and appears as a large retroperitoneal mass with macroscopic fat.

Lymphoma

Renal lymphoma is usually a part of systemic disease and associated with adenopathy or involvement with other organs such as liver and GIT. Extranodal spread of lymphoma often affects the genitourinary system with the kidneys, being most commonly involved organ. Non-Hodgkin's lymphoma is more common than Hodgkin's lymphoma in renal involvement.

Renal involvement is often asymptomatic, detection usually occurs at imaging studies. The incidence at autopsy being as high as 41.6 percent. Despite the high prevalence, imaging studies demonstrate involvement in only 3-8 percent of patients.

Renal lymphoma has a variety of imaging appearances depending on the pattern of tumor proliferation. Malignant lymphocytes reach the renal parenchyma by means of hematogenous spread and proliferate within the interstitium, using nephrons, tubules and blood vessels as scaffolding for further growth. If it follows this infiltrative pattern, kidneys enlarge, maintaining the reniform shape. In many cases there is focal proliferation giving rise to single or more commonly bilateral renal expansile masses. Some tumors spread by means of contiguous extension from the retroperitoneal disease, penetrating the renal capsule. Renal involvement is usually bilateral, in form of nodules or diffuse infiltration, bulky single tumor, invasion from perirenal disease or microscopic invasion.

IVU is insensitive and findings when present occur late in the disease. On IVU, renal lymphoma may present as diffuse enlargement or multiple masses. Hydronephrosis or hydroureter may be seen due to displacement or obstruction to renal pelvis or ureter by lymph nodes. Poor function occurs due to diffuse and extensive involvement.

Ultrasonography[20] reveals hypo echoic solid lesions. Lymphoma masses tend to formed by large number of uniform cells. This results in a homogeneous, nearly anechoic appearance on US. This may mimic renal cysts, but there is no through transmission and subtle low level echoes may be seen. This sonographic pattern is unique to renal lymphoma (Figs 11.21A and B). It may also detect hydroureteronephrosis, adenopathy and other foci in liver and spleen. The sinus fat surrounding the central pelvicaliceal echoes may completely disappear. Large retroperitoneal nodes may be seen encasing the vessels.

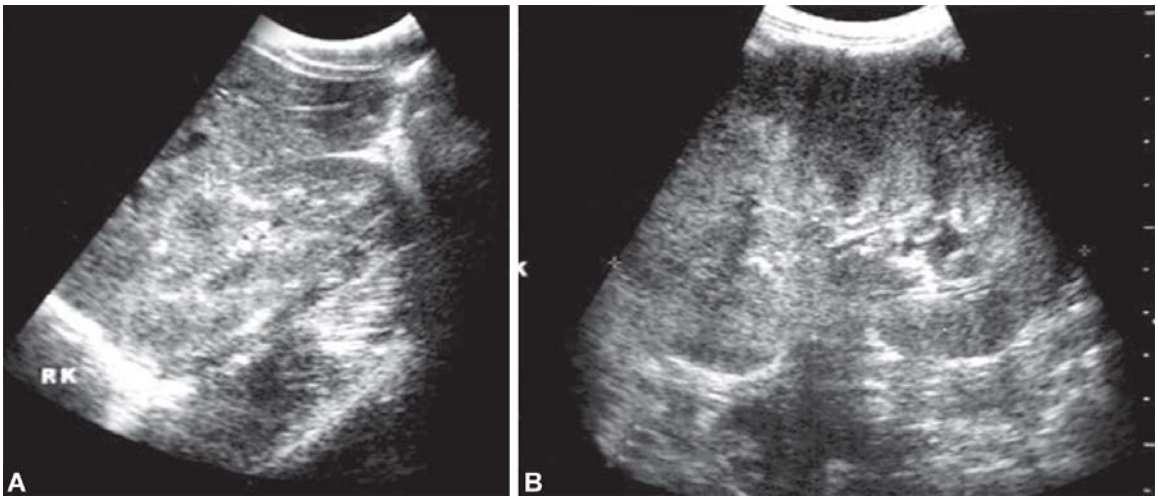

Figs 11.21A and B: USG bilateral renal enlargement with poorly defined hypo/anechoic nodules giving a homogeneous appearance—lymphoma

CT is more sensitive than ultrasound in detection of renal lymphoma. There are few common presentations.[21-23] The most common (50-60%) being of multiple focal masses which have attenuation similar or only slightly less than renal parenchyma on unenhanced images (Figs 11.22A and B). Nephrographic phase contrast CT is essential as many lesions are small and affect the medullary part of the kidney and may be missed on CM phase. After IV contrast, it enhances less than normal parenchyma. Heterogeneity and necrosis may be seen with larger lesions. Calcification is usually not seen, unless there has been therapy. Invasion into renal vein and IVC is rare.

Renal lymphoma manifests as solitary mass in 10-25 percent of patients. They characteristically demonstrate less enhancement following IV contrast differentiating them from RCC.

Contiguous involvement to kidneys or perinephric space from large retroperitoneal masses is the second most common pattern (25-30%). Perinephric involvement is noted in approximately one-third of patients, most

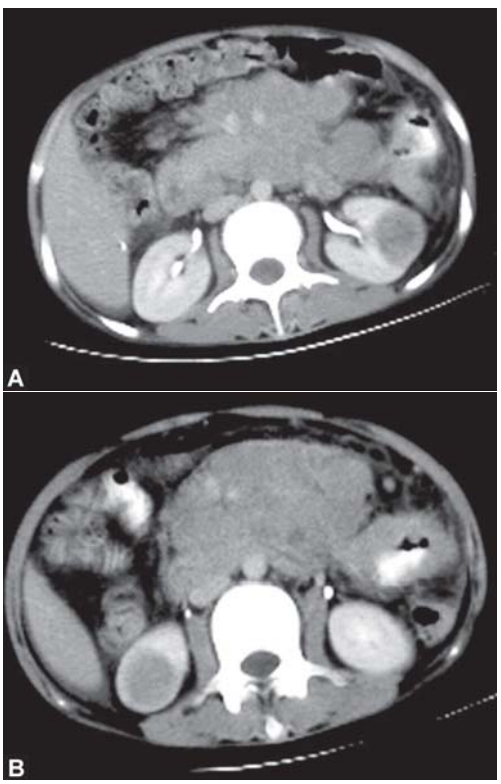

Figs 11.22A and B: Contrast enhanced CT showing well-defined focal hypodense masses in both kidneys with significant retroperitoneal adenopathy and bowel thickening—a case of lymphoma

of whom also have parenchymal involvement (Fig. 11.23).

Another appearance of renal lymphoma in a perinephric ring of soft tissue is noted around the kidney without a focal parenchymal lesion; the soft tissue is of low attenuation, compresses the renal parenchyma without significant impairment of renal function.

Diffuse renal enlargement may be seen in the infiltrative form (Fig. 11.24). There is a low attenuation mass expanding the kidney with predominent, involvement of the renal medulla, with relative sparing of cortical margins. This is more common in Burkitt's lymphoma, either disseminated or limited to the kidneys. Heterogeneous enhancement of the kidneys, with loss of normal differential enhancement is seen.

Lymphoma can affect the renal sinus preferentially. CT shows, the normal sinus fat is replaced by homogeneous soft tissue mass. The mass usually causes encasement of the renal vessels leading to poor enhancement.

Massive retroperitoneal adenopathy is often coexistent with renal lymphoma.

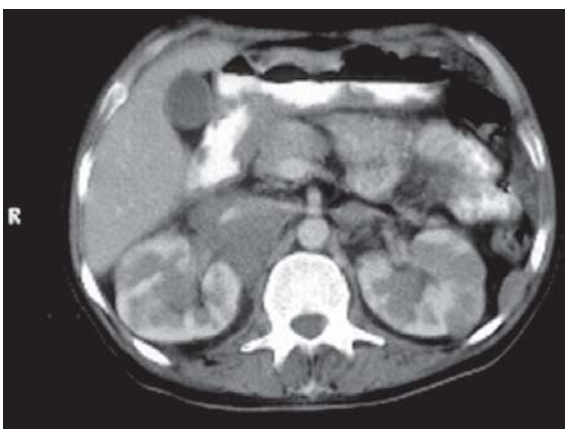

Fig. 11.23: Renal lymphoma—CECT shows multiple nodules in both kidneys with perirenal disease on the right side

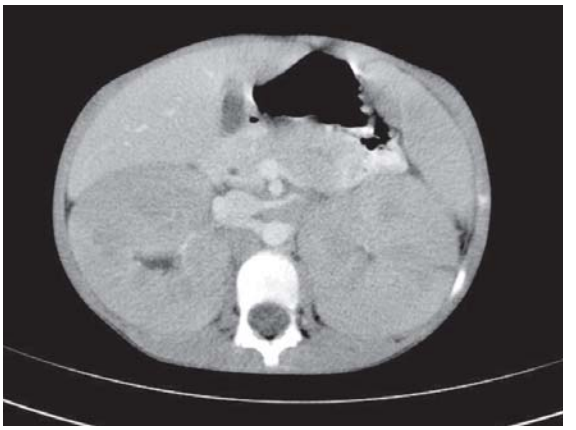

Fig. 11.24: CT abdomen—bilateral kidneys are enlarged with loss of corticomedullary differentiation—a case of Burkitts lymphoma

The morphological appearance of lymphoma on MRI is similar to that on CT. Renal lymphoma is slightly hypointense to renal parenchyma on unenhanced T1-weighted images and mildly hyperintense on T2-images. There is mild heterogeneous enhancement on post-gadolinium images, the enhancement being less than that of the normal parenchyma.

Primary renal lymphoma is extremely rare, due to lack of lymphatic tissue within the kidney. The tumor is aggressive and shows bilateral renal involvement in majority of cases. The tumor is usually a B-cell non-Hodgkin's lymphoma and affects patients who are middle aged or older. Rapid improvement and decrease in renal size is noted following the initiation of chemotherapy. In chronic lymphatic leukemia, kidney may be involved in 90 percent of cases and is associated with membranous glomerulonephritis.

In suspected cases of lymphoma FNAC or biopsy may be indicated for differentiating from other tumors. The distinction is important as lymphoma is usually treated medically.

Renal Metastasis[23]

Renal metastasis is present in approximately 10 to 20 percent of patients, in setting of other metastatic disease. Most renal metastasis are hematogeneous, although a few may be due to direct invasion (adrenal, colonic and pancreas). The most common site of primary, being lung, colon, breast, melanoma and reproductive organ malignancies. Melanoma, when present frequently metastasizes to kidney.

Metastasis are usually asymptomatic, may rarely present as hematuria.

On ultrasonography, they may be seen as hypoechoic lesions. On CT, the common appearance is of bilateral renal masses, though solitary renal metastasis are not uncommon. The lesions measure 20 to 44 HU on enhanced CT and have minimal enhancement after IV contrast of 5 to 15 HU. Large solitary renal metastasis disrupt renal cortical margins) may be associated with breast, lung or colon carcinomas. Direct involvement of perinephric space by metastasis, representing usually lymphatic spread is noted in metastasis from melanoma and lung carcinoma. Hemorrhagic renal metastasis is seen in melanoma and pheochromocytomas.

There may a diagnostic dilemma between RCC versus metastasis (Figs 11.25A and B). Renal metastasis are usually bilateral (50%), solitary metastasis may resemble RCC, which however has no necrosis. Hyperenhancement and renal vein involvement favors RCC. The margination of metastasis is often less well defined than in RCC.

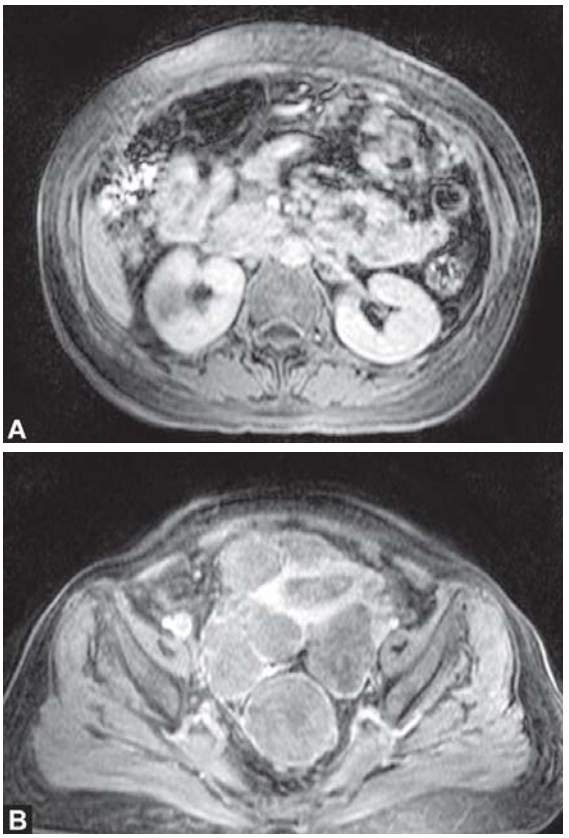

Figs 11.25A and B: MRI T1 vibe post contrast a focal poorly enhancing mass in the right kidney **(A)**, Renal metastasis from disseminated ovarian malignancy **(B)**

Oncocytoma

Renal oncocytoma is a benign solid non-fat containing renal mass, accounting for about 5 percent of renal cortical neoplasm. It is a benign renal epithelial tumor, arising from proximal tubule with many characteristics of RCCs. Oncocytomas are histologically composed of large cells (oncocytes) with mitochondria rich cytoplasm. The appearance of a typical oncocytoma cannot be reliably differentiated from RCC.[3,24,25]

Most oncocytomas are asymptomatic (80%), but few may present with hematuria pain or mass. The peak age of incidence is in the seventh decade with a male preponderance. The incidence of oncocytomas is higher in incidentally discovered renal masses, as compared with patients who have urinary symptoms. They may be quite large at time of presentation. Oncocytoma appear

as well demarcated, unencapsulated, fairly homogeneous renal cortical tumors. Bilateral multiple oncocytomas are seen in hereditary syndromes of renal oncocytosis.

Ultrasonography may show a central stellate scar within a solid hematogenous mass. On CT, they are solid, well-marginated tumors, slightly hypodense to renal parenchyma on unenhanced images. Some may exhibit a central low attenuation scar seen with branched appearance. However, central necrosis with RCC may mimic this. Renal capsular pathological invasion into perinephric fat occurs in 11 percent. There should be no adenopathy or vascular invasion. The presence of a central scar, absence of calcification or necrosis and hemorrhage suggests the diagnosis, though there is no specific CT finding to differentiate oncocytoma from RCC, and surgery is usually performed for these (Fig. 11.26).

The MRI appearance is of a hypo- to isointense (22%) mass on T1W images with high signal on T2WI, enhancing homogeneously after IV gadolinium and may exhibit spokewheel pattern of enhancement. The central scar, if present is hypointense on T2 vis-a-vis hyperintensity of necrotic RCCs on T2W images. A spokewheel pattern of feeding arteries associated with a homogeneous nephrogram is a characteristic finding on catheter angiography.

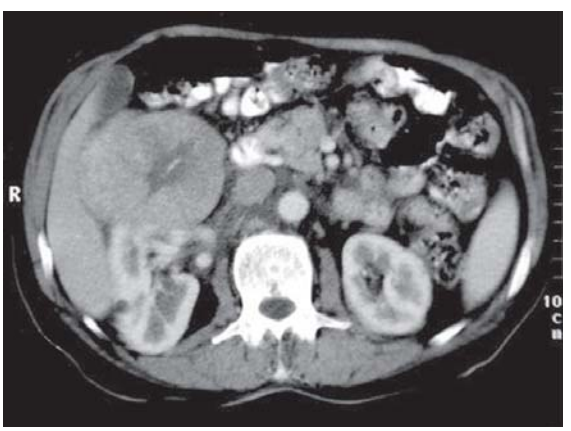

Fig. 11.26: CT-well defined, homogeneously enhancing mass right renal with a central scar-oncocytoma

In absence of previously and documented oncocytoma or stability of lesion, nephron sparing surgery is done.

Renal Adenomas

Papillary adenomas are the most common renal epithelial neoplasm. According to autopsy series, approximately 40 percent of patients above the age of 70 harbor renal adenoma. Papillary adenoma are also found in patients with acquired renal cystic disease and in those undergoing long-term hemodialysis. They are seen in about 15 percent of kidneys at autopsy and usually occur as cortical sub-capsular tumors less than 1 cm. They are indistinguishable from RCCs. According to some authors, renal adenoma is an earlier stage of evolution of renal cell carcinoma. By definition, papillary adenomas measure 5 mm or less.[26,27]

Metanephric adenoma is a benign neoplasm with a peak age in 5th-6th decades. Polycythemia, a characteristic finding seen in 10 percent disappears after surgery. Metanephric adenoma typically occurs as a well-defined, unencapsulated, solitary solid mass. Metanephric adenomas display hypovascularity and delayed, minimal enhancement.

MIXED EPITHELIAL AND STROMAL TUMORS (MESTs)[3,26]

This comprises of tumors previously referred to as hamartoma, adult mesoblastic nephroma. They are seen almost exclusively in perimenopausal women, most patients receiving estrogen therapy. Most present incidentally and are believed to be a hormonally dependent tumor. MESTs are characte-

rized by variegated imaging patterns including complex cysts, mixed solid cystic masses that show delayed and heterogeneous enhancement. On MR imaging the degree of delayed enhancement and T2 hypointense signal is dependent on the stromal component.

CYSTIC NEPHROMA

These are rare benign neoplasms that also show a female preponderance. Most patients are asymptomatic. Cystic nephromas are predominantly unilateral, well circumscribed cystic lesions with thin septations. Hemorrhage or urinary obstruction may be caused by the prolapse of the cystic mass into the renal pelvis.

ANGIOMYOLIPOMA

These benign lesions are mesenchymal neoplasms (hamartomas), representing excess growth of mature fat, smooth muscle and thick walled blood vessels, the amount of each component being variable. AMLs are now grouped under a family of tumors characterized by the proliferation of perivascular epitheloid cells (PEComas).[28]

Tuberous sclerosis is the most commonly associated syndrome. Multiple and bilateral angiomyolipomas should suggest the diagnosis of TS. Approximately 80 percent of patients with TS have angiomyolipoma, only 20 percent of cases of angiomyolipomas, subsequently are diagnosed TS. Angiomyolipomas may rarely be associated with NF-I, von Hippel Lindau or ADPKD. TS associated AML are asymptomatic, young patients without sex predilection. AML associated with TS are often multiple, bilateral and larger at the time of presentation. These are also likely to grow and be symptomatic. They may be sporadic tumors, commonly detected in females in 5th to 7th decades.

AML may originate from the cortex or the medulla. The tumor is usually well defined, and calcification and necrosis. They appear as large, heterogeneous masses with varying amount of macroscopic fat, intralesional aneurysms and hypervascular soft tissue. Angiomyolipomas are composed of thick walled inelastic blood vessels, risk of intratumoral and perinephric hemorrhage is higher in lesion > 4 cm diameter.

Plain abdominal radiography may show distinctive radiolucency, within a large soft tissue mass with lot of fat, in 10 percent of patients. Ultrasonography reveals highly, echogenic circumscribed mass (more echogenic than central fat). It may appear as echogenic fat within a tumor or isolated foci of echogenicity (Figs 11.27A and B, 11.28A and B). If fat content is less or admixed with hemorrhage, the echogenicity of tumor is diminished, and may appear as any other renal mass. Recent work has suggested that 32 percent of renal carcinomas are also highly reflective, although there are other pointers towards RCC such as hyporeflective rim or focal small spotty areas of reduced central reflectivity. Another feature that helps in distinguishing an angiomyolipoma from a small RCC is posterior shadowing, seen in approximately 30 percent of AML, but is not seen in small hyper-reflective renal carcinomas.

CT is the most accurate imaging technique for detection and characterization of angiomyolipomas.[29,30] The lesions show low attenuation with fat measurements and presence of gross fat being typical for these. The ROIs are typically less than –10 HU. Thin slices are necessary to demonstrate fat in small AMLs because of volume averaging. Higher specificity may be obtained with threshold measurements of –15 to –30 HU.

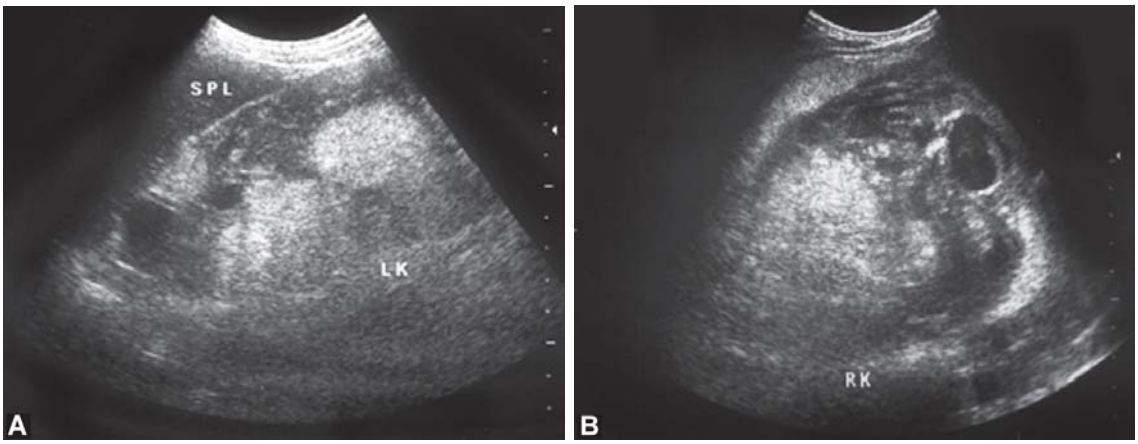

Figs 11.27A and B: Multiple well defined homogeneously hyperechoic lesions with no perilesional halo in both left and right kidneys—Angiomyolipomas

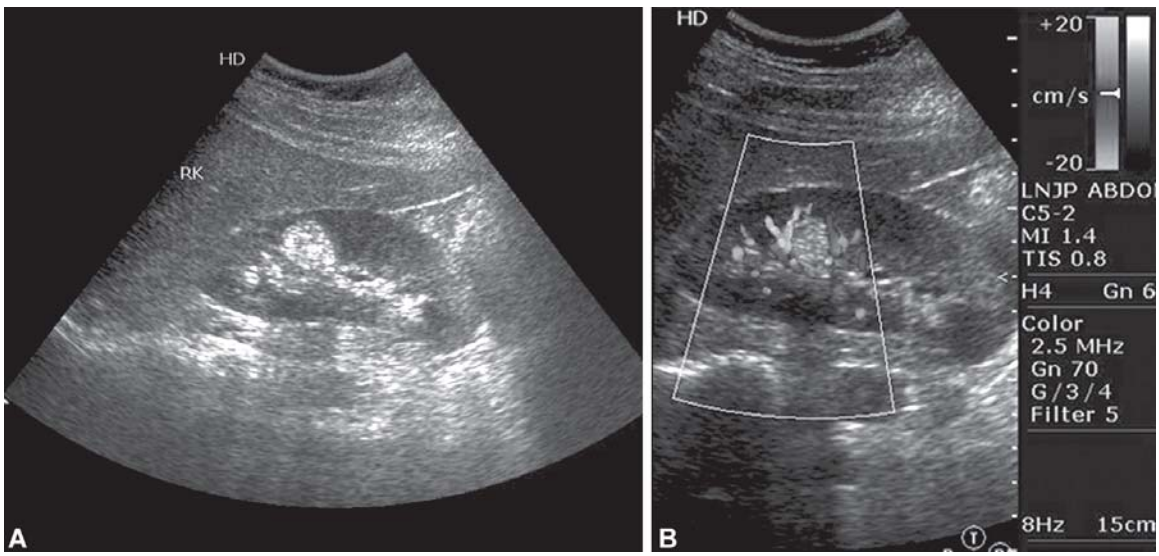

Figs 11.28A and B: USG **(A)** and color Doppler **(B)** show a small well-defined hyperechoic lesion in the right kidney with peripheral vascularity—Angiomyolipoma *(For color version see Plate 16)*

The fat may be interposed with solid components. A subset of lesions will not meet fat attenuation criteria due to volume averaging or hemorrhage, others are fat poor and rarely a well-differentiated RCC can mimic this appearance. CT pixel mapping[31], over a region of interest within the tumor may be useful to detect small quantities of fat. With pixel mapping, three to six contiguous pixels with negative Hounsfield units averaging below –20 HU indicates intratumoral fat (Figs 11.29 to 11.31A and B).

The presence of typical AML in the contralateral kidney helps in the diagnosis. AMLs are usually well-marginated, but do not have a true capsule, the lesion is usually at the margin of the kidney and may expand beyond as a small hypodense wedge-shaped defect

in the renal parenchyma. This wedge-shaped defect is diagnostic of angiomyolipoma. These lesions are vascular, large vessels may be identified. Intratumoral aneurysms may be present and AML's exhibit moderate enhancement after IV contrast. Homogeneous and prolonged enhancement is a valuable predictor for differentiating AML with minimal fat from RCC.

MRI will also demonstrate fat component of an angiomyolipoma. On MRI, AMLs have a characteristic high T1-signal and on fat saturated images exhibit a drop in signal. The use of in –phase and opposed phase imaging is also helpful in the diagnosis of angiomyolipoma. In AML, a characteristic India Ink artifact is seen at the interface between the mass and the normal renal parenchyma on opposed phase T1 images, whereas the central part of the lesion does not demonstrate changes in signal intensity compared with in phase images. This is useful in very small lesions in which direct comparison with T1 images with and without fat suppression may be difficult (Figs 11.32A to F). The appearance of AML on T2-weighted images is variable and depends on bulk fat present

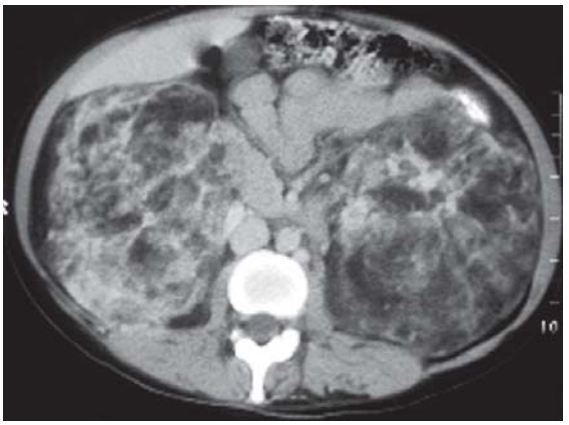

Fig. 11.30: CECT showing large heterogeneous soft tissue masses in both kidneys with fat density scattered throughout and enlarged vessels—a case of tuberous sclerosis

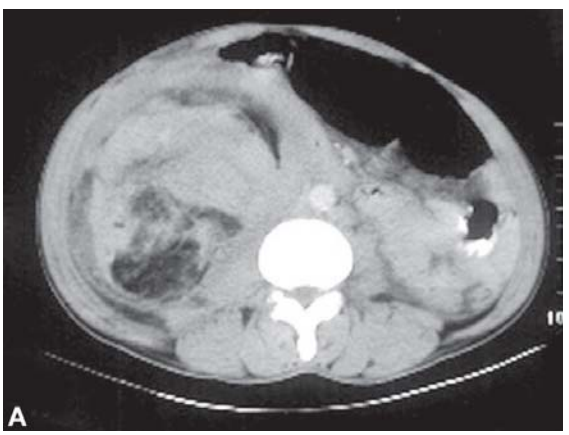

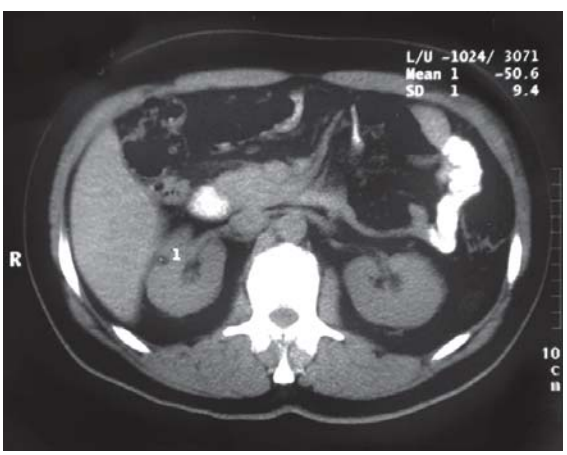

Fig. 11.29: CT shows a small pinhead lesion in right kidney with fat attenuation S/o AML

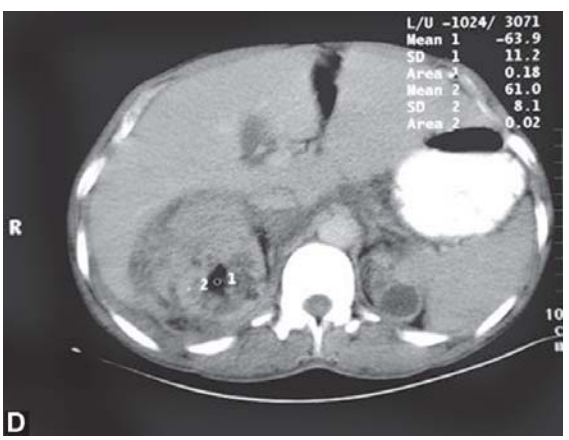

Figs 11.31A and B: CT showing bilateral large fat attenuation lesions with enhancing soft tissues and perilesional hemorrhage—AML

in the lesion. An AML composed of predominantly fat would demonstrate homogeneous high-signal at T2 single shot images. Lipid poor angiomyolipomas are frequently hypointense on T2-weighted images. This may help to differentiate from RCC which will be T2 hyperintense.[32]

Angiography may demonstrate multiple aneurysms and onion layer appearances. Approximately 58 to 75 percent of these lesions grow with time. Growth of an isolated AML without TS is less than those with TS and multiple lesions. Annual follow-up is recommended for asymptomatic lesions < 4 cm. For larger lesions, due to risk of hemorrhage, semiannual evaluation is suggested. Even small AMLs may rarely bleed. For large symptomatic lesions embolisation may decrease risk of hemorrhage.

Pathological differentiation between a well differentiated liposarcoma from a angiomyolipoma may be difficult, unless radiological appearance is considered.[33] Liposarcomas, are rare, seen in older patients, are larger at time of diagnosis and are centered at perinephric space or capsule rather than intraparenchymal like AML. They are hypovascular, without enlarged vessels and aneurysms. The renal parenchymal defect in AML as stated earlier is not seen in well-differentiated liposarcomas, which will displace, compress and distort the kidney, but will not invade renal parenchyma. It is important to assess the relationship of fat to remainder of tumor, such that fat is intratumoral and not perirenal fat engulfed by a growing RCC.

PNET OF THE KIDNEY

This is a highly aggressive renal neoplasm, belonging to the Ewing's family of tumors. Patient is usually a young adult. Although radiological features, such as presence of tumor thrombus, proximity to neural foramina have been described,[34] diagnosis is based on histology and immunocytohistochemistry.

Biopsy[2,3,35]

Traditionally, percutaneous biopsy has played a limited role in evaluation of all solid renal tumors. This procedure is usually reserved done for patient with known extrarenal malignancy and a solitary renal mass. This will enable differentiation from RCC, which is to be treated surgically, from a solitary metastasis which can be treated nonsurgically. Percutaneous biopsy is to be avoided in renal infiltrating neoplasms, as there is a risk of needle track seeding, especially in transitional cell carcinomas. Percutaneous biopsy should not be relied upon completely to differentiate between benign and malignant tumors. This is especially so for differentiation of oncocytoma and RCCs, for some RCCs contain oncocytic components that are indistinguishable from those in benign oncocytoma. The results may be inconclusive in excluding RCC. Recent studies have, however shown that image guided biopsy of a solid enhancing renal mass is a highly diagnostic procedure. When percutaneous renal mass biopsy is indicated, it has been shown that core needle biopsy is more accurate than FNACs.

Incidental Solid Renal Mass

The increased incidence of incidental renal masses with cross sectional imaging poses problems to the radiologist and the physician. When encountering a renal mass, a benign lesion like angiomyolipoma needs to be

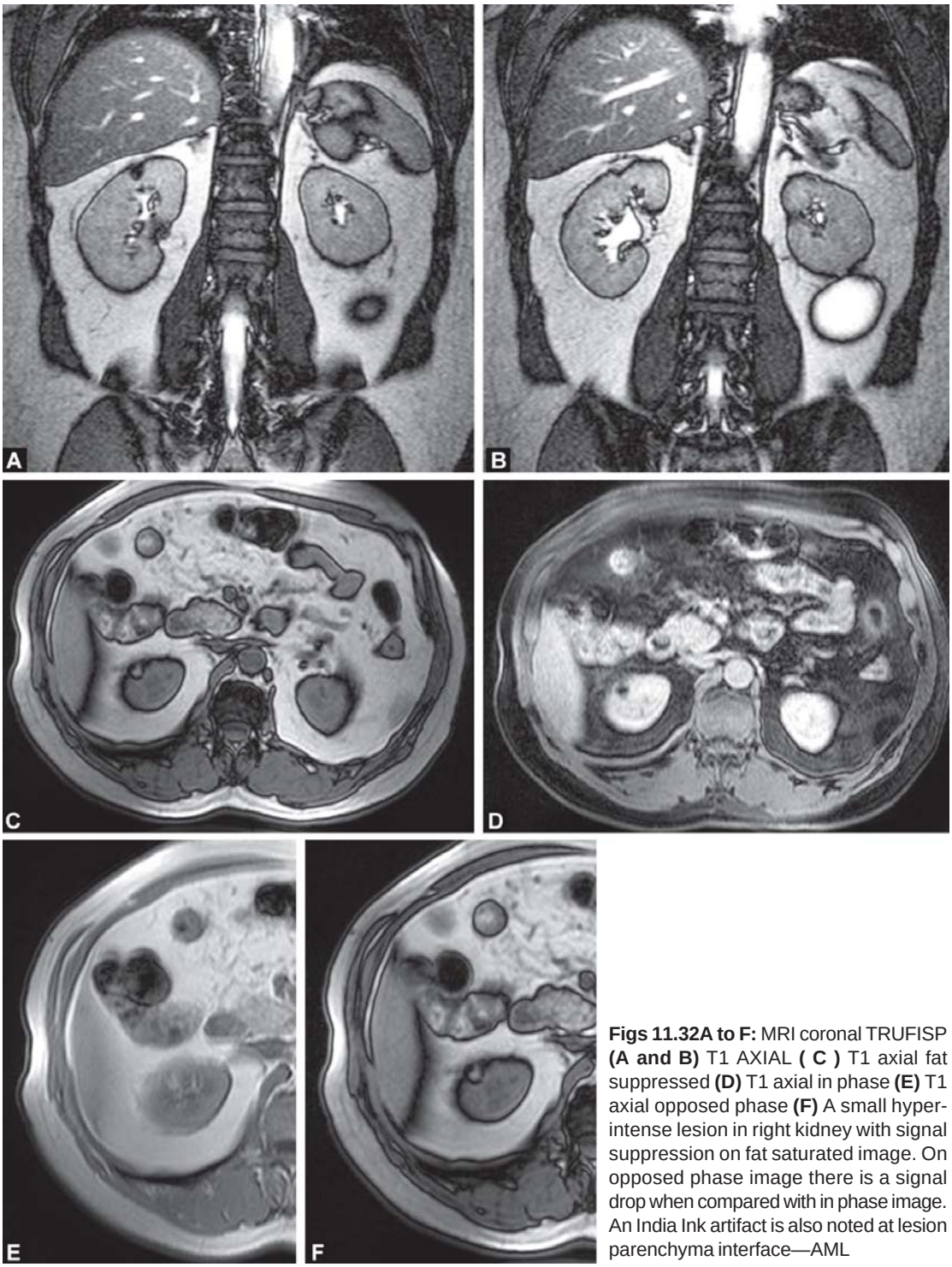

Figs 11.32A to F: MRI coronal TRUFISP **(A and B)** T1 AXIAL **(C)** T1 axial fat suppressed **(D)** T1 axial in phase **(E)** T1 axial opposed phase **(F)** A small hyperintense lesion in right kidney with signal suppression on fat saturated image. On opposed phase image there is a signal drop when compared with in phase image. An India Ink artifact is also noted at lesion parenchyma interface—AML

excluded. Differentiation from a RCC is necessary. CT, thin section CT, for small lesions and MRI including chemical shift imaging may be required. Hyperattenuating enhancing lesions may represent other benign tumors like, oncocytoma, metnephric adenoma.

If a large >3 cm solid mass is discovered, renal cell carcinoma (provided there is no fat on CT/MR protocols) is the most probable diagnosis and surgery is recommended. If the tumor is 1-3 cm in size, RCC is most likely though percutaneous biopsy may be required. Very small lesions < 1 cm are more likely to be benign; thin sections (< 3 mm) may help. Obsevation and follow up CT/MR at 3-6 months, then at 12 months and then yearly may be done.[36]

CT is the imaging modality of choice for evaluating renal tumor. When a proper technique is used CT provides a high degree of accuracy in detecting renal mass. Certain imaging features and enhancement pattern may help distinguish various subtypes of renal tumors. It also provides diagnostic information for treatment planning and follow up. MR imaging is a rapidly evolving tool, currently valuable as a problem-solving tool.

REFERENCES

1. Eble JN, Sauter G, Epstein JI, Sesterhenn IA (Eds). World Health Organisation Classification of Tumors: Pathology and Genetics of Tumors of the Urinary System and Male Genital Organs. Lyon, France IARC Press, 2004.
2. Zhang J, Lefkowitz RA, Bach A. Imaging of kidney career. Radiol Clin North Am 2007; 45-119-47.
3. Maki DD, Birhbaum BA, Chakraborty DP, et al. Renal cyst pseudo enhancement: Beam hardening effects on CT numbers. Radiology 1999; 213(2):468-72.
4. Welch TJ, LeRoy AJ. Helical and electron beam CT scanning in the evaluation of renal vein. Involvement in patients with renal cell carcinoma. J Comput Assist Tomogr 1997;21(3):467-71.
5. Pedrosa I, Sun MR, Spencer M, et al. MR imaging of renal masses: correlation with findings at Surgery and pathologic analysis. Radiographics 2008;28:985-1003.
6. Pedrosa I, Chou MT, Ngo L, et al. MR classification of renal masses with pathological correlation. Eur Radiol 2008;18:365-75.
7. Zang J, Tehrani YM, Wang C, et al. Renal masses: characterisation with diffusion weighted MR imaging—a preliminary experience. Radiology 2008;247(2):458-64.
8. Ramdave S,Thomas GW, Berlangieri SU, et al. Clinical role of F18 flurodeoxyglucose positron emission tomography for the detection and management of renal cell carcinoma. Urol 2001; 166(3):825-30.
9. Johnson CD, Dunnick NR, Lohan RH, et al. Renal adenocarcinoma: CT staging of 100 tumors. Am J Roentgenal 1987;148:59-63.
10. Levine E. Renal cell carcinoma Radiological diagnosis and staging: Semin Roentgenol 1987;22:248.
11. Hallscheidt PJ, Bock M, Riedasch G, et al. Diagnostic accuracy of staging renal cell carcinomas using multidetector row computed tomography and magnetic resonance imaging : a prospective study with histopathological correlation. J Comput Assist Tomogr 2004; 2833-39.
12. Boss A, Clasen S Kuczyk M, et al. Image guided radiofrequency ablation of renal cell carcinoma. Eur Radiol 2007;17:725-33.
13. Gatewood OM, Goldman SM, Marshall FF, et al. Computerised tomography in the diagnosis of transitional cell carcinoma of the kidney. J Urol 1982;127(5):876-87.
14. Parienty RA, Ducellier R, Pradel J, et al. Diagnostic valve of CT number in pelvicaliceal filling defects. Radiology 1982;145(3):743-47.
15. Leo ME, Petrou SP, Barrett DM. Transitional cell carcinoma of the kidney with vena caval involvement: Report of 3 cases and a review of the literature. J Urol 1992;148(2 Pt 1):398-400.
16. Hulnick DH, Bosniak MA. 'Faceless kidney' CT sign of renal duplicity. J Comput Assit Tomogr 1986;10:771-72.

17. Daniels RE. The Goblet Sign (3rd). Radiology 1999;210:737-38.
18. Peyromaure M, Thiounn N, Scotte F, et al. Collecting duet carcinoma of the kidney: A clinicopathological study of 9 cases. J Urol 2003; 170:1138-40.
19 Swartz MA, Karth J, Schneider DT, et al. Renal medullary carcinoma : Clinical pathological immunohistochemical and genetic analysis with pathogenetic implications. Urology 2002; (6016):1083-89.
20. Ruchman RB, Yeh HC, Mitty HA, et al. Ultrasonographic and computer tomographic features of renal sinus lymphoma. J Clin Ultrasond 1988;16:35-40.
21. Reznek RH, Mootoosamy I, Webb JA, et al. CT in renal and perirenal lymphoma: A further look. Clin Radiol 1990;42(4):233-38.
22. Urban BA, Fishman EK. Renal Lymphoma: CT patterns with emphasis on helical CT. Radiographics 2000;20:197-212.
23. Choyke PL, White EM, Zemen RK, et al. Renal metastasis: Clinicopathological and radiological correlation. Radiology 1992;159(6):1229-34.
24. Quinn MJ, Harlman DS, Friedman AC, et al. Renal oncocytoma: New observations. Radiology 1984;153:49-53.
25. Dyer R, Disantis MD, Mc clennan BL. Simplified approach for evaluation of the solid renal mass in adults. Radiology 2008;247(2):331-43.
26. Prasad SR, Surabhi VR, Menias CO, et al. Benign renal neoplasms in adults: Cross-sectional imaging findings AJR 2008;190:158-64.
27. Kiyoshima K, Oda Y, Nakamura T, et al. Multicenteric papillary renal cell carcinoma associated with renal adenomatosis. Pathol int 2004;54:266-72.
28. Prasad SR, Mino Kneudson M, Narra VR, et al. Neoplasms of the perivascular epitheloid cell including the abdomen and pelvis: Cross sectional imaging findings. J Comput Assist Tomogr 2007;31(5):688-96.
29. Bosniak MA, Meigbow AJ, Hulnick DH, et al. CT diagnosis of renal angiomyolipomas: The importance of detecting small amounts of fat. Am J Roentgenol 1988;151(3):497-501.
30. Silverman SG, Mortele KJ, Tuncali MD, et al. Hyperattenuating renal masses: Etiologies, pathogenesis and imaging evaluation. Radiographics 2007;27:1131-43.
31. Takahashi K, Honda M, Okubo RS, et al. CT pixel mapping in the diagnosis of small angiomyolipomas of the kidneys. J Comput Assist Tomogr 1993;17:98-101.
32. Isreal GM, Bosniak MA. Pitfalls in renal mass evaluation and how to avoid them. Radiographics 2008;28:1325-38.
33. Israel GM, Bosniak MA, Slywotzky CM, et al. CT differentiation of large exophytic renal angiomyolipomas and perirenal liposarcoma. Am J Roentgenal 2002;179(3):769-73.
34. Chu WC, Reznikov B, Lee YN, et al. PNET of the kidney—a rare renal tumor in adolescents with seemingly characteristic radiological features. Paediatr Radiol 2008;38(10):1089-94.
35. Maturen KE, Ngheim HV, Caoili EM, et al. Renal mass core biopsy: Accuracy and impact in clinical management. AJR Am J Reontgenol 2007; 188:563-70.
36. Silverman SG, Israel GM, Herts BR, Richie JP. Management of the incidental renal mass. Radiology 2008;249(1):16-31.

Chapter 12

Imaging of the Urinary Bladder and Urethra

Anupam Lal, Paramjeet Singh

ANATOMY

Urinary Bladder

The urinary bladder is a musculomembranous sac which acts as a reservoir for the urine; and its size, position, and relations vary according to the amount of fluid it contains. The empty bladder assumes the form of a flattened tetrahedron and when distended with fluid it becomes round or oval in shape. In adults, the normal bladder capacity is highly variable but is usually between 500 and 600 mL. The normal wall of the bladder is smooth and should be regular and uniform in thickness (typically 2-3 mm in fully distended bladder) not exceeding 6 mm in adults.

The bladder lies in the anterosuperior portion of the pelvic cavity which is separated anteriorly from the pubic rami by the fatty Retzius' space. Superiorly, the bladder is enveloped by peritoneum, which continues posteriorly and is then reflected onto the anterior surface of the rectum (anterior surface of uterus in females). The bladder is surrounded by perivesical fat; laterally, it is bordered by the obturator internus muscles and inferiorly by the prostate gland. The superoanterior portion of the bladder, the apex, is attached to the anterior abdominal wall by the median umbilical ligament, a remnant of the urachus. The posteroinferior wall, referred to as the base, is continuous with the bladder neck. The urinary bladder wall consists of smooth muscle, lamina propria, submucosa and mucosa. The muscular component of the bladder wall is composed of longitudinal and circular smooth muscle bundles that form distinct layers near the bladder neck.

The mucous membrane consists of multilayered transitional epithelium, which over the greater part of the viscus is loosely attached to the muscular coat, and appears wrinkled or folded when the bladder is contracted. Over a small triangular area, termed the 'trigone', immediately above and behind the internal orifice of the urethra, the mucous membrane is firmly bound to the muscular coat, and is always smooth. The anterior angle of the trigone is formed by the internal orifice of the urethra: its posterolateral angles by the orifices of the ureters. A ridge of muscle, the interureteric ridge, extends between the ureteral orifices and forms the posterior aspect of the trigone. In the contracted bladder the ureteric orifices are about 2.5 cm apart and about the same

distance from the internal urethral orifice; in the distended viscus these measurements may be increased to about 5 cm.

The bladder is connected to the pelvic wall by the endopelvic fascia which is strengthened by the pubovesical and rectovesical ligaments.

The arteries supplying the bladder are the superior, middle, and inferior vesical arteries, derived from the anterior trunk of the internal iliac artery. The obturator and inferior gluteal arteries also supply small visceral branches to the bladder, and in the female additional branches are derived from the uterine and vaginal arteries. The veins form a complicated plexus on the inferior surface, and fundus near the prostate, and end in the hypogastric veins. Lymphatic drainage of the bladder is primarily to the external iliac chain of lymph nodes.

Urethra

The urethra is composed of mucous membrane, supported by a submucous tissue which connects it with the various structures through which it passes.

The Male Urethra

The male urethra varies from 17.5 to 20 cm in length. It presents a double curve in the ordinary relaxed state of the penis and consists of anterior and posterior portions, each of which is subdivided into two parts. The anterior urethra extends from the external meatus to the inferior edge of the urogenital diaphragm, coursing through the corpus spongiosum. The anterior urethra is conventionally divided into the penile (or pendulous) and bulbous parts at the penoscrotal junction on the basis of clinical and imaging findings. The pendulous portion terminates in the glans penis to form the fossa navicularis, which is 1–1.5 cm long. The proximal portion of the bulbous urethra is dilated and termed the "sump" of the bulbous urethra; just proximal to the sump, the bulbous urethra assumes a conical shape at the bulbomembranous junction. This portion of the bulb is known as the "cone." The anterior urethra has periurethral Littré glands, which are more numerous at the dorsal aspect of the penile urethra and in the bulbous urethral sump. The Cowper glands are two pea-sized glands that lie within the urogenital diaphragm on each side of the membranous portion of the posterior urethra. The ducts of the Cowper glands are 2 cm long and empty into the bulbous urethral sump on either side of midline.

The posterior urethra is divided into the prostatic and membranous urethras. The prostatic urethra, the widest and most dilatable part of the canal, is about 3-3.5 cm. long, It runs almost vertically through the prostate from its base to its apex, lying nearer its anterior than its posterior surface; the form of the canal is spindle-shaped, being wider in the middle than at either extremity, and narrowest below, where it joins the membranous portion. A longitudinal ridge of smooth muscle (urethral crest) extends from the bladder neck to the membranous urethra on the posterior wall of the posterior urethra. This longitudinal ridge continues into the verumontanum, an ovoid mound (from 15 to 17 mm. in length, and about 3 mm. in height) that lies in the posterior wall of the prostatic urethra.

In the center of the verumontanum lies the prostatic utricle, a small saccular depression that is a vestigial remnant of the müllerian duct. Just distal and lateral to the utricle are the orifices of the paired ejaculatory ducts. The prostatic glands empty directly into the prostatic urethra via multiple

small openings that surround the verumontanum. The prostatic urethra then tapers distally into the membranous urethra, which is approximately 1–1.5 cm long and ends at the inferior aspect of the urogenital diaphragm.

The membranous urethra is the shortest, least dilatable, and, with the exception of the external orifice, the narrowest part of the canal. It extends downward and forward, with a slight anterior concavity, between the apex of the prostate and the bulb of the urethra, perforating the urogenital diaphragm about 2.5 cm below and behind the pubic symphysis.

The proximal (internal) urethral sphincter extends from the bladder neck through the prostatic urethra above the verumontanum. Although it is similar to the detrusor muscle, it has different neurogenic innervation. The distal (external) sphincter has both intrinsic and extrinsic components. The "intrinsic" urethral sphincter is a concentric muscular structure and lies in the distal third of the prostatic urethra below the mound of the verumontanum and surrounds the membranous urethra. Both the internal and intrinsic sphincters are composed of smooth muscle and function as muscles that maintain passive continence. The internal sphincter functions as the primary continence sphincter and the intrinsic sphincter as the secondary continence sphincter. The extrinsic sphincter is a paraurethral, striated, voluntary muscle with contributions from the levator ani complex. The sphincter surrounds the membranous urethra and is involved in active continence.

The Female Urethra

The female urethra is 4 cm long and extends from the bladder neck at the urethrovesical junction to the vestibule, where it forms the external meatus between the labia minora. It is placed behind the symphysis pubis, imbedded in the anterior wall of the vagina, and its direction is obliquely downward and forward; it is slightly curved with the concavity directed forward. Its diameter when undilated is about 6 mm. It perforates the fascia of the urogenital diaphragm, and its external orifice is situated directly in front of the vaginal opening and about 2.5 cm. behind the clitoris. Many small periurethral glands open into the urethra. Distally, these glands group together on either side of the urethra (Skene glands) and empty through two small ducts to either side of the external meatus. The proximal part of the urethral wall is made up of two layers of smooth muscle (inner longitudinal and outer circular) that are contiguous with the smooth muscle of the bladder neck. The outer portion of the urethra is composed of striated muscle, which, in the upper two-thirds of the urethra, is primarily circular and extends proximally to blend with the bladder base. The lower portion of the urethra is intimately situated next to the anterior vaginal wall and enveloped by common musculature (the urethrovaginal sphincter), which extends to the inferior pubic ramus above the urogenital diaphragm.

IMAGING MODALITIES

Various imaging modalities available for imaging of the urinary bladder and urethra include the following:

- Plain films
- Cystography
- Retrograde Urethrography (RGU)
- Voiding Cystourethrography (VCUG)
- Urodynamic studies
- Ultrasonography (US)

- Computed tomography (CT)
- Magnetic resonance Imaging (MRI)
- Radionuclide imaging

Plain Films

The role of plain films is in the detection of radiopaque calculi or foreign bodies, calcification, abnormal gas pattern and in identification of soft tissue and the bony abnormalities. A plain radiograph or fluoroscopic examination is mandatory before starting the contrast studies to identify any radiopacity (calculi, calcification or foreign body) that may be obscured with contrast subsequently. Radiolucent foreign bodies can be seen if these get encrusted with calcium. Causes of bladder wall calcification include tuberculosis, tumors, radiation cystitis, cyclophosphamide induced cystitis, alkaline incrustation cystitis, amyloidosis and schistosomiasis.[1] Bladder neoplasms may be suggested on detection of stippled calcification.

In emphysematous cystitis, the plain film typically shows gas within the bladder lumen and irregular streaky radiolucencies within the bladder wall. The presence of gas within the ureter may be seen in the setting of emphysematous pyeloureteritis or emphysematous pyelonephritis. Plain films may occasionally be helpful for the detection of metastases, spinal abnormalities in cases of neurogenic bladder and diastasis of the pubic symphysis in patients with exstrophy/epispadias anomaly.

Retrograde Urethrography (RGU)

Retrograde urethrography is considered to be the best initial study for urethral and periurethral imaging in men and is indicated in the evaluation of urethral injuries, strictures, and fistulas. The patient is placed in a supine 45° oblique position. The penis should be placed laterally over the proximal thigh with moderate traction. The patient should be reassured about the discomfort that is experienced during balloon inflation. Then, 20–30 mL of 60 percent iodinated contrast material is injected under fluoroscopic guidance through the 16- or 18-F Foley catheter (having the bulb gently inflated in fossa navicularis) so that the anterior urethra is filled. Commonly, spasm of the external urethral sphincter will be encountered, which prevents filling of the deep bulbar, membranous, and prostatic urethras. Slow, gentle pressure is usually needed to overcome this resistance. Spot radiographs are obtained when there is visual confirmation of contrast material flowing into the bladder. During RGU opacification of the prostatic ducts, Cowper ducts, and periurethral Littré glands is often, but not necessarily, associated with urethral inflammatory and stricture disease.[2] If the integrity of the urethral mucosal lining is disrupted by increased pressure during contrast material injection, intravasation of contrast material with opacification of the corpora and draining veins may occur (Fig. 12.1).

Voiding Cystourethrography (VCUG)

VCUG is the most commonly used imaging method in the evaluation of the female urethra and male posterior urethra. Voiding urethrography is usually performed after the bladder is filled with contrast material via a transurethral or suprapubic catheter. After the transurethral catheter is withdrawn, the patient voids under fluoroscopic observation and spot radiographs of the bladder and urethra are obtained. During active voiding, the bladder neck opens widely and becomes funnel shaped in both male and female

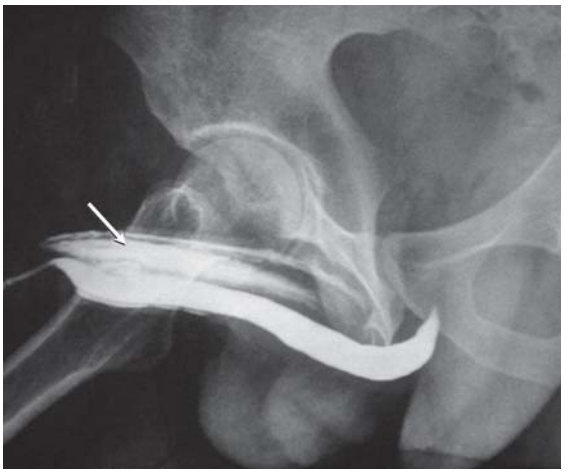

Fig. 12.1: RGU image showing opacification of the corpora (arrow) and draining veins due to increased pressure of injection

patients by means of the internal sphincter mechanism. In male patients, the verumontanum appears elongated and the proximal bulbar urethra has a less conical appearance. However, the membranous urethra remains the narrowest segment between these parts of the urethra, even though it may dilate up to 6 or 7 mm in diameter during voiding.[2] Voiding cystourethrography may not demonstrate certain abnormalities of the male anterior urethra because the normal anterior urethra is not fully distended to the degree seen at retrograde urethrography. A retrograde study is the most appropriate way to evaluate the anterior part of the urethra, and a voiding study is the most appropriate way to evaluate the posterior part of the urethra.

Cystography

Cystography (excretory, retrograde and suprapubic) is a well-established modality for urinary bladder evaluation. The best cystogram is obtained by the retrograde method. Meglumine salts of diatrizoate and iothalmate are now universally used for cystography. Solution of 15 percent is generally adequate for cystography. In the excretory cystogram, bladder can be evaluated simultaneously along with upper urinary tracts, but it is not possible to recognize the presence of reflux.

In patients with renal failure having lesions in the bladder, retrograde cystography has a role. Cystography and micturating cystography is indicated for demonstration of the ability of the bladder to contract and control of the micturation, with assessment of vesical diverticulae and anatomic abnormalities of the bladder neck and urethra. However, the examination is contraindicated in presence of acute infections of the bladder and urethra.

Contrast cystogram can distinctly demonstrate intraluminal calculi, hematomas, tumors (Fig. 12.2) and wall irregularities. In traumatic injury of the bladder, cystogram depicts the

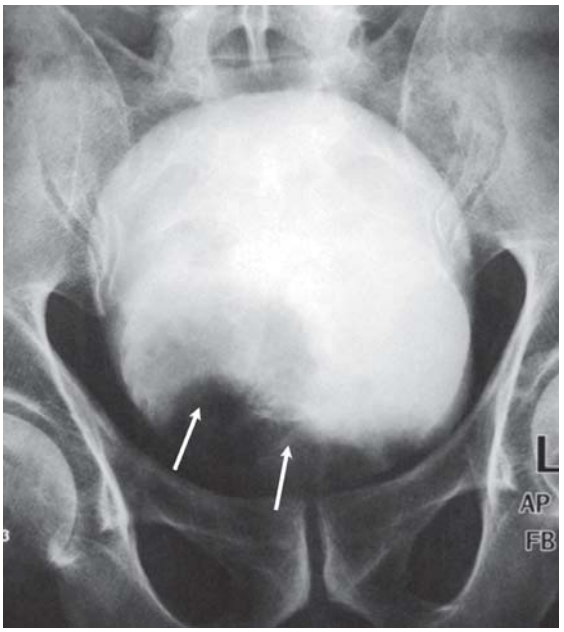

Fig. 12.2: Excretory cystogram showing irregular lobulated filling defect (arrows) at bladder base due to malignant growth

type of bladder rupture (extraperitoneal or intraperitoneal), in addition to detection of pelvic fractures.

Extrinsic compression of the bladder can be produced by pelvic hematoma or lipomatosis resulting in appearance of bladder that has been referred to as "teardrop bladder". In such pathologies, ultrasound and CT play an important role in evaluating the cause of extrinsic compression.

Urodynamic Studies of the Lower Urinary Tract

Urodynamic studies are considered to be among the most definitive tests for determining the source of symptoms involving the lower urinary tract, including the bladder and the urethra. A variety of urodynamic tests can help to evaluate the bladder and urethra and how they are functioning in their task of storing and releasing urine. These tests can help to pinpoint the anatomic or neurologic source of symptoms such as leakage, frequent urination, problems starting a stream, dribbling, painful urination, problems completely emptying the bladder, and recurrent urinary tract infections. The types of tests that are administered depend on the patient's symptoms and may include one or more of the tests like uroflowmetry, cystometry, electromyelogram, pressure studies for stress incontinence, VCUG, Video urodynamics and assessment of postvoid residual urine etc.

Ultrasonography (US)

Real-time ultrasonography is a versatile modality in the detection of bladder lesions, and is frequently employed as the primary imaging modality for its evaluation. US of the urinary bladder can be carried out by transabdominal, endorectal or endovaginal approach. However, transabdominal approach is the simplest and the easiest. Bladder must be examined when it is comfortably distended. In the majority of patients this means a volume of about 350 ml. The bladder appears as a thin-walled smooth anechoic structure almost rectangular in configuration on transverse scanning with no intravesical filling defects.

Bladder ultrasonography is used to assess the following:

1. Bladder wall anatomy:
   a. Thickening of the wall and focal abnormalities
   b. Presence of trabeculation
   c. Diverticulae
2. Capacity of the bladder and postmicturation residual volume,
3. Anatomy of bladder base and urethral opening,
4. Distal ureteric anatomy,
5. Intravesical filling defects and extraluminal masses causing bladder compression.

Radiolucent calculi, which may be missed on plain radiographs, are easily picked up on US. Blood clots and sediments are usually freely mobile within the lumen. In obese patients and those with peritonitis in whom palpation of the bladder is difficult, ultrasound is very useful in determining whether the bladder is full enough to allow safe suprapubic catheterization. Transrectal US (TRUS) is useful in defining the plane between the prostate, seminal vesicles and the bladder, in posterior wall masses. Ultrasound cystodynamogram can be performed in patients with symptoms of voiding disorders.

Sonography of the urethra is has mostly been used for diagnosis of urethral diverticula and strictures and is usually performed by using a broadband 5–10 MHz linear array

for transpenile or transperineal scanning and a broadband 5–9-MHz curved array for transvaginal or transrectal scanning. Endourethral sonography is performed with a 12.5-MHz, 6.2-F, catheter-based transducer on an intravascular US machine. Disadvantages of this technique include the need for a dedicated expensive intravascular US machine, a single use urethral catheter, and limited field of view.

Sonourethrography has been shown to be accurate, sensitive, and specific for the diagnosis and assessment of penile and bulbar urethral strictures. RGU and sonourethrography are equally efficacious in detection of anterior urethral strictures (Fig. 12.3). Further characterization of strictures in terms of length, diameter and periurethral pathologies, like spongiofibrosis and false tracts, is done with greater sensitivity using sonourethrography as compared with RGU, with the added benefit of lower incidence of complications.[3]

Computed Tomography (CT)

The role of CT is in identification of size and number of distal ureteric, vesical or urethral calculi, pelvic trauma and in staging of vesicle or urethral malignancy.

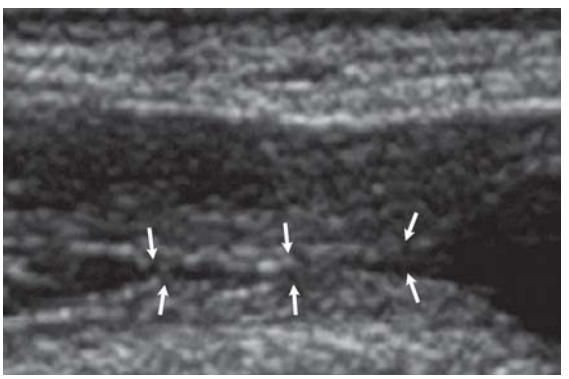

Fig. 12.3: Sonourethrogram showing a stricture (arrows) of penile urethra

On CT scan, the urinary bladder is seen as a homogeneous midline structure of water density. The size and configuration varies greatly depending on the amount of urine present. The outer margin of the bladder wall is smooth and usually well-delineated by the perivesical fat. Although urine is of near water density, the bladder wall has soft tissue attenuation. In contrast enhanced CT scan, opacified urine usually occupies the dependent portion of the bladder and unopacified urine layers above it. However, this relationship may be reversed in patients with glycosuria or infectious debris in the bladder, where the unopacified urine may have higher specific gravity than the excreted opacified urine.[4] Scans obtained before and after administration of contrast medium can detect subtle vesical and perivesical abnormalities. Dense opacification of the lumen may obscure small tumors or calculi and can produce scan artifacts which degrade the image (Figs 12.4A and B). In the male pelvis, the seminal vesicles are seen posterior to the urinary bladder, cephalad to the rectum. They are oval to tear shaped structures. A small amount of fat is usually present between the seminal vesicle and posterior wall of the urinary bladder. This relationship may be distorted by a distended rectum or when the patient is prone. The prostate gland is located just posterior to the symphysis pubis and anterior to the rectum. Masses seen on intravenous urography compressing or displacing the bladder are readily evaluated by CT. True masses are easily distinguished from bladder impression produced by the bowel loops present in the pelvis, if the loops are adequately filled with contrast material. Alteration in the shape of the bladder can be produced by retroperitoneal fibrosis, pelvic

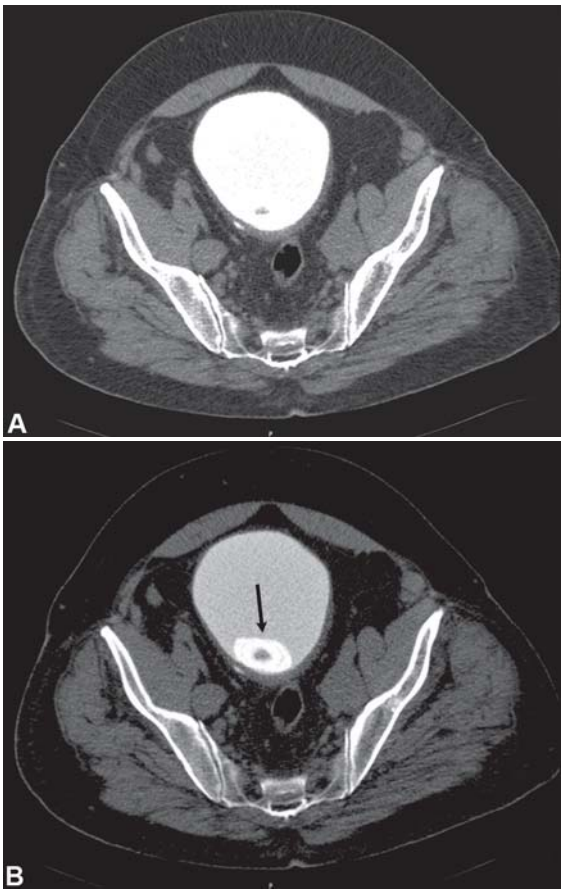

Figs 12.4A and B: Bladder calculus: Dense opacification of bladder in CT axial image completely obscuring the calculus **(A)**, which is visualized (arrow) in wide window setting **(B)**

lipomatosis, hematoma and lymphoceles, etc. In these benign conditions, CT reveals elevation and narrowing of the bladder (*pear-shaped bladder).*

Contrast-enhanced CT with delayed imaging or retrograde bladder filling (CT cystography) has been shown to be highly accurate and equivalent to conventional cystography in the detection of bladder rupture.[5]

MR Imaging (MRI)

In patients with congenital anomalies, MR imaging is reserved for cases of intersex anomalies or complex genitourinary anomalies, in which evaluation of internal organs is essential. MR imaging may demonstrate diverticula that are not seen on radiographic contrast-enhanced studies or inflammatory infiltration around the urethra and presence of a periurethral abscess or sinus tract. In cases of trauma, it is helpful in assessing the presence and extent of anterior or posterior urethral injury and predicting the occurrence of complications. On MR imaging, a fistula can be seen as a direct communicating channel with an adjacent organ. In patients with urethral tumors, the major role of MR imaging is in local staging.[6]

MR images provide an excellent insight into the anatomy and pathology of the urinary bladder. T1- and T2- weighted spin echo (SE) sequences are both useful in imaging of the bladder. Muscle layer has an intermediate signal intensity equal to that of skeletal muscle on T1-weighted images and low signal intensity on T2-weighted images (Fig. 12.5). On proton density weighted images, the mucosa and lamina propria can sometimes be distinguished from the muscle layer, because the mucosa and lamina propria have higher signal intensity.

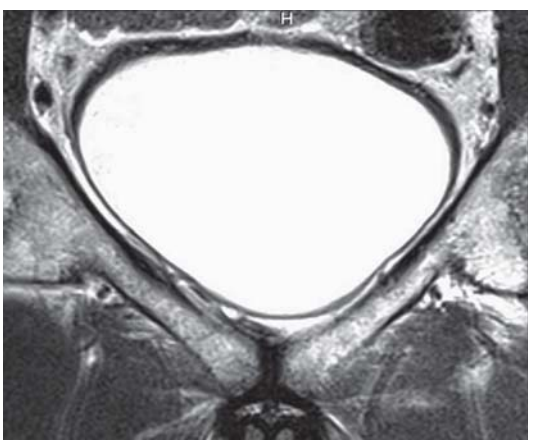

Fig. 12.5: MR: Coronal T2 image of urinary bladder. Note low signal intensity of detrusor muscle

Fast SE sequences provide superior quality in T2 weighted MR images with a threefold to fivefold reduction of examination time compared with conventional SE sequences. At the moment, fast SE is the state of art for obtaining T2-weighted images of the pelvis. Three-dimensional (3D) techniques with offline reconstruction of high resolution images in any arbitrary plane are also very useful. The introduction of short TR(< 10 msec) gradient echo sequences that use a preparation pulse, such as turbo FLASH (fast low angle shot), snapshot FLASH and MP-RAGE (magnetization prepared rapid gradient echo) and fast spin echo (FSE) sequences significantly reduce imaging time without compromising signal to noise ratio. For T1-weighted 3D imaging, the use of an MP-RAGE sequence has been described. Also, use of phased array multicoils and endorectal coils improves resolution. Dynamic contrast enhanced MR provides the best information to help differentiate malignant from benign lesions.

Development of oral intestinal MR contrast agents such as ferrite particles has improved the delineation of small bowel loops and para-aortic region.

The urethra can be evaluated in orthogonal planes (axial, sagittal, and coronal) or imaged obliquely along its course. Both T1- and T2-weighted imaging are often needed to evaluate the male and female urethra. In male patients, the membranous urethra is best evaluated in the axial plane and the relation between the membranous and bulbous urethra (particularly in cases of trauma) is best evaluated in the coronal or sagittal plane. For imaging of the anterior urethra, the penis should be positioned anteriorly in the supine position and taped to the abdominal wall beneath the surface coil (Fig. 12.6). In female patients, axial images are essential.[7]

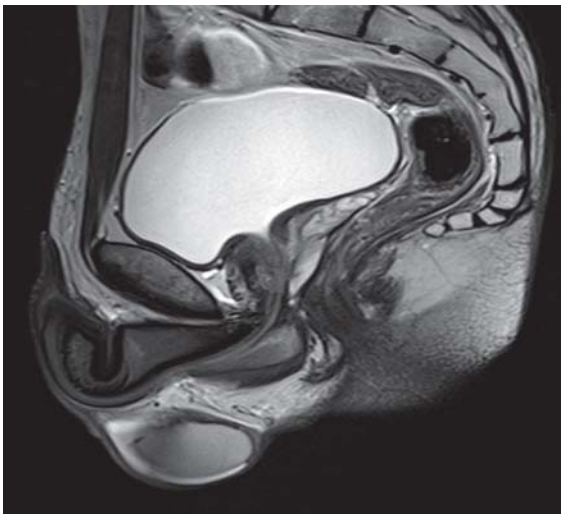

Fig. 12.6: MR: Sagittal T2 image showing the entire extent of urethra

For evaluation of a urethral diverticulum or spread of urethral cancer, a combination of axial and sagittal or coronal imaging may be helpful.

A thin section thickness (3-5 mm) and a small intersection gap (1-2 mm) are desirable for imaging the urethra. The signal-to-noise ratio can be improved by using surface coils or endovaginal or endorectal coils. Although endocavitary coils may improve the spatial resolution, the small field of view may limit the area of imaging and the high signal intensity in the near field may degrade image quality. Use of intravenous contrast media is beneficial in selected cases, particularly in patients with extensive tumors or inflammation.

Radionuclide Imaging

Radionuclide cystography has been accepted as the technique of choice for evaluation and follow-up of children with urinary tract infection and reflux. The advantages being

simplicity, lower radiation dose and no catheterization needed. Radionuclide cystography is more sensitive than voiding cystography in detecting vesico-ureteric reflux; however, this has poor anatomical resolution than the conventional VCUG. Direct and indirect radionuclide cystography are interesting alternatives to the radiograph technique and are integrated into the process of diagnosis and follow-up of vesicoureteral reflux.[8]

SPECIFIC DISEASES OF THE URINARY BLADDER

Bladder Diverticulae

Bladder diverticulae refer to pouch like eversion or evagination of the bladder wall. These may be congenital, but are more commonly acquired as a result of bladder outlet obstruction. Congenital bladder diverticulae develop as a result of herniation of bladder mucosa through the detrusor muscle, usually at a location slightly above and lateral to the ureteric orifice (Hutch diverticuli). These may vary from small to quite large and may cause either obstruction of, or reflux into the ipsilateral ureter. Diverticulae are sites of urinary stasis and thus lead to infection.

On cystogram, bladder diverticulae are seen as outpouchings from the bladder which may show persistence of contrast in the postmicturition phase. On US these appear as well-defined, thin-walled fluid containing structures communicating with the bladder lumen. The most important use of US is to detect the complications, i.e. stone or tumor in the diverticulum, which is not always possible to assess on cystography or endoscopy.

Urachal Anomalies

The urachus develops from the superior portion of the urogenital sinus and connects the dome of the bladder to the allantoic duct during fetal life. It lies behind the abdominal wall and anterior to the peritoneum in the space of Retzius. Normally, it obliterates before birth forming the fibrous median umbilical ligament. In absence of complete obliteration urachus persists in one of the following four types:

Urachal anomalies	*Entity*
1. Completely patent urachus	Vesicocutaneous fistula between bladder and umbilicus
2. Patent caudal portion opening into the bladder	Vesicourachal diverticulum
3. Patent cephalic portion opening into the umbilicus	Urachal sinus
4. Midportion is patent, both cephalic and caudal ends closed	Urachal cyst

Patent urachus is usually diagnosed in the newborn when there is leakage of urine from the umbilicus. It can be directly demonstrated by retrograde injection of contrast into umbilical orifice. It may also fill up during voiding cystourethrogram, best demonstrated in the lateral projection. Urachal cyst is not delineated on conventional urography studies. An urachal diverticulum is identified as urine filled anterosuperior protrusion of the bladder dome on cystography.

In adults the urachal diverticulum may be complicated with infection or malignancy (Figs 12.7 and 12.8). Urachal anomalies can be delineated on US, CT and MRI. US reveals a tubular, anechoic structure in the lower, mid anterior abdominal wall. MRI is very helpful as it permits multiplanar imaging especially in the sagittal plane.

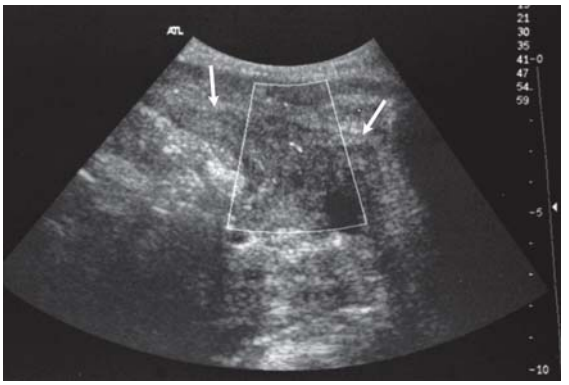

Fig. 12.7: Urachal diverticulum (arrow) complicated with infection: US image showing thickening of diverticular wall with increased vascularity

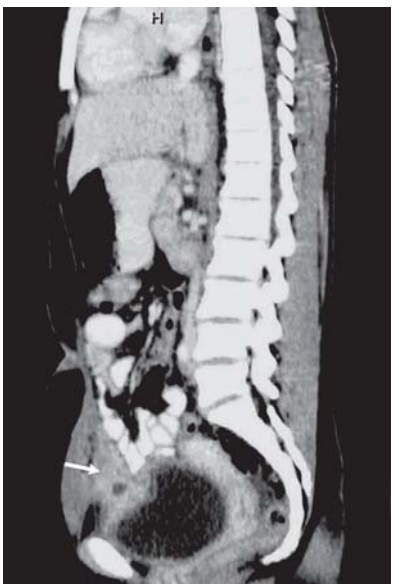

Fig. 12.8: Sagittal 3D reformatted CT image of the same patient as in Fig. 12.7 showing thickening and enhancement of urachus

Exstrophy

Exstrophy of the bladder is a spectrum of defects in the formation of the anterior abdominal wall caused by varying degrees of failure of midline fusion of mesodermal tissue below the umbilicus. Classical exstrophy includes epispadias, separation of pubic

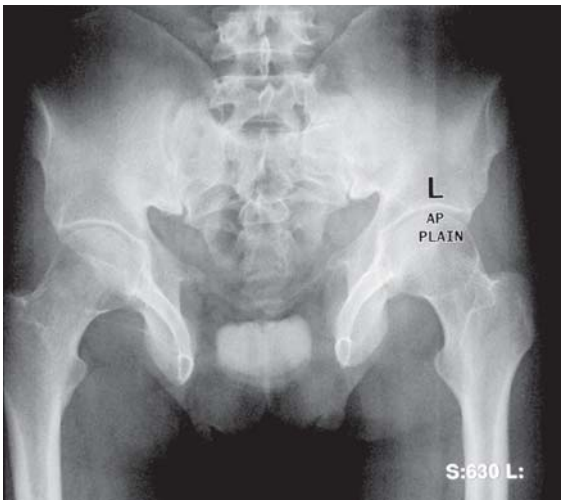

Fig. 12.9: Exstrophy of bladder: Radiograph showing diastasis of pubic symphysis

bones (more than 10 mm) and communication of bladder with the anterior skin surface (Fig. 12.9). On excretory urography, there is a wide lateral curve of the pelvic portion of the distal ureters, which then turn upwards and medially, passing through the bladder wall in a perpendicular direction. Cystogram is performed in postoperative follow up of these patients.

Other Anomalies

Other major anomalies include, bladder agenesis and hypoplasia which are associated with urethral and other congenital anomalies, which when severe may even be incompatible with life. Duplication of the bladder may be partial or complete with two separate bladders, lying side by side separated by a peritoneal fold. Each bladder receives the ipsilateral ureter and empties into a separate urethra. This can be associated with anomalies of the gastrointestinal tract, genital system and lower spine. Anatomy of duplication can be well-demonstrated on US and MRI.

Neurogenic Bladder

Neurogenic bladder dysfunction may be caused by spinal dysraphism, cord compression or cord injury. Cystography is very helpful in diagnosis of neurogenic bladder. US is also useful to assess bladder size, shape, volume, post void residue, renal parenchymal changes and secondary calculi.

In the condition called as detrusor-external sphincter dyssynergia (DSED), contraction of the external sphincter occurs involuntarily at the same time as detrusor contraction thus impeding urinary flow and resulting in bladder outlet obstruction. In this condition bladder is often vertically oriented, with an irregular contour with trabeculation; frequently with multiple diverticulae and is referred to as "Christmas tree" or "pine tree" bladder. On voiding cystourethrography, there may or may not be vesicoureteral reflux. In detrusor areflexia voiding cysto-urethrography often reveals a smooth, thin-walled bladder with increased capacity, occasionally upto several liters and extending high into the abdomen. Significant post void residue is seen in both these conditions.

Infections

Acute Cystitis

Acute cystitis due to bacterial infection is most commonly the result of transurethral infection, and is common in females. *Escherichia coli* is the most common pathogen. Cystography is contraindicated in acute infection. US is the most useful modality allowing evaluation of the upper tracts as well as the bladder. On US, cystitis show thickened and less distinct bladder wall with internal echoes or debris. Cobble-stone appearance of bladder wall can be seen in severe bladder edema due to acute cystitis. Contour irregularity due to bladder mucosal edema can also be seen in radiation cystitis, cyclophosphamide cystitis and eosinophilic cystitis, and these can be associated with hemorrhage.

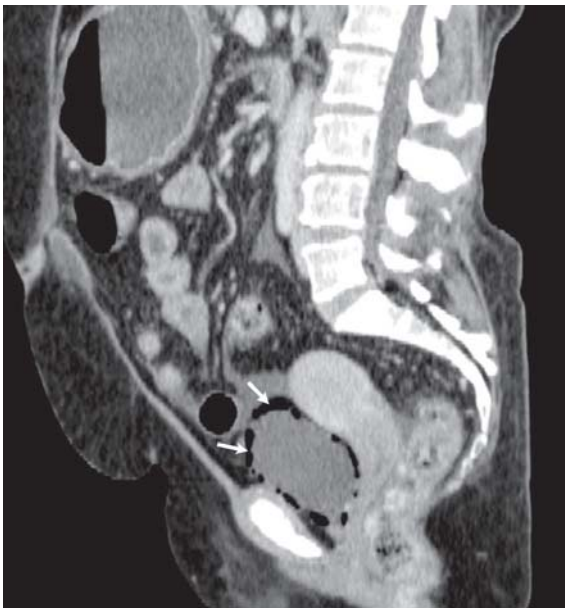

Fig. 12.10: Emphysematous cystitis: Sagittal reformatted CT image showing air pockets (arrows) within the bladder wall

Emphysematous cystitis is almost always seen in diabetic or immunocompromised patients and *E. coli* is the most common pathogen (Fig. 12.10).

Chronic Cystitis

The hallmark of chronic cystitis is thickening, calcification and irregularity of the bladder wall associated with trabeculation and often diminished bladder capacity. Tubercular infection of the bladder has been discussed in detail in the chapter on Tubercular Infection of the Urinary Tract.

Cystitis Cystica

Cystitis cystica is a benign condition commonly seen in women with recurrent or chronic cystitis, or in chronically irritated bladders such as those catheterized for long periods or with calculus disease of the bladder. Multiple round contour defects at the bladder base can be seen in cystitis cystica and malakoplakia, on cystogram and US.

Malakoplakia

Malakoplakia is an uncommon granulomatous response to an infection of the urinary tract, predominantly with *E. coli*. Submucosal granulomas containing macrophages with inclusion bodies known as 'Michaelis-Gutmann bodies' are characteristic. It may affect any part of the urinary tract. Radiographically, these are seen as single or multiple mural filling defects especially in the trigone and bladder base. Accompanying bladder wall thickening may also be seen, simulating carcinoma.

Schistosomiasis

Schistosomiasis or bilharziasis is a parasitic infection caused by Schistosoma hematobium, producing polypoidal bladder wall thickening, which is nonspecific in appearance. In late stages fibrosis leads to a small capacity bladder with focal or curvilinear dense wall calcification.

Extravesical Processes

Appendicitis, diverticulitis and pelvic abscesses may produce reactive thickening of the bladder wall and mucosal irregularities.

Bladder Tumors

Primary bladder tumors are mostly epithelial in origin, less than 10 percent arising from a nonepithelial source. All epithelial tumors are malignant, majority being transitional cell type with squamous cell carcinoma and adenocarcinoma being relatively uncommon. Nonepithelial tumors may be benign (e.g. leiomyoma, fibroma) or malignant (e.g. leiomyosarcoma and rhabdomyosarcoma). Various other primary tumors or masses may occur including pheochromocytoma, hemangioma, leukoplakia, lymphoma and endometriosis. The bladder can also rarely be the site of metastases. The staging system most often used for bladder cancer is the **TNM** system (Adapted from: International Union Against Cancer (UICC). TNM [tumor nodes metastasis] classification of malignant tumors. 5th ed. Geneva (CH):UICC; 1997.)

Ta	Noninvasive papillary carcinoma
Tis	Carcinoma *in situ*
T1	Invades subepithelial connective tissue
T2	Muscular invasion
T2a	Inner half
T2b	Outer half
T3	Invades perivesical tissues
T3a	Microscopic disease
T3b	Macroscopic disease
T4	Invades adjacent organs, pelvic–abdominal wall
T4a	Prostate, uterus or vagina
T4b	Pelvic or abdominal wall
N1	Single lymph node < 2 cm
N2	Single lymph node > 2–5 cm, multiple < 5 cm
M0	No distant metastasis
M1	Distant metastasis

The clinical staging (with deep fractioned transurethral resection) is much less accurate in staging invasive (Stages T2-T4) tumors. Cystogram cannot detect an early growth, extent of extravesical spread or status of the adjacent organs (Fig. 12.11).

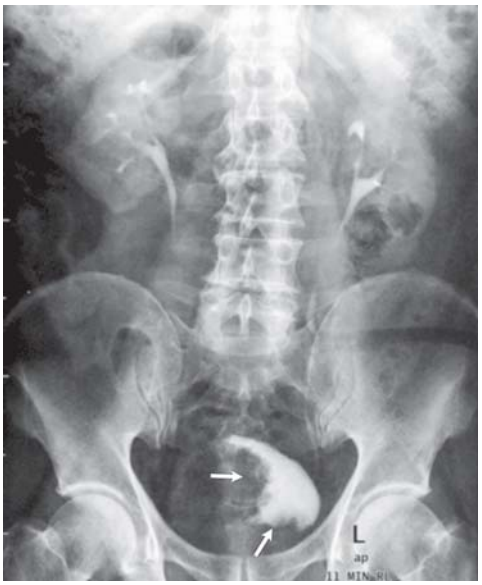

Fig. 12.11: TCC of bladder: IVU image showing large polypoidal filling defects (arrows) within the bladder

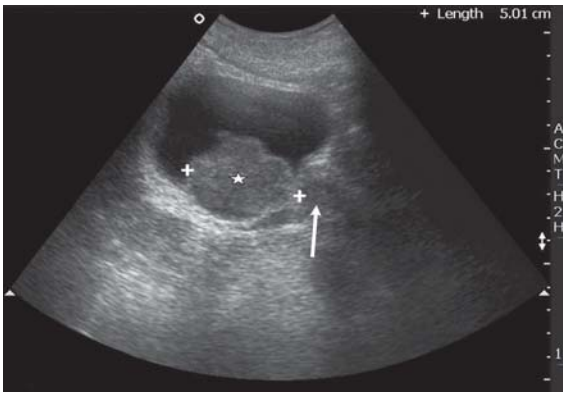

Fig. 12.12: TCC of bladder: US image showing intraluminal polypoidal mass within the bladder with invasion of left ureter (arrow)

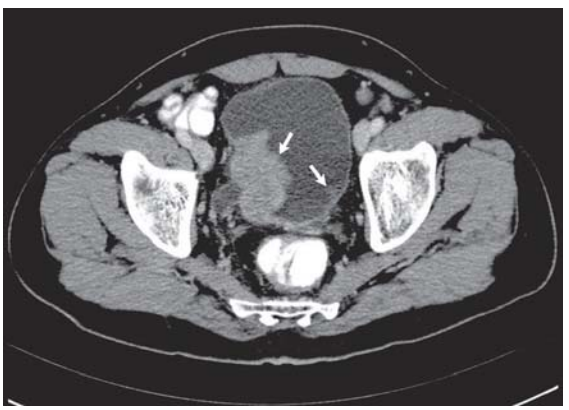

Fig. 12.13: TCC of bladder: CT axial image showing a large polypoidal growth (arrow) along right lateral wall and base of bladder causing ureteric obstruction. A small tumor is also seen along left lateral wall (arrow)

Although the intravesical position of many tumors can be visualized on US, an accurate assessment of the depth of penetration of the bladder wall cannot be done with US (Fig. 12.12). The diagnostic accuracy of the transabdominal US for depth of infiltration ranges from 55 to 95 percent. Perivesical invasion cannot be frequently determined, however, extravesical spread may be recognized by the asymmetry due to infiltration.

Tumors involving the posterior bladder wall and neck; prostate and seminal vesicles may be visualized better with transrectal approach. Finally, none of the ultrasound methods optimally assesses the regional nodal status.

The major role of CT in carcinoma of the bladder is to stage rather than detect the primary neoplasm. However, CT is not accurate for the early stages, and its reliability increases with more advanced disease (Fig. 12.13). CT cannot differentiate between the various layers of the bladder wall and cannot therefore distinguish lesions limited to the lamina propria (T1) from those invading the superficial (T2) and deep (T3a) muscles. CT is useful for detecting extravesical extension characterized by poor definition of the outer aspect of the bladder wall with an increase in density of the perivesical fat. Tumor involvement of the pelvic side wall is characterized by a soft tissue mass extending into the obturator internus muscle or by strands of soft tissue extending from the main tumor mass to the pelvic wall.

Tumor invasion of the seminal vesicles should be suspected if a soft tissue mass obliterates the seminal vesicle angle. This should be interpreted with caution because the normal seminal vesicle angle may be lost if the rectum is over distended or if the patient is scanned in prone position. CT is useful in detecting lymph node metastases, involvement being judged by the size of the node. Nodes greater than 10 mm in short axis are considered malignant. The obturator and external iliac lymph nodes are involved first. CT has limited accuracy in detecting perivesical infiltration and lymph node metastasis in invasive bladder carcinoma[9,10](accuracy of CT varies from 40 to 90 percent for staging, 65-85 percent for detection of perivesical extension and 65-97 percent for lymph node detection).

On MR, T1-weighted images are the best sequences for evaluating tumor extension into the adjacent bright fat, lymphadenopathy detection, and bone marrow involvement.[11] There is better delineation of bladder cancer from urine with T2-weighted images. When compared with 2-dimensional T1-weighted spin echo (SE) imaging, 3-dimensional magnetization prepared rapid gradient echo (MP-RAGE) imaging improved bladder carcinoma staging by 15 percent.[12] When compared with SE, fast SE sequences significantly reduced acquisition time by 3-fold to 5-fold without compromising T2-weighted image quality.[13] Presently, fast SE is state of the art for obtaining T2-weighted images of the pelvis. Contrast administration and fast dynamic imaging improves the ability of MRI to detect and stage bladder cancers. Most carcinomas enhance intensely following intravenous contrast material administration. Tumor tissue generally enhances earlier (average 6.5 s) than post-biopsy granulation tissue (13.5 s).[14]

MRI is the most accurate staging technique in invasive tumors. T2-weighted or contrast enhanced T1-weighted sequences are needed to evaluate the infiltrating component of the tumor. Visualisation of the low intensity line on T2-weighted images representing the uninvolved bladder wall between the tumor and perivesical fat is an important feature in MRI staging, differentiating stage T3a from stage T3b. Disruption of the low signal intensity muscle layer of the bladder, irregularity of the outer bladder wall and perivesical stranding indicate stage T3b disease (Figs 12.14 to 12.17).

The demonstration of direct tumor invasion into adjacent organs is facilitated by multiplanar imaging. A sagittal image is needed for evaluation of uterine or vaginal invasion. Assessment of invasion of the seminal vesicles is also facilitated by use of the sagittal image, invasion being demonstrated by an increase in vesicular size, decrease in signal intensity on T2-weighted images and obliteration of the angle between seminal vesicle and the posterior bladder wall.

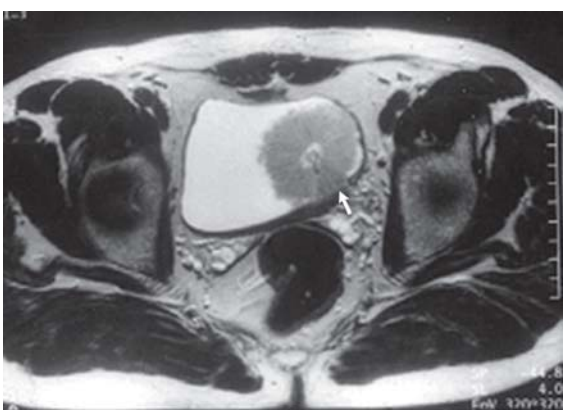

Fig. 12.14: TCC of bladder: Axial T2-weighted image of a papillary transitional cell carcinoma shows a intraluminal mass which is intermediate in signal intensity. The pedicle is clearly seen (arrow). The muscle wall is not infiltrated. Perivesical enlarged vessels are noted adjacent to the tumor on left side

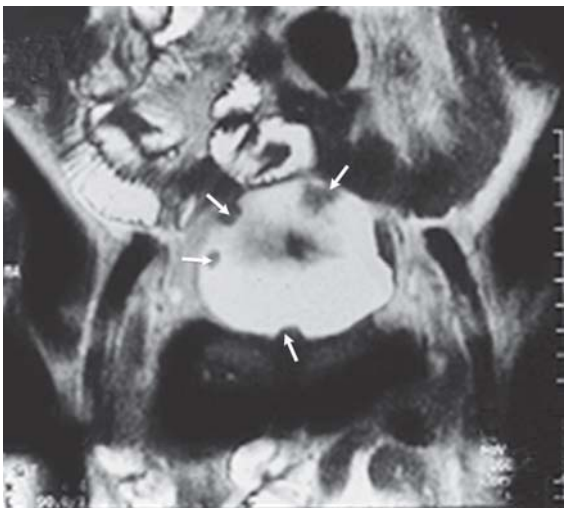

Fig. 12.15: TCC of bladder: Coronal T2-weighted image showing superficial masses in diffuse multifocal cancer (arrows) which appear relatively hypointense compared to bright urine. There is no perivesical extension

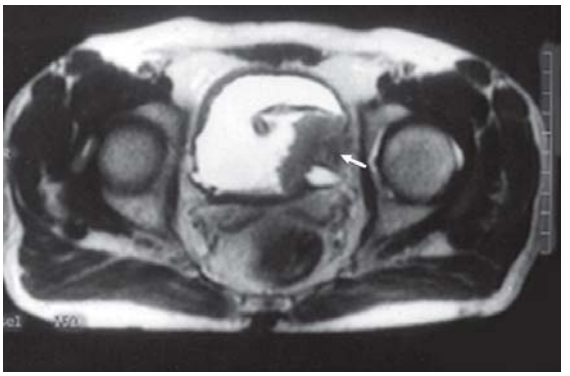

Fig. 12.16: TCC of bladder: T2 axial section shows left posterolateral wall tumor (TCC) with deep muscle infiltration leading to ureteric obstruction. Early perivesical spread is seen as stranding of fat along left posterolateral aspect (arrow)

Invasion of the prostate and rectum is seen as direct tumor extension with an increase in signal intensity on T2-weighted images. Because of multiplanar imaging capability, MR is especially useful for evaluation of tumors at the bladder dome or base.

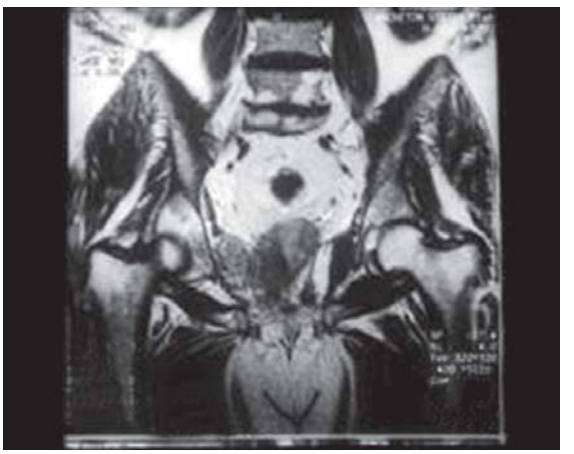

Fig. 12.17: TCC of bladder: Stage T4 disease with infiltration of the right pelvic side wall muscles (arrow) by bladder cancer. Note normal marrow signal of the pelvic bones on this T1 image

T1 weighted images are more suitable for imaging lymph nodes which as these have lower signal intensity than the surrounding fatty tissue. MRI with ultra-small superparamagnetic iron oxide agents have shown potential for detecting metastases in normal size nodes and in differentiating reactive enlarged nodes from those with metastases.[15]

All modalities have limitation in determining extent of tumor growth in the muscle layer of the bladder wall, i.e. differentiation between stages T2 and T3a. The use of endorectal surface coils or phased-array multicoils in combination with IV contrast agents or T2-weighted fast SE sequences might solve the problem of differentiating stage T2 from stage T3 tumors.

Other newer imaging modalities like fluorescence cystoscopy, optical coherence tomography and narrow-band imaging are under evaluation and may prove useful in staging of early bladder cancer.[16] Virtual cystoscopy may allow non-invasive tumor diagnosis, treatment planning and surveillance.

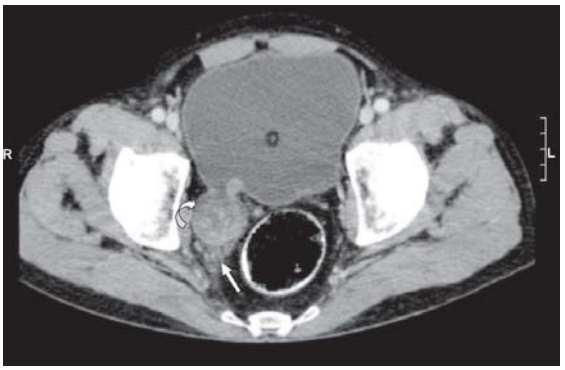

Fig. 12.18: TCC of bladder diverticulum: Axial CT image shows an enhancing mass almost completely filling the bladder diverticulum (curved arrow) along right posterolateral wall. Note extravesical extension of the tumor (arrow)

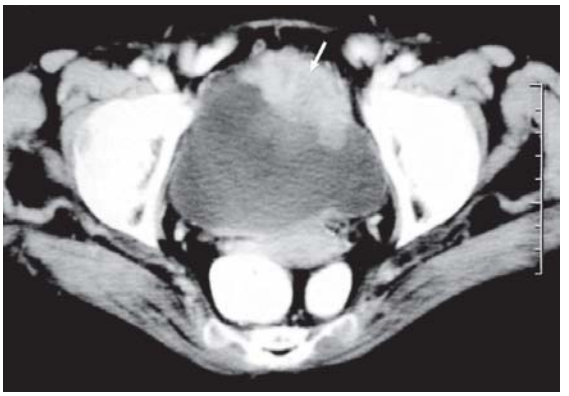

Fig. 12.19: Urachal carcinoma: Axial CT image showing a polypoid tumor mass (arrow) along the anterosuperior aspect of bladder

Because of urinary stasis and chronic inflammation, there is a 2 to 10 percent increased incidence of carcinoma that develops within bladder diverticula.[17] Most neoplasms of bladder diverticulum are of urothelial origin. By definition the detrusor muscle is absent in diverticula; therefore, tumors often have invaded the perivesical fat at the time of diagnosis (Fig. 12.18). A narrow diverticular neck or unusual location can preclude adequate visualization at cystoscopy; therefore, imaging has an important role in identifying such occult neoplasm.

Most urachal carcinoma are mucin-producing adenocarcinomas of the juxtavesical segment of the urachus.[18] Diagnosis is often facilitated by the characteristic midline location of the mass anterosuperior to the bladder, which is optimally delineated in the sagittal and coronal planes (Fig. 12.19).

Chronic stasis and inflammation predispose to squamous cell carcinoma (SCC). Schistosomiasis (bilharziasis) is associated with a higher incidence of vesical SCC.

SPECIFIC DISEASES OF URETHRA

Gonococcal and Nongonococcal Urethritis

Gonococcal urethritis is associated with the gram-negative diplococcus, *Neisseria gonorrhea. Chlamydia trachomatis* is the most common pathogen of nongonococcal urethritis, accounting for 30 to 50 percent of cases. Patients with gonococcal urethritis usually present with purulent urethral discharge. Urethral discharge associated with nongonococcal urethritis is usually scant. The diagnoses of acute gonococcal or nongonococcal urethritis are usually made by means of clinical and laboratory findings. No imaging studies are necessary for noncomplicated urethritis. Complications associated with gonococcal urethritis are more common and more serious than those associated with nongonococcal urethritis and include urethral stricture, periurethral abscess, and periurethral fistula.

The typical urethrographic finding in gonococcal urethral stricture is an irregular urethral narrowing several centimeters long

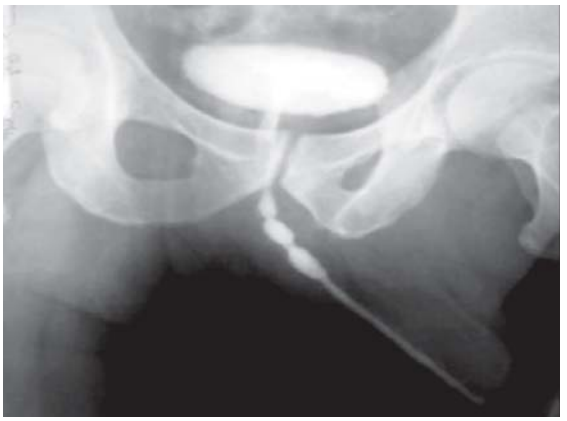

Fig. 12.20: Gonococcal urethral stricture: RGU image showing a panurethral stricture

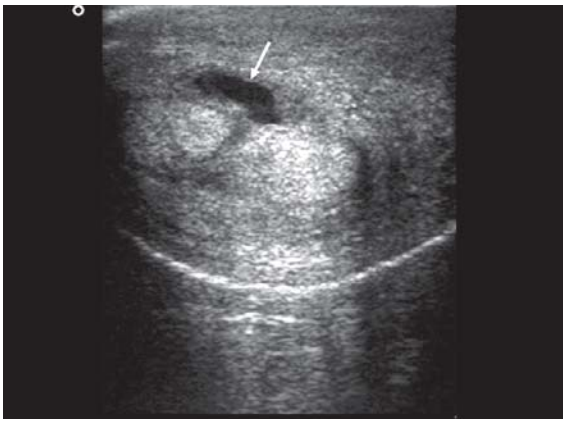

Fig. 12.21: Periurethral abscess: US image shows an abscess cavity (arrow) in relation to the penile urethra

(Fig. 12.20). An estimated 15 percent of men with gonococcal urethritis go on to develop stricture, with an interval of 2-30 years between infection and the onset of obstructive symptoms.[19] Hard fibrous scars are present at the distal portion of the bulbous urethra in 70 percent of patients. These scars are due to less effective flushing by urination and the preponderance of Littré glands in this area. Associated dilatation of Littré glands may be present at urethrography. If the proximal coneshaped bulbar urethra appears to be narrowed, elongated, asymmetric, irregular, or absent, the stricture is seen to extend into the membranous urethra in more than 90 percent of cases.[20] This radiologic finding is of prime importance to the urologist because surgical treatment may involve cutting the scar tissue and, consequently, the distal sphincter, which could result in iatrogenic incontinence.

Periurethral abscess arises initially when a Littré gland becomes obstructed by inspissated pus or fibrosis (Fig. 12.21). The most common infecting organisms are gram-negative rods, enterococci, and anaerobes. Periurethral abscess is a life-threatening infection of the male urethra and periurethral tissue and frequently a sequelae of gonococcal infection, urethral stricture disease, or urethral catheterization. Pseudodiverticulum formation results from urethral communication with a periurethral abscess. Because the tunica albuginea of the penis prevents the dorsal spread of infection, the abscess tends to track ventrally along the corpus spongiosum, where it is confined by the Buck fascia. However, when the Buck fascia is perforated, there can be extensive necrosis of the subcutaneous tissue and fascia. Rapid diagnosis and treatment are essential. Imaging studies may be indicated if the diagnosis is not established clinically. An abscess that drains into the urethra may be demonstrated at urethrography. Ultrasonography (US) can demonstrate the presence of periurethral abscess, and CT and MR imaging are helpful for assessing the extent of the periurethral abscess and complications such as fasciitis and Fournier gangrene.

Urethroperineal fistulas are most often the consequence of a periurethral abscess. In general, the initial abscess cavity contracts by means of healing fibrosis, which leaves only the narrow fistulous tract from the urethra to the perineum. Consequently, urination usually occurs through the perineal fistulas,

which results in the so-called "watering can perineum".[21] Urethroperineal fistulas are usually the result of tuberculosis and schistosomiasis infections.

Condyloma Acuminata (venereal warts)

Condyloma acuminata are caused by viral infection and produce soft, sessile, squamous papillomas on the penile glans and shaft and the prepuce. Urethral involvement occurs in 0.5 to 5 percent of male patients. On occasion, condyloma acuminata may extend to the prostatic urethra and bladder. The diagnostic procedure of choice is voiding cystourethrography. However, the diagnosis is often not suspected until retrograde urethrography has been performed. The typical urethrographic findings are multiple papillary filling defects in the anterior urethra.

Tuberculosis

Usually, genital tuberculosis is a descending infection and renal tuberculosis is evident. The prostate is involved in 70 percent of patients with genital tuberculosis. Prostatic abscess may rupture into any surrounding structure, which results in prostatorectal and prostatoperineal urethral fistulas (Fig. 12.22). In the acute phase, there is urethral discharge with associated involvement of the epididymis, prostate, and other parts of the urinary system. In the chronic phase, diagnosis becomes difficult because patients present with obstructive symptoms secondary to urethral strictures. Tuberculous urethral strictures result in periurethral abscesses, which, unless treated, produce numerous perineal and scrotal fistulas resulting in watering can perineum. Retrograde urethrography typically demonstrates an anterior urethral stricture associated with multiple prostatocutaneous and urethrocutaneous fistulas. Simultaneous fistulography may be useful for assessing the entire urethra.

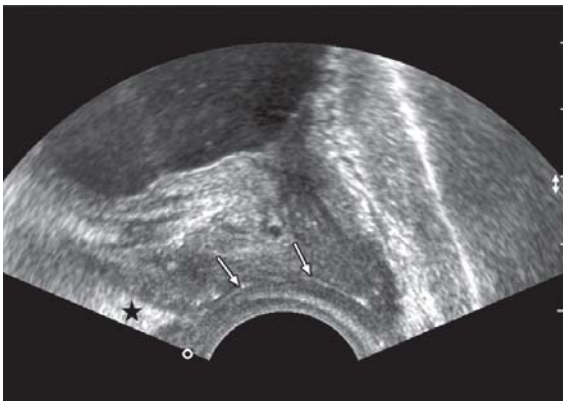

Fig. 12.22: Rectourethral fistula in a young male who had tuberculous prostatic abscesses and presented with pneumaturia: Transrectal US image shows the echogenic fistulous tract (arrows) between the rectum (star) and the prostatic urethra

Urethral Strictures

Most urethral strictures are the result of infection, instrumentation, or other iatrogenic causes. The causes of anterior urethral strictures may be inflammatory (e.g., infectious urethritis, balanitis xerotica obliterans), traumatic (straddle injury, iatrogenic instrumentation) or congenital. The most common external cause of traumatic stricture is straddle injury. Iatrogenic trauma to the urethra may result from pressure necrosis at fixed points in the urethra from indwelling catheters (Fig. 12.23). Instrumentation-related strictures usually occur in the bulbomembranous region and, less commonly, at the penoscrotal junction.

Alternatively, posterior urethral stricture is often an obliterative process that occurs as a result of urethral distraction or disruption caused by either trauma or surgery (Fig. 12.24). Post-traumatic posterior urethral

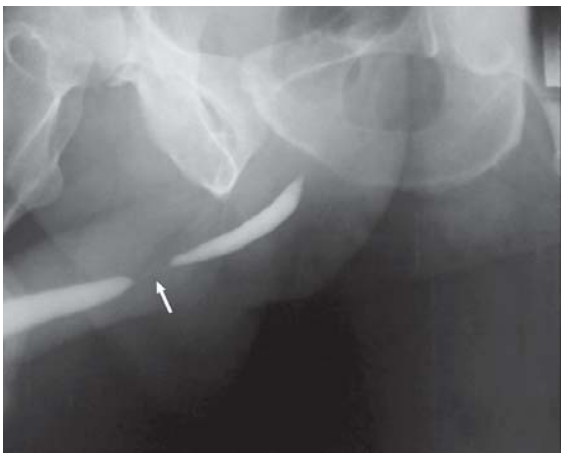

Fig. 12.23: Posttraumatic anterior urethral stricture: RGU image showing a penile urethral stricture due to instrumentation for transurethral resection of prostate

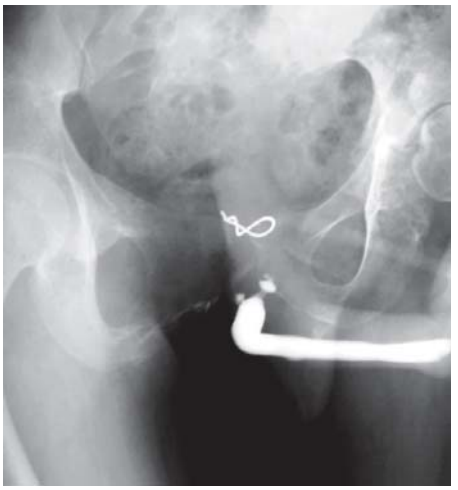

Fig. 12.24: Posttraumatic posterior urethral stricture: RGU image showing a tight posterior urethral stricture at membranous urethra due to pelvic trauma

stricture is often associated with resultant displacement of the urethral axis, which results in obliteration from intervening fibrosis. Iatrogenic stricture of the prostatic posterior urethra ("bladder neck contracture") usually occurs after transurethral resection of the prostate or open radical prostatectomy.[22]

Urethral Diverticulum

Acquired urethral diverticulum occurs more frequently in female patients and is rare in male patients. Most commonly, it occurs in the midurethra and on the posterolateral wall rather than on the anterior wall. It is thought to result from inflammation and trauma of the periurethral Skene glands and ducts, leading to local glandular dilatation and subsequent rupture into the urethra. It may arise in association with a congenital anomaly, such as cloacal epithelium or a wolffian or müllerian duct remnant. Urethral diverticulum has been reported in 1.4 percent of women with stress urinary incontinence.[23] Another common cause is disruption of the periurethral fascia during bladder neck suspension surgery for stress incontinence, which results in focal posterior urethral prolapse. The diagnosis is usually made with voiding cystourethrography or cross-sectional imaging (Fig. 12.25). Voiding cystourethrography has an overall accuracy of 65 percent.[24]

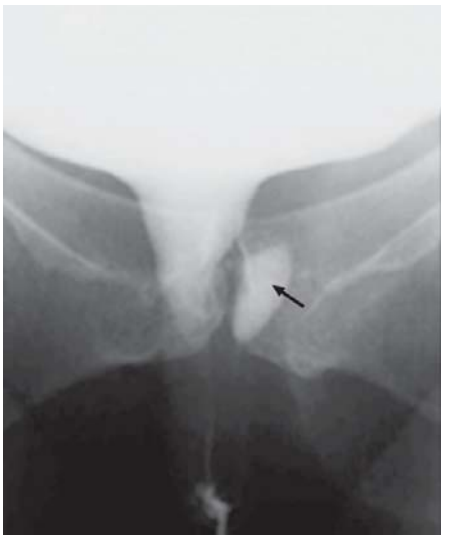

Fig. 12.25: Urethral diverticulum in an elderly female: VCUG image showing the urethral diverticulum (arrow)

US can demonstrate a relatively echo-free cavity adjacent to the urethra and may also demonstrate intracavitary debris or surrounding inflammatory edema. MR imaging is more sensitive than voiding cystourethrography and double balloon urethrography in the detection of urethral diverticula, particularly in the detection of narrow-neck noncommunicating urethral diverticula.[25] The differential diagnosis of a urethral diverticulum includes vaginal cyst (Gartner duct cyst, paramesonephric or müllerian duct cyst, epithelial inclusion cyst), ectopic ureterocele, endometrioma, and urethral tumors.[26]

Urethral diverticula may be complicated by infection, stone formation, and malignant degeneration. Adenocarcinoma is the most frequently diagnosed tumor in female urethral diverticula.

Urethral Calculi

Most urethral calculi consist of small stones expelled from the bladder into the urethra during voiding (migrant calculi). Rarely, primary (native) formation of a stone occurs in the urethra when stricture is present, or it may be associated with a urethral diverticulum. On a preprocedural low abdominal radiograph, the stone may be identified before contrast material is injected. Retrograde urethrography will usually depict a rounded filling defect in the urethra (Figs 12.26A and B).

Tumors of the Male Urethra

Benign tumors of the urethra are very rare. They may be of epithelial or mesenchymal origin and manifest as filling defects, with biopsy often being necessary to establish the correct diagnosis. Malignant tumors comprise of less than 1 percent of all urologic cancers, and usually occur after 50 years of age. The most common symptom at presentation is a palpable mass in the perineum or along the shaft of the urethra with or without obstructive voiding symptoms. Urethral stricture

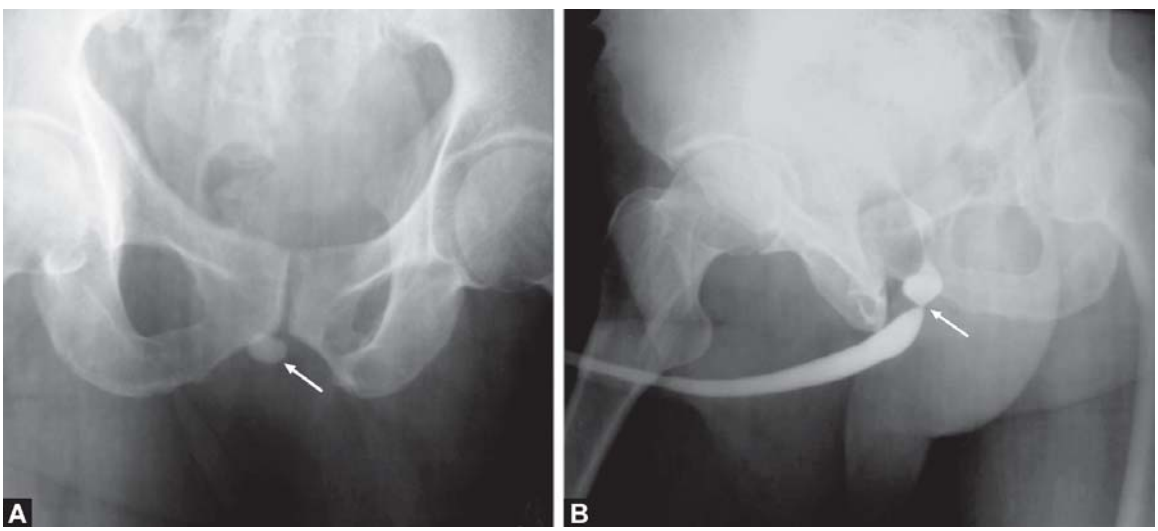

Figs 12.26A and B: Urethral calculus: Radiograph showing a calculus (arrow) in expected location of prostatic urethra, **(A)**. RGU image showing the stricture (arrow) at bulbar urethra distal to the impacted calculus, **(B)** Note the calculus is obscured by injected contrast

or bleeding, obstructive symptoms, serosanguinous discharge, urethral fistula, periurethral abscess, or perineal pain in an elderly man is suggestive of urethral carcinoma.

The bulbomembranous urethra is involved most frequently (60% of cases), followed by the penile urethra (30%) and the prostatic urethra (10%).[27] Overall, 80 percent of male urethral carcinomas are squamous cell carcinoma, 15 percent are transitional cell carcinoma, and 5 percent are adenocarcinoma or undifferentiated carcinoma. The histologic subtype of urethral cancers also varies according to anatomic location. The prostatic urethra is involved by transitional cell carcinomas in 90 percent of patients and by squamous cell carcinomas in 10 percent. The bulbomembranous urethra is involved by squamous cell carcinomas in 80 percent of patients, transitional cell carcinomas in 10 percent, and adenocarcinomas or undifferentiated carcinomas in 10 percent. The penile urethra is involved by squamous cell carcinomas in 90 percent of patients and by transitional cell carcinomas in 10 percent (Figs 12.27 and 12.28). Adenocarcinoma arises from the Littré or Cowper glands. More than one-half of patients with a carcinoma of the urethra have a history of urethral stricture disease, and almost one-fourth have a history of sexually transmitted disease.

Male urethral carcinoma can spread by direct extension to adjacent structures or metastasize to regional lymph nodes. Stage I urethral tumor is confined to the subepithelial connective tissue. Stage II tumor invades the corpus spongiosum, prostate, or periurethral muscle. Stage III tumor invades the corpus cavernosum and bladder neck or beyond the prostatic capsule. Stage IV tumor invades other adjacent organs. The lymphatic vessels from the anterior urethra drain into the superficial and deep inguinal lymph nodes and, occasionally, into the external iliac lymph nodes. Tumors of the posterior urethra most commonly spread to the pelvic lymph nodes. Carcinomas of the bulbomembranous urethra may invade the urogenital diaphragm, prostate, perineum, and scrotal skin. Hematogenous dissemination is uncommon until

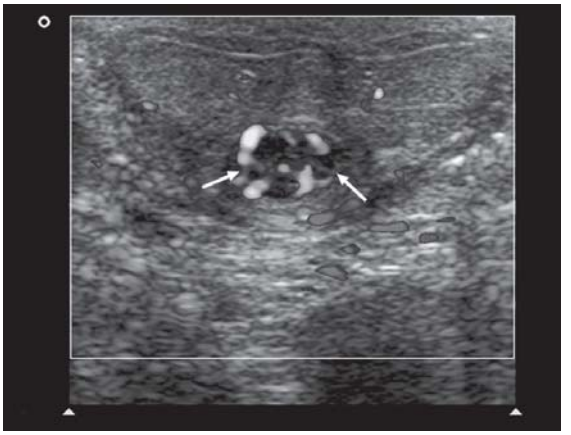

Fig. 12.27: Urethral TCC in an elderly male: US power Doppler image shows a hypoechoic hypervascular mass (arrows) at penile urethra *(For color version see Plate 16)*

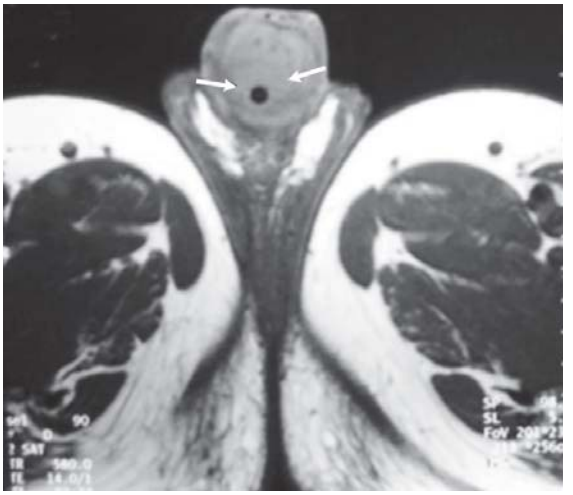

Fig. 12.28: Urethral SCC: CEMR axial image showing a hypoenhancing periurethral mass (arrow) of penile urethra. Note, the urethral outline can be clearly made due to presence of urinary catheter

advanced local disease is present or in primary transitional cell carcinoma of the prostatic urethra. In general, anterior urethral carcinoma is more amenable to surgical control and has a better prognosis than posterior urethral carcinoma, which is often associated with extensive local invasion and distant metastasis.

The diagnosis of urethral tumors is usually suggested clinically at physical examination. Urethrography can be helpful in making the diagnosis of urethral carcinoma, usually showing focal irregular narrowing of the urethra. The typical MR finding in urethral carcinoma is a mass with decreased signal intensity relative to the normal corporal tissue at both T1- and T2-weighted imaging. MR imaging can depict invasion of the corpora cavernosa and is useful for demonstrating tumor location and size and local staging.[28]

Tumors of the Female Urethra

Although carcinoma of the female urethra is more common than that of the male urethra, with a female-to-male ratio of 4:1, it accounts for less than 0.01 percent of all malignancies occurring in women. Most patients are over 50 years old. Causes associated with the development of urethral cancers in women include chronic irritation, urinary tract infection, and proliferative lesions such as caruncles, papillomas, adenomas, polyps, and leukoplakia of the urethra. Most patients present with urethral bleeding, urinary frequency, obstructive symptoms, and a palpable urethral mass or induration. Female urethral cancer is classified as either "anterior" urethral cancer or "entire" urethral cancer.[27] Anterior tumors of the female urethra are located exclusively in the distal third of the urethra and account for 46 percent of urethral tumors. Entire urethral carcinomas tend to be high grade and locally advanced, most frequently with squamous cell carcinoma (60% of patients), followed by transitional cell carcinoma (20%), adenocarcinoma (10%), undifferentiated tumor and sarcoma (8%), and melanoma (2%). Local extension of the primary lesions into the bladder neck, vagina, or vulva is not uncommon, and, therefore, differentiation of the primary urethral lesions from those of the vulva or vagina may be difficult.

The diagnosis of urethral tumor in a woman is usually made at clinical examination. Urethrography demonstrates irregular narrowing of the urethra. MR imaging has been reported to be accurate for evaluating local urethral tumors in 90 percent of patients. Urethral tumors typically appear hypointense on T1-weighted images and relatively hyperintense on T2-weighted images. Tumor extent is best evaluated on sagittal T2-weighted images.

Metastatic Tumors of Urethra

Secondary tumors of the male urethra are uncommon. Bladder transitional cell carcinomas may spread to the anterior urethra by means of seeding during urethral instrumentation or at cystectomy; these lesions are usually seen as multiple small mucosal nodules during urethrography. Contiguous spread of carcinoma of the prostate, rectum, spermatic cord, and testis may involve the corpus spongiosum, which causes extensive urethral narrowing and irregularity. Hematogenous metastases to the corpora cavernosa and corpus spongiosum are occasionally seen with malignant melanoma and primary prostate, bladder, colonic, testicular, and renal malignancies.

REFERENCES

1. Pollack HM, Banner MP, Martinez LO, Hodson CJ. Diagnostic considerations in urinary bladder wall calcification.AJR 1981;136:791-97.
2. McCallum RW. The adult male **urethra**: normal anatomy, pathology, and method of urethrography. Radiol Clin North Am 1979;17:227-44.
3. Choudhary S, Singh P, Sundar E, Kumar S, Sahai A. A comparison of sonourethrography and retrograde urethrography in evaluation of anterior urethral strictures. Clin Radiol 2004; 59:736-42.
4. Kim SH, Han MC. Reversed contrast-urine levels in urinary bladder: CT findings. Urol Radiol 1992;13:249-52.
5. Chan DP, Abujudeh HH, Cushing GL Jr, Novelline RA. CT cystography with multiplanar reformation for suspected bladder rupture: experience in 234 cases. AJR 2006;187: 1296-302.
6. Ryu J, Kim B. MR imaging of male and female urethra. Radiographics 2001;21:1169-85.
7. Tan IL, Stoker J, Zwamborn AW, Entius KA, Calame JJ, Laméris JS. Female pelvic floor: endovaginal MR imaging of normal anatomy. Radiology 1998;206:777-83.
8. Piepsz A, Ham HR. Pediatric applications of renal nuclear medicine. Semin Nucl Med 2006;36:16-35.
9. M Jinzaki, A Tanimoto, H Shinmoto, Y Horiguchi, K Sato, S Kuribayashi, SG Silverman. Detection of Bladder Tumors with Dynamic Contrast-Enhanced MDCT. AJR 2007;188: 913-18.
10. Baltaci S, Resorlu B, Yagci C, Turkolmez K, Gogus C, Beduk Y. Computerized tomography for detecting perivesical infiltration and lymph node metastasis in invasive bladder carcinoma. Urol Int 2008;81:399-402. Epub
11. Lee JK, Rholl KS. MRI of the bladder and prostate. AJR 1986;147:732-36.
12. Barentsz JO, Jager G, Mugler JP 3rd. Staging urinary bladder cancer: value of T1-weighted three dimensional magnetization prepared-rapid gradient echo and two dimensional spin-echo sequences. AJR 1995;164:109-15.
13. Barentsz JO, Ruijs SH, Strijk SP. The role of MR imaging in carcinoma of the urinary bladder. AJR 1993;160:937-74.
14. Barentsz JO, Jager GJ, van Vierzen PB. Staging urinary bladder cancer after transurethral biopsy: value of fast dynamic contrast-enhanced MR imaging. Radiology 1996;201:185-93.
15. Deserno WM, Harisinghani MG, Taupitz M, et al. Urinary bladder cancer: preoperative nodal staging with ferumoxtran-10-enhanced MR imaging. Radiology 2004;233:449-56.
16. Goh AC, Lerner SP. Application of new technology in bladder cancer diagnosis and treatment. World J Urol 2009. [Epub ahead of print]
17. Dondalski M, White EM, Ghahremani GG, et al. Carcinoma arising in urinary bladder diverticula: imaging findings in six patients. AJR 1993;161:817-20.
18. Sheldon CA, Clayman RV, Gonzalez R, et al. Malignant urachal lesions. J Urol 1984;131:1-8.
19. DiSantis DJ. Inflammatory conditions of the urethra. In: Pollack AH, McClennon BL, eds. Clinical Urography (2nd ed). Philadelphia, Pa: Saunders, 2000;1041-57.
20. Gallentine ML, Morey AF. Imaging of the male urethra for stricture disease. Urol Clin North Am 2002;29:361-72.
21. Sharfi AR, Elarabi YE. The 'watering-can' perineum: presentation and management. Br J Urol 1997;80:933-36.
22. Pansadoro V, Emiliozzi P. Iatrogenic prostatic urethral strictures: classification and endoscopic treatment. Urology 1999;53:784-89.
23. Fortunato P, Schettini M, Gallucci M. Diverticula of the female urethra. Br J Urol 1997;80:628-32.
24. Keefe B, Warshauer DM, Tucker MS, Mittelstaedt CA. Diverticula of the female urethra: diagnosis by endovaginal and transperineal sonography. AJR Am J Roentgenol 1991; 156:1195-97.
25. Daneshgari F, Zimmern PE, Jacomides L. Magnetic resonance imaging detection of symptomatic noncommunicating intraurethral wall diverticula in women. J Urol 1999;161:1259-61.
26. Hahn WY, Israel GM, Lee VS. MRI of female urethral and periurethral disorders. AJR Am J Roentgenol 2004;182:677-82.
27. Donat SM, Cozzi PJ, Herr HW. Surgery of penile and urethral carcinoma. In: Walsh PC, Reitik AB, Vaughan ED, Jr, Wein AJ, eds. Campbell's urology. 8th ed. Philadelphia, Pa: Saunders, 2002;2983-99
28. Vapnek JM, Hricak H, Carroll PR. Recent advances in imaging studies for staging of penile and urethral carcinoma. Urol Clin North Am 1992;19:257-66.

Chapter

13

Imaging of the Prostate Gland

Paramjeet Singh, Anupam Lal

INTRODUCTION

The prostate gland is a common cause of urinary symptoms in elderly men. Two such important diseases of ageing men are carcinoma and hyperplasia of the gland. In addition, a number of congenital and inflammatory pathologies also affect the gland. The advent of modern cross-sectional imaging techniques like ultrasonography (US) and magnetic resonance imaging (MRI) has made it possible to directly visualize the prostate, assess its size accurately and also evaluate any suspicious lesion that may warrant a biopsy.

ANATOMY

The prostate is a chestnut-shaped gland surrounded by a fibrous capsule. Proximally its base is adjacent to the bladder neck and distally its apex lies on the urogenital diaphragm. The seminal vesicles are paired saccular structures lying posterosuperiorly and in continuity with ampullae of the vasa efferentia as they taper medially towards the prostate. The urethra traverses the gland in an angular manner. Detailed anatomic dissection of the prostate reveals zonal anatomy, whereby the prostate is divided into four glandular zones surrounding the prostatic urethra: The peripheral zone, transition zone, central zone, and the periurethral glandular area.[1] In the normal gland sonography can rarely identify these zones unless a pathologic condition is present. On sonography, it is useful to separate the prostate into a peripheral zone and the inner gland which encompasses the transition and central zones and the periurethral glandular area. A nonglandular region on the anterior surface of the prostate is termed the anterior fibromuscular stroma.[2] The peripheral zone, the largest of the glandular zones occupies the posterior, lateral and apical regions of the gland and contains approximately 70 per cent of the prostatic glandular tissue and is the site of most prostate cancers. It surrounds the distal segment of prostatic urethra and is separated from the transition zone and central zone by the surgical capsule, which is often hyperechoic as a result of corpora amylacea or calcification. The transition zone, in the normal patient contains approximately 5 percent of the prostatic glandular tissue and is the exclusive site of origin of benign prostatic hyperplasia. It is seen as two small glandular areas located adjacent to the proximal prostatic urethra and continues with

periurethral glandular tissue encircling the proximal urethra. The periurethral glands form about 1 percent of the glandular volume and are embedded in the longitudinal smooth muscle of the proximal urethra, also known as the internal prostatic sphincter. The central zone constitutes approximately 25 percent of the glandular tissue and is located at the prostatic base. The ducts of the vas deferens and seminal vesicles enter the central zone, and the ejaculatory ducts pass through it. The central zone is relatively resistant to disease processes and is the site of origin of only 5 percent of prostate cancers.

Prostate is supplied by the prostatic arteries which are branches of prostaticovesical arteries arising from the internal iliac arteries on each side. The prostatic artery gives rise to urethral and capsular arteries. The urethral artery supplies about one-third of the prostate while the capsular branches supply the remainder of the gland. Neurovascular bundle containing cavernous nerve from pelvic plexus passes posterolateral to the gland.

Most often the prostate is elliptical in shape, and using the formula for a prolate ellipse (0.523 × transverse × anteroposterior × cephalocaudal diameter) prostatic volume can be calculated. The normal prostate gland volume in the adult is approximately 20 cm^3.

IMAGING MODALITIES[3]

Ultrasound (US)

The prostate can be imaged sonographically by transabdominal, transperineal, transurethral and transrectal approach. Correlative studies have shown that volumetric evaluation of the prostate with suprapubic ultrasound is accurate and that a gram of prostate tissue is equivalent to 1 cm^3. The suprapubic approach allows for gross evaluation of the prostate size but does not offer images of sufficient quality to visualize the zonal anatomy. Transperineal method is compromised by beam scattering but may be useful in patients following abdominoperineal resection. Transurethral approach using 7.5 to 10 MHz transducer affords enhanced visualization of the transitional zone but has poor resolution of the peripheral zone and is an invasive technique. Transrectal ultrasonography (TRUS) is currently the preferred method because of its ability to demonstrate the zonal anatomy, the ejaculatory ducts and seminal vesicles. The most commonly used commercially available probes (with a transducer frequency ranging from 5 to 8 MHz) fire from the end and the longitudinal and axial scans are obtained by rotating the transducer through a 180° axis. Other probe designs include 360° radial scanners paired with end viewing probes for a sagittal image and paired side viewing axial and sagittal probes. The advantages of end-viewing probe designs include patient con-venience, ease of use, and biopsy capability at the time of the diagnostic examination. The central and peripheral zones form the bulk of prostate gland and appear uniformly hyperechoic with only subtle differentiation in their echogenicity. The hypoechoic peri-urethral area corresponds to the transitional zone. Seminal vesicles appear slightly less echogenic than prostate. Grey scale ultra-sound relies on morphology and echogenicity for detection of pathology. To improve ultrasound as an imaging modality of the prostate, many new technologies, such as color and power Doppler, 3-dimensional ultrasound of the prostate and contrast-enhanced ultrasound has been developed. In addition, treatment modalities using high intensity

focused ultrasound (HIFU) for the treatment of BPH and localized prostatic cancer have been developed.[4]

Computed Tomography (CT)

The prostate appears as homogeneous dense structure on computed tomography. Though CT provides a rough assessment of prostatic size and contour, it is not possible to differentiate normal from hyperplastic gland or detect the cancer when it is confined within the prostate gland.

Magnetic Resonance Imaging (MRI)

MRI allows detailed visualization of normal zonal anatomy of the prostate, the prostatic capsule, periprostatic structures and also pelvic lymph nodes.

On T1W images the zonal anatomy is not very clear and the gland is of uniform low-signal intensity. T1W images are useful for detection of hemorrhage (post-biopsy) and to differentiate cyst from an abscess. Internal architecture of the prostate is best appreciated on T2W image. The peripheral zone has high-signal intensity while the central and transitional zones have relatively low-signal intensity. However, central and transitional zones cannot be differentiated from each other, and both together are termed as central gland (Fig. 13.1). In young men, the central gland predominantly consists of central zone. In older men, with prostatic hyperplasia most of the central gland consists of transitional zone. The anterior fibromuscular stroma is dark on all pulse sequences. Seminal vesicle fluid appears bright on T2W image while the walls are hypointense. The periprostatic fat is hyperintense on both T1WI and T2WI and allows easy assessment of periprostatic spread of growth.

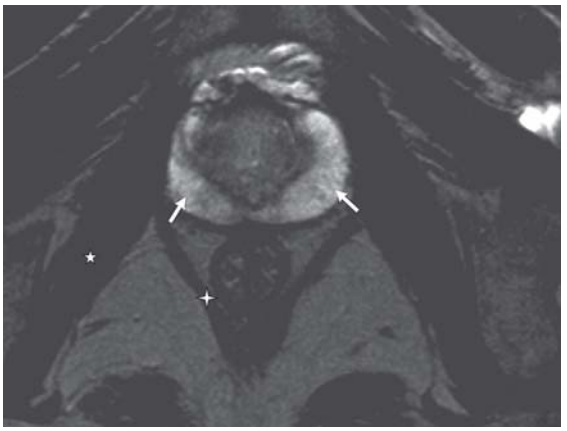

Fig. 13.1: Transverse T2-weighted image of prostate showing hyperintense peripheral zone (arrows) and relatively hypointense central gland. The obturator internus (star) and levator ani (cross) muscles are seen as hypointense structures

BENIGN PROSTATIC HYPERPLASIA (BPH)

Enlargement of the prostate gland is common in older men; however the gland size does not always correlate with symptoms of prostatism. BPH starts in the form of nodules in the transition zone which enlarge in size and number, eventually impinging on the adjacent central and peripheral zones.

Ultrasonography (US)

The sonographic appearance of benign prostatic hyperplasia is varied and depends on the histopathologic changes. Distinct nodules or diffuse enlargement can be present in the transition zone, the periurethral glandular tissue, or both. The typical sonographic feature of BPH is enlargement of the inner gland, which appears relatively hypoechoic to the peripheral zone. The border between central and peripheral gland which is indistinct in young men, becomes more distinct due to presence of BPH (Fig. 13.2). The echo pattern of central gland depends on the

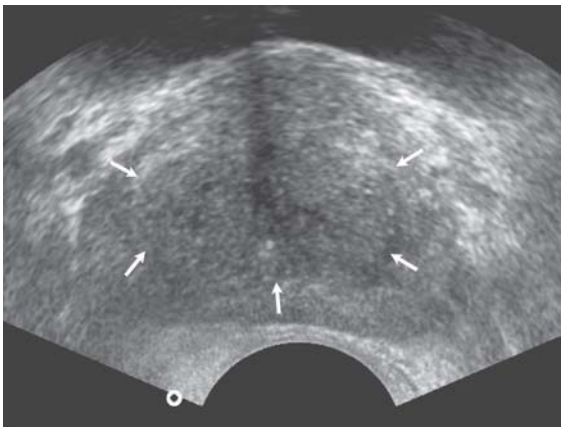

Fig. 13.2: BPH: Transrectal US shows enlarged heterogeneous central gland (between arrows)

admixture of glandular and stromal elements. Nodules may be fibroblastic, fibromuscular, muscular, hyperadenomatous, and fibroadenomatous.[4] Depending on the combination; the nodules may appear either isoechoic, hyperechoic or hypoechoic. Calcifications may also be seen in the central zone.

Because the growth of the gland is primarily anterior, the volume or weight cannot be estimated well by digital palpation. Prostatic ultrasound provides an accurate and reproducible method to determine the prostatic volume and the effect of the hyperplasia on the anterior urethra that correlates with the symptoms of prostatism.

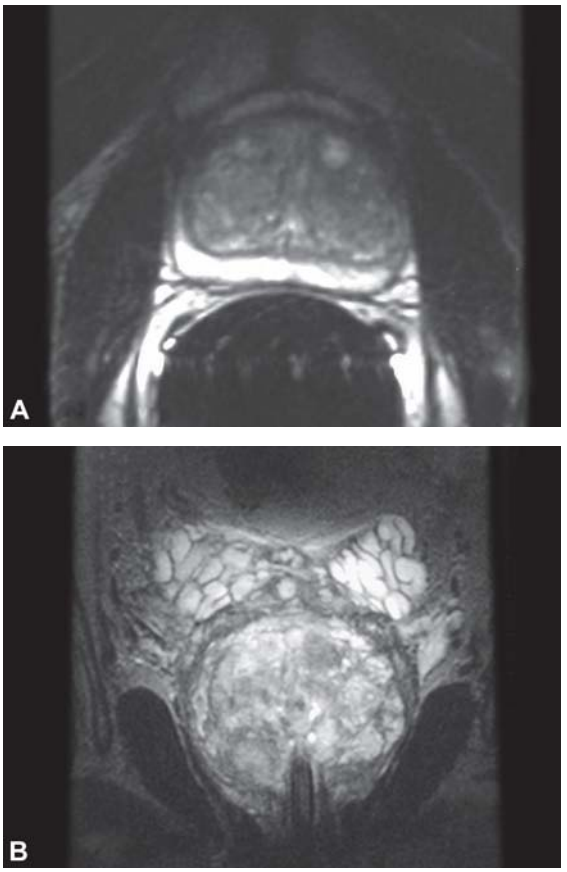

Figs 13.3A and B: T2-weighted axial image **(A)** shows zonal anatomy, i.e. hyperintense peripheral gland and heterogeneous central zone due to hyperplastic changes. The bright nodule represents glandular hyperplasia and dark areas being stromal hyperplasia. The surgical and anatomical capsules are seen as hypointense structures. **(B)** Coronal T2 section shows changes of BHP with enlarged TZ nearly totally effacing the central zone

Magnetic Resonance Imaging (MRI)

T2W endorectal coil imaging of the prostate allows differentiation of glandular (high signal intensity) from the stromal component (low to intermediate signal intensity) in BPH. Surrounding central and peripheral zones are compressed forming a pseudocapsule around the hyperplastic gland (corresponding to the surgical capsule) (Figs 13.3A and B). On T1WI, nodules of BPH are isointense with the remainder of prostate. MR imaging provides excellent resolution of internal prostatic anatomy, the information with respect to the ratio of glandular to stromal tissue in the prostate and an accurate estimate of prostate volume; however, is not routinely used in patients with BPH because of high cost and limited availability.

Other Imaging Modalities

Intravenous urography (IVU) is no longer routinely performed and is generally performed to evaluate other associated symptoms like hematuria, pyuria, and urinary calculi. Retrograde and voiding cystourethrography can provide anatomic information regarding bladder neck contracture, residual tissue, and urethral stricture disease in postprostatectomy patients. CT is hardly ever indicated for uncomplicated BPH as it provides little relevant information, other than prostatic volume determination.

PROSTATE CANCER

Cancer of the prostate is the most common cancer and ranks as the second most common cause of cancer death in men.[5] Adenocarcinoma is the most common histologic type, encountered in approximately 95 percent of patients. Around 70 percent of the prostatic cancer originates in the peripheral zone, 10 to 20 percent in the transitional zone, and 5 to 10 percent in the central zone. Multicentricity of the tumor is quite common. Approximately 30-46% men above 50 years of age may harbor a cancer focus but less than 20% of those develop clinical disease which is largely related to variability in aggressiveness. Imaging has little role in early detection of cancer but has a vital part in local and distant staging of the disease (Table 13.1). Diagnostic tests for local staging must aim to differentiate organ confined disease from locally invasive disease extending beyond capsule (ECS) into periprostatic fat, lymphatics and vessels (stage 3) or adjacent organs (stage 4). Due to proximity, invasion of seminal vesicles and bladder base superiorly, membranous urethra distally and rarely rectum posteriorly should be looked for. Patients with metastatic disease fare worst and a lymph nodal and distant metastasis work-up is part of routine evaluation.

Table 13.1: Prostate adenocarcinoma—TNM staging classification

Stage	*Extent of cancer*
T1	Clinical localized: Tumor not palpable on digital rectal examination
T1a	Focal tumor (< 5% of resected tissue on TURP) and low grade
T1b	Diffuse tumor (> 5% of resected tissue on TURP) and high grade
T2	Clinically localized: Tumor palpable
T2a	Tumor involves < 0.5 lobe
T2b	Tumor involves > 0.5 lobe
T2c	Tumor involves both lobes
T3	Locally invasive beyond prostatic capsule: Tumor palpable
T3a	Unilateral extracapsular extension
T3b	Bilateral extracapsular extension
T3c	Seminal vesicle invasion
T4	Invades adjacent tissue (e.g. bladder, rectum, levator ani muscles)
N/M	Metastatic disease
N 1-4	Metastases to lymph nodes
M 1	Distant metastases

Confined disease (T2) is treated with surgery or radiotherapy while extracapsular spread or SV invasion (T3) is treated with radiation and /or hormonal therapy (Table 13.2). The Gleason scoring system, which was first described in 1966, is based on the architectural growth patterns of prostatic adenocarcinoma. The histologic patterns are grouped into five grades, which are viewed as a continuum. It was found that tumors behaved more like the "average" grade rather than the highest grade present; therefore, Gleason developed a "score" based on the grade of the predominant pattern added to the grade of the second most prevalent pattern.[6] Clinical staging with digital rectal examination (DRE), serum PSA and biopsy tumor grade (Gleason score) remains the standard of practice though it under stages ECS in up to 30-60% cases.[7] However, definitive therapy also takes into

consideration patient's life expectancy, his general health, tumor prognostic factors and presence of metastasis. Particularly, patients at increased risk for metastatic disease (Gleason score 8-10, serum PSA >20 ng/ml or clinical stage T3-4) must undergo imaging work-up before definitive therapy.[7] On the other hand, patients with intermediate risk (Gleason score 5-7 and PSA 10-20) need further elucidation of prognostic factors by newer techniques estimating metabolic information, i.e. spectroscopy, angiogenesis by color Doppler and perfusion imaging and cellularity, i.e. diffusion imaging.

Table 13.2: Treatment decisions by prostate cancer stage

Stage	*Possible treatment options*
T1 Gleason score 2-4	Consider watchful waiting
T1 Gleason score 5-10	Radical prostatectomy, XRT
T2-b Gleason score < 8 and PSA < 20 ng/mL	Radical prostatectomy, XRT
T2-b, Gleason score 8-10 or PSA> 20 ng/mL	Radical prostatectomy or XRT
T2C	Radical prostatectomy or XRT
T3-4	XRT or hormonal therapy, if patient not candidate for radiation
N 1-4	XRT and hormonal therapy
Local recurrence	Consider XRT, if surgical failure, hormonal therapy
Metastatic disease	Palliative XRT, hormonal therapy

Transrectal Ultrasonography (TRUS)

Initially considered as a primary screening test for prostatic cancer, the role of TRUS has now been replaced by prostate specific antigen (PSA) and digital rectal examination (DRE). TRUS alone has limited potential to identify prostatic cancer because of frequent

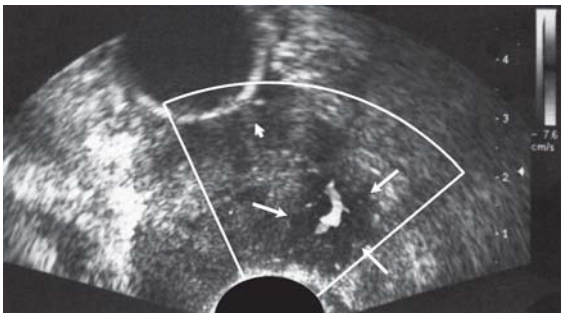

Fig. 13.4: Carcinoma prostate: Transrectal US with color Doppler shows increased vascularity within the tumor mass (arrows) in left PZ

multifocality of cancer within the prostate, the variable sonographic appearance of prostatic tumors, the poor specificity of focal ultrasonic abnormalities, and the substantial percentage of isoechoic prostate cancers which cannot be differentiated from adjacent benign tissues with imaging.[8] Color Doppler and power Doppler has been added to TRUS in an attempt to increase the sensitivity and specificity of prostate ultrasound and ultrasound-guided biopsy. Preliminary reports suggest that increased vascularity in a prostatic lesion correlates with high grade cancer and can suggest the lesion to be biopsied[9] (Fig. 13.4). The indications for TRUS in patients with known or suspected prostate cancer are:

1. Evaluation of the patient with an abnormal digital rectal examination
2. Evaluation of the patient with abnormal laboratory test results indicative of prostate cancer, including PSA, acid phosphatase, or other evidence of metastatic disease
3. Guidance for biopsy
4. Monitoring response to treatment for prostate cancer.

Against the background of normal peripheral zone glandular tissue, small prostatic cancer usually appears hypoechoic because

of closely packed cells in the tumor nodule. Larger tumors may appear isoechoic or hyperechoic. This appearance may be caused by a desmoplastic response of surrounding normal tissue or due to infiltration of the neoplasm into a background of benign prostatic hyperplasia.[7] When an isoechoic tumor is present, it can be detected by presence of secondary signs including glandular asymmetry and capsular bulging. When the cancer totally replaces an entire zone or the entire gland, its identification becomes difficult. Such diffuse lesions must be identified based on the expected echo-genicity of the area examined rather than its relation to surrounding structures. Peripros-tatic extension may be suspected when there is disruption of capsule echogenicity, and irregularity or bulging of the capsular margin (Fig. 13.5). Seminal vesicle extension can be defined sonographically by enlargement, cystic dilatation, asymmetry, anterior displacement, hyperechogenicity, and loss of the seminal vesicle beak. A comparison from the other normal side can be helpful. Because of the high frequency transducers and thus limited depth of penetration, TRUS does not permit pelvic lymph node assessment. Sensitivity of TRUS for local extension into the capsule or seminal vesicles in different studies range from as high as 90 percent and as low as 40 to 60 percent and specificities for invasion range from 46 to 90 percent, depending on the size of primary tumor.[10,11]

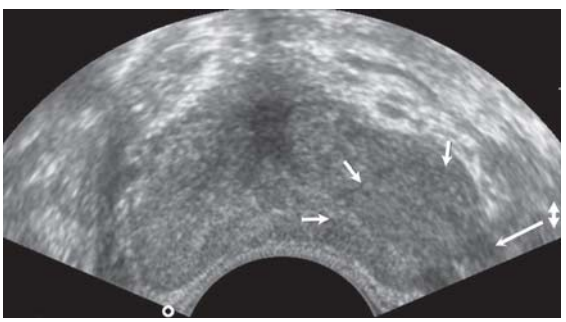

Fig. 13.5: Carcinoma prostate: Transrectal US image shows large hypoechoic mass in left PZ (arrows) with extracapsular extension (long arrow)

Newer developments in TRUS equipment over the past decade include the use of power Doppler, higher frequencies, broad bandwidth technologies, harmonic, contrast harmonic, and pulse inversion imaging. All these improvements may enhance detection of subtle focal sonographic abnormalities within the prostate. Ultrasonic contrast agents can aid visualizations of subtle alterations in prostatic echotexture by highlighting changes in microvasculature. It is possible that Doppler's techniques and contrast agents have the potential to reveal prognostic information about cancer in individual patients by differentiating high grade from low grade tumors.[9]

Computed Tomography (CT)

CT has a limited role in the evaluation of patients with prostatic cancer. Although it can accurately evaluate lymph node and distant metastases and is inaccurate in local staging of the tumor nor helps in biopsy.[10]

Magnetic Resonance Imaging

Most prostatic cancers show low signal intensity relative to normal peripheral zone on T2WI (Fig. 13.6). Central zone cancer detection is problematic due to fibrous stroma having low signal. Tumours with large mucin content, however, may be hyperintense. Low signal intensities are also seen in bacterial or granulomatous prostatitis, post-biopsy hemorrhages and prostatic hyperplasia. The proposed sensitivity, specificity, positive- and negative-predictive values, and overall accuracy of MR imaging in the detection of cancer of prostate and of

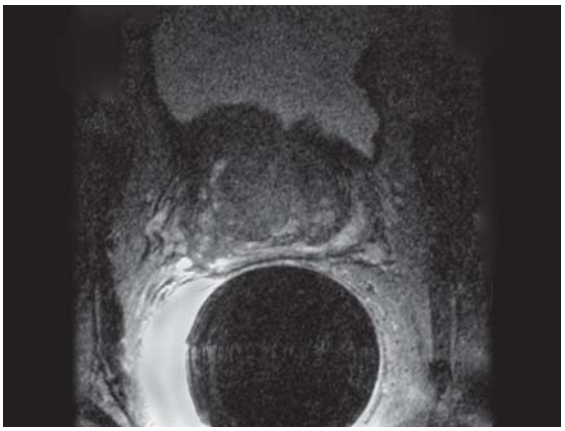

Fig. 13.6: Low-signal infiltrating cancer of the right posterolateral peripheral zone is seen on this endorectal coil axial T2 section of prostate gland

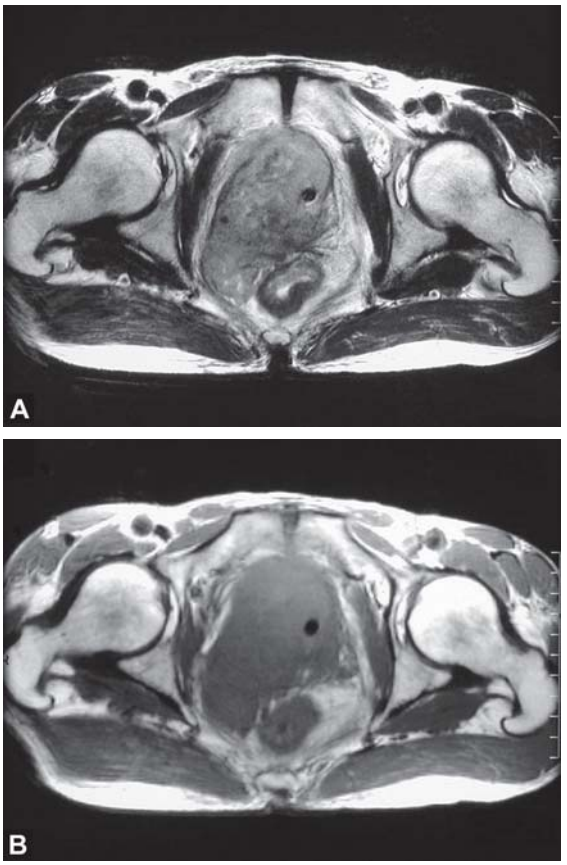

Figs 13.7A and B: Axial T2 (A) and T1 (B) sections of prostate in a case of cancer. Extracapsular extension of cancer through the right neurovascular bundle is seen replacing the normal periprostatic fat

local extracapsular disease in different studies have a wide range of estimates (e.g. 64–98% accuracy has been reported).[11-16] A very high accuracy is precluded by (*a*) the frequency of microscopic regions of capsular invasion that are below even the best spatial resolution of MR imaging; (*b*) the wide differential diagnosis for the findings that frequently connote tumor; and (*c*) the inescapable technical difficulties relating to patient motion, postbiopsy changes, and other factors. As a very general rule, local staging of prostate tumor on the basis of transrectal MR imaging findings will be correct in approximately three-quarters of cases. Currently MRI is the imaging modality of choice for preoperative staging of the prostate cancer. It is more advantageous than ultrasound in detecting local invasion in form of capsular disruption or irregular bulging. Infiltration of low-signal intensity prostatic carcinoma into high-signal intensity seminal vesicles on T2WI can be detected prior to alteration in their size and contour. MRI can also evaluate involvement of the periprostatic neurovascular bundle in form of asymmetry (Figs 13.7A and B). The NVB if uninvolved can be spared during surgery**.** Faster sequences with high resolution like turbo spin echo, use of endorectal coil and multiplaner imaging improve staging.

Newer advances in MR imaging of the prostate include diffusion/perfusion imaging and MR spectroscopy. Normal spectra on Proton MR spectroscopic imaging (MRSI) show choline/creatinine, polyamines and citrate. Peripheral zone shows highest citrate concentration due to glandular elements. A reduction in citrate/ polyamines and increase in choline resulting in high Ch-Cr/cit ratio is

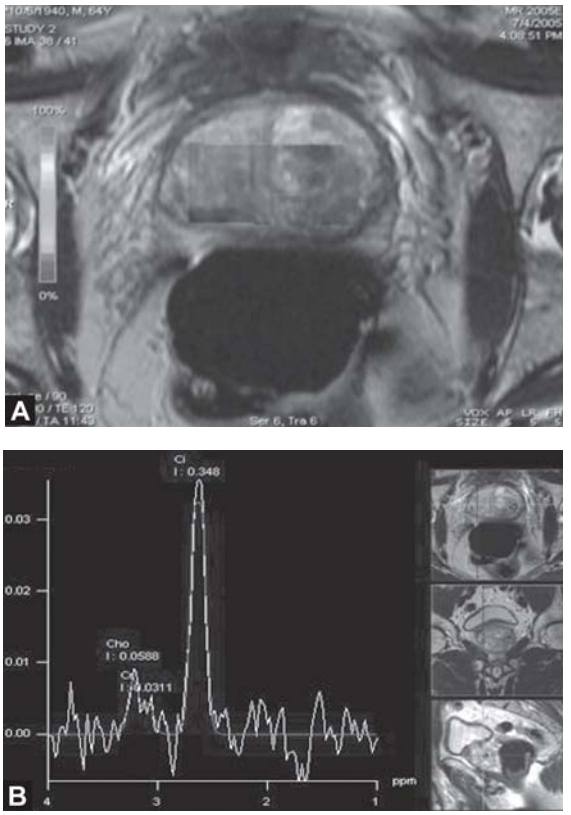

Figs 13.8A and B: Proton MR spectroscopic imaging. Normal spectrum of prostate tissue shows dominant citrate peak at 2.6 ppm and choline/creatinine complex at 3-3.2 ppm *(For color version see Plate 17)*

seen in cancers due to high phospholipids cell membrane turn over in proliferating malignant tissue (Figs 13.8A to 13.9C). Sensitivity and specificity in cancer detection goes up to 91 and 95% respectively when MRSI is combined with routine MR imaging. Assessment of tumor volume, ECE, correlation with Gleason score, cancer detection in patients with prior negative biopsies and risk prediction are all improved with MRSI.[17] However, postbiopsy areas, fibrous stroma of hyperplastic nodules and prostatitis may yield false positive results.

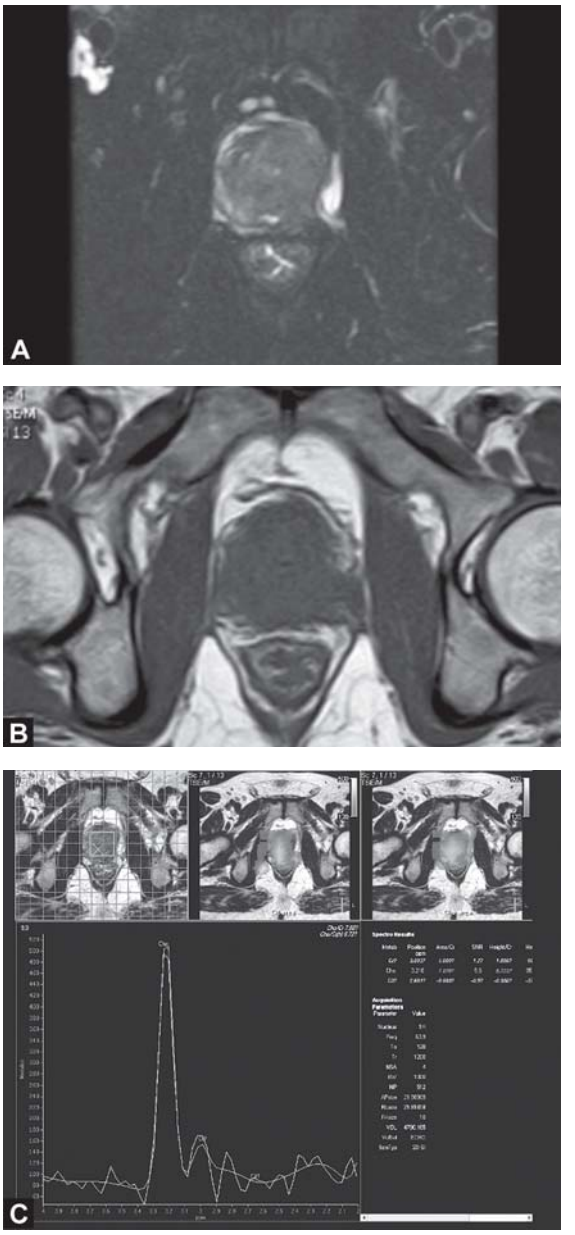

Figs 13.9A to C: T2 **(A)** and T1 **(B)** weighted axial sections of prostate showing loss of signal in left posterolateral peripheral zone with early neurovascular bundle extension suggesting cancer. **(C)** Proton MRSI with multivoxel spectra and metabolite maps overlaid on the anatomical images (upper panel). The spectrum (lower panel) shows high Cho-Cr complex with near total absence of citrate *(For color version of Fig. 13.9C see Plate 17)*

Diffusion imaging may reveal restriction of diffusion in cancers (1.30-1.35 × 10^{-3}) due to high cellularity vs benign tissue (1.60-1.96 × 10^{-3}) particularly in peripheral zone which normally shows higher ADC. Central zone may show variable diffusion. DWI currently suffers from low SNR and needs to be compared with other techniques.[18] Dynamic contrast-enhanced MR imaging, assesses neoangiogenesis a hallmark of higher grade tumors. The data can be evaluated in a semiquantitative (contrast arrival, time-to-peak, peak enhancement and wash-in-washout gradient) or quantitative approach using pharmacokinetic modeling method. It has been shown to detect 93% clinically important cancers.[18] It has lower sensitivity for central gland cancers and should be read along with T2WI. It is particularly important in assessing tumor recurrence.

A combination of these newer techniques (multiparametric imaging with image overlay) has potential to improve the yield of prostate cancer detection and staging, but require further validation. High field 3T imaging offers greater SNR and dynamic range facilitating these newer applications.

Positron Emission Tomography (PET)

PET scanning using various pharmaceuticals like [18F] deoxyglucose, carbon-11 labeled choline and [11C] acetate has been used for both primary and metastatic prostatic cancers but the experience is largely experimental. FDG has limitations for evaluation of prostate cancer patients and therefore alternative tracers are being investigated. To date, the best results have been obtained with 11C-choline and 11C-acetate PET, which seem to demonstrate similar values in this field. At present, the only clinical indication for imaging prostate cancer with 11C-choline-PET is evaluation of suspected recurrence after treatment.[19]

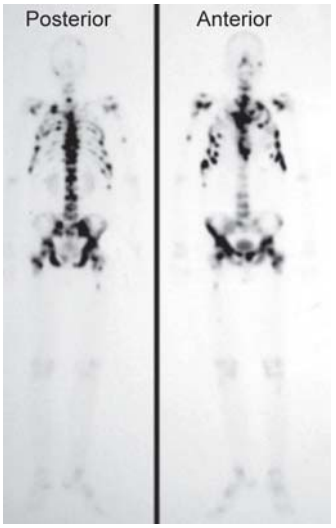

Fig. 13.10: Nuclear scan anterior and posterior views showing multiple osteoblastic metastatic deposits involving axial skeleton from cancer prostate

EVALUATION OF THE METASTASES

Bone scintigraphy is a sensitive method for detecting bone metastases and should be a routine part of the staging process (Fig. 13.10). However, the bone scan has little specificity, and abnormal (hot) areas must be further studied radiographically to allow differentiation between metastases and benign disorders such as fractures, degenerative arthritis and Paget's disease. MRI has shown to be more sensitive than radionuclide scan in detection of skeletal metastases (Fig. 13.11). A chest radiograph remains essential for evaluation of the intrathoracic metastases.

PROSTATITIS AND PROSTATIC ABSCESS

Acute focal or diffuse suppurative inflammation of the prostate (acute prostatitis) occurs most commonly due to ascent of bacteria from the urethra, less often by descent from the upper urinary tract or bladder, and

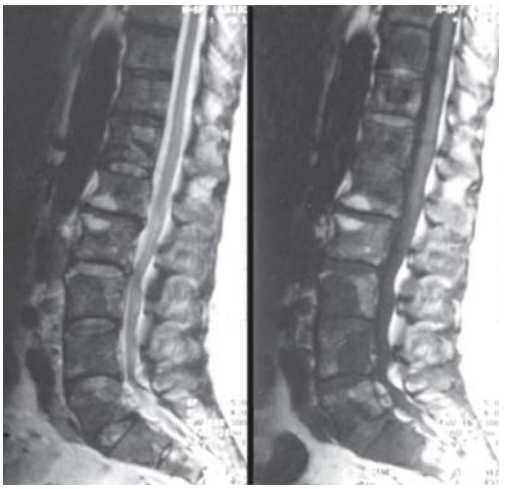

Fig. 13.11: T1 SE and T2 TSE sagittal scans showing blastic marrow deposits appearing hypointense on T1 and T2 images involving dorsolumbar spine

occasionally by lymphogenous or hematogenous spread from a distant focus of infection. The common pathogens are those which cause urinary tract infection like *E.coli, Klebsiella, Proteus, Pseudomonas,* etc. Chronic prostatitis is caused in much the same way and by the same bacterial pathogens as the acute prostatitis, however, it may be associated with certain abacterial pathogens such as *Chlamydia* or *Mycoplasma* organisms. In acute prostatitis, generally the glands are hypoechoic. Color Doppler shows a very vascular focus in areas of prostatitis, mimicking carcinoma. The development of an anechoic mass with or without internal echoes suggests the development of an abscess (Fig. 13.12), which on color Doppler shows a highly vascular wall. The abscess cavity may also contain air due to gas producing organisms (Fig. 13.13). In doubtful cases contrast-enhanced MRI can show the abscess cavity with enhancement of its wall (Figs 13.14A to C). Sonographic findings of chronic prostatitis include focal masses of different degrees of echogenicity, ejaculatory

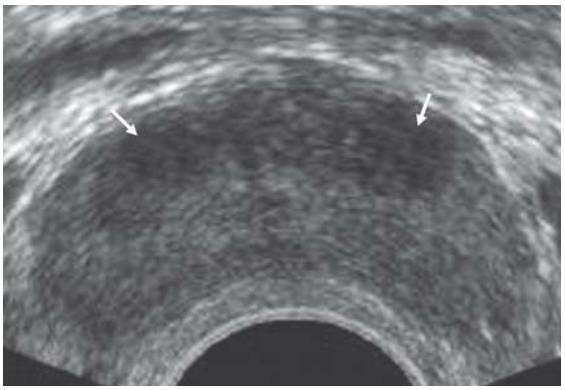

Fig. 13.12: Acute prostatitis with developing abscesses: Transrectal US show hypoechoic areas within the central gland (arrows)

duct calcifications, capsular thickening or irregularity, and periurethral glandular irregularity. In addition dilatation of periprostatic veins and distended seminal vesicles may be seen. Chronic granulomatous prostatitis can mimic sonographic features of prostatic carcinoma. Solitary or multiple diffuse large or small hypoechoic zones may be seen.

MRI appearance of chronic or granulomatous prostatitis can mimic prostatic carcinoma; however, low-signal intensity areas that do not deform the contour favor the diagnosis of chronic prostatitis.[20] Granulomatous prostatitis does not show contrast

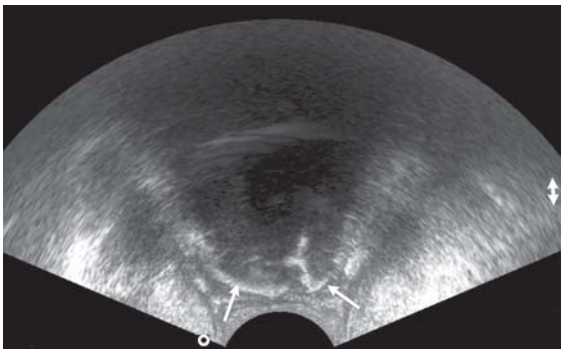

Fig. 13.13: Prostatic abscesses: Transrectal US shows large prostatic abscesses containing air (arrows)

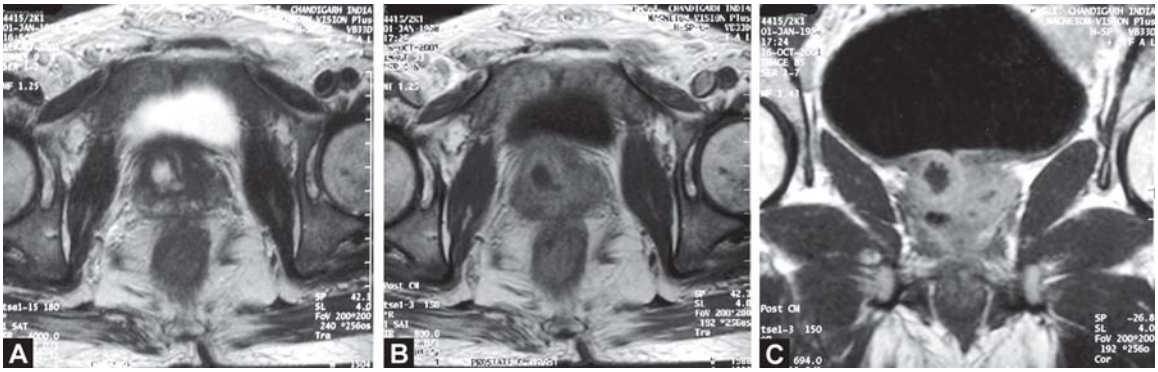

Figs 13.14A to C: T2 axial **(A)**, T1 postcontrast axial **(B)** and coronal **(C)** sections show a bacterial intraprostatic abscess appearing hyperintense on T2 and showing enhancing peripheral margins in the right half of the gland

enhancement whereas prostatic carcinoma does. MRI is very helpful in suspected prostatic abscess since abscess has very high-signal intensity on T2WI and shows intense enhancement of its walls on contrast studies.

PROSTATIC CYSTS

Midline prostatic cysts can be Müllerian duct cysts or utricle cysts. Müllerian duct cysts do not contain sperms and can cause infertility due to compression of the ejaculatory ducts. Utricle cysts contain sperms but unlike former do not extend beyond prostate (Figs 13.15 and 13.16A and B). The paramidline cysts are Wolffian cysts, seminal vesicle cysts or ejaculatory duct cysts which

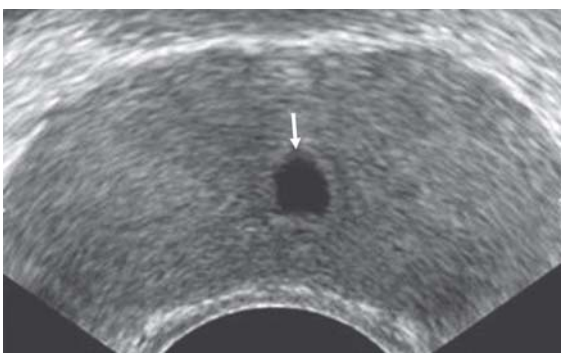

Fig. 13.15: Prostatic utricle cyst: Transrectal US shows the utricular cyst (arrow) in midline

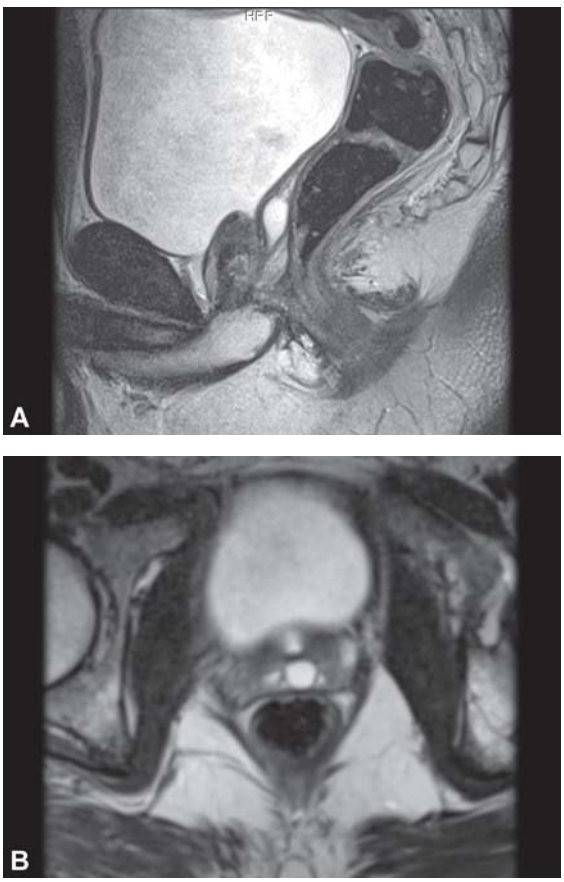

Figs 13.16A and B: T2 sagittal and axial images **(A, B)** shows a Müllerian duct cyst on posterior aspect of the prostate appearing hyperintense. Note the extension beyond the capsular margin

contain sperms. Associated Wolffian duct anomalies, i.e. renal anomalies may be seen in these patients. Peripheral cysts are acquired retention cysts and may be associated with BPH. Cowper's gland cysts are also acquired cysts associated with urogenital diaphragm. Cystic lesions appear smooth walled, hypoechoic on USG and hyperintense on T2WI unless complicated by infection or hemorrhage.[21]

REFERENCES

1. McNeal JE. The zonal anatomy of the prostate. Prostate 1981;2:35-49.
2. Kaye KW, Richter L. Ultrasonographic anatomy of normal prostate gland: Reconstruction by computer graphics. Urology 1990;35:12-17.
3. Amiel GE, Slawin KM. Newer modalities of ultrasound imaging and treatment of the prostate. Urol Clin North Am 2006;33: 329-37.
4. Shinohara K, Scardino PT, Carter SS, Wheeler TM. Pathologic basis of the sonographic appearance of the normal and malignant prostate. Urol Clin North Am 1989;16:675-91.
5. Jemal A, Siegel R, Ward E, Murray T, Xu J, Thun MJ. Cancer statistics 2007. CA Cancer J Clin 2007; 57:43-66.
6. Gleason DF. Histologic grading of prostate cancer: A perspective. Hum Pathol 1992;23:237-79.
7. Yu KK, Hricak H. Imaging prostate cancer. Radiol Clin North Am 2003;38:59-85.
8. Clements R. The role of transrectal ultrasound in diagnosing prostate cancer. Curr Urol Rep 2002;3:194-200.
9. Inahara M, Suzuki H, Nakamachi H, Kamiya N, Shimbo M, Komiya A, Ueda T, Ichikawa T, Akakura K, Ito H. Clinical evaluation of transrectal power doppler imaging in the detection of prostate cancer. Int Urol Nephrol 2004;36: 175-80.
10. Rifkin MD, Dähnert W, Kurtz AB. State of the art: Endorectal sonography of the prostate gland. Am J Roentgenol (AJR) 1990;154: 691-700.
11. Hamper UM, Sheth S, Walsh PC, Holtz PM, Epstein JI. Carcinoma of the prostate; value of transrectal sonography in detecting extension into the neurovascular bundle. Am J Roentgenol (AJR) 1990;155:1015-19.
12. Chelsky MJ, Schnall MD, Seidmon EJ, Pollack HM. Use of endorectal surface coil magnetic resonance imaging for local staging of prostate cancer. J Urol 1993;150:391-95.
13. Jager GJ, Barentsz JO, de la Rosette JJ, Rosenbusch G. Preliminary results of endorectal surface coil magnetic resonance imaging for local staging of prostate cancer. Radiologe 1994; 34:129-33.
14. Bartolozzi C, Menchi I, Lencioni R, et al. Local staging of prostate carcinoma with endorectal coil MRI: Correlation with whole-mount radical prostatectomy specimens. Eur Radiol 1996; 6:339-45.
15. Fütterer JJ, Engelbrecht MR, Jager GJ, Hartman RP, King BF, Hulsbergen-Van de Kaa CA, Witjes JA, Barentsz JO. Prostate cancer: Comparison of local staging accuracy of pelvic phased-array coil alone versus integrated endorectal-pelvic phased-array coils. Local staging accuracy of prostate cancer using endorectal coil MR imaging. Eur Radiol 2007;17:1055-65.
16. Beyersdorff D, Taymoorian K, Knösel T, Schnorr D, Felix R, Hamm B, Bruhn H. MRI of prostate cancer at 1.5 and 3.0 T: Comparison of image quality in tumor detection and staging. AJR Am J Roentgenol 2005;185:1214-20.
17. Kurhanewicz J and Vigneron D. Advances in mR spectroscopy of the prostate Mag Reson Imaging Clin N Am 2008;16:697-710.
18. Somford DM, Futterer JJ, Hambrock T, Barentsz JO. Diffusion and perfusion MR Imaging of the prostate. Mag Reson Imaging Clin N Am 2008; 16:685-95.
19. Farsad M, Schiavina R, Franceschelli A, Sanguedolce F, Castellucci P, Bertaccini A, Brunocilla E, Manferrari F, Concetti S, Garofalo M, Rocca C, Borghesi M,Franchi R, Fanti S, Nanni C, Martorana G. Positron-emission tomography in imaging and staging prostate cancer. Cancer Biomark 2008;4:277-84.
20. Shukla-Dave A, Hricak H, Eberhardt SC, Olgac S, Muruganandham M, Scardino PT,Reuter VE, Koutcher JA, Zakian KL. Chronic prostatitis: MR imaging and 1H MR spectroscopic imaging findings—initial observations. Radiology 2004; 231:717-24.
21. Parsons RB, Fisher AM, Bar-Chama N, Mitty HA. MR imaging in male infertility. Radiographics 1997;17:627-37.

MISCELLANEOUS URINARY TRACT LESIONS

Chapter 14

Renal Cystic Diseases

Veena Chowdhury

INTRODUCTION

Renal cystic diseases continue to present a diagnostic challenge to the radiologist despite recent advances in imaging technology. Cystic disease of the kidney can be divided into two broad categories: congenital or developmental disorders and acquired disorders. The congenital disorders include autosomal dominant and autosomal recessive polycystic disease, tuberous sclerosis, von Hippel-Lindau disease and medullary sponge kidney.[1] Statistically, most cystic lesions of the kidney are simple benign cortical cysts with classic imaging characteristics. Occasionally, however these masses defy diagnosis because of overlap in appearance between benign and malignant lesions. Masses with calcification, high attenuation or high signal intensity or thin septations are probably benign and need a follow up while a multiloculated lesion with enhancing walls or nodularity suggest an aggressive nature and require surgery. Therefore, the most important task for the radiologist is making the critical differentiation between atypical benign cysts and cystic tumors.[2]

EMBRYOLOGY

The kidneys and ureters develop from the intermediate mesoderm. The permanent kidney or metanephros develops following the contact of the metanephric diverticulum or ureteric bud with the metanephric mesoderm. During the fourth week of gestation, a dorsal bud of the metanephric diverticulum grows out of the mesonephric duct into the mass of metanephric mesoderm; thus, during the fifth week of gestation, the metanephros is induced to develop metanephric tubules in its caudal portion. The tip of the ureteric bud becomes the renal pelvis and calyces. The metanephric collecting tubules then develop from the renal calyces. The blind end of the collecting tubules then induce clusters of mesenchymal cells to develop into metanephric tubules of the nephron. Further development of the permanent kidney occurs through both, the growth in the absolute number of nephrons and via the gradual ascent and rotation of the kidney.

The developmental process initially begins as a solid mass of cells which later cannulates to form the lumen. Most congenital cystic

disorders are the result of an arrest in cannulation and communication at various stages of development.[3]

CLASSIFICATION

Renal cystic disease comprises a diverse group of heritable, developmental and acquired disorders. An awareness of the pathology of each cystic disease is helpful in the understanding of the corresponding radiological images. Because of their diverse etiology, histology and clinical presentation, no single universally accepted classification exists, but a practical working classification composed of major categories and most clinically significant renal cystic diseases is as follows:[4-6]

Nongenetic	*Genetic*
1. **Acquired disorders** a. Simple renal cysts; typical, atypical, complicated. b. Acquired cystic disease in renal failure and hypokalemia c. Multilocular cystic nephroma d. Hydronephrotic multicystic kidney	1. **Autosomal dominant** a. Autosomal dominant polycystic kidney disease b. Tuberous sclerosis complex c. Von Hippel Lindau disease d. Medullary cystic disease e. Glomerulo cystic disease
2. **Developmental disorders** a. Multicystic dysplastic kidney b. Pyelocalyceal cysts	2. **Autosomal recessive** a. Autosomal-recessive polycystic kidney disease b. Nephrophthisis
3. **Miscellaneous cystic disease** a. Cystic renal carcinoma b. Inflammatory cysts	

Bosniak Classification System

To characterize cystic lesions of the kidney in 1986 Bosniak developed a classification system based on CT features, recognizing four basic types:

I. Category I lesions are simple cysts of water density (0-20 HU), sharply defined from the adjacent renal parenchyma with no perceptible wall thickness. They are homogeneous and do not show calcification or contrast enhancement (Fig. 14.1).

II. Category II lesions are minimally complicated benign cysts and are of three types
   a. Cysts with thin delicate calcification in the wall or septum.

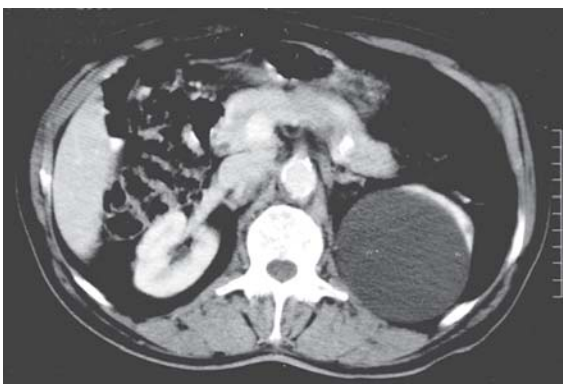

Fig. 14.1: Contrast-enhanced CT showing multiple simple cysts and a large smoothly marginated lesion of homogeneous fluid density in left kidney with cortical "beak" sign typical of simple cyst

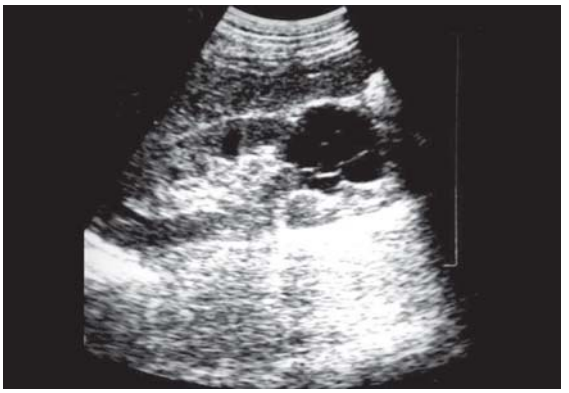

Fig. 14.2: Gray-scale sonogram of right kidney showing a complicated cyst with few thin internal septations (Bosniak's category II lesion)

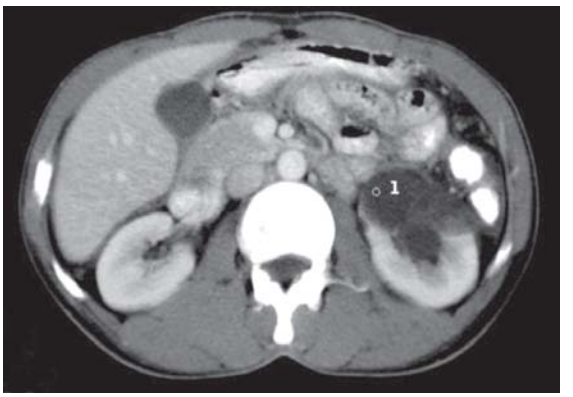

Fig. 14.3: CECT showing a multiloculated cystic mass arising from left kidney with nodular mural thickening and irregularity causing splaying and attenuation of pelvicalyceal system – cystic RCC (Bosniak's category IV lesion)

b. Cysts containing one or two nonenhancing thin internal septae (< 1 mm wall thickness) with no thickened elements. Presence of delicate calcification can be seen in septated cysts (Fig. 14.2).
c. Hyperdense cysts showing uniform, nonenhancing high attenuation on a noncontrast CT examination. If a lesion with attenuation value of 50-90 Hounsfield units is large (>3 cm), irregular, inhomogeneous or has any other noncystic characteristics, it cannot be considered as a category II lesion and should be evaluated surgically to exclude renal carcinoma or should be followed up at three monthly intervals to ensure that the lesion is not growing or changing.

Lesions falling into category I and II a and b are considered benign and do not require follow-up.

III. Category III lesions are masses with more numerous or thickened septae (>1 mm), thick wall, thick and irregular calcification or multiloculated lesions. Surgical management is indicated in these cases. Approximately half of these lesions may prove to be benign e.g. aggregates of simple cysts, multilocular cystic nephroma, lymphangioma or hydatid disease.
IV. Category IV lesions have more obviously malignant characteristics such as inhomogeneity, solid elements, wall thickening, or enhancing components and are regarded as unequivocally malignant, requiring standard surgical management (Fig. 14.3).

Diagnosis and management is clear in category I and IV lesions but difficult in category II and III lesions. Computed tomography helps to differentiate these two.[6]

In 1993, Bosniak revised the classification system to include a subset of minimally complicated lesion with dense calcifications under category 2 which could be managed with follow up. The risk of malignancy in these lesions is approximately 5 percent. All imaging strategies are based on the principles of Bosniak classification.[7]

IMAGING MODALITIES

Conventional Radiography

Plain radiography and excretory urography (EU) are indirect imaging modalities. EU has the additional advantage of assessing the gross functional status of the kidney. Cystic masses of the kidney often reveal:

a. Abnormality of the renal contour or adjacent fascial planes, displacement of bowel loops or splaying of ribs.
b. Curvilinear or rim calcification in cyst wall
c. Filling defects in the opacified cortex during the nephrographic phase of urography.
d. Splaying and distortion of opacified collecting system (Fig. 14.4).

Ultrasonography (US)

Gray scale, realtime sonography is the primary imaging modality for evaluation of renal cystic disorders. It is a noninvasive, multiplanar direct imaging modality, which requires no patient preparation, and unlike excretory urography it shows the mass lesion itself, along with changes in the renal parenchyma and tubular anatomy. It can almost always differentiate a cystic from a solid mass and simple cyst from cystic dysplasias associated with complications. However, obesity and excessive bowel gas can obscure the kidneys.

Tissue harmonic imaging is useful for identifying isoechoic lesions and small renal cysts which may be indistinguishable from normal renal parenchyma on the fundamental mode. Colour Doppler flow imaging and Duplex Doppler sonography can aid in determining the presence or absence of vascularity and flow patterns which provide a clue regarding the benign versus malignant nature of renal cystic masses.

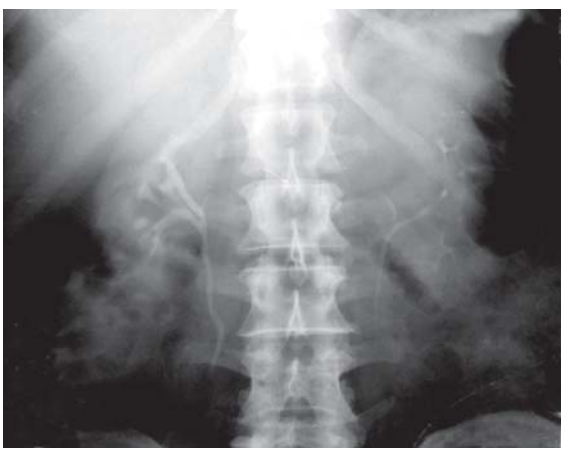

Fig. 14.4: Excretory urogram showing enlarged kidneys with splaying and stretching of pelvicalyceal system (spidery calyces) in a patient with polycystic kidney disease

Computed Tomography (CT)

Computed tomography is the main modality for imaging and characterizing cystic renal lesions.

A lesion that contains fluid and has no blood supply remains water dense after contrast administration but solid tumors appear relatively dense in contrast to enhancing parenchyma. Enhancement is dependent on the dose and rate of administration of iodinated contrast and the timing of imaging. The unenhanced CT, corticomedullary phase, nephrographic phase and excretory phase are obtained. The nephrographic phase is the most valuable for detecting mass lesions less than 3 cm which include clinically insignificant renal cysts and renal cell carcinomas.

A change of less than 10 HU from pre to post contrast images is considered typical of a benign cyst. Very rarely, cystic tumors may enhance less than 10 HU. Majority of pathologic lesions are more than 15 HU. An enhancement between 10 and 15 HU is

considered suspicious but not diagnostic of a tumour. However, morphological features such as wall thickening or nodule make the lesion suspicious even without enhancement especially in the case of papillary cancers.

Spiral CT and multislice helical CT have improved the detection and characterization of renal masses smaller than 10 mm. This is of great significance in patients with very small cysts which may contain foci of malignancy as in von Hippel-Lindau disease. Differentiation of angiomyolipomas (AML) from RCC in small lesions with minimal fat is best possible with helical CT. Excellent 3-D reconstructions using maximum intensity projection (MIP), surface shaded display (SSD) or volume rendering techniques depict the cysts precisely.[5-7]

Magnetic Resonance Imaging (MRI)

Multiplanar imaging capability and angiographic capabilities with excellent soft tissue contrast resolution have made MRI a useful method for evaluating the kidneys. The high field strengths, breathhold imaging, fat suppression techniques and use of MR contrast agents help in differentiating tumor from cysts. The multiplanar imaging capability of MRI makes it easier to assess polar lesions and coronal images make it simple for the urologist to visualize the relative position of a small lesion if a wedge resection or partial nephrectomy is to be planned. MR contrast agents do not have significant nephrotoxicity, hence can be used in patients with renal failure or iodinated contast sensitivity. MRI has a limitation in evaluating cystic lesions with calcification.

Conventional spin-echo sequences may be used for evaluating the kidneys. T1 and T2 weighted images are acquired in the axial planes and often in the coronal and sagittal planes as well. The newer fast imaging sequences reduce motion artifacts. Gradient-echo fast low angle shot (FLASH) sequences acquired during a single breathhold are very useful for evaluating renal lesions.[2,8]

Angiography

Prior to the advent of newer imaging modalities like US, CT and MRI, angiography was commonly used for evaluation of renal mass lesions. However, in the present era it is mainly indicated for interventional procedures of vascular and mass lesions of the kidney. It also serves as a "road map" before renal sparing surgery. Actively bleeding tumors such as angiomyolipomas can be treated with selective angiography by embolization of the intrarenal supply of the tumor.[9]

Cyst Puncture/Cystography

The radiologist plays a key role in the conclusive diagnosis of cystic renal lesions since percutaneous cyst aspiration under US or CT guidance is therapeutic in simple cystic lesions and the biochemical and cytological examination of cyst fluid aids in the differentiation of complex cysts.

SIMPLE RENAL CYST

A renal cyst is a dilated fluid-filled segment of a nephron or collecting tubule, which represents the most common renal mass in an adult, occurring in 50 percent of the population over the age of 50 years. A cystic kidney contains three or more cysts.[4]

Pathology

The pathologic characteristics of a simple nephrogenic cyst include one or more

chambers lined by low cuboidal or flattened epithelium; a 1-2 mm thick fibrous wall; and a serous fluid content that is clear, slightly yellow, and may contain a small amount of protein. Uncommonly, thin septa divide the cyst into multiple chambers that may or may not communicate with each other. Calcium may deposit in the wall or septa of a simple nephrogenic cyst in the absence of any complication such as hemorrhage or infection.[10]

Although it is believed that simple cysts are acquired due to either tubular obstruction or medullary interstitial fibrosis, their exact pathogenesis is unknown. Occasionally, solid renal tumors may obstruct the tubules of adjacent normal parenchyma resulting in tubular dilatation and secondary cyst formation. Such cysts have been referred to as sentinel cysts. Therefore whenever a simple cyst is detected, the adjacent parenchyma should be carefully evaluated for the presence of an adjacent solid mass.

Clinical Features

Most cysts are asymptomatic especially when small. Large cysts may present as palpable mass, flank discomfort/pain, occasionally with hematuria or hypertension, proteinuria or polycythemia. Renal function is generally preserved in the host kidney regardless of size or position of the cyst.

Imaging Features

Excretory urography with tomography can detect renal cysts with a diameter of 2 cm or greater. Simple uncomplicated cysts present as round, smooth, radiolucent filling defect in the nephrogram and frequently show a beak at the interface of the cyst with the rest of the parenchyma and no definable wall is present. Large or centrally located cysts distort and splay the collecting structures. Because abscesses and hypovascular renal cell carcinomas may resemble simple cysts on urography, a cystic mass should be investigated further by ultrasound.[10]

Sonographic studies show simple cysts to be round and uniformly echo-free internally, with a well-defined posterior wall and strong acoustic shadowing. One or more thin, delicate septations may be present (Figs 14.5 and 14.6). If these features are present, a simple cyst can be diagnosed and no further follow-up or intervention is required, provided there are no complicating clinical features to suggest the possibility of other

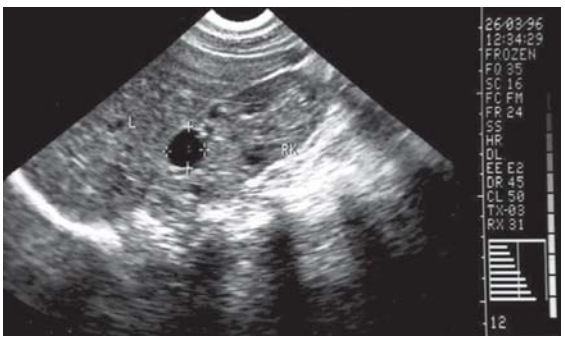

Fig. 14.5: US of kidney showing a well-marginated anechoic lesion with distal enhancement — simple cortical cyst

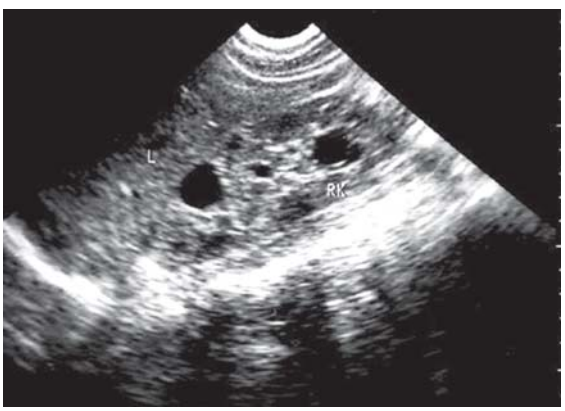

Fig. 14.6: Sonogram showing multiple simple cysts in the right kidney

significant lesion. On Doppler examination simple cysts show lack of colour flow.

Computed tomographic scans shows cysts to be masses of water density (0-20 HU) sharply defined from the adjacent renal parenchyma with no perceptible wall thickness. They are homogeneous and do not show calcification or enhancement after intravenous contrast is administered.

Lesions that fulfill these criteria are simple cysts and require no further intervention. When a renal lesion is not entirely cystic by strict US or CT criteria, a dedicated thin-section CT examination of the kidneys before and after IV contrast administration should be undertaken. To minimize errors in measurement created by partial volume averaging, the slice thickness should be less than half the diameter of the lesion. Enhancement is identified as an increase of at least 10 HU over baseline. Helical CT scanning, which allows for rapid continuous scanning of the kidneys during a single breath-hold, also helps reduce the potential for errors of interpretation due to breathing misregistration.[10,11]

Sampling of fluid from a cystic renal lesion is easily accomplished percutaneously with ultrasound or CT guidance.

On MR imaging, simple cysts contain fluid that appears as uniformly low signal intensity on T1- and high signal intensity on T2-weighted sequences (Figs 14.7A and B). MR diagnosis is based on the same morphologic criteria used to assess lesions by CT. As calcification is not detected on an MR scan, the modality is less effective in evaluating one of the key features distinguishing atypical lesions.[7,8]

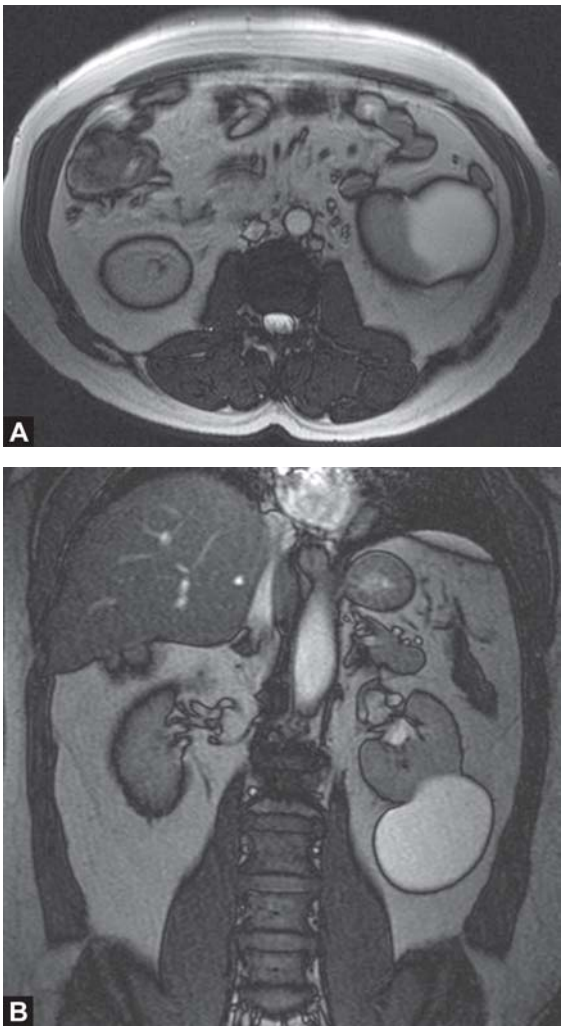

Figs 14.7A and B: TRUFISP axial **(A)** and coronal **(B)** MR images reveal a homogenous sharply marginated lesion with imperceptible wall thickness and high signal arising exophytically from the left kidney – An exophytic simple cortical cyst

Complicated Simple Renal Cyst

A simple cyst may be complicated by
i. hemorrhage
ii. infection
iii. rupture
iv. neoplasia

Hemorrhagic Cyst

It refers to any cystic renal mass filled primarily with blood. It may result from

hemorrhage into a simple cyst or organization of a liquefied hematoma. Approximately 6 percent of simple cysts are complicated by hemorrhage, which is usually the result of trauma, varicosities in the cyst wall or a bleeding diathesis.

Imaging Features

On excretory urography, a hemorrhagic cyst presents as a lucent mass. In cases of trauma, the mass may communicate with the collecting system. In chronic cases, thick calcified walls may be present. An acute hemorrhagic cyst may be impossible to differentiate from an uncomplicated simple cyst on US. With chronicity, internal echoes are seen which represent debris and clot. Later, a thick calcified wall may be seen and the cyst may become multiloculated.

When acute hemorrhage into a cyst has occurred, CT reveals a homogeneous hyperdense mass measuring 70-90 HU, which appears relatively hypodense on postcontrast scans (flip-flop phenomenon) (Fig. 14.8). As the blood liquefies and organizes, there may be a decrease in attenuation and increase in wall thickness with heterogeneous internal contents due to clot and debris.

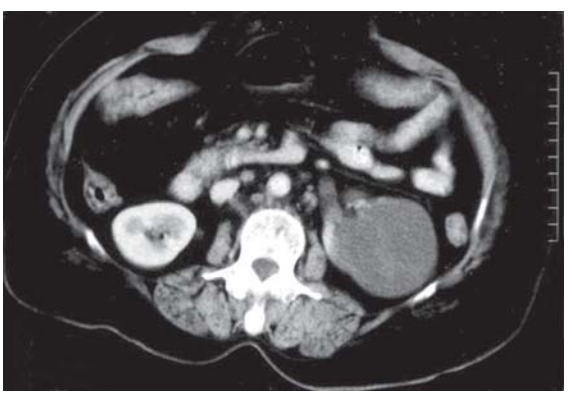

Fig. 14.8: Contrast-enhanced CT showing thin walled septated hyperdense cystic lesion with an exophytic component arising from left kidney — complicated hemorrhagic cyst

On MRI variable signal intensity patterns may be seen in hemorrhagic cysts depending on the hemoglobin degradation products present. The methemoglobin in a hemorrhagic cyst alters its appearance, so that the lesion has an intermediate to high signal intensity on T1-weighted images. Signal intensity on T2-weighted images varies depending on whether red cell lysis has occurred. The overlapping, variable signal intensities of hemorrhagic cysts and tumors with hemorrhage blur the distinction between benign and malignant cystic masses. MR diagnosis is based on the same morphologic criteria used to assess lesions by CT.[4,7]

Infected Cyst

A cyst may become infected by the following routes:

a. Hematogenous dissemination
b. Vesicoureteric reflux
c. Surgical manipulation
d. Cyst puncture

Flank pain and fever may occur but symptoms may be absent.

Pathology

Infected cysts often have markedly thickened walls that are occasionally calcified. Their contents consist of varying amounts of inspissated pus and fluid as well as calcified and noncalcified debris.

Imaging Features

EU demonstrates a mass with thick walls. Rarely, an airfluid level may be seen when the cyst is infected by a gasforming organism. Sonography reveals a thick walled cystic mass

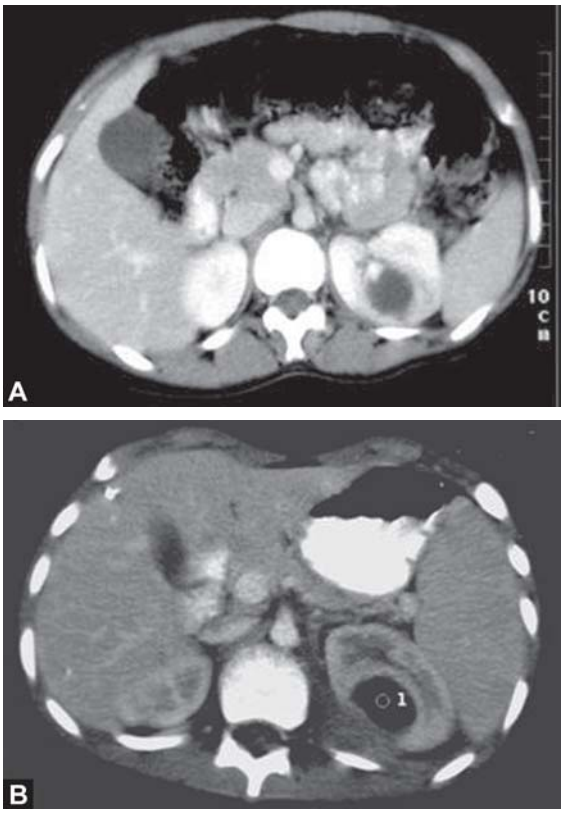

Figs 14.9A and B: Contrast enhanced CT scans showing a hypodense cystic lesion in the left kidney with inhomogenous appearance of the cyst fluid **(A)**. Another case showing a hypodense cystic lesion in the left kidney with involvement of the ipsilateral psoas muscle **(B)**. Infected renal cysts

with internal echoes. Gas transmits the sonographic beam poorly and is suspected when intense specular echoes and illdefined shadowing are recognized.

CT reveals cyst with thick walls, internal septations, debris fluid level, airfluid level and an inhomogeneous appearance of the cyst fluid (Figs 14.9A and B). On MRI, an infected cyst is more intense than a simple uncomplicated cyst but will usually appear less intense than a subacute hemorrhagic cyst although it may be indistinguishable from a chronic hemorrhagic cyst.

Cyst Rupture

It is an uncommon complication of a simple renal cyst. Cyst rupture may be clinically silent or may be accompanied by severe pain and abdominal tenderness. Hematuria is common and the condition is usually diagnosed on the basis of EU, which often demonstrates the collecting system communicating with the cyst.

US and CT can demonstrate fluid or blood in the perinephric and retroperitoneal spaces. Management in such cases is conservative.

Carcinoma in Wall of a Pre-existing Cyst

Rarely, a carcinoma arises from the epithelial lining of a pre-existing simple cyst in the form of a discrete nodule at the base of the cyst.

Imaging Features

The cyst fluid provides an excellent acoustic window for visualizing the tumor nodule on sonography. CECT demonstrates focal wall thickening or a discrete tumor nodule that often enhances. MRI may reveal a focal mass or wall thickening. On angiography, it may be recognized as a focal blush in a larger hypovascular mass.

ATYPICAL SIMPLE CYSTS

Occasionally, simple cysts are atypical in their radiographic or clinical presentation. In these differentiation from cystic neoplasms, infectious diseases and other renal cystic disorders may be difficult.

Calcified Cyst

About 1-3 percent of cysts are calcified and the calcification is usually peripheral and curvilinear. US is unreliable owing to shadowing and reverberation artifacts due

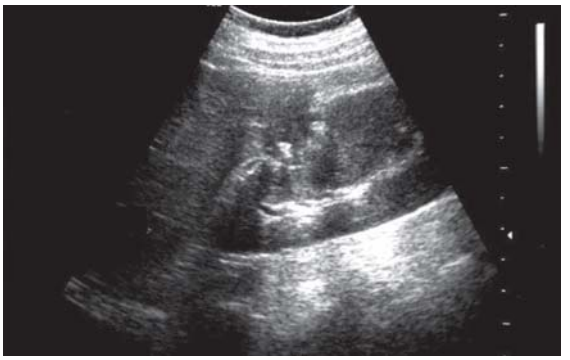

Fig. 14.10: Gray-scale sonogram shows peripheral curvilinear calcification causing distal shadowing in a complicated cyst

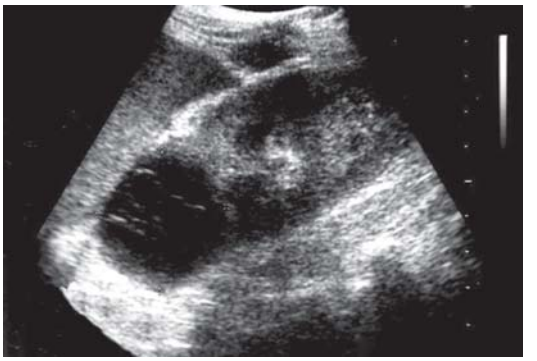

Fig. 14.11: US image showing multiseptated complex cystic mass within upper pole of left kidney distorting the renal contour and central sinus echoes – atypical septated cystic metastases from carcinoma lung

to calcification (Fig. 14.10). CT is the most sensitive method of detecting calcification within a cyst however, a confident radiological diagnosis of a calcified simple cyst from a cystic RCC is often extremely difficult and may be achieved only after careful histological examination.

Hyperdense Cyst

Hyperdense cyst is a homogeneous, cystic appearing mass measuring 50-100 HU on unenhanced scans and demonstrating no significant contrast enhancement. It is thought to represent hemorrhage into a cyst while other explanations for a hyperdense cyst include high protein content, high viscosity and solidified colloid. Careful examination is required because some hyperdense masses may be secondary to either a primary or a secondary neoplasm. A measurement or washout of contrast material from a lesion at 15 minutes allows differentiation between hyperdense cysts and renal tumor. There is no change in hyperdense cysts while tumors show a decrease in attenuation or "deenhancement".

Septated Cysts

Occasionally one or more septa are identified within a renal cyst, which may be a manifestation of two adjacent cysts sharing a common wall or a cyst, complicated by hemorrhage or infection. A septated cyst can be considered nonsurgical if the septae are 1 mm or less without any associated nodularity. The presence of multiple, thick septae should mandate further evaluation to rule out a cystic neoplasm (Fig. 14.11).

Multiple Simple Cysts

They may occur in one or both kidneys and are often misdiagnosed as bilateral polycystic kidney disease. Features favouring the diagnosis of multiple simple cysts against PCKD are normal renal function, absence of family history and absence of cysts in other organs.

Localized Cystic Disease

These represent dilated ducts and tubules which vary in size from a few millimeters to several centimetres. Between the cysts normal renal parenchyma without neoplastic or dysgenetic stroma is seen. On sonography, multiple small cysts often present as one large multiloculated mass. Individual smaller cysts are often recognised in the parenchyma

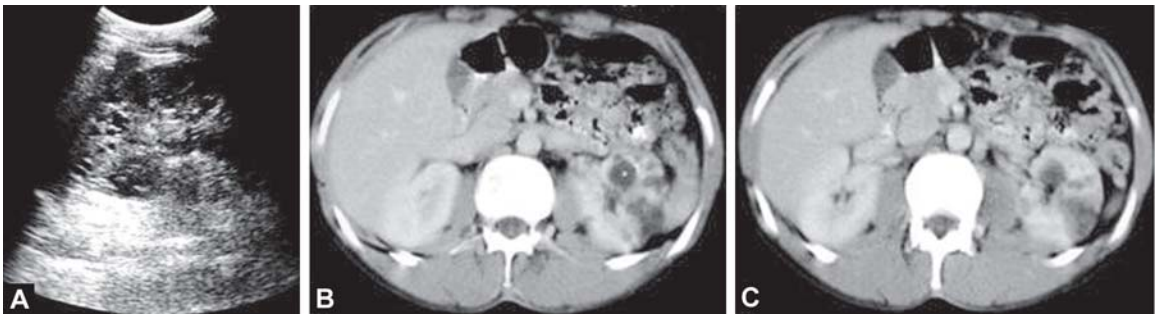

Figs 14.12A to C: Sonogram **(A)** showing multiple small cysts in the upper pole of the left kidney seen as a multiloculated mass. Contrast enhanced CT scans **(B and C)** revealing multiple cysts in the upper pole of the left kidney separated by enhancing bands of renal parenchyma – Unilateral localized cystic disease

adjacent to the main multiloculated mass (Figs 14.12A to C). The most important differential diagnosis is a multiloculated neoplasm which can be differentiated by the absence of capsule between the cluster of cysts and normal parenchyma and the presence of several small parenchymal cysts not contained within the main cluster of cysts. These findings are best appreciated on CT.[12]

POLYCYSTIC KIDNEY DISEASE

Autosomal Dominant Polycystic Kidney Disease (ADPKD)-(Potter Type III)

ADPKD is the most common of the hereditary diseases (1:1000). It is a systemic hereditary disorder that is characterized by cyst formation in ductal organs, particularly the kidney and liver, and by gastrointestinal, cardiovascular and musculoskeletal abnormalities.

About 85 percent of cases are due to a dominant gene located on the short arm of chromosome 16 (the ADPKD-1 gene) whereas 5-10 percent of cases are due to an abnormal gene located on the long arm of chromosome 4 (the ADPKD-2 gene), which causes a milder form of the disorder.[4,5]

Patients with a positive family history of ADPKD and no imaging evidence of renal cysts can be further evaluated using gene-linkage analysis. It is proposed that the disorder results from failure of union of the branches of ureteral bud with metanephros which, deprived of the organizing influence form cysts.

Pathology

There is cystic dilatation of nephrons involving all segments from proximal convoluted tubule to collecting duct due to epithelial hyperplasia leading to redundancy and predisposing to cyst formation.

With minimal disease, the kidneys are normal in size with smooth surface but with increase in the size and number of cysts, the kidneys are asymmetrically enlarged with bosselated surface contour, however, the reniform shape is maintained.

Although multiple bilateral renal cysts are the most important manifestation, ADPKD is really a systemic disease and is associated with many other organ abnormalities including intracranial aneurysms, cardiac valvular abnormalities, liver and pancreatic cysts and colonic diverticulae.[4]

Clinical Features

Most affected individuals present in the fourth or fifth decade with flank pain, palpable masses, hypertension, hematuria,

urinary tract infection, proteinuria or polycythemia. Progressive azotemia ensues as renal parenchyma is destroyed and renal failure occurs in most patients by the age of 60 years. Complications include superimposed infection, cyst hemorrhage, uric acid stones and hypertension.

Imaging Features

In a patient with a family history of ADPKD, screening for the disease with sonography, CT or MR imaging often helps to establish the diagnosis. Ultrasound is the modality of choice for primary evaluation of most patients with suspected ADPKD.

Plain films reveal bilateral enlarged kidneys with lobulated margins causing displacement of surrounding structures, like colonic flexures. Calcification may be curvilinear or amorphous and presence of renal calculi often signifies superimposed infection. The "nephrogram" phase of the EU is characterized by numerous, smoothly marginated radiolucencies throughout the cortex and medulla, which have been likened to the appearance of " Swiss cheese". An appearance of spidery collecting system with stretched and crescentric calyces may be noted.

On US, cysts of varying sizes are noted in enlarged kidneys with a lobulated outline (Figs 14.13A and B). Similar cysts may be seen in liver, pancreas and the spleen. Antenatal diagnosis is possible on demonstration of enlarged cystic kidneys, ascites and hepatomegaly. The presence of atleast two renal cysts (unilateral or bilateral) in individuals at risk and younger than 30 years may be regarded as sufficient to establish a diagnosis; among those aged 30-59 years, the presence of at least two cysts in each kidney may be required; and among those aged 60 years and above, at least four cysts in each kidney should be present.[4]

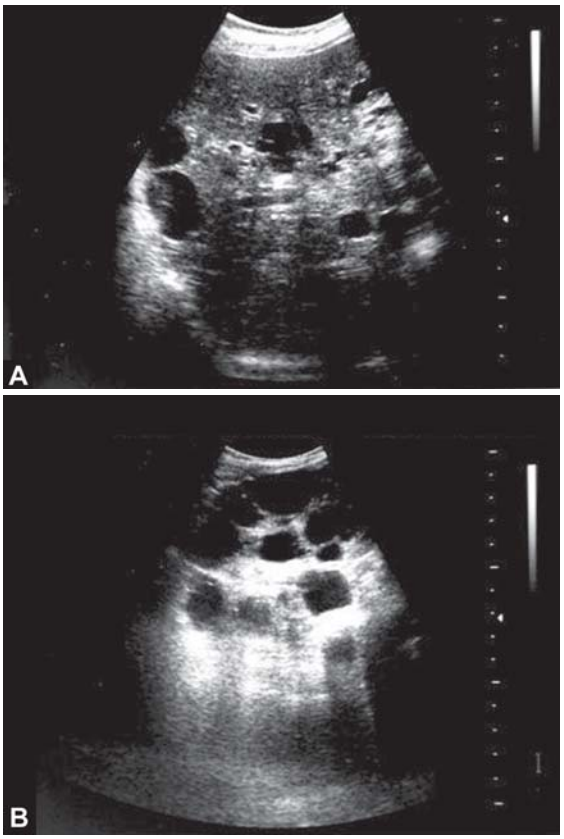

Figs 14.13A and B: Sonography showing multiple noncommunicating cysts of varying sizes replacing the renal parenchyma and distorting the central sinus echoes – ADPKD. Cysts are also seen in the liver

The sensitivity of CT scan is greater than that of ultrasound in detecting renal cysts and thus, may establish the diagnosis at an earlier age and more definitively (Figs 14.14A and B) (Fig. 14.15). On MRI, the renal cysts are hypointense on T1 weighted and hyperintense on T2 weighted images, with infected and proteinaceous cysts showing intermediate signal intensities(Fig. 14.16) and (Fig. 14.17).

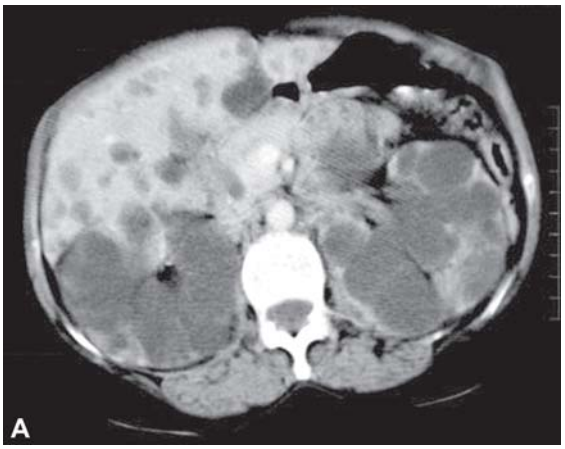

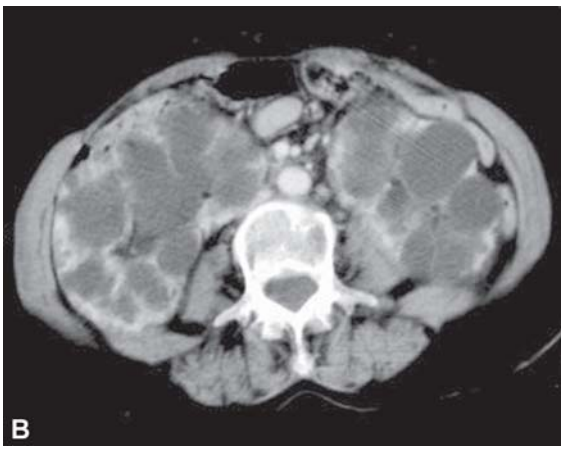

Figs 14.14A and B: Contrast enhanced CT scans revealing multiple non-communicating cysts in both kidneys. Cysts are also seen in the liver – ADPKD

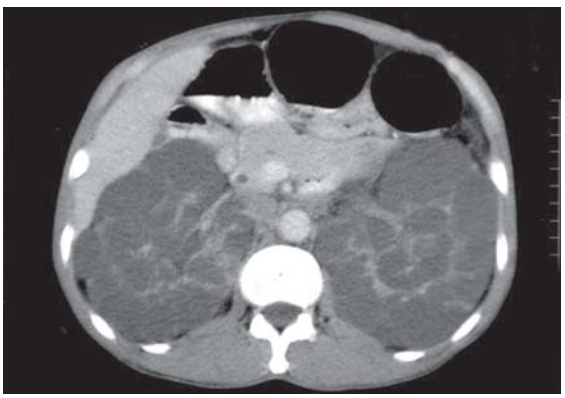

Fig. 14.15: CECT scan in another case showing multiple non-communicating cysts in both kidneys – ADPKD

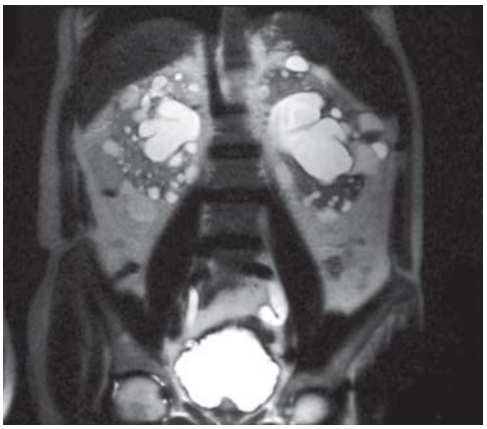

Fig. 14.16: T2W coronal MR image showing both kidneys to be enlarged with multiple cysts of varying sizes having fluid signal intensity studding the renal parenchyma of both kidneys consistent with polycystic kidney disease. Note is also made of bilateral hydronephrosis and back pressure changes in the bladder due to bladder outflow obstruction

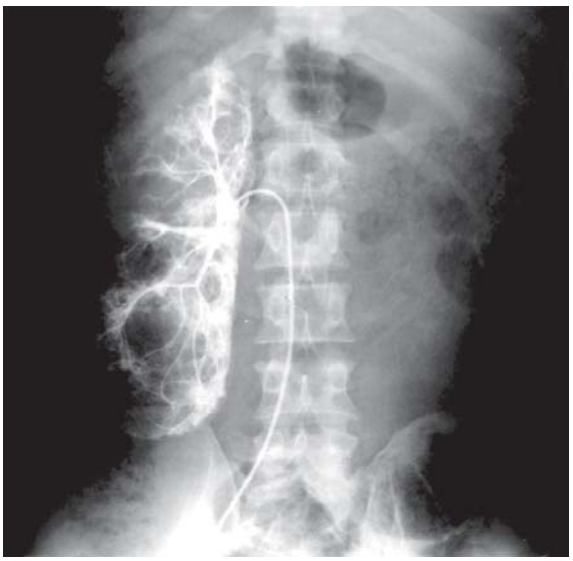

Fig. 14.17: Selective renal angiogram in a case of polycystic kidney disease showing avascular areas with splaying of the normal renal vessels around consistent with cysts

Autosomal Recessive Polycystic Kidney Disease (ARPKD) (Potter Type I)

Of all the renal cystic diseases, ARPKD is the most common heritable disease manifesting in infancy and childhood. The two constant

features of ARPKD are involvement of the kidney and liver. Its frequency has been reported as between 1 in 6000 and 1 in 55000 births and the responsible gene has been mapped to chromosome 6.[13]

Clinicopathologic Features

ARPKD is a disease of tubular malformation and ectasia. In the kidney, the disorder manifests as nonobstructive collecting duct ectasia, usually in a bilaterally symmetric fashion with enlargement of the kidneys. Fibrosis develops in the renal interstitium resulting in impairment of renal function and consequent hypertension, dilute urine and renal failure. The liver shows hepatic fibrosis and biliary ectasia.

The perinatal form of ARPKD is the most common and it usually presents with severe renal failure and bilateral renal enlargement. In infancy or childhood the hepatic abnormalities secondary to congenital hepatic fibrosis predominate with milder renal disease. Portal hypertension can result due to severe periportal fibrosis. Marked cystic dilatation of the intrahepatic biliary ducts "Caroli's disease" is also associated with ARPKD. Generally, the hepatic and renal involvement are inversely proportional to each other in individual patients.[13]

Imaging Features

Antenatal diagnosis of ARPKD can be made. Bilateral symmetrically enlarged kidneys with severe oligohydramnios and a nondistended fetal bladder with thoracic cage compression are typical features seen in the third trimester.[5]

In neonates and infants with moderate to severe renal disease, the kidneys are smoothly enlarged. Plain films reveal abdominal distension with centrally placed gas filled bowel loops. With severe kidney disease, the baby may be born with pulmonary hypoplasia and a small thorax with evidence of pneumothorax.

On US, the kidneys are smoothly enlarged and diffusely echogenic with loss of corticomedullary differentiation. The bladder is usually small.

On unenhanced CT, the kidneys are smooth, enlarged and low in attenuation. Focal liver cysts and features of portal hypertension may be present. Recently bilateral renal calcifications have been reported on CT and the degree of calcification is related to the severity of renal disease.[14] After IV contrast administration, the kidneys show a "striated nephrogram", which represents accumulation of contrast material in the dilated tubules. On MR imaging, there is increased signal intensity of the renal parenchyma on T2 weighted images.

MEDULLARY SPONGE KIDNEY (MSK)

MSK is an uncommon, benign cystic disorder of the renal medulla characterized by dilatation of the terminal portion of the collecting ducts (ducts of Bellini). The disorder is typically bilateral, although it may be unilateral or rarely involves only one pyramid. Its true prevalence in the general population is unknown but is estimated to be 1 in 5000 persons.[4]

Clinicopathologic Features

Renal size is normal to slightly enlarged with a smooth renal contour. It is characterized by dilatation of the papillary portions of the ducts with presence of small intraluminal calcification. Calcification is either due to distal renal tubular acidification defect or due to urinary stasis in the dilated collecting ducts.

Patients usually present in the third or fourth decade with renal colic, hematuria, dysuria and fever. Male/female ratio is 2:1. The association of MSK with other rare diseases suggests a hereditary pattern. It is associated with congenital hemihypertrophy, Ehlers Danlos syndrome, parathyroid adenoma, Caroli's disease, Marfan's syndrome and ADPKD.[4]

Imaging Features

The diagnosis of MSK is made with EU, which shows a characteristic pattern of medullary nephrocalcinosis with multiple discrete calculi clustered in the renal pyramid on plain films. On contrast administration, the cystically dilated collecting ducts appear as clusters of small rounded opacities in the papillae, which may become distorted with splaying of the calyceal cups (Fig. 14.18).

Ureteral obstruction may result when calculi are extruded into the collecting system. A brush or fan appearance of discrete linear densities may be seen. On sonography, the medulla may be hyperechoic from calcific deposits. Occasionally, cystic cavities and hydronephrosis may be detected.

CT scan is sensitive in the detection of medullary nephrocalcinosis, but insensitive in diagnosing MSK because there are many causes of medullary nephrocalcinosis.

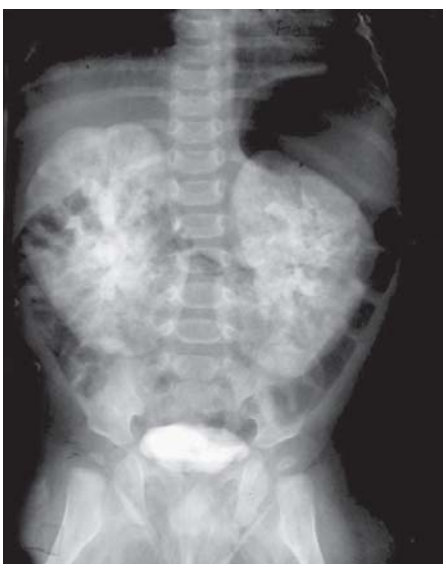

Fig. 14.18: Excretory urogram in a child with medullary sponge kidneys showing enlarged kidneys with medullary nephrocalcinosis and characteristic "Swiss cheese" nephrogram

MEDULLARY CYSTIC DISEASE

It is a rare disease process characterized by progressive renal failure, renal tubular atrophy, secondary glomerular sclerosis and cysts of the renal medulla and corticomedullary junction.[15]

Clinical Features

This disease complex can be separated into 2 distinct groups by age of onset and mode of inheritance. In the juvenile form inherited as an autosomal recessive disorder, the children present with hyposthenia, anemia and growth retardation and it is associated with ophthalmologic and neurologic abnormalities, congenital hepatic fibrosis and related dysplasia. The adult form presents in the 2nd to 4th decades, typically with no extrarenal manifestations and is inherited as an autosomal dominant mode. Both forms progress to renal failure; haematuria typically is not present.

Imaging Features

Plain film shows normal to small kidneys with no calcifications. EU shows poor visualisation of normal to small kidneys with a smooth contour.

On USG, small fluid filled medullary cavities and smooth kidneys of increased echogenicity are noted.[15] CT demonstrates kidneys that are bilaterally small and smooth

with presence of cysts in the medulla and corticomedullary junction.

MULTICYSTIC DYSPLASTIC KIDNEY (MCDK)- [POTTER TYPE II]

MCDK is a developmental, nonhereditary anomaly with multiple, smooth nonfunctioning, non-communicating cysts. It is one of the most common abdominal masses in the newborn and is typically unilateral, otherwise asymptomatic. The bilateral form of MCDK is usually associated with congenital gastrointestinal and cardiac abnormalities. This form has a poor outcome due to accompanying oligohydramnios and pulmonary hypoplasia.[16]

Pathology

The kidney is composed of multiple cysts held together by connective tissue with little or no normal renal parenchyma. Most often, there is atresia of the ureter and renal pelvis (pyeloinfundibular atresia). The hydronephrotic form is seen if incomplete but severe obstruction occurs early in nephrogenesis resulting in a dilated renal pelvis.

Potter described two subtypes of renal dysplasia depending on the size of renal cysts. In Potter type II a the kidney is enlarged due to polymorphic and multilocular cysts while in Potter type II b the kidney is smaller. These two types can be differentiated on sonography.[3]

Imaging Features

The diagnosis is made most often with antenatal or neonatal sonography. MCDK can be diagnosed in utero from as early as 15 weeks. A paraspinal mass with internal cysts of varying shapes and sizes without identifiable communication is seen and the renal pelvis and ureter are usually not visible. Oligohydramnios with bilateral MCDK is a poor prognostic sign (Figs 14.19A and B).

A hydronephrotic MCDK tends to have a more reniform shape and a dilated renal pelvis should be seen. Doppler waveforms have been reported to be markedly abnormal in MCDK with a reduced peak systolic frequency shift or no diastolic flow present. In the older child or adult, radiographic

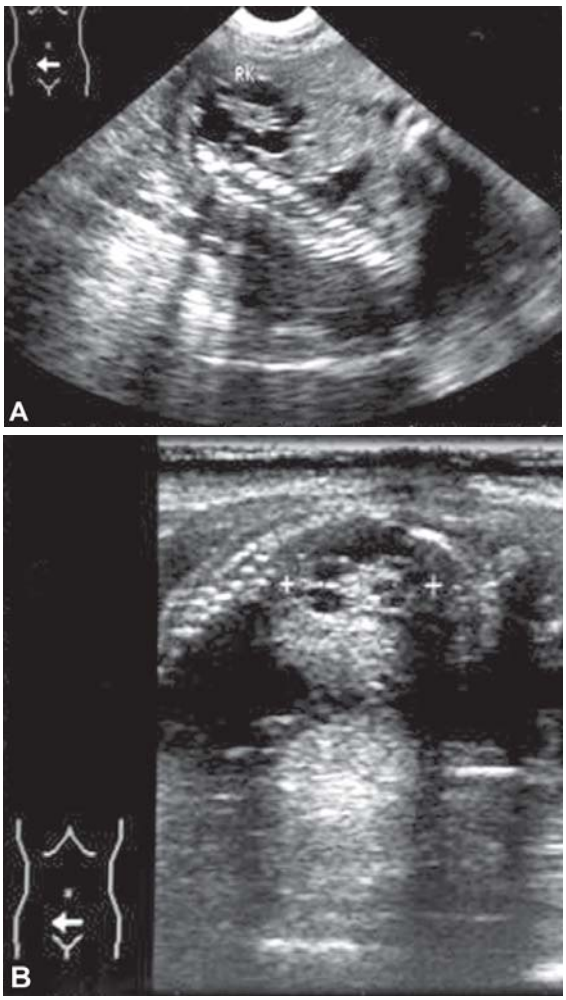

Figs 14.19A and B: Antenatal sonogram showing multiple non-communicating cysts in an enlarged fetal kidney – multicystic dysplasia

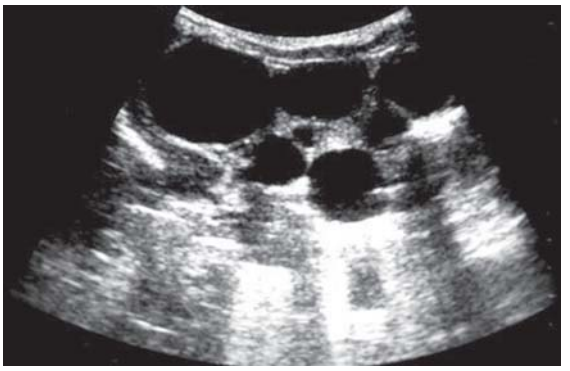

Fig. 14.20: US of right kidney in a four-year-old child shows multiple cysts of varying sizes distorting the reniform contour – MCDK

studies show nonfunctioning kidney with evidence of ring calcification(s) in the renal region (Figs 14.20 and 14.21A and B). Radionuclide scan is used to assess the functional activity when the diagnosis is in question. 99mTc mercaptoacetyltriglycine uptake is seen in an obstructed kidney but not in MCDK.[4]

CYSTIC DISEASE ASSOCIATED WITH RENAL NEOPLASM

Acquired Cystic Kidney Disease (ACKD)

ACKD is characterized by the formation of multiple renal cysts in patients with endstage renal disease, who have no history of hereditary cystic disease. It is seen in 40-50 percent of patients on long term hemodialysis. After 3 to 5 years of dialysis, the prevalence of ACKD is 40 to 60 percent, rising thereafter to reach 90 percent between 5 and 10 years on dialysis.[4]

Multiple, bilateral small cysts that involve both the renal cortex and medulla are seen. ACKD is also associated with an increased incidence of renal neoplasms. Factors causing renal cyst and tumor formation in end stage renal disease are unknown but the two are interrelated. It is postulated that with progressive destruction of functioning renal

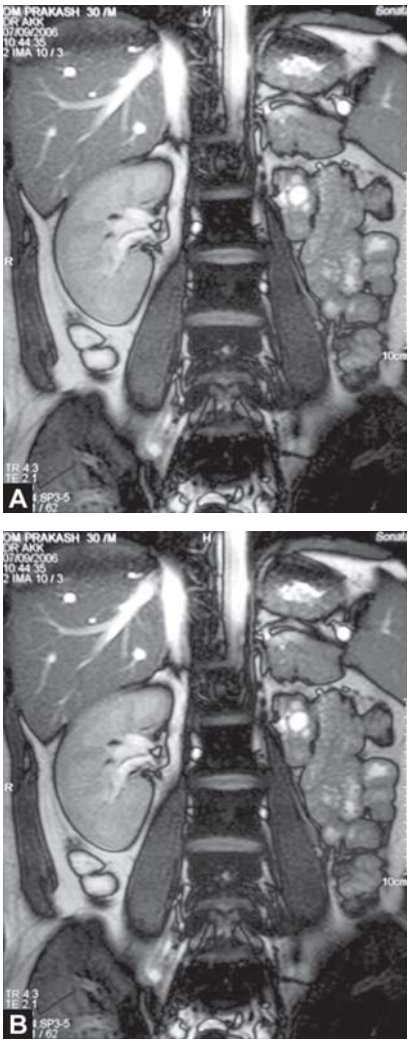

Figs 14.21A and B: Coronal true FISP MR images reveal a small dysplastic left kidney replaced by multiple noncommunicating cysts showing hyperintensity on T2W image with compensatory hypertrophy of right kidney – adult MCDK

tissue cystogenic substances accumulate and cause hypertrophy and hyperplasia of epithelial cells. The tubular epithelium proliferates and cystic dilatation of tubules occurs. Subsequently there is a continuum from single layered epithelial cysts to multilayered cysts to renal cell carcinomas. Tumors can be multiple and bilateral.[8,17,18]

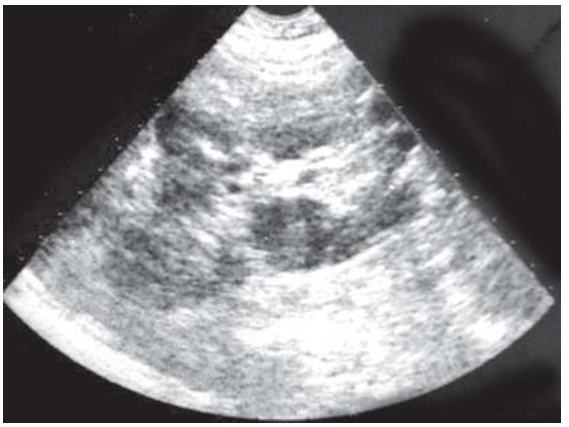

Fig. 14.22: US in a patient with chronic renal failure on long term hemodialysis showing shrunken echogenic kidney with loss of corticomedullary differentiation and multiple small cortical cysts – ACKD

Clinical Features

Most patients with ACKD are asymptomatic, however, increase in hemoglobin due to raised erythropoetin levels, hematuria and renal neoplasia, may be seen.

Imaging Features

On US, bilateral small kidneys with increased echogenicity and multiple cysts are seen (Fig. 14.22). Solid or complex renal tumors may also be diagnosed (Figs 14.23A and B). CT reveals small kidneys with multiple cysts; cyst wall calcification is common. High density cysts and renal tumors are easily diagnosed and CT is the most useful study for ACKD.[19]

On MRI, simple cysts can be distinguished from hemorrhagic cysts (high SI on both T1 and T2WI). Furthermore, solid tumors showing inhomogeneous signal intensity more than that of renal parenchyma on T2WI can be well delineated.

von Hippel-Lindau Disease (VHL)

This is a relatively rare autosomal dominant disorder caused by an abnormal gene on short

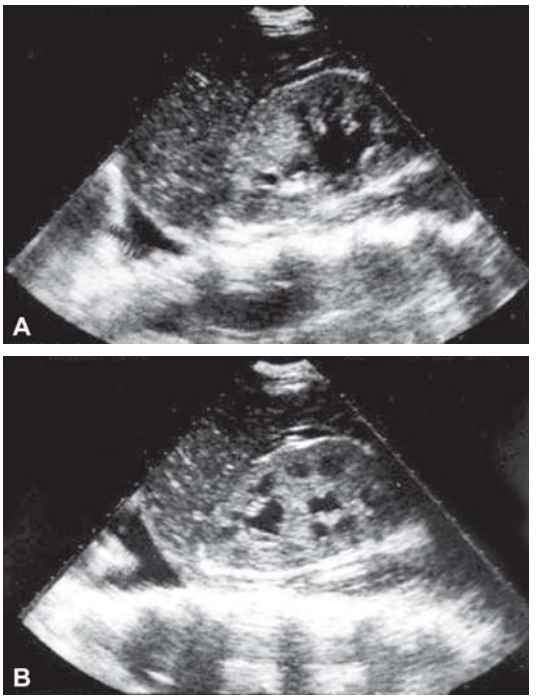

Fig. 14.23A and B: US in a patient with renal failure showing shrunken echogenic kidneys with multiple small cortical cysts. Hydronephrosis is seen in the right kidney

arm of chromosome 3. This disorder is associated with hemangioblastomas of the CNS, retinal angiomatosis, pheochromocytomas and cysts and tumors of the kidney and pancreas and papillary cystadenomas of the epididymis. Clinically, the patient presents with abdominal mass, flank pain and haematuria.[20]

Pathology

Bilateral, multiple small cortical cysts are seen without causing renal enlargement. Extensive disease can mimic ADPKD. Bilateral and multifocal renal cell carcinomas are also noted.

Imaging Features

On EU, renal cortical cysts are seen bilaterally, causing distortion of the renal

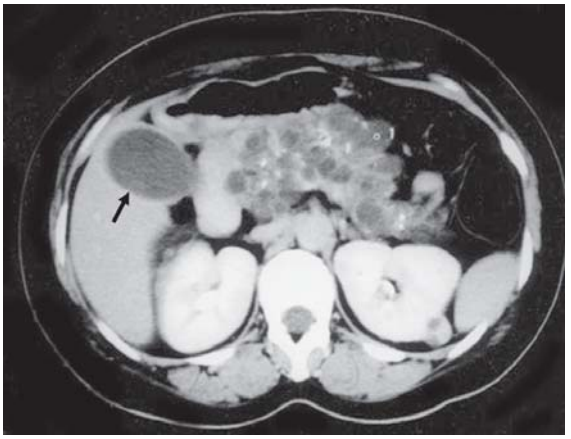

Fig. 14.24: CECT sections showing a solid enhancing mass and cyst in the left kidney with multiple cysts and calcifications in the pancreas – von Hippel-Lindau disease

architecture. USG is highly sensitive for detection of renal cysts; however, small renal tumors may not be seen. CT is more sensitive than USG for the detection and characterization of renal masses and small, solid renal masses can be precisely defined (Fig. 14.24).

MR imaging is indispensable for the diagnosis of neurological neoplasms seen in patients with VHL. Furthermore, small RCC's can be detected on CEMR. Large tumors can be evaluated and characterized on non-enhanced scans and tend to be more heterogeneous.[21]

TUBEROUS SCLEROSIS (TSC)

It is a genetically transmitted neurocutaneous syndrome with sporadic occurrence. Genetic markers have been identified at 9q34(TSCI) and 16p13(TSCZ) although they account for only 50 percent of TSC families. The true incidence of TSC is difficult to measure though its birth incidence ranges from 1 per 5800 to 1 per 10,000. It has an autosomal dominant mode of inheritance and is characterized by mental retardation, seizures and cutaneous lesions. This disorder is associated with multiple hamartomas in the brain (cortical tubers), retina, skin, heart (rhabdomyomas), kidney (angiomyolipomas) and other organs.[22]

Renal cystic disease also occurs in TSC and the occurrence of both angiomyolipomas and renal cysts is virtually diagnostic of TSC. Angiomyolipomas are benign masses consisting of varying amounts of abnormal blood vessels, smooth muscle and fat.

Imaging Features

On abdominal radiographs, lucency suggesting fat within an AML can occasionally be detected. On EU, the findings vary with the size and number of renal cysts and the presence of AML's. Multiple nonopacifying renal masses causing distortion of the collecting system are seen. On sonographic examination, multiple renal cysts and AML's, showing hyperechoic reflections may be seen.[23]

On CT, fat containing AML's with low attenuation values and intralesional hemorrhage may be noted along with renal cysts (Figs 14.25A and B). MR imaging aids in diagnosing AML's by showing high signal intensity on both T1 and T2 images.[8]

CYSTS OF RENAL SINUS

Peripelvic cysts, parapelvic cysts, parapelvic lymphatic cysts and parapelvic lymphangiectasia have been used variably to describe cysts of the renal sinus (Fig. 14.26). The term renal sinus cyst is preferred for fluid filled masses in the renal sinus, either solitary or multiple, that are usually detected as an incidental finding in the older patients. Diagnosis may be incidental or during investigation of hematuria/hypertension.

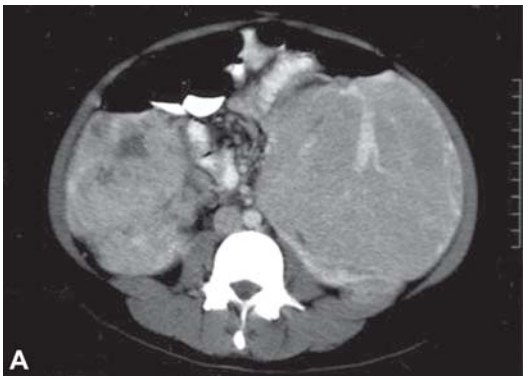

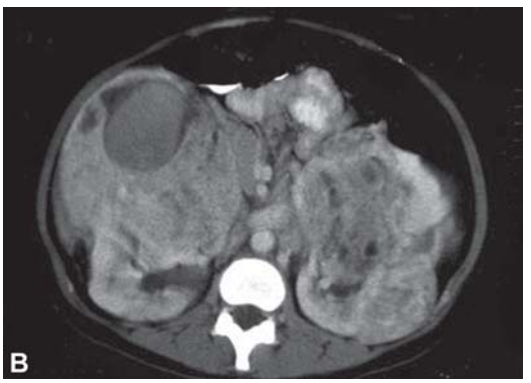

Figs 14.25A and B: Contrast enhanced CT scan showing heterogeneous masses involving both the kidneys. The masses show fat attenuation values and cystic areas within. The lesions show intralesional vacularity – bilateral angiomyolipomas

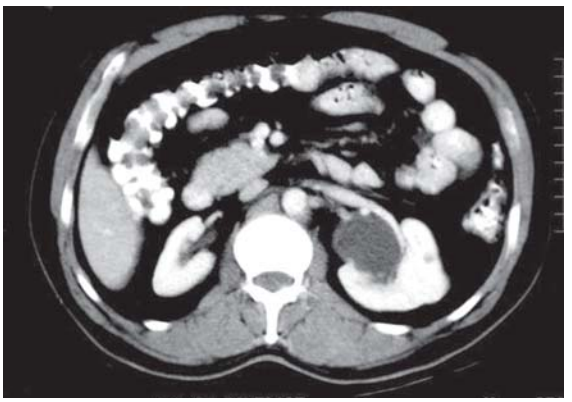

Fig. 14.26: Contrast enhanced CT scan showing a solitary fluid filled lesion in the renal sinus detected as an incidental finding in this patient – A parapelvic cyst

Features are nonspecific and the treatment is cyst puncture.[6]

MISCELLANEOUS CYSTIC DISEASE

Inflammatory

Hydatid Cysts

The kidney can also be involved by hydatid disease; the patient is usually asymptomatic until the cyst has grown large enough to cause pressure symptoms or rupture.

Imaging Features

Plain radiography may reveal a localized bulge on the renal contour or evidence of calcification in a degenerated cyst; which may be eggshell or sunburst in appearance. On EU, an intact cyst with a complete pericyst is seen as filling defect in the kidney. When there is reposition of the pericyst, there is interposition of contrast medium between the ectocyst and pericyst. There is interposition of contrast medium between the ectocyst and pericyst producing the "goblet or wine glass or surraco's sign". In the open type, when there is a communication between the hydatid cyst and collecting system, the contrast medium gives a mottled appearance and may also produce the "crescent sign".[6]

On US, calcific cysts or hydatid sand may be seen. Parallel echogenic stripes formed when membranes of dead daughter cysts become adherent, are very suggestive of hydatid cyst. CT shows unilocular, low attenuation cyst or daughter cysts arranged within the mother cyst, giving a rosette appearance (Figs 14.27A to C).

Pyogenic Cyst

These are usually secondary to acute pyelonephritis. Excretory urography reveals

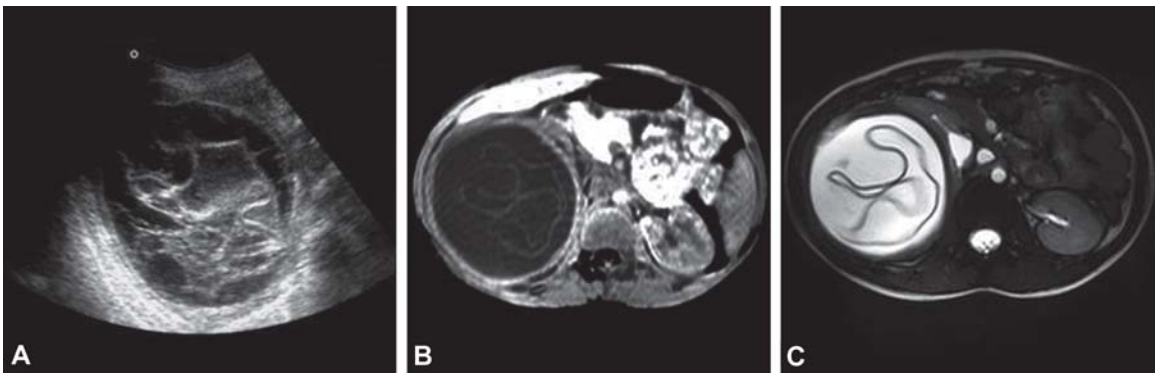

Figs 14.27A to C: Sonogram **(A)** showing a cyst replacing the right kidney with multiple serpentine linear structures / membranes within s/o ruptured hydatid cyst. T1W MR axial image **(B)** showing the cyst replacing the right kidney. The cyst is hypointense on T1. T2W MR image **(C)** shows the cyst to have high signal. The membranes are seen as linear areas of low signal within – Ruptured hydatid cyst of the right kidney

filling defects or irregular cavities communicating with the pelvicalyceal system. On sonography, thick walled cystic lesions with low level internal echoes are seen. CECT shows low attenuation masses with rim enhancement and thickening of perirenal fascia.

Tuberculous Cysts

The most common route of spread of *Mycobacterium TB* to the kidney is hematogenous seeding from the lungs. A tuberculous focus is usually located in the renal cortex and may develop a communication with the tubular system and the pyramids, which can rupture into the calyces.

EU reveals extensive calcification and papillary necrosis with multiple irregular cavities. End stage tubercular kidneys usually do not excrete contrast medium at urography. On US, multiple renal cavities can be seen.

Focal calyceal changes are seen on CT as calyceal enlargement, pericalyceal areas of early cavitation, infundibular strictures and loss of perirenal fat planes. Late features of calcification or hydronephrosis secondary to strictures may be seen.

Pleuricystic Kidney Disease

It applies to entities when one or more renal cysts are present in syndromes of multiple malformations. The degree of renal cyst formation in each syndrome is variable and reflects different responses to the underlying abnormality.

Glomerulocystic Disease

This is a rare congenital disease characterized by dilatation of Bowman's space and adjacent tubules. The kidneys are enlarged with multiple small cortical cysts leading to progressive renal failure.[6] This entity is nonfamilial and not related to other renal cystic diseases.

Microcystic Disease

Infants with congenital nephrotic syndrome can have cystic dilatation of proximal convoluted tubules. However, no discernible radiological changes are noted.

CYSTIC RENAL CELL CARCINOMAS

They are seen in 5 to 10 percent cases of RCC. Four patterns are commonly seen and these

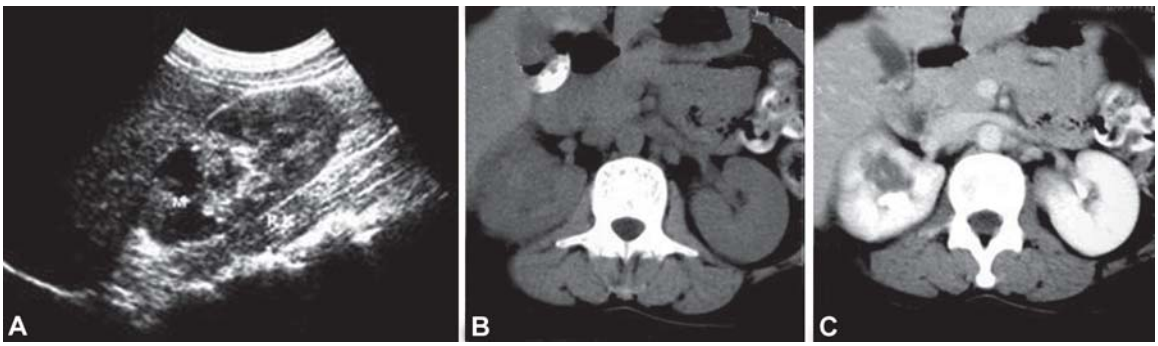

Figs 14.28A to C: Sonogram **(A)** showing a complex cystic mass in the upper pole of the right kidney with thick septations. Non contrast CT **(B)** showing an ill-defined hypodense mass in the right kidney. Contrast enhanced CT scan in the nephrogram phase **(C)** showing significant enhancement of the cystic lesion (enhancement > 20 HU) consistent with a malignant cystic neoplasm

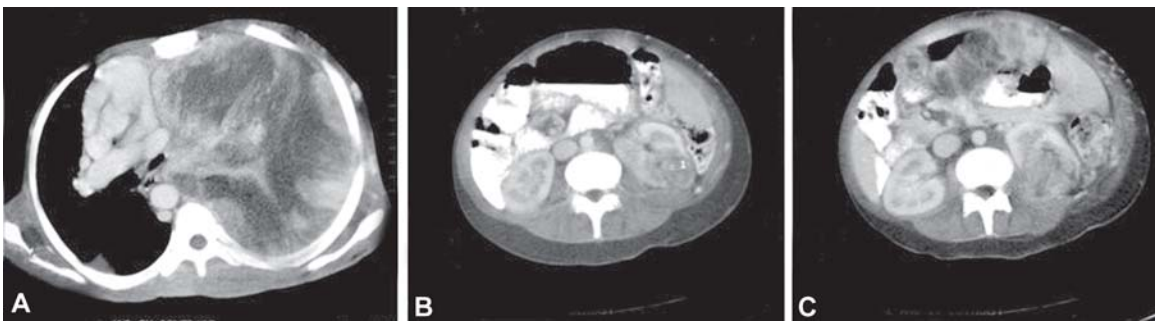

Figs 14.29A to C: Contrast enhanced CT of the chest revealing pulmonary sarcoma **(A)** with collapse of the left lung. Contrast enhanced CT scan **(B and C)** showing a solid appearing hypodense lesion in the left kidney – Renal metastasis

are: intrinsic multilocular growth, cystic necrotic tumor, unilocular cystadenocarcinoma and tumor found within a cyst wall. The most common appearance is that of a macrocystic multilocular cyst with large or small cystic components. This appearance is indistinguishable from a complicated cyst or benign multilocular cystic nephroma on sonography and CT (Figs 14.28A to C). The microcystic multilocular RCC however appears solid on sonography and CT because the cystic spaces are smaller than 5 mm in diameter (Figs 14.29A to C). Rarely unilocular renal cell carcinoma may occur (Figs 14.30A and B). Papillary renal cell carcinoma a subtype of renal malignancy can appear as a homogenous hyperattenuating mass.

Another cystic type of RCC occurs when a solid lesion outgrows its blood supply and becomes necrotic. This is seen as a hemorrhagic complex cystic mass. The imaging appearances depend on the degree of necrosis present.[24]

In conclusion, any fluid-filled renal mass not fulfilling the imaging criteria of an uncomplicated cyst should be considered a cystic lesion. When multiple features are present the mass should be managed according to the most aggressive finding. Most multiloculated cystic masses with wall thickening, nodularity or enhancement would require surgery to establish a final diagnosis.

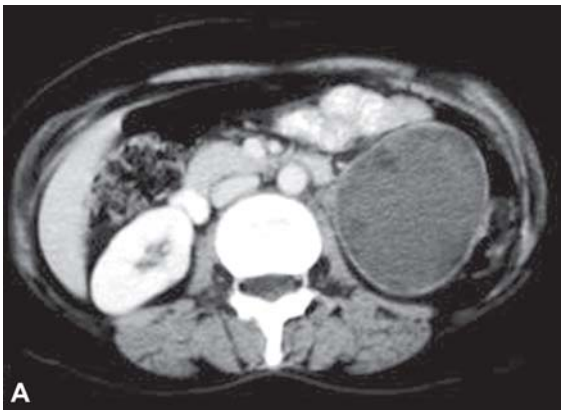

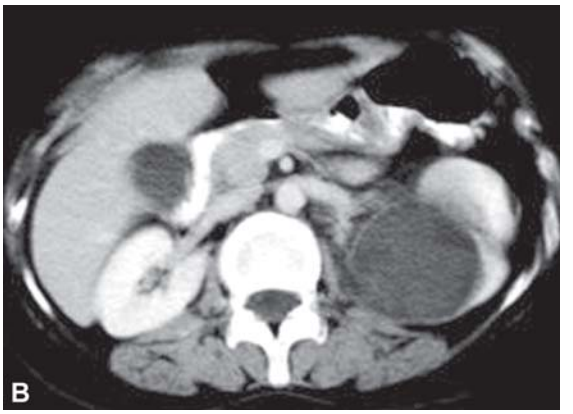

Figs 14.30A and B: Contrast enhanced CT scan showing a unilocular cyst in the left kidney. The cyst has inhomogeneous fluid content and shows solid elements within – cystic RCC (L) kidney

REFERENCES

1. Tantravahi JR, Steinman TI: Acquired cystic kidney disease. Seminars in Dialysis 2000;13(5): 330-34.
2. J Stuart Wolf: Evaluation and management of solid and cystic renal masses. The Journal of Urology 1998;159:1120-33.
3. Friedmann W, Vogel M, Dimer JS, et al. Prenatal differential diagnosis of cystic kidney disease and urinary tract obstruction: anatomic, pathologic, ultrasonographic and genetic findings. Eur J Obs and Gyn and Rep Biol 2000;89:127-33.
4. Levine E, Hartman DS, Meilstrup JW, et al. Current concepts and controversies in imaging of renal cystic diseases. UCNA 1997;24(3): 523-43.
5. Thomsen HS, Levine E, Meilstrup JW, et al. Renal cystic diseases. Eur Radiol 1997;7:1267-75.
6. Hartman DS: Cystic disease. In Pollack HM (Ed): Clinical urography. Philadelphia: WB Saunders, 1990;1059-1185.
7. Bosniak MA. Problems in radiological diagnosis of renal parenchymal tumors. Urol, Clin North Am 1993;20:217-30.
8. Gladys M, Torres, Pablo R Ros: Kidney. In Stark DD, Bradley WG (Eds): Magnetic Resonance Imaging, second edition, Mosby Year-Book, Inc.1999.
9. Reichard EAP, Roubidoux MA, Dunnick NR: Renal neoplasms in patients with renal cystic diseases. Abdom Imaging 1998;23:237-48.
10. Davidson AJ, Hartman DS, Choyke PL: Radiologic assessment of renal masses: Implications for patient care. Radiology 1997;202:297-305.
11. Levine E: The Kidney. In Haaga JR (Ed): Computed Tomography and Magnetic Resonance Imaging of the Whole Body, third edition, Mosby-Year Book, Inc. 1994.
12. Hwang DY, Lee JG, Kim SH, et al. Unilateral renal cystic disease in adults. Nephrol Dial Transplant 1999;14:1999-2003.
13. Lonergan GJ, Rice RR, Suarez ES: Autosomal recessive polycystic kidney disease: Radiologic-pathologic correlation. AFIP Archives Radiographics 2000;20:837-55.
14. Lucaya J, Enriquez G, Nieto J: Renal calcifications in patients with autosomal recessive polycystic kidney disease. Prevalence and cause. AJR Am J Roentgenol 1993;160:359-62.
15. Rego JD Jr, Laing FG, Jeffrey RB: Ultrasonic diagnosis of medullary cystic disease. J Ultrasound Med 1983;2:43.
16. Mentser, Mahan J, Koff S: Multicystic dysplastic kidney. Pediatr Nephrol 1994;8:113.
17. Henson JHL, Al-Hilli A, Penry JB: The development of acquired renal cystic diseases and

neoplasia in a chronic haemodialysis patient. Br J Radiol 1985;58:1215-17.

18. Diana L. Farmer. Urinary tract masses. Seminars in Pediatric Surgery 2000;9(3):109-14.
19. Levine E, Grantham J, Slusher S. CT of acquired cystic kidney disease and renal tumors in long-term dialysis patients. AJR 1984;142:125-31.
20. Choyke PL, Glenn GM, Walther MM. von Hippel-Lindau disease: Genetic, clinical and imaging features. Radiology 1995;194:629.
21. Rominger M, Kenney P, Morgan D. Gadolinium-enhanced MR imaging of renal masses. Radiographics 1992;12:1097-16.
22. Povey S, Burley M, Attwood J. Two loci for tuberous sclerosis: one on 9q34 and one on 16p13. Ann Hum Genet 1994;58:107.
23. Durham DS. Tuberous sclerosis mimicking ADPKD. Aust NZJ Med 1987;17:71.
24. Ooi GC,Sagar G, Lynch D. Cystic renal cell carcinoma: Radiological features and clinico-pathological correlation. Clin Rad 1996;51:791.

Chapter

15 Renovascular Hypertension

Niranjan Khandelwal, Anupam Lal, Manphool Singhal

INTRODUCTION

Hypertension defined as blood pressure of 140/90 mmHg or more, is a common medical problem affecting as much as one-third of the population. It is a leading cause of mortality and morbidity. In most cases (93-94%) hypertension is idiopathic and is labelled as essential hypertension. In a minority of patients, a specific etiology can be identified and such patients are said to have secondary hypertension. The major aetiologies implicated in this category include renovascular, renal parenchymal, endocrine and neurologic with renovascular hypertension being the most common. Its prevalence is estimated at 1-5 percent of the general hypertensive population.[1,2]

Renovascular hypertension (RVH) denotes the casual relationship between a renal artery stenosis (RAS) and its clinical consequences, namely, hypertension or renal failure.[3] It is also defined as hypertension that improves or resolves after correction of renal artery stenosis.[4]

Diagnosing renovascular hypertension is important because treatment of renal artery stenosis may cure patient's hypertension. Renal artery stenosis is also an important cause of ischemic nephropathy and end stage renal disease (ESRD) which can be prevented by early and appropriate intervention.[5-7] Also in view of the widespread use of angiotensin converting enzyme inhibitors (ACE), it is important to exclude the presence of RAS as these agents may precipitate renal failure in the presence of bilateral renal artery stenosis or stenosis of renal artery in a solitary functioning kidney.

PATHOPHYSIOLOGY

Renal artery stenosis causes a decrease in perfusion pressure and glomerular filtration rate (GFR) by decreasing the hydrostatic pressure in the afferent arterioles. Regardless of the cause of stenosis, the accompanying reduction in intrarenal arterial pressure is sensed by the juxtaglomerular apparatus of the afferent arterioles. The renin angiotensin aldosterone system is triggered in an attempt to maintain glomerular filtration pressure. Renin secreted by juxtaglomerular apparatus of the kidney, converts plasma angiotensinogen to angiotensin I. This is converted by angiotensin converting enzyme in the lungs to angiotensin II. Angiotensin II is a potent vasoconstrictor and increases blood

pressure by direct effect on arterioles and by stimulating aldosterone secretion leading to salt and water retention. Angiotensin II also causes vasoconstriction of the efferent arterioles in an attempt to restore glomerular filtration to normal.

In patients with unilateral renal artery stenosis increased levels of angiotensin II causes not only vasoconstriction of afferent arterioles of the affected kidney but also a decrease in GFR and sodium excretion by the contralateral kidney. The nonaffected kidney also demonstrates marked decrease in renin secretion. Increased blood pressure ultimately results in pressure natriuresis from the contralateral kidney resulting in the classic 'high renin-normal volume' pattern of unilateral RAS.[8,9]

In patients with bilateral stenosis or a solitary kidney with renal artery stenosis the entire mass of nephrons is ischemic, resulting in increased renin, excess angiotensin II and aldosterone, which by counter regulatory mechanisms, decrease renin production. Since pressure natriuresis cannot occur from either kidney, there is volume retention. The overall picture in bilateral renal artery stenosis is a mixed one with both renin and volume factors typically being involved. Because of volume overload these patients are prone to recurrent sudden 'flash' pulmonary edema.[8,9]

If RAS is untreated, prolonged exposure of renal vasculature to vasopressor agents may alter renal hemodynamics and result in nephrosclerosis, and subsequent removal of offending RAS does not relieve hypertension. This is called 'renoprival effect' and is indicated clinically by inability of the kidney to excrete sodium and water. Recently 'azotemic renovascular disease' is the preferred term for these changes as changes in the effected are not necessarily due to ischemic changes.[10] In animal models it has shown that due to critical renal artery stenosis oxidative stress pathways develops with stimulation of tissue fibrogenic pathways leading to acute tubular injury and subsequent irreversible interstitial fibrosis-fibrogenic cascade.[11-14] It is imperative therefore that renovascular hypertension is diagnosed and treated prior to these irreversible changes.[8]

ETIOLOGY OF RENAL ARTERY STENOSIS

Renal artery stenosis may be broadly categorized as atheromatous or nonatheromatous. The various causes are listed in Table 15.1.

Atherosclerosis, fibromuscular dysplasias and in our subcontinent, non-specific aortoarteritis (Takayasu's disease) account for

Table 15.1: Causes of renovascular hypertension

I. Renal artery stenosis
- Atherosclerosis
- Fibromuscular dysplasia
- Nonspecific aortoarteritis/Takayasu's arteritis
- Vasculitis
- Dissection
- Vasospasm
- Coarctation syndrome
- Neurofibromatosis
- Congenital rubella
- Syphilitic arteritis
- Tuberous sclerosis
- Extrinsic compression
- Middle aortic syndrome
- Williams syndrome

II. Other causes of renovascular hypertension
- Aneurysm of renal artery
- Renal artery embolus
- AVF – renal artery
- Irradiation
- Renal transplant
- Trauma

most of the cases. Chugh et al[15] found that nonspecific aortoarteritis was responsible for 61 percent of patients, fibromuscular dysplasia for 28 percent and atherosclerosis for 8 percent patients with RVH in India. The incidence of atherosclerosis is rising in the urban population.[16]

Atherosclerosis

Atherosclerosis accounts for approximately two-thirds of patients of renal artery stenosis in the western world. It occurs more commonly in men over the age of 50 years. Obstruction usually results from aortic plaque engulfing the renal ostium (i.e. within 4 mm of aortic lumen). Less frequently plaque develops independently in the proximal third of the renal artery. The stenosis is often circumferential but may be eccentric and is commonly associated with calcification. Differentiation between proximal and ostial lesions is important because of their different response to angioplasty. Because atherosclerosis is a generalized process both renal arteries are frequently affected. If atheromatous lesions are left untreated there is a high probability of progression to complete occlusion.[17-19]

Fibromuscular Dysplasia

Fibromuscular dysplasia (FMD) has only been recognized for the past 30 years or so but accounts for almost a third of the patients with of renovascular hypertension according to western literature. It typically occurs in young women. It may involve any layer of the artery and is classified as intimal, medial or adventitial.[20,21]

1. *Intimal fibroplasia* There is concentric accumulation of collagen beneath the internal elastic membrane which causes focal smooth stenosis usually in the mid-portion of renal artery. It is more common in children and is progressive.
2. *Medial dysplasia* This is the most common type of dysplasia and accounts for approximately 95 percent cases.
   a. *Medial fibroplasia*: This is the most common type of medial dysplasia in which there is replacement of smooth muscle by collagen. These alternate with small areas of dilatation due to aneurysm formation and result in the classic 'string of beads' appearance. It is more common in women between 20 to 50 years of age and is progressive. It usually responds to angioplasty (Figs 15.1A and B).

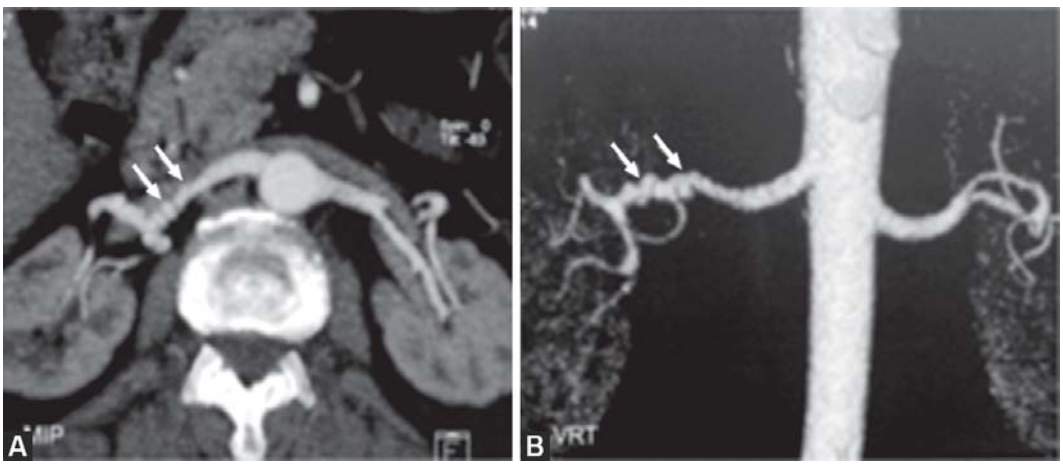

Figs 15.1A and B: CT angiography images (MIP and VRT) showing classical 'string of beads' appearance (arrows) involving right renal artery and its divisions in a case of fibromuscular dysplasia (Medial fibroplasia)

b. *Perimedial fibroplasia*: Collagen infiltrates outer layer of media. A beaded appearance similar to medial fibroplasia is seen but the 'beads' are smaller as aneurysms do not develop.
c. *True medial hyperplasia:* Uncommon media is replaced by hyperplastic smooth muscle and fibrous tissue. A tubular smooth narrowing of the vessels is seen on angiography.
d. *Medial dissection*: Also uncommon. A new channel is formed in the outer one-third of the media with visualisation of a false channel in media on angiography.

3. *Adventitial dysplasia* Collagenous infiltrate surrounds the adventitia, producing a tubular smooth narrowing on the angiogram.

FMD is not confined to renal arteries but is also seen in visceral and peripheral arteries. It also involves the carotid and vertebral arteries, but tends to spare the intracranial vessels.

Nonspecific Aortoarteritis/Takayasu's Arteritis[22-24]

Nonspecific aortoarteritis also known as Takayasu's disease is a granulomatous arteritis that commonly involves the aorta and its major branches. In the acute phase the media and adventitia are filled with giant cells and granulomata. Destruction of the entire vascular wall and progressive adventitial fibrosis lead to luminal narrowing, occlusion, dilatation or formation of aneurysms. The disease tends to affect young females (mostly less than 35 years of age) particularly from South East Asia and India. In the active stage the disease is associated with clinical features like fever and increased sedimentation rate. Hypertension in Takayasu's disease may be caused by coarctation of aorta or main renal artery stenosis (Fig. 15.2).

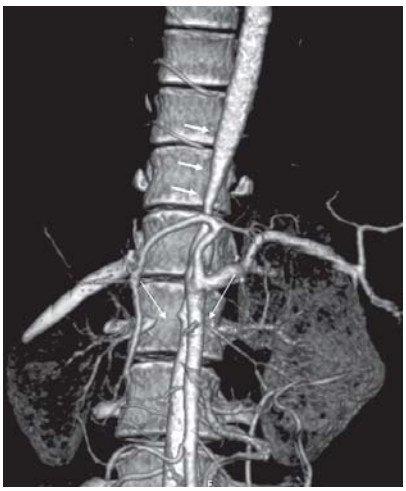

Fig. 15.2: CTA (VRT) image showing narrowing of abdominal aorta (arrows) and near total occlusion of bilateral renal artery (long arrows) in a case of Takayasu's aortoarteritis *(For color version see Plate 17)*

It may be classified into four types.

Type I—Narrowing of aortic arch or great vessels arising from arch.

Type 2—Descending thoracic and upper abdominal aorta involvement.

Type 3—Involvement of aortic arch vessels, abdominal aorta and major branches.

Type 4—Pulmonary artery involvement.

Middle Aortic Syndrome[25-27]

A rare syndrome of diffuse narrowing of abdominal aorta often affects visceral and renal arteries. It typically occurs in young patients, most often in the second decade. Various aetiologies including chronic inflammatory aortitis, atherosclerosis, neurofibromatosis and cystic medial necrosis are implicated. According to some authors there is no clear distinction between this condition and nonactive Takayasu's disease. The renal arteries are commonly affected with long stenosis.

SCREENING FOR RENOVASCULAR HYPERTENSION

Hypertension is common but RVH is not, therefore screening should be reserved for patients at moderate to high-risk for RVH. The following criteria have been proposed, in the presence of which prevalence of RVH is 20-30 percent:[8,9]

Clinical

- Patients presenting with accelerated/malignant hypertension.
- Hypertension uncontrolled by triple drug therapy.
- Onset of hypertension less than 20 years or more than 50 years of age, or a sudden worsening of their condition.
- Unilateral small kidney discovered with any clinical study.
- Impairment of renal function after treatment with an Angiotensin-converting enzyme (ACE) inhibitor.
- Patients with long history of smoking.
- Patients with symptoms of peripheral vascular disease.

Physical signs that suggest RVH include the following:

- Abdominal or flank bruit (systolic or diastolic)
- Grade 3 or 4 fundoscopic changes of hypertension.

Laboratory tests that may indicate reno vascular disease include:

Blood urea nitrogen	> 20 mg/dl
Serum potassium	< 3.4 mEq/L
Proteinuria	

There is no perfect screening test for the detection of renovascular hypertension. The situation is further complicated by the fact that the presence of renal artery stenosis (RAS) may not always indicate a causal relationship. Not every RAS leads to renovascular hypertension and patients with essential hypertension may also develop RAS. The degree of stenosis that causes renovascular hypertension has not been established although most investigators treat stenosis measuring 50 percent or greater.[28,29] Physiologically, RAS is defined as inadequate renal blood flow leading to reduction in GFR and loss of renal parenchyma, hence it becomes prudent to establish the functional significance of RAS before proceeding to revascularization.[30]

Clinical and Biochemical Tests

Clinical/nonradiological tests that have been used for the diagnosis of RVH include: Plasma renin activity, ACE inhibitor challenge test, aspirin challenge test and 24 hours ambulatory blood pressure monitoring.

IMAGING MODALITIES FOR ASSESSMENT OF RAS

In the clinically suspected patients having RAS as a cause of RVH it becomes necessary to identify those patients, preferably through non-invasive methods, who have truly hemodynamically significant RAS and can benefit from interventional or surgical revascularization.[31-33]

Radionuclide renal scintigraphy especially with ACE inhibitors is highly sensitive and accurate in detection of unilateral RAS but its accuracy decreases in patients suffering from bilateral RAS or azotemia and in patients with single functioning kidney.[34]

Doppler ultrasound is widely available and performed imaging modality for determination of renal size, morphology and

allows direct evaluation of the renal arteries as well as transrenal Doppler waveform analysis, but it remains operator dependent.

Intravascular ultrasound (IVUS) is the best modality for the correct evaluation of stenosis and plaque morphology, but it being invasive and expensive it is unlikely to become a screening modality.[35]

Computed tomography angiography (CTA) with the advent of multidetector CT (MDCT) and contrast enhanced magnetic resonance angiography (CE-MRA) are widely used for the initial evaluation of RAS with sensitivity and specificity equivalent to digital subtraction angiography (DSA).[36] However after published reports of nephrogenic systemic fibrosis (NSF) following gadolinium-based contrast agent in patients with deranged renal functions, CE-MRI as a screening test is being avoided.[37,38] It is of great importance that radiologists be aware of this serious disease and exercise caution when considering the use of Gd-based contrast media in patients with moderate (glomerular filtration rate < 60 ml/min/1.73 m^2) to severe (glomerular filtration rate < 15 ml/min/1.73 m^2) renal disease. In this situation various other MR techniques which can assess renal arterial morphology, perform functional measurements of arterial flow and parenchyma perfusion without the administration of gadolinium are being investigated and found useful in patients with deranged renal functions. These techniques are non-contrast studies such as time-of-flight (TOF), phase contrast (PC), steady-state free precession (SSFP), and arterial spin labeling (ASL).[38] These advancements explains why renal MRI is evolving as the first-line imaging modality for the evaluation of renovascular disease.

An ideal renal artery imaging study should answer the following questions:[39]

1. Localization and number of arteries
2. Characterization of renal stenosis, including etiology of stenosis, localization, and poststenotic dilatation
3. Hemodynamic and functional significance of the stenosis
4. Further pathologies or variants that might have an influence on treatment planning

Radionuclide Renal Scintigraphy

Radionuclide imaging of the kidney is the most widely performed screening test for the diagnosis of renovascular hypertension I^{131} orthoiodohippurate (OIH) was used in the past. Currently technetium 99m (99mTc) diethylenetriamine pentaacetic acid (DTPA) and mercaptoacetic triglyceride (MAG 3) are commonly used for isotope renography.[8]

The standard renogram reflects the salt and water retention on the ischemic side by demonstrating slow transit and excretion of radiotracer. The classic appearance is that of a small kidney with decreased uptake and delayed tracer transit and excretion. In its original form the test had an unacceptably high rate of both false positives and false negatives and was not significantly better than hypertensive urography hence was not used.[40] An incidental observation by Majd et al in 1983[41] led to the emergence of captopril renography which has since become the standard screening test in the diagnosis of this condition. Captopril renal scintigraphy can be used as a screening test, to establish the hemodynamic significance of RAS, to predict the outcome of revascularisation and in the follow-up after successful revascularization.

Principles of Angiotensin Converting Enzyme Inhibitor (Captopril) Scintigraphy

In a patient with a significant RAS the efferent arterioles of the glomeruli are constricted by angiotensin II to maintain glomerular filtration pressure in the face of diminished afferent arteriolar pressure. Administration of ACE inhibitor decreases this angiotensin related constriction of efferent arterioles which reduces glomerular filtration and hence urine flow. ACE inhibitor does not affect GFR in patients with normal renal arteries or those with essential hypertension.[8]

Protocol

ACE inhibitor scintigraphy is performed 1 hour after the oral dose of 25 mg of captopril or 15 minutes after an intravenous dose of 0.04 mg/kg of enalpril maleate. Patients are well-hydrated, are taken off antihypertensive medication 2-5 days prior to the study according to the half life. Resting blood pressure is monitored. After a baseline study, the scan is repeated 30 minutes after administration of ACE inhibitor. Time-activity curves are generated from renal cortex and pelvis.

Results

A positive result is said to be present if there is a decrease in uptake and delayed clearance by the affected kidney on the post-captopril study compared to the baseline study or if there is exaggeration of the baseline asymmetry between the normal and abnormal kidney in patients with unilateral RAS (Fig. 15.3).

The exact findings depend on the radioisotope used. 99mTc DTPA is mainly excreted by glomerular filtration and captopril

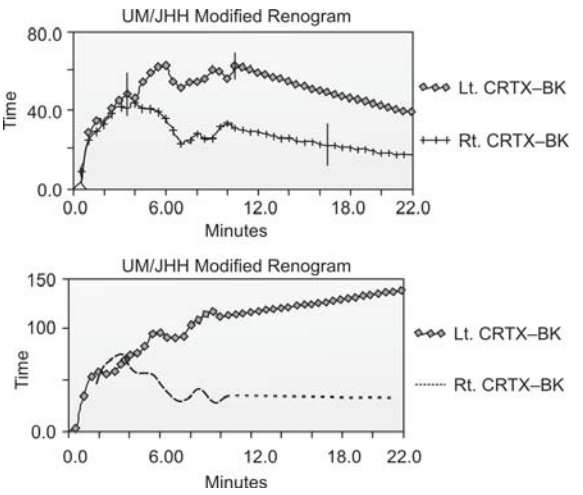

Fig. 15.3: Pre-(above) and postcaptopril (below) radionuclide renograms generated from cortical activity demonstrate asymmetric peak activity and cortical retension on the left side with exaggeration of abnormality on the postcaptopril scan

causes a decrease in renal uptake and excretion. On the other hand OIH I^{131} and MAG 3 are excreted predominantly by tubular secretion so that captopril administration predominantly acts by prolonging transit time through the kidney. There is little difference reported in literature in the ability of various radiotracers to detect RVH. However, MAG 3 produces good images even in patients with impaired renal function.[42]

The overall sensitivity and specificity of the test exceeds 90 percent in most series with a few exceptions.[43] Advantages include low cost, relative reliability, and noninvasive nature. A positive captopril renography may suggest a cure or improvement in blood pressure after intervention. It may also be used in the follow up of patients after intervention.[44] Disadvantages and pitfalls include low sensitivity in patients with azotemia or underlying renal dysfunction and, in patients

with bilateral RAS. Branch artery stenosis cannot be diagnosed. It has a low spatial resolution and provides functional not anatomic data. In patients who develop severe hypotension in response to captopril, bilateral symmetric parenchymal retention may be seen (false positive). Symmetrical retention even in the absence of hypotension is usually a false positive finding.[8,42] Presence of pelvic retention may complicate interpretation of cortical retention and scintigraphy must be interpreted with caution in the presence of pelvic retention.[45]

Ultrasound

A normal appearance of the kidneys on ultrasound does not exclude a significant unilateral or bilateral renal artery stenosis. Renal size and shape may be normal unless the stenosis is greater than 60 percent when a small decrease in size may be found.[46]

Color Doppler Flow Imaging (CDFI)

The advent of Doppler and more recently contrast enhanced Doppler have provided important diagnostic tools in the evaluation of renal artery stenosis.[8]

Two approaches are used with Doppler ultrasound. The first is the direct visualization and interrogation of the stenotic segment of the renal artery. The second is an assessment of the arterial waveform distal to the stenosis within segmental renal vessels (Fig. 15.4).

Direct Approach

This requires evaluation of the entire main renal artery, spectral traces are then obtained from areas of stenosis identified on color Doppler. The aorta is also interrogated and peak systolic velocity (PSV) obtained at the level of renal origins. An anterior or anterolateral approach usually allows insonation of both the arteries. A coronal approach can be used when bowel gas is present (Fig. 15.5). The criteria used to diagnose significant stenosis or occlusion of a renal artery is as follows: [3,8,47]

1. An increase in peak systolic velocity (Thresholds commonly applied in current literature to diagnose RAS include PSV (max) in the renal artery > 150-180 cm/sec. Fig. 15.6).

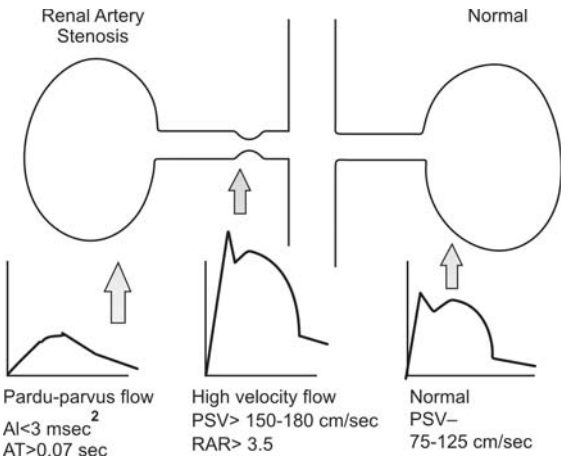

Fig. 15.4: Schematic diagram of the renal artery Doppler tracings showing the normal renal artery trace on the left side. On the right side high velocity at the site of stenosis and 'tardus parvus' waveform is seen distal to the stenosis

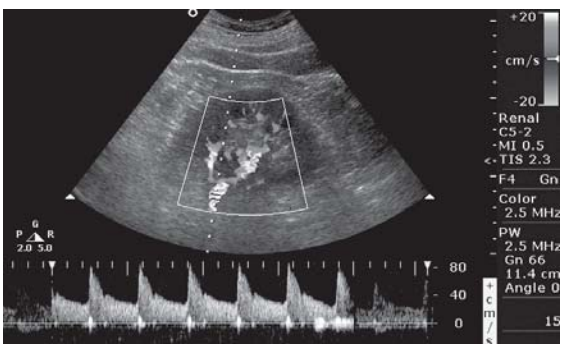

Fig. 15.5: Color Doppler image through coronal approach show normal spectral trace of main renal artey *(For color version see Plate 17)*

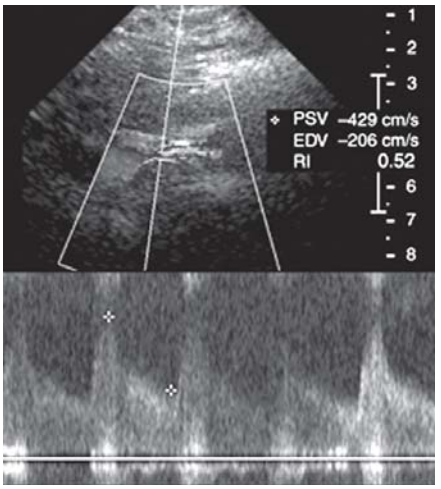

Fig. 15.6: Spectral trace at the site of stenosis of renal artery shows increased peak systolic velocities

2. Renal artery/aortic ratio (RAR ratio) > 3.5 calculated as:

$$\frac{\text{PSV max renal arteries}}{\text{PSV aorta at the origin of renal arteries}}$$

3. Turbulent flow in the post stenotic area
4. Visualization of the renal artery without detectable Doppler signal, a finding that indicates occlusion.

Although theoretically simple in practice these measurements often cannot be obtained, as main renal arteries may not be visualized in upto 42 percent cases. The procedure is time consuming and operator dependent. Accessory renal arteries (present in upto 40% cases) may not be visualized. Branch artery stenosis cannot be diagnosed. In cases of renal artery occlusion collaterals may be sampled. The use of sonographic contrast media like Levovist has been found to enhance the visualization of main renal vessels resulting in higher technical success rates.

Indirect Approach

Arterial wave forms from the segmental renal arteries from the upper, mid and lower poles are evaluated. The normal waveform from these vessels shows a steep systolic upstroke with a peak in early systole referred to as early systolic peak (ESP). The early systolic acceleration seems to be the best predictor of RAS and should be measures along the initial portion of the systolic rise and should not include the late compliance peak.[48,49] In contrast the waveform in patients with RAS lacks both these features and is known as 'tardus-parvus' waveform. Tardus refers to the slowed systolic acceleration and parvus refers to the low amplitude of the systolic peak (Fig. 15.7).

There are two quantitative measurements that are used (i) the acceleration time (AT) (ii) the acceleration index (AI). Acceleration time is the time from start of systole to peak systole and a value greater than 0.07 sec is significant. 'AI' is the slope of the systolic upstroke which is reduced to less than 3 m/sec^2 in significant RAS. Some authors have shown that simple pattern recognition of 'tardus-parvus' waveform is more accurate

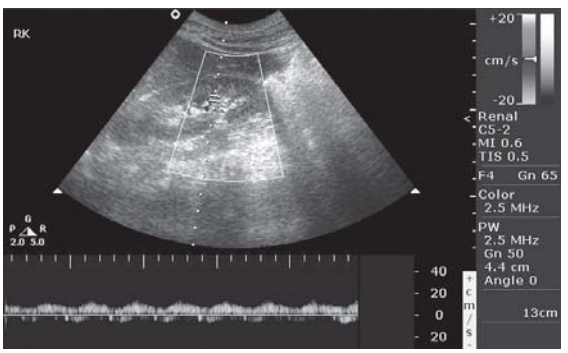

Fig. 15.7: Color Dopper image showing 'parvus tardus' waveform in interlobar artery due to main renal artery stenosis *(For color version see Plate 17)*

than calculation of 'AT' and 'AI'.[50] The waveform may also demonstrate a decrease in resistive index (RI) and pulsatility index.[51]Administration of captopril in individuals with significant RAS produces measurable changes in Doppler waveform which increases the degree of pulsus tardus and decreases the RI. [52]

These criteria only detect stenosis of greater than 70-80 percent reliably. The shape of the waveform is not simply related to the pressure drop across the stenosis but also compliance of renal arteries.[37] Coexisting parenchymal disease may also affect the waveform due to changes in peripheral resistance. The technique also cannot distinguish between high grade stenosis and complete occlusion with collateral flow. Tardus parvus waveform may also be produced by abdominal coarctation.[53]

Doppler sonography may also be used to predict the outcome of therapy for RAS.[54] A 'RI' of more than 80 probably identifies patient with RAS in whom angioplasty or surgery will not improve renal function or blood pressure.

The sensitivity of Doppler US when compared with DSA has varied significantly ranging from as high as 92 percent to as low as 50 percent. Recent studies indicate a specificity of 91-95 percent.[8]

CT Angiography (CTA)

CTA offers a noninvasive technique for obtaining angiographic images. The advent of spiral CT and more recently multidetector CT (MDCT) has revolutionized computed tomography and CTA. MDCT has made possible the acquisition of isotropic data with high spatial and temporal resolution; this coupled with new softwares is providing angiograms comparable to catheter angiography. Data acquisition with MDCT is acquired craniocaudally with section thickness of 1mm with a pitch of 1.5 after an intravenous injection of 90-150 ml of contrast medium (300 mg I/ml) at the rate of 3-6 ml/sec using bolus tracking techniques. [36]

The axial images are reconstructed in multiple planes using multiplanar reconstruction (MPR), maximum intensity projection (MIP) or real time volume rendering techniques (VRT) for morphological evaluation of kidneys and main renal arteries (Fig. 15.8).

The sensitivity of CTA in identifying main renal arteries has been 100 percent; accessory arteries are also almost always detected with any area of narrowing. The sensitivity and specificity for diagnosis of RAS has ranged between 90-95 percent[36, 55-57] CTA is more sensitive than Doppler ultrasound for detection of stenosis of main renal arteries (96 vs 63%) but specificity of the two techniques is similar (88 vs 89%).[44]

CTA can demonstrate the wall of the aorta unlike angiography which only visualizes the lumen of the vessel, important in cases of atherosclerosis (Fig. 15.9) and also aorto-

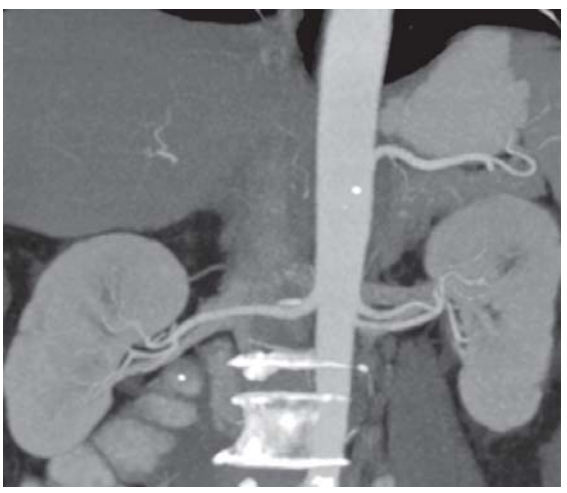

Fig. 15.8: MDCT angiographic image (MIP) showing normal caliber single renal artery on right side and two on left side

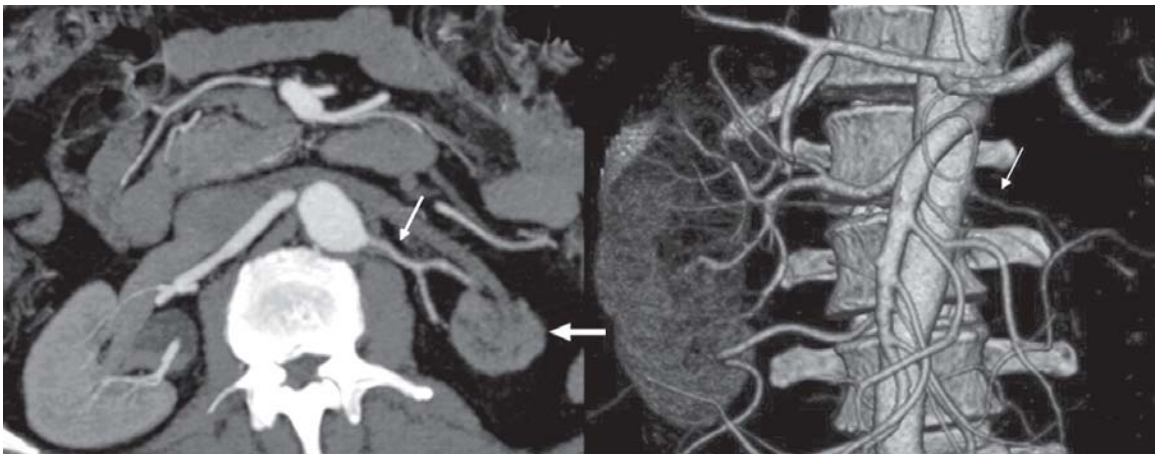

Fig. 15.9: CTA (MIP and VRT) images showing atherosclerotic narrowing of left renal artery(arrows) with asymmetric mural thickening renal artery near the ostium. Note atrophy of left kidney (thick arrow) *(For color version see Plate 18)*

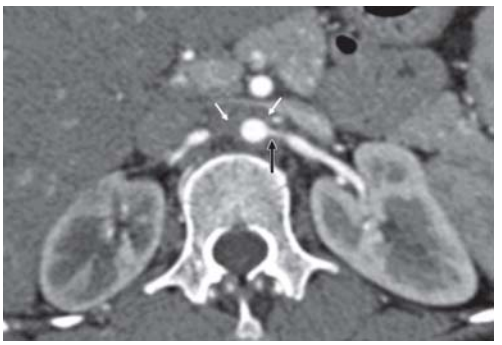

Fig. 15.10: Takayasu's aortoarteritis: CTA (MIP image) showing symmetric circumferential mural thickening of aorta at the origin of renal arteries (white arrows) with stenosis of renal arteries (black arrow)

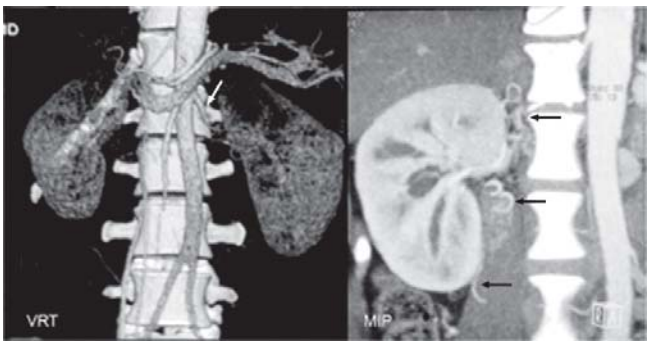

Fig. 15.11: CTA (VRT and MIP) images showing complete occlusion of right renal artery. The left renal artery in normal (white arrow). MIP image shows normal size of the right kidney and multiple arterial collaterals (black arrows) perfusing the kidney

arteritis (Fig. 15.10) where the lumen may appear angiographically normal in places but may show vessel wall involvement in cross-sectional studies. It easily demonstrates the extent of plaque projecting into the vessel lumen, aiding in determining the form of intervention planned such as angioplasty vs primary stent placement.[58] CTA has high efficacy for diagnosis of ostial stenosis—the most difficult place to evaluate during arteriography and improves the differentiation between ostial and truncal stenosis. MDCT CTA can also detect collaterals in the presence of renal artery occlusion (Fig. 15.11). Unlike MR angiography, CTA can also be used to examine the patency of vessels that have been dilated by intravascular stents.[59] In a recent study MDCT produced interpretable multiplanar images of the renal artery even with a metallic stent in place and was adequate for determining stent patency, however intrastent diameter was underestimated in most patients as compared to catheter angiography.[60]

Disadvantages with CTA include relatively high cost and use of large amount of iodinated contrast medium precluding its use in renal insufficiency. Mural calcification in the aorta or renal artery may result in overestimation of stenosis. In various series the overestimation of the renal artery stenosis varied from 3-7 percent.[57]

Magnetic Resonance Angiography (MRA)

Magnetic resonance angiography has the ability to visualize renal arteries non-invasively with or without the use of contrast medium. The CE-MRA is the preferred technique for the detection of RAS.[61] However with the reports of nephrogenic systemic fibrosis the use of gadolinium is restricted for the patients having deranged renal functions.[37] In such cases non-contrast enhanced MR imaging of renal arteries should be done.[38]

It is essential to mention here that before analysis of renal arteries morphological assessment of kidneys in respect of their size, corticomedullary differentiation, and presence of any mass lesion or abnormalities of collecting system should be done.

Contrast Enhanced MRA (CE-MRA)

Recent advances in the magnetic resonance gradient hardware with availability of 3.0 T, acquisition of isotropic data with submillimeter resolution is allowing the detection of renal artery narrowing with high accuracy.[62,63] Moreover, it is now possible to demonstrate the functional consequences of RAS, such as a decline in renal perfusion and glomerular filtration.[64]

Intravenous gadolinium is used in a dose of 0.1-0.3 mmoles/kg with bolus tracking. With the advent of 3.0T the amount of contrast can be reduced because of increase in T1 of tissue. Entire acquisition is performed during a single breath hold. In patients unable to withhold breath for long time parallel imaging technology provides high resolution images with shorter acquisition times. Three-dimensional contrast MRA overcomes the limitations of noncontrast MRA. As a result renal arteries are assessed in their entirety, including the major segmental branch vessels, as well as small accessory renal arteries. In addition, speed, operator independence, high spatial and contrast resolution and lack of side effects have contributed to making 3D contrast MRA a well-suited screening alterative for detection of renovascular disease. The technique has sensitivities of 93-100 percent and a specificity of 90-100 percent (Fig. 15.12).

In several centers contrast enhanced MRA is complemented by 3D-PC acquisition. Areas

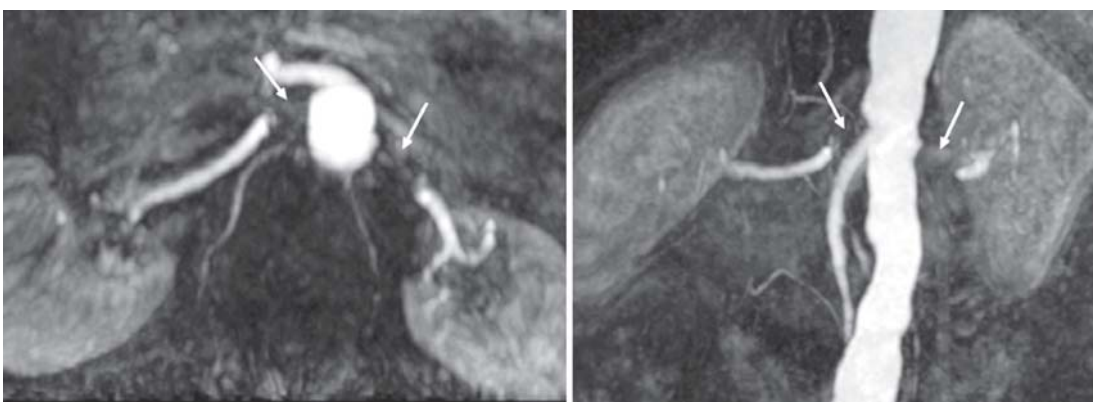

Fig. 15.12: CE-MRA (MIP axial and coronal images) showing severe stenosis of bilateral renal arteries near origin (arrows)

of hemodynamically significant stenosis are detected by their associated turbulence seen as a signal void on 3D-PC images. The presence of a signal void at or immediately downstream from a stenosis suggests pressure drop across the stenosis. For 3D–PC MRA to be optimally sensitive to turbulent flow echo time should be approximately 8 ms and velocity encoded value (VENC) should be kept at 25-50 cm/sec.

The major advantages of MRA are absence of ionizing radiation, production of arteriographic images that unlike CTA are not affected by calcified plaques. Images can be viewed in multiple planes with facilities for temporal processing as well. Phase contrast studies can provide information about blood flow velocity also (as phase is related to time).

The drawbacks of MRA include its high cost and limited availability. Artifacts caused by motion and bowel peristalsis also tend to reduce usefulness of the study.

The MRI is also being evaluated in acquiring the functional data that can provide comprehensive assessment of renal morphology and renal function prior to any intervention.[64] Dynamic contrast-enhanced (DCE)-MRI is fastly emerging technique in which fast repetitious imaging of the kidney is performed using first pass of the contrast agent. In the recently published series from different centers significant correlations between raising serum creatinine levels and decreasing renal perfusion parameters are found indicating that renal first pass perfusion may reflect, atleast to a certain degree, renal function.[63,65] In an another study significant reduction of the cortical perfusion and medullary perfusion and of the accumulation of contrast media in the medulla were found in patients with renal failure.[66] The DCE-MRI can evaluate the kidneys after the placement of stents which otherwise cannot be assessed due to susceptibility artifacts. In such situations demonstration of normal perfusion parameters proves the patency of stent.[63]

Noncontrast-Enhanced MR Imaging of the Renal Arteries

Since the established link between gadolinium-based contrast agents and nephrogenic systemic fibrosis in patients suffering from severe renal insufficiency CE-MRA is not considered safe in such patients. Various noncontrast MRA techniques have evaluated such as time of flight (TOF), phase contrast (PC), steady-state free-procession (SSFP), and arterial spin labeling (ASL).

TOF MRA

Signal in TOF MRA is produced by unsaturated blood flowing into the plane of imaging (flow related enhancement). TOF MRA is not an useful technique for the evaluation of renal arteries because of the following reasons.

1. It tend to overestimate the degree of stenosis, in particular 2D techniques do not compensate for vessel tortuosity and therefore tend to overestimate vessels stenosis,
2. Loss of signal in slow flow when vessel in oriented in axial plane (in-plane saturation),
3. Inherently a slow technique requiring several minutes, causing breathing related degradation or extremely long scan times for signal averaging, and
4. Poor visualization of the distal arterial segment where flow is slow.

Phase Contrast (PC) MRA

Phase Contrast (PC) MRA depicts not only the morphologic nature of a stenosis, but also provides quantitative analysis of flow

dynamics in RAS.[67] Combining phase contrast with cardic gating , a 2D velocity map can be obtained, which is termed as "quantitative" or "q" flow.[68] With this flow maps similar to Doppler ultrasound can be generated and analyzed.

Steady-state Free Precession Magnetic Resonance Angiography

Three dimensional steady-state precession (SSFP) is the most promising non-contrast bright blood technique for evaluation of renal arteries as it is intrinsically fast, high in signal-to-noise ratio (SNR), and flow compensated in all the three axis.[38] In the recent reported studies this sequence has 100 percent sensitivity and 100 percent negative predictive value.[69-71] Based on these studies SSFP either breath hold or navigator-gated can be performed as a first line MRA technique to rule out RAS especially in patients in risk of NSF. If SSFP is negative for high grade RAS (> 50%), RAS can be excluded without using any gadolinium based contrast agents, vie-a-versa if SSFP is positive, then further studies (CE-MRI, DSA, CTA) can be done for better delineation of stenosis.[38]

Arterial Spin Labeling

Arterial spin labeling (ASL) uses blood as an endogenous contrast agent to obtain angiograms with an advantage to obtain tissue perfusion as well. The perfusion parameters are being investigated and initial reports suggest a good correlation with scintigraphy.[72]

Renal Angiography

Conventional angiography (or digital subtraction angiography) is the gold standard against which all other modalities for diagnosing renal artery stenosis are compared. Intraarterial DSA results in reliable depiction of main renal arteries and branch vessels, with less contrast material and with use of smaller lumen catheters than conventional angiography. Angiography plays a limited role as the preliminary screening test for RAS, however, all patients proceeding to percutaneous treatment of RAS initially undergo diagnostic angiography as part of the procedure.[8]

Angiographic evaluation should include aortography and bilateral selective renal arteriography. The initial aortogram is necessary to evaluate the renal artery ostia, identifying accessory renal arteries and avoid mistaking guide wire induced arterial spasm for fixed disease.

Flush aortography is usually adequate to demonstrate main renal arteries and any proximal renal stenosis. When intrarenal or branch artery stenosis are suspected selective injections are necessary. Because the origin of right renal artery is anterolateral and left renal artery is posterolateral an ostial lesion may be missed on an AP aortogram due to overlap by the opacified aorta, superimposition of intrarenal vessels may also mask stenosis. Depending on the site of stenosis oblique/lateral view, cranial/caudal angulation or magnification views may be required to optimally delineate stenosis.[73-75]

Features of RAS on Arteriography

Atherosclerosis produces irregular circumferential or eccentric narrowing of the ostium or proximal third of the renal arteries. Bilateral disease is common and infrarenal aortic involvement usually exists (Fig. 15.13).

FMD typically involves middle to distal renal arteries and less commonly intrarenal branches. Bilateral disease may be seen in

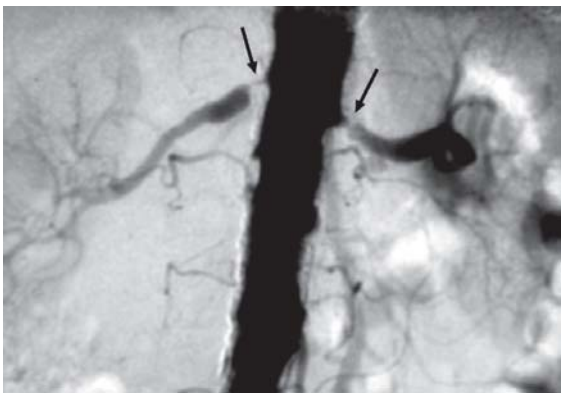

Fig. 15.13: DSA aortogram showing atherosclerotic stenosis (arrows) of bilateral renal arteries

about two-third of cases. The right kidney is affected more commonly than the left. The classic appearance of the common medial fibroplasia type of FMD is a string of beads. Other forms may show different morphologies as already discussed. With FMD aorta is usually disease free.

The morphological pattern of involvement in aortoarteritis shows racial and geographical differences.[76] In Japan thoracic aortic involvement is more common and neck vessels are most often involved.[77] In most other Asian countries abdominal aorta is most often affected particularly renal and subclavian arteries.[76] Pulmonary artery involvement is less frequently seen in Indian patients. Steno-occlusive lesions are the most common type of lesions found in the north Indian population, dilating lesions are less common.[76]

After a stenosis has been identified, its hemodynamic significance must be proved by one of the following criteria.[78]

- Reduction in luminal diameter > 75 percent.
- Systolic pressure gradient across the stenosis > 15-25 mmHg or > 20 percent of aortic systolic pressure.
- Evidence of collateral circulation into distal vessel.
- Pharmacologic manipulation of collateral vessel flow (epinephrine restricts flow to the kidney and makes collaterals more apparent).

A stenosis with 50 to 75 percent reduction in luminal diameter may be hemodynamically significant but in such cases other signs must be sought. Pressure gradients are the most accurate indicator of hemodynamic significance.

Advantages of conventional angiography / DSA include the high resolution of the technique making it the only modality capable of adequately visualizing branch renal artery stenosis. Pressure gradients can be measured to assess hemodynamic significance and selective renal catheterization may be followed by appropriate intervention in the same sitting.

Angiography is, however, not without limitations. It is expensive and invasive and carries the added risks that come with the use of iodinated contrast. Angiography only provides intraluminal information; no intramural information is gained about the vessel wall or plaques. There is a low but definite risk of complications which may be at the puncture site such as hematoma, pseudoaneurysm or at the level of renal arteries because of selective catheterization. The most serious of these are vessel dissection, arterial puncture and cholesterol embolization leading to renal failure. Transient decrease in renal function may occur in upto 5 percent patients.

In the future intravascular ultrasound or angioscopy may be useful in high-risk patients.[35,79]

TREATMENT

Atherosclerotic Disease

There are in principle three modes of treatment for renovascular hypertension—medical therapy, surgery and angioplasty. An antihypertensive drug by lowering the arterial pressure may further reduce renal perfusion pressure causing renal damage hence some type of revascularisation is preferred.

Percutaneous Transluminal Renal Angioplasty (PTRA) and Stenting

Since PTRA was first reported by Gruntzig[80] in 1978 there has been a continuous refinement in technique and it has generally been accepted as a valuable first line therapy for RVH. Renal artery stenting has further extended the role of PTRA and both techniques can be considered complementary. Percutaneous techniques offer a minimally invasive alternative to surgery and properly performed are not preclusive of future surgical treatment.[81]

PTRA is best suited to discrete tight concentric, short segment stenosis located away from ostium and branches of renal arteries. Eccentric, long segment and calcified lesions, occlusion in tortuous vessels, stenosis adjacent to an aneurysm and occlusion or stenosis with a thrombus increase the risk of complications and reduce the likelihood of success.

Indications: Percutaneous revascularisation of renal arteries is indicated for (1) Refractory hypertension (2) Preservation of renal function (3) Prevention of 'flash' pulmonary edema especially in patients on calcium channel blockers (4) Preservation of renal artery patency.

PTRA and stenting are justified in selected patients who have both normal renal function and normal blood pressure because of the natural history of renal artery stenosis to progress and ultimately result in impaired renal function.[82]

Before PTRA is performed the salvage ability of the procedure must be established. The commonly used criteria are (1) residual function-single kidney GFR by radionuclide studies (2) kidney size of 8-9 cm (3) renal biopsy showing preservation of glomeruli and tubule (4) presence of collateral circulation to intrarenal vessels confirmed by arteriography. Revascularisation is usually not beneficial in patients with severe renal failure (S. creatinine > 4.0 mg/dl).[78]

Renal Artery Stenting

Angioplasty failure is an absolute indication for stenting. The criteria for angioplasty failure include–residual stenosis of more than 30 percent, residual aortorenal pressure gradient of > 20 mmHg, acute occlusive, flow limiting dissection flap and late restenosis (recurrent stenosis > 50%).[82]

In selected patients in whom the risk of intervention or anatomic considerations make a repeat procedure in the future unlikely primary stenting is justifiable. It should be the technique of choice for ostial atherosclerotic RAS[83] (Figs 15.14A to C).

Complications: Complication rate in PTRA varies from 3-6 percent. Complications include those related to the arteriographic procedure and those due to angioplasty and stenting.[81,82] These include renal artery injury, guidewire perforation of kidney, flow limiting renal artery dissection, renal artery thrombosis, renal artery rupture.

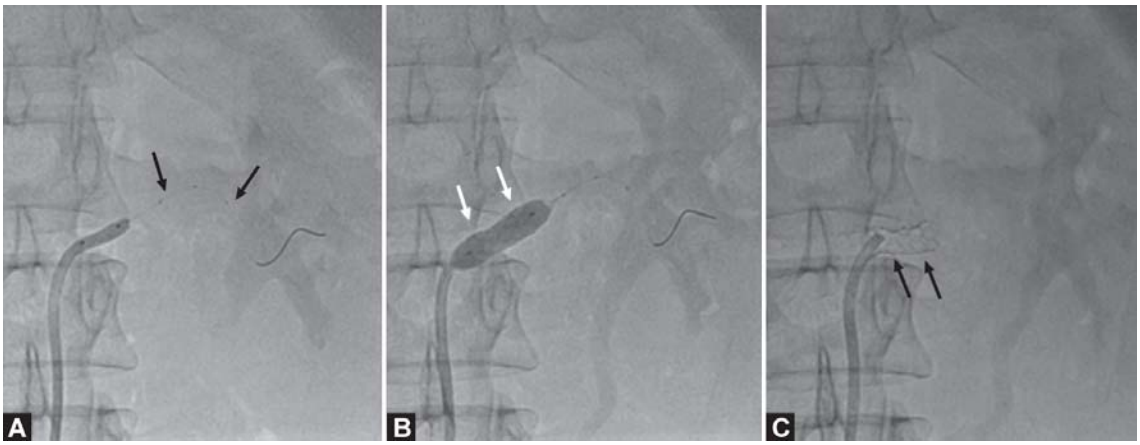

Figs 15.14A to C: Stenting of left renal artery stenosis: The guide wire (arrows) is negotiated across the stenotic segment **(A)**, The balloon expandable stent is deployed across the stenosis and inflated (arrows) **(B)**, final position of the stent across the stenosis (arrows) **(C)**, *Image courtesy: Department of Cardiology, PGIMER, Chandigarh*

Stent related complications include stent malposition, misdeployment of stent, endovascular infection, and cholesterol embolization.

Outcome: Success in renal revascularisation can be judged by the technical success of angioplasty and by the clinical response.[84,85]

Angiography is considered to be technically successful if the residual stenosis is < 30 percent, at least 50 percent enlargement in arterial diameter as compared to pre-angioplasty diameter and pressure gradient of less than 20 mmHg or reduction in pressure gradient by at least 15 mmHg from the pre-treatment gradient

Clinical results are judged as cured: diastolic blood pressure < 90 mmHg without medication**,** improvement: equal or reduced medication required to maintain the diastolic blood pressure below 90 mmHg or a 15 mm Hg reduction in blood pressure with the same or reduced number of medicines and failed: no change in blood pressure after the procedure.

In patients treated for renal salvage a reduction in serum creatinine levels of > 20 percent may be considered successful treatment.

The results of PTRA depend on the type of lesion, indication for treatment, and factors such as age, coexistent essential hypertension and nephrosclerosis.

The results in FMD are uniformly good. Technical success is achieved in 90-100 percent patients. Hypertension is cured or improved in 98 percent patients.[82] Intimal FMD may require much greater pressures than medial fibroplasia type of FMD. Restenosis is uncommon in these patients and primary patency at 15 months is 92 percent.

For atherosclerotic lesions both angiographic and clinical results for nonostial stenosis are superior to those for ostial stenosis (within 2-10 mm of aortic lumen). Technical success occurs in 75-95 percent cases, although some authors have reported lower rates of 43 percent for nonostial lesions and 29 percent for ostial lesions. Long-term

clinical benefit is seen in 76 percent patients with ostial lesions and 83 percent patients with nonostial lesions.[86] Van der Van *et al* showed that PTA with stenting improved the outcome for ostial lesions.[83]

Lesser success can be expected in patients with bilateral RAS, generalized atherosclerosis, with heavily calcified or segmental artery lesion.

For renal salvage the results are less favorable and improvement is seen in 40-60 percent cases.

Future Management of RAS

A paradigm shift in thinking in the treatment of RAS is being undertaken worldwide as conventional wisdom to dilate or stent the renal arteries having stenosis more than 50 percent was challenged in 2000, where no significant change was found in patients who had RAS and were treated either by medical antihypertensive therapy and angioplasty.[33] Based on this observation large trials such as STAR (The Dutch benefit of stent placement and blood pressure and lipid lowering for the prevention of progression of renal dysfunction caused by atherosclerotic ostial stenosis of renal artery) with 2 years follow-up, ASTRAL study (The large-scale angioplasty and stent for renal artery stenosis), CORAL study (Cardiovascular outcomes with renal atherosclerotic lesions) were undertaken and their final outcomes are expected soon.[87-89]

Takayasu's Arteritis/Nonspecific Aortoarteritis

The widespread nature of the disease and complexity of pathological changes in the vessel wall make surgical revascularisation difficult. Graft occlusion is also common. These problems make percutaneous revascularisation techniques extremely attractive.

Specific technical difficulties may be encountered during PTRA for aortoarteritis because of the tough noncompliant nature of the stenosis which is difficult to cross and resists repeated prolonged balloon dilatation. Patients may also develop hypotension and backache during the procedure.[85]

However, reports have shown high rate of technical success and frequently good clinical response.

Following angioplasty for any cause at least 3-6 months of follow up is required to assess durability of clinical response.

Surgical Therapy

Surgical revascularization is now indicated only in situations where PTRA fails or is contraindicated. Techniques include aortorenal, lienorenal, ileorenal arterial bypass, nephrectomy and autorenal transplantation.

Renal Artery Stenosis in Children[27,90]

Although RAS is uncommon in children the incidence is much higher in children with hypertension than in adults. About 4-20 percent of children with hypertension have RAS.

Causes

Fibromuscular dysplasia The classical string of beads appearance is rarely seen with intimal fibroplasia being the most common type of lesion. The lesions are more often found in boys unlike adults. Branch artery stenosis is also more common.

Neurofibromatosis Stenosis of proximal renal artery is seen, these may be associated with hypoplasia of abdominal aorta.

Nonspecific aortoarteritis and middle aortic syndrome are other important causes.

Because of the higher incidence of RAS in children with hypertension patients with a strong clinical suspicion often undergo DSA.

PTRA is being used with increasing frequency in children, however, the success rate is lower than adults for two reasons—smaller size of vessels and more frequent vasospasm make children more difficult to angiogram and dilate. Adult FMD and atherosclerosis respond well to PTRA while children have a more fibrotic process that cannot be adequately dilated.

CONCLUSION

Diagnosis of renovascular hypertension is complex because of the low prevalence and lack of strong causal relationship between renal artery stenosis and renovascular hypertension. Hence main aim should not to detect RAS of 50 percent or more in diameter but to identify stenosis which likely to get benefit from revascularization. Another concern is avoidance of unnecessary diagnostic angiography, especially in patients with renal failure.

Patients with a strong clinical suspicion are most often investigated by captopril renal scintigraphy or Doppler ultrasound. In good hands Doppler ultrasound proves to be cost effective with results near equal to scintigraphy. Patients with positive results may proceed directly to non-invasive angiography. However, patients with bilateral RAS or patient with significant renal impairment in addition to RVH may be missed if renal scintigraphy is the only screening test used.

The choice of the second screening test depends on local availability, expertise and patient's renal functional status. CTA/CE-MRA may be used, but after the insurgence of nephrogenic systemic fibrosis (NSF) in patients with deranged renal functions gadolinium based contrast agents should be avoided and so are the iodinated contrast agents for CTA. In such situations new MRI techniques such as SSFP, ASL is being investigated with satisfactory results.

Angiography remains the gold standard for diagnosis. However, with advances in non- invasive imaging particularly MRA and CTA, angiography may only be necessary as a prerequisite for percutaneous intervention.

REFERENCES

1. Dunnick NR, Sfakianakis GN. Screening for renovascular hypertension. Radiol Clin North Am 1991;29:497-50.
2. Silverman J, Friedman M, Van Allan R. Detection of main renal artery stenosis using phase contrast Cine MR angiography. AJR 1996; 166:1131-37.
3. Soulez G, Oliva VL, Turpin S, et al. Imaging of Renovascular Hypertension: Respective Values of Renal Scintigraphy, Renal Doppler US, and MR Angiography. Radiographics 2000;20: 1355-68.
4. Heaton CM, Farber JM. Magnetic resonance imaging of the renal arteries, Seminars in Interventional Radiology 2001;18:3-10.
5. National High Blood Pressure Education Program Working Group 1995 update on chronic renal failure and renovascular hypertension. Arch Intern Med 1996;156:1938-43.
6. Rimmer JM, Gennai FJ. Atherosclerotic renovascular disease and progressive renal failure. Ann Intern Med 1993;118:712-19.
7. Jacobson HR. Ischemic renal disease: An overlooked clinical entity? Kidney Int 1988; 34:729-43.
8. Ahmad I, Ray CE. Diagnosing renovascular hypertension. Seminars in Interventional Radiology 2001;18:11-21.
9. Pickering TG, Blumfenfeld JD. Renovascular hypertension and ischemic nephropathy in the kidney 2000;2007-34.
10. Textor SC, Wilcox CS. Renal artery stenosis: A common, treatable cause of renal failure? Annu Rev Med 2001;52:421-42.
11. Chade AR, Rodriguez-Porcel M Grande JP, et al. Distinct renal injury in early atherosclerosis and renovascular disease. Circulation 2002; 106:1165–71.

12. Chade AR, Rodriguez-Porcel M, Grande JP,et al. Mechanisms of renal structural alterations in combined hypercholesterolemia and renal artery stenosis. Arterioscler Thromb Vasc Biol 2003;23:1295–01.
13. Nath KA, Croatt AJ, Haggard JJ, et al. Renal response to repetitive exposure to heme proteins: Chronic injury induced by an acute insult. Kidney Int. 2000;57:2423-33.
14. Vesna D. Garovic, MD, Stephen C, et al. Renovascular Hypertension and Ischemic Nephropathy Circulation 2005;112:1362-74.
15. Chugh KS, Jain S, Sakhuja V: Renovascular hypertension due to Takayasu's arteritis among Indian patients. Quarterly J Med 1992;85: 833-43.
16. Sharma S, Khosla A, Rajani M, et al: Coronary arteriographic profile in young north Indian patients with coronary heart disease. Asian Medical Journal 1989;32: 531-37.
17. Ram CV, Clagett GP, Radford LR. Renovascular hypertension, Semin Nephrol 1995;15:152-74.
18. Schreiber MJ, Pohl MA, Navick MC. The natural history of atherosclerotic and fibrous renal disease. Urol Clin North Am 1984;11:383-92.
19. Jaff MR, Olin JW. Atherosclerotic stenosis of the renal arteries. Tex Heart Inst J 1998;25:34-39.
20. Harrison EG Jr, Mc Cormack LJ. Pathologic classification of renal arterial disease in renovascular hypertension. Mayo Clin Proc 1971; 46:161-67.
21. Luescher TF, Lic JT, Stanson AW: Arterial fibromuscular dysplasia. Mayo Clin Proc 1987;62:931.
22. Matsunaga N, Hayashi K, Sakamoto L, et al. Takayasu arteritis: Protean radiologic manifestations and diagnosis. Radiographics 1997; 17:579-94.
23. Keer GS. Takayasu's arteritis rheum. Dis Clin North Am 1995;21:1041-58.
24. Lagneau P, Michel JB. Renovascular hypertension and Takayasu's disease. J Urol 1985;134: 876-79.
25. Conolly JE, Wilson SE. Middle aortic syndrome: Distal thoracic and abdominal coarctation, a disorder with multiple etiologies. J Am Coll Surg 2002;194:774-81.
26. Sumboonnanonda A. Middle aortic syndrome clinical radiological findings. Arch Dis Child 1992;64:501-05.
27. Greene JF, Fitzwater J, Burgers J. Arterial lesions associated with neurofibromatosis. Am J Clin Pathol 1974;62:481-87.
28. Harden PN. Effect of renal artery stenting on progression of renovascular renal failure. Lancet 1997;349:1133-36.
29. Van Jaarsveld BC. The Dutch renal artery stenosis intervention cooperative (DRASTIC) study. Abstract presented at the Interventional Society of Hypertension meeting, Amsterdam, The Netherlands, August 1998.
30. Preston RA, Epstein M. Ischemic renal disease: An emerging cause of chronic renal failure and end stage disease. J Hypertens 1997;15:1365-77.
31. Dorros G, Jaff M, Muthiak L, et al. Four year-year follow-up of Palmaz-Schatz stent revascularization as treatment for atherosclerotic renal artery stenois. Circulation 1998;98:642-47.
32. Watson PS, Hadjipetrou P, Cox SV, et al. Effect of renal artery stenting on renal function and size in patients with atherosclerotic renovascular disease. Circulation 2000;102:1671-77.
33. van Jaarsveld BC, Krijen P, Pieterman H, et al. The effect of balloon angioplasty on hypertension in atherosclerotic renal-artery stenosis. Dutch Renal Artery Stenosis Intervention Cooperative Study Group. N Engl J Med 2000;342:1007-14.
34. Huot SJ, Hansson JH, Dey H, et al. Utility of captopril renal scans for detecting renal artery stenosis. Arch Intern Med 2002;162:1981-84.
35. De Scheerder I, De Man F, Herregods MC, et al. Intra-vascular ultrasound versus angiography for measurement of luminal diameters in normal and diseased coronary arteries. AM Heart J 1994;127:243-51.
36. Willmann JK, Wildermuth S, Roos JE, et al. Aortoiliac and renal arteries: Prospective intraindividual comparison of contrast-enhanced three-dimensional MR angiography and multi-detector row CT angiography. Radiology 2003;226:798–811.
37. Grobner T. Gadolinium. A specific trigger for the development of nephrogenic fibrosing dermopathy and nephrogenic systemic fibrosis? Nephrol Dial Transplant 2006;21:1104-08.
38. Potthast S, Maki JH. Non-Contrast-enhanced MR angiography of the renal arteries. Magn Reson Imaging N Am 2008;16:573-84.

39. Dellegrottaglie S, Sanz J, Rajajagopalan S. Technology insight: Clinical role of magnetic resonance angiography in the diagnosis and management of renal artery stenosis. Nat Clin Pract Cardiovasc Med 2006;3:329-38.
40. Mitty HA, Shapiro RS, Parsons RB, et al. Renovascular Hypertension. Radiol Clin North Am 1994;21:227-34.
41. Majd M, Potter BM, Guzzetta PC. Effect of captopril on efficacy of renal scintigraphy in detection of renal artery stenosis (abstract). J Nucl Med 1983;24:23.
42. Fine EJ. Diuretic Renography and Angiotensin Converting Enzyme inhibitor renography. Radiol Clin North Am 2001;39:979-95.
43. Van Jaarsrel B, Krijnen P, Derks F. The place of renal scintigraphy in diagnosis and treatment of renal artery stenosis, fifteen years clinical experience. Arch Intern Med 1997;157:226-34.
44. Nally JV, Barton DP. Contemporary approach to diagnosis and evaluation of renovascular hypertension. Urol Clin North Am 2001;28: 781-91.
45. Krijnen P, Dei MY, Claessens RA. Interobserver agreement on captopril renography for assessing renal vascular disease. J Nucl Med 2002;43:380-87.
46. Gutzman RP, Zierler RE, Issacson JA. Renal atrophy and arterial stenosis: A prospective study with duplex ultrasound. Hypertension 1994;23:346-50.
47. Haan DC, Kroon AA, Flobbe K. Renovascular disease in patients with hypertension: Detection with duplex ultrasound. J Hum Hypertens 2002;16:501-07.
48. Kliewer MA, Tupler RH, Carroll BA, et al. Renal artery stenosis: Analysis of Doppler waveform parameters and tardus-parvus pattern. Radiology 1993;189:779–87.
49. Oliva VL, Soulez G, Lesage D, et al. Detection of renal artery stenosis with Doppler sonography before and after administration of captopril: Value of early systolic rise. AJR Am J Roentgenol 1998;170:169–75.
50. Stavros AT, Packer SH, Yakes WF. Segmental stenosis of the renal artery Pattern recognition of the tardus and parvus abnormalities with duplex sonography. Radiology 1992;184:487-92.
51. Schwerk B, Restrepo K, Stellwaag W. Renal artery stenosis grading with image directed Doppler US evaluation of renal resistive index. Radiology 1996;190:785-90.
52. Rene PC, Oliva VI, Rao TB. Renal artery stenosis evaluation of Doppler US after inhibition of angiotensin converting enzyme with captopril. Radiology 1995;196:675-79.
53. Bude O, Rubin M. Detection of renal artery stenosis with Doppler sonography: It is more complicated than originally though? Radiology 1995;196:612-13.
54. Radermacher J, Charan A, Bleck J. Use of Doppler ultrasonography to predict the outcome of therapy for renal artery stenosis. N Engl J Med 2001;344:410-16.
55. Olbricht CT, Paul K, Prokop M. Minimally invasive diagnosis of renal artery stenosis by spiral computed tomography angiography. Kidney Int 1995;48:1332-37.
56. Galanski M, Prokop M, Charan A. Renal artery stenosis: Spiral CT angiography. Radiology 1993;189:185-92.
57. Kaatce R, Beek F, Lange E. Renal artery stenosis detection and quantification with spiral CT angiography versus optimised digital substraction angiography. Radiology 1997; 205: 121-27.
58. Halpern EJ, Rutter CM, Gardiner GA Jr. Comparison of Doppler US and CT angiography for evaluation of renal artery stenosis. Acta Radiol 1998;5:524-32.
59. Harish A, Khatri P, Priyadarshini H, et al. Accuracy of 64-slice coronary CT angiography in predicting percentage diameter stenosis. Indian Heart J 2008;60:296-301.
60. Behar JV, Nelson RC, Zidar JP, et al. Thin-section multi detector CT angiography of renal artery stents. AJR 2002;178:1155-59.
61. Schoenberg SO, Prince MR, Knopp MV, et al. Renal MR angiography. Magn Reson Imaging N Am 1998;6:351-70.
62. Leiner T. Magnetic resonance angiography of abdominal and lower extremity vascukature. Top Magn Reson Imaging 2005;16:21-66.
63. Michaely HJ, Sourbron S, Dietrich O et al. Functional renal imaging: An overview. Abdom Imaging 2006.[epub ahead of print]
64. Leiner T, Michaely H. Advances in contrast-enhanced MR angiography of the renal arteries. Magn Reson Imaging N Am 2008;16:561-72.
65. Michoux N, Montet X, Pechere A, et al. Parametric and quantitative analysis of MR

renographic curves for assessing the functional behavior of the kidney. Eur J Radiol 2005;54: 124-35.
66. Michaely HJ, Herrmann KA, Nael K, et al. Functional renal imaging: Nonvascular renal disease. Abdom Imaging 2007;32:1-16.
67. Debatin JF, Ting RH, Wegmuller H, et al. Renal artery blood flow: Quantitation with phase contrast MR imaging with and without breath holding. Radiology 1994;190:371-8.
68. Schoenberg SO, Knopp MV, Londy F, et al. Morphologic and functional magnetic resonance imaging of renal artery stenosis: a multireader tricenter study. J Am Soc Nephrol 2002;12: 158-69.
69. Herborn CU, Watkins DM, Runge VM, et al. Renal arteries: comparison of steady-state free procession MR angiography and contrast-enhanced MR angiography. Radiology 2006; 239:263-68.
70. Spuentrup E, Manning WJ, Bornert P, et al. Renal arteries: Navigator-gated balanced fast field-echo projection MR angiography with aortic spin labeling: Initial experience. Radiology 2002; 225:589-96.
71. Katoh M, Buecker A, Stuber M, et al. Free-breathing renal MR angiography with steady-state free-precession (SSFP) and slab-selective spin inversion: Initial results. Kidney Int 2004;66:1272-78.
72. Michaely HJ, Schoenberg SO, Ittrich C, et al. Renal disease: Value of functional magnetic resonance imaging with flow and perfusion measurements. Invest Radiol 2004;39:698-705.
73. Verschuyl EJ, Kaalec R, Beek FJA. Renal artery origins best angiographic projection angles. Cardio Vasc Radiol 1997;205:115-20.
74. Gerlock AJ, Goncharenki V, Oplis M, et al. Right posterior oblique: The projection of choice in aortography of hypertensive patients. Radiology 1978;127:45-48.
75. Harrington DP, Levin DC, Garnic JC, et al. Compound angulation for the angiographic evaluation of renal artery stenosis. Radiology 1083;146:829-31.
76. Sharma S, Rajani M, Talwar KK. Angiographic morphology in non specific aortoarteritis (Takayasu's arteritis) a study of 126 patients from north India. Cardiovasc Intervent Radiol 1992;15:160-65.
77. Yamato M, Ceeky JW, Hiramatsu K, et al. Takayasu's arteritis; radiographic and angiographic findings in 59 patients. Radiology 1986;161:329-34.
78. Valji K. Vascular and interventional radiology. Renal Arteries and Veins. WB Saunders 1999; 154-81.
79. Caramella N, Bisogni C, Laiolo E. Detection of accessory renal arteries with virtual vascular endoscopy of the aorta. Cardiovasc Intervent Radiol 1999;22:1-6.
80. Gruntzig A, Khulmann K, Vetterr W. Treatment of renovascular hypertension with percutaneous transluminal dilatation of renal artery stenosis. Lancet 1978;1:801-02.
81. Miller G, Ford K, Braun S. Percutaneous transluminal angioplasty versus surgery for renovascular hypertension. AJR 1985;144:447-50.
82. Sanctis JTD. Renal artery Angioplasty and stenting. Seminars in Interventional Radiology 2001;18: 23-35.
83. Van de Ver P, Kaatie R. Geutler Arterial stenting and balloon angioplasty in ostial atherosclerotic renovascular disease: A randomised trial. Lancet 1999;353:282-86.
84. Sharma S, Saxena A, Talwar KK. Renal artery stenosis caused by nonspecific aortoarteritis (Takayasu's disease): Results of treatment with percutaneous transluminal angioplasty. AJR 1992;158:417-22.
85. Martin LG, Cork RD, Kaufman SL. Long-term results of angioplasty in 110 patients with renal artery stenosis. J Vasc Interv Radiol 1992;3:619.
86. Eldrup-Horgensen J, Harvey R, Sampson L. Should percutaneous transluminal renal artery angioplasty be applied to ostial renal artery atherosclerosis? J Vasc Surg 1995;21:909-15.
87. Bax L, Mali WP, Buskens E, et al. The benefit of stent placement and blood pressure and lipid lowering for the prevention of progression of renal dysfunction caused by Atherosclerotic ostial stenosis of the renal artery. The STAR-study: rationale and study design. J Nephrol 2003;16:807-12.
88. Mistry S, Ives N, Harding J, et al. Angioplasty and stent for renal artery lesions (ASTRAL trial): Rationale, methods and results so far. J Hum Hyperten 2007;21:511-15.
89. Murphy TP, Cooper CJ, Dworkin LD, et al. The cardiovascular outcomes with renal atherosclerotic lesions (COREL) study: Rationale and methods. J Vasc Inter Radiol 2005;16:1295-300.
90. Robinson L, Yedroye W, Reidy J. Saxton II Renal artery stenosis in children. Clin Radiol 1991; 44:376-82.

Chapter

16

Renal Parenchymal Disease and Renal Failure

Anupam Lal, Hina Arif Mumtaz

Disorders of renal function are ubiquitous in contemporary practice of medicine. Kidney disease manifestations may vary from complete asymptomatic cases to life threatening emergencies. Insight into the causes and consequences of medical renal disease has progressively increased over the last decade, and radiological imaging has played a pivotal role in this improved understanding.

DEFINITION AND CLASSIFICATION OF RENAL FAILURE

The term renal failure encompasses the spectrum of diseases from acute and reversible to chronic and irreversible. It is broadly divided into two categories:

Acute Renal Failure (ARF)

This is defined as a rapid deterioration in renal function characterized by progressive azotemia (best measured by serum creatinine) which may or may not be accompanied by oliguria (urine output<400ml/d). The cardinal feature of ARF is a decline in glomerular filtration rate (GFR). There is sudden and often temporary loss of renal function, which is frequently reversible, with less than 20 percent cases ultimately requiring renal replacement therapy.[1] Imaging is, therefore, directed at identifying correctable causes of acute renal insult. Most common causes include acute tubular necrosis, severe dehydration, tubular blockade, infection and obstruction.

Chronic Renal Failure (CRF)

The diagnosis of CRF implies a persistent abnormality in GFR with a wide range of causes. Slow progressive loss of kidney function over a span of years occurs, resulting in permanent kidney damage. Chronic kidney disease is defined as sustained kidney damage greater than 3 months duration resulting in a GFR of less than 60 ml/min/1.73 m^2.[2]

For purposes of diagnosis and management, renal failure can be divided into three categories:

1. Prerenal: Diseases caused by any process that decreases perfusion to kidneys in which the integrity of renal parenchymal tissue is preserved.
2. Intrarenal: Diseases affecting renal parenchymal tissue (which can be further divided into vascular, glomerular and tubular diseases).

3. Postrenal: Diseases associated with obstruction of the urinary tract or venous blood flow. It is also known as "surgical renal failure" as it is often amenable to correction.

This chapter is designed to give a contemporary insight of the intrarenal causes of acute and chronic renal failure - *'Medical Renal Diseases'*.

Various causes of acute and chronic renal failure are enumerated in Tables 16.1 and 16.2.[1]

ROLE OF IMAGING IN RENAL FAILURE

Overlapping imaging findings are seen in renal failure. Comprehensive evaluation should be done in a particular case which includes clinical profile, laboratory findings and histopathology along with imaging to arrive at a conclusive diagnosis.

The role of imaging in renal failure is to segregate the surgical and medical conditions resulting in renal insufficiency.[1] Goal for radiological studies in renal failure is:

a. Exclusion of correctable causes of acute renal failure (eg.: obstruction, thrombosis)
b. Estimation of renal size to differentiate acute parenchymal disease from chronic parenchymal disease.

Once obstruction is excluded, prerenal and postrenal causes of renal failures can be managed medically.

Radiological Approach to Renal Parenchymal Disease

Most diseases affecting the parenchyma of the kidney may produce lesions detectable only by electron or light microscopy, or by deranged renal function. However, some pathological processes manifest as renal morphological abnormalities and may be diagnosed by radiological imaging.

Morphological criteria are useful to categorize the wide spectrum of renal parenchymal diseases. Evaluation is done based on renal size, contour and laterality of involvement (Table 16.3).

Renal size is an important diagnostic criterion. Large kidneys result from accumulation of fluid, deposition of protein, inflammatory or neoplastic infiltrates, glomerular or microvascular proliferation and cellular hypertrophy. Small kidneys result from loss of renal substance due to hypoplasia, necrosis, atrophy or fibrosis. Renal contour is another useful indicator. If a disease causes global reduction in renal mass, parenchymal bulk is uniformly lost and its size decreases with smooth contour. This is ascertained by preserved interpapillary line, which is a useful landmark for evaluating loss of renal parenchyma. Interpapillary line is drawn through the tips of papilla (base of the calyces) (Fig. 16.1), the distance from this line to lateral surface of kidney is the renal parenchymal thickness which averages to 2.5 to 3 cm. It is greater at polar calyces ranging upto 3.5 cm. Distances less than 2 cm are suggestive of parenchymal loss while those greater than 3.5 cm indicate mass lesion or infiltration. [3]

Assessment of renal contour may show a deviation when there is focal loss or regional expansion. Laterality indicates nature of the disease. Bilateral renal lesions are usually found in systemic disorders in which total renal mass is affected.[4,5]

Radiological imaging in renal parenchymal disease is usually targeted to reach a set of differential diagnosis, with distinct morphological description. Bilateral large smooth kidney' constitutes to the group of acute renal parenchymal disease, while 'bilateral small smooth kidney' fall into description of chronic renal parenchymal disease.

Table 16.1: Causes of acute renal failure

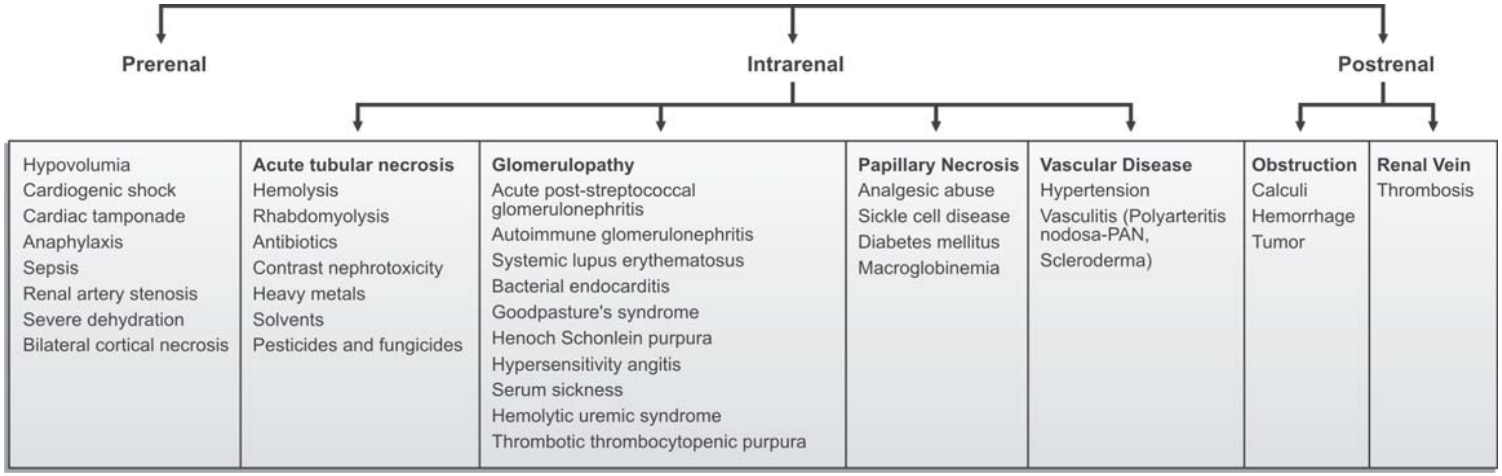

Table 16.2: Causes of chronic renal failure

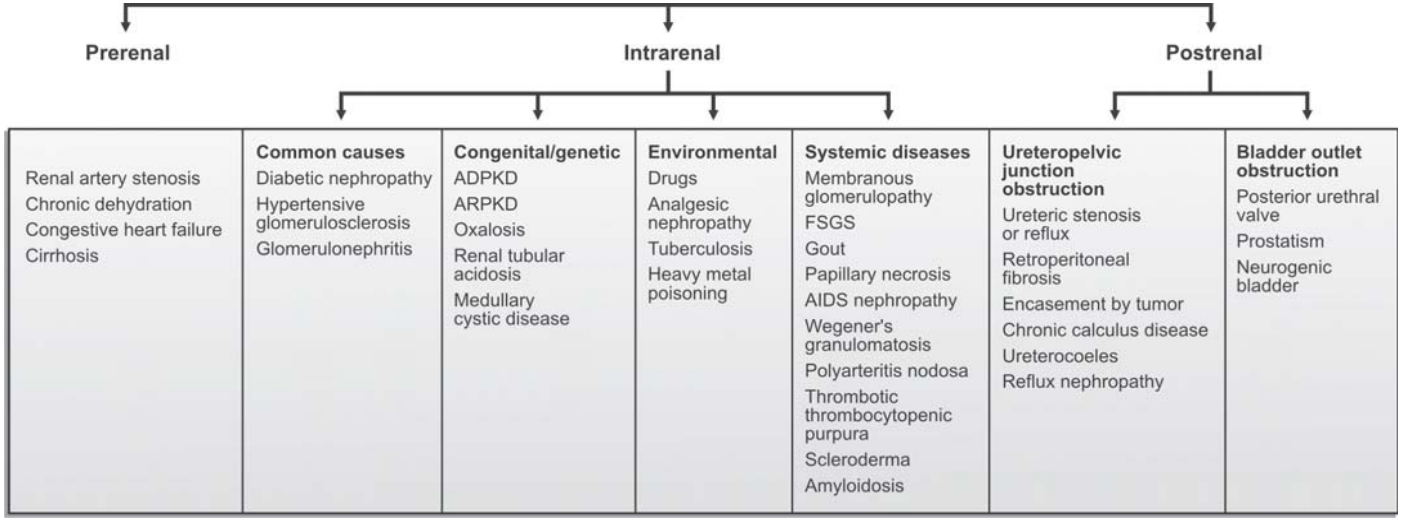

Table 16.3: Morphological criteria to categorize renal parenchymal disease (Size, contour, laterality). List of differential diagnosis of these morphological sets are given in Tables 16.4 to 16.6

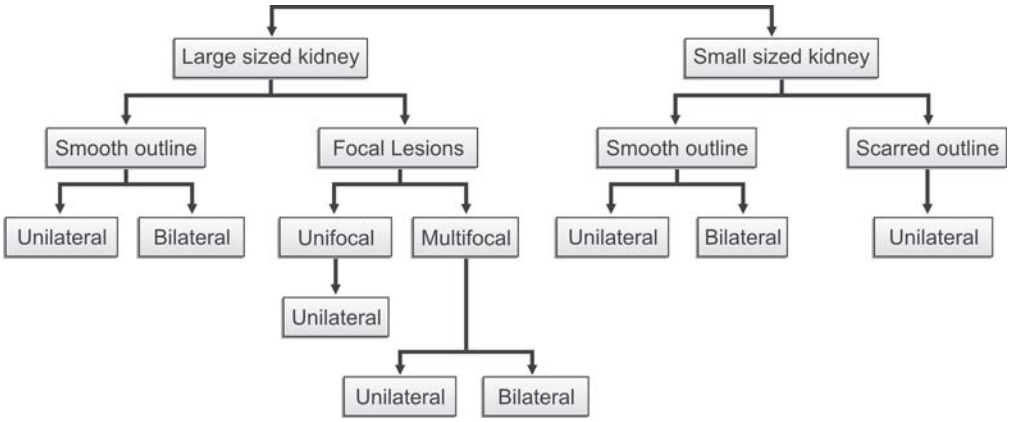

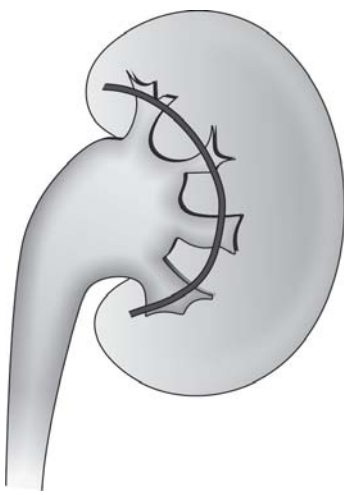

Fig. 16.1: Schematic diagram of normal interpapillary line: This line is drawn by joining the tips of renal papillae; smooth uninterrupted interpapillary line is seen in normal kidney

Imaging Techniques

Recent advancements in all the fields of imaging have led to better evaluation of renal cases and their improved management. Imaging studies performed for evaluating the kidneys provide not only anatomic but also functional and metabolic information. To reach a diagnosis for a particular case, it is important to know the benefits and the limitations along with the diagnostic yield of each modality.

Plain Radiography and Urography

The plain film also known as KUB, has been used for years as the first step in the evaluation of the kidneys, however it gives little significant information on its own. Role of plain radiography is to detect renal parenchymal calcification and calculi. Renal size and contour may be estimated if the renal outlines can be visualized. Renal size is approximately equal to 3 to 4 lumbar vertebral body height. Normal kidney measures 10-14 cm in men and 9-13 cm in women on conventional radiography and 1-2 cm less on ultrasonography. Generally, right kidney is smaller than the left by about 0.5 cm. In clinical setting, discrepancy in renal size of more than 2 cm is considered significant.[3]

In this era of cross-sectional imaging, urography is more of historic importance; however, interesting abnormal nephrographic patterns present in certain sets of diseases, were described by Fry and Cattell, which are:[6]

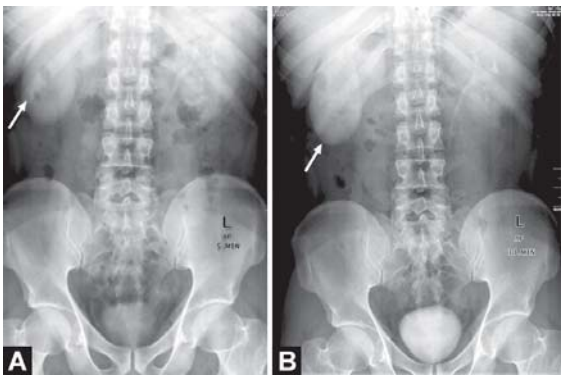

Figs 16.2A and B: Increasing dense nephrogram: IVU shows increased nephrographic density (arrow) on 2-hour film as compared to 5-minute nephrographic phase. Patient had right sided urinary obstruction because of a small tumor near the right vesicoureteric junction

1. Immediate faint persistent nephrogram – Chronic glomerular disease.
2. Increasingly dense nephrogram – Acute renal obstruction, hypotension, renal ischemia, acute glomerular disease, intratubular obstruction and acute renal vein thrombosis (Figs 16.2A and B).
3. Immediate dense persistent nephrogram – Acute tubular necrosis and severe inflammatory renal disease.

Striated nephrogram—is a variant of obstructive nephrogram which may also be encountered in other conditions like pyelonephritis, polyarteritis nodosa (PAN), trauma and medullary cystic kidney disease. Prominent cortical nephrons are seen extending into the medulla as 'medullary rays'.

Ultrasonography

Ultrasonography is initial imaging modality for azotemia as it is non-invasive and readily differentiates between obstructive (surgical) and non-obstructive (medical) causes of renal failure (Fig. 16.3A)[5]. Renal sizes, cortical thickness, echogenicity of the kidneys and the presence or absence of hydronephrosis are easily assessed on ultrasonography. Renal size and parenchymal thickness are useful parameters to assess chronicity of renal disease (Fig. 16.3B). Enlarged kidneys indicate an acute parenchymal lesion while contracted small kidneys suggest a chronic disease. Renal cortical echogenicity is an important indicator for the diagnosis of renal parenchymal disease. Normally the echogenicity of renal cortex is less than liver or spleen; the demonstration of increased echogenicity of the renal cortex under standard scanning techniques may be useful in suggesting the presence of renal parenchymal (medical renal) disease. Renal corticomedullary differentiation may be preserved, obliterated or accentuated depending on the severity of renal cortical echoes[7,8] (Figs 16.3 C to F).

Increased cortical echogenicity with preserved corticomedullary differentiation may be seen in glomerulonephritis, nephrosclerosis, amyloidosis, acute leukemia, ATN and Alport's syndrome while cortical echogenicity is decreased in lymphoma, acute pyelonephritis and renal vein thrombosis. Increased medullary echotexture is found in gouty nephropathy, medullary nephrocalcinosis and medullary sponge kidney. Interestingly, some authors recognize the altered state of hydration at the time of scanning as one of determining factors influencing the renal cortical echotexture of the patient.[8,9] An extracapsular hypoechoic rim of edema may surround the kidneys in renal failure. This finding when present is usually bilateral and is called as 'kidney sweat sign'.[10]

Ultrasound examination is also valuable for assessing the kidneys for follow-up of renal parenchymal disease. Changes in renal size, progression as well as resolution of the

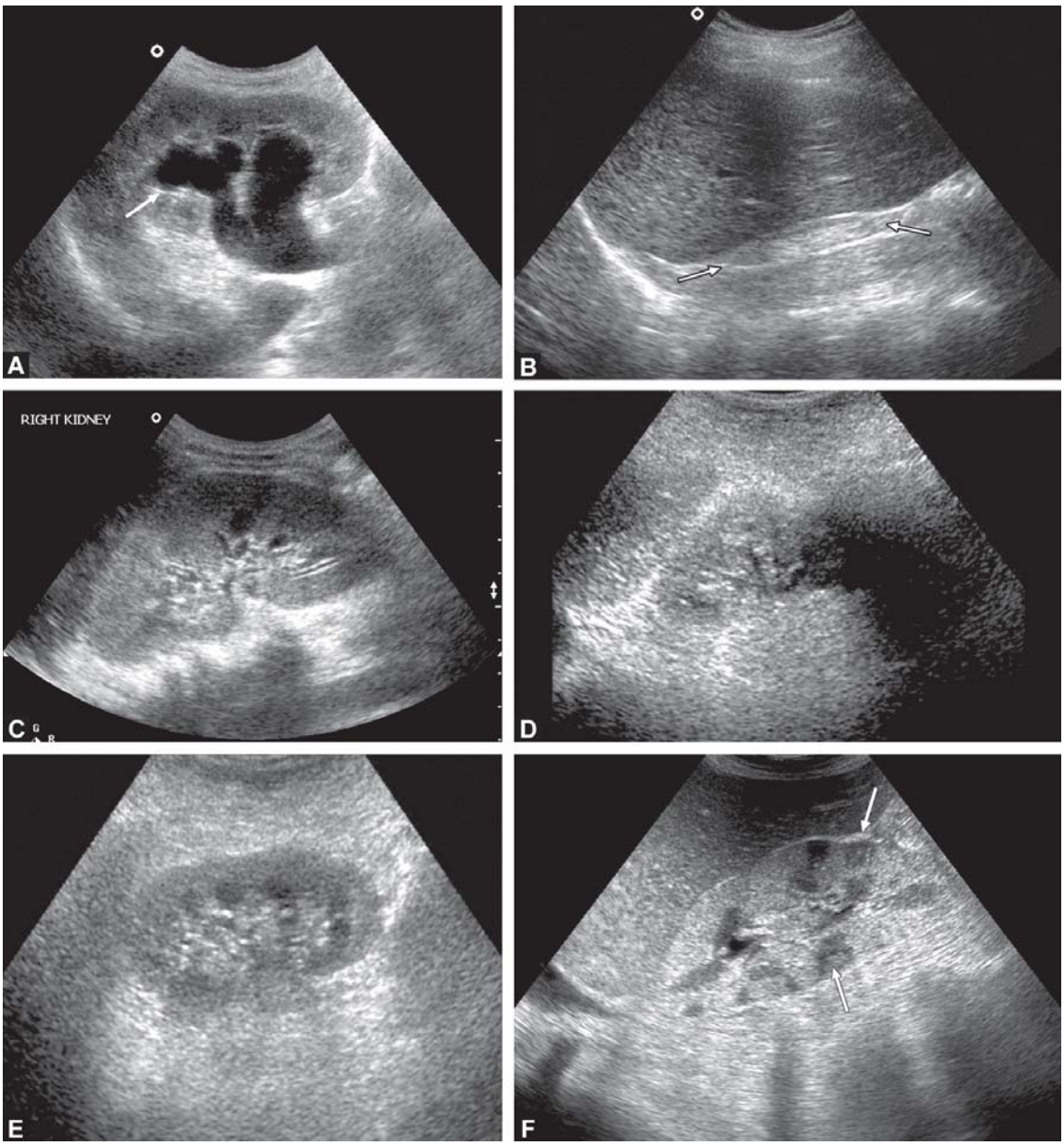

Figs 16.3A to F: (A) Obstructive renal failure in a man with distal ureteric calculus: Longitudinal ultrasound image depicts marked dilatation of the pelvicalyceal system (arrow). Note the upper ureter is also dilated. **(B)** Chronic Renal Failure: Ultrasound image shows small smooth kidney with markedly decreased renal parenchymal thickness. **(C–F)** Acute renal parenchymal disease US images: **(C)** Slightly raised cortical echogenicity and lack of renal corticomedullary differentiation. **(D)** Markedly increased parenchymal echoes nearing to that of renal sinus resulting in loss of corticomedullary differentiation. **(E)** Hyperechoic renal cortex, relatively prominent renal medulla with accentuated corticomedullary differentiation. **(F)** Complicated pyelonephritis with multiple renal abscesses: Severely raised cortical echoes and few hypoechoic well-defined parenchymal lesions (abscesses)(arrows) with right pleural effusion

disease can easily be monitored on ultrasonography .

Color Doppler

Color Doppler is a handy, easily available and non-invasive tool for evaluation of renal blood vessels. Normal renal arterial branching pattern is well-appreciated on color flow imaging. Assessment of spectral wave pattern and flow indices of renal arteries can be done. Vascular resistance (Resistive Index: RI) and pulsatility (Pulsatility Index) along with absolute flow velocities of the main, intralobar and arcuate arteries may be calculated. Out of these indices Resistive Index is most commonly used. It is calculated as:

Resistive Index (RI) =

$$\frac{\text{Peak systolic velocity} - \text{Lowest diastolic velocity}}{\text{Peak systolic velocity}}$$

Normal resistive index is less than 0.7. Parenchymal diseases with tubulointerstitial or vascular involvement cause increased resistive index (>0.7), while glomerular diseases do not cause any significant increase in this parameter.[11] Elevated RI correlates with the severity of disease in SLE , HUS, diabetes and hepatorenal syndrome[5] (Fig. 16.4).

Computed Tomography

Computed tomography has a specific role in evaluation of renal failure. In acute renal failure non-contrast CT scan of kidneys may show parenchymal calcification. Renal parenchyma, however, appears homogenous in attenuation on NCCT. Various nephrographic patterns are demonstrated after the administration of contrast. Differential diagnosis of the nephrographic patterns used on urography is similarly applied to CT nephrogram. Excretory function can further be assessed on sequential dynamic imaging.[12]

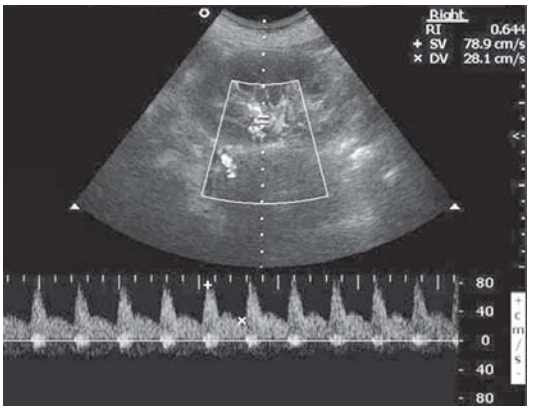

Fig. 16.4: Normal Doppler ultrasound: Doppler spectra obtained in the area of interlobar arteries show a sharp systolic peak and prominent antegrade flow during diastolic phase. Resistive index in this patient is 0.64, which is normal *(For color version see Plate 18)*

Magnetic Resonance Imaging

Routine MRI evaluation of the kidney includes axial and coronal T1 weighted and T2 weighted spin echo sequences, with or without fat suppression. Corticomedullary differentiation (CMD) is distinctly seen on T1W and T2W images. In normal kidney, the cortex is slightly higher in signal intensity than the medulla on T1W images while renal medulla is hyperintense to cortex on T2W images. (Figs 16.5A to D). In a normal well-hydrated kidney, sharp corticomedullary differentiation is seen on T1W sequence due to high signal of cortex as compared to medulla. Wide variety of renal medical diseases cause decrease in cortical signal and subsequent loss of CMD. Loss of corticomedullary differentiation on T1W spin echo sequences is a sensitive indicator of parenchymal diseases and correlates with elevated serum creatinine levels >3.0 mg/dl. Dynamic contrast enhanced T1 weighted

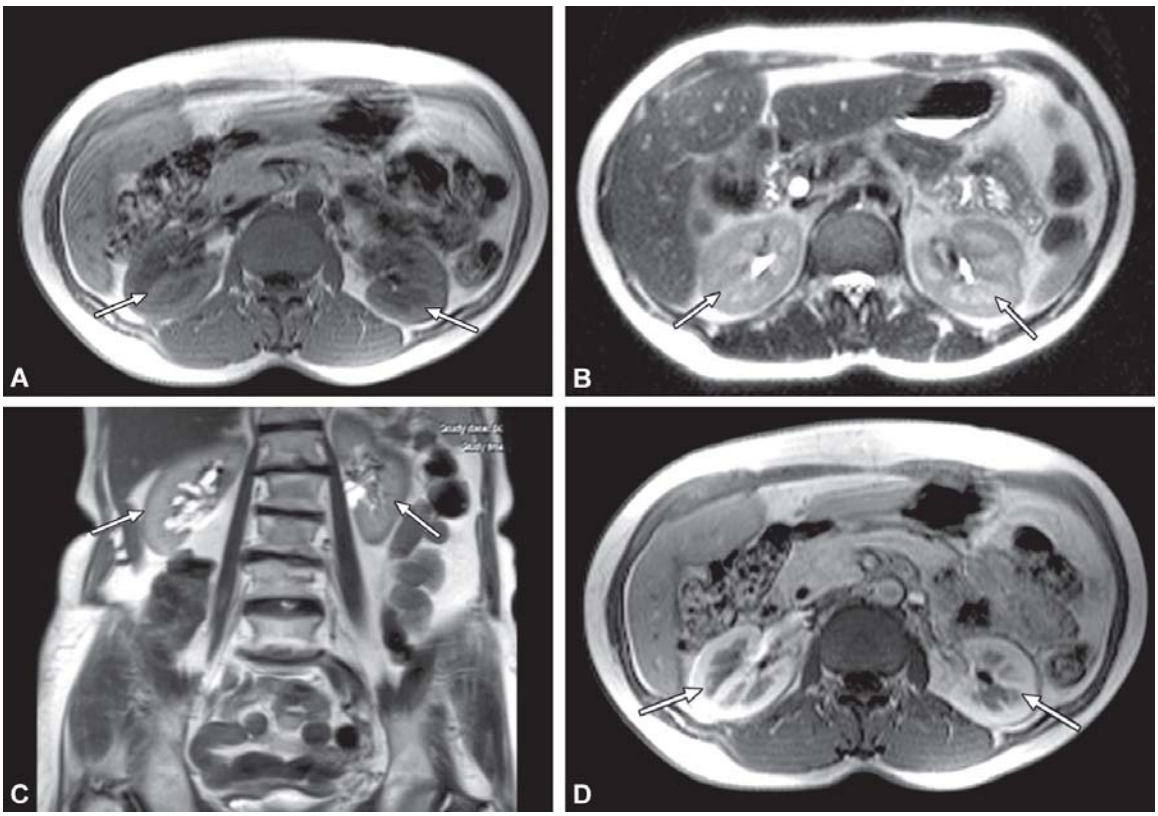

Figs 16.5A to D: Normal spin echo magnetic resonance imaging findings: **(A)** T1W axial image shows corticomedullary differentiation resulting from high signal intensity of normal renal cortex and lower signal intensity of renal medulla(arrows). **(B and C)** T2W axial and coronal MR images depict the hyperintensity of normal renal medulla as compared to renal cortex (arrows). **(D)** Postgadolinium dynamic MR in cortical phase reveals the striking distinction between renal cortex and medulla (arrows)

sequences can also be done. CMD is lost on post-gadolinium dynamic MR imaging when serum creatinine is >8.5 mg/dL.[13] Some pilot studies are exploring the use of diffusion weighted MR imaging to demonstrate low values of ADC in renal cortex and medulla in patients of renal failure as compared to healthy volunteers.[14] When gadolinium was introduced as intravenous contrast agent for magnetic resonance imaging it was initially regarded as nonnephrotoxic and was possibly recommended to replace iodinated contrast agents in patients at risk for acute renal failure. However, contrast induced nephropathy has been associated with gadolinium, especially in patients with advanced renal disease. Further research can clarify the renal effects of gadolinium in patients with renal insufficiency.[15]

Renal Angiography

Renal angiography has limited role in renal parenchymal disease as it is an invasive procedure and usually requires large amount of iodinated contrast medium. Characteristic appearances like aneurysmal dilatation of medium and small sized vessels on arteriography are seen in conditions like PAN,

Wegener's granulomatosis and SLE. Pruned, tortuous vessels with slow flow with thinned renal cortex are demonstrated. Lucent or mottled nephrogram may be seen.

Renal artery stenosis is most accurately diagnosed on angiography and can be treated by angioplasty.[16]

Radionulceotide Imaging

Scintigraphy provides imaging based diagnostic information on renal structure and function. Radionucleotide agents are excreted by kidneys; hence, they should be judiciously employed in patients with renal failure. ^{99m}Tc-DTPA is excreted solely by the glomerular filtration, therefore it should not be used frequently. Tubular secretion of ^{99m}Tc-MAG3 and Hippuran I-131 occurs, hence these may be utilized in severe renal insufficiency.[17]

Contrast Medium Associated Nephropathy

The presence of renal failure may pose some limitations on the choice of an individual imaging modality. Iodinated contrast media may cause exacerbation of renal insufficiency.

Contrast medium associated nephropathy (CAN) is one of the common causes of hospital acquired ARF. The exact mechanism of CAN is still unknown, but it is thought to be multifactorial.[18] CAN is defined as a rise of ≥ 0.5 mg/dl of serum creatinine (above a baseline value) within 48 hours of the administration of intravascular contrast material when no other cause of renal injury is readily apparent.[19] The rise in serum creatinine usually peaks at 3 to 5 days and return to baseline within 10 to 14 days. The most important risk factor is pre-existing renal insufficiency (serum creatinine > 1.5-2.0 mg/dL), followed by diabetes mellitus, advancing age, congestive heart failure, dehydration, high dose of contrast media and furosemide. Adequate hydration, dose reduction and use of non-ionic contrast media are recommended as preventive measures.[5]

IMAGING IN RENAL PARENCHYMAL DISEASE

Acute Renal Parenchymal Disease

Radiographic appearance of 'Bilateral, large, smooth' kidneys is usually seen in the setting of renal failure of recent onset. When obstruction is ruled out a similar picture of enlarged smooth kidneys with normal or effaced collecting system is seen that indicates parenchymal disease of recent origin, which is possibly reversible. Tables 16.4 and 16.5 enumerate the causes of renomegaly based on morphological criteria[4].

However, in some conditions certain characteristic appearances are seen imaging which shall be discussed in the next section of this chapter. Infections, cystic renal diseases, obstructions, renal vascular diseases and tumors are not included here as they are covered in other chapters in this book.

Acute Tubular Necrosis (ATN)

ATN is the most common reversible cause of renal failure. Renal hypoperfusion and ischemic injury (due to shock, severe dehydration, burns and crush injury) are the leading causes of ATN. The incidence of ATN related to nephrotoxic drugs (contrast media, aminoglycosides and other antibiotics) and agents (heavy metals, solvents and pesticides) is also rising. ATN is also commonly seen in the transplanted kidney.[20]

The pathogenesis of ATN is still debatable, but some authors have proposed that direct tubular damage is the primary event leading to necrosis of the epithelium and obstruction of the tubular lumen with cellular debris. [20]

Table 16.4: Causes of bilateral large smooth kidneys[4]

Proliferative/necrotizing disorders
Acute glomerulonephritis
Polyarteritis nodosa (microscopic form)
Systemic lupus erythematosus
Wegener's granulomatosis
Allergic angitis
Diabetic glomerulosclerosis
Lung hemorrhage and glomerulonephritis (Goodpasture's syndrome)
Anaphylactoid purpura (Henoch- Schonlein syndrome)
Thrombotic thrombocytopenic purpura
Focal glomerulonephritis associated with subacute bacterial endocarditis
Plasma cell dyscrasias
Multiple myeloma
Waldenstrom's macroglobulinemia
Amyloidosis
Abnormal glycogen deposition
von Gierke's disease (Glycogen storage disease Type-I)
Abnormal lipid deposition
Fabry's disease
Abnormal fluid accumulation:
Acute tubular necrosis
Acute cortical necrosis
Leukemia
Acute interstitial nephritis
Acute blockage of tubules
Acute urate nephropathy
Tamm - Horsfall protein
Acute myeloma nephropathy
Acromegaly
Nephromegaly associated with cirrhosis, hyperalimentation and diabetes mellitus
Hemophilia
Homozygous-S disease
Tyrosinosis Type I
Infectious mononucleosis
Autosomal recessive polycystic kidney disease
Physiological response to contrast material and diuretics

The oliguric (urine output < 500 ml/day) or anuric phase usually begins less than 24 hours after the inciting incident and may last for 1 to 3 weeks. Dark urine and proteinuria may be present during this duration. It is followed by diuretic phase, a harbinger of renal recovery. [21]

Imaging Features

In ATN, both kidneys are enlarged and smooth in outline. Contrast enhanced studies are not recommended in ATN. If IV contrast is inadvertently given, persistent dense nephrogram is seen on urography which may persist for more than 24 hours. As tubules are filled with cellular infiltrates, contrast

Table 16.5: Large kidney with focal lesion[4]

Unifocal unilateral		Multifocal	
		Bilateral	Unilateral
Solid masses Malignant neoplasms Renal cell carcinoma Adult nephroblastoma Sarcoma Metastatic deposits Invasive transitional cell carcinoma Benign neoplasms Hamartoma Adenoma Mesenchymal tumor Inflammatory mass	**Fluid-filled masses** Simple cyst Focal hydronephrosis Multilocular cystic nephroma Arteriovenous malformation	Autosomal dominant polycystic kidney diseases Hodgkin's lymphoma Metastases Acquired cystic kidney disease Cystic disease associated with von Hippel-Lindau disease Cystitis and angiomyolipomas associated with tuberous sclerosis	Xanthogranulomatous pyelonephritis Malakoplakia Multicystic kidney disease (Potter's Type II)

leaks into the interstitium through the damaged basement membrane, hence, faint or non-opacification of pelvicalyceal system occurs. Variable appearances of ATN on ultrasonography have been proposed by different authors, which are:[22]

- Normal cortical and medullary echogenicity–Ischemic ATN,
- Increase in cortical echogenicity with maintained corticomedullary differentiation–Drug related ATN,
- Normal cortical echogenicity with echogenic pyramids–associated with precipitation of Tamm-Horsfall protein .

Increased resistive index (>0.7) on Doppler imaging is present in majority of patients with ATN.[23]

Bilateral renomegaly with patchy nephrogram is seen on CT scan. Gadolinium enhanced MRI demonstrates compartmental renal involvement of cortex, inner and outer medulla and give complementary information about the pathological condition of the kidney. Perfusion abnormalities were also shown in experimentally induced ATN. Blood oxygen level dependent MRI (BOLD MRI) assesses intrarenal oxygen bioavailability which reflects tissue deoxyhemoglobin levels. Ischemia and hypoperfusion in ATN results[24] in reduced tissue oxygen bioavailability which is utilized to discriminate between acute rejection and acute tubular necrosis that may follow renal transplantation.[25]

Acute Cortical Necrosis (ACN)

Acute cortical necrosis is a rare form of acute renal failure which is characterized by ischemic necrosis of renal cortex, including renal column of Bertini with sparing of renal medulla, and thin rim of subcapsular cortex. Both kidneys are involved either diffusely or in patchy distribution; in both instances peripheral renal cortex is spared as it is supplied by the preserved capsular vessels.[5]

More than two-thirds of cases are associated with pregnancy and its complications – abruptio placenta, septic abortion and placenta previa. Other causes include severe trauma with shock, sepsis, transfusion reaction, severe dehydration, burns, peritonitis and toxins (e.g. snake venom). Although large numbers of conditions are associated with acute cortical necrosis, the pathophysiology unfortunately remains unclear. Ischemia following vasospasm is probably the initiating event which results due to constriction of small intracortical blood vessels. This may follow exposure to toxins, circulating hormones, or neural stimuli.[25]

Diffuse involvement of both the kidneys may result in complete renal failure requiring either dialysis or transplantation for survival, whereas patchy involvement leads to renal insufficiency.

Imaging Features

Imaging findings depend on the stage of illness. In the acute stage, urographic findings are non-specific. Kidneys are diffusely enlarged with faint opacification of collecting system. For those surviving the early phase, smooth renal shrinkage occurs over several months. Radiographically, distinctive tram like or egg shell calcification of cortex may be seen which start appearing as early as 24 days after the onset of disease.[20]

On ultrasonography, enlargement of both kidneys and loss of the normal corticomedullary differentiation with a circumferential hypoechoic zone corresponding to the necrotic cortex is seen. Ultrasound is useful for follow up. Calcification of cortex causes dense cortical echoes with distal acoustic shadowing.

Specific appearance of acute cortical necrosis is described on contrast enhanced CT scan. The three diagnostic features are (a) enhancement of the medulla, (b) non-enhancement of the renal cortex, and (c) lack of excretion of contrast medium into the collecting system. Enhanced subcapsular cortex, the distinctive 'Cortical rim sign' on contrast-enhanced CT scan suggests the sparing of the most peripheral region of renal

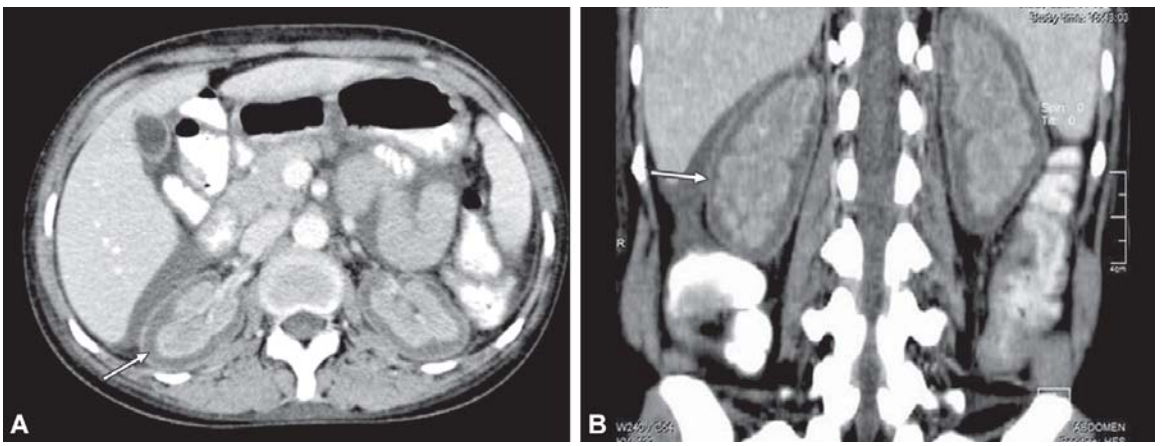

Figs 16.6A and B: Acute cortical necrosis in a female patient with septic abortion: Axial and coronal post-contrast CT scan (corticomedullary phase) demonstrate absence of contrast enhancement in the cortex and relatively hyperdense medulla and subcapsular cortex, the characteristic 'Cortical rim sign'

cortex (Figs 16.6A and B). 'Cortical rim sign' is also seen in other conditions which result in hemodynamic derangement like renal infarction, renal vein thrombosis and ATN.[26-28]

MRI also shows these representative findings. Kidneys are enlarged in the early phase. Low signal intensity of the inner renal cortex and the columns of Bertin on every MR imaging sequence is the major characteristic finding of renal cortical necrosis. Swelling of both kidneys with increased signal intensity of the cortex on T2-weighted images instead of T1-weighted images is another feature of renal cortical necrosis at MR imaging. Later a thin rim of low signal intensity (T1WI and T2WI) may be seen along the border of kidneys due to calcification.[29]

Leukemia

Leukemia (predominantly lymphocytic leukemia) is the most common malignant cause of bilateral renal enlargement in children. Renal enlargement occurs due to infiltration of kidneys by leukemic cells. Usually, markedly large kidneys are seen, however, sometimes asymmetrical renal involvement or focal renal mass may be seen. (Figs 16.7A and B).

Imaging Features

In leukemic infiltration of kidney, the nephrogram is faint and the collecting system is attenuated. Pelvicalyceal system is often filled with blood clots or uric acid stones which appear as filling defects.[20]

Acute Interstitial Nephritis (AIN)

Acute interstitial nephritis is an acute hypersensitivity reaction, mediated through immunologic mechanisms. It may result following an exposure to drugs or non- renal infection (e.g: infectious mononucleosis). However, an idiopathic variety is also described. The most common cause of AIN are drugs particularly—methicillin, penicillin, amphotericin, NSAID, sulfonamides, phenytoin, and thiazide.[30]

Fever, skin rashes, eosinophilia, oliguria and protienuria are the common clinical signs and symptoms of drug induced AIN which appear between 5 days to 5 weeks of

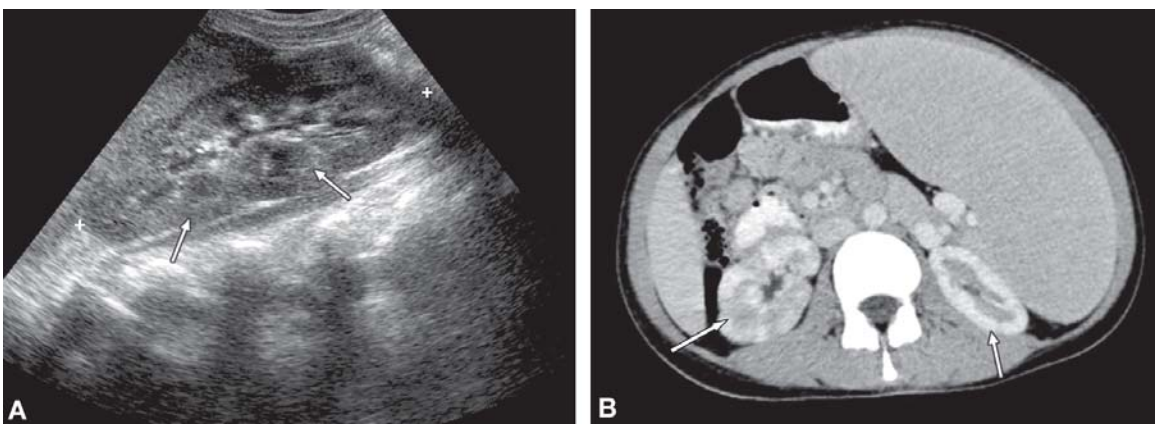

Figs 16.7A and B: Renal manifestation of leukemia: **(A)** Ultrasonography of kidney shows focal, well-defined, hypoechoic masses. **(B)** CECT axial image in another patient also shows bilateral, multiple, focal hypodensities suggestive of leukemic deposits. Massive splenomegaly is also seen

exposure. Patient recovers with the withdrawal of the causative agent.[31]

Imaging Features

Bilateral renomegaly with diminished to normal opacification of collecting system is seen on urography. Ultrasound shows increased cortical echogenicity with renal enlargement. Enhanced uptake of Gallium citrate in the kidneys on renal scintigraphy is also reported.[30] Kidneys may become shrunken and irregular as the disease progresses to a chronic course. Calcification of renal papillae may occur in analgesic induced nephritis. Interstitial fibrosis leads to low signal intensity of renal cortex on T1W MRI.

Amyloidosis

Amyloidosis is a diverse group of diseases that have extracellular deposition of an insoluble fibrillar proteinaceous substance with a beta sheath configuration.

Amyloidosis can be classified as follows:[32]

1. Primary Amyloidosis: Without pre existing or co-existing disease.
2. Amyloidosis associated with multiple myeloma.
3. Secondary or Reactive amyloidosis associated with chronic infections (like tuberculosis, osteomyelitis, leprosy) chronic inflammatory disease (rheumatoid arthritis, ankylosing spondylitis) and malignancies (Hodgkin's lymphoma , renal cell carcinoma).
4. Heredofamilial amyloidosis associated with familial mediterranean fever. Neurological, renal and cardiovascular involvement is seen.
5. Localized amyloidosis without systemic involvement.
6. Dialysis-related amyloidosis.
7. Amyloidosis associated with aging.

Older men are more affected than women,[33] usually presenting with non-specific symptoms like weight loss, fatigue and weakness.

Multiorgan involvement is present in more than 85 percent of cases. Kidney is affected in 80 percent patients with secondary amyloidosis and 35-40 percent patients with primary disease. Isolated involvement of the renal pelvis, ureter bladder, urethra, prostate seminal vesicle, and retroperitoneum can occur.[34]

Imaging Features

In acute phase bilateral renal enlargement is seen. Decrease in size occurs with progression of disease process, smooth outline is, however, maintained. Nephrogram is diminished with variable excretion into normal pelvicalyceal system. Cortical echogenicity is raised as seen in other parenchymal diseases.Rapid deterioration in renal function or sudden onset nephrotic syndrome indicates renal vein thrombosis, a complication of amyloidosis. Thrombosed renal vein is demonstrated on color Doppler, CT scan or MRI.

MRI shows reduced cortical signal intensity on T1 weighted images with subsequent loss of corticomedullary differentiation. Bilateral increased delayed uptake of Gallium 67 when other causes of abnormal gallium activity are excluded.[34]

Amyloidosis of Renal Pelvis

Isolated involvement of renal pelvis can occur in amyloidosis. Interesting radiological appearance of calcification or ossification in the amyloid deposits may be seen. These

deposits are usually located in the submucosa of the pelvicalyceal system. A lucent band of mucosa separates the IV contrast density from calcification in the pelvis on IVU. Other causes for calcification of pelvicalyceal system are tuberculosis, leukoplakia primary carcinoma of renal pelvis and renal calculus.[34] Submucosal amyloid deposits appear hypointense on T1and T2 weighted MR images.

Multiple Myeloma

Multiple myeloma is a plasma cell disorder which originates in the bone marrow and is characterized by involvement of the skeleton at multiple sites. The neoplastic plasma cells produce excess immunoglobulins and Bence-Jones proteins are characteristically present in the urine. Abnormal proteins precipitate in the renal tubules resulting in renal insufficiency in 30-50 percent of such patients.

Nausea, vomiting, anorexia, weight loss and progressive weakness are the presenting features. Nephrocalcinosis resulting from hypercalcemia, uric acid calculi, renal infections and amyloidosis may further complicate the illness.

Imaging Features

Urography shows enlarged smooth kidneys with faint opacification indicating impaired renal function. Collection system is attenuated. Injection of iodinated contrast media is hazardous in patients of multiple myeloma as it precipitates myeloma proteins in the renal tubules. Dehydration has to be avoided to reduce the risk of complications. Ultrasonography shows nephromegaly with reduced cortical echotexture. CT scan and radionucleotide study demonstrates impaired renal function.[21]

Paroxysmal Nocturnal Hemoglobinuria (PNH)

In PNH complement mediated erythrocyte damage results in hemolysis with release of hemoglobin in plasma. Hemolysis is precipitated by infections, drugs immunization and exercise. Patient presents with hemoglobinuria, iron deficiency anemia and venous thrombosis.

Imaging Features

Non-contrast CT may show high density of renal cortex due to hemosiderin pigments. Paramagnetic effects of hemosiderin results in markedly reduced signal in the cortex in both T1W and T2W images but it is more pronounced on T2W sequences. Similar imaging features are seen in intravascular hemolysis like in malfunctioning prosthetic valves, sickle cell anemia, hereditary spherocytosis and thalassemia.[35]

Chronic Renal Parenchymal Disease

In contrast to the capacity of kidney to regain back its function following acute renal insult, renal injury of more prolonged nature often leads to progressive and irreversible loss of nephrons. Such reduction in renal mass subsequently results in bilaterally small smooth kidneys. The uremic kidney shrinks globally reflecting the inherent tissue loss. Renal contour may be smooth or irregular. The echogenicity can be normal or increased. Radiological features, like those in acute renal parenchymal disease are overlapping in most of the causes of chronic renal parenchymal disease. However, some conditions show interesting radiological appearances and are discussed here. The various causes of bilateral small smooth

kidneys are listed in Table 16.6, the conditions leading to morphologically small, unilateral kidneys are also cited.[4] Figs 16.8 to 16.11 show imaging in cases of chronic renal failure.

Renal Papillary Necrosis

Necroses of the renal papillae not only have many causes but also many radiological forms. Parenchymal diseases affecting the

Table 16.6: Causes of small kidney

Smooth		Scarred U/L
Unilateral	**Bilateral**	
Ischemia due to focal arterial disease	Generalized arteriosclerosis	Reflux nephropathy
Chronic infarction	Benign and malignant nephrosclerosis	Lobar infarction
Renal vein thrombosis (late)	Atheroembolic renal disease	
Radiation nephritis	Chronic glomerulonephritis	
Congenital hypoplasia	Papillary necrosis	
Post-obstructive atrophy	Hereditary nephropathies	
Post-inflammatory atrophy	Hereditary chronic nephritis (Alport's syndrome)	
Reflux atrophy	Medullary cystic disease	
Partial nephrectomy	Amyloidosis (late)	
	Arterial hypotension	
	Cortical necrosis (late)	

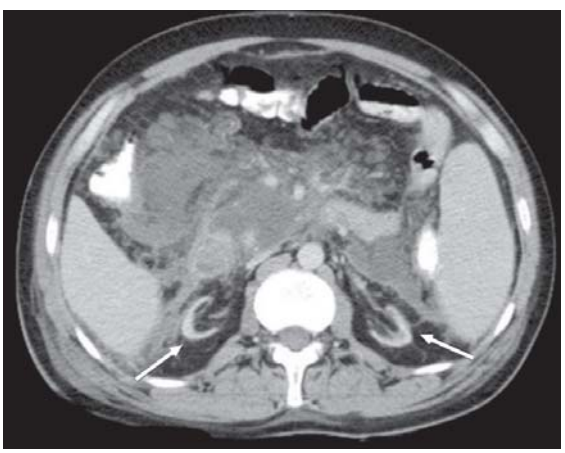

Fig. 16.8: End stage renal disease: CECT axial image shows bilateral smooth shrunken kidneys in a patient of CRF with pancreatitis. Peripancreatic inflammatory fluid collections are also present

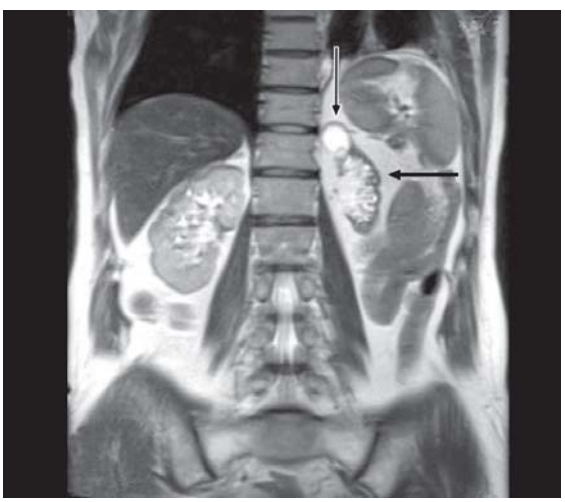

Fig. 16.9: Unilateral small smooth kidney: T2W Coronal MR image reveals small, contracted left kidney with thinned renal parenchyma and indistinct CMD, subsequent to left renal artery stenosis (arrow). Note made of simple cortical renal cyst in left upper pole (short arrow)

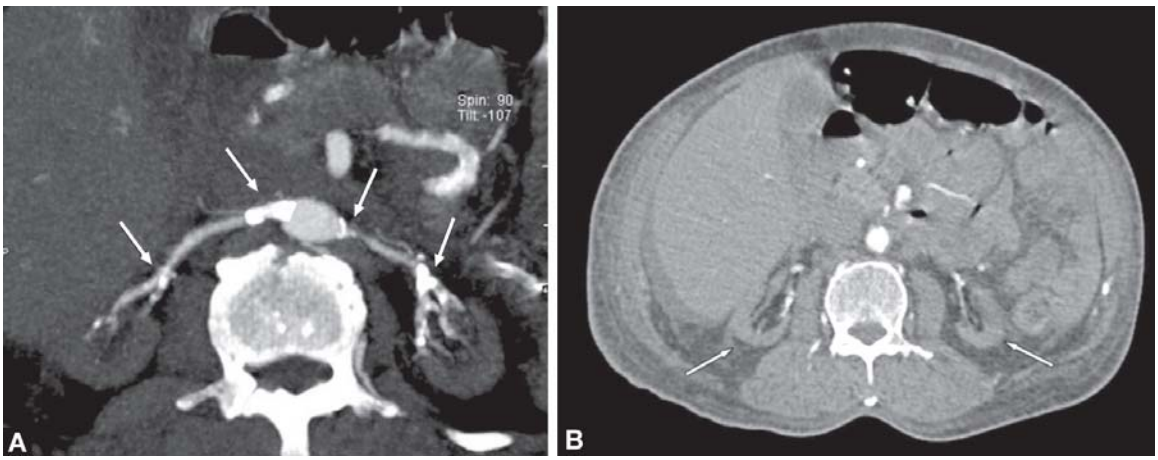

Figs 16.10A and B: Bilateral small smooth kidneys: CT angiography **(A)** shows calcified arthero-thrombotic plaques involving both main renal arteries and their ostia **(B)** smooth globally shrunken kidneys, in a patient of severe bilateral renal artery stenosis. Mild peri hepatic fluid is seen

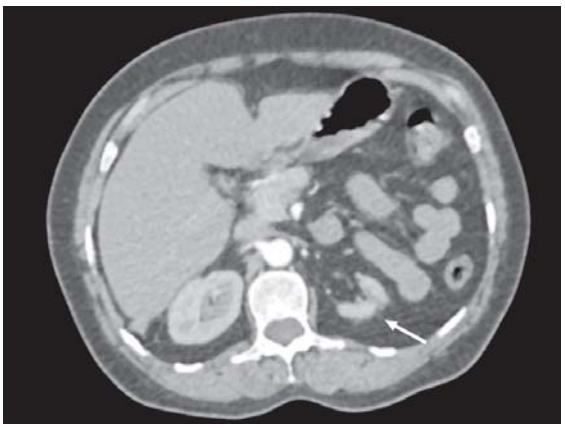

Fig. 16.11: Unilateral small scarred kidney: CECT axial image in cortical phase of enhancement shows small left kidney with irregular outline with parenchymal defect at interpolar region

papillae and calyces are diagnosed on urography. In mild cases the kidney size and function are normal, and the abnormality is limited to the papillae only. In advanced disease there is global shrinkage of kidney with impaired renal function. Most common cause of renal papillary necrosis is analgesic abuse nephropathy. Other causes are diabetes, sickle cell nephropathy, obstruction with infection, renal vein thrombosis, dehydration and prolonged hypotension.[5] (Pneumonic to remember causes of renal papillary necrosis- ADIPOSE: Analgesic nephropathy, diabetes, Infant in shock, Pyelonephritis, obstruction, sickle cell disease and ethanol).

In early papillary necrosis ischemia occurs in the renal papillae due to compression of the medullary vessels by inflammatory changes in the interstitium. If the phase of temporary spasm passes, normal circulation is restored and the involved tissues may recover. However, if ischemia continues and perfusion is not restored, irreversible coagulation necrosis, tubular fibrosis and lobar infarcts result.

Urographic findings during this period of early ischemic change are usually normal. On MDCT, the ischemic changes that lead to renal papillary necrosis can be demonstrated best on nephrographic phase as small, poorly marginated areas of diminished enhancement at the tip of the medullary pyramid.

In advanced stage of necrosis, clefts originate from the fornices and extend to the

medullary pyramids and papillae, ultimately causing the papillae to slough (Fig. 16.12). Caliceal deformities in renal papillary necrosis occur in three forms:

1. **Medullary:** Central necrosis takes place at the tip of the pyramid. Detachment of necrotic papillae starts in the central part of the calix, opening into a round or oval cavity.
2. **Papillary:** Detachment of necrotic papillae usually begins in the region of the caliceal fornices, and the resulting defect is triangular in shape also termed as lobster claw appearance.
3. **In situ:** When papillae fail to separate (necrosis *in situ*) calyces appear normal, they later calcify to give appearance of nephrocalcinosis.

In the healing phase, the papilla may epithelialize, and its tip takes a blunted appearance. In addition, shrinkage of the kidney may occur with reduction of parenchymal thickness. This is the common sequel of renal papillary necrosis. Moreover, the loss of renal cortex is associated hypertrophy of the renal columns resulting in a typical irregular wavy renal outline.[36]

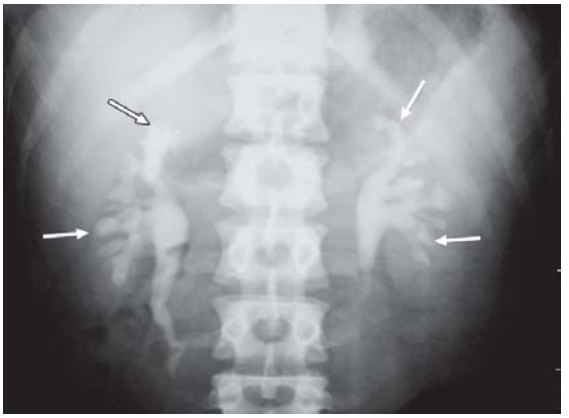

Fig. 16.12: Renal papillary necrosis: IVU film showing irregular and distorted calyces of both kidneys, with contrast excavation and formation of multiple cavities. Few amputated calyces are also seen

In advanced disease, after the sloughing of necrotic papillae, cavities are seen that are continuous with calices in renal medullary areas. Their differentiation with other cystic lesions in the renal medullae should be done (like hydronephrosis, congenital megacalices, parapelvic cysts, and caliceal diverticula).[37]

Alport's Syndrome

Alport's syndrome is progressive hereditary nephritis that manifests as hematuria and proteinuria, and is frequently associated with nerve deafness and variety of ocular abnormalities. It is often preceded by upper respiratory tract infections. Syndrome affects males more frequently than females. Progressive renal insufficiency occurs.

Imaging Features

Kidneys are severely shrunken in advanced stage, but maintain their smooth outline. Poor excretion of nephrographic contrast is noted. Renal echogenicity is increased on USG with loss of CMD. Hyperechogenicity due to nephrocalcinosis is present which is due to chronic glomerulonephritis. Non-specific pruning and tortuosity of interlobar arteries is seen on angiography.[37,38]

Benign and Malignant Nephrosclerosis

Nephrosclerosis affects the renal arterioles. The disease courses over many years but it rarely leads to kidney failure on its own. Malignant nephrosclerosis, however, progresses very rapidly and damages the arteries. These damaged arteries are unable to provide enough oxygen to the kidney tissues, resulting in kidney failure. The incidence of hypertensive nephrosclerosis increases with advancing age.[39]

Imaging Features

Kidneys are small and smooth in benign nephrosclerosis; occasionally shallow infarcts can be seen. Normal nephrographic opacification, and excretion into pelvicalyceal system is seen on urography.

On ultrasonography, increased central sinus echogenicity due to fat deposition may be seen. Subcapsular and perirenal hemorrhages may be detected as hypoechoic or anechoic fluid collections. High density fluid (blood) can be better detected on noncontrast CT scan. Blood degradation product may also be identified on MR imaging.[40]

Renal Osteodystrophy

A number of skeletal abnormalities may coexist in the metabolic bone disease due to renal failure. The primary radiologic bone changes reflect:

a. Deficiency in active form of vitamin D due to impaired renal function: Rickets.
b. Impaired clearance of calcium leading to increased parathormone secretion: Secondary hyperparathyroidism.

The spectrum consists of secondary hyperparathyroidism along with rickets, osteomalacia, osteosclerosis, and osteoporosis.

Inability of the kidney to adequately excrete phosphate, leads to hyperphosphatemia and increased osteoclastic activity. It can be categorized by resorption of bone at subperiosteal, cortical, subchondral, trabecular, endosteal, and subligamentous locations. Radiographic appearance of subperiosteal resorption has been described as a lacelike irregularity of the normal cortical margin, which may progress to areas of scalloping and spiculation. The earliest involvement is often seen along the radial aspects of the middle phalanges of the index and middle fingers, beginning in the proximal metaphyseal region. The terminal tufts may also demonstrate subperiosteal resorption. Additional sites of subperiosteal bone resorption include the upper medial tibia, humerus, and femur; superior and inferior ribs; and lamina dura (Fig. 16.14).

Loss of trabecular sharpness occurs with trabecular resorption. This is well seen in the skull, described as a granular salt-and-pepper appearance, with loss of distinction between the inner and outer tables. Common sites of subchondral resorption are the distal clavicle and acromioclavicular joint, sacroiliac joint, sternoclavicular joint, symphysis pubis, and posterior patella (Figs 16.13A and B).[14] Osseous resorption may also occur at sites of ligamentous and tendinous attachments. Brown tumors are rare.

Osteosclerosis has a strong predilection for the axial skeleton, where cancellous bone predominates over cortical bone. In the vertebral bodies, bandlike areas of sclerosis involving the superior and inferior end plates with intervening normal osseous density are classically seen, which resemble the stripes on rugby jerseys called as rugger jersey spine.

Changes of rickets can be seen in children with a general delay in bone age, bowing of long bones, scoliosis, diffuse concave impressions at multiple vertebral end plates, basilar invagination of the skull, "triradiate pelvis" deformity and rachitic rosary. In children, epiphyseal displacement (slipped epiphysis) in children is also seen. Osteomalacia in adults may manifest as looser zones. Metastatic soft tissue and vascular calcification can be seen in ocular tissues, arteries, subcutaneous and periarticular soft tissues, and viscera.[41]

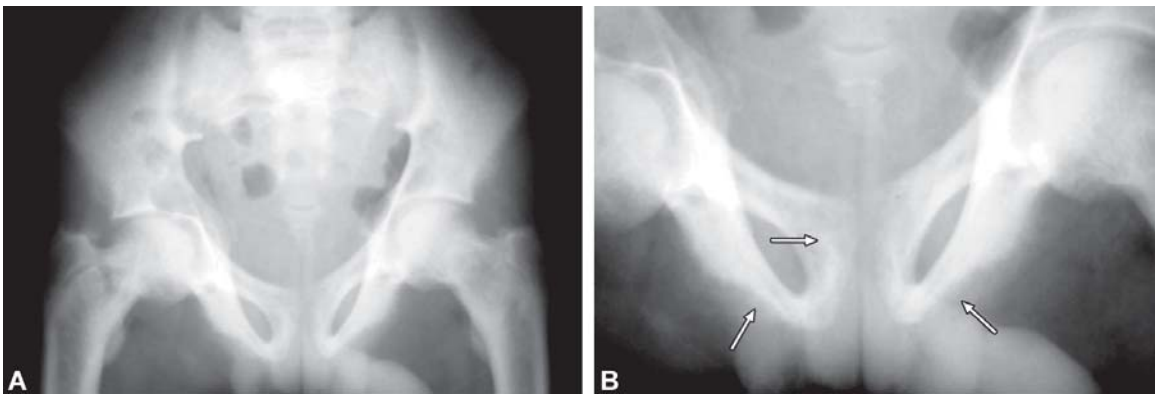

Figs 16.13A and B: Renal osteodystrophy in a patient of tuberculosis: Antero-posterior view of pelvis shows osteopenic triradiate pelvis. Subchondral resorption of bone is seen at the pubis symphysis, ischial tuberosities and sacroiliac joint (arrow)

CONCLUSION

Imaging and management of renal failure continues to evolve with the development of newer imaging modalities and attainment of better cost effectiveness. Despite these achievements radiological imaging still has limitations in evaluation of renal parenchymal disease and renal failure. Radiological imaging techniques are rapidly expanding and are expected to grow even further. The future possibly holds improved methods to readily identify the causes of reversible acute renal failure and plan treatment strategies to combat chronic renal failure. The combination of better diagnostic methods and management strategies will lead to improved quality of life in patients with renal failure.

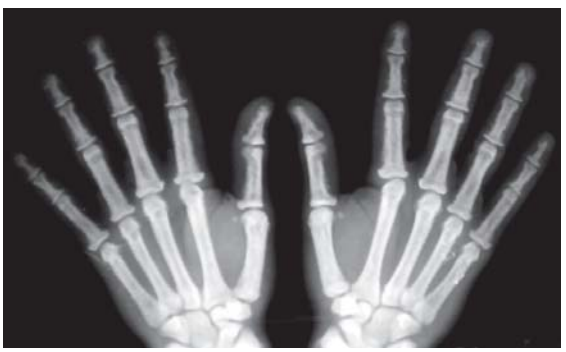

Fig. 16.14: Radiographs of hands in a patient of hyperparathyroidism in renal osteotrophy: Characteristic subperiosteal resorption phalanges including terminal tufts is seen. Subchondral and intracortical resportion is also seen

REFERENCES

1. P L Choyke, Zeiessman H A. Imaging of renal failure. In: Pollack HM, McClennan BL, ed. Clinical Urography, 2nd Ed. Philadelphia, Pa: WB Saunders, 2000;3:3029-31.
2. National Kidney Foundation: K/DOQ1. Clinical practice guidelines for chronic kidney diseases: Evaluation, classification, stratification. Am J Kidney Disease 2002;1:39.
3. Friedenberg RM, Dunbar JS. Excretory urography. In: Pollack HM, McClennan BL, ed, Clinical Urography, 1st ed, Philadelphia, Pa: WB Saunders, 1990,2264-76,100-245.
4. Davidson AJ, Hartman DS. A systemic approach to Radiological Diagnosis of Renal Parenchymal Disease. In: Davidson AJ, Hartman DS, eds. Radiology of Kidney and Urinary Tract, 2nd ed, Philadelphia, Pa: WB Saunders, 1990;1:101-243.
5. Kim SH, Kim B, Renal Parenchymal Disease. In: Pollack HM, McClennan BL, ed, Clinical Urography,2nd ed , Philadelphia, Pa: WB Saunders, 2000;3:2654-84.

6. Fry IK, Cattell WR. The nephrographic pattern during excretion urography.Br Med Bull 1972;28:227-32.
7. Ritche WW, Vick CW, Glocheski SK, Cook DE. Evaluation of azotemic patients: Diagnostic yield of initial US examination. Radiology 1998; 167:245-47.
8. Hungtington DK, Hill SC, Hill MC. Sonographic manifestations of medical renal disease. Semin Ultrasound CT MR 1991;12:290-307.
9. Manley JA, O'Neill C. How echogenic is echogenic? Quantitative acoustics of the renal cortex. Am J Kidney Dis 2001; 37:706-11.
10. Yasa NA, Peng M, Ralls PW. Perirenal lucency ('Kidney sweat'): A new sign of renal failure. AJR 1999;173:1075-79.
11. Platt JF, Ellis JH, Rubin JM, et al. Intrarenal arterial Doppler sonography in patients with non-obstructive renal disease: Correlation of resistive index with biopsy findings. AJR 1990;157:1223-27.
12. Saunder HS, Dyer BB, Shifrin RY, et al. The CT nephrogram: Implications of evaluation of urinary tract disease. Radiographics 1995;15: 1069-95.
13. Chung JJ, Semelka RC, Martin DR. Acute renal failure: Common occurrences of preservation of corticomedullary differentiation on MR images. Magn Reson Imaging 2001; 19:789-93.
14. Thoeny HC, Keyzer FD, Oyen RH, Peeters RR. Diffusion-weighted MR Imaging of Kidneys in Healthy Volunteers and Patients with Parenchymal Diseases: Initial Experience. *Radiology* 2005;235:911-17.
15. Ledneva E, Karie S, Launay – Vacher V, Janus N, Deray G. Renal Safety of Gadolinium Based Contrast Media in Patients with Chronic Renal Insufficiency. 2009;250:618-28.
16. Abrams HA, Grassi CJ. Renal angiography in hypertension. In: Baums (Ed). Abrams Angiography: Vascular and Interventional Radiology 4th ed. Boston, Little Brown. 1997;1244-89.
17. Maisey M, Briton KE. Nuclear Imaging in Nephrology. In, Davidson AM, Cameron JS, Grunfeld JP, et al. In: Oxford textbook of clinical nephrology. 2nd edn. Oxford, Oxford University press.1998;137-50.
18. Tublin ME, Murphy ME, Tessler FN. Current concepts in contrast media induced nephropathy. AJR 1998;171:933-39.
19. Barrett BJ, Cariske EJ. Metanalysis of relative nephrotoxicity of high and low osmolality Iodinated Contrast Media Radiology. 1993; 188:171-78.
20. Dunnick RN, Sandler CM, Newhouse JH, et al. Renal failure and medical renal disease, In: Textbook of Uroradiology. Lippincott Williams and Wilkins.2001;230-41.
21. Davidson A. Acute Renal Parenchymal Disease. In: Pollack HM, McClennan BL, edn, Clinical Urography, 1st ed, Philadelphia, Pa: WB Saunders, 1990,2264-76.
22. Rosenfeld AT, Zeman RK, Cicchetti DV, et al. Experimental acute tubular necrosis: US appearance Radiology 1985;157:771.
23. Platt JH, Rubin JH, Ellis JH. Acute renal failure: Possible Role of Duplex Doppler US in Distinction between Acute Pre-renal Failure and acute tubular necrosis. Radiology 1991;179:419.
24. Han F, Xiao W, Xu Y, et al. The significance of BOLD MRI in differentiation between renal transplant rejection and acute tubular necrosis. Nephrology Dialysis Transplantation 2008;23: 2666-72.
25. Gormsen H, Iverson P, Raaschou I. Kidney biopsy in acute anuria: with case of acute, bilateral cortical necrosis. Am. J .Med 1955;19: 209-11.
26. Jordan J, Low R, Jeffrey RB Jr. CT findings in acute renal cortical necrosis. J Comput Assist Tomogr 1990;14:155-56.
27. Wang MT, Wu RH, Chen JC. CT Findings of Acute Renal Cortical Necrosis. Chin J Radiol 2007;32:103-06.
28. Hnn L, Pfister RC. Renal subcapsular rim sign: New etiologies and pathologenesis. AJR 1982;138:51-54.
29. Jeong JY, Kim SH, Lee HJ, Sim JS. Atypical Low - Signal - Intensity Renal Parenchyma: Causes and Patterns. Radiographics. 2002;22:833-46.
30. Ten RM, Torres VE, Milliner DS, et al. Acute interstitial nephritis: immunologic and clinical aspects. Mayo clin Proc 1988;63:921.
31. Davidson AJ, Hartman DS. Diagnostic set: Large smooth, bilateral. In Davidson AJ, Hartman DS eds, Radiology of Kidney and Urinary Tract, 2nd ed, Philadelphia, Pa: WB Saunders, 1990; 157-186.
32. Sipe JD, Cohen AS. Amyloidosis. In: Fauci AS, Braunwald E, Isselbacher KJ, et al. (Eds)

Harrison's principle of internal medicine. New York, McGraw-Hill, 1998;1856-60.
33. Cohen AS: Amyloidosis. In: Pertersdrof RG, Adams RD, Braunwald E, et al. (Eds), Harrison's principle of internal medicine. NewYork, McGraw-Hill, 1983;368-71.
34. Amendola RA. Amyloidosis of the urinary tract. In Pollack HM, ed, Clinical urography: An atlas and textbook of urologic imaging, Philadelphia, Pa : WB Saunders 1990;2493-2500.
35. Kim SH, Han MC, Lee JS, Kim SP. Paroxysmal nocturnal hemoglobinuria: Case report of MRI and CT findings. Acta Radiol 1991;32:315-16.
36. Jung DC, Kim SH, Jung S, Hwang S, Kim SH. Renal Papillary Necrosis: Review and Comparison of Findings at Multi–Detector Row CT and Intravenous Urography. Radiographics 2006;26:1827-36.
37. Davidson A. Chronic renal failure. In: Pollack HM, McClennan BL, ed, Clinical Urography, 1st ed, Philadelphia, Pa: WB Saunders, 1990; 2279-90.
38. Chuang VP, Reuters SR. Angiographic features of Alport's syndrome: Hereditary nephritis .AJR 1974;121:539-43.
39. Davidson AJ, Hartman DS. Diagnostic set: Small, Smooth, bilateral . In Davidson AJ, Hartman DS eds, Radiology of Kidney and Urinary Tract, 2nd ed, Philadelphia, Pa: WB. Saunders, 1990; 135-86.
40. Ono H, Ono Y. Nephrosclerosis and hypertension. Medical Clinics of North America. 1997;6:81.
41. Murphey MD, Sartoris D, Quale JL, Minim N, et al. Musculoskeletal manifestations of chronic renal insufficiency. Radiographics 1993;13: 357-79.

Chapter

17

Renal Transplant

Ajay Gulati, Manavjit Sandhu

INTRODUCTION

Renal transplantation as a treatment of choice, is well-established for patients with end stage renal disease (ESRD) and leads to recovery of the normal renal function, cure of the uremic syndrome, and full rehabilitation from the renal disease. This has been made possible by improved surgical techniques, development of effective immunosuppressive medications, and better donor-recipient matching.

Renal function impairment of the transplant kidney can be secondary to parenchymal abnormality or due to surgical complications. Depending upon the clinical findings appropriate diagnostic studies are carried out. Renal biopsy remains the definitive way to diagnose the parenchymal abnormalities.

TECHNIQUE

The transplanted kidney is usually placed extraperitoneally in patient's right iliac fossa with the pelvis lying anteriorly. In cadaveric renal transplants an aortic patch (Carrel patch) is commonly removed with main renal artery. With live donors, only the main renal artery is harvested and anastomosed commonly in end to side manner with recipient's external iliac artery. The donor renal vein is always anastomosed end-to-side with external iliac vein. The current preferred method of re-establishing continuity of urinary tract is by creation of ureteroneocystostomy (commonly by using a submucosal tunnel to decrease the incidence of vesicoureteric reflux).[1,2]

Post-transplantation complications are characterized as either early or late. Early complications appear in the first few weeks and are generally due to surgical difficulties. Late complications appear some weeks later and are normally due to medical problems (usually due to immunosuppression or due to drug toxicity).

Early complications include acute rejection, acute tubular necrosis, hematoma, pyelonephritis, abscess, urinoma, acute ureteral obstruction and vascular complications. Late complications include chronic rejection, lymphocele, cyst formation, malignancies and opportunistic infections of transplant kidney.[3]

The greatest risk in the early post-transplant period is of early graft failure which presents with oliguria. To diagnose this early, there is a routine policy of clinical surveillance complimented with laboratory tests and imaging.[4]

COMPLICATIONS

Various complications of the renal transplant are as follows:

Acute Tubular Necrosis (ATN)

Acute tubular necrosis (ATN) occurs due to renal ischemia and presents with anuria immediately or within first few days after an initial diuresis. The patients remain constitutionally well and urine Na^+ is high. It is usually self-limiting with renal function returning to normal within few days to weeks. It is almost exclusively seen in cadaveric transplants.[4]

Rejection

Acute rejection remains one of the most serious and common complications. Virtually every patient experiences some degree of rejection and differentiating rejection from other causes of graft dysfunction remains a challenging clinical problem.

Clinically, there are three distinct types of rejection: (i) Hyperacute, (ii) Acute (iii) Chronic. Hyperacute rejection (due to circulating antibodies) usually occurs within hours to one or two days after the transplantation. It is characterized by the presence of fibrin thrombi in small arteries with cortical necrosis. The treatment is only the graft removal.

Acute rejection (mediated through CMI) is seen most frequently in first one to three weeks. It is characterized clinically by oliguria with systemic symptoms like pyrexia, hypertension, graft tenderness and swelling. The urine Na^+ is usually low (c.f, ATN in which urine Na^+ is high). If diagnosed early it may be reversed by steroids or by antibody therapy.[4]

Chronic rejection manifests as slow deterioration in renal function over a period of weeks or months. It does not respond to increased immunosuppressive therapy. Removal of the graft is required in majority of the patients.

Renal Artery Thrombosis

Renal artery thrombosis is a rare complication and results in loss of the graft. It is due to hyperacute or acute rejection and improper vascular anastomosis.

Renal Artery Stenosis

Renal artery stenosis is a well-recognized complication occurring in 3 to 12 percent of the transplants. It presents clinically as hypertension with or without deterioration of the renal function. Percutaneous transluminal angioplasty is the preferred mode of therapy with surgical correction reserved for the patients with unsuccessful angioplasty.

Pseudoaneurysm

Pseudoaneurysm is an uncommon complication which may present as hypertension because of the compression of the renal artery by the aneurysm.

Renal Vein Thrombosis

Renal vein thrombosis is rare, but may by due to twisting or kinking at the time of surgery or secondary to thrombosis of the iliac veins.

Arteriovenous Fistula

Arteriovenous fistula (AVF) occurs most commonly after percutaneous needle biopsy. Most small fistulae close spontaneously, while large fistulae may require embolization or nephrectomy.

Peritransplant Fluid Collections

In the early postoperative period, the fluid collections around transplant kidney are

hematoma, abscess or urinoma. Lymphocele generally occurs later (4-8 weeks after surgery).[5] Ultrasound-guided percutaneous aspiration can provide the definitive diagnosis.

Urinary Complications

These include urinary leak, obstruction, vesicoureteral reflux and nephrolithiasis. Urinary leak is the most frequent urinary complication in early postoperative period. This commonly occurs at the level of ureterovesical anastomosis secondary to ischemia of the distal ureter.

Urinary obstruction is commonly due to ureteric stricture in the distal one-third. It can also occur due to blood clot within the ureter or extrinsic compression by lymphoceles. The hydronephrosis can be due to obstruction or VUR. If RI > 0.5, then hydronephrosis is generally due to obstructive causes.

Reflux is an important cause of recurrent urinary tract infections and makes the transplant at increased risk of pyelonephritis.

Calculi formation is a late complication of renal transplantation. It may occur de novo or as a result of hypercalcemia, hyperparathyroidism, steroid therapy, chronic infection, etc.[6-8]

Malignancy

Immunosuppressive therapy places the transplant recipient at 100 times the normal risk for developing cancers particularly of the skin, cervix, rectum, Kaposi's sarcoma and lymphoma.[6,7]

Post-transplantation lymphoproliferative disorder (PTLD), a potentially malignant process, is a complication that is associated with Epstein-Barr virus and occurs in approximately 1 percent of allograft recipients. The most common radiological feature is diffuse lymphadenopathy. In addition single or multiple extranodal masses can involve the liver, spleen, lung, CNS and GIT. It can even affect the graft itself with predilection for the renal hilum.[3,8,9]

Renal cell carcinoma also shows increased prevalence in transplant recipients with 90 percent occurring in the native kidneys and 10 percent in the transplant kidney.[8]

IMAGING TECHNIQUES

Impaired renal allograft function during the post-transplant period warrants an immediate and thorough evaluation to distinguish between the parenchymal and surgical complications.

The various imaging techniques and their indications are as follows:

Radiography

Plain Radiography

Plain radiographs are useful in demonstrating radiopaque calculi and gas in the renal parenchyma and collecting system in rare cases of emphysematous pyelonephritis.

Intravenous Urography

Intravenous urography was a useful study when ureteral obstruction or extravasation was suspected in a transplant recipient with adequate renal function. Presently it is not indicated due to the availability of ultrasonography and radionuclide imaging.

Cystography

Cystography is indicated to rule out vesicoureteral reflux in patients with persistent or recurrent urinary tract infection.

Radionucleotide Imaging (RIA)

RIA is the most useful modality for assessing the renal function both qualitatively and

quantitatively while screening for common complications. Obtaining a baseline scan in the immediate postoperative period is extremely important.[5] Serial radionuclide scans allow early detection of rejection and can be used to monitor the recovery from ATN. The commonest technique used is dynamic renal imaging using ^{99}Tc DTPA.[1]

Ultrasonography (US)

Sonography is a simple, inexpensive and readily available imaging modality that has become an essential component of the management of renal transplantation. High frequency transducers (5 MHz or higher) provide excellent details of the transplant kidney because of the superficial location. Several sonographic findings are seen in patients with graft dysfunction including enlargement of kidney, poor corticomedullary differentiation, reduced amplitude of sinus echoes and enlarged pyramids. Real time ultrasonography combined with duplex doppler or color and power flow imaging techniques is the most frequently used examination to evaluate worsening renal function in the post-transplantation period. Color Doppler is used to assess patency of vessels and detect any focal area of color aliasing which would indicate focal stenosis. Studies have shown that power Doppler sonography is superior to duplex Doppler sonography in screening patients with acute rejection. On spectral analysis, peak systolic velocity (PSV), acceleration time (AT), pulsatility index (PI) and resistive index (RI) are assessed. The upper limit of normal PSV in renal artery is 200-250 cm/s. The RI is considered to be normal if it is less than 0.7, indeterminate between 0.7 and 0.8 and elevated, if greater than 0.8 (Figs 17.1A to 17.2C).

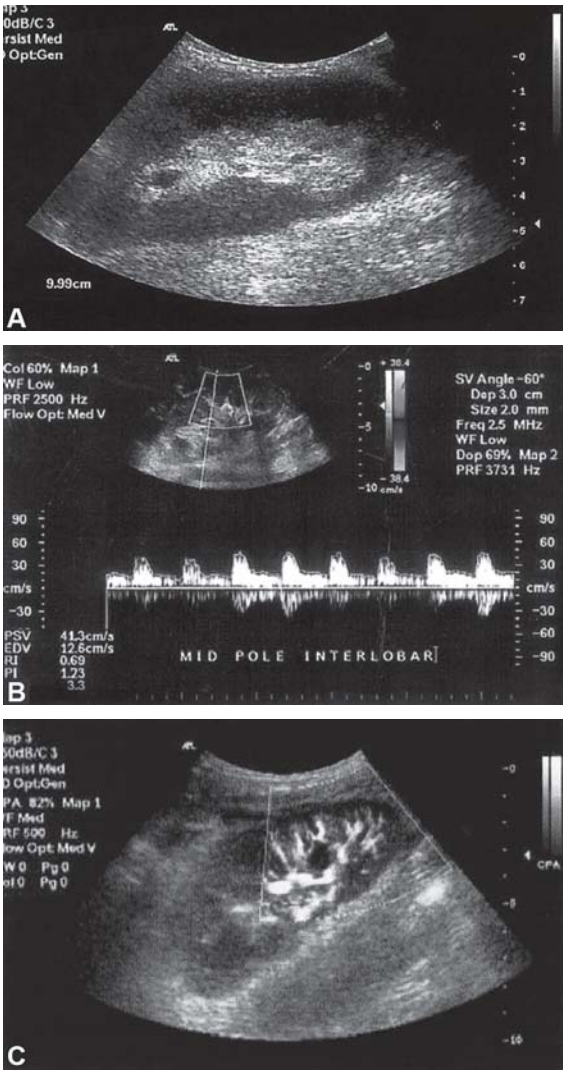

Figs 17.1A to C: USG and Doppler images of the normal transplant kidney: **(A)** Gray scale sonogram showing normal size, outline, echogenicity, corticomedullary differentiation and pelvicalyceal system. **(B)** Duplex Doppler from interlobar artery shows normal low resistance flow with RI of 0.69 (< 0.8) and PI of 1.23 (< 1.5). **(C)** Power Doppler image shows normal cortical perfusion showing reaching upto the periphery of the renal cortex *(For color version of Figs 17.1B and C see Plate 18)*

US also easily detects hydronephrosis and perinephric fluid collections (Figs 17.3A to C and 17.4). Minimal dilatation of the collecting

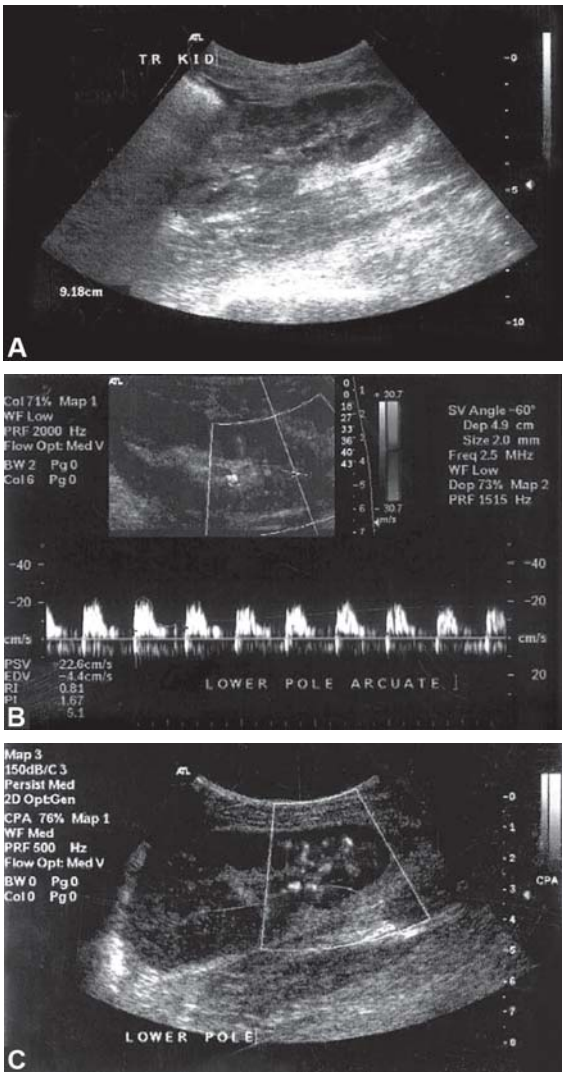

Figs 17.2A to C: USG and Doppler images of the transplant kidney with acute rejection (confirmed on renal biopsy) : **(A)** Gray scale sonogram shows normal renal length and echogenicity with indistinct CMD and reduced renal sinus echoes. **(B)** Duplex Doppler from interlobar artery shows raised RI of 0.81and PI of 1.67. **(C)** Power Doppler image shows reduced cortical perfusion *(For color version of Figs 17.2B and C see Plate 19)*

system in the immediate postoperative period is acceptable and is usually due to edema at the ureteroneocystostomy site. Hydronephrosis may be secondary to the ureteral

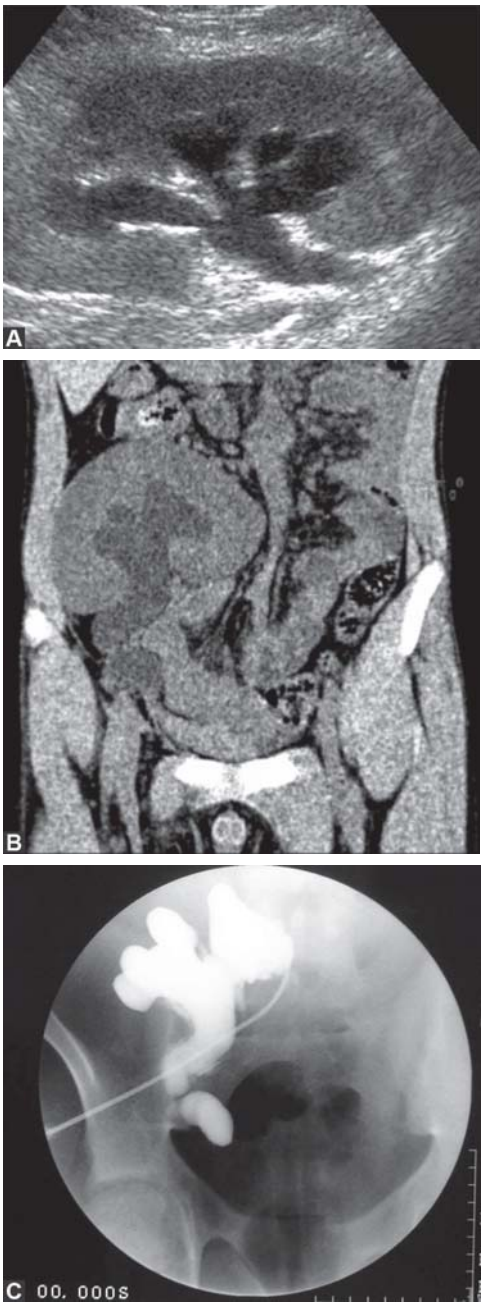

Figs 17.3A to C: Hydroureteronephrosis with ureteric stricture: **(A)** US image of the renal transplant shows moderate hydronephrosis. **(B)** Coronal reformatted CT image shows hydroureteronephrosis with ureteric stricture. **(C)** Antegrade urogram shows hydroureteronephrosis with ureteric stricture

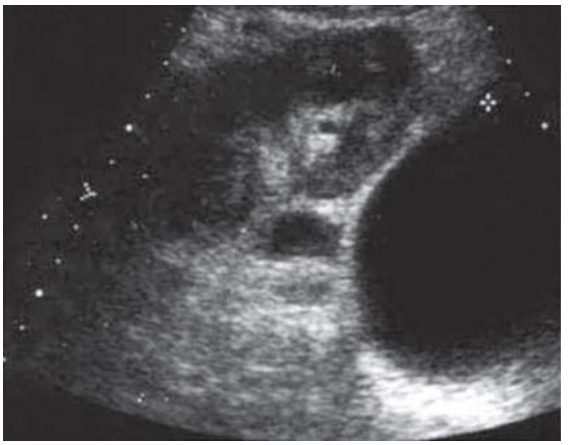

Fig. 17.4: Urinoma: Saggital US image shows a large anechoic fluid collection seen posterior to the kidney. Note the dilatation of the ureter is attributable to the compression by the urinoma

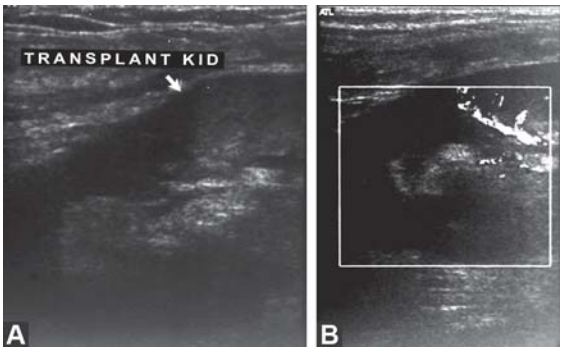

Figs 17.5A and B: Renal Infarction: **(A)** US images shows well demarcated hypodensity involving the renal parenchyma. **(B)** Power Doppler shows absence of flow in the involved renal parenchyma

stricture or peritransplant fluid collections. Ultrasonography is sensitive for detection of the peritransplant fluid collections but it is not specific for fluid type, and aspiration of the fluid collection with ultrasound guidance is helpful in the management. US guidance minimizes the risk and discomfort of the percutaneous renal transplant biopsy. Vascular complications of transplantation, i.e. infarction, arteriovenous fistulae, pseudoaneurysms, arterial or venous thrombosis, and stenosis are readily identified by color and Duplex Doppler sonography.[8,10-12] (Figs 17.5A and B).

A new technique for the quantification of vascularity based on the analysis of color Doppler images is described.[13] In this technique the velocity information obtained directly from cineloops is transferred to a computer for off-line analysis. This methodology is used in transplanted kidneys to assess parenchymal vascularity on the basis of percentage color pixel density and mean flow velocity in midkidney cross-sectional regions of interest and the distance from the most peripheral color pixels to the capsule of the kidney. In normally functioning transplants, the mean maximum color pixel density was 34.7+/– 13.4 percent, the mean flow velocity was 5.2 +/– 0.9 cm/second, and the mean distance to the capsule was 3.3 +/–1.1 mm. This technique can reliably detect allograft nephropathies.[13]

Computed Tomography (CT)

Helical CT is an accurate, noninvasive technique which can depict parenchymal, perirenal, renal sinus, pyeloureteral and vascular diseases in renal transplant in great detail (Figs 17.6A to F). It helps to differentiate acute rejection from obstructive uropathy, urinary fistula, perinephric fluid collections, mass lesions, etc. Dynamic CT has been used in the evaluation of physiological status of the renal transplants. It often delineates fluid collections and their anatomic relationship to adjacent structures better than USG. It can also distinguish the nature of fluid collections (Fig. 17.7). Fresh blood in the form of hematoma has the highest attenuation value (55 – 66 HU), lymphoceles are between 10 to 20 HU, and the abscesses between 20 to 30 HU. In addition, drainage can be performed with CT guidance when

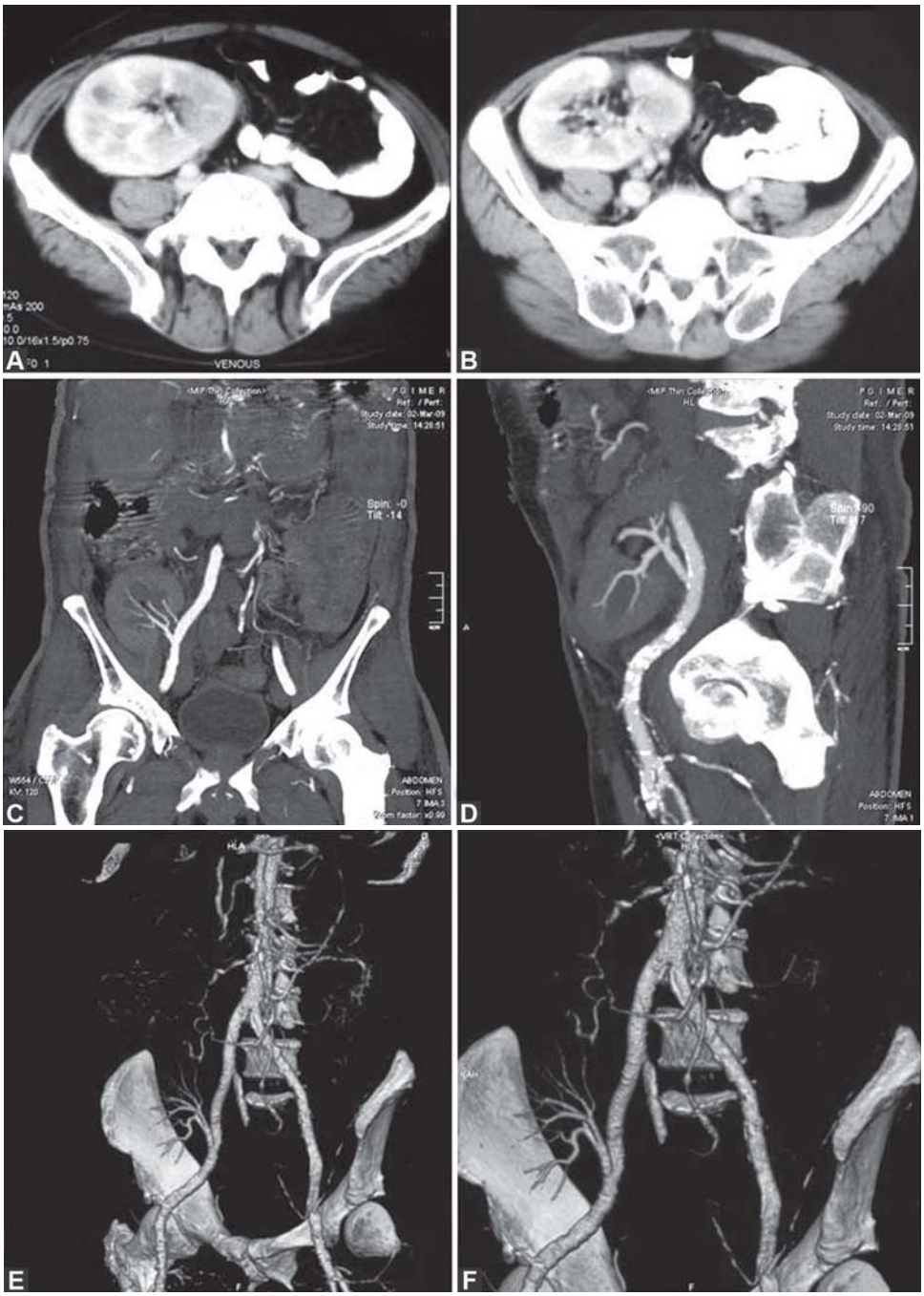

Figs 17.6A to F: Normal transplant kidney: **(A and B)** Contrast-enhanced venous phase show uniformly enhanced parenchyma of the transplant kidney. Note made of a simple cyst. **(C and D)** Vascular MIP reformatted images depict the transplant renal artery anastomosed to the external iliac artery. **(E and F)** Volume rendered images show the end to side anastomoses of the graft artery and the external iliac artery *(For color version of Figs 17.6E and F see Plate 19)*

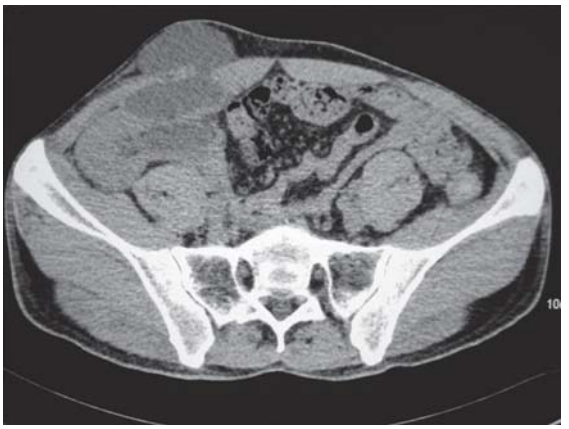

Fig. 17.7: Urinoma: NCCT KUB shows hydronephrosis with perinephric urinoma extending into the anterior abdominal wall

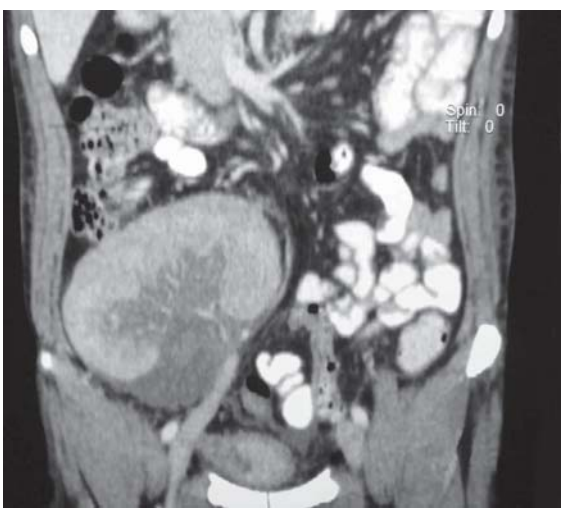

Fig. 17.8: PTLD involving renal transplant: Coronal reformatted CT image shows infiltrating mass in the renal hilum surrounding the graft pedicle

USG cannot clearly define the relationship to the bowel (Figs 17.8 to 17.11). In assessing the complex problems such as detection of malignancy or sites of infection or sepsis, CT is the most useful modality. CT angiography with 3D reformatted images allows accurate imaging of the vascular diseases such as stenosis, thrombosis, pseudo aneurysms and arteriovenous fistulae when US studies are inconclusive.

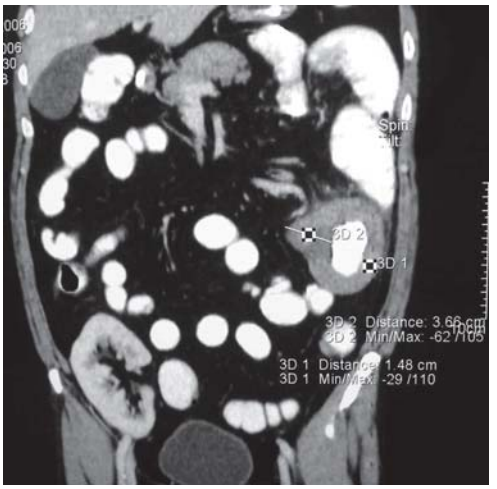

Fig. 17.9: Post-transplantation lymphoma: Coronal reformatted CT image shows homogeneous circumferential mural thickening involving the jejunum

Magnetic Resonance Imaging (MRI)

MR Imaging allows rapid global assessment of the renal transplant arterial system, renal parenchyma and peritransplant region. It can also detect or exclude various of the causes of renal transplant failure (e.g. stenosis or occlusion of transplant vessels, peritransplant fluid collections and ureteral obstruction).[14]

From the renal safety perspective, the lack of nephrotoxicity seen with the currently available gadolinium contrast media makes MR imaging a very useful and attractive alterative for evaluating renal transplant patients.[15]

A dynamic MR performed with 3D fat saturated gradient echo T1-weighted sequence provides adequate information regarding the vessels and functional status of the transplant. HASTE T2-weighted acquisition also provides rapid assessment of the anatomy along with the detection of hydronephrosis, perirenal collections and malignancy, if present (Figs 17.12A and B).

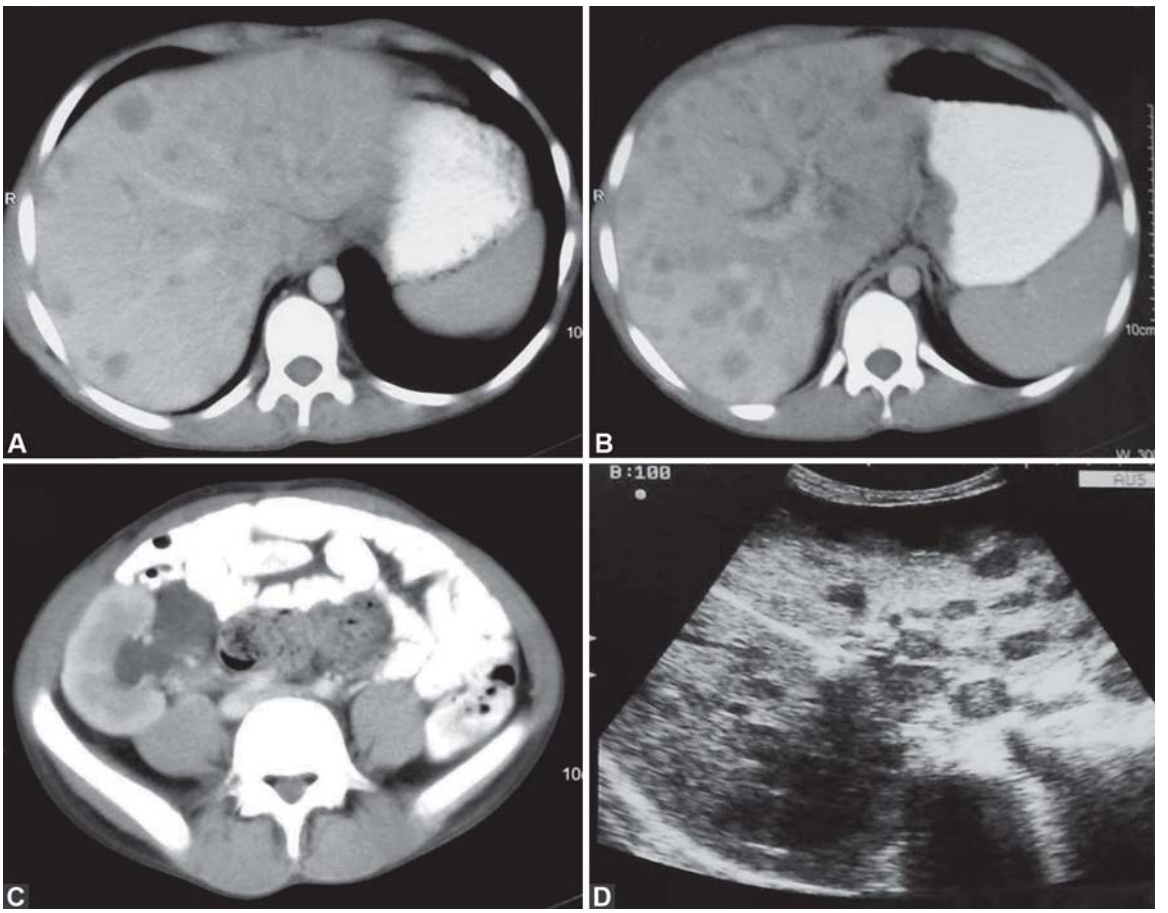

Figs 17.10A to D: Hepatic PTLD: **(A and B)** Contrast-enhanced CT scan shows multiple hypodense lesions involving both the lobes **(C)** CT scan at lower level shows hydronephrosis in renal transplant secondary to narrowing at ureterovesical anastomoses. **(D)** US image shows multiple well-defined hypoechoic lesions in the liver parenchyma

The role of MRI in renal transplant dysfunction is rapidly evolving. Decreased or absent CMD on T1-weighted images is seen in majority of patients with acute rejection. However, this finding is not specific and can also be seen in allograft infection, cyclosporine toxicity and infiltrative or diffuse parenchymal diseases. On dynamic Gd-enhanced imaging, there is a blunted uprise and delayed peak in the cortical signal intensity curves. The medulla also show decreased enhancement in acute rejection.[15]

Preliminary reports indicate that phosphorus 31 MR spectroscopy may be useful in differentiating the rejection from other causes of the renal transplant failure. The use of MR spectroscopy for evaluating the phosphorus metabolism of allografts is still under development and has been reported to be useful. The long-term assessment of post-transplant renal prognosis with ^{31}P magnetic resonance spectroscopy has been recently evaluated and a beta-adenosine triphosphate/inorganic phosphate (beta-ATP/Pi)

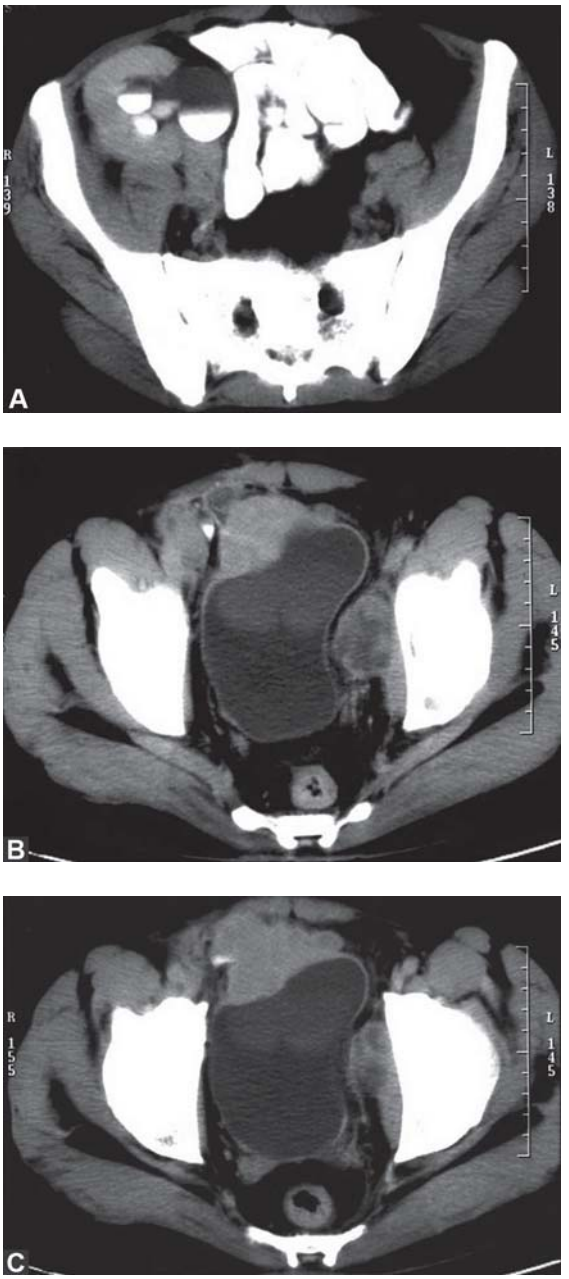

Figs 17.11A to C: Lymphoma in renal allograft recipient involving ureterovesical anastomoses:**(A)**Contrast-enhanced CT scan demonstrates hydroureteronephrosis. **(B and C)** Contrast-enhanced scans obtained at lower levels shows homogeneous soft tissue mass lesion at the ureterovesical anastomoses

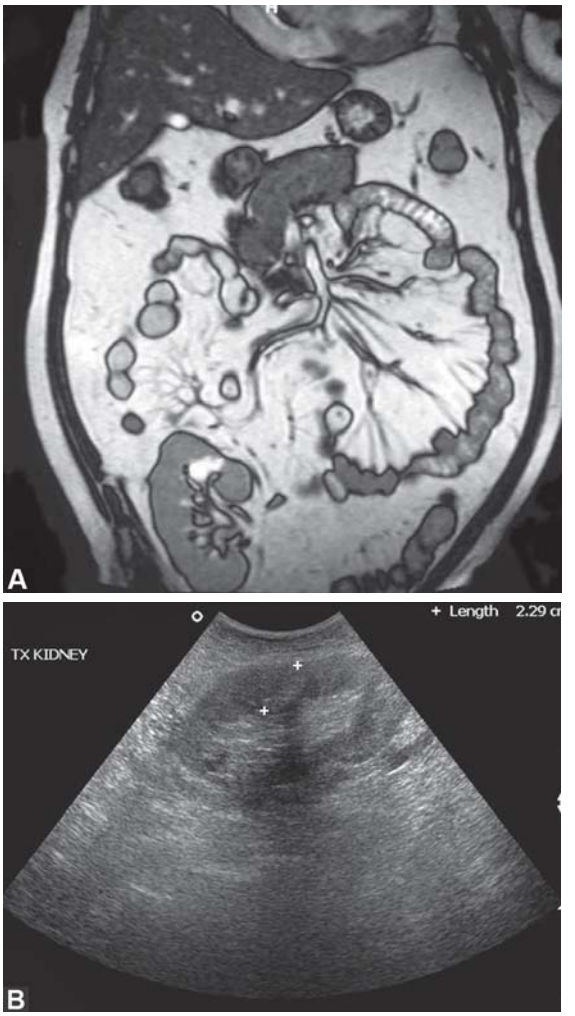

Figs 17.12A and B: Renal cell carcinoma in a renal graft: **(A)** Coronal MR T2WI shows focal hyperintense lesion in the transplant kidney. **(B)** US image shows the lesion is iso- to-hypoechoic to the renal parenchyma

ratio above 1.2 suggests a high probability of 3-year renal survival, whereas a value over 2.5 indicates that the transplanted kidney could survive over 5 years.[16]

MR is an excellent modality for screening of renal artery stenosis and other vascular complications (Fig. 17.13). MR angiographic examination can help in avoiding unnecessary catheter angiographies in majority of cases.

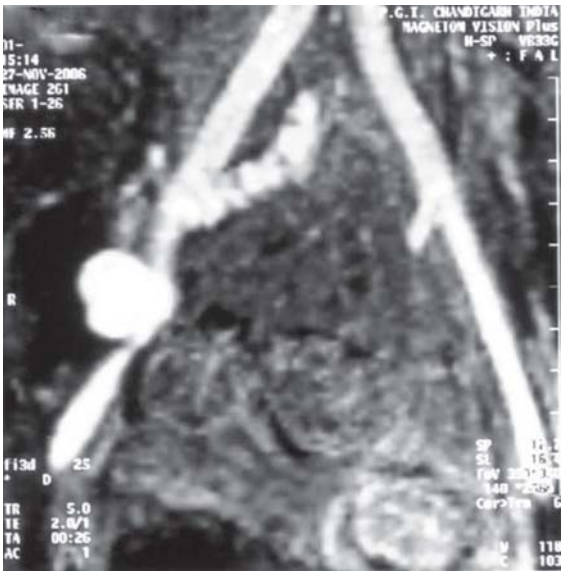

Fig. 17.13: Pseudoaneurysm: MIP reformatted MR angiogram depicts stenosis involving the external iliac artery with a pseudoaneurysm at the anastomotic site

Angiography

Some important indications of renal transplant angiography are acute anuria, hypertension not responding to medication and functional deterioration of the allograft, in which confirmatory evidence of rejection or renal artery stenosis is necessary in order to proceed with the definitive surgery.[17,18] In acute rejection, there is a pruned-tree appearance secondary to the loss of second and third order branches. The arteriogram is essentially normal in acute tubular necrosis. In chronic rejection, arteriography demonstrates small graft size with irregularity, attenuation and occlusion of interlobar arteries and a patchy nephrogram secondary to the areas of cortical infarction.

Angiography is indicated in patients with hypertension not responding to the medical therapy. Angiography in such situation may demonstrate degree of renal artery stenosis. Percutaneous transluminal angioplasty can also be attempted to correct the arterial stenosis.

Transcatheter embolization is the treatment of choice for both symptomatic AVF's and enlarging pseudoaneurysms. Superselective embolization performed with metallic coils minimizes the loss of functioning allograft tissue (Figs 17.14A to C). It allows the occlusion of targeted vessels in a precise and definitive manner, unlike embolization with particles that may reflux into nontargeted branches. Surgery is the treatment of last resort, with partial or total nephrectomy being the two options.

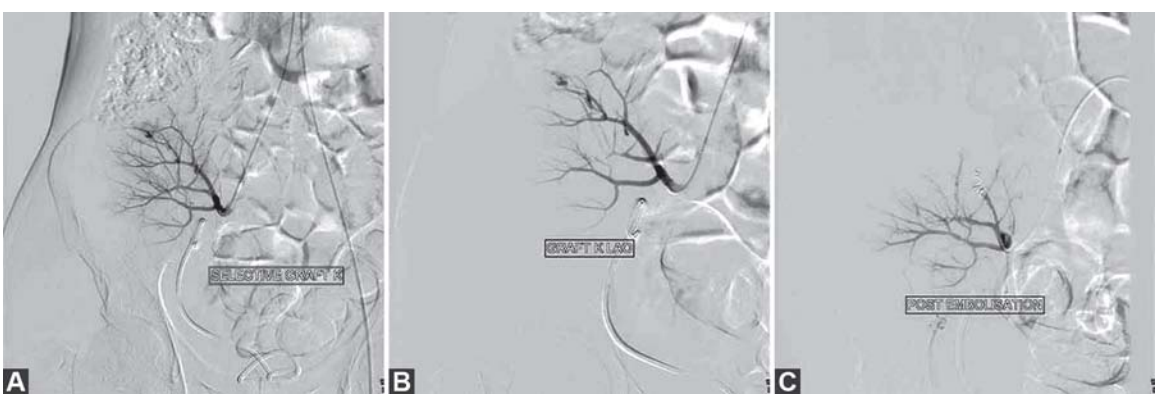

Figs 17.14A to C: Transcatheter embolization of pseudoaneurysm: **(A and B)** Angiogram of transplant renal artery (AP and LAO projection) show a pseudoaneurysm in upper segmental artery. **(C)** Angiogram obtained after coil embolization shows successful obliteration of the aneurysm with preservation of the flow in the rest of the renal parenchyma

Percutaneous Interventional Techniques

Percutaneous interventional radiological techniques play an important role in management of the renal transplant patient and the timely use of these techniques may obviate surgery in some cases.

Antegrade pyelography is the most accurate and informative examination for the demonstration of ureteral stricture as well as the site of ureteral leak (Refer Fig. 17.3C). Nephrostomy drainage catheter is placed in patients with urine leak and ureteral obstruction. Ureteral strictures can be dilated percutaneously by using angioplasty catheter, and indwelling ureteral stents left in place. Renal stone extraction through a percutaneous nephrostomy in a renal transplant patient can also be successfully accomplished.

ACKNOWLEDGMENTS

Sincere thanks to Dr Anupam Lal and Dr Manphool Singhal for contributing to the images of the chapter.

REFERENCES

1. Rankin S. Renal parenchymal disease, including renal failure, renovascular disease (Ed) and transplantation in Grainger RG. Allison DJ (Ed). Diagnostic Radiology (5th edn): Churchill Livingstone (I): 851-55.
2. Oliver JH. Clinical indications, recipient evaluation, surgical considerations, and the role of CT and MR in renal transplantation. Radiol Clin N Am 1995;33:435-44.
3. Sebastria C, Quiroga S, Boye R, Cantarell C, et al. Helical CT in renal transplantation: Normal findings and early and late complications. Radiographics 2001;21:1103-17.
4. Kabala JE, Roobottom C. The kidneys and ureters. Sutton D (Ed). Textbook of Radiology and Imaging (7th edn). Churchill Living Stone (II):982-86.
5. Brown ED, Chen YM, Wolfman NT, Ott DJ, et al. Complication of renal transplantation: Evaluation with US and Radionuclide Imaging Radiographics 2000;20:607-22.
6. Akbar SA, Jafri ZH, Amendola MA, Madrazp BL, et al. Complications of renal transplantation. Radiographics 2005;25:1335-56.
7. Kumar R, Wilson DD, Santa Cruz FR. Postoperative urological complications of renal transplantation. Radiographics 1984;(4)3:531-47.
8. Langer JE, Jones LP, et al. Sonographic Evaluation of the renal transplant. Ultrasound Clin 2007;2:73-88.
9. Sandhu MS, Kalra N, Sidhu R. Post-transplant lymphoproliferative disorder (PTLD) localised near the allograft mimicking a collection. Indian J of Radiol and Imaging 2002;12:132-33.
10. O'neill WC, Baumgarten DA. Ultrasonography in renal transplantation. Am J Kidney Diseases 2002;39:663-78.
11. Tublin ME, Dodd GD. Sonography of renal transplantation. Radiol Clin N Am 1995;33: 447-59.
12. Datta R, Sandhu M, Saxena AK, Sud K, et al. Role of duplex Doppler and power Doppler sonography with acute renal parenchymal dysfunction. Australasian Radiology 2005;49: 15-20.
13. Gruenewald S, Skerrett D, Dolimier D, et al. Technique of Colour Doppler quantification of vascularity in transplanted kidneys. J Clin Ultrasound 2002;30:151-57.
14. Hohenwalter MD, Skowlund CJ, Erickson SJ, Hariharan S, et al. Renal Transplant evaluation with MR angiography and MR Imaging. Radiographics 2001;21:1505-17.
15. Pedrosa I, Rofsky NM, Kidneys. Clinical Magnetic Resonance Imaging. Edelman RR, Hesselink JR, Zlatkin MB, Crues JV (3rd edn). Saunders (III);2851-52.
16. Seto K, Ikechira H, Obata T, et al. Long-term assessment of post transplant renal prognosis with 31P magnetic resonance spectroscopy. Transplantation 2001;72:627-30.
17. Orons PD, Zajko AB. Angiography and interventional aspects of renal transplantation. Radiol Clin N Am 1995;33:461-71.
18. Kobayashi K, Censullo ML, Rossman LL, Kyriakides PN, et al. Interventional Radiologic Management of Renal Transplant Dysfunction:Indications, limitations, and technical considerations. Radiographics 2007;27:1109-30.

Chapter

18

Imaging of Obstructive Uropathy and Diseases of Ureter

Mahesh Prakash, Mandeep Kang

INTRODUCTION

Obstructive uropathy is a general term that describes obstructive changes in any part of the urinary tract. The renal structural and functional alterations caused by obstruction are termed as obstructive nephropathy.[1] Despite remarkable advances in diagnosis and treatment, obstruction remains a leading cause of damage to the urinary tract. Urinary obstruction affects patients of all ages and is responsible for thousands of hospital admissions and surgical procedures. Obstruction predisposes to urinary tract infection and renal failure. Early diagnosis and treatment of urinary obstruction can reverse the renal damage.

PATHOPHYSIOLOGY

When the ureter is acutely obstructed, the pressure of the collecting system proximal to the obstruction rises. Initially the renal blood flow (RBF) rises transiently, but over the next 6-12 hours, the RBF drops upto 30 percent due to increase of renal vascular resistance.[2] There are two mechanisms that come into play to temporarily decompress the nephron. First is pyelosinus and pyelovenous backflow and second is enhanced absorption of fluid from the tubules. Both mechanisms are responsible for continuing but reduced glomerular filtration. There is sufficient evidence to show that preglomerular arteriolar resistance develops in acute obstruction. This resistive index measure by doppler has been used with variable success to confirm intra-renal vascular resistance in acute obstruction.[3,4] The elevated intrarenal resistance produces diminished diastolic flow eventually causing ischemia. The elevated intrarenal pressure also causes mechanical atrophy of tubules. After several days of total ureteric obstruction, less glomerular filtrate is produced so the intrapelvic pressure begins to fall. In 6-8 weeks time, the intrapelvic pressure returns to normal or subnormal levels however the glomerular filtration rate (GFR) is severely compromised.[1]

Relief of total but short lived obstruction leads to full restoration of the GFR. Longer period of total obstruction causes progressive nephron loss called obstructive atrophy.[2] Relief of obstruction that has already caused renal atrophy is followed by improvement in renal function but not to normal levels. The kidney often shrinks in size with blunting of the calyces and impaired ability of urinary concentration and acidification.[2]

These semi-recovered kidneys showing the anatomical and functional sequelae are said to exhibit postobstructive atrophy.

If the obstruction is partial and chronic, its effect to renal function is less predictable. Structural changes can occur in the medulla with impairment of the ability to concentrate urine. Sometimes partial obstruction can exist for years without causing any functional impairment.

IMAGING OF ACUTE OBSTRUCTION

Intravenous Urography (IVU), ultrasound (US), nuclear studies and Computed Tomography (CT) are the various modalities used for the assessment of urinary obstruction. The use of MR has been limited. IVU has conventionally been the initial imaging technique to evaluate possible renal obstruction. More recent studies however have shown the usefulness of ultrasound and non-contrast CT scan.

Plain X-ray

A single supine radiograph of the KUB region may reveal a radiopaque calculus as the cause of obstruction; however, nonradio-opaque calculi cannot be detected.

Intravenous Urography (IVU)

IVU historically has been the initial technique in evaluation of possible urinary obstruction with assessment of both the anatomical and physiological components of the kidney. The signs indicative of acute obstructive process are (1) prolonged dense nephrogram, (2) renal enlargement, (3) dilatation of the collecting system, (4) delayed pyelogram, (5) ureteric dilatation, and (6) pyelosinus extravasation.

If the obstruction is mild, then the nephrogram and calyceal opacification may be normal with minimal dilatation of the ureter. With more severe obstruction, the nephrogram is delayed in onset and becomes more dense and persistent (Figs 18.1A to D). The nephrogram may demonstrate faint radial striations due to contrast in the collecting ducts and tubules.[5] The kidney is often larger than normal. The opacification of calyces and ureter is delayed and depends upon the degree of obstruction. A completely obstructed kidney that has become anuric may not show any opacification of the collecting system, however once the opacification of the collecting system begins, additional radiographs are required to demonstrate the site of obstruction. For taking additional radiographs, the rule of eight can be helpful to prevent multiple exposures. If no contrast appears in the collecting system by 15 minutes after injection, there is little reason to obtain next film until two hours later.[6]

The collecting system and ureter are mildly dilated in acute obstruction. High obstructions cause more pelvicalyectasis then low ones. Extravasation of contrast medium from the kidney is demonstrated by IVU in upto 24 percent of obstructed patients.[7] Forniceal rupture occurs and opacified urine dissects through the tissues of the renal sinus. Minimal extravasation of contrast causes a smudged appearance of the calyces however, when there is extensive leakage, contrast medium tracks around the renal pelvis and along the psoas muscles causing outlining of the ureter. Rarely, pyelolymphatic and pyelosubcapsular extravasation can occur. Unrelieved obstruction with continued extravasation of urine may result to a retroperitoneal collection called urinoma.[7] These collections are best visualized on USG, CT or MRI.

There has been a significant decline in the use of IVU as the dominant imaging technique

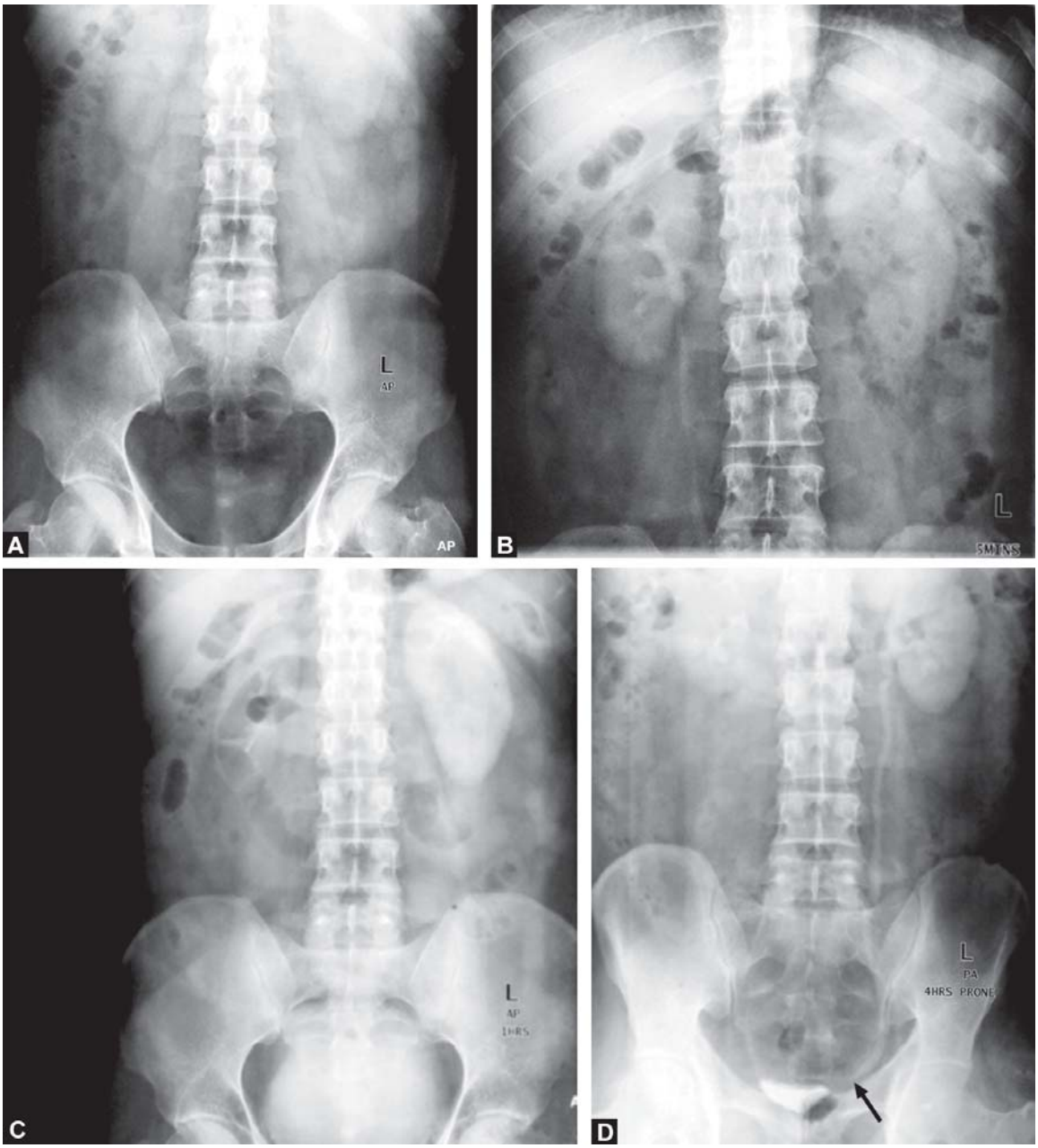

Figs 18.1A to D: Serial IVU images of acute obstruction showing obstructing nephrogram. Plain film **(A)** five minute film **(B)** and 1 hour film **(C)** shows increasingly dense left nephrogram. Delayed **(D)** film well depicted the left lower ureter calculus as the cause of obstruction (Arrow)

in acute obstruction. This change has been driven by fear of contrast induced nephrotoxicity and by growth of renal sonography and particularly low-dose CT. The main drawback of IVU is that it can be time consuming because of the serial delayed films

which may be required to be obtained until the level of obstruction is delineated. This may require many hours and repeated films. Acute side effects of iodinated contrast and contrast induced nephrotoxicity are also partly responsible for the decline in the use of IVU.[8]

Sonography (USG)

Conventional gray scale sonography is a good screening method for detecting subacute and chronic obstruction as demonstrated by pyelocaliectasis however in acute obstruction, pyelocaliectasis is minimal or absent. Another drawback is its inability to reliably distinguish mild hydronephrosis from normal or prominent extrarenal pelvis.[9] The routine gray scale US misses approximately 30 percent of acute obstruction as pelvicaliectasis is usually mild to nonexistent. Grading of hydronephrosis as mild, moderate or severe is useful for descriptive purposes but it cannot be equated with either the presence or degree of obstruction. Urine debris levels or dependent echogenic material within the dilated collecting system have been reported in kidneys with pyonephrosis; however, a dilated pyelocalyceal system free of internal echoes does not rule out pyonephrosis.[6] If hydronephrosis is seen with dilated ureter, an attempt should be made to follow the ureter caudally to the point of obstruction.

Duplex and Color Doppler Sonography

Investigations with duplex and color doppler ultrasound have yielded advances in three areas:

1. Distinguishing mild pyelectasis from prominent central renal blood vessels.
2. Detecting high grade acute ureteric obstruction through analysis of ureteral jets.
3. Establishing renal resistive index as an independent hemodynamic measure of urinary obstruction.

In certain cases normal renal vessels produce separation of the renal sinus echopattern which can mimic mild pelvicaliectasis. In this situation, color doppler offers a quick and effective distinction between these two conditions. Normal ureteral jets are bilaterally symmetrical. The demonstration of ejection of the urine from ureter into urinary bladder excludes total obstruction.[10] The ureters with low-grade obstruction or non-obstructive ureterolithiasis may show normal or near normal ureteral jet pattern. Because of technical limitations and inconsistent findings in partial obstruction, evaluation of ureteral jets has limited clinical usefulness.

Resistive index (RI) is a measure of resistance to blood flow through the kidney and is defined as peak systolic velocity minus end diastolic velocity divided by peak systolic velocity. Normal intrarenal resistance in adults is less than 0.7. The RI may increase in acute obstruction (Figs 18.2A and B). The criteria suggested to diagnose obstruction include:[3,4]

1. Elevation above a threshold value.
2. Intrarenal RI difference of more than 0.06 to 0.10 with unilateral obstruction.
3. Abnormal RI response to diuretic challenge: there is increase of intrarenal RI with diuretic challenge in case of significant obstruction while normal kidneys with non-obstructive dilatation or partial obstruction show no change.

Computed Tomography (CT)

CT scan has emerged as an effective initial imaging tool in the evaluation of acute renal obstruction. CT scan adds value in the following conditions in the context of urinary obstruction:

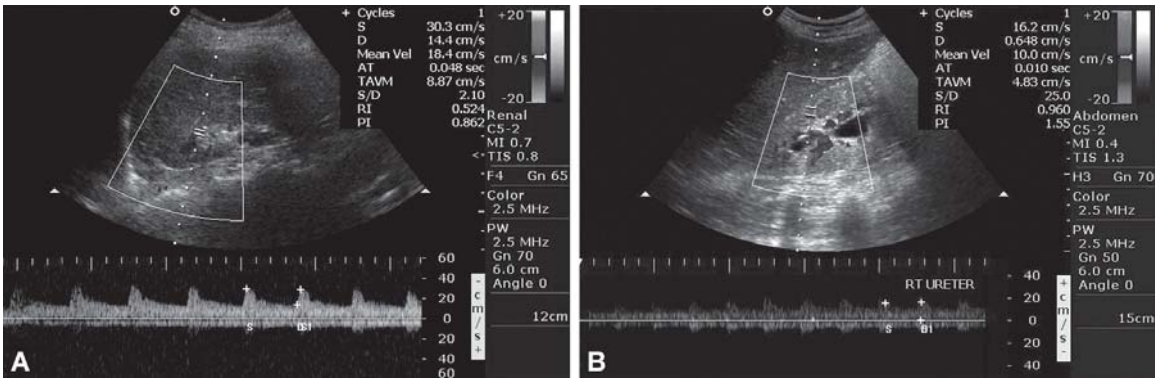

Figs 18.2A and B: Doppler tracing of normal kidney **(A)** and in acute obstruction **(B)**.The Resistive index is increased in acute obstruction *(For color version see Plate 19)*

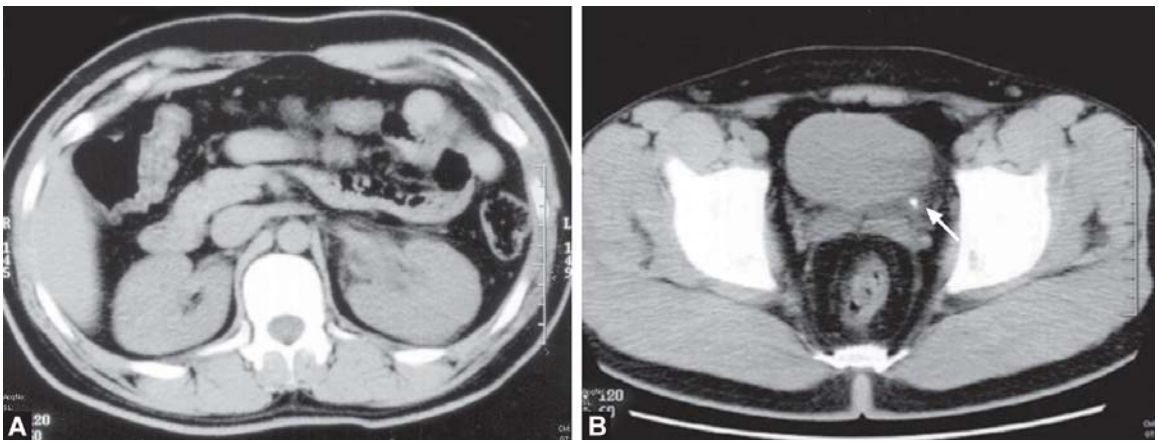

Figs 18.3A and B: Low dose non contrast CT scan (NCCT) of young male presented with acute loin pain. Axial section at the level of kidneys **(A)** shows minimal calyceal separation and perinephric stranding on left side and lower section at the level of bladder **(B)** shows obstructed calculus in lower ureter (arrow)

1. Screening patients with acute flank pain.
2. Screening patients with azotemia who are strongly suspected as having obstruction.
3. Establishing the etiology of ureteral obstruction when other investigations have failed.

Previously, CT was not routinely used in the evaluation of ureteric obstruction because of ionizing radiation, need for intravenous contrast, increased expense and non-availability in many institutions. Today, CT scan is widely available, very quick and can be done without contrast. Noncontract CT (NCCT) scan is useful in determining the presence or absence of obstruction and have higher sensitivity for detection of ureteric stones as compared with IVU.[11] The disadvantage of NCCT is higher radiation dose to patient however Tack et al reported that low dose (30 mAs) NCCT gives a diagnostic quality image for detection of urinary stones and hence significantly reduces the radiation dose to patient[12] (Figs 18.3A and B). The secondary CT signs of obstruction that may be present in patients with ureteric stones are ureteral dilatation, pyelocaliectasis, perinephric stranding and renal enlargement.

The early corticomedullary differentiation is prolonged when contrast enhanced CT is performed in acute obstruction. Gradual opacification of the medulla follows over minutes to hours, resulting in persistent homogenously dense or diffusely mottled nephrogram. If obstruction is unrelieved, the medullary pyramids may actually become more densely opacified then the cortex, creating the reverse corticomedullary nephrogram.

CT is extremely useful for diagnosing the cause of obstruction. Non-opaque filling defects in the renal pelvis or ureter seen on IVU deserve non-contrast CT to distinguish urate calculi from other lesions. Urate and xanthine stones always have high attenuation value.[13] CT is particularly useful in determining the etiology when IVU shows extrinsic ureteric obstruction. Lymphadenopathy, primary and secondary retroperitoneal malignancy, retroperitoneal fibrosis and perianeurysmal fibrosis are some of the common examples which can be easily visualized on CT. In a minority of patients, the cause of obstruction may not be seen as there may not be an intra-luminal or peri-ureteral mass. Secondary signs of obstruction include stranding of perinephric fat, dilatation of intrarenal collecting system, and unilateral increase in cortical thickness.[8]

Radionuclide Renography

The role of nuclear medicine in the evaluation of acute obstruction is limited. Use of technetium DTPA or MAG-3 permits evaluation of arrival, uptake, transit and elimination of radiopharmaceutical from the kidney. DTPA is a glomerular agent whereas MAG-3 operates by tubular secretion. MAG-3 is being increasingly used because of its better renal uptake even in the presence of in renal insufficiency. In obstruction, activity in the parenchyma may rise at a slower rate and persist for a longer time than the non-obstructed kidney. Activity in the collecting system also proceeds down the ureter at a slower rate.

Radionuclide renography however lacks precise anatomical delineation of obstruction as well as ability to define the cause of obstruction. Its major use is in the differentiation of a dilated non-obstructed system from a partially obstructed system. The diuretic renogram, using frusemide after DTPA or MAG-3 study can separate these two entities.[14] If the system is dilated but not obstructed, the collecting system activity washes out within 10 minutes after frusemide administration. If obstructed, no or partial response to the diuretic challenge is seen depending on the severity of obstruction.

MR Imaging

At present, MR imaging has limited role to in the evaluation of urinary obstruction. Magnetic resonance urography (MRU) is an ideal technique in pregnancy, where there is contrast allergy, renal failure patients and if radiation dose is an issue. The level of obstruction is always identified.[15] Ureteric abnormalities are poorly defined especially if they are less than 4 mm in size and that includes stones. MR imaging remains more expensive and not readily available.

IMAGING OF CHRONIC OBSTRUCTION

The plain radiograph may reveal radio-opaque stones that could be responsible for obstruction. A grossly hydronephrotic kidney may be visible as a soft tissue mass in the renal fossa.

Intravenous Urography (IVU)

The urographic pattern varies in chronic obstruction.[16] The kidney size is small in untreated complete obstruction however long standing partial obstruction can result in enlargement of the collecting system and kidney. The obstructive nephrogram is usually not seen in cases of chronic obstruction as tubular concentrating ability and GFR are reduced. The nephrographic density may be normal, faint or none depending upon the residual functioning parenchyma. The renal parenchyma is usually atrophied. When parenchymal thickness is reduced to 1-2 cm, but the renal function is relatively preserved then calyceal crescents are sometimes seen during nephrogram (Fig. 18.4A). The crescents are thin, curved collections of contrast denser than the nephrogram, located in the medulla. They represent realigned collecting tubules running perpendicular to their usual orientation.[17] They parallel the cortical margin of the ballooned calyces, located just 1-2 mm peripheral to the calyces. These crescents remain fixed regardless of patient position. The opacification of extremely thin parenchyma over the dilated calyceal sac produces a "Rim" or shell nephrogram.

Chronic obstruction produces varying degree of pyelocalyceal dilatation. As contrast medium enters the dilated system, it glides to the dependent portion of calyces. With the patient supine, rounded puddles of contrast appear separated from the surrounding nephrogram by a boundary of nonradioopaque urine, this picture has been called the **ball pyelogram** (Fig. 18.4B).

Chronic obstruction may lead to nonvisualized kidney on urogram. The ureter becomes dilated proximal to the obstructing lesion, elongated and tortuous, and in extreme cases it may resemble a segment of small intestine. This is called giant hydroureter or giant megaureter.

Sonography (USG)

Ultrasound is highly reliable in the detection of chronic ureteral obstruction by demonstrating

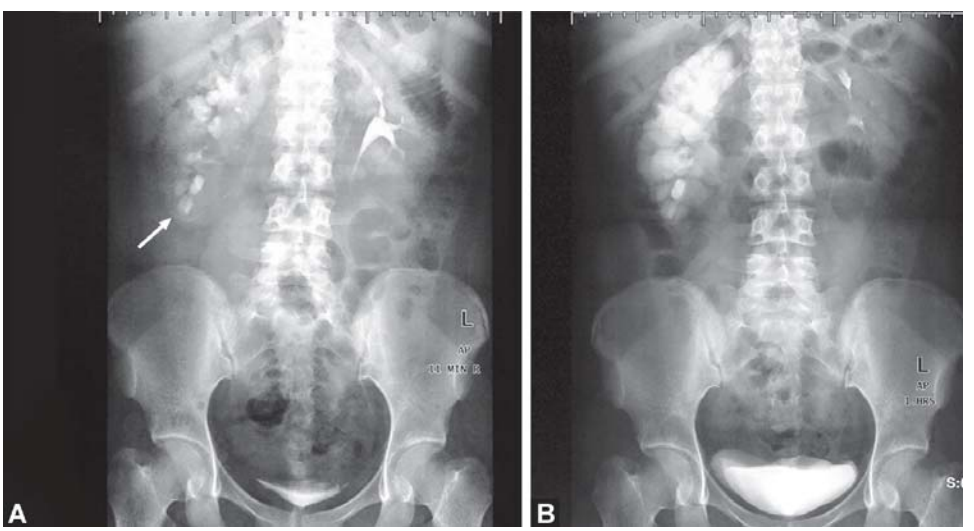

Figs 18.4A and B: IVU study of chronic hydronephrosis due to ureteric stricture . 11 minute film **(A)** shows crescents (Arrow) and 1 hour film **(B)** shows ball pyelogram

pyelocaliectasis with reported sensitivities ranging from 93-100 percent.[18] The ureter is dilated proximal to the obstruction in most of the cases. Resistive index (RI) may be abnormal but it is less reliable in chronic obstruction then acute obstruction. Ultrasound may show false positives as the collecting system may appear dilated in patients with extrarenal pelvis, vesicoureteric reflux, and persistent change due to obstruction that has been relieved.

Computed Tomography

CT shows the same findings as visualized on urography. Abnormal renal dimensions, varying degree of parenchymal thinning and pyelocaliectasis are seen. With moderate or severe hydronephrosis, urine-contrast layers in the dependent portion of the collecting system which are only occasionally demonstrated at IVU are commonly seen on CT. When the hydronephrosis is accompanied by parenchymal thinning, obstructive atrophy is diagnosed (Figs 18.5A and B). The CT version of the shell or rim nephrogram is a thin band of opacified parenchyma surrounding the dilated pelvicalyceal system. Following relief of obstruction, the kidney may shrink remarkably as a manifestation of post obstructive atrophy. Hydronephrosis with parenchymal signs of pyelonephritis, perinephric abscess or thickened renal pelvis can suggest pyonephrosis. CT is a modality of choice for demonstration, if the obstruction is caused by extrinsic process.[18] The concept of CT urography is attractive because both the renal parenchyma and urothelium can be evaluated at single comprehensive examination. CT urography is very useful in urinary obstruction as it simultaneously evaluates the functional status of the kidney, detects dilatation of the pelvicalyceal system as well as the level and cause of obstruction. The limitations of CT urography are the higher radiation dose and longer scan time.

Magnetic Resonance Imaging

The morphological characteristics of a chronically obstructed kidney may be demonstrated by MRI. The cortico-medullary distinction usually seen on T1 weighted images may disappear because of atrophy or destruction of medulla. The dilated pelvicalyceal system is seen as hypointense region

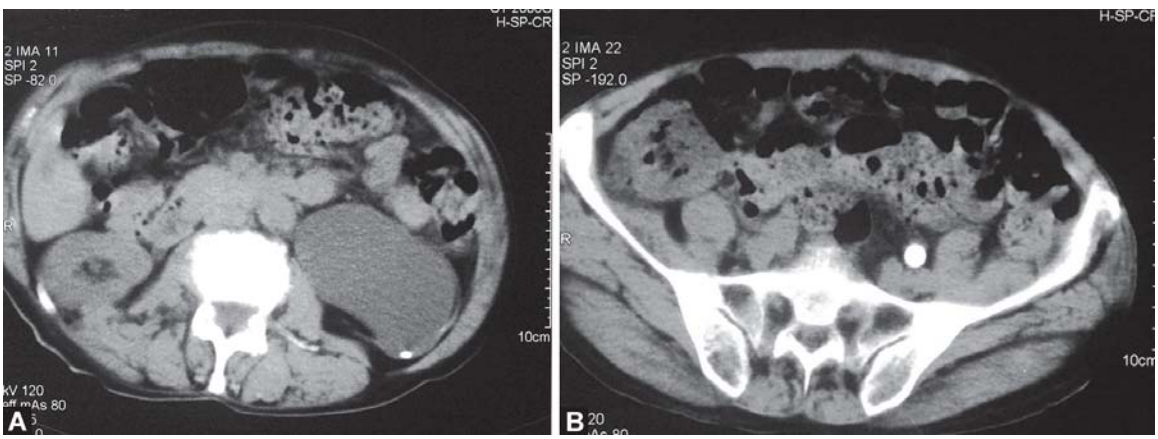

Figs 18.5A and B: NCCT axial images shows gross hydronephrosis with obstructive atrophy and left renal calculus **(A)**, lower sections shows obstructing calculus in lower ureter **(B)**

on T1 and hyperintense on T2 weighted images.

INVASIVE TECHNIQUES IN URINARY OBSTRUCTION

Antegrade Pyelography

This study is done by puncturing the collecting system percutaneously under fluoroscopy. Sonographic guidance facilitates placement of a small caliber needle into the intrarenal collecting system. Once correct placement is ensured by urine aspiration, contrast is injected under fluoroscopic control for opacification of the PCS and ureter.

The usual indications are:[6]

1. To localize the collecting system before percutaneous nephrostomy or Whitaker test
2. To pinpoint the level of obstruction in a dilated urinary system not adequately opacified by an IVU.
3. To opacify the urinary system after failed retrograde ureteropyelogram.
4. To obtain renal urine for bacteriological or cytological examination.

Retrograde Pyelography

This test is particularly valuable when IVU is suboptimal owing to poor renal function and in cases where IV contrast administration is contraindicated. Imaging with retrograde pyelography defines the level and degree of obstruction. It also clarifies whether the obstruction is intraluminal or not.

CAUSES OF OBSTRUCTION AND DISEASES OF URETER

In children, obstruction is commonly due to congenital causes whereas in adults most cases are due to acquired causes. Obstruction may also be classified by location as intra-renal, post-renal, supra-vesical or infra-vesical.

Congenital Ureteric Obstruction

Primary megaureter and obstruction associated with duplication are common causes of congenital ureteric obstruction. The major causes are given in Table 18.1.

Table 18.1: Congenital causes of ureteric obstruction[6]

UPJ obstruction
Primary megaureter
Ureterocele
Ureteric valve
Distal ureteric stenosis
Ureteric atresia
Circumcaval ureter

Ureteropelvic Junction (UPJ) Obstruction

Congenital obstruction of the UPJ is a common anomaly of the urinary tract. It results due to deficiency and derangement of the ureteric smooth muscle fibers resulting in failure of normal peristalsis in the affected segment and subsequent functional obstruction. Males and the left side are commonly affected. Dilated renal pelvis and calyces are demonstrated on urography. Delayed radiographs are usually necessary for demonstrating the point of obstruction at UPJ. With long standing or high grade obstruction the kidney may become nonfunctional. When there is insufficient contrast excretion or the ureter is not visualized, the diagnosis can be established by antegrade pyelography. Ultrasound usually shows hydronephrosis and dilated renal pelvis with a nondilated ureter. In patients with equivocal UPJ obstruction, diuresis renography and Whitaker procedure may be employed to assess functional obstruction.

Primary Megaureter

Primary megaureter or congenital megaureter is an uncommon entity probably caused by functional abnormality of the juxtavesical ureter, which is less distensible and fails to transmit normal peristalsis. Primary megaureter may be seen in both children and adults and typically remains asymptomatic in many cases.[19] Males are affected more than females. A characteristic beak-like configuration of the distal ureteral segment is seen on urography with proximal dilatation of ureter (Fig. 18.6). The dilatation may extend proximally to calyces.

Primary megaureter may be associated with UPJ obstruction, contralateral renal agenesis and vesicoureteric reflux. Ultrasound readily detects PCS and ureteral dilatation. An MCU is required to determine whether vesico-ureteric reflux is present or not. In the absence of reflux, the obstructive nature of the megaureter should be evaluated by diuretic urogram.

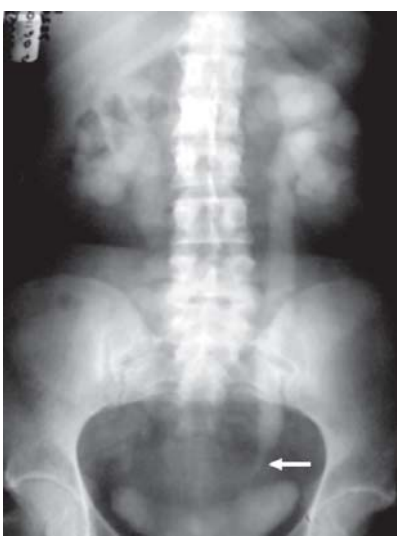

Fig. 18.6: Delayed IVU image (1 hour) shows bilateral hydro-ureteronephrosis with smooth tapering of lower ureter suggestive primary megaureter (Arrow)

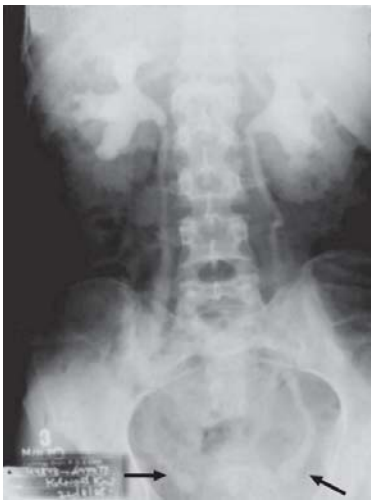

Fig. 18.7: IVU (30 min film) shows bilateral hydronephrosis with fusiform dilatation (arrow) of lower most portion of ureters suggestive of ureterocele

Ureterocele

The term ureterocele means saccular dilatation of the intramural portion of ureter as it passes through the bladder wall (Fig. 18.7). It may be of two types—simple (orthotopic) and ectopic. The ureters of a simple ureterocele drain a nonduplex kidney and insert into the bladder at their normal position at the trigone. An ectopic ureterocele frequently occurs in a duplex kidney. Ureterocele typically appear on urography and cystography as smooth, rounded or ovoid filling defect in the bladder.

Circumcaval Ureter

Circumcaval ureter results when the supracardinal vein persists and forms the major portion of the inferior vena cava. Embryonically, the subcardinal vein lies ventral to the ureter. The right ureter is carried medially by the migration of the subcardinal vein towards the developing IVC. The typical pattern on urography is a tortuous, dilated proximal right ureter and associated hydronephrosis.

The proximal ureter has a characteristic reverse-J course before it crosses behind and around the IVC and then descends medial to the ipsilateral lumbar pedicle. The confirmation of the diagnosis can be made with CT, which shows the ureter passing posterior and medial to the IVC.

Acquired Ureteric Obstruction

The causes of acquired ureteric obstruction can be intraluminal or extraluminal.

Intraluminal Causes

Abnormalities may develop within the ureteral lumen without any attachment to the uroepithelial lining. The common causes are calculi, blood clots, tissue slough, fungus ball and foreign material.

Ureteric Calculus

Approximately 90 percent of urinary stones contain calcium (calcium oxalate, magnesium ammonium phosphate) and 10 percent are calcium free (uric acid, cystine and xanthine). Oxalate and cystine calculi are radio-opaque however pure uric acid calculi are radiolucent on plain radiography. Calculi in the ureters can be difficult to visualize on plain X-rays in view of the fact that a third of the ureter may overlie bone. IVU is performed to establish whether or not a concretion seen on plain films lies in the urinary tract, if so, whether it is the cause of ureteric obstruction.

Stones, except for those composed of matrix are well seen on sonography. Strong echoes with a sharply marginated acoustic shadow are the distinguishing features that distinguish stones from other filling defects in the ureter.

Computed tomography plays a major role in the differential diagnosis of nonopaque filling defects in the ureter. Stones that are nonopaque (uric acid) or faintly opaque (cystine) are visualized as dense as calcium containing stones, however their actual attenuation values are lower than calcium stones. Helical CT is of particular value in detecting acute obstruction caused by ureteric calculus. Noncontrast contiguous sections from kidney to bladder permit identification of the ureter as well as obstructing calculus.[20]

Blood clots: Blood clots in ureter are secondary to trauma, tumors, nephritis, vasculitis and bleeding disorders. Blood clots exhibit radiographic features that are common to other non-radiopaque lesions. The location of clot varies with time or with change in position of patient. When clot persists as a mass of fibrin, calcification may develop that resembles stones or uroepithelial tumors.[21] Sonography shows a mass-like filing defect with low level echoes. The CT attenuation value of clot varies with time. When the clot is fresh, its attenuation value exceeds that of soft tissue. Within a week its attenuation decreases. Blood clot does not enhance after intravenous contrast administration.

Tissue slough: Necrosed papilla and cholesteaotoma can slough and cause obstruction of ureter with proximal dilatation. Urography shows features of nonopaque filling defect. Calcium is sometime deposited along the periphery of a sloughed papilla. Sonography and CT demonstrate hypoechoic and hyperdense mass lesion respectively.

Fungus ball: Most fungus balls or mycetomas are caused by Candida albicans and Aspergillus. Fungal infection of the urinary tract occurs in the setting of altered host resistance like HIV, steroid intake, severe debilitating disease and antineoplastic drug

intake. The fungus balls fill the renal pelvis or ureter with a nonopaque mass. Sometime contrast material insinuates into the interstices of the mass causing lacelike radiodense pattern during IVU.[22] The fungus ball appears as an echogenic mass on sonography while CT shows soft tissue attenuation filling defects. Neither sonography nor CT can differentiate fungus ball from other intraluminal soft tissue.

Intramural Causes

Ureteral Tumors

Primary ureteral tumors are relatively rare, accounting for approximately 1 percent of all urinary tract tumors. Tumors arising from epithelium are commonest however they can arise from mesoderm. Males are affected more than females with the usual age of presentation being in the 5th to 8th decades. The most common tumor of ureter is transitional cell carcinoma. Rare tumors include squamous carcinoma, adenocarcinoma, sarcoma and metastasis.

Transitional Cell Carcinoma (TTC)

Transitional cell carcinoma occurs more frequently in males and has a peak incidence in the seventh decade. Certain epidemiological factors have been associated with increased risk for development of transitional cell carcinoma. These include exposure to chemicals, dye, petroleum, rubber and cable industries. Tobacco, coffee, artificial sweetener, chronic inflammation and infection are additional risk factors. There is increased prevalence of TCC in analgesic and Balkan nephropathy. Squamous cell carcinoma occurs in older age and is generally associated with chronic infection and leukoplakia of urinary tract. Adenocarcinoma occurs in patients with severe infection and stone disease.

Radiological findings

IVU: The lesion appears as a smooth or lobulated, polypoidal filling defect in the ureter which maintains a constant relationship with the ureteric wall (Figs 18.8A and B). There is usually proximal obstruction dilatation of the ureter. The ureter just distal to the tumor is also often slightly dilated. The combination of distal margin of soft tissue mass invaginating into the distended segment of opacified ureter constitutes the **Chalice or Bregman's** sign.[23] This sign is useful in distinguishing tumor from nonopaque stone as the ureter is not dilated distal to a stone.

Sonography: Tumors of the ureter may be seen as a soft tissue mass situated at the distal end of a slightly dilated ureter. USG examination does not reliably distinguish between ureteric tumor and blood clot.

CT: Computed tomography defines the contour and mural attachment of tumor following ureteral opacification. The tumor may enhance after intravenous contrast administration. The tumor may project into the ureteric lumen with circumferential or eccentric mural thickening. The lesion may infiltrate into the periureteric fat. CT is important in the staging of a documented ureteric tumor as it detects periureteral extension as well as lymph node enlargement.[24] MR may be used in patients in whom CT cannot be done.

Benign Tumors

Benign tumors of urothelium constitute approximately 20 percent of ureteral neoplasms. The commonest is a papilloma which presents as a solitary filling defect attached to the ureter by a stalk.

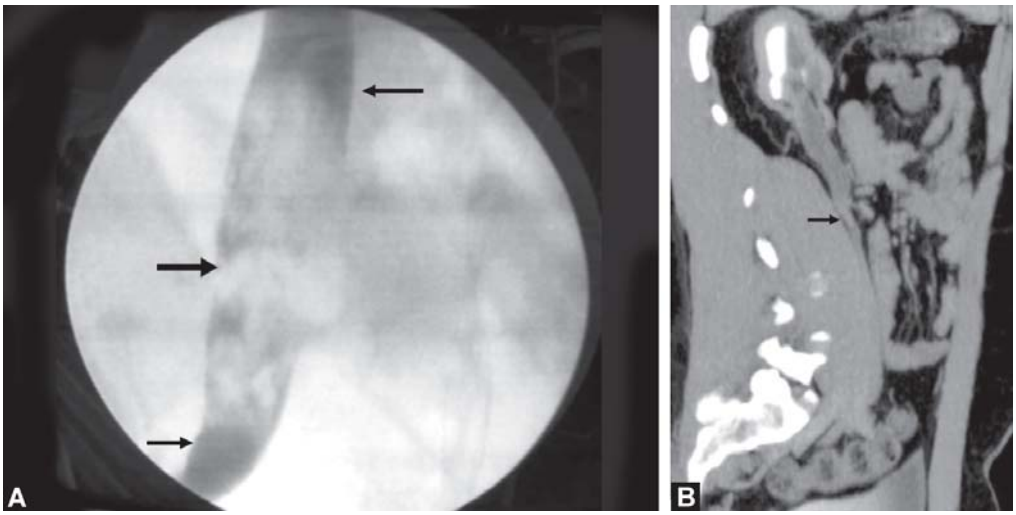

Figs 18.8A and B: Transitional cell carcinoma of ureter (TCC). Fluoroscopic spot of nephrostogram **(A)** shows irregular filling defect (thick arrow) in mid-ureter with dilatation of ureter (thin arrows) proximal as well as distal to the lesion (Bregman's sign). Another patient with TCC: Contrast enhanced CT with sagittal reconstruction **(B)** showing circumferential mural thickening (arrow) of ureter with proximal hydroureteronephrosis. These findings may mimic inflammatory lesion of ureter

Nonepithelial Tumors

Fibroepithelial polyp is the most common nonepithelial tumor. These typically occur in patients in the 20-40 years age group. The usual location is the proximal one-third of the ureter. The lesion is usually solitary but multiple lesions can rarely be seen. The lesion can present as a mobile, smooth, cylindrical, slightly mobile, filling defect. Sometimes the lesion can be frond like.

Secondary Tumors and Contiguous Infiltration

These are more common than primary ureteric tumors. Direct extension of tumor from primary sites such as cervix, prostate and bladder can cause ureteric obstruction. Malignant retroperitoneal lymphadenopathy also causes obstruction to the ureter. Some tumors invoke an intense periureteric desmoplastic reaction causing ureteric obstruction. In such cases, imaging may demonstrate a soft tissue mass like retroperitoneal fibrosis. Rarely, hematogenous malignant deposit can occur to the ureters. The common primaries responsible are melanoma, renal cell carcinoma, breast, lung and prostate.[25]

Inflammatory Lesions of Ureter

Inflammatory conditions of the ureter include a wide variety of disorders. Primary inflammation of the ureter is rare in the absence of systemic or regional disease in urinary tract, retroperitoneum, pelvis or peritoneum. Inflammation of ureteral wall may originate from inflammatory elements excreted in the urine, hematogenous embolism or contiguous spread from adjacent areas within the urinary tract and abdomen. The general responses of the ureter to inflammation are loss of ureteric peristalsis, dilatation, ulceration, irregularity, pseudopolyposis, edema and desmoplasia leading to stricture and calcification.[26]

Radiological imaging radiology plays an important role in diagnosing and characterizing inflammatory conditions of the ureter. This information supplements that from other clinical diagnostic tools including urinalysis, urine culture, urine cytology and cystoureteroscopy.

Malakoplakia: Malakoplakia is a benign chronic granulomatous disorder more commonly seen in women than men. It can be seen at any level of the urinary tract but has a predilection for the bladder and lower ureter. It is seen in association with chronic *Escherichia coli* or *Proteus mirabilis* infection and is found more frequently in diabetics and immunosuppresed patients. On urography, the lesions are rounded to flat, coalescent filling defects lending an irregular contour to the ureteral margin.[27] Ureteric obstruction may be present. The imaging features overlap with ureteritis cystica but the lesions are usually rounder and the ureter is not dilated in the latter condition.

Ureteritis cystica: This disease entity is usually asymptomatic but may present with hematuria or symptoms of urinary tract infection. Histologically, this condition consists of multiple, small, subepithelial, fluid-filled cysts in the ureteric wall. Ureteritis cystica does not cause ureteric obstruction. The disease has a slight predilection for the upper ureter. The typical radiographic appearance is that of multiple, small, filling defects with scalloping of the ureteral margin. The differential diagnosis includes air bubbles, hemorrhage into ureteric wall, and papillary neoplasm.[28] The condition may or may not regress with treatment of the underlying inflammatory condition.

Leukoplakia: Leukoplakia is a rare inflammatory condition which more commonly involves the urinary bladder than the ureter. It results from squamous metaplasia of the urothelium and is frequently associated with chronic urinary tract infection or long standing stone disease. The imaging features include diffuse, irregular; filling defects. There may be ridging of the mucosa with ureteric dilatation. Differentiation from malakoplakia or ureteral malignancy is difficult on imaging.

Schistosomiasis: Schistosomiasis is a chronic indolent infestation caused by the trematode *Schistosoma hematobium*. The parasite lays its eggs in the veins of the bladder and lower ureter stimulating chronic inflammatory reaction resulting in cystitis and ureteritis and eventually scarring and calcification. Schistosomiasis commonly affects the bladder and ureteric involvement is seen in one-third of patients. The ureters are bilaterally asymmetrically involved with predominant involvement of the lower ureter. The disease usually affects a younger age group. Imaging findings are characteristic. Calcification of the ureter is seen in 75 percent of cases which is usually linear or tram-track in appearance. There is a characteristic deformity of the distal ureters consisting of medial and cephalic displacement which may resemble cow's horns.[29] There is varying degree of stenosis and dilatation and the ureter may show a beaded appearance which can resemble tubercular ureteritis.

Tubercular ureteritis: Tuberculosis of the urinary tract is usually due to hematogenous dissemination of *Mycobacterium tuberculosis*. Ureteral involvement is usually due to descending renal infection. The symptoms are nonspecific and include constitutional symptoms and lower urinary tract symptoms like frequency, dysuria, and suprapubic pain. The patients may present with hematuria and

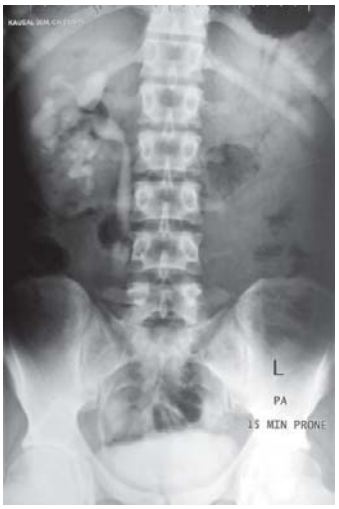

Fig. 18.9: IVU film (15 min) shows hydronephrosis, forniceal stenosis, cavitary changes in right kidney with ureteric narrowing. All these features suggest tubercular involvement of urinary tract

sterile pyuria. When the infection affects the ureteral wall, the first changes are those of ulceration and wall edema with thickening which progress to strictures and calcification. These changes may lead to proximal dilatation of the ureter and PCS. Plain films of abdomen may show evidence of ureteric calcification with or without calcification of the kidney. Characteristic urographic findings include alternating areas of dilatation and short strictures of the ureter (beaded appearance), long straight stricture (pipestem ureter) or isolated stricture (Fig. 18.9). The ureter is shortened and straightened due to periureteral fibrosis.[30] The CT scan is useful in demonstrating ureteric wall thickening and presence of lymph nodes if any. The bladder may show poor distensibility owing to irritative spasm or fibrosis within the wall (Figs 18.10A and B).

Radiation ureteritis Radiation can lead to early and late changes in the ureteric wall, ultimately leading to fibrosis and stricture. Fibrosis continues to develop long after radiotherapy has been completed. IVU may demonstrate mucosal irregularity and a short or long distal ureteric stricture. CT may demonstrate these findings as well as thickening and stranding of the wall of the ureter.

Inflammatory Bowel Disease

Genito-ureteric complications may occur in up to one-fourth of patients with inflamma-

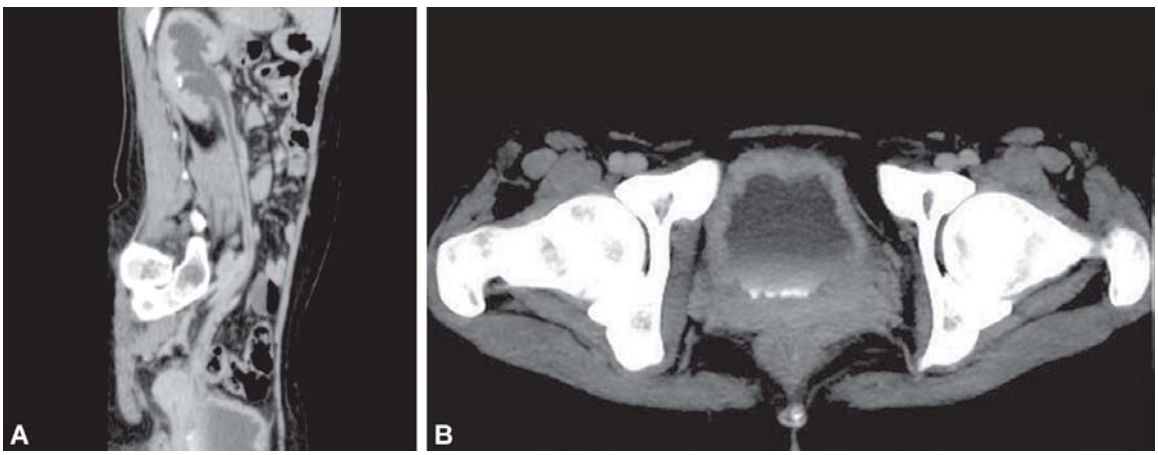

Figs 18.10A and B: CT scan of urinary tract tuberculosis. Multiplanar reconstruction (MPR) **(A)** shows hydronephrosis of kidney with thickened ureteric wall **(B)** and irregular thickening of urinary bladder with reduced capacity

tory bowel disease. Obstruction due to direct ureteral involvement is the second most common complication, the first being nephrolithiasis. Ureteric involvement by Crohn's disease is usually at the level of the pelvic brim and the right ureter is more commonly involved.[31] On urography, the ureter shows a smooth area of narrowing with varying degree of obstruction. CT scan shows an inflammatory soft tissue mass with narrowing and mural thickening of the ureter.

Endometriosis Ureteral involvement generally occurs in cases with widespread pelvic disease however cases of isolated ureteral involvement have been reported. Two forms of ureteral endometriosis have been described. Extrinsic involvement is four times more common than the intrinsic variety. The distal ureter is commonly involved. Ureteral involvement may result in narrowing of ureter, hydronephrosis and occasionally an intraluminal mass.[32] The stricture is usually smooth but abruptly tapered and may show medial sharp angulation. CT may demonstrate a soft tissue mass or endometrioma causing encasement of the ureter (Figs 18.11A to D).

Extrinsic Causes of Ureteral Obstruction

The extrinsic causes of ureteral obstruction are given in Table 18.2.

Retroperitoneal Fibrosis

Retroperitoneal fibrosis (RPF) is an important cause of obstructive uropathy leading to renal failure. It encompasses a range of diseases characterised by the presence of fibro-inflammatory tissue, which usually surrounds the abdominal aorta and iliac arteries and extends into the retroperitoneum to envelop neighbouring structures including the ureters. RPF may be idiopathic (Ormond's disease) or secondary to a wide variety of stimuli which includes both benign and neoplastic causes.

The classic triad of delayed renal contrast excretion with unilateral or bilateral (60% of cases) hydronephrosis and proximal hydroureter secondary to ureteral involvement, medial deviation of the middle-third of both ureters and tapering of the ureteral lumen at the L4–L5 vertebral level, though less frequently seen than previously thought is still useful in the identification of RPF. When there is insufficient contrast excretion on urography,

Table 18.2: Extrinsic causes of ureteral obstruction[6]

Retroperitoneal tumors	Lymphoma, sarcoma, metastases, cysts
Pelvic tumors	Uterine leiomyomas, malignancies of cervix; ovary, bladder, prostate, colorectum
Retroperitoneal fibrosis Pelvic lipomatosis	Idiopathic, secondary
Pregnancy related	Hydronephrosis of pregnancy, ovarian vein thrombophlebitis, ovarian vein syndrome
Gynecologic conditions	Pelvic inflammatory disease, endometriosis, uterine prolapse, hydrocolpometra
Gastrointestinal diseases	Crohn's disease, diverticulitis, appendicitis, Pancreatic and gastric malignancies
Miscellaneous	Amyloidosis, Reaction to foreign material (barium, surgical suture, etc.)

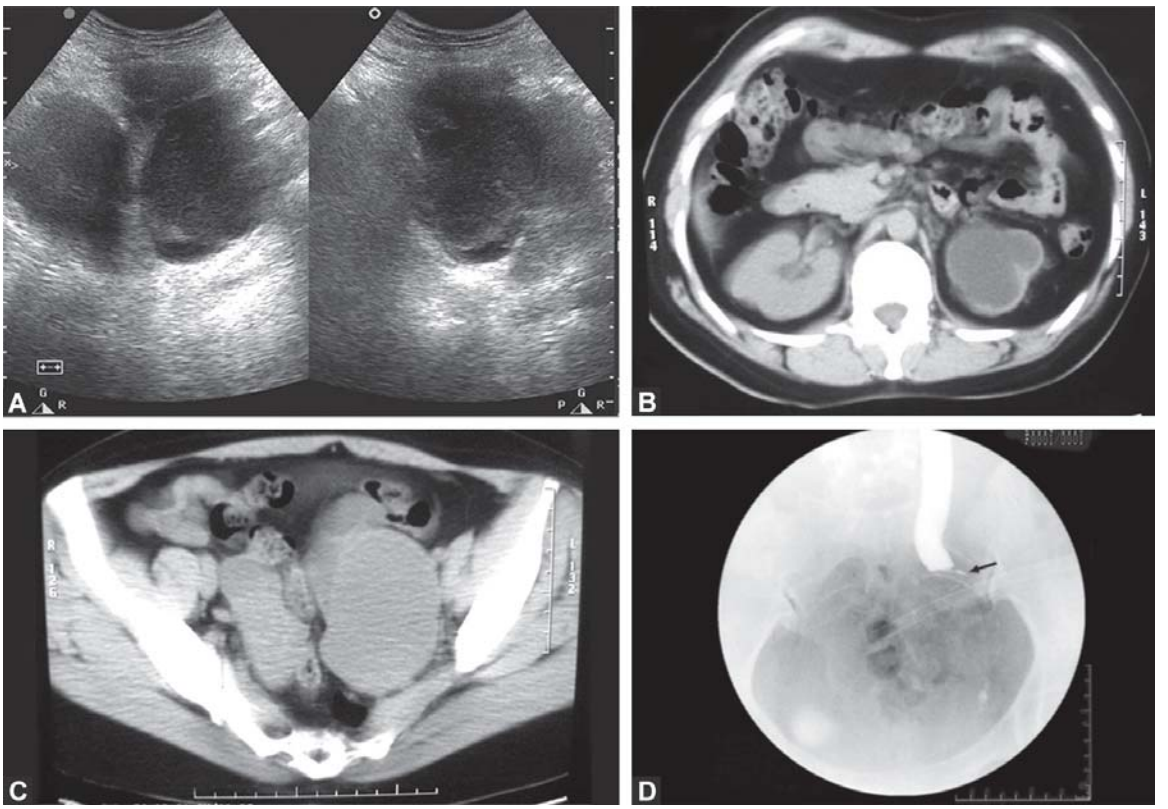

Figs 18.11A to D: Obstructive uropathy due to endometriosis. USG image **(A)** shows complicated cyst with in left adnexa. CT scan axial scan at the level of pelvis **(C)** shows adnexal mass encasing lower ureter resulting obstructive atrophy of kidney **(B)**.The nephrostogram **(D)** of the same patients shows displacement and stricture of lower ureter (arrow)

retrograde or antegrade pyelography is required to demonstrate the characteristic ureteral changes.[33] CT scan demonstrates sheet like soft tissue mass in retroperitoneum with encasement of ureters (Figs 18.12A to C) CT may help in the identification of disease activity with the degree of soft-tissue enhancement correlating with the activity of the fibrotic process. Retroperitoneal fibrosis has signal characteristics similar to those of other fibrotic processes, with a tendency toward diffusely low signal intensity on T1-weighted MR imaging. T2 signal is a reflection of the degree of associated active inflammation (and thus edema) with high signal indicating early inflammatory phase of benign RPF or malignancy while low signal signifies chronic phase of benign RPF. Chronic, inactive fibrosis will have little edema and thus be visualized as having low signal on both T1- and T2-weighted imaging. This feature may also prove valuable in assessing a patient's response to treatment; decreasing T2-signal indicating a favorable therapeutic response.[33,34]

Retroperitoneal Neoplasms

Extraureteral malignancies causing obstructive uropathy are much more common than primary ureteral neoplasms. The ureter is very prone to involvement as it is near many

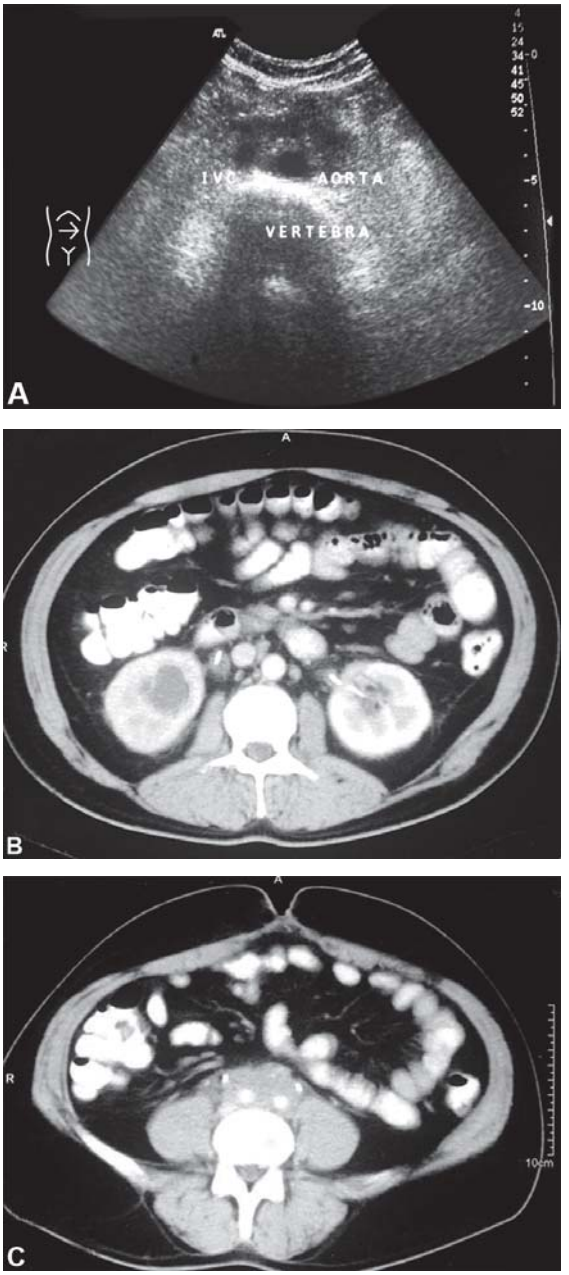

Figs 18.12A to C: A young patient of idiopathic retroperitoneal fibrosis presented with obstructive uropathy. Ultrasound image **(A)** and contrast enhanced CT scan **(B and C)** shows retroperitoneal mass encasing major vessels and bilateral ureter. Note made of bilateral DJ stents

structures in the retroperitoneum that frequently harbor malignancies. In many cases, obstruction may result from direct extension of neoplasms from primary sites like the bladder, prostate, endometrium, sigmoid colon, rectum and cervix (Figs 18.13A to 18.14B). In other cases there may be metastasis to the periureteral tissues especially the lymph nodes by distant tumors which causes uropathy by direct infiltration of one or both the ureters or by compression and mechanical obstruction. Bulky lymph nodes seen in lymphomas may cause similar manifestations.

Primary retroperitoneal tumors arising in the vicinity of the ureters may also lead to mechanical obstruction. CT scores over sonography in the detection and possible classification of these tumors. Malignancies may incite an intense periureteral desmoplastic reaction resembling retroperitoneal fibrosis leading to ureteral obstruction. This is especially seen in metastases from carcinomas of lung, breast, pancreas, colon, stomach and sometimes lymphoma.[35] Patients who have received radiation therapy in the vicinity may also experience obstructive symptoms. This was initially thought to be due to radiation induced ureteric stricture but lately it has been realized that the ureter is relatively resistant to radiation. An obstruction in this case usually means that the tumour had involved the ureteral wall before radiation or there has been a recent relapse.

Pelvic Lipomatosis

It is an unusual disease resulting from proliferation of mature fibroadipose tissue in the pelvis. Usually seen in males, it may require surgery if it is causing obstructive

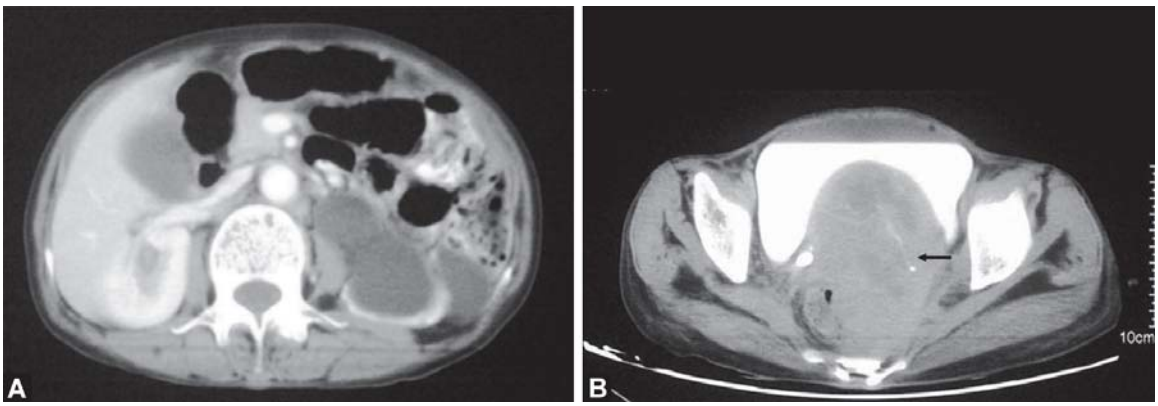

Figs 18.13A and B: Carcinoma of cervix causing obstructive uropathy. Contrast enhanced CT (CECT) axial section **(A)** shows obstructive atrophy of left kidney. Delayed section at the level of pelvis **(B)** shows large heterogeneous cervical mass causing encasement of lower ureter (Arrow)

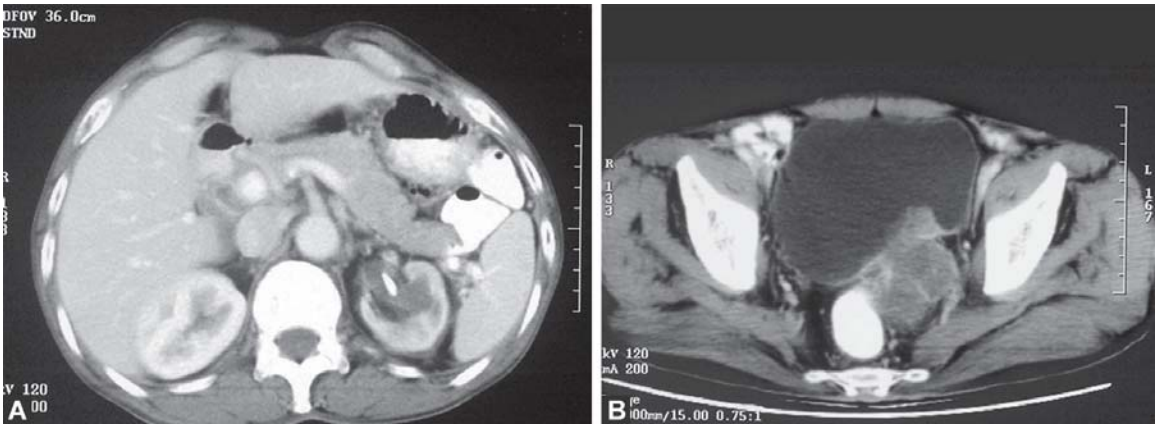

Figs 18.14A and B: Ureteric obstruction caused by urinary bladder malignancy. Contrast CT axial section (A) shows left hydroureteronephrosis with large calculus in renal pelvis. Inferior section (B) shows large lobulated mass arising from urinary bladder with exophytic component causing left ureteric involvement

uropathy by ureteral compression. Radiographic findings include relative hyperlucency of the pelvic cavity on plain radiographs. Contrast studies may show displacement and compression of rectosigmoid and urinary bladder leading to 'tear drop' or 'pear' shaped bladder.[36] The distal ends of the ureters are displaced medially in the majority of cases with presence of hydroureter or hydroureteronephrosis. Identical appearance of the bladder can also be seen with pelvic lymphadenopathy, diffuse pelvic carcinomatosis, pelvic/perivesical liposarcoma and pelvic fibrosis (resembling retroperitoneal fibrosis).

Pregnancy Related Dilatation of Ureter

Variable degree of ureteral dilatation is often seen during pregnancy which is most marked in the third trimester with predominant involvement of the right side. In most of the cases the dilatation progressively disappears in the postpartum period. The ureteral segments below the pelvic brim do not show

dilatation indicating that partial mechanical obstruction by the gravid uterus accounts for the major changes of hydroureter seen during pregnancy.

Sonography forms the initial and mainstay imaging modality in these conditions. If the sonographic findings are equivocal, MR urography should be performed which can show tapered narrowing of the lumbar portion of the ureter which is being compressed by the gravid uterus against the iliac artery at the sacral promontory.[37] An obstructing calculus is usually above or below this level.

Gynecological Causes

Various gynecologic causes disorders may cause extrinsic compression on the ureter leading to proximal dilatation of the urinary system. Tubo-ovarian abscesses in pelvic inflammatory disease (PID) may cause extrinsic ureteric compression or surround the ureter with inflammation leading to partial obstruction with lateral displacement of the ureter below the pelvic brim. Pneumohydronephrosis may rarely develop due to fistula formation between the abscess and the ureter. Uterine and bladder prolapse are important causes of reversible and preventable renal failure. Obstruction is usually bilateral and is often associated with UTI. Sonography along with IVU studies helps in the easy identification of the disease. Other gynecologic causes disorders like hydrometrocolpos and hydrocolpometra may also cause ureteral compression.

Gastrointestinal Diseases

Various diseases related to the GIT may lead to indirect involvement of the urinary tract by contiguous involvement of the ureters. Retroperitoneal extension of inflammation and fibrosis may occur in inflammatory bowel disease especially Crohn's disease as well as in complicated colonic diverticulitis with predominant involvement of the right and left ureters respectively. In Crohn's disease, the ureter usually displays a sharply tapered, smooth area of narrowing over several centimeters leading to varying degree of obstruction. Pancreatic and appendiceal inflammation similarly may directly spread to the ureter, commonly on the right side leading to obstructive symptoms.

Miscellaneous Diseases of Ureter

Ureteral Injury

The causes of ureteric injury can be iatrogenic and external trauma. Radical hysterectomy, gynecological surgery and obstetric trauma are common causes of iatrogenic injury. Penetrating injury and fall from height are common causes for external trauma. Most surgically induced ureteric injuries go unsuspected at the time of injury, because they are often not a direct injury but the result of ischemia. Excretion intravenous urography may demonstrate extravasation of urine and hydronephrosis (Figs 18.15A and B). The complications of ureteric injury include hydronephrosis/pyonephrosis secondary to stricture, calculus formation, ureteric fistula, urinomas and renal failure.

Ureteral Herniation

Herniation of ureter is rare. Inguinal, femoral and sciatic hernias may include the ureter. Herniation of ureter can be recognized on urography, e.g. in sciatic herniation, the pelvic ureter extends laterally through the sacrosciatic notch, producing a hairpin shaped redundancy.[38]

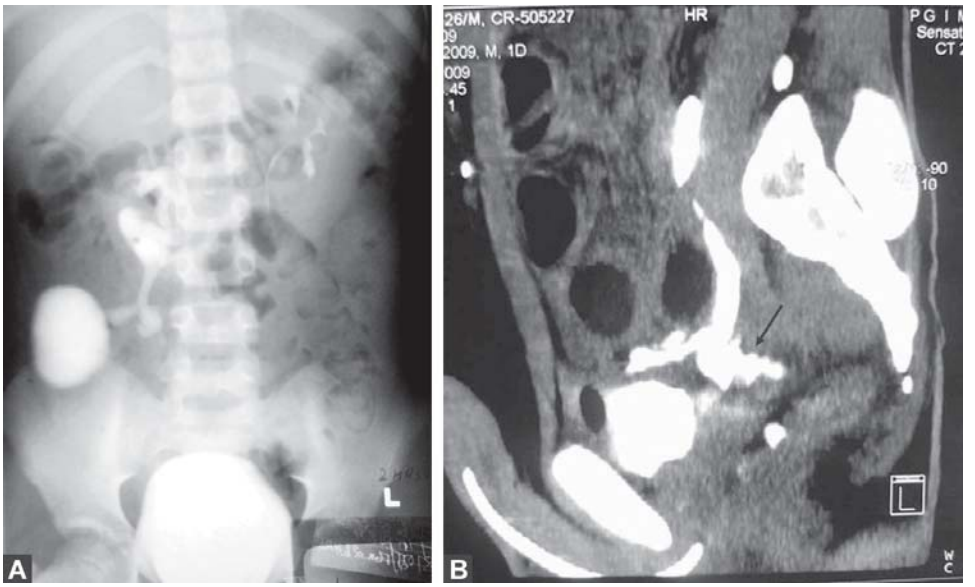

Figs 18.15A and B: Ureteric trauma. Delayed IVU film(2 hours) **(A)** shows extravasation of contrast from right upper ureter. **(B)** CT reformation in another patient shows contrast leak from lower ureter suggestive of ureteric trauma (Arrow)

Ureteral Fistula

The common causes of ureteral fistulae are penetrating trauma, complicated ureteral surgery and inflammatory or malignant disease.[39] Ureteral fistula usually presents with urinary tract infection and clinical evidence of flow through the fistula. The diagnosis of fistula is usually made by ureterography. Rarely, an ureteroenteric fistula may be demonstrated during contrast study of the gastrointestinal tract. CT may demonstrate the primary lesion and the fistulous tract.

REFERENCES

1. Wilson DR. Pathophysiology of obstructive nephropathy. Kidney Int 1980;18:281-92.
2. Hodson CJ. Experimental obstructive nephropathy in the pig.Br J Urol(suppl) 1969;41:5-20.
3. Tublin ME, Dodd GD III, Verdile VP. Acute renal colic; diagnosis with duplex doppler US. Radiology 1994;193:697-701.
4. Cronan JJ, Tublin ME. Role of resistive index in the evaluation of acute renal obstruction AJR1995;164:377-78.
5. Bigongiari LR, Davis RM, Nowak WG et al. Visualization of medullary rays on excretory urography in experimental ureteric obstruction AJR 1977;129:89-93.
6. Talner LB. Urinary obstruction. In Grainger and Allison's Diagnostic Radiology (3rd edn). Chuchil Livingstone, 1997.
7. Bernardino ME, McClennan BL. High dose urography: incidence and relationship to spontaneous peripelvic extravasation. AJR 1976;127:373-76.
8. Koelliker SL, Cronan JJ. Acute urinary tract obstruction: imaging update. Urologic Clinics of North America 1997;24:571-81.
9. Kamholtz RG, Cronan JJ, Dorfman GS. Obstruction and the minimally dilated renal collecting system: US evaluation. Radiology 1989;170: 51-53.
10. Burge HJ, Middleton, WD, McClennan B et al. Ureteral jets in healthy subjects and in patients with unilateral ureteric calculi: comparison with color doppler US. Radiology 1975;180:437-42.

11. Smith RC, Rosenfield AT, Choe KA et al. Acute flank pain:Comparison of noncontrast enhanced CT and intravenous urography.Radiology 1995;194:789-94.
12. Tack D, Sourtzis S, Delpierre I et al. Low dose unenhanced mutidetector CT of patients with suspected renal colic. Am J Roentgenol 2003; 180:305-11.
13. Pollack HM, Arger PH, Banner MP. Computed tomography of renal pelvic filling defects. Radiology 1981;138:645-51.
14. O'Reilly PH. Diuresis renography eight years later:an update.J Urol 1986;136:993-99.
15. Hussain S,O'Mally M, Jara H. MR urography. Magn Reson Imaging North Am 1997;5:95-106.
16. Elkin M. Obstruction and dilatation of urinary tract.In:Elkin M (Ed). Radiology of urinary system. Little Brown: Boston, 1980.
17. Dunbar JS, Nogrady MB. The calyceal crescent – a roentgenographic sign of obstructive hydronephrosis. AJR 1970;110:520-28.
18. Dunnick NR, Sandler CM. Textbook of Uroradiology(3rd ed). Lippincot press.
19. Pfister RC, Hendren WH. Primary megaureter in children and adults. Urology 1978;12:160-66.
20. Dalrymple NC, Verga M, Anderson KR. The value of unenhanced helical computerized tomography in the management of acute flank pain. J Urol 1998;159:735-40
21. Thomas J, Stey A, Abouker P. Calculi on blood clots. J Uro (Paris) 1976;82:496.
22. Margolin HN. Fungus infection of urinary tract.Semin Roentgenol 1971;6:323-28.
23. Bergman H, Friedenberg RM, Sayegh V. New roentgenologic sign of carcinoma of ureter. AJR 1961;86:707-10.
24. Kenney PJ, Stanley RJ. Coputed tomography of ureteral tumor. J Comput Assit Tomogr 1987;11:102.
25. Winalski CS, Lipman JC, Tumeh SS. Ureteral neoplasms. Radigraphics 1990;10:271.
26. Wasserman NF. Inflammatory disease of the ureter.Radiol Clinic North Ameri 1996;34: 1131-56.
27. Elliot GB, Moloney PJ, Clement JG. Malacoplakia of urinary tract. AJR 1972;116:830.
28. Menedez B, Sala X. Cystic pyeloureteritis:Review of 34 cases. Radiology aspects and differential diagnosis. Urology 1997;50:31-37.
29. Young SW, Khalid KH, Farid Z et al. Urinary tract lesions of schistosoma hematobium. Radiology 1974;111:81.
30. Royalance N, Penry JB, Davies ER et al. The radiology of tuberculosis of urinary tract. Clin Radiol 1970;21:163.
31. Banner MP. Genitourinary complication s of inflammatory bowel disease. Radiol Clin North Am 1987;25:199.
32. Kane C, Dronin P. Obstructive uropathy associated with endometriosis. Amer J Obst Gynecol 1985,151:207.
33. Cronin CG, Lohan DG, Blake MA et al. Retroperitoneal fibrosis: a review of clinical features and imaging findings. AJR Am J Roentgenol 2008;191:423-31.
34. Vaglio A, Salvarani C, Buzio C. Retroperitoneal fibrosis. Lancet 2006;367:241-51.
35. Winalski CS, Lipman JC, Tumeb SS. Ureteral neoplasms. Radiographics 1990;10:271.
36. Heyns CF. Pelvic lipomatosis: A review of its diagnosis and management. J Urol 1991;146:267.
37. Grenier N, Pariente JL, Trillaud H et al. Dilatation of collecting system during pregnancy: physiologic vs obstructive dilatation. Eur Radiol 2000;10:271-79.
38. Tsai PJ, Lin JT, Wu TT et al. Ureterosciatic hernia causes obstructive uropathy. Chin Med Assoc 2008;71:491-93.
39. Moon SG, Kim SH, Lee HJ, et al. Pelvic fistulas complicating pelvic surgery or diseases: spectrum of imaging findings. Korean J Radiol 2001;2:97-104.

Chapter

19

Urinary Tract Trauma

Atin Kumar, Shivanand Gamanagatti

INTRODUCTION

Approximately 10 percent of all traumatic injuries involve the urinary tract, most often the kidney.[1] Although trauma to the urinary tract is seldom the cause of death but serious morbidity can result if such injuries are missed. An accurate radiographic and imaging evaluation is important to determine the presence and extent of injury for the proper management of the patients. Evaluation of the urinary tract trauma should be integrated into the overall management of the trauma patient.

Blunt trauma accounts for 80 to 90 percent of all renal injuries.[1] These are primarily due to deceleration injuries in motor vehicle accidents, falls or assault. In approximately 10 to 20 percent of the patients, penetrating injuries result due to gunshot or knife wounds. Pre-existing kidney lesions, e.g. renal tumors, hydronephrosis, polycystic kidney disease and horseshoe kidneys make the kidney more susceptible to the injury. In 80 percent of the patients with penetrating trauma and 75 percent of blunt trauma patients, associated injuries, e.g. splenic rupture, liver laceration and injuries to the small and large bowel are seen.[2] In about 50 percent of these patients, bone fractures are present. Iatrogenic causes such as surgery, interventional procedures and biopsies are also associated with trauma to the urinary tract.

RENAL TRAUMA

Since the late 1980s, the prevailing techniques of imaging and clinical management of renal trauma have changed dramatically. Consensus has been building towards a conservative approach and successful clinical management must be based on an accurate assessment of the extent of injury.

Imaging Work-up in a Patient with Suspected Renal Trauma

Trauma to the kidney may be suspected to be minor or significant on the basis of clinical picture, nature and site of injury. An unstable patient may undergo no imaging work up if an immediate surgery is indicated on clinical grounds. In a clinically stable patient with abdominal trauma and with suspected abdominal organ injury and/or hypotension, kidneys are imaged as part of a standard abdomen and pelvic CT. The current globally accepted indications specifically for radiological evaluation of urinary tract in trauma patients are:[2-5]

- Gross hematuria
- Microscopic hematuria with hypotension (BP < 100 Hg at any time during evaluation)
- Injuries associated with renal injury such as direct contusion or hematoma of flank soft tissues, fractures of lumbar spine, lower rib and transverse process
- Penetrating trauma with any degree of hematuria.

Earlier children with any degree of hematuria were also an indication for radiological evaluation, but recently there has been a trend to have an approach similar to adult patient. Renal imaging is not required in a patient with minor trauma having microhematuria without shock.

An approach to a patient having significant trauma can be outlined as shown in the algorithm (Fig. 19.1).

Role of Radiography (Plain Radiographs)

Widespread availability and use of CT and ultrasound has replaced abdominal radiography for evaluation of renal trauma. However radiographs have a role in the setting of penetrating abdominal trauma.

Role of Ultrasound

Specific visceral injuries are poorly assessed on ultrasonography. The value of sonography is primarily in rapid establishment of presence of hemoperitoneum in an unstable

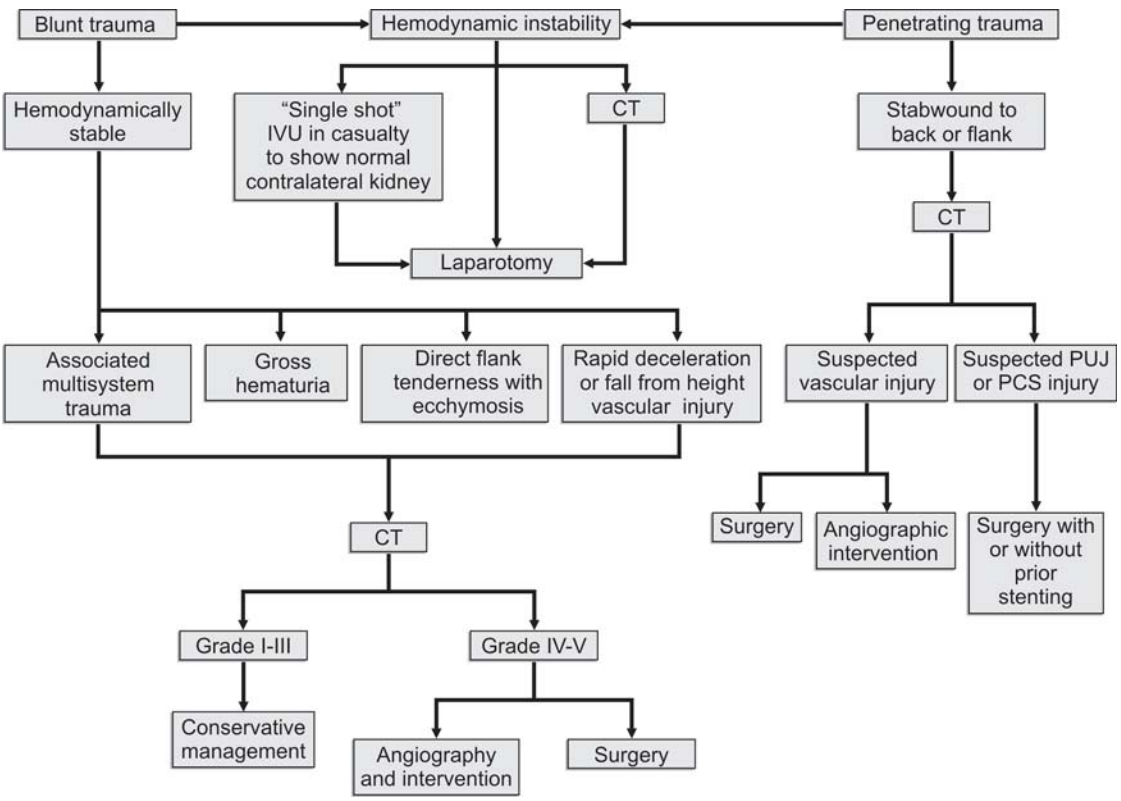

Fig. 19.1: Imaging work-up in suspected renal trauma

patient. In the setting of abdominal trauma it is usually done with FAST (Focussed Assessment with Sonography in Trauma) protocol. It is insensitive to detect retroperitoneal blood and renal parenchymal injuries.

Role of Intravenous Urography (IVU)

The role of intravenous urogram (IVU) in suspected renal trauma is limited. It has been replaced by CT which is now easily available and is more sensitive than IVU for parenchymal injuries, urinary contrast extravasation as well as for other abdominal injuries. However, IVU still has a role, depending on the preference of the surgeon, to establish gross function and evaluation of the uninjured contralateral kidney in hemodynamically unstable patients going for surgery and for urological evaluation of patients who are already in the operating room.[2,3] The technique followed is usually a tailored "single shot" study with a radiograph obtained 10 minutes after administration of intravenous contrast. However, if time and condition of patient permits, a precontrast plain radiograph and delayed radiographs may be taken for assessment of urinary contrast extravasation and for delayed function.

Role of CT

Contrast-enhanced CT scan is currently the investigation of choice for radiological evaluation of patients with blunt abdominal trauma.[4,5] It has replaced IVU for evaluation of renal trauma. The current trend of conservative management of blunt renal trauma has further enhanced the role of CT because 80 percent of renal injuries seen on CT are self-limiting. Helical CT avoids misregistration artifacts and allows a dual phase acquisition in two phases of renal enhancement. This technique distinguishes contrast extravasation due to vascular injury (seen in the early images), from that due to pelvi-calyceal injury (seen in the delayed images). Multislice CT has reduced the time required for CT evaluation still further and this is valuable in patients who are in need of immediate surgery.

CT accurately assesses all the criteria essential for management of renal trauma *viz.* extent of damaged nonviable tissue, amount of perirenal hemorrhage, extravasation of urine and evidence of renal pedicle or vascular injury.

CT technique: The technique needs to be tailored to the patient's specific condition.

- Noncontrast images of the kidney are optional.
- 100-150 ml of intravenous contrast is injected, ideally at a rate of 2-4 ml, using a pressure injector.
- The scanning parameters are variable depending upon the multislice capability of the scanner.
- The first set of images is obtained after 70-90 seconds delay.
- A second set of images is obtained after 3-5 minute delay for detection of pelvi-calyceal contrast extravasation.
- A further delayed set of images may be obtained after 10-15 min to delineate urinary contrast extravasation if there is significant perinephric or periureteric fluid.

Multiplanar reformatted images and three-dimensional images including CT urographic images can significantly aid in the evaluation.

Role of Angiography

CT can have characteristic findings in main renal artery occlusion or avulsion. Surgery can thus be undertaken solely on the basis of CT findings after blunt trauma.

The role of angiography is primarily in penetrating trauma with vascular injury suspected clinically or on CT. Also, late development of gross hematuria following blunt injury may signify an overlooked vascular injury or formation of a pseudoaneurysm. Catheter angiography accurately delineates the vessel changes which may occur due to injury, i.e. occlusion, laceration, pseudoaneurysm and AV fistula.

In this setting, there is an increasing role of therapeutic angiographic interventions as a nonsurgical therapy for transcatheter embolization of ongoing hemorrhage in renal trauma in hemodynamically stable patients and also for vascular complications of injury including post-traumatic pseudoaneurysms, arteriovenous fistulas, vascular stent placement for renal artery intimal injury and even thrombolysis of renal artery thrombosis.

Role of Retrograde Pyelography

Retrograde pyelography has a role in the specific setting of suspected renal pelvic, ureteropelvic junction or ureteral injury which has not been adequately excluded on CT. However, it is often not practically possible in emergent situation and also does not characterize renal injuries.

Role of Radionuclide Renal Scintigraphy

With widespread availability of CT, radionuclide scintigraphy is rarely used in acute trauma setting. It may have a role in demonstrating function of an injured kidney in patients allergic to iodinated contrast and in follow-up of repair of renovascular trauma.

Role of MRI

MRI may have a role in patients where CT is contraindicated or not available. However, it is usually not practical in acute trauma setting. It can demonstrate renal parenchymal injuries as well as renal function after contrast administration.

Radiological Findings

The most commonly accepted classification of renal injuries is given by the American Association for the Surgery of Trauma based on the depth of injury and involvement of vessels or the collecting system.[6] It classifies the renal trauma into 5 grades as follows:

Grade 1

Grade 1 renal injuries account for approximately 75-80 percent of all renal injuries. They include:

- *Contusion*: Focal illdefined area of hypodensity which shows decreased enhancement as compared to adjacent normal renal parenchyma (Figs 19.2A and B). They are differentiated from infarct by the presence of some contrast enhancement as contrast from latter which has absent contrast enhancement. A global contusion may show a striated nephrogram, or spidery collecting system (due to parenchymal edema).
- *Subcapsular hematoma*: A non-expanding, hyperattenuating (40-60 HU) fluid collection indenting the adjacent renal parenchyma (Figs 19.3A and B). It does not enhance on contrast administration.

Grade 2

Grade 2 renal injuries include:

- *Perinephric hematoma*: A nonexpanding illdefined hyperattenuating fluid collec-tion in perinephric space between the renal parenchyma and gerota's fascia (Figs 19.4A and B). It occurs after laceration of renal capsule.

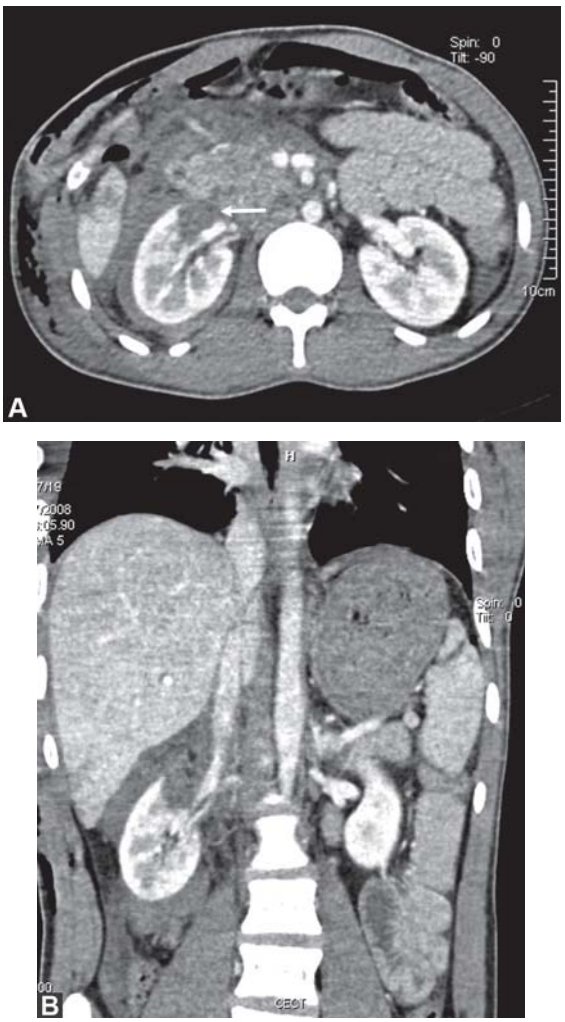

Figs 19.2A and B: Axial **(A)** and multiformatted coronal **(B)** CECT shows a focal hypodense area (arrows) in anterior part of right kidney suggestive of contusion

- *Laceration*: A superficial (< 1cm deep), irregular or linear, low attenuation area within the renal parenchyma which may contain blood or clot. It does not enhance after contrast administration.

Grade 3

Grade 3 renal injuries include:

- *Lacerations*: > 1 cm in depth but do not involve the collecting system (Fig. 19.5).

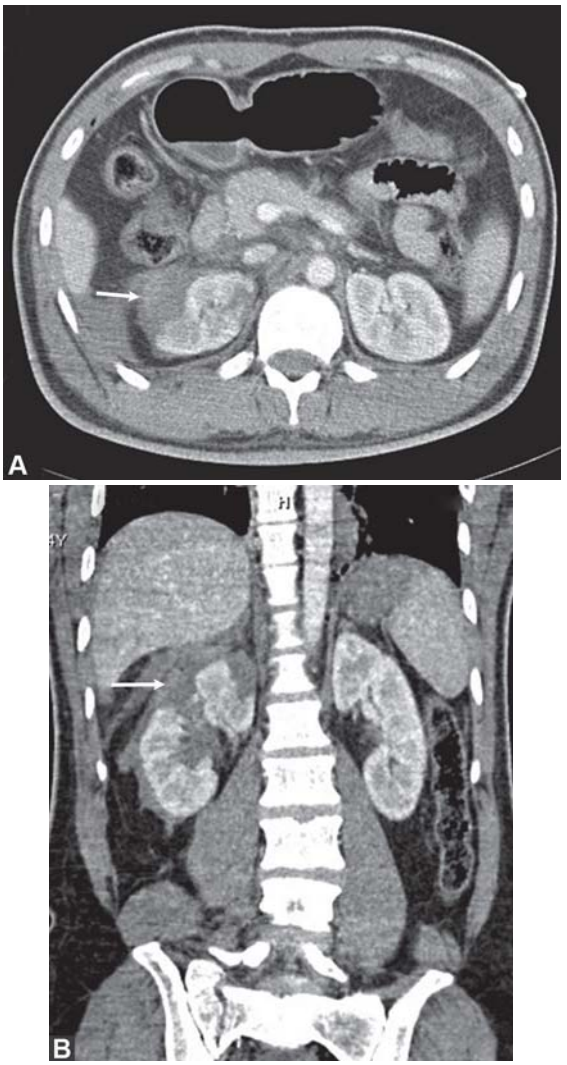

Figs 19.3A and B: Axial **(A)** and multiformatted coronal **(B)** CECT shows a hyperdense nonenhancing subcapsular hematoma (arrows)

Grade 4

Grade 4 renal injuries include:

- *Lacerations*: Deep lacerations extending through the kidney into the collecting system. It commonly leads to extravasation of urine and urinary contrast. Delayed phase CT in excretory phase is important to demonstrate urinary contrast extravasation (Figs 19.6A to D).

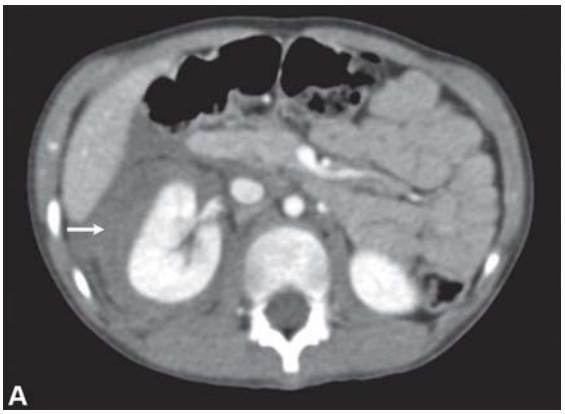

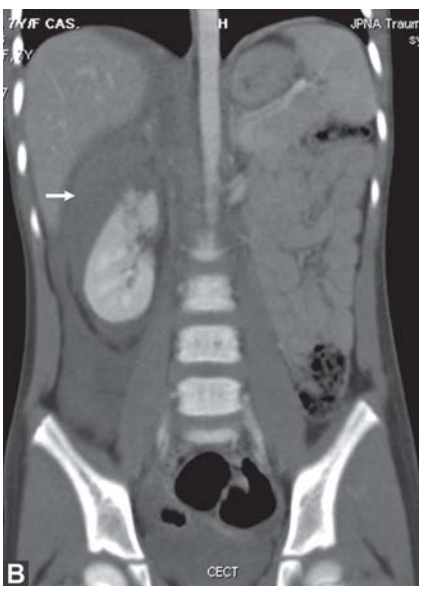

Figs 19.4A and B: Axial **(A)** and multiformatted coronal **(B)** CECT shows perinephric hematoma (arrows) around right kidney

- *Vessel injury*: Injury to main renal artery or vein with contained hemorrhage.
- *Segmental infarction without associated laceration*: Occurs due to dissection, thrombosis or laceration of segmental arteries. Usually associated with other renal injuries. On CT it is seen as peripherally based, well circumscribed, wedge shaped focal nonenhancing area through the renal parenchyma in a radial or segmental orientation (Figs 19.7A and B).

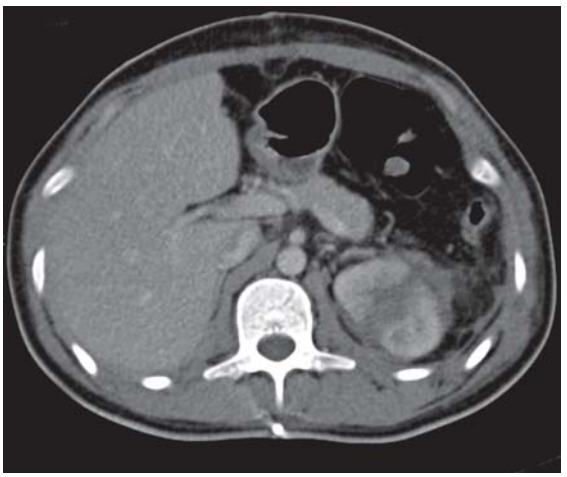

Fig. 19.5: Axial CECT abdomen shows a linear hypodense nonenhancing laceration involving upper pole of left kidney

Grade 5

Grade 5 renal injuries include:

- *Shattered kidney*: It refers to gross renal parenchymal disruption secondary to multiple renal lacerations associated with devitalized areas due to renal infarction (Figs 19.8A and B).
- *Devascularized kidney:*
  - Main renal artery may get thrombosed secondary to intimal tear following blunt renal trauma. It occurs due to stretching of the renal artery between the artery origin anchored to aorta and mobile kidney. It leads to global renal infarction (Figs 19.9A and B). CT reveals abrupt termination of renal artery after its origin with nonenhancing renal parenchyma except for a cortical rim sign which usually appears few days later and retrograde opacification of renal vein from IVC. Perinephric hematoma is characteristically absent in such cases. Renal angiography with thrombolysis may be done in selected cases, ideally within 12 hours after trauma or in a patient

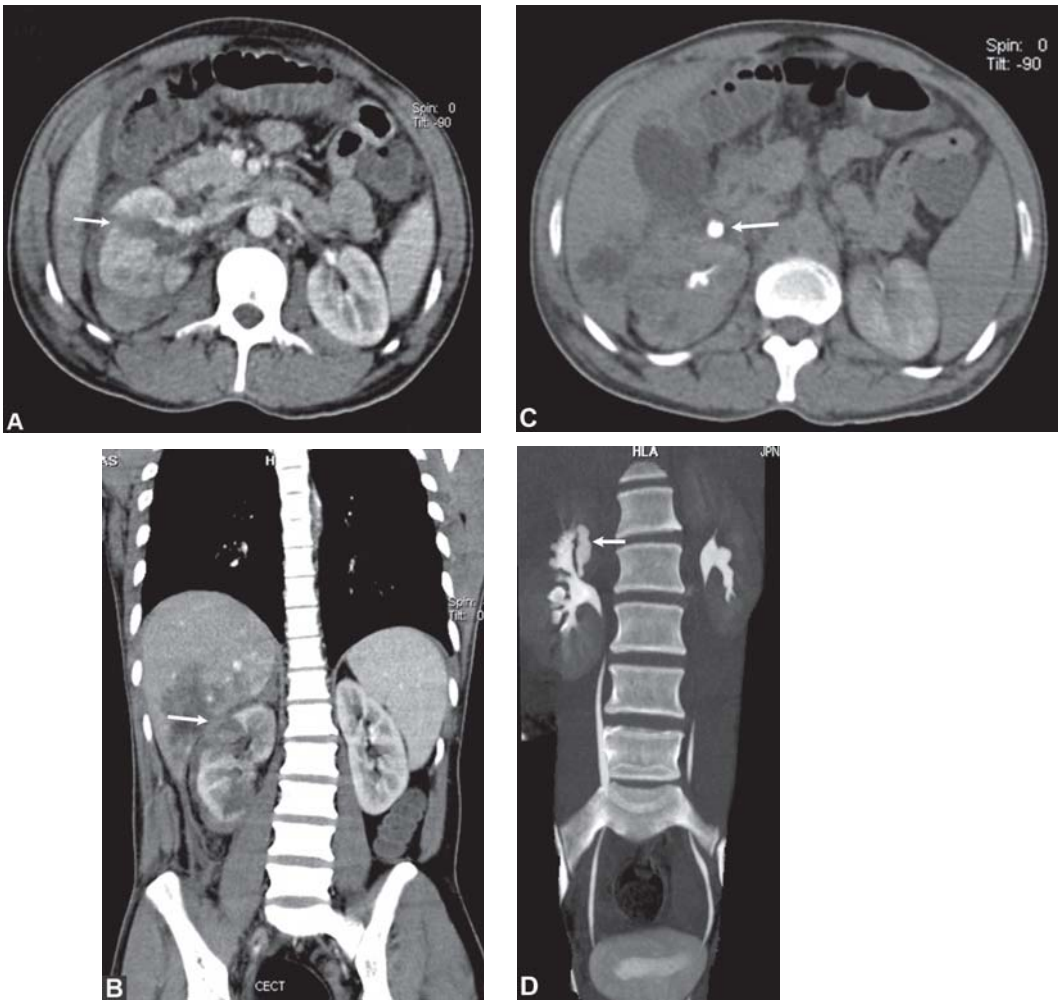

Figs 19.6A to D: Axial **(A)** and multiformatted coronal **(B)** CECT shows a deep laceration (arrows) in upper pole of right kidney extending into pelvicalyceal system with perinephric hematoma. Delayed phase axial CT **(C)** shows contrast lying outside the kidney on its anterior aspect signifying urinary contrast extravasation. Reformatted coronal MIP image **(D)** clearly shows the extravasated contrast from upper calyceal injury

with only one kidney or bilateral renal artery thrombosis.

- Renal artery may also get avulsed after blunt trauma. CT reveals global renal infarction with extensive medial perinephric hematoma with or without active arterial contrast extravasation.
- Renal vein may get lacerated or thrombosed. CT reveals intraluminal thrombus with features of renal vein occlusion including increased size of kidney, diminished or delayed enhancement and delayed excretion (Figs 19.10A and B).

- *Ureteropelvic junction injuries*: Complete avulsion or partial tear. The injury occurs primarily in children who lack retroperitoneal fat to cushion the kidney during rapid deceleration. Usually the

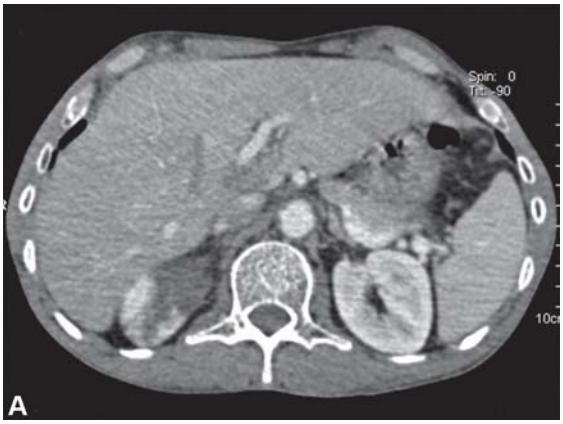

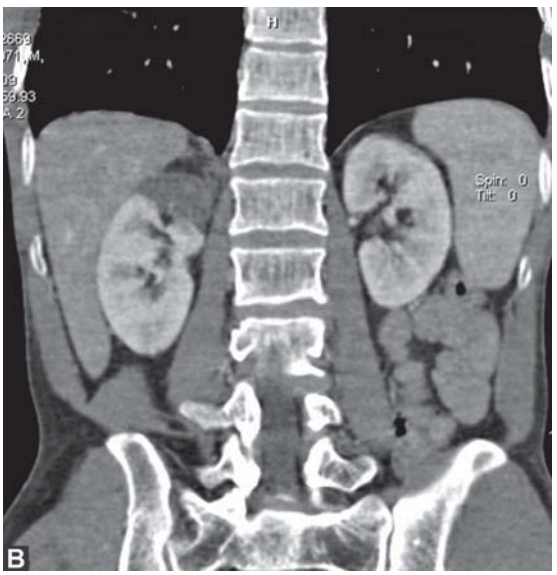

Figs 19.7A and B: Axial **(A)** and multiformatted coronal **(B)** CECT shows a well defined peripheral based wedge shaped nonenhancing area in upper pole of right kidney suggestive of a segmental infarct

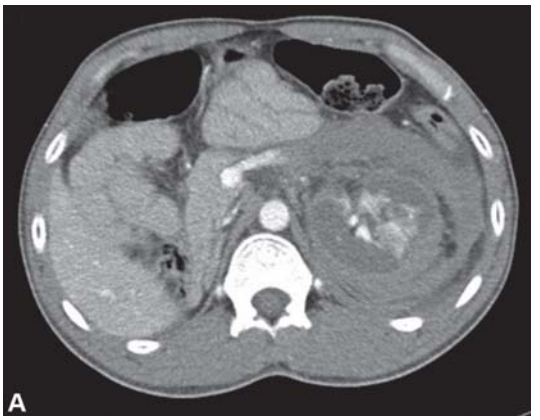

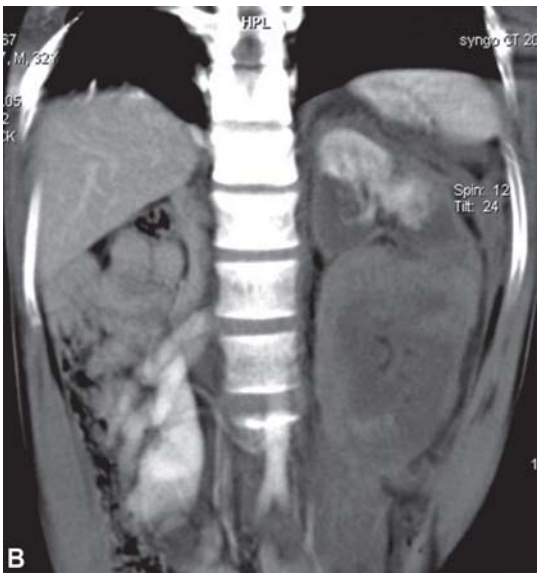

Figs 19.8A and B: Axial **(A)** and multiformatted coronal **(B)** CECT shows completely shattered left kidney with large devitalized (nonenhancing) areas

patient presents late with fever, flank pain and anuria. CT shows medial or circumferential urinoma with extravasation of urinary contrast into the urinoma on delayed phase images (Figs 19.11A and B). Partial tear can be differentiated from complete avulsion by presence of contrast within the distal ureter. Retrograde pyelography may be required for definitive diagnosis to demonstrate the distal ureter if CT or IVU fail to demonstrate distal ureteric filling.

Vascular Contrast Extravasation

It is seen as focal or diffuse areas of enhancement paralleling the attenuation of vessel seen within the parenchyma or in the perinephric hematoma (Figs 19.12A to C). It may be contained hemorrhage or pseudoaneurysm which is well circumscribed and

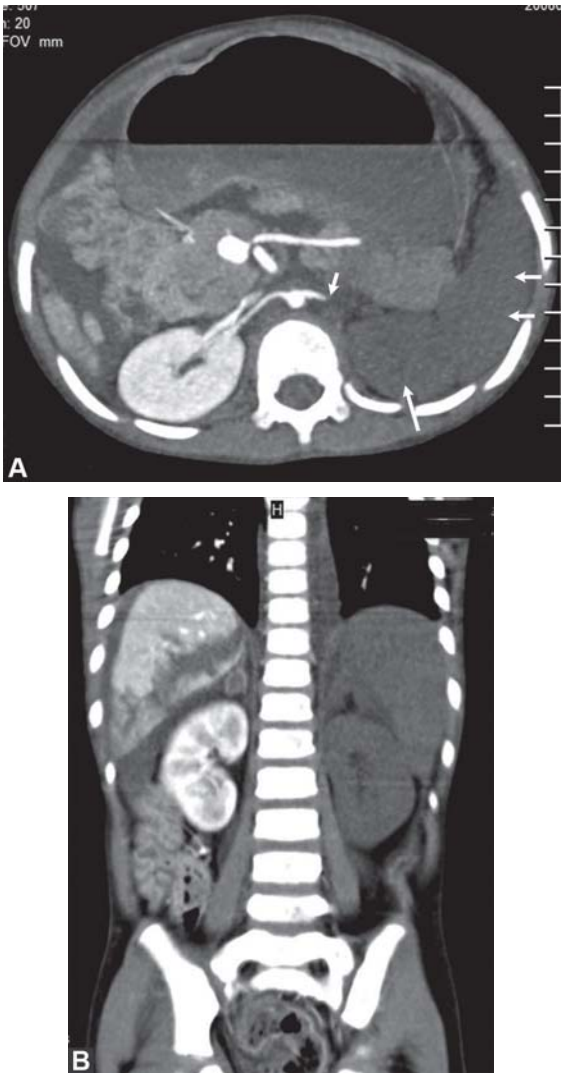

Figs 19.9A and B: Axial MIP **(A)** and multiformatted coronal **(B)** CECT shows nonenhancing left kidney (long arrow) with abrupt termination of left renal artery (short arrow). Also note devascularized spleen (medium arrows in **(A)** and large liver laceration **(B)**

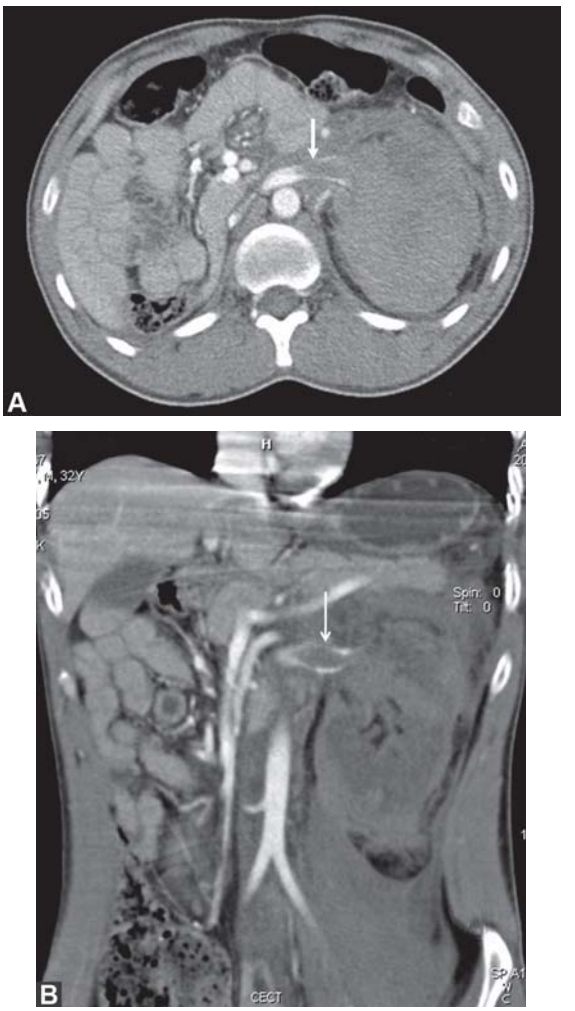

Figs 19.10A and B: Axial **(A)** and multiformatted coronal **(B)** CECT shows an enlarged nonenhancing left kidney with large perinephric hematoma with a hypodense thrombus in the left main renal vein (arrows)

seen usually within a laceration. Active hemorrhage is illdefined, within an associated acute hematoma which tends to track into surrounding tissues on delayed phase images. When seen, it indicates the need for urgent surgical or angiographic intervention.

Renal Trauma with Pre-existing Abnormality

Kidney harboring a pre-existing abnormality is at more risk for injury in blunt abdominal trauma especially in children.[7] Hydronephrosis or extrarenal pelvis is at more risk of rupture. Cysts and tumors can also frequently hemorrhage after trauma. An

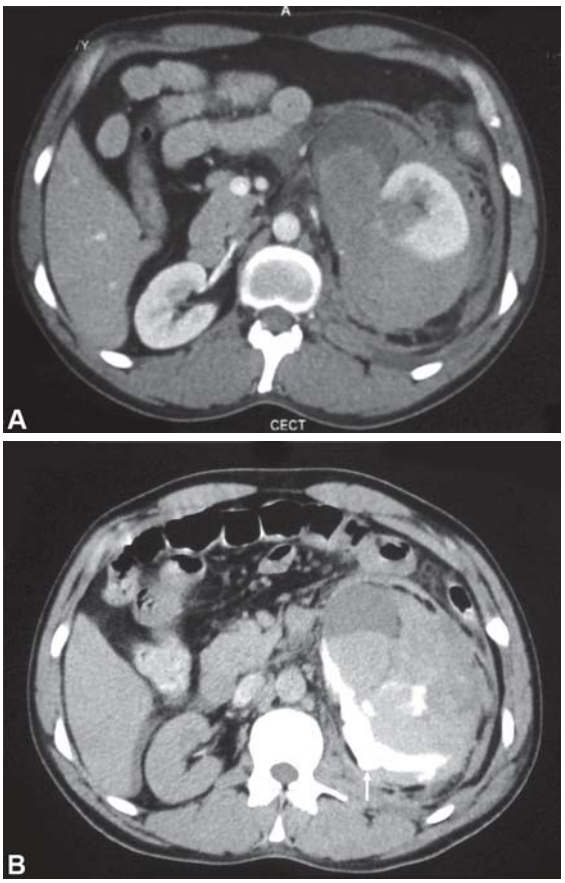

Figs 19.11A and B: Axial CECT abdomen **(A)** shows extensive left perirenal hematoma/fluid collection. Delayed phase axial image **(B)** shows urinary contrast extravasation in medial perinephric space (arrow) signifying renal pelvic avulsion

ectopic or horseshoe kidney is also more prone to trauma because it is less protected (Figs 19.13A and B).

Management of Renal Trauma

The classification of renal trauma into grades correlates with the need for surgery. In general the trend is towards nonoperative management for all but most severe injuries.[8] Grade 1-3 injuries, which constitute >90 percent of all renal injuries, are almost always managed conservatively. The only absolute indication for active intervention in these

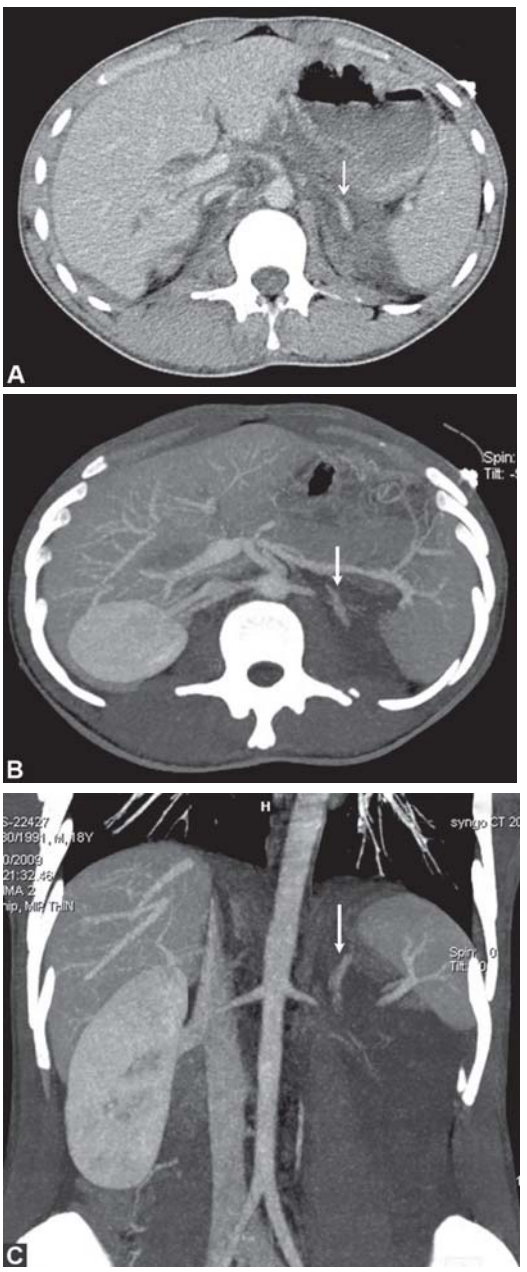

Figs 19.12A to C: Axial CECT abdomen **(A)** shows a focal hyperattenuating area (arrow) in left suprarenal location within a hypodense hematoma. Axial **(B)** and reformatted coronal **(B)** MIP images clearly shows the arterial contrast extravasation (arrows) within the left perinephric hematoma. Note the abrupt termination of transected left renal artery and nonenhancing left kidney

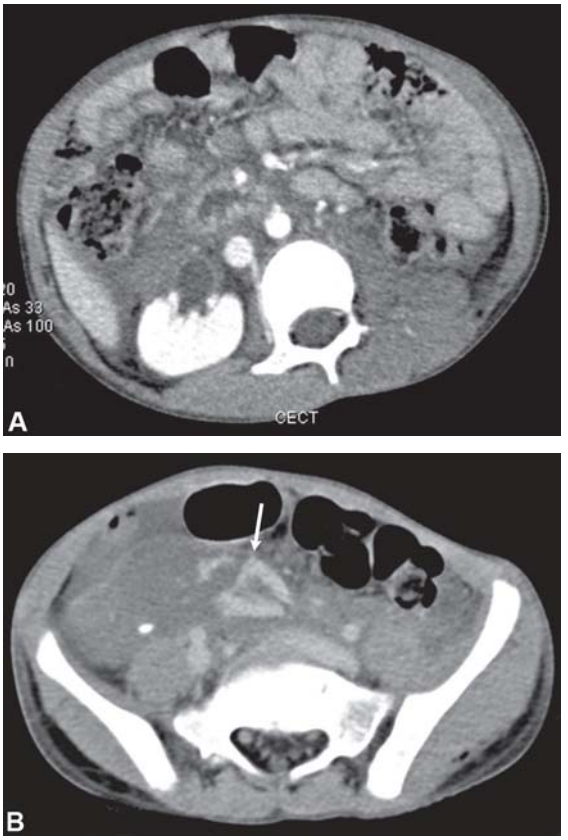

Figs 19.13A and B: Axial CECT (A) at the level of kidneys shows left kidney is not present in left renal fossa. Axial image through the pelvis (B) shows extensive lacerations of ectopic left kidney (arrow)

grade patients is presence of life-threatening active hemorrhage which may be dealt with angiographic embolization (Figs 19.14A and B) or surgical exploration.[4] Most of grade 4 injuries can also be managed conservatively. Even large urinary extravasations resolve spontaneously on conservative management sometimes helped by percutaneous drainage of these collections with or without percutaneous nephrostomy and/or ureteric stent placement.[3,9] If they fail to resolve, surgical repair may be warranted. Grade 4 injuries with significant devitalized tissue (> 50%) especially with concomitant injuries or urine leak usually require surgical debridement or

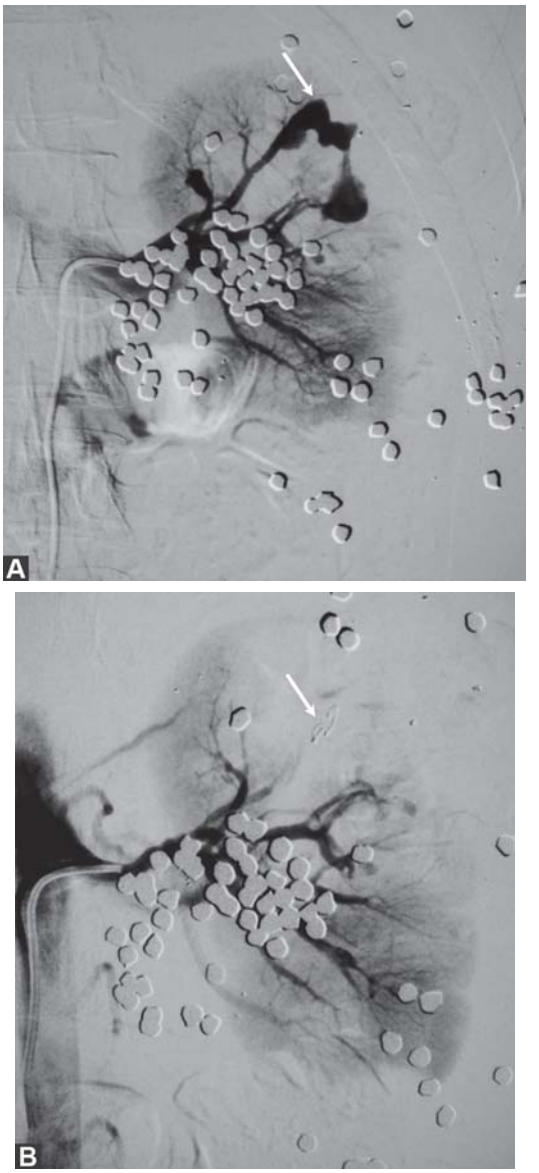

Figs 19.14A and B: DSA image **(A)** of selective left renal artery injection in a patient injured with multiple pellets shows pseudoaneurysm formation with active bleed (arrow) in upper pole of left kidney. The involved upper polar segmental branch was selectively embolized with coil (arrow in **B**) resulting in thrombosis of pseudoaneurysm

repair to prevent later development of urinoma, abscess or infection which may warrant nephrectomy. With aggressive

monitoring and increasing use of angiographic embolisation and percutaneous drainage, overall < 10 percent of grade 3-4 injuries require surgical intervention.[9] Grade 5 injuries with complete avulsion of ureteropelvic junction require surgical repair whereas partial tears may resolve on conservative management or stenting and proximal drainage.[2,3] Devascularization of kidney may be managed conservatively in a stable patient but requires nephrectomy in case of active bleed or major parenchymal disruption. Surgical repair or angiographic thrombolysis of acute renal artery thrombosis can be done to try to preserve the renal function but is shown to have best results usually within few hours of injury.[10] Renal hypertension developing weeks to months after renal trauma is a frequent finding which usually can be managed medically but may occasionally require nephrectomy.

To summarize, the only absolute indication for surgical exploration (or angiographic embolisation) is life-threatening active hemorrhage.[4] Relative indications for operative management include the presence of (a) > 50 percent of renal parenchyma devitalization, (b) arterial thrombosis, and (c) urinary extravasation which is not controlled by conservative management including proximal drainage and stenting.

URETERAL TRAUMA

Iatrogenic surgical trauma accounts for 95 percent of all ureteral injuries and usually occurs in association with gynecological procedures[11]. In gynecological surgery, majority of ureteral injuries are discovered postoperatively (84%) with an average delay of 65 days after the procedure. The patients present with flank pain, fever, hematuria and occasionally anuria. The emergence of endoscopic and laparoscopic surgery and endourological diagnostic and therapeutic interventions in the last two decades have further contributed to the increased incidence of iatrogenic ureteral trauma.[12] In urologic surgery, iatrogenic ureteral injuries occur in open surgery in 21 percent and 79 percent in endoscopic procedures. Recognition of the injury during surgery or the endoscopic procedure leads to immediate repair or placement of double J-stent for conservative management.

Gunshot wound, stabbing, and blunt trauma account for rest 5 percent of the ureteral injuries. Penetrating trauma to ureter is frequently associated with injuries to other organs.[13] Hematuria is usually present but may be absent. Blunt trauma in children with deceleration injury may occasionally lead to ureteral avulsion.

Imaging Work-up

Role of IVU

Traditionally IVU has been used as a follow up study to identify ureteric injury following trauma. However with widespread availability of CT, its role has become limited. IVU still has a role in the form of one-shot study in unstable patients who require emergency surgery.[14] IVU demonstrates extravasation at the site of injury or obstruction proximal to the site of injury (Fig. 19.15). Patients in whom ureteral injury is missed, urinary extravasation, hydronephrosis and abscess formation can result. Demonstration of a mature fistulous tract or a large urinoma at a later stage is much more likely (90-100%). Hydronephrosis is seen at a later stage in 90 percent patients after ureteral injury. Ureteral avulsion may be diagnosed by contrast extravasation medial to the kidney.

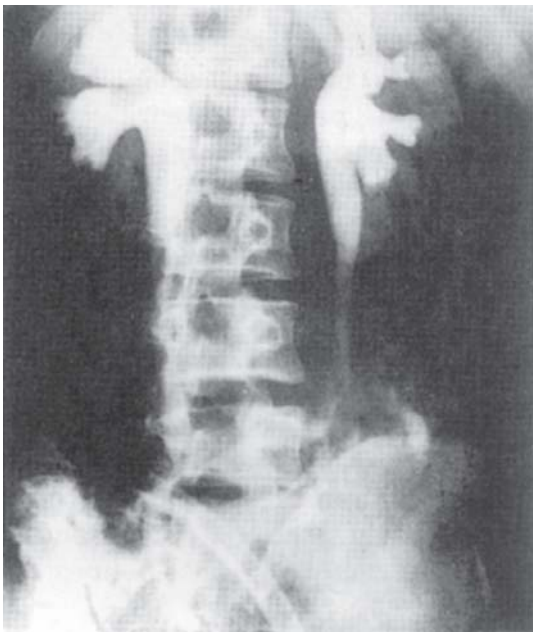

Fig. 19.15: IVU showing left ureteral injury with extravasation of contrast opposite L5 vertebra

Role of CT

Delayed phase CT has an important role in detection of ureter avulsion at UPJ in acute blunt trauma.[15] The diagnosis depends on demonstration of contrast extravasation medial to the kidney and lack of distal ureter opacification. CT is also useful in accurate assessment of the size of the associated perirenal hematoma which helps the surgeon in deciding on the need for surgery.

Role of Antegrade and Retrograde Ureterograms

Ureterograms obtained *via* the antegrade or retrograde route are considered the gold standard for confirming the presence of ureteral injury. The ureterogram clearly defines the type and location of the injury as also its magnitude. Any associated fistulae and communicating urinomas are also delineated.

Classification

Ureteral injuries have been classified into following grades:[16]

Grade 1: hematoma only
Grade 2: laceration < 50 percent of circumference
Grade 3: laceration > 50 percent of circumference
Grade 4: complete tear < 2 cm of devascularization
Grade5: complete tear > 2 cm of devascularization

Management

Injuries detected during surgery are treated immediately by either surgical repair or endourologic interventions.[16,17] Injuries recognized later are treated by percutaneous nephrostomy for urinary diversion and antegrade or retrograde stent placement. Stenting may be preceded by balloon dilatation or endoureterectomy for strictures. In ureteral avulsion, stenting is coupled with drainage of urinoma which prevents fibrosis and facilitates passage of guide wire antegradely across the dehiscence. Fistulae are also managed with nephrostomy and stenting. Disruption of pelvic ureter can be managed by antegrade ureteroneocystostomy and stenting for 1-3 months for which a curved transjugular intrahepatic portosystemic shunt (TIPS) needle sheath can be used.

BLADDER TRAUMA

Bladder injury is relatively rare and constitutes only 2 percent of all abdominal injuries that require surgical repair. It may be due to blunt, penetrating or iatrogenic trauma. Majority of the patients of bladder trauma have associated fracture of pelvis most commonly of the anterior pubic arch.[18] A distended bladder is more prone to injury.

The patient presents with suprapubic pain or tenderness and/or hematuria. In such cases the recommendation is to first exclude urethral injury by a retrograde urethrography (RGU) followed by insertion of a foley's catheter. If a urethral injury is found, a suprapubic cystostomy is usually done. This is followed by cystography which may be conventional technique or CT cystography. However with increasing use of CT scan, CT cystography has become the investigation of choice which can be done at the same sitting if the patient is undergoing CT scan for abdominal injuries.[19] Delayed scanning of the bladder after intravenous contrast administration so as to allow the contrast excreted by kidneys to opacify the bladder is no substitute for CT cystography as it has been shown to miss a significant number of bladder ruptures.[19,20] Conventional cystography may be done if CT is not available.

Cystography

Conventional Cystography

Technique

- 300-400 ml of dilute contrast is instilled into the bladder *via* the urethral (if urethral injury excluded) or the suprapubic route.
- The initial film is taken after 100 ml contrast is instilled to check gross extravasation.
- Films are then taken after the entire contrast is instilled.
- A postdrainage film excludes extravasation hidden by a distended bladder.

CT Cystography

The technique recommended is retrograde filling of the bladder with contrast (same as with conventional cystography) followed by a computed tomogram of the pelvis. With this technique, the diagnostic accuracy is comparable to that of conventional cystography. The CT cystography may be done at the time of initial examination simultaneously with acquisition of abdomen and pelvis after intravenous contrast administration. Postdrainage scans are not required. According to current recommendations, CT cystography should be done in all patients with known pelvic fractures or in patients with gross hematuria or severe pelvic trauma with no known pelvic fractures.

Classification

Blunt Trauma

A classification of bladder injury after blunt pelvic trauma has been described by Sandler et al.[18]

Type 1 Bladder contusion
Type 2 Intraperitoneal injury
Type 3 Interstitial bladder injury
Type 4 Extraperitoneal injury
  A Simple
  B Complex
Type 5 Combined bladder injury

Bladder contusion (Type 1): This consists of a self-limiting, incomplete mural tear with localized echymosis. CT cystography is normal, showing a well-distended uniformly hyperattenuating thin walled bladder with no contrast leakage. No specific therapy is required. A perivesical hematoma may be associated with major pelvic fractures even when no evidence of actual bladder tear is seen on cystography. Accumulated blood compresses upon the extraperitoneal part of the bladder narrowing it at the base. An "inverted tear drop" or "inverted pear sign" may be seen on cystogram.

Intraperitoneal injury (Type 2): Intraperitoneal rupture usually occurs after a blow to the lower abdomen in the presence of distended bladder. Rupture occurs at the dome due to increased intravesical pressure. This is the weakest point of the bladder and also the peritonealized portion of the bladder wall. Urine will thus enter the peritoneal cavity. On cystography, contrast material may be seen outlining the abdominal viscera, loops of bowel, mesenteric folds, paracolic gutters or pouch of Douglas (Figs 19.16A and B). The contrast material may track to upper abdomen also. The locations of free intraperitoneal contrast are predictable with well-defined boundaries as compared to extraperitoneal rupture.

Interstitial injury (Type 3): This represents a dissecting rupture of the bladder wall without frank perforation. On CT cystography a mural hematoma/defect may be seen. Occasionally intramural contrast may be seen. But there is no contrast extravasation outside the bladder. Such defects may involve both extraperitoneal and intraperitoneal portions of the bladder wall. Hence interstitial rupture was designated as a separate category in this classification.

Extraperitoneal injury (Type 4): This is the most common injury to the bladder (80-90% of cases) and usually occurs in association with a fractured pelvis or in penetrating trauma. Earlier it was thought that the tear was caused by direct penetration of the bladder by bone fragments. However, now it is postulated that this type of injury may be either a type of bursting or shearing injury resulting from the force of pelvic ring disruption.

In **simple** (Type 4 A) extraperitoneal rupture, extravasation is confined to the perivesical space. On CT cystography, flame-shaped areas of extravasation are noted in the perivesical spaces and in the prevesical space (space of retzius) where it can track cranially upto umbilicus. The ill-defined contrast in the prevesical space is said to have a 'molar tooth' appearance.

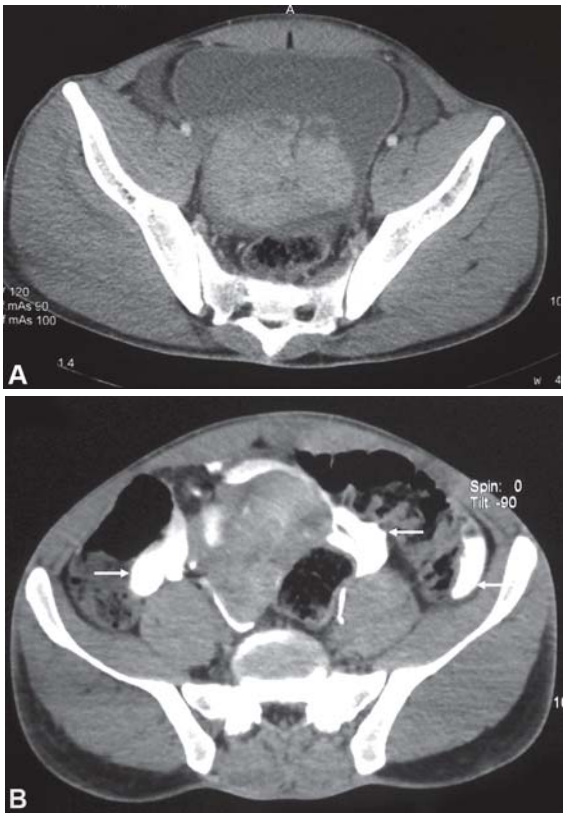

Figs 19.16A and B: Axial CECT image **(A)** through urinary bladder shows a hyperdense clot within the bladder. Axial CT cystography image **(B)** shows extravasation of contrast outside the bladder in the peritoneal cavity outlining the bowel loops (arrows)

A **complex** (Type 4B) extraperitoneal rupture is diagnosed when contrast extravasation extends beyond the perivesical space into the scrotum, thigh, perineum, hip joint and anterior abdominal wall (Fig. 19.17). It occurs secondary to rupture of urogenital diaphragm. Contrast may also track upwards into the paranephric spaces.

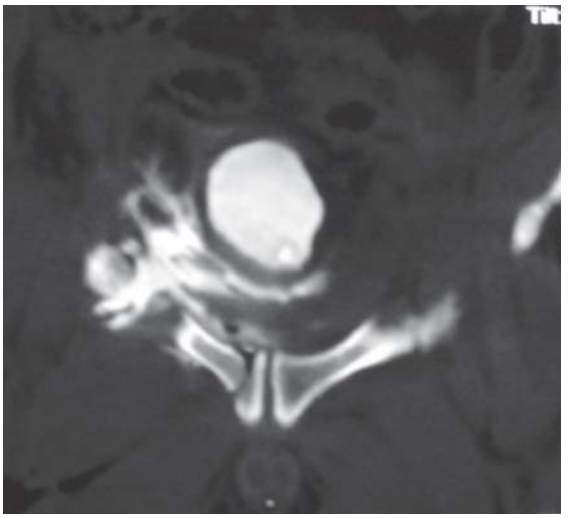

Fig. 19.17: Reformatted coronal MIP CT cystography image shows complex extraperitoneal rupture of urinary bladder with contrast lying in extraperitoneal spaces in perineum extending into right hip joint

It is important to differentiate intraperitoneal rupture from extraperitoneal rupture of bladder because the former requires surgical repair where the latter is usually managed conservatively with foley's catheter placement.

Combined extra and intraperitoneal bladder injury (Type 5): An injury may result in rupture of both intraperitoneal and extraperitoneal portions of the bladder wall. On CT cystography, both patterns of contrast extravasation may be seen.

Penetrating Bladder Trauma

Injury may result from gunshot or knife wounds and may result in extraperitoneal, intraperitoneal or combined bladder injury. There is a high incidence of associated bowel or other visceral injury and exploratory surgery is required in virtually every patient.

Iatrogenic Bladder Trauma

Bladder injuries may be due to urologic, gynecologic or obstetric procedures. Bladder perforations or vesicovaginal and vesicouterine fistulae may form. Cystography and hysterosalpingography help in the diagnosis. Migration of surgical devices like drains, catheters, contraceptives or orthopedic prostheses can sometimes perforate the bladder.

Management of Bladder Trauma

Type 1, 3 and 4 injuries are managed conservatively with placement of a foleys catheter. However intraperitoneal rupture of bladder requires surgical repair. Hence type 2 and 5 injuries are managed surgically.

URETHRAL TRAUMA

Posterior urethral injuries result from pelvic fractures and gunshot wounds. Injury associated with pelvic fracture mostly involves the urethra near the urogenital diaphragm. Anterior urethral injuries are much less common and are more commonly due to iatrogenic cause, straddle injury or gunshot wound. The lifelong consequences in males include incontinence, strictures and impo-tence. Female urethra injury is rare.

The clinical signs suggestive of urethral injury in a male patient with pelvic trauma include gross hematuria, blood at urethral meatus, inability to void, swelling or hematoma of the perineum or penis and a high riding prostate on per rectal examination associated with pelvic fracture.[21] The clinical signs in a female patient include difficulty in micturition, blood at meatus, hematuria, labial edema, vaginal bleeding or urine leak per rectum. If the above signs are present in a patient with pelvic trauma, urethrography should be done for evaluation of urethra before insertion of a Foleys catheter.

Radiology

The urethra is best evaluated with retrograde urethrography or voiding cystourethrography.

Technique of Urethrography

- Dynamic retrograde urethrography, ideally under fluoroscopy, is used for the evaluation of urethral injury.
- Steep oblique films are obtained, at the end of injection of 25-30 ml of 50 percent contrast.
- If the urethra appears intact, a catheter is passed into the bladder for cystography and a voiding urethrogram is obtained.

Blunt Urethral Trauma

Urethral injuries are classified anatomically as anterior or posterior urethral injuries. Posterior urethral injury occurs in 4-14 percent of patients with pelvic fracture and upto 20 percent of these have associated bladder laceration.[22] Anterior urethral injury commonly results from straddle pelvic injury secondary to the patient falling astride a blunt object or direct blow to the perineum. However, more commonly, anterior urethral injuries may be iatrogenic due to instrumentation.

Posterior Urethral Injuries Associated with Pelvic Fracture

- Commonly, prostato-membranous urethral injury above the urogenital diaphragm results.
- A high riding urinary bladder is seen on excretory urography. This is due to disruption of puboprostatic ligaments and hematoma in retropubic and perivesical spaces.
- Contrast extravasation will be seen adjacent to the posterior urethra and sometimes into the pelvic extraperitoneal space.

Anterior Urethral Injury

Straddle injuries resulting from the patient falling astride a blunt object or direct blow to the perineum may lead to anterior, mostly bulbous, urethral injuries. More commonly, anterior urethral injuries may be iatrogenic due to instrumentation. In partial rupture, extravasation of contrast occurs on urethrogram but continuity of the urethra is preserved. In complete rupture, no contrast is seen in the proximal urethra. Venous intravasation is seen commonly. Treatment is by suprapubic urinary diversion and delayed surgery.

Classification

Based on findings of urethrography, the following types of urethral injuries have been described by Goldman *et al*[23] who have modified the initial classification given by Colapinto and McCallum.[24]

Type I

- Stretched, but intact posterior urethra is seen (Fig. 19.18).
- In this type of injury the prostate is detached from the urogenital

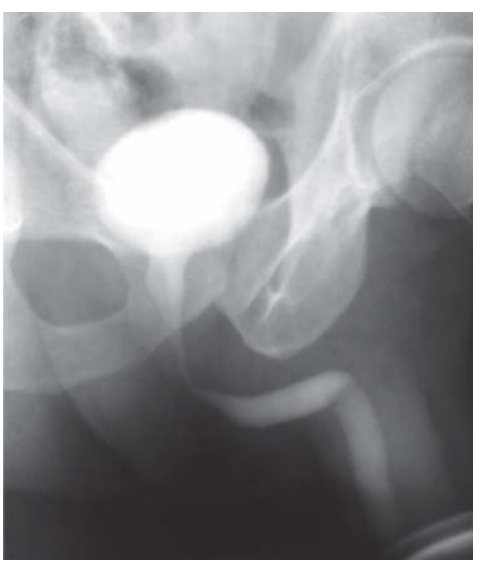

Fig. 19.18: MCU shows a stretched posterior urethra in a patient with multiple pelvic fractures

diaphragm with an elevated bladder seen on cystography due to retropubic hematoma and rupture of puboprostatic ligaments.

- No extravasation is seen on the urethrogram.

Type II

- Seen in around 15 percent of cases.
- Urethra is ruptured at the membrano-prostatic junction above the urogenital diaphragm which is intact (Fig. 19.19).
- Contrast extravasation is seen into the pelvic extraperitoneal space above the urogenital diaphragm but not in the perineum.

Type III

- Most common type.
- Membrano-bulbous urethral rupture is seen with disruption of urogenital diaphragm.
- Contrast extravasation both above and below urogenital diaphragm, i.e. into pelvis and the perineum (Fig. 19.20).

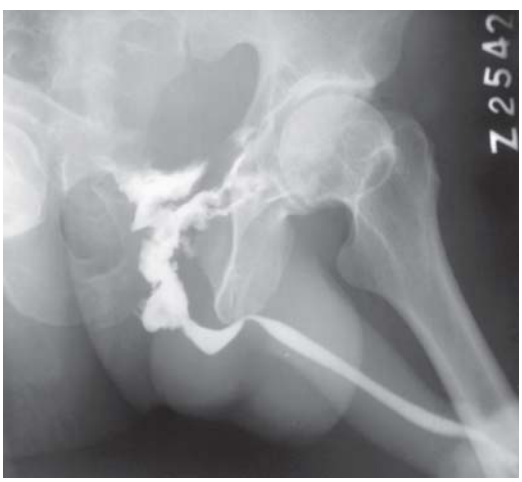

Fig. 19.19: RGU shows a type II urethral injury with contrast extravasation from posterior urethra above the urogenital diaphragm

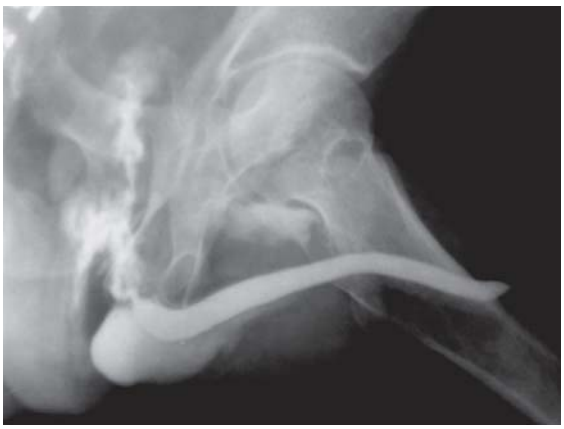

Fig. 19.20: RGU shows a type III urethral injury with contrast extravasation from posterior urethra both above and below the urogenital diaphragm

Type IV

- There is bladder neck injury with extension into the posterior urethra.
- Contrast extravasation is seen in the pelvic extraperitoneal space with disruption of bladder neck (Fig. 19.21).

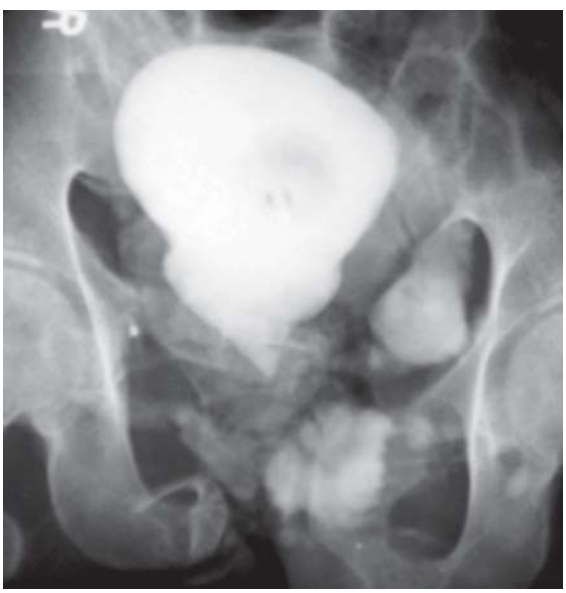

Fig. 19.21: MCU showing elongated injured bladder neck with contrast extravasation around the prostatic urethra

Type IVa
- Extraperitoneal bladder base injury simulating a bladder neck injury.
- Radiologically indistinguishable from type IV injury.

Type V
- Caused by straddle injury.
- Anterior urethra, most commonly bulbous urethra, injury is seen which may be partial or complete.
- Contrast extravasation is seen into the penile soft tissues (Fig. 19.22).

Management of Urethral Trauma

Type 1 injuries are managed conservatively with placement of a urethral or suprapubic catheter. In general partial disruptions are also managed conservatively with suprapubic or urethral catheterization whereas complete disruptions of the urethra are managed either by endoscopic realignment or delayed urethroplasty. Bladder neck injuries involve internal sphincter and hence are treated surgically to prevent development of incontinence. However, type IVa injury may be treated conservatively since it does not involve the bladder neck.

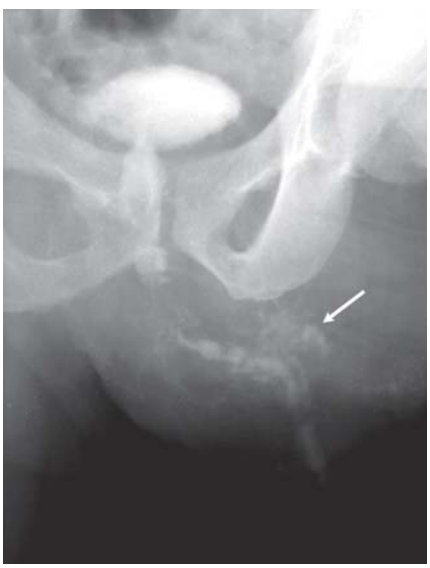

Fig. 19.22: RGU showing contrast extravasation in penile tissues from anterior urethral injury (arrow)

Evaluation before Delayed Urethroplasty

- A combined voiding cystourethrogram and a retrograde urethrogram is obtained.
- The bladder is filled with 30 percent dilute contrast through the suprapubic cystostomy.
- The patient is then asked to void.
- A simultaneous retrograde urethrogram is performed.
- This technique demonstrates proximal and distal extent of the stricture. This enables the surgeon to decide between a transperineal and transpubic approach for urethroplasty.
- Recently reports have shown the potential of MRI to demonstrate length of the urethral injury along with amount of displacement of the prostatic apex. This information is helpful in preoperative planning of the surgical approach.

Penetrating Injury

Penetrating trauma to the urethra may be secondary to knife or gunshot wounds. The diagnosis is established by retrograde urethrography. Early surgery is the treatment of choice.

Iatrogenic Injury

Iatrogenic urethral injury may result from pelvic surgery, urethral instrumentation or indwelling catheters.

Female Urethra

Injury to the female urethra is rare because of its mobility. Excretory urography or

cystourethrography may show extravasation of contrast at the site of rupture.

REFERENCES

1. McAninch JW. Renal injuries. In: Gillenwater JY, Grayhack JT, Howards SS, Duckett JW (Eds). Adult and pediatric urology. 3rd ed. St. Louis, Mo: Mosby 1996;539-53.
2. Kawashima A, Sandler CM, Corl FM, et al. Imaging of renal trauma: A comprehensive review. Radiographics 2001;21:557-74.
3. Smith JK, Kenny PJ. Imaging of renal trauma. Radiol Clin N Am 2003;41:1019-35.
4. Harris AC, Zwirewich CV, Lyburn ID, Torreggiani WC, Marchinkow LO. CT findings in blunt renal trauma. Radiographics 2001; 21:S201-S14.
5. Park SJ, Kim JK, Kim KW, Cho KS. MDCT findings of renal trauma. AJR 2006;187:541-47.
6. Moore EE, Shackford SR, Patcher HL, et al. Organ injury scaling: Spleen, liver and kidney. J trauma 2001;50:195-200.
7. Pollack HM, Wein AJ. Imaging of renal trauma. Radiology 1989;172:297-308.
8. Knudson MM, Maull KI. Nonoperative management of solid organ injuries:past, present and future. Surg Clin of N Am 1999;79:1357-71.
9. Brandes SB, McAninch JW. Reconstructive surgery for trauma of the upper urinary tract. Urol Clin of N Am 1999;26:183-99.
10. Peterson NJ. Genitourinary trauma. In: Feliciano DV, Moore EE, Mattox KL (Eds). Trauma (3rd edn). Stamford, Conn: Appleton & Lange, 1996; 661-94.
11. Assimos DG, Patterson LC, Taylor CL. Changing incidence and etiology of iatrogenic ureteral injuries. J Urol 1994;152:2240-46.
12. Campbell EW Jr, Filderman S, Jacobs SC. Ureteral injury due to blunt and penetrating trauma. Urology 1992;40:216-20.
13. Pitts JC, Peterson NE. Penetrating injuries of the ureter. J Trauma 1981;21:978-82.
14. Lynch TH, Matnz-NL, Las, et al. European Association of urology: Guidelines on urological trauma. Eur Urol 2005;47:1-15.
15. Kenney PJ, Panicek DM, Witanowski LS. Computed tomography of ureteral disruption. J Comput Assit Tomogr 1987;11:480-84.
16. Bent C, Iyngkaran T, Power N, et al. Urological injuries following trauma. Clin Radiol 2008; 63:1361-71.
17. Lask D, Abarbanel J, Luttwak Z, et al. Changing trends in the management of iatrogenic ureteral injuries. J Urol 1995;154:1693-95.
18. Sandler CM, Hall JT, Rodriguez MB, et al. Bladder injury in blunt pelvic trauma. Radiology 1986; 158:633-38.
19. Vaccaro JP and Brody JM. CT cystography in the evaluation of major bladder trauma. Radiographics 2000;20:1373-81.
20. Power N, Ryan S, Hamilton P. Computed tomographic cystography in bladder trauma: pictorial essay. Can Assoc Radiol J 2004;55(5):304-08.
21. Patel U. Lower urinary tract trauma. In: Patel U, Rickards D, eds. Imaging and urodynamics of the lower urinary tract. London, England: Taylor & Francis, 2005;115-21.
22. Kawashima A, Sandler CM, Wasserman NF, LeRoy AJ, King BF, Goldman SM. Imaging of urethral disease: A pictorial review. Radiographics 2004;24:S195-S216.
23. Goldman SM, Sandler CM, Corriere JN Jr, et al. Blunt urethral trauma: A unified anatomical mechanical classification. J Urol 1997;157:85-89.
24. Colapinto V, McCallum RW. Injury to the male posterior urethra in fractured pelvis—a new classification. J Urol 1977; 118:575-80.

Chapter 20

Imaging the Adrenal Gland

Raju Sharma, Ashu Seith Bhalla, Arun Kumar Gupta

INTRODUCTION

Thomas Addison first described a clinical entity resulting from adrenal dysfunction in 1855 but it took nearly half a century for the scientific community to accept that adrenals are essential to life. Remarkable progress has since been made in defining the structure and function of the adrenal gland. Adrenal glands are small but their common involvement in many disease processes has made cross-sectional imaging modalities essential to detect abnormal morphological and functional alterations. Radiology also plays a critical role in the characterization of adrenal mass lesions. Therefore, it is important to first understand the normal anatomy and functional characteristics of the adrenal gland.

ANATOMY AND PHYSIOLOGY

The adrenal gland is named for its location adjacent to the kidney. It lies within perirenal fascia, embedded in perirenal fat. Each gland measures 3 to 5 cm in length, 2 to 3 cm in width, 5.0 mm in thickness and weighs around 3.5 to 5.0 gm. Both glands differ in shape. The right adrenal is pyramidal in shape and its relations are liver laterally, upper pole of right kidney inferiorly, right crus of diaphragm posteromedially and inferior vena cava anteromedially. The left adrenal gland is crescent-shaped and its relations are upper pole of left kidney posterolaterally, left crus of diaphragm posteromedially, anteriorly stomach in upper two-third and pancreatic body with splenic vessels in lower one-third. Each adrenal gland receives its blood supply from three arteries namely, superior adrenal artery a branch of inferior phrenic, middle adrenal artery arising from descending aorta and inferior adrenal artery, a branch of renal artery. There is a single adrenal vein on either side, the right adrenal vein drains into inferior vena cava and left one into left renal vein.

The adrenal gland is made of an outer cortex that is derived from mesoderm and an inner medulla, derived from neural crest. The cortex forms almost 90 percent of total adrenal mass; the medulla contributes only 10 percent. The adrenal cortex is histologically comprised of three distinct zones – zona glomerulosa, zona fasciculata and zona reticularis from outside to inside. The adrenal cortex secretes three groups of steroid hormones. Zona glomerulosa constitutes 10 to 15 percent of the cortex and

secretes mineralcorticoids, aldosterone being the most important. Zona fasciculata constitutes 80 percent of the cortex and secretes glucocorticoids, while zona reticularis contributing only 5 to 10 percent of cortex, secretes androgens. Zona glomerulosa is mainly involved in aldosterone biosynthesis whereas fasciculata-reticularis zone is the site for cortisol and androgen biosynthesis.

The adrenal medulla secretes epinephrine and norepinephrine, which form an integral part of sympathetic autonomic nervous system and play an important role in the regulation of vital functions and many metabolic processes.

IMAGING MODALITIES

A number of imaging modalities are available for evaluation of the adrenals. Before the advent of imaging modalities of US, CT and MRI, the radiological techniques available for evaluation of adrenals were plain X-ray abdomen, excretory urography, invasive techniques of perirenal air insufflation, adrenal venography and angiography. Most of these techniques have become obsolete. Angiography may be sometimes indicated to look for extra-adrenal pheochromocytoma in situations when Metaiodobenzylguanidine (MIBG) scintigraphy is not available. Adrenal venous sampling may be recommended in patients with aldosteronism, both for distinguishing unilateral from bilateral disease and for localizing unilateral tumor. However, this technique is invasive, technically difficult to perform and requires long fluoroscopy time with resultant high radiation dose and needs hospitalization. Procedural complications include adrenal infarction, adrenal vein thrombosis, adrenal hemorrhage, hypotensive crises and adrenal insufficiency. Therefore, adrenal venous sampling is best reserved for patients with equivocal findings on cross-sectional imaging modalities.

Ultrasound is seldom used in imaging suspected adrenal pathology. CT and MRI remain the imaging modalities for evaluation of structural changes in the diseased adrenal whereas scintigraphy provides functional assessment of the gland. F-18 fluorodeoxyglucose positron emission tomography (F-18 FDG PET) has played an important role in defining physiological and pathological conditions of the adrenal glands. Integrated information obtained from anatomic and functional imaging is essential for characterization of adrenal disease.

Percutaneous biopsy of the adrenal lesion under USCT guidance has an accuracy of 80-90 percent. Minor complications include abdomi-nal pain, hematuria or small pneumothorax. Major ones requiring treatment occur in 3-5 percent of the patients and include hemorrhage and pneumothorax.

Ultrasound (US)

Despite availability of high-resolution real time ultrasound scanners, normal adrenal gland or small adrenal lesions remain difficult to be visualized on sonography, especially in obese patients. Therefore, ultrasonography is seldom indicated for adrenal lesion, although large adrenal mass may be detected incidentally during abdomi-nal ultrasound examination. Ultrasound is however useful in evaluation of suspected adrenal hemorrhage in neonates. It may also be used as a screening modality in suspected pheochromocytoma, due to the easy availability of the examination. US guidance suffices for sampling of large adrenal lesions.

Computed Tomography (CT)

CT remains the first choice of imaging modality for evaluation of most of the adrenal

diseases. The widespread availability of CT in clinical practice makes it an ideal non invasive technique for evaluating adrenal gland morphology owing to the speed with which examination can be performed, its superior spatial resolution and quantification of contrast washout patterns.[1-3] The introduction of spiral CT and more recently multidetector-row helical CT (MDCT), has allowed rapid thin slice imaging of the adrenal glands during various phases of contrast enhancement. Small adrenal lesions can be detected and accurate density measurements of lesions can be done.

CT technique should be tailored according to the clinical indication. In general, when CT is used to study the adrenal glands the entire abdomen through the aortic bifurcation is scanned. This is helpful for staging or for evaluating possible ectopic adrenal lesions.[4] Five hundred ml of 2 percent of oral contrast is given 15 minutes prior to scanning to opacify the bowel loops. Oral contrast material is helpful so that unopacified loops of bowel are not confused as adrenal lesions. A nonenhanced CT examination should be done first. This may be followed by enhanced and delayed enhanced CT examination when required in a situation, where adenoma needs to be differentiated from metastasis.

While evaluating adrenal glands for suspected hyperplasia or adenoma, in a clinical setting of functioning tumors (e.g. Cushing's disease, Conn's syndrome, Congenital adrenal hyperplasia), then thin sections are obtained through the adrenals. For these scans, intravenous contrast material is not required.[4]

In the search for pheochromocytoma, CT should be done from lower thorax to symphysis pubis. Pericardium is a rare site but can be easily included on CT. Large sporadic pheochromocytomas are easily detected on CT and contrast administration is usually unnecessary. However syndromic pheochromocytoma may be small, multiple and extra-adrenal. In order to optimize visualization of tumors, contrast injection maybe necessary. It is debatable if IV contrast is safe in this setting. It is extremely rare for IV contrast to precipitate hypertensive crisis in patients of pheochromocytomas. Most authorities consider it unnecessary to give prophylactic alpha and beta adrenergic blockade prior to IV contrast.[5]

The adrenal gland has a characteristic inverted Y or V shape on CT and is seen as an anteromedial ridge with two posterior limbs, medial limb being shorter than the lateral limb and limbs have normally straight or concave outline (Figs 20.1A and B). The adrenal measurements on CT are taken as anteroposterior diameter from the tip of the anteromedial ridge to the posterior tip of the longest limb, length by calculating the number of sequential scans in which the gland is visualized (Fig. 20.2). The criteria for enlargement of adrenal are taken as length more than 4.0 cm, anteroposterior diameter of more than 3.0 cm and limb thickness of more than 6.0 mm or more than adjacent diaphragmatic crus. Besides these absolute measurements, any alteration in the contour, focal bulge, calcification, pattern of enhancement, CT attenuation values on non-enhanced, enhanced and delayed enhanced techniques, and displacement of surrounding structures should be evaluated.

Magnetic Resonance Imaging (MRI)

The intention of most MRI techniques used so far has primarily been distinction of benign

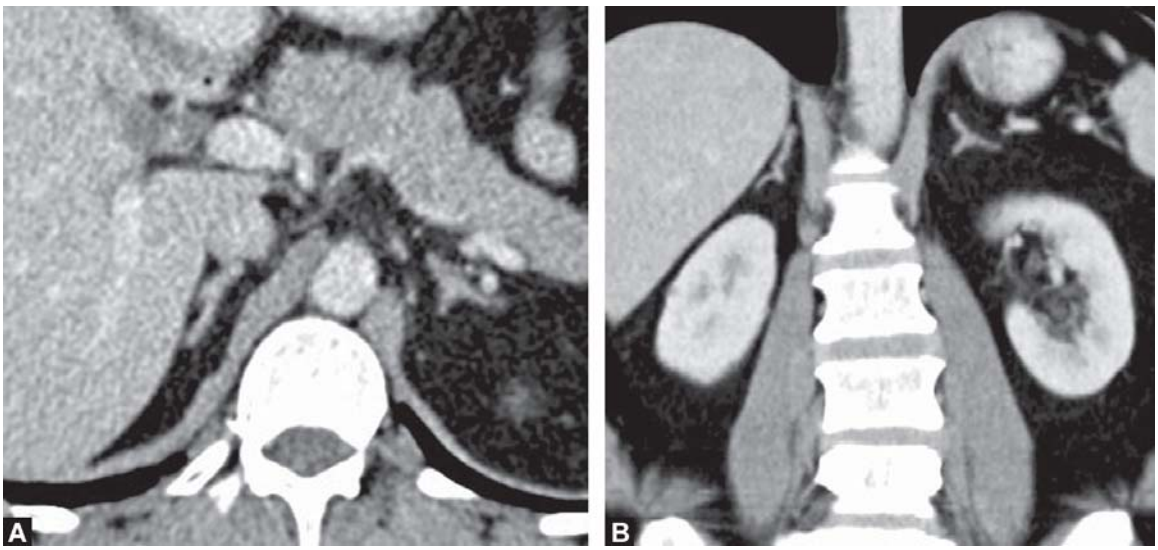

Figs 20.1A and B: Axial **(A)** and coronal **(B)** CT images showing the normal adrenal glands

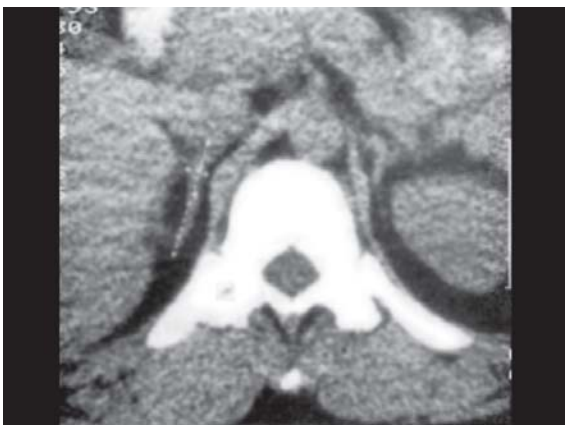

Fig. 20.2: Normal adrenal measurements (1) Anteroposterior diameter, and (2) Limb thickness

from malignant disease. The most reliable in this context is the combined use of in-phase and out-of-phase gradient-echo (GRE) techniques for adenoma vs metastasis distinction. The best approach is to use 2D or 3D gradient-echo sequences, without fat suppression. The only variation between sequences should be the echo-time (TE), with T.E of 4.2-4.5 ms for in-phase imaging and TE of 2.2-2.7 ms for out-of-phase imaging at I.5 T. On the newer MR systems, double echo (in phase and out of phase) sequences are available that allow more accurate comparison.[6] The normal adrenal cortex contains abundant lipid, which however is not enough to be demonstrated on in-phase and out-of-phase imaging.

Serial post-gadolinium gradient echo may also be used for benign vs malignant differentiation. The capillary-phase postgadolinium images are most useful.[7] As in the case of CT, the incidence of hypertensive crisis following gadolinium in suspected pheochromocytomas is extremely rare.[5]

T2-weighted images provide information on fluid-content of lesions.T2-weighted imaging hence is most useful in the search for pheochromocytomas which have a high fluid content. T2-weighted sequences also supplement benign vs malignant differentiation, although substantial overlap exists.[8] Normal adrenal gland may demonstrate cortico-medullary differentiation on T2WI.

As no single technique is more than 90 percent accurate, it is useful to combine in-phase and out-of-phase images with other

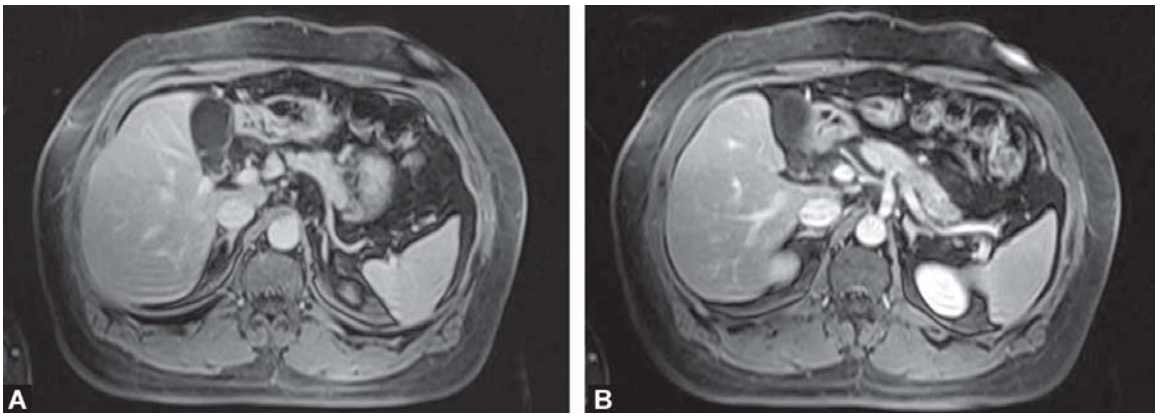

Figs 20.3A and B: Gradient echo T1W axial images showing the normal inverted 'V' configuration of the adrenal gland

techniques to increase confidence of lesion characterization, especially capillary-phase gadolinium enhanced imaging.[6,8]

Normal adrenal glands and small adrenal masses are well-demonstrated on T1 weighted fat suppressed images (Figs 20.3A and B).[9] The demonstration of cortico-medullary differentiation on either noncontrast T1W fat-suppressed images or immediate post-gadolinium GE images is helpful in distinguishing adrenal from renal tumors.[10] Sagittal plane is more useful than coronal plane in this regard. The use of thin section 3D-GRE sequences in one plane of acquisition, allows reconstructions in other planes for defining tumor location.

Radionuclide Imaging

This technique is primarily used as a problem solving modality for lesions not adequately characterized on CT and MR imaging. It provides functional imaging of the adrenal cortex and medulla. Radiolabelled analogues of cholesterol, e.g. 75 Se selenomethyl norcholesterol, 59 NP beta iodomethyl–19-norcholesterol can localize mass causing adrenal cortical dysfunction, the latter one is particularly useful in the work up for suspected aldosteronism. The advances made with CT and MRI have largely eliminated the use of 59 NP imaging for adrenal. Iodine-131 Metaiodobenzylguanidine (MIBG) is concentrated in sympathoadrenal tissue and is used for imaging adrenal medullary lesion, especially to evaluate for pheochromocytoma and to screen the whole body for extra-adrenal pheochromocytoma.

Positron Emission Tomography (PET)

Recently positron emission tomography (PET) has become available as a possible tool for evaluating the adrenal. FDG-PET has shown promise in differentiating benign from malignant mass. However, in literature only limited data on the role of 18-FDG PET/PET-CT in characterization of adrenal lesions in oncology population is available, that too involving a relatively small sample size.[11] F18-FDG PET imaging has been found to be a reliable non-invasive imaging technique to differentiate benign from malignant adrenal masses. It has demonstrated a high-sensitivity, specificity and overall accuracy for detecting adrenal metastases in patients with malignancy.

The common causes of false positive adrenal lesions on F18-FDG PET imaging are

benign adenomas and pheochromocytoma.[12,13] All the benign and malignant pheochromocytomas have been shown to accumulate F18-FDG, although uptake is found in a greater concentration in malignant as compared to benign pheochromocytoma.[12] The common causes of false negative F18-FDG PET results, are small size lesions, necrotic metastasis, and metastases from neuroendocrine tumors.[13] Small metastatic lesions can be missed because of the limited resolution of F18-FDG PET/PET-CT or the absence of sufficient tumor cells with increased glycolysis.

Adrenal Diseases

Diseases of the adrenal may become manifest as a result of hormone excess or deficiency. The adrenal diseases may be considered under the following three groups.

Group I : Adrenal hyperfunctional diseases.
Group II : Adrenal insufficiency.
Group III : Adrenal diseases with normal function.

Group I : Adrenal Hyperfunctional Diseases

Hyperfunctioning adrenal diseases occur either from the adrenal cortex (Cushing's syndrome, Conn syndrome, hyperandrogenism) or the adrenal medulla (pheochromocytoma). The clinical features depend on the type of hormone produced and its target organs.

Cushing's Syndrome

Cushing's syndrome is caused by adrenocorticotropic hormone (ACTH) overproduction in 75 percent of patients and by excess of cortisol production from adrenal neoplasms in 25 percent. ACTH overproduction results from either pituitary adenoma or from ectopic ACTH producing nonendocrine tumors. Ectopic ACTH producing nonendocrine tumors include bronchial carcinoid tumor, islet cell tumor of the pancreas, medullary carcinoma of thyroid, thymic carcinoid tumor and pheochromocytoma (Figs 20.3A and B).

The diagnosis of Cushing's syndrome depends predominantly on the clinical features and biochemical findings. It presents an easily recognizable clinical picture of truncal obesity, moon facies, cutaneous striae, buffalo hump, hypertension, muscles weakness, fatigability, osteoporosis, profound emotional changes and amenorrhea in women.

Appropriate work-up of patients with Cushing's syndrome includes plasma cortisol and 24 hours urine for cortisol estimation followed by dexamethazone suppression test. The abnormal test establishes the diagnosis of Cushing's syndrome. The purpose of imaging is to identify the source of excess ACTH either from a pituitary tumor or an ectopic source and to detect or exclude adrenal mass. The adrenal appearances in Cushing's syndrome depend on the etiology of the syndrome. CT is the primary modality used in this setting. Visualization of adrenal pathology on CT is aided by the large amount of retroperitoneal fat that is usually present in these patients. MRI plays a secondary role.[14]

ACTH dependent Cushing's syndrome: This results from pituitary cause in 85 percent of patients and rest from ectopic ACTH secretion. The adrenals show changes of hyperplasia in the form of smooth thickened limbs or multiple small nodules of varying size involving one or both limbs.

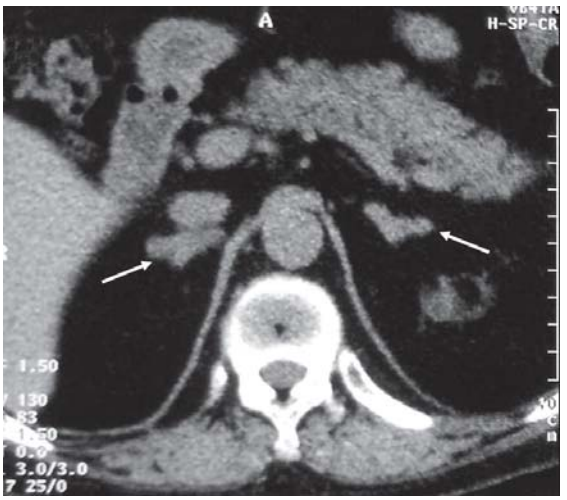

Fig. 20.4: NCCT of adrenal glands of a 20 years old male patient presenting with Cushing's syndrome showing bilateral adrenal hyperplasia (arrows) with proliferation of perirenal and mesenteric fat

These changes may be seen in one or both adrenals (Figs 20.4 and 20.5A and B). MRI signal intensity in adrenal hyperplasia closely follows that of the normal adrenal gland.

ACTH Independent Cushing's Syndrome

Adrenocortical adenoma accounts for 10 to 20 percent of patients with Cushing's syndrome. It is seen as a solitary, well-defined homogeneous mass, usually around 2-3 cm in diameter (Figs 20.6A to C). However, when large, it shows focal areas of necrosis and hemorrhage. These adenomas are larger than those seen in Conn's syndrome, and are usually lipid rich.[4] The contralateral gland is normal but occasionally atrophic. *Adrenal carcinoma* accounts for 10 to 15 percent of patients with Cushing's syndrome. Also, only 10 percent of adrenal carcinomas function to a level that results in *Cushing's* syndrome.[4] It is generally seen as a large mass often more than 6.0 cm, heterogeneous with areas of necrosis and calcification, with features of local invasion, regional lymphadenopathy and distant spread (Figs 20.7, 20.8A and B).

Rockall et al[15] while reporting findings in 37 patients with primary adrenal Cushing's

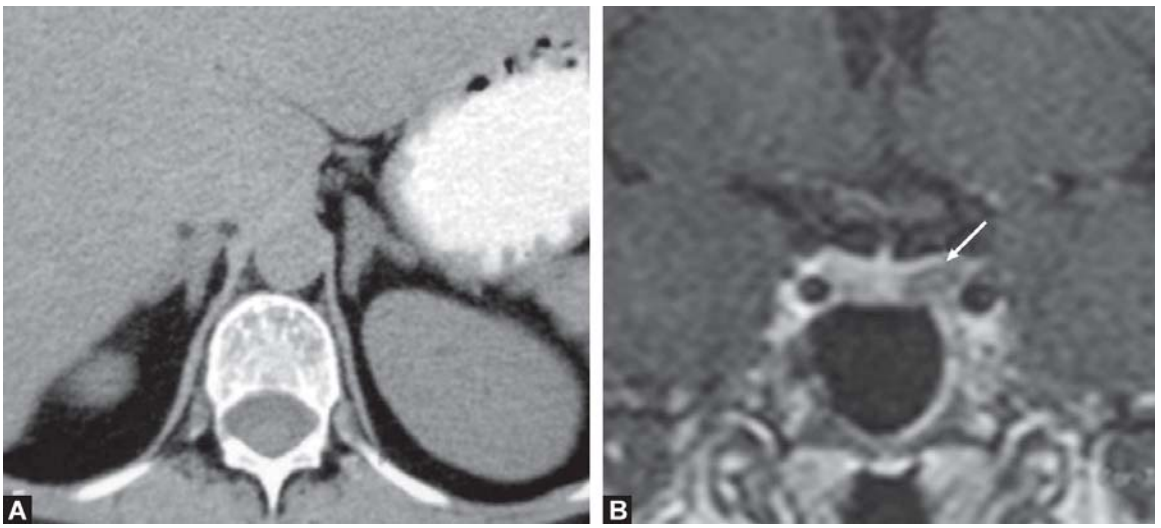

Figs 20.5A and B: NCCT of adrenal glands **(A)** of a 32 years old female patient presenting with Cushing's syndrome showing nodular, bilateral adrenal hyperplasia. Post contrast T1W coronal image of MRI sella of the same patient reveals a microadenoma on left side of anterior pituitary (arrow)

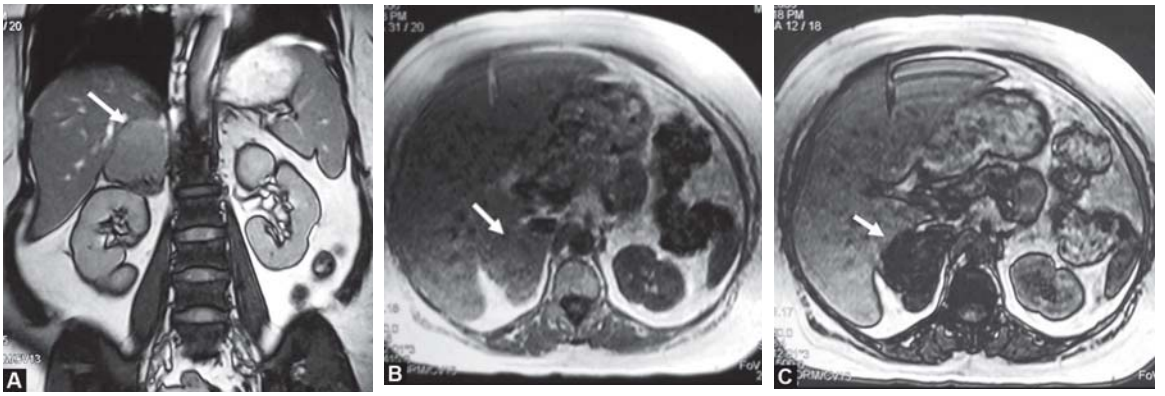

Figs 20.6A to C: MRI of a 44 years old female with Cushingoid features. TRUFISP coronal image **(A)** shows an intermediate signal intensity mass in the right adrenal gland. T1 FLASH in-phase **(B)** and opposed-phase **(C)** images reveal significant signal drop in the opposed-phase images, suggesting adrenal adenoma

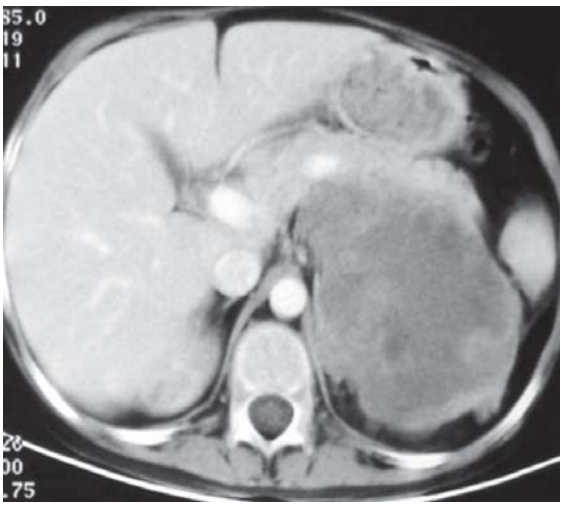

Fig. 20.7: Axial CECT of a 12 years old boy with Cushingoid features showing a heterogeneously enhancing mass arising from the left adrenal, suggesting adrenal carcinoma

syndrome found hyperfunctioning adenomas (n = 24) and functioning carcinomas (n = 10), accounted for 92 percent of cases. Adenomas had a significantly smaller mean size (3.5 vs 14.5 cm) and lower mean unenhanced CT attenuation value (11 vs 28 HU) than did carcinomas. The presence of necrosis, hemorrhage, and calcification favored a diagnosis of carcinoma. Six of 10 carcinoma patients had metastases at presentation. Two adenomas were seen within a myelolipoma. Two adenomas were of uncertain malignant potential. Bilateral disease—primary pigmented nodular adrenal dysplasia (PPNAD) (n = 2) and ACTH-independent macronodular adrenal hyperplasia (AIMAH) (n = 1), had characteristic imaging features. In PPNAD, multiple tiny (2–5 mm) nodules were visible bilaterally, with no overall glandular enlargement and normal intervening adrenal tissue. In AIMAH, both glands were grossly enlarged and contained nodules up to 3 cm in diameter.

Aldosteronism

Aldosteronism (Conn's syndrome) is associated with excess of mineralocorticoids and characterized clinically by hypertension, muscle weakness, polyuria, polydipsia and persistent hypokalemia. It is caused by adrenal adenoma in about 80 percent of patients while adrenal gland hyperplasia in the rest. Adrenal carcinoma is extremely rare, accounts for less than 1 percent of patients, as a cause of aldosteronism. In patients with unilateral adenoma, unilateral adrenalectomy is the treatment of choice. On the other hand,

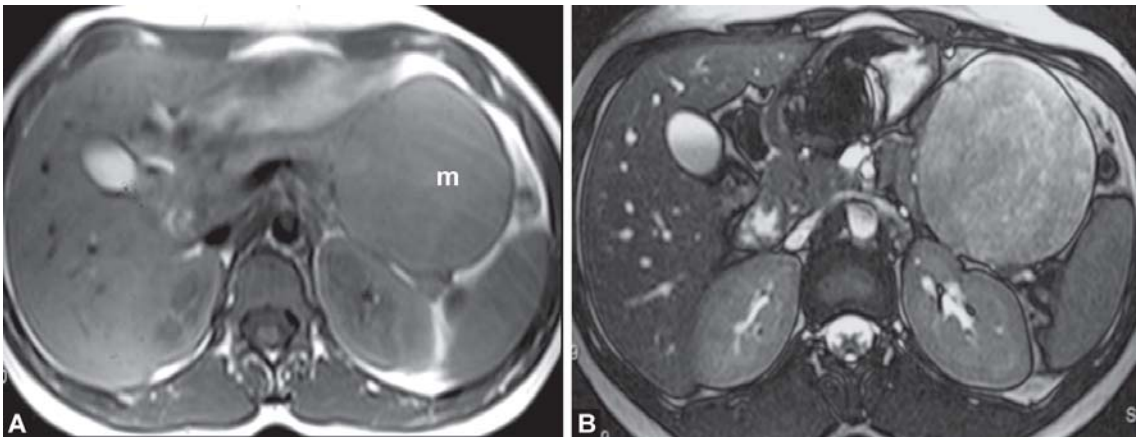

Figs 20.8A and B: Axial T1W **(A)** and T2W **(B)** MR images of a 28 years old female with clinical and biochemical features of Cushing's syndrome, reveal a well encapsulated mass (m), hypointense on T1W and heterogeneously hyperintense on T2W, arising from left adrenal gland. On biopsy, it was a carcinoma

cases of bilateral adrenal gland hyperplasia are treated medically with pharmacological agents.[16] The imaging approach hence is to distinguish between these two entities.

Aldosterone producing adenoma is small with a mean size of 1.6-1.8 cm and may have central low attenuation due to high lipid content (Fig. 20.9). A dedicated CT examination with thin sections is required for localizing the adenoma.

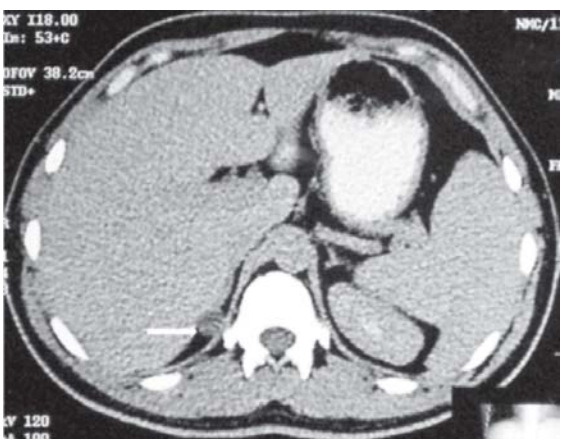

Fig. 20.9: NCCT of a 28 years old male with hypertension shows a low attenuating nodule in the right adrenal (arrow) with attenuation value of 4HU. Conn's syndrome due to adrenal adenoma

If CT examination is inconclusive, adrenal cortical scintigraphy with NP-59 may be done. On NP-59 scintigraphy, both adrenals are normally visualized on 5th day or later, following injection of radiopharmaceuticals. Bilateral adrenal visualization before 5th day suggests adrenal gland hyperplasia while unilateral adrenal visualization before 5th day indicates an adenoma. If clinically strongly suspected and negative CT examination the other alternative study is adrenal venous sampling to determine lateralization of aldosterone secretion to one side suggesting adenoma or both sides suggesting bilateral hyperplasia. NP 59 scintigraphy has long procedural time of nearly two weeks with an accuracy of 71 percent in contrast to adrenal venous sampling with an accuracy of 95-100 percent.

Androgenital Syndrome

Androgenital syndrome is a consequence of excessive secretion of sex hormones. It causes virilization, feminization or precocious puberty depending upon the age and sex of the patient. The commonest form is virilization, occurring in females.[4] The characteristic

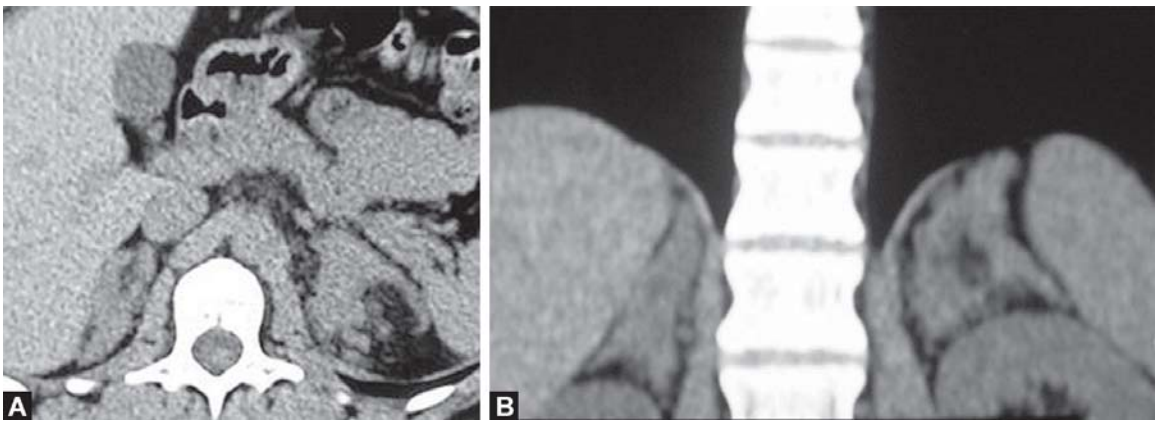

Figs 20.10A and B: Axial **(A)** and coronal **(B)** NCCT scans of a 13 years old girl with features of virilization shows bilateral nodular adrenal hyperplasia

clinical features are amenorrhea, hirsuitism, clitoromegaly, deepening of voice.

The adrenal causes of androgen excess include congenital adrenal hyperplasia in children and virilizing tumors (adenoma or carcinoma) in adults. Congenital adrenal hyperplasia (CAH) occurs due to deficiency of enzymes involved in the synthesis of steroid hormones. Each different enzyme deficiency results in a different form of congenital adrenal hyperplasia. The clinical manifestations are determined by the degree of deficiency of cortisol or aldosterone and by the biological properties of the biochemical intermediates that are formed and secreted in excess.

Androgen producing tumors are rare and include adenoma or carcinoma, and occur in both males and females at a later age. In general, in adults a higher proportion of malignant tumors result in adrenogenital syndrome than benign lesions.[4]

MRI is preferred to CT to image adrenals as well as ovaries particularly in children to detect tumors because of MRI being non-ionising. CT is however often the initial and only modality performed in evaluation of suspected CAH, due to easy availability and short examination times (Figs 20.10A to 20.11B).[17]

The tumors are usually more than 2.0 cm in size and show imaging characteristics described above (Figs 20.12A and B). Occasionally adrenal and gonadal venous sampling may be necessary to locate the source of excessive androgens.

Pheochromocytoma

Pheochromocytomas are catecholamine producing tumors which arise from ganglion cells anywhere in the autonomic nervous system. Ninety percent of pheochromocyto mas originate in the adrenal medulla, while 10 percent are extra-adrenal, the common sites being paravertebral sympathetic ganglia, organ of Zuckerkandl, urinary bladder, neck or mediastinum. Ten percent of pheochromocytomas are bilateral and 10 percent are malignant. Five to ten percent are inherited as autosomal dominant either alone or in combination with other abnormalities such as multiple endocrine neoplasia, (MEN Type II or III), neuro-fibromatosis, von Hippel-Lindau's retinal and cerebellar hemangioblastomas.

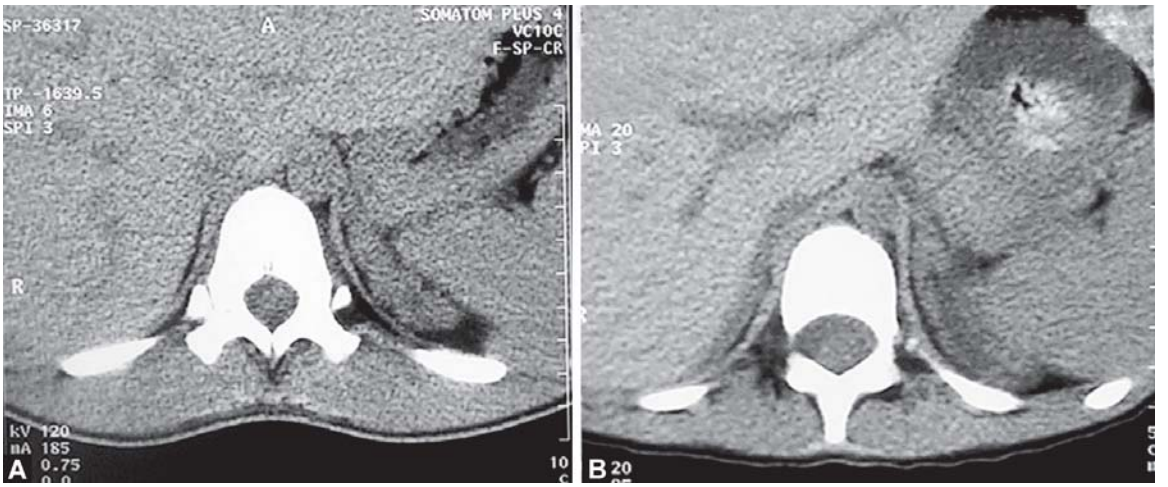

Figs 20.11A and B: Axial NCCT of 11 years old brother of the patient shown in Fig 10**(A**), presenting with precocious puberty and 5 years old sister with virilization **(B)** also show features of congenital adrenal hyperplasia

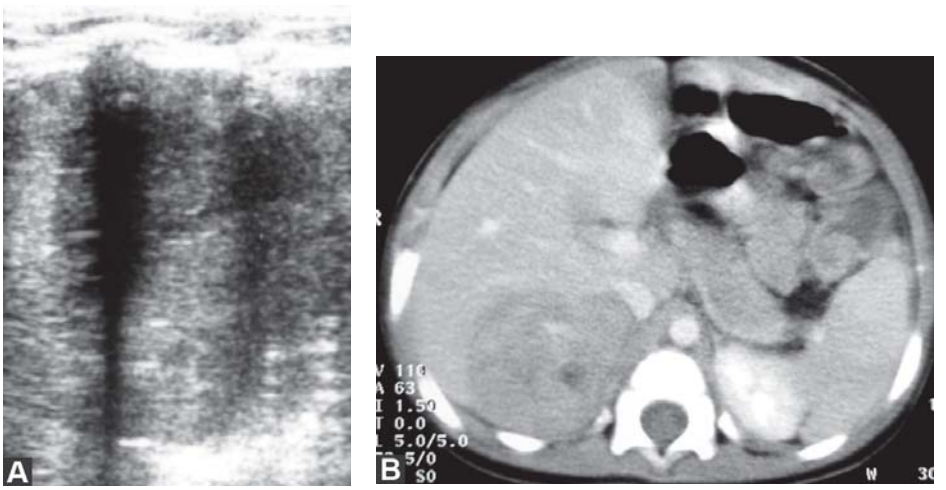

Figs 20.12A and B: Ultrasound (A) and axial CECT **(B)** of a 1.5 years girl child with feature of virilization show a large heterogeneous mass arising from the right adrenal, suggesting a carcinoma

Clinical features of hypertension, paroxysmal attacks of palpitation, headache, sweating and biochemical tests of plasma catecholamine levels and 24 hours urine vanillylmandelic acid level can provide the diagnosis. Imaging is required to locate the tumor. CT is the technique of choice to confirm adrenal mass. It is seen as soft tissue density mass with contrast enhancement on CECT (Figs 20.13A to C). On MRI, it is isointense or hypointense on T1 weighted image and extremely hyperintense on T2 weighted image. Although this finding is almost universally seen with pheochromocytomas, a percentage of adrenal metastases have overlapping findings.[4,6,18] Gadolinium–DTPA

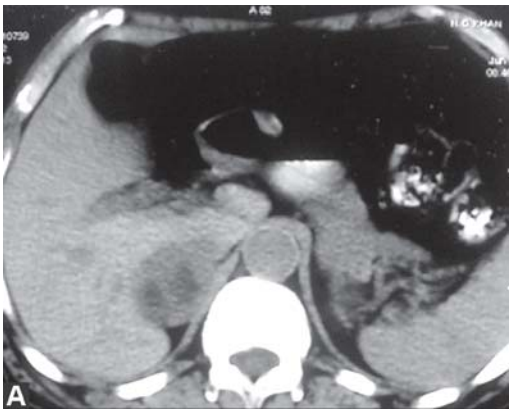

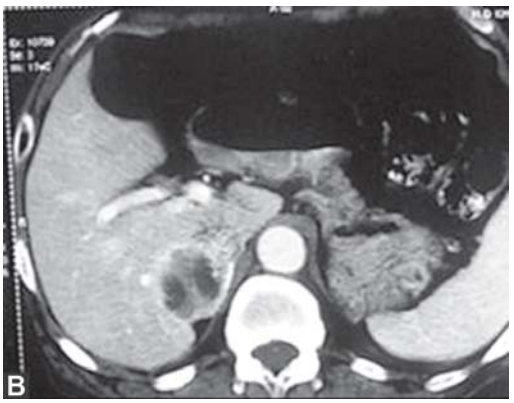

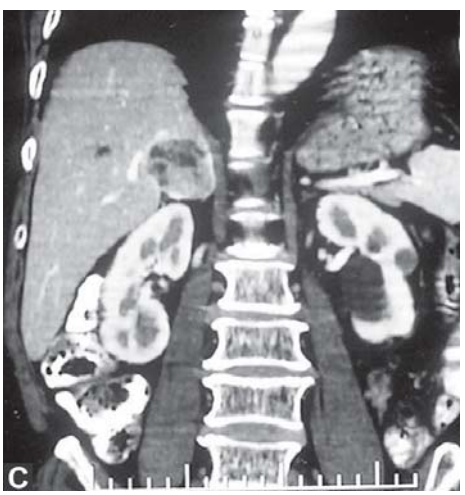

Figs 20.13A to C: (A) NCCT scan of a young hypertensive male showing a mass in the right adrenal. Axial **(B)** and coronal **(C)** CECT reveal intense enhancement with central areas of necrosis

(diethylenetriamine penta-acetic acid) produces marked enhancement with slower wash sout of contrast as compared to adenoma (Figs 20.14A to D). Pheochromocytomas show insignificant signal drop on out of phase GRE images. It may show variable necrosis but calcification in pheochromocytoma is rare (Figs 20.15A and B). The initial imaging findings in benign and malignant pheochromocytomas are nearly identical. Only the presence of metastases can clearly define a pheochromocytoma as malignant.[4]

CT and MRI can detect adrenal pheochromocytoma equally well. However, MRI is better for detecting extra-adrenal pheo-

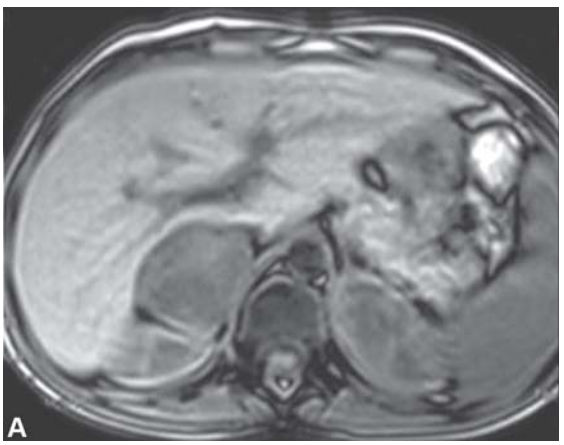

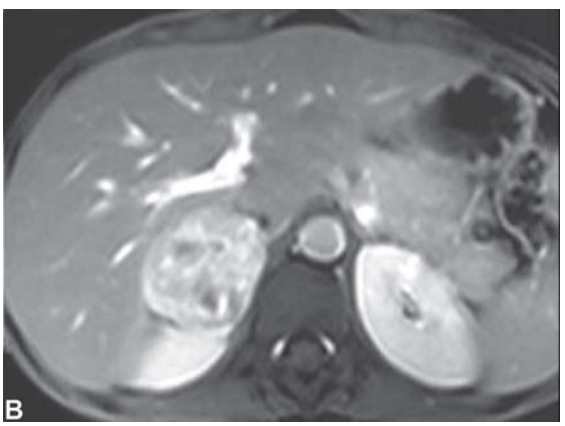

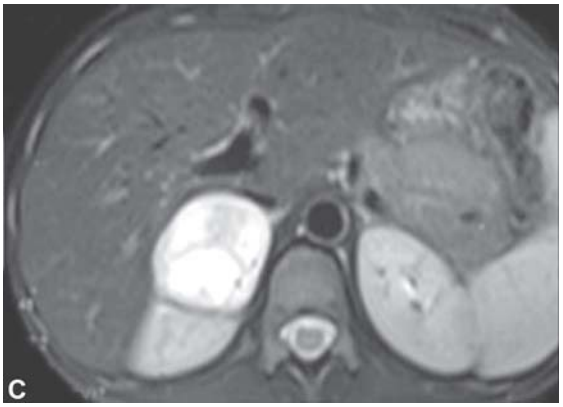

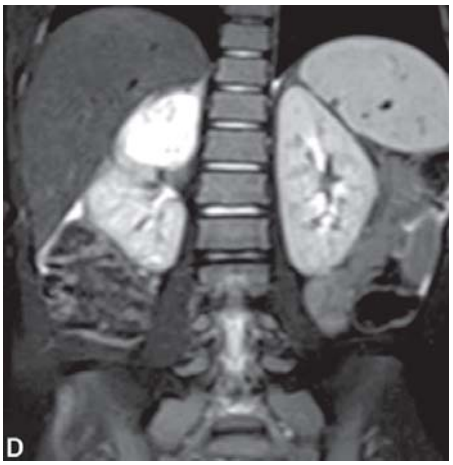

Figs 20.14A to D: T1W pre **(A)** and post-gadolinium **(B)** axial images of 15 years old male with hypertension reveals an intensely enhancing right adrenal mass. T2W axial **(C)** and coronal **(D)** images reveal the typical hyperintensity of a pheochromocytoma

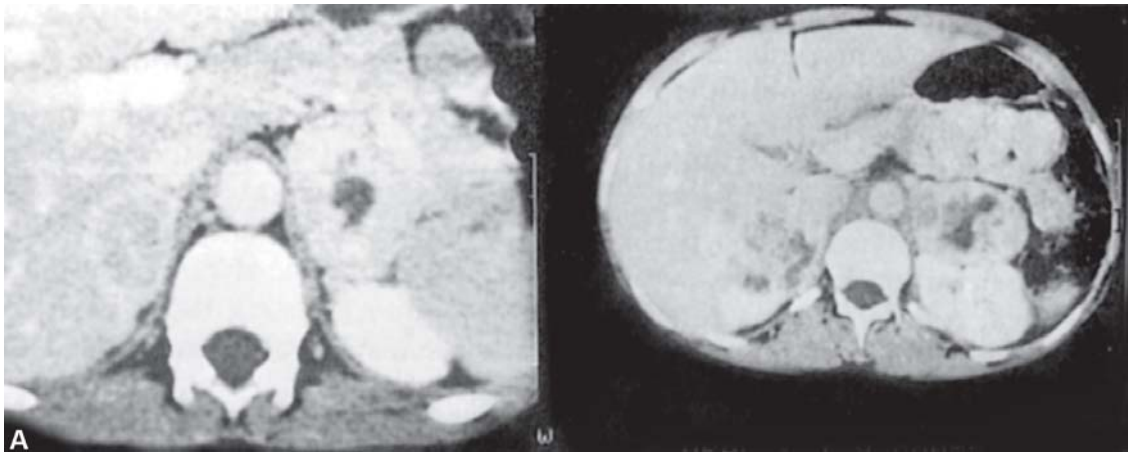

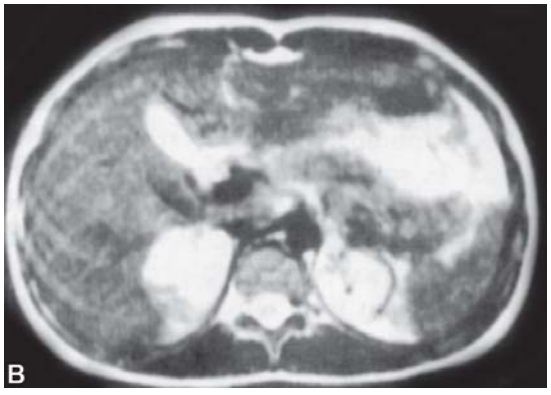

Figs 20.15A and B: Bilateral pheochromocytoma (different patient). **(A)** Bilateral adrenal masses showing intense enhancement and variable necrosis on CECT. **(B)** Bilateral pheochromocytoma: Hyperintense on T2W image with round areas of low intensity within, suggests flow voids of intratumoural vessels in left adrenal

chromocytoma and recurrence after surgery. On sonography, pheochromocytoma is seen as well-defined hypoechoic mass which may show areas of necrosis or hemorrhage. The accuracy of ultrasonography in detecting pheochromocytoma is less than CT and MRI, particularly if the tumor is small and extra-adrenal.

In patients with strongly suspected pheochromocytoma, but no adrenal mass identified on CT or MRI, MIBG scintigraphy is the technique of choice to detect ectopic location and is also indicated for metastatic or locally recurrent disease. It is seen as focal areas of abnormal activity. The sensitivity of MIBG scintigraphy for detecting pheochromocytoma is 80-90 percent with a specificity of 90-100 percent but a positive MIBG scintigraphy should always be correlated with CT or MRI.

Group II : Adrenal Insufficiency

Adrenal hypofunction refers to disorders of the adrenal cortex. It is classified as primary or secondary. Primary form is due to destruction of the adrenal cortex, while the secondary form results from pituitary causes. Usually 85-90 percent of the adrenal cortex must be destroyed before the clinical syndrome manifests.[4] Primary adrenal insufficiency or Addison's disease presents with weakness, hypotension, weight loss with or without pigmentation.

The causes of Addison's disease include idiopathic atrophy, chronic granulomatous infections, e.g. tuberculosis, histoplasmosis, blastomycosis and adrenal hemorrhage. Other causes include autoimmune diseases and drugs.

Of the chronic infections, tuberculosis accounts for more than 60 percent of patients in India. This is in contrast to the west where idiopathic adrenal insufficiency accounts for almost 90 percent of the patients. CT is an important imaging modality to define size and morphology.[19] In patients with idiopathic atrophy, the glands are often too small to be identified (Fig. 20.16). The CT morphology in tuberculosis includes bilateral asymmetrical adrenal enlargement with or without calcification or necrosis, small gland with calcification involving one or both adrenals, or small gland with no calcification (Figs 20.17A to 20.19C). There may be evidence of associated pulmonary tuberculosis. Follow up studies in these patients on treatment, have shown reduction in size of the adrenals and presence of calcification (Figs 20.17A and B).

In histoplasmosis, adrenals may show bilateral asymmetrical enlargement but often normal configuration and usually no calcification (Figs 20.14A to D). Histoplasmosis in India is not as rare as reported in the Indian literature. Because of lack of awareness and investigative facilities, many of these patients are probably treated for tuberculosis.

Bilateral adrenal hemorrhage is usually associated with anticoagulant therapy or with stress caused by surgery, sepsis or hypotension.

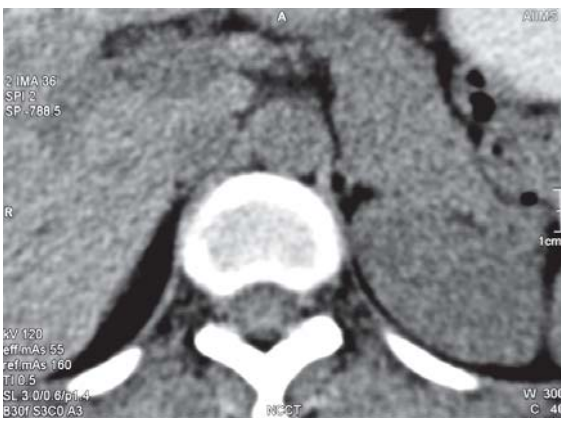

Fig. 20.16: NCCT scan of patient with Addison's disease showing bilateral atrophic adrenal glands

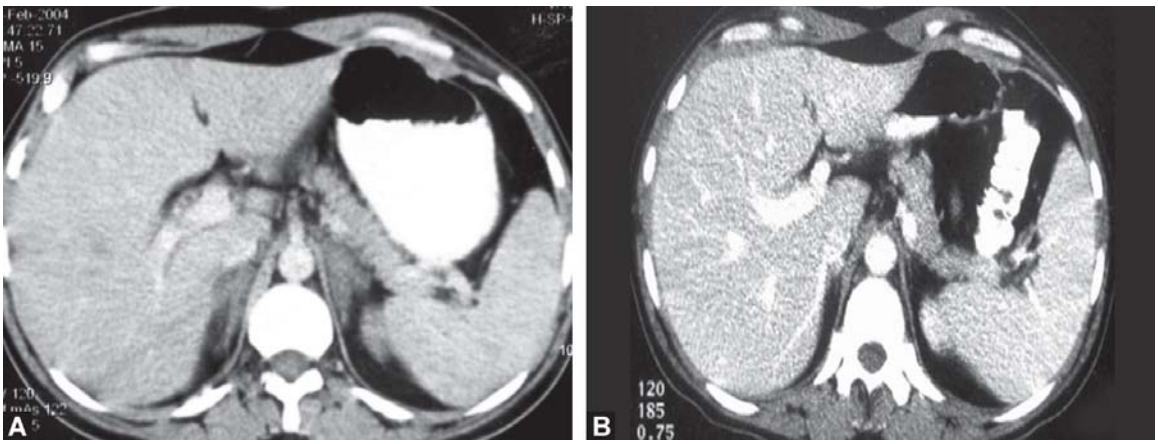

Figs 20.17A and B: CECT scan **(A)** of a patient with fever and biochemical evidence of adrenal insufficiency shows bilateral asymmetric (left > right) enlargement of the adrenal glands. Few ill-defined focal are seen in the liver and spleen also suggesting disseminated tuberculosis. Patient was put on ATT. CECT obtained 1 year later **(B)** reveals small, atrophic adrenal glands

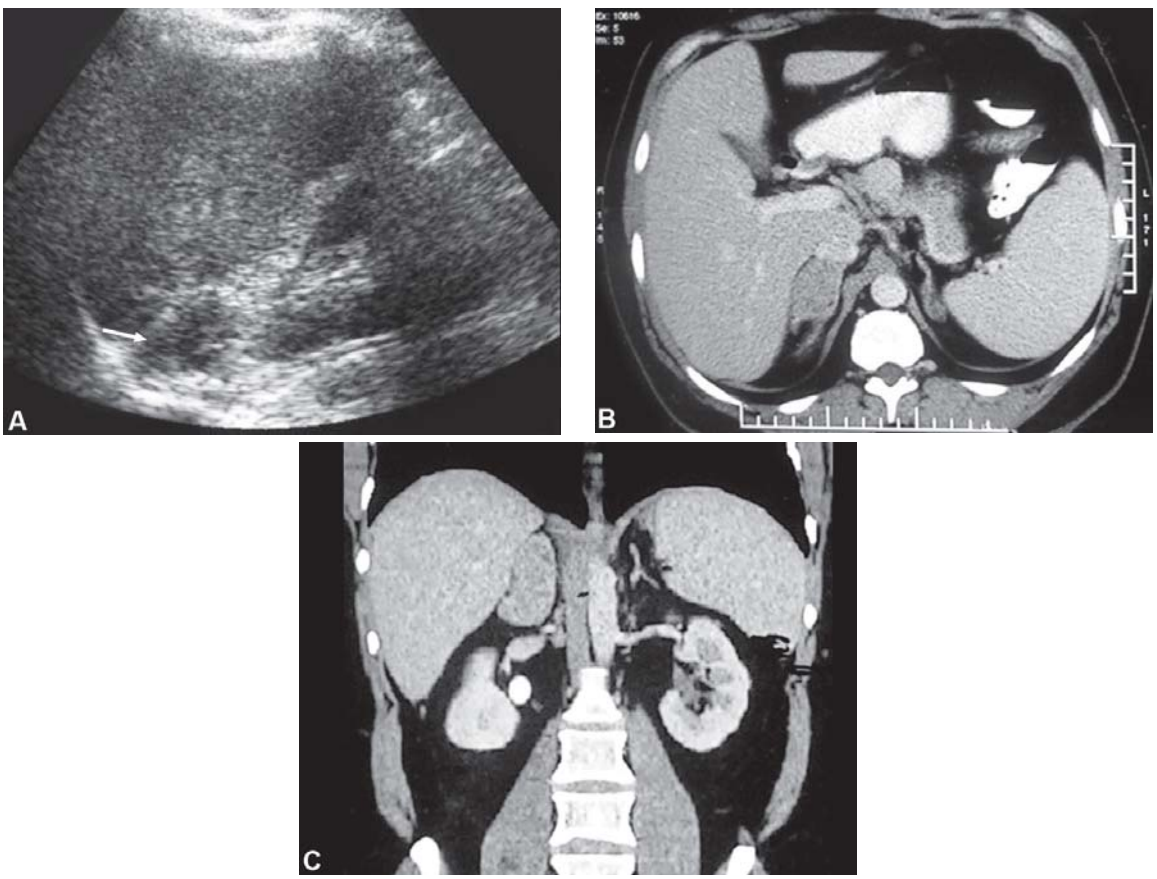

Figs 20.18A to C: US **(A)** Axial CECT **(B)** and coronal MPRs **(C)** reveal an enlarged, heterogeneous right adrenal gland. Biopsy: Tuberculosis

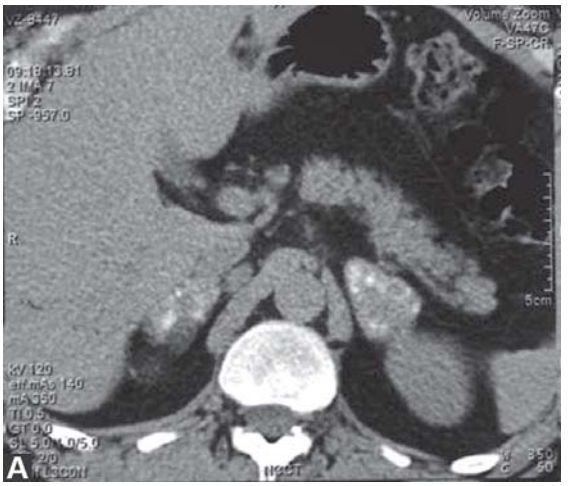

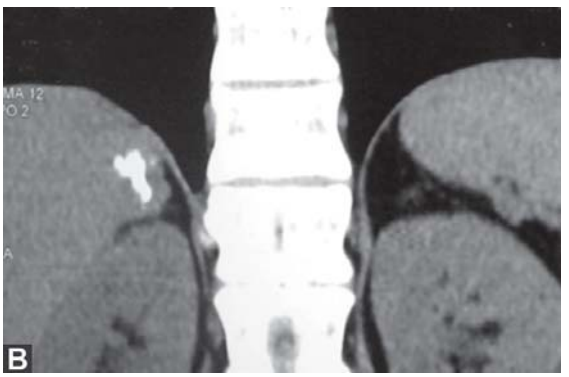

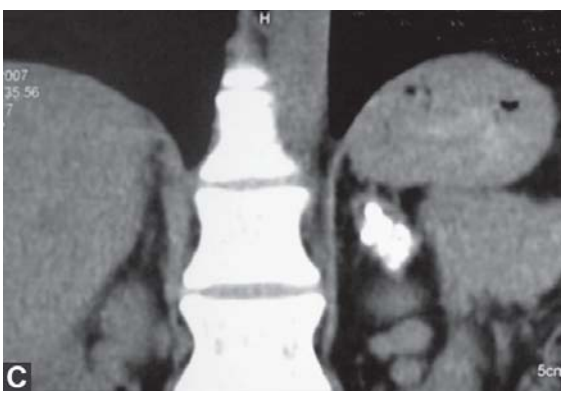

Figs 20.19A to C: Axial CECT **(A)** and coronal MPRs **(B, C)** of two different patients with Addisons's disease reveal bilateral, calcified adrenal glands, suggesting granulomatous involvement

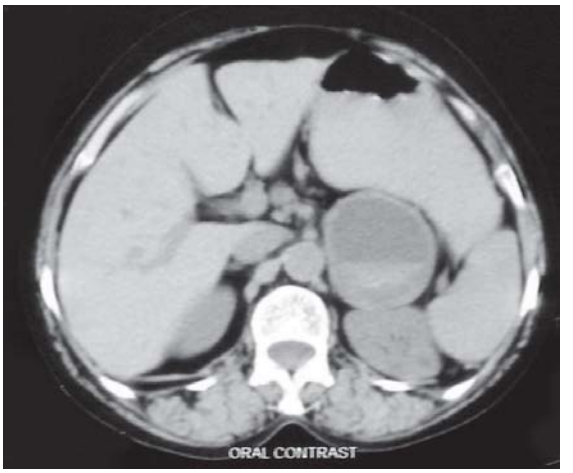

Fig. 20.20: Axial CT showing a low attenuating left adrenal mass with blood-fluid level suggestive of adrenal hemorrhage

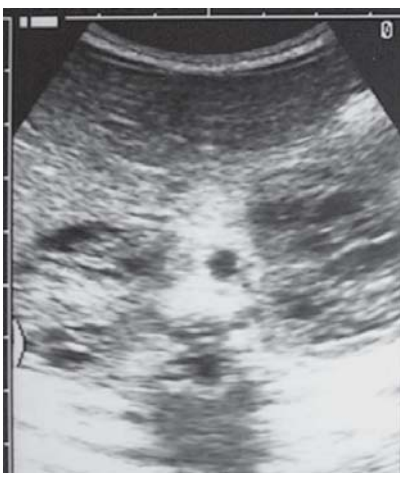

Fig. 20.21: US of a preterm neonate showing bilateral enlarged adrenal glands, suggesting adrenal hemorrhage

Less commonly, it is caused by trauma or hypoxia during delivery. CT may show asymmetrical adrenal enlargement with areas of high attenuation or blood-fluid level (Fig. 20.20). Neonates, especially preterm infants may also show bilateral adrenal hemorrhage (Fig. 20.21). Follow-up studies after appropriate treatment show diminution in size and

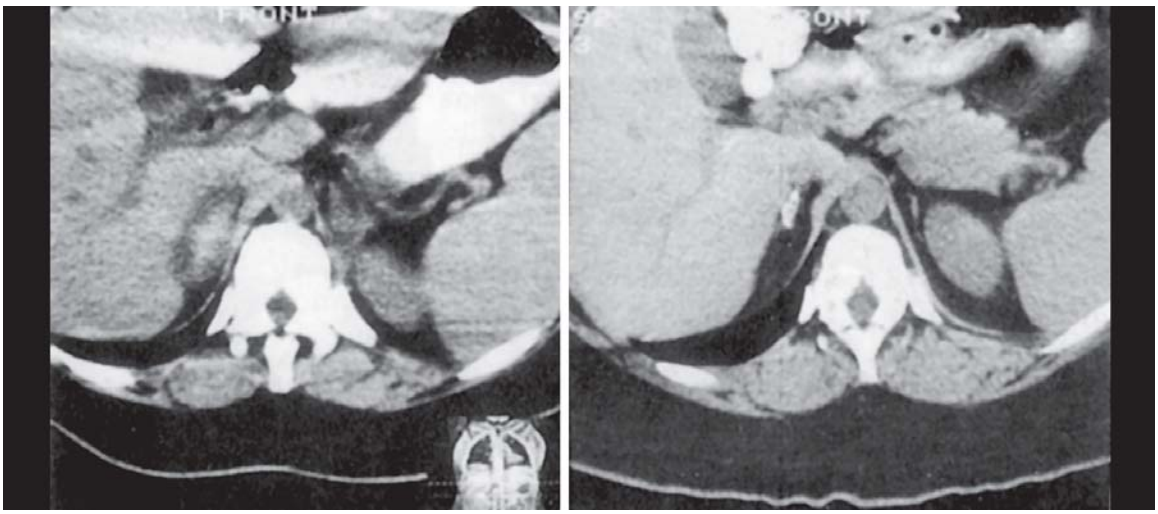

Fig. 20.22: Adrenal hemorrhage: CT shows asymmetrically enlarged adrenals with heterogeneous attenuation but no calcification. Follow up CT after five years shows small right adrenal with dense calcification and atropic left adrenal

decrease in attenuation thereby suggesting resorption (Fig. 20.22).

In the older child and adult, unilateral adrenal hemorrhage is usually caused by blunt abdominal trauma, and often involves the right adrenal. Unilateral adrenal hemorrhage has also been recently reported in patients undergoing liver transplantation. The excision of a segment of recipient's inferior vena cava necessitates ligation and division of right adrenal vein, this may result in venous infarction and hemorrhage in right adrenal. CT features are similar to those seen in bilateral hemorrhage.

Group III: Adrenal Diseases with Normal Function

A number of diseases may involve the adrenals which do not alter the adrenal function. Most of these disease entities are detected incidentally as adrenal mass or patients may present with vague abdominal pain or discomfort. These include non-functional adenoma or carcinoma, metastasis, lymphoma, neuroblastoma, adrenal cyst and myelolipoma. In some of these entities a specific diagnosis can be made from characteristic features on CT, e.g. adrenal cyst, myelolipoma. In some, CT may show nonspecific features but correlation with clinical features may suggest the possible etiology, e.g. neuroblastoma, metastasis.

Incidentaloma

These are adrenal nodules or masses discovered during imaging done for indications other than adrenal disease (Figs 20.23 to 20.26A and B). They are seen in 4-7 percent of the imaged population and majority of them are benign in the non-oncology population.[20,21] On the other hand almost 50 percent of incidentally detected adrenal lesions in patients with known malignancy represent metastatic disease.[2,4] Characterization of such incidental masses remains an important clinical problem when a unilateral non-functional adrenal mass is present; the differential diagnosis rests between adenoma and carcinoma or metastasis. In a patient with known malignancy, it is very essential to differentiate such incidental adrenal

mass as adenoma or metastasis because this will greatly affect patient's management and prognosis.

Adenoma vs Metastasis

Adenomas are thought to represent non-neoplastic overgrowth of adrenocortical cells of zona fasciculata. They consist of cholesterol laden clear cells and contribute little to steroid production. The imaging features of functional and nonfunctional adenomas on CT or MRI are similar (Figs 20.23 to 20.26A and B) except the functional ones are usually smaller at the time of presentation than non-functional tumors. They account for almost 90 percent of all incidentalomas.[5]

Tumors of the lung, kidney, breast, digestive tract, ovary and melanoma are the most common primary sites to metastasize to adrenals.[4,5] Metastases are well-defined with heterogeneous density and a thin irregular enhancing rim following intravenous contrast injection, commonly unilateral and usually larger than adenoma (Figs 20.27A to D). On MRI, they are hypointense on T1 weighted image and hyperintense on T2 weighted

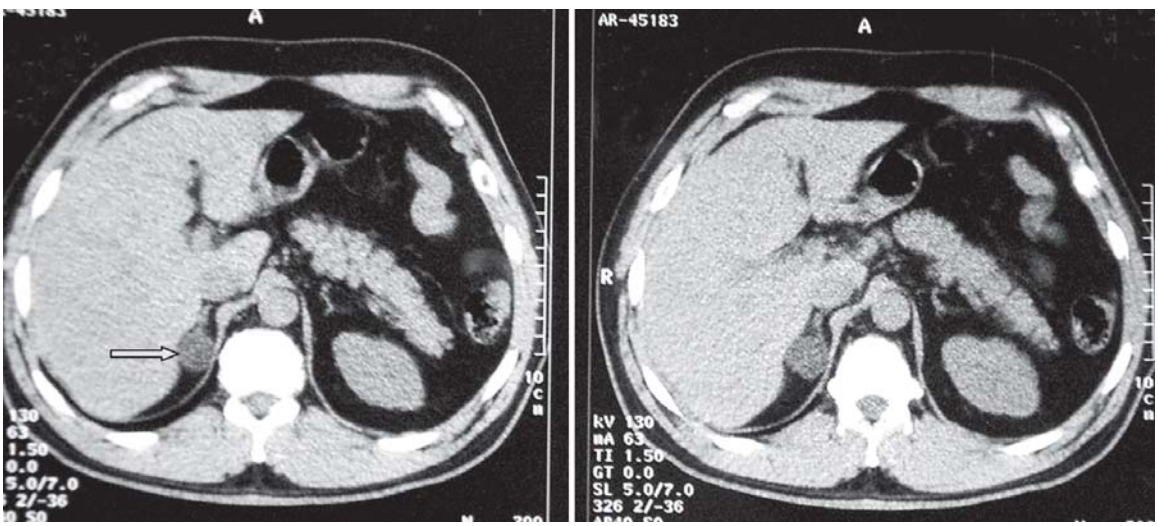

Fig. 20.23: Adrenal adenoma. NCCT shows a low attenuating well-defined mass in the right adrenal (arrow). The attenuation value was 6 HU

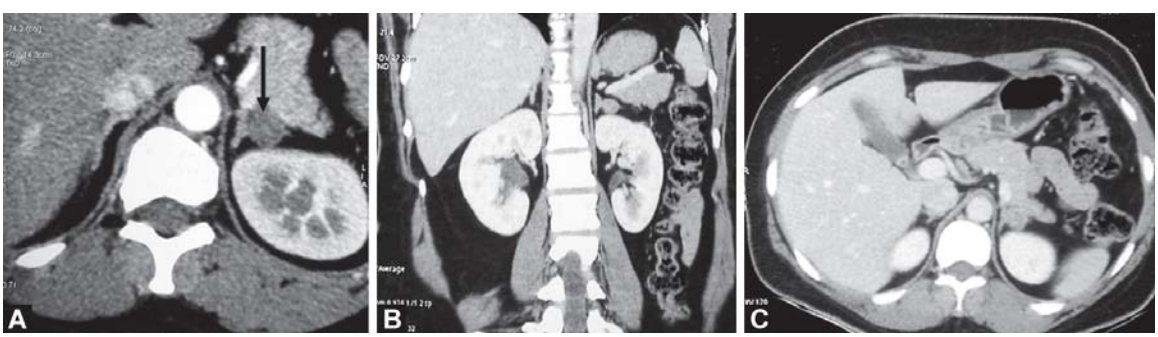

Figs 20.24A to C: Adrenal Adenoma. CECT **(A)** coronal MPR **(B)** and 15 minute delayed CT scan **(C)** show a mass in left adrenal gland (arrow) which showed 65 percent wash-out on the delayed scan

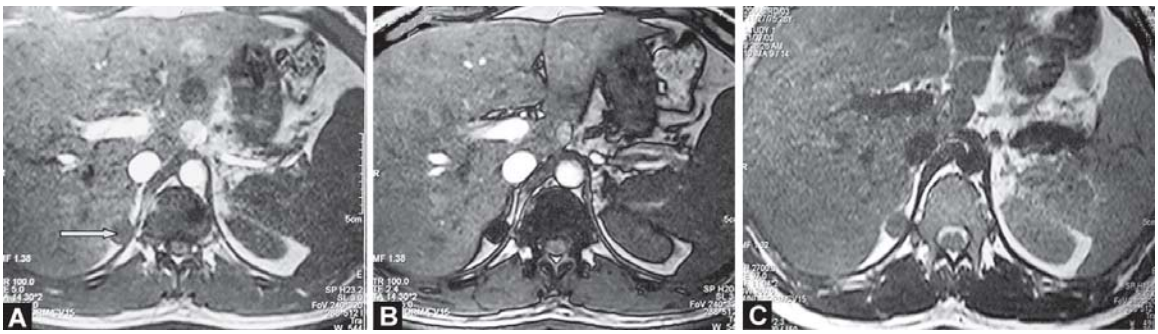

Figs 20.25A to C: Incidentally detected adrenal adenoma. Gradient echo T1W in-phase image **(A)** shows a hypointense nodule in right adrenal (arrow) which shows marked signal loss on the opposed phase image **(B)** The lesion is hypointense on T2W scan **(C)** also

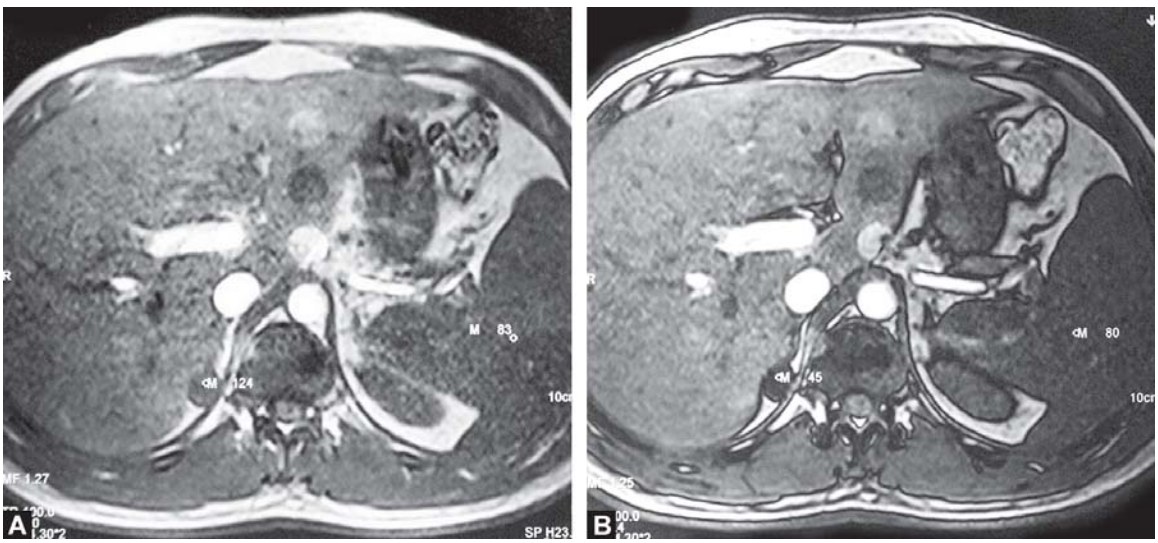

Figs 20.26A and B: Adrenal adenoma. GRE T1W in-phase **(A)** and opposed phase image **(B)** showing drop in signal intensity of right adrenal lesion from 124 to 45 whereas spleen signal intensity changes from 83 to 80 only

image, relative to liver intensity. It has been reported that 27 percent of patients with known malignancy have microscopic adrenal metastasis. However, the detection of an adrenal mass in a patient with known malignancy does not necessarily indicate metastatic disease and it may be a non-functional adenoma.

CT features of adenoma include size less than 5.0 cm and well-defined margins with smooth contour (Figs 20.23 to 20.24C). Adrenal metastasis may show large mass with heterogeneous density and irregular shape (Figs 20.27A to D). However, these features are not specific. It has been also reported that size alone is a poor discriminator between benign adenoma and malignant mass.[5,6]

In recent years, several studies have reported two imaging criteria based on attenuation value and differences in vascular enhancement pattern to differentiate benign adenoma from adrenal metastasis.[2,20]

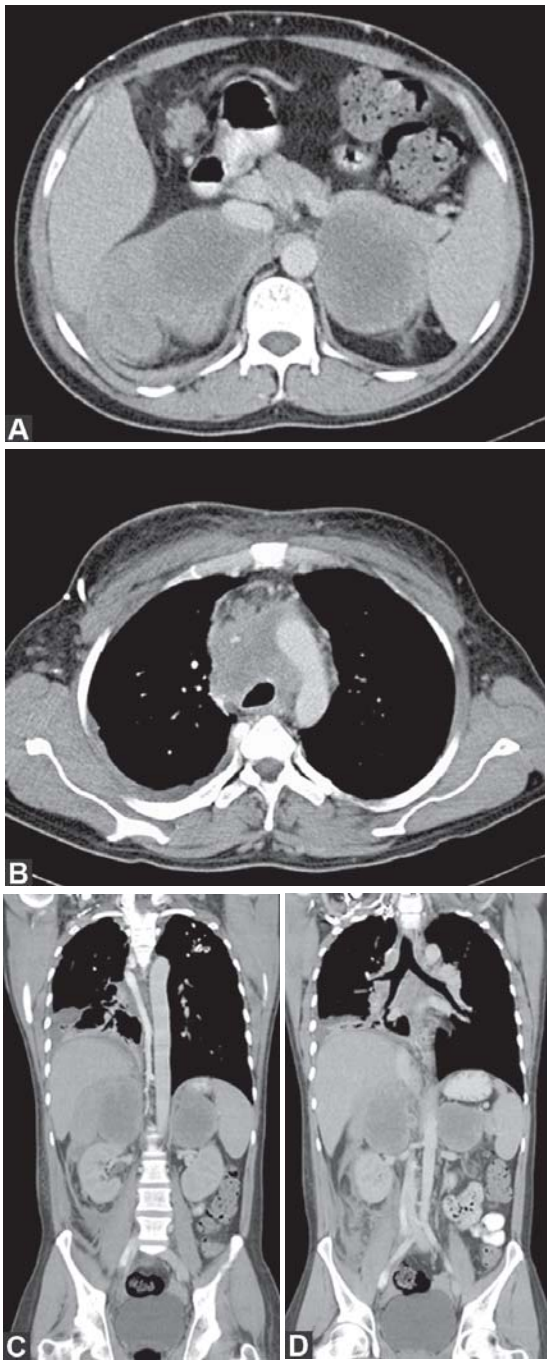

Figs 20.27A to D: Adrenal Metastases. CECT abdomen **(A)** shows bilateral solid adrenal masses. CECT chest **(B)** and coronal MPRs **(C,D)** show mediastinal adenopathy in a patient of bronchogenic carcinoma

Adenomas have abundant intracytoplasmic fat and therefore show low attenuation on non-contrast CT (Fig. 20.23). On the other hand metastases have little intracytoplasmic fat and thus do not show low attenuation. A large region of interest covering the adrenal mass should be used but should not include periadrenal fat for measuring attenuation value. It has been reported that a threshold of 10 HU has 71 percent sensitivity and 98 percent specificity for characterizing adenoma versus metastasis.[22] This specificity may be increased further if other features of size, shape and morphology are considered. Although 70 percent of adenomas have abundant lipid, the remaining are lipid poor and are difficult to characterize on a non-contrast scan.

If attenuation of the adrenal mass on non-contrast CT is 10 HU or less (Figs 20.9 to 20.23), the diagnosis is lipid rich adenoma and no further evaluation is required. If attenuation is more than 10 HU, the mass is indeterminate and requires further evaluation by contrast enhanced CT and 15 minutes delayed enhanced CT scan (Figs 20.24A to C).[23]

Adenomas enhance rapidly with intravenous contrast media and show rapid wash out. Metastasis also enhance rapidly but the wash out is delayed when compared to adenoma.[18,20] It has been speculated that this difference in enhancement wash out in non--adenoma is possibly due to disturbed capillary permeability, with prolonged retention of contrast in the effective extracellular space.

Adrenal masses with an attenuation value less than 30-40 HU on 15 minute delayed contrast enhanced CT are almost always adrenal adenomas.[1,24] In addition to the delayed CT attenuation itself, it is also possible to calculate the percentage washout of initial enhancement. The patient is first scanned without contrast, then again at

70 seconds, and then 15 minutes after contrast administration. Contrast wash-out can be quantified using Relative percentage wash out (RPW) and Absolute percentage wash out (APW) as follows:

RPW= 100 × (Enhanced HU- Delayed HU)/ Enhanced HU

APW=100 × (Enhanced HU- Delayed HU)/ Enhanced HU-Non-enhanced HU

If the APW is greater than 60 percent and the RPW is greater than 40 percent[20,23,24] lesion is labeled benign. This technique has a sensitivity of 88 percent and a specificity of 96 percent for the diagnosis of adenoma.[1,20] On the other hand, metastases and adrenocortical carcinoma have relative contrast retention on delayed contrast-enhanced CT.

It has been said that the relative washout percentage is more accurate for the differentiation of lipid poor adenomas from metastases than are the absolute attenuation values on delayed contrast enhanced scans.[25]

Dual energy CT: This is an emerging technique which has been used for determining bone mineral density and for evaluation of fatty liver. The difference in CT attenuation images acquired at 140 and 80 Kvp is measured, and if the difference between the two KVp is more than 6 HU, it is suggestive of fat containing lesion.[2]

Magnetic resonance imaging: In recent years, MRI has become a problem solving modality for the characterization of indeterminate adrenal masses. When results on CT examination are equivocal, MRI is the next imaging modality for characterizing the lesion. Due to increased fluid content in adrenal cancer and metastases, these appear bright on T2 weighted MRI images. However, there is significant overlap between T1 and T2 weighted MRI images of adenoma and metastases. With the introduction of higher field strength magnets (1.5T), chemical shift imaging and dynamic gadolinium enhanced MR imaging has shown promising results with adrenal gland lesions characterization. Confident diagnosis of adenomas on MRI requires the addition of chemical shift imaging to the protocol.

Chemical shift MR imaging has been used to differentiate adenoma from metastasis. This technique is based on the different resonance frequency rates of protons in fat and water molecules in a magnetic field. Two breath hold T1 weighted acquisitions are taken, first using a short echo time (TE 2.1 ms at 1.5Tesla) when the fat and water protons are out of phase and second in-phase acquisition using long echo time (TE 4.2 ms at 1.5Tesla). On most current MR scanners the in and opposed phase images can be obtained by one dual echo breath hold gradient echo sequence. The signal intensity on the in-phase image is derived from the signal of water plus fat protons while in the out of phase image, MR signal of water and lipid protons cancel each other out within a voxel. Therefore a mass containing intracellular lipid and water will show loss of signal in the out of phase images when compared with in-phase image (Figs 20.25A to C). Thus adenoma appears darker on out of phase image than on in-phase image, while metastasis will show no significant signal loss on out of phase image and the signal intensity remains unchanged.[2,8,9]

The sensitivity and specificity ranging from 81 to 100 percent and 94 to 100 percent respectively on chemical shift MR imaging for differentiating adenoma from metastasis have been reported.[6,9,20] The loss of signal can be assessed visually using spleen as the internal control (Fig. 20.26). The liver should not be used as the internal reference as it may also show signal loss on opposed phase image when there is steatosis.

The chemical shift change can also be detected by quantitative methods. Two ratios have been defined in CSI.

$$\text{SI Index} = \frac{1 - [\text{SI(in)} - \text{(opp)}]}{\text{SI(in)}}$$

and

Adrenal to spleen ratio

$$= \frac{\text{SI adrenal (opp)}}{\text{SI spleen (opp)}} \Big/ \frac{\text{SI adrenal (in)}}{\text{SI spleen (in)}}$$

SI index of > 16.5 percent and adrenal to spleen ratio of < 0.71 is suggestive of adenoma/ benign adrenal lesions. For a benign adrenal lesion characterization, the reported sensitivity and specificity using these two ratios were 87-100 percent and 92-100 percent respectively, whereas failure rate for diagnosis of lipid poor adenomas has been 13 to 17 percent.[20]

On dynamic MRI, contrast enhancement characteristics of adrenal masses is similar to that on CT with adenomas showing rapid contrast washout and metastases and carcinoma showing retention of contrast.

Diffusion weighted MRI (DWI): Which provides insight into water composition and cellularity in a tumor may provide an additional tool to distinguish benign from malignant adrenal masses. Malignant tumors have an increased cellularity which manifests as restricted diffusion, and a decrease in the apparent diffusion coefficient. There are no major published studies specifically on the adrenal, but extrapolating from data on liver, kidney etc this may be a promising technique in the future to distinguish between benign and malignant masses.[2]

Positron emission tomography (PET): Due to the limitations of CT and MR imaging, functional imaging modalities like F-18 FDG PET are now increasingly used for further characterization of an adrenal lesion.

F-18-fluorodeoxyglucose positron emission tomography (F-18 FDG PET) is an imaging modality that permits acquisition of functional information and when fused with CT imaging, results in accurate localization and metabolic characterization of adrenal lesions. In PET-CT, 18-Fluorodeoxyglucose is used as a glucose analogue which is taken up preferentially by malignant cells because of their increased glucose metabolism. Due to relative lack of glucose-6-phosphatase in the cancer cells as compared to cells of normal tissues, there is a focal intracellular accumulation of FDG, resulting in high tumor uptake values as compared to the background uptake values. However, in literature only limited data on the role of 18-FDG PET/PET-CT in characterization of adrenal lesions in oncology population is available, that too involving a relatively small sample size.[11] The results of all these studies are encouraging and justify the use of PET for metastatic disease evaluation in cancer patients. Although, PET results are encouraging, several inherent problems are associated with FDG-PET imaging viz. small adrenal lesions are difficult to image owing to poor resolution, and uptake in other abdominal structures, such as renal pelvis, can obscure the adrenal gland.

18F-FDG uptake is taken as abnormal when it is higher than background liver uptake.[11,13] T. If a lesion shows F18-FDG uptake less than that of the liver, or shows uptake that is significantly higher than the liver, the study can be interpreted with high confidence unless the patient has pheochromocytoma, which can be excluded by biochemical markers.[13]

In evaluation of adrenal masses with F18-FDG PET/CT, combined information from

the F18-FDG PET and unenhanced CT portions of a PET/CT study is more specific than F18-FDG PET information alone.[26] A SUV cut-off value of 3.1 has been used to differentiate malignant lesions and adenomas. PET data using a SUV cut-off of 3.1 to differentiate malignant adrenal masses from adenomas, yielded a sensitivity, specificity, positive predictive value and negative predictive value of 98.5 percent, 92 percent, 89.3 percent, and 98.9 percent respectively.[26]

Adrenal Carcinoma

Adrenal carcinomas are rare neoplasms, and are more common in women. They are usually larger than 10 cm at the time of presentation and are invasive. Only 10 percent are clinically functional which usually manifests as Cushing's syndrome, or virilization in females. CT or MRI show large solid masses with areas of degeneration and cystic changes, and 33 percent contain calcification (Figs 20.28A to 20.29F).[2,5,20] They tend to be locally invasive, especially into adrenal or renal veins and inferior venacava. They are hypointense on T1 and hyperintense on T2 weighted scans (Figs 20.28D to F) and show variable enhancement. Differential diagnosis includes adenoma, metastases, lymphoma, exophytic liver tumors, or upper polar renal masses.

Adrenal Lymphoma

Primary Lymphoma of the adrenal gland is unusual, but its involvement in disseminated lymphoma is common. The latter is more often seen in Non-Hodgkin lymphoma.[27] The most common presentation is diffuse bilateral enlargement of the gland, and the shape is usually maintained (Figs 20.30A to D). The tumor is hypovascular and shows only mild enhancement after contrast.

Adrenal Collision Tumor

This is a very rare entity characterized by coexistence of two contiguous but histologically different tumors. Both tumors may be malignant or one may be benign, other malignant or both may be benign. Imaging may show two distinct morphological features within the same mass. This entity should be suspected when only focal decrease in signal intensity of a mass is seen on opposed phase images or a focus of bright enhancement is seen within a mass which otherwise looks like an adenoma. Such an appearance may suggest a metastatic deposit within an adrenal adenoma.[5,28]

Adrenal Cyst

Adrenal cysts are rare and usually seen in females. They are derived from endothelium in 45 percent of patients and the rest are epithelial, parasitic or pseudocysts from prior hemorrhage. CT shows characteristically well-defined round low attenuating lesion suggesting fluid with rim enhancement (Fig. 20.31A). Rim calcification may be noted (Fig. 20.31B). The attenuation values may be mixed in the presence of debris or hemorrhage. On MR, adrenal cysts are hypointense on T1 weighted image and hyperintense on T2 weighted image. The complications of adrenal cysts include hemorrhage, infection and rupture.[20,29]

Myelolipoma

Myelolipoma is a benign tumor of the cortex, comprised of mature fat and hematopoietic elements. Patients are usually asymptomatic and the lesion detected incidentally. It accounts for about 7-15 percent of all incidentalomas. Imaging appearance may vary depending on which histological component is dominant. Ultrasonography and CT

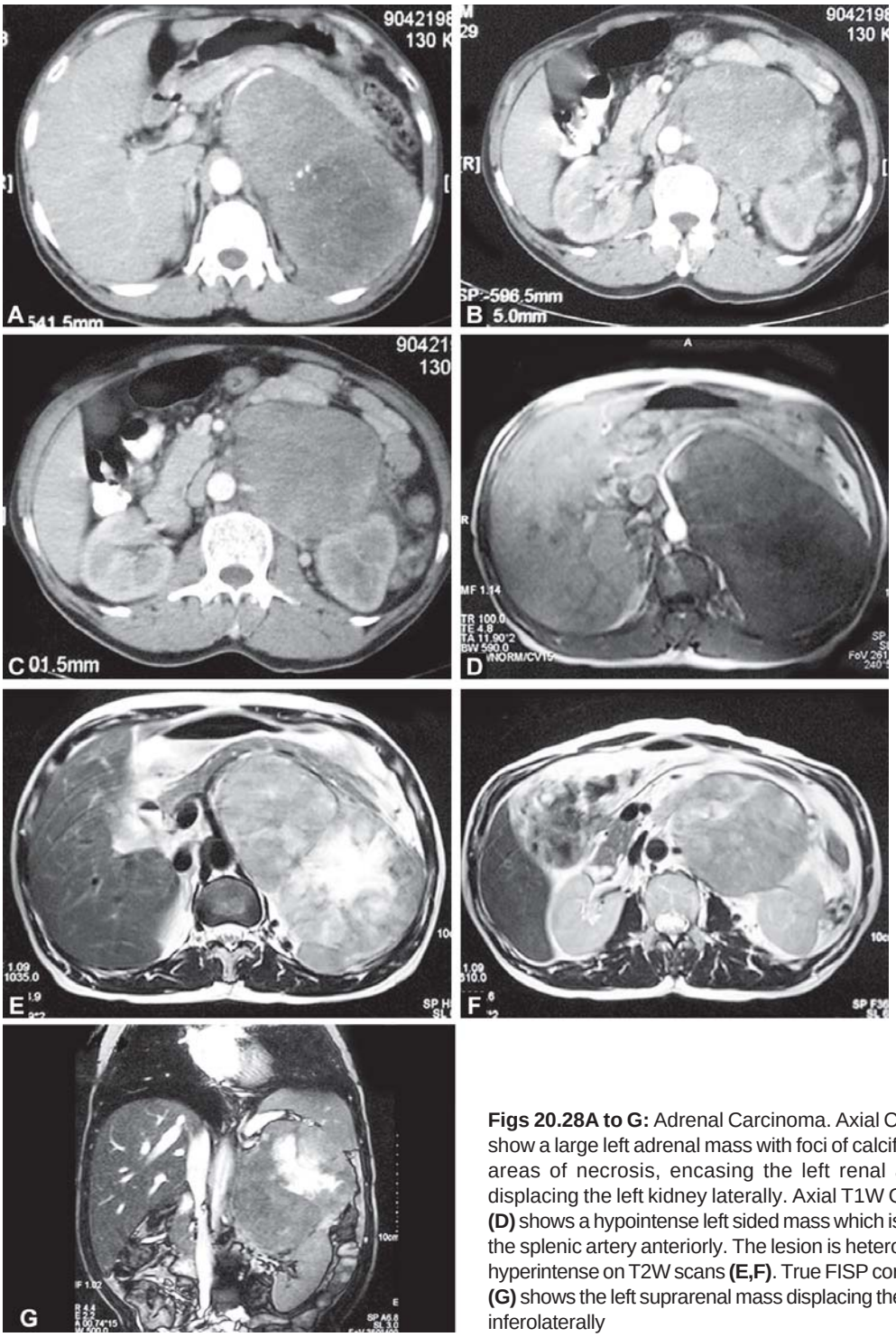

Figs 20.28A to G: Adrenal Carcinoma. Axial CECT **(A-C)** show a large left adrenal mass with foci of calcification and areas of necrosis, encasing the left renal artery and displacing the left kidney laterally. Axial T1W GRE image **(D)** shows a hypointense left sided mass which is displacing the splenic artery anteriorly. The lesion is heterogeneously hyperintense on T2W scans **(E,F)**. True FISP coronal image **(G)** shows the left suprarenal mass displacing the left kidney inferolaterally

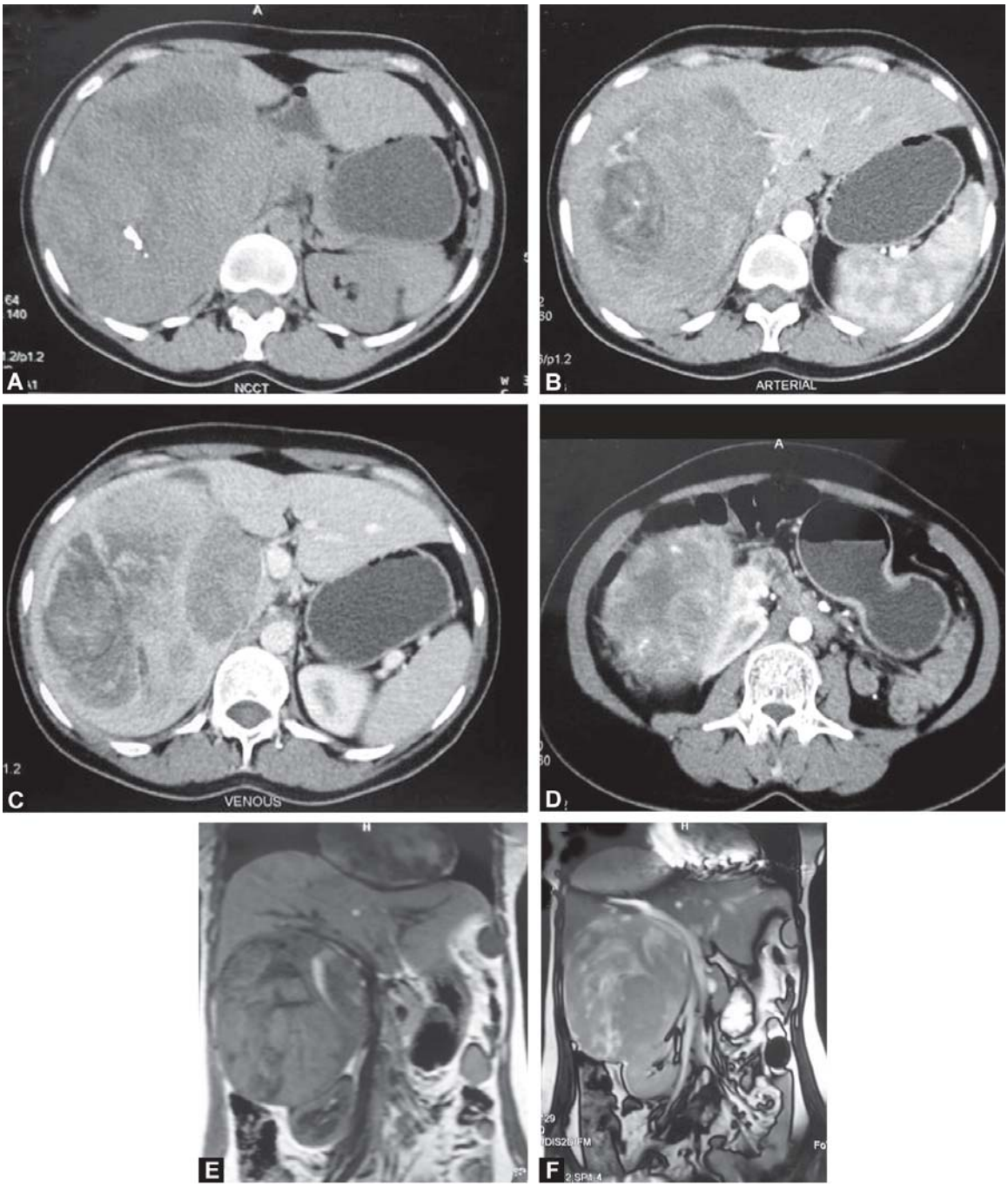

Figs 20.29A to F: Adrenal carcinoma. Axial NCCT **(A)** and CECT **(B-D)** show a large right adrenal mass with foci of calcification. It mimics an exophytic liver mass. GRE T1W **(E)** and true-FISP coronal **(F)** MR image of same patient show the right adrenal mass displacing the kidney inferomedially

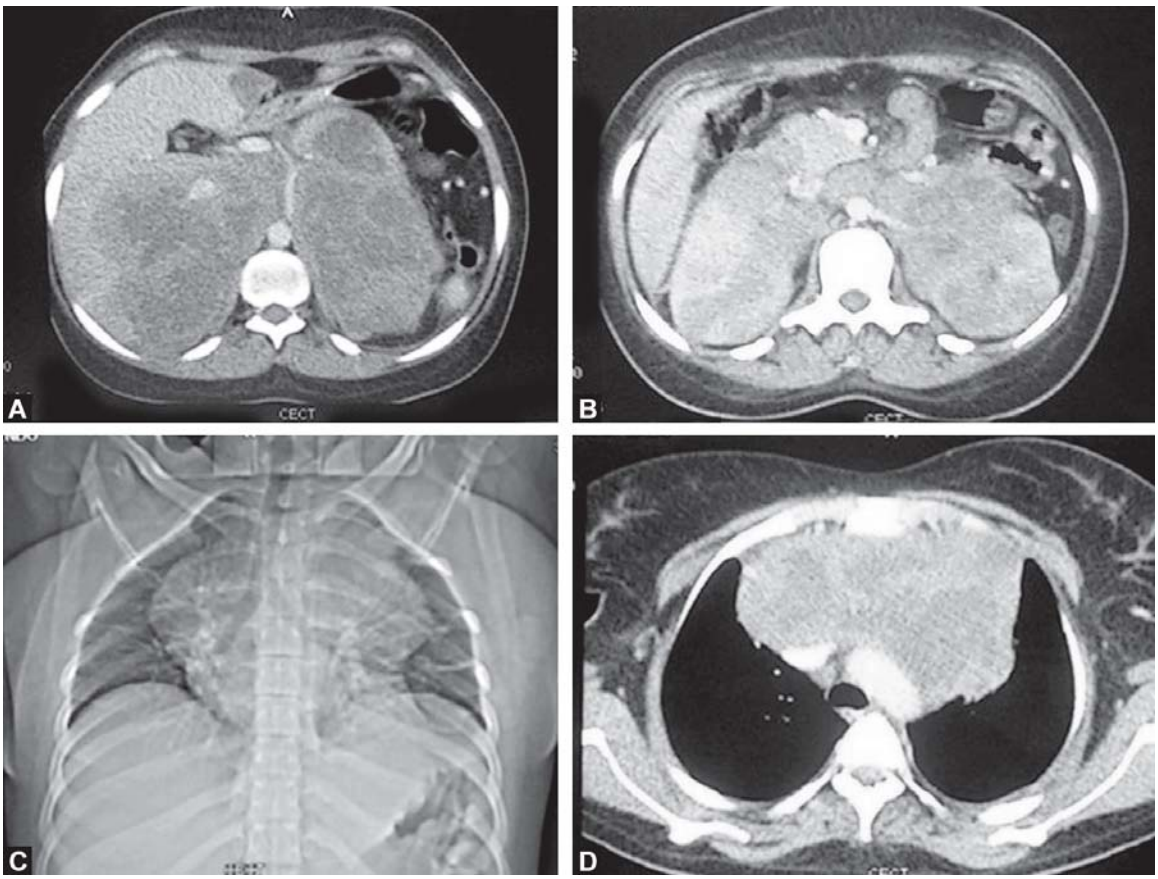

Figs 20.30A to D: Adrenal involvement in Non-Hodgkin lymphoma. Axial abdomen CECT **(A, B)** show bilateral adrenal masses, retroperitoneal adenopathy and focal renal lesions. Chest radiograph **(C)** and CECT chest **(D)** show bulky mediastinal adenopathy

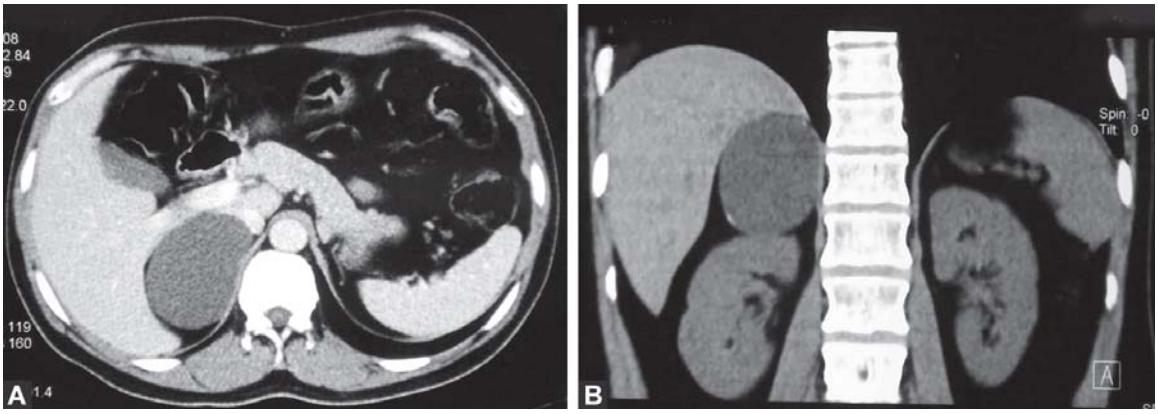

Figs 20.31A and B: Adrenal Cyst. Axial CT **(A)** and coronal MPR **(B)** show a fluid attenuating right adrenal mass with rim calcification

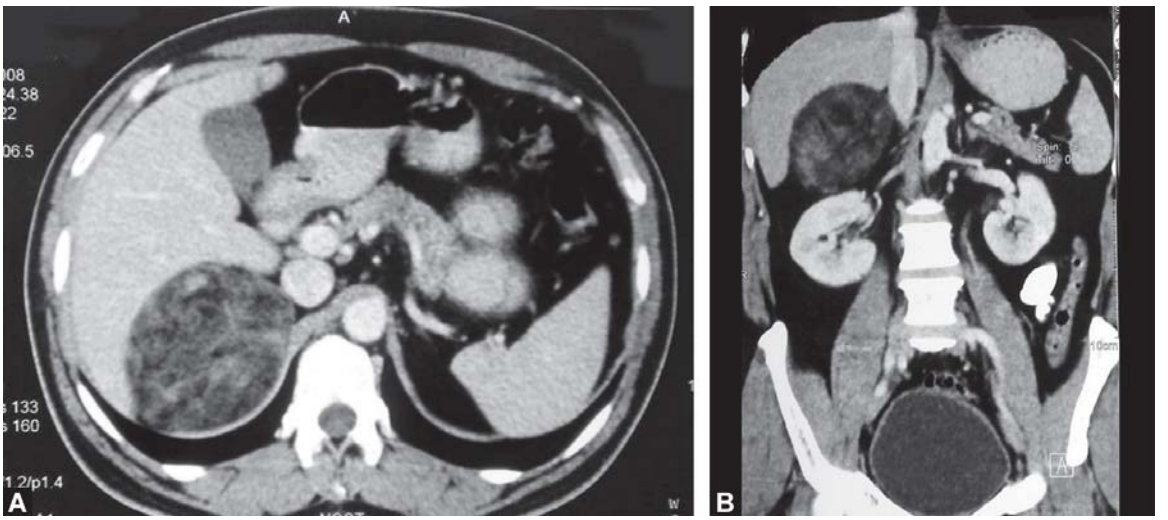

Figs 20.32A and B: Adrenal Myelolipoma. Axial CECT **(A)** and coronal MPR **(B)** show a mixed attenuating right adrenal mass with fat and soft tissue attenuation

features are quite characteristic and diagnostic. Ultrasonography shows well-defined echogenic or heterogeneous adrenal mass, which may be associated with apparent posterior displacement of the diaphragm due to propagation speed artifact resulting from slow speed of sound through the fat. CT confirms presence of intratumoral fat (Figs 20.32A and B). Punctate calcification may be seen in 20 percent of cases.[4,5] MRI can also characterize the lesion by identification of presence of fat which appears hyperintense on both T1 and T2 weighted images, and shows loss of signal on fat suppression techniques (Figs 20.33A to D).[6] Marrow elements show low signal on T1 and moderate signal on T2W images. Differential diagnosis includes adrenal adenoma, and large myelolipomas may mimic retroperitoneal lipoma or liposarcoma.

Neuroblastoma

Neuroblastoma is one of the most common tumor of childhood with 80 percent occurring below the age of 5 years. Most neuroblastomas arise from adrenal medulla but may also arise from sympathetic chain, posterior mediastinum being the second most common site. Seventy five percent occur in the abdomen, and two-thirds of these are in the adrenal gland. Symptoms are related to the primary tumor and to metastases, which are present in more than 50 percent patients at the time of diagnosis. Children can present with a palpable mass, bone pain and opsomyoclonus. Common sites of metastases are lymph nodes, cortical bone, marrow, skin and liver.[4,5]

Ultrasonography almost always shows a mass which must be distinguished from nephroblastoma. Neuroblastoma is seen typically as large mass with heterogeneous echogenicity with scattered hyperechoic areas due to presence of calcification. CT shows soft tissue mass with areas of low attenuation and scattered coarse or mottled calcification, seen in almost 85 percent of the patients. The tumor enhances with intravenous contrast. Unlike Wilm's tumor, which usually has a well defined pseudocapsule,

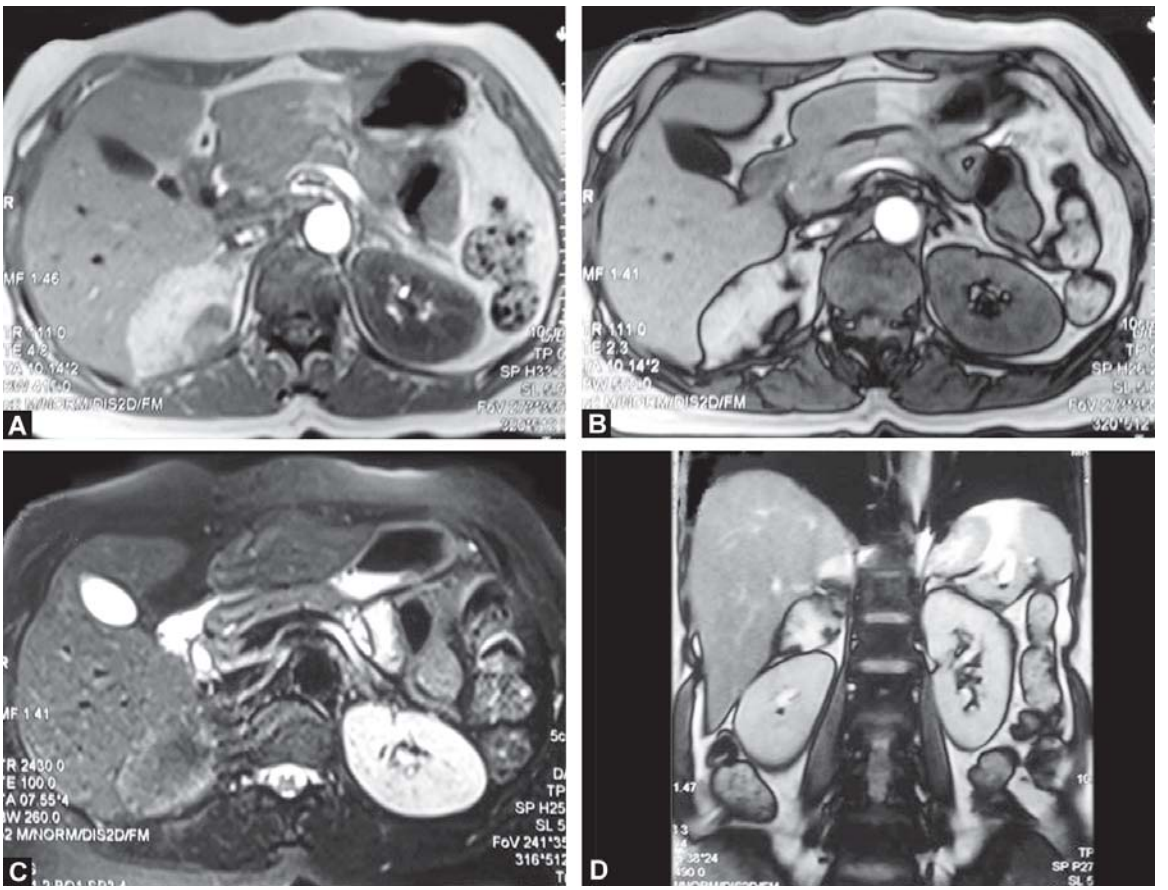

Figs 20.33A to D: Adrenal Myelolipoma. GRE T1W in-phase **(A)** and opposed phase **(B)** image show a hyperintense right adrenal mass which shows no drop in signal intensity but is suppressed on T2W fat suppressed image **(C)**. Coronal true-FISP image **(D)** shows a hyperintense right adrenal mass

neuroblastoma invades adjacent structures and encases the aorta and its branches (Fig. 20.34) early in the course of disease. On MRI, neuroblastoma shows low signal intensity on T1 weighted image and increased intensity on T2 weighted image, relative to liver intensity. Tumor heterogeneity is seen best on T2 weighted sequence and reflects calcification and necrosis.

MRI is better than CT for defining vascular encasement, metastasis and intraspinal extension which occurs in 15 percent of patients. Therefore, MRI is the single best imaging modality for accurately staging the extent of the disease.[6] Neuroblastoma may also take up MIBG, which may detect bony metastasis more accurately than CT or MRI. The presence of skeletal metastasis in association with an adrenal mass in a child strongly suggests the diagnosis of neuroblastoma.

SUMMARY

With the widespread use of cross-sectional imaging techniques detection of an adrenal mass has increased over the years. However,

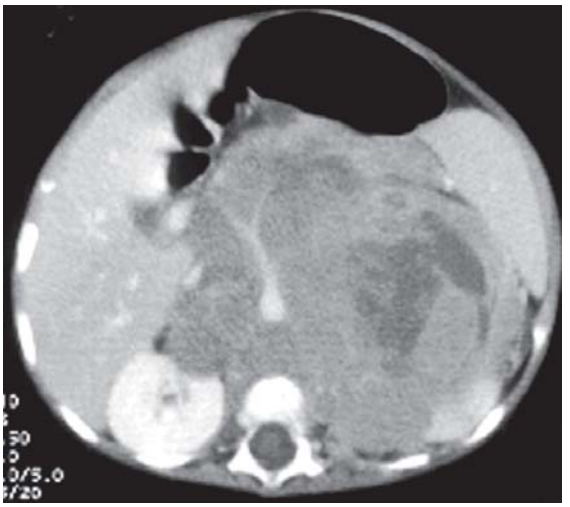

Fig. 20.34: Neuroblastoma. Axial CECT abdomen of a 2-year-old child shows a large left adrenal mass which is extending posterior to the aorta and inferior vena cava and encasing the celiac axis

clinical and appropriate biochemical tests in adrenal lesions, especially for functional diseases remain the most vital and initial mode of evaluation, followed by CT. The role of CT has continued to expand in both detection and characterization of an adrenal mass as benign or malignant. Based on size criteria and tumor morphology, it is not always possible to suggest benignity or malignancy. Follow up studies are very necessary in equivocal cases. Necrosis in the tumor is related directly to prognosis. More necrosis carries worse prognosis. All attempts should be made to characterize an incidental adrenal mass as adenoma or metastasis in a patient with known malignancy. Lipid rich adenoma can be characterized with attenuation value of 10 HU or less on non-contrast CT. Lipid poor adenoma can be differentiated from metastasis on delayed enhanced CT with percentage enhancement wash out of more than 50 percent. If the mass remains indeterminate, chemical shift MRI is the next imaging modality for further characterization. If all these modalities still fail to characterize the lesion in a patient with known malignancy, having no other evidence of metastatic deposit, adrenal biopsy under CT guidance should be performed to establish a definitive diagnosis.

REFERENCES

1. Korobkin M. CT characterization of adrenal masses: The time has come. Radiology 2000; 217:629-32.
2. Blake MA, Holalkere NS, Boland GW. Imaging techniques for adrenal lesion characterization. Radiol Clin N Am 2008;46:65-78.
3. Gross MD, Korobkin M, Hussain H, et al. Adrenal gland imaging , in Jameson JL, DeGroot LJ (Eds): Endocrinology (5th edn). Philadelphia, WB Saunders 2005;2425-53.
4. Welch TJ, Sheedy PF. The adrenal glands, in CT and MR imaging of the whole body (4th edn), 2003. Haaga, Lanzieri, Gilkeson Eds, Mosby, St Louis, USA,
5. Adrenal anatomy and imaging issues, in Diagnostic Imaging-Abdomen 2004: Federle MP, Jeffrey RB, Desser TS, et al (Eds). Amirsys, Salt Lake City, Utah.
6. Kelekis NL, Semelka RC, Firat RT. Zeynep. Adrenal glands in Abdominal-pelvic MRI. Ed Semelka RC, 2nd edition, John Weley and Sons, New Jersey USA 2006;865-916.
7. Chung JJ, Semelka RC, Martin Dr. Adrenal adenomas. Characteristic post gadolinium capillary blush on dynamic MR imaging. J Mag Reson Imaging 2001;13:242-48.
8. Reinig JW, Stutley JE, Leonhardt CM, Spicer KM, Margolis M, Caldwell CB. Differentiation of adrenal masses with MR imaging: Comparison of techniques. Radiology 1994;192:41-46.
9. Lee MJ, Mayo-Smith WW, Hahn PF, et al. State-of-the-art MR imaging of the adrenal gland. Radiographics 1994(14);1015-29, discussion 1029-32.
10. Bilbey JH, Mc Louglin RF, Kurkjian PS, et al. MR imaging of adrenal masses; value of chemical-shift imaging for distinguishing adenomas from other tumors. Am J Roentgenol 1995;164: 637-42.

11. Blake MA, Slattery JMA, Kalra MK, Halpern EF, Fischman AJ, Mueller PR, Boland GB. Adrenal lesions: Characterisation with Fused PET/CT image in patients with proved or suspected malignancy—Initial Experience. Radiology 2006;238:970-77.
12. Shulkin BL, Thompson NW, Shapiro B, Francis IR, Sisson JC. Pheochromocytomas: Imaging with 2-[18F]fluoro-2-deoxy-D-glucose PET. Radiology 1999;212:35-41.
13. Yun M, Kim W, Alnafisi N, Lacorte L, Jang S, Alavi A. 18F-FDG PET in characterizing adrenal lesions detected on CT or MRI. J Nucl Med 2001;42:1795-99.
14. Lumachi F, Zucchetta P, Marzola MC, et al. Usefulness of CT scan, MRI and radiocholesterol scintigraphy for adrenal imaging in Cushing's syndrome. Nuclear Medicine Communications 2002;23:469-73.
15. Rockall AG, Babar SA, Sohaib SAA, et al. CT and MR Imaging of the Adrenal Glands in ACTH-independent Cushing Syndrome. Radiographics 2004;24:435-52.
16. Doppman JL, Gill JR Jr, Miller DL, et al. Distinction between hyperaldosteronism due to bilateral hyperplasia and unilateral aldosteronoma: Reliability of CT. Radiology 1992;184: 677-82.
17. Harinarayana CV, Gupta R, Ammini AC, et al. Computed tomography in untreated congenital adrenal hyperplasia. Paed Radiol 1991;21: 103-05.
18. Mayo-Smith WW, Boland GW, Noto RB, et al. State of the art adrenal imaging. Radiographics 2001;21:995-1012.
19. Ammini AC, Gupta R, Mukhopadhya C, et al. Computed tomography morphology of adrenal gland of patients with Addison's disease. Austral Radiol 1996;40:38-42.
20. Boland GW, Blake MA, Hahn PF, Mayosmith WW. Incidental Adrenal lesions: Principles, techniques, and algorithms for imaging characterization. Radiology 2008;249(3):756-75.
21. Young WF Jr. The incidentally discovered adrenal mass. N Engl J Med 2007;356:601-10.
22. Boland GW, Lee MJ, Gazelle GS, et al. Characterization of adrenal masses using unenhanced CT: An analysis of CT literature. Am J Roentgenol 1998;171:201-04.
23. Caoili EM, Korobkin M, Francis IR, et al. Adrenal masses: characterization with combined unenhanced CT and delayed enhanced CT. Radiology 2002;222:629-33.
24. Korobkin M, Brodeur FJ, Yutzy GG, et al. Differentiation of adrenal adenomas from nonadenomas using CT attenuation values. Am J Roengenol 1996;166:531-36.
25. Pena CS, Boland GW, Hahn PF, Lee MJ, Mueller PR. Characterization of indeterminate (lipid-poor) adrenal masses: Use of washout characteristics at contrast enhanced CT. Radiology 2000;217-798-802.
26. Metser U, Miller E, Lerman H, Lievshitz G, Avitla S, Even-Sapir E. 18F-FDG PET/CT the evaluation of adrenal masses. J Nucl Med 2006;47:32-37.
27. Paling MR, Williamson BR. Adrenal involvement in non-Hodgkin lymphoma. Am J Roengenol 1983;141:303-05.
28. Schwartz LH. Collision tumor of the adrenal gland: demonstration and characterization at MR imaging. Radiology 1996;201(3):757-60.
29. Tung GA, Pfister RC, Papanicolaou N, Yoder IC. Adrenal cysts: Imaging and percutaneous aspiration. Radiology 1989;173:107-11.

Chapter

21 The Retroperitoneum

Smriti Hari, Atin Kumar

The retroperitoneum is the portion of the abdomen located posterior to the peritoneal cavity. It extends from the diaphragm superiorly to the pelvis inferiorly. An understanding of the complex anatomy of the retroperitoneum is imperative for predicting the distribution of inflammatory fluid collections, extravasated blood, and solid masses in this region. This chapter describes the computed tomography (CT) and magnetic resonance imaging (MRI) manifestations of diseases involving the retroperitoneal spaces, aorta, inferior vena cava (IVC) and retroperitoneal lymph nodes. Disease processes confined to the retroperitoneum including, primary retroperitoneal tumors, retroperitoneal fibrosis, and abnormalities related to the iliopsoas compartment are also discussed.

NORMAL ANATOMY

The retroperitoneum is divided into three main compartments: An anterior pararenal space that is continuous across the midline, a perirenal space on each side, and a posterior pararenal space on each side (Fig. 21.1). The anterior pararenal space contains the pancreas, the second, third, and fourth segments of the duodenum, the ascending and descending colon, lymph nodes, and fat. This space is bordered anteriorly by the posterior parietal peritoneum, posteriorly by the anterior renal fascia (Gerota's fascia), and laterally by the lateroconal fascia, which is a continuation of the posterior renal fascia (Zuckerkandl fascia).[1] The perirenal space lies between the anterior and posterior renal fascia and contains the kidney, adrenal gland, renal pelvis, proximal ureter, renal hilar vessels, lymph nodes, and fat.[2] The fascia of Gerota blends anteriorly with the connective tissue surrounding the aorta and inferior vena cava. The posterior pararenal space extends from the posterior renal fascia to the transversalis fascia and contains only a small amount of fat. Although it is located posterior to the kidneys, it continues anterolaterally as the properitoneal fat stripe.

The renal and lateroconal fascia are laminated, potentially expansile planes composed of apposed layers of embryonic mesentery: The retromesenteric plane between the leaves of the anterior pararenal fascia, the retrorenal plane formed by splitting of posterior pararenal fascia and the lateroconal plane between the leaves of the lateroconal fascia. Whereas most collections remain confined to

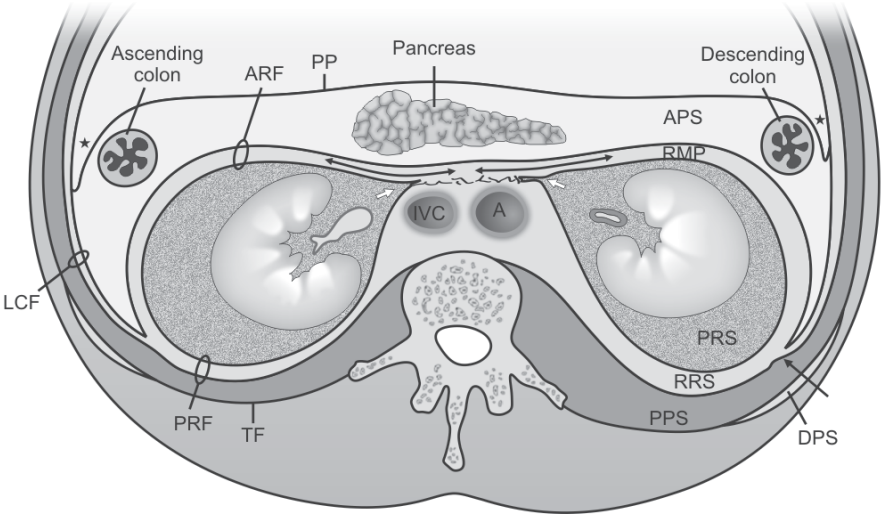

Fig. 21.1: Retroperitoneal and interfascial planes. Drawing at level of renal hila shows that perirenal and lateroconal fascia are laminated planes composed of apposed layers of embryonic mesentery. Note that thickness of interfascial planes is exaggerated to illustrate potentially expansile nature. Also note that perinephric spaces are closed medially *(open arrows).* Retromesenteric plane is continuous across midline *(bidirectional arrows).* Retromesenteric plane, retrorenal space, and lateroconal space communicate at fascial trifurcation *(arrow).* Dorsal pleural sinus may extend inferiorly to lie posterolateral to posterior pararenal space and transversalis fascia. A = aorta, APS = anterior pararenal space, ARF = anterior renal fascia, DPS = dorsal pleural sinus, IVC = inferior vena cava, LCF = lateroconal fascia, PP = parietal peritoneum, PPS = posterior pararenal space, PRF = posterior renal fascia, PRS = perinephric space, RMP = retromesenteric plane, RRS = retrorenal space, TF = transversalis fascia, ***** = posterior peritoneal recess

the retroperitoneal compartment in which they originate, CT observations and cadaveric dissections suggest that rapidly accumulating collections can dissect and decompress through these retroperitoneal fascial planes themselves.[3]

Inferior to the cone of renal fat, anterior and posterior renal fascia fuse, effectively sealing the caudal perinephric space, preventing the inferior extension of perirenal fluid into the pelvis.[4] The communicating retromesenteric, retrorenal and the lateroconal fascial planes continue downwards into the true pevis anterolateral to the psoas muscle.[5] Thus, the interfascial fluid unlike perinephric fluid can spread from the abdominal retroperitoneum into the pelvis.[6] Superiorly, both layers of renal fascia blend with the diaphragmatic fascia to form the cephalic limit of the retroperitoneum. The normal anterior and posterior renal fascia measure 1-3 mm in thickness and are well-visualized on CT scan except when abdominal fat is scanty. The posterior renal fascia is thicker and more frequently visualized than the anterior. Thickening of the retroperitoneal fascia is a sensitive but nonspecific indicator of adjacent disease, and is seen in both inflammatory (Fig. 21.2) and neoplastic disorders.

IMAGING MODALITIES

Multidetector CT is currently the preferred imaging modality for evaluating the retroperitoneum. It accurately displays its anatomical limits and clearly defines individual spaces separated by various fascial

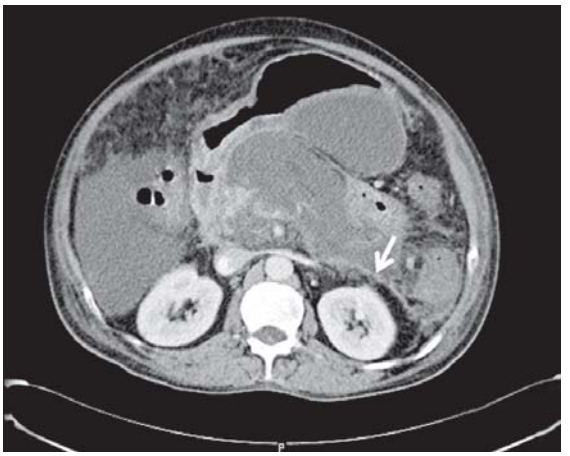

Fig. 21.2: Thickening of the left anterior renal fascia (arrow) in a patient of acute pancreatitis

layers. Isotropic multiplanar reconstructions (MPRs) of thin overlapping slices in the coronal and sagittal plane provide excellent delineation of the location and extent of retroperitoneal masses. It is a useful modality for making initial diagnosis of various pathological conditions and for follow-up. The introduction of multidetector technology has substantially improved the quality and ease of performing CT angiography. The simultaneous acquisition of multiple thin collimated slices in combination with enhanced gantry rotation speed offers thin slice coverage of extended volumes without any loss in spatial resolution. Multidetector CT angiography (MDCTA) is increasingly being used for assessing diseases affecting the vasculature of the abdominal organs, for treatment planning and post therapy follow-up.[7] CT scanners with 16 or more detectors enable full abdominal coverage from the diaphragm to the groin with high spatial resolution. These scanners permit excellent evaluation of the whole arterial visceral vasculature (e.g. hepatic vessels, mesenteric vessels, renal arteries) and the aortic-iliac axis in a single data acquisition (Fig. 21.3).

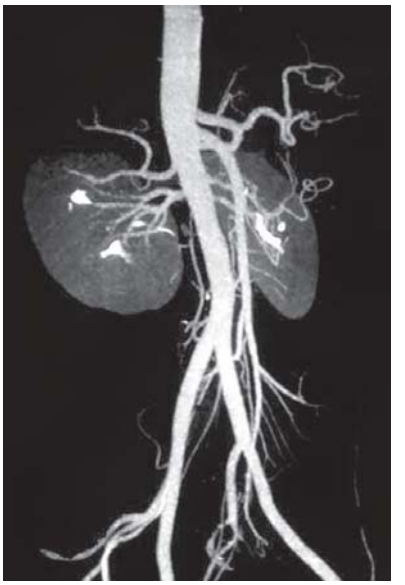

Fig. 21.3: Normal MDCT angiogram of the abdominal aorta. Maximum-intensity-projection (MIP) image shows good delineation of the entire abdominal aorta and its branches.The aorta has smooth walls and tapers gradually to the level of the aortic bifurcation

MRI may provide additional information about retroperitoneal abnormalities because of its multiplanar capability and excellent soft tissue resolution. The MR imaging protocol should be devised to maximize the signal intensity differences between pathologies and the background tissues. Typical sequences used are pre-contrast T1-weighted spoiled gradient echo (SGE), fat-suppressed T2-weighted and post-gadolinium fat-suppressed T1-weighted SGE images. In the investigation of retroperitoneal hemorrhage, precontrast fat-suppressed T1-weighted SGE sequence should be obtained because it has the greatest sensitivity for subacute hemorrhage. Both T1-weighted and T2-weighted sequences are important for delineation and characterization of retroperitoneal masses, abscesses, and fibrosis. Image acquisition in two orthogonal planes permits direct evaluation of the extent of retroperitoneal

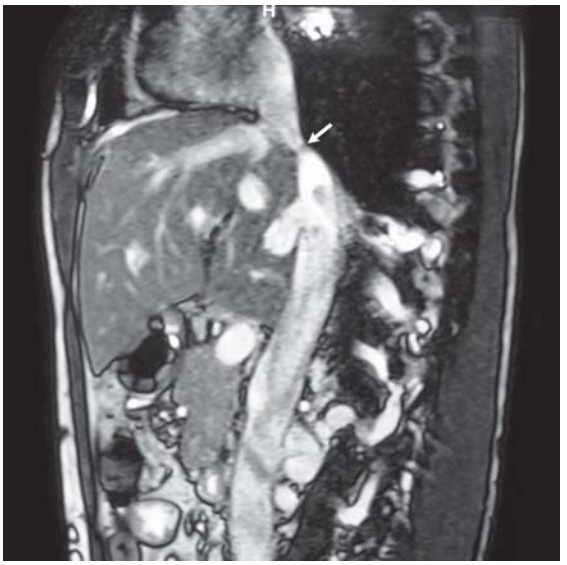

Fig. 21.4: Membranous obstruction of the intrahepatic IVC. Sagittal balanced steady-state (true FISP) MR image shows segmental occlusion of the IVC just below the cavoatrial junction

disease. Applications include evaluation of patients with suspected IVC thrombosis or Budd-Chiari syndrome (Fig. 21.4), intravascular extension of renal, adrenal, or hepatic tumors, and evaluation of anatomic anomalies of the IVC and systemic veins.[8]

Magnetic resonance angiography (MRA) has an important role to play in the imaging of aorta and IVC. Three-dimensional (3D) gadolinium-enhanced MRA can visualize the entire aorta with a single acquisition, allowing accurate determination of the extent of aneurysm, dissection, and other abnormalities. Vascular contrast is excellent, and data can be viewed in any projection, which facilitates surgical planning.[9] Typically 0.1 to 0.2 mmol/kg body weight of gadolinium is injected intravenously as a bolus with an automatic injector at a rate of 2 to 4 ml/s, followed by 20 cc of saline to clear lines and veins. For aortic imaging, the time interval between initiating contrast injection and initiating the imaging sequence can be determined using a test bolus technique. 1–2 ml of contrast is injected as a test bolus and the aorta is scanned approximately once per second. The travel time can be directly observed and then used to calculate the correct scan delay. Alternatively, automated triggering may be employed in which the aorta is continuously scanned until the contrast material bolus is directly observed or the signal intensity reaches a specified level, at which time the 3D sequence is begun. The acquired dataset can be postprocessed either by MPRs or by 3D maximum intensity projection (MIP) (Fig. 21.5). It is important to remember that arterial-phase MIP images demonstrate contrast material within the patent lumen and therefore may not accurately depict the true diameter of an aneurysm. The walls of vessels can usually be identified on source images or axial reformatted images. In addition, axial T1-weighted spoiled gradient-echo or spin-echo MR sequences following angiography are very useful in determining the diameter of the aneurysm and the extent of intraarterial plaque or thrombus. Likewise, it is important

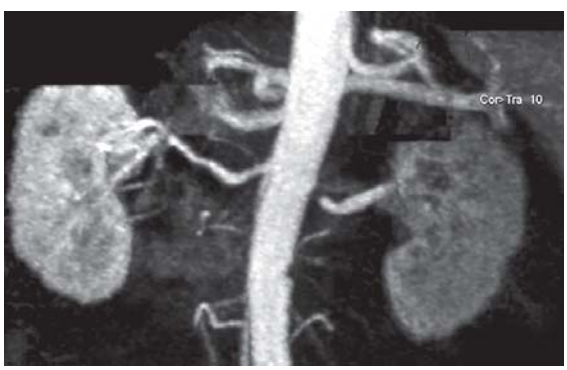

Fig. 21.5: Maximum intensity projection of 3D, gadolinium-enhanced MR angiogram depicting left renal artery stenosis

to scrutinize source images or thin-section reformatted images in patients who may have a dissection; an intimal flap can easily be missed if only MIP images are viewed.

Positron-emission tomography (PET) scanning has shown very high sensitivity and specificity for detection of retroperitoneal diseases. PET with 2-(fluorine-18) fluoro-2-deoxy-D-glucose (FDG) allows detection of small malignant nodes not identified or not meeting size criteria for malignancy with CT (Figs 21.6A and B) and tumor recurrences in surgical beds that are otherwise difficult to assess because of altered anatomy, surgical clip artifacts, and scar issue.[10] However, evaluation of retroperitoneal malignancies or adenopathy with FDG-PET can be complicated by urinary and colonic activity or anatomic variants. Urinary artifacts are avoided with intravenous hydration, administration of furosemide, and catheterization and retrograde filling of the bladder with saline solution. Colonic artifacts are avoided by cleansing the bowel with an isosmotic solution. FDG-PET is useful in assessing the retroperitoneum for adenopathy in malignancies such as testicular cancer; lymphoma; and rectal, ovarian or cervical cancer that spread along retroperitoneal lymphatics.

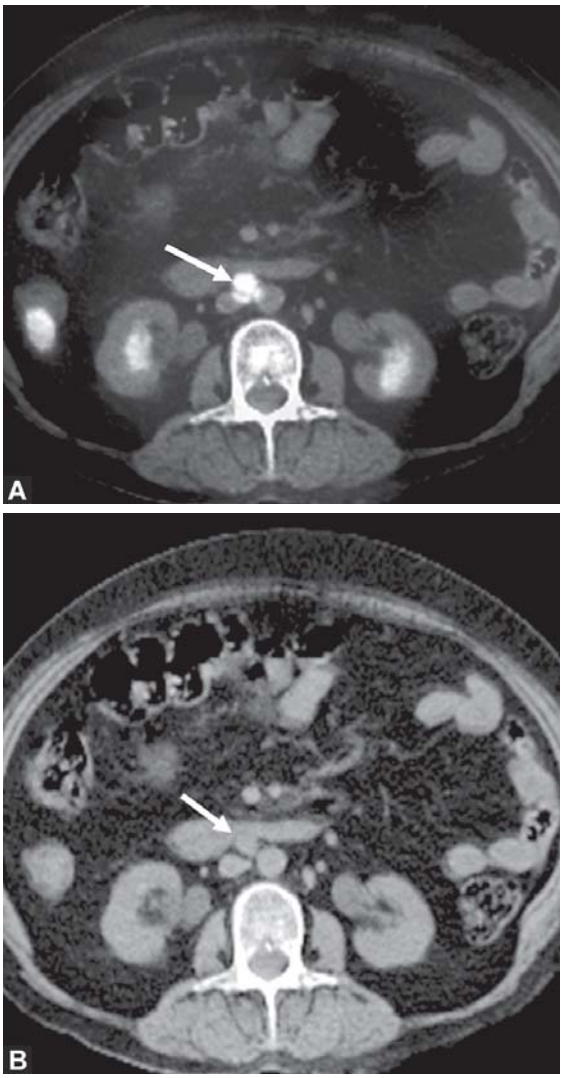

Figs 21.6A and B: (A) FDG-PET image in a patient of carcinoma ovary shows increased uptake in a subcentimetric aortocaval lymph node (arrow). **(B)** Comparison CT image also shows the node (arrow), which was considered insignificant by the size criteria *(For color version of Fig. 21.6A see Plate 20)*

RETROPERITONEAL COLLECTIONS

Fluid collection in the retroperitoneum occurs in a variety of conditions. The important conditions are acute pancreatitis, urinary tract disruption with urinoma formation, hematoma and abscess. Although the clinical presentations differ, they all share a tendency to dissect within the well-defined fascial planes in the retroperitoneal space. Most of these appear on CT as water density collections and are frequently indistinguishable from one another.

Fluid collections in the anterior pararenal space often result from acute pancreatitis (Fig. 21.7).[11] Fluid collections arise within or adjacent to the pancreas in about 40 percent and resolve spontaneously without leaving any clinical sequelae in over 50 percent of

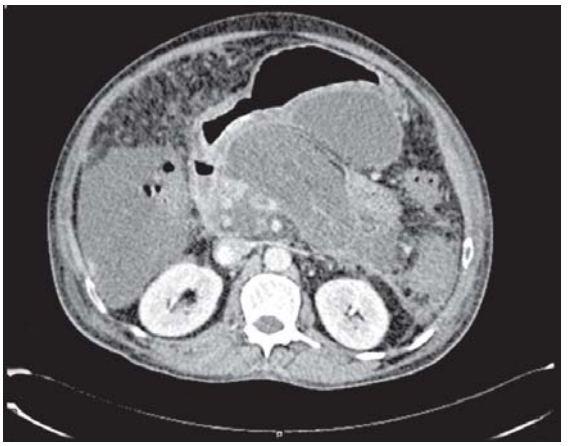

Fig. 21.7: Fluid collection in the anterior pararenal space. CT image in a patient with acute pancreatitis demonstrates peripancreatic fluid in the left anterior pararenal space

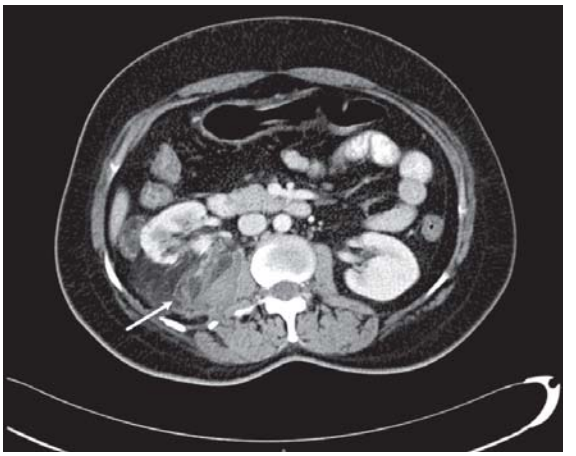

Fig. 21.8: Perirenal hemorrhage. Axial CT image shows right perirenal hemorrhage (arrow) that occurred spontaneously from rupture of underlying renal angiomyolipoma

these patients. In others, the fluid collections persist, develop a fibrous capsule and are often associated with a variety of complications including secondary infection, perforation and erosion into the spleen, liver or vascular system. Both infected and noninfected fluid collections and pseudocysts can be treated effectively by image guided percutaneous catheter drainage.

Abscesses, hematomas, and urinomas can all develop in the perirenal space. Perirenal hemorrhage is usually caused by blunt trauma, rupture of an aortic aneurysm, bleeding disorders, anticoagulant therapy or spontaneous bleeding within a renal tumor (Fig. 21.8). On CT characteristically, a hyperdense, ill-defined collection originating from the disrupted vessels and extending into the interfascial planes is seen. Loculated blood can mimic a complex cyst or neoplasm. CT attenuation of hematoma varies with time, ranging from hyperdense fresh blood, typically > 50 HU to near water density within several weeks. Bleeding may be intermittent resulting in a heterogeneous appearance. MRI is more useful in determining the content of retroperitoneal fluid collections as it is more sensitive and specific for detection of blood products. An acute hematoma is isointense on T1-weighted and hyperintense on T2w images. Within several days the signal gradually becomes hyperintense on T1-weighted images and a hematoma is then hyperintense on both T1- and T2-weighted images with a developing, hypointense hemosiderin rim (Figs 21.9A and B).

Abnormal perirenal fluid may be in either of two locations: within the renal capsule (subcapsular) or outside the capsule in the perinephric fat. Subcapsular fluid collections usually produce distortion of the renal parenchyma whereas perinephric collections do not. Urinomas result from obstructive uropathy and less frequently from abdominal trauma and surgical or diagnostic instrumentation.

Retroperitoneal abscesses are particularly difficult to diagnose, because they may not exhibit the classic clinical features, i.e. fever, chills and an elevated white blood cell count.

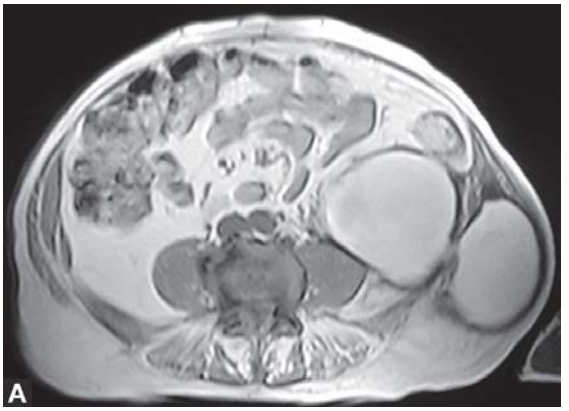

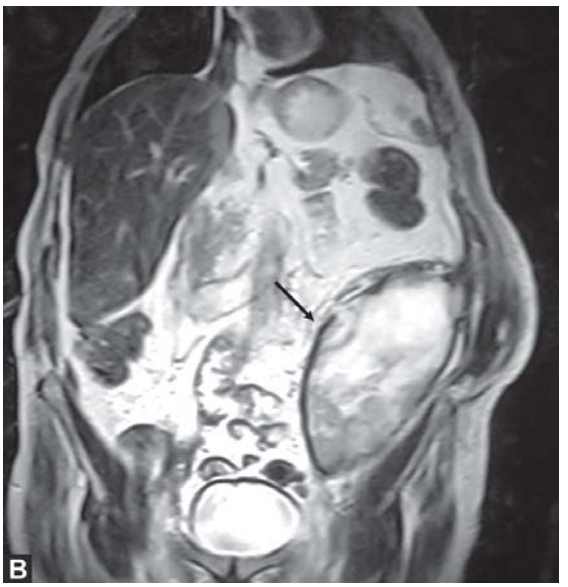

Figs 21.9A and B: Spontaneous retroperitoneal hemorrhage in a patient on anticoagulant therapy. **(A)** Axial T1-weighted MR image shows a well-defined hyperintense lesion anterior to the left psoas. It is partially decompressing into the parietes. **(B)** Coronal T2-weighted image shows heterogeneous, predominantly high signal intensity within the mass. There is a markedly hypointense peripheral rim (arrow) due to hemosiderin deposition. These T1 and T2 signal intensities are diagnostic of a subacute hematoma

When an abscess is mature, its wall is thick and generally hypervascular. On contrast enhanced CT, there is enhancement of the wall and the fluid is usually homogeneous and does not enhance. Many abscesses contain multiple septations. There may be substantial reactive inflammation in the surrounding fat.

Abnormalities in the posterior pararenal space are much less common than abnormalities in the anterior pararenal space or the perirenal space. When present, these are most commonly the result of spread of pathologic processes in the pelvis. Causes can include hematoma, infection, and neoplasm.

AORTA

The most important abdominal aortic abnormalities are aneurysm formation and aortic dissection. MDCTA and MRA have gradually replaced conventional angiography as the procedures of choice for detailed evaluation of the aorta.

Aortic Aneurysm

Most abdominal aortic aneurysms result from atherosclerosis. Other causes include trauma, infection, Takayasu's arteritis, cystic medial necrosis and syphilis. The infrarenal aorta is the most common site of abdominal aortic aneurysms accounting for 95 percent of cases. If untreated, these aneurysms may enlarge and rupture with a mortality of 50 to 90 percent.[12]

The abdominal aortic aneurysm may show curvilinear calcification on plain abdominal radiography. On ultrasonography (US), CT and MRI the aneurysm is identified as focal area of dilatation exceeding 3 cm in size. Spontaneous rupture is a frequent complication of aneurysms measuring 6 cm or more in diameter. Therefore, most aneurysms larger than 6 cm require surgery. Important diagnostic information needed for management includes location, diameter of aneurysm, its longitudinal length, its

relationship to the renal, common iliac and femoral arteries and assessment of the periaortic tissues for perianeurysmal fibrosis.[13] US is a good modality for initial evaluation of aortic aneurysm. It may also be used for follow-up of patients who do not undergo surgical repair. However, CT and MRI are preferred techniques for evaluating the size, extent and complications of aneurysms. At several centers, CT angiography has replaced conventional angiography because it is less invasive and can provide all the necessary information required for the management. Angiography frequently underestimates the dimensions of an aneurysm because it shows only the flowing blood in the lumen and does not show mural thrombus, which is detected on CT (Fig. 21.10). Contrast enhanced 3D Gradient echo MRA demonstrates the full extent of the aneurysm and its relationship to aortic branches.

Aneurysm rupture or leak is associated with a high morbidity and mortality if not promptly treated. CT findings of ruptured abdominal aortic aneurysms are often straightforward. Most ruptures are manifested as a retroperitoneal hematoma accompanied by an abdominal aortic aneurysm. Periaortic blood may extend into the perirenal space, the pararenal space, or both. Intraperitoneal extravasation may be an immediate or a delayed finding. Discontinuity of the aortic wall or a focal gap in otherwise continuous circumferential wall calcifications may point to the location of a rupture. There usually is a delay of several hours between the initial intramural hemorrhage and frank extravasation into the periaortic soft tissues. Contained or impending ruptures are more difficult to identify. A small amount of periaortic blood may be confused with the duodenum, perianeurysmal fibrosis, or adenopathy. Imaging features suggestive of instability or impending rupture include increased aneurysm size, a low thrombus-to-lumen ratio, and hemorrhage into a mural thrombus. A peripheral crescent-shaped area of hyperattenuation within an abdominal aortic aneurysm represents an acute intramural hemorrhage and is another CT sign of impending rupture. Draping of the posterior aspect of an aneurysmal aorta over the vertebrae is associated with a contained rupture.[14]

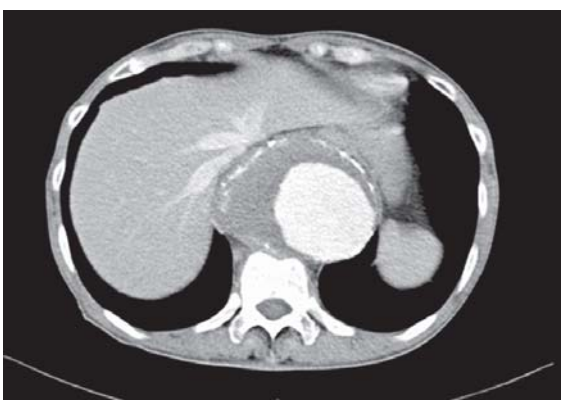

Fig. 21.10: Abdominal aortic aneurysm. Dynamic, contrast-enhanced axial CT image shows markedly dilated abdominal aorta with a large eccentric thrombus. A conventional angiogram on this patient would significantly underestimate the size of the aneurysm as only the patent part of the lumen containing flowing blood would be opacified

The preferred surgical treatment of abdominal aortic aneurysms is an end-to-end anastomosis with aortic graft repair. Complications of abdominal aortic surgery that can be detected on CT include graft infections, aorto-enteric fistulae, anastomotic aneurysms, graft leak or rupture.

Aortic Dissection

Aortic dissection usually originates in the thorax but sometimes extends into the

abdomen. Mortality rate of untreated dissection is very high approaching 25 percent at 1 day, 50 percent at 1 week and 75 percent at 1 month.[15] The strategy for therapy depends on the type of dissection, the site of entry, the extent of dissection, involvement of aortic branches, patency of the false lumen, and the presence of thrombus in the false lumen.

Currently, the noninvasive modalities that are most frequently used to identify aortic dissections are US, CT and MRI. US, including transthoracic echocardiography and transesophageal echocardiography, is widely available and can be performed quickly and easily at the bedside. Thus, US can be used in most patients with aortic dissections, even in relatively unstable patients. However, US has major shortcomings, namely, a limited field of view and a diagnostic accuracy that largely depends on the investigator's experience. Furthermore, US does not provide images that can be used to plan therapy. Multidetector CT has the advantages of shorter scanning times, wide availability, and high diagnostic accuracy and has, therefore, classically been the modality of choice for the evaluation of aortic dissection. In the past, emergency MR imaging evaluation of aortic dissection has been impossible owing to prolonged examination times, but the advent of 3D contrast–enhanced MRA has changed this paradigm. Contrast-enhanced MR angiography has largely replaced unenhanced MR angiographic techniques and has dramatically shortened the total examination time required for confident diagnosis of aortic dissections; however, it is more suitable for stable patients. In principle, contrast-enhanced MR angiography is similar to CT angiography. Both modalities provide excellent evaluation of aortic dissections. In patients without contraindications for either modality, at most centers, the use of each modality is based on equipment availability, the personal preference of the radiologist or referring physician, and patient acceptance.

Confident diagnosis and correct classification of aortic dissection is based on the detection of an intimal flap in the aorta that separates the true and false lumina (Fig. 21.11). Such a flap manifests as a hypointense line with a linear, arc, or S shape in the axial plane. The true and false lumina can be differentiated on the basis of signal intensity, morphologic features, the relationship between the lumina, and the appearance of thrombosis.

- Signal intensity: Similar to CT angiography, contrast-enhanced MRA shows the true lumen with higher signal intensity than the false lumen owing to a higher concentration of contrast material during the arterial phase.
- Morphologic features: The true lumen is usually smaller than the false lumen and would be thin or flat from being pressed, appearing oval in the axial plane. The false

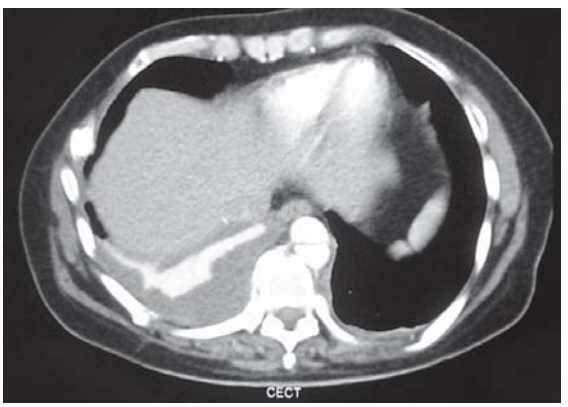

Fig. 21.11: Thoracoabdominal aortic dissection. Axial CT angiogram easily demonstrates the linear intimal flap between the anterior true lumen and posterior false lumen. Active extravasation into the retroperitoneum is also seen

lumen is expanded or very large, appearing crescentic or winding around the true lumen in the axial plane.
- Relationship between the lumina: The lumina may be parallel to each other, the false lumen may wind around the true lumen, or the true lumen may look like a ribbon floating in the false lumen.
- Appearance of thrombosis:The false lumen usually contains a thrombus, especially at the retrograde end of the initial entry site, whereas the true lumen contains no thrombus in most cases.

INFERIOR VENA CAVA

Mostly a routine CT or an MR abdominal protocol employing pre- and postcontrast SGE images provides sufficient evaluation of the IVC for patient management. At least one MR sequence should be performed in the sagittal or coronal plane, because it permits direct visualization of the longitudinal extent of IVC. However, when detailed evaluation of retroperitoneal veins is required, it is prudent to obtain CT or MR venography.

Congenital Anomalies

Congenital abnormalities of the IVC and related veins are common. Preoperative knowledge of the presence of these anomalies is helpful, particularly in patients undergoing a portasystemic shunt procedure, aortic surgery or nephrectomy, and reduces the risk of major venous hemorrhage associated with these anomalies.[16]

CT and MRI are well suited to determine whether rounded or tubular retroperitoneal structures are vascular in nature. Some of the developmental anomalies of inferior vena cava are: Interruption of inferior vena cava with azygos and hemiazygos vein continuation (Fig. 21.12), left sided inferior vena cava, duplication of the inferior vena cava, and anomalies of the left renal vein, e.g. circum-aortic or retro-aortic left renal vein.[17]

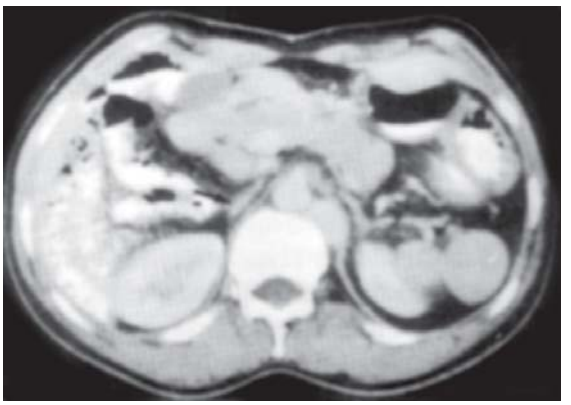

Fig. 21.12: Congenital polysplenia with IVC anomaly. CT scan shows multiple splenenculi and interrupted IVC with hemiazygos venous continuation. Linear density (arrow) seen lateral to the right crus is part of the right adrenal gland

Retrocaval Ureter is thought to be due to persistence of right posterior cardinal vein with failure of development of the infrarenal right supracardinal vein. It occurs with a frequency of 0.2 per thousand population. In retrocaval ureter the proximal right ureter courses medially behind the inferior vena cava, usually at L3 vertebral level and then courses anteriorly around the cava to partially encircle it. The anomaly is characterised by hydronephrosis and medial deviation (fish hook deformity) of the middle ureteral segment.

Venous Thrombosis

Inferior vena caval thrombus may result from proximal extension of thrombi from lower extremity, pelvis or renal veins. Intracaval tumor extension may occur via veins draining neoplasms such as renal cell carcinoma, hepatoma or adrenal carcinoma. CT and MRI perform well in evaluating IVC thrombosis

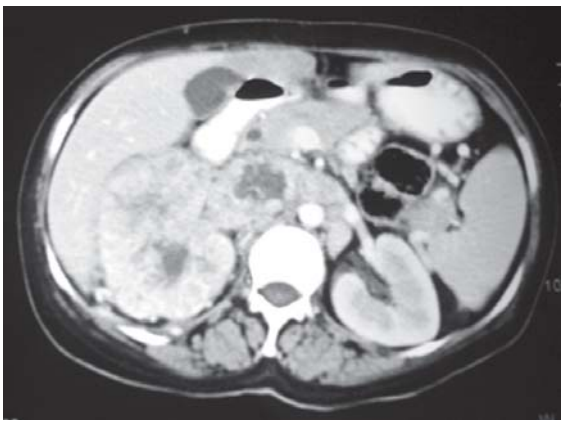

Fig. 21.13: IVC thrombus: Axial contrast-enhanced CT image in a 57-year-old man shows a large right renal cancer extending into the right renal vein and the IVC. The mass within the distended IVC is of the same attenuation as the primary tumor

and distinguishing tumor from bland thrombus.[18] Tumor thrombus shows anatomic contiguity and an enhancement pattern identical to that of primary tumor (Fig. 21.13). The bland thrombus does not enhance with contrast. Depiction of the supradiaphragmatic extent of the thrombus into the right atrium is important for surgical planning as it requires combined thoracoabdominal surgery, whereas thrombus that ends below the hepatic veins may require only an abdominal approach.[19]

In cases of chronic venous thrombosis the affected vessel may not be identified if the thrombus is organized and contacted. In these cases careful evaluation reveals the absence of a vein in the expected location in combination with the presence of collateral vessels.

Primary Tumors of the IVC

Primary tumors of the inferior vena cava are rare. Leiomyoma, endothelioma or leiomyosarcoma may arise as a primary neoplasm of the caval wall.[20] The tumor is usually seen as a filling defect, which may be associated with venous expansion and enhancement of the tumor wall on CT scan (Fig. 21.14). Signal intensity of these tumors is moderately low on T1-weighted images and mixed to high on T2-weighted images. Areas of intermixed tumor and blood products may show bright signal intensity on T1-weighted images. MPRs in the sagittal or coronal plane are

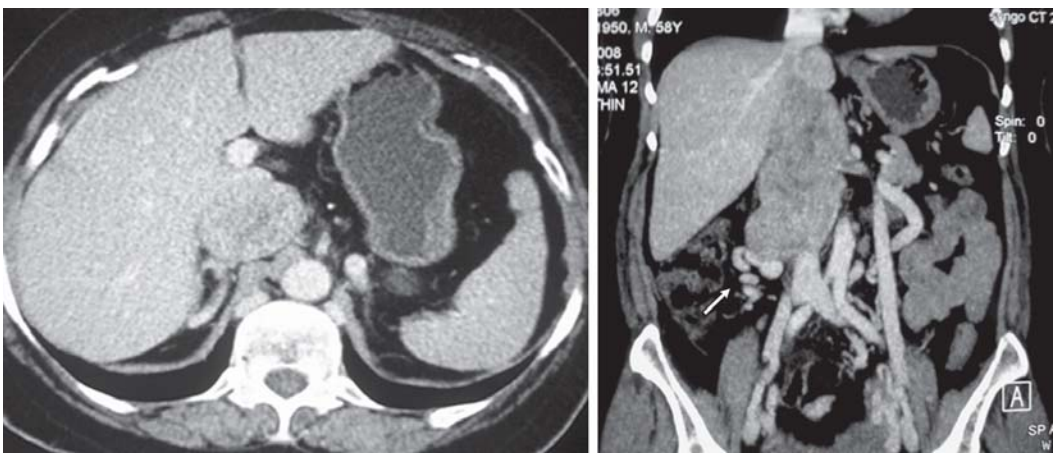

Fig. 21.14: IVC leiomyosarcoma. Contrast-enhanced CT scan of the upper abdomen shows a large, mildly enhancing mass within the hepatic portion of the IVC. Coronal multiplanar image reconstructed from CT data better depicts the craniocaudal extent of the mass and the dilated venous collaterals (arrow)

useful for demonstrating the craniocaudal extent of the tumor. Collateral vessels such as azygous and hemiazygous veins may be enlarged.

LYMPH NODES

Normal lymph nodes appear as small, rounded soft tissue masses adjacent to the great vessels. Retrocrural, paraceliac, gastrohepatic para-aortic, aortocaval, periportal, peripancreatic, external and internal iliac groups together constitute the retroperitoneal nodes. Presently, CT is the most frequently used imaging technique for evaluation of enlarged retroperitoneal nodes. The diagnosis of lymph node abnormalities on CT is based on size and image morphology. Size of a node is best determined by measuring its short axis diameter. The retroperitoneal lymph nodes are considered abnormal if their size is more than 10 mm, except in the retrocrural space where the upper limit is 6 mm. A variety of retroperitoneal structures can be confused with enlarged lymph nodes, including unopacified loops of bowel, vascular collaterals, dilated lymphatics, and retroperitoneal fibrosis. Careful evaluation of serial CT images after oral and intravenous contrast is helpful in distinguishing between these structures.

MR sequences suited for detection of lymph nodes include precontrast T1-weighted spin-echo or SGE, fat-suppressed T2-weighted turbo spin-echo and contrast-enhanced fat-suppressed sequences. The enlarged lymph nodes appear low in signal on precontrast SGE in a background of high-signal fat, and nodes are moderately high in signal on fat-suppressed T2-weighted and contrast-enhanced T1-weighted images. Fat-suppressed T2-weighted images are very sensitive for the detection of lymph nodes and perform better than CT, particularly in pediatric patients or other patients with paucity of retroperitoneal fat.

Benign Lymphadenopathy

Benign lymphadenopathy may occur secondary to inflammatory or infectious disease. Lymphadenopathy is the most common manifestation of abdominal tuberculosis.[21]

The mesenteric, omental, and peripancreatic lymph nodes are most commonly involved. The nodes commonly demonstrate peripheral enhancement with central areas of low attenuation after intravenous contrast administration (Fig. 21.15). Discrete homogeneous lymph nodes may also be seen in some cases. Calcification is frequently seen in tubercular lymph nodes. Enlarged lymph nodes with low density centers may also be seen in pyogenic infections, Whipples disease, lymphomatous or metastatic nodes following radiotherapy and chemotherapy.

Enlarged retroperitoneal nodes have also been observed in 30 percent of patients with sarcoidosis.[22] The periportal, paraceliac and

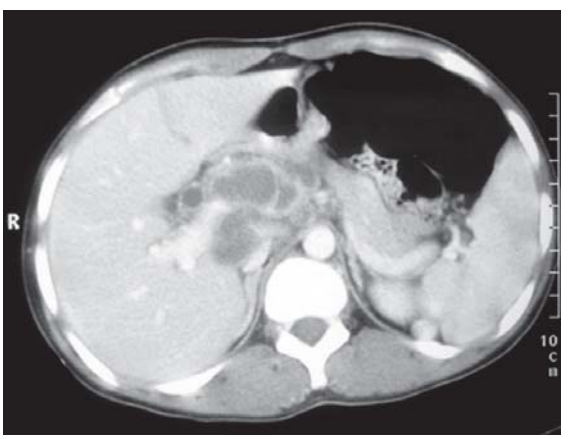

Fig. 21.15: Retroperitoneal tubercular lymphadenopathy. Axial CT image shows enlarged periportal and portocaval lymph nodes with characteristic central necrosis and peripheral rim enhancement

para-aortic groups are most often involved. On CT, the nodes affected by sarcoidosis generally show homogeneous soft-tissue attenuation and remain discrete. Nodal calcification is unusual in sarcoidosis.

Castleman disease is occasionally also associated with retroperitoneal lymph node enlargement. Mostly the CT or MR appearance of these enlarged lymph nodes is not specific. However, identification of intense and uniform contrast enhancement in lymph nodes can suggest the diagnosis (Fig. 21.16).[23]

Lymphangioleiomyomatosis is a rare cause of bulky retroperitoneal lymphadenopathy. This is a progressive disease involving the lung, lymphatic trunks and lymph nodes, typically affecting young women of childbearing age. Sometimes it can primarily involve retroperitoneum with or without subsequent development in the lungs.[24] On CT scans the enlarged lymph nodes may show cystic, low-attenuation components.

Lymphoma

Abdominal lymph nodes are involved in 50 percent of the non-Hodgkin's lymphoma (NHL) patients as against 25 percent of those with Hodgkin's disease (HD) at presentation.[25] Mesenteric involvement is seen in more than half of the NHL patients (versus 5 percent of those with HD). The patterns of lymphadenopathy are also markedly different, slight enlargement of upper para-aortic nodes and contiguous spread being characteristic of HD. NHL on the other hand manifests with bulky lymph nodes in multiple locations.

The enlarged lymph nodes may appear as discrete masses or as confluent soft tissue mass obliterating the retroperitoneal fat (Fig. 21.17). Lymphomas are 'soft' tumors and frequently surround the adjacent vessels (floating aorta sign) and ureters without compressing their lumina. Lymphomas are homogeneous, with minimal contrast enhancement and relatively low signal intensity at T2 weighted images representing densely packed cellular components. Nodes are rarely calcified (<1%) in untreated patients.[26]

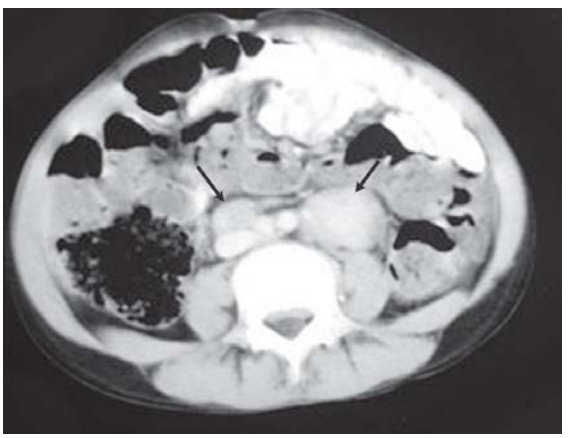

Fig. 21.16: Castleman disease. Contrast enhanced axial CT image shows large, well-defined, markedly enhancing para-aortic lymph nodes (arrow) compatible with the diagnosis of Castleman disease in an 8-year-old boy

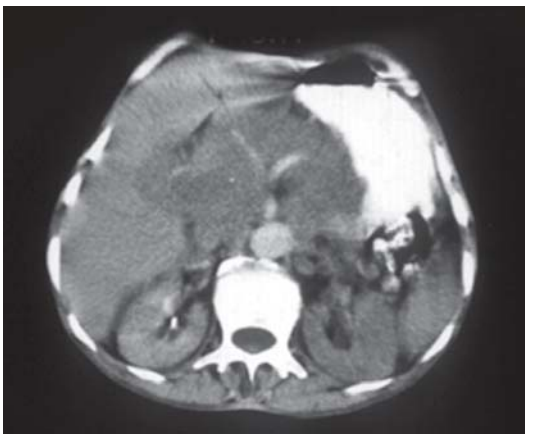

Fig. 21.17: Non-Hodgkin lymphoma. Contrast enhanced Axial CT image shows large, confluent lymph nodal mass in the preaortic location. The celiac axis branches are engulfed by the mass but their patency is preserved

CT is also used for follow-up of disease after treatment. Response to treatment is usually indicated by reduction in the retroperitoneal lymph node enlargement. In some patients lymph nodes may become hypodense as an appropriate response to treatment with or without reduction in lymph node size. Occasionally there may be post-treatment dystrophic calcification of the lymphomatous masses.

Persistent lymph nodal masses may be seen in some patients even after treatment. These may represent residual tumor, post-treatment inflammation or fibrosis. Unfortunately there are no reliable CT characteristics that can differentiate between malignant and benign residual masses. Several studies have suggested that MRI may be helpful in distinguishing late post therapy fibrosis (hypointense on T2-weighted images) from viable lymph nodes (hyperintense or heterogeneous on T2-weighted images). Also chronic fibrotic tissue shows minimal MR enhancement postcontrast while recurrence generally enhances markedly.

FDG-PET has proved to be very useful in the clinical management of lymphomas. It is now considered the most accurate tool for the assessment of treatment response and prognosis in patients with Hodgkin lymphoma and aggressive non-Hodgkin lymphoma.[27] FDG-PET can detect metabolically active disease by its increased glycolysis that is proportional to the tumor mitotic activity. It can separate high from low-grade tumors and aid in prognostication. FDG-PET at the end of treatment seems to aid considerably in differentiating between residual masses with or without residual lymphoma. An early interim FDG-PET scan after 1 to 3 cycles of chemotherapy is a very strong predictor of outcome, and trials are now in progress testing treatment modifications on this basis.[28] Like other imaging modalities, PET has its own drawbacks including inability to detect very small lesions (< 5 mm) and reduced specificity due to increased uptake in metabolically active inflammatory and infective tissues.

HIV Lymphadenopathy

Enlarged lymph node are present in most (> 60%) patients with HIV infection but in more than half of these patients the short-axis diameter of the largest node measures only 10-15 mm.[29] Although sometimes the nodal enlargement results only from reactive hyperplasia, many other diseases may be responsible. These include disseminated mycobacterial infections (Fig. 21.18), histoplasmosis, lymphoma and Kaposi's sarcoma. When lymph node enlargement is massive, AIDS-related lymphoma should be suspected. Intense enhancement of lymph nodes suggests a diagnosis of Kaposi's sarcoma.

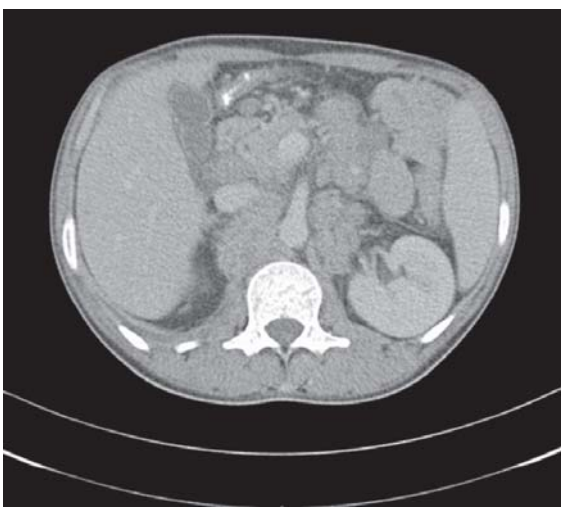

Fig. 21.18: *Mycobacterium tuberculosis* infection in a 35-year-old man with HIV infection. Axial CT image shows multiple, enlarged, low attenuation lymph nodes in the portocaval and paracelic regions

Metastatic Lymphadenopathy

Metastatic lymph nodes show varied morphological patterns, but the diagnosis is usually straightforward due to the presence of a known primary. Neoplasms of the stomach, colon, pancreas, kidney, testis, ovary, uterus, bladder and prostate may all metastasize to retroperitoneal lymph nodes. Calcification in the metastatic nodes suggests mucin producing primary from the ovary or gastrointestinal tract.

Testicular neoplasms tend to metastasize via lymphatics rather than via bloodstream. Lymphatics from the testes drain into ipsilateral lymph nodes, which follow the course of the gonadal veins. Typically, left sided neoplasms spread to involve lymph nodes in the left renal hilum, as the left gonadal vein drains into the left renal vein. Right sided neoplasms spread to paracaval lymph nodes, an area where the right gonadal vein joins the IVC. While metastatic retroperitoneal nodes from some testicular tumors appear quite homogeneous on CT, others particularly from non-seminomatous neoplasms often appear heterogeneous containing low attenuation central areas of necrosis and rim enhancement (Figs 21.19A and B). Seminomas may present with bulky masses whereas non-seminomatous germ cell tumor often metastasize to normal sized nodes. On MR metastatic lymph nodes show low-intermediate signal intensity on T1-weighted images, and high signal intensity on T2-weighted images. Low signal intensity masses after treatment usually represent fibrosis.

CT and MRI use the nonspecific criterion of size and are limited in their ability to differentiate benign from malignant lymph nodes. Contrast enhanced MR lymphography is a promising technique in differentiating benign from metastatic lymph nodes and

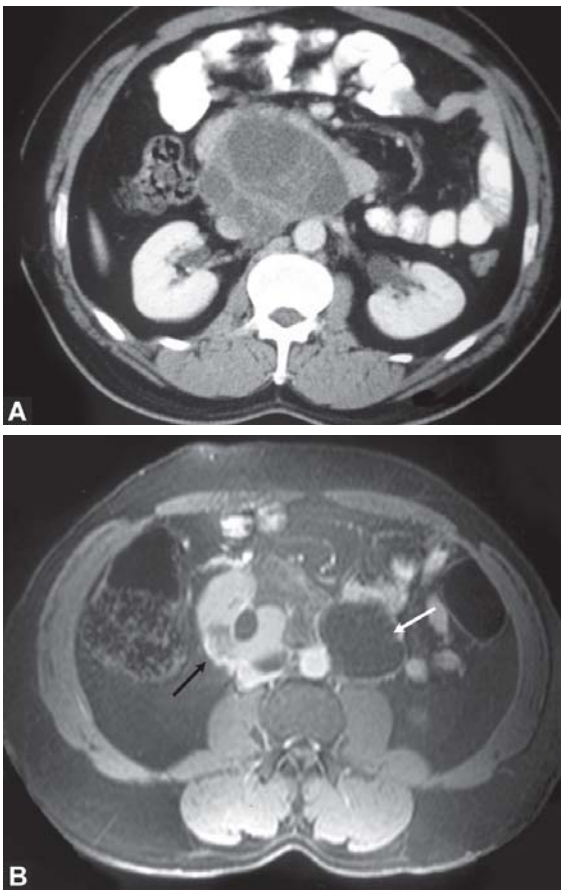

Figs 21.19A and B: Metastatic testicular germ cell tumor. **(A)** Axial CT image shows massive, low attenuation retroperitoneal lymphadenopathy. **(B)** Postchemotherapy contrast enhanced T1-weighted axial MR image in another patient shows enhancing viable tumor (black arrow) and the non-enhancing necrotic component (white arrow)

providing information on lymph node morphology and function. Ultrasmall super paramagnetic iron oxide (USPIO) particles with a long plasma circulation time are suitable as MR contrast agents for MR lymphography. MR imaging is typically performed 24 to 36 hours after intravenous infusion of USPIO particles. Normal lymph nodes decrease in signal intensity on enhanced T2-weighted and T2-weighted

gradient echo images, indicating uptake of this contrast agent. Nodes infiltrated by tumor have no appreciable USPIO uptake and thus reveal no signal change on pre-and postcontrast images.[30]

FDG-PET may be more sensitive and specific than CT for certain retroperitoneal metastases depending on the primary. Non-seminomatous germ cell tumors with well differentiated components are not very FDG-avid.

PRIMARY NEOPLASMS

Primary retroperitoneal neoplasms are rare tumors that originate in the retroperitoneal space but outside the major organs within that compartment. These neoplasms are generally derived from mesenchymal cells, neurogenic cells, or embryonic rests and may be benign or malignant. Diagnosis of these tumors is often challenging for radiologists and consists of several steps, including determining tumor location (characterizing the retroperitoneal space and identifying the organ of origin) and recognizing specific features of various retroperitoneal tumors (evaluating patterns of spread, tumor components, and vascularity).

To decide whether the tumor is located within the retroperitoneal space, it is useful to observe the displacement of normal anatomic structures. Anterior displacement of retroperitoneal organs (e.g, kidneys, adrenal glands, ureters, ascending and descending colon, pancreas, portions of the duodenum) strongly suggests that the tumor arises in the retroperitoneum (Figs 21.20A and B). Major vessels and some of their branches are also found in the retroperitoneal cavity, so that displacement of these vessels can be helpful as well. Before a tumor can be described as primarily retroperitoneal, the possibility that the tumor originates from a retroperitoneal organ must be excluded. Some radiologic signs that are helpful in determining tumor origin include the "beak sign," the "phantom (invisible) organ sign,"

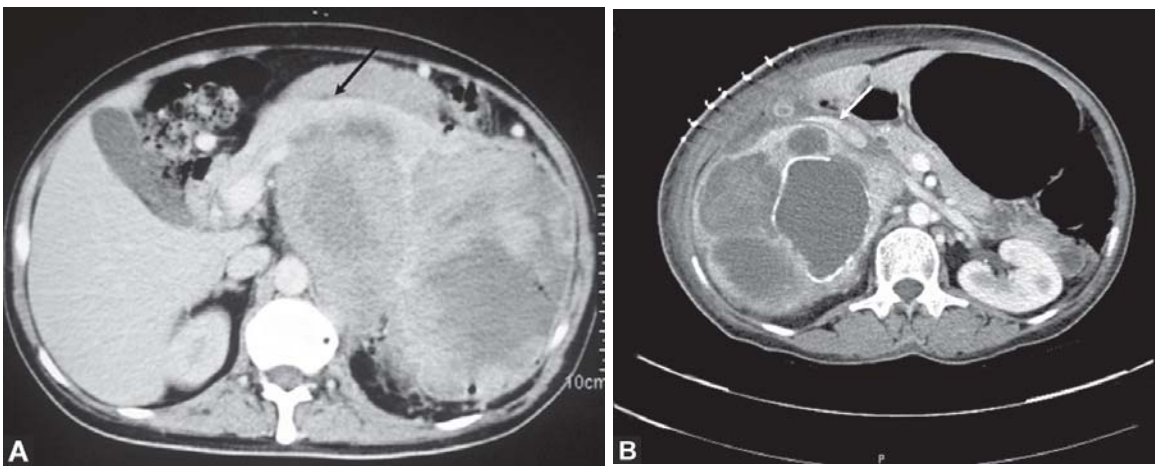

Figs 21.20A and B: (A) Anterior displacement of pancreas. Axial CT image shows a large mass that is difficult to localize at first glance. However, anterior displacement of pancreas (arrow) confirms it to be in the retroperitoneal space. **(B)** Anterior displacement of the IVC. Axial CT image reveals a large, heterogeneous partially cystic right hypochondriac mass with septal calcification on the right. Its retroperitoneal location is suggested by the anterior displacement and stretching of the IVC (arrow). Histopathology revealed a diagnosis of paraganglioma

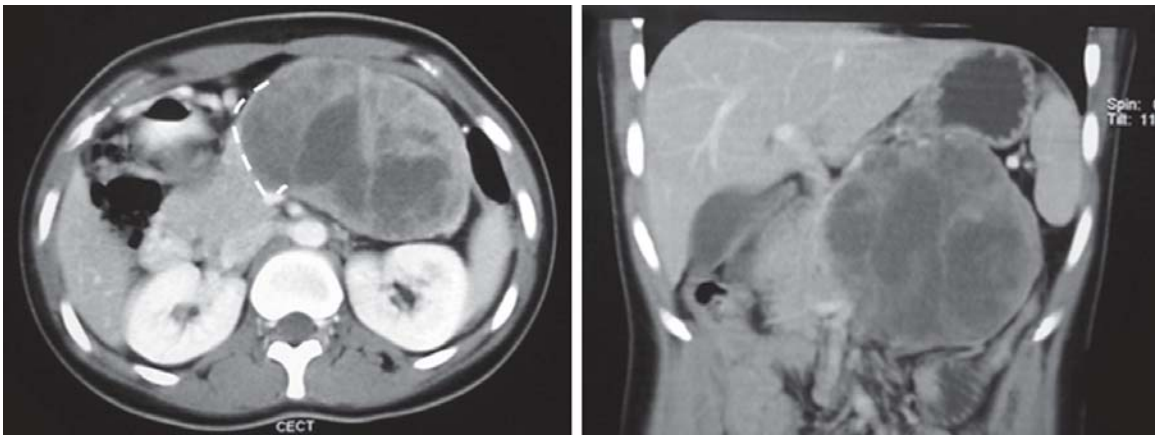

Fig. 21.21: Beak sign. Axial CT image shows a large cystic tumor with the beak sign in its contact surface with the pancreas (broken white line). This finding represents mucinous cystadenocarcinoma of the pancreas

and the "embedded organ sign".[31] When there is no definite sign that suggests an organ of origin, the diagnosis of primary retroperitoneal tumor becomes likely.

Beak Sign—When a mass deforms the edge of an adjacent organ into a "beak" shape, it is likely that the mass arises from that organ (Fig. 21.21). On the other hand, an adjacent organ with dull edges suggests that the tumor compresses the organ but does not arise from it.

Phantom (Invisible) Organ Sign—When a large mass arises from a small organ, the organ sometimes becomes undetectable. This is known as the phantom organ sign. However, false-positive findings do exist, as in cases of huge retroperitoneal sarcomas that involve other small organs such as the adrenal gland.

Embedded Organ Sign—When a tumor compresses an adjacent plastic organ (e.g. gastrointestinal tract, inferior vena cava) that is not the organ of origin, the organ is deformed into a crescent shape. In contrast, when part of an organ appears to be embedded in the tumor (positive embedded organ sign) at the contact surface, it is likely to be the organ of origin (Fig. 21.22).

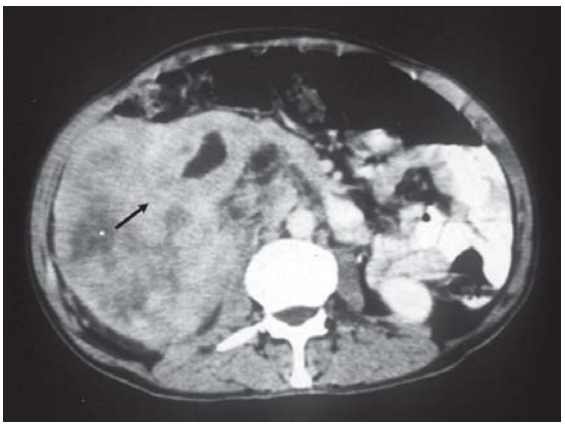

Fig. 21.22: Embedded organ sign. CT image shows a huge heterogeneous mass in the right side of abdomen. The lumen of the duodenum is stretched toward the mass, and the wall of the duodenum appears embedded in the mass at the contact surface (arrow). These findings represent gastrointestinal stromal tumor of the duodenum with a positive embedded organ sign

Malignant Neoplasms

Malignant tumors of the retroperitoneum are roughly four times more frequent than benign lesions, in sharp contrast to neoplasms

occurring elsewhere in the body, where benign lesions predominate.[32]

Liposarcoma is the most frequent primary retroperitoneal malignant tumor followed by malignant fibrous histiocytoma.[33] Leiomyosarcomas are encountered slightly less often, and a variety of other neoplasms (fibrosarcomas, malignant teratomas, rhabdomyosarcomas, and hemangiopericytomas) are seen only occasionally. Most primary retroperitoneal tumors arise in front of the plane of the spine and psoas muscle and despite their retroperitoneal location some may project forward as far as the anterior abdominal wall. Less commonly tumors arise in the paraspinal or posterior pararenal part of the retroperitoneal space.

Percutaneous core biopsy is often required for the complete histological analysis of these tumors and their distinction from lymphoma. Although biopsy may identify the cell type of a retroperitoneal tumor, treatment and prognosis are not affected by specific cell type. Only surgical resectability and tumor grade affect patient survival. The only consistently effective treatment for primary retroperitoneal sarcomas is operative resection. The role of imaging is to determine the tumor location and extent. It is essential to determine which organs are definitely or possibly invaded by the tumor for planning appropriate therapy.

Primary retroperitoneal sarcomas have a high rate of recurrence after local resection, even when the surgical margins are negative for tumor. Seventy five percent of recurrences typically appear within 2 years of initial surgery. The most effective treatment of recurrent retroperitoneal sarcomas is additional surgical resection. Therefore it is beneficial to have a close imaging follow-up so that recurrences can be identified when still small in size, improving the likelihood of complete resection. All patients should undergo baseline imaging CT or MRI 6 months after the initial surgical resection. Subsequently patients with grade I tumors should undergo annual imaging and patients with grade II or III tumors should undergo biannual imaging for 5 years. Thereafter, all patients should undergo annual imaging because recurrences of low- and high-grade tumors may appear late in some patients.[34]

Liposarcomas

CT or MRI can suggest a diagnosis of liposarcoma when fat is detected within a retroperitoneal mass. The amount of fat seen in liposarcomas varies widely. Three types of retroperitoneal liposarcomas are encountered, viz. well-differentiated also known as lipogenic liposarcomas, myxoid and undifferentiated.[35] On CT well-differentiated liposarcomas are predominantly of fat density and contain irregular strands of higher density (Figs 21.23A and B). The tumors often merge imperceptibly with adjacent normal fat and usually displace rather than invade adjacent organs. Myxoid liposarcomas have density less than muscle but greater than fat. Undifferentiated liposarcomas are indistinguishable from nonfatty soft tissue sarcomas (Figs 21.24A and B). It may not be possible to definitively differentiate retroperitoneal liposarcomas from benign lipomas, although some CT or MRI findings suggest that a fatty mass is more likely to be malignant than benign. These findings include identification of soft tissue septa more than 2mm thick within a fatty retroperitoneal mass, septal irregularity or bulging, and obvious enhancement.[36]

Leiomyosarcomas

Leiomyosarcomas are large, heterogeneous masses with foci of hemorrhage, necrosis and

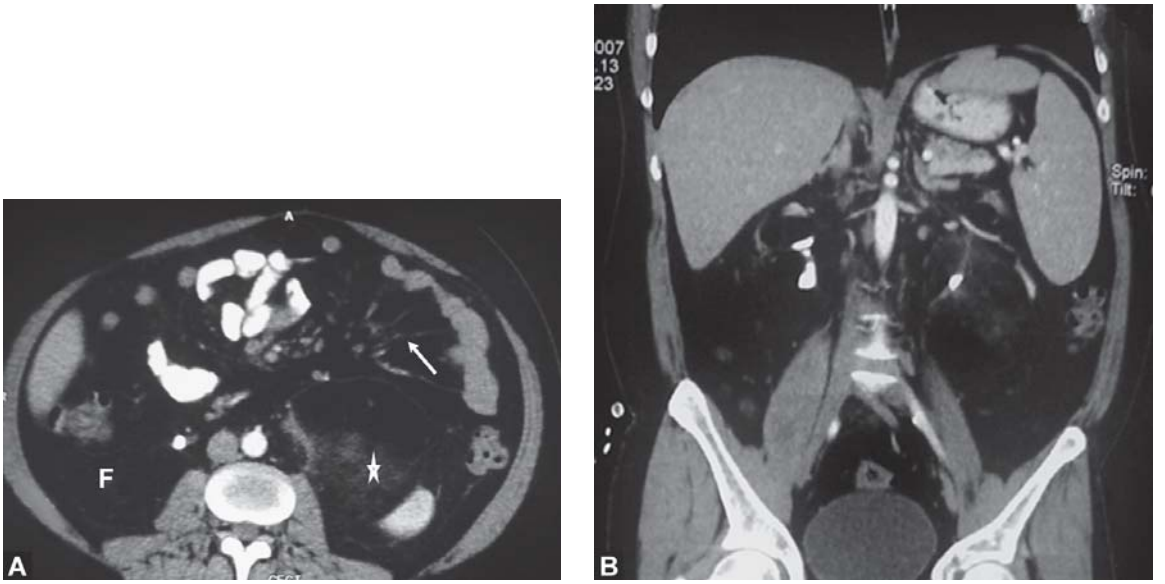

Figs 21.23A and B: Retroperitoneal well-differentiated liposarcoma in a 60-year-old man with a history of increasing abdominal girth. Axial and coronal CT images show a diffusely infiltrative, retroperitoneal and abdominal mass composed of fat (F) with Hounsfield (HU) measurements of –80 to –120. There are multiple thick septa (arrow) and a posterior soft tissue component (star) with mildly higher attenuation

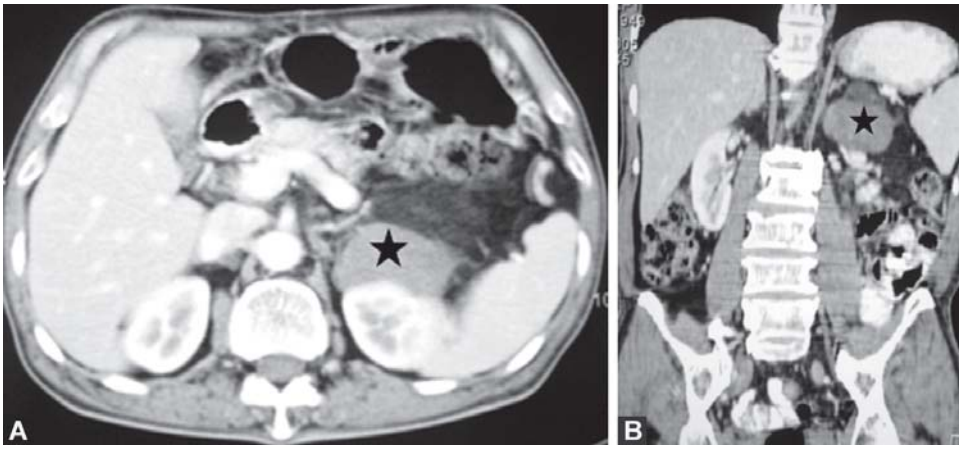

Figs 21.24A and B: Poorly-differentiated retroperitoneal liposarcoma. Axial and coronal CT images show a predominantly homogeneous soft tissue density mass (star) anterior to the left kidney. The CT appearance is indistinguishable from other retroperitoneal soft tissue sarcomas. Histopathology revealed a diagnosis of poorly-differentiated liposarcoma

cystic degeneration (Fig. 21.25).[37] They do not contain fat or calcification. Not infrequently, retroperitoneal leiomyosarcomas extend into the retroperitoneal veins and IVC.

Malignant Fibrous Histiocytomas

Malignant fibrous histiocytomas are high grade connective tissue tumors. They are multilobulated, infiltrative, unencapsulated

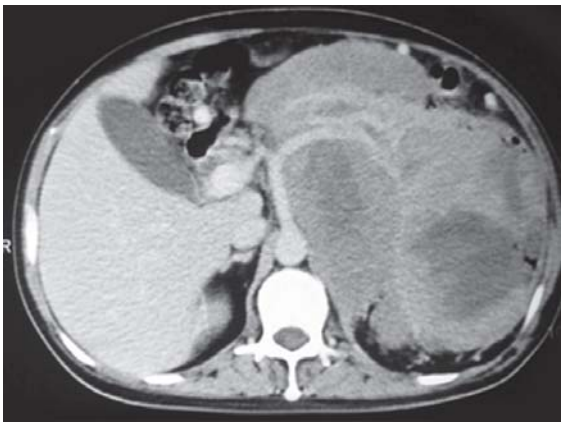

Fig. 21.25: Retroperitoneal leiomyosarcoma. Axial CT image shows a huge, heterogeneous, soft tissue density retroperitoneal mass on the left. Biopsy revealed it to be a leiomyosarcoma. Any non-fat containing retroperitoneal malignancy may have this appearance

but deceptively well circumscribed masses. They may contain myxoid stroma, fibrous tissue, hemorrhage, and necrosis giving rise to a typical mosaic of mixed low, intermediate and high signal intensity on T2-weighted MRI images. Although both myxoid stroma and necrosis have similar T1 and T2 signal intensity, differentiation may be possible as myxoid stroma shows delayed enhancement in contrast to the nonenhancing necrotic areas. Up to 25 percent of malignant fibrous histiocytomas contain dystrophic calcification, a finding that is extremely uncommon in other retroperitoneal malignancies.[33]

Hemangiopericytomas

Hemangiopericytomas are highly vascular tumors thought to arise from blood vessel walls. They may demonstrate areas of intratumoral hemorrhage and multiple flow voids on MRI. Hemangiopericytomas enhance rapidly and intensely on dynamic contrast-enhanced CT or MRI.

Other Malignancies

Fibrosarcomas and neurofibrosarcomas are usually heterogeneous and thus identical in appearance to leiomyosarcomas, some liposarcomas and malignant fibrous histiocytomas. Neuroblastomas and ganglioneuroblastomas often contain calcification. They are usually seen in children. Rhabdomyosarcomas are rare, heterogeneous tumors, also seen in pediatric patients.

Benign Neoplasms

Most benign lesions originate from neural tissue or neural crest remnants (neurofibroma, schwannoma, ganglioneuroma, and paraganglioma). Hemangioma, lymphangioma, lipoma, teratoma and desmoid tumors are the other benign tumors encountered in the retroperitoneum.

Paragangliomas

Majority of paragangliomas (extra-adrenal pheochromocytoma) lie in the retroperitoneum, in the immediate para-aortic region, from the level of the adrenal glands to the aortic bifurcation. Paragangliomas are well defined soft tissue masses, usually quite large at the time of diagnosis (Figs 21.26A and B). Paragangliomas are homogeneous when small, but become increasingly heterogeneous as they grow due to central necrosis, hemorrhage and even calcification.[38] On MR images, Paragangliomas often demonstrate extremely high signal intensity on T2 weighted images. Paragangliomas are generally hypervascular, and most enhance briskly after injection of IV contrast material.

Neurogenic Tumors

Neurogenic tumors are often located adjacent to the vertebral column or deep to the psoas

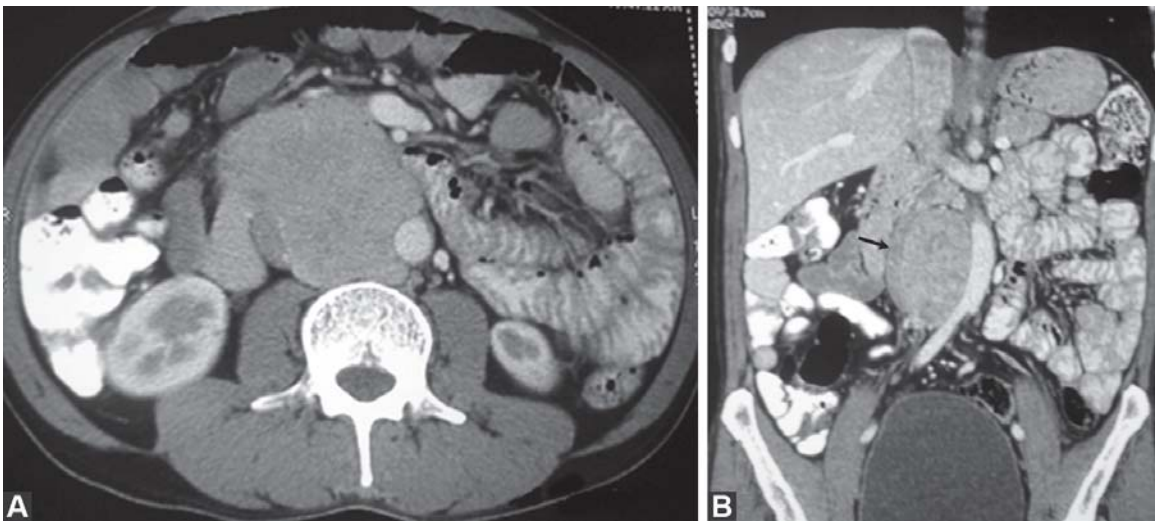

Figs 21.26A and B: Retroperitoneal paraganglioma: **(A)** Axial CT image shows large homogeneous soft tissue density mass in the aortocaval region. **(B)** Coronal image shows the IVC draping around the right lateral margin of the mass (arrow)

muscles. MRI is the imaging modality of choice for imaging of these tumors as it detects tumor extension into the neural foramina, a common feature of neurogenic tumors (Fig. 21.27). MRI also helps in the characterization of these masses, as they tend to have high signal intensity on T2 weighted, due to the myxoid stroma they contain. Central low to intermediate signal intensity may be seen corresponding to fibrous tissue and is referred to as the 'target sign'. Sometimes a whorled appearance consisting of linear or curvilinear structures of low signal intensity is seen on T2 weighted images. At histopathological analysis, this finding corresponds to bundles of Schwann cells and collagen fibres within the mass. Varying degrees of contrast enhancement in neurogenic tumors have been reported, from slight to moderate to marked with delayed heterogeneous uptake of contrast. These enhancement features are explained by the presence of abundant myxoid material in these tumors, resulting in delayed progressive accumulation of contrast material in the extracellular space.[39]

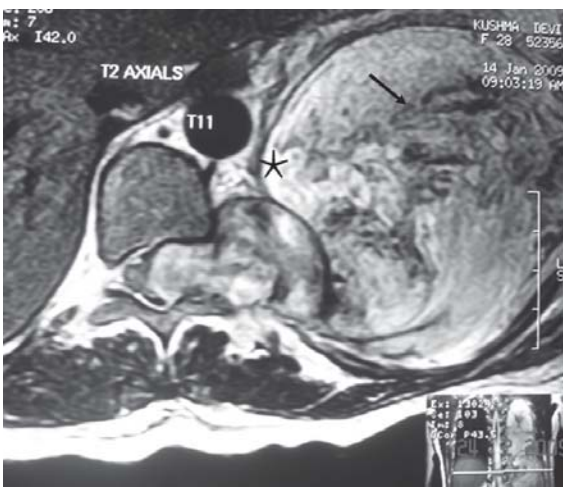

Fig. 21.27: Intraspinal extension of schwannoma. T2-weighted axial MR image shows a smoothly encapsulated, large heterogeneous intensity mass in the left paraspinal location. It has extended inside the extradural compartment of the spinal canal. The markedly hyperintense area (star) represents myxoid stroma. The linear, low signal intensity areas, having a somewhat whorled appearance (arrow), correspond to bundles of Schwann cells and collagen fibers within the mass

Schwannomas are the most common neurogenic soft tissue tumors occurring in the retroperitoneum. They usually appear as well-defined, heterogeneous soft tissue

masses. Although they may contain cystic areas, they usually have large solid components. Retroperitoneal *neurofibromas* are commonly seen in patients with neurofibromatosis. On CT, neurofibromas appear as well-defined, sharply marginated, homogeneous masses that demonstrate near-water attenuation. *Ganglioneuromas* arise from sympathetic ganglia and are composed of mature Schwann cells, ganglion cells, and nerve fibers. Predominantly children and young adults (60% of cases) are affected and the prognosis is excellent, recurrence being rare after surgical resection. At CT or MRI, ganglioneuromas appear as well-circumscribed oval, crescentic, or lobulated masses. These tumors tend to partially or completely surround major blood vessels, with little or no compromise of the lumen. At unenhanced CT, the tumors appear homogeneous, with attenuation less than that of muscle. They contain calcification in about 20 percent of cases. The calcifications are discrete and punctate rather than amorphous and coarse as in neuroblastomas.

Teratomas

Teratomas are congenital neoplasms containing components of all three germ layers. CT often shows calcification or even osseous elements. Fat may be seen on both CT and MRI (Fig. 21.28). Sometimes a dermoid plug is identifiable as a soft tissue mural nodule projecting into a cyst. The incidence of malignant degeneration is rare (< 1%), and usually occurs in the dermoid plug in postmenopausal women.

Lipoma

Lipoma is a benign mesenchymal tumor that resembles normal fat. Lipomas typically demonstrate homogeneous fatty attenuation at CT and homogeneous signal intensity identical to that of fat with all MR imaging sequences. Thin fibrous septa of low signal intensity on T1- and T2-weighted images may traverse the lesion. Some lipomas have prominent fibrous septa and nodularity and may mimic well-differentiated liposarcomas at imaging.

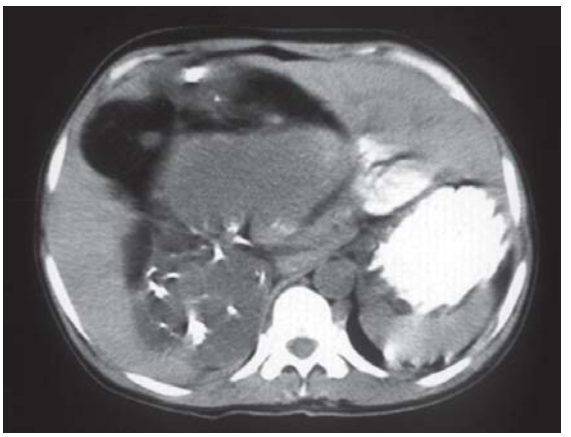

Fig. 21.28: Retroperitoneal teratoma. Axial CT image reveals a large heterogeneous mass containing elements that show the attenuation of fluid, fat, soft tissue and calcification

RETROPERITONEAL FIBROSIS

Retroperitoneal fibrosis results from proliferation of fibrous tissue in the midline and paraaortic distribution. Approximately 70% cases of retroperitoneal fibrosis are idiopathic and are known as Ormond's disease. Other causes include various drugs (e.g. methysergide), previous abdominal surgery or radiation therapy, aortic hemorrhage, aortitis, aortic atherosclerosis, extravasation of urine, nonspecific gastrointestinal inflammation including appendicitis and diverticulitis, infective pathologies including tuberculosis, histoplasmosis, syphilis and actinomycosis. Retroperitoneal fibrosis may be a part of multifocal fibrosclerosis in which fibrous

pseudotumor of the orbit, Riedel's thyroiditis, sclerosing cholangitis and mediastinal fibrosis may also occur. Retroperitoneal malignancy especially metastases may also produce retroperitoneal fibrosis by producing a desmoplastic reaction to the tumor cells.[40]

Idiopathic retroperitoneal fibrosis most commonly occurs in patients between 40 and 60 years of age. Males are affected twice as commonly as females. Fibrous plaque typically extends from below the level of the kidneys to the bifurcation of great vessels. The fibrous tissue may involve the inferior vena cava, aorta, ureters and occasionally the iliac and renal veins in a symmetric or asymmetric distribution. Microscopically, collagen fibroblasts and inflammatory cells characterize idiopathic retroperitoneal fibrosis.

The clinical and laboratory findings of idiopathic retroperitoneal fibrosis are nonspecific and include fever, back pain and raised erythrocyte sedimentation rate. Most patients have impaired renal functions.

Excretory urography typically demonstrates bilateral hydronephrosis, which may be asymmetric and sometimes even unilateral. Retrograde studies demonstrate smooth tapering of the ureters that is most pronounced at the pelvic brim (Fig. 21.29). The involvement may vary from focal to a long segment of ureter. Despite ureteral narrowing, there is no obstruction to retrograde passage of catheter in the ureter.

US demonstrates retroperitoneal fibrosis as a poorly demarcated periaortic mass that is typically echo-free or hypo-echoic. Associated hydronephrosis may be seen. CT appearance of the fibrous plaque varies considerably: It can be midline or asymmetric, well circumscribed or poorly defined, localized or extensive (Figs 21.30A to C).

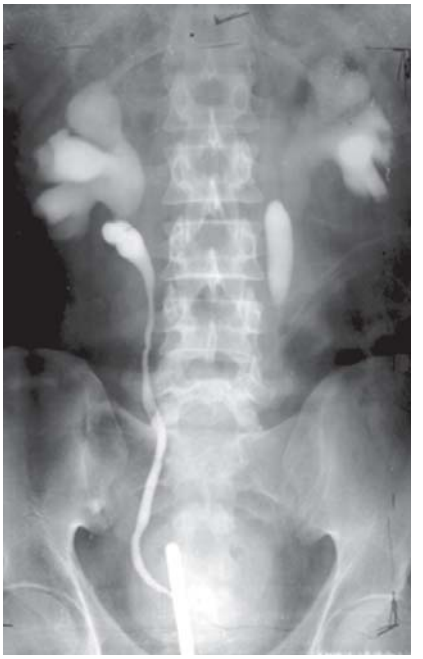

Fig. 21.29: Retrograde pyelography showing medial deviation of both ureters with hydroureteronephrosis in a patient with idiopathic retroperitoneal fibrosis

Contrast enhancement varies with the age of the process, while increased enhancement is seen in early stages due to vascularity of the immature fibrosis, chronic fibrosis does not enhance appreciably. MRI may permit distinction between benign or non-neoplastic retroperitoneal fibrosis and malignant retroperitoneal fibrosis. In non-malignant retroperitoneal fibrosis low or intermediate signal intensity on T1 and T2 weighted images has been reported in contrast to higher signal intensity in most malignancies on T2W images (Fig. 21.31). However, it has been recognized that benign retroperitoneal fibrosis also can have high signal intensity on T2-weighted images when it is in the active, inflammatory stage. MRI also demonstrates effect of the fibrotic mass on the aorta and inferior vena cava.

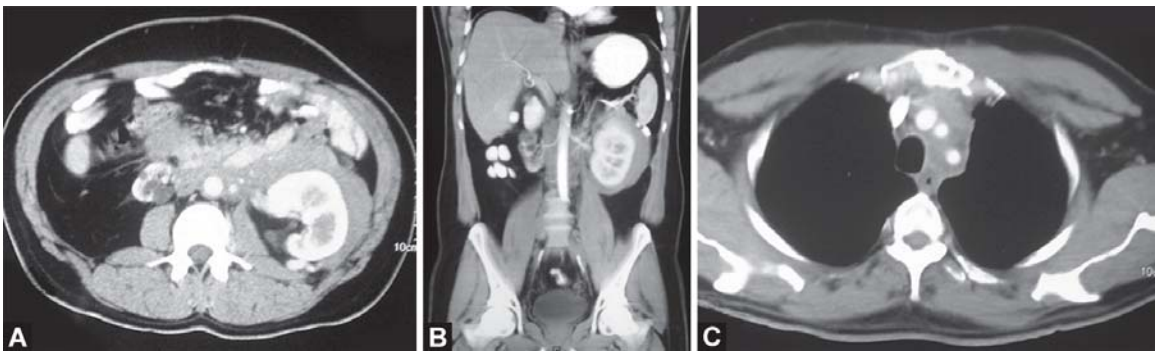

Figs 21.30A to C: Retroperitoneal fibrosis. **(A)** Contrast-enhanced axial CT image shows hypodense, nonenhancing, infiltrating mass surrounding the aorta and IVC and extending into the left perirenal space. Right kidney is shrunken and hydronephrotic. **(B)** Coronal image shows the entire extent of the plaque like, perirenal soft tissue. Appearance is nonspecific, and differentials include malignancy such as lymphoma. Diagnosis was confirmed by biopsy. **(C)** CT scan though the chest shows evidence of mediastinal fibrosis, a frequent association of retroperitoneal fibrosis

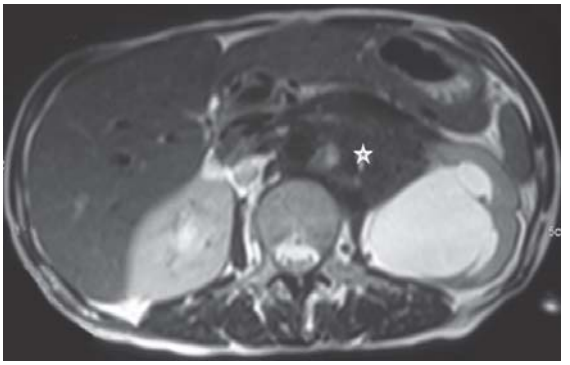

Fig. 21.31: Retroperitoneal fibrosis. Axial T2-weighted MR image shows a very hypointense mass (star), a finding consistent with the presence of mature fibrous tissue with little or no active inflammation

Iliopsoas Muscle Compartment

Diseases affecting the iliopsoas muscle more commonly originate from adjacent structures and involve the muscle by direct extension. These include hemorrhage, infections and tumors of the spine, kidneys, bowel, pancreas and retroperitoneal lymph nodes. The iliopsoas is well evaluated by both CT and MRI. Coronal or sagittal planes provide direct evaluation of the full craniocaudal extent of the muscle.

Tuberculous spondylitis and lumbar discitis are the commonest cause of an iliopsoas abscess in our country. Iliopsoas inflammatory masses display a variety of appearances, ranging from diffuse homogeneous enlargement to discrete masses containing central areas of low CT attenuation or high signal intensity on T2-weighted MR images. Postcontrast images show abscesses as expansile lesions with non-enhancing necrotic centers, intense peripheral enhancement and enhancement of the surrounding tissues (Figs 21.32A and B). Calcification is detected occasionally on CT in inflammatory masses, particularly in patients with tuberculosis. MRI scores over CT in detecting intraspinal extension of the inflammatory granulation tissue and cord compression.

Neoplastic involvement of psoas muscle may occur with contiguous spread from metastatic lymph nodes from primary neoplasms (of kidney, testis, bladder and cervix), lymphoma, renal cell carcinoma and retroperitoneal sarcoma. Primary Neoplasms of the psoas muscle are rare. Iliopsoas malignancies often appear similar to other pathologies on imaging. The affected muscle

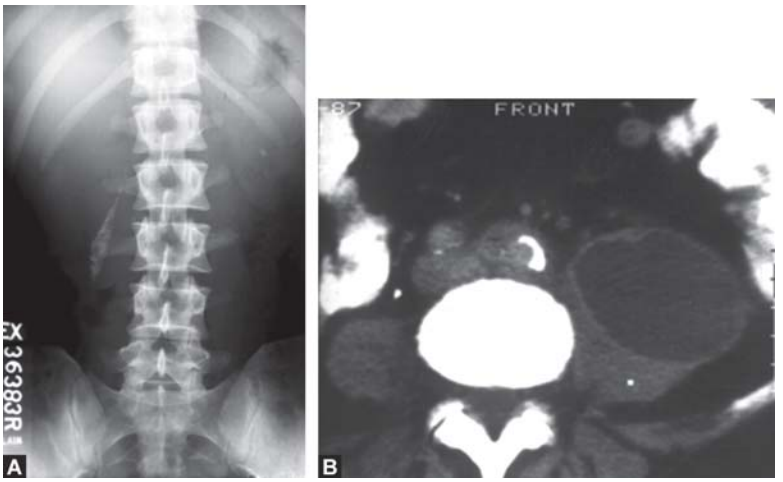

Figs 21.32A and B: Psoas abscess. CT image shows a well-defined, fluid density lesion in the left psoas muscle. It has a thin, peripheral enhancing rim and large necrotic center

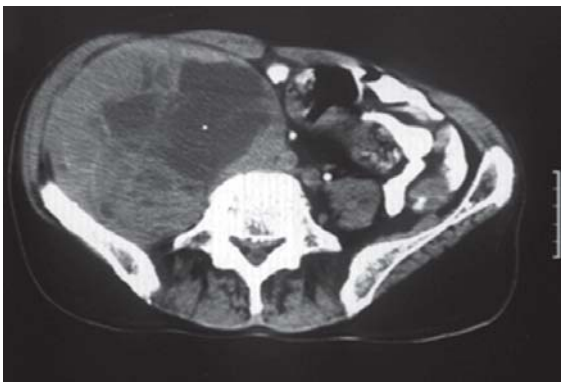

Fig. 21.33: Anaplastic carcinoma iliopsoas. Axial CT image shows a large het mass involving the right iliacus muscle. The large, irregular, solid component (arrow) within the mass raises a possibility of malignancy

is usually enlarged. As with abscesses, iliopsoas tumor may have enhancing peripheral rims and central necrosis (Fig. 21.33). A specific diagnosis is possible only when a large solid enhancing component is seen.

REFERENCES

1. Korobkin M, Silverman PM, Quint LE, Francis IR. CT of the extraperitoneal space: normal anatomy and fluid collections. Am J Roentgenol 1992;159:933-42.
2. Raptopoulos V, Kleinman PK, Marks S Jr, Snyder M, Silverman PM. Renal fascial pathway: posterior extension of pancreatic effusions within the anterior pararenal space. Radiology 1986;158(2):367-74.
3. Molmenti EP, Balfe DM, Kanterman RY, Bennett HF. Anatomy of the retroperitoneum: observations of the distribution of pathologic fluid collections.Radiology 1996;200(1):95-103.
4. Raptopoulos V, Lei QF, Touliopoulos P, Vrachliotis TG, Marks SC JR. Why perirenal disease does not extend into the pelvis: the importance of closure of the cone of the renal fasciae. Am J Roentgenol 1995;164 (5):1179-84.
5. Aizensterin RL, Owens C, Sabris S, et al. The perinephric space and renal fascia. Review of normal anatomy, pathology and pathways of disease spread. Crit Rev Diagnost Imaging 1997;38:325-67.
6. Gore RM, Balfe DM, Aizenstein RI, Silverman PM. The great escape: interfascial decompression planes of the retroperitoneum. AJR Am J Roentgenol 2000;175(2):363-70.
7. Kang PS, Spain JW. Multidetector CT angiography of the abdomen. Radiol Clin North Am 2005;43(6):963-76.
8. Kandpal H, Sharma R, Gamangatti S, Srivastava DN, Vashisht S. Imaging the inferior vena cava: a road less traveled. Radiographics 2008;28(3): 669-89.
9. Glockner JF. Three-dimensional gadolinium-enhanced MR angiography: applications for

abdominal imaging. Radiographics 2001; 21(2):357-70.
10. Vesselle HJ, Miraldi FD. FDG PET of the retroperitoneum: normal anatomy, variants, pathologic conditions, and strategies to avoid diagnostic pitfalls. Radiographics 1998;18(4): 805-23.
11. Ishikawa K, Idoguchi K, Tanaka H, Tohma Y, Ukai I, Watanabe H, Matsuoka T, Yokota J, Sugimoto T. Classification of acute pancreatitis based on retroperitoneal extension: application of the concept of interfascial planes. Eur J Radiol 2006;60(3):445-52.
12. Missiroli C, Singh AK. Nontraumatic emergencies of abdominal aorta. Semin Ultrasound CT MR 2008;29(5):369-77.
13. Taneja K, Sharma S, Das B, et al. Aortic aneurysms and dissections: Imaging with computerised tomography. Indian Journal of Thoracic and Cardiovascular Surgery 1994;10: 52-56.
14. Rakita D, Newatia A, Hines JJ, Siegel DN, Friedman B. Spectrum of CT findings in rupture and impending rupture of abdominal aortic aneurysms. Radiographics 2007;27(2):497-507.
15. Anagnostopolous CE, Prabhakar MJ, Kittle CF. Aortic dissections and dissecting aneurysm. Am J Cardiol 1972;30:263-73.
16. Aljabri B, MacDonald PS, Satin R, Stein LS, Obrand DI, Steinmetz OK. Incidence of major venous and renal anomalies relevant to aortoiliac surgery as demonstrated by computed tomography. Ann Vasc Surg 2001;15(6):615-8.
17. Onba_ O, Kantarci M, Koplay M, Olgun H, Alper F, Aydinli B, Zirek H, Ceviz N. Congenital anomalies of the aorta and vena cava: 16-detector-row CT imaging findings.Diagn Interv Radiol 2008;14(3):163-71.
18. Cuevas C, Raske M, Bush WH, Takayama T, Maki JH, Kolokythas O, Meshberg E. Imaging primary and secondary tumor thrombus of the inferior vena cava: multi-detector computed tomography and magnetic resonance imaging. Curr Probl Diagn Radiol 2006;35(3):90-101.
19. Lawrentschuk N, Gani J, Riordan R, Esler S, Bolton DM. Multidetector computed tomography vs magnetic resonance imaging for defining the upper limit of tumour thrombus in renal cell carcinoma: a study and review. BJU Int 2005;96(3):291-5.
20. Alfuhaid TR, Khalili K, Kirpalani A, Haider MA, Wilson SR, Daneman A. Neoplasms of the inferior vena cava—pictorial essay. Can Assoc Radiol J 2005;56(3):140-7.
21. Hulnick D, Megibow A, Naidich D, et al. Abdominal tuberculosis: CT evaluation. Radiology 1985;157:199-204.
22. Warshauer DM, Lee JK. Imaging manifestations of abdominal sarcoidosis. Am J Roentgenol 2004;182(1):15-28.
23. Gossios K, Nikolaides C, Bai M, Fountzilas G. Widespread. Castleman disease: CT findings. Eur Radiol 1996;6(1):95-8.
24. Kehagias D, Pafiti A, Vaos N, Samanidis L. Retroperitoneal lymphangioleiomyomatosis: CT appearance. Eur Radiol 1998.
25. Sheth S, Fishman EK. Non-Hodgkin lymphoma: pattern of disease at spiral CT. Crit Rev Diagn Imaging 2001;42(6):307-56.
26. Apter S, Avigdor A, Gayer G, Portnoy O, Zissin R, Hertz M. Calcification in lymphoma occurring before therapy: CT features and clinical correlation. Am J Roentgenol 2002;178(4): 935-8.
27. Schöder H, Moskowitz C. PET imaging for response assessment in lymphoma: potential and limitations. Radiol Clin North Am. 2008; 46(2):225-41.
28. Specht L. 2-[18F] fluoro-2-deoxyglucose positronemission tomography in staging, response evaluation, and treatment planning of lymphomas. Semin Radiat Oncol 2007;17:190-7.
29. Radin R. HIV infection: analysis in 259 consecutive patients with abnormal abdominal CT findings. Radiology 1995;197:712.
30. Bellin MF, Lebleu L, Meric JB. Evaluation of retroperitoneal and pelvic lymph node metastases with MRI and MR lymphangiography. Abdom Imaging 2003;28:155-63.
31. Minami M, Ohmoto K, Charnsangavej C, KawauchiN, Itai Y, Sasaki S. Origin of abdominal tumors: useful findings and signs on tomographic imaging. Radiology 1996;201:491-9.
32. Lane RH, Stephens DH, Reiman HM. Primary retroperitoneal neoplasms: CT findings in 90 cases with clinical and pathologic correlation. AJR Am J Roentgenol 1989;152(1):83-9
33. Cohan RH, Baker ME, Cooper C, Moore JO, Saeed M, Dunnick NR. Computed tomography of primary retroperitoneal malignancies. J Comput Assist Tomogr 1988;12(5):804-10.

34. Gupta AK, Cohan RH, Francis IR, Sondak VK, Korobkin M. CT of recurrent retroperitoneal sarcomas. Am J Roentgenol 2000;174:1025-30.
35. Craig WD, Fanburg-Smith JC, Henry LR, Guerrero R, Barton JH. Fat-containing lesions of the retroperitoneum: radiologic-pathologic correlation. Radiographics 2009;29:261-90.
36. Song T, Shen J, Liang BL, Mai WW, Li Y, Guo HC. Retroperitoneal liposarcoma: MR characteristics and pathological correlative analysis. Abdom Imaging 2007;32:668-74.
37. Hartman DS, Hayes WS, Choyke PL, Tibbetts GP. From the archives of the AFIP. Leiomyosarcoma of the retroperitoneum and inferior vena cava: radiologic-pathologic correlation. Radiographics1992;12:1203-20.
38. Lee KY, Oh YW, Noh HJ, Lee YJ, Yong HS, Kang EY, Kim KA, Lee NJ. Extraadrenal paragangliomas of the body: imaging features. Am J Roentgenol 2006;187:492-504.
39. Rha SE, Byun JY, Jung SE, Chun HJ, Lee HG, Lee JM. Neurogenic tumors in the abdomen: tumor types and imaging characteristics. Radiographics 2003;23:29-43.
40. Carmel G Cronin, Derek G Lohan, Michael A. Blake, Clare Roche, Peter McCarthy, Joseph M. Murphy Retroperitoneal Fibrosis: A Review of Clinical Features and Imaging Findings. Am J Roentgenol 2008;191:423-431.

Chapter 22

Nonvascular Interventions in the Urinary Tract

Mandeep Kang, Anupam Lal, Naveen Kalra

INTRODUCTION

The past few decades have witnessed a revolution in the development of minimally invasive procedures, with interventional radiology being in the forefront of these developments. All percutaneous procedures under image guidance are based on the premise that a skinny needle (21-22 gauge) can be inserted into almost any organ part in the body with safety and accuracy. Nonvascular interventions in the urinary tract are well established procedures with the initial description of a percutaneous nephrostomy having appeared in literature more than half a century ago.[1] Propelled by technological advances, minimally invasive uroradiological interventional therapies have altered the day-to-day practice of urology.

PERCUTANEOUS NEPHROSTOMY

Percutaneous nephrostomy (PCN) is the basic technique in interventional uroradiology which provides a direct access to the urinary tract.[2] Besides urinary diversion in an obstructed system, the access can be used to create large bore tracks through which various endourological procedures can be safely performed with fewer complications than open surgical procedures.[3]

Indications

1. Supravesical urinary tract obstruction
   a. Calculus disease
   b. Neoplasm
   c. Ureteral/anastomotic stricture
   d. Pyonephrosis
   e. Assessment of recoverable renal function in chronic obstruction
2. Urinary diversion for management of a urinary leak or fistula
3. Access for subsequent interventions
   a. Antegrade ureteric stenting
   b. Nephrolithotomy/lithotripsy
   c. Stone dissolution
   d. Ureteral occlusion for urinary fistula
   e. Biopsy of urothelial lesion/fulguration
   f. Foreign body or fungal ball removal
   g. Whitaker test

There is no absolute contraindication for PCN with the only relative contraindication being coagulopathy which should be corrected prior to the procedure.

Anatomy Relevant to Percutaneous Renal Entry

Knowledge of renal anatomy is essential for selection of a safe route through the kidney for percutaneous nephrostomy. The main renal artery divides into anterior and

posterior divisions with further segmental branches. The anterior division supplies the anterior two-thirds of the renal parenchyma while the posterior division supplies the posterior third. There is a zone of relative avascularity between the two vascular territories known as the Brödel's line of bloodless incision which lies just posterior to the lateral convex border of the kidney (Fig. 22.1). The ideal access to the collecting system should be through this relatively avascular plane.[4] Because of the normal rotation of the kidneys about their horizontal axis, the posterior calyces are directed posterolaterally with their long axis pointing to this avascular zone; these calyces should ideally be targeted at percutaneous nephrostomy. In the hilum of the kidney, the renal vein, artery and pelvis are located in an antero-posterior orientation. Central puncture of the collecting system should be avoided, only the calyces (which are completely surrounded by renal parenchyma) should be punctured.

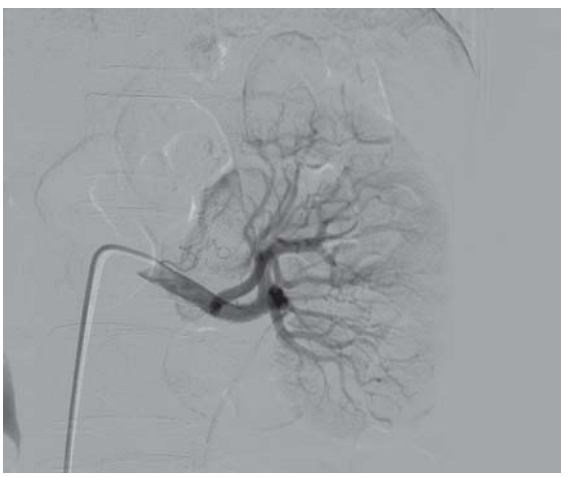

Fig. 22.1: Vascular anatomy of the kidney: Selective left renal arteriogram 25° left posterior oblique view shows bifurcation of the main renal artery into dorsal and ventral branches. The avascular plane of Brödel lies along the plane of division of these vascular territories

Central puncture can lead to two problems. Firstly, a major vessel can be injured leading to severe bleeding; secondly, there may be urinary leakage from the catheter tract due to inadequate sealing by renal tissue.[5]

The site of renal entry depends upon the indication for access. A lower pole posterior calyx can be safely accessed using a subcostal approach to avoid transgression of the pleura.[5] However, a posterior calyx of the upper pole or interpolar region provides the easiest access to the pelvi-ureteric junction for subsequent ureteral interventions. In cases of complex stone disease, entry through the posterior calyx of the upper pole allows visualization of most parts of the collecting system.[3]

Technique

An informed consent must be obtained from the patient after explaining in detail the need for the procedure, the procedure itself and the potential complications which can occur. A coagulogram must be performed and abnormalities if any, must be corrected prior to the procedure. Urine analysis to screen for possible urinary infection should also be performed. Prophylactic broad-spectrum antibiotics should be started prior to the procedure in patients with known or potential urinary infection (urinary conduit diversions, obstruction with or without fever, urinary leaks).

PCN is usually performed under fluoroscopic or ultrasound guidance. In certain cases, CT guidance may be used for example in emphysematous pyelonephritis when air in the collecting system obscures visualization on ultrasound. The use of MR guidance has also been described.[6]

The patient is placed prone on the fluoroscopy table with a bolster under the abdomen

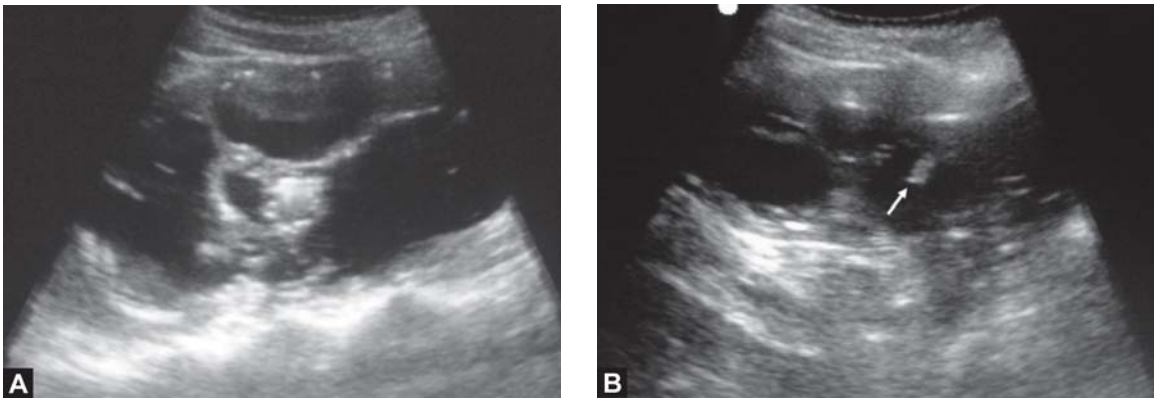

Figs 22.2A and B: Percutaneous nephrostomy. **(A)** Longitudinal sonogram shows gross hydronephrosis with internal echoes suggestive of pyonephrosis. **(B)** The lower pole calyx has been punctured using an 18 G needle. Needle tip is seen in situ (arrow)

to fix the kidneys against the posterior abdominal wall and prevent their anterior displacement during the procedure. The back and flanks are cleansed and draped. The calyx to be punctured is chosen depending upon the indication and local anesthetic is infiltrated into the skin and subcutaneous tissues. This is generally adequate for pain relief during the procedure, however, conscious sedation may be required in apprehensive or noncooperative patients. Infants and young children will require general anesthesia.

The chosen calyx can be punctured with an 18G needle under ultrasound guidance in a dilated system. After removing the stylet, a urine sample should be aspirated for culture. A small volume of iodinated contrast is injected to opacify the collecting system. A 0.035" guidewire is then passed through the needle and negotiated into the pelvis. After a stab incision along the needle tract, the needle is removed and the tract dilated using fascial dilators. For drainage of non-infected urine, catheters of 8-10 F are usually sufficient. The catheter is placed over the guidewire and coiled in the pelvis (Figs 22.2A to 22.3D). A check injection of contrast should be done to confirm position of all side holes of the cathe-

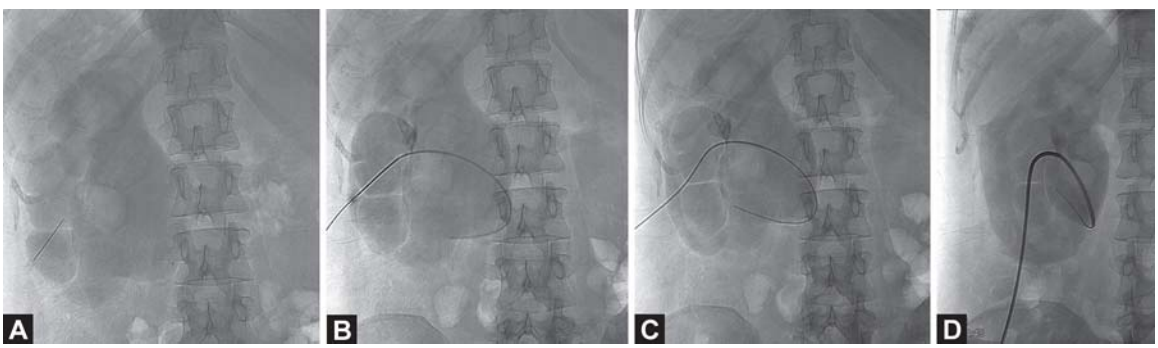

Figs 22.3A to D: Percutaneous nephrostomy. **(A)** The grossly dilated calyces are opacified due to a CECT abdomen done the previous day. These have been directly punctured by an 18G needle under fluoroscopic guidance. **(B)** A stiff guide-wire has been negotiated into the pelvis. **(C)** The puncture needle has been withdrawn and the track is being dilated using fascial dilators. **(D)** An 8F catheter is being threaded over the guide-wire to coil in the pelvis

ter within the collecting system. Pigtail catheters with or without locking devices may be used. The catheter is stabilized at the skin using sutures or other retention devices, connected to a urine collection bag and allowed to drain under gravity.

A variety of techniques may be used for the initial puncture. Some workers inject intravenous iodinated contrast to opacify the collecting system followed by direct puncture of the pelvis under fluoroscopic guidance with a 22 G needle. Iodinated contrast (with or without room air or carbon dioxide) is then injected under fluoroscopic control to opacify the collecting system to a degree necessary to find a suitable calyx. The selected calyx can then be punctured from the posterolateral aspect with an 18 G needle, with the subsequent steps being the same as described before. Another variation of this "two-stick" technique is to use a 22 G needle for the second puncture as well, a 0.014" hydrophilic guidewire is passed through this needle over which a 5F percutaneous access set is placed and the guidewire exchanged for a 0.035" stiff or super-stiff Amplatz guidewire.[3,6-8] Regardless of the technique used, care has to be taken not to over-distend the collecting system so as to avoid pyelovenous reflex, particularly in infected systems.

Occasionally, external urinary diversion is necessary in non-dilated collecting systems (e.g. in urinary leak or fistulas). These kidneys can be punctured using the double stick technique with initial opacification of the collecting system with intravenous injection of iodinated contrast.[9] Alternatively, these kidneys can also be accessed using sonographic guidance after intravenous injection of frusemide. Even if the calyces do not dilate adequately to be visualized on ultrasound, the renal pelvis can be seen and punctured with a skinny needle, iodinated contrast or saline injected to distend the calyces and a definitive calyceal puncture made with fluoroscopic or US guidance.[10]

Postprocedure Care

Vital signs should be frequently monitored in the immediate post procedure period as there is a potential for on-going blood loss or the development of septicemic shock (due to pyelovenous reflux and bacteremia) in patients at risk. Ideally, the patient should be admitted overnight for observation after the procedure, during which time the tube should be gently flushed with saline every four hours. Hematuria is initially present after percutaneous nephrostomy in virtually all patients, this usually gradually settles within 24-48 hours. The PCN tube output should be recorded to assess for adequacy of drainage. Appropriate analgesics, including narcotics if required (particularily for patients with intercostal entry) should be provided. The patients should be instructed regarding tube care, especially if long-term drainage is anticipated. The dressing around the catheter should be changed daily. The catheters need to be changed every 6-8 weeks.

Results

Placement of a nephrostomy tube is technically successful in 93-99 percent of cases in dilated systems. The success rate is lower in patients with non-dilated systems, complex stone disease, anatomical variants and renal cysts. Use of CT guidance may improve the technical success in patients with anatomical variants or renal cysts.[11,12]

Complications

These may be divided into local and systemic complications.

Systemic Complications

The most common systemic complication which can at times be fatal is sepsis. Every obstructed system is potentially infected. Manipulation of guidewires, catheter and injection of contrast all lead to an increase in the pressure in the collecting system which can lead to pyelovenous reflux. The incidence of septic complications has been reported to be between 1 and 2.5 percent.[11,13,14] The incidence rises to 7 percent in the setting of pyonephrosis.[12] One should avoid overdistention of the system by limiting the amount of contrast injected and also keeping manipulation to a minimum in the initial procedure. Complicated or prolonged procedures should be avoided in an infected system; further imaging and manipulation should be undertaken only 48-72 hours after the initial procedure when the system is adequately decompressed.[3,5,14]

Prone position of the patient during the PCN procedure may lead to respiratory insufficiency, especially in infants or young children under sedation. Good patient monitoring is essential.[5]

Local Complications

The most common local complication is bleeding which may occur from the renal parenchymal vessels or the intercostal vessels. Transient hematuria is observed in almost every patient. Severe bleeding which requires transfusion or intervention is seen in 1-3 percent of patients.[11] Bleeding noticed at the time of PCN can often be controlled by tamponade of the track with a larger bore nephrostomy catheter. If bleeding persists for 2-3 days, a nephrostogram should be obtained to check for malposition of the catheter. Severe bleeding developing several days after catheter insertion requires further evaluation. A track fistulogram can be obtained by exchanging the nephrostomy catheter with an introducer sheath over a stiff guidewire. The sheath is then gradually withdrawn while injecting contrast. At times, the venous or arterial source of bleed may fill with contrast. Angiographic evaluation for identification of a renal arteriovenous fistula, pseudoaneurysm or vessel laceration should be scheduled without delay in patients with persistent or severe bleeding. Most of these vascular injuries can be managed by the endovascular route, surgical intervention is rarely necessary.[15] Bleeding can lead to a perinephric hematoma which can cause a Page kidney with subsequent deterioration in renal function. This should be drained percutaneously.

Adjacent organs may be inadvertently punctured. A retro-renal colon, an uncommon anatomic variant may be transgressed leading to a nephrocolic fistula. Treatment is conservative and consists of ensuring adequate urinary drainage by placement of an antegrade or retrograde ureteric stent, and withdrawing the nephrostomy catheter into the colon to allow the nephrocolic track to heal.[16] Pleural complications in the form of pneumothorax, pleural effusion, emphysema or hemothorax may occur in 0.1-0.2 percent of cases. The incidence rises with intercostal entry or complex endourologic procedures.[17]

Catheter block or dislodgement are technical complications which may occur. The blocked catheter should be cleaned with a guidewire and changed. Replacement of a dislodged catheter is usually possible through the previous tract. Many times the whole tract can be opacified by a small amount of dilute contrast injected via a sheath placed at the site of urine leak on the skin. A hydrophilic guidewire is then used to probe the tract which usually finds its way into the collecting system.

Overall, when major and minor complications are considered together, the complication rate is between 10 and 15 percent. The mortality rate for percutaneous nephrostomy varies from 0.046 to 0.3 percent.[3,5]

Extended Applications of Percutaneous Nephrostomy

Antegrade Ureteric Stenting

The most common extension of PCN is placement of a ureteric stent for obstruction or fistula. It is often much easier to negotiate areas of narrowing, fistulae or discontinuity in the ureter in an antegrade rather than retrograde manner. The stenting is usually performed under local anesthesia and conscious sedation. After the initial PCN, a safety guidewire is placed through an access sheath to avoid losing renal access during the subsequent manipulation of the working guidewire. Negotiation of an obstructed segment is often facilitated by the use of curved angiographic catheters and hydrophilic guidewires. Once the stricture has been negotiated, the guidewire-catheter combination can be coiled within the bladder and the hydrophilic guidewire exchanged for a super-stiff Amplatz wire (Figs 22.4A to D). Determination of the correct length of the ureteric stent required can be done by using the bent guidewire technique. Balloon dilatation of strictures, placement of ureteric stents, postprocedure drainage of the upper urinary tract and subsequent nephrostograms can all be performed via the initial PCN tract. The percutaneous external urinary catheter is left in place for 24 hours after the procedure, after which it is capped. Thereafter, if there is no hydronephrosis on sonography and contrast injection shows free flow down the double J stent, the external catheter is removed.

Balloon dilatation of benign ureteric strictures may provide durable relief in up to 50 percent of cases. Following the dilatation, the ureter is supported with a stent. In case repeated entry into the ureter may be required, an internal-external stent can be placed for preserving percutaneous access as well as providing mechanical support.[17] Anastomotic strictures after cystectomy and ureteric diversion to an ileal conduit can also be mana-

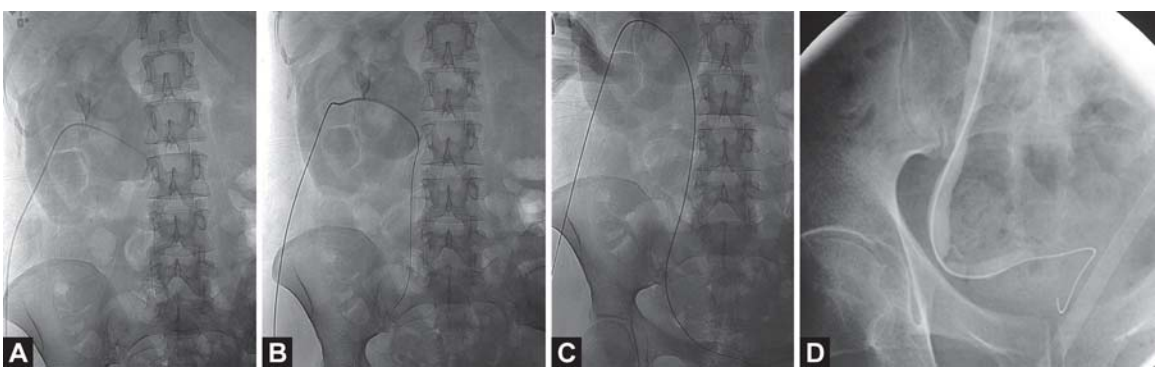

Figs 22.4A to D: Antegrade stenting in a patient with carcinoma of the urinary bladder. **(A)** The PCN catheter has been exchanged for a curved angiographic catheter over a stiff guide-wire. **(B)** A hydrophilic guide-wire has been introduced through the catheter and is being negotiated down the ureter. **(C)** The catheter guide-wire combination has been advanced into the urinary bladder. **(D)** The hydrophilic guide-wire has been exchanged for a super-stiff Amplatz guide-wire after negotiating a tight stricture at the uretero-vesical junction. The ureteric stent is then placed over the stiff guide-wire

ged through an antegrade percutaneous approach.[18] Internal-external stents are also placed in cases of ureteric leaks or fistulas because of the anticipated need for multiple percutaneous ureteral interventions and prolonged urinary drainage to allow healing. One should ensure that a solid portion of the tube traverses the site of leak with side-holes above and below.

In patients with fistulas of the ureters or lower urinary tract associated with advanced inoperable pelvic malignancies, external drainage with a PCN catheter and urinoma drainage catheter may not provide adequate urinary diversion. Ureteral occlusion can be done using stainless steel or platinum coils deployed in the ureter above the level of leak along with a PCN to provide relief from the distressing symptoms.[19] Other materials which can be used for ureteral occlusion include gelatin sponge, n-butyl cyanoacrylate, detachable balloons or radiofrequency electro-cautery.[20] The major drawback is the permanent nature of the occlusion and need for life-long nephrostomy catheter.

Large Bore Track Creation

PCN forms the first step for creation of a large diameter track which may be necessary for percutaneous stone therapy, nephroscopy, or antegrade ureteroscopy.[21] Tracks of 30F or larger can be created by using balloon dilatation systems, coaxial dilators or combined balloon-sheath systems. Following the procedure, a large diameter tube (24-30F) is inserted through the sheath into the kidney to provide urinary drainage and track tamponade and the sheath is removed.

SCLEROTHERAPY FOR RENAL CYSTS

Benign renal cysts (cortical or parapelvic) are found in approximately 50 percent of males above the age of 50 years. Renal cysts vary in size and are frequently multiple. They are usually silent, but large, infected or hemorrhagic cysts can cause symptoms. Large cysts can also cause obstruction of the pelvicalyceal system, pressure atrophy of the adjacent parenchyma and stone formation in obstructed calyces.[7,22]

A symptomatic renal cyst is managed with a combination of percutaneous drainage and sclerotherapy. Various agents which have been used to induce sclerosis of the epithelial lining of the cyst include hypertonic dextrose, hypertonic water-soluble contrast, iophandylate, absolute alcohol, tetracycline and sodium tetradecyl sulphate. The technique consists of puncture of the cyst under sonographic guidance and aspiration of the cyst contents. Contrast is then injected to demonstrate the internal appearance of the cyst and to rule out any communication of the cyst with the collecting system. If no communication is demonstrated and the cyst is small, sclerosant can be injected amounting to about one-third of the aspirated contents of the cyst. The sclerosant is left in place for 15-20 minutes with frequent postural changes of the patient to ensure contact with all the walls of the cyst and then reaspirated. If the cyst is larger, a 5F percutaneous drainage catheter can be placed in the cyst and left to drain for 24-48 hours before sclerotherapy. Larger cysts may require multiple sessions of sclerotherapy.

If a cyst is communicating with the renal collecting system sclerosant should not be injected as it can cause strictures in the pelicalyceal system. An infected cyst is managed like an abscess with percutaneous catheter drainage. Good outcomes of sclerotherapy in renal cysts are reported with success rates of 75-100 percent.[7,22]

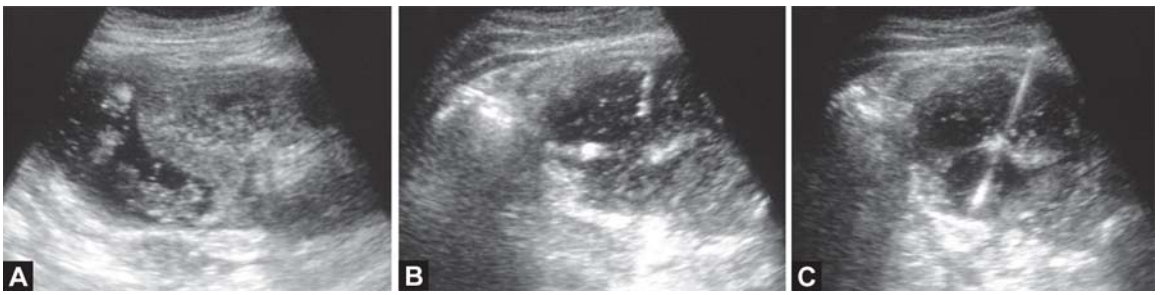

Figs 22.5A to C: (A) An irregular collection with debris and internal echoes is seen in the upper pole of the kidney suggestive of renal abscess. **(B)** The abscess has been punctured with an 18 gauge needle. **(C)** Guide-wire is seen coiled in the abscess

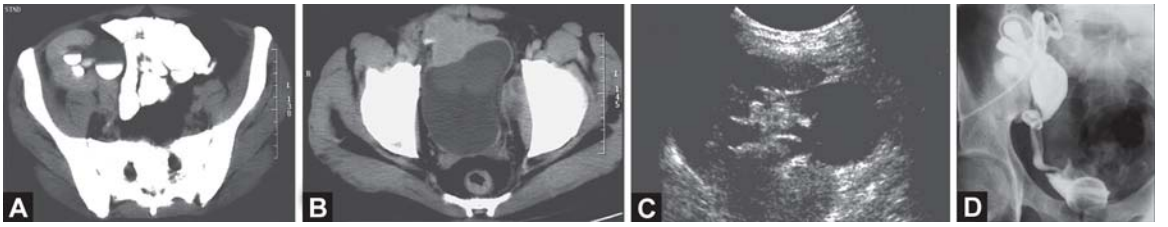

Figs 22.6A to D: Anatomotic stricture in a transplant kidney. **(A)** CECT Abdomen axial image showing hydroureteronephrosis in the transplant kidney. **(B)** There is a large, lobulated mass involving the uretero-vesical anastomotic site engulfing the ureter. **(C)** Ultrasound image showing dilatation of the pelvis with minimal dilatation of the calyces. **(D)** Nephrostogram obtained after percutaneous nephrostomy demonstrates the stricture at the anastomotic site. This was successfully stented

PERCUTANEOUS CATHETER DRAINAGE

Percutaneous catheter drainage (PCD) can be done to drain renal or perirenal abscesses, collections, lymphoceles or urinomas. The basic technique is similar to PCN consisting of needle puncture under imaging guidance, guidewire insertion, track dilatation and catheter placement (Figs 22.5A to C). The size and type of drainage catheter should be chosen according to the nature of fluid to be drained.

BIOPSIES

Core biopsy with an automated gun is more common than fine needle aspiration (FNA) in the genitourinary tract. Renal biopsy with a 16-18G gun is used in cases of renal parenchymal disease. Biopsy or FNA can be performed for genitourinary tumors. Transrectal ultrasound guided biopsy of the prostate is useful in suspected cases of prostatic carcinoma.

THE COMPLICATED RENAL TRANSPLANT

Common complications in renal transplant recipients include graft rejection, perigraft or pelvic fluid collections (urinomas, lymphoceles, etc.), ureterovesical anastomotic strictures and focal parenchymal lesions. The percutaneous procedures required in this group of patients are similar to those required in native kidneys. The transplant kidney is approached from the lateral aspect with the patient supine (Figs 22.6A to D). These patients are usually very sick and immunocompromised, therefore, meticulous attention should be paid to antiasepsis.

RADIOFREQUENCY ABLATION OF RENAL TUMORS

The incidence of renal cell carcinoma (RCC) has been seen to rise in recent years. This is probably due to the increasing use of abdominal imaging and improvements in CT and MR technology resulting in the incidental detection of small, asymptomatic renal tumours in patients undergoing imaging for other indications. Recent studies have indicated that RCC may be incidentally detected at cross-sectional imaging in up to 60 percent of patients.[23,24] Patients with RCC that have not spread outside the renal parenchyma have an excellent prognosis for cure if the RCC can be resected. In the past, radical nephrectomy has been the conventional treatment for RCC. Over the last two decades, nephron-sparing surgery has become an oncologically viable alternative in patients who would be rendered anephric by a radical nephrectomy. Nephron-sparing surgery has also been shown to be an equally effective curative treatment for patients with a single, small (< 5 cm), and clearly localized RCC and a normal contralateral kidney.[23] However, nephron-sparing surgery requires more technical skills than radical nephrectomy with higher intraoperative blood loss. Many patients may be poor surgical candidates due to presence of significant comorbidities and advanced age. In addition, some patients may have multiple, bilateral tumors or poor renal function. In these patients, less invasive nephron-sparing surgical techniques have been applied including laparoscopic partial nephrectomy, radiofrequency ablation and cryoablation. Percutaneous approaches to treatment of RCC reported include radiofrequency ablation, cryotherapy, microwave therapy and high intensity focused sonography. Radiofrequency ablation (RFA) has been successfully used for primary and metastatic hepatic tumors. The first reports on the use of RFA in the treatment of renal tumors appeared in 1997 and it is widely used as an effective curative treatment option today.[25]

Ablation Process

In RFA, a high-frequency, alternating current with a wavelength of 460-500 kHz is passed through an electrode placed within the target tumor tissue. Grounding pads placed around the patients thighs complete the electrical circuit. Deposition of radiofrequency energy results in the heating of cells near the site of energy deposition. When human tissue is heated to beyond 49°C, cell death occurs within minutes due to loss of enzymatic function, melting of cell membranes, and destruction of cytoplasm. Temperatures in excess of 60°C cause immediate cell death. When the temperature exceeds 100°C, the cells boil releasing gas vapors and causing tissue charring. These in turn inhibit the dispersion of radiofrequency energy decreasing the effectiveness of the procedure. Hence, ideal RFA devices should produce prolonged heating of target tissue between 50°C and 100°C.[25] Various modifications developed towards this purpose include: (i) Pulsed energy deployment, (ii) Expansion of electrode surface, (iii) Intraparenchymal injection of iron compounds or saline before and during RF application, and (iv) Internal cooling of the needle electrode with saline.

Equipment

All RFA devices consist of an electric generator, needle electrode and grounding pad. Among the commercially available systems, the RITA RF system (RITA Medical Systems, Inc, Fremont, CA, USA) contains a 14-gauge

insulated outer needle and 4-9 internal curved prongs which deliver the RF electrical energy while affixing the needle in place. The latest RITA StarBurst Xli-Enhanced electrode, which has saline infusion capability, allows a maximum treatment volume of 7 cm. Radionics (Burlington, Mass, USA) offers the Cooltip system which has a 17-gauge straight electrode with a beveled tip with internally circulating saline for controlling the temperature at the needle tip (<20°C), to reduce tissue charring, build-up of impedance and maximize energy deposition. A cluster of three straight electrodes arranged 0.5 cm apart in a triangular pattern is also available. The Radiotherapeutics RF 3000 system (Radiotherapeutics Corporation, Natick, MA, USA) has a 17-gauge LeVeen needle electrode consisting of an insulated metal cannula and 12 expandable wire tines which reach a diameter of 4 cm when fully deployed. Different devices use a slightly different approach to maximize energy delivery and monitor thermal destruction. The theoretical maximum size of the ablated area is twice the length of the energy emitting segment of the electrode in the long axis of the treatment zone. The maximum in the transverse axis is up to two-thirds of the long axis of the treatment zone. Practically, the ablated area is smaller than the theoretical zone. Flowing blood, large fluid containing spaces, or circulating air can decrease the effective size of the treatment zone due to the "heat-sink" effect.[26]

Patient Selection and Preprocedure Evaluation

RFA can be performed in patients with a renal tumor suggestive of RCC on the basis of the imaging findings, and who have marginal renal function, serious comorbidities that make them high-risk surgical candidates, or are at high risk for developing additional RCCs (e.g. von Hippel-Lindau disease). Contraindications are relative and include uncorrected coagulopathy and an ongoing acute illness such as sepsis.[25, 27]

All patients should undergo a contrast enhanced CT or MR of the abdomen before the procedure. The tumor should still be Robson's stage I or II to achieve curative results. Spread of the tumor beyond the renal fascia, into renal vein or lymph nodes or distant metastases are contraindications for RFA. There is no absolute size criterion for RFA, however, the likelihood of complete ablation increases in smaller tumours. Tumors larger than 7 cm are unlikely to be successfully ablated and should only be considered for cytoreduction. Peripherally located tumors are also more likely to be successfully ablated in comparison to centrally located tumors due to the heat-sink effect of the vessels in the renal hilum.[27,28] Due to the insulation offered by the perinephric fat, subcapsular or exophytic tumors can usually be completely ablated.[24]

Laboratory investigations to be performed prior to the procedure include serum creatinine, platelet count and coagulation profile. Biopsy of the tumor before ablation is usually not performed if the imaging findings are characteristic, however some authors routinely perform a biopsy for tissue diagnosis prior to the procedure. Prophylactic antibiotics are usually administered.

Guidance

Imaging guidance for the procedure can be with the help of sonography, CT or MR. Sonography plays an important role in the guidance of both percutaneous and intraoperative procedures. It provides real time imaging

without any hazards of ionizing radiation, it's easy availability and portability offer further advantages. Needle positioning can be accurately checked using 3D US. However, dissolved gases (primarily nitrogen) are released during tissue heating which form microbubbles in the tissue cause obscuration of lesion due to their hyperechogenicity.[26] This is particularly important when the tumor is more than 3 cm in size and requires multiple, overlapping ablations. In some patients, it may be difficult to visualize very small renal tumors with sonography. Air-filled bowel close to the tumor also may not be adequately visualized on US. In most cases, RFA of renal lesions is performed under CT guidance. CT offers the following advantages:(i) it can demonstrate small RCCs; (ii) there is no obscuration of the lesion after ablation; and (iii) a contrast enhanced CT can be performed after the procedure to assess adequacy of ablation before terminating the procedure.[25] MR has also been used for guidance for RFA. It provides better soft tissue contrast without need for intravenous contrast. Its multiplanar capabilities without radiation hazards and provision of MR fluoroscopy sequences makes it optimally suited for guiding RFA procedures.

Procedure

The procedure can be performed on an out patient basis. A written informed consent should be obtained. The procedure is usually performed under local anesthesia with conscious sedation. General anesthesia may be required in certain cases such as deep seated, difficult to access lesions where precise respiratory control is required.

The technique of placing the electrode is similar to that of performing an imaging-guided biopsy of a focal lesion. The goal is to ablate the target tumor tissue as well as a 0.5-1 cm circumferential rim of adjacent normal parenchyma, therefore an appropriate electrode size should be selected. The electrode is advanced to the deep margin of the tumor as there is little ablation beyond the electrode tip in some cases. The ablation is usually performed for 10-15 minutes per ablative cycle. Multiple, overlapping ablations need to be done in larger tumors. In literature, technical success rates for renal RFA range from 92 to 100 percent with clinical success rates for small renal tumors (mean diameter - 1.7-3.5 cm) reported as between 86 to 100 percent.[24-28]

Postprocedure and Follow-up

All patients should be kept under observation for 4-6 hours after the procedure. Antibiotics should be continued for at least five days postprocedure. Appropriate analgesics should be prescribed for ensuring adequate analgesia.

A contrast enhanced biphasic CT should be obtained immediately after the procedure to determine adequacy of ablation. Thereafter a contrast enhanced CT or MR should be obtained at one, three, six, and twelve month intervals to look for residual or recurrent tumor. Imaging after the first year can be done at 6-9 month intervals. CT is more often used for postablation follow-up because of its lower cost and wider availability, however, MR may be used in patients with renal insufficiency (Figs 22.7A to C).

Immediately after ablation, the ablated tumor usually appears larger than the preablation size because a peripheral margin of 0.5-1 cm of normal tissue is also ablated. On follow-up imaging, ablated tumors appear as focal, non-enhancing masses which show decrease in size with time. Soft tissue stranding may be seen in the peri-nephric fat. At times, a curvilinear, hyperattenuating area or halo is seen surrounding the ablated lesion.[24]

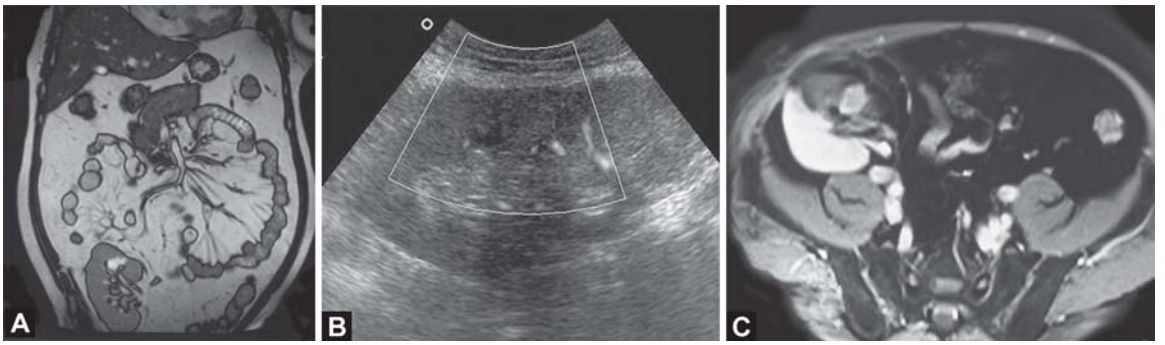

Figs 22.7A to C: Radiofrequency ablation of a renal cell carcinoma in a transplant kidney. **(A)** Pre-procedure MR coronal T2 weighted image shows a focal area of hyperintensity in the upper pole of the transplant kidney. **(B)** Follow-up Doppler image after six weeks shows absence of flow to the region of the ablated tumor. **(C)** MR axial post-gadolinium T1 image one month after RFA shows absence of enhancement of the renal parenchyma in the region of ablation. Note the defect is larger than the original tumor size due to ablation of a rim of normal parenchyma around the tumor

Nodular enhancement in the ablated tumor or an increase in the size of lesion is considered to represent residual or recurrent tumor. On MR, the area of necrosis appears hypointense on T2 weighted images. It usually appears hyperintense relative to the renal cortex on T1 weighted images, though it may occasionally appear iso to hypointense. Rim enhancement of the ablated lesion may be seen early after ablation but this gradually resolves over 3 months. Residual viable tumor tissue appears hyperintense on T2 weighted images and shows nodular enhancement post gadolinium on T1 images.[24]

Complications

Few complications have been reported after RFA in renal lesions. Hematuria occurs rarely, is usually self-limited and commonly resolves within 24-48 hours. Thermal necrosis of adjacent bowel has been reported. At a minimum, there should be at least 5 mm of intervening fat between the target tumor and bowel to avoid thermal injury. If bowel abuts the target, sterile water can be injected to displace the bowel and ensure safe ablation of the RCC. RFA of lesions adjacent to the adrenal gland can cause release of vaso-active catecholamines which requires administration of alpha blockers. Perirenal hemorrhage is common but is rarely clinically significant. Needle track seeding and development of ureteric strictures are other rare complications. Overall, the rate of major complications after RFA of renal lesions is estimated to be approximately 1 percent.[25,29]

Other Applications of RFA

RFA has been successfully used to treat intractable hematuria in cases of unresectable RCCs. It has also been used for the treatment of recurrent RCC after surgery. The surgical resection of isolated distant metastases from RCC has been reported to be associated with prolonged survival rates. RFA has been used to successfully ablate pulmonary metastases from RCC.

To summarise, the use of RFA for the treatment of RCC is a very promising technique that should be considered as a therapeutic option for patients with early-stage RCC who are poor surgical candidates.

REFERENCES

1. Goodwin WE, Casey WL, Woolf W. Percutaneous trocar (needle) nephrostomy in hydronephrosis. JAMA 1955;157:891-94.
2. Banner MP, Ramchandani P, Pollack HM. Interventional procedures in the upper urinary tract. Cardiovascular Intervent Radiol 1991; 14:267-84.
3. Dyer RB, Regan JD, Kavanagh PV, Khatod EG, Chen MY, Zagoria RJ. Percutaneous Nephrostomy with Extensions of the Technique: Step by Step. Radiographics 2002;22:503-25.
4. Papanicolou N. Renal anatomy relevant to percutaneous interventions. Semin Intervent Radiol 1995;12; 163-72.
5. Hausegger KA, Portugaller HR. Percutaneous nephrostomy and antegrade ureteral stenting: technique – indications – complications. Eur Radiol 2006;16(9):2016-30.
6. Karniemi J, Sequeiros RB, Ojala R, Tervonen O. MRI guided percutaneous nephrostomy: a feasibility study. Eur Radiol 2008 Nov [Epub ahead of print].
7. Park BK, Kim SH, Moon MH. Nonvascular interventions of the urinary tract. J Korean Med Sci 2002;17:727-36.
8. Funaki B, Vatakencherry G. Comparison of single-stick and double-stick techniques for percutaneous nephrostomy. Cardiovasc Intervent Radiol 2004;27:35-7.
9. Patel U, Hussain FF. Percutaneous nephrostomy of nondilated renal collecting systems with fluoroscopic guidance: Technique and results. Radiology 2004;233:226-33.
10. Gupta S, Gulati M, Suri S. Ultrasound guided percutaneous nephrostomy in nondilated pelvicalyceal sytem. J Clin Ultrasound 1998; 26:177-9.
11. Farrell TA, Hicks ME. A review of radiologically guided percutaneous nephrostomies in 303 patients. J Vasc Intervent Radiol 1997;8:769-74.
12. Ramchandani P, Cardella JF, Grassi CJ, et al. Quality improvement guidelines for percutaneous nephrostomy. J Vasc Interventional Radiol 2003;14:277-81.
13. Wah TM, Weston MJ, Irving HC. Percutaneous nephrostomy insertion: outcome data from a prospective multi-operator study at a UK training centre. Clin Radiol 2004;59:255-61.
14. Zagoria RJ, Dyer RB. Do's and don'ts of percutaneous nephrostomy. Acad Radiol 1999;6(6):370-77.
15. Vignali C, Lonzi S, Bargellini I, Cioni R, Petruzzi P, et al. Vascular injuries after percutaneous renal procedures: treatment by transcatheter embolization. Eur Radiol 2004;14:723-9.
16. Gerspach JM, Bellman GC, Stoller ML, Fugelso P. Conservative management of colon injury following percutaneous renal surgery. Urology 1997;49:831-6.
17. Seymour H, Patel U. Ureteric stenting: current status. Semin Intervent Radiol 2000;17:351-65.
18. Tal R, Bachar GN, Baniel J, Belenky A. External Internal nephro-ureteral-ileal stents in patients with an ileal conduit: long term results. Urology 2004;63:438-41.
19. Titton RL, Gervais DA, Hahn PF, Harisinghani MG, Arellano RS, Mueller PR. Urine leaks and urinomas: Diagnosis and imaging-guided intervention. Radiographics 2003;23:1133-47.
20. Avritscher R, Madoff DC, Ramirez PT, Wallace MJ, Ahrar K, et al. Fistulas of the lower urinary tract: Percutaneous approaches for the management of a difficult clinical entity. Radiographics 2004;24 Suppl1:S217-36.
21. Bhattacharya T, Kumaradevan J, Watkinson AF. Percutaneous nephrolithotomy: State of the art. Semin Intervent Radiol 2000;17:341-9.
22. Hanna RM, Dahniya MH. Aspiration and sclerotherapy of symptomatic simple renal cysts: value of two injections of a sclerosing agent. AJR Am J Roentgenol 1996;167:781-3.
23. Kawamoto S, Permpongkosol S, Bluemke DA, Fishman EK, Solomon SB. Sequential changes after radiofrequency ablation and cryoablation of renal neoplasms: role of CT and MR imaging. Radiographics 2007;27:343-55.
24. Farrell MA, Charboneau WJ, DiMarco DS, Chow GK, Zincke H, et al. Imaging-guided radiofrequency ablation of solid renal tumours. AJR Am J Roentgenol 2003;180:1509-13.

25. Zagoria RJ. Imaging-guided radiofrequency ablation of renal masses. Radiographics 2004; 24:S59-71.
26. Chiou SY, Liu JB, Needleman L. Current status of sonographically guided radiofrequency ablation techniques. J Ultrasound Med 2007; 26:487-99.
27. Liu KW, Gervais DA, Arellano RA, Mueller PR. Radiofrequency ablation in renal cell carcinoma. Clin Radiol 2003;58:905-13.
28. Boss A, Clasen S, Kucyzk M, Schick F, Pereira PL. Image guided radiofrequency ablation of renal cell carcinoma. Eur Radiol 2007;17: 725-33.
29. Rhim H, Dodd GD III, Chintapalli KN, et al. Radiofrequency thermal ablation of abdominal tumours: lessons learned from complications. Radiographics 2004;24:41-52.

Chapter

23 Vascular Interventions in the Genitourinary Tract

Shivanand Gamanagatti, Deep Narayan Srivastava

INTRODUCTION

Interventional vascular radiology has grown over the past two to three decades and has placed the radiologist to play an important role in patient's management. With the current advances in technology allowing more accurate and controlled deployment of embolic agents, embolotherapy has now become the procedure of choice for the management of visceral and solid organ aneurysms and also percutaneous renal revascularization has become an accepted procedure of choice for renal artery stenosis.

Various vascular interventional procedures in genitourinary practice are directed towards vascular dilatation or vascular embolization. The commonly performed procedures include:

- Renal artery angioplasty
- Renal artery stenting
- Renal artery embolization
- Uterine artery embolization
- Vaginal AVMs embolization
- Varicocele embolization
- Scrotal AVM embolization

RENAL ARTERY ANGIOPLASTY

Renal artery stenosis (RAS) is the most common cause of secondary hypertension, seen with a 14 percent prevalence among patients with chronic renal failure. Among the various causes of RAS, atherosclerosis is the most common etiology, others being fibromuscular dysplasia, Takayasu arteritis, neurofibromatosis, etc. Medical therapy and surgical treatment including renal vascularization and nephrectomy are traditional methods of treatment for renovascular hypertension. These methods, however, have several disadvantages. The lowering of blood pressure by medical therapy further reduces renal blood flow and further deterioration of renal function even in controlled blood pressure. The surgical revascularization methods are considerably beneficial to most patients but considering the associated morbidity and operative mortality rate of 8 percent, surgery should be done only on carefully selected patients. Presently, percutaneous transluminal renal angioplasty (PTRA) is the first line of treatment for renal artery stenosis due to its relatively lower morbidity and mortality compared to surgical methods. The Society of Cardiovascular and Interventional Radiology (SCVIR) has laid down guidelines for the renal artery angioplasty. Various pathological lesions are shown in following table:

Cause	*Affected Segment*	*Incidence %*
Atherosclerosis	Ostium and Proximal 1/3	90
Fibromuscular dysplasia	Mid and Distal 1/3	10
Takayasu Arteritis	Ostium and proximal part	<1
NF-1	All	<1
Radiation	All	<1
Trauma	All	<1

According to the SCVIR guidelines, above lesions can be divided into four categories as follows:[1]

Category-I Lesions are those for which balloon angioplasty alone is the procedure of choice. It includes fibromuscular dysplasia of the renal artery and unilateral short (< 3 cm) and non-ostial atherosclerosis (Figs 23.1 and 23.2).

Category-II Lesions are well-suited for angioplasty and are atherosclerotic bilateral non-ostial stenosis, postoperative anastomotic stenosis, stenoses associated with worsening renal function (Fig. 23.3).

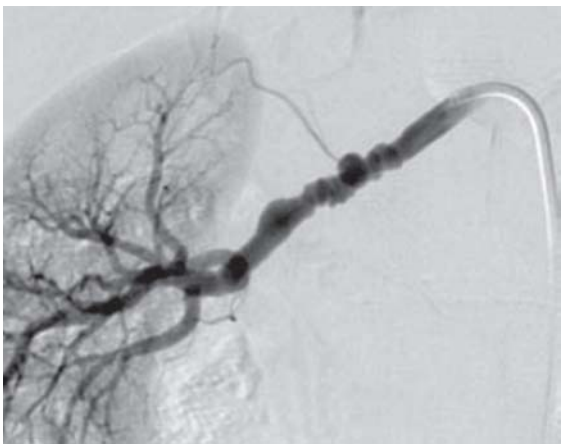

Fig. 23.2: Selective renal angiogram showing classic string-of-pearls appearance of right renal artery suggestive of fibromuscular dysplasia (Category-I lesions)

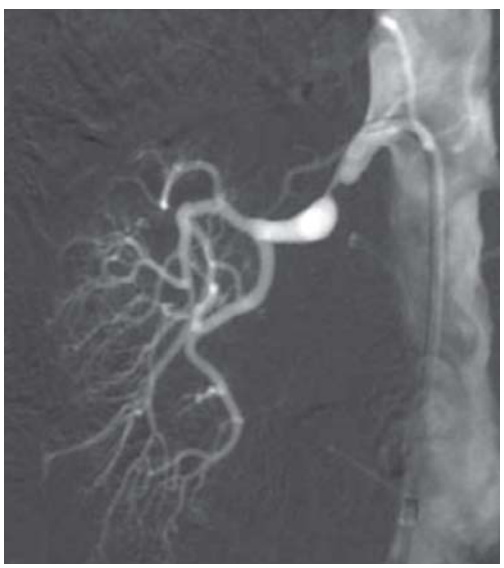

Fig. 23.1: Selective renal angiogram showing non-ostial short segment narrowing with post stenotic dilation of right renal artery (Category-I lesions)

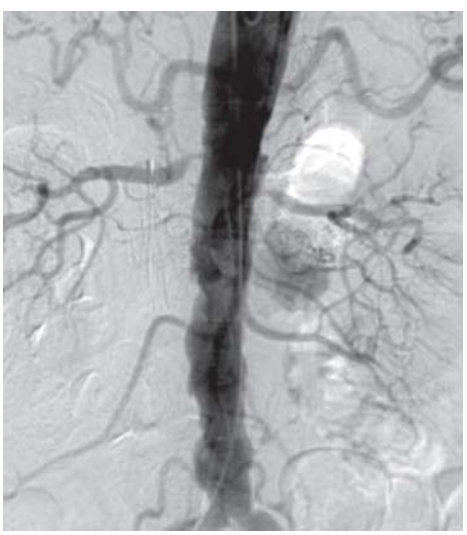

Fig. 23.3: Flush aortogram showing diffuse atherosclerotic abdominal aorta and ostial narrowing of bilateral renal arteries (Category-II lesions)

Category-III Lesions have a moderate chance of technical success or long-term benefits compared to bypass surgery and are atherosclerotic renal ostial stenosis, non-atheromatous lesions involving the proximal renal arteries

Category-IV Lesions have a low technical success rate. This includes renal artery stenoses in vessels that arise from an aneurysmal or severely diseased aortic segment or stenoses associated with renal artery aneurysm.

Imaging the Renal Arteries

Conventional angiography is still considered the best anatomic study for evaluating patients with renal artery stenosis. Duplex ultrasonography can be very helpful and should be the first imaging study in patients suspected of having renal artery stenosis. The quality of renal ultrasonography depends on the operator and on other variables such as body habitus, but even so, the sensitivity of duplex scanning has been reported to be 98 percent, with 98 percent specificity and high positive and negative predictive values.[2]

Computed tomography angiography (CTA) is now replacing conventional angiography for evaluating renal arteries. The images are comparable to those of conventional angiography, vessels can be evaluated in three dimensions, and CTA offers options for clarifying anatomy which may be better than with conventional angiography. Exposure of the patient to radiation from renal CTA is comparable to that of catheter angiography.[2]

Magnetic resonance angiography (MRA) is also used to evaluate the anatomy of the renal arteries. It has lower resolution than CTA or conventional angiography but is excellent for patients with impaired renal function because the contrast agent (gadolinium) is relatively nonnephrotoxic.[2,3]

Endovascular treatment of renal artery stenosis involves either percutaneous transluminal angioplasty or a combination of angioplasty and stent placement.

Technique[4-6]

Renal Artery Angioplasty

The procedure is most commonly performed through a femoral artery approach. However, if indicated by patient's anatomy (for example presence of iliac artery occlusions or a very steeply angled renal artery), the brachial approach can be used. A 6-F sheath is inserted into the femoral artery. It will be very helpful if a long (typically 35-cm) sheath is used as guiding catheter. A preshaped catheter is then used to access the renal artery. The catheter is used in combination with a guidewire to cross the lesion. A hydrophilic guidewire such as a Terumo can be very helpful, especially in lesions that are difficult to cross, though many would also use the soft tipped Bentson guidewire. Having crossed the lesion, heparin and an antispasmodic drug are administered. The author uses 3000 units of heparin and 300 mg of isosorbide dinitrate, respectively.

With the catheter across the stenosis, the guidewire is changed to a specialist guidewire such as the Jindo. The guidewire itself is very stiff, providing good support for the angioplasty balloon. The atraumatic nature of the tip is very important, as it can be placed in a cortical branch without significant danger of causing spasm. An angioplasty balloon is then introduced over the guidewire and angioplasty performed (Figs 23.4A to C). After con-firming the proper position of balloon, it is inflated and left for 30 seconds.

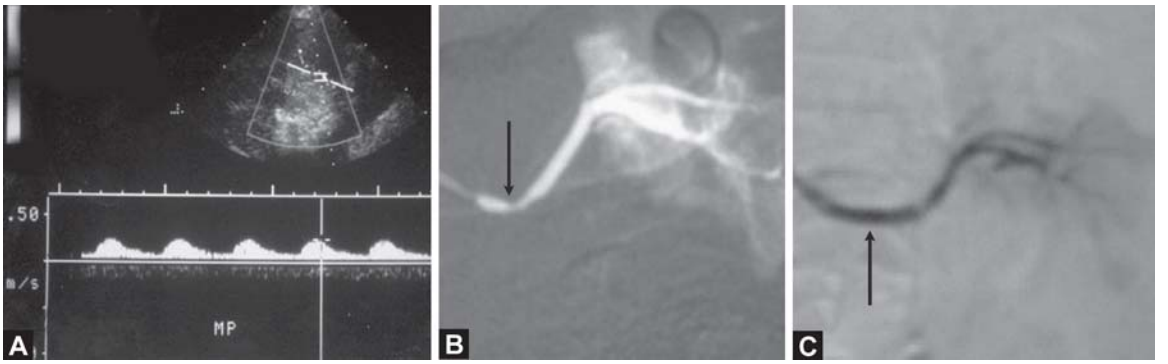

Figs 23.4A to C: A case of renal artery stenosis treated by angioplasty: **(A)** renal doppler showing classic pulsus parvus et tardus wave form of renal artery stenosis. **(B)** selective renal angiogram showing focal narrowing of left renal artery. **(C)** Post angioplasty angiogram showing successful dilatation of renal artery and 0 percent residual stenosis

Balloons are not oversized, but should instead be the same diameter as the artery distal to the stenosis. Typical balloon diameters will vary between 5 and 7 mm. Loin pain with balloon inflation is common, but should not be severe. In the event of the latter, vessel rupture may occur, and dilation should be stopped and a smaller balloon used. After dilation the balloon is removed and the guidewire left in place, and a check angiogram performed through the long sheath or guiding catheter. If there has been a complication or further dilation is required, access has thus been maintained to allow additional intervention. The angioplasty is considered technically successful if after the angioplasty the arterial lumen had less than 30 percent residual stenosis and the pressure gradient is less than 20 mm Hg. The clinical results can be assessed by the effect on blood pressure control and improvement of renal function.

RENAL ARTERY STENTING

The renal artery stent placement is now an established method of adjunctive treatment to renal angioplasty. Several problems related with renal angioplasty such as flow compromising dissection, residual stenosis greater than 30 percent with a trans-stenotic pressure gradient greater than 20 mm Hg or restenosis, can be successfully treated with stenting. The renal artery stenting has shown better technical results, long-term patency and a lower rate of restenosis than that of PTRA. Stents are almost exclusively placed in the renal arteries by using an angioplasty balloon (balloon-expandable rather than self-expanding stents). In many respects insertion of renal artery stents is performed in a similar way to renal angioplasty. However, stents are normally inserted at the ostium of the renal artery because they are used for the treatment of atheromatous disease. It is therefore essential to have a clear idea of the exact location of the ostium to facilitate accurate stent placement. Prior to stent insertion it is of value to predilate the stenosis with a 4-mm balloon to ease the passage of the stent across the stenosis. Although many recommend the use of a guiding catheter, modern long sheaths also perform very well. Use of either allows angiograms to be performed whilst finally positioning the stent prior to deployment. There are no reported adverse consequences associated with leaving the stent projecting 2 mm or so into

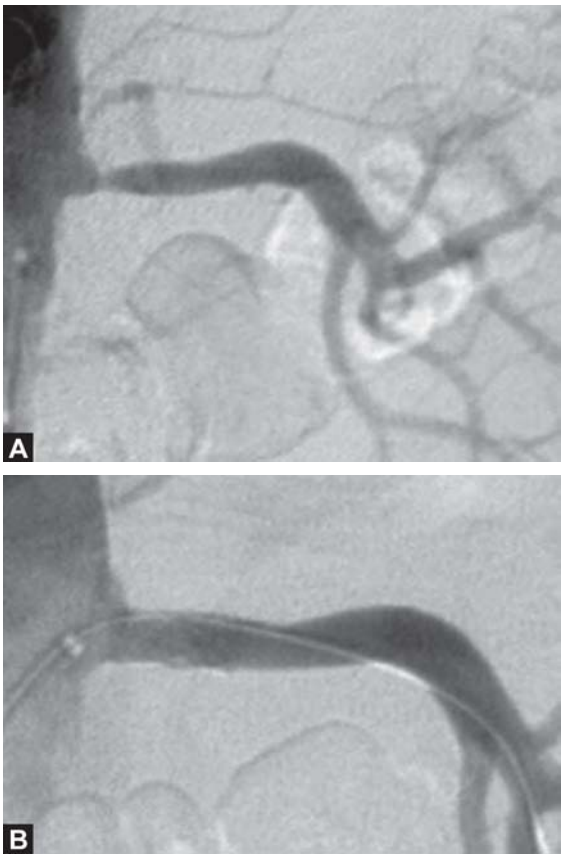

Figs 23.5A and B: A case of renal artery ostial narrowing treated by stenting: **(A)** Renal angiogram showing ostial narrowing of left renal artery. **(B)** Post stenting angiogram showing 0 percent residual stenosis

the aorta. Positioning the stent in this manner ensures that the entire lesion is stented. Some time it may be necessary to perform renal arterial intervention from a brachial approach, for example when femoral access is not possible or if the renal arteries are sharply angulated inferiorly (Figs 23.5A and B).

Outcome

Compared with the relatively good outcomes after angioplasty for fibromuscular dysplasia, balloon angioplasty alone has not been as successful in treating atherosclerotic renal artery stenosis. This is most likely because of the high degree of elastic recoil in atherosclerotic arteries compared with that encountered in fibromuscular webs.

The restenosis rate after angioplasty alone varies widely but has been reported to be from 10 to 46 percent.[5] Angioplasty (without stent placement) has a higher technical success rate when applied to atherosclerotic lesions in the mid portion of the main renal artery (72-82%) than in ostial lesions (success rate ≈60%).

Stents are now almost uniformly used for all ostial lesions and almost all atherosclerotic renal artery stenosis. One current report quotes a technical success rate for stents of 94 to 100 percent and a restenosis rate of 11 to 23 percent, with an improvement in blood pressure control in 50 to 80 percent and stabilization of renal function in 60 to 70 percent.[5,6]

Renal function at the time of stent placement strongly predicts patency and expected survival after intervention. In patients with normal renal function, 3-year survival is 94 percent, 74 percent if serum creatinine is between 1.5 and 2.0 mg/dL, and 52 percent if serum creatinine is greater than 2.0 mg/dL.[6]

Renal Artery Intervention in Renal Transplants

Although technically angioplasty and stenting are similar in many ways to procedures in native kidneys, the management of transplant renal artery stenosis involves some important differences. Cadaveric transplants are generally anastomosed to the recipient external iliac artery, because it is possible to obtain the full length of renal artery and renal vein stump. These procedures are seperately described in the chapter on imaging of renal transplant.

Complications

The complications can be divided into major (renal insufficiency, renal artery occlusion, renal artery damage including rupture etc.) and minor (temporary renal insufficiency, retroperitoneal hematoma, femoral artery complications etc).

RENAL ARTERIAL EMBOLIZATION

The various indications are embolization of renal neoplasms, renal pseudoaneurysms (secondary to either traumatic or iatrogenic injury), end-stage kidney, etc.

Technique

There are three different types of renal embolization: proximal (occlusion of main/segmental renal artery), distal (occlusion of lobular or arcuate arteries) and capillary (occlusion of arterioles and glomeruli). Depending upon the type of embolization the catheter is advanced into the renal artery branches. The super-selective embolization with a coaxial catheter can save part of renal parenchyma. The selection of embolizing material also depends upon the purpose of occlusion (temporary or permanent). The various materials used for embolization are particles (gelfoam, polyvinyl alcohol), liquid agents (alcohol, sclerosants), steel coils and detachable balloons.

TRANSCATHETER EMBOLIZATION OF RENAL NEOPLASMS

The current role of renal embolization in carcinoma of the kidney is uncertain.

The most important aim of preoperative embolization of the renal artery is to prevent migration of tumor cells from being flooded out.

The various indications are:

1. To relieve symptoms such as pain, hematuria, polycythemia, congestive heart failure.
2. To facilitate surgical resection by preoperative embolization to reduce the tumor vascularity
3. To inhibit tumor growth and to reduce tumour mass.
4. To stimulate an immune response by decreasing the tumor load
5. Prophylactic embolotherapy in angiomyolipomas to avoid risk of hemorrhage

The impact of the renal embolization as palliative method of treatment on the survival time is difficult to estimate but improvement in local symptoms such as hematuria and pain is evident.

Varieties of embolizing agents have been used such as gelatin sponge, stainless steel coil, N-butyl cyanoacrylate, absolute alcohol, autologus blood clot. But the embolization material of choice is ethanol. Ethanol is widely used for permanent embolization. The optimal dose is 0.5 ml/kg of body weight with upper limit of 1ml/kg and at the rate of 2 ml/sec. the advantage of alcohol over other permanent embolizing material are complete tissue necroses with permanent arterial occlusion, milder post infarction syndrome, less chances of infection and simple to use.

Technique for delivery of absolute alocohol to renal artery includes balloon occlusion technique and superselective technique.[7,8] Balloon occlusion technique serves several purposes like, it prevents reflux of alcohol into aorta, prolongs contact period of alcohol with endothelium.

In superselective technique, endhole catheter is advanced superselectively into lobar braches and the alcohol is injected to

prevent reflux. This is then followed by large vessel embolization with coils. Mechanism of action of alcohol proposed to be combination of perivasculat necrosis, sludging of erythrocytes in small arteries and glomeruli and endothelial damage.

Rate of injection has serious impact over the success of embolization. Injection rate of 1-5ml/sec, leads to perivascular necrosis, sludging of erythrocytes in small arteries and glomeruli indicating direct tissue toxicity. Where as at slow rate of injection 0.1 ml//sec, causes endothelial damage and less tissue toxicity. Hence, slow rate of injection is desirable in benign conditions like AVM, angiomyolipomas, where permanent arterial occlusion with minimal tissue damage is desirable.[7]

Angiographic findings of successful embolization include ,all arteries smaller than major segmental arties must be occluded, stagnation of flow and extravazation of contrast material into adjacent renal parenchyma (Figs 23.6A to F).

Care must be taken when embolizing with absolute ethanol due to the vigorous thrombosis it causes by denaturing proteins. Ethanol can cause seizures and intoxication if it reaches the systemic circulation. It can also permeate the tissues and cause injury to adjacent structures such as bowel and nerves.

Transcatheter Embolization of Renal Pseudoaneurysms

Incidence

Incidence of aneurysm formation differs for the various etiologies of renal artery aneurysms. However, literature suggests that incidence ranges between 0.015 percent and 9.7 percent.[9] Poutasse have classified renal artery aneurysms into saccular, fusiform, dissecting, and pseudoaneurysms.[10] The natural history of these aneurysms is not well defined in the literature. However, the incidence of rupture rate, ranges from 0 percent to 14 percent.[10] Renal artery aneurysms that are treated surgically are approached by nephrectomy, ex vivo repair and reimplntation.[9-11]

Causes

Typically, pseudoaneurysm formation in the renal artery distribution is either iatrogenic or traumatic. Other causes of aneurysm formation include fibromuscular dysplasia, polyarteritis nodosa, amphetamine abuse, angiomyolipoma (either with or without associated tuberous sclerosis) and neurofibromatosis.

Risks Posed by the Aneurysm

Rupture is a rare risk of these aneurysms. However, pregnant women are more prone to rupture which is similar to splenic artery aneurysms rupture.

Anatomic/Physiologic Considerations

The vascular supply to the kidney is considered endorgan,and hence infarction is common after embolization. Therefore, in patients with renal insufficiency or underlying diseases such as tuberous sclerosis or von Recklinghausen's disease, nephron-sparing procedures are vital. Superselective embolization is advisable in all cases of renal artery embolization unless partial or total nephrectomy is planned.

Technique

The renal arteries arise at the L2 level from the abdominal aorta. A LAO view during a flush injection of the aorta will often provide the best view of the origins. Careful exami-

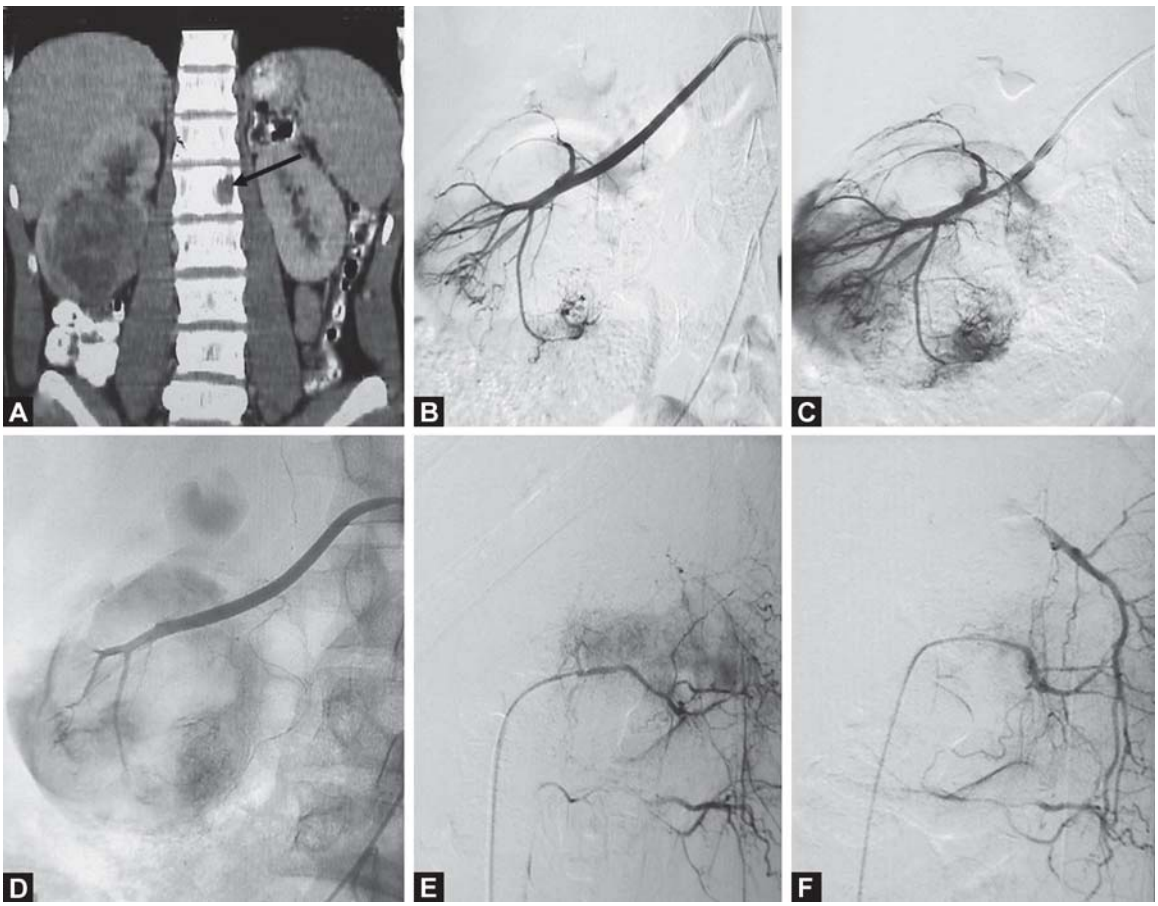

Figs 23.6A to F: A case of renal cell carcinoma with vertebral metastasis treated by absolute alcohol. **(A)** Coronal MPR image showing large mass lesion in lower pole of right kidney. Note: destructive lytic lesion in L1 vertebra (arrow), **(B)** selective angiogram showing tumor neovascularity in lower polar region **(C)** delayed angiogram showing tumor blush and no arteriovenous shunting. **(D)** postembolization angiogram showing stasis of contrast, persistent tumor staining and obliteration of tumor vascularity. **(E)** selective angiogram of paraspinal artery showing tumor blush supplying the L1 vertebral lesion. **(F)** following embolization with PVA particles (500-700 μ) showing obliteration of tumor vascularity

nation for accessory renal arteries is necessary. A renal double curve or Cobra catheter will easily select the main renal ostium. A Rosen wire is an atraumatic guidewire that allows for secure exchange or upsizing to a guiding catheter or Balkin sheath. Selective injection should be performed to identify the feeding vessel or vessels. This can be done through the sheath. Many embolization techniques can be used in this setting depending on the type, number, and location of the aneurysms. Commonly pseudoaneurysms are embolized superselectively by using coils (Figs 23.7A to D). Sometime, aneurysms of the main renal artery maybe amenable to stent graft placement, thus allowing distal perfusion to be maintained. However, until stent graft placement is perfected, surgical repair by resection, aneurysmorraphy, and autotransplantation is more commonly performed in this setting.

More peripherally located aneurysms can be selectively coil embolized using microcatheter technique (Figs 23.8A to D). Both

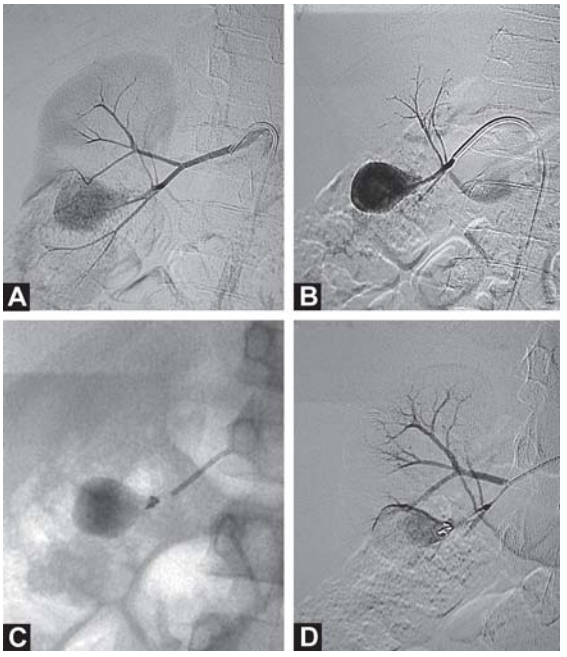

Figs 23.7A to D: Post PCNL renal artery pseudoaneurysm treated by coil embolization: **(A and B)** selective renal angiogram showing large pseudoaneurysm arising from lower polar artery, **(C)** spot image showing coil at the neck of pseudoaneurysm **(D)** post embolization angiogram showing non filling of pseudoaneurysm

distal and proximal control is not always possible, and may not be necessary due to the vascular anatomy. In the presence of multiple aneurysms from a lesion such as an angiomyolipoma, a combination of particle and coil embolization can be performed. If actively bleeding, the aneurysms are coiled first, followed by occlusion of the feeding vessels to the tumor with PVA or embospheres. Gelfoam can be sandwiched between coil nests to assist thrombosis.[12-15]

Results of Embolization

The technical success is quite high once the renal artery is securely accessed. If superselective techniques are used, very little ischemia results and there is very little chance of inducing renal failure.

Complications

Although rare, dissection or perforation of the renal arteries and their branches can occur. Rupture may lead to rapid development of retroperitoneal hemorrhage. Both dissection flaps and rupture can be immediately controlled with balloon tamponade. Although dissection flaps can often be tacked down, rupture typically requires emergent surgery. Even perforation of smaller branch vessels can occur if a guidewire is passed too far into the periphery.

The Embolization of End-stage Kidney

The non functional kidney may manifest by pain, hypertension, albuminuria and other symptoms. In such cases embolization procedure can replace surgical nephrectomy (Figs 23.9A to D).

Technique

Absolute alcohol is a very effective 'permanent' agent for occluding capillaries. The embolization material is injected cautiously through an endhole catheter under fluoroscopic control to avoid reflux into the aorta. The embolization is considered complete when there is stasis of contrast medium in the major renal arteries without any flow of contrast material into the distal branches. There is therefore residual opacification of the parenchyma of the embolized kidney. During the embolization patients commonly experience severe flank pain on the side of the kidney being infarcted and intravenous opiate analgesia is required for pain control. This limits the procedure to embolization of a single kidney at any one sitting. Patients must be then carefully monitored for 24 hours and kept in the hospital until their pain and any associated pyrexia has settled.[7,8]

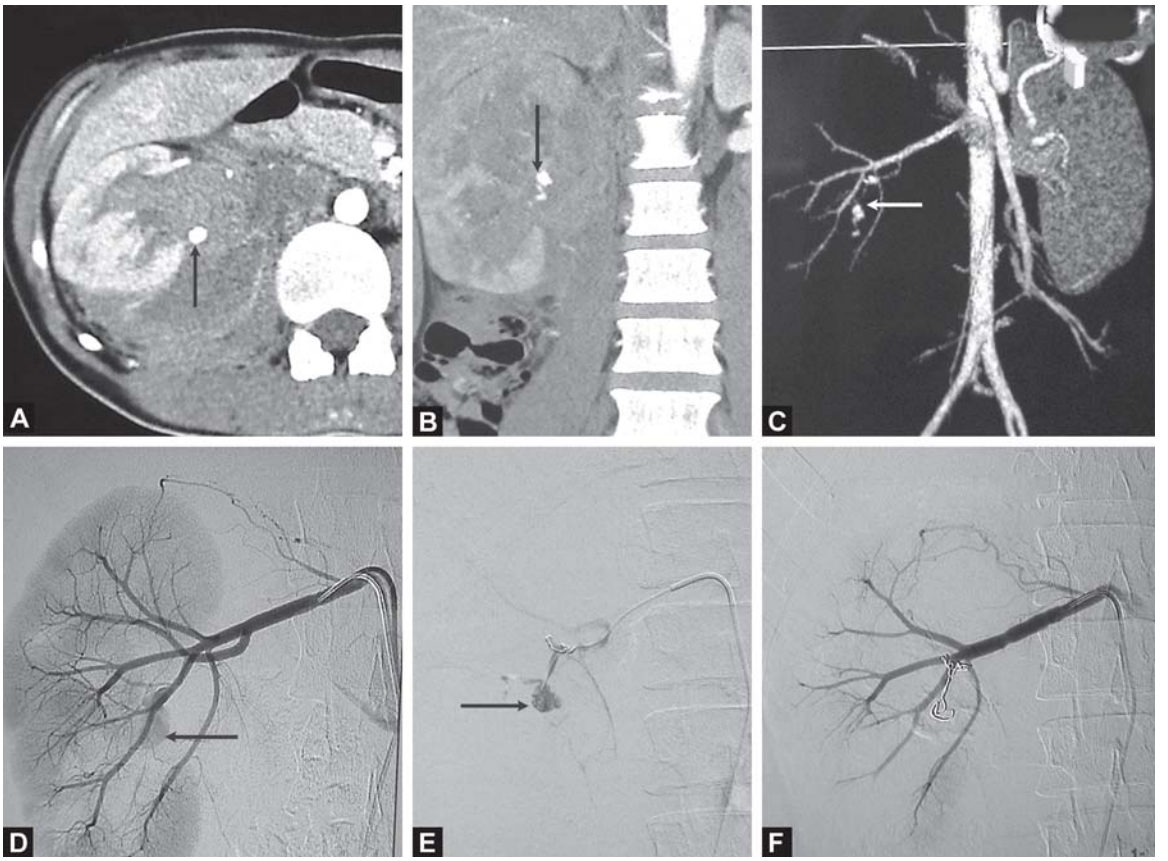

Figs 23.8A to F: Post PCNL renal artery pseudoaneurysm treated by microcoils using microcatheter coaxial technique: **(A, B, C)** contrast enhanced CT images showing small extrarenal pseudoaneurysm with surrounding large hematoma formation. **(D)** selective renal angiogram showing filling of pseudoaneurysm supplied by lower polar branch of right renal artery **(E)**. superselectively getting access into the branch supplying pseudoaneurysm using microcatheter **(F)** post embolization angiogram showing non filling of pseudoaneurysm

The complications are mainly postembolization syndrome in the form of flank pain for few days, fever, nausea, vomiting, etc. There may be hypertension in the first few hours. Majority of these symptoms are self-limited and are resolve without any specific treatment. Rarely there may be major complications like renal failure, renal abscess and testicular infarction. The results of embolization are quite encouraging in most of the clinical situations.

Arteriovenous Fistulas and Malformations

Acquired arteriovenous fistulas in the kidney are usually the result of trauma, especially percutaneous biopsy. Massive renal arteriovenous fistulas can cause high-output heart failure. Congenital AVMs of the kidney are exceedingly rare. These lesions consist of numerous dilated, tortuous vessels within the subepithelium of the collecting system. When symptomatic, they usually present with gross hematuria and less commonly are associated with hypertension or an abdominal bruit. Color Doppler sonography, CT, and MR imaging are useful in detecting some of these lesion.

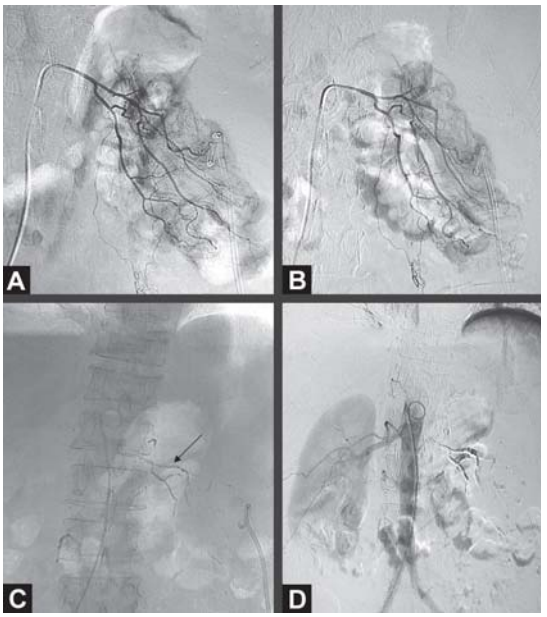

Figs 23.9A to D: Glue embolization of non functioning kidney. **(A, B)** selective renal angiogram showing tortuous intrarenal branches, **(C)** spot image showing glue cast in the intrarenal branches, **(D)** post embolization flush aortogram showing complete obliteration of left renal artery and no parenchymal blush seen

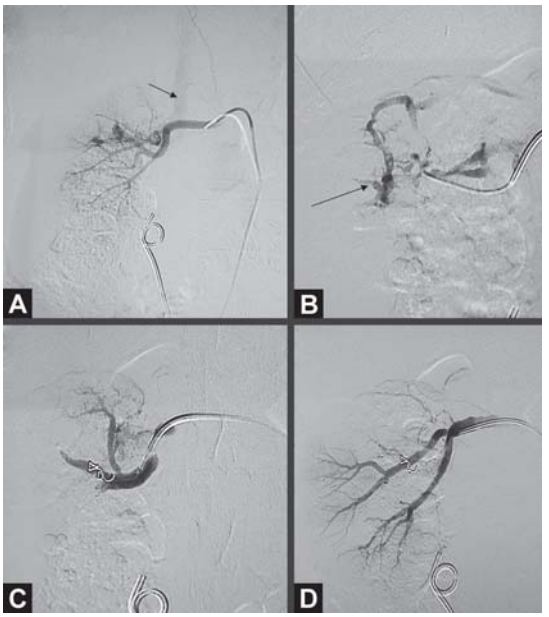

Figs 23.10A to D: Post PCNL AV fistula treated by coil embolization. **(A)** selective right renal angiogram showing small contrast filled structure supplied by upper polar artery with early draining vein, **(B)** superselective angiogram showing getting close to the site of AV fistula (arrow), **(C)** coil embolization of the AV fistula site, **(D)** post embolization angiogram showing obliteration of the AV fistula

At angiography, an arteriovenous fistula produces dilatation of the feeding branch and early filling of the draining vein. Numerous segmental or interlobar arteries feed the renal AVM, which is composed of dilated, tortuous channels with rapid shunting into renal vein and IVC.

Transcatheter embolization is the first-line of treatment for most of these lesions. Coils are effective for treatment of fistulas (Figs 23.10A to D). In AVMs, the nidus should be obliterated using a liquid agent such as cyanoacrylate (glue).[16-19]

UTERINE ARTERY EMBOLIZATION (UAE)

Indications

Uterine artery embolization has become an extremely valuable therapy for patients with gynecological and obstetric diseases. The various indications where it can be used are uterine leiomyoma, arteriovenous malformations (AVMs) and postpartum and postoperative hemorrhage. UAE can also control bleeding following radiotherapy treatment in cases of carcinoma cervix.

Uterine Leiomyoma

UAE is the minimally invasive therapy in the management of uterine fibroids. The common indications for treatment are menorrhagia leading to anemia, abdominal pain, uterine enlargement with mass effect, infertility and late miscarriages. The advantages of UAE compared to operative therapies are that the patient retains the uterus, all the myomas are treated together in the same sitting and

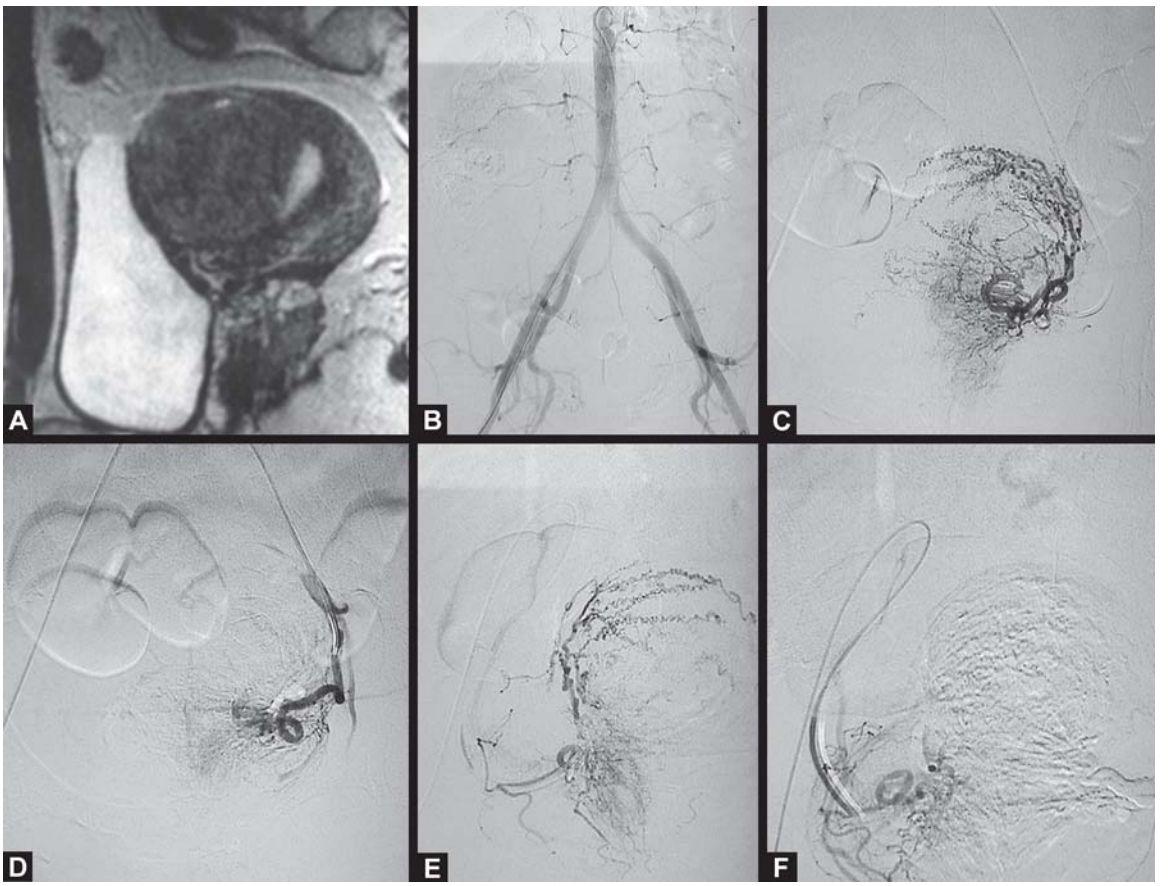

Figs 23.11A to F: Uterine artery embolization of uterine fibroid. **(A)** Sagittal T2W MR image showing fibroid in fundal region **(B)** Flush aortogram to look for any ovarian artery supply, **(C)** selective left uterine artery angiogram showing increased vascularity supplying the fibroid, **(D)** post embolization angiogram showing reduction in vascularity following embolization with PVA particles (500-700 μ), **(E, F)** right uterine angiogram followed by embolization using PVA particles and uterine Robert's catheter

therapy is less invasive (Figs 23.11A to 23.12D). The disadvantages are vaginal expulsion of necrotic fibroid if the fibroid is submucosal, postembolization syndrome and a procedure which is not a fully curative treatment since the mean reduction of fibroid is about 40 per cent or so.

Uterine Arteriovenous Malformations (AVMs)

The AVMs may either be congenital due to faulty development of arteries, veins, capillaries, lymphatics or are acquired as a result of inter-villous space enlargement at the site of myometrial scar. The predisposing factors for acquired AVMs are previous uterine surgery, dilatation and curettage, intrauterine contraceptive devices, previous pregnancy, genital tuberculosis and trophoblastic disease.

Congenital AVMs are usually seen in women of child bearing age who often present with spontaneous abortion because of bleeding. The clinical presentation in

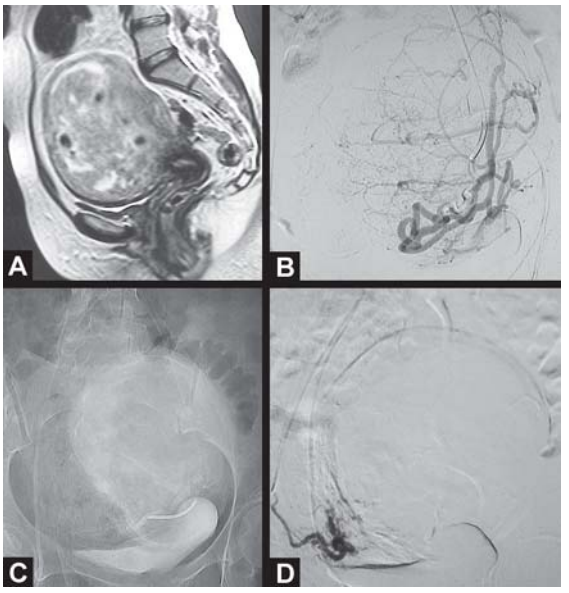

Figs 23.12A to D: Uterine artery embolization of large uterine fibroid. **(A)** Sagittal T2W MR image showing large fibroid in fundal region **(B)** selective left uterine artery angiogram showing increased vascularity supplying the fibroid and splaying of branches by the large fibroid **(C)** post embolization angiogram showing reduction in vascularity and stasis following embolization with PVA particles (500-700 μ) **(D)** right uterine angiogram after the embolization showing reduction in vascularity

acquired AVMs is profuse, intermittent repetitive bleeding. UAE has shown good results in the treatment of these lesions with the added advantage that patient also maintains fertility (Figs 23.13A to F).

Postsurgical and Postpartum Hemorrhage (Figs 23.14A to D)

Role of interventional radiology in the management of PPH has gained wide acceptance in the obstetric-gynecologic community as an alternative to uterine artery ligation or hemostatic hysterectomy.

The postsurgical hemorrhage due to vascular leak can be treated with gelfoam embolization of uterine or anterior division of internal iliac artery. The various causes of post-partum hemorrhage are abnormal placentation, retained products of conception, birth canal laceration, uterine atony or rupture of uterus. All such catastrophic bleeding conditions can be treated by angiographic embolization of uterine artery by using various embolizing materials.

Patient Selection: The choice between endovascular and operative treatment should be made jointly by the patient, gynecologist, and intervention radiologist after the current status of all available treatment modalities has been considered and presented in a forthright fashion. Only symptomatic patients in whom other causes for disease have been excluded (including a recent Papanicolaou test) should undergo this treatment. The intervention radiologist is obligated to become the primary physician caring for the patient in Preprocedure consultation, hospital recovery, and all outpatient management. Adenomyosis also may respond to UAE.[20,21]

Absolute or relative contraindications include pregnancy, active or chronic pelvic infection, gynecologic malignancy (unless palliative or as an adjunct to operation), uncorrectable coagulopathy, severe contrast allergy, and prior pelvic surgery or radiation therapy. The effect of UAE on fertility has not been established, although pregnancy can occur after the procedure. Pedunculated fibroids with relatively narrow stalks are prone to detachment after UAE and may require operative removal.

Technique

UAE for fibroids was first reported by Ravina and coworkers.[22] A pelvic arteriogram with the catheter positioned in the infrarenal abdominal aorta is obtained as a road map. Selective catheterization of the anterior divisions of the internal iliac arteries is

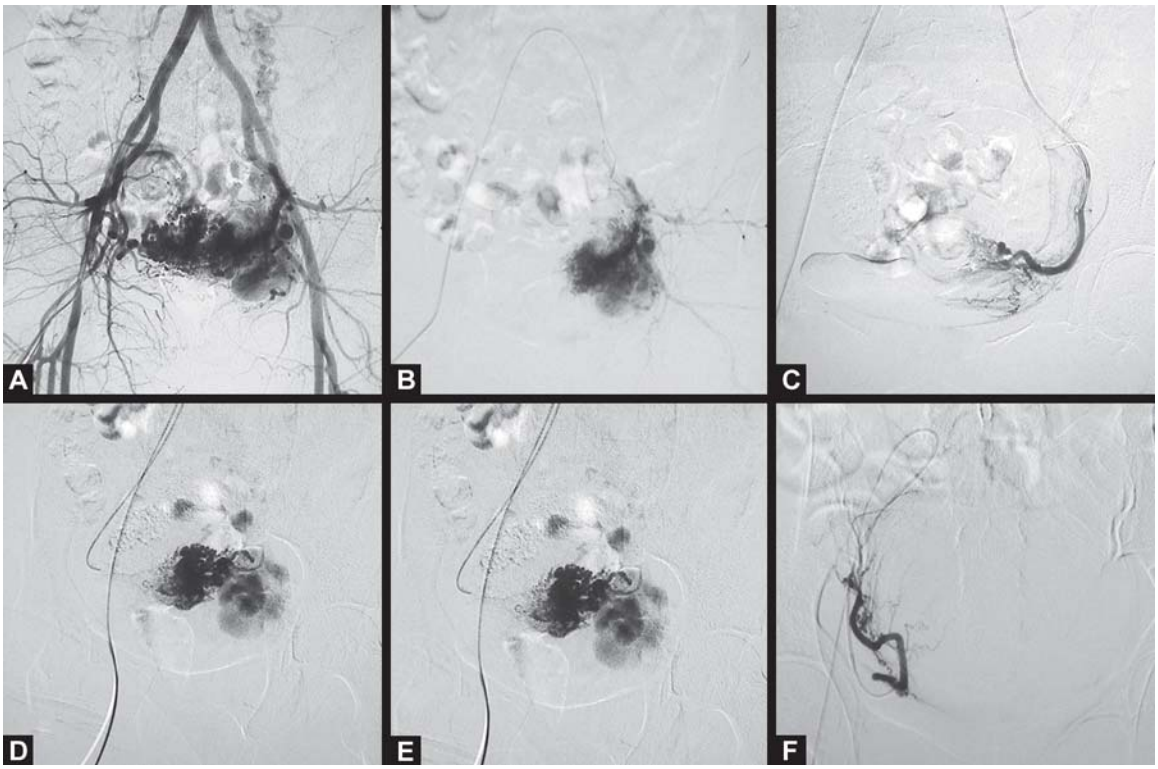

Figs 23.13A to F: Uterine arterio-venous malformation treated by angioembolization **(A)** flush aortogram showing large vascular blush in the pelvis **(B)** selective angiogram of left uterine artery showing large vascular blush with nidus **(C)** post embolization angiogram following embolization with PVA particles 700-1000 μ) showing complete obliteration of the vascular blush on left side. **(D, E)** selective angiogram of right uterine artery showing residual vascular blush with nidus which was obliterated with PVA particle embolization **(F)**

performed with a cobra or ultra-long reverse-curve (e.g. Roberts) catheter. Once the uterine artery is identified and selected, angiography shows the markedly dilated spiral arteries feeding the uterus. Tumor hypervascularity and vessel displacement is seen. In some cases, the descending portion of the uterine artery can be engaged with the 5-French diagnostic catheter. However, vasospasm may be a problem, so that coaxial placement of a microcatheter directed well into the uterine artery often is required. The preferred agents for embolization are small-caliber particulate matter,-including polyvinyl alcohol (PVA) particles (350 to 500 or 500 to 700 pm), tris-acryl gelatin microspheres (Embospheres, 700 to 900 pm), and Gelfoam pieces. There does not appear to be any significant difference in clinical efficacy between the two agents. Proximal embolization (e.g., with coils) is inadvisable, because collateral vessels are very likely to develop and which will continue to feed the tumor. Embolization with particulate slurry (made with diluted contrast material) is continued until there is no flow in uterine artery branches ("pruned-tree" appearance). Regardless of the location of fibroids, bilateral embolization is necessary to prevent development of collateral vessels.[23-26]

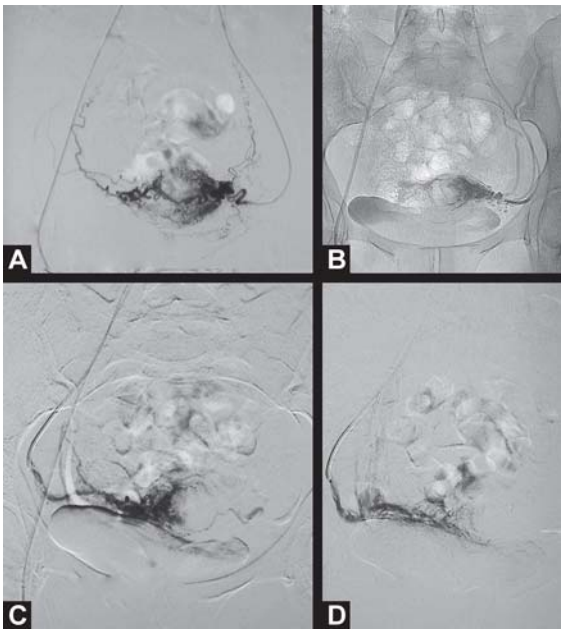

Figs 23.14A to D: Post MTP continuous uterine bleeding treated by angioembolization. **(A)** selective angiogram of left uterine artery showing vascular blush **(B)** post embolization angiogram following embolization with PVA particles 700-1000 μ) showing complete obliteration of the vascular blush and stasis of contrast, **(C)** selective angiogram of right uterine artery showing vascular blush which was obliterated with PVA particle embolization **(D)**

Bilateral completion internal iliac arteriograms are obtained to identify any additional vessels feeding the tumors. The interventionalist should be observant of variant arterial anatomy and important collateral vessels. In most cases, the ovarian arteries contribute to fibroids through anastomoses with the main uterine artery. In about 10 percent of patients, the uterine artery is the major blood supply to the ovary, or the ovarian artery has significant direct communication with the fibroid. Embolization of these vessels theoretically increases the risk of ovarian infarction and infertility. Any other collateral vessels that feed the tumor must also be occluded. This is particularly true in women who have undergone prior pelvic surgery, had other tuba1 pathology, or have fundal fibroids. Postprocedure care should be directed by the interventionalist who performed the UAE. A postembolization syndrome consisting of pain, nausea and vomiting, and low-grade fever is to be expected. Most patients require overnight hospitalization. Pain must be aggressively managed with IV, and later with oral narcotic. Antiemetics are given prophylactically or as needed. Discharge medications include antiinflammatory drugs (e.g. ketorolac) and potent oral narcotics. Follow-up is done by the interventionalist, including routine clinic evaluation at 1 to 3 weeks after the procedure.[27]

Results

Bilateral UAE is successful in about 95 percent of cases. Incomplete infarction of fibroids may be associated with the potential for continued growth. Clinical success with substantial improvement in symptoms is seen in about 80 to 90 percent of women. Submucosal lesions and small lesions seem to respond better than other tumors. Failure or recurrence is noted in about 6 percent of cases. If symptoms continue and leiomyomas persist or enlarge on imaging studies, repeat UAE (with aggressive search for collateral vessels including the ovarian arteries) is often warranted.

Complications

Intra and postprocedure pain is a common problem after UAE. Important complications after UAE are intrauterine infection, uterine ischemia and necrosis, pulmonary embolism, and expulsion of pedunculated submucosal lesions. The overall complication rate is about 5 percent while major complications occur in about 1 percent. Most patients do not have a

significant change in follicle stimulating hormone level after the procedure though this is more likely to occur in women older than 45 years of age. Amenorrhea (which is often transient) occurs in less than 10 percent of cases, but it is much more likely in patients older than 45 to 50 years of age. Serious infections as complications are observed in 1 percent of treated women. Less than 2 percent require subsequent hysterectomy for any complications of UAE.[28-30]

The reasons for uterine artery embolization failure are incomplete embolization, presence of important collaterals (e.g. ovarian arteries), large fibroids and recanalization of embolized arteries.

VAGINAL AVM EMBOLIZATION

Vaginal arteriovenous malformations are rare entities and their most common presentation is vaginal hemorrhage and rarely dyspareunia. These lesions can be successfully treated by angioembolization of the supplying vessels using polyvinyl alcohol particles. Angioembolization being safe and effective should be the first treatment of choice for symptomatic vaginal vascular malformation (Figs 23.15A to C).

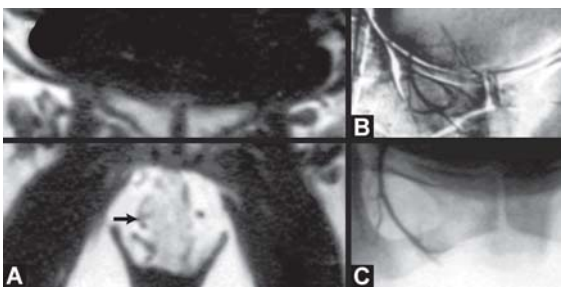

Figs 23.15A to C: Vaginal AVM treated by angioembolization. **(A)** MR image showing abnormal vascular channels(flow voids) on right side of vagina (small arrow) **(B)** selective angiogram of right internal pudendal artery showing vascular blush, which was obliterated using PVA particles **(C)**

SCROTAL AVM AND TESTICULAR TUMOR EMBOLIZATION

Scrotal arteriovenous malformations are rare entity. The scrotal arteriovenous malformations and the paratesticular masses may occasionally present with uncontrollable bleeding. These lesions can be successfully treated by angioembolization of the supplying vessels using either Glue or PVA particles depending upon the situations (Figs 23.16A to 23.17D). Angioembo-lization being safe and effective should be considered as choice of treatment for the treatment of symptomatic scrotal vascular malformation.

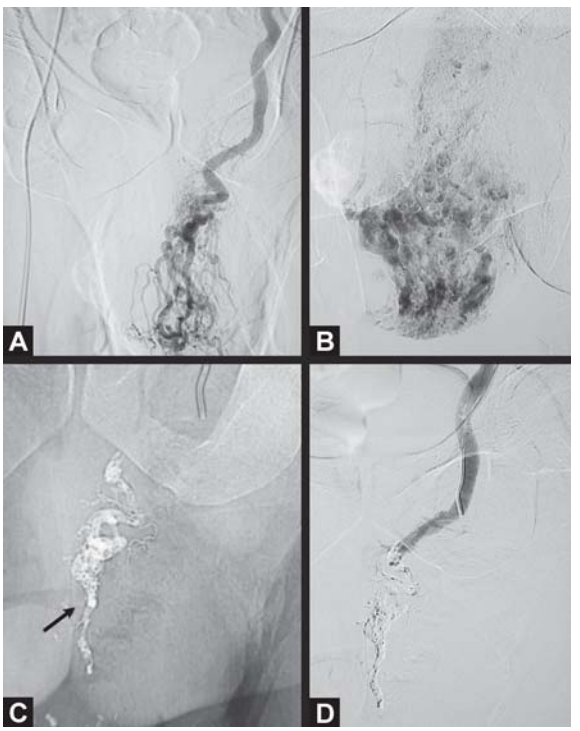

Figs 23.16A to D: Scrotal AVM treated by glue embolization. **(A,B)** selective left internal pudendal artery angiogram showing hypertrophied artery and large nidus, **(C)** Spot image showing glue cast obliterating the nidus **(D)** Post embolization angiogram showing complete obliteration of the vascular nidus

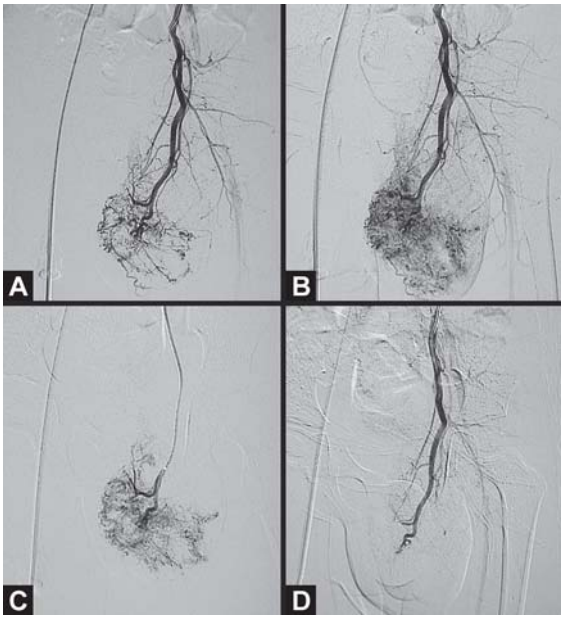

Figs 23.17A to D: Left paratesticular mass in 5-year-old child with scrotal bleeding treated by angioembolization. **(A,B)** Selective left internal pudendal artery angiogram showing hypertrophied artery and large tumor blush, **(C)** catheter brought close to the tumor blush, **(D)** post embolization angiogram following embolization using PVA particles 300-500 μ, showing complete obliteration of tumor blush

VARICOCELE EMBOLIZATION

Varicocele is an important cause of male infertility. Varicocele embolization is indicated in an individual who have been infertile for at least two years and having oligoasthenospermia without an apparent cause of infertility. The embolization is done after placing catheter deep into the internal spermatic vein. Various embolizing materials like steel coils, PVA particles, gelfoam are used.[31-33]

In conclusion, renal artery aneurysms can be life-threatening if hemorrhage occurs. Following aneurysm rupture, surgical morbidity and mortality are fairly high. Aggressive management by the interventional radiologist therefore is paramount since these patients are in any case too sick for major revascularization procedures, making endovascular techniques a more desirable approach. Embolization of dysfunctioning organs using various embolization techniques and regimens in the management of hypertension or protein wasting in end-stage renal disease has replaced surgical nephrectomy. The evolution of uterine fibroid embolization has established the role of embolotherapy as a viable alternative to hysterectomy, and undoubtedly revolutionized the management of postpartum bleeding. A variety of methods for embolization are described in the literature. The type of treatment should be tailored to each individual case as the anatomy will typically dictate the therapy best suited.

REFERENCES

1. Cicuto KP, McLean GK, Oleaga JA, et al. Renal artery stenosis. Anatomical classification for percutaneous transluminalangioplasty. AJR Am J Roentgenol 1981;137:599-01
2. Rountas C, Vlychou M, Vassiou K, Liakopoulos V, Kapsalaki E, Koukoulis G, Fezoulidis IV, Stefanidis I. Imaging modalities for renal artery stenosis in suspected renovascular hypertension: prospective intraindividual comparison of color Doppler US, CT angiography, GD-enhanced MR angiography, and digital substraction angiography. Ren Fail. 2007;29(3):295-302.
3. Tan KT, van Beek EJ, Brown PW, et al. Magnetic resonance angiography for the diagnosis of renal artery stenosis. A metaanalysis.Clin Radiol. 2002;57:617-24.
4. Hoffman O, Carreres T, Sapoval MR, et al. Ostial renal artery stenosis angioplasty. Immediate and mid-term angiographic and clinical results. J Vasc Interv Radiol 1998;9:65–73.
5. Matsumoto AH, Tegtmeyer CJ, Fitzgerald EK et al. Percutaneous transluminal angioplasty of visceral arterial stenoses: results and long-term clinical follow-up. J Vasc Interv Radiol 1995; 6:165–74.
6. Moss JG and Hamilton G. Renal and visceral artery intervention. In: Dyet JF, Nicholson AA,

Ettles DF, Wilson SE (Eds): Textbook of endovascular procedures. Churchill Livingston, Philadelphia, pp 2000;151-73.
7. Park JH, Kim WS, Han MC, Lee CW. Renal arterial embolization with absolute ethanol. J Korean Med Sci 1987;2(1):13-8.
8. Park JH, Kim SH, Han JK, Chung JW, Han MC. Transcatheter arterial embolization of unresectable renal cell carcinoma with a mixture of ethanol and iodized oil. Cardiovasc Intervent Radiol 1994 ;17(6):323-7.
9. Martin RS 3rd, et al. Renal artery aneurysm: Selective treatment for hypertension and prevention of rupture. J Vasc Surg 1989;9: 26-34.
10. Poutasse EF. Renal artery aneurysms. Their natural history and surgery. J Urol 1966;95:297–306.
11. Poutasse EF. Renal artery aneurysms. J Urol 1975;113:443-49.
12. Liguori G, et al. Percutaneous management of renal artery aneurysm with a stent-graft. J Urol 2002;167:2518-19.
13. Pershad A, Heuser R. Renal artery aneurysm: successful exclusion with a stent graft. Catheter Cardiovasc Interv 2004;61:314-16.
14. Rundback JH, et al. Percutaneous stent-graft management of renal artery aneurysms. J Vasc Interv Radiol 2000;1189-93.
15. Schneidereit NP, et al. Endovascular repair of a ruptured renal artery aneurysm. J Endovasc Ther 2003;10:71–74.
16. Crotty KL, Orihuela E, Warren MM. Recent advances in the diagnosis and treatment of renal arteriovenous malformations and fistulas. J Urol 1993;150:1355.
17. Takebayashi S, Aida N, Matsui K. Arteriovenous malformations of the kidneys: diagnosis and follow-up with color Doppler sonography in six patients. AJR Am J Roentgenol 1991;157:991.
18. Allione A, Pomero F, Valpreda S, et al. Worsening of hypertension in a pregnant women with renal arteriovenous malformation. A successful superselective embolization after delivery. Clin Nephrol 2003; 60:211
19. Takebayashi S, Hosaka M, Ishizuka E, et al. Arteriovenous malformations of the kidneys: ablation with alcohol. AJR Am J Roentgenol 1988;150:587.
20. Andrews RT, Spies JB, Sacks D, et al. Patient care and uterine artery embolization for leiomyomata. J Vasc Interv Radiol 2004;15:115.
21. Siskin GP, Tublin ME, Stainken BF, et al. Uterine artery embolization for the treatment of adenomyosis: clinical response and evaluation with MR imaging. AJR Am J Roentgenol 2001;177:297.
22. Ravina JH, Herbreteau D, Ciraru-Vigneron N, et al. Arterial embolisation to treat uterine myomata. Lancet 1995;346:671.
23. Worthington-Kirsch RL, Andrews RT, et al. Uterine fibroid embolization: technical aspects. Tech Vasc Intent Radio l 2002;5:17.
24. Banovac F, Ascher SM, Jones DA, et al. Magnetic resonance imaging outcome after uterine artery embolization for leiomyomata with use of tris-acryl gelatin microspheres. J Vasc Interv Radiol 2002;13:681.
25. Pelage JP, Le Dref O, Beregi JP, et al. Limited uterine artery embolization with tris-acryl gelatin microspheres for uterine fibroids. J Vasc Interv Radiol 2003;14:15.
26. Pelage JP, Le Dref O, Soyer P, et al. Arterial anatomy of the female genital tract: variations and relevance to transcatheter embolization of the uterus. AJR Am J Roentgenol 1999;172:989.
27. Siskin GP, Bonn J, Worthington-Kirsch RL, et al. Uterine fibroid embolization: pain management. Tech Vasc Interv Radiol2002;5:35.
28. Pelage JP, Walker WJ, Dref OL. Uterine necrosis after uterine artery embolization for leiomyoma. Obstet Gynecol 2002;99:6767.
29. Spies JB, Spector A, Roth AR, et al. Complications after uterine artery embolization for leiomyomas. Obstet Gynecol2002;100:873.
30. Spies JB, Roth AR, Gonsalves SM, et al. Ovarian function after uterine artery embolization for leiomyomata. assessment with use of serum follicle stimulating hormone assay. J Vasc Interv Radiol 2001;12:437
31. Lima SS, Castro MP, Costa OF. A new method for the treatment of varicocele. Andrologia 1978;10:103-06.
32. Trombetta C, Salisci E, Deriu M, Paoni A, Sanna M, Ganau A, Belgrano E. Echo-flowmetric control 6 years after percutaneous treatment of varicocele. Arch Ital Urol Androl 1993;65: 363-67.
33. Usuki N, Nakamura K, Takashima S, Takada K, Kaminoh T, Tsubakimoto M, Matsuoka T, Nakatsuka H, Oda J, Minakuchi K, et al. Embolization of varicocele with ethanol. Nippon Igaku Hoshasen Gakkai Zasshi 1994;54:870-875 (Japanese).

Chapter

24

Imaging in Female Infertility

Rashmi Dixit

Infertility is generally defined as one year of unprotected intercourse without conception and is one of the most prevalent chronic health disorders involving young adults[1] Overall, infertility is estimated to occur in up to 20 percent of couples. The ability to diagnose and treat various causes of infertility is rapidly progressing and the radiologist is becoming increasingly involved in both the diagnosis and treatment of these patients.[1] Earlier evaluation and treatment is indicated in women with 1) age over 35 yrs 2) history of oligo/amenorrhea 3) known or suspected uterine/tubal disease or endometriosis 4) a partner known to be subfertile.[2] Infertility is referred to as primary when the patient has never conceived and secondary when there is a history of previous pregnancy.

CAUSES OF INFERTILITY

Although statistics vary, a male factor is attributable in 40 percent cases, female factor 40 percent of the times and in about 20 percent cases there may be combined or unexplained causes. [3]

Evaluation of the infertile couple begins with a complete history and examination.[4] A careful history and physical examination can identify symptoms or signs suggesting a specific cause for infertility and thereby help to focus subsequent diagnostic evaluation on the factor (s) most likely responsible. [2]

The six most common factors causing infertility should be carefully assessed. These are the cervical, the endometrial- uterine, the tubal, the ovarian, the peritoneal, and the male factors.[4-7]

Imaging Modalities

Imaging medalities used in evaluating female infertility include:

1. Hysterosalpingography or HSG
2. Sonography including transvaginal sonography (TVS) and sono hystero-salpingography.
3. Magnetic resonance imaging (MRI)

Hysterosalpingography (HSG) [8,9]

HSG is performed during the first 7-12 days of menstural cycle and is best scheduled during the 2-5 day interval immediately following the end of menses to minimize the risk for infection, avoid interference from intrauterine blood clot, and prevent any possibility that an HSG might be performed in a not yet recognized conception cycle. HSG does not require any specific preparation,

although pretreatment with an NSAID (approximately 30 minutes before) is helpful to limit discomfort associated with the procedure. Although usually unnecessary, prophylactic antibiotic treatment may also be considered to minimize post procedure infection. HSG is best avoided altogether for at least several weeks following any episode of acute PID to minimize risk of infectious complications.

The basic technique for performing an HSG is quite standard. The study should be performed using image intensification fluoroscopy with a limited number of radiographs. The average HSG requires only 20-30 seconds of fluoroscopic time with minimal radiation exposure and has very low risk. Usually, only 3-4 basic films are required —a scout, one film during early filling, third film to document the uterine contours with the uterus fully distended and assess tubal patency, and a fourth film to detect free intra peritoneal spill not seen earlier or any areas of contrast loculation (Figs 24.1A, 24.2A and B).

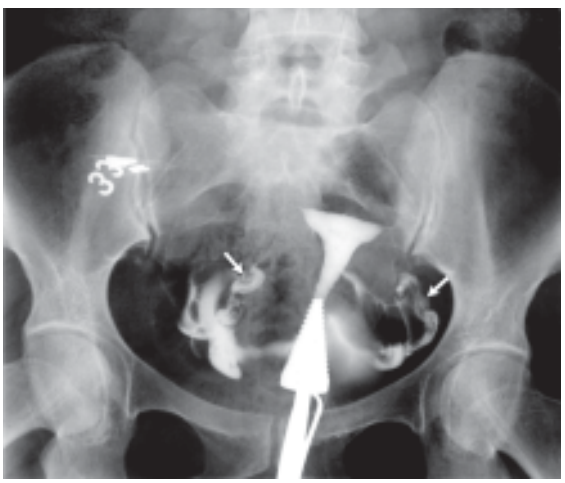

Fig. 24.1: Normal HSG : showing an inverted triangle shaped smooth uterine outline. Both fallopian tubes are well outlined by contrast. Note the presence of longitudinal rugal folds in the ampullary portion (arrows). Free intraperitoneal spill is seen on both sides outlining the bowel loops

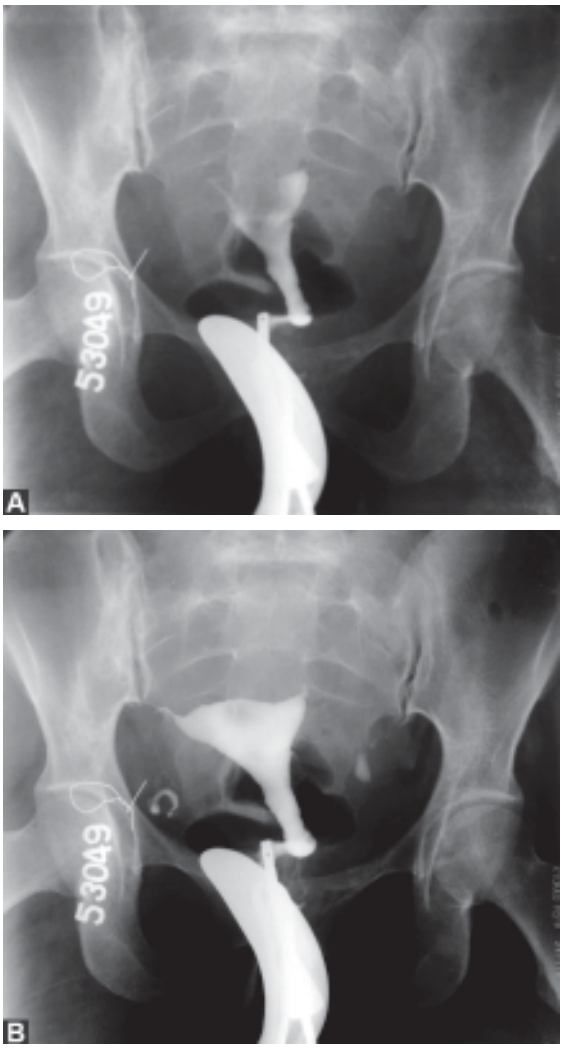

Figs 24.2A and B: Uterine filling defect due to a fundal fibroid is much better appreciated on the early filling film (A) as compared with (B) where the uterine cavity is fully distended with contrast and the filling defect is much less apparent

Additional films may be needed when the uterus obscures the tubes or the uterine cavity appears abnormal. Contrast can be introduced using a common metal "acorn" cannula or via a balloon catheter. In general, the latter technique requires less fluoroscopic time and smaller volumes of contrast,

produces less pain, and is easier to perform. Slow injection of contrast (typically 3-10 mL) helps to minimize the discomfort associated with HSG.

Watersoluble contrast media are generally used. Oil based contrast media have also been used in the past but these are generally too viscous to reveal internal tubal architecture (having prognostic significance) disperse poorly in pelvis, so adnexal adhesions cannot be detected and are associated with significant risk of granulomatous reaction, venous intravesation and embolism. Those advocating oil soluble contrast media say that these adverse reactions are rare and numerous studies have shown that oil based contrast media increase fertility in the months immediately following HSG in women with patent tubes, however, this has been challenged by a subsequent randomized clinical trial[10-13] and these agents are generally not used.

Complications following an HSG are relatively rare but may include – light spotting after the procedure (usually lasting less than 24 hours), infection and pain. Rarely systemic reactions to contrast media and uterine or fallopian tube perforation have been reported.[8]

Transvaginal Sonography

While evaluating patients for infertility by TVS, especially for follicular monitoring or oocyte retrieval normal condoms with spermicidal gels should be avoided. [15] Even ultrasound gels may have a detrimental effect on sperm and embryo and should not be used during oocyte retrieval or embryo transfers.[16]

Sonohysterosalpingography

Sonohysterosalpingography refers to a technique that evaluates the uterus and fallopian tubes after the uterine cavity has been distended with sonographic contrast media. Saline is the most commonly used agent, other contrast media include air and positive contrast agents such as echovist. It is a sensitive technique to detect uterine synechiae, endometrial polyps and can also be used to evaluate for tubal patency. [14,15]

The Normal Menstrual Cycle[1]

A basic understanding of the normal menstrual cycle is important before trying to image female infertility.

The normal menstrual cycle can be divided into three major stages: the follicular phase, ovulation, and luteal phase. The cycle is under the control of the hypothalamic- pituitary-ovarian axis. Day 1 of the average 28-day cycle is the start of menstruation. The plasma follicle stimulating hormone (FSH) level begins to increase, stimulating growth of the ovarian follicles and beginning the follicular phase. Usually one follicle becomes the dominant or graafian follicle. The developing follicles secrete estradiol, which stimulates endometrial proliferation; therefore, the follicular phase is also called the proliferative phase. Estradiol peaks about 12 hours before the luteinizing hormone (LH) ovulatory surge. This peak in estradiol causes in an increase in LH/FSH levels, stimulating ovulation on or about day 14. After ovulation, the luteal or secretory phase begins, during which the ruptured graafian follicle becomes the corpus luteum. The corpus luteum produces progesterone, which primes the endometrium for the fertilized egg. If conception does not occur, the corpus luteum degenerates, causing a decrease in estradiol/progesterone levels and sloughing of the endometrial lining, i.e. menstruation.

Cervical Factor

The cervical factor refers to the properties of cervical mucus and sperm transport. The hospitality of the cervix to the sperm is not evaluated by imaging the cervical anatomy but is best determined by the post coital test. Although some controversy exists regarding how and when to perform the post coital test most authors recommend that it should be as close to ovulation as possible and at least 8 hours after intercourse. [1,4] Imaging plays a limited role in this evaluation except for monitoring follicle development which helps to optimize the timing of the test and avoid false positive results.[1] In recent years its utility and predictive value have been seriously questioned[2,17] but some still consider it a useful diagnostic test.[2,18]

Cervical stenosis may occasionally be the cause of infertility. The normal size and appearance of the cervix are variable and therefore diagnosis based on appearance alone is difficult. An internal os region of less than 1 mm in diameter by hysterosalpingography in a woman with painful periods may indicate cervical stenosis.[3]

Endometrial–Uterine Factor

Fewer than 10 percent of cases of infertility are caused by uterine and endometrial abnormalities.[1,4,5] Although a relatively uncommon cause of infertility they should always be considered because they can adversely affect the outcome of pregnancies achieved by successful treatment of other more common factors. The abnormalities can be classified into two categories: anatomic e.g. adhesions, leiomyomas, congenital uterine malformations and physiological i.e. lack of normal endometrial response to hormonal stimulation.

There are four basic methods for evaluating the uterine cavity : HSG, Standard TVS or TVS with saline contrast (sonohysterography) MRI and hysteroscopy. The choice of the investigation needs to be tailored to the individual patient. HSG is the traditional method and still the best initial method because it also evaluates tubal patency. However, in women with no risk for tubal disease and whose tubal status is already known (say from previous laparoscopic surgery for some other cause) TVS offers a better tolerated and simpler alternative than can also reveal suspected ovarian pathology (cyst /endometrioma) with no radiation exposure. When uterine cavity detail is critical or when congenital anomalies are suspected sonohysterography or MRI may be used. Hysteroscopy is the most definitive method but may be safely reserved for treatment of abnormalities identified by other less invasive methods. [9]

Endometrial Adhesions or Synechiae

Endometrial adhesions or synechiae cause infertility either by obstructing the cervical os or fallopian tube or by providing a sub optimal environment for embryo implantation. Synechiae are usually the sequelae of infection including tuberculosis or prior dilatation and curettage. Asherman's syndrome is the association of synechiae with hypomenorrhea or amenorrhea and infertility.

Hysterosalpingography is the imaging study of choice in the evaluation of synechiae. Synechiae appear as multiple irregular filling defects in the uterine cavity.[1] They are generally linear and irregular and extend from one uterine wall to the opposite which allows the contrast agent to flow around them only in one dimension. For this reason, they

are more easily defined than polyps, myomas or other masses that generally allow contrast agent to flow around them in two dimensions.[3] Adhesions at the margins of the cavity may distort the uterine outline or obscure cornua.[9] (Fig 24.3) Adhesions are difficult to visualize on TVS, but when seen can appear as echogenic bridges in the endometrial cavity or as irregularities of the endometrium surrounded by cystic spaces.[1,5] Synechiae are easier to identify on sonohysterography where they appear as linear echogenic bridges in the fluid filled endometrial cavity.

Leiomyoma

Leiomyoma (fibroid) is the most common neoplasm of the uterus found in up to 25 percent of women. Leiomyomas are rarely a primary cause of infertility and treatment should be considered only after other potential causes have been excluded.[1,4,5] Available evidence suggests that pregnancy and implantation rates are significantly lower in women with submucous myomas but not in those with subserosal or intramural myomas that do not encroach or clearly distort the endometrial cavity, especially when modest in size (5-7 cm). Proposed mechanisms by which myomas might adversely affect fertility include cornual occlusion by myomas that involve or compress the interstitial segment of the tube, dysfunctional uterine contractility interfering with ovum or sperm transport or embryo implantation and poor regional blood flow resulting in focal endometrial attenuation or ulceration.[9]

On hysterosalpingography, leiomyomas generally appear as filling defects in the endometrial cavity with enlargement of cavity when sufficiently large. (Fig. 24.4) Care must be taken to differentiate between leiomyomas and other filling defects, including polyps, blood clots, mucus, and air bubbles. On ultrasound, fibroids have a variable appearance. They commonly are hypoechoic, but they also can be isoechoic or hyperechoic. Additionally, shadowing from calcification may be present. The reported sensitivity of

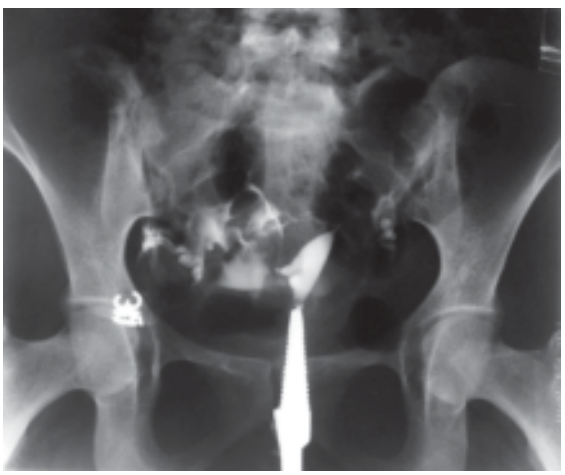

Fig. 24.3: HSG in a patient with secondary infertility following prior dilatation and curettage shows a distorted uterine cavity with irregular filling defects in the region of right cornu suggestive of intrauterine adhesions

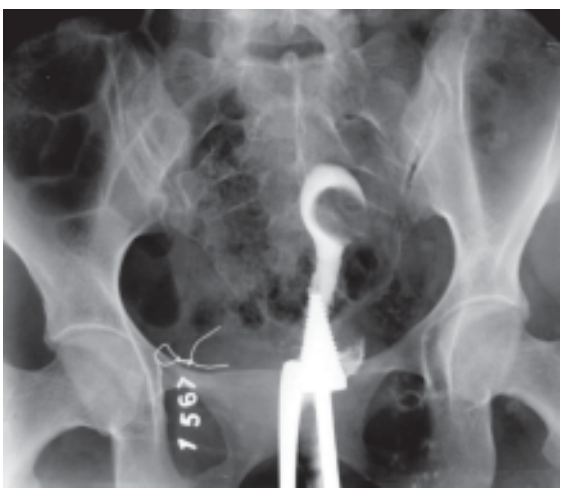

Fig. 24.4: A globular uterine cavity with a well-defined rounded filling defect consistent with a fibroid

ultrasound in detecting fibroid ranges from 65 to 93 percent. Limitations of ultrasound in evaluating fibroids include failure to detect small leiomyomas and difficulty in exact localization due to unfavorable uterine position, and poor uterine visualization because of patient body hapitus. MRI has the highest sensitivity for detecting fibroids. [1,19] Fibroids generally show low to intermediate signal intensity on T1 weighted images and low signal intensity on T2 weighted images; however, if they have de-generated, the signal characteristics can be variable. (Fig. 24.5) Distinct advantages on MRI include the ability to differentiate leiomyomas from adenomyosis, and improved preoperative localization for surgical planning and predicting treatment outcome. Submucosal fibroids may be resected via a hysteroscope rather than laparotomy. When submucous myomas are single and small, the benefits of hysteroscopic myomectomy generally outweigh the few associated risks. When these are multiple and large, hysteroscopic myomectomy requires much greater technical expertise and poses greater risks including severe postoperative uterine adhesions.[1,20] Leiomyomas with an intramural component may be treated by uterine artery embolization (UAE). In these patients high signal intensity on T1W images is a negative predictor of volume reduction. It is hypothesized that such leiomyomas have already undergone hemorrhagic degeneration and loss of vascular supply so that they show poor response to UAE.[21] Gadolinium enhanced MR may be useful in predicting the outcome to hormonal (GnRH) therapy. [21]

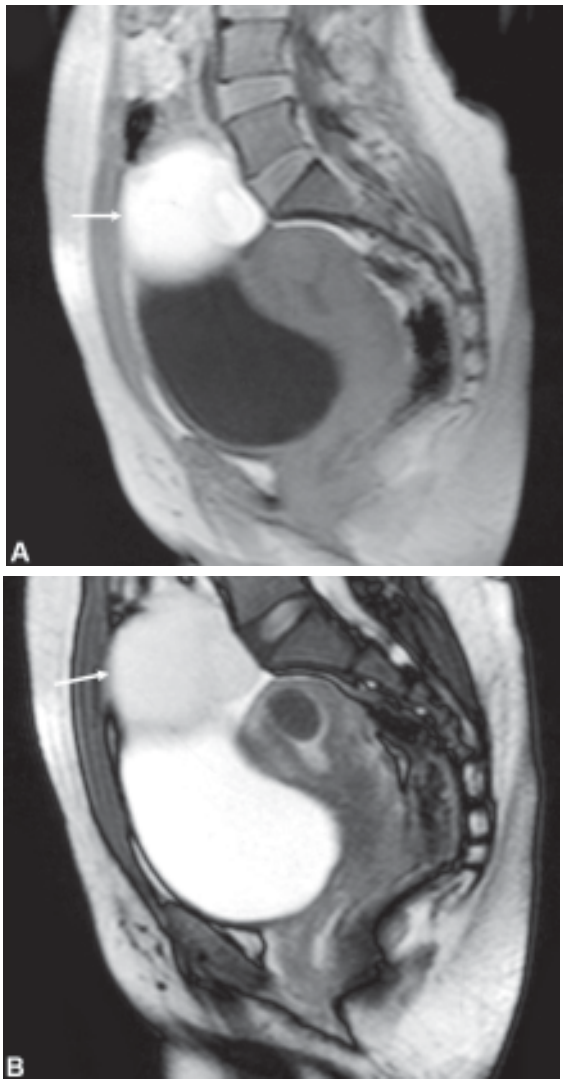

Figs 24. 5A and B: T1(A) and T2(B) weighted sagittal MR images reveal a small submucous fundal fibroid appearing iso intense on T1 and hypointense on T2W images with distortion of the endometrial cavity. Note the presence of hemorrhagic cyst in one of the ovaries lying superior to the bladder and the uterus appearing hyperintense on both T1W and T2W images (arrows)

Endometrial Polyps[9]

Endometrial polyps can be identified by HSG or TVS. The sensitivity of sonohysterography for diagnosis of endometrial polyps is greater and that of HSG and nearing hysteroscopy but false positive results due to blood clot,

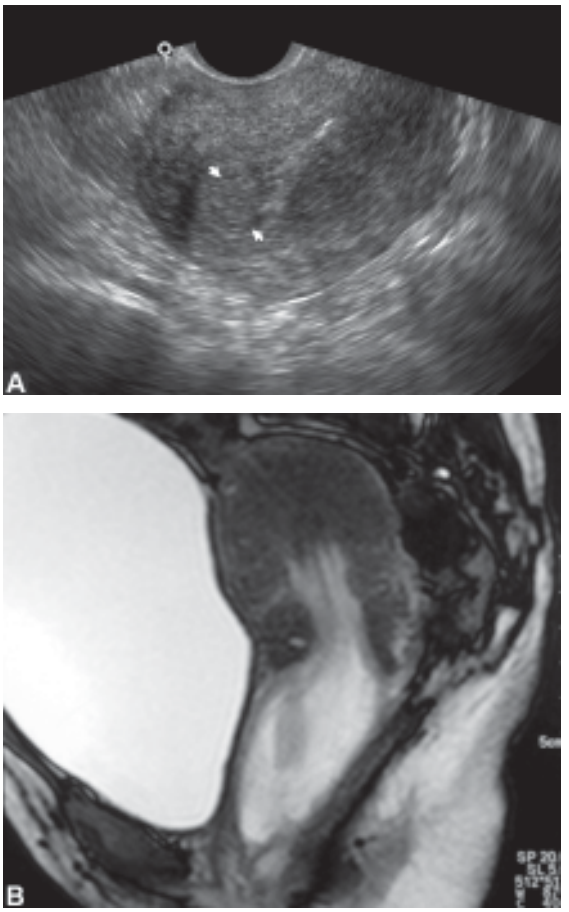

Figs 24.6A and B: (A) TVS reveals a relatively well-defined hypoechoic mass within the upper endometrial cavity (arrows) due to an endometrial polyps which was hysteroscopically removed, (B) Sagittal T2W MR image (in another patient) reveals a large hyperintense endometrial polyp coming out through the cervix and bulging into the vagina

mucus plug and shearing of normal endometrium are not uncommon. (Figs 24.6A and B).

Mullerian Duct Abnormalities (MDAs)[1,9,21,22]

Mullerian duct abnormalities (MDAs) result form congenital nondevelopment or fusion abnormalities of mullerian ducts, MDAs affect 1 to 5 percent of all women and although they have long been associated with pregnancy loss and complications the ability to conceive is generally not affected. The anomalies have been classified into seven groups based on their prognosis for future fertility and surgical treatment. Among the MDAs septate uterus carries the highest rate of pregnancy loss (67 percent). Because the treatment of MDAs is dependent on the type of abnormality and because certain treatment options like IVF, super ovulation are associated with multifetal gestation which presents even greater risk to women with uterine malformations, a correct diagnosis is paramount. The most consistently accurate imaging technique for evaluating MDAs is MRI. Combining transvaginal sonography with hysterosalpingography has been reported to result in diagnostic accuracy rates as high as 90 percent. 3D ultrasound is comparable in accuracy to MR in evaluation of congenital malformations.[23,24]

HSG evaluates mainly the internal morphology of the endometrial cavity and is less accurate it cannot reliably distinguish a *septate from a bicornuate uterus*. Both these appear as two diverging endometrial cavities. A more obtuse angle (>105°) favors a bicornuate uterus and an acute angle (<75 °) favours a septate uterus, but there is considerable overlap. (Figs 24.7A to C). The external contour must be evaluated to make the correct diagnosis (a septate uterus has a normal contour, whereas a bicornuate uterus is heart-shaped). Using T2-weighted MR images parallel to the long axis of the uterus, both the internal and external uterine contour can be evaluated simultaneously. Not only does simultaneous internal and external visualization differentiate a bicornuate from

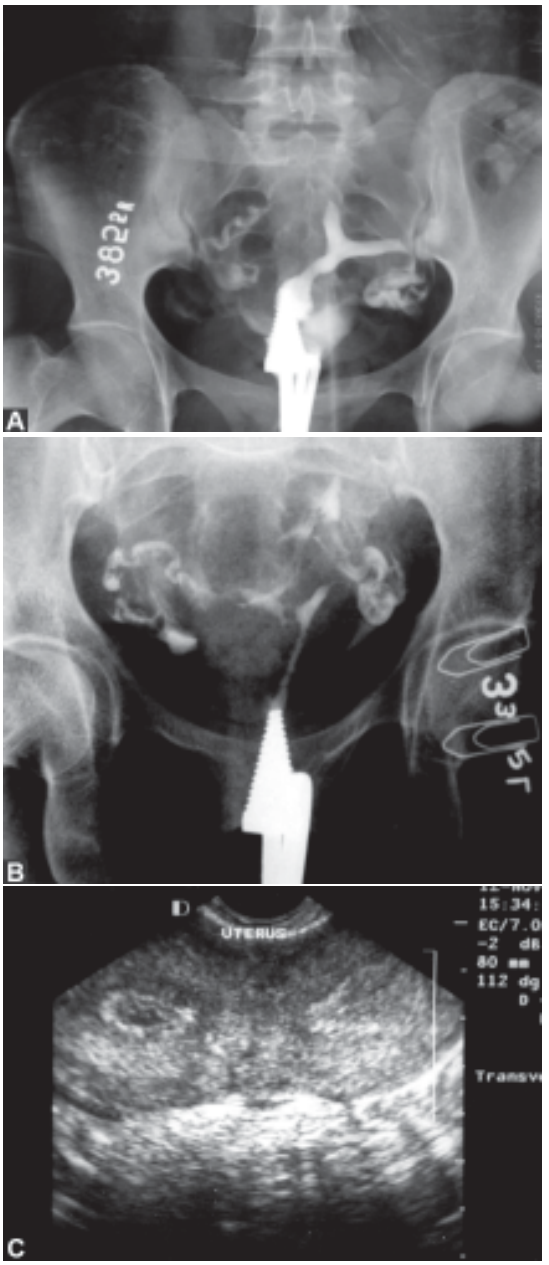

Figs 24.7A to C: HSG demonstration of septate versus bicornuate uterus- **(A)** spot radiography shows two uterine horns with an indeterminate angle of divergence which could represent a septate or bicornuate uterus.**(B)**Widely divergent uterine horns in another patient suggesting bicornuate morphology. **(C)**TVS image of the same patient as (B) showing two widely divergent uterine horns fluid is present in the right horn : Bicornuate uterus

a septate uterus, but it also helps in treatment planning. On MR the bicornuate uterus has divergent uterine horns with an intercornual distance exceeding 4 cm, concavity of the fundal contour or a cleft more than 1 cm deep (heart shaped) whereas in a septate uterus the contour is normally convex, flat or minimally indented by less than 1 cm. The septum may be a combination of fibrous tissue myometrium or both.[21] (Fig. 24.8) Septoplasty via hysteroscopy is generally done for septate uterus. An incompetent cervix is often

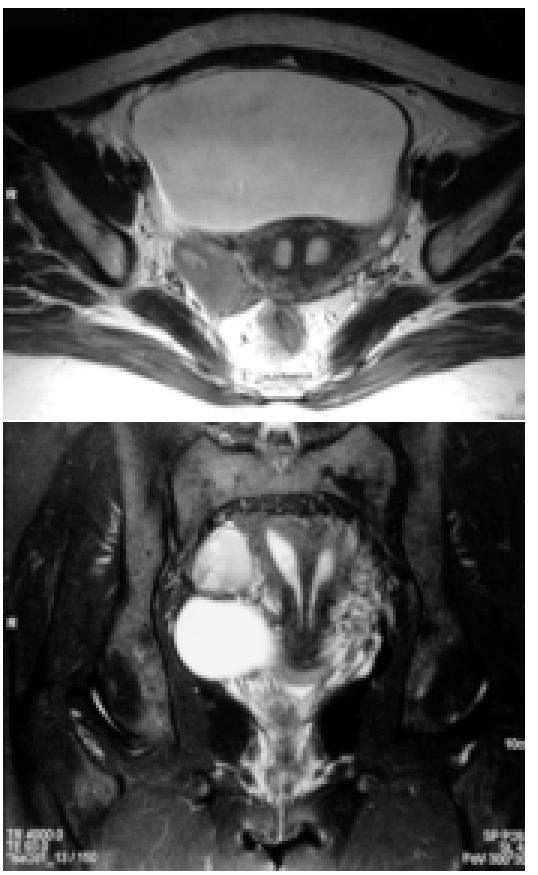

Fig. 24.8: T2W axial and coronal MR images in a patient with complete uterine septum. Two uterine cavities are seen which are separated by a septum showing signal isointense to myometrium in its upper part and an inferior fibrous component which is T2 hypointense extending into the cervix. The external fundal contour is only mildly indented. Note the cyst in the right ovary: Septate uterus

associated with bicornuate uterus and serial scanning during pregnancy may be helpful. [3]

MRI is also helpful in delineating other less common MDAs including arcuate, unicornuate uterus, uterus didelphys or uterine agenesis. Among the MDAs, uterus didelphys is associated with the highest possibility of successful pregnancy. Spontaneous abortion and premature labor may occur in pregnancies with a *unicornuate uterus*. Some of these patients have a rudimentary horn on the contralateral side. When this is non-communicating, endometrial tissue is expelled retrogradely resulting in increased frequency of endometriosis. This makes surgical resection of the horn necessary.

Arcurate uterus usually has no effect on fertility. It has been proposed that when a ratio of less than 10 percent between the height of fundal indentation and distance between the lateral apices of the horns is calculated on HSG, an adverse reproductive outcome is not anticipated.[22-27] However a defining depth of indentation to differentiate an arcurate configuration from a broad based septum has not been established. On MR images the normal external uterine contour is maintained with a smooth myometrial fundal indentation. The signal intensity of this is similar to normal myometrium (Figs 24.9A and B).

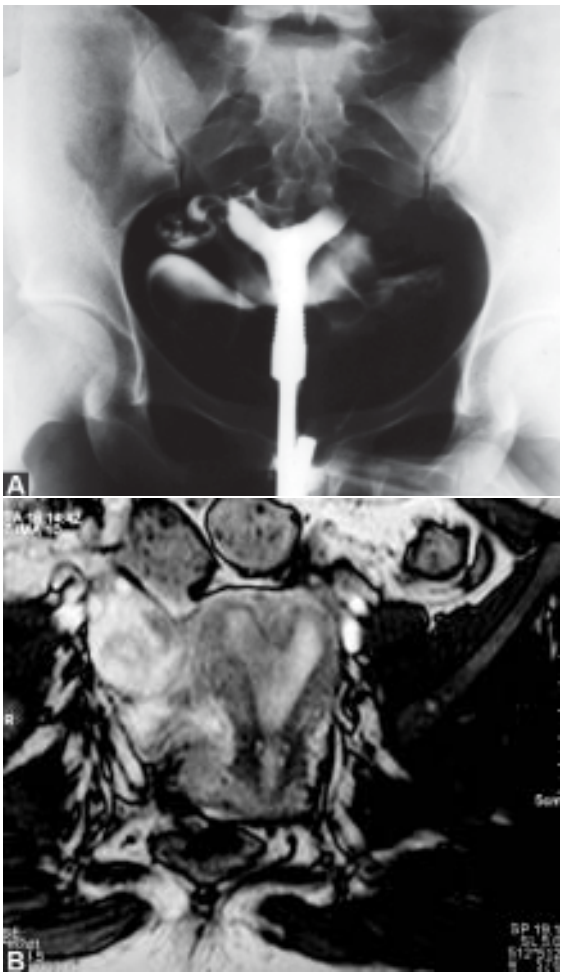

Figs 24.9A and B: (A) HSG showing a broad saddle shaped indentation of fundal outline representing an arcurate deformity **(B)** TSE-T2W MR image of the same patient demonstrates a normal external uterine contour with a smooth broad myometrial indentation at the fundus

Endometrial ossification is a rare condition which acts like an IUCD. It appears as a highly reflective echo on USG.[15]

Adenomyosis

Adenomyosis is not a common cause of infertility and generally manifests as pelvic pain or bleeding. It is most commonly detected with MR Imaging or ultrasound. [15] The relevant ultrasound findings are thickening and assymetry of anterior or posterior uterine walls with a pooly defined area of increased, decreased or heterogeneous echogenicity or myometrial cysts (Fig. 24.10). MR reveals a myometrial mass of low signal on both T1 and T2W images with indistinct margins, focal widening of the junctional zone (>12 mm) and punctuate high signal intensity foci.[21] (Fig. 24.11) Adenomyosis may occasionally be imaged

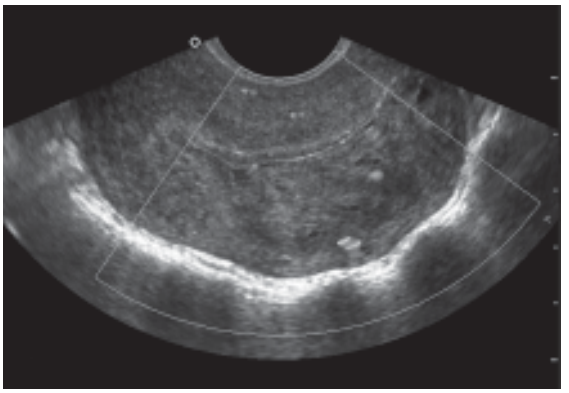

Fig. 24.10: TVS (CDFI) showing a poorly defined area of decreased echogenicity in the anterior myometrium with no abnormal vascularity: adenomyosis *(For color version see Plate 20)*

with HSG when nests of endometrial tissue connect to the uterine cavity. At HSG adenomyosis appears as small diverticulae extending in to the myometrium.[8] (Fig. 24.12)

The only functional uterine[9] abnormality that is of particular interest in the evaluation of infertility is chronic endometritis. Some may view defects of endometrial receptivity including luteal phase deficiency (LPD) as another but controversies exist regarding the existence mode of diagnosis and of LPD.

Nontubercular Chronic Endometritis

Nontubercular chronic endometritis[9] is an enigmatic condition of uncertain persistence from one cycle to next and often of uncertain bacterial origin. The diagnosis is usually made histologically but in florid cases TVS may reveal thin echogenic endometruim that does not thicken as follicular phase advances.

Sonography has also been used to study the normal developmental response of the endometrium to try and predict implantation. In the menstrual phase the endometrium is a thin echogenic interface which thickens during the proliferative phase is relatively hypo to isoechoic yielding a prominent trilaminar pattern. During the secretory phase the endometruim does not thicken further but becomes more echogenic. Researchers have attempted to correlate endometrial thickness and appearance and volume (using 3D ultrasound) in an effort to predict optimal implantation times, however, neither allowed a reliable prediction of subsequent implantion. [28]

Spiral and uterine artery Doppler indices have been studied to evaluate endometrial

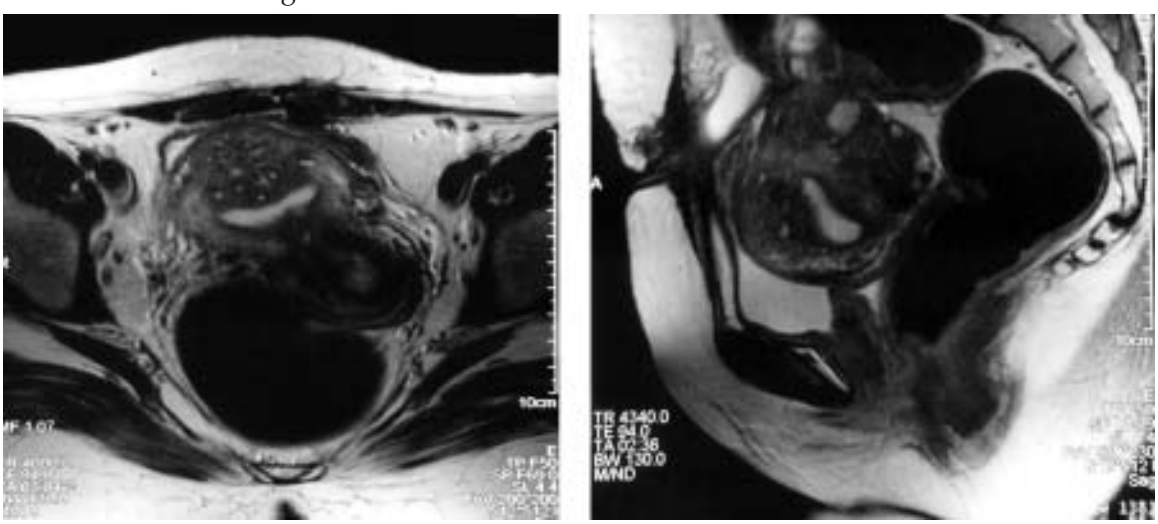

Fig. 24.11: Axial and sagittal T2W MR images reveal ill defined myometrial masses with indistinct margins, myometrial cysts and focal widening of junctional zone : adenomyosis

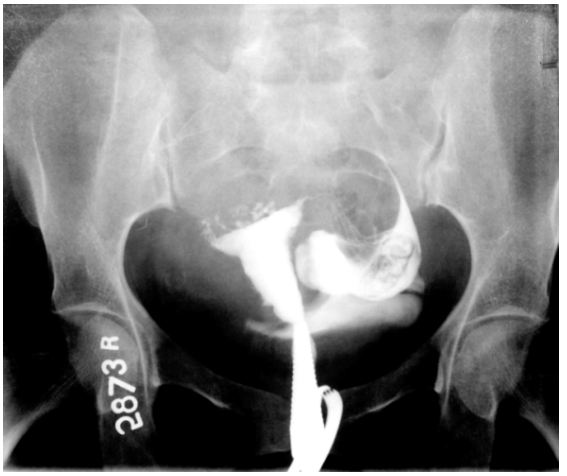

Fig. 24.12: HSG in a known case of adenomyosis showing multiple small irregular diverticulae in the region of fundus filling with contrast : Right sided tube is not visualized. (Cornual block) Left tube is normal

receptivity but the results have again been conflicting. Some authors have reported that a uterine artery PI to >3 correclates with poor chance of implantation[1,29] while others have shown that Doppler evaluation of the spiral or uterine arteries has little predictive value.[28] Recently researchers have shown that presence of both endometrial and sub endometrial blood flow on the day of embryo transfer (ET) is indicative of good endometrial receptivity whereas absence of both represents a poor uterine environment.[30] As a result of conflicting results routine US or Doppler evaluation of the endometruim has no proven value in management of patients with infertility. According to a recent study the relevant studies in literature differs in patient's characteristics, the day of ultrasound examination and selection of sub-endometrial region and further studies are required especially in the late follicular to the early luteal phase. [31]

Tubal Factor

The fallopian tubes connect the peritoneal cavity to the external environment via the uterus, cervix and vagina. Their function and their anatomy is complex and includes conduction of sperm from the uterine end towards the ampulla, conduction of ova in the other direction from the fimbriated end to the ampulla, and support of the early embryo and conduction of the early embryo from the ampulla into the uterus for implantation. The normal fallopian tube ranges in length from 7 to 16 cm, with an average length of 12 cm. The tube is composed of a ciliated mucosal epithelial layer surrounded by three smooth muscle layers and is divided into four regions: (1) the intramural or interstitial portion, which lies in the wall of the uterine fundus and is 1 to 2 cm long; (2) the isthmic portion, which is approximately 2 to 3 cm long; (3) the ampullary portion, which is 5 to 8 cm long; and (4) the infundibulum, which is the trumpet-shaped distal end of the tube that terminates in the fimbria.[3]

Fallopian tube pathology in the cause of infertility in up to 40 percent women and is among the most common causes of infertility. Tubal obstruction is a common sequelae of infection or endometriosis. Another cause of tubal infertility commonly described in the western literature is salpingitis isthmica nodosa (SIN).[1,3]

Evaluating tubal patency is an essential part of the infertility workup. The methods available to evaluate the tubes include HSG, sonohysterosalpingography and laparoscopy. HSG remains the most common initial imaging technique used to evaluate the fallopian tubes. Compared with laparoscopy (which is the gold standard test for tubal patency). HSG has only moderate sensitivity

but relatively high specificity. The clinical implications are that when HSG reveals obstruction there is still a relatively high probability (approx 60 percent) that the tube is infact open, but when HSG demonstrates patency there is little chance that the tube is actually occluded (approx 5 percent). In these cases, contrast in a dilated tube or vaginal formix may be mistaken for peritoneal spill.[9] Sonohysterosalpingography and 3D ultrasound and Doppler techniques have been used to evaluate the tubes. However the techniques provide no information reqarding tubal anatomy and whether one or both tubes are patent. Although 3D-ultrasound and Doppler techniques have improved visualization of fluid movement through fallopian tubes but it is unlikely that they will replace traditional HSG anytime soon. [9]

On HSG, the interstitial portion of the fallopian tube may be delicate and thread-shaped or may be funnel shaped, assuming the configuration of a small triangle or diamond. The isthmic portion is normally thread-shaped. Diameter of both these regions is approx 1 mm. *Proximal tubal obstruction*[1,3] is obstruction in the first 3 to 4 cm of the tube. Hysterosalpingography shows obstruction of the proximal end of the fallopian tube in 20 percent of cases. The cause of proximal tubal obstruction is frequenly unclear, but infection and subsequent inflammation are leading causes in all reported series. Histopathologic findings in resected proximal tubal segments include plugs of amorphous debris, chronic inflammation, obliterative fibrosis, and salpingitis isthmica nodosa (SIN). Together these lesions account for majority of anatomic occlusions at the uterotubal junction. Other causes include granulomatous or "giant cell" salpingitis from tuberculosis, foreign bodies, and some parasitic infestations. Intraluminal endometriosis occurs in approximately 10 percent of tubes resected for proximal occlusion and may exist without relation to visible lesions elsewhere in the pelvis. Mullerian anomalies of the fallopian tube are rare, but cornual occlusion is seen with variants of unicornuate uterus, where atresia of tubal segments, including the proximal isthmus, can occur.

Another cause of proximal tubal obstruction on HSG is "tubal spasm". The cornual portion of the fallopian tube is encased by smooth muscle of the uterus. If there is spasm of the muscle during HSG, one or both tubes may not fill beyond the interstitial portion. Administration of a spasmolytic agent such as glucagon can occasionally result in uterine muscle relaxation and consequent tube opacification. However no reliable antispasmodic has been discovered.[32] According to some authors, however, tubal spasm is the cause of proximal tubal obstruction much less often than originally proposed. They postulate that temporary non visualization of the tube may be explained by some easily dislodged entity such as amorphous debris in tubal lumen. [32,33] Placing the patient prone and waiting for 5 minutes before slowly reinjecting contrast may help in some cases. If proximal tubal obstruction persists despite these maneuvers tubal catheterization with selective salpingography can be performed.

Fluoroscopically guided selective salpingography can diagnose and treat proximal tubal obstruction.[3,34-36] Selective salpingography is a minimally invasive method during which the tip of the catheter is placed in the tubal ostia and contrast is injected directly into the tube. Often the obstruction can be cleared by the injection alone. If the obstruction persists, a guidewire can be directed into the tube fluoroscopically

through the catheter. Recanalization of the tube, either by forceful injection of contrast or by clearing the obstruction with a guidewire, is possible in up to 95 percent of patients.[36] Pregnancy rates after one year are comparable to surgery. Complications are also similar to surgery, including a reocclusion rate 30 percent and an ectopic pregnancy rate of 10 percent.[36] Sonographic guidance has also been performed for this technique in a small number of patients. [1]

Salpingitis isthmica nodosa (SIN) is another tubal pathology commonly described in western literature. There is an association between SIN and pelvic inflammatory disease however, it is not clear whether SIN is caused by pelvic inflammation or it is congenital and predisposes to inflammation. It is mostly affects the isthmic portion occasionally interstitial and ampullary segments. On HSG it is seen as characteristic multiple small diverticule involving the proximal two thirds of the tube. In addition to causing infertility it also increases the risk of ectopic pregnancy. Tuberculous salpingitis can have the same appearance but may be associated with calcified lymph nod es or calcifications of the tube itself.[1] SIN associated with tubal obstruction may be treated by fluoroscopically guided tubal catheterization and recanalization. [1,3]

The *ampullary portion* is the longest portion of the tube. It gradually widens from 1 to 2 mm at its proximal end to approxi-mately 15 mm, where it joins the fimbriated infundibular portion. Subtle ampullary rugal folds can be demonstrated by salpingography, and occasionally the fimbriae are outlined by contrast material. Abnormal rugal folds imply damage of the epithelium from infection and usually coexist with a dilated and sometimes distally obstructed tube. Abnormal rugal folds can occur in a patent tube, and they indicate reduced chances for conception. The visualization of abnormal rugal folds requires optimal tubal imaging, because the normal rugal folds are subtle. Rugal folds may be best seen before the dilated tube is fully distended with contrast i.e. during early filling. [3]

Obstruction of the *fimbrial portion* of the tube is characterized by dilation of the ampullary portion of the tube, which sometimes can be massive, and no free spill of contrast agent into the peritoneal cavity despite adequate filling of the tubes and rolling the patient. (Fig. 24.13) It may be occasionally difficult to differentiate a dilated tube from loculated spill of contrast agent. The amount of dilation of the tube does not necessarily predict surgical results. A dilated tube may be soft and pliable with an intact epithelium and offer an opportunity for surgical correction. An obstructed but

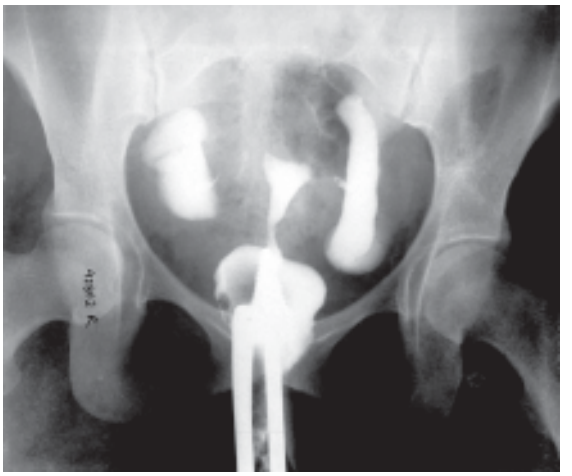

Fig. 24.13: HSG in a patient with bilateral fimbrial block shows markedly dilated ampullary segments (hydrosalpinx) with absence of free intraperitoneal spill

minimally dilated tube may have an indurated and thickened wall that cannot be reconstructed. The visualization of normal ampullary rugal folds probably improves the chances for successful tubal reconstruction. Dilation of the ampullary portion of the tube in the absence of complete occlusion indicates perifimbrial phimosis, or adhesions around the fimbria that impede egress of fluid. Fimbrial phimosis can be mild or severe, but generally the presence of at least a pinpoint opening in the distal tube carries a more favorable surgical prognosis that complete occlusion. It also increases the risk of post-HSG peritonitis.

Although ultrasound is unable to visualize normal fallopian tubes blockage of the fallopian tube with fluid accumulation (hydrosalpinx) is easily seen on ultrasound. (Fig. 24.14) The distended tube coiled around the ovary with folds producing septa which do not completely cross the lumen. (Fig. 24.15) A hydrosalpinx may occasionally be visible on ultrasound, distended with fluid only at midcycle, under the estrogenic influence of a preovulatory follicle. [37]

A woman with severly damaged fallopian tubes but a normal uterine cavity is a good candidate for *in vitro* fertilization and embryo transfer. However presence of hydrosalpinx in a woman being treated by IVF is associated with poor embryo uptake which may be improved after treatment of hydrosalpinx. Even a unilateral hydrosalpinx is capable of disrupting natural fertility and preventing the success of IVF.[37-39] The mechanism is as follows: Estradiol produced by the preovulatory and ovulating follicle stimulates both ampullary transudation of fluid and isthmic secretion of dense mucus which along with an estrogen medicated increase in isthmic myosalpingeal tone functionally occludes the tube's communication with the cavity of the uterus. Thus the hydrosalpinx gathers fluid. With ovulation, increasing progesterone

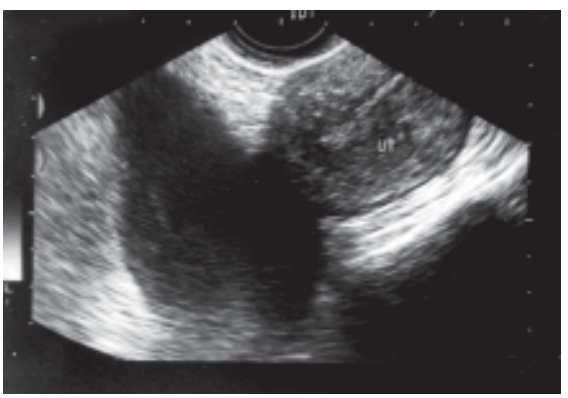

Fig. 24.14: USG showing a cystic hypoechoic retort shaped dilated tube with incomplete reptations : Hydrosalpinx

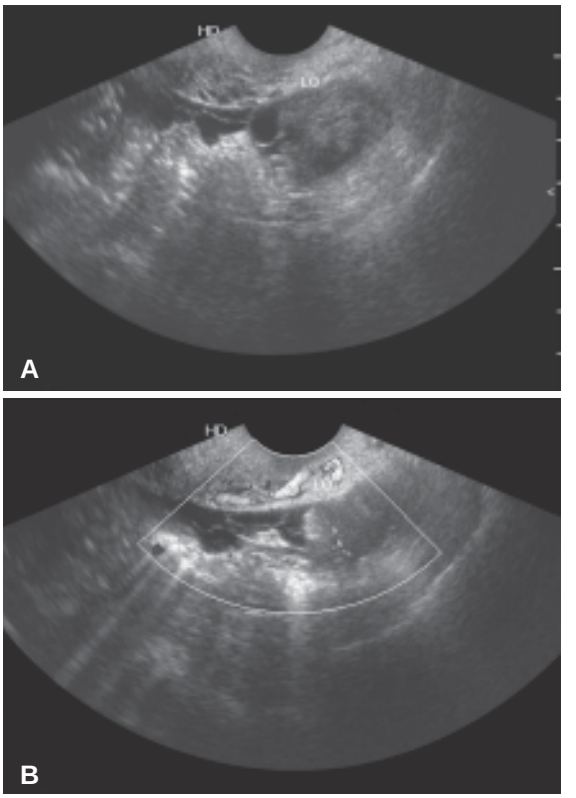

Figs 24.15A and B: TVS (grey scale CDFI) showing a mildly dilated left fallopian tube seen to extend up to the left ovary *(For color version of Fig. 24.15B see Plate 20)*

secretion from the luteinizing follicle relaxes the isthmus, allowing passage of accumulated hydrosalpinx fluid down the endometrial cavity just at the time that a normal tube allows passage of pre-embryo to the uterus. This cascade from a single tube is likely to displace any pre-embryos that might have reached through the contralateral patent one or through IVF and transcervical transfer.

Conceptions rates following salpingostomy are less than 25 percent if the hydrosalpinx has a thickwall or a diameter greater than 15 mm.[15,40]

Peritoneal Factor

The peritoneal factor responsible for infertility relates to the presence of pelvic adhesions from previous infection, endometriosis or surgery.[1,3,4] Adhesions can cause problems in oocyte pick up and transfer due to distortion of the normal anatomy, limitation of fimbrial motility and obstruction of fallopian tubes. Imaging techniques are limited in their ability to diagnose pelvic adhesions. Laparoscopy is the gold standard for visualization of pelvic adhesions and endometriosis.[1]

With HSG the presence of peritubal adhesions and endometriosis is under diagnosed with reported sensitivities ranging from 34 to 75 percent. Peritubal adhesions can be suggested if loculated spill of contrast is seen in the peritoneal cavity, or it is seen to track along the outside of the tube producing "a halo effect" or double contour appearance to tubal wall.[41] Peritubal adhesions can also be diagnosed if a persistently convoluted, kinked, stretched or vertically oriented fallopian tube is seen. (Fig. 24.16) Delayed films or film obtained after rolling the patient may be useful to confirm loculated spill in doubtful cases. Normally the contrast should flow freely to outline the bowel loops.[1,3,42] A tug and release maneuver has also been described to confirm the presence of adhesions. If traction is applied on the HSG system both a fixed laterodeviated uterus (due to adhesions) as well as a normal non median uterus initially follow the traction direction, however, during the releasing phase the fixed laterodeviated uterus tends to keep the original deviated position while the non median uterus keeps the pelvis midline. [41]

Ultrasound especially TVS may also allow detection of pelvic adhesions and loculated fluid collections in the adnexae. Adhesions may be suggested by *enmasse* movement of tethered organs when pressure is applied simultaneously by the operator's hand transabdominally and by the probe transvaginally. However, the sensitivity is low[42,1].

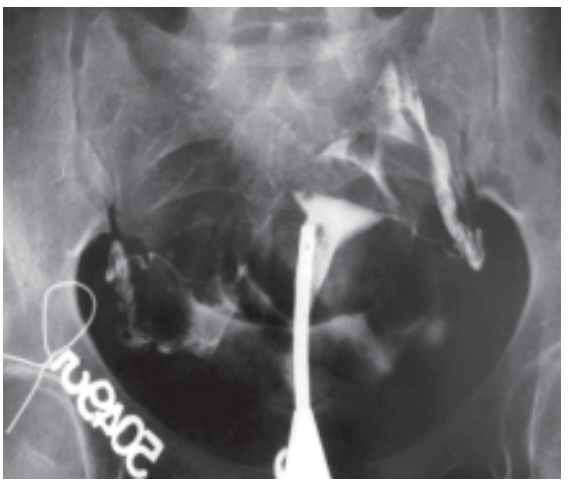

Fig. 24.16: HSG film reveals an irregular filling defect in the uterine body just adjacent to the cannula due to adhesions. An air bubble is seen in the right cornu. The ampullary portion of the left fallopian tube is vertically stretched with evidence of both peritubal and free spill due to peritubal adhesions

Endometriosis

Endometriosis is found in 25-50 percent of infertile women and 30-50 percent of women with endometriosis are infertile.[43] Endometriosis is the result of ectopic foci of secretory endometrium located outside the uterus. In addition to causing adhesions, it can impair fertility through hormonally medicated mechanisms. Endometriosis occurs as diffuse peritoneal implants or focal endometriomas (chocolate cysts). Transvaginal sonography is the preferred technique to identify ovarian endometriomas which are seen as complex adnexal or cul de sac masses. Diffuse low level internal echoes may be seen. However TVS has limited ability to identify generalized disease producing subtle changes such as obliteration of margins between pelvic organs and a generalized increase in echogenicity.[21,42]

On MR imaging endometriomas may be seen as adnexal cysts with high signal on both T1W and T2W images or high signal on T1 and low signal on T2W images (shading) and indistinct margins due to adhesions. Evaluation of adhesions is limited and these may be seen as low signal intensity stranding that obscures organ interfaces, post displacement of uterus, kissing ovaries, angulated bowel loops, an elevated posterior vaginal fornix, loculated fluid collections and hydro/hematosalpinx (Figs 24.17A to C). Hormonal therapy is occasionally used to treat endometriosis and shading on T2W images is the most important negative predictor for volume reduction with medical treatment, such therapy should be discontinued should low T2 signal be seen in a case on hormonal treatment.[21] It is important to remember that small implants and adhesion[6] that may cause infertility are

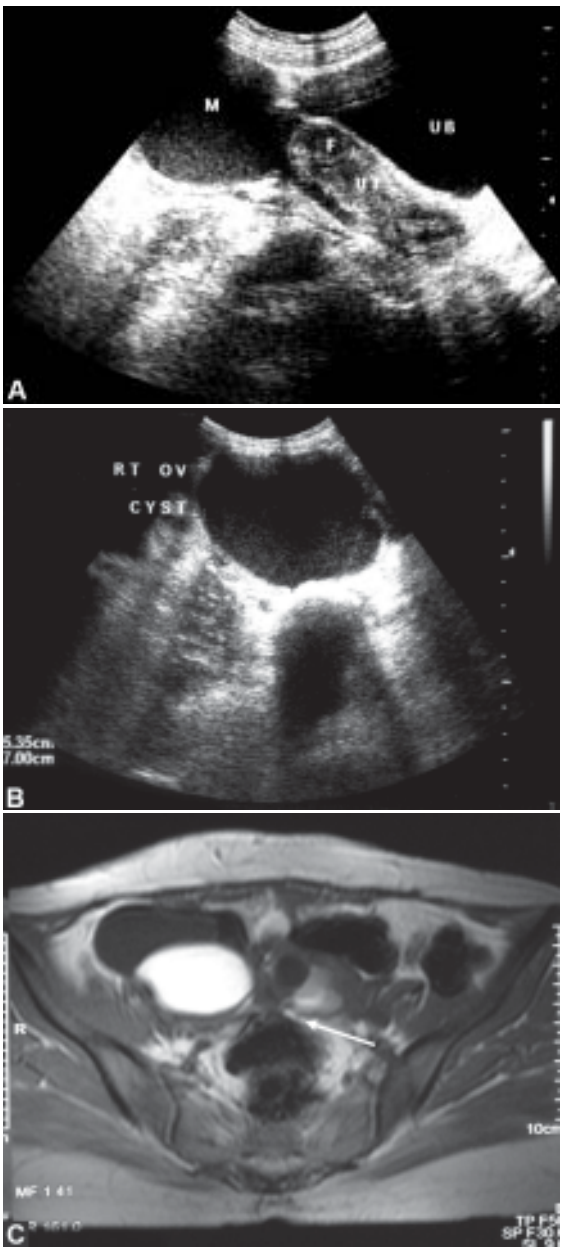

Figs 24.17A to C: Endometriotic cysts; Ultrasound (A and B) showing a cystic mass with low level internal echoes replacing the right ovary. A small fibroid is also seen in the uterine fundus. T1W MR image (C) reveals B/L adnexal cysts with high signal due to hemorrhage and angulation of the anterior rectal surface due to adhesions (arrow)

not well visualized by any imaging technique. Laparoscopy remains the gold standard for diagnosis and staging of endometriosis and is also the mainstay for diagnosis. [2,3]

Genital Tuberculosis

About 18 percent of female infertility in India is attributed to genital tuberculosis.[44] Tuberculosis commonly results in changes in the endometrium, the fallopian tubes and pelvic peritoneum.

Scarring in uterine tuberculosis is well-demonstrated by HSG. This can take few specialized forms namely : T-shaped uterus, asymmetric uterus and pseudounicornuate uterus.[45] A T-shaped uterus has been observed in a significant number of patients with uterine TB and in the appropriate setting it is virtually diagnostic of uterine TB. In the Western literature, a T-shaped uterus has usually been labelled as a diethylstilbestrol (DES) uterus. The DES and the tuberculous uterus both reveal irregular margins. However, tubal changes are not noted in DES uteri, whereas tubal changes are invariably seen in T-shaped uteri due to TB. The normal uterine cavity has a triangular appearance with either straight or concave lateral walls. In tuberculous endometritis due to scarring along the long as well as the short axis of the uterus; this triangular shape is converted into a T-shape.[45]

Scarring is also recognizable by the asymmetric uterine contour it produces. An asymmetric, small sized uterine cavity is usually due to TB. Occasionally the scarring may be more unilateral which may lead to obliteration of that side of the uterine cavity leading to a unicornuate uterus-like appearance—"the pseudounicornuate uterus". Comparison with previous films, laparoscopy, and awareness about this type of scarring would be essential in excluding TB in a true unicornuate uterus. A good pointer towards endometrial TB is myometrial extravasation and / or venous intravasation. This finding along with any other endometrial or tubal change (Fig. 24.18 and 24.19) is very suggestive of a tuberculous etiology of endometritis[45].

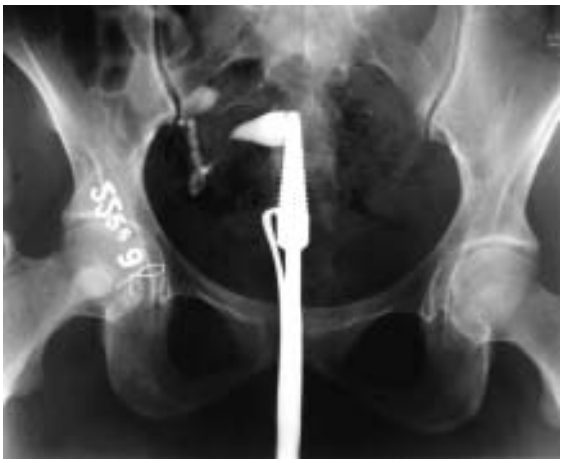

Fig. 24.18: A HSG showing a mildly dilated beaded right fallopian tube with evidence of loculated spill. Left tube is not visualized due to cornual block: Sequelae of tuberculosis

Ovarian Factor

Upto 20 percent of infertility cases are caused by ovarian factors.[1,7,46] Normal ovarian follicular development, ovulation and formation of a functional corpus luteum are needed for adequate reproductive function and these represent the ovulatory factors that must be evaluated in an infertility investigation. The imaging modality used to evaluate the ovaries is TVS which is used to detect both ovarian pathology and monitor ovulation. Functional ovarian cysts or other benign ovarian cysts and tumors like dermoid cysts or fibromata may occasionally interfere

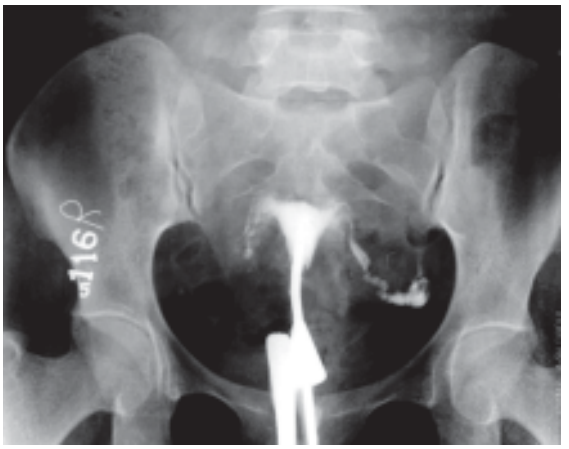

Fig. 24.19: HSG demonstrating a beaded left fallopian tube with no free spill. Only the proximal (isthmic and interstitial portion) of the right fallopian tube is visualized. Note the presence of myometrial extravasation suggestive of tubercular involvement

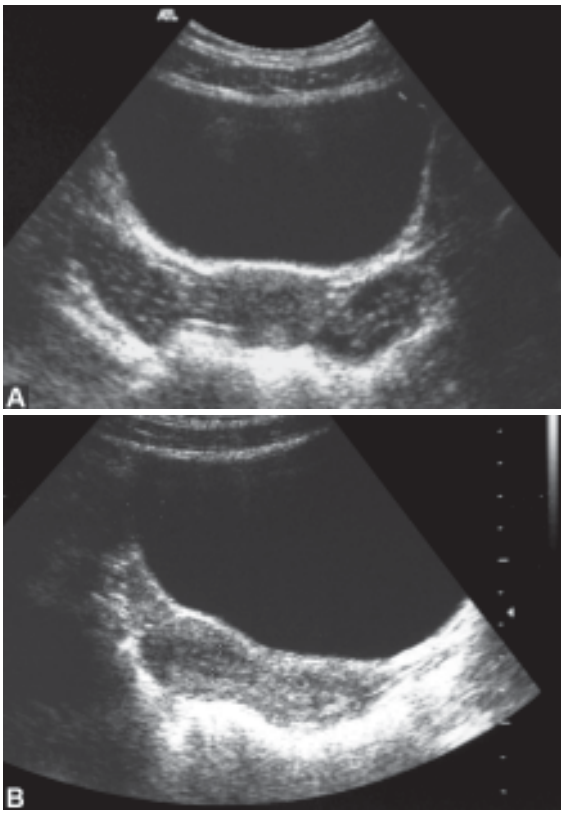

Figs 24.20A and B: Transverse (A) and longitudinal (B) US images reveal markedly enlarged ovaries with multiple small diffusely scattered cysts. Note the presence of endometrial thickening in the uterus:Polycystic ovarian disease

with ovarian function particularly when large. Endometriomas have already been discussed.

Polycystic Ovarian Syndrome (POD)

Another condition commonly found during evaluation for infertility is Polycystic ovarian syndrome (POD).[1,47-51] It is a complex endocrine disorder of unknown etiology also called Stein-Leventhal syndrome. It is characterized by multiple small (<1 cm) ovarian cysts. These cysts are thought to represent graafian follicles that persist in arrested stages of development because of low levels of FSH. The classic sonographic features of polycystic ovaries are round, enlarged ovaries, with multiple 2 to 6 mm cysts, absence of cysts greater than 1.5 cm in diameter, smooth contours and hyperechoic ovarian stroma. The small cysts may be peripherally located or dispersed throughout the ovarian parenchyma. The present of a thickened echogenic endometrium (due to estrogen excess) also supports the diagnosis of POD (Figs 24.20A and B). One third of patients with clinical manifestations of POD have normal ovaries.

Distinct from polycystic ovaries are the more chaotically distributed multiple follicles seen in what has come to be called multifollicular ovaries. The ovulatory pattern in these patients is often irregular, reminiscent of the post-menarcheal or premenopausal states, and premature menopause is common among these patients. Their response to ovarian stimulation for

assisted conception can be unpredictable; many respond poorly. The ultrasound appearance of variably sized follicles, irregularly dispersed, and often larger than usually seen, is not always convincingly different from normal. (Figs 24.21A and B) A multifollicular morphology can also be seen in patients recovering from anorexia.[37]

Follicular Monitoring

Ovulation is initially monitored using simple tests like BBT mid luteal serum progesterone and urinary LH. However, when a more accurate estimation of ovulation is necessary, ultrasound is used to monitor follicular development in both natural and stimulated cysts.[9] Observation of a developing follicle, the prediction of impending ovulation allow procedure such as post coital testing, HCG administration, intercourse, donor and husband insemination and egg collection to be timed optimally. Patients not shown to be ovulating may be treated by ovulation induction agents.

Spontaneous Cycles[15,52]

Beginning with menarche, during spontaneous cycles there is usually development of one or sometimes two dominant follicles. Sonography can depict developing follicles beginning at the time they measure 3 to 5 mm. In the spontaneous cycle by unknown mechanisms one or at the most two follicles that develop to approximately 10 mm. At this time (about 7 days before LH surge) a dominant follicle takes over and there is a very little further growth of other follicles. Occasionally two dominant follicles develop. During the five days prior to ovulation the dominant follicle grows at the rate of 2-3 mm/day. As a follicle reaches maturity its inner dimensions range from 17 to 25 mm. However within the same individual the size of the mature follicle is relatively constant cycle to cycle.

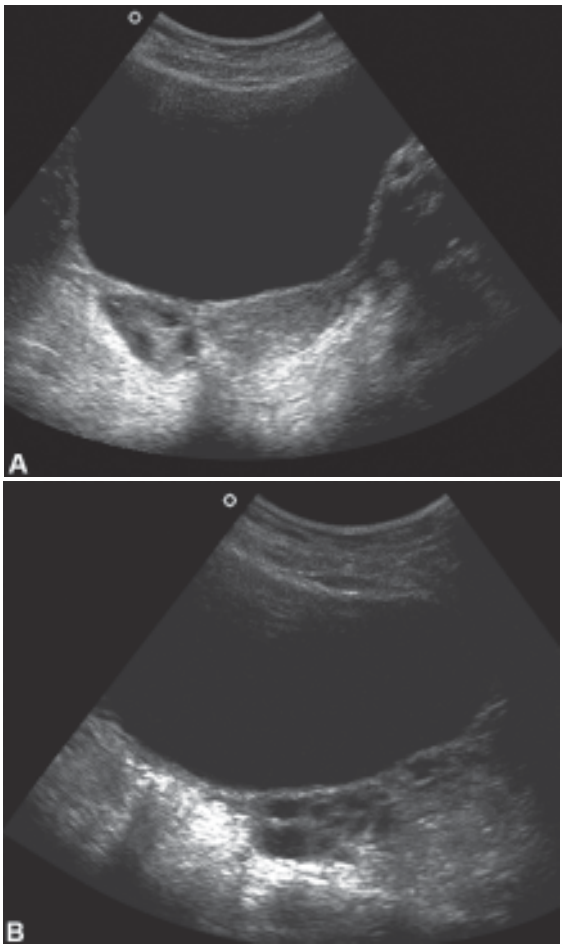

Figs 24.21A and B: Multifollicular ovarian morphology seen in a patient recovering from anorexia. Ovaries are only mildly enlarged with multiple variably sized follicles irregularly dispersed on the left side (B)

Induced Cycles[2,15]

In patients in whom infertility can be attributed to an ovulation abnormality or anovulation, ovulation induction is indicated. Ovulation induction or super ovulation therapy is also used in women with normal ovulation before assisted conception

techniques such as IVF-ET or GIFT to increase the number of oocytes aspirated. This increases the number of fertilized concepti that may be transferred thereby increasing the chances of pregnancy.

Before starting treatment a baseline scanning of the pelvis should be done. Presence of one or more cysts larger than approximately 2 cm in diameter particularly if accompanied by serum estradiol concentration of more than 100 pg/ml may interfere with treatment and induction may be postponed to the next cycle or cysts treated by aspiration.

The two medications that are most commonly used for ovulation induction include clomiphere citrate and hMG (human menopausal gonadotropin). Patients undergoing ovulation induction are usually examined every other day beginning at day 10. Patients undergoing IVF-ET are examined by sonography starting earlier and usually daily in an attempt to carefully monitor their follicular development.

Clomiphene citrate is an estrogen antagonist that acts to indirectly promote secretion of FSH and LH. Because the process of selection and dominance in overridden, multiple relatively synchronous follicles develop. In some women elevated serum FSH and LH results in ovulation without further therapy. In other patients, human chorionic gonadotrophin may be needed to induce ovulation. [1] Follicular development with clomiphere citrate can be quite different from that observed in natural cycles. Each follicle seems to develop at an individual rate and at times may be accelerated or slowed down. Therefore, the larger follicles on a given date may not be the same one that is the largest 2 days later and it may not even be the same one that is most mature. Furthermore correlation of estradiol levels (E2) and follicle size is poor and maximum pre ovulatory diameter can range from 19 to 24 mm. In clomiphere stimulated cycles the growth rate in the last few days preceding ovulation is higher.

As opposed to clomiphene citrate treatment with hMG does not require an intact hypothalamic-pitutary axis. This contains both FSH and LH and induces follicle development. Human chorionic gonadotrophin (hCG) is then given to induce ovulation of mature follicles. Although follicle growth can be assessed by serial measurement of serum or urinary estradiol levels, multiple, small, immature follicles may produce as much estradiol as a large mature follicle. Therefore, TVS is used to predict the optimal by timing for administering an ovulation inducing dose of hCG.[1,53-55] Sonographic delineation of follicle size is critical because hCG is best administered once follicles reach 15 to 18 mm.[1]

Prediction of Ovulation [1,15,52]

Follicular rupture occurs at a wide range of diameters between 2 to 2.7 cm. In the unstimulated ovary follicles are approximately spherical. They may, however, be flattened in one plane by either pressure of the transducer or bladder so a mean of the maximum diameter in three planes is a better estimate of follicular size than measurements only in two planes. [15] In super-ovulation cycles pressure from abutting follicles distorts the follicle so exact measurements are often difficult. Serial follicular measurement is best done by the same observer using the TVS route. In a recent study assessment of follicular volume using 3D ultrasound was found to correlate better with oocyte retrieval than 2D ultrasound alone. The authors found that a follicular size of > 22 mm or a

volume > 5 ml was correlated with poor oocyte retrieval probably due to post mature follicle.[56]

Ovulation can also be predicted by collapse of a previously seen follicle, development of internal echoes within the follicle, crenation of follicular walls, visualization of cumulus, peri follicular halo and visualization of fluid in the cul-de-sac (if not previously seen). However, fluid may commonly be seen in the pouch of Douglas in the periovulatory period and only a small percentage of women have a detectable increase with ovulation. Contrary to propular belief ovulation need not alternate between two ovaries. Unfortunately the variable appearance of ovulation make the use these of ultrasound signs problematic in the management of infertility.[15]

Ultrasound Doppler studies reveal an increase in blood flow to the ovary carrying the dominant follicle[57-60] (and later, the corpus luteum) – an increase that precedes other indicators of follicular dominance. With maturation of the follicle, increased flow is directed to the follicle itself within the dominant ovary. Intrafollicular neovascularization occurs over the hours preceding ovulation and becomes massive after follicular collapse as blood vessels invade the luteinizing follicular (or granulose) cells and the corpus luteum forms and impedance in intra ovarian arterioles drops while velocities reach up to 40 cm/s. These changes do not occur in non ovulatory cycles. Recently, a study[61] was undertaken to investigate if corpus luteal function could be improved by increasing CL blood flow in women with LPD and high CL-RI (> 0.51). They concluded that Vit E or L-arginine treatment improved luteal function by decreasing CL blood flow impedance.

Luteinized Unruptured Follicle (LUF) [3,15]

The corpus luteum formed after ovulation may have a variety of ultrasound appearances. It may be imperceptible from the surrounding ovarian stroma, it may show a small cystic component with echoes or may be large (> 40 mm) and be hemorrhagic.[15]

Failure to detect follicular collapse but with infilling of the follicle suggests luteinization without ovulation. The LUF syndrome occurs more commonly in infertile patients than in fertile patients and may be a cause of unexplained infertility. However, ultrasound diagnosis has a 15 percent false positive rate. Great care should be taken in diagnosing this condition because ovulation may be associated with an increase in size of follicles and these cystic corpora lutea may indicate a conception cycle.

Ovarian Hyperstimulation Syndrome (OHSS)

OHSS is potentially the most serious complication of ovulation induction with gonadotrophins. It occurs after hCG administration to patient with a large number of immature follicles and high serum estradiol levels and is more likely to occur in those with a polycystic ovarian morphology.[1,62,63]

Two mechanisms may be responsible: excessive serum levels of gonadotrophins or hypersensitivity of the ovaries to these hormones. The ovarian hyperstimulation syndrome occurs when hyperstimulation of the ovaries is accompanied by an aberration of the fluid balance. This syndrome is characterized by third-space fluid accumulation and electrolyte disturbances. The severity of the syndrome varies, but it is generally more severe if pregnancy follows ovulation. The clinical features that

cause concern are nausea, vomiting, ascites, pleural and peri-cardial effusion. These worsen hemoconcentration causing hyper-viscosity and hyper coagulability which predispose to thrombosis, embolism and renal failure.[15]

Ultrasound is used to detect patients potentially likely to develop OHSS and in hyperstimulation patients to categorize the severity of the disease and to assess the size of the ovaries.[62,63] Mild cases are characterized by minimal weight gain and ovarian enlargement to a maximum dimension of 5 cm. Moderate cases are classified as weight gain of up to 10 lb and ovarian size not exceeding 10 cm. These patients may have some ascites. In severe cases, weight gain exceeds 10 lb, the ovaries are greater than 10 cm in size, ascites is readily apparent, and pleural effusions may be present. In all cases of ovarian hyperstimulation, sonographic examination shows ovarian enlargement with a myriad of cysts. These cysts vary in size and are separated by thick septae. Follow-up scans will show gradual regression in size and number of cysts, as well as resolution of the ascites and pleural effusions (Figs 24.22A and B).

TREATING INFERTILITY

The last decade has seen a transformation in the approach to treating infertility. Increasingly assisted conception with IVF or one of its related therapeutic modalities is being used to treat infertility. These acronyms are summarized in Table 24.1

Table 24.1: Acronyms used in assisted conception[37]

IVF	*In vitro* fertilization Recovered eggs are fertilized with prepared sperm in the laboratory and transferred back to the genital tract after usually several days' culture.
GIFT	Gamete intrafallopian transfer Recovered eggs are almost immediately transferred, with prepared sperm, into the fallopian tubes, so that fertilization and early development occur in the normal situation; generally, a higher pregnancy rate than after IVF, provided the tube used is normal and normal sperm function can be assumed.
ZIFT	Zygote intrafallopian transfer IVF in which 1 day fertilized eggs, or zygotes, are transferred to the fallopian tube.
Uterine ET	Uterine embryo transfer Conventional procedure with IVF: 2-day pre-embryos are transferred through the cervix to the endometrial cavity.

Contd....

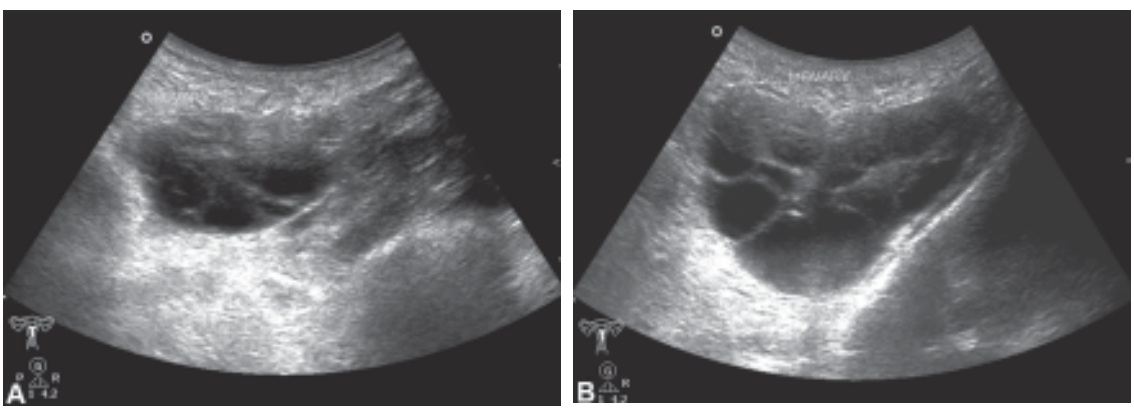

Figs 24. 22A and B: TVS scans of both ovaries in a patient on ovulation induction reveals enlarged ovaries with a myriad of cysts varying in size consistent with ovarian hyperstimulation syndrome (OHSS)

Contd....

FET, FrET	Frozen embryo transfer Transfer of IVF pre-embryos previously cryostored.
TEST	Tubal embryo-stage transfer 2-day IVF pre-embryos are transferred to the tube instead of to the uterus.
ICSI	Intracytoplasmic sperm injection Laboratory refinement for IVF in cases of severely depressed sperm function, in which a single sperm is selected and microinjected into each egg.
MESA	Microepididymal sperm aspiration A means of obtaining sperm for ICSI in men with obstructive azoospermia.
TESE	Testicular sperm extraction A means of obtaining sperm cells from testicular tubules for ICSI in some men with non-obstructive azoospermia.

Imaging has become inseparable from all modern assisted conception practices. Besides detecting pathologies like hydrosalpinx which are likely to affect the success of IVF, imaging especially TVS is crucial for the safety of ovulation induction and is widely used in oocyte retrieval.

Follicle Aspiration[15,64,65]

In the first successful *in vitro* fertilization, oocytes were collected during laparoscopy which is an expensive procedure associated with complications like peri ovarian adhesions, hemorrhage infection, etc.

Ultrasound directed follicle aspiration (UDFA) has reduced costs considerably and can be done as an out patient technique. Various approaches have been used in the past for follicular aspiration including direct transabdominal, transabdominal through full bladder, transvaginal, transvaginal/transvesical and per urethral.[15]

Oocyte collection using TVS, first described by Wikland in 1985[64] has become the technique of choice however the actual method used can be tailored according to each patient depending on where the ovaries are situated. With all these aspiration techniques, a long (30 cm) 18-gauge needle is used that is scored at the tip, which results in its enhanced sonographic visualization. The aspiration procedure is performed under local anesthesia and with supplemental intravenous or intramuscular medication.

For the transvaginal aspiration with transvaginal transducers, a needle guide is attached to the transducer/probe. This allows the needle to transverse in the beam path of the transducer. The cursor is displayed on the scanning screen, which indicates the path of the needle. After a condom containing sterile gel is placed over the transducer and a sterile needle guide is attached, the operator manipulates the transducer to optimally delineate the ovary. The desired follicle is brought into the "line of sight" and the needle is introduced transvaginally. After the initial aspiration, the follicle may be filled with buffered medium and flushed so that chances of retrieving a mature oocyte are maximized.

The technique has been associated with low complication rates which include vaginal hemorrhage and pelvic infection. When a transvesical or transurethral approach is used postoperative clot retention or occasionally urine extravasation may occur.

Ultrasound has also been used to guide embryo transfer to the uterine cavity to assist accurate placement of the embryos in the uterine cavity rather than cervical canal.

CONCLUSION

It is clear that imaging studies contribute greatly to the diagnosis and management of infertility in women. Hysterosalpingography remains the first-line radiologic examination

for most women undergoing an infertility investigation. It can show intrauterine synechiae tubal morphology such as hydrosalpinx, myomas and congenital anomalies may also be suggested. MR imaging is the most accurate examination for detection and localization of myomata and characterization of congenital malformations. This is clinically important because the location, number, and size of myomata affect the treatment of these lesions, and the correct classification of a developmental abnormality can prevent unnecessary laparoscopy and aid in appropriate surgical management. Sonography plays a vital role in monitoring ovarian follicular development in spontaneous and induced cycles and is invaluable as a guidance procedure in reproductive techniques such as oocyte collection and gamete transfer *in vitro* fertilization programs.[42.]

REFERENCES

1. Collins JI and Woodward PJ. Radiological Evaluation of Infertility : Seminars in Ultrasound, CT and MRI 1995,16(4):304-16.
2. ASRM Practice Committee. Optimal evaluation of the infertile female : Fertil Steril 2006;86(4): 264-67.
3. Thurmond AS. Imaging of female infertility Radiol Clin N Am 2003;41:757-67.
4. Jaffe SB, Jewlewicz R. The basic infertility investigation Fertil Steril 1991;56:599-613.
5. Krysiewicz S. Infertility in Women: Diagnostic evaluation with hysterosalpingography and other imaging techniques. AJR Am J Roentgenol 1992;159:253-61.
6. Winfield AC, Wentz AC. Diagnostic Imaging of Infertility. Baltimore, MD, Williams and Wilkins, 1987.
7. Moghissi K (ed). Current concepts in infertility. Clin Obstet Gynecol 1989;22:9-189.
8. Simpson WL, Beitia LG, Mester J. Hystero salpingography:A reemerging study. Radiographics 2006;26:419-31.
9. Speroff L and Fritz MA. Female Infertility. In Clinical gynecologic endocrinology and infertility. Leon Speroff and Marc A Fritz(Eds) 7th edition 2005;1013-67.
10. Grosskinsky CM, Clark RL, Wilson PA, Novotny DB. Pelvic granulomata mimicking endometriosis following the administration of oil-based contrast media for hysterosalpingography. Obstet Gynecol; 1994;83:890.
11. Nunley WC, Jr. Bateman BG, Kitchin JD, 3rd Pope TL, Jr., Intravasation during hysterosalpingography using oil-based contrast medium-a second look. Obstet Gynecol 1987;70:309.
12. Vandekerckhove P, Watson A, Lilford R, Harada T, Hughes E. Oil-soluble versus water-soluble media for assessing tubal patency with hysterosalpingography or laparoscopy in subfertile women. Cochrane Database Syst Rev: CD000092, 2000.
13. Spring DB, Barkan HE, Pruyn SC Potential therapeutic effects of contrast materials in hysterosalpingography: a prospective randomized clinical trail. Kaiser Permanente Infertility Work Group. Radiology 2000:214:53.
14. Fleicher AC, Parsons AK, Cullinan JA. Special imaging procedures in gynecology. In clinical gynecologic Imaging Fleischer AC. (Eds) Lippincott –Raven, Philadelphia 1997;315-31.
15. Steer CV, Parsons JH. Infertility In Ultrasound in Obstetrics and Gynaecology, Dewbury K, Meire H, Cosgrove D, Farrant P (Eds.) Churchill Livingstone. 2nd Edition 2001;99-122.
16. Hill LM. Transvaginal Sonography in an assisted conception program in Gyneologic imaging. John C. Anderson Eds 1999;585-599.
17. Oei SG, Helmerhorst FM, Bloemenkamp KW, Hollants FA, Meerpoel DE, Keirse MJ. Effectiveness of the postcoital test : randomized controlled trial. BMJ 1998; 317:502-5.
18. Glatstein IZ, Harlow BL, Hornstein MD. Practice patterns among reproductive endocrinologists: further aspects of the infertility evaluation. Fertile Steril 1998;70:263-9.
19. Dudiak CM, Turner DA, Patel SK et al. Uterine leiomyomas in the infertile patient : Preoperative localization with MR imaging versus US and hysterosalpingography. Radiology 1988;167: 627-30.
20. Woodward PJ. Wagner BJ, Farley TE. MR imaging in the evaluation of female infertility. Radiographics 1993:13;293-310.

21. Imaka I, Wada A, Matsuo M, et al. MR imaging of disorders associated with female infertility:use in diagnosis, treatment and management. Radiographics 2003;23:1401-21.
22. Troiano RN, Mc Carthy SM. Mullerian Duct Anomalies : Imaging and Clinical Issues Radiology 2004; 233:19-34.
23. Olphin JD, Heilbrum M. Imaging of Mullerian duct anomalies Clin Obstet Gynaecol 2007; 52(1): 40-56.
24. Deutch TD, Abuhamad AZ. The Role of 3D-USG and MR imaging in the diagnosis of MDA: a review of literature. J Ultrasound Med 2008;27(3):413-23.
25. Homer HA, Li TC, Cooke ID. The septate uterus: a review of management and reproductive outcome. Fertil Steril 2000; 73:1-14.
26. Ott DJ, Fayez JA, Zagoria RJ, (Eds). "Congenital anomalies" in hysterosalpingography: a text and atlas. 2nd edition. Baltimore, Md:Williams & Wilkins, 1998; 59-69.
27. Stampe Sorensen S. Fundal contour of the uterine cavity in the new syndrome of minor mullerian duct anomalies and oligomenorrhea : a prospective controlled study. Am J Obstet Gynecol 1983; 145:659-67.
28. Schild RL, Knobloch C, Dorn C, et al. Endometrial receptivity in an in vitro fertilization program as assessed by spiral artery blood flow; endometrial thickness, endometrial volume and uterine artery blood flow. Fertile Stezil 75(2) 2001;361-66.
29. Steer CV, Campbell S ,Tan SL, et al. The use of transvaginal colour flow imaging after in vitro fertilization to identify optimum uterine conditions before embryo transfer. Fertil Steril 1992;576;372-376.
30. Chen LW, An H.K, Chen PL, et al., Assessment of uterine receptivity by the endometrial, subendometrial blood flow distribution pattern in women undergoing in vitro fertilization – embryo transfer Fertil Steril 2002;78(2):245- 251.
31. Alcazar JL. Three Dimensional Ultrasound assessment of endometrial receptivity : a review Reprod. Biol. Endocrinol 2006; 4-56.
32. Thurmond AS, Novy MJ, Rosch J. Terburaline in diagnosis of interstitial fallopian tube obstruction. Invest Radiol 1988;23:209-10.
33. Sulak PJ, Letterie, GS, Coddington CC, et al. Histology of proximal tubal occlusion. Fertil Steril 1987;48: 437-40.
34. Thurmond AS. Selective salpingography and fallopian tube recanalization AJR. AmJ. Roentgenol 1991;156:33-38.
35. Rosch J. Thurmond AS, Vchida BT et al : Selective transcervical fallopian tube catherterization – Technique update. Radiology 1988;168:1-5.
36. Thurmond AS, Rosch J. Nonsurgical fallopian tube recanalization for treatment of infertility Radiology 1990;174:371-74.
37. Jansen RPS, Ramsay PA. Imaging in gynecologic infertility. In Gynecologic Imaging. John C. Anderson(Eds) 1999;567-80.
38. Strandell A, Waldenstrom U, Nilsson L, Hamberger L. Hydrosalpinx reduces in vitro fertilization/embryo transfer pregnancy rates. Hum Reprod 1994; 9:861-63.
39. Andersen AN, Yue Z, Meng FJ, Petersen K. Low implantation rate after in-vitro fertilization in patients with hydrosalpinges diagnosed by ultrasonography. Hum Reprod 1994;9: 1935-38.
40. Donnez J, Casanas–Roux E. Prognostic factors of fimbrial microsurgery. Fertil Steril 1986;46: 200-04.
41. Valentini AL, Muzuil L, Marana R. Improvement of hysterosalpingographic accuracy in the diagnosis of peritubal adhesions. AJR 2000; 175:1173-76.
42. Krysiewicz S. Infertility in women : Diagnostic evaluation with hysterosalpingography and other imaging techniques. AJR 1992;158:253-61.
43. Schenken RS. Endometeriosis in Scott JR, Di Saia PJ, Hammona CB, Spellacy WN eds. Danforths obstetrics and gynaecology. 8th edition. Philadelphia PA: Lippincott Williams and Wilkins, 1999; 669-75.
44. Das P, Ahuja A, Gupta SD. Incidence, etiopatho genesis and pathological aspects of genitourinary tuberculosis in India : A journey revisited. Indian J Urol 2008; 24: 356-61.
45. Merchant SA: Tuberculosis of the genitourinary system Ind J. Radiol Imag 1993;3:253-74.
46. Daly DC, Reuter K, Cohen S, et al: Follicle size by ultrasound versus cervical mucus quality: Normal and abnormal patterns in spontaneous cycles. Fertil Steril 1989;51:598-603.
47. Mendelson EB, Friedman H, Neiman HL, et al. The role of imaging in infertility management. AJR AM J Roentgenol 1985;144:415-20.

48. Parisi L, Tramoniti M, Derchi LE, et al. Polycystic ovarian disease: Ultrasonic evaluation and correlations with clinical and hormonal data. J Clin Ultrasound 1984;12:21-26.
49. El Tabbakh GH, Lofty I, Azab I, et al. Correlation of sonographic ovarian disease and the clinical, hormonal, and laparoscopic findings. Am J Obstet Gynecol 1986;154:892-95.
50. Yeh H-C, Futterweit W, Thornton JC. Polycystic ovarian disease: US features in 104 patients. Radiology 1987;163:111-16.
51. Pache TD, Wladimiroff JW, Hop WCJ, et al. How to discriminate between normal and polycystic ovaries: Transvaginal US study. Radiology 1992;183:421-23.
52. Fleischer AC, Daniell JF, Rodein J, et al. Sonographic monitoring of ovarian follicular development. J.Clin Ultrasound 1981;9:275.
53. Fleischer AC Herbert CM,GA, et al. Transvaginal sonography of the endometrium during induced cycles. J Ultrasound Med 1991;10:93-95.
54. Haning RV, Zwiebel WJ: Ultrasound assistance in clinical management of infertility. Semin Ultrasound CT MR 1983;4:226-34.
55. Hann LE, Crivello M, McArdle C, et al. In vitro fertilization: Sonographic perspective. Radiology 1987;163:665-68.
56. Shmorgun D, Hughes e E, Mohida P, Roberts R. Prospective cohort study of three versus two dimensional ultrasound for prediction of oocyte maturity. Fertil Steril 2009 Jan. E pub ahead of print.
57. Campbell S, Bourne TH, Waterstone J, et al. Transvaginal colour blood flow imaging of the periovulatory follicle. Fertil Steril 1993;60:433-38.
58. Taylor KJW, Wells PNT, Conway Pl. Ultrasound Doppler flow studies of the ovarian and uterine arteries. Br J Obstet Gynaecol 1985;92:240-46.
59. Deutinger J, Reinthaller A, Bernaschek G. Transvaginal pulsed Doppler measurement of blood flow velocity in the ovarian arteries during cycle stimulation and after follicle puncture. Fertil Steril 1989;51:466-70.
60. Collins W, Jurkovic D, Bourne T, et al. Ovarian morphology, endocrine function and intra-follicular blood flow during the peri-ovulatory period. Hum Reprod 1991;6:319-24.
61. Takasaki A, Gamura H, Taniguchi K, et al. Luteal blood flow and luteal function. J. Ovarian Res. 2009; 2:1.
62. Cowan BD: Ovarian hyperstimulation syndrome. Female Patient 1991;16:37-44.
63. Ranking RN, Hutton LC. Ultrasound in the ovarian hyperstimulation syndrome. J Clin Ultrasound 1981;9:473-476.
64. Wikland M, Lenmart E, Hamberger L Tranvesical and transvaginal approaches for the aspiration of follicles by the use of ultrasound. NY Sci 1985;442:182.
65. Fleishcer AC, Vasquez JM, Kepple DM. Transvaginal Sonography in gynaecologic fertility disorders. In clinical gynecologic Imaging Fleischer AC. (Eds.) Lippincott –Raven, Philadelphia 1997;273-314.

Chapter

25

Benign Diseases of the Female Pelvis

Alpana Manchanda, Veena Chowdhury

Ultrasonography is the primary modality for evaluating gynecological abnormalities as it adequately depicts normal and pathological anatomy. Ultrasound provides useful information in confirming the presence or absence of a pelvic mass, determining its site of origin and precise relationship to other pelvic organs, and evaluating the morphologic characteristics of the mass along with delineating ascites or adenopathy or other features suggesting malignancy. The diagnostic sensitivity and specificity of sonography has increased with the advent and increased use of high resolution transvaginal probes.

Color Doppler sonography (CDS) and sonohysterography (SHG) are useful adjuncts to conventional grey scale ultrasonography in the evaluation of gynecologic disorders and can be helpful in clarifying the etiology of some of the masses with nonspecific morphological features. CT often provides diagnostic information in patients who have suspected pelvic masses in whom the initial ultrasound has proved equivocal as it is capable of detecting adenopathy, assessing fat planes and extent which are important in the staging of malignancy.

Magnetic resonance imaging (MRI) can reliably diagnose several benign lesions such as congenital anomalies of the uterus, leiomyomas, adenomyosis, dermoid cysts and in some cases of endometriomas.

BENIGN UTERINE LESIONS

Congenital Uterine Anomalies

Congenital uterine anomalies represent a spectrum of morphological abnormalities that result from nondevelopment or varying degrees of nonfusion of the mullerian ducts and occur in 1 percent-15 percent of women.[1] The clinical classification of mullerian duct anomalies follows the guidelines proposed by Buttrams and Gibbons.[2] The classification was modified by the American Fertility Society in 1988 (now the American Society of Reproductive Medicine ASRM) and is the most widely accepted scheme for classifying Mullerian duct anomalies[3] (Table 25.1).

Classification

Congenital anomalies of the female reproductive tract are frequently associated with renal anomalies, especially renal agenesis or ectopia.[4] Renal anomalies may be present in upto 50 percent of patients.[5] Therefore, in individuals with suspected mullerian duct anomalies, the kidneys should be evaluated as well. Patients with uterine anomalies may

Table 25.1: American fertility society (AFS) classification of congenital uterine anomalies

Class	*Anomaly*	*% of Anomalies*
Class I	Agenesis/hypoplasia	10%
Class II	Unicornuate uterus	15-20%
Class III	Uterus didelphys	5-7%
Class IV	Bicornuate uterus	10%
Class V	Septate uterus	55%
Class VI	Arcuate uterus (considered a normal variant)	
Class VII	Uterine anomalies associated with DES exposure	1%

be completely asymptomatic as in uterus didelphys or they may result in infertility or spontaneous abortion. Septate uterus is associated with a higher rate of reproductive failure.[6,7] Patients may present at puberty with primary amenorrhea, pelvic mass or pain. MR is helpful in these patients of primary amenorrhea as it can determine the presence or absence of the vagina, cervix or uterus. In addition, MR can reveal the level of obstruction and whether retrograde menstruation has resulted in hematosalpinx.[3]

Hysterosalpingography (HSG) and ultrasound have been the primary imaging modalities, but each has its own-limitations. HSG permits the contour of the endometrial cavity to be defined, but its relationship to the myometrium cannot be determined. Hence HSG cannot always differentiate between a septate and bicornuate uterus (Fig. 25.3A). Conventional two-dimensional sonography is helpful in identifying two horns of a uterus, but the distinction between the above two conditions cannot be generally made. Before the advent of MRI, diagnosis was often possible only on laparoscopy or surgery. MRI has proved to be an accurate and noninvasive means of evaluating patients with congenital anomalies, allowing precise classification. The introduction of three-dimensional ultrasound allows identification of congenital uterine anomalies, thus replacing the use of MRI in this field.

Class I: Mullerian Agenesis or Hypoplasia

Uterine agensis or hypoplasia results from non-development or rudimentary development of the mullerian ducts. A subtype of uterine agenesis is the Meyer–Rokintansky–Kuster–Hauser(MRKH) syndrome which has an incidence of approximately 1 in 5,000.[8] This syndrome results in failure of development of upper two-thirds of vagina, cervix and uterus. Ovaries are intact and are associated with variable anomalies of the urinary tract and skeletal system. [5] The T2-weighted sagittal images are most useful for identifying the presence of a uterus. Vaginal agnesis is best characterized on the axial plane with no normal vaginal zonal anatomy identified between the rectum and the urethra (Figs 25.1A to C). The main advantage of MRI compared with other modalities is its ability to differentiate complete from segmental uterine agenesis. Uterine hypoplasia is diagnosed when the uterus is small in size and the myometrium is of lower than normal signal intensity. In addition, the endometrial cavity is small and inter cornual diameter is less than 2 cm with poorly differentiated zonal anatomy. [9]

Class II: Unicornuate Uterus

A unicornuate uterus results from non-development or rudimentary development of one mullerian duct while the other one elongates normally. The characteristic appearance on MRI is the "*banana*" shaped uterine cavity with maintained zonal anatomy although the uterine volume is reduced.[2] If a rudimentary horn is present,

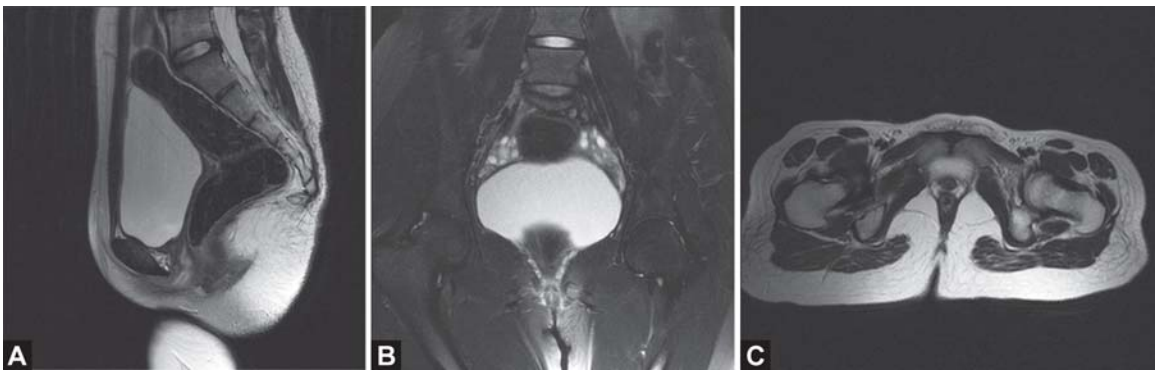

Figs 25.1A to C: (A and B) T2 W sagittal and coronal MR images show absence of uterus and cervix with normal morphology of both ovaries. **(C)** T2 W axial image shows lower one-third of vagina between the bladder and rectum – uterine agenesis

MRI can usually distinguish it from an adnexal mass suspected on ultrasound, as well as determine if there is endometrium contained within it and if it communicates with the unicornuate uterus.

Women with a non-communicating rudimentary horn are at a risk of endometriosis while an ectopic or ruptured pregnancy may result if the rudimentary horn communicates with the opposite normal horn. Thus, a rudimentary horn should be removed to prevent these complications.[8] Renal agenesis or other anomalies when present are generally located ipsilateral to the small or absent uterus.

Class III: Uterus Didelphys

The didelphys uterus results from non-fusion of the two mullerian ducts. Two separate normal sized uteri and cervices are demonstrated on MRI, with a septum extending upto the upper vagina. The two uteri are usually widely separated with preservation of the endometrial and myometrial widths and no communication between the endometrial cavities. While the horns in uterus didelphys are widely divergent, the cervices are often closely approximated and may show a minor degree of fusion along their medial margins. A longitudinal vaginal septum is present in 75 percent of cases and occasionally a transverse vaginal septum may be present causing obstruction of the hemi uterus resulting in hematometrocolpos[3] (Fig. 25.2A to C).

Class IV: Bicornuate Uterus

Partial fusion of the mullerian ducts produces the bicornuate uterus, with the resulting septum being composed of myometrium. It may be bicornuate unicollis in which the myometrial septum extends to the internal os or bicornuate bicollis where it extends as far as the external os. On T2-weighted axial MR images, two uterine horns are visualized, each containing an endometrial cavity, with the separating myometrium having a high signal intensity. In addition, MR may also document an outward fundal concavity in bicornuate uterus as opposed to the convexity seen in a normal uterus. The depth of the intervening cleft separating the uterine horns in the external fundal myometrium is greater than 1 cm (Figs 25.3A to C).[3] Normal zonal anatomy is seen in each horn.

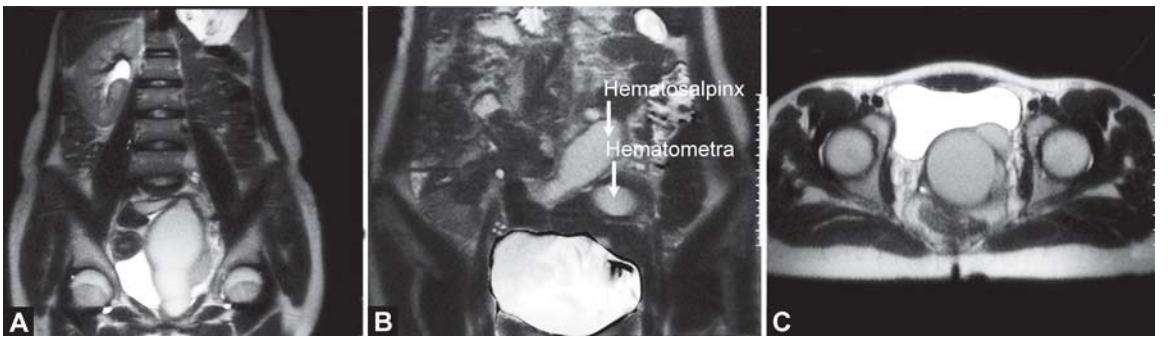

Figs 25.2A to C: (A) T2 W coronal MR image reveals complete duplication of uterus with normal morphology of right sided uterus. The left uterus and vagina are distended with hyperintense contents – Hematometrocolpos. Left kidney is absent. **(B)** T2 W coronal shows a hyperintense tubular structure on the left side - hematosalpinx along with hematometra. **(C)** Axial T2W image shows complete duplication of vagina with hematocolpos on the left with normal vagina on the right with thin, central luminal hyperintensity: Uterus didelphys with obstructed left side system with associated developmental absence of left kidney

Class V: Septate Uterus

Septate uterus is the most common congenital anomaly representing approximately 55 percent of all anomalies. Septate uterus is due to incomplete resorption of the final fibrous septum between the two mullerian ducts. It may be complete or partial. Complete septate uterus is one wherein the septum extends to the external os. While in partial septate uterus, septum extends to any level proximal to the external os. The external uterine contour is convex, flat or mildy concave, with the fundal indentation less than or equal to 1 cm.[3] The uterine septum is of low signal intensity on both T1 and T2 weighted images in contrast to the medium to high signal intensity myometrium separating the two endometrial cavities in the bicornuate uterus (Figs 25.4A and B). The differentiation between septate uterus and bicornuate uterus is clinically significant because of their different complications and different treatment.

Evaluation of the external fundal contour is the most important feature for distinguishing a bicornuate uterus from a septate uterus. This can be well defined by transvaginal sonography, 3D ultrasonography and magnetic resonance imaging, which show both the external contour of the fundus as well as the nature of the dividing tissue.

Table 25.2 lists the differentiating features between septate and bicornuate uteri.

Table 25.2: Distinguished features between septate and bicornuate uteri

Features	*Septate Uterus*	*Bicornuate Uterus*
1. Depth of fundal cleft	≤ 1cm	> 1cm
2. Fundal contour	convex/flat	Deep fundal concavity
3. Intercornual angle	< 75°	>105°
4. Intercornual distance (T2 W coronal MR image)	< 4 cm	> 4 cm
5. Intercornual tissue	Fibrous or myometrial	Myometrial tissue

The nature of tissues separating the two endometrial cavities has been used to distinguish between septate and bicornuate uteri but has been found to be a less reliable feature than the external shape of the uterus. Typically a fibrous septum defines the septate uterus which whill appear hypoechoic compared to myometrium on TVS and

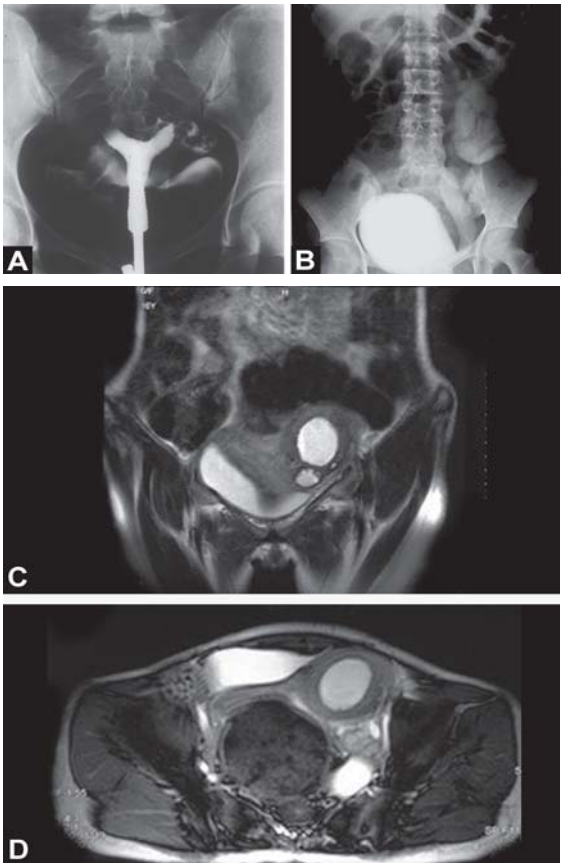

Figs 25.3A to D: (A) HSG showing two separate uterine cavities. The left fallopian tube is visualized with intraperitoneal spill while the right tube is not visualized Bicornuate/septate uterus. **(B)** IVP in another patient reveals malascended left kidney with Grade IV HUN with ectopic low insertion of left ureter in retropubic region. **(C and D)** Coronal and axial T2W MR images of same showing two separate uterine horns with dilated and high SI endometrial collection in left horn suggestive of hematometra with small right horn with thinned endometrium. Fundal contour is concave, best appreciated on the coronal image-Bicornuate uterus

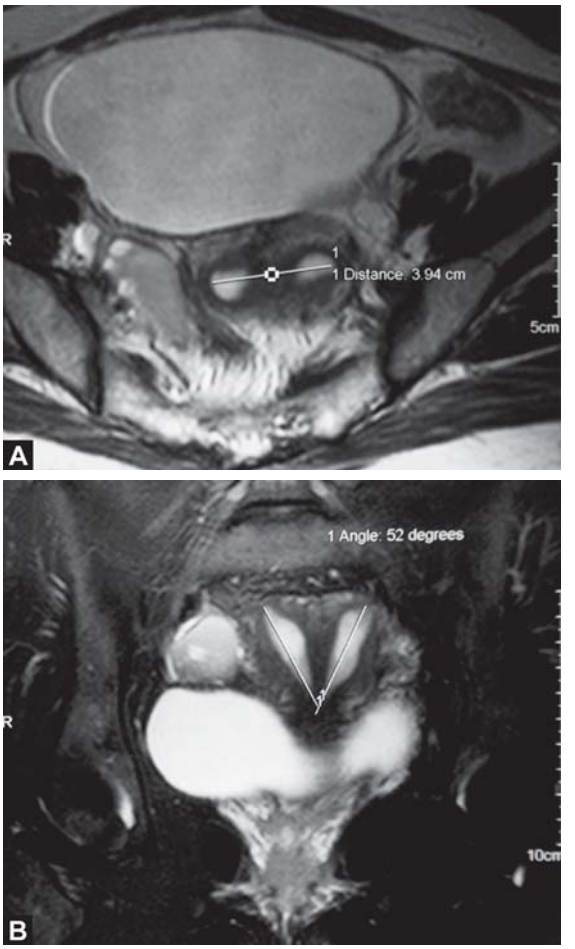

Figs 25.4A and B: (A) T2 W axial MR image shows two endometrial cavities with an intercornual distance < 4cm with hypointense septum separating them. **(B)** T2 W coronal image depicts the two uterine cavities separated by a vertical septum extending from the fundus to above the internal os with an intercornual angle < 75°. Also seen is a right hemorrhagic ovarian cyst –Septate uterus

hypointense on all MR pulse sequences. In contrast, a myometrial septum occurs only in a bicornuate uterus and would appear isoechoic or isointense to myometrium. However, a considerable overlap in the imaging features of the dividing tissues in these two entities have been found.[9]

Class VI: Arcuate Uterus

An arcuate configuration of the uterus is considered a normal variant and is not associated with an increase risk of infertility or pregnancy loss. It results from a near complete resorption of the uterovaginal

septum, leaving a mild concave indentation at the level of the fundus. On imaging, the external uterine contour is usually flat or convex, though it may be slightly concave. There is a broad, smooth indentation of the myometrium on the endometrium in the fundal region with normal zonal anatomy being maintained. Also there is no evidence of a low signal appearing fibrous component.

Class VII: Diethylstilbestrol Exposed Uterus

Diethylstilbestrol (DES) is a synthetic estrogen that was used in the 1950's and 1960's to prevent recurrent spontaneous abortions and poor reproductive outcomes in patients. This drug has been associated with congenital anomalies of the female genital tract in the offspring of women exposed in the first trimester. Uterine malformations include narrowed, irregular endometrial cavities with constriction bands ("T" configuration), small hypoplastic uterus. Fallopain tubes can demonstrate stenosis, sacculations and shortening.[3] These anomalies of uterine shape are demonstrable by hysterosalpingography and MR imaging. They are not associated with any urinary tract abnormalities.[10]

Leiomyomas

Leiomyoma (fibroid) of the uterus is the most common gynecologic disorder occurring in 20 to 40 percent of all women during their reproductive years. It is a benign uterine tumor and consists of predominantly smooth muscle with varying amounts of fibrous and connective tissue.[11] These tumors are estrogen-dependent, hence there is an increased prevalence of leiomyomas in patients with diseases associated with hyperestrogenism such as endometrial hyperplasia, endometrial cancer, anovulatory states.[10] Leiomyomas may increase in size during pregnancy and decrease in size after menopause. Most women with leiomyomas are asymptomatic although some may have signs and symptoms of pelvic mass, pain, abnormal bleeding and pressure effect on adjacent pelvic organs. They are usually well-circumscribed and surrounded by a pseudocapsule. Majority of the leiomyoma are found within the uterine body (90%), with a small proportion found within the cervix or broad ligament. Myoma may be solitary or multiple and occur in submucosal, intramural or subserosal locations (Figs 25.5A and B). It often calcifies in postmenopausal women and large tumors may develop hyaline, myxomatous, cystic or hemorrhagic degeneration.

The sonographic appearance of uterine fibroid depends on its relative composition of smooth muscle and fibrous tissue and on the presence and nature of degeneration. These masses may be difficult to detect with ultrasonography because of variable patterns of echogenicity which may range from hypoechoic to echogenic, homogeneous to heterogeneous, with or without acoustic shadowing. It may present with uterine enlargement or distort the uterine contour. The most common appearance of a leiomyoma is that of a well-marginated, hypoechoic round or oval mass within the uterine body.[5] Intense shadowing may represent calcification.[12,13] Calcified myoma have a typical appearance on plain radiograph of the abdomen(Fig. 25.6).

Distortion of the endometrial complex is helpful in identifying a submucosal component. Submucosal leiomyomas may mimic endometrial lesions and sonohysterosalpingography may help in differentiating the

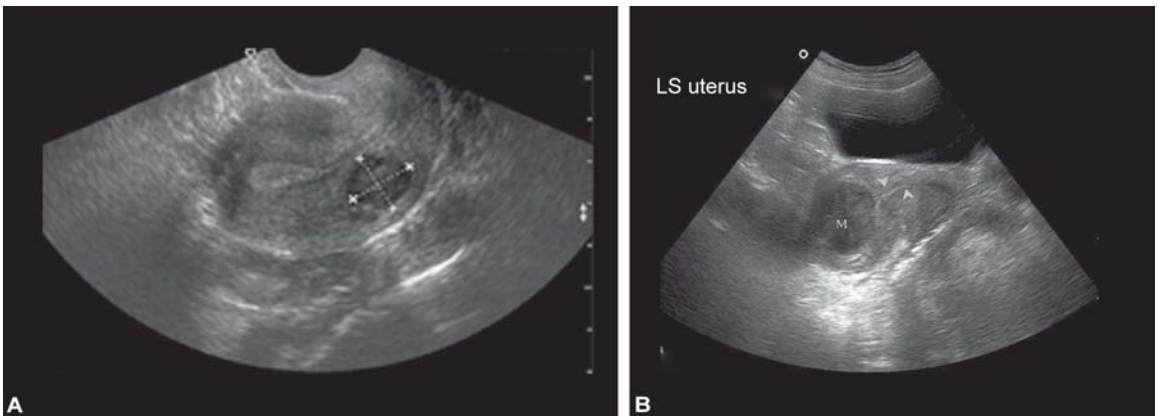

Figs 25.5A and B: Uterine fibroids– TVS shows **(A)** Well-defined, round, hypoechoic mass in posterior myometrium – Intramural fibroid. **(B)** LS of the uterus reveals homogeneous, hypoechoic well marginated round to oval mass lesion in the fundus of uterus displacing the endometrium inferiorly – Submucosal fibroid

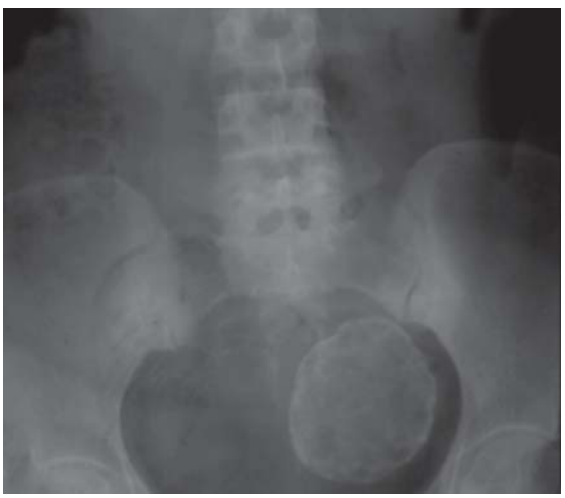

Fig. 25.6: Plain X-ray pelvis shows a large calcified fibroid in the pelvis

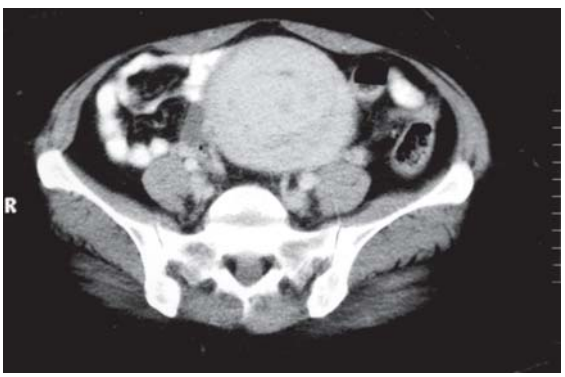

Fig. 25.7: CT scan through the lower abdomen shows leiomyoma as a well-defined rounded lesion with homogeneous contrast enhancement with few small hypodense areas within

two. Submucosal fibroids are usually broad based hypoechoic masses with an overlying layer of echogenic endometrium.[14]

The characteristic CT features of uterine leiomyoma is an enlarged uterus with solid enhancing mass (Fig. 25.7) having a lobulated contour with speckled, whorled, streaked or curvilinear calcification. The presence of dystrophic calcification is the most specific sign of leiomyoma.[15] However, calcification is only seen in 10 percent of cases. Other CT features suggestive of a uterine leiomyoma are soft tissue masses that distort or obliterate the uterine cavity and irregular low density areas within uterine masses representing degeneration of a leiomyoma.[16] However, if there is no calcification, myoma cannot be distinguished from carcinoma on the basis of attenuation values. In the absence of calcification both ultrasound and MRI are superior to CT for demonstrating myomas.

MRI is indicated when the ultrasound examination is indeterminate or limited as in retroflexed uterus.[17]

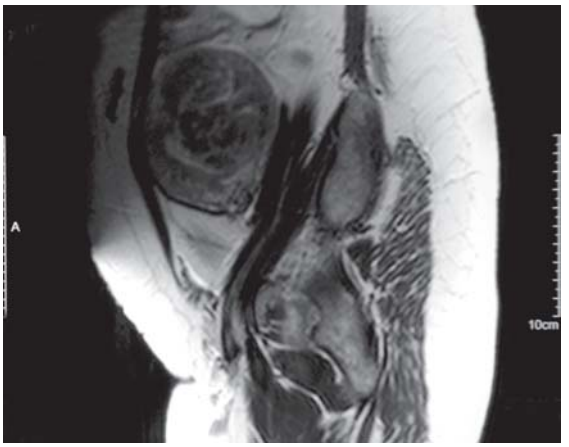

Fig. 25.8: T2W sagittal image of pelvis reveals a large, well-defined low signal intensity mass in the posterior myometrium with typical whorled internal appearance abutting the endometrium – Intramural fibroid

Magnetic resonance imaging offers the most sensitive imaging of leiomyomas, being able to identify lesions as small as 0.3 cm. Leiomyoma is typically seen as sharply marginated homogeneous areas of very low signal intensity on T2-weighted sequences and isointense to myometrium on T1-weighted sequences (Fig. 25.8). The characteristic low signal intensity on T2- W1 is due to the presence of compact, smooth muscle myoma cells and a paucity of intercellular matrix.[7] They are well circumscribed with well defined margins. The appearance of leiomyoma after the administration of gadolinium is variable. On postcontrast T2-weighted images, leiomyoma most often appear of lower signal intensity relative to the myometrium or endometrium. The presence of calcification usually causes areas of signal void on both T1 and T2-weighted images, but unlike CT the finding is not specific. Thin, hyperintense rims are sometimes seen, as well as internal signal heterogeneity due to hyaline or myxoid degeneration.[18]

MR imaging facilitates the differentiation of a pedunculated leiomyoma from an adnexal mass on basis of typical signal intensity and morphology.[19] An MR feature of exophytic leiomyomas is the "bridging vessel sign" which refers to the presence of flow voids on T1 and T2 weighted images from branches of the uterine artery that are localized between the mass and the uterus. This indicates that the tumour is supplied by branches of the uterine artery. It is the only non-invasive means available for differentiating a leiomyoma from adenomyosis and is useful in patients considered for myomectomy as it precisely determines the location and number of leiomyomas.[20]

Hemorrhagic, cystic and fatty degeneration are the three types of degeneration in fibroids that have suggestive MR features. Hemorrhagic degeneration of fibroids is uncommon and is associated with leiomyomas during pregnancy. Leiomyoma with hemorrhagic "red degeneration" often reveal peripheral or central high SI on T1-W images secondary to methemoglobin and show minimal enhancement[8] 5 percent of fibroids have foci of cystic degeneration which on MR imaging appears as very high SI on T2 W images and also do not enhance after contrast. Falty degeneration of a leiomyoma into a lipoleiomyoma is rare and has an incidence of less than 0.5 percent.[8] The fat tissue within the myoma can be detected and characterised using fat suppression techniques. CT is also very sensitive in identifying fat attenuation within a lipoleiomyoma (Fig. 25.9).

Malignant degeneration is rare (0.1-0.6%) but should be suspected if a leiomyoma enlarges suddenly,[21] or if an indistinct border or irregular contour is noted on MR imaging.[22]

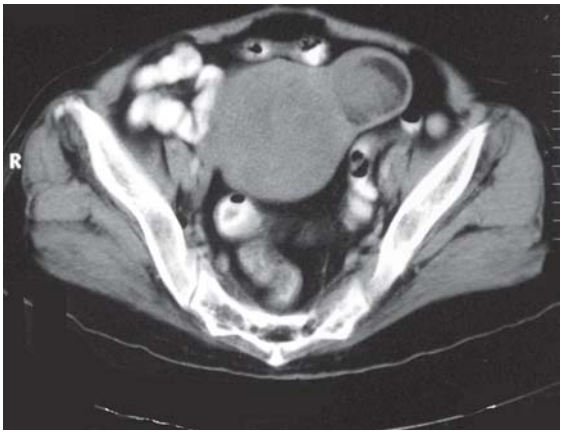

Fig. 25.9: CT scan of the pelvis showing a lobulated uterine mass with fatty degeneration–Lipoleiomyoma

Treatment of uterine leiomyomas – Most leiomyomas are asymptomatic and therefore do not require any treatment. Multiple treatment options are available for women who are symptomatic. The surgical options include hystrectomy and myomectomy. Myomectomy can be via laprotomy, laproscopic or hysteroscopic route. Non surgical treatments include uterine artery embolization (UAE) and medical therapy. Hystrectomy is an effective treatment for symptomatic fibroids and routinely performed in patients with pain and abnormal bleeding. Patients with one or two submucosal myomas are likely to benefit from hysteroscopic resection following which a cessation of excess bleeding and restoration of fertility may be seen.

UAE has become an alternative noninvasive treatment of symptomatic uterine fibroids. When compared with myomectomy, it has been found to be a better treatment option for fibroid related menorrhagia and equivalent method for reducing pain.[23]

MR angiography provides information to determine which patients are potential candidates for UAE therapy. MR can document the size, number, location and vascularity of uterine leiomyomas. Women with large (> 10 cm) leiomyomas have been found to have equally good results after UAE as those with smaller myomas. One sub-type that has shown poor response to UAE is leiomyomas with high SI on T1W images and minimal or no enhancement.[24] This is likely because the high SI myomas have already undergone ischemia/hemorrhagic necrosis and will not lose additional vascularity or volume with additional embolization.[25] Conversely, the best response to UAE therapy is seen in those myomas that show marked enhancement after contrast administration.

Contrast enhanced MR angiography (CE-MRA) can reveal the presence of normal uterine arteries. If a separate gonadal arterial supply to the uterus is seen on CE MRA, then one should consider embolizing the gonadal artery at the time of UAE. Failure to embolize the gonadal artery that directly supplies the uterus, has been seen to be a cause of UAE failure. [26]

After UAE, MR can document a decrease in size and enhancement of fibroids, preserved enhancement of remainder of the uterus and lack of visualization of the uterine arteries on an MRA study. An MR performed immediately after UAE showing decreased enhancement of the fibroids correlates, with a subsequent successful clinical response.[25] A decrease in volume of fibroids by 40 to 60 percent and a decreased enhancement of fibroids has been documented by MR following UAE correlating with the successful necrosis.[24]

OTHER BENIGN MESENCHYMAL TUMORS

Fatty or mixed mesenchymal tumors such as fibromyolipoma, myolipoma and lipoma of

the uterus are rare benign tumors.[27] They may arise from metaplasia of connective tissue or smooth muscle cells.

Sonographically, lipoma is seen as a rounded lesion of central increased echogenicity with a hypoechoic rim.[28] On CT, the encapsulated fat density of uterine lipoma mimics the more common ovarian dermoid (benign cystic teratoma).[29] Proper diagnosis of these lesions is important because teratomas are generally managed by surgical excision, whereas lipomatous uterine tumors require no therapy unless symptomatic.

Adenomyosis

Adenomyosis is the presence of ectopic endometrial glands and stroma with surrounding smooth muscle hyperplasia within the myometrium. It occurs due to direct invasion of the basal endometrium into the myometrium and may be microscopic, focal or diffuse.[30] Diffuse form is more common and is composed of widely scattered foci of adenomyosis distributed asymmetrically within the myometrium, while the focal or nodular form is composed of circumscribed nodules called adenomyomas within the inner myometrium.[14] Adenomyosis is frequently accompanied by additional pelvic abnormalities such as uterine myomas and it occurs concomitantly in 6-20 percent patients with endometriosis.[30] It is frequently diagnosed in multiparous, premenopausal women, with clinical presentation mimicking leiomyomas or dysfunctional bleeding. Establishing the correct diagnosis is essential, as treatment of these three entities differs markedly. The definitive treatment of adenomyosis is hysterectomy, dysfunctional uterine bleeding may be controlled with dilatation and curettage and symptomatic leiomyomas may be removed via myomectomy.

Sonography shows an enlarged uterus without focal masses, more often seen to involve the posterior uterine wall.[31] The uterus has a globular configuration. On transabdominal sonography, the features suggestive of adenomyosis are a diffuse uterine enlargement with a normal contour, normal endometrial and myometrial texture. Other findings that have been described are thickening of the posterior myometrium with the involved area being slightly more anechoic than normal myometrium.[14] Transvaginal sonography (TVS) has been found to be more accurate in the diagnosis of adenomyosis.[32] On TVS the findings include (i) poorly defined hypoechoic myometrium, (ii) heterogeneous myometrial echotexture, (iii) assymmetrically thickened myometrial wall (iv) shaggy endometrium with poor definition between endometrium and myometrium, (v) scattered small (< 5 mm) myometrial cysts.[33]

The focal and nodular involvement of the myometrium is called adenomyoma. Two sonographic features used to characterize an adenomyoma are indistinct margin and presence of hypoechoic lacunae in the hyperechoic myometrium with several cysts.[33] These two criteria have enabled correct diagnosis with TVS in 95 percent cases.

MR can detect and characterise adnomyosis accurately. On T2-weighted images, focal adenomyosis appears as an ill-defined poorly marginated area of low signal intensity within the myometrium but continuous with the junctional zone–JZ (inner myometrium). The junctional zone may be evenly or irregularly thickened with a thickness of > 12 mm considered abnormal.[34] Occasionally small foci (2-4 mm)of increased signal intensity in both T1 and T2-weighted images are seen within the thickened

junctional zone that pathologically correspond to small foci of hemorrhagic endometrium (Figs 25.10A to C). MR imaging is highly accurate in diagnosing adenomyosis from leiomyomas.[35,36] MR can more accurately diagnose adenomyosis than can TVS, especially in women with coexistent leiomyomas.[8] Focal adenomyosis often has an ill-defined border and is always contiguous with the junctional zone which is frequently thicker than 12 mm, whereas the border around leiomyomas is sharp.[35] An irregular interface between endometrium and adenomyosis is typical. T2W images will show a relatively homogeneous, low intensity mass, but the SI is not as low as that with leiomyomas. [10] Adenomyosis is often oriented parallel to the endometrial stripe and has minimal mass effect on the endometrial canal while leiomyomas do show mass effect.[37]

The Table 25.3 below shows the differentiating features between adenomyosis and leiomyomas.

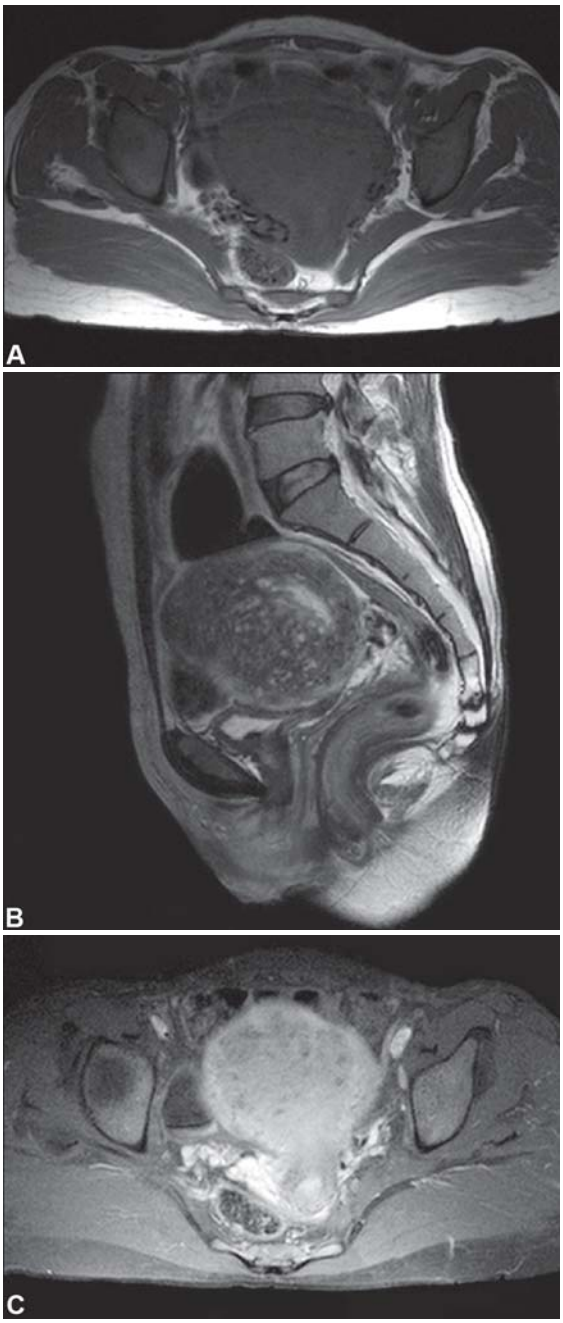

Figs 25.10A to C: Axial and sagittal T1, T2 and postcontrast images reveal bulky uterus with thickening and heterogeneity of junctional zone (JZ), poorly defined endomyometrial junction, multiple small T2 hyperintense foci in JZ showing heterogeneous contrast enhancement – Diffuse adenomyosis

Endometrial Polyps

Endometrial polyps are localized hyperplastic overgrowth of endometrial glands and stroma which are covered by endometrium and almost always benign. Endometrial polyps may be sessile or pedunculated and are usually attached to the uterine fundus. They may be small or so large as to protrude through the cervical os into the endocervical canal (Fig. 25.11A and B). There are three types of polyps: hyperplastic (resembling glands of endometrial hyperplasia), atrophic (cystically dilated atrophic glands), and functional (undergo cyclical endometrial changes). Endometrial polyps are common, being found in perimenopausal and postmenopausal women, with 20 percent to be multiple in the affected women. Most polyps are asympto-

Table 25.3: Differentiating features between adenomyosis and leiomyomas

Features	*Adenomyosis*	*Uterine leiomyoma*
Margins	Poorly defined	Well circumscribed
Center	Junctional zone	Any layer of uterus, originates in myometrium
Appearance	Focal or diffuse	Focal
T2 signal intensity	Small hyperintense foci	Hypointense unless degeneration present
Thickened junctional Zone	Yes (>12mm)	No
Mass effect on endometrium	Minimal or none	+ if intracavitary or submucosal

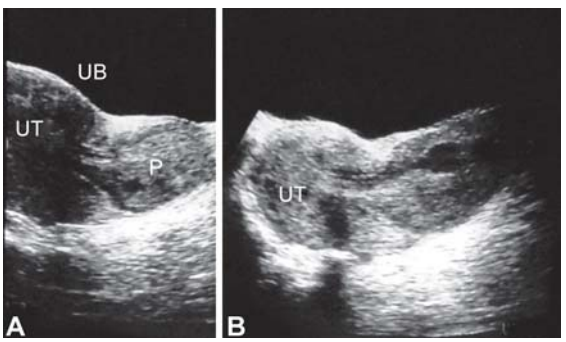

Figs 25.11A and B: (A) TAS showing a well defined oval mass in the cervix with its stalk extending into the endometrial cavity – Endometrial polyp. **(B)** small cyst is seen in the lower part of the polyp with multiple myometrial fibroids

matic, however when symptomatic, may cause menorrhagia, intermenstrual bleeding or postmenopausal bleeding. Women on tamoxifen therapy for breast cancer treatment have an increased relative risk for developing endometrial polyps. A spectrum of endometrial abnormalities like proliferative changes, hyperplasia, polyps and cancer have been reported with tamoxifen.[3]

Ultrasound features include nonspecific thickened endometrium, a focal echogenic area in the endometrium or occasionally an endocavitary mass surrounded by fluid indistinguishable from carcinoma.[38] Sonohysterography is an ideal technique for demonstrating a polyp. This is because a polyp seen as a round echogenic mass within the endometrial cavity is much more easily identified when there is fluid in the endometrial cavity outlining the mass. A submucosal fibroid may mimic an endometrial polyp but may be differentiated by a broader base and more irregular contour of the former on sonohysterography. A normal layer of endometrium is seen overlying a submucosal fibroid while the polyp can be seen arising from the endometrium.[14] Cystic areas may be see within a polyp, representing the histologically dilated glands. With Color Doppler, a feeding artery may be seen in the pedicle of the polyp.[39] On MR imaging, endometrial polyps have a variable appearance and may be seen as low/intermediate signal masses within the endometrial cavity on T2W images and appear isointense to the endometrium on T1W images. Contrast enhanced MRI has been reported to improve the sensitivity of their detection, polyps generally enhancing less than the surrounding endometrium, but more than the myometrium[40] (Figs 25.12A to C). Most endometrial polyps can be reliably differentiated from submucosal leiomyomas on MR imaging with leiomyomas appearing lower in signal intensity than polyps and being myometrial in origin. However, in case of a degenerated submucosal fibroid, the signal intensity of the two may overlap.[3]

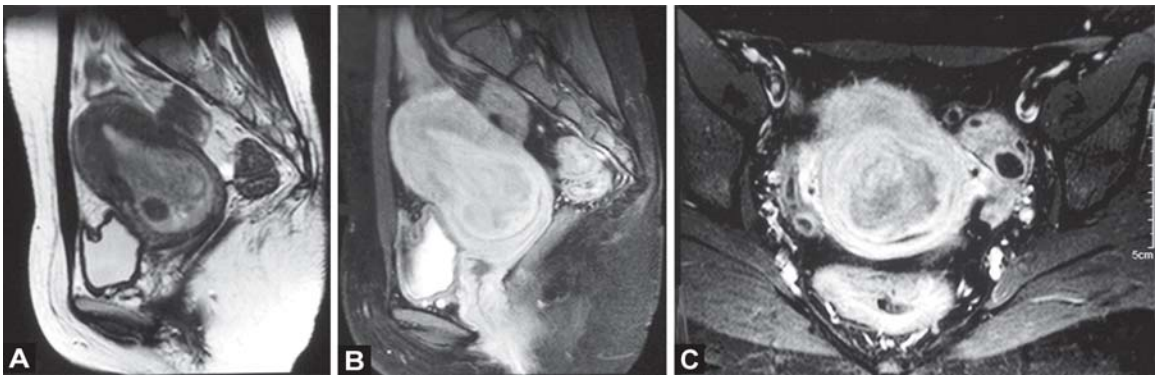

Figs 25.12A to C: T2 sagittal and T1 postgadolinium images reveal a large, round to oval well-circumscribed polypoid mass hyperintense on T2W image in the endometrial cavity with widening of the cavity and extending into the lower uterine segment with heterogeneous contrast enhancement–Endometrial polyp

Endometrial Hyperplasia

Endometrial hyperplasia is the excessive proliferation of the endometrial glands, with an increase in endometrial gland-to-stromal raito when compared with normal proliferative endometrium.[14] It may be focal or diffuse and is most often the result of unopposed estrogen stimulation (chronic anovulatory states, obesity, tamoxifen therapy) Women with endometrial hyperplasia commonly present with postmenopausal bleeding. Histologically, endometrial hyperplasia can be divided into hyperplasia without cellular atypia and hyperplasia with cellular atypia(atypical hyperplasia) with 25 percent of the latter sub-group progressing to endometrial cancer. Each of these types may be further subdivided into simple (cystic) or complex (adenomatous) hyperplasia depending on the glandular complexity. In simple (cystic) hyperplasia, there is cystic dilatation of the glands with surrounding abundant cellular stroma while in complex (adenomatous) hyperplasia, the glands are crowded with little intervening stroma.

The cut-off value for normal versus abnormal endometrial thickeness is controversial, but is a function of the patients hormone status [i.e. premenopausal, postmenopausal with or without hormone replacement therapy (HRT)]. On ultrasonography, a bilayer endometrial width greater than equal to 5 mm is regarded as abnormal in symptomatic postmenopausal women. In asymptomatic postmenopausal women on HRT, cut off values range from < 5 to > 8 mm while in premenopausal women an endometrial thickness greater than 8 mm in the proliferative phase and greater than 16 mm in the secretory phase is considered abnormal. [41]

Both TVS and sonohysterography are the modalities of choice for screening of endometrial pathology. A focal or diffuse thickening of the endometrium is seen which is usually thick and echogenic (Fig. 25.13). Small cysts may be seen within the endometrium in cystic hyperplasia. As the sonographic appearance is non-specific, biopsy is necessary for diagnosis.

On MR imaging, endometrial hyperplasia appears as a diffuse widening of the endometrium with the signal intensity of the hyperplastic endometrium appearing hypo to isointense relative to normal endometrium. Small, high signal intensity cystically dilated

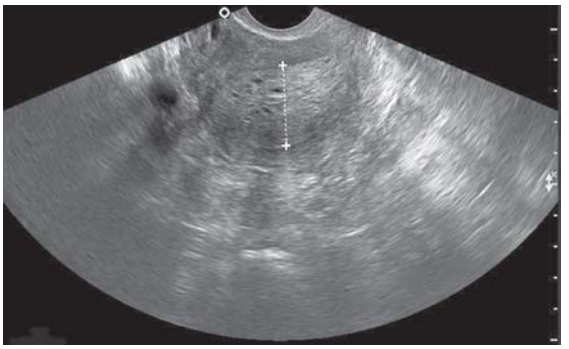

Fig. 25.13: TVS reveals diffuse thickened echogenic endometrium with small cysts within–Endometrial hyperplasia

glands may be seen within it. Follwing contrast administration, the endometrial hyperplasia enhances less than the adjacent myometrium.[3]

Endometrial Synechiae

Endometrial synechiae/adhesions (Asherman's syndrome) are bridging bands of tissue in the endometrial cavity which occur in response to trauma (post-curettage), infection or inflammation. They may be a cause of infertility or recurrent pregnancy loss. The sonographic diagnosis is difficult unless fluid is distending the endometrial cavity. The endometrium usually appears normal on transabdominal sonography. On TVS, adhesions may be seen as irregular, hypoechoic bridgelike bands within the endometrium which are best seen during the secretory phase when the endometrium is more hyperechoic.[42] Sonohysterography is a technique which demonstrates adhesions very well and should be performed in all cases of suspected adhesions. Adhesions appear as bridging bands of tissue that distort the cavity or as thin undulating membranes best seen on realtime sonography. Hysterosalpingography (HSG) is the other primary method for diagnosis followed by division of the adhesions under hysteroscopy. MR imaging is complementary and provides information on the etiology of synechiae. [43] On T2 weighted images, synechiae appear as low signal intensity bands that traverse the endometrial cavity and enhance after contrast administration, especially in the early phase. MR is a useful technique as it provides information of the endometrial cavity above the adhesions which is a blind spot for hysteroscopy, and has both therapeutic and prognostic significance.[44]

UTERINE ARTERIOVENOUS MALFORMATION

Uterine arteriovenous malformations (AVMs) are uncommon and may be congenital, traumatic, malignant or idiopathic in origin. Congenital AVMs are considered to be undifferentiated vascular structures resulting from the arrest of embryonic development at various stages. Acquired AVMs are usually caused by procedures such as curettage, uterine surgery or may be secondary to trauma or neoplasm.[45]

On grey-scale imaging, appearance of AVMs is non-specific and include subtle, myometrial inhomogeneity, tubular spaces within the myometrium or prominent parametrial vessels. Doppler findings reveal a low resistance flow with high peak systolic velocities. Spectral analysis of venous flow also depict high flow velocities and systolic velocity peaks similar to arterial pattern, suggesting an arteriovenous shunting.[46]

Both CT and MR can accurately assess the size, extent, vascularity of AVMs and the degree of adjacent organ involved. On MR imaging, AVMs appear as focal uterine masses or as disruption of the junctional zones with serpiginous flow related signal voids within the myometrium, showing intense enhance-

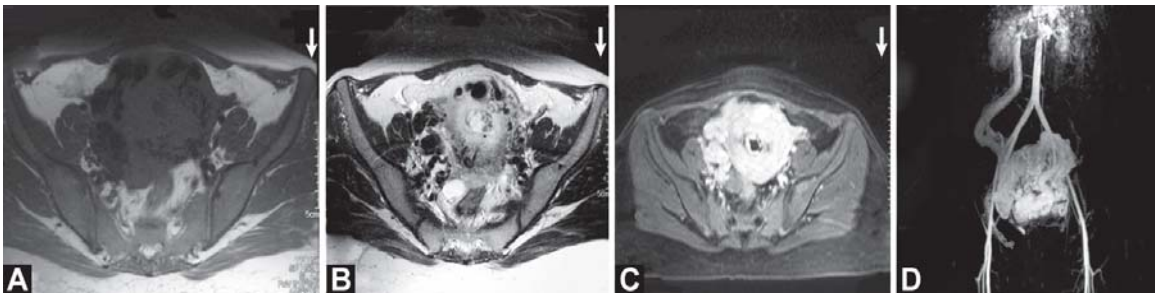

Figs 25.14A to D: (A and B) T1W and T2W axial MR images reveal a bulky uterus with multiple, large tortuous flow voids within the myometrium and bilateral parametrial regions showing. **(C)** intense enhancement on postgadolinium images. **(D)** MRA reveals prominent arterial feeder channels arising from anterior division of the internal iliac arteries. Enlarged, tortuous venous channels are seen draining into the iliac vein with early filling of the IVC – Uterine arteriovenous malformation

ment on postgadolinium imaging (Figs 25.14A to D). Treatment of uterine AVM consists of either surgery or transcatheter embolization. The extent of involvement of adjacent pelvic viscera is a major criteria in deciding between the two treatment options. [45]

BENIGN OVARIAN MASSES

Sonographic morphology of benign ovarian masses include either the masses being completely cystic or complex .

BENIGN CYSTIC MASSES OF PELVIS

In general, most cystic masses that arise within the pelvis are of ovarian origin. Cystic adnexal masses on sonography include physiological ovarian cysts (follicular cysts, corpus luteum cysts, and theca lutein cysts), hemorrhagic ovarian cysts, simple ovarian cysts, polycystic ovarian disease, hydrosalpinx, cystadenoma, parovarian cysts, peritoneal inclusion cysts and endometriomas.

FUNCTIONAL CYSTS

Follicular Cysts

Follicular cysts develop when a follicle fails to ovulate or involute They occur in all age groups but are most common in women of reproductive age-group. It is a simple cyst and its diagnosis is based purely on ultrasound findings—a unilocular, round, anechoic structure with a thin and regular walls causing posterior acoustic enhancement.[47] The size of the cyst varies from 3-5 cm. CT is not the investigation of choice for evaluation of ovarian cysts, but are common incidental finding on CECT of the the pelvis wherein they are well defined, rounded, unilocular, homogeneous, water density mass with smooth thin walls and low attenuation contents.[48]

On MR imaging, they are well-circumscribed, homogeneous, intermediate to low signal intensity masses on T1 weighted images and very high signal intensity on T2 weighted images. The cyst wall is imperceptible on T1 weighted images and enhances following administration of gadolinium.[3]

Simple follicular cysts usually resolve spontaneously. Follow up ultrasound is recommended 6 weeks after initial imaging evaluation to see for cyst resolution. It should preferably be done in the first of week of the menstrual cycle in order to avoid confusion with other follicular cysts.

The differential diagnosis of follicular cysts include nonfunctional cysts and cystic neoplasm. Nonfunctional cysts include

surface epithelial inclusion cysts, rete cysts and parovarian or paratubal cysts. Parovarian cysts are indistinguishable from functional cysts by imaging criteria except by location. A diagnosis of parovarian cyst can be made when the ipsilateral ovary is seen close to but separate from the cyst.

Simple ovarian cysts are common in premenopausal women and with increasing use of ultrasound are also seen in upto 20 percent of postmenopausal women.[49] They should be followed by serial ultrasonography to see for cyst resolution and any change in cyst morphology. Earlier it was advocated that postmenopausal cysts > 5cm in size should be removed. However, studies have shown that postmenopausal simple cysts upto 10 cm in size can be followed by serial sonographic evaluation and do not warrant an immediate laprotomy as risk of malignancy is very rare (< 1%).[50]

Corpus Luteum Cyst

Corpus luteal cysts are normal physiological ovarian structures formed after ovulation by the dominant follicle when the follicular wall becomes vascularized, thickened and partially collapsed. The changes in the follicular wall are known as luteinization. While they are not pathological, they can cause periovulatory pain that may require radiological evaluation. Corpus luteal cysts are less common than follicular cysts but tend to be larger and symptomatic. They are usually unilateral and more prone to hemorrhage and rupture. If the ovum is fertilized, the corpus luteum continues as the corpus luteum of pregnancy. Maximum size is reached at 8-10 weeks and by 12-16 weeks the cyst usually resolves spontaneously. It represents the most common adnexal mass in pregnancy.[3]

Sonographically, corpus luteal cysts have a thicker hyperechoic and crenulated wall. The contents are usually hyperechoic and represents some bleeding into the follicle that has ovulated. A higher fat content of the cyst wall is a likely cause for the hyperechogenic wall of the corpus luteal cyst.[47] On color Doppler sonography, corpus luteal cyst shows a typical " ring of fire appearance" (Figs 25.15 A and B).

As computed tomography (CT) is increasingly being used as a primary modality for the radiological evaluation of patients with lower abdominal or pelvic pain, therefore;

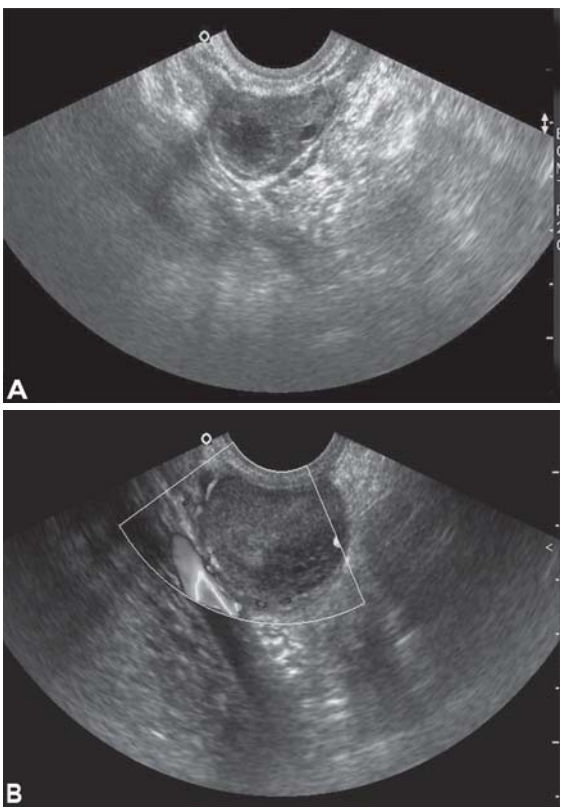

Figs 25.15A and B: (A) Corpus luteum cyst showing thick wall with crenulated appearance within the ovarian parenchyma. **(B)** CDS showing "ring of fire" appearance around corpus luteum cyst with internal echoes due to hemorrhage *(For color version of Fig. 25.15B see Plate 20)*

recognition of CT appearance of corpus luteal cysts is desirable. They are unilocular cysts, typically less than 3 cm in diameter with thick, crenulated, hyperdense or enhancing walls. This appearance corresponds to the histopathological changes of corpus luteal cysts seen after ovulation.[48]

The characteristic appearance of corpus luteum cyst on MR allows it to be differentiated from other ovarian masses. The inner wall of the cyst wall may be seen as a line of high signal intensity on T1-weighted images and a line of low signal intensity on T2 – weighted images representing hemosiderin deposited along its wall. [51] The thickened cyst wall enhances avidly following administration of gadolinium. Internal debris and hemorrhage can be present within the corpus luteum but lack of internal enhancement rules out the possibility of ovarian malignancy.[3]

The above described characteristic appearances of corpus luteal cyst on imaging allows distinction from other ovarian masses and often obviates the need for follow-up. When in doubt, correlation with recent ultrasound and follow-up imaging is helpful as corpus luteal cysts should exhibit rapid change in size. A large amount of hemorrhage into a cyst can mimic an endometrioma, but on follow-up imaging the corpus luteum cyst will resolve whereas an endometrioma will persist.

Hemorrhagic Cyst

The most common complication of a functional cyst is hemorrhage. Hemorrhage can occur in any ovarian cyst, but most commonly seen in corpus luteal cysts. Women with hemorrhagic cysts frequently present with acute onset of pelvic pain. Hemorrhagic cysts show a spectrum of findings as a result of variable sonographic appearance of blood. The sonographic appearance depends on the amount of hemorrhage and the time of hemorrhage relative to the time of sonographic examination. Various sonographic findings include diffuse echogenic material, diffuse echoes with visible fibrin strands, retracting thrombus and fluid-fluid level.

The internal characteristics of a hemorrhagic cyst are much better appreciated on TVS because of its superior resolution. Hemorrhagic ovarian cysts typically contain fine linear echoes which represent strands of fibrin. Fibrin within the internal architecture of clot is responsible for this appearance. The fibrin strands need to be differentiated from true septations which are a feature of ovarian neoplasm. Usually, fibrin strands are innumerable, discontinuous, cannot be traced on multiple frames, whereas septations are continuous, thick, linear structures seen in multiple frames on sonography.[47]

A retracting thrombus adherent to the wall of the hemorrhagic cyst is another sonographic feature. This finding may occasionally be confused with a focal mural nodule, a feature of a neoplastic ovarian mass. A retracting clot has a typically concave margin, whereas, mural nodules have a convex margin. Also, retracting clots appear to have a variable central echogenic pattern, while most mural nodules appear isoechoic in relation to the wall of the cyst. Color Doppler sonography does not reveal any blood flow within the fibrin strands or retracting thrombus thereby supporting the diagnosis of hemorrhage[47] (Figs 25.16A and B).

Hemorrhagic ovarian cysts have a very specific appearance in the vast majority of cases, and the presence of multiple, thin, linear fibrinous strands within the cyst has been typically described as "Fish Net" appearance[49] (Fig. 25.16C). When a unilocular

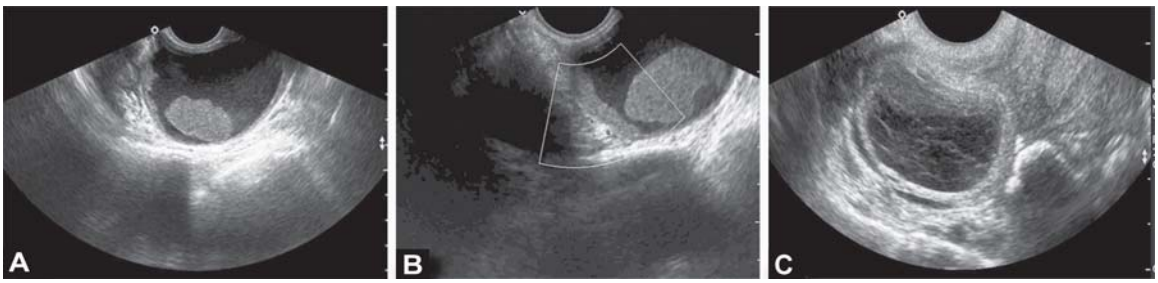

Figs 25.16A to C: Hemorrhagic ovarian cysts showing **(A)** Presence of retracting clot with wall thickness and irregularity. **(B)** CDS showing absence of blood flow in both. **(C)** "Fishnet appearance"

smooth walled cyst with the above mentioned appearance is identified, it is 200 times more likely to be a hemorrhagic ovarian cyst than any other possibility.[49]

On MR imaging, signal intensities vary according to the age of hemorrhage. Most frequently hemorrhagic cysts demonstrate high signal intensity on T1and T2 weighted images due to intracellular methemoglobin in the late sub acute phase.[3] Apart from hemorrhage, fat containing lesions also appear bright on T1 weighed images. The two can be differentiated on fat suppressed T1 weighted images, wherein signal intensity of hemorrhage remains unchanged while that of fat is suppressed. This feature helps in the distinction of haemorrhagic cysts from dermoid cysts.

The cyst wall is thin and smooth and demonstrates intense enhancement after gadolinium administration. Contrast-enhanced images may help differentiate adherent clot from a mural nodule because clot will not enhance after the administration of gadolinium. Hemorrhagic cyst may be difficult to differentiate from other hemorrhagic adnexal lesions, especially endometriomas. However, hemorrhagic cyst tends to be solitary and is usually brighter on T2 weighted images than endometriomas, which typically has more profound T2 shortening, described as shading.[52]

It is important to remember that hemorrhagic cysts almost always represent non-neoplastic cysts that resolve spontaneously and grey-scale ultrasound is the investigation of choice for diagnosing the same. The main features to note are the presence of fibrin strands or retracting clot, with absence of suspected septations and wall irregularity as secondary helpful findings. Also, follow-up ultrasound should be performed 4-6 weeks after the initial sonography, preferably in the first week of menstruation to allow time for resolution of the cyst and to avoid confusion with new physiologic cysts.[52]

Theca Lutein Cysts

Theca lutein cysts are the largest of the functional cyst group. They result from over-stimulation by high levels of circulating human chorionic gonadotropin (HCG) in trophoblastic disease or from iatrogenic hyperstimulation with exogenous HCG in the treatment of infertility. On ultrasonography, theca lutein cysts appear as bilateral, large multilocular cysts and may persist for days or weeks after withdrawl of the stimulus (Fig. 25.17). These cysts may undergo hemorrhage, rupture or torsion.[14]

Polycystic Ovarian Disease

Polycystic ovarian disease is a complex endocrinological disorder resulting from

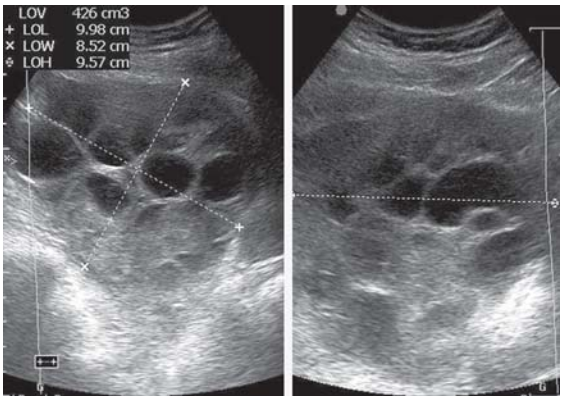

Fig. 25.17: TAS showing a large multilocular cysts in left ovary in a patient of OHSS – Theca lutein cyst

chronic anovulation clinically characterised by amenorrhea or oligomenorrhea, infertility, hirsuitism and obesity. The luteinising hormone to follicle-stimulating hormone (LH to FSH ratio) is more than 2 with increased androgen levels. Acylic production of estrogen results in appropriately elevated levels of LH and decreased levels of FSH. Increased LH leads to stimulation of ovarian theca and stroma and decreased FSH is responsible for chronic anovulation.

TVS has been used to distinguish the polycystic ovary from the healthy one. Classic sonographic and MR features are bilateral ovarian enlargement with multiple (10 or more) small peripheral follicles of uniform size measuring 2-8 mm in diameter (Fig. 25.18). Two patterns of cyst distribution have been described. In the peripheral cystic pattern, the cysts are present beneath the ovarian capsule, leading to a "string of pearls" appearance. In the general cystic pattern, the cysts can be seen both in the subcapsular and stromal parts of the ovary and can vary in size. In general, the polycystic ovary contains twice the number of antral follicles which are usually less than 4 mm in diameter and have twice

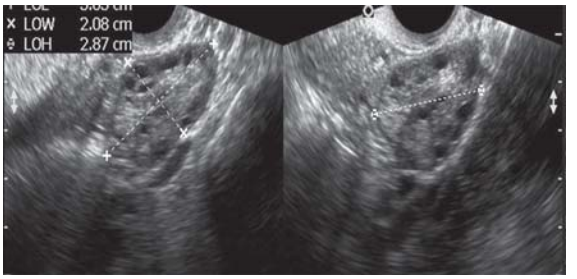

Fig. 25.18: PCOD – Bilateral enlarged ovaries with stromal echogenicity and multiple peripheral follicles

the volume of the normal ovary.[10] The cysts show uniform high signal on T2W images. Hypertrophied ovarian stroma is depicted as broad central areas of low T1 and T2 signal intensity and appears echogenic on sonography. The ratio of ovarian stroma to ovarian area has been found to be the best predictor of polycystic ovaries by sonography.[53] However, with respect to ovarian volume and follicular number, there is considerable overlap with healthy subjects. In almost one-third of the patients with clinical and endocrinological evidence of PCOD, the ovaries show normal morphology and volume.[10]

Peritoneal Inclusion Cyst

Peritoneal inclusion cysts occur predominantly in premenopausal women with a history of previous abdominal surgery, trauma, pelvic inflammatory disease or endometriosis. The normal peritoneum absorbs fluid produced by the ovaries. This ability is lost following inflammation or adhesions. Fluid may accumulate within adhesions and entrap the ovaries leading to a large cystic adnexal mass with multiple septations with the ovary lying centrally or in the wall of the cyst.[54] The patient may present with pain or pelvic mass. Peritoneal inclusion cysts are lined by mesothelial cysts

and they are also referr to as benign cystic mesothelioma or benign encysted fluid.

On sonography, peritoneal inclusion cysts are multiloculated, cystic adnexal masses. The diagnostic finding is an intact ovary amid septations and fluid indicating the extraovarian origin of the mass.[55] The ovary may be located centrally or displaced peripherally with, margins of the cystic mass following the contour of the pelvis (Figs 25.19A to C).

Peritoneal inclusion cysts have a characteristic appearance on MR imaging depicting a cystic mass with thin septations, no distinct wall and bordered by the pelvic sidewall (Figs 25.19D and E). Usually, there is no mass effect on adjacent structures, although this can be seen in large lesions. Typically they are of low signal intensity on T1 and high signal on T2- weighted images. If protein content of the cyst is high or hemorrhage has occurred into the cyst, the cyst may be intermediate to hyperintense on T1 weighted images.[3]

Peritoneal inclusion cysts need to be differentiated from parovarian cysts and hydrosalpinx. While all these conditions are extra-ovarian, parovarian cysts are separate from the ovary, whereas the ovary lies inside or in the wall of a peritoneal inclusion cyst.[56] Parovarian cysts are usually round to ovoid and are not associated with a history of pelvic surgery, trauma or inflammation. Hydrosalpinx appears as a tubular cystic structure with visible folds and the ovary is seen to be outside the cystic structure. Peritoneal inclusion cyst may be mistaken for a cystic ovarian neoplasm and patient may undergo multiple surgeries. Accurate diagnosis of the same is essential because it is known to recur after extensive surgery in 30 to 50 percent cases.[3] Hence, treatment is conservative. Peritoneal inclusion cysts have no malignant potential.

Hydrosalpinx

Hydrosalpinx occurs when an inflammatory process produces adhesions of the fimbriated end of the fallopian tube, trapping the intraluminal secretions and dilatation of the ampullary and infundibular portions of the tube. Dilated fallopian tubes are depicted as tubular, fluid-filled structures that are folded upon themselves to form a C or S shape or, at times, a multilocular mass. The diagnosis of simple hydrosalpinx is typically made by sonography. Multiplanar imaging can be helpful in confirming the tubular nature of an adnexal mass or demonstrating incomplete septations, thus confirming it to originate from the fallopian tube.[3]

Most cases of hydrosalpinx have a typical appearance and can be easily distinguished from ovarian abnormalities. The most consistent sonographic feature described by Tessler and colleagues is a tubular, elongated extra-ovarian structure with folded configuration (incomplete septation)[57] (Figs 25.20A and B).

Recently, Patel et al have described a combination of tubular shape and "waist sign" as being specific for the diagnosis of hydrosalpinx.[49]

Sonographically, a dilated tube is seen as a fusiform, anechoic adnexal mass with lack of peristalsis which allows differentiation from small bowel loops. Timor-Tritsch et al have described three appearances of tubal wall structure[14] (i) "Cogwheel " sign which is anechoic cogwheel shaped structure visible in the cross-section of the tube with thick walls, (ii) "beads on a string" sign, which are hyperechoic mural nodules of 2 to 3 mm in size and seen on the cross-section of the fluid-filled distended tube. (iii) incomplete septa which are hyperechoic septa that originate as a triangular protrusion from one of the walls, but do not reach the opposite wall.

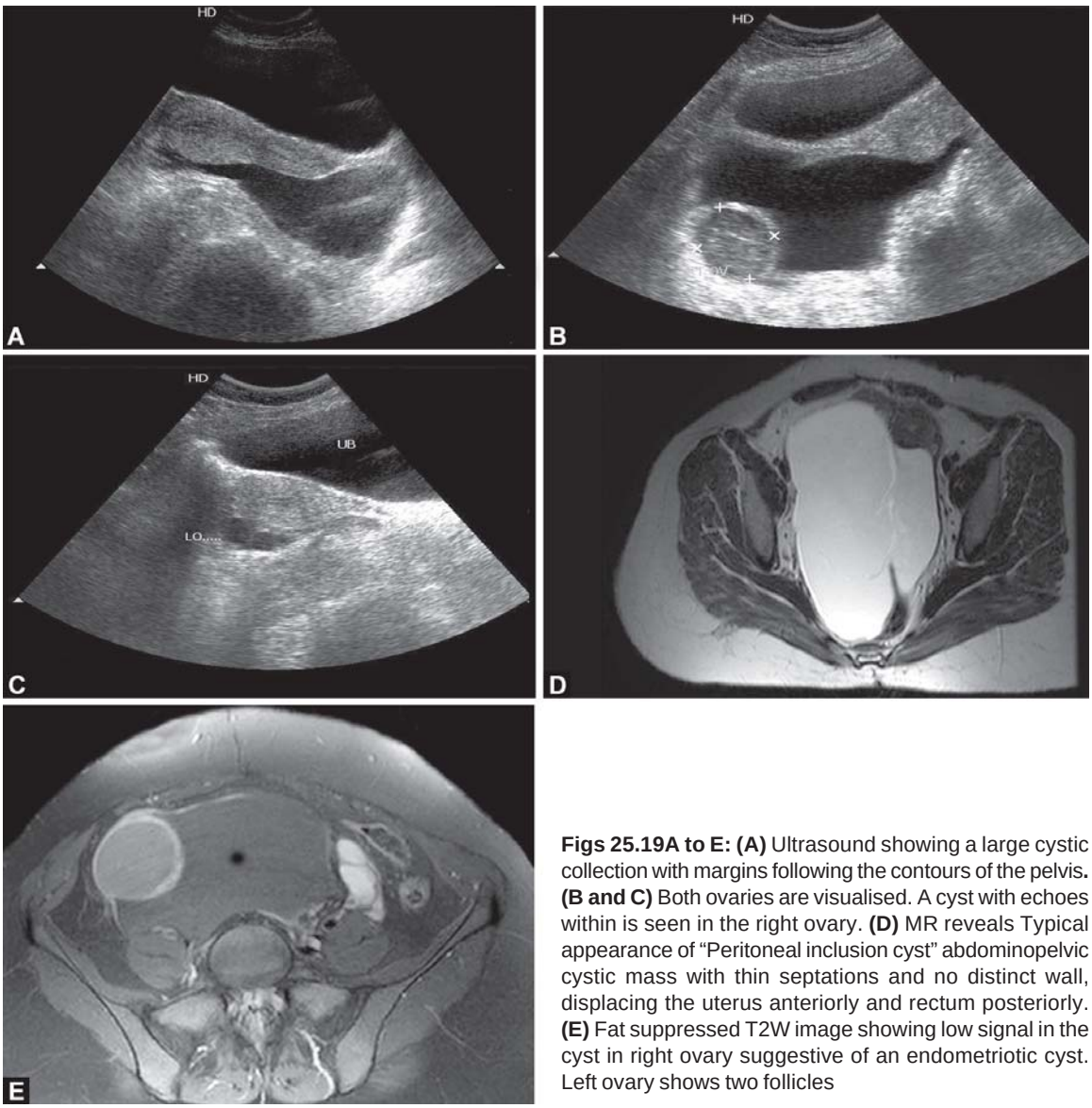

Figs 25.19A to E: (A) Ultrasound showing a large cystic collection with margins following the contours of the pelvis**. (B and C)** Both ovaries are visualised. A cyst with echoes within is seen in the right ovary. **(D)** MR reveals Typical appearance of "Peritoneal inclusion cyst" abdominopelvic cystic mass with thin septations and no distinct wall, displacing the uterus anteriorly and rectum posteriorly. **(E)** Fat suppressed T2W image showing low signal in the cyst in right ovary suggestive of an endometriotic cyst. Left ovary shows two follicles

In case of a complex cystic adnexal mass it may not be possible to establish the tubular nature of the process by sonography and MR can help in demonstrating incomplete septations and a separate normal ovary (Figs 25.21 A and B). MR can also help in determining the etiology of hydrosalpinx. If hydrosalpinx is due to endometriosis, signal intensity characteristics of the tubal fluid are similar to those in endometriomas (high T1 and low T2 signal intensities). In a patient with adhesions, signal intensity of the dilated tube follows that of simple fluid (low T1 and high T2 signal intensities).[3]

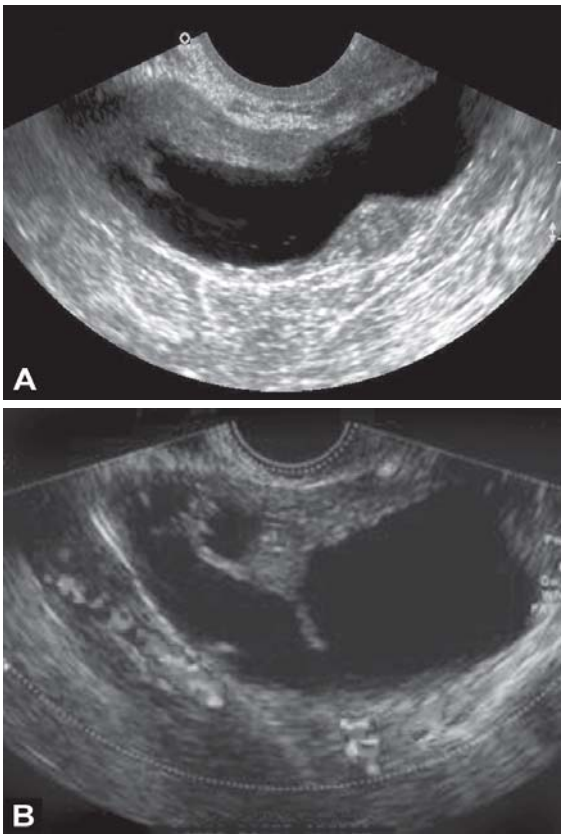

Figs 25.20A and B: (A) TVS reveals tubular elongated extraovarian structure. **(B)** Incomplete septation and absence of vascularity on CDS - Hydrosalpinx *(For color version of Fig. 25.20B see Plate 20)*

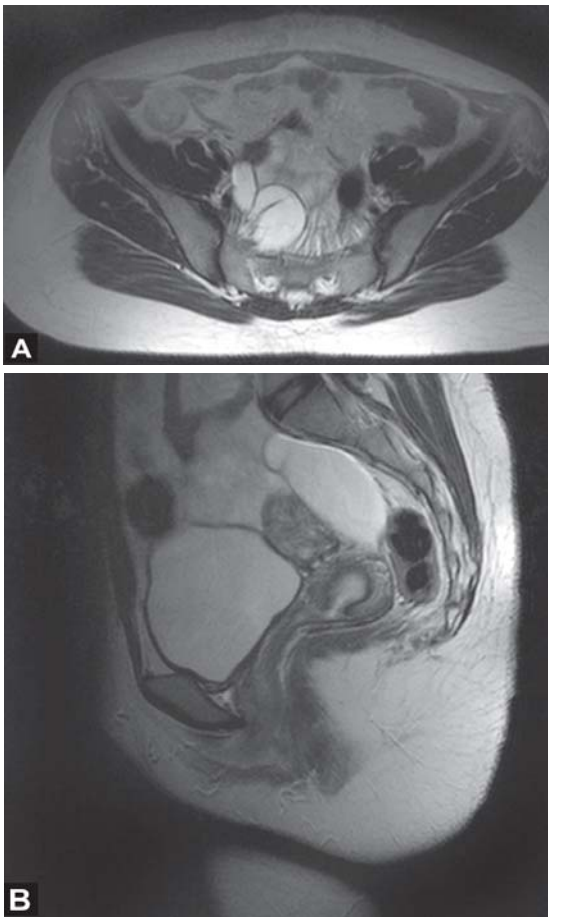

Figs 25.21A and B: T2W axial and sagittal images showing a hyperintense tubular structure with folded configuration in the right adnexa – Hydrosalpinx

Parovarian Cysts

Parovarian or paratubal cysts arise from mesonephric (Wolffian) or paramesonephric (Mullerian) structures. They represent 10 percent of all adnexal masses and most commonly occur in the 3rd to 4th decade. The hydatid of Morgagni is the most common paramesonephric cyst and is found arising from the fimbrial end of the fallopian tube.[47] They are frequently located superior to the uterine fundus.[14]

They are usually large and unilocular. Parovarian cyst are not physiological, hence its dimensions remain constant throughout menstrual cycle. Sonographically, they are round to oval, anechoic with good sound transmission and morphologically indistinguishable from simple functional cysts. A specific diagnosis is not possible unless a normal ovary is seen separately from the cyst[58] (Fig. 25.22). On sonography, a complicated parovarian cyst may resemble an endometrioma, serous cystadenoma or a hemorrhagic cyst. The cyst may undergo torsion and rupture similar to other cystic masses. Malignancy is rare in cysts less than 5 cm. Benign neoplasms such as cystadenomas and cystadenofibromas of parovarian origin are also uncommon.[14]

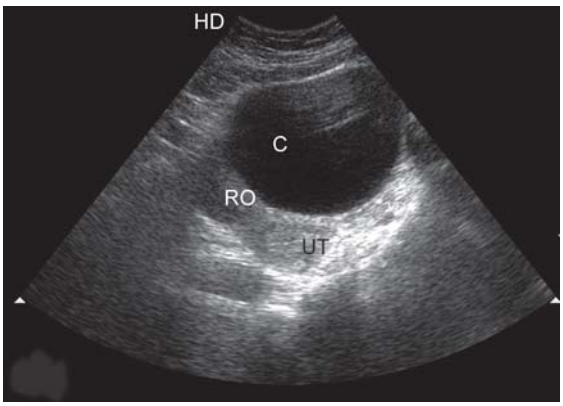

Fig. 25.22: Ultrasound of the right adnexa showing a unilocular smooth walled anechoic cyst with normal appearing right ovary adjacent and separate from it – Parovarian cyst

CYSTADENOMAS

Cystadenomas are benign epithelial tumors arising from the surface epithelium of the ovary. They are of two types-serous and mucinous.

Serous cystadenomas account for 25 percent of all benign ovarian neoplasms with 20 percent of them being bilateral. The peak incidence of presentation is in the fourth and fifth decades. Sonographically, serous cystadenomas are large, thin-walled, unilocular cystic masses with a mean size of around 10 cm. They may be multilocular in which case the septations are thin (Fig. 25.23A). Papillary projections may be seen occasionally. Usually the cysts contain simple fluid with low signal intensity on T1 and high signal intensity on T2 weighted images. Rarely, the cyst contents may be complex due to high protein content or hemorrhage. On post-contrast T1 weighted images, the cyst wall and septa enhance with no evidence of any solid component.[3]

In contrast, mucinous cystadenomas are less common and occur most often in the third to fifth decades. They are less frequently bilateral than their serous component (only 3% bilateral) Sonographically, mucinous cystadenomas are larger, measuring upto 15 to 30cm having a multilocular appearance. Multiple thin septae are present and low level echoes due to mucoid material may be seen in the dependent portions of the mass. In many of the mucinous cystadenomas, the imaging appearance of the individual locules may vary as a result of difference in degree of haemorrhage or protein content. The sonographic feature of variable echogenicity in the contents of an multilocular adnexal cyst is strongly suggestive of a mucinous tumor[47] (Fig. 25.23B). The difference in chemical composition of fluids rather than their difference in viscosity is responsible for the different sonographic echogenicities. This sign may not be seen in all mucinous tumours as some may have small differences in the chemical composition of contents. Also, some of the mucinous tumours may be unilocular and have one type of mucin.[47] Papillary projections are less frequently seen than in their serous counterpart. On MR imaging, the thick mucinous content of the cyst may result in a high signal on T1 and low signal on T2 weighted images. The loculations in these cysts vary giving a "stained glass" appearance.

Preoperative knowledge of the mucinous nature of the tumour is important because penetration of the tumor capsule or rupture may lead to intraperitoneal spread of mucin-secreting cells that may fill the peritoneal cavity with a gelatinous material. This condition is known as pseudomyxoma peritonei and apart from mucinous cystadenoma and cystadenocarcinoma, can result from a ruptured mucocoele of the appendix and mucinous tumours of the appendix and colon (Fig. 25.23C).

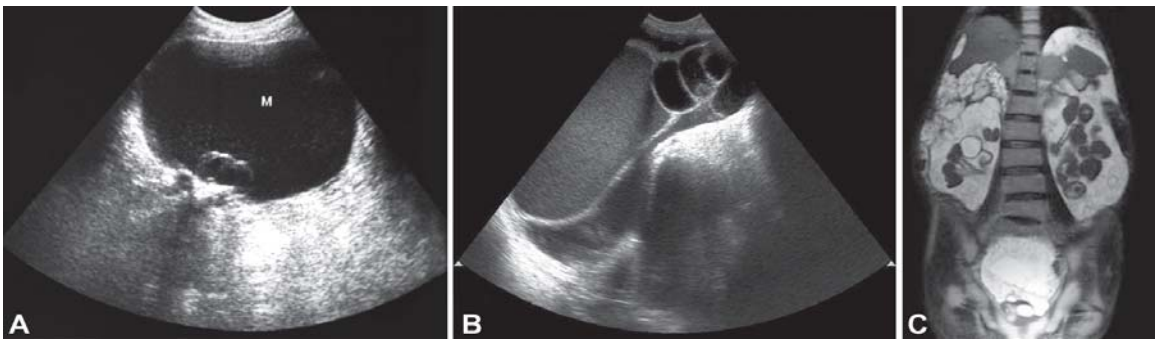

Figs 25.23A to C: (A) TAS reveals a large unilocular thin walled cystic mass with thin septations within – Serous cystadenoma. **(B)** Characteristic appearance of Mucinous cystadenoma showing "variegated echogenicity sign" in the loculi of a large multiloculated cystic mass. **(C)** T2W and coronal image showing mucinous implants on peritoneal surfaces with typical scalloping of liver surface secondary to ruptured mucinous tumour – Pseudomyxoma peritonei

Color Doppler sonography (CDS) has been used along with conventional unltrasound to characterise cystadenomas and other adnexal masses. CDS does not improve actual detection of a mass, but seems to improve specificity in differentiating benign from malignant masses. Presence of colour flow in echogenic portion of the cyst is indicative of malignancy while its absence indicates benignancy.[59]

Spectral Doppler analysis has been seen to be of limited value in predicting malignancy as a number of physiological (corpus luteum) and benign (inflammatory) masses have a low PI (≤ 1) similar to that seen in ovarian malignancy.[60]

Benign and malignant ovarian neoplasms can be differentiated by sonographic characteristics of the mass. Features suggestive of a benign ovarian mass is a cystic mass (usually < 5 cm) with thin, wall defined walls and thin septations. On analysis of Doppler spectrum, a benign mass generally shows no flow or a high resistance flow. In contrast, features that suggest malignancy in an adnexal mass are a large size (> 10 cm) with thick, ill-defined or irregular walls, large solid component, thick or irregular septations (> 3 cm) with evidence of peritoneal, lymphatic, hematogenous spread or local invasion. Doppler features indicative of a malignancy are presence of vascular nodules within the mass with low resistance flow in them.

The diagnosis of cystadenoma is usually made by ultrasound wherein a combination of sonographic morphology and Doppler characteristics help in differentiating a benign from malignant ovarian mass. MR is helpful in the evaluation of indeterminate adnexal masses on ultrasound due to its superior tissue characterization.[3]

COMPLEX MASSES

Complex masses are those that contain both solid and cystic areas and include tubo-ovarian abscess, endometriosis, dermoid cyst, ovarian torsion and ectopic pregnancy.

Tubo-ovarian Abscess

Tubo-ovarian abscess is a result of ascending infection that spreads to involve the endometrium and fallopian tubes. The ovaries are relatively resistant to infection and are involved only in more severe cases. Bilateral adnexal involvement is the rule, and abscess

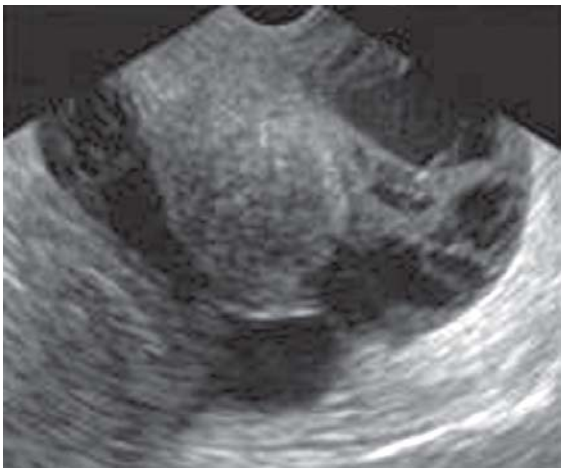

Fig. 25.24: TVS reveals bilateral multilocular complex adnexal masses with septations and associated free fluid–Tubo-ovarian abscesses

formation tends to occur with late or inadequate treatment. Tubo-ovarian abscess has a variable appearance on sonography. It is typically a unilocular or multilocular complex mass with irregular borders and thickened wall.[61] Multiple internal septations may be present (Fig. 25.24). Normal ovarian stroma with follicles is often identifiable as part of the conglomerate mass. Anechoic or hypoechoic areas represent collection of frank pus. On CT, tubo-ovarian abscess is seen as thick-walled, complex adnexal mass with centers of low attenuation and shaggy margins.[62] If air is present within the mass, a diagnosis of an abscess can be made confidently, but when no gas is present, differentiation of abscess from neoplasm is usually not possible without a percutaneous fine needle aspiration.[63] Abscess on MR imaging appears as unilocular or multilocular cystic mass with a thicker wall than that seen in functional ovarian cyst. The abscess fluid has variable signal but usually is of very high signal intensity on T2-weighted image and low signal intensity on T1-weighted image.[64] The abscess wall and adjacent inflammatory changes enhance intensely with gadolinium showing thickened irregularly enhancing wall and septations. Infiltration of pelvic fat surrounding the mass may be evident.

Actinomycosis is an uncommon pelvic infection usually seen in the presence of an intrauterine device. The mass in actinomycosis consists predominantly of a solid lesion with low signal intensity on T2 weighted images, Cystic elements are seen less commonly. Diffuse infiltration of the uterus, adnexa and pelvic musculature with transgression of fascial planes is the hall mark of the disease. The presence of a foreign body such as an intrauterine contraceptive device (IUCD) further corroborates to the diagnosis. Following guided aspiration, indentification of sulphur granules within the aspirate is diagnostic of an actinomycotic infection.[3]

The diagnosis of tubo-ovarian abscess is typically made by clinical examination and ultrasound. Both transabdominal and TVS are useful. The transabdominal approach is helpful in assessing the extent of the disease, while TVS is superior in detecting dilated tubes, periovarian inflammatory change and internal characteristics of tubo-ovarian abscesses. Sonography is also helpful in following the response to antibiotic therapy. MR has been demonstrated to have a higher accuracy compared to TVS for making the diagnosis. [3] In chronic cases, multiple pelvic organs may be involved and inflammatory signs can be absent, making differentiation from malignancy difficult.

Endometriosis

Endometriosis is defined as the presence of functioning endometrium located outside the uterus. The sites of implantation of ectopic endometrium in decreasing order of fre-

quency are ovary, utero-sacral ligaments, cul-de-sac, posterior wall of lower uterine segment, fallopian tube, rectovaginal septum and sigmoid colon. Ectopic endometrium may be diffuse or focal, more commonly being diffuse with minute endometrial implants involving pelvic viscera and their ligamentous attachments. It is a disease of women in the reproductive age group who may present with chronic lower abdominal pain, pelvic and back pain, dysmenorrhea, irregular bleeding and infertility. However there is no direct relationship between the severity of symptoms and extent of the disease. Sonography is insensitive in evaluating diffuse endometrial implants and plaques as these lesions are too small to be imaged. [65]

Endometriomas are internal hemorrhages within an area of endometriosis resulting in endometrial cysts. 80 percent of pelvic endometriosis is found in the ovary. They are bilateral in 30-50 percent of cases and are frequently multilocular. On sonographic evaluation, endometriomas appear as ovarian cysts ranging from anechoic to solid, depending on the amount of blood and its organization.[47] They have wide range of manifestations from cystic to complex and may have a solid appearance.

The classic appearance of an endometrioma on ultrasound is a cystic mass with homogeneous low level echoes[65] (Figs 25.25A and B). 95 percent of endometriomas exhibit diffuse low level internal echoes. Though the absence of this finding does not exclude an endometrioma, it significantly decreases the likelihood of diagnosis.[49] Repeated episodes of bleeding and rebleeding may result in development of irregular walls and echogenic mural nodules. Fluid-fluid levels or fluid debris levels represent blood products. These appearances are much less specific and can

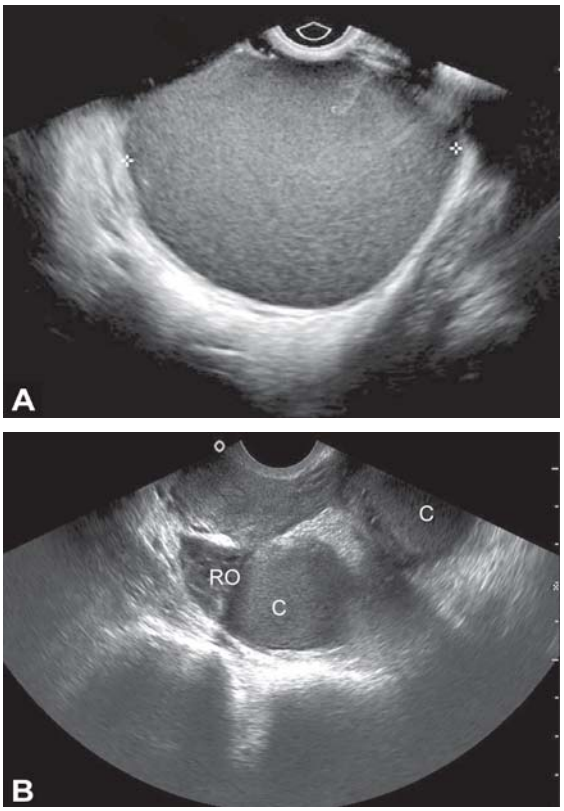

Figs 25.25A and B: (A) TVS showing a unilocular ovarian cyst with low level internal echoes – characteristic of Endometrioma. **(B)** Bilateral endometriotic cysts in another patient depicting typical ground glass appearance

be mimicked by hemorrhagic cysts, tubo-ovarian abscesses and cystadenomas. Presence of thick septations and walls, irregular mural nodules may sometimes make it difficult to differentiate from malignant ovarian neoplasms. In addition, multilocular appearance and punctate echogenicities in the wall of the endometrioma are seen less commonly but add specificity to the appearance of the lesions. These hyperechoic wall foci represent focal deposits of cholesterol secondary to degeneration and breakdown of cell membranes. A smooth walled mass with homogeneous ground glass

internal echoes and co-existing hyperechoic wall foci has been described to be 32 times more likely to be an endometrioma than any other adnexal mass.[49] Doppler waveform analysis is not helpful in differentiating endometrioma from other masses. Low resistance waveform resembling malignancy are encountered in endometrioma. CT appearance of endometriosis and endometrioma is nonspecific and easily mimicked by PID and benign and malignant ovarian tumors.[66] MR improves diagnostic accuracy with endometrial cyst typically appearing as high signal intensity on T1-weighted sequence with shading or low signal intensity on T2-weighted sequence due to presence of blood products[67,68] (Figs 25.26A to D). The "Shading sign" is a distinguishing feature of an endometrotic cyst at MR imaging which consists of T2 shortening in an adnexal cyst that is hyperintense on T1 W images. It is most commonly manifested as a complete loss of signal intensity or dependent layering with a hypointense fluid level in an endometrioma.[69]

Its precise mechanism is complex. Endometriotic cysts are highly viscous and have a high concentration of protein and iron from recurrent hemorrhage. The concentration of iron is 10-20 times higher than in blood. The high iron and protein within the lesion leads to T2 shortening and contribute to signal intensity loss described as 'shading'. These lesions are more often multiple, with angular margins or distorted shape. Fat saturation sequence does not suppress the signal intensity of the cyst which was bright on T1-weighted sequence confirming that hemorrhage, not fat is present. This signal characteristic differentiates endometrioma from fatty adnexal masses such as dermoids.

MR can diagnose endometriomas with 91 to 96 percent accuracy if MR features of multiple lesions with high signal intensity on T1 weighted images without fat suppression are noted and demonstrate low signal intensity on T2 weighted images.[3] The wall of an endometrioma is thick and can contain foci of low signal intensity on T1 and T2 weighted images due to a combination of fibrosis and hemosiderin—laden macrophages. On contrast enhanced T1 weighted images endometriomas show early wall enhancement.

In contrast, endometrial implants are often difficult to identify on imaging studies as they appear as small, flat lesions having variable T1 and T2 signal characteristics.[3] Implants commonly manifest as solid masses with low signal intensity on T2 weighted images due to fibrosis surrounding the glandular islands and demonstrate enhancement following contrast administration. Small hemorrhagic implants have been seen to become more conspicuous on fat-saturated T1 weighted sequences, appearing bright against the background of suppressed fat, thereby increasing the accuracy in staging the disease.

A rare complication of endometriosis is the development of clear cell carcinoma which occurs in 0.04 percent cases. About 25 percent of clear cell carcinomas arise in endometriomas and 50 to 70 percent are associated with pelvic endometriosis.[3]

As small implants and adhesions are not well-evaluated on imaging and MR may underestimate the extent of disease, therefore, laproscopy remains the standard of reference for diagnosis and staging. MR has a role in detecting lesions inaccessible to laproscopy due to dense adhesions. In addition, MR can be used for staging the disease, differentiating endometriomas from other adnexal masses and evaluating the response to treatment. Larger endometriomas with pronounced T2

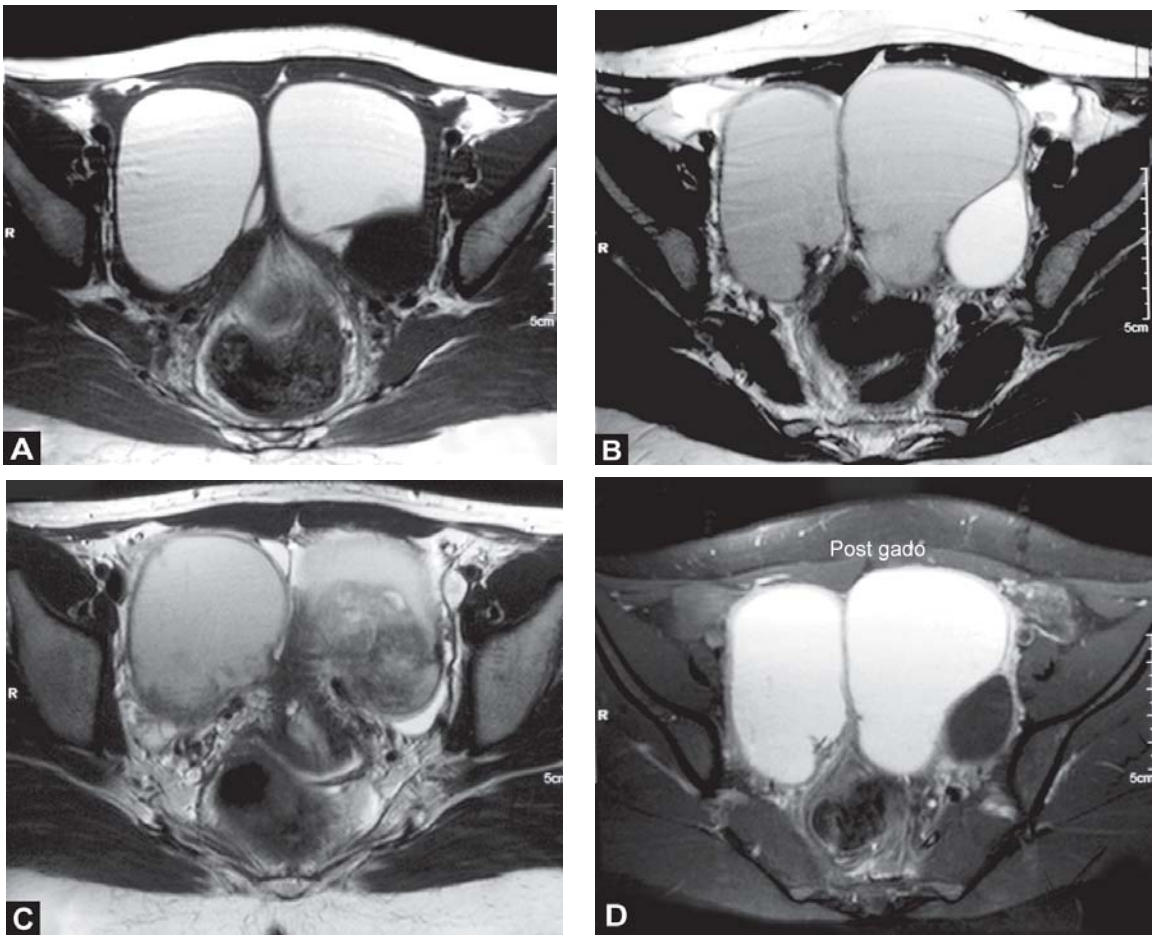

Figs 25.26A to D: MR imaging in endometriomas. **(A and B)** Bilateral endometriotic cysts appearing as large well defined cystic lesions in B/L adnexal regions with predominantly high SI on T1W and low SI on T2W images. One of the cysts has a low signal on T1W and high signal on T2W image. **(C)** T2W axial image shows hypointense debris in dependant part of cysts. **(D)** T1 Post-gadolinium fat-sat image showing early wall enhancement with lack of suppression of T1 bright signal – Confirms diagnosis of endometrioma

shading have been reported to benefit less from medical treatment. This may be related to the more concentrated blood products in older endometriomas.[3]

The differential diagnosis of endometriomas on MR imaging include other lesions which have a high signal intensity on T1 weighted sequences. These are fat containing tumors such as dermoid cysts which are reliably differentiated as they get suppressed on fat saturated sequences while the bright signal of endometriomas persist. Hemorrhagic lesions like hemorrhagic cyst and corpus luteum cyst may be difficult to differentiate from an endometrioma on imaging alone, but are generally solitary, the wall of a hemorrhagic cyst being thin while that of a corpus luteum cyst being slightly thicker and convoluted. Also, as there is no repeated hemorrhage into these lesions, marked loss of signal intensity on T2 weighted images is generally not observed.

Dermoid Cyst/Mature Cystic Teratoma

Dermoid cyst is a mature benign form of teratoma and occurs in women in their reproductive years. It is a common cause of adnexal mass accounting for approximately 20 percent of all ovarian neoplasms and 99 percent of germ cell tumors. It is bilateral in 10-15 percent cases.

Dermoid cyst contain all three germ layers, however the ectodermal layer predominates. Most tumors are discovered incidently on physical examination or imaging studies. If clinical symptoms are present, they are often nonspecific like pelvic mass or pain. Most common complication is ovarian torsion, seen in 16 percent of cases.

On plain radiograph, around 40 percent of ovarian teratoma shows diagnostic characteristics with presence of teeth or fat in the pelvis.[70] Variable sonographic appearances of ovarian dermoids have been described depending on the internal composition. The classic US appearance is a complex cystic mass with solid mural component called "dermoid plug"[71] (Fig. 25.27). The dermoid plug usually contains hair, teeth or fat and is usually echogenic and frequently casts an acoustic shadow. This is seen in almost 90 percent of cystic teratomas.

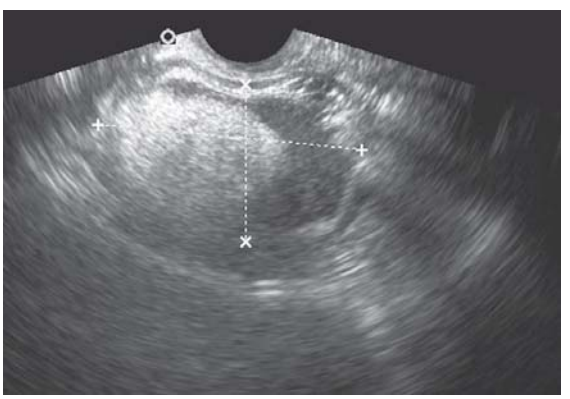

Fig. 25.27: Cystic ovarian mass with an echogenic mural nodule in the periphery representing "dermoid plug" – Cystic teratoma

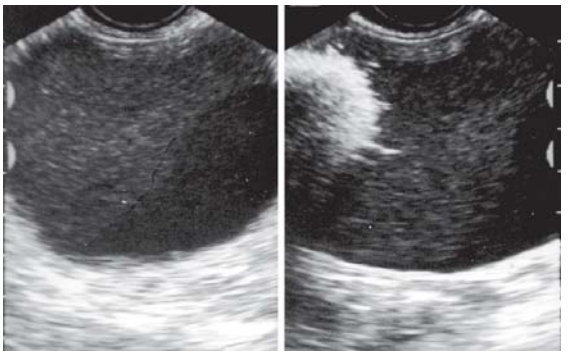

Fig. 25.28: Transvaginal view of a Dermoid with a fluid-debris level, probably produced by interface between sebum and cellular debris. Highly reflective mass in the periphery with partial shadowing represent hair in the dermoid within the ovary

Other sonographic findings associated with dermoids are high amplitude achoes within the mass. This is seen in 60 percent of cystic teratomas and is due to presence of sebum. Presence of hyperechoic lines and dots within the mass, so called 'dermoid mesh' is caused by hair and also seen in 60 percent of cystic teratomas.[49]

A fat-fluid or hair fluid level may be seen and is considered specific (Fig. 25.28). However these findings are seen in only one-third of cases. Echogenic dermoids may mimic bowel gas and may be missed on US. When a dermoid produces ill-defined acoustic shadowing that obscures the posterior wall of the lesion, it is termed as "Tip-of-the-iceberg-sign". This is produced by a mixture of matted hair and sebum which is highly echogenic because of multiple tissue interfaces. Often hematomas, abscesses or endometriomas cannot be distinguished ultrasonographically from teratomas. The diagnosis is commonly made on US. CT can provide a definitive diagnosis in majority of cases.[72] The characteristic CT features include detection of fat (–130 to

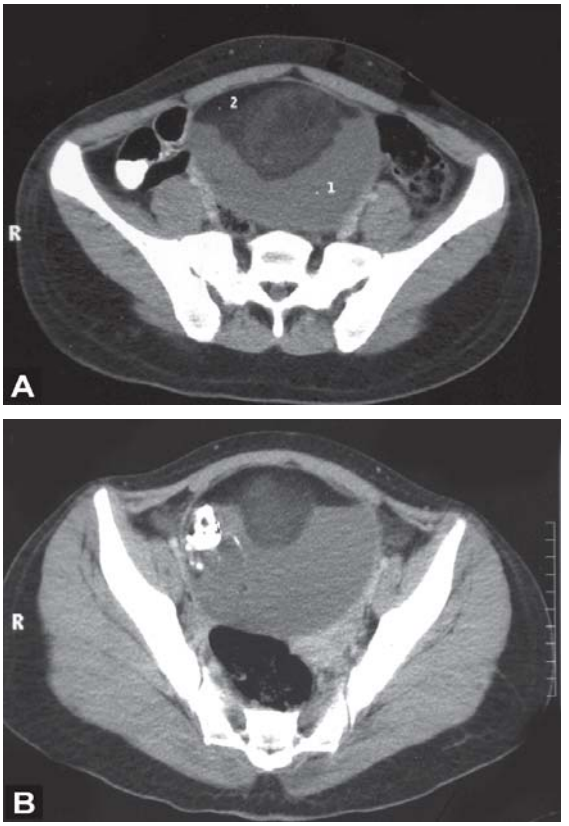

Figs 25.29A and B: Right ovarian cystic teratoma: **(A)** CT shows a large abdominopelvic mass of fat attenuation, with fat fluid level and a central hair ball. **(B)** The mass shows areas of calcification

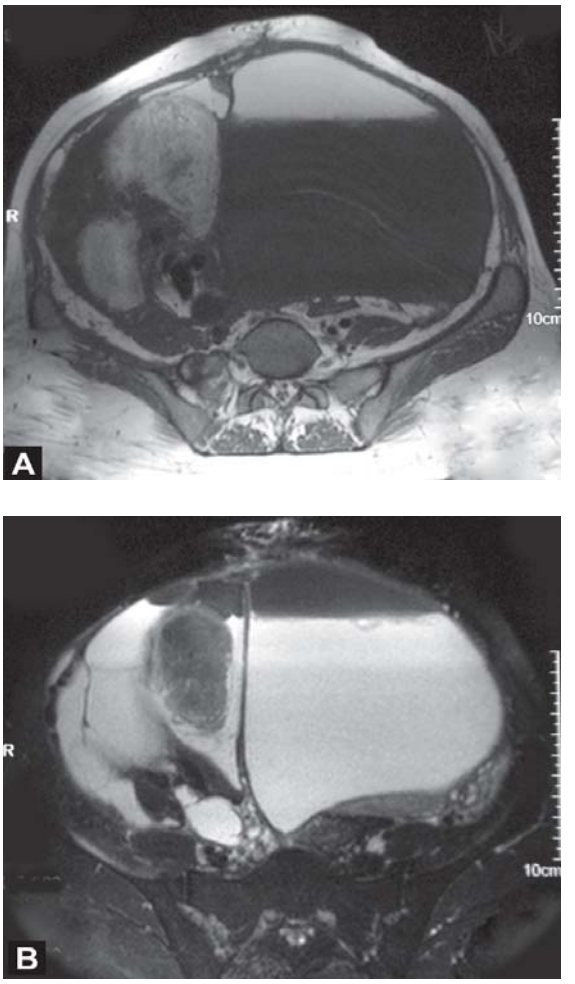

Figs 25.30A and B: MR Imaging in bilateral dermoid cysts. **(A)** B/L complex masses with bright signal of fat anteriorly on T1W image. **(B)** T1W fat-suppressed image showing suppression of fat signal with chemical shift artifact at fat-fluid interface

–90 HU), hair, teeth and fat-fluid level (Figs 25.29A and B). Although malignant teratomas are rare, CT detection of an irregular solid component greater than 5 cm strongly suggests the diagnosis.[73]

Cystic teratomas are well-defined, heterogeneous masses and identification of fat within an adnexal mass is the key to diagnosis of a dermoid cyst on MRI.[74] On MRI, fat is identified when the signal intensity of the mass (or part of it) is isointense to subcutaneous fat on both T1 and T2 weighted sequences and internal or external chemical shift artefact indicating fat water interface is present. On fat saturation sequence, suppression of signal that was of high signal intensity on T1 weighted sequence; confirms the presence of fat within the mass[75] and thereby helps in differentiating from an endometrioma or hemorrhagic cyst (Figs 25.30A and B).

Ovarian Torsion

It is an acute condition requiring prompt surgical intervention caused by partial or complete rotation of the ovarian pedicle on its long axis. Ovarian torsion is most commonly associated with an adnexal mass, usually a dermoid cyst, but may also occur spontaneously. On ultrasound, the salient finding is unilateral ovarian enlargement which is edematous with multiple small cystic structures at the periphery, which is due to transudation of fluid into the follicles from circulatory impairment. Small amounts of fluid may be seen in the cul-de-sac secondary to obstructed veins and lymphatics.[76]

Color Doppler may facilitate specific diagnosis of ovarian torsion by demonstrating lack or severe restriction of arterial flow. The ovary has a dual blood supply, and torsion may effect one arterial blood supply more than the other, resulting in partial arterial flow on CDS. The arterial waveform may exhibit a lack of diastolic flow with a "spike" configuration of the systolic peak. Studies have shown that while arterial flow may be present even in non-viable ovaries, absent venous flow may be sensitive of non-viability.

MR is not a primary imaging modality but can be helpful if sonographic findings of torsion are indeterminate. The most common finding on MR imaging is an adnexal mass with deviation of the uterus to the side of the torsion. Engorged vessels leading towards the vascular pedicle can be identified between the mass and uterus.[77] Hemorrhage in the torsed ovary can be seen as a high signal intensity ring in the periphery of the lesion, while hemorrhagic infarction is identified as low signal intensity on T1 and T2 weighted images due to interstitial hemorrhage. The most specific feature of infarction is lack of enhancement on T1 weighted contrast enhanced images.[3]

The treatment of choice for ovarian torsion is laparoscopic detwisting of the adnexa and resection of any enlarged cysts. Ovaries can remain viable upto 36 hours after twisting and thus oophorectomy can be avoided in most women.[78]

Ectopic Pregnancy

Ectopic pregnancy is one of the most common gynecological emergencies, presenting with amenorrhea followed by vaginal bleeding or pelvic pain. The diagnosis is usually reached by a combination of clinical presentation, hCG levels and findings on ultrasonography. On transabdominal and TVS, it appears as a complex cystic adnexal mass representing the ectopic gestational sac and hematoma, usually separate from the ovary.

The most common site for ectopic pregnancy is the fallopian tubes, occurring in up to 97 percent of cases of which 75-80 percent are located in the ampullary region.[79] The ovary, cervix are other less common sites of ectopic pregnancy. As most often fallopian tube is the site for an ectopic pregnancy, it is important to scan above or below the ovary and between the ovary and uterus.

The sonographic finding which is most specific for ectopic pregnancy is the presence of a live extrauterine pregnancy. However, it is positive is only 8-26 percent of ectopic pregnancies on TVS.[80] The next most specific sign is the presence of an extrauterine gestation sac containing a yolk sac, with or without an embryo.[81] The "tubal ring" of ectopic pregnancy is another finding which has been found to be 40-68 percent sensitive for ectopic pregnancy.[79] The tubal ring represents an extrauterine gestation sac with trophoblastic tissue. But the most common,

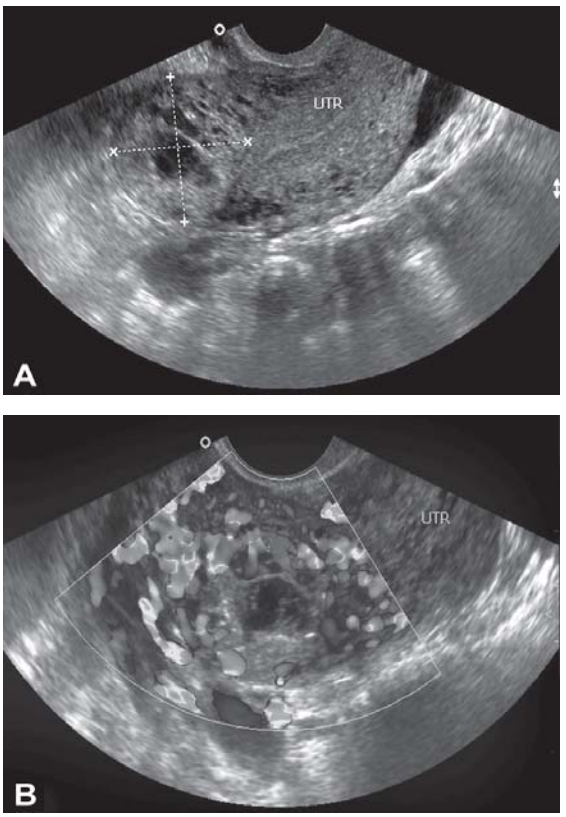

Figs 25.31A and B: TVS reveals a complex cystic mass in right adnexa separate from the right ovary with increased vascularity due to vascular trophoblastic tissue – Ectopic pregnancy *(For color version of Fig. 25.31B see Plate 20)*

but slightly less specific finding of an ectopic pregnancy is a complex adnexal mass separate from the ovary. The use of color doppler shows a "ring of fire" pattern and a high-velocity, low-impedance flow which is compatible with placental perfusion (Figs 25.31A and B). However, the corpus luteum is also very vascular and shows a similar appearance on color flow imaging from which it needs to be differentiated.

In a patient with suspicion of an ectopic pregnancy one should routinely screen the upper abdomen for free fluid in the Morrison's pouch or flanks. Presence of echogenic free fluid does not always signify a ruptured ectopic pregnancy, though more the fluid, greater is the possibility of finding a ruptured ectopic pregnancy. [47]

BENIGN SOLID OVARIAN MASSES

Solid ovarian masses are less common as compared to the frequency of solid masses representing uterine leiomyoma. Benign solid ovarian masses include thecomas, fibromas and fibrothecomas which arise from ovarian stroma. They are part of sex cord–stromal tumors with 80 percent of these tumors producing hormones, although fibromas do not. Fibromas usually arise in postmenopausal women, are mostly asymptomatic until they cause pelvic pressure or produce torsion. Ascites is seen up to 50 percent of patients with fibroma larger than 5 cm in diameter.[14] Meig's syndrome represents the rare triad of ovarian fibroma, ascites and pleural effusion. Sonographically, these fibrous tumors have a characteristic appearance of a hypoechoic mass with marked posterior attenuation of the sound beam seen separate from the uterus and a non-visualized ovary.[14] MR is helpful if the sonographic appearance is non-specific or the ovarian origin of the lesion is questionable.

On MR fibromas are usually well-defined solid tumors, with low signal intensity on both T1 and T2-weighted images. The low signal intensity results from abundant collagen content of these tumors and is relatively diagnostic of fibromas.[82] Hyalinisation and myxomatous changes in the solid masses may occasionally show irregular areas of high signal intensity on T2-weighted images. The differential diagnosis of a solid adnexal mass includes ovarian neoplasm, pedunculated uterine leiomyoma, metastasis, non-Hodgkin lymphoma.

An adnexal mass that is of low signal intensity on both T1 and T2 weighted images is most likely to be a pedunculated leiomyoma. The diagnosis is further confirmed if a stalk is seen connecting to the uterus or two normal ovaries are identified. Ovarian fibromas also present with low signal intensity on T1 and T2 weighted images, but on T1 weighted images, fibromas often have lower signal intensity than leiomyomas.[83] Fibroids have a discrete round margin and characteristic whorled internal structure and typically enhance intensely with gadolinium (Figs 25.32A to C). In contrast, benign ovarian stromal tumors have homogenous internal structure and show a lesser degree of enhancement.[84]

A Brenner tumor is an uncommon surface epithelial stromal tumor consisting of transitional cells in prominent fibrous connective tissue. In one-third of cases they are associated with other ovarian tumors. Sonographically they are hypoechoic solid masses usually smaller than 2 cm.[14] It is the predominantly fibrous content of Brenner tumor that results in a relatively low SI on T2 weighted images. Otherwise, ovarian fibroma and Brenner tumor may be indistinguishable by imaging.

CONCLUSION

Ultrasonography, especially transvaginal sonography is the modality of choice in detection and characterization of pelvic masses due to its superior resolution. It gives a detailed assessment of morphology of a mass on the basis of its internal contents thereby suggesting the possible etiology. Masses can be cystic, complex or solid on sonographic evaluation. It is the complex or solid masses that need a thorough evaluation. Though MR has a lower resolution than ultrasound, it has a wide range of tissue

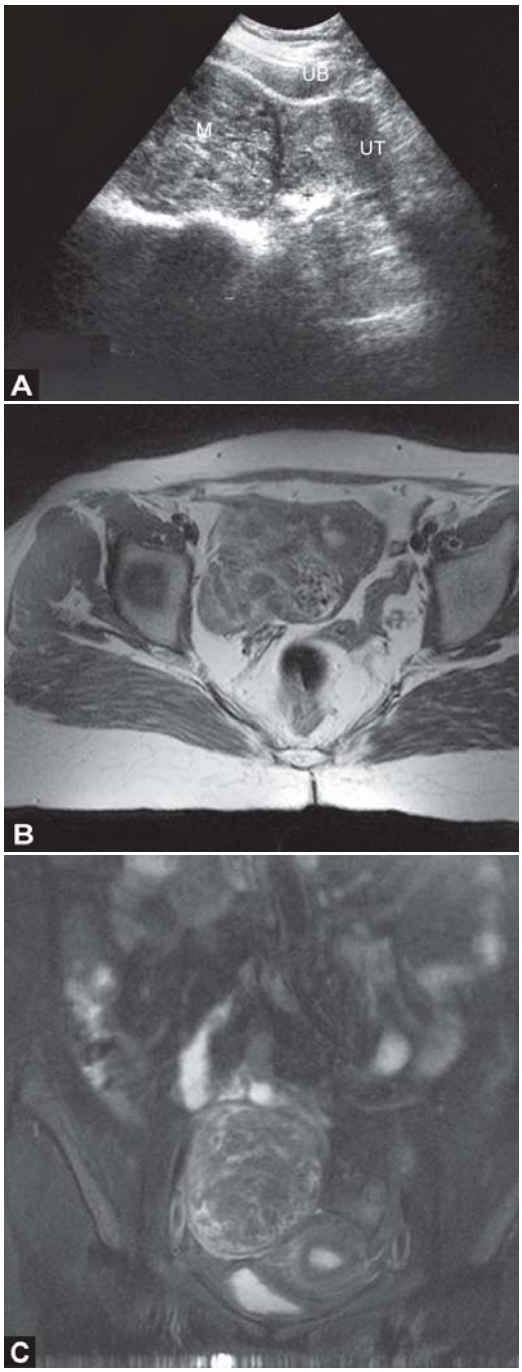

Fig. 25.32A to C: (A) Solid adnexal mass with characteristic whorled internal pattern – Broad ligament fibroid. **(B and C)** T2 axial and coronal MR images in another patient showing well-defined, rounded hypointense mass—Exophytic fibroid

specificity and a much larger field of view.[83] MR can be used to definitely characterize simple fluid, blood, fat and fibrous tissue and the enhancement properties of solid tissues can be measured following contrast administration. The larger field of view and multiplanar capability of MR is useful for characterizing large pelvic masses and evaluating their origin (ovarian/uterine) when the adnexal anatomy is significantly disorted.

REFERENCES

1. Sorenson SS. Estimated prevalence of mullerian anomalies. Acta Obstet Gynecol Scan 1988;67:441.
2. Buttram VC, Gibbons WF. Mullerian anomalies, a proposed classification (an analysis of 144 cases). Fertil Steril 1979;32:40-46.
3. Ascher SM, Siewert B, Toriano R, et al. Benign conditions of the Female Pelvis, In Edelman RR, Hesselink JR, Zlatkin MB (Eds): Clinical MRI Vol 3 (3rd edition), Saunders, Elsiever 2006; 2988-3046.
4. Woolf RB, Allen WM: Concomitant malformations: The frequent simultaneous occurrence of congenital malformations of the reproductive and urinary tract. Obstet Gynecol 1953;2:236.
5. Sala E, Allison S, Ascher S, et al. Imaging in Gynaecology, In Adam A; Dixon AK (Eds): Grainger and Allison's Diagnostic Radiology and Textbook of Medical Imaging Vol 2 (5th edition), Churchill livingstone 2008;1217-41.
6. Buttram VC. Mullerian anomalies and their management. Fertil Steril 1983;60:159.
7. Golan A, Langer R, Bukovsky I, et al. Congenital anomalies of the mullerian system. Fertil Steril 1989;51:747.
8. Siegelman ES. MRI of the Female Pelvis. In Siegelman ES (Ed): Body MRI (Ist edition), EIsiever Saunders 2005;269-342 .
9. Carrington BM, Hricak H, Nuruddin RN et al. Mullerian Duct Anomalies: MR Imaging Evaluation. Rad 1990;176:715-20.
10. Zagoria RJ. The Female Genital Tract. In Zagoria RJ (Ed): The Requisites—Genitourinary Radiology (2nd edn), Mosby 2004;256-311.
11. Hendrickson MR, Kempson RL (Eds). Surgical Pathology of the Uterine Corpus Philadelphia, WB Saunders, 1980;452.
12. Gross BH, Silver TM, Jaffe MH. Sonographic features of uterine leiomyomas: Analysis of 41 proven cases. J Ultrasound Med 1983;2:4013.
13. Walsh JW. Grey-scale ultrasound in 204 proven gynecologic masses: Accuracy and specific diagnostic criteria. Radiology 1979;130:391.
14. Salem S, Wilson SR. Gynaecologic Ultrasound. In Rumack CM, Wilson SR, Charbonean JW (Eds): Diagnostic Ultrasound. Vol 1(3rd edition), Elsevier Mosby 2005;527-87.
15. Karasick S, Lev-Toaff AS, Toaff ME. Imaging of uterine leiomyomas. AJR 1992;158:799-805.
16. Tada S, Tsukioka M, Ishii C, et al. Computed tomographic features of uterine myoma. J Comput Assist Tomogr 1981;5:866-69.
17. Weinreb JC, Barkoff ND, Megibow A. The value of MR imaging in distinguishing leiomyomas from other solid pelvic masses when sonography is indeterminate. AJR 1990;154:295.
18. Hricak H, Tscholakoff D, Heinrichs L. Uterine leiomyomas: Correlation of MR, histopathologic findings and symptoms. Radiology 1986;158:385.
19. Aubel S, Wozney P, Ediwards RP. MRI of female uterine and juxta-uterine masses: Clinical application in 25 pattients. Magn Reson Imaging 1991;9:485.
20. Zwain M, McCartty S, Scoutt LM, et al. High-field MRI and US evaluation of the pelvis in women with leiomyomas. Magn Reson Imaging 1990;8:371.
21. Muto MG, Friedman AJ. The uterine corpus. In Ryan KJ, Berowitz RS and Barbieri RL, (Eds): Kistner's Gyncology, St Louis; Mosby 1995.
22. Pattani SJ. MRI of uterine leiomyosarcoma. Imagn Reson Imaging 1995;13(2):331.
23. Razavi M K, Hwang G, Jahed A , et al. Abdominal myomectomy versus uterine fibroid embolisation in the treatment of symptomatic uterine leiomyomas. AJR 2003;180:1571-75.
24. Burn PR, Mc Call J M, Chinn RJ, et al. Uterine fibroleiomyoma: MR imaging appearances before and after embolisation of uterine arteries. Rad 2000;214:729-34.
25. de Souza NM, Williams AD. Uterine arterial embolisation for leiomyomas: Perfusion and volume changes at MR imaging and relation to clinical outcome. Rad 2002;222:367-74.

26. Nikolic B, Spies JB, Abbara S, et al. Ovarian artery supply to uterine fibroids as a cause of treatment failure after uterine artery embolisation: a case report. J Vasc Interv Radiol 1999;10:1167-70.
27. Soyer P, Harry G, Cazier A. Uterine fibromyolipoma: Uncommon imaging features. Eur J Radiol 1991;13:67.
28. Houser LM, Carrasco CH, Shelhan LR. Lipomatous tumour of the uterus: Radiographic and ultrasonic appearance. BJR 1979;52:992.
29. Lehrman BJ, Nisenbaum HL, Glasser SA. Uterine myolipoma: Magnetic resonance imag-ing, computed tomographic, and ultrasound appearance. J Ultrasound Med 1990;9:665.
30. Azziz R. Adenomyosis: Current perspectives. Obstet Gynecol Clinics North Am 1989;16:221.
31. Bohlman ME, Ensor RE, Sander RC. Sonographic findings in adenomyosis of the uterus. AJR 1987;148:765.
32. Hulka CA, Hall DA, Mc Carthy K, et al. Sonographic findings in patients with adenomyosis: Can sonography assist in predicting extent of disease? AJR 2002;179;379-83.
33. Dimitrios Botsis, Dimitrios Kassasnos, George Antomou. Adenomyoma and Leiomyoma: Differential diagnosis with Transvaginal Sonography. J Clin Ultrasound 1998;26:21-25.
34. Kido A, Togashi K, Koyama T, et al. Diffusely enlarged uterus: evaluation with MR imaging. Radiographics 2003;23:1423-39.
35. Mark AS, Hricak H. Adenomyosis and leiomyoma: Differential diagnosis by means of Magnetic resonance imaging. Radiology 1987; 163:527.
36. Togashi K, Ozasa H, Konishi I. Enlarged uterus: Differentiation between adenomyosis and leiomyoma with MRI. Radiology 1989;171:531.
37. Ascher SM, Jha RC, Reinhold C. Benign myometrial conditions: Leiomyomas and adenomyosis. Top Magn Reson Imaging 2003;14:281-304
38. Johnson MA, Graham MF, Cooperberg PL. Abnormal endometrial echoes: Sonographic spectrum of endometrial pathology. J Ultrasound Med 1982;1:161-66.
39. Sheth S, Hamper UM, Kurman RJ. Thickened endometrium in the post-menopausal woman : Sonographic pathologic correlation. Rad 1993;187:135-39.
40. Hricak H, Frick S, Honda G. MR imaging in the evaluation of benign uterine masses. Am J Roent 1992;158:1043.
41. SmithBindman R, Kerlikowske K, Feldstein VA, et al. Endovaginal ultrasound to exclude endometrial cancer and other endometrial abnormalities. JAMA 1998;280:1510-1617.
42. Fedele L, Bianchi S, Dorta M, et al. Intrauterine adhesions: Detection with transvaginal US. Rad 1996;199:757-59.
43. Letterie GS, Haggerty MR. Magnetic resonance imaging of intrauterine synechiae. Gyaecol Obstet Invest 1994;37:66-68.
44. Bacclar AC, Wilcock D, Powell M, et al. The value of MRI in the assessment of traumatic intrauterine adhesions (Asherman's syndrome) Clin Radiol 1995;50:80-83.
45. Dixit R, Prakash A, Chowdhury V, et al. Pelvic Arterio-Venous Malfaormation. Radiological quiz – GU Imaging IJRI 2000;10:177-79.
46. Huang MW, Muradali D, Thurston WA, et al. Uterine arterio-venous malformation. Grey-scale and Doppler US features with MR imaging correlation. Radiology 1998;206(I):115.
47. Joshi M, Ganeshan K, Munshi HN. Ultrasound of Adnexal masses. Semin Ultrasound CT MRI 2008;29:72-97.
48. Siddall KA, Rubens DJ. Multi-detector CT of the Female Pelvis. RCNA 2005;43:1097-1118.
49. Patel MD. Practical Approach to the Adnexal Mass. RCNA 2006;44:879-99.
50. Giede KC. Ovarian Cysts in Postmenopausal Women : When to worry. The Canadian Journal of CME 2007;21-24.
51. Togashi K. MR imaging of the ovaries: Normal appearance and benign disease. RCNA 2003;41: 799-811.
52. Scoutt LM, Mc Carthy SM, Lange R. MR evaluation of clinically suspected adnexal masses. J Comput Assist Tomogr 1994;18(4):609.
53. Fulgheshu AM, Ciampelli M, Belosi C, et al. A new ultrasound criteria for the diagnosis of polycystic ovary syndrome: The ovarian stroma/total area ratio. Fertil Steril 2001;76: 326-31.
54. Hoffer FA, Kozakewich H, Colodny A, et al. Peritoneal inclusion cysts: Ovarian fluid in peritoneal adhesions. Rad 1988;169:189-91.
55. Jain KA. Imaging of Peritoneal inclusion cysts AJR 2000;174;1559-63.
56. Sohaey R, Gardner TL, Woodward PJ, et al. Sonographic diagnosis of peritoneal inclusion cyst. J Ultrasound Med 1995;14:913-17.

57. Tessler FN, Perrella RR, Fleischer AC, et al. Endovaginal sonographic diagnosis of dilated fallopian tubes. AJR 1989;153:523-25.
58. Athey PA, Cooper NB. Sonographic feature of parovarian cysts. AJR 1985;144:83-86.
59. Fleischer AC, Cullinan JC. Pelvic masses. Chap 6, Pg 61-70 In Copel JA, Reed KL (Eds): Doppler ultrasound in Obstetrics and Gynecology, Raven Press, Ltd 1995.
60. Buy JN, Ghossain MA, Hugol D. Characterisation of adnexal masses: Combination of Colour Doppler and Conventional Sonography Compared with Spectral Doppler Analysis Alone and Conventional sonography alone. AJR 1996;166:385-93.
61. Coleman BG. Transvaginal sonography of adnexal masses. In The Female Pelvis *RCNA* 30(4): 1992.
62. Wilbur A. Computed tomography of tubovarian abscesses. J Comput Assist Tomogr 1990;14(4):625-28.
63. Shamam OM, Bennel WF, Teteris NJ, et al. Primary fallopian tube adenocarcinoma presenting as a hydrosalpinx. CTappearance. J Comput Assist Tomogr 1988;12(4):674-75.
64. Mitchell DG, Mintz MC, Spritzer CE. Adnexal masses: MR imaging observations at 1.5 T, with US and CT correlation. Radiology 1987;162:319.
65. Friedman H, Vogelzang RL, Mendelson EB. Endometriosis detection by US with laparoscopic correlation. Radiology 1985;157:217-20.
66. Fishman EK. Computed tomography of endometriosis. J Comput Assist Tomogr 1983;7: 257-64.
67. Togashi K, Nishimura K, Kimura I. Endometrial cysts: Diagnosis with MR imaging. *Radiology* 1991;180:73.
68. Outwater EK, Dunton CJ. Imaging of the ovary and adnexa: Clinical issues and applications of MR imaging. Radiology 1995;194:1.
69. Glastonbury CM. The shading sign. Rad 2002;224:199-201.
70. Sloan RD. Cystic teratomas (dermoid) of the ovary. Radiology 1963;81:847.
71. Quinn SF, Erickson S, Black WC. Cystic ovarian teratomas: The sonographic appearance of the dermoid plug. Radiology 1985;155:477-78.
72. Friedman AC, Pyatt RS, Hartman DS. CT of benign cystic teratomas. *AJR* 1982;138:659.
73. Buy JN. Cystic teratoma of the ovary: CT detection. Radiology 1989;171:697-701.
74. Togashi K, Nishimura K, Itoh K. Ovarian cystic teratomas. MR imaging. Radiology 1987;162:669.
75. Mitchell DG. Chemical shift magnetic resonance imaging: Applications in the abdomen and pelvis. Top Magn Reson Imaging 1992;4(3):46.
76. Graif H, Shalev J, Strauss S. Torsion of the ovary: Sonographic features. AmJ Roentgenol 1984; 143:1331.
77. Rha SE, Byun JY, Tung SE, et al. CT and MRI imaging findings of adnexal torsion. Radiographics 2002;22:283-94.
78. Argenta PA, Yeagley TJ, Ott G, et al. Torsion of the uterine adnexa: pathological correlations and current management trends. J Reprod Med, 2000;45:831-36.
79. Eyvazzadeh AD, Levine D. Imaging of Pelvic Pain in the First Trinester of Pregnancy RCNA 2006;44:863-77.
80. Nuberg DA, Mack LA, Jeffrey RBJr, et al. Endovaginal sonographic evaluation of ectopic pregnancy: A prospective study AJR, 1987;149: 1181-86.
81. Russel SA, Filly RA, Damato N. Sonographic diagnosis of ectopic pregnancy with endovaginal probes. What really has changed? Ultrasound Med 1993;12:145-51.
82. Jeong YY, Outwater EK, Kang HK. Imaging Evaluation of Ovarian Masses: Radiographics 2000;20:1445-70.
83. Funt SA, Hann LE. Detection and characterisation of adnexal masses. RCNA 2002;40:591-608.
84. Lee SI. Radiological Reasoning: Imaging characterisation of bilateral adnexal masses. AJR 2006;187:S460-66.

Chapter

26

Imaging in Gynecological Malignancies

Sanjay Thulkar, Smriti Hari

GYNECOLOGICAL MALIGNANCIES IN INDIA

The incidence of various gynecological cancers in India is different from that of the developed countries. The incidence of cervical cancer is high in India and that of the endometrial cancer and ovarian cancer is low as compared with the western population. Socioeconomic and environmental factors are mainly responsible for this phenomena.[1] Annual age adjusted incidence (AAR) of cervical cancer in India ranges from 13 (Mumbai) to 24.8 (Chennai) per 100,000 women per year.[2] It used to be the most common cancer in females in India, however, now the breast cancer has taken over this position in most population based cancer registries of India. The incidence of ovarian cancer is 2.2 to 8 and that of endometrial cancer is 0.7 to 9.5 per 100,000 women per year.

CARCINOMA OF CERVIX

Peak incidence of carcinoma of cervix occurs between 30 and 50 years of age. Main risk factors for the cervical cancer include early age at first coitus, multiple sexual partners and sexually transmitted human papilloma virus (HPV) infection.[3] Widespread screening and early detection of cervical cancer has been made possible with Papanicolaou (PAP) smear examinations.

Approximately, 90 percent of cervical cancers are squamous cell carcinomas, others include adenocarcinomas and sarcomas.[3] Cervical carcinoma develops through various stages of dysplasia of cervical epithelium. It is designated as cervical intraepithelial neoplasia (CIN). Highest grade of CIN is called carcinoma *in situ* which is still limited by basement membrane. Breach of the basement membrane leads to invasive carcinoma. Clinically, patients present with vaginal bleeding and discharge. Patients with advanced disease may complain of pelvic pain and other symptoms related to lower urinary tract.

Spread of cervical cancer occurs through direct extension into parametrium and the pelvic lymph nodes. Direct invasion of uterus and upper vagina also occurs. Involvement of urinary bladder, rectum and pelvic sidewalls occurs late. Hematogenous spread to lungs, bone, liver and brain is uncommon and late feature in the course of the cervical cancer. Invasive cervical cancers are staged according to International Federation of

Gynecologists and Obstetricians (FIGO) staging system into four stages (Table 26.1). The staging is clinical and may include findings of hysteroscopy, cystoscopy, proctoscopy, curettage, biopsy, IVP and X-rays. Prognosis depends on patient's age, tumor size and lymph node status as well histopathological type and grade of the tumor. Lymph node status is an important prognostic factor; the 5 years survival rates are 90 percent for node negative and 50 percent for node positive diseases.[4,5]

Imaging Modalities

Conventional Radiography

International Federation of Gynecologists and Obstetricians (FIGO) staging system uses the findings on chest radiography, IVP and barium enema. The demonstration of urinary obstruction on IVU is classified as stage III B. The findings on IVU include delayed nephrogram, hydro-ureteronephrosis or extrinsic compression or deviation of ureters. Involvement of rectum and sigmoid colon can be seen on barium enema as irregularity of outline, ulceration and fistula formation. Presently, IVU and barium enema are not routinely performed, instead cross-sectional imaging modalities such as US, CT and MRI are preferred.[4] These may be supplemented with sigmoidoscopy and cystoscopy.

Table 26.1: Staging of the carcinoma of cervix

Stage 0:	**Carcinoma *in situ***
Stage I:	**Invasive tumor confined to cervix.** IA: Preclinical (subdivided into IA1 when stromal invasion is < 3 mm deep and 7 mm wide and IA2 when it is greater) IB: Clinically detectable (subdivided into IB1, if < 4 cm and IB2, if > 4 cm)
Stage II:	**Spread beyond uterus** IIA: Involvement of upper third of vagina IIB: Involvement of parametrium not extending to side wall
Stage III:	**Extension to the pelvic side wall/ lower 3rd of vagina/ hydronephrosis** IIIA: Involvement of lower third of vagina IIIB: Involvement of pelvic side wall and/ or hydronephrosis
Stage IV:	**Pelvic visceral involvement or distant metastases** IVA: Involvement of bladder or rectum IVB: Distant metastases

Ultrasonography

Cervical tumors are usually isoechoic to normal cervix and hence are not readily identified on ultrasonography.[4] Transvaginal and transrectal ultrasonography may show nonspecific enlargement of the cervix.[6] Transvaginal color Doppler imaging does not offer any improvement in detection and characterization of cervical cancer.[7] Large necrotic tumors are hypoechoic and hence these can be identified on ultrasonography. Presence of hydro/pyometra suggests obstruction of endocervical canal by the tumor. Ultrasonography readily detects hydronephrosis.

CT

Cervical cancer is poorly depicted on CT. The mass may not be seen or seen as nonspecific enlargement of the cervix. When mass is demonstrated, it is hypodense and heterogeneous, often with peripheral enhancement[4,8] (Fig. 26.1) CT does not accurately detect early parametrial invasion. Features suggestive of early parametrial invasion include irregular margins of the cervix and stranding in parametrium. However, these findings can also be caused by reactive or inflammatory changes without tumor extension. Advanced parametrial invasion on CT is suggested by soft tissue mass in

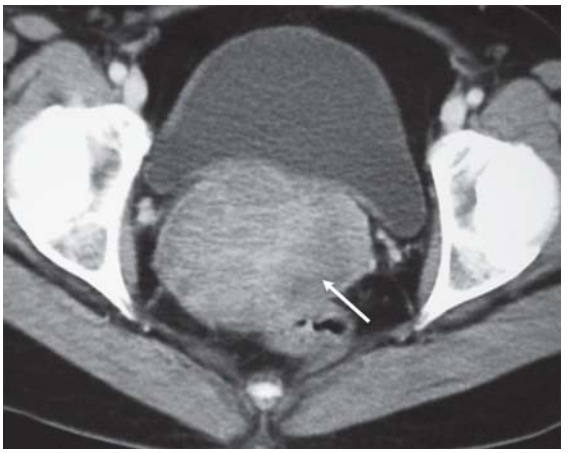

Fig. 26.1: Carcinoma of cervix: CECT of pelvis shows a bulky heterogeneously enhancing mass (arrow). It is confined to cervix as there is smooth interphase with the myometrium

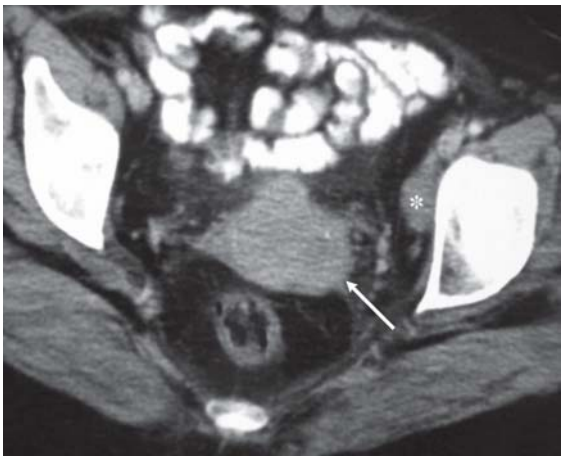

Fig. 26.2: Carcinoma of cervix: CECT shows isodense cervical mass with irregularity of the outline and extension of soft tissue (arrow) in left parametrium suggestive of parametrial invasion. Enlarged left opturator lymph node (asterisk) is also seen

parametrial fat, encasement of ureter or thickening and nodularity of uterosacral ligament[9] (Figs 26.2 and 26.3). CT findings suggestive of pelvic sidewall invasion include extension of the tumor within 3 mm of lateral wall of pelvis, encasement of iliac vessels, invasion of obturator internus or pyriformis muscles or bone destruction.[4] Ureteric obstruction is reliably detected by CT, thereby obviating the need for IVU (Fig. 26.3). Invasion of urinary bladder or rectum occurs late in course of the disease. On CT, this may be seen as loss of fat plane and irregular wall thickening.

CT is fairly accurate in evaluation of lymph nodal metastases (Figs 26.2 and 26.3). Presence of central necrosis in the lymph nodes is highly specific for metastatic involvement.[10] Distant metastases may be seen in lungs, liver and bones. Peritoneal metastases may also occur in carcinoma of cervix. These are seen as peritoneal nodules, thickening and ascites.

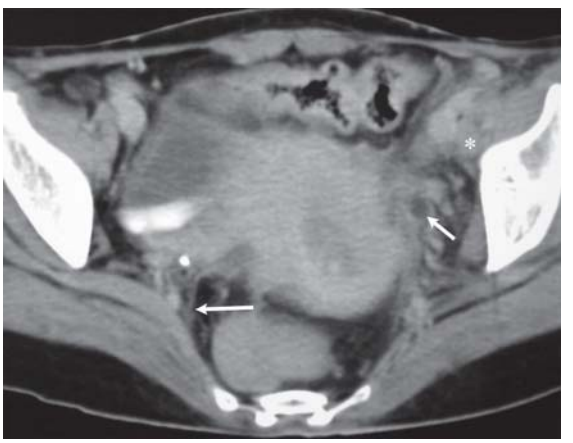

Fig. 26.3: Carcinoma of cervix: Delayed pelvic image of the CECT shows large cervical mass with soft tissue stranding involving the right pyriformis muscle (arrow) suggestive of pelvic wall invasion. Urinary bladder and right ureter is opacified, however, left ureter is dilated and unopacified (small arrow) suggestive of poorly functioning left kidney. Enlarged left external iliac lymph node (asterisk) is also seen

MRI

Superior contrast resolution has made MRI the imaging modality of choice for evaluation of cervical cancer. Indications of MRI include

pre-treatment evaluation of local tumor extent and nodal involvement, assessment of treatment response and detection of recurrent disease.[9]

T1, T2 and contrast enhanced T1-weighted images are normally obtained in axial and sagittal planes. Excellent contrast between tumor and the cervical tissue allows accurate delineation and measurement of tumor size on these images.[11] On T2W image, the tumor is seen as a hyperintense mass surrounded by hypointense cervical stroma. On contrast enhanced T1W image, small tumors enhance homogeneously (Figs 26.4A and B). Large tumors may be necrotic and do not enhance, however, they often have enhancing rim surrounding them. Demonstration of intact peripheral fibrous layer of the cervix, which is normally seen as a hypointense ring on T2W images (Fig. 26.4A), has 95% negative predictive value for parametrial invasion.[5,12] Disruption of stromal ring suggests full thickness stromal invasion but not necessarily parametrial invasion. Various MRI features of parametrial invasion include nodular or irregular tumor signal intensity extending into the parametrium (Figs 26.5A and B), focal tumor bulge into the parametrium, encasement of ureter or periuterine vessels and thickening and nodularity of uterosacral ligament.[4,9] Parametrial invasion may be overestimated on T2W images in large size tumors because of stromal edema caused by tumor compression.[5]

Lateral pelvic wall involvement is suggested by tumor proximity (less than 3 mm) or hyperintensity of muscles on T2W images, encasement of iliac vessels or bony destruction. MRI is highly accurate for detection of the invasion of urinary bladder, vagina and rectum.[9,11] Bladder invasion is suggested by disruption of low signal intensity bladder wall, irregularity of bladder wall or mass protruding into the lumen. Rectal invasion is rare and seen as segmental thickening or loss of anterior rectal wall.[13]

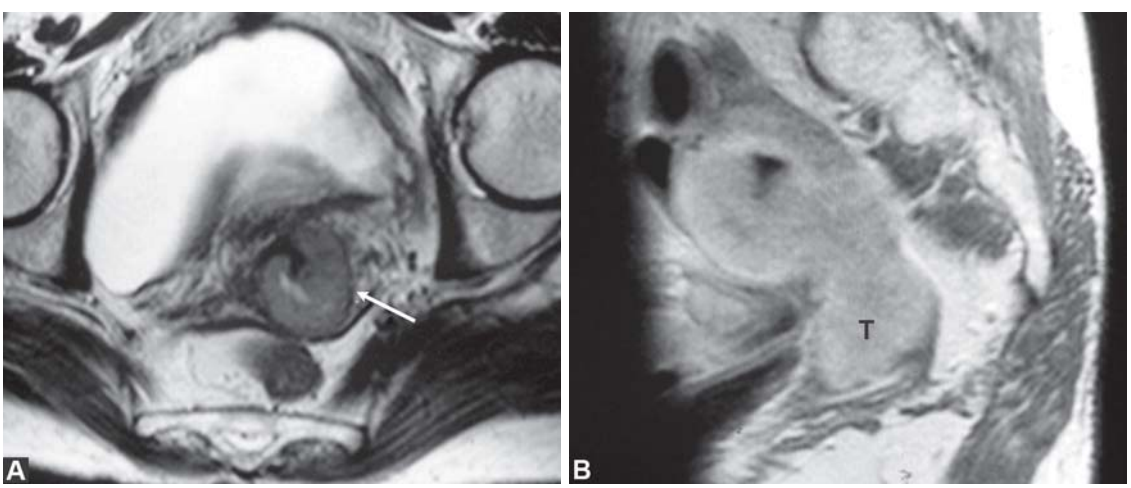

Figs 26.4A and B: Carcinoma of cervix: **(A)** T2W axial MR image shows hyperintense mass in the cervic surrounded by the hypointense rim of cervical stroma (arrow) **(B)** contrast enhanced sagittal T1 W image shows extension of the tumor (T) in lower part of the body of the uterus

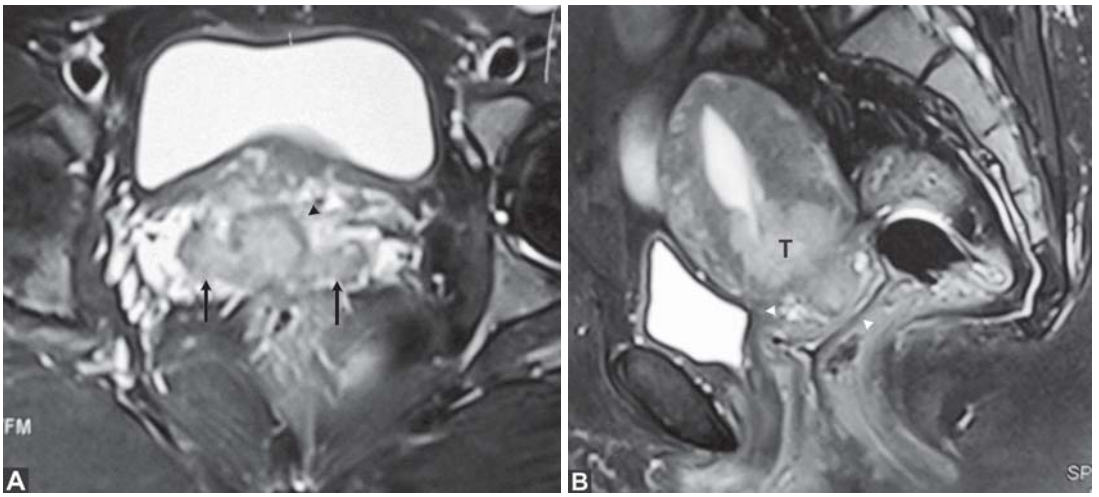

Figs 26.5A and B: Carcinoma of cervix: **(A)** T2W axial MR image shows hyperintense mass in the cervix. It is surrounded by hypointense stromal ring anteriorly (black arrowhead), however, this ring is disrupted posterolaterally with tumor sensity soft tissue extension in bilateral parametrium (arrows). **(B)** Contrast-enhanced sagittal T1W images shows enhancing tumor (T) in the cervix. Preserved hypointense walls of urinary bladder and rectum (arrowheads) exclude their invasion by the tumor

Imaging Strategies in Cervical Cancer

Imaging has no role in the diagnosis of cervical cancer. Routine pretreatment work up includes clinical examination, laboratory studies and chest radiography. FIGO staging system is clinical and it has several limitations. Estimation of tumor size and spread may not be always accurate on clinical examination. Lymph node status is not included in staging. Findings on chest X-ray, IVP or barium enema are included in staging but not the USG, CT or MRI. Even though cross-sectional imaging findings have been shown to improve the accuracy of staging.[14,15] FIGO guidelines prohibits the use of US, CT or MR imaging findings for staging purpose.[3] In practice however, cross-sectional imaging findings are often used to choose most appropriate treatment options without changing the clinical stage.

In early cervical cancers (clinically stage IA) with tumor size less than 2 cm, chances of local or lymphatic spread are minimal and hence no cross-sectional imaging is necessary. MRI is the investigation of choice when clinical stage is 1B or higher.[13] In advanced disease (stage II or more), both MRI and CT can be used for evaluation, MRI being the preferred modality.[16] MRI is also recommended when clinical examination and staging is equivocal. Imaging assessment of the tumor and its spread assist in correct therapeutic decisions. Patients with clinically occult bulky tumors (> 4 cm) or lymphadenopathy may receive chemoradiation instead of upfront surgery.

For parametrial invasion, overall sensitivity of CT is 55 percent and that of MRI is 74 percent.[17] Early parametrial invasion however, is better assessed clinically.[18] IVP and barium enema have now become obsolete in staging work-up as same information can also be obtained with CT or MRI. Absence of rectal and bladder involvement on MRI has

100 percent negative predictive value and this can obviate the cystoscopy and sigmoidoscopy in patients with cervical cancer[19] (Fig. 26.5B).

Accuracy of MRI in detection of lymph nodal metastases is similar to CT. It is up to 85 percent for CT and 89 percent for MRI.[9] The sensitivity is poor as metastases in normal sized lymph nodes cannot be identified using size criteria. Use of lymph node specific contrast agent, such as ultra small super paramagnetic iron oxide (USPIO) can significantly improve the sensitivity of MRI in detection of lymph node involvement.[20]

PET

PET imaging is not routinely obtained in cervical cancer; however, it is a useful adjunct to CT and MRI for the evaluation of lymph nodes, detection of distant metastases and assessment of treatment response.[9] PET has sensitivity and specificity of 84 percent and 95 percent for para-aortic lymph nodes and 79 percent and 99 percent for pelvic lymph nodes.[21] It is more sensitive than MRI for this purpose.[22] FDG uptake in primary tumor is also an independent predictor of the disease free survival.[23] Hence, PET is useful imaging modality in patients with advanced cervical cancer for making treatment decisions and determining the prognosis.

Treatment and Follow-up

Early cervical cancers (up to stage II-A) can be treated with both surgery and radiotherapy, surgery being the preferred modality for younger women. Those with positive margin or nodes on surgery also receive postoperative chemoradiotherapy. Radiotherapy is the primary treatment modality for most patients with advanced (stage II-B or more) disease.[3]

After radiation treatment, the tumor and uterus normally decrease in size and the cervix shows low signal intensity on T2W images.[9] However, sometimes edema or necrosis may appear hyperintense mimicking residual tumor. Patients are normally followed up for five years with clinical examinations, lab studies, PAP smear and chest radiography.

Recurrence of carcinoma of cervix is most commonly detected within first two years after the treatment.[3] It is uncommon after five years. Vaginal vault and lymph nodes are the most common sites of the local recurrence. These may invade, pelvic sidewall, bladder or rectum. Recurrence at distant metastatic sites includes metastases in liver, lung, bone adrenals and peritoneal carcinomatosis.[13] Both CT and MRI demonstrate the recurrences but it is better assessed with MRI. Recurrence is seen on T2W images as heterogeneous mass and enhancement on post-contrast T1W images. However, early radiation changes and infection may also show similar findings.[13] MRI has high sensitivity (90-91%) but low specificity (22-38%) for detection of recurrence.[9] PET is a better investigation for detection of recurrence with sensitivity and specificity of more than 80 percent and its use may improve the management of recurrent cervical cancer in many patinets.[24,25]

CARCINOMA OF ENDOMETRIUM

Prolonged estrogen stimulation is the main risk factor for endometrial cancer.[4] An increased incidence of endometrial carcinoma is seen in women taking estrogen such as for oral contraception or postmenopausal hormone replacement therapy. Increased incidence is also noted in postmenopausal women taking tamoxifen as a part of

hormonal therapy for breast cancer. Other risk factors include nulliparity, obesity, diabetes. The peak incidence of endometrial carcinoma is between the ages of 55 and 65 years.

Most patients present with postmenopausal vaginal bleeding or discharge, however, it can also occur in premenopausal women. In less than 5 percent of patients, the tumor is detected incidentally on cervical cytology or histopathology of uterus removed for benign causes.[3] The diagnosis of endometrial carcinoma in suspected patients is made by histopathological examination of endometrial biopsy and curettage. Up to 90 percent of the endometrial cancers are adenocarcinoma, the rest include adenosquamous carcinoma, clear cell carcinoma and papillary serous carcinoma.[13]

Spread and Staging

Endometrial carcinoma typically arises from body of uterus (upper uterine corpus). The early growth is exophytic into the endometrial cavity followed by progressive invasion of myometrium. This pattern causes uterine enlargement. The tumor spreads caudally to involve cervix and vagina and axially to involve adnexa, parametrium and other pelvic organs. Lymphatic spread of the endometrial carcinoma is complex in nature and hence any group of pelvic lymph nodes or retroperitoneal para-aortic lymph nodes may be involved.[4] Hematogenous spread to lungs, liver, bones and brain occurs late in the course of the disease. Endometrial cancer is staged according FIGO staging system (Table 26.2). It is a surgico-pathological staging system.

Table 26.2: Staging of the carcinoma of endometrium

Stage I:	**Tumor confined to the body of uterus** IA: Limited to endometrium IB: Invade less than half of myometrium IC: Invade half or more of myometrium
Stage II:	**Tumor involving cervix** IIA: Endocervical invasion only IIB: Cervical stromal invasion
Stage III:	**Tumor extending outside uterus but not outside true pelvis** IIIA: Involement of serosa, adnexa or malignant ascites IIIB: Vaginal involvement IIIC: Pelvic or para-aortic lymph nodes
Stage IV:	**Bladder/rectum invasion or distant metastases** IVA: Bladder or bowel involvement IVB: Distant metastases

Imaging Modalities

Conventional Radiography

Chest radiographs are routinely obtained in all patients diagnosed to have endometrial carcinoma. Skeletal radiography or scintigraphy can be performed if bone metastases are suspected. Similar to the carcinoma of cervix, IVU and barium studies are obsolete in evaluation of endometrial carcinoma.[4]

Ultrasonography

Ultrasonography is an important modality for screening, diagnosis as well as staging of endometrial carcinoma. Transvaginal sonography is more accurate than trans-abdominal sonography for this purpose. Normal endometrium is seen as an echogenic stripe in the uterine cavity. It is surrounded by inner myometrium, which is seen as hypoechoic layer around the echogenic endometrium (endometrial halo).

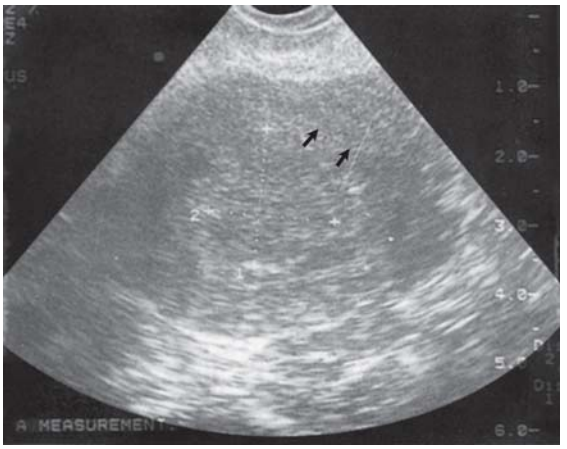

Fig. 26.6: Carcinoma of endometrium: Transvaginal sonogram shows thickened endometrium with loss of subendometrial halo (arrowheads) by endometrial carcinoma

Early endometrial cancers typically appear as widening of endometrial layer (Fig. 26.6). Double layer endometrial thickness of greater than 5 mm in postmenopausal women is considered abnormal.[26] Exception to this is women on estrogen therapy in whom endometrial stripe thickness up to 7 mm is considered normal.[4] In premenopausal women, the upper limit of endometrial thickness is 15 mm. Thickening of endometrium can also be seen in endometrial hyperplasia or polyps. Saline infusion sonohysterography improves the accuracy of the diagnosis.[27] Color Doppler shows diffusely increased vascularity in multivessel pattern in endometrial cancer, in contrast to the pedicle artery sign seen in polyps.[28] Transvaginal sonography along with endometrial aspiration samplings can be used for screening of endometrial cancer in high-risk women.

Obliteration of endometrial halo (produced by inner myometrium) or irregularity of endometrium-myometrium interphase on transvaginal sonography is suggestive of myometrial invasion.[9] Larger tumors cause enlargement and distortion of the echotexture of the uterus (Fig. 26.7A). Sonography is not suitable to detect extrauterine spread of the tumor and lymph nodal metastases.

CT

Endometrial cancer appears as diffuse or focal enlargement of endometrium. The tumor enhances less than the adjacent myometrium (Fig. 26.7B). Irregularity of uterine outline and stranding of parametrium is suggestive of an extrauterine spread. CT readily demonstrates lymph nodal enlargement, peritoneal deposits and distant metastases.[9] Myometrial invasion of the tumor is difficult to assess on the CT. Both false positive and false negative errors are common with CT.

MRI

This imaging modality is the technique of choice for evaluation of endometrial carcinoma. It provides an excellent morphological display of uterus and adjacent structures. T2W and gadolinium enhanced T1W axial and sagittal images are mostly used. The zonal anatomy is best demonstrated on T2W image. Endometrium appears hyperintense and is surrounded by hypointense rim of junctional zone representing inner myometrium. The outer myometrium shows medium signal intensity.

Endometrial cancer appears isointense on T1W and hyperintense on T2W images when compared with myometrium (Figs 26.8A and B). Large tumors are often seen as polypoidal masses expanding the endometrial cavity. Presence of normal hypointense junctional zone seen on T2W images excludes myometrial invasion. Obliteration of

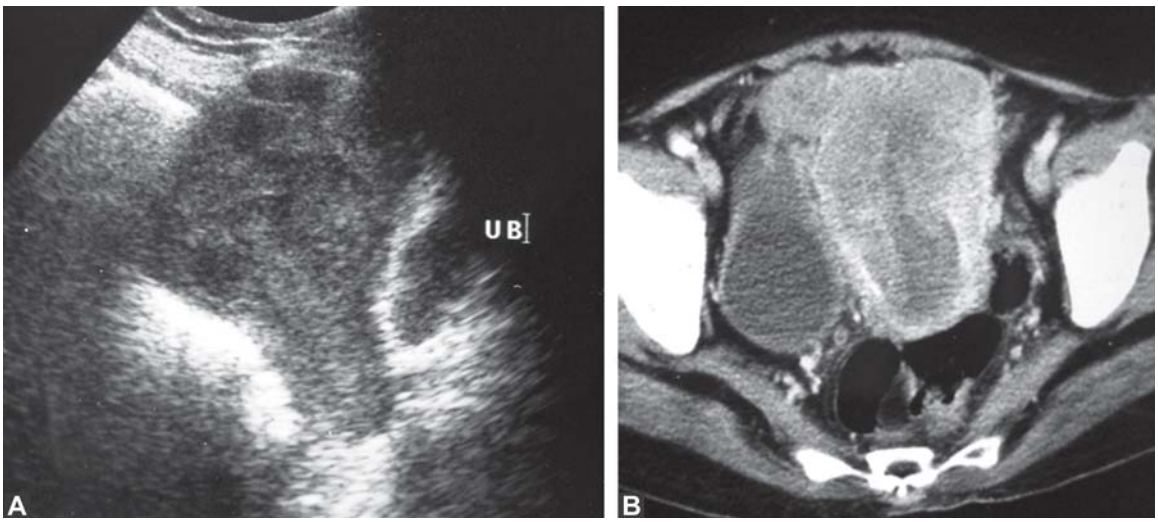

Figs 26.7A and B: Carcinoma of the endometrium: **(A)** Sonography shows enlarged, distorted and heterogeneous uterus. **(B)** CECT also shows the similar findings. The tumor enhancement is lesser than that of the myometrium

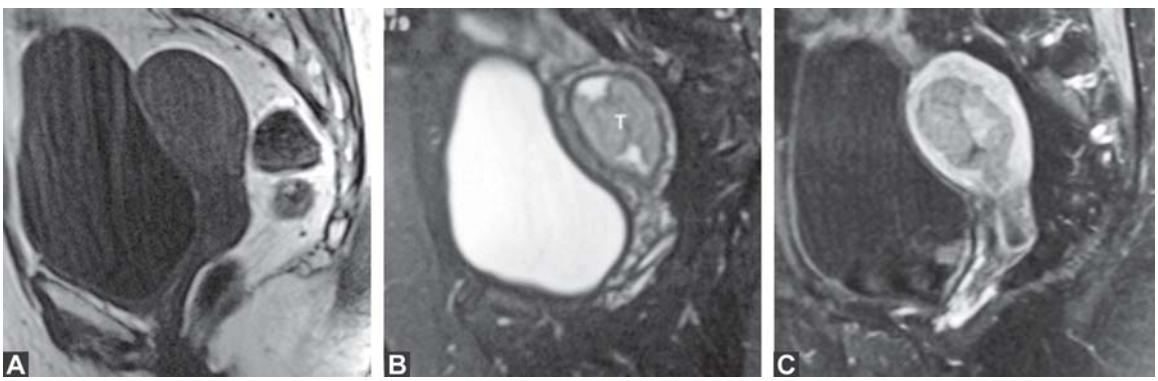

Figs 26.8A to C: Carcinoma of endometrium: Sagittal T1W MRI shows nonspecific enlargement of the uterus as the tumor is isointense. (B) Sagittal fat suppressed T2W MR image shows large tumor (T) distending the uterine cavity. It is moderately hyperintense as compared with surrounding myometrium. The junctional zone is indistinct in this atrophic uterus (C) On contrast enhanced T1W MR image, the tumor enhances less than the myometrium

junctional zone or irregularity of endometrium-myometrium interphase suggests myometrial invasion[9] (Fig. 26.9). After intravenous gadolinium, endometrial carcinoma shows less enhancement compared to myometrium (Fig. 26.8C). Dynamic contrast enhanced studies are more useful in detection of small tumors and to assess myometrial invasion. Early phase (0-1 minute) shows better contrast between inner and outer myometrium, the former enhances earlier. Deep myometrial invasion is best assessed at equilibrium (2-3 minutes) as tumor myometrium contrast is highest at this time. Presence of low signal intensity tumor in outer myometrium suggests deep invasion

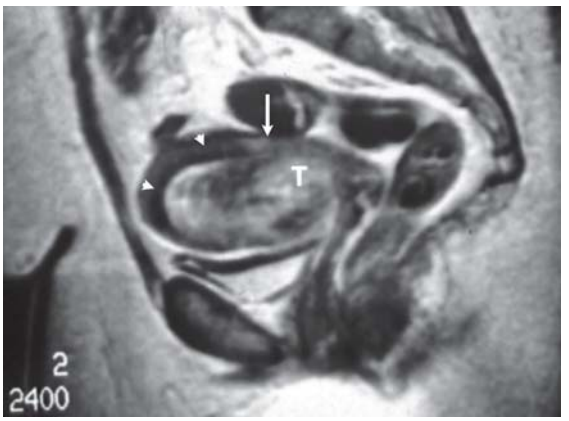

Fig. 26.9: Carcinoma of endometrium: T2W sagittal MR images shows hyperintense endometrial tumor (T). The junctional zone, seen as hypointense rim, is intact in fundus (arrowheads), however, it is obliterated in lower part with tmor extension into deep myometrium (arrow)

(Stage 1C) disease. Cervical invasion (Stage II) is better assessed at delayed (4-5 minutes) phase.[13] Spread to parametrium (Stage IIIA) is seen as disruption of serosal outline and direct toumor extension into the parametrium. Vaginal involvement (Stage IIIB) is seen as segmental loss of the low intensity vaginal wall.

Imaging Strategies in Endometrial Cancer

Transvaginal sonography is the most useful modality for detection of endometrial cancer. Patients with abnormal findings on sonography then undergo dilatation and curettage or endometrial biopsy for definitive diagnosis. Transvaginal sonography is also useful to determine the extent of myometrial invasion, however, MRI provides more accurate information about the degree of invasion and locoregional extent of the disease.

Determining the presence and depth of myometrial invasion on MRI is important. There is six-seven fold increased prevalence of lymphadenopathy if depth myometrial invasion is more than 50 percent (Stage 1C) when compared with patients with less than 50 percent (Stage 1B) or absent (Stage 1A) myometrial invasion. The preoperative assessment of myometrial invasion helps to plan the extent of lymph node sampling.[9] MR evaluation of endometrial cancer may be difficult in elderly women with atrophic uterus as junctional zone may be indistinct (Fig. 26.8B). The junctional zone is also difficult to evaluate when it is irregular and thickened in women with adenomyosis and in presence of myometrial distortion by large tumor or fibroid. MRI has 87 percent sensitivity and 91 percent specificity in assessment of myometrial invasion, however, sensitivity for detection of lymph node involvement is only 50 percent.[29]

Treatment and Follow-up

Carcinoma of the endometrium is surgically stagzed and treated tumor. All patients with early (Stage I and II) endometrial cancers are treated with hysterectomy and bilateral salpingo-oophorectomy. After surgery, those with high risk of recurrence receive adjuvant radiotherapy. Tumor grade and stage, depth of myometrial invasion, cervical stromal invasion and lymph node status are important prognostic indicators in this regard. Advanced (Stage III and IV) tumors are treated with pelvic radiotherapy. After radiotherapy, patients with resectable tumors are operated for removal of residual tumor. Rests of the patients are subjected to extended field radiotherapy or chemotherapy.[4]

Patients are followed with clinical examination. Recurrence can be local or at distant metastatic sites. Almost all recurrences occur within three years.[30]

Local recurrences usually develop in vaginal vault and these are detected on follow-up clinical examinations. Hence, routine imaging for follow-up is not required. CT and MRI are performed only when pelvic examination is abnormal or distant metastases are suspected.[4]

OVARIAN MALIGNANCIES

Carcinoma of the ovary is the second most common gynecological malignancy. This is classified according to tissue of origin. Majority are epithelial tumors. Others include germ cell tumors, stromal-sex cord tumors and metastatic cancers from extra-ovarian primary sites. Incidence of these types varies widely. As per ten years data at author's institute, epithelial tumors constitute 83 percent while germ cell tumors constitute 9.5 percent of ovarian tumors. 3.2 percent each are stromal tumors and metastatic carcinomas of the ovary.[31]

Epithelial Ovarian Carcinoma

These account for up to 90 percent of all malignant ovarian cancers. These are separated into two major categories; invasive (80%) and noninvasive or borderline (20%) tumors. Epithelial invasive cancers are further classified into serous cystadenocarcinoma, mucinous cystadenocarcinoma, endometroid carcinoma, clear cell carcinoma and undifferentiated tumor.[32] Ovarian carcinoma predominantly occurs in postmenopausal women and up to 85 percent of them present with peritoneal spread.[33] (Stage III). About 10 percent of epithelial ovarian cancers are hereditary. These include women with breast ovarian cancer syndrome (with BRCA1 and BRCA2 mutations) and hereditary nonpolyposis colorectal cancer syndrome. These women have up to 60 percent lifetime risk of developing ovarian cancers and the risk can be reduced with prophylactic bilateral salpingo-oophorectomy after childbearing.[34]

Patients usually present with abdominal pain, distention or symptoms related to gastrointestinal tract/ or and genitourinary tract compression or nonspecific constitutional symptoms. A pelvic mass may be evident on abdominal palpation or pelvic examination but it is usually detected or confirmed on initial sonographic examination.

Spread of the tumor is transcoelomic and follows the pathways of peritoneal fluid circulation. Accordingly, deposits in right subdiaphragmatic region and para-colic gutters occur early along with ascites. Eventually all peritoneal surfaces, omentum and mesentery may be involved. Metastases to the para-aortic and pelvic lymph nodes also occur.

Ultrasonography

Ultrasonography is the first imaging modality to diagnose or confirm the clinically suspected adnexal mass. It is also used to characterize the adnexal masses based on their morphological features. Transvaginal sonography is better than transabdominal approach for characterization of adnexal masses. Large, bilateral, complex solid-cystic masses are usually malignant. Cysts with thick walls, irregular thick septation (more than 3 mm), papillary projections or mural nodules favor malignancy (Fig. 26.10A). Ovaries enlarged for the age are also suspicious for malignancy. Presence of ascites, peritoneal deposits and lymph node enlargement are other supportive evidences. Physiological hemorrhagic cysts may some-

times have suspicious appearances on ultrasound and hence it is important to follow these with ultrasound and only persistent lesions should be considered abnormal.[32]

Doppler studies are important in evaluation of adnexal masses. Nonhyperechoic mass with central vascularity on color Doppler is suggestive of malignancy.[35,36] On pulsed Doppler, malignant tumors have abnormal neovascularity and low resistance flow pattern. Low pulsatility index (1.4 or less) and low resistive index (0.4 or less) suggest malignancy. Positive predictive value of 98 percent has been reported for the diagnosis of ovarian malignancy using these features.[37] However, subsequent studies found that characterization of the adnexal masses based on Doppler studies only is unreliable as similar findings may also be seen in inflammatory diseases and physiological cysts.[38,39] A large meta-analysis of the studies concluded that combined morphological and Doppler transvaginal sonographic evaluation provides the best results in detection of ovarian cancer.[40]

Screening for Ovarian Cancer

The five-year survival rates up to 90 percent for stage I cancers as compared to 15-20 percent in stage III or IV cancers and the fact that most patients present with advanced disease make screening important option.[41] Transvaginal ultrasound, Doppler studies and serum CA 125 measurement can be used in combination for screening of the ovarian cancer.

There are several difficulties for screening of ovarian cancer. Ultrasound features are nonspecific. This leads to several false positive results and unnecessary surgeries. CA 125 is elevated in only 50 percent of stage 1 epithelial cancers and it is relatively insensitive for mucinous tumors.[34] Also, there is low incidence of ovarian cancer in general population and the cost of screening is high. Currently, a large screening trial is going on in USA (PLCO or prostate, lung, colorectal and ovary) but the results and recommendations will be available only after a decade.[34] At present, there is no evidence that screening reduces the mortality from

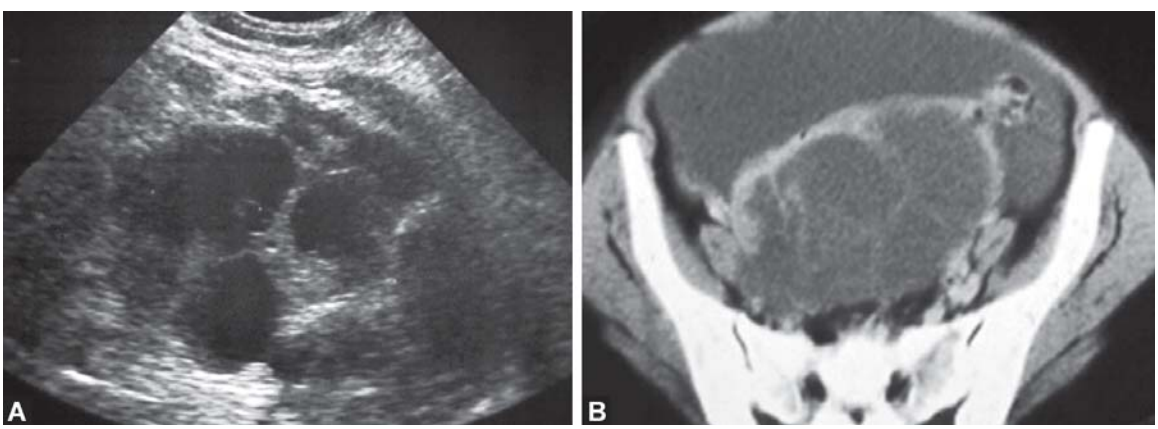

Figs 26.10A and B: Carcinoma of ovary: **(A)** Ultrasonography shows complex cystic pelvic mass with irregular thick septations and solid component. **(B)** CECT of pelvis shows similar findings

ovarian cancer and hence not recommended for women with or without family history of ovarian cancer.[42] The exception may be women with BRCA mutations in whom screening may be performed until prophylactic bilateral oophorectomy after childbearing.[43]

CT

CT is the main stay of preoperative evaluation of ovarian cancer. The CT features of ovarian cancer show varied morphological patterns: A multilocular cyst, thick wall or internal septations, solid mural nodules, complex cystic-solid mass or lobulated papillary mass (Figs 26.10 to 26.12). Solid looking areas that do not enhance may represent blood or mucinous fluid with high protein content.[32,33] Normal size ovaries which are large for the age, especially when these show papillary excrescences are also suspicious for malignancy (Fig. 26.13). Calcification is occasionally seen in papillary serous adenocarcinoma and Brenner tumor (Fig. 26.14). Ancillary findings of malignancy such as ascites, peritoneal deposits, lymphadenopathy and pleural effusion may also be present. Although CT is not normally used for differentiation of benign and malignant adnexal masses, it is equivalent to ultrasonography for this purpose.[44]

Involvement of uterus, rectum, colon and small bowel by the tumor is well-demonstrated on CT (Figs 26.12 and 26.14). It can also detect deposits on peritoneum, liver or bowel surfaces. Peritoneal deposits are seen as soft tissue nodules or plaque like thickening and enhancement of the peritoneum (Figs 26.15 and 26.16). These may coalesce to form large masses. Peritoneal deposits are more commonly seen at the peritoneal reflections where the peritoneal fluid tends to accumulate. Accordingly, common sites are pouch

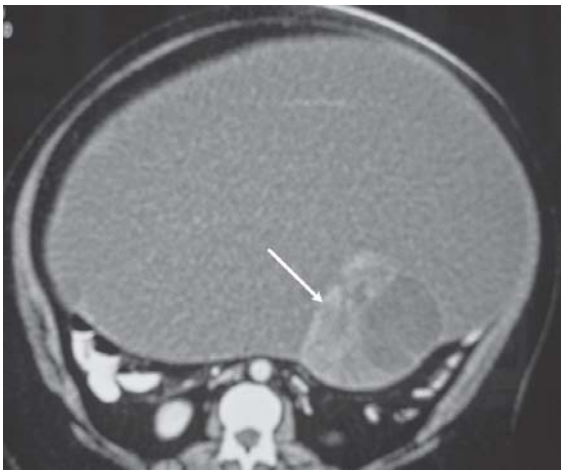

Fig. 26.11: Carcinoma of ovary: CECT of pelvis shows clear cell carcinoma of ovary as a large cyst with solid mural nodule (arrow)

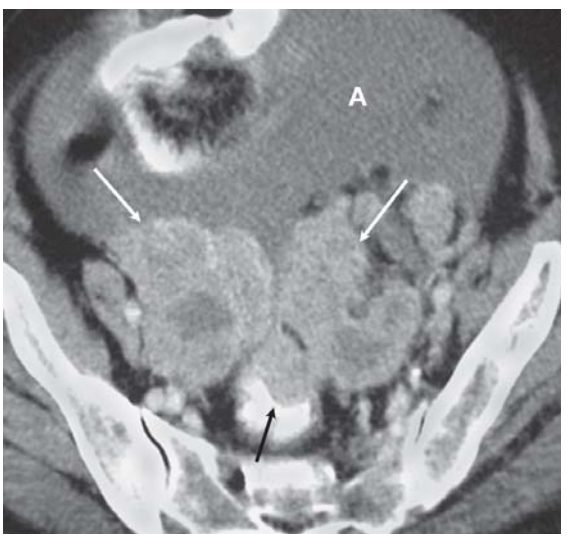

Fig. 26.12: Carcinoma of ovary: CECT shows bilateral complex solid cystic adnexal masses (white arrows) with invasion of the rectum (black arrow) seen as wall thickening and luminal bulge. Ascites (A) is also seen

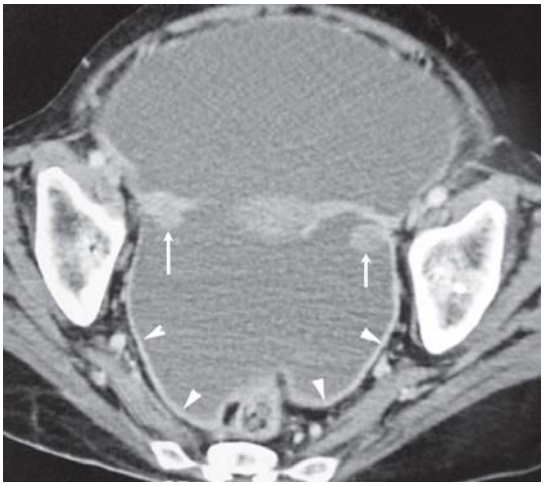

Fig. 26.13: Carcinoma of ovary: Bilateral normal-sized but irregular ovaries (arrows) are definitely abnormal for this elderly woman with atrophic uterus. Gross ascites as well as peritoneal deposits are present. The later is seen as enhancing and thickened peritoneum in pouch of Douglas (arrowheads)

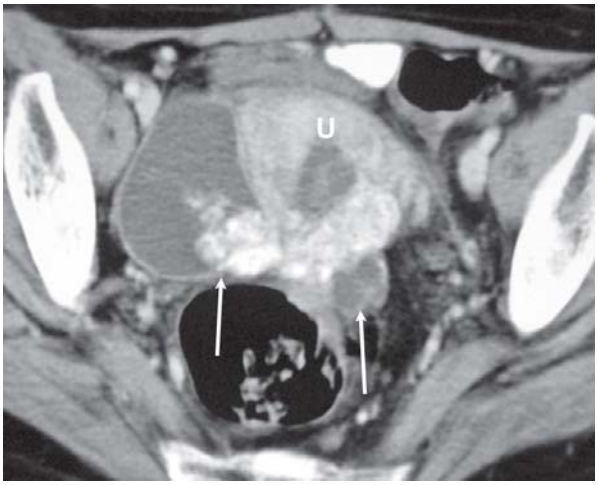

Fig. 26.14: Carcinoma of ovary: CECT shows bilateral complex cystic masses (arrows) with calcifications in solid component are seen. Invasion of the uterus (U) and the rectum is also seen

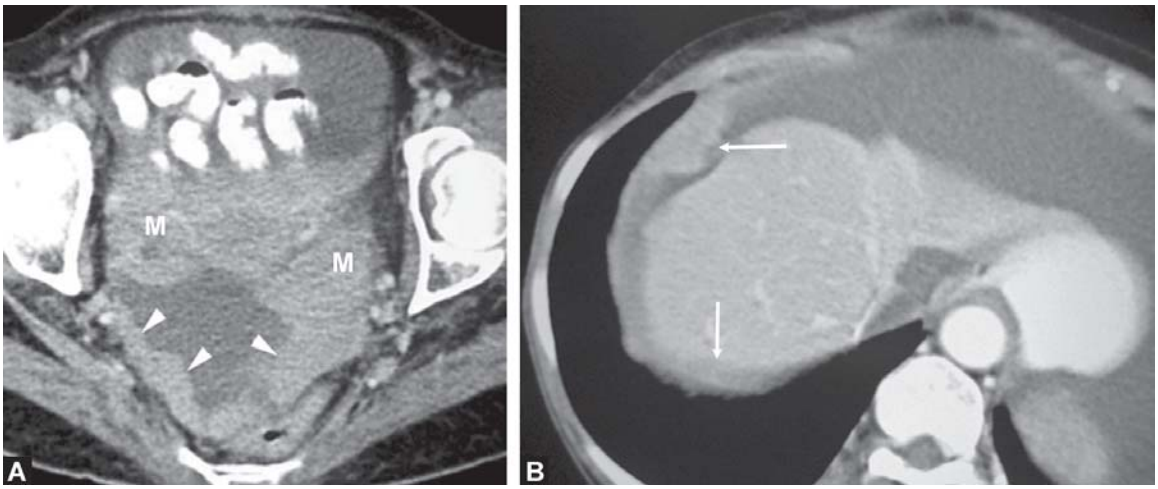

Figs 26.15A and B: Carcinoma of ovary with peritoneal deposits: **(A)** CECT of the pelvis shows bilateral adnexal masses (M) and ascites with plaque like peritoneal deposits (arrowheads) in pouch of Douglas. **(B)** Peritoneal deposits are also seen of the surfaces of liver and diaphragm (arrows)

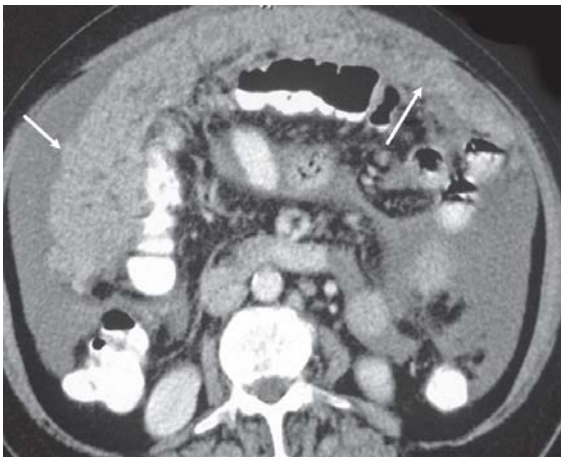

Fig. 26.16: Carcinoma of ovary: Multiple omental deposits coalesce to form a characteristic solid omental cake (arrows)

of Doglous, paracolic gutters, right subdiaphragmatic space and liver surface.[45] The sensitivity of CT in detection of peritoneal deposits is moderate, conventional CT scanners detected only up to 50 percent of peritoneal deposits that are 5 mm or less in size. The multidetector CT scanners have improved sensitivity in detection of small peritoneal deposits, especially in upper abdomen.[46] CT detection of peritoneal or liver surface deposits is facilitated by presence of ascites (Fig. 26.15B). Small foci of peritoneal calcifications may also represent deposits, especially, if it is a new finding.

Omental deposits are initially seen as multiple nodular lesions in omental fat. Later, they coalesce to form a solid 'omental cake', which is seen along the greater curvature of stomach or anterior to transverse colon or small bowel (Fig. 26.16). It may be seen beneath the anterior abdominal wall located anywhere from upper abdomen to pelvis and at times, mistaken for unopacified bowel loops. Mesenteric metastases are seen as rounded, ill-defined soft tissue masses surrounded by small bowel loops or as thickening along the mesenteric vessels and lymphatics.[33] CT accurately detects paraaortic and pelvic lymph node enlargement. Superior diaphragmatic (paracardiac) lymphadenopathy is a characteristic finding some advanced ovarian cancers and these are associated with poor prognosis.[47] Intrahepatic metastases are rare and occur late in the course of the disease. Ovarian cancer is one of the few primary cancers to have splenic metastases.

Although it is not possible to suggest specific histological diagnosis on CT, some features are considered typical for various types.[32] Seorus cystadenocarcinoma, endometroid carcinoma and undifferentiated carcinoma are frequently bilateral. Serous cystadenocarcinomas are usually seen as bilateral complex masses of irregular shape with papillary excrescences on the surface (See Fig. 26.13). Endometroid cancers are usually bilateral masses which can be both cystic as well as completely solid (Fig. 26.18). Concomitant endometrial hyperplasia, endometriosis or endometrial carcinoma may be associated. Undifferentiated tumors are usually solid masses with areas of necrosis. Mucinous adenocarcinomas and clear cell

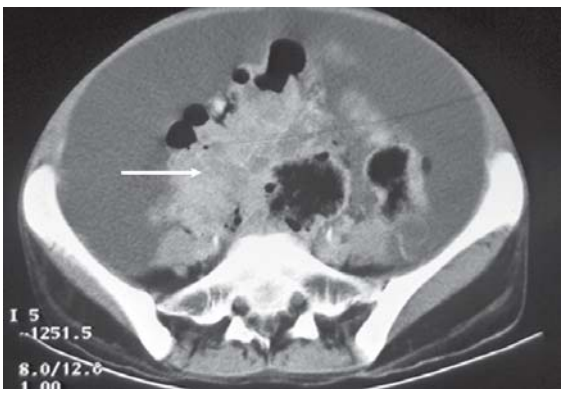

Fig. 26.17: Carcinoma of ovary: Large conglomerate mesenteric deposits (arrow) are seen in the mesentery involving multiple bowel loops

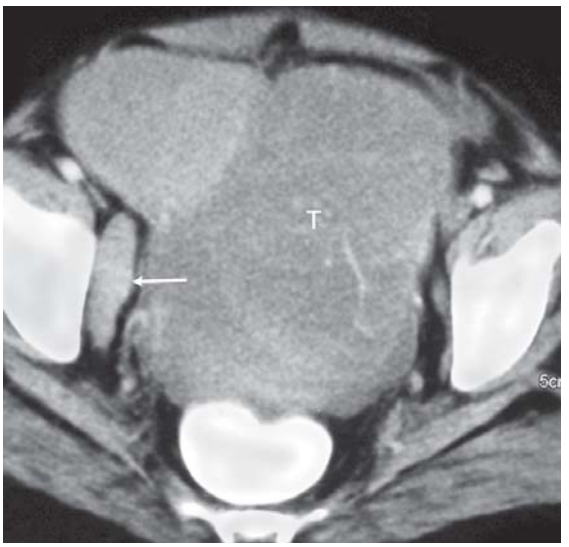

Fig. 26.18: Endometroid carcinoma of the ovary: CECT of the pelvis shows solid well defined adnexal mass (T) with minimal contrast enhancement. Enlarge right obturator lymph node (arrow) is also seen

carcinomas are more commonly unilateral and seen in comparatively younger age group. The mucinous tumor typically manifests as multiloculated cystic solid mass with variable densities in different locules. Clear cell carcinoma is characterisitically seen as unilateral cystic lesion with solid mural nodule in relatively younger women (see Fig. 26.11). Unlike endometrial counterpart of this tumor, ovarian clear cell carcinoma has a better prognosis.

MRI

The morphological features of ovarian cancer on MRI are similar to those seen on sonography or CT, but because of excellent soft tissue contrast, the details are better demonstrated. T1W fat suppressed, T2W and gadolinium enhanced T1W sequences are important in ovarian cancer. Most tumors are low or intermediate in signal intensity on T1W and high in signal intensity on T2W images (Figs 26.19A and B). Contrast enhancement helps to differentiate solid component of the tumor from blood clot or debris which do not enhance. MRI is better than other modalities in determining the

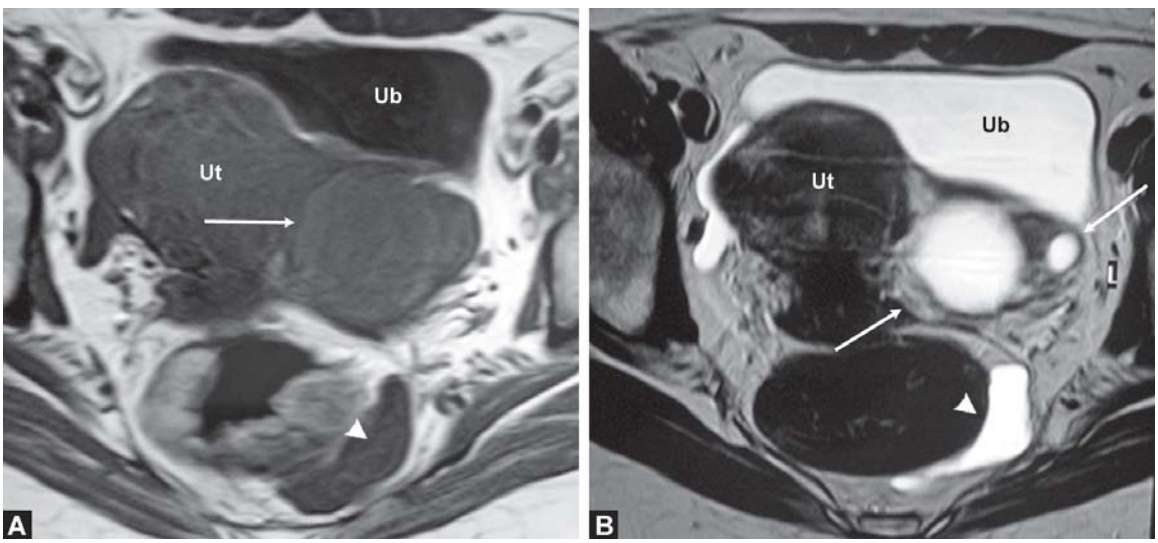

Figs 26.19A and B: Carcinoma of ovary: (A) T1W and (B) T2W MR images show left adnexal mass which is homogenously isointense on T1W image and heterogeneously hyperintense on T2W image (arrows). A large uterosacral ligament deposit is seen on left side (arrowhead) with signal intensity similar to the primary tumor

origin of a pelvic mass as well as its characterization into benign and malignant.[33,48] Hence, it is used as a problem solving tool in the settings of indeterminate mass on sonography.[32] MR signal characteristic do not help in differentiation of benign versus malignant lesions, instead, morphological features are used for this purpose. MR features favoring malignancy are same as those for ultrasonography and CT: Size more than 4 cm, large, wall or septal thickness of more than 3 mm, solid component or nodularity and presence of necrosis.[32,49] Ancillary features supporting the diagnosis of malignancy include invasion of other pelvic structures, peritoneal deposits, ascites and lymphadenopathy. These features have accuracy of 91 percent in characterization of malignant ovarian tumors. Necrosis in a solid mass and vegetations in cystic masses are most reliable predictors of malignancy on MR imaging of adnexal masses.[50] MR is also accurate in demonstration of direct involvement of other pelvic structures by the ovarian tumor.

PET

PET scanning is of limited use in characterization of ovarian masses. Physiological uptake in ovaries in different phases of menstruation is a limitation in detection and characterization of ovarian cancer on PET.[51] Various benign conditions like corpus luteum cysts, dermoid and benign cystadenomas may also show FDG uptake leading to false positive result.[52] On the other hand, mucinous cystadenocarcinomas may not show uptake on PET. Hence, PET is not useful for detection and characterization of the adnexal masses.

Staging and Treatment

The prognosis and management depends on type and stage of the disease. Staging is surgical and it is done according to FIGO guidelines into four stages (Table 26.3).

Table 26.3: Staging of carcinoma of the ovary

Stage I:	**Tumor limited to ovaries**
	IA: Limited to one ovary
	IB: Limited to both ovaries
	IC: IA or IB with malignant ascites
Stage II:	**Pelvic extension**
	IIA: Involvement of uterus and/ or fallopian tubes
	IIB: Involvement of other pelvic organs
	IIC: IIA or IIB with malignant ascites
Stage III:	**Peritoneal deposits/ lymphadenopathy**
	IIIA: Microscopic deposits
	IIIB: Macroscopic (< 2 cm) deposits
	IIIC: Large (> 2 cm) deposits and/or lymphadenopathy
Stage IV:	**Distant metastases**

In standard surgical procedure both staging as well as therapeutic resection of the tumor are combined. The complete surgical procedure includes total abdominal hysterectomy with bilateral salpingo-oophorectomy, omentectomy, retroperitoneal lymph node sampling, peritoneal biopsies and cytology of peritoneal washings. The aim of the surgery is to stage the disease as well to achieve optimal debulking of the tumor, because adjuvant therapy is effective only if the residual tumor is less than 1 cm in size. If residual tumor is more than 1 cm, the survival of patients is poor and similar regardless of the size of the residual tumor.[34,53]

Although only 10-15 percent patients present with early stage (Stage I and II) diseases, high cure rate is achieved with surgery and adjuvant (postoperative) chemotherapy. Platinum and taxane based chemotherapy is normally used in combination. Patients with advanced diseases (Stage III and IV) are also treated with

surgery and adjuvant (postoperative) chemotherapy, however, relapses are common and most patients eventually develop resistance to the treatment.[34] Neoadjuvant (preoperative chemotherapy) is given to the patients in whom optimal cytoreductive surgery may not be possible. Many of these patients can then undergo optimal surgery.[31]

Imaging Strategies in Carcinoma of Ovary

Role of imaging in ovarian cancer is to detect and characterize adnexal masses, recognize unusual findings that may suggest atypical or alternative diagnosis, demonstrate metastases in order to prevent surgical understaging and detect specific sites of the disease that may be unresectable.[45]

Ultrasound is the primary modality is important to detect and characterize the adnexal masses in patients who are clinically suspected to have ovarian cancer. MRI may be used in equivocal cases.[32,33]

Although staging of the ovarian cancer is always surgical, preoperative CT is recommended and it is now routinely obtained. Preoperative estimation of the gross extent of the disease on imaging may guide the referral to appropriate speciality. Demonstration of GIT and urinary tract involvement helps to modify the surgical plan.[45] Preoperative CT can also accurately predict the surgical outcome and hence has important role in deciding the management of ovarian cancer. Findings that suggest unresectable disease include greater than 1-2 cm deposits at porta hepatis, fissure for falciform ligament or ligamentum teres, GB fossa, diaphragm, gastrohepatic ligament, lesser sac and root of the mesentery (Figs 26.15B, 26.17 and 26.20). Invasion of pelvic sidewall and ureters as well as presence of retroperitoneal lymphadenopathy encasing aorta or lymphadenopathy located above the renal hilum also suggest unresectable disease. Such patients can be spared of surgery and put on neoadjuvant chemotherapy, as optimal debulking of the disease is unlikely to be achieved in these patients.[45,54,55] Detection of distant metastases on imaging help to prevent surgical under staging, although it does not necessarily makes the patient inoperable.

In few patients with clinically diagnosed carcinoma of ovary, imaging may suggest alternative diagnosis and hence, change the management. Metastatic ovarian cancer is often similar to primary ovarian cancer in clinical presentation as well as imaging features, hence, careful search to exclude other primary site should be made on CT. The identification of different primary with metastases to ovary on imaging may change the treatment from surgery to chemotherapy.

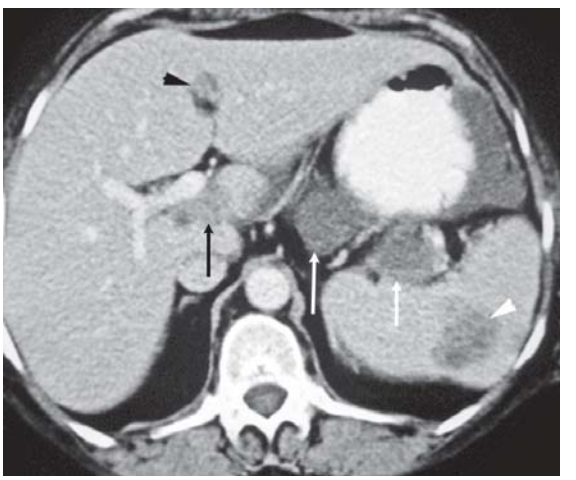

Fig. 26.20: Carcinoma of ovary with multiple unresectable deposits: CECT shows multiple deposits at falciform ligament (black arrowhead), porta hepatis (Black arrow), lesser sac and splenic hilum (white arrows). A parenchymal deposit is also seen in the spleen (White arrowhead)

Similarly, identification of benign or less aggressive tumors like germ cell tumors on CT also change the management as these are treated with more conservative surgery.[45]

Although CT is the primary imaging modality for preoperative staging, MRI may be equal to CT.[56] At present, use of MRI in ovarian cancer limited primarily because of long imaging time required for MRI evaluation of entire abdomen and pelvis, high cost and limited availability.[32]

Borderline Epithelial Carcinoma

About 20 percent of all epithelial ovarian cancers are borderline tumors, also known as tumors of low malignant potential. Histologically these can be serous or mucinous and characterized by absence of stromal invasion.[34] Most patients present with stage I disease and have good prognosis. Imaging features are similar to invasive epithelial cancers and hence imaging cannot differentiate between stage I invasive cancers and borderline cancers. Borderline tumors are treated with surgical excision and staging. Fertility preserving unilateral oophorectomy or cystectomy can also be performed. Such patients require prolonged imaging follow-up to detect recurrences.[32]

Pseudomyxoma Peritonei

Pseudomyxoma peritonei occurs due to rupture of mucinous adenocarcinoma into the peritoneal cavity leading to gelatinous deposits throughout the peritoneum.[33] Primary is often unclear and may be located in ovary, appendix or elsewhere.[57] On CT, it resembles high density ascites. Mass effect of the gelatinous material may result in characteristic scalloping of liver, spleen and bowel surfaces and septations within the fluid[45,57] (Fig. 26.21). Prognosis is generally poor.

Primary Papillary Serous Carcinoma of the Peritoneum

Some cases of serous adenocarcinoma in women with raised serum CA-125 may demonstrate extensive peritoneal carcinomatosis but no adnexal masses. Ovaries may be normal or not visualized. Calcifications may also be present. These tumors are considered to have arisen from extraovarian peritoneum and the condition is called primary papillary serous carcinoma of the peritoneum.[58] The management however, is same as that of ovarian cancer.[34] Peritoneal tuberculosis may also mimic peritoneal carcinomatosis and the differentiation from malignancy is possible only on histopathology.[59]

Follow-up Imaging

Recurrence rate is high in ovarian cancer even after complete remission. The patients are followed up with pelvic examination, serum

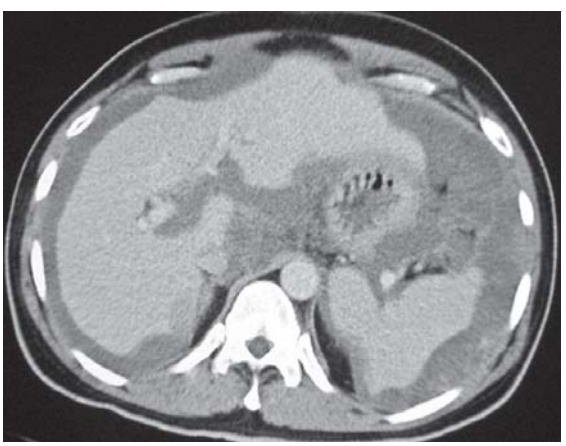

Fig. 26.21: Pseudomyxoma peritonei: CECT shows presence of high density ascites with indentations and scalloping on the surfaces of liver and spleen

tumor markers (CA-125), and CT of abdomen and pelvis every 3-4 months for 2 years.[33] Less frequent follow-up is required after that. After completion of the treatment, a surgical exploration of the asymptomatic patient (second look laparotomy—SLL) was the standard procedure to document pathological complete remission. This procedure is now uncommonly performed, as CT with tumor markers is adequate for majority of the patients.

Both CT and MRI are useful in detection of macroscopic recurrences. On CT and MRI, recurrences can be seen in various forms; pelvic or vault masses, peritoneal deposits, ascites, lymphadenopathy or rarely, hematogenous metastases to various distant organs. Peritoneal deposits may be cystic or solid (Fig. 26.22). These can be easily mistaken for unopacified bowel loops and hence, careful search on CT is essential. The recurrences are also common at the sites of previous lesions and hence; review of preoperative CT scans is desirable while evaluating the follow-up CT scans. Careful search for the recurrences should be made at these sites. PET CT is also useful to detect recurrences; especially in patients with rising tumor markers and normal CT scan.[60] Recurrent disease may be treated with surgery and/or chemotherapy. The CT criteria suggesting unresectability of recurrent disease are same as those for primary disease. In addition, presence of pelvic sidewall invasion, hydronephrosis and bowel obstruction are important findings which preclude the pelvic exenteration.[61]

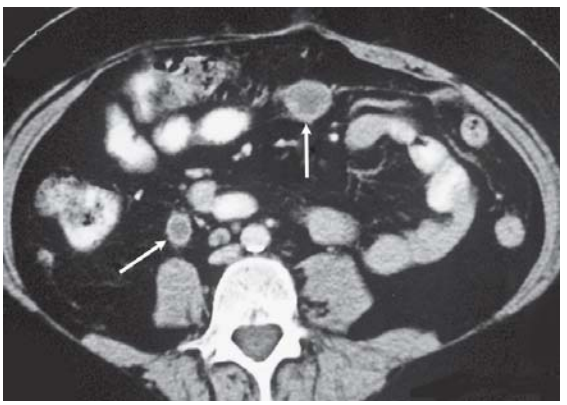

Fig. 26.22: Recurrent carcinoma of ovary: Multiple small cystic peritoneal deposits with enhancing nodular walls are seen (arrows). These resemble unopacified bowel loops and hence, can get overlooked

Germ Cell Tumors of the Ovary

Germ cell tumors (GCT) of the ovary are rare. These constitute only 2-3 percent of ovarian cancers in west but up to 15 percent of ovarian cancers in Asia.[34] These affect young women below 30 years of age. GCT is commonest ovarian tumor in pediatric age group. Commonest of these tumors is dysgerminoma, which is a histological counterpart of seminoma in males. Others include immature teratoma, embryonal tumor, endodermal sinus (yolk sac) tumor, choriocarcinoma and mixed germ cell tumors, which is any combination of the other tumors.

Patients often present early when the tumor is sill confined to the ovary. Most present with abdominal pain, mass or with acute abdomen because of torsion, rupture or hemorrhage in the tumor mass. Tumor markers such as AFP, hCG and LDH are elevated. These help to diagnose yolk sac tumor (AFP only), choriocarcinoma (hCG only) and embryonal cell carcinoma (both AFP and hCG). Patients with pure immature teratoma have normal AFP and hCG levels.[34] FIGO staging of the GCT is same as that of epithelial ovarian cancer.

On cross-sectional imaging, germ cell tumors are unilateral, solid and well-defined, however cystic, necrotic or hemorrhagic areas may also be seen (see Fig. 26.10). These tumors are often quite large but well-defined

at presentation. Spread of most germ cell tumors occur by direct extension into adjacent organs and/or by lymphatic or hematogenous dissemination. Ascites and peritoneal deposits may also be seen with germ cell tumors. Metastases to the lymph nodes, liver and lungs are more common with germ cell tumors than with epithelial carcinomas.

Dysgerminoma is the most common ovarian malignancy in children and young adults; with 80 percent of patient under 30 years of age.[33] It is seen as large, unilateral, well defined solid mass (Figs 26.23A and B). It is usually homogenous however, varying degree of necrosis or hemorrhage may be present. Numerous fibro-vascular septe are present within the mass. Prominent arterial flow may be demonstrated in these septe on color Doppler.[62] On MRI, these septe are hypointense on T2W images and show strong enhancement.[63]

Immature teratoma is usually a unilateral solid mass with coarse calcifications and rarely intratumoral fat (Fig. 26.24). Mature teratoma element may coexist in same or contralateral ovary.[32] Peritoneal spread is common. Gliomatosis peritonei is a condition when multiple benign or low grade malignant deposits of immature teratoma are seen throughout the peritoneal cavity. After chemotherapy, some of the immature teratoma disappear while other may transform into mature (benign) teratoma.

Yolk sac or endodermal sinus tumor is a highly malignant ovarian tumor characterized by rapid growth and early metastases. On CT and MRI, these are seen as complex cystic or solid tumors with heterogenous and intense contrast enhancement (Fig. 26.25). Areas of necrosis and hemorrhages are often present.

Pure embryonal cell carcinomas and choriocarcinomas (non-gestational) are rare and most often these are part of other germ cell tumors, i.e. mixed germ cell tumors. Imaging features are nonspecific.

Most patients with germ cell tumors present with early stage disease and hence, prognosis is usually good. Surgery with unilateral salpingo-oophorectomy and preservation of uterus and contralateral ovary can be performed in most patients, thus preserving the fertility. Advanced diseases are treated

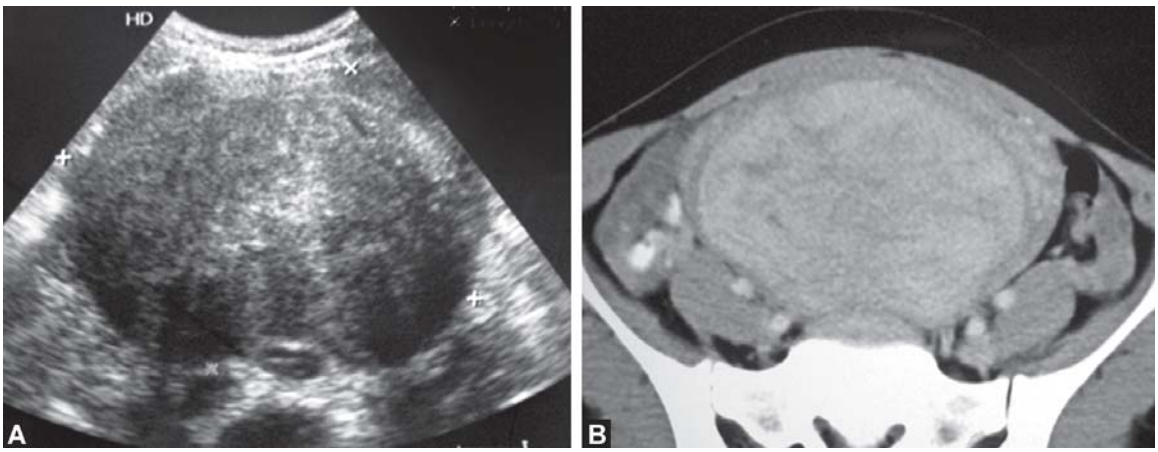

Figs 26.23A and B: Dysgerminoma: **(A)** ultrasonography of pelvis in a young woman shows a large, well-defined, homogeneous mass. **(B)** CECT shows moderately enhancing mass with same morphological features

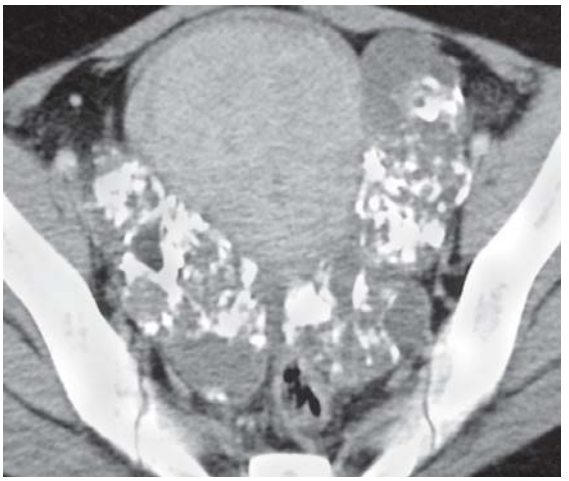

Fig. 26.24: Immature teratoma: CECT shows bilateral solid adnexal masses with coarse calcifications

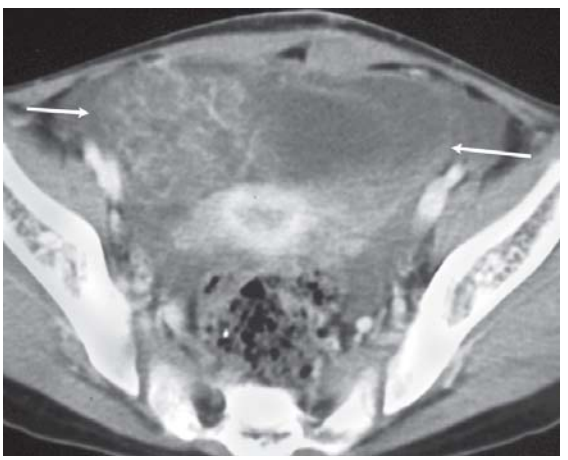

Fig. 26.25: Yolk sac tumor: CECT of pelvis of a female child shows large heterogenous pelvic mass (bounded by arrows) with areas of necrosis and invasion of the uterus

with surgery and chemotherapy. Dysgerminoma, like seminoma, are radiosensitive and can be treated with radiotherapy if preservation of fertility is not the main concern.[64] Patients are followed with periodic physical examination, serum tumor markers and sonography. CT is performed if sonographic examination is equivocal or tumor markers are rising. Functional ovarian cyst are often seen in normal ovary after fertility preserving surgery and these evoke anxiety and fear of recurrent disease, however, these can be safely followed up.[64] Recurrences after complete remission of GCTs are uncommon and occur in 10-20 percent of patients. Most of these occur in first two years and late relapses are extremely rare.

Stromal-sex Cord Tumors

Neoplasms arising from sex cord or stromal cells constitute 1-2 percent of ovarian malignancies.[32] Commonest of these is granulosa cell tumor, which is almost always malignant, while fibromas, thecomas and sertoli-leydig cell tumors, which usually behave in benign fashion. Histology of stromal-sex cord tumors can not accurately predict the clinical behavior and actual grade of malignancy cannot be defined. These tumors occur either in postmenopausal women or in pre-pubertal girls. Majority of these tumors secret estrogen and hence cause sexual precocity in girls or resumption of menses in postmenopausal women. These tumors are usually diagnosed at early stage, treated surgically and have good prognosis.

On imaging, granulosa cell tumor is usually seen as predominantly solid and multilobulated adnexal mass. MRI may show characteristic sponge like appearance as well as extensive intratumoral hemorrhages.[65] These tumors enhance heterogenously after intravenous contrast on CT or MRI. Associated uterine enlargement and endometrial hyperplasia may also be seen. Granulosa cell tumors also have high propensity for local invasion and sacral involvement is may be present.[33] Fibro-thecomas solid benign tumors but rarely, these can be malignant.

Because of the high fibrous content, these show low signal intensity in T2W MRI.[65]

Metastatic Ovarian Tumors

Upto 15 percent of ovarian malignancies are metastatic in nature.

Common primary sites are stomach, colon and breast. Uncommon primary sites include lung, gallbladder and pancreas. 'Krukenberg tumor' is the term used for specific histological pattern of mucin secreting signet cells with sarcomatous stroma, usually from a gastric primary.[66] Clinical presentation in metastatic ovarian tumors is variable. About one-third of the patients present with pelvic mass and not with the symptoms of primary site. Melanoma usually secondarily involves ovaries, however, primary malignant melanoma of the ovary also occurs.[67]

On cross-sectional imaging, ovarian metastases are usually seen as bilateral, large, lobulated solid or complex cystic masses (Fig. 26.26). These are indistinguishable from primary ovarian carcinoma; although multilocularity on ultrasound or MRI is uncommon with metastases.[33,68] Ascites, peritoneal nodules and omental deposits are also seen both in primary as well as metastatic ovarian tumors. Hematogenous spread to liver is rare with primary ovarian carcinoma but common with metastatic ovarian disease. Hence, presence of intra-hepatic metastases should warrant a search for primary tumor in stomach or colon. Possibility of metastatic ovarian tumor must be considered in any patient with ovarian mass if there is a known extra-ovarian primary cancer or liver metastases.

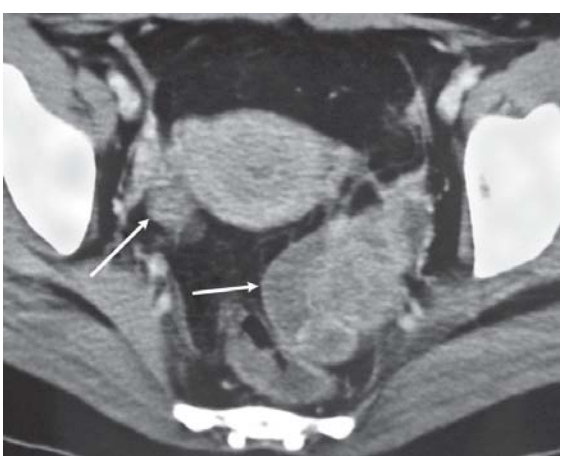

Fig. 26.26: Metastases to ovary: CECT of a pelvis in a woman with metastatic breast cancer shows bilateral cystic solid adnexal metastases (arrows). The appearance is indistinguishable from that of primary ovarian carcinoma

Rare Ovarian Tumors

Brenner tumors are epithelial tumors of ovary. These are usually benign, however, some of them can be borderline or frankly malignant. Malignant Brenner tumors are also known as transitional cell carcinoma of the ovary. An imaging benign Brenner tumors are seen as homogenously solid or unilocular cystic lesions. Malignant Brenner tumor however, is indistinguishable from other epithelial carcinomas on imaging.[65,69] These may also contain calcifications.[45] Primary ovarian carcinoid and neuroendocrine tumors are rare ovarian malignancies which are related to teratoma. Hepatoid adenocarcinoma is a rare tumor which involves ovary and occasionally, the uterus. These are aggressive tumors and believed to be type of yolk sac tumors. These histologically resemble hepatocellular carcinoma and serum AFP may also be elevated. Imaging findings are nonspecific and range from solid to complex cystic-solid masses.

MISCELLANEOUS GYNECOLOGICAL MALIGNANCIES

Carcinoma of Vagina and Vulva

Secondary involvement of vagina and vulva by adjacent tumors like rectum, cervix or

urinary bladder is more common than the primary carcinoma.[70] Vaginal and vulval carcinomas are rare and seen in old women. Majority of these are squamous cell carcinomas. Others include clear cell adenocarcinoma, melanoma and leiomyosarcoma.[71]

Vaginal carcinomas usually occur in upper third of the vagina. They may spread to involve adjacent structures like urinary bladder and rectum (Fig. 26.27). Involvement of pelvic lymph nodes and hematogenous metastases may also be seen. Vulval tumors commonly involve labia majora and uncommonly, labia minora, clitoris and perinium.

These tumors are diagnosed and staged using FIGO staging similar to that of carcinoma of cervix. MRI is the preferred modality to determine the site of origin as well as extent of the tumor when this is difficult to assess clinically. Most tumors are seen as hyperintense masses on T2W and contrast enhanced T1W images. As majority of these tumors are treated with radiotherapy, MRI facilitates the treatment planning by defining the extent of the tumor.[71]

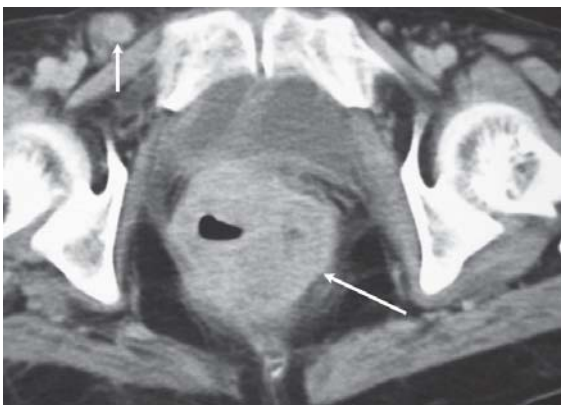

Fig. 26.27: Carcinoma of vagina: CECT shows enhancing pelvic floor mass involving vagina and rectum (large arrow). Enlarged right inguinal lymph node is also seen (small arrow)

Sarcoma of the Uterus

Uterine sarcoma are highly malignant tumors and account for 1-3 percent of all gynecological malignancies. These include endometrial stromal sarcoma, malignant mixed mullerian tumor (carcinosarcoma) and leiomyosarcoma. These can also arise from ovaries. Prior pelvic irradiation is associated with increased risk for the development of uterine sarcomas. Imaging features of uterine sarcomas are nonspecific and may be similar to the endometrial carcinoma or fibroids. However, these are often large at presentation and it may be difficult to determine the organ of origin on imaging. Areas of necrosis and hemorrhage, myometrial invasion and peritoneal deposits are usually seen on imaging.[13]

Rhabdomyosarcoma of uterus, cervix or vagina occurs in children and have nonspecific imaging features. Clear cell adenocarcinoma of vagina is associated with diethyl stilbesterol exposure. The characteristic imaging finding is multicystic, expansile mass in the vagina.

Fallopian Tube Carcinoma

Fallopian tube carcinoma is extremely rare. On imaging it is seen as solid or cystic adnexal masses similar to ovarian tumors.[72] Serum CA-125 may also be elevated in cases of fallopian tube carcinoma. Hence preoperative diagnosis of fallopian tube carcinoma is rarely made.

Gestational Trophoblastic Neoplasms

Gestational trophoblastic disease includes hydatidiform mole, invasive mole, placental site trophoblastic tumor and choriocarcinoma. These are associated with elevated serum hCG. Hydatidiform mole or molar pregnancy

is not a neoplasm. Gestational Trophoblastic neoplasms include placental site trophoblastic tumor and choriocarcinoma. Placental site trophoblastic tumor is a slow growing tumor and remains localized in uterus for long before metastasizing while choriocarcinoma is an aggressive variant characterized by rapid growth, widespread dissemination and propensity for hemorrhage.

Choriocarcinoma may evolve from a molar pregnancy or a full-term pregnancy. Patients usually present with vaginal bleeding and there is elevated serum hCG. On sonography, uterus is enlarged. Endometrial cavity contains echogenic solid mass with numerous small cystic spaces and the placenta (Fig. 26.28). Associated theca lutin cysts of the ovaries are seen in 20-50 percent cases.[73] Myometrial invasion in choriocarcinoma is seen as hyperechoic nodules, thickening and hypervascularity of the myometrium. CECT may show enlarged uterus with heterogeneous mass in endometrial cavity (Fig. 26.29A). On T2W MR images, distension of the uterus by high signal intensity mass is seen. Myometrial invasion is also better appreciated on MRI. If myometrial invasion is not seen on imaging, appearance is same as that of hydatidiform mole. Purpose of imaging however, is to establish the presence of gestational trophoblastic disease in appropriate clinical setting and to determine its extent and spread.

Choriocarcinoma spreads hematogenously. The metastases can be seen in lungs (Fig. 26.29B), vagina, liver, spleen, GIT or brain. Few patients present with metastases from occult primary. Treatment with surgery and chemotherapy results in rapid improvement, even with widespread metastases. Choriocarcinoma should be considered in any women in reproductive age, even without a history of sexual activity, who present with abnormal bleeding, enlarged uterine cavity or metastases with occult primary. Imaging evaluation and serum hCG estimation are essential part of diagnostic work up in these patients. Nongestational choriocarcinoma are part of germ cell tumors of the ovary and usually seen as part of mixed germ cell tumors rather than pure choriocarcinoma.

Lymphoma of the Female Genital Tract

Secondary involvement of the female genital tract as a part of disseminated non-Hodgkin's lymphoma is more common than primary involvement. Infiltration of the uterus causes its diffuse enlargement (Fig. 26.30). On MRI, the signal intesity is homogenous with preserved normal junctional zone.[74] Lymphoma of the ovary is usually seen as bilateral, solid, large adnexal masses with little contrast enhancement.[32] On MRI, it is homogenously hypointense on T1W images with only minimal increase in signal intensity on T2W images.[75] Ovary is the commonest organ of female genital tract to be involved

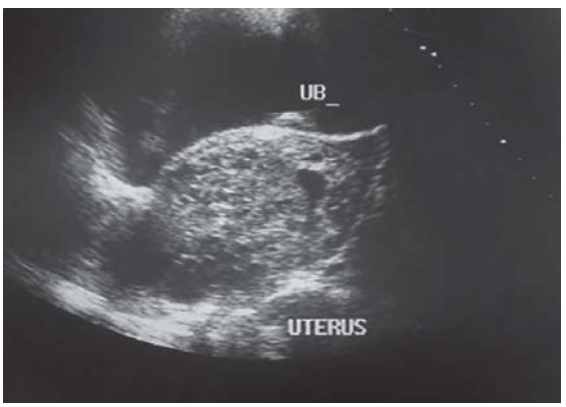

Fig. 26.28: Chroriocarcinoma: Ultrasonography shows enlarged uterus distended with echogenic mass containing numerous tiny cystic spaces. The appearance is similar to hydatidiform mole

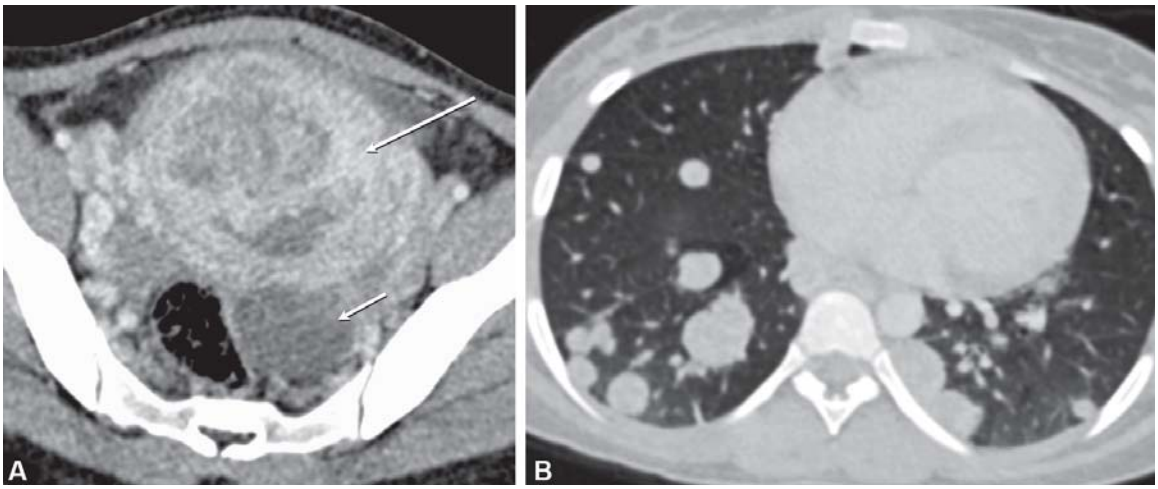

Figs 26.29A and B: Choriocarcinoma: **(A)** CECT shows enlarged uterus distended with heterogeneously enhancing mass (large arrow), associated theca lutin cyst is also seen (small arrow). **(B)** Lung window of the chest CT shows characteristic cannonball metastases

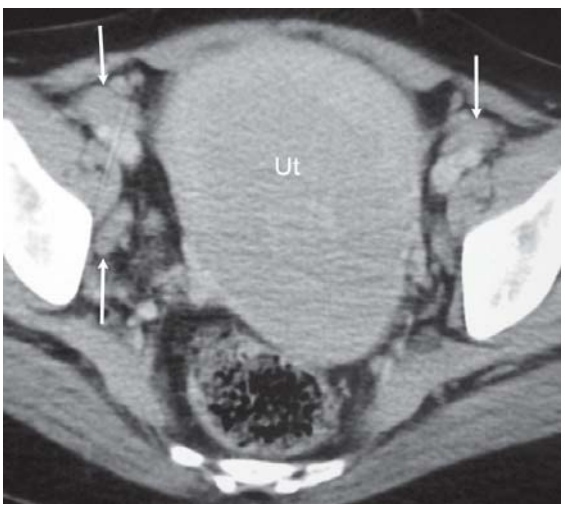

Fig. 26.30: Lymphoma of the uterus: CECT of the pelvis of a woman with disseminated non Hodgkin lymphoma shows diffuse homogeneous enlargement of the uterus (ut). Multiple enlarged pelvic lymph nodes are also seen (arrows)

in leukemia, in the form of granulocytic sarcoma.[76] On imaging, these are seen as lobulated solid or complex cystic solid adnexal masses with variable contrast enhancement, similar to the primary ovarian carcinoma.[77]

REFERENCES

1. Shanta V. Perspectives in gynecological oncology. In: Lalit Kumar (Ed). Current trends in gynecologic oncology. 1st edition, Mumbai, Himalaya Publishing House 1999;1-15.
2. Indian Council of Medical Research: Consolidated report of population based cancer registries 2001-2004. At: http://icmr.nic.in/ncrp/report.pop_2001-04.
3. Eifel PJ, Berek JS, Markman MA. Cancer of the cervix, vagina and vulva. In: Devita VT, Lawrence TS, Rosenberg SA. Cancer: Principles and practice of oncology. Lippincot, Wiliams and Wilkins, Philadelphia, 8th edition, 2008; 1496-1543.
4. Boles SM, Hricak H, Rubin P. Carcinoma of the cervix and endometrium. In: Bragg DG, Rubin P, Hricak H (Eds) Oncologic Imaging, (2nd edn). Philadelphia, WB Saunders 2002;523-48.
5. Kaur H, Silverman M, Iyer RB, et al. Diagnosis, staging and surveillance of cervical carcinoma. AJR 2003;180:1621-31.
6. Innocenti P, Pulli F, Sarini L. Staging of cervical cancer: Reliability of trans-rectal US. Radiology 1992;185:201-05.
7. Carter JR. Cervical tumor characterization by transvaginal colour flow Doppler ultrasound. Int J Gyn Ca 1999;9:279-84.

8. Pannu HK, Corl FM, Fishman EK. CT evaluation of cervical cancer: Spectrum of disease. Radiographics 2001;21:1155-68.
9. Akin O, Mironav S, Taskar NP, et al. Imaging of uterinecancer. Radiol Clin N Am 2007;45: 167-82.
10. Yang WT, Lam WW, Yu MY, et al. Comparison of dynamic helical CT and Dynamic MR imaging in evaluation of pelvic lymph nodes in cervical carcinoma. AJR 2000;175:759-66.
11. Sheu MH, Chang CY, Wang JH, et al. Preoperative staging of cervical carcinoma with MR imaging: A reappraisal of diagnostic accuracy and pitfalls. Eur Radiol 2001;1:1828-33.
12. Lien HH, Blomlie V, Iverson T, Clinical stage 1 carcinoma of cervix: Value of MR imaging in determining parametrial invasion. Acta Radiol 1993;34:130-32.
13. Sala E, Wakely S, Senior E, et al. MRI of malignant neoplasms of the uterine corpus and cervix. AJR 2007;188:1577-87.
14. Hricak H, Lacey CG, Sandles LG, et al. Invasive cervical carcinoma: Comparison of MR imaging and surgical findings. Radiology 1998;166: 623-31.
15. Ozsarlak O, Tjalma W, Schepens E, et al. The correlation of preoperative CT, MR imaging and clinical staging with histopathology in primary cervical carcinoma. Eur Radiol 2003;13:2338-45.
16. Hricak H, Powel GB, Yu KK. Invasive cervical carcinoma: Role of MR imaging in pretreatment work up: Cost minimization and diagnostic efficacy analysis. Radiology 1996;198:403-09.
17. Bipat S, Glas AS, Van Der Valden J, et al. Computed tomography and magnetic resonance imaging in staging of uterine cervical carcinoma: A systematic review. Gynecol Oncol 2003;91:59-66.
18. Hanke K, Heilman V, Straka P, et al. Pretreatment staging of cervical cancer: Is imaging better than palpation? Role of CT and MRI in preoperative staging of cervical cancer: Single institution results for 255 patients. Ann Surg Oncol 2008:15:2856-61.
19. Rockall AG, Ghosh S, Alexander SF, et al. Can MRI rule out bladder and rectal invasion in cervical cancer to help select patients for limited EUA? Gynecol Oncol 2006;101:244-49.
20. Rockall AG, Sohaib SA, Harsinghani MG, et al. diagnostic performance of nanoparticle enhanced magnetic resonance imaging in the diagnosis of lymph node metastases in patients with endometrial and cervical cancer. J Clin Oncol 2005;23:2813-21.
21. Havrilesky LJ, Kulasingam SL, Matchar DB, et al. FDG-PET for management of cervical and ovarian cancer. Gynecol Oncol 2005:97;183-91.
22. Choi HJ, Roh JW, Seo SS, et al. Comparison of accuracy of magnetic resonance imaging and positron emission tomography/computed tomography in presurgical detection of lymph node metastases in patients with uterine cervical carcinoma: A prospective study. Cancer 2006;106:914-22.
23. Xue F, Lin LL, Dehdashti F, et al. F-18 fluorodeoxyglucose uptake in primary cervical cancer as an indicator of prognosis after radiation therapy. Gynecol Oncol 2006;101:147-51.
24. Chung HH, Jo H, Kang WJ, et al. Clinical impact of integrated PET/CT on the management of suspected cervical cancer recurrence. Gynecol Oncol 2007;104:529-34.
25. van der Veldt AA, Buist MR, van Baal MW, et al. Clarifying the diagnosis of clinically suspected recurrences of cervical cancer: Impact of 18FDG PET. J Nucl Med 2008;49:1936-43.
26. Smith-bindman R, Kerlikoweske K, Feldstien VA, et al. Endovaginal ultrasound to exclude endometrial cancer and other endometrial abnormalities. JAMA 1998;280:1510-17.
27. Bree RL, Bowerman RA, Bohm-Velez M, et al. US evaluation of the uterus in patients with postmenopausal bleeding: A positive effect on diagnostic decision-making. Radiology 2000; 216:260-64.
28. Alcazar JA, Ajossa S, Floris S, et al. Reproducibility of endometrial vascular patterns in endometrial diseased as assessed by transvaginal power Doppler sonography in women with post-menopausal bleeding. J Ultrasound Med 2006;25:159-63.
29. Manfredi R, Mirk P, Maresca G, et al. Local-regional staging of endometrial carcinoma: Role of MR imaging in surgical planning. Radiology 2004;231:372-78.
30. Shumskey AG, Stuart GC, Brasher PN, et al. An evaluation of routine follow ups of the patients treated for endometrial carcinoma. Gynecol Oncol 2004;55:231-35.
31. Kumar L, Janga D, Berge S, et al. chemotherapy for advanced epithelial ovarian cancer.

Indian Journal of Medical and Pediatric Oncology 2004;25:21-25.
32. Mironov S, Akin O, Taskar NP, et al. Ovarian cancer. Radiol Clin N Am 2007;45:149-66.
33. Ascher SM, Imauka I, Jha RC. Tumors of adnexa. In: Bragg DG, Rubin P, Hricak H (Eds). Oncologic Imaging, (2nd edn). Philadelphia, WB Saunders, 2002;549-74.
34. Cannistra SA, Gershenson DM, Recht A. Ovarian cancer, fallopian tube carcinoma and peritoneal carcinoma. In: Devita VT, Lawrence TS, Rosenberg SA (Eds). Cancer: Principles and practice of oncology. Lippincot, Wiliams and Wilkins, Philadelphia, 8th edition 2008;1568-94.
35. Brown DL, Doubilet PM, Miller FH, et al. Benign and malignant ovarian masses: Selection of the most distinguishing grey scale Doppler sonographic feature. Radiology 1998;208:103-08.
36. Guerriero S, Alcozar JL, Coccia ME, et al. Complex pelvic masses: A target of evaluation of vessel distribution by color Doppler sonography for the diagnosis of adnexal malignancies: Results of a multicenter European study. J Ultrasound Med 2002;21:1105-11.
37. Kurjak A, Zalud I, Alfirec Z. Evaluation of adnexal masses with transvaginal color Doppler ultrasound. J Ultrasound Med 1991;10:295-97.
38. Levine D, Feldstein VA, Babcock CJ, et al. Sonography of ovarian masses: Poor sensitivity of resistive index for identifying malignant lesions. AJR 1994;162:1355-59.
39. Liu J, Xu Y, Wang J. Ultrasonography, computed tomography and magnetic resonance imaging for the diagnosis of ovarian carcinoma. Eur J Radiol 2007;62:328-34.
40. Kinkel K, Hricak H, Ying L, et al. US characterization of ovarian masses: A meta-analysis. Radiology 2000;217:803-11.
41. Neelam, Banerjee S, Kriplani A. Screening for ovarian cancer. In : Kumar L (Ed). Current trends in gynecologic oncology. 1st edition, Mumbai, Himalaya Publishing House 1999; 80-87.
42. Sterling D, Evans GR, Pichert GR, et al. Screening for familial ovarian cancer: Failure of current protocols to detect ovarian cancer at an early stage according to the international federation of gynecology and oncology system. J Clin Oncol 2005;23:5588-96.
43. Kauf NT, Satagopan JM, Robson ME, et al. Risk reducing salpingo-oophorectomy in women with BRCA1 or BRCA 2 mutations. N Engl J Med 2002;346:1609-15.
44. Zhang J, Mironov S, Hricak H, et al. Characterization of adnexal masses using feature analysis at contrast enhanced helical computed tomography. J Comput Assist Tomogr 2008;32: 533-40.
45. Cookley FV. Staging ovarian cancer: Role of imaging. Radiol Cin N Am 2002; 40:609-36.
46. Pannu HK, Horton KM, Fishman EK, et al. Thin section dual phase multidetector row computed tomography detection of peritoneal metastases in gynecologic cancers. J Comput Assist Tomogr 2003;27:333-40.
47. Holloway BJ, Gore PH, Hern RP, et al. The significance of paracardiac lymph nodes enlargement in ovarian cancer. Clin Radiol 1997;52: 692-97.
48. Kurtz AB, Tsimikas JV, Tempany CM, et al. Diagnosis and staging of ovarian cancer: Comparative values of Doppler and conventional US, CT and MR imaging correlated with surgery and histopathologic analysis –report of the Radiology Diagnostic Oncology group. Radiology 1999;212:19-27.
49. Sohaib SA, Sahdev A, Van Trappen P, et al. Characterization of adnexal mass lesions on MR imaging. AJR 2003;180:1297-304.
50. Hricak H, Chen M, Coakely FV, et al. Complex adnexal masses: Detection and characterization with MR imaging-multivariate analysis. Radiology 2000;214:39-46.
51. Subhas N, Patel PV, Pannu HK, et al. Imaging of pelvic malignancies with in-line FDG PET-CT: Case examples and common pitfalls of FDG PET. Radiographics 2005;25:1031-43.
52. Frenchel S, Grab D, Nuesle K, et al. Asymptomatic adnexal masses: Correlation of FDG PET and histologic findings. Radiology 2002;223: 780-88.
53. Hoskins WJ. Epithelial ovarian carcinoma: Principle of primary surgery. Gynecol Oncol 1994;55:S91-96.
54. Nelson BE, Rosenfield AT, Schwartz PE. Preoperative abdominopelvic computed tomography prediction of optimal cytoreduction in epithelial ovarian carcinoma. J Clin Oncol 1993; 11:166-72.

55. Qayyum A, Coakley FV, Westphalen AC, et al. Role of CT and MR imaging in predicting optimal cytoreduction of newly diagnosed primary epithelial ovarian cancer. Gynecol Oncol 2005;96:301-06.
56. Tempany CM, Zou KH, Silverman SG, et al. Staging of advanced ovarian cancer: Comparison of imaging modalities-report from Radiological Diagnostic Oncology Group. Radiology 2000;215:761-67.
57. Zissin R, Gayer G, Fishman A, et al. Synchronous mucinous tumors of the ovary and appendix associated with pseudomyxoma peritonei: CT findings. Abdom Imaging 2000; 25:311-16.
58. Chopra S, Laurie LR, Chintapally KN, et al. Primary papillary serous carcinoma of the peritoneum: CT–pathologic correlation. J Comput Assist Tomogr 2000;24:395-99.
59. Ha HK, Jung JL, Lee MS, et al. CT differentiation of tubercular peritonitis and peritoneal carcinomatosis. AJR 1996;167:743-78.
60. Murakami M, Miyamato T, Lida T, et al. Whole body positron emission tomography and tumor marker CA 125 for detection of recurrence in epithelial ovarian cancer. Int J Gynecol Cancer 2006;16:99-107.
61. Funt FA, Hricak H, Abu Rustum N, et al. Role of CT in the management of recurrent ovarian cancer. AJR 2004;182:393-98.
62. Kim SH, Kang SB. Ovarian dysgerminomas: Colour Doppler ultrasonographic findings and comparison with CT and MR findings. J Ultrasound Med 1995;14:843-48.
63. Tanaka YO, Kurosaki Y, Nishida M, et al. Ovarian dysgerminoma: MR and CT appearance. J Comput Assist Tomogr 1994;18:443-48.
64. Kumar L, Kumar S, Kriplani A, et al. Malignant germ cell tumors of ovary In: Kumar L (Ed). Current trends in gynecologic oncology. (1st ed); Himalaya Publishing House Mumbai , 1999; 100-17.
65. Imaoka I, Wada A, Kaji Y, et al. Developing and MR imaging strategy for diagnosis of ovarian masses. Radiographics 2006;26:1431-48.
66. Ha HK, Back SY, Kim SH, et al. Krukenbergs's tumor of the ovary: MR imaging features. AJR 1995;164:1435-39.
67. Vimla N, Kumar L, Thulkar S. Primary malignant melanoma in ovarian cystic teratoma. Gynecol Oncology 2001; 82:380-83.
68. Brown DL, Zou KH, Tempany CM, et al. Primary versus secondary ovarian malignancy: Imaging findings of adnexal masses in radiology diagnostic oncology group study. Radiology 2001;219:213-18.
69. Oh SN, Rha SE, Jung SE, et al. Transitional cell tumor of the ovary: Computed tomographic and magnetic resonance imaging features with pathologic correlation. J Comput Assist Tomogr 2009;33:106-12.
70. Parikh JH, Barton DP, Ind TE, et al. MR imaging features of vaginal malignancies. Radiographics 2008;28:49-63.
71. Chang SD. Imaging of vagina and vulva. Radiol Clin N Am 2002;40:637-58.
72. Slanetz PJ, Whitman GJ, Halpern EF, et al. Imaging of fallopian tube tumors. AJR 1997; 169: 1321-24.
73. Green CL, Angtuaco TL, Shah HR. Gestational trophoblastic disease: A spectrum of radiologic diagnosis. Radiographics 1996;16:1371-84.
74. Kim YS, Cho O, Song S, et al. MR imaging of primary uterine lymphoma. Abdom Imaging 1997;22:441-44.
75. Ferrozzi F, Tognini G, Bova D, et al. Non-Hodgkin lymphomas of the ovaries: MR findings. J Comput Assist Tomogr 2000;24: 416-20.
76. Kamble R, Sharma A, Thulkar S, et al. Granulocytic sarcoma of uterine cervix as presentation of acute myeloid leukemia: A case report and review of literature. J Obstet Gynecol Res 1997; 23:261-66.

Scrotum and Male Sexual Dysfunction

Chapter 27

Imaging of Scrotum

Anupam Lal, Manphool Singhal

Anatomy

The scrotum is a cutaneous pouch which contains the testes and parts of the spermatic cords. It is formed by the fusion of two scrotal sacs separated by an inner septum that corresponds to a midline ridge or raphé on the surface, which is continued forward to the under surface of the penis, and backward, along the middle line of the perineum to the anus. Of these two lateral portions the left hangs lower than the right, to correspond with the greater length of the left spermatic cord. The scrotal wall is composed of the following structures, listed from the superficial to the deep layers: Rugated skin, superficial fascia, dartos muscle, external spermatic fascia, cremasteric fascia, and internal spermatic fascia. The testes are suspended in the scrotal sac by the spermatic cord and are anchored to scrotal wall caudally by gubernaculum testis. It is a cord like structure located caudal to the testis and guides the testicular descent.

Each testis is of an oval form, compressed laterally, and having an oblique position in the scrotum; the upper extremity is directed forward and a little lateralward; the lower, backward and a little medialward; the anterior convex border looks forward and downward, and the posterior or straight border, to which the cord is attached, backward and upward. The anterior border and lateral surfaces, as well as both extremities of the organ, are convex, free, smooth, and invested by the visceral layer of the tunica vaginalis. The posterior border, to which the cord is attached, receives only a partial investment from that membrane. Lying upon the lateral edge of this posterior border is the long, narrow and flattened body of epididymis. Visceral and parietal layers of tunica vaginalis surround the testis and epididymis. Between these two layers lies vaginal cavity containing small amount of serous fluid and is derived from the 'saccus vaginalis' of the peritoneum. In the fetus, saccus vaginalis precedes the descent of the testis from the abdomen into the scrotum. The testicular capsule is formed by tunica albuginea. Tunica albuginea is covered by the tunica vaginalis, except at the points of attachment of the epididymis to the testis, and along its posterior border, where the spermatic vessels enter the gland. It is applied to the tunica vasculosa over the glandular substance of the testis, and, at its posterior border, is reflected into the interior of the gland, forming an incomplete vertical septum,

called the mediastinum testis. From the mediastinum, numerous fibrous septa extend into the testis, dividing it into 250-400 lobules, each of which consists of one to three seminiferous tubules supporting the sertoli cells and spermatocytes that give rise to sperm. These tubules contain loose interstitial tissue that contains Leydig cells, which are responsible for testosterone secretion.

All tubules drain into larger ducts called tubuli recti. These tubuli recti converge to form the rete testis, an anastomosing network of draining tubules, and enter into mediastinum testis, which caries the sperms from testis to the epididymis. The mediastinum testis consists of invagination of tunica albuginea and the rete testis. It also contains branches of testicular arteries, centripetal veins and lymphatics of the testis and hence is the anatomical hilum of the testis.

Testicular size depends on age and stage of sexual development. At birth, the testis measures approximately 1.5 cm in length and 1 cm in width. Before the age of age 12 years, testicular volume is about 1-2 cm^3. Clinically, a male individual is considered to have reached puberty once the testis achieves a volume of 4 cm^3. The average dimensions of the postpubertal testis are from 4 to 5 cm in length, 2.5 cm in breadth, and 3 cm in the antero-posterior diameter; its weight varies from 10.5 to 14 gm.

The epididymis consists of a central portion or body; an upper enlarged extremity, the head (globus major); and a lower pointed extremity, the tail (globus minor). The head of the epididymis (globus major) lies cephalad to the testis and is composed of 8-12 efferent ducts converging into a single larger duct in the body and tail (globus minor). This single duct becomes the vas deferens and continues in the spermatic cord.

Four testicular appendages have been described: the appendix testis, the appendix epididymis, the vas aberrans, and the paradidymis. These are remnants of embryonic ducts.[1] The appendix testis and the appendix epididymis are usually seen at scrotal US. The appendix of the testis (hydatid of Morgagni) is a minute oval, sessile body seen on the upper extremity of the testis, just beneath the head of the epididymis. It is the remnant of the upper end of the Müllerian duct. On the head of the epididymis is a second small stalked appendage (sometimes duplicated); it is named the appendix of the epididymis (pedunculated hydatid), and is usually regarded as a detached efferent duct. The spermatic cord is composed of arteries (the internal and external spermatics; and the artery to the ductus deferens), veins, lymphatics, nerves, and the excretory duct of the testis. These structures are connected together by areolar tissue, and invested by the layers brought down by the testis in its descent.

The arteries supplying the coverings of the testes are: The superficial and deep external pudendal branches of the femoral, the superficial perineal branch of the internal pudendal, and the cremasteric branch from the inferior epigastric artery. The veins follow the course of the corresponding arteries. The lymphatics end in the inguinal lymph glands. The nerves are the ilioinguinal and lumboinguinal branches of the lumbar plexus, the two superficial perineal branches of the internal pudendal nerve, and the pudendal branch of the posterior femoral cutaneous nerve.

IMAGING MODALITIES

Ultrasonography (US) with a high-frequency (7.5–10-MHz) transducer has become the imaging modality of choice for examination of the scrotum. Sonography combined with

color Doppler and power Doppler has evolved into an all-encompassing scrotal imaging technique as both structural and perfusion abnormalities can be detected. The ability of color and power Doppler US to demonstrate testicular perfusion aids in reaching a specific diagnosis in patients with acute scrotal pain. MRI and nuclear scan are other important complementary modalities. CT scan and MRI have important role in staging of testicular cancer and for the localization of testis in patients with cryptorchidism.

Technique of Sonography

Scrotal US are performed with the patient in the supine position and the scrotum supported by a towel placed between the thighs. Optimal results are obtained with a 7–10 MHz high-frequency linear-array transducer. A stand-off pad can be used for evaluation of superficial lesions. The testes are examined in at least two planes, along the long and transverse axes. The size and echogenicity of each testis and the epididymis are compared with those on the opposite side. In patients being evaluated for an acute scrotum, the asymptomatic side should be scanned initially in order to set the gray-scale and color Doppler gain settings to allow comparison with the affected side. In patients with small palpable nodules, scans should include the area of clinical concern. A finger should be placed beneath the nodule and the transducer placed directly over the nodule for scanning, or a finger can be placed on the nodule and the transducer opposite to confirm imaging of the lesion. Scrotal skin thickness (normal 2–8 mm, depending on the state of contraction of the cremasteric muscle) should be evaluated. The structures within the scrotal sac are examined to detect extratesticular masses or other abnormalities. Additional techniques such as use of the Valsalva maneuver or upright positioning can be used as needed for venous evaluation.

Prepubertal testes are of low to medium echogenicity, whereas pubertal and postpubertal testes are of medium homogeneous echogenicity, reflecting the development of germ cell elements and tubular maturation.[2] The mediastinum testis is identified as an echogenic band of variable thickness and length extending in a caudocranial direction (Fig. 27.1). The space between the two leaves of the tunica vaginalis normally contains small amounts of fluid, seen as a thin echo-free rim in the area adjacent to the head of the epididymis. This normal amount of fluid should not be misinterpreted as hydrocele. The epididymis is best evaluated in a longitudinal view when the epididymal head (globus major) can be seen as a pyramidal structure 5-12 mm in maximum length lying atop the superior pole of the testis. The head of the epididymis is usually isoechoic to the testis, and its echotexture may be coarser than that of the testis.[3] The narrow body of the epididymis (2-4 mm in diameter), when

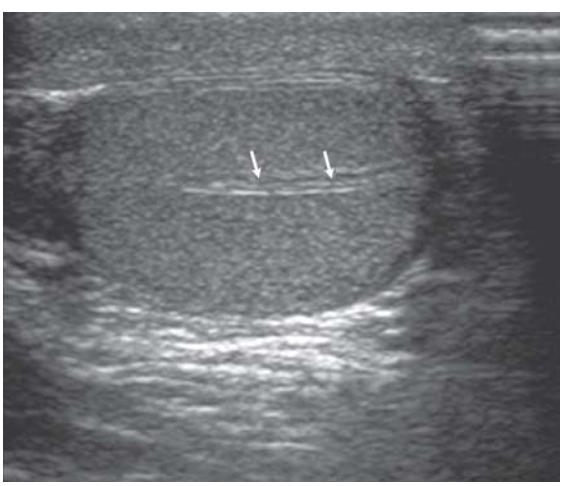

Fig. 27.1: US image of the testis in its long axis showing echogenic line of mediastinum testes (arrows)

normal, is usually indistinguishable from the surrounding peritesticular tissue. The tail of the epididymis (globus minor) is approximately 2-5 mm in diameter and can be seen as a curved structure at the inferior pole of the testis, where it becomes the proximal portion of the ductus deferens.

The spectral waveform of the intratesticular arteries characteristically has a low-resistance pattern,[4] with a mean resistive index of 0.62 (range, 0.48-0.75);[2] however, this is not true for a testicular volume of less than 4 cm,[3] as is often found in prepubertal boys, when diastolic arterial flow may not be detectable.[5]

MRI of Scrotum

MRI of the scrotum is extremely valuable as a problem solving modality. The MR examination is performed in supine position with scrotum supported by towel. Symmetric placement of testis is important for optimal coronal scans. The scrotum is then covered by small cloth or gauze and the surface coil is placed over it in a flat position. T1 and T2-weighted spin echo images are obtained in coronal and axial planes. Contrast-enhancement or fat suppression sequences are also obtained when further tissue characterization is required. Optimum coverage is provided by thin (4-5 mm) slices with 1-2 mm inter-slice gaps and 8-20 cm field of view. The scan area must be extended to lower pole of kidneys when looking for undescended testis and upto the diaphragm when MRI is performed for staging of testicular cancer.

On MRI, the testis is seen as an oval, sharply defined structure with homogeneous intermediate signal intensity on T1W images and high-signal intensity on T2W images (Fig. 27.2). The tunica albuginea is seen as a thin hypointense rim around the testis.

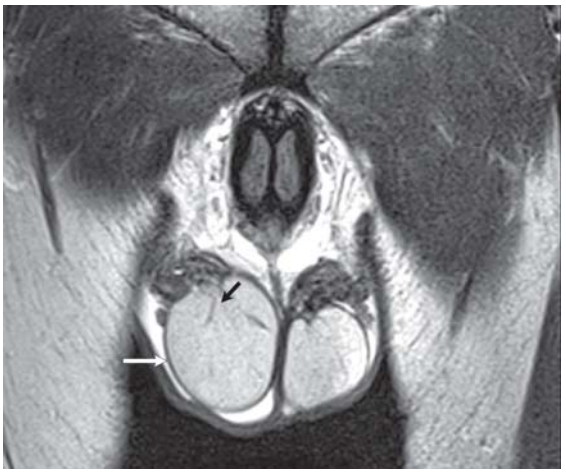

Fig. 27.2: T2 coronal MR image of the scrotum showing testes as high signal intensity structures within the scrotum. Note the hypointense rim of tunica albuginea (white arrow) around the testes and the mediastinum testis (black arrow) within it

The mediastinum testis is also hypointense and it is seen as a dark stripe invaginating into the testis. The signal intensity of the epididymis is similar to testis on T1W images and much lower on T2W images. The pampiniform plexus is seen as a tortuous tubular structure extending from upper pole of testis upto the inguinal canal. Vas deferens can sometimes be seen as a low intensity tubular structure that can be traced from tail of the epididymis to the inguinal canal.

CONGENITAL ANOMALIES OF THE TESTIS

Cryptorchidism

Cryptorchidism, where either one or both testes fails to migrate to the base of the scrotum, affects 4 to 5 percent of full-term and 9 to 30 percent of premature males at birth. The testis can be found in any position along its usual line of descent (the position can be abdominal, inguinal, prescrotal, or gliding);

however, about 80 percent of non-palpable undescen-ded testis are located in inguinal canal and remaining 20 percent are intra-abdominal.[6] Early correction, from 3 to 6 months of age, is currently advised. Normal complete descent is necessary for full maturation of the testis. Complications of undescended testis include infertility, malignant degeneration, torsion and inguinal hernia. Orchiopexy performed later, even after puberty, is advocated for better surveillance of the testis. If orchiopexy is not feasible, orchidectomy is considered in patients after puberty. Recent epidemiologic studies indicate a 2.5 to 8 times greater risk of developing malignancy in cryptorchid testis.[7] Seminoma is the most common malignancy in the cryptorchid testis. Orchiopexy does not change the risk of malignant degeneration of the once cryptorchid testis, but it does allow easier surveillance. If seminoma does occur in one testis, prompting unilateral orchiectomy, the remaining testis remains at a higher risk for the development of cancer.

Ultrasound examination is indicated for the localization of undescended testis and also for the follow-up after orchiopexy. The undescended testis is often smaller and iso or hypoechoic in echogenicity. Identification of mediastinum testis helps in differentiating this with other similar appearing structures like lymph nodes. The undescended testis is most commonly located distal to external inguinal ring anterior to the pubic tubercle. Even small rudimentary testis can be identified if it is located here and hence, sonography is the primary imaging modality used for the localization of undescended testis (Fig. 27.3). If testis is not located in the inguinal canal or base of the scrotum, then suprapubic, perineal and femoral regions should also be scanned. Intra-abdominal testis is difficult to locate on sonography.

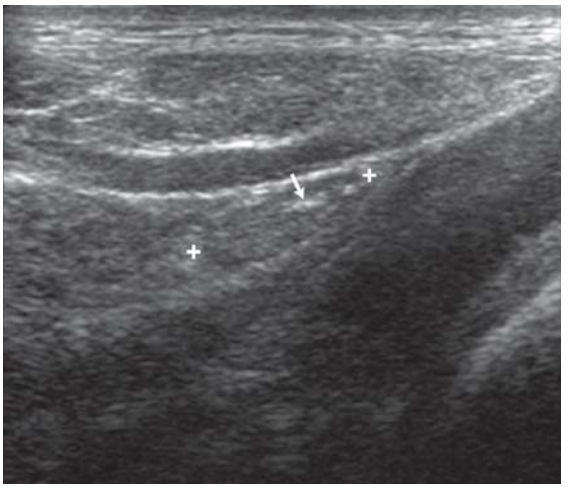

Fig. 27.3: US image of left undescended testis in a 24-year male: the testis is atrophic and located distal to external inguinal ring anterior to the pubic tubercle. Mediastinum testes is identified within the testis (arrow)

MRI is an excellent modality for demonstration of penoscrotal or intracanalicular testis, but is not very satisfactory for demonstration of high intra-abdominal testis. Bladder should be emptied before the scanning. Fast T1W and T2W axial and coronal images are obtained from scrotum to above the seminal vesicles. The examination is extended upto lower pole of the kidneys if testis is not located in the pelvis. The undescended testis can be easily identified with its characteristic signal intensity pattern. It tends to be oval in inguinal canal and round in intra-abdominal position. Sometimes the gubernaculum testis may be misdiagnosed as the undescended testis. While testis typically is hypointense on T1W and hyperintense on T2W images, the gubernaculum testis is hypointense on both T1W and T2W images. Hypertrophied inguinal lymph nodes may also have the signal characteristics similar to the testis, however, typical location of the nodes (adjacent to vessels or below the inguinal ligament) and

demonstration of mediastinum in undescended testis help to differentiate testis from the lymph nodes. CT, like MRI, also allows precise identification of the undescended testis.

Miscellaneous Congenital Anomalies

Retractile or migratory testis is common in boys 5-6 years old and is due to a hyperactive cremaster muscle reflex. The testis slides back and forth between scrotum and external inguinal ring. These usually take normal intrascrotal position by puberty and no treatment is required. The ectopic testis, i.e. location outside the descent path, is rare and the usual sites of testicular ectopia are perineum, femoral canal, superficial inguinal pouch (lateral to external inguinal ring), suprapubic area, and contralateral scrotal pouch.[8] The etiology is believed to be misdirected attachment to the scrotum. Unilateral absence of testis (monorchia) is usually left sided.[9] Unlike cryptorchidism, the testis in the patients with monorchia is not at increased risk of malignancy. Polyorchidism or testicular duplication is very rare and only few cases have been reported.[8]

ACUTE SCROTUM

Acute scrotum is a clinical condition characterized by sudden onset of pain, swelling and redness of the scrotum that may occur alone or in any combination. It is essential to differentiate as early as possible the conditions such as testicular torsion or rupture that require immediate surgery from those that are managed conservatively such as epididymitis. Clinical examination alone may not be helpful or it may be difficult to perform in patients with acute tender scrotum. Acute inflammation and testicular torsion are most important causes of acute scrotal pain. Other causes include torsion of appendix of testis or epididymis, trauma, tumor, incarcerated inguinal hernia and thrombophlebitis of the pampiniform plexus.

Epididymitis and Orchitis

Epididymitis is the most common cause of acute scrotum in postpubertal adults. Acute epididymitis is almost always caused by descending lower urinary tract infection. In children and older men *E. coli*, *Proteus* and *Pseudomonas* are the usual causative organisms. In young men, sexually transmitted organisms such as *gonococci* and *Chlamydia* are responsible. Rare causes such as sarcoidosis,[10] brucellosis,[11] tuberculosis, *Cryptococcus*, and mumps may also cause epididymitis and orchitis. Drugs such as amiodarone hydrochloride may also cause epididymitis (chemical epididymitis).[12] Direct extension of the inflammation in testis, resulting in epididymo-orchitis occurs in about 20 percent of patients with epididymitis.[13] Isolated orchitis is rare except when caused by viral infections such as *mumps* and *AIDS*.[14] Complications of acute epididymitis include chronic pain, infarction, abscess, gangrene, infertility, atrophy, and pyocele.

Patients present with insidious pain and scrotal swelling. Fever, dysuria and urethral discharge may also be present. Clinically, scrotal pain associated with epididymitis is usually relieved when the testes are elevated over the symphysis pubis (the Prehn sign).[15] Gray-scale US findings of acute epididymitis include an enlarged hypoechoic or hyperechoic (presumably secondary to hemorrhage) epididymis[2] (Fig. 27.4). Indirect signs of inflammation, such as reactive hydrocele or pyocele with scrotal wall thickening, are present in most cases. Diffuse testicular

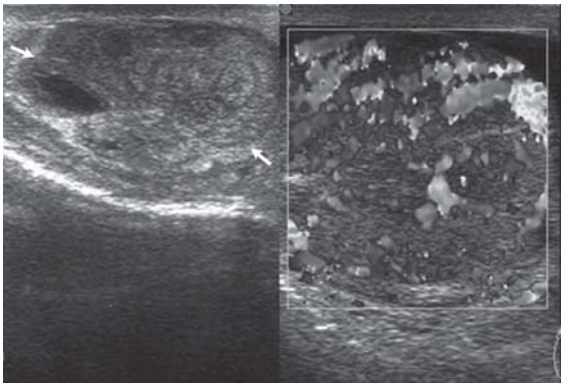

Fig. 27.4: US and color Doppler image of acute epididymitis: Showing enlarged heterogeneous epididymal head with increased vascularity *(For color version see Plate 21)*

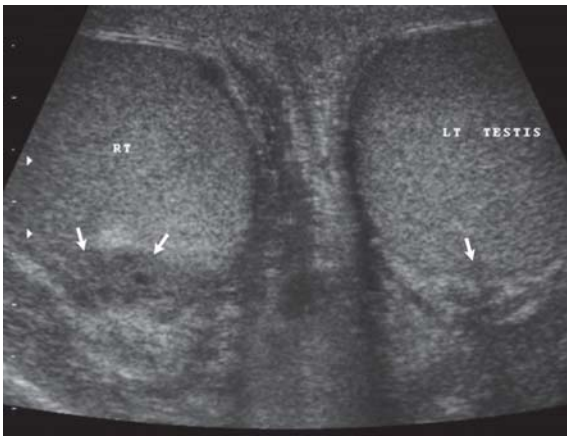

Fig. 27.5: Bilateral epididymorchitis: US image showing enlarged heterogeneous epididymis posterior to both testes and hypoechoic areas within the testes (arrows)

involvement is confirmed by the presence of testicular enlargement and an inhomogeneous testicular echotexture. Orchitis is characterized by edema of the testes contained within a rigid tunica albuginea, resulting in heterogeneous echogenicity.[16] The process may be seen as diffuse or focal, with the latter manifesting as multiple hypoechoic lesions within the testicular parenchyma (Fig. 27.5). Leukemia and lymphoma of the testis have a similar appearance and are often (but not always) bilateral, whereas infection (excluding mumps) is usually unilateral.

The sensitivity of color Doppler US imaging in detecting scrotal inflammation is nearly 100 percent.[17] In acute epididymitis, there are an increased number and concentration of identifiable vessels with hyperemia, resulting in a high-flow, low-resistance pattern.[18] Analysis of the spectral waveform and resistive index can also provide useful information. In the testes of a healthy volunteer, the resistive index is rarely less than 0.5, but in more than half of patients with epididymo-orchitis, the resistive index is less than 0.5.[19] Use of a peak systolic velocity threshold of 15 cm/sec results in a diagnostic accuracy of 90 percent for orchitis and 93 percent for epididymitis.[20] Reversal of flow during diastole in acute epididymo-orchitis is suggestive of venous infarction.[21] Follow-up sonography is necessary in patients who do not respond to therapy. However, it is not required in patients with uncomplicated epididymitis.

In acute epididymitis, enlarged epididymis with high-signal intensity on T2W images is seen on MRI. Areas of hemorrhages and hypervascularity (in the form of engorged vessels with signal void) can also be demonstrated. The inflamed epididymis shows marked enhancement on postcontrast images. Associated orchitis, if present, is seen as homogeneous or heterogeneous hypointense areas in testis on T2W images.

The sonographic findings in chronic epididymitis are non-specific and diagnosis is usually made on the basis of clinical findings. This condition is characterized by persistent pain in the scrotal area. At gray-scale US, it is characterized by an enlarged epididymis and increased echogenicity.[22] There may be

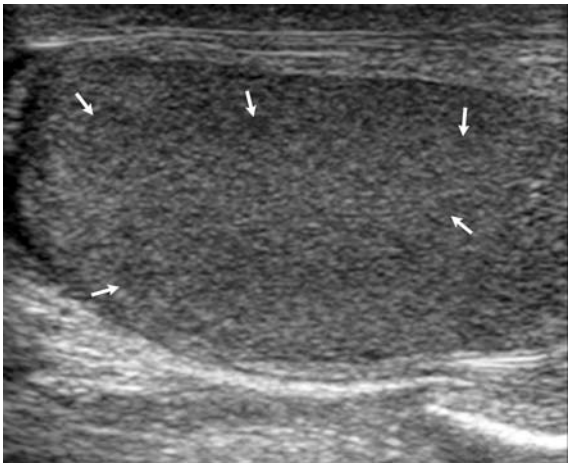

Fig. 27.6: Granulomatous orchitis in a case of syphilis: US image showing multiple illdefined hypoechoic lesions (arrows) within the testis

calcifications within the epididymis. Granulomatous epididymo-orchitis can be seen in cases of tuberculosis, brucellosis, sarcoidosis, leprosy, and syphilis (Fig. 27.6).

Torsion

Testicular torsion occurs due to rotation of testis on the longitudinal axis of spermatic cord. Initially venous drainage is stopped resulting in edema and hemorrhages. Subsequently arterial flow is also impaired resulting in ischemia and hemorrhagic necrosis of the gonad. It is a surgical emer-gency, as delay in diagnosis and intervention leads to irreversible damage to the testis. The extent of testicular ischemia depends on the degree of torsion, which ranges from 180 to 720° or greater. The testicular salvage rate depends on the degree of torsion and the duration of ischemia. A nearly 100 percent salvage rate exists within the first 6 hours after the onset of symptoms; a 70 percent rate, within 6–12 hours; and a 20 percent rate, within 12-24 hours.[23]

There are two types of testicular torsion - Extravaginal and intravaginal. Extravaginal torsion is rare and occurs almost exclusively in neonates. It occurs when testis and gubernaculum are not fixed and are free to rotate in the scrotum. The entire vaginal sac including testis rotates at the level of external inguinal ring. It often presents as a mass in the groin in newborns. Intravaginal torsion occurs within the vaginal sac. It results from anomalous suspension of testis by a long stalk of spermatic cord and most commonly occurs in boys around the puberty. There is ten-fold increased incidence of torsion in undescended testis after orchiopexy.[24]

Approximately two-third of the cases of torsion occur between 12 and 18 years of age. Patients with acute torsion present after a sudden onset of pain followed by nausea, vomiting, and a low-grade fever. Physical examination reveals a swollen, tender, and inflamed hemiscrotum. US is considered the first step in evaluation. US findings vary with the duration and degree of rotation of the spermatic cord. Gray-scale images are nonspecific for testicular torsion and often appear normal if the torsion has just occurred. Testicular swelling and decreased echogenicity are the most commonly encountered findings 4-6 hours after the onset of torsion

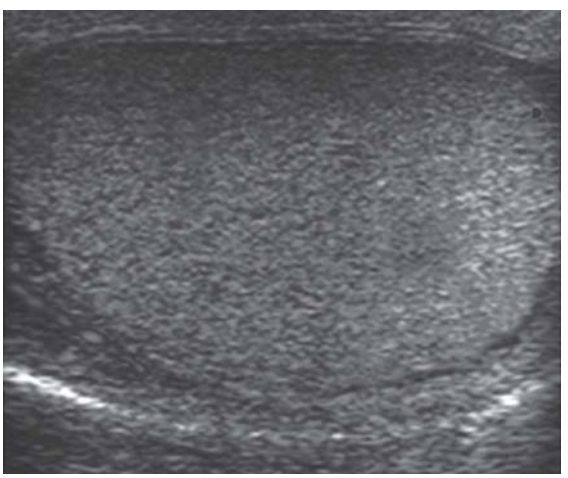

Fig. 27.7: Power Doppler US image showing heterogeneous appearing testis with reduced intratesticular flow in a case of torsion of testis *(For color version see Plate 21)*

(Fig. 27.7). At 24 hours after onset, the testis has a heterogeneous echotexture secondary to vascular congestion, hemorrhage, and infarction (late or missed torsion). An enlarged hypoechoic epididymal head may be visible because the deferential artery supplying the epididymis is often involved in the torsion.[25] In the setting of testicular torsion, normal testicular echogenicity is a strong predictor of testicular viability. Other indicators include the presence of scrotal wall thickening and reactive hydrocele.

Torsion is not an all-or-none phenomenon but may be complete, incomplete, or transient. Cases of partial or transient torsion present a diagnostic challenge. The ability of color Doppler US imaging to enable accurate diagnosis of incomplete torsion remains undetermined. The presence of color or power Doppler signal in a patient with the clinical manifestation of torsion does not exclude torsion.[26]

For accurate diagnosis the scanner should be optimized for detection of slow flow and be adjusted for the lowest repetition frequency and the lowest possible threshold setting. The threshold should be set just above the level for detection of color noise. By using the absence of identifiable intratesticular flow as the only criterion for detecting testicular torsion, color Doppler US is 86 percent sensitive, 100 percent specific, and 97 percent accurate in the diagnosis of torsion and ischemia in painful scrotum.[17] Color Doppler US and scintigraphy are comparable with regard to diagnosis of torsion in adolescent and adult populations.[17] Scintigraphy remains a reasonable alternative for evaluation of acute scrotal pain and should be used when color Doppler US sensitivity for low-velocity, low-volume testicular blood flow is inadequate and the diagnosis of torsion remains in question (Fig. 27.8).

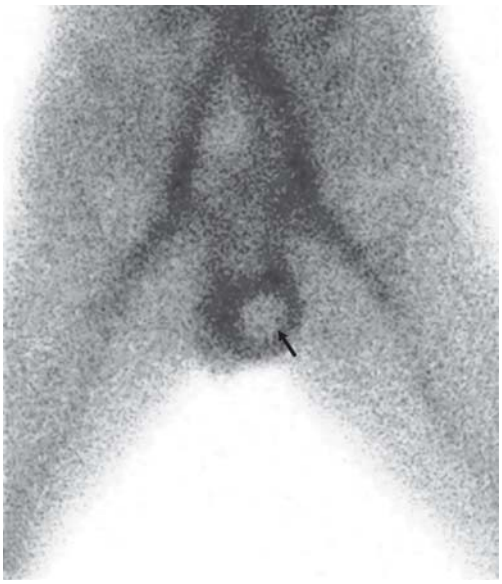

Fig. 27.8: Tc-99m pertechnetate scan showing photopenic area arrow in scrotum due to torsion of left testis *(For color version see Plate 21)*

Patients with torsion of the appendix testis and appendix epididymis present with acute scrotal pain, but there are usually no other physical symptoms. The classic finding at physical examination is a small firm nodule that is palpable on the superior aspect of the testis and exhibits bluish discoloration through the overlying skin; this is called the "blue dot" sign.[27] Approximately 91 to 95 percent of twisted testicular appendices involve the appendix testis and occur most often in boys 7-14 years old. US evaluation of torsion of the appendages of the testes usually reveals a hyperechoic mass with a central hypoechoic area adjacent to the testis or epididymis. Reactive hydrocele and skin thickening are common in these cases. Increased peripheral flow may be seen around the twisted testicular appendage at color Doppler US.[17] These cases are managed conservatively, with attention to pain management. The pain usually resolves in

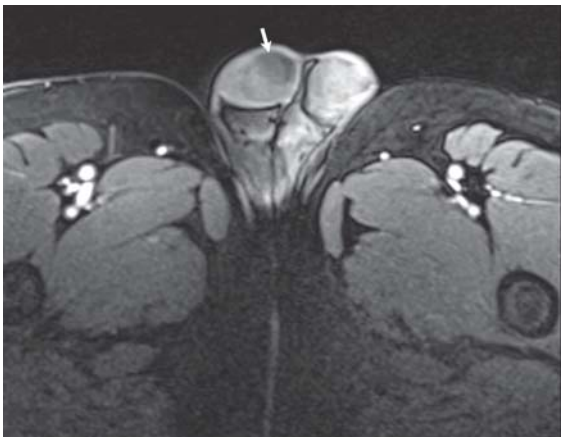

Fig. 27.9: Intermittent torsion: CEMR axial image showing hypoenhancing area within the right testis (arrow)

2-3 days, with atrophy of the appendix, which may calcify. The role of US examination in torsion of testicular appendages is to exclude testicular torsion and acute epididymo-orchitis.

MRI in testicular torsion can show twisted cord as multiple low intensity curvilinear structures radiating in a 'whirlpool' pattern. The torsion knot may be seen as an area of signal void. In patients with intermittent torsion, the testis is enlarged and hyperintense on both T1 and T2 weighted images owing to subacute hemorrhages (Fig. 27.9). Phosphorus MR spectroscopy has been reported to be helpful in evaluation of acute torsion. It demonstrates decreased levels of beta-ATP and phosphomonoester and increased levels of inorganic phosphorus.[13]

Scrotal Trauma

Scrotal trauma usually results from either direct injury or from straddle injuries. History is very helpful in the diagnosis, however, marked scrotal swelling, pain and open injuries limit adequate clinical examination. Patients with open and penetrating scrotal injuries undergo immediate surgery and are not candidates for scrotal sonography.

In cases of blunt trauma, sonography is used to confirm or exclude testicular rupture, differentiate a hematoma from hematocele and for follow-up of patients undergoing conservative management. Testicular rupture is a surgical emergency and such patients are taken up for immediate surgery whereas patients with small hematomas or hematocele are managed conservatively. Hence scrotal sonography has a decisive influence on clinical management.[28]

On sonography, intratesticular hematoma is seen as sharply defined hypoechoic space occupying lesion (SOL). Irregularities of testicular contour and hypo or hyperechoic heterogeneous areas suggest testicular rupture. These parenchymal areas correspond to hemorrhages and infarction. Visualization of solid and cystic intrascrotal mass and absence of testis like structure is a characteristic feature of testicular fragmentation. Sometimes a distinct fracture line may also be identified. Hematocele usually accompany testicular rupture but its absence does not exclude the possibility of rupture.[14] Scrotal hematoma between the layers of scrotal wall is seen as non-specific soft tissue thickening. If the urethra is injured, extravasation of urine between the layers of scrotal wall produces 'onion peel' thickening of scrotal wall.

Acute hematocele or accumulation of blood in vaginal sac contains numerous small internal echoes. In chronic hematocele, thick septae and wall-thickening is demonstrated.

MRI may be required in patients with scrotal injury when satisfactory sonographic examination is not possible. It is also indicated if testicular rupture cannot be confidently excluded on the sonography. The diagnosis of testicular rupture is facilitated by unequivocal depiction of tunica albuginea on MRI.

The integrity of tunica albuginea is best assessed on T2W or contrast enhanced T1W images. Intratesticular injuries demonstrate decreased contrast enhancement. MRI is also valuable in demonstration of hematomas.

TESTICULAR TUMORS

Testicular cancer represents 1 per cent of all cancers in men. It is the most common malignancy affecting young men of 20 to 34 years of age. However, developments in diagnostic and therapeutic modalities during past decade have led to high cure rate, even for patients who present with metastatic disease.[16] Risk factors for testicular cancer include cryptorchidism, testicular atrophy (e.g. mumps), testicular microlithiasis, Klinefelter's syndrome, Down syndrome and maternal use of diethyl stilbesterol.[29]

Patients with testicular cancer commonly present with a painless mass or vague discomfort in the scrotum. The principal role of US examination in the diagnosis of testicular cancer is to help distinguish intratesticular from extratesticular lesions, because the majority of extratesticular masses are benign and intratesticular masses are more likely to be malignant.[30] Gray-scale US is nearly 100 percent sensitive for detection of testicular tumors.[31] There are a variety of benign intratesticular processes, such as hematoma, orchitis, abscess, infarction, and granuloma that mimic testicular malignancy and must therefore be considered in the differential diagnosis. Color Doppler and power Doppler US demonstrate increased vascularity in the majority of malignant tumors and help to better define testicular involvement.

Testicular tumors are divided in germ cell and non-germ cell tumors.

Germ Cell Tumors

Germ cell tumors account for 90 to 95 percent of testicular cancer. Other malignant testicular tumors include those of gonadal stromal origin, lymphoma, leukemia, and metastases. Germ cell tumors are divided into two groups: Seminomatous and nonseminomatous germ cell tumor (NSGCT). The later includes embryonal cell carcinoma, teratoma, choriocarcinoma, endodermal sinus tumor or any combination of these tumors. This distinction determines treatment and prognosis.

Serum tumor markers are important in diagnosis, staging and follow-up. These include LDH (lactose dehydrogenase), AFP (alpha-fetoprotein) and hCG (human chorionic gonadotrophin). LDH may increase in any type of tumor and it correlates well with the extent of the disease. The α-fetoprotein level is never elevated in patients with pure seminoma. If histologic results suggest seminoma in the presence of an elevated-fetoprotein level, the tumor is treated as nonseminomatous.[32] hCG is elevated in all patients of choriocarcinoma, majority of NSGCT and only in few patients with seminomas.[29]

Seminomas

Seminomas are the most common type of testicular tumor and account for approximately 50 percent of all germ cell tumors. They occur most often in men aged in their 40s and almost never in infants.[33] Seminomas are associated with the best prognosis of the germ cell tumors because of their high sensitivity to radiation and chemotherapy.[7] There are three subtypes of seminomas: Typical seminomas account for 85 percent of the total number; anaplastic, for 5 to 10 percent; and

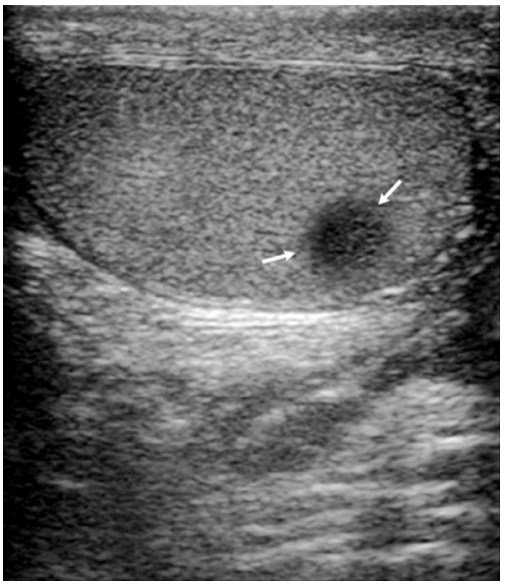

Fig. 27.10: US image showing a nonpalpable seminoma (arrow) of testis

spermatocytic, for 4 to 6 percent. Spermatocytic seminomas occur most often in men aged in their 60s and 70s and are associated with an excellent prognosis. On gray-scale US scans, seminoma appears as a homogeneous hypoechoic lesion, which corresponds to the smooth uniform appearance of the gross specimen (Fig. 27.10). The entire testis is replaced by tumor in more than half the cases. In one prospective study,[34] 10 percent of seminomas had cystic components. Seminomas are usually confined by the tunica albuginea and rarely extend to peritesticular structures. Lymphatic spread to retroperitoneal lymph nodes and hematogenous metastases to lung, brain, or both are evident in about 25 percent of patients at the time of presentation.

Nonseminomatous Germ Cell Tumors (NSGCTs)

Nonseminomatous germ cell tumors (NSGCTs) occur most often in men-aged in their 30s, have multiple histologic patterns in 40 to 60 percent of cases.[30] Some common patterns are (a) teratoma, embryonal carcinoma, yolk sac tumor, and human chorionic gonadotrophic hormone–containing syncytiotrophoblast; (b) teratoma and embryonal carcinoma (teratocarcinoma); and (c) seminoma and embryonal carcinoma. The macroscopic and US appearance of tumors with a multihistologic pattern depend on the proportions of each component. They often have an inhomogeneous echotexture (71%), irregular or ill-defined margins (45%), echogenic foci (35%), and cystic components (61%).[34] Echogenic foci represent areas of hemorrhage, calcification, or fibrosis. Approximately 60 percent of NSGCTs manifest with advanced disease.[30]

Embryonal carcinoma Embryonal carcinoma occurs most often in men aged in their 30s and is more aggressive than are seminomas. Three percent of NSGCTs are pure embryonal carcinomas; however, 45 percent of tumors of mixed histologic characteristics contain embryonal components. Unlike seminomas, a pure embryonal carcinoma is often small and does not cause enlargement of the scrotum. At US, embryonal carcinomas are predominantly hypoechoic lesions with poorly defined margins and an inhomogeneous echotexture. Echogenic foci commonly appear and represent hemorrhage, calcification, or fibrosis. Twenty percent of embryonal carcinomas and 89 percent of teratocarcinomas have cystic components. Tumor invasion of the tunica albuginea is common and may distort the contour of the testis.[7]

Yolk sac tumor Yolk sac tumors are also known as endodermal sinus tumors or infantile embryonal carcinomas. These neoplasms occur most often in children younger than 5 years of age and produce fetoprotein

exclusively.[33] Yolk sac elements are frequently seen in tumors with mixed histologic features in adults and thus indicate poor prognosis. The US appearance of yolk sac tumor is usually inhomogeneous and may contain echogenic foci secondary to hemorrhage.

Choriocarcinoma It is a highly malignant testicular tumor seen as microscopic foci in 16 percent of mixed germ cell tumors. Pure choriocarcinomas are rare, however, and represent only 0.3 percent of all testicular tumors. Microscopic vascular invasion is common, which explains the tendency of this tumor for early hematogenous metastasis, especially to the lungs, when the primary tumor is relatively small.[30] Many choriocarcinomas show extensive hemorrhagic necrosis in the central portion of the tumor; at US, this appears as mixed cystic and solid components.[35]

Teratoma Teratomas are composed of all three germ cell layers—endoderm, mesoderm, and ectoderm and can occur in any age group. Pure teratoma is the second most common testicular tumor in prepubertal boys. In adults, pure teratoma represents 2 to 3 percent of testicular neoplasms,[30] but teratomatous components are seen in over 50 percent of mixed germ cell tumors. Mature teratoma in children is often benign, but teratoma in adults, regardless of age, should be treated as malignant. At US, these tumors tend to be very large and markedly inhomogeneous masses (Fig. 27.11). Echogenic foci represent calcification, cartilage, immature bone, and fibrosis. Cystic components are more commonly seen in these than in other NSGCTs.

Burned-out germ cell tumor Burned-out germ cell tumor of the testis, usually teratocarcinoma or choriocarcinoma, occurs secondary to rapid tumor growth and results in the tumor outstripping its blood supply and in subsequent tumor regression. Histologic examination reveals no tumor cells, only fibrosis and scar tissue. The US appearance ranges from small echogenic foci to a relatively hypoechoic mass and corresponds to the tumor appearance at gross examination.[36]

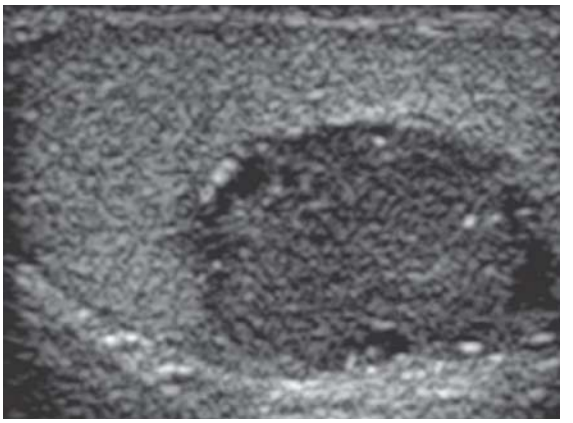

Fig. 27.11: US image: showing teratoma of testis. Note small cystic areas and foci of calcification within the lesion

Non-germ Cell Testicular Tumors

These include tumors of gonadal stroma (Leydig cell tumors, Sertoli cell tumors and gonadoblastoma), lymphoma, leukemia, metastases and other rare tumors. Majority of stromal tumors are benign. These may be endocrinally active and hence patients may present with precocious puberty, gynecomastia or other endocrinopathies. Leydig cell tumor is the most common type of sex cord—stromal tumor of the testis and can occur in any age group. Children often present with symptoms of precocious puberty due to production of androgens by the tumor. Adults with this tumor present with scrotal enlargement (42.5%) and gynecomastia (30%), which usually precedes testicular swelling.[37] Malignant Leydig cell tumors are uncommon.

Gonadoblastoma (contains both germ cell and stromal cell elements) is rare and is almost exclusively seen in intersex problems and gonadal dysgenesis. Eighty percent are phenotypically female.

Sonographically stromal tumors are seen as small, smoothly demarcated, homogeneous hypoechoic intratesticular masses[29] (Fig. 27.12).

Lymphomas constitute 5 percent of testicular tumors and are almost exclusively diffuse non-Hodgkin's lymphoma B-cell tumors (Fig. 27.13). In men older than 60 years, lymphoma is the most common testicular neoplasm and accounts for 50 percent of cases.[38] Sonographically these tumors resemble seminomas but asynchronous involvement of the contralateral testis and involvement of the spermatic cord and epididymis suggests lymphoma more than it does seminoma. Leukemic infiltration to the testis has been found at autopsy in 40 to 65 percent of patients with acute leukemia and in 20 to 35 percent of patients with chronic leukemia.[39] In boys with acute lymphoblastic leukemia, testicular involvement is reported in 5 to 10 percent of patients, with the majority found during clinical remission. Bilateral testicular involvement is seen in about 50 percent of the patients. Sonographically, lymphoma/leukemia deposits are seen as focal or diffuse hypoechoic areas. The testis is usually enlarged. A blood-testis barrier limiting the effect of chemotherapeutic agents in the testes explains the persistence of leukemia in the testes after remission.

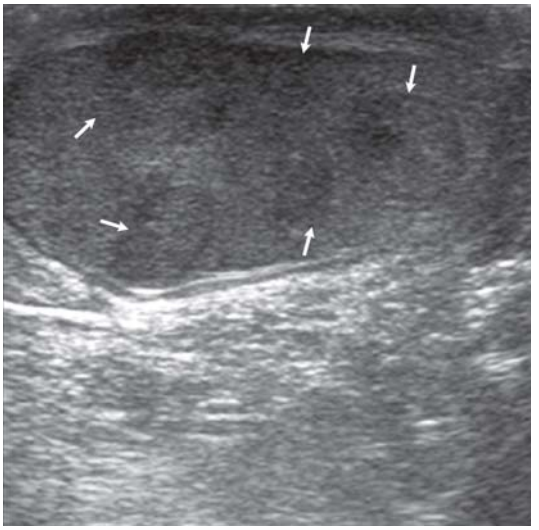

Fig. 27.12: US image showing multicentric rhabdomyosarcoma of testis

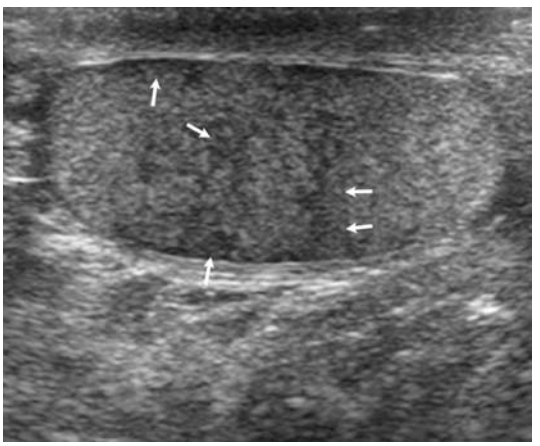

Fig. 27.13: US image showing sheet like hypoechoic areas within the testis (arrows) due to lymphoma (NHL)

Intrascrotal metastases from tumors of other organs are rare and are usually found in older patients. Most frequent primaries are from lung, kidney, prostate and melanoma.[14] Sonographic appearances are nonspecific.

Staging or Testicular Cancer

Testicular cancer is staged using the TNM system created by the American Joint Committee on Cancer (AJCC).

Primary Tumor (T)

TX: The primary tumor cannot be assessed.

T0: There is no evidence of primary tumor.

Tis: Carcinoma *in situ* (noninvasive cancer cells).

T1: The tumor has not spread beyond the testicle and the narrow tubules next to the

testicles where sperm undergo final maturation (epididymis). Cancer cells are not found inside blood vessels or lymph vessels next to the tumor. The cancer may have grown through the inner layer surrounding the testicle (tunica albuginea) but not the outer layer covering the testicle (tunica vaginalis).

T2: Similar to T1 except that the cancer has spread to blood vessels, lymphatic vessels, or the tunica vaginalis.

T3: The tumor invades the spermatic cord (which contains blood vessels, lymphatic vessels, nerves, and the vas deferens).

T4: The tumor invades the skin surrounding the testicles (scrotum).

Regional Lymph Nodes (N)

NX: Regional (nearby) lymph nodes cannot be assessed.

N0: No metastasis (spread) to regional lymph nodes is seen on X-rays.

N1: There is metastasis in at least one lymph node, but no lymph node is larger than 2 cm (about 3/4 inch) in any dimension.

N2: There is metastasis in at least one lymph node that is larger than 2 cm but is not bigger than 5 cm (2 inches) in any dimension.

N3: There is metastasis to at least 1 lymph node that is larger than 5 cm in any dimension

If the lymph nodes were taken out during surgery, there is a slightly different classification:

pNX: Regional (nearby) lymph nodes cannot be assessed.

pN0: There is no metastasis to regional lymph nodes.

pN1: There is metastasis (spread) to 1 to 5 lymph nodes, with no lymph node larger than 2 cm (about 3/4 inch) across in greatest dimension.

pN2: There is metastasis in at least one lymph node that is bigger than 2 cm but not larger than 5 cm; or metastasis to more than 5 lymph nodes that aren't bigger than 5 cm (one inch) across (in greatest dimension); or the cancer is growing out the side of the lymph node.

pN3: There is metastasis to at least one lymph node that is bigger than 5 cm.

Distant Metastasis (M)

MX: Distant metastasis cannot be assessed.

M0: There is no distant metastasis (no spread to lymph nodes outside the area of the tumor or other organs, such as the lungs).

M1: Distant metastasis is present.

M1a: The tumor has metastasized to distant lymph nodes or to the lung.

Serum Tumor Markers (S)

	LDH (U/liter)	*hCG (mIU/ml)*	*AFP (ng/ml)*
Sx	Marker studies not available or not performed.		
S0	Normal	Normal	Normal
S1	<1.5 X Normal	<5,000	<1,000
S2	1.5-10 X Normal	5,000-50,000	1,000-10,000
S3	> 10 X Normal	>50,000	>10,000

LDH = lactate dehydrogenase (measured in units per liter)
hCG = human chorionic gonadotropin (measured in milli-International units per milliliter [ml])
AFP = alpha-fetoprotein (measured in nanograms per milliliter [ml]

Stage grouping

Stage	*T*	*N*	*M*	*S*
Stage 0	Tis (in situ)	N0	M0	S0
Stage I	T1-4	N0	M0	SX
Stage IA	T1	N0	M0	S0
Stage IB	T2-T4	N0	M0	S0
Stage IS	Any T	N0	M0	S1-3
Stage II	Any T	N1-3	M0	SX
Stage IIA	Any T	N1	M0	S0-1
Stage IIB	Any T	N2	M0	S0-1
Stage IIC	Any T	N3	M0	S0-1
Stage III	Any T	Any N	M1	SX
Stage IIIA	Any T	Any N	M1a	S0-1
	Any T	Any N	M1a	S1
Stage IIIB	Any T	N1-3	M0	S2
	Any T	Any N	M1a	S2
Stage IIIC	Any T	N1-3	M0	S3
	Any T	Any N	M1a	S3
	Any T	Any N	M1b	Any S

M1b: The tumor has metastasized to organs, such as liver, brain, bone, and others.

Another application of the TNM system used for advanced disease takes into account the markers and classifies the cancer as low, medium, and poor outlook.

Risk Status	*Nonseminoma*	*Stages*	*Seminoma*	*Stages*
Good outlook	No non-lung spread	IS (S1)		
	Good markers	II A (S1)	No non-lung spread	IIC
	AFP < 1,000	II B (S1)	AFP normal	IIIA
	hCG < 5,000	IIC (S1)	hCG and LDH can be any level	IIIB IIIC
	LDH < 1.5	IIIA		
	No non-lung spread			
	Intermediate markers	IS (S2)	Non-lung spread	IIIC with non-lung spread
Intermediate outlook	AFP 1,000-10,000	IIC (S2)	AFP normal	
	hCG 5,000-50,000	IIIB	hCG and LDH can be any level	
	LDH 1.5-10			
	Non-lung spread			
	High markers	IS (S3)		
Poor outlook	AFP > 10,000	IIC (S3)	None (seminoma is never classified as poor outlook)	
	hCG > 50,000	All IIIC		
	LDH > 10			

Imaging in Evaluation of Testicular Cancer

MRI

MRI is used as a problem solving modality. MRI of scrotum is more sensitive than sonography for detection of testicular tumors, however, the findings are variable and non-specific. Most testicular tumors are iso- intense to testis on T1W images and hypo-intense on T2W images. On dynamic gadoli-nium enhanced MRI, the tumor enhancement is often earlier and greater than the normal testicular parenchyma. Similar to their sonographic appearances, seminomas tend to be homogeneous, whereas NSGCTs are heterogeneous on MRI. Lymphoma and leukemia are characterized by testicular enlargement with diffuse, homogeneous decrease in signal intensity on T2W images. MRI is also useful in staging work-up of testicular tumors when CT is inconclusive or contraindicated. It is also useful for follow-up after the treatment.

CT

CT is the most commonly used modality in evaluation of tumor spread, staging and follow-up. CT is useful for detection of enlarged retroperitoneal or mediastinal lymph nodes as well as extranodal metastases in lungs and liver. In testicular carcinoma, nodes smaller than 1 cm should be considered suspicious, if they are located in the regional nodal drainage site (e.g. renal hilum on the left or aorto-caval region on right side (Fig. 27.14). Cut-off nodal diameter of 7 mm has been suggested as more useful for testicular cancer.[29] The enlarged lymph nodes may demonstrate necrotic center or heterogeneous contrast enhancement, particularly in NSGCTs. After completion of the treatment, some lymph nodes may not decrease in size and instead, develop more necrosis and fibrotic strands. Majority of such lymph nodal masses do not contain viable tumor, however, it cannot be ruled out on the basis of CT alone.

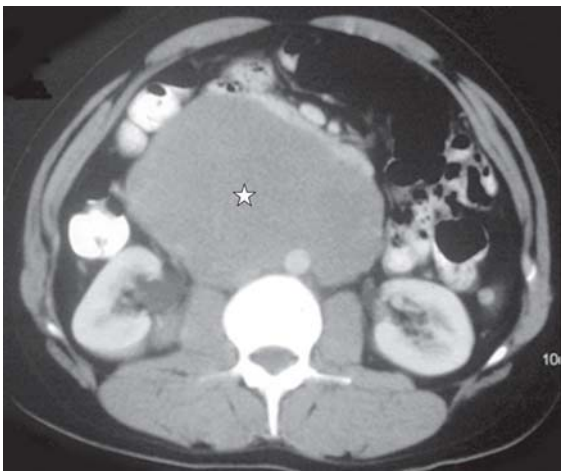

Fig. 27.14: Axial CECT image at the level of renal hilum showing a large metastatic homogeneous lymph nodal mass (star) in a case of seminomas testis

PET

The role of fluoro-D-deoxyglucose positron-emission tomography (FDG-PET) in testicular malignancies has been examined in various studies primarily in three specific settings: (i) Differentiation of active disease from fibrosis/mature teratoma in patients with residual mass following chemotherapy and evaluation of the response to treatment; (ii) Initial staging and disease assessment after orchidectomy identification of suspected recurrences in the context of elevated circulating serum markers; and (iii) Predicting response to treatment. In patients with residual masses or raised marker levels following therapy, positron-emission tomography (PET) appears sensitive and specific for detecting recurrent disease, at suspected and unsuspected sites.[40] Fewer

studies are available investigating its usefulness for staging at diagnosis and this requires further investigation to determine its eventual place as an imaging modality in this setting. Its precise role in disease prognostification is yet to be clearly defined in this malignancy but the initial results are promising.

BENIGN INTRATESTICULAR LESIONS

Cysts

Testicular cysts are incidentally detected on sonography. These need to be differentiated from cystic tumors. Symptomatic or palpable testicular cysts or those with suspicious solid component need further evaluation and/or exploration. Others can be followed-up. Two types of simple benign cysts can be identified—cysts of tunica albuginea and simple testicular cysts. Tunica albuginea cysts are typically small (less than 5 mm) and are usually palpated as firm nodular masses. These are located at the periphery. Simple testicular cysts are usually located near the mediastinum testis and are not palpable.

Tubular ectasia of rete testis may be mistaken for tumors. These are typically located at the mediastinum testis and consist of areas of multiple tiny cystic spaces with no flow on CDFI (Fig. 27.15). It is usually associated with epididymal obstruction. Epidermoid and dermoid cysts of the testis are rare and these are also seen as palpable simple cysts with characteristic echogenic margins. They do not have malignant potential.

Adrenal Rests

Aberrant adrenal tissue rests may be found in testis in about 8 percent of patients with congenital adrenal hyperplasia. Pathogenesis may be related to the common embryonic origin of adrenals and gonads. On sonography, they are seen as multifocal and often bilateral hypoechoic lesions.

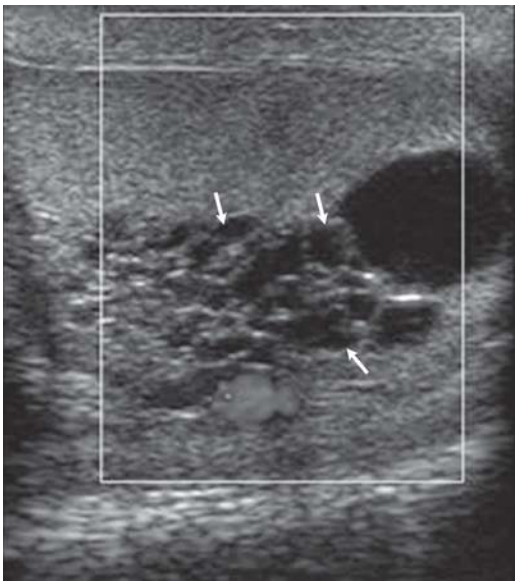

Fig. 27.15: US showing tubular ectasia of rete testis (arrows). Note absence of flow of color Doppler *(For color version see Plate 21)*

Calcifications

Testicular microlithiasis (TM) is an uncommon condition in which multiple, fine calcifications are present within seminiferous tubules. Sonography demonstrates innumerable, small, hyperechoic foci scattered throughout the testicular parenchyma, which rarely show acoustic shadowing (Fig. 27.16). The presence of five or more foci per transducer field in one testis is abnormal.[13] Testicular microlithiasis has been associated with testicular neoplasia in 18 to 75 percent of cases.[41] The exact prevalence of testicular tumors associated with TM is unknown. Currently, there is no evidence that TM is either a premalignant condition or a causative agent in testicular neoplasia; however, in view

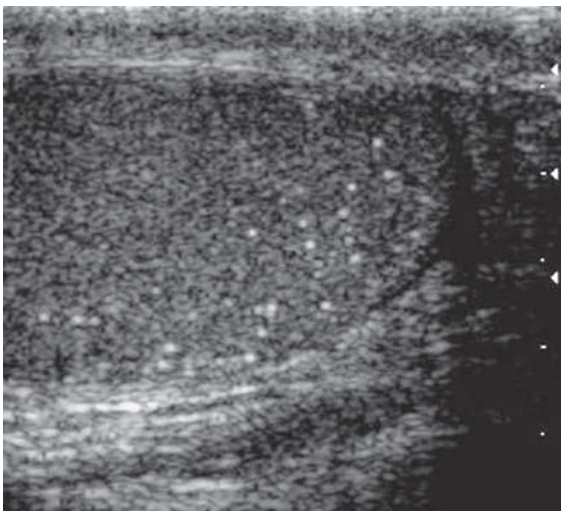

Fig. 27.16: US image showing multiple punctate hyperechoic nonshadowing foci of testicular microlithiasis

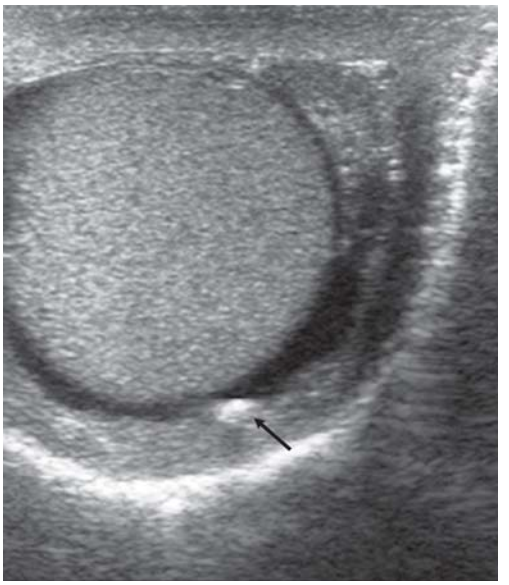

Fig. 27.17: US image showing a scrotal pearl (arrow)

of its reported associations with testicular neoplasia, annual US follow-up is recommended for at least several years after the diagnosis.[41]

Extratesticular scrotal calculi or *scrotoliths* (scrotal pearls) may represent a loose body caused by torsion of the appendix testis or epididymis.[16] The presence of a small quantity of fluid around the testis at US examination facilitates the diagnosis of scrotoliths (Fig. 27.27). Intratesticular macrocalcifications raise the suspicion of large cell calcifying Sertoli cell tumor, burned-out germ cell tumor, or post-traumatic change.

EXTRATESTICULAR PATHOLOGIES

Fluid Collections

Hydrocele is an abnormal accumulation of serous fluid in vaginal cavity. The congenital type is seen in infants and it is due to persistent communication between scrotal sac and the peritoneum. Acquired hydrocele is idiopathic or secondary to inflammation, torsion, trauma or tumor. Sonographically, a clear fluid is seen surrounding the testis. However, fine mobile echogenic concretions or a few thin septations can be seen in any long-standing hydrocele and it does not necessarily suggests complicated collection. Rarely, the concretion may be fairly large when it gives a 'bull's eye' appearance with central calcification surrounded by the hypo-echoic layer.

Hematocele and pyocele result from haemorrhage and abscess formation respectively. Both contain multiple septations and echogenic debris. Thickening of scrotal skin and calcifications may be seen in both of these conditions[13] (Fig. 27.18).

Inguinoscrotal hernia is usually diagnosed on the basis of clinical examination. Hernia may contain small bowel, large bowel and/or omentum. Sonographically, hernia is seen as echogenic structure of varying shapes, which moves in the inguinal canal with breathing. Sometimes bowel loops with their mucosal folds and peristalsis can also be identified. The presence of realtime peristalsis

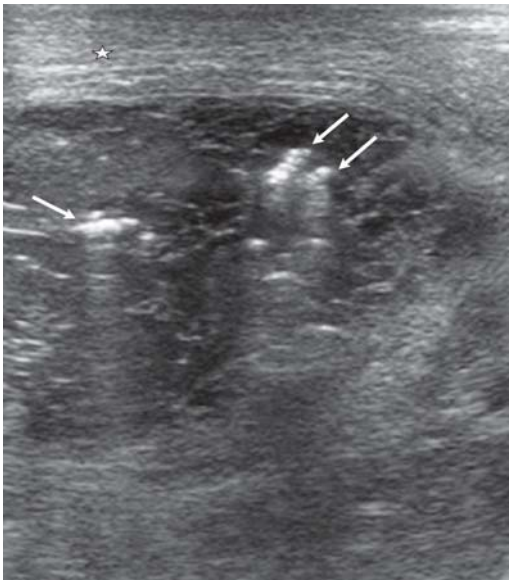

Fig. 27.18: Pyocele of scrotum: US image showing echogenic fluid collection within the scrotum and air foci (arrows) trapped within thin septations. Note the thickened skin of scrotum (star)

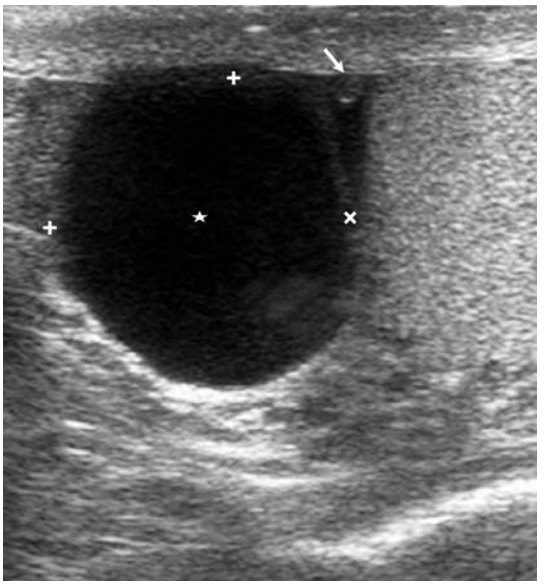

Fig. 27.19: US image showing an epididymal cyst. Appendix of testis (arrow) is seen between the cyst and the testis

is diagnostic for the presence of bowel. Bowel strangulation is more common in indirect than in direct inguinal hernia. An akinetic dilated loop of bowel observed at US in the hernial sac or hyperemia of scrotal soft tissue and bowel wall are suggestive of strangulation.[2] The testis and epididymis are separately seen and they retain their normal appearance.

Epididymal Cysts

Epididymal cysts and spermatoceles are the most common scrotal lesions and these may be encountered in upto 70 percent of all patients subjected to scrotal sonography.[12] Spermatoceles contains debris and sperms in addition to serous fluid and occur secondary to the obstruction of spermatic pathway. These are usually located in the head. Epididymal cysts are less common than spermatoceles and do not contain sperms. These are usually smaller in size and are located anywhere in the epididymis. Spermatoceles and epididymal cysts are identical on sonography and are seen as anechoic, well-circumscribed cysts with no or few internal echoes (Fig. 27.19). Sperm granulomas may be found in patients with epididymal obstruction or after vasectomy.[12] On sonography, these are seen as hypoechoic epididymal lesions, sometimes with focal calcification.

Postorchidectomy Scrotum

After orchidectomy, small amount of clear fluid is usually seen in the empty hemiscrotal sac, which resolves gradually. The scrotal wall appears thickened because of contraction. Hematomas are common in early postoperative period. Fresh hematomas are echogenic. These become hypoechoic or cystic as these resolve after five to six weeks. Tumor recurrence may be suspected if the mass develops several months after the orchidectomy.

On sonography, the recurrence is seen as a poorly defined hypoechoic lesion. Color Doppler, MRI or sonography guided biopsies are useful to differentiate recurrent tumor from hematoma.[42]

Testicular prosthesis is usually made up of silicone. On sonography, it is seen as a sharply defined, anechoic structure, frequently with excessive reverberations.[42]

Extratesticular Tumors

Extratesticular scrotal tumors are mostly benign and usually involve the epididymis. The most common is adenomatoid tumor constituting 30 percent of these tumors. It arises in epididymis or spermatic cord. On sonography, it is generally seen as solitary, well-defined, round to oval, small mass with variable echogenicity.[14] It may occasionally invade adjacent testicular parenchyma. Other benign paratesticular tumors include hemangioma, lipoma, neurofibroma and leiomyoma. Malignant paratesticular tumors include liposarcoma, fibrosarcoma and lymphoma in adults and rhabdomyosarcoma in children. The sonographic appearances of these tumors are nonspecific.[13]

Varicocele

Varicocele is an abnormal dilatation and tortuosity of the veins of the pampiniform plexus. It is described in detail in Chapter on Male Infertility.

REFERENCES

1. Trainer TD. Testis and the excretory duct system. In Sternberg S, (Eds). Histology for pathologists. New York, NY: Raven, 1992; 744-46.
2. Siegel MJ. The acute scrotum. Radiol Clin North Am 1997;35:959-76.
3. Bree RL, Hoang DT. Scrotal ultrasound. Radiol Clin North Am 1996; 34:1183-1205.
4. Middleton WD, Thorne DA, Melson GL. Color Doppler ultrasound of the normal testis. AJR 1989;152:293-97.
5. Paltiel HJ, Rupich RC, Babcock DS. Maturational changes in arterial impedance of the normal testis in boys: Doppler sonographic study. AJR Am J Roentgenol 1994;163:1189-93.
6. Friedland GW, Chang P. The role of imaging in the management of the impalpable undescended testis. AJR 1988;151:1107-11.
7. Heiken JP. Tumors of the testis and testicular adnexa. In: Pollack HM, McClennan BL, (Eds). Clinical Urography. Philadelphia, Pa: Saunders, 2000;1716-41.
8. Hricak H: Congenital anomalies of the testis. In: Hricak H, Hamn B, Kim B (Eds). Imaging of Scrotum. New York: Raven press1995;1:37-48.
9. Levitt SB, Konyan SJ, Engel RM. The impalpable testis: A rational approach to management. J Urol 1978;120:515-20.
10. Toyoshima M, Chida K, Masuda M. Testicular sarcoidosis. Nihon Kokyuki Gakkai Zasshi 2000;38:63-66.
11. Bayram MM, Kervancioglu R. Scrotal gray-scale and color Doppler sonographic findings in genitourinary brucellosis. J Clin Ultrasound 1997;25:443-7.
12. Cook JL, Dewbury K. The changes seen on high-resolution ultrasound in orchitis. Clin Radiol 2000;55:13-18.
13. Gorman B, Carroll BA. The scrotum. In Rummak CM, Wilson SR, Charhoneau JW (Eds). Diagnostic Ultrasound. Mosby: St Louis 2005;3: 849-88.
14. Oyen RH. Scrotal ultrasound. Eur Radiol 2002;12:19-34.
15. Noske HD, Kraus SW, Altinkilic BM, Weidner W. Historical milestones regarding torsion of the scrotal organs. J Urol 1998;159:13-16.
16. Dewbury KC. Scrotal ultrasonography: An update. BJU Int 2000;86:143-52.
17. Burks DD, Markey BJ, Burkhard TK, Balsara ZN, Haluszka MM, Canning DA. Suspected testicular torsion and ischemia: Evaluation with color Doppler sonography. Radiology 1990; 175:815-21.
18. Horstman WG. Scrotal imaging. Urol Clin North Am 1997;24:653-71.
19. Jee WH, Choe BY, Byun JY, Shinn KS, Hwang TK. Resistive index of the intrascrotal artery in

scrotal inflammatory disease. Acta Radiol 1997;38:1026-30.
20. Brown JM, Hammers LW, Barton JW, et al. Quantitative Doppler assessment of acute scrotal inflammation. Radiology 1995;197: 427-31.
21. Sanders LM, Haber S, Dembner A, Aquino A. Significance of reversal of diastolic flow in the acute scrotum. J Ultrasound Med 1994;13: 137-39.
22. Rifkin MD. Inflammation of the lower genitourinary tract: The prostate, seminal vesicles, and scrotum. In: Pollack HM, McClennan BL (Eds): Clinical Urography 2nd ed. Philadelphia, Pa: Saunders, 2000;1058-87.
23. Patriquin HB, Yazbeck S, Trinh B, et al. Testicular torsion in infants and children: Diagnosis with Doppler sonography. Radiology 1993;188:781-85.
24. Williamson RCN. Torsion of the testis and allied conditions. Br J Surg 1976;63:465-76.
25. Berman JM, Beidle TR, Kunberger LE, Letourneau JG. Sonographic evaluation of acute intrascrotal pathology. AJR Am J Roentgenol 1996;166:857-61.
26. Dogra VS, Sessions A, Mevorach A, Rubens DJ. Reversal of diastolic plateau in partial testicular torsion. J Clin Ultrasound 2001;29:105-08.
27. Skoglund RW, McRoberts JW, Ragde H. Torsion of testicular appendages: Presentation of 43 new cases and a collective review. J Urol 1970; 104:598-600.
28. Kratzik C, Hainz A, Kuber W. Has ultrasound influenced the therapy concept of blunt scrotal trauma. J Urol 1989;142:1243-46.
29. Hari A, Grossfeld G, Hricak A. Tumors of the scrotum. In Bragg DG, Rubin P, Hricak H (Eds): Oncologic Imaging. Philadelphia: WB Saunders Co. 2002;2:603-28.
30. Geraghty MJ, Lee FT, Jr, Bernsten SA, Gilchrist K, Pozniak MA, Yandow DJ. Sonography of testicular tumors and tumor-like conditions: A radiologic-pathologic correlation. Crit Rev Diagn Imaging 1998;39:1-63.
31. Rifkin MD, Kurtz AB, Pasto ME, Goldberg BB. Diagnostic capabilities of high-resolution scrotal ultrasonography: Prospective evaluation. J Ultrasound Med 1985;4:13-19.
32. Guthrie JA, Fowler RC. Ultrasound diagnosis of testicular tumours presenting as epididymal disease. Clin Radiol 1992;46:397-400.
33. Cotran RS, Kumar P, Collins T. The male genital tract In: Robbins Pathologic Basis of Disease. 6th ed. Philadelphia, Pa: Saunders 1999;1011-34.
34. Schwerk WB, Schwerk WN, Rodeck G. Testicular tumors: Prospective analysis of real-time US patterns and abdominal staging. Radiology 1987;164:369-74.
35. Comiter CV, Renshaw AA, Benson CB, Loughlin KR. Burned-out primary testicular cancer: Sonographic and pathological characteristics. J Urol 1996;156:85-88.
36. Hamm B. Differential diagnosis of scrotal masses by ultrasound. Eur Radiol 1997;7: 668-79.
37. Kim I, Young RH, Scully RE. Leydig cell tumors of the testis: A clinicopathological analysis of 40 cases and review of the literature. Am J Surg Pathol 1985;9:177-92.
38. Nonomura N, Aozasa K, Ueda T, et al. Malignant lymphoma of the testis: histological and immunohistological study of 28 cases. J Urol 1989;141:1368-71.
39. Richie JP. Neoplasms of the testis. In Walch PC, Retik AB, Vaughan ED, Wein AJ, (Eds). Campbell's urology. (7th edn) Philadelphia, Pa: Saunders, 1998;2411-52.
40. Basu S, Rubello D. PET imaging in the management of tumors of testis and ovary: Current thinking and future directions. Minerva Endocrinol 2008;33:229-56.
41. Ganem JP, Workman KR, Shaban SF. Testicular microlithiasis is associated with testicular pathology. Urology 1999;53:209-13.
42. Eftekhari F, Smith JK. Sonography of scrotum after orchiectomy: normal and abnormal findings. AJR 1993;160;543-47.

Chapter

28

Male Infertility and Erectile Dysfunction

Deep Narayan Srivastava, Sanjay Thulkur

MALE INFERTILITY

Defects in male partner may be responsible for infertility in up to 50 percent of the infertile couples.[1] These defects account for a reduction in the quantity and quality of the semen. The evaluation of infertile male begins with a careful history and physical examination of the patient. This is followed by semen analysis in which ejaculate volume and its pH, sperms count, their motility and morphology are studied. Average sperm count in normal fertile man is 70 to 80 million sperms per ml and it contains more than 60 percent motile sperms. Sperm count of less than 20 million per ml is termed as oligospermia, however, significant decrease in pregnancy rates occur only at sperm concentration of less than 5 million per ml. Oligospermia is present in 80 percent and azoospermia is present in another 15 to 20 percent of the infertile men.[1]

Etiology

Male infertility results from many diverse conditions. Congenital anomalies include cryptorchidism, Klinefelter's syndrome, agenesis of vas deferens and/or seminal vesicles and congenital ejaculatory duct cyst. Endocrinal abnormalities are uncommon causes of the male infertility and these are diagnosed primarily on the basis of clinical examination and laboratory findings. Luiteinizing hormone secreted by the pituitary gland regulates the *testosterone* secretion by Leydig cells of the testis. Low testosterone affects spermatogensis, growth of the prostate and seminal vesicle secretion.[2]

Acquired testicular abnormalities such as trauma, tumor, infection and paratesticular abnormalities such as varicocele and epididymitis are responsible for infertility in significant number of patients. Tuberculosis and gonorrhea cause inflammation and obstruction of the ductal transport system. Other diseases such as mumps and syphilis may affect seminiferous tubules in the testicular parenchyma.

Primary or secondary neoplastic infiltration of testes, as occurs in lymphoma and leukemia, may affect fertility. Chemotherapy; especially with cisplatin or alkylating agents can produce irreversible damage to germinal epithelium. Radiotherapy of more than 15 Gy also produces testicular damage. Testicular tumors and hematological malignancies are common neoplasms in young males and infertility counseling before treatment is

mandatory in these patients. Cryopreservation of sperms is a preferred option.[3]

Imaging Approach in Male infertility

Normal volume (more than 1 ml), fructose positive ejaculate with azoospermia or oligospermia is usually caused by lesions of the testis or of paratesticular structures such as varicocele and epididymal diseases.[4] These lesions can be satisfactorily evaluated with scrotal ultrasonography, supplemented with color Doppler flow imaging. Although clinical examination is an integral part of diagnostic work-up in these patients, upto 67 percent of scrotal pathologies detected on sonography and responsible for infertility are not apparent clinically.[5]

Low volume ejaculate (less than 1 ml) is caused by stenosis, obstruction or congenital anomalies of distal sperm transport system, which include vas deferens, seminal vesicles, ejaculatory duct and prostate. Abnormalities in these structures result in decreased semen volume and blockage of flow of sperms into the ejaculate leading to azoospermia or oligospermia. These abnormalities include agenesis of vas deferens or seminal vesicles or both, inflammatory strictures and obstruction of seminal vesicles and vas deferens, ejaculatory duct cysts and obstruction. Vasography is the traditional modality for evaluation of distal ductal system. It is an invasive technique and requires surgical exploration of the vas deferens in scrotum. The procedure itself may cause iatrogenic scarring and obstruction of the vas.[6] Transrectal ultrasonogrpahy (TRUS) has now replaced vasography as the primary imaging modality for distal ductal system.[1,7] It is now widely used to diagnose congenital and other obstructive lesions that produce low volume ejaculate and azoospermia. MRI is indicated only if TRUS findings are inconclusive.[8]

Varicocele

Varicocele is the most common surgically correctable cause of male infertility. There is abnormal dilatation of veins of the pampiniform plexus, which is due to venous reflux in these veins. The incidence of varicocele is 15 percent in general population and 35 to 40 percent in men presenting with infertility.[9,10] Primary varicocele is seen in young men and is due to incompetent testicular vein. It is mostly left-sided or bilateral. Left testicular vein is maximally predisposed to develop varicocele. Various factors responsible include right-angled entry of left testicular vein into left renal vein, the intermittent compression of left renal vein between aorta and the superior mesenteric artery (nutcracker syndrome) and pressure of the left colon.[11] Secondary varicocele results from compression of testicular veins by adjacent masses such as tumor, lymph nodes or hydronephrosis.[12] Cross communications exist between veins of the pampiniform plexus and cremasteric veins as well as external spermatic veins and veins of vas deferens. In patients, subjected to high ligation, these communications may lead to recurrence.

Although most men with varicocele are not infertile, varicocele is present in up to 40 percent of infertile men. Repair of varicocele improves quality of semen in majority of patients.[13] Proposed mechanisms by which varicocele causes testicular dysfunction include hormonal imbalance, hypoxia secondary to venous stasis, reflux of adrenal and renal metabolites and elevated testicular temperature.[14] During adolescence, when the testis is growing rapidly, it may be very susceptible to harmful effects of varicocele.

The simplest and most widely used method for diagnosis of varicocele is physical examination; however, subclinical varicocele cannot be diagnosed with physical examination alone. Ultrasonography with color duplex flow imaging is the preferred imaging modality for evaluation of varicocele. Thermogrpahy and venography are rarely performed for diagnostic purpose.[13] The patient is examined in supine and erect position during quite breathing, deep breathing and Valsalva maneuver before interpreting the examination as normal.[9] Vessels are scanned on each side from the scrotal neck to the lower pole of testis. As the flow in pampiniform plexus is very slow, Doppler parameters must be adjusted to detect very slow flow during color Doppler examination. On grey scale ultrasonography, visualization of three or more dilated veins with at least one of them having a diameter of 3 mm or more is suggestive of varicocele.[13] These tortuous venous channels are easily compressible as opposed to other cystic abnormalities in this region. On color Doppler study, continuous retrograde flow towards testis during Valsalva maneuver, is taken as a positive sign for varicocele[13,15] (Figs 28.1A and B). A brief reflux in veins of pampiniform plexus followed by cessation of flow is physiological. Pulsed Doppler is not required for the diagnosis of varicocele.[13] Some varicoceles can be demonstrated in erect position of the patient only and hence scanning in erect position is mandatory before the study is interpreted as normal.[13] Intratesticular varicocele is rare and always associated with paratesticular varicocele. It is usually located in subcapsular location or in the mediastinum testis.[16]

Size of the varicocele does not correlate with degree of impairment of spermatogenesis. Thus a small varicocele detected only on radiological assessment may have a profound effect on spermatogenesis.[17] The treatment of subclinical varicocele in infertility is still controversial, however, it has been demonstrated that sperm motility improvement after varicocele surgery is comparable in patients with both clinical and subclinical varicocele.[18]

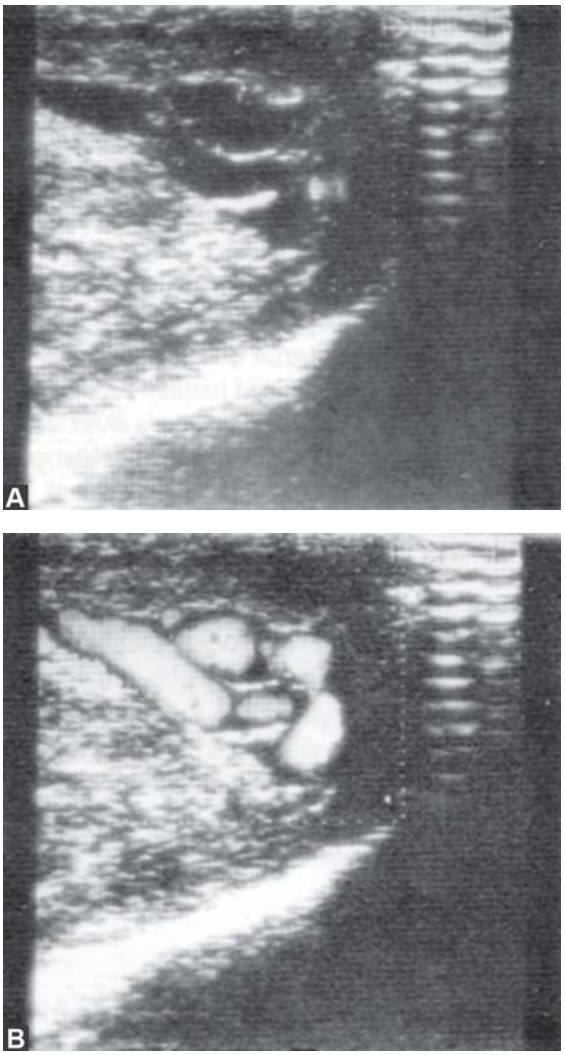

Figs 28.1A and B: Varicocele: **(A)** Multiple dilated vascular channels with minimal detectable flow is seen at the lower pole of testes on this black-and-white image of colour Doppler scan. **(B)** Significant increase in flow is seen during Valsalva maneuver

Spermatic venography is the gold standard for diagnosis of varicocele. When compared with venography, color Doppler ultrasonography had a sensitivity of 93 percent and specificity of 80 percent in a group of infertile patients with normal physical examinations.[19] In addition to the diagnosis, spermatic venography has therapeutic application for embolization of varicocele. In this technique, an angiographic catheter is placed into the testicular vein via transfemoral venous route. About 5 to 10 ml of contrast is injected during Valsalva maneuver and radiographs of abdomen and pelvis are taken. The venography can be followed by embolization performed using coils or sclerosants such as sodium tetradecyl sulfate foam.[13] Correct identification of all venous collaterals with their selective embolization is necessary. High technical success rate with significant improvement in semen quality can be achieved with this technique.[20] This technique is especially suitable for post-surgical recurrent varicocele.[21]

Testis

Sonographic examination of the testis is important in the evaluation of infertile male, specifically for measurement of testicular size for atrophy or for tumor identification. Normal adult testis is homogenous with low to medium echogenicity and measures 3-5 cm in length, 2-3 cm in width and 2-3 cm in antero-posterior thickness. Testicular volume in cc can be calculated using the formula of length × width × thickness × 0.53. The normal volume of adult testis is 15 to 20 cc and testis is symmetrical on both sides.[21]

Cryptorchoidism occurs in approximately 0.8 percent of all one-year-old boys and if left untreated can represent a congenital cause of male infertility.[22] Progressive germ cell damage occurs in the cryptorchoid testis secondary to the increased temperature at its extra scrotal location. Significant germ cell damage occurs by two years of age and untreated post-pubertal undescended testis may be completely devoid of germ cells. It also has a deleterious effect on contralateral normal descended testis. Pregnancy rates in men who have undergone pre pubertal treatment of unilateral cryptorchoidism ranges between 65 to 80 percent.[22] In addition to infertility, undescended testis is highly susceptible for malignant transformation.

Most of the undescended testes are located at or close to the inguinal canal and ultrasonography is very sensitive to identify their location. Ultrasonography is less accurate in detection of undescended testis when it is located in the retroperitoneum. CT or MRI scans of abdomen and pelvis from the level of inguinal rings to lower poles of the kidney are required for testicular localization in such situations. MRI is more accurate because of its high soft tissue contrast and multi planner capabilities. The characteristic high signal intensity of testis on T2 weighted sequences aid in easy recognition of undescended testis. MRI scores over ultrasonography and CT in localization of atrophic undescended testis.

Testicular tumors are most common in the same age group in which fertility disorders of male are most prevalent. Testicular tumors may be identified in-patients presenting with oligospermia or azoospermia.[23] Seminomas are the most common testicular tumours and are usually homogeneously hypoechoic on sonography. Non seminomatous tumors are complex and heterogeneous in echotexture. Testicular tumors are described in details in the chapter on imaging of scrotum.

Testicular torsion occurs most frequently during adolescence and therefore has the potential impact on fertility of affected young males. Acute testicular torsion is an emergency and torsed testis must be salvaged at the earliest. The degree of ischemic damage due to torsion depends on the duration of testicular torsion. There are good chances of salvage when patients are operated within seven hours. If it is delayed for more than 24 hours, virtually all testicular function is lost. On sonography, the affected testis is hypoechoic and may be enlarged. Color Doppler shows decreased vascularity, which is best appreciated when compared with contralateral normal testis.

Testicular trauma has less impact on male fertility than the other testicular factors such as torsion or cryptorchoidism.[22] Spermatogenic dysfunction may develop in testicular trauma patients, secondary to direct cell injury and the formation of anti sperm antibodies from disruption of blood-testis barrier in them. Ultrasonography with color Doppler is most suitable investigation to determine the extent of testicular trauma; however, satisfactory ultrasonography examination may not be possible in acutely traumatized and painful scrotum. In such situations, MRI is more accurate to detect disruption of the testicular capsule; however, most of these patients will need surgical exploration.

Higher incidence of testicular microlithiasis is found on scrotal ultrasonography in infertile men; however, its relationship with infertility is not known.[10]

Epididymis

The epididymis is located along the posterolateral aspect of testis and runs parallel and posterior to the mediastinum testis. The head of the epididymis is pyramidal in shape and it is larger than rest of the epididymis. The head measures 5 to 12 mm in thickness.

Infertile man may have infection or inflammation of the epididymis. The normal epididymis has the echogenicity similar to the testis. In acute epididymitis, epididymis is enlarged and hypoechoic with increased vascularity on color Doppler. Chronic inflammation results in an enlarged and heterogeneously hyperechoic epididymis, sometimes with foci of calcification.[12] Scarring in chronically inflamed epididymis may result in epididymal obstruction, which can be avoided with early and aggressive treatment of epididymitis.

Epididymal cysts and spermatoceles are usually located at the head of the epididymis and these can be easily detected on sonography. Most epididymal cysts do not cause obstruction, however, rarely, these may compress the epididymal tubules and cause epididymal obstruction, especially if large, and produce oligo or azoospermia, Very large epididymal cysts may occasionally be difficult to differentiate from hydrocele on sonography, however, compression of epididymis and adjacent testicular margin and presence of the fluid at one end of the testis instead of surrounding the testis help to differentiate large epididymal cyst from hydrocele (Fig. 28.2).

TRUS Evaluation of Distal Genital Ductal System

TRUS is indicated in infertile men with suspicion of obstructive pathology in distal sperm transport system. This is suggested by low volume ejaculate with oligo or azoospermia and palpable abnormality on digital rectal examination. The conditions that produce low volume ejaculate with oligo or azoospermia include agenesis of vas deferens

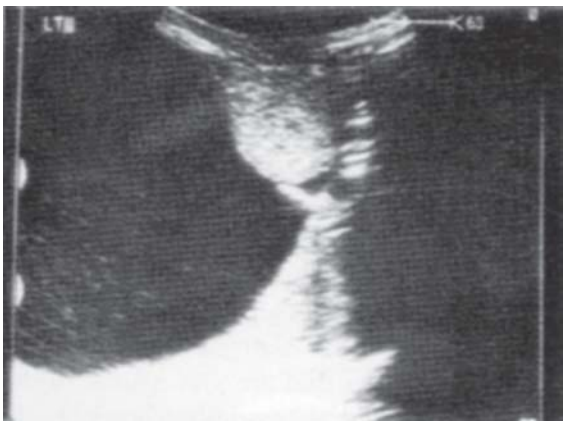

Fig. 28.2: Large epididymal cyst at the upper pole of testis seen on scrotal ultrasonography. Nonvisualization of normal epididymal head and eccentric displacement of testis instead of being surrounded by fluid helps to differentiate this condition from hydrocele

and seminal vesicle, ejaculatory duct obstruction and urethral strictures.[1,7] Other indications of TRUS include hematospermia, painful ejaculation, severe sperm motility defects and azoospermia in normal volume ejaculate without testicular atrophy.[24]

On TRUS, normal prostate is a symmetric, triangular and ellipsoid structure with homogeneous echogenicity surrounded by a thin layer of echogenic capsule. Normal seminal vesicles are paired, well defined, sacular, elongated hypoechoic organs, situated cranial to the prostate and posterior to urinary bladder with 'bow-tie' appearance on axial images. These may vary in size, shape and degree of distention; however, usually these are symmetrical. On axial plane, ampulla of vasa deferentia are seen as round or oval tubular structures that are just cranial to prostate and medial to seminal vesicles. In sagittal plane, these can be seen behind prostate projecting medially towards seminal vesicles. Ejaculatory ducts are difficult to visualize on TRUS in normal men. These may sometimes be seen as tubular structures obliquely traversing the prostate and entering the urethra at verumontanum.[1]

Seminal Vesicles and Vas Deferens

Seminal vesicle secretions contribute about 80 to 90 percent of sperm volume. They also secrete fructose and maintain an acidic pH of semen. Congenital anomalies and obstructive lesions of seminal vesicles result in decreased semen volume, low pH and low fructose levels.

Wolffian duct anomalies include renal agenesis, agenesis of vas deferens, agenesis or atrophy of seminal vesicles and cysts of seminal vesicles. Seminal vesicle atrophy or agenesis may be unilateral or bilateral.[2] It occurs in all patients with agenesis of vas deferens. Bilateral absence of seminal vesicles may be seen in up to 40 percent of patients with low volume azoospermia.[4] It can be diagnosed with semen analysis and clinical examination in most patients.[25] Large number of these patients also has associated renal anomalies. Another strong association is with cystic fibrosis in which 98 percent of men have agenesis of seminal vesicles and vas deferens.[4] On TRUS or MRI, seminal vesicle is considered atrophic if it measures less than 7 mm in width and dilated (as in ejaculatory duct obstruction) when it measures more than 15 mm.[2,8] Diagnosis of seminal vesicle and vas agenesis is made when these are not visualized (Fig. 28.3).

Cysts of seminal vesicles may be congenital or acquired. Congenital cyst of seminal vesicle results from an ectopic ureter insertion into the seminal vesicle and is associated with a hypoplastic kidney on the same side. This cyst may compress ejaculatory duct and produce obstruction. Acquired cysts of seminal vesicles are secondary to infection. Chronic inflammation produces cystic dila-

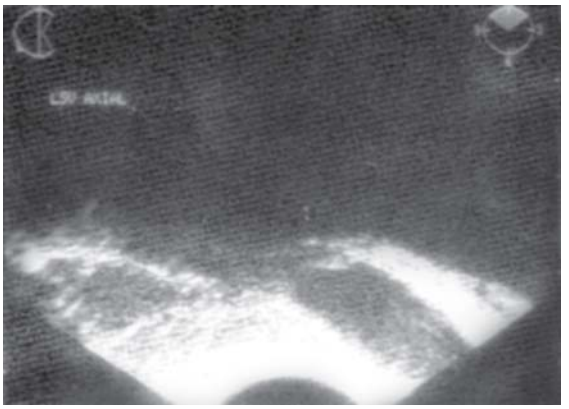

Fig. 28.3: Agenesis of seminal vesicle. TRUS shows absence of seminal vesicle on right side on axial scan. Normal left seminal vesicle is seen as hypoechoic elongated structure behind the urinary bladder

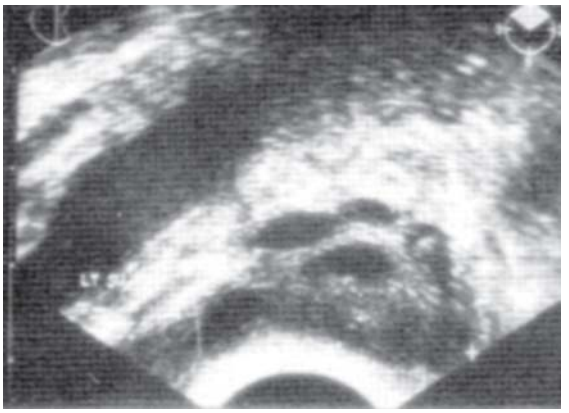

Fig. 28.4: Multiple post-inflammatory seminal vesicle cysts are seen on axial TRUS scan

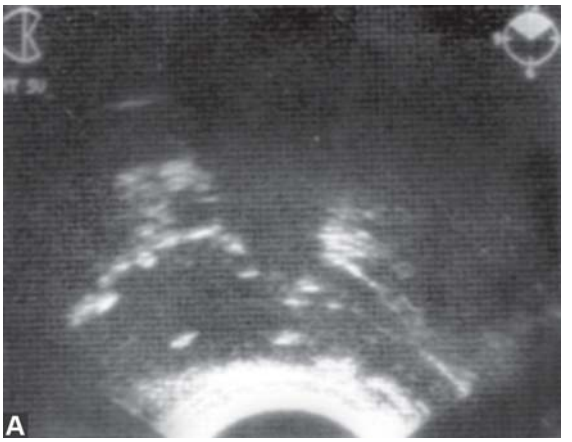

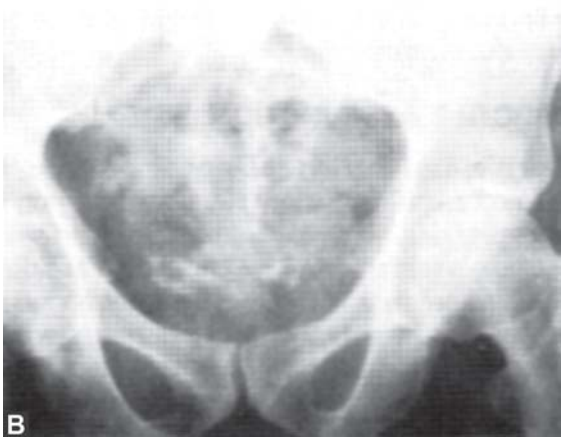

Figs 28.5A and B: Seminal vesicle calculi: **(A)** Axial TRUS scan, **(B)** AP radiograph of pelvis

tation with scarring and obstruction of the lumen of the seminal vesicles and causes infertility (Fig. 28.4). Stone formation in dilated seminal vesicles can be readily demonstrated on TRUS (Figs 28.5A and B), however, this appears to be secondary to stasis rather than cause of the obstruction.[8,26]

Ejaculatory Ducts

These are formed by confluence of seminal vesicles and terminal ampullary portion of the vas deferens and hence, ejaculatory duct obstruction results in decreased semen volume with absence of seminal fructose. TRUS may demonstrate ejaculatory duct cysts, dilatation of ejaculatory ducts (Fig. 28.6) or calcification in ejaculatory ducts along with dilated seminal vesicles 4.[27] Any of these findings strongly suggest ejaculatory duct obstruction.

Many of these conditions can be treated with transurethral resection of the ejaculatory duct (TURED).[27] Specificity of TRUS in the diagnosis of ejaculatory duct obstruction is unsatisfactory, hence, TRUS-guided seminal vesicle aspiration followed by vesiculography

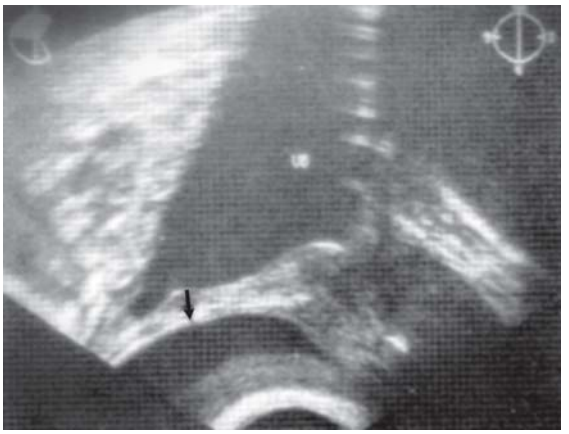

Fig. 28.6: Ejaculatory duct obstruction: cystic dilatation of ejaculatory duct (arrow) is seen on sagittal TRUS image

is useful before TURED.[28,29] TRUS-guided seminal vesicle aspiration is performed with a 21G needle introduced transrectally. Presence of motile sperms in seminal vesicle fluid strongly suggests ejaculatory duct obstruction because sperms are not normally seen in seminal vesicles. The aspiration is followed by injection of 5 to 20 ml of dilute non-iodinated contrast under fluoroscopic guidance and images are obtained to study the seminal vesicles and ejaculatory ducts. Pelvic and inguinal portions of vas deferens may also be visualized with this technique.[24]

Prostate

Mullerian duct cyst and utricle cyst are congenital prostatic cysts which may be indistinguishable from each other. When large, these may compress and produce ejaculatory duct obstruction.[2] On imaging, both are seen as midline cyst in prostate. Mullerian duct cysts do not communicate with urethra and when large, may extend above the prostate. Utricle cysts communicate with urethra and do not extend above prostate. Acquired prostatic cysts like parasitic and prostatic retention cysts are usually located peripherally. These may produce obstruction to semen flow within the prostate and subsequent infertility. Chronic prostatitis may produce scarring, atrophy of seminal vesicles and strictures of ejaculatory duct which may lead to infertility.[2] These can be identified on TRUS as disorganization of normal anatomy produced by scarring of prostatic tissue and occasional stone formation.[4]

MRI in Infertility

Scrotal MRI is the most important adjunct to ultrasonography in evaluation of testicular and paratesticular abnormalities. It is highly accurate in cryptorchidism, testicular tumors, trauma and infection. Scrotal MRI is described in details in the chapter on 'Imaging of Scrotum'.

MRI is recommended for the evaluation of distal genital tract when TRUS findings are equivocal.[8,26] Various abnormalities of prostate and seminal vesicles such as cysts of seminal vesicles and ejaculatory duct, dilatation of vas deferens and seminal vesicles secondary to ejaculatory duct obstruction can be satisfactorily demonstrated. On MRI, absence or atrophy of seminal vesicles with very small size and loss of normal high-signal intensity is seen in upto 40 percent of patients.[26] Agenesis of vas may be demonstrated. MRI is particularly advantageous in suspected case of ejaculatory duct obstruction as demonstration of normal ejaculatory ducts rules out presence of ejaculatory duct obstruction.[30]

Imaging in Assisted Fertilization

Scrotal sonography is also useful in the work up of assisted fertilization. Testicular volume as calculated on sonography can predict the outcome of testicular biopsies for sperm

retrieval. Chances of successful sperm retrieval are significantly higher in patients with testicular volume more than 12 cc.[31] Similarly, sonography guided testicular sperm aspiration is more accurate and it has less complications when compared with the blind aspiration as sonography allows good visualization of testicular parenchyma, easy sampling and avoidance of prominent vessels.[32] In patients with ejaculatory duct obstruction, sperms can also be aspirated from seminal vesicles under TRUS guidance. Intra operative use of TRUS is helpful in identification of obstructing cyst and determining the depth of resection during trans urethral resection of ejaculatory duct for the treatment of ejaculatory duct obstruction.[33]

ERECTILE DYSFUNCTION

Erectile dysfunction (ED) or impotence is defined as inability to achieve and/or maintain an erection for satisfactory sexual intercourse.[34] Its prevalence increases with age and affects up to 52 percent men between age group of 40-69 years.[35] ED is broadly classified into two categories; organic and psychologic. Vasculogenic impotence is the most common cause of organic impotence and may be a marker for occult cardiovascular disease.[36] Vascular ED does not rule out the presence of contributing psychological factors, but merely means that vascular factors are predominant cause of ED. Vascular ED has two different mechanisms; obstruction in penile inflow tract, termed as arterial ED and the inability to trap the incoming blood in the cavernosa, termed as veno-occlusive ED.

Anatomy and Physiology of Penile Erection

The paired internal pudendal arteries give rise to common penile arteries which divide into four branches, one each to spongiosa, cavernosa, proximal urethra and the dorsum of the penis (deep dorsal artery). The cavernosal artery provides blood to cavernosa through multiple helicine arteries that open directly into the cavernosal sinusoids. Venules located within the subtunical space between the periphery of erectile tissue and the tunica albugenia provide venous outflow channel from corpora cavernosa via peripheral lacunae. These vein pierce tunica albuginea and drain into cavernosal and then into deep dorsal vein.

Penile erection is a neurovascular phenomenon in which neurological stimulus via parasympathetic nerves from sacral 2,3,4 leads to arterial response. It is initiated by relaxation of smooth muscles of helicine arteries leading to vasodilatation. The phase of arterial response is followed by the phase of tumescence, in which relaxation of trabecular smooth muscles and increased arterial flow lead to increase in size and length of the penis. The phase of erectile response follows when subtunical venules are compressed against tunica albuginea due to dilatation of sinusoids and increase in intracavernosal pressure. If this veno-occlusive mechanism is intact, the arterial inflow leads to increase in intracavernosal pressure to the levels of mean arterial blood pressure. Perineal muscles contractions generate further increase in pressure, which leads erectile response to rigidity.

Parameters of quality of the arterial response are peak systolic velocity and acceleration time as measured by pharmacopenile duplex ultrasonography (PPDU) and cavernosal artery occlusion pressure as measured by cavernosometry. Parameters to assess the quality of veno-occlusive mechanism are end diastolic velocity and resistive index on PPDU and maintenance flow and pressure loss on cavernosometry.

Evaluation of Erectile Dysfunction

Psychologic factors or systemic illnesses are responsible for erectile dysfunction in majority of patients. Careful history, clinical examination and routine laboratory tests are extremely important for the evaluation of ED as these can identify the underlying cause in up to 80 percent of patients.[37] Such work-up may detect reversible cause of ED or unmask the systemic illness responsible for ED. With advent of effective oral pharmacotherapy, the diagnostic approach has significantly changed over past decade. A good erectile response to these drugs excludes significant arterial or vascular disease as a cause of ED. Hence, most patients are first given a therapeutic trial and only those with failure are referred for invasive diagnostic tests like PPDU, cavernosography or angiography.[34]

Pharmacopenile Duplex Ultrasonography (PPDU)

Pharmacopenile duplex ultrasonography (PPDU) is most widely used investigation to define vascular ED and to differentiate between arterial insufficiency and defective veno-occlusive mechanism.

The different vasoactive agents used for PPDU are papaverine, combination of papaverine and phentolamine and prostaglandin PGE_1 (Trimix).[34] Papaverine may lead to false negative erectile response in some patients and persistent painful erection (priapism) may occur in other. Prostaglandin PGE_1 has better erection rate and less incidence of priapism.[38] Genital self-stimulation, visual erotic stimulus or application of penoscrotal tourniquet may augment the erectile response. Gadgets like virtual glasses with facility for audio-visual erotic stimulus improve the erectile response and Doppler waveform, thereby eliminating the false positive results of PPDU examination.[39]

Technique of PPDU: The examination must be conducted in an atmosphere of privacy. The ultrasonographic evaluation begins with scanning of flaccid penile shaft in transverse plane to measure the diameter of cavernosal artery. It ranges from 0.2 to 1 mm.[34] Although the arterial flow in the flaccid penis is difficult to demonstrate, Doppler flowmetry of flaccid penis has the potential to detect arteriogenic ED. Peak systolic velocity of less than 10 cm/sec in the cavernosal artery of flaccid penis is suggestive of arteriogenic ED.[40] Later, intracavernosal injection of 60 mg of papaverine is made with 30 G needle in either of the cavernosa as cross communications exist between both sides. Care must be taken not to inject into a vessel or urethra. The erectile response is graded visually from E0 to E5 as suggested by Broderick et al[41] (Table 28.1). Grade E4 and E5 are sufficient for penetration.

Table 28.1: Visual grading of penile erection during PPDU

E0	:	No response
E1	:	Elongation of shaft only
E2	:	Moderate tumescence, no rigidity
E3	:	Full tumescence, no rigidity, easily bendable
E4	:	Full erection, partial rigidity
E5	:	Full rigidity for at least 20 minutes

After evaluating the erectile response, scanning is started from the base at the penoscrotal junction to distal part, both in transverse and longitudinal planes. Dorsal scanning in saggital plane is necessary to identify cavernosal collaterals and penile deformities such as Peyronie's disease. The post injection diameter of both cavernosal arteries is measured. Angle corrected flow velocities are measured as proximal as possible in cavernosal arteries. Most accurate flowmetry values are obtained at the time of

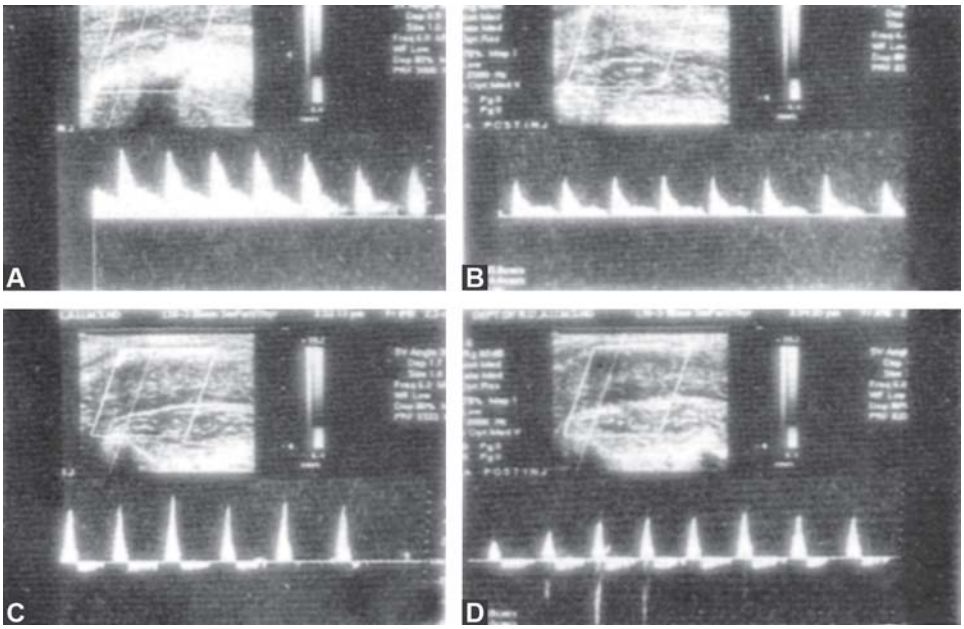

Figs 28.7A to D: Normal spectral waveform progression of PPDU: **(A)** Early tumescence, **(B)** Late tumescence, **(C)** Early rigidity, **(D)** Peak rigidity

peak rigidity, however, this time is highly variable. Hence, flowmetry values are normally obtained at 0, 5,10 and 20 minutes after the injection.

Post papaverine injection normal spectral waveform has been described to have five phases[42] (Figs 28.7A to D). Phase 1 is characterized by increase in both systolic and diastolic velocities. In phase 2, there is progressive decrease in end diastolic velocity and appearance of a diachrotic notch. Patients with severe venous leakage do not progress beyond phase 2. In phase 3, diastolic flow approximates zero and it is reversed in phase 4. Phase 5 is characterized by eventual loss of both systolic and diastolic signals.

Various parameters studied on flowmetry are peak systolic velocity (PSV), end diastolic velocity (EDV), acceleration time (AT), and resistive index (RI). Mild variations are seen in cutoff values described in different studies. PSV of more than 35 cm/sec rules out arterial insufficiency and PSV of 25 cm/sec is highly suggestive of the same. Lot of overlap is seen between these two values in normal and abnormal individuals.[2] Currently acceptable reference values to interpret the examination as normal are given in Table 28.2.[34,38]

Table 28.2 : Normal reference values for PPDU

PSV	:	25 cm/sec or more
EDV	:	5 cm/sec or less
AT	:	0.11 sec or less
RI	:	0.85 or more

In a study of 32 men without evidence of vascular ED conducted at AIIMS, the mean PSV was 61.3 cm/sec, the mean EDV was –1.2 cm (minus sign denotes flow reversal) and the mean AT was 0.06 sec.[43] Mean RI was 0.93 in whom diastolic flow reversal was not achieved. Another interesting observation was the linear relationship between PSV and ages of the individuals, which implies that use of single cut-off value for all ages may be debatable.

Abnormal PSV (less than 25 cm/ sec) and AT (more than 0.11 sec) are suggestive of arterial disease. Similarly, any increase in the cavernosal artery diameter by less than 75 percent of the baseline diameter also indicates possibility of arterial disease. Abnormal EDV (more than 5 cm/ sec) and RI (less than 0.85) denote venous leakage. RI is considered more reliable than EDV for assessment of veno occlusive mechanism.[43] If arterial disease is present, intracavernosal pressure remains below systemic pressure and veno-occlusion cannot occur, even if this mechanism is intact, and diastolic flow will continue to persist. Therefore, veno-occlusive mechanism cannot be assessed with EDV and RI in presence of arterial disease.

PPDU with oral sidenafil: Sidenafil citrate (Viagra) has been studied as an alternative to intracavernosal injection of vasoactive drugs for PPDU, in order to make the examination non-invasive. However, the results are inconsistent.[44,45] Oral dose of 50 or 100 mg is normally used. Unlike intracavernosal agents, sidenafil alone cannot achieve erection and it must be supplemented with audiovisual sexual stimulation. Effect of sidenafil is also slow and peak erection is usually achieved between 60 to 75 minutes after its oral administration. The quality of erection and the PSV achieved with sidenafil is lower than the same parameters achieved after intracavernosal injection. This may lead to false positive PPDU results in some patients.[45] With these limitations, oral sidenafil has failed to replace intracavernosal injections of vasoactive drugs for PPDU. A recent study has suggested that best results are obtained with combination of oral sidenafil and intracavernosal injection of trimix during PPDU.[46]

Peyronie's Disease

This is a benign condition resulting from inelastic scar of tunica albuginea, which produces curvature deformities of penis and the ED. It is traumatic in origin in majority of the patients and the ED in these patients is primarily because of penile deformities, painful erection or associated vascular disorders.[47] On sonography, the penile plaques are seen as echogenic focal thickenings of tunica, which may displace or encase dorsal vasculature. Dense plaques may contain calcifications and cause acoustic shadowing (Fig. 28.8), however, shadowing can be seen even without evidence of calcification on plain radiographs. Most plaques are located in the middle third of the shaft of the penis.[38]

Cavernosometry

Cavernosometry is a primary modality available for quantifying and mapping of veno-occlusive dysfunction. However, because of its invasive nature, it is reserved for patients with suggestion of venous leakage on PPDU if surgical repair is being considered for them. In cavernosometry,

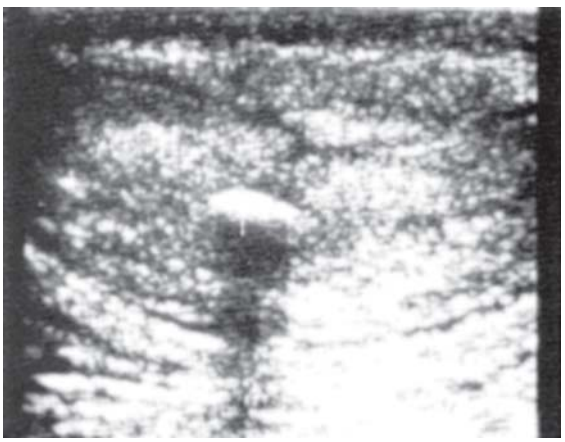

Fig. 28.8: Peyronie's disease: Dense echogenic plaque of tunica albuginea with distal shadowing is seen on PPDU

venous outflow resistance is assessed by determining the intracavernosal flow rate required to sustain an erection in a state of complete sinusoidal relaxation.

In this technique, two 19G needles are introduced, one in each cavernosa. One needle is connected to the infusion pump and the other needle to a pressure monitor. A mixture of 30 mg of papaverine and 1 mg of phentolamine is infused. The intracavernosal pressure rises gradually and then remains steady. After this, the infusion flow rate is gradually increased to demonstrate linearly proportional increase in intracavernosal pressure. Linear relationship between cavernosal pressure and infusion rate is suggestive of a state of complete sinusoidal relaxation. If a nonlinear relationship is observed, a second dose of papaverine may be given to achieve complete sinusoidal relaxation.

Maintenance flow rate is considered as the most important parameter of cavernosometry and it involves recording of minimum flow rate, which is required to maintain intra cavernous pressure at 150 mm Hg. Maintenance flow rate of more than 3 ml per minute is suggestive of venous leakage. After this, the infusion is stopped and the rate of fall of cavernosal pressure is observed for 30 seconds. The rate of fall, termed as 'pressure loss', of more than 1.5 mm Hg per second is considered abnormal.[38]

Gravity cavernosometry is a simple and cost effective modification of the above technique in which the inflow needle is connected to heparinized normal saline kept at the height of 160 cm. The infusion produces increase in cavernosal pressure which subsequently reaches at a pleatuea, termed as 'steady state pressure'. Steady state pressure of less than 97 mm Hg is considered abnormal.[48]

Cavernosography

Patient can be taken up for cavernosography after cavernosometry in the same sitting. About 40 ml of iodinated contrast is injected in infusion line while keeping intra cavernosal pressure just above mean arterial pressure. Spot films of penis and pelvis are obtained under fluoroscopic guidance in AP and both oblique projections (Figs 28.9A and B). Normally draining veins are not opacified. In case of venous leakage, veins are visualized draining

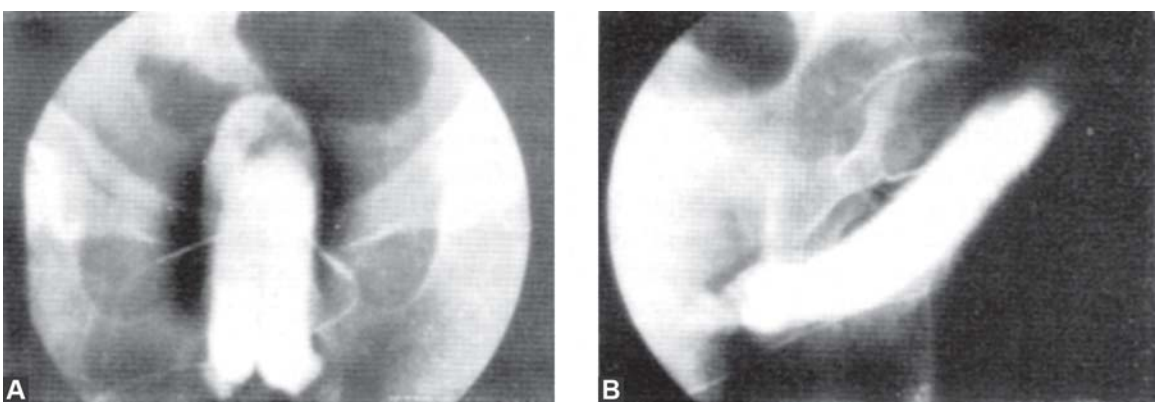

Figs 28.9A and B: Normal cavernosogram: **(A)** AP and **(B)** oblique views show homogeneous opacification of bilateral cavernosa without visualisation of any vein in victinity

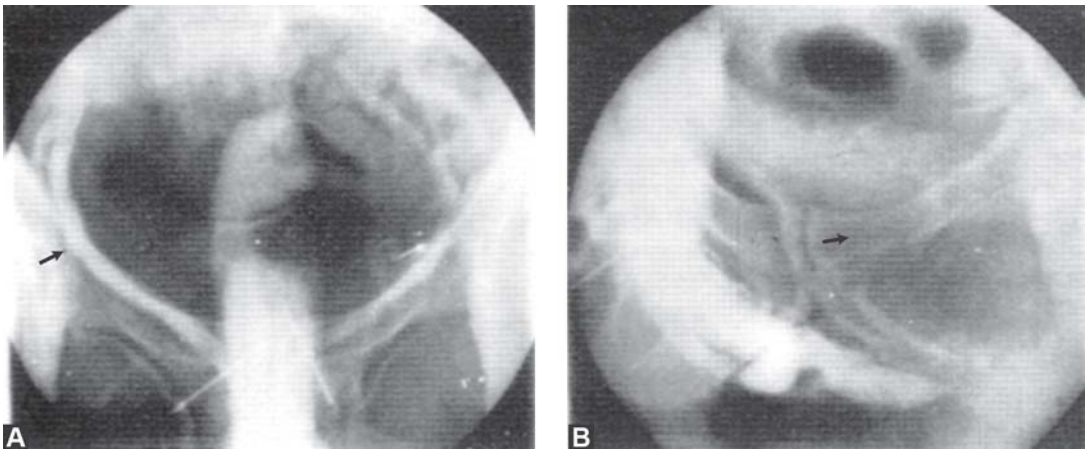

Figs 28.10A and B: Cavernosogram: Veno-occlusive ED: **(A)** AP view shows venous leak into internal pudendal vein (arrow). **(B)** Oblique view shows venous leak into deep dorsal vein in the cavernosogram of another patient

from the veins of corpus spongiosum, the deep dorsal, cavernosal and crural veins (Figs 28.10A and B). More than one site is present in most patients, with deep dorsal and cavernosal veins being the most common combination.[49]

Penile Angiography

Internal pudendal angiography is indicated in younger patients with suspected isolated arterial disease, such as post-traumatic narrowing, who may benefit from surgical repair rather than in elderly patients with diffuse atheromatous involvement. Patency of common iliac, internal iliac and internal pudendal arteries is established on initial angiographic films. Later, 60 mg of papaverine is injected in cavernosa followed by selective angiography of anterior division of internal pudendal artery. Contrast is injected at the rate of 3-4 ml per second and images are obtained in posterior oblique projection. In majority of the patients, anatomy of the penile arterial supply and the precise location of the arterial lesion is demonstrated which allows planning of appropriate surgical approach (Figs 28.11A and B).

Priapism

The most common complication during the diagnostic work-up and especially during PPDU and cavernosometry is papaverine induced prolonged and painful erection or priapism. The incidence can be as high as 11 percent.[34] Chances of priapism are high if PSV of more than 66 cm/s or RI of more than 1 (diastolic flow reversal) is observed.[50] It is prudent to observe the patient for at least 2 hours after the procedure. Not all priapism cases require specific treatment as penis detumescence generally occurs within few hours. In case the duration of erection exceeds six hours, the corpora cavernosa are drained to decrease the pressure and 10 microgram of adrenaline is injected intracavernosally to induce cavernosal smooth muscle contraction, effective venous drainage and restriction of arterial flow. Compression bandage is also applied for few minutes. In case of recurrence of erection, the procedure is repeated.

Broadly, priapism is divided into high flow and low flow priapism. High flow priapism is usually associated with trauma. The patients have painless erection and venous

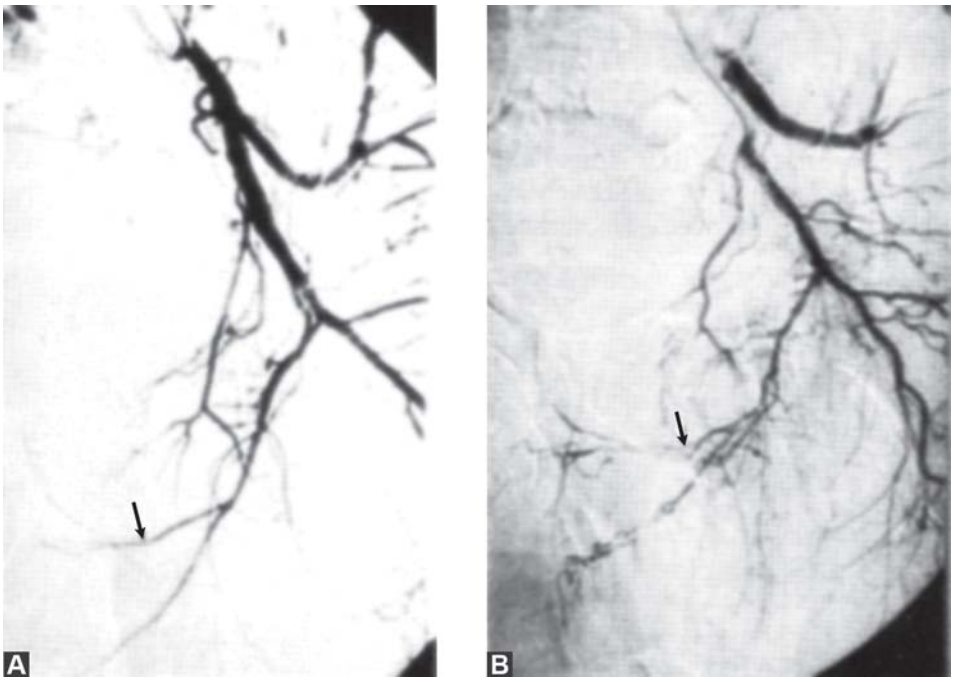

Figs 28.11A and B: Internal pudendal angiogram: **(A)** Normal internal pudendal and common penile (arrow) arteries. **(B)** Internal pudendal angiogram of another patient shows post-traumatic narrowing of common penile artery (arrow) as a cause of arteriogenic ED

outflow is usually maintained. The diagnosis of high flow priapism is usually clinical but color Doppler US may provide useful information. No cavernosal injection is required for the study. A hypoechoic area may be seen in cavernosa on grey scale US which suggest laceration. Color Doppler study may demonstrate the cavernosal artery tear and arterial-lacunar fistula. Selective embolization of the torn artery with blood clots, coils or PVA is the treatment of choice to treat these lesions.[51]

Low flow or ischemic priapism is seen as complication of intracavernosal injection of drugs or leukostasis in leukemic patients. The diagnosis is clinical and imaging is not required before surgical intervention. The condition is considered as an urologic emergency. US and color Doppler findings are same as that of normal rigid erection.

REFERENCES

1. Kuligowska E. Transrectal ultrasonography in diagnosis and management of male infertility: In Jaffe R, Pierson RA, Abramowics JS (Eds): Imaging in Infertility and Reproductive Endocrinology, JB Lippincot Co. Philadelphia, 1994;217-29.
2. Parsons RB, Fisher AM, Bar-Chama N, et al. MR imaging in male infertility. Radiographics 1997;17:627-37.
3. Colpi GM, Contalbi GF, Nerva F, et al. Testicular function following chemoradiotherpay. Eur J Obstet Gynecol Reprod Biol 2004;113 Suppl: S2-6.
4. Cornund E, Amar E, Hamida K, et al. Ultrasound findings in male hypofertility and impotence. Eur Radiol 2001;11:2126-36.
5. Pierik FH, Dohle GR, Muiswinkel JM, et al. Is routine scrotal ultrasonography advantageous in infertile men? J Urol 1999;162:1618-20.
6. Jarrow JP. Transrectal ultrasonography of infertile men. Fertil Steril 1993;60:1035-39.

7. Raviv G, Mor Y, Levron J, et al. Role of transrectal ultrasonography in the evaluation of azoospermic men with low volume ejaculate. J Ultrasound Med 2006;25:825-9.
8. Engin G, Kadioglu A, Orhan I, et al. Transrectal US and endorectal MR imaging in partial and complete obstruction of the seminal duct system. A comparative study. Acta Radiol 2000; 41:288-95.
9. Dhabuwala CB, Parulkar BG: Doppler flow analysis and conventional ultrasonography for evaluation of the infertile male: In Jafe R, Pierson RA, Abramowics JS (Eds): Imaging in Infertility and Reproductive Endocrinology, JB Lippincot Co. Philadelphia, 1994;207-16.
10. Qublan HS, Al-Okoor K, Al-Ghoweri AS, et al. Sonographic spectrum of scrotal abnormalities in infertile men. J Clin Ultrasound 2007;35: 437-41.
11. Howards SS: Varicocele. Infertil Reprod Med Clin N Am 1992;3:429-41.
12. Dambro TJ, Stewart RR, Carroll BA, et al. The scrotum. In: Rumack CM, Wilson SR, Charboneau JW (eds). Diagnostic ultrasound. 2nd edition, St Louis, Mosby. 1998;719-822.
13. Beddy P, Geoghegan T, Browne RF, et al. Testicular varicocele. Clin Radiol 2005;60: 1248-55.
14. McLure RD, Hrickak H. Scrotal ultrasound in infertile man: detection of subclinical unilateral and bilateral varicocele. J Urol 1986;135:711-14.
15. Kokacok E, Serhatlioglu S, Kiris S, et al. Colour Doppler sonographic evaluation of of interrelations between diameter, reflux and flow volume of testicular veins in varicocele. Eur J Radiol 2003;47:251-6.
16. Kessler A, Meirsdorf S, Graif M, et al. Intratesticular varicocele: grey scale and color Doppler sonographic appearance. J Ultrasound Med 2005;24:1711-16.
17. Dubin L, Amelar R. Varicocele size and results of varicocelectomy in selected infertile men with a varicocele. Fertil Steril 1970;21:606-9.
18. McLure R, Kho D, Dale R, et al. Subclinical varicocele- the effectiveness of varicocelectomy. J Urol 1991;145:786-90.
19. Gonda RL Jr, Kaw JJ, Forte KA et al. Diagnosis of subclinical varicocele in infertility. AJR 1987; 148:71-5.
20. Gandini R, Konda D, Reale CA, et al. Male varicocele: transcatheter foam sclerotherapy with sodium tetradecyl sulfate- outcome in 244 patients. Radiology 2008;246:612-8.
21. Halden W, White RI: Outpatient embolotherapy of varicocele. Urol Clin N Am 1987;14:137-40.
22. Thompson ST: Prevention of male infertility – an update. Urol Clin N Am 1994;21:365-76.
23. Simon SD, Lee RD, Mulhall PP. Should all infertile males undergo urologic evaluation before assisted reproductive technologies? Fertil Steril 2001;75:1226-7.
24. Kim Ed, Lipshultz LI: Role of ultrasound in assessment of male infertility. J Clin Ultrasound 1996;24:437-53.
25. Kumar R, Thulkar S, Kumar V, et al. Contributions of investigations to the diagnosis of bilateral vas aplasia. ANZ J Surg 2005;75:807-9.
26. Kim MJ, Lee JT, Lee MS, et al. MR imaging of male infertility with an endo rectal surface coil. Abdom Imaging 1997;22:348-53.
27. Fisch H, Lambert SM, Goluboff ET. Management of ejaculatory duct obstruction. Etiology, diagnosis and treatment. World J Urol 2006; 24:604-10.
28. Colpi GM, Negri L, Nappi RE, et al. Is transrectal ultrasonography a reliable diagnostic approach in ejaculatory duct sub obstruction? Hum Reprod 1997;12:2186-91.
29. Purohit RS, Wu DS, Shinohara K, et al. A prospective comparison of three diagnostic methods to evaluate ejaculatory duct obstruction. J Urol 2004;171:232-5.
30. Schnall MD, Pollack HM, Arsdalen KV, et al. The seminal tract in patients with ejaculatory dysfunction: MR imaging with an endo rectal surface coil. AJR 1992;159:337-41.
31. Toov JH, Fait G, Houser R, et al. Can Doppler ultrasonographic measurements of the testis predict spermatozoa retrieval in azoospermic patients undergoing testicular biopsy? Fertil Steril 2001;76:1276-7.
32. Belenky A, Avrech CM, Bacher GN, et al. Ultrasound guided testicular sperm aspiration in azospermic patient: a new sperm retrieval method for intra cytoplasmic sperm injection. J Clin Ultrasound 2001;6:339-43.
33. Belker AM, Steinbock GS: Transrectal prostate ultrasonography as a diagnostic and therapeutic aid for ejaculatory duct obstruction. J Urol 1990; 144:356-8.
34. Mihmanli I, Kantarci F. Erectile dysfunction. Semin Ultrasound CT MRI 2007;28:274-86.

35. Aroujo AB, Mohr BA, McKinley JB. Changes in sexual function in middle aged and older men: longitudinal data from the Massachusetts Male Aging Study. J Am Geriatr Soc 2004;52:1502-09.
36. Montorsi F, Briganti A, Salonia A, et al. Erectile dysfunction prevalence, time of onset, and association with risk factors in 300 consecutive patients with acute chest pain, and angiographically documented coronary artery disease. Eur Urol 2003;44:360-64.
37. Hatzichristan D, Hatzimouratidis K, Bekas M, et al. Diagnostic steps in evaluation of patients with erectile dysfunction. J Urol 2002;168:615-20.
38. Meuleman E, Diemont WL. Investigation of erectile dysfunction. Urol Clin N Am 1995;22: 803-19.
39. Park K, Kwon DD, Oh BR, et al. Efficacy of virtual glasses in audio-visual sexual stimulation during penile colour duplex Doppler ultrasonography. Eur Urol 2002;41:62-5.
40. Roy C, Saussine C, Tuchman C, et al. Duplex Doppler sonography of flaccid penis: potential role in the evaluation of impotence. J Clin Ultrasound 2000;28:290-94.
41. Broderick GA, Arger P. Duplex Doppler ultrasonography: noninvasive assessment of penile anatomy and function. Semin Roentgen 1993; 28:43-56.
42. Shwartz AM, Lawe M, Berger RE, et al: Assessment of normal and abnormal erectile function-color Doppler sonography versus conventional techniques. Radiology 1991;180:105-9.
43. Bhargava R, Srivastava DN, Thulkar S, et al. Colour duplex Doppler ultrasonography evaluation of non-vasculogenic male erectile dysfunction: an Indian perspective. Australas Radiol 2002;44:170-73.
44. Arslan D, Esen AA, Secil M. A new method for evaluation of ED: Sidenafil plus Doppler ultrasonography. J Urol 2001;166:181-4.
45. Copel L, Ktz R, Blacher A, et al. Clinical and duplex US assessment of effects of sidenafil on cavernosal arteries of the penis: comparison with intracavernosal injection of vasoactive agents-initial experience. Radiology 2005;237:986-91.
46. Park JK, Park JS, Jeon SB, et al. Why a combined intracavernosal injection with trimix and oral sidenafil is reliable therapy in ultrasonic evaluation of erectile dysfunction. BJU Int 2008;102:993-97.
47. Gholami SS, Lue TF. Peyronie's disease. Urol Clin N Am 2001;28:377-90.
48. Meulman EJ, Wijkstra H, Doesbury WH, et al: Comparison of diagnostic values of pump and gravity cavernosometry in the evaluation of cavernous veno-occlusive mechanism. J Urol 1991;146:1266-70.
49. Shabsingh R, Fishman IJ, Toombs BD et al. Venous leaks: Anatomical and physiological observations. J Urol 1991;146:1260-64.
50. Metawea B, El-Nashar AR, Gad-Allah A, et al. Intracavernos papaverine phentolamine induced priapism can be accurately predicted with colour Doppler ultrasonography. Urology 2005;66: 858-60.
51. Campliani S, Savoca G, Buttazi L, et al. High flow priapism: treatment and long term follow-up. Urology 2002;59:110-13.

INDEX